비매품/무료
93500
9 788957 083567
ISBN 978-89-5708-356-7

WINDOWS INTO SAUROPSID AND SYNAPSID EVOLUTION
Essays In Honor of Louis L. Jacobs
Yuong-Nam Lee, *editor*
DINOSAUR SCIENCE CENTER PRESS

Microsteiromys jacobsi

WINDOWS INTO SAUROPSID AND SYNAPSID EVOLUTION

Essays In Honor of Louis L. Jacobs

Yuong-Nam Lee, *editor*

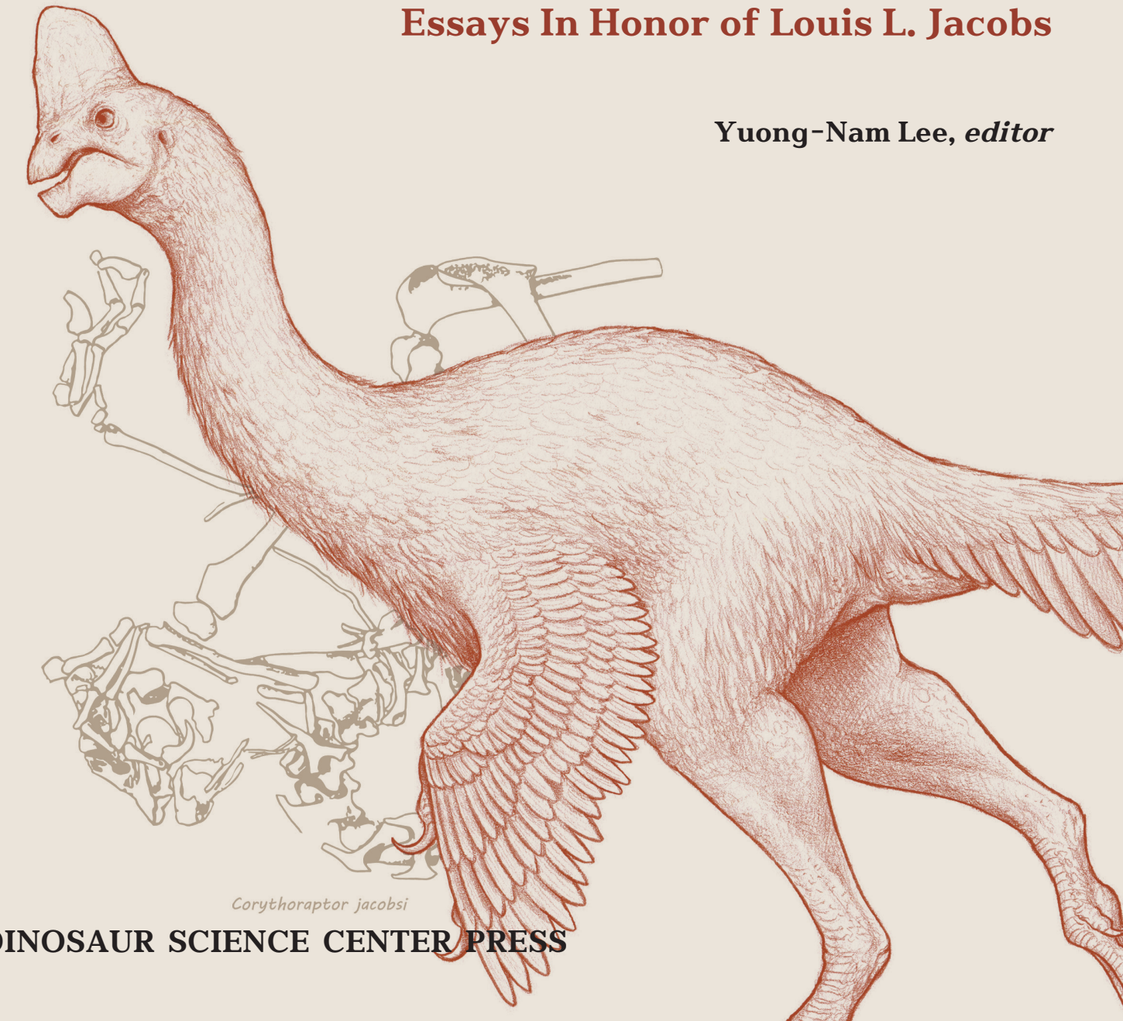

Corythoraptor jacobsi

DINOSAUR SCIENCE CENTER PRESS

WINDOWS INTO SAUROPSID AND SYNAPSID EVOLUTION

Essays In Honor of Louis L. Jacobs

Yuong-Nam Lee, *editor*

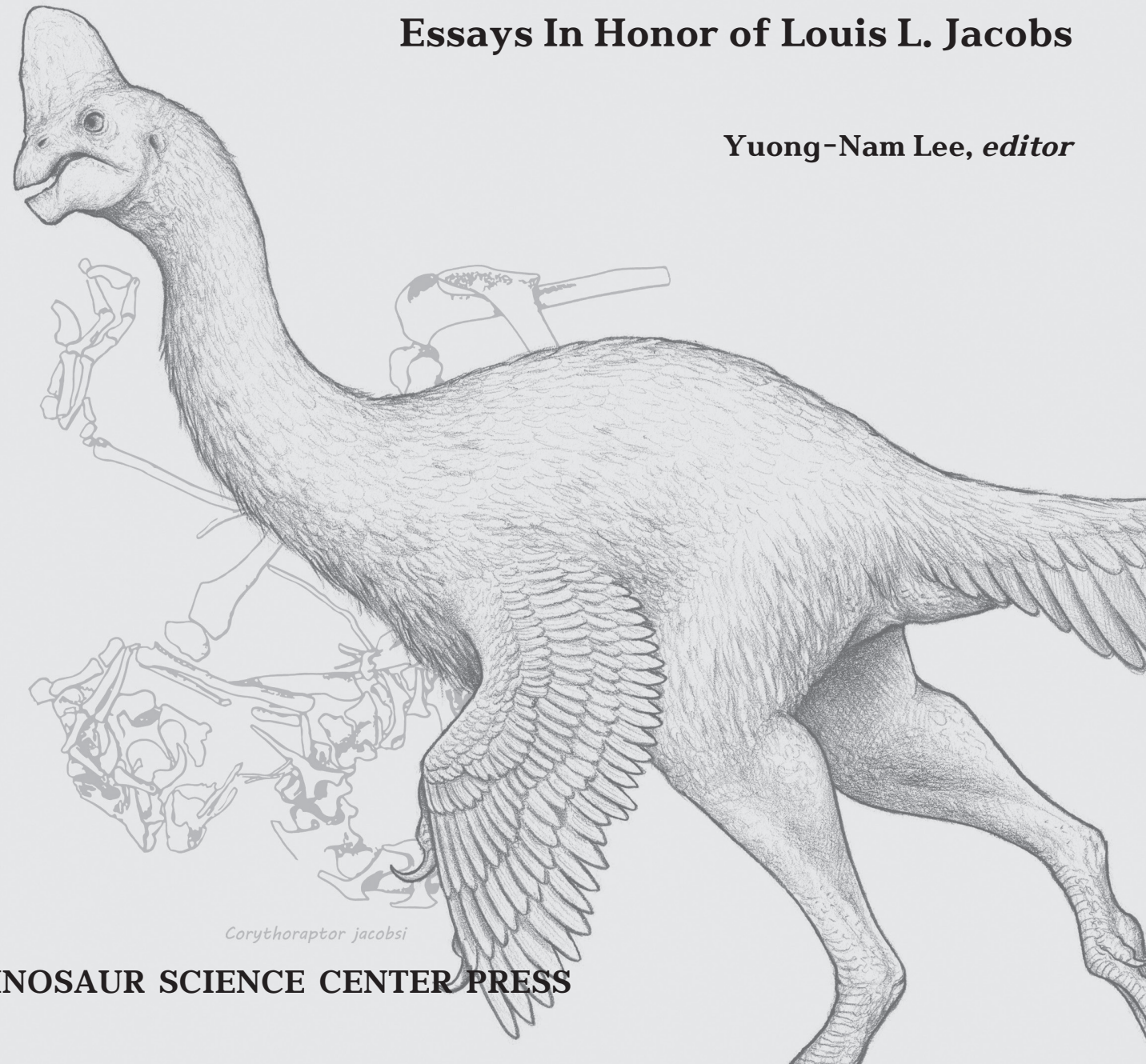

DINOSAUR SCIENCE CENTER PRESS

비매품/무료
93500
9 788957 083567
ISBN 978-89-5708-356-7

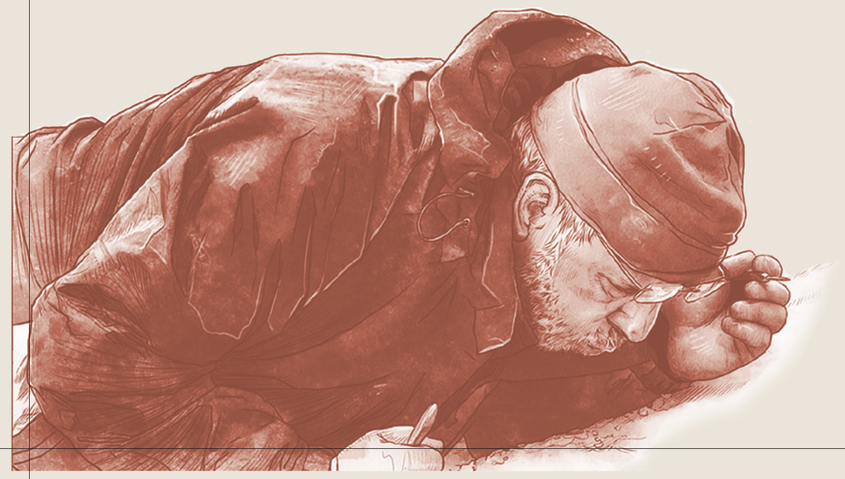

WINDOWS INTO SAUROPSID AND SYNAPSID EVOLUTION

Essays In Honor of Louis L. Jacobs

Yuong-Nam Lee, *editor*

DINOSAUR SCIENCE CENTER PRESS

Microsteiromys jacobsi

WINDOWS INTO SAUROPSID AND SYNAPSID EVOLUTION

Essays In Honor of Louis L. Jacobs

Yuong-Nam Lee, *editor*

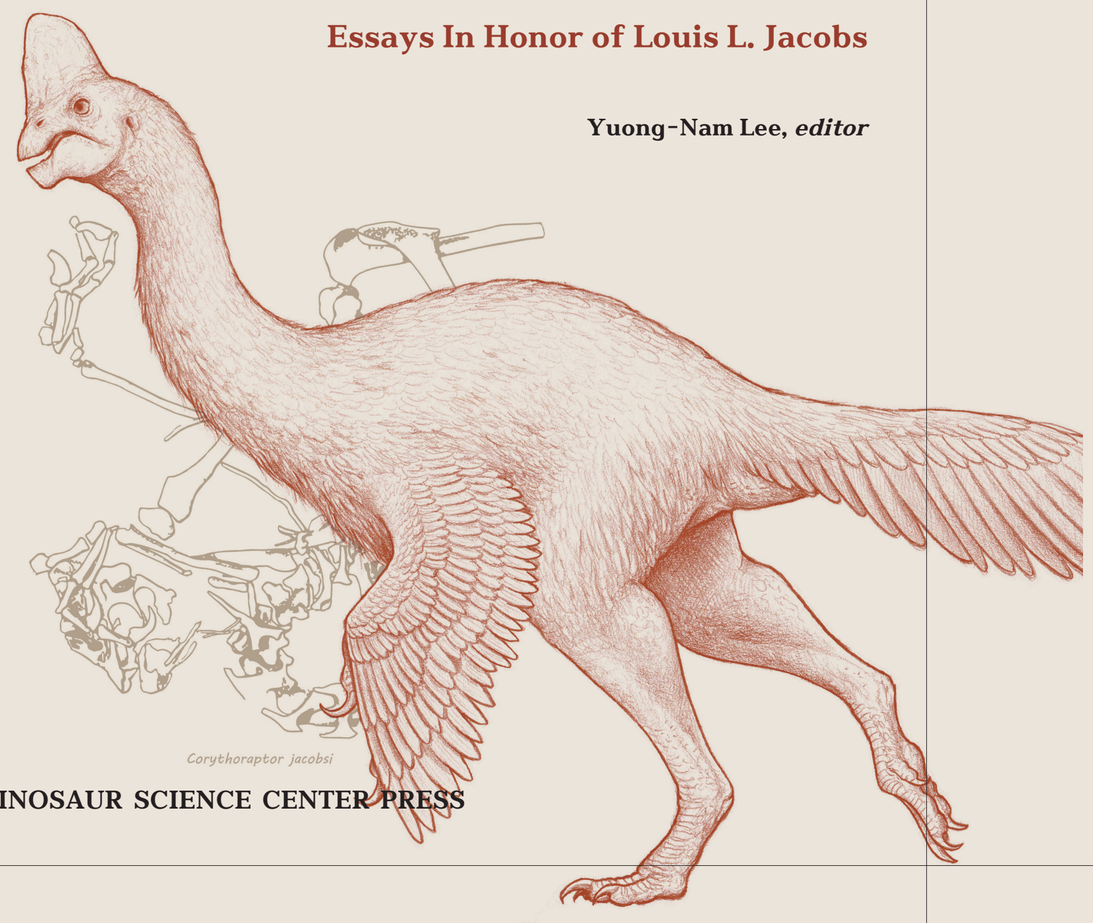

Corythoraptor jacobsi

DINOSAUR SCIENCE CENTER PRESS

WINDOWS INTO SAUROPSID AND SYNAPSID EVOLUTION

Essays

In honor of

Prof. Louis L. Jacobs

Yuong-Nam Lee, *editor*

DINOSAUR SCIENCE CENTER PRESS

WINDOWS INTO SAUROPSID AND SYNAPSID EVOLUTION

ISBN: 978-89-5708-358-1 (paper)
978-89-5708-356-7 (cloth)

Printed by Hanrimwon Co., Ltd.

South Korea

To

Louis L. Jacobs

TABLE OF CONTENTS

WINDOWS INTO SAUROPSID EVOLUTION

WINDOWS INTO SYNAPSID EVOLUTION

LIST OF CONTRIBUTORS

Thomas L. Adams
Witte Museum,
San Antonio, TX 78209, U.S.A

Kate A. Andrzejewski
Kansas Geological Survey,
University of Kansas,
Lawrence, Kansas 66047, U.S.A

K. D. Angielczyk
Negaunee Integrative Research Center,
Field Museum of Natural History,
Chicago, Illinois 60605, U.S.A

R. Araújo
Instituto de Plasmas e Fusão Nuclear,
Universidade de Lisboa,
Portugal

Zorigt Badamkhatan
Institute of Paleontology,
Mongolian Academy of Sciences,
Ulaanbaatar 15160, Mongolia

Rinchen Barsbold
Institute of Paleontology,
Mongolian Academy of Sciences,
Ulaanbaatar 15160, Mongolia

Jon Baskin
Department of Biological and Health Sciences,
Texas A&M University-Kingsville,
Kingsville, Texas 78363, U.S.A

C. Browning
Iziko South African Museum,
Cape Town, South Africa

Kentaro Chiba
Department of Biosphere-Geosphere Science,
Okayama University of Science,
Okayama 700-0005, Japan

Tsogtbaatar Chinzorig
Department of Biological Sciences,
North Carolina State University,
Raleigh, North Carolina 27607, U.S.A

Philip J. Currie
Department of Biological Sciences,
University of Alberta,
Edmonton, Alberta T6G 2E9, Canada

R. David
Natural History Museum,
London, United Kingdom

Stephanie K. Drumheller
Department of Earth and Planetary Sciences,
University of Tennessee,
Knoxville, Tennessee 37996, U.S.A

David C. Evans
Department of Ecology and Evolutionary Biology,
University of Toronto,
Toronto, ON, Canada

S. Ferreira-Cardoso
Institut des Sciences de l'Evolution de Montpellier (ISEM),
CNRS, IRD, EPHE,
Université de Montpellier,
Montpellier, France

Leonardo S. Filippi
CONICET-Museo Municipal "Argentino Urquiza",
Rincón de los Sauces, Neuquén, Argentina

Anthony R. Fiorillo
New Mexico Museum of Natural History & Science,
Albuquerque, New Mexico 87104, U.S.A

Lawrence J. Flynn
Department of Human Evolutionary Biology,
Harvard University,
Cambridge, MA 02138, U.S.A

Gregory F. Funston
Department of Natural History,
Royal Ontario Museum,
Toronto, Ontario M5S 2C6, Canada

António Olímpio Gonçalves
Departamento de Geologia, Faculdade de Ciências,
Universidade Agostinho Neto,
Luanda, Angola

Louis L. Jacobs
Roy M. Huffington Department of Earth Sciences,
Southern Methodist University,
Dallas, TX 75275, U.S.A

Yusuf M. Juwayeyi
Department of Social Sciences,
Long Island University,
Brooklyn, New York, U.S.A

Purevdorj Khatanbaatar
Institute of Paleontology,
Mongolian Academy of Sciences,
Ulaanbaatar 15160, Mongolia

Yuri Kimura
Department of Geology and Paleontology,
National Museum of Nature and Science,
Tsukuba, Ibaraki 305-0005, Japan

Yoshitsugu Kobayashi
Hokkaido University Museum,
Hokkaido University,
Sapporo, Hokkaido 060-0810, Japan

Satoshi Konishi
Department of Biosphere-Geosphere Science,
Okayama University of Science,
Okayama 700-0005, Japan

D. J. P. Kortje
Iziko South African Museum,
Cape Town, South Africa

Kewal Krishan
Department of Anthropology,
Panjab University,
Chandigarh 160014, India

Katsuhiro Kubota
Museum of Nature and Human Activities,
Hyogo 669-1546, Japan

Rohit Kumar
Department of Geology,
Panjab University,
Chandigarh 160014, India

Yuong-Nam Lee
School of Earth and Environmental Sciences,
Seoul National University,
Seoul 08826, South Korea

Lu Li
Institute of Vertebrate Paleontology and Paleoanthropology,
Chinese Academy of Sciences,
Beijing 100044, China

Junchang Lü (deceased)
Institute of Geology,
Chinese Academy of Geological Sciences,
Beijing, China

Buuvei Mainbayar
Institute of Paleontology,
Mongolian Academy of Sciences,
Ulaanbaatar 15160, Mongolia

Z. Macungo
Evolutionary Studies Institute,
University of the Witwatersrand,
Johannesburg, South Africa

A. Massingue
Museu Nacional de Geologia,
Maputo, Mozambique

Paul J. McCarthy
Department of Geosciences,
University of Alaska,
Fairbanks, Alaska, 99775, U.S.A

Ariel H. Méndez
Instituto Patagónico de Geología y Paleontología
(CCT CONICET-CENPAT),
Puerto Madryn, Chubut, Argentina

Logan Micucci
Department of Earth Sciences,
Ottawa-Carleton Geoscience Centre,
Carleton University,
Ottawa, ON, Canada

Andreas Möller
Department of Geology,
University of Kansas,
Lawrence, Kansas 66045, U.S.A

Christopher R. Noto
Deparment of Biological Sciences,
University of Wisconsin-Parkside,
Kenosha, Wisconsin 53141, U.S.A

Rajeev Patnaik
Department of Geology,
Panjab University,
Chandigarh 160014, India

Ariana Paulina-Carabajal
Instituto de Investigaciones en Biodiversidad y Medioambiente
(CONICET-Universidad Nacional del Comahue),
S. C. de Bariloche 8400, Argentina

David Pilbeam
Department of Human Evolutionary Biology,
Harvard University,
Cambridge, MA 02138, U.S.A

Michael J. Polcyn
Roy M. Huffington Department of Earth Sciences,
Southern Methodist University,
Dallas, TX 75275, U.S.A

Zhuding Qiu
Institute of Vertebrate Paleontology and Paleoanthropology,
Chinese Academy of Sciences,
Beijing 100044, China

Hanika Rizo
Department of Earth Sciences,
Ottawa-Carleton Geoscience Centre,
Carleton University,
Ottawa, ON, Canada

Michael J. Ryan
Department of Earth Sciences,
Ottawa-Carleton Geoscience Centre,
Carleton University,
Ottawa, ON, Canada

Mototaka Saneyoshi
Department of Biosphere-Geosphere Science,
Okayama University of Science,
Okayama 700-0005, Japan

Anne S. Schulp
Naturalis Biodiversity Center,
Leiden, The Netherlands

Emily Schwing
New Mexico Museum of Natural History & Science,
Albuquerque, New Mexico 87104, U.S.A

Bahadur Singh
Department of Anthropology,
Panjab University,
Chandigarh 160014, India

R. M. H. Smith
Evolutionary Studies Institute,
University of the Witwatersrand,
Johannesburg, South Africa

Laura Stelson
Katmai National Park and Preserve,
King Salmon, AK 99613, U.S.A

Corwin Sullivan
Department of Biological Sciences,
University of Alberta,
Edmonton, Alberta T6G 2E9, Canada

Keiichi Takahashi
Lake Biwa Museum,
Kusatsu, Shiga 525-0001, Japan

Kohei Tanaka
Faculty of Life and Environmental Sciences,
University of Tsukuba,
Tsukuba, Ibaraki 305-8572, Japan

Louis H. Taylor
4931 W. Rowland Avenue,
Littleton, Co 80128, U.S.A

François Therrien
Royal Tyrrell Museum of Palaeontology,
Drumheller, Alberta T0J 0Y0, Canada

Yukimitsu Tomida
National Museum of Nature and Science,
Tsukuba, Ibaraki 169-0073, Japan

Khishigjav Tsogtbaatar
Institute of Paleontology,
Mongolian Academy of Sciences,
Ulaanbaatar 15160, Mongolia

Karen Ulloa-Guaiquín
Instituto de Investigaciones en Biodiversidad y Medioambiente
(CONICET-Universidad Nacional del Comahue),
S. C. de Bariloche 8400, Argentina

Alberto Valenciano
Departamento de Estratigrafía, Geodinámica y Paleontología,
Facultad de Ciencias Geológicas,
Universidad Complutense de Madrid,
Madrid, Spain

Yan-Yin Wang
Department of Biological Sciences,
University of Alberta,
Edmonton, Alberta T6G 2E9, Canada

Alisa J. Winkler
Roy M. Huffington Department of Earth Sciences,
Southern Methodist University,
Dallas, TX 75275, U.S.A

Wenyu Wu
Institute of Vertebrate Paleontology and Paleoanthropology,
Chinese Academy of Sciences,
Beijing 100044, China

Yudai Yamamoto
Department of Biosphere-Geosphere Science,
Okayama University of Science,
Okayama 700-0005, Japan

Darla K. Zelenitsky
Department of Geoscience,
University of Calgary,
Calgary, Alberta T2N 1N4, Canada

PREFACE

This volume is a tribute to the professional life of Dr. Louis L. Jacobs. While no single book can replace a lifetime of accomplishments by a great vertebrate paleontologist, everyone who knows him will feel the meaningful value of this volume, even if it comes late.

His career in vertebrate paleontology, which began in graduate school in 1970, has been passionately and successfully pursued for the past 53 years and will continue in the future. His extensive and significant research achievements are well reflected in his bibliography. However, Louis remains highly passionate and actively engaged in vertebrate paleontology, indicating that his scholarly accomplishments will continue for a long time.

The essays in this volume were presented by Louis' friends, colleagues, and students. Sixty-eight professionals from 16 countries willingly contributed to this volume. It demonstrates that Louis has a close network of professionals from all around the world. Louis began his professional career focusing on rodent fossils but expanded his expertise to various reptiles, including dinosaurs and mosasaurs. Accordingly, the organization of this book is divided into sauropsids and synapsids, reflecting the significant contributions of Louis to the study of the evolution of these two major groups in vertebrate paleontology, and the title of the book is a tribute to his achievements.

We have discussed this volume for the past 15 years, with the intention to publish it in line with Louis' retirement. However, it was postponed several times. At last, this year, the 5th Asia Dinosaur International Symposium, sponsored by Hwaseong City, South Korea, allowed us to publish this book. We reached out to Louis' colleagues, friends, and students to participate in this project. In each contributor's acceptance responses, we could feel how successful Louis' life has been. We are especially grateful to Dr. Lawrence Flynn, who introduced us to Louis' longtime colleagues and friends in the field of mammal fossil studies. We would also like to express our gratitude to Dr. Louis Taylor, a member of 'Red Fireballs' and one of Louis' closest friends, who reached out to us first, expressing his desire to write a detailed biography of Dr. Louis Jacobs.

Finally, all of us (someone called us 'Asian Mafia' as a joke) are deeply grateful for the golden times in our lives at SMU, thanks to Dr. Louis Jacobs, and we take very pride in being his students. We are very fortunate we have him as our mentor. We learned from him what friends are for when watching Louis, who brought Will Downs' ashes to the Flaming Cliffs in 2006.

Louis has significantly contributed to studying rodents in Pakistan and Kenya and researching dinosaurs and marine reptiles in Malawi and Angola. However, the five years of KID expeditions with us in the Gobi Desert of Mongolia will forever remain cherished memories of happy times.

We have been very delighted and honored to organize a tribute for 'a wonderful human being' as one contributor referred to Louis.

Yuong-Nam Lee
School of Earth and Environmental Sciences,
Seoul National University,
Seoul, South Korea

Yoshitsugu Kobayashi
Hokkaido University Museum,
Hokkaido University,
Sapporo, Japan

[§]*Junchang Lü*
Institute of Geology,
Chinese Academy of Geological Sciences,
Beijing, China
[§]deceased

8 November 2023

Junchang Lü, Louis L. Jacobs, Yoshitsugu Kobayashi, Yuong-Nam Lee at Flaming Cliffs in 2006

BIBLIOGRAPHY
(THROUGH NOVEMBER, 2023)
OF
LOUIS L. JACOBS

Refereed Articles and Monographs in Journals, Books, and Symposium Volumes

Jacobs, L.L. 1977. Rodents of the Hemphillian age Redington local fauna, San Pedro Valley, Arizona. Journal of Paleontology, 5(3):505-519.

Jacobs, L.L. 1977. A new genus of murid rodent from the Miocene of Pakistan and comments on the origin of the Muridae. Paleobios, 25:1-11.

Butler, R.F., Lindsay, E.H., Jacobs, L.L., and Johnson, N.M. 1977. Magnetostratigraphy of the Cretaceous-Tertiary boundary in the San Juan Basin, New Mexico. Nature, 267:318-323.

Pilbeam, D., Barry, J., Meyer, G., Shah, S.M.I., Pickford, M.H.L., Bishop, W.W., Thomas, H., and Jacobs, L.L. 1977. Geology and paleontology of Neogene strata of Pakistan. Nature, 270:684-489.

Jacobs, L.L. 1978. Fossil rodents (Rhizomyidae and Muridae) from Neogene Siwalik deposits, Pakistan. Museum of Northern Arizona Bulletin Series, 52:1-103.

Lindsay, E.H., Jacobs, L.L., and Butler, R.F. 1978. Biostratigraphy and magnetostratigraphy of Paleocene terrestrial sediments in the San Juan Basin, New Mexico. Geology, 6:425-429.

Jacobs, L.L. 1979. Homology of tooth cusps in murid rodents based on Miocene fossils from Pakistan. Casopis pro Mineralogii a Geologii (Praha), 24(3):301-304.

Jacobs, L. L. 1979. Small mammals: Insectivora, Tupaiidae, Chiroptera, and Rodentia. In Pilbeam, D.R., Behrensmeyer, A.K., Barry, J.C., and Shah, S.M.I. (eds.), Miocene sediments and faunas of Pakistan. Postilla, 179:33-34.

Jacobs, L.L. 1980. Additions to the Triassic vertebrate fauna of Petrified Forest National Park, Arizona. Arizona-Nevada Academy of Science Journal, 12:247.

Jacobs, L.L. 1980. Siwalik fossil tree shrews. In Luckett, W.P. (ed.), Comparative biology and evolutionary relationships of tree shrews. Plenum Publ. Corp., New York, pp. 205-216.

Jacobs, L.L. and Murry, P. 1980. The vertebrate community of the Triassic Chinle Formation near St. Johns, Arizona. In Jacobs, L.L. (ed.), Aspects of vertebrate history: essays in honor of Edwin Harris Colbert. Museum of Northern Arizona Press, Flagstaff, pp. 55-71.

Jacobs, L.L. and Pilbeam, D. 1980. Of mice and men: fossil-based divergence dates and molecular “clocks.” Journal of Human Evolution, 9:551-555.

Jacobs, L.L. 1981. Miocene lorisid primates from the Pakistan Siwaliks. Nature, 289(5798):585-587.

Jacobs, L.L., Cheema, I.U., and Shah, S.M.I. 1981. Zoogeographic implications of early Miocene rodents from the Bugti Beds, Baluchistan, Pakistan, Geobios, 15(1):101-103

Jacobs, L.L., and Lindsay, E.H. 1981. *Prosigmodon oroscoi*, a new sigmodont rodent from the late Tertiary of Mexico. Journal of Paleontology, 55:425-430.

Rose, K.D., Walker, A., and Jacobs, L.L. 1981. Function of the mandibular tooth comb in living and extinct mammals. Nature, 289(5798):583-585.

Barry, J.C., Lindsay, E.H., and Jacobs, L.L. 1982. A biostratigraphic zonation of the middle and upper Siwaliks of the Potwar Plateau of northern Pakistan. Palaeogeography, Palaeoclimatology, Palaeoecology, 37:95-130.

Dehm, R., Jacobs, L.L., Wessels, W., de Bruijn, H., and Hussain, S.T. 1982. Fossil rodents from the type area of the Chinji Formation, Siwalik Group, Pakistan. Koninklijke Nederlandse Akadademie van Wetenschappen, Proceedings, Series B, 85(3):259-263.

Flynn, L.J., and Jacobs, L.L. 1982. Effects of changing environments on Siwalik rodent faunas of northern Pakistan. Palaeogeography, Palaeoclimatology, Palaeoecology, 38:129-139.

Jacobs, L.L., and Li Chuan-kuei. 1982. A new genus (*Chardinomys*) of murid rodent (Mammalia, Rodentia) from the Neogene of China, and comments on its biogeography. Geobios, 15(2):255-259.

Flynn, L.J., Jacobs, L.L., and Sen, S. 1983. La diversité de *Paraulacodus* (Thryonomyidae, Rodentia) et des groupes apparentés pendant le Miocene. Annales de Paléontologie, Paris, 69(4):355-366.

Jacobs, L.L., and Lindsay, E.H. 1984. Holarctic radiation of Neogene muroid rodents and the origin of South American cricetids. Journal of Vertebrate Paleontology, 4(2):265-272.

Jacobs, L.L. 1985. The beginning of the Age of Murids in Africa. Acta Zoologica Fennica, 170:149-151.

Flynn, L.J., Jacobs, L.L., and Lindsay, E.H. 1985. Problems in muroid phylogeny: relationship to other rodents and origin of major groups. In Luckett, W.P., and Hartenberger, J.L. (eds.), Evolutionary relationships among rodents. Press, New York, pp. 589-616.

Barry, J.C., Johnson, N.M., Raza, S.M., and Jacobs, L.L. 1985. Neogene mammalian faunal change in Southern Asia: Correlations with climatic, tectonic, and eustatic events. Geology, 13:637-640.

Jacobs, L.L., Flynn, L.J., and Li, C.K. 1985. Comments on rodents from the Chinese Neogene. Bulletin of the Geological Institutions of the University of Uppsala, N.S., 11:59-78.

Lindsay, E.H., and Jacobs, L.L. 1985. Pliocene small mammal fossils from Chihuahua, Mexico. Revista, Instituto de Geologia Universidad National Autonoma Mexico, Paleontologia Mexicana 51:1-53.

Hill, A., Drake, R., Tauxe, L., Monaghan, M., Barry, J., Behrensmeyer, A.K., Curtis, G., Jacobs, B. Fine, Jacobs, L.L., Johnson, N., and Pilbeam, D. 1985. Neogene paleontology and geochronology of the Baringo Basin, Kenya. Journal of Human Evoluton, 14:759-773.

Flynn, L.J., Jacobs, L.L., and Cheema, I.U. 1986. Baluchimyinae, a new Ctenodactyloid rodent subfamily from the Miocene of Baluchistan. American Museum Novitates, 2841:1-58.

Cifelli, R. L., Ibui, A., Jacobs, L.L., and Thorington, R.W., Jr. 1986. A giant tree squirrel from the late Miocene of Kenya. Journal of Mammalogy, 67(2):274-283.

MacPhee, R.D.E., and Jacobs, L.L. 1986. *Nycticeboides simpsoni* and the morphology, adaptations, and relationships of Miocene Siwalik Lorisidae. In Flanagan, K.M., and Lillegraven, J.A., (eds.), Vertebrates, phylogeny, and philosophy. Contributions to Geology, University of Wyoming, Special Paper 3, pp. 131-161.

Barry, J.C., Jacobs, L.L., and Kelly, J. 1986. An early middle Miocene catarrhine from Pakistan with comments on the dispersal of catarrhines to Eurasia. Journal of Human Evolution, 15:501-508.

Jacobs, L.L., Anyonge, W., and Barry, J.C. 1987. *Ndamathaia kubwa*: a giant tenrecid from the Miocene of Kenya. Journal of Mammalogy, 68(1):10-16.

Flynn, L.J., Brillanceau, A., Brunet, M., Coppens, Y., Dejax, J., Duperon-Laudoueneix, M., Ekodeck, G., Flanagan, K.M., Heintz, E., Hell, J., Jacobs, L.L., Pilbeam, D.R., Sen, S., and Djallo, S. 1987. Vertebrate fossils from Cameroon, West Africa. Journal of Vertebrate Paleontology, 7(4):469-471.

Winkler, D.A., Murry, P.A., Jacobs, L.L., Downs, W.R., Branch, J.R., and Trudel, P. 1988. The Proctor Lake Dinosaur Locality, Lower Cretaceous of Texas. Hunteria, 2(5):1-8.

Brunet, M., Dejax, J., Brillanceau, A., Congleton, J., Downs, W., Duperon, M., Eisenman, V., Flynn, L., Heintz, E., Hell, J.,

Jacobs, L., Jehenne, Y., Ndjeng, E., Mouchelin, G., and Pilbeam, D. 1988. Mise en 'evidence d'une sedimentation precoce d'age Barremien dans le fosse de la Benoue en Afrique occidentale (Bassin du Mayo Oulo Lere, Cameroun), en relation avec l'ouverture de l'Atantique sud. Comptes Rendus de l'Académie des Sciences, Paris, 306:1125-1130.

Jacobs, L.L., Congleton, J.D., Brunet, M., Dejax, J., Flynn, L.J., Hell, J.V., and Mouchelin, G. 1988. Mammal teeth from the Cretaceous of Africa. Nature, 336 (6195):158-160.

Brunet, M., Jacobs, L., Congleton, J., Coppens, Y., Dejax, J., Flynn, L., Hell, J., Jehenne, Y., Mouchelin, G., and Pilbeam, D. 1988. Premiere decouverte d'un fragment de mandibule de Mammifere dans le Cretace inferieur d'Afrique (Cameroun, Bassin de Koum). Comptes Rendus de l'Académie des Sciences, Paris, 307, II:1675-1680.

Clark, J.M., Jacobs, L.L., and Downs, W.R. 1989. Mammal-like dentition in a Mesozoic rocodylomo. Science, 244:1064-1066.

Jacobs, L.L., Flanagan, K.M., Brunet, M., Flynn, L.J., Dejax, J., and Hell, J.V. 1989. Dinosaur footprints from the Lower Cretaceous of Cameroon, West Africa. In Gillette, D.D., and Lockley, M.G. (eds.), Cambridge University Press, pp. 349-351.

Jacobs, L.L., Flynn, L.J., and Downs, W.R. 1989. Neogene rodents of southern Asia. In Black, C.C., and Dawson, M.R. (eds.), Papers on Fossil Rodents in Honor of Albert Elmer Wood. Natural History Museum of Los Angeles County, Science Series, 33:157-177.

Jacobs, L.L., Winkler, D.A., and Murry, P.A. 1989. Modern mammal origins: Evolutionary grades in the Early Cretaceous of North America. Proceedings of the National Academy of Sciences USA, 86:4992-4995.

Brunet, M., Coppens, V., Dejax, J., Flynn, L., Heintz, E., Hell, J., Jacobs, L., Jehenne, Y., Mouchelin, G., Pilbeam, D., and Sudre, J. 1990. Nouveaux mammiferes du Cretace inferieur du Cameroun, Afrique de L'Ouest. Comptes Rendus de l'Académie des Sciences, Paris, 310:1139-1146.

Colin, J.-P., and Jacobs, L.L. 1990. L'age des Couches a Dinosaures du Malawi: apport des ostracodes. Comptes Rendus de l'Académie des Sciences, Paris, 311:1025-1029.

Flynn, L.J., and Jacobs, L.L. 1990. Preliminary analysis of Miocene small mammals from Pasalar, Turkey. Journal of Human Evolution, 19:423-436.

Flynn, L.J., Pilbeam, D., Jacobs, L.L., Barry, J.C., Behrensmeyer, A.K., and Kappelman, J.W. 1990. Time and faunas in a Miocene terrestrial setting. Journal of Geology, 98:589-604.

Jacobs, L.L., Flynn, L.J., Downs, W.R., and Barry, J.C. 1990. Quo Vadis *Antemus*? The Siwalik Muroid Record. In Lindsay, E.H., Fahlbusch, V., and Mein, P. (eds.), European Neogene Mammal Chronology. Plenum Press, New York, pp. 573-586.

Jacobs, L.L., Winkler, D.A., Kaufulu, Z.M., and Downs, W.R. 1990. The Dinosaur Beds of Northern Malawi, Africa. National Geographic Research, 6:196-204.

Winkler, D.A., Murry, P.A., and Jacobs, L.L. 1990. Early Cretaceous (Comanchean) fossil vertebrates of central Texas. Journal of Vertebrate Paleontology, 10(1):95-116.

Barry, J.C., Morgan, M.E., Winkler, A.J., Flynn, L.J., Lindsay, E.H., Jacobs, L.L., and Pilbeam, D. 1991. Faunal interchange and Miocene terrestrial vertebrates of southern Asia. Paleobiology, 17(3):231-245.

Jacobs, L.L., Winkler, D.A., and Murry, P.A. 1991. On the age and correlation of Trinity mammals, Early Cretaceous of Texas, USA. Newsletters on Stratigraphy, 24:35-43.

Murry, P.A., Winkler, D.A., and Jacobs, L.L. 1991. An azhdarchid pterosaur humerus from the Lower Cretaceous Glen Rose Formation of Texas. Journal of Paleontology, 65(1):167-170.

Winkler, D.A., Jacobs, L.L., Congleton, J.D., and Downs, W.R. 1991. Life in a sand sea: biota from Jurassic interdunes. Geology, 19:889-892.

Congleton, J.D., Flynn, L.J., Jacobs, L.L., Brunet, M., Dejax, J., Hell, J., and Pilbeam, D. 1992. Preliminary correlation of continental sediments of the Koum Basin, northern Cameroon. In Mateer, N.J., and Chen Pei-ji (eds.), Aspects of nonmarine Cretaceous Geology, China Ocean Press, Beijing, pp. 213-219.

Mateer, N.J., Wycisk, P.J., Jacobs, L.L, Brunet, M., Luger, P., Dina, A., Hendriks, F., Weissbrod, T., Gvirtzman, G., Arush, M., Mbede, E., Hell, J., and El-Nakhal, H.A. 1992. Correlation of nonmarine Cretaceous strata of Africa and the Middle East. Cretaceous Research, 13(3):273-318.

Colin, J.K., Brunet, M., Congleton, J.D., Dejax, J., Lynn, L.J., Hell, J., and Jacobs, L.L. 1992. Ostracodes lacustres des bassins d'age Cretace Inferieur du nord Cameroun: Hama-Koussou, Koum et Barbouri-Figuil. Revue de Paleobiologie, 11(2):357-372.

Jacobs, L.L., Winkler, D.A., Downs, W.R., and Gomani, E.M. 1993. New material of an Early Cretaceous titanosaurid sauropod dinosaur from Malawi. Palaeontology, 36(3):523-534.

Jacobs, L.L., Winkler, D.A., Murray, P.A., and Maurice, J.M. 1994. A nodosaurid rocodylo from the Texas shore of the Western Interior Seaway. In Horner, J.R. and Carpenter, K. (eds.), Dinosaur Eggs and Babies. Cambridge University Press, pp. 337-346.

Jacobs, L.L., and Downs, W.R. 1994. The evolution of murine rodents in Asia. In Tomida, Y., Li, C., and Setoguchi, T. (eds.), Rodent and Lagomorph Families of Asian Origins and Diversification, National Science Museum, Tokyo, Monograph Series, pp. 149-156.

Jacobs, L.L., Winkler, D.A., and Gomani, E.M. 1996. Cretaceous dinosaurs of Africa: Examples from Cameroon and Malawi. Memoirs of the Queensland Museum, 39(3):505-610.

Xu, Xiaofeng, Winkler, A.J., and Jacobs, L.L. 1996. Is the rodent *Acomys* a murine? An evaluation using morphometric techniques. In Stewart, K.M., and Seymour, K.L. (eds.), Palaeoecology and palaeoenvironments of late Cenozoic mammals. University of Toronto Press, Toronto, pp. 660-675.

Winkler, D.A., Murry, P.A., and Jacobs, L.L. 1997. A. Primitive *Tenontosaurus* (Ornithopoda, Dinosauria) from the Early Cretaceous of Texas. Journal of Vertebrate Paleontology, 17(3):330-348.

Jacobs, L.L., and D.A. Winkler. 1998. Mammals, archosaurs, and the early to late Cretaceous transition in north-central Texas. In Tomida, Y., Flynn, L.J., and Jacobs, L.L. (eds.) Advances in Vertebrate Paleontology and Geochronology in honor of Everett H. Lindsay. National Science Museum, Tokyo, Monograph 14:253-280.

Gomani, E.G., L.L. Jacobs, and D.A. Winkler. 1999. Comparison of the African titanosaurian, *Malawisaurus*, with a North American Early Cretaceous sauropod. National Science Museum, Tokyo, Monograph 15:223-233.

Flynn, L.J., and Jacobs, L.L. 1999. Late Miocene small mammal faunal dynamics: the crossroads of the Arabian Peninsula. In Whybrow, P.J., and Hill, A. (eds.), Fossil vertebrates of Arabia. Yale University Press, pp. 412-419.

Jacobs, L.L., Murry, P.A., Downs, W.R., and El-Nakhal, H.A. 1999. A dinosaur from the Republic of Yemen. In Whybrow, P.J., and Hill, A. (eds.), Fossil vertebrates of Arabia. Yale University Press, pp. 454-459.

Jacobs, B.F., Kingston, J., and Jacobs, L.L. 1999. Origin of grass-dominated ecosystems. Annals of the Missouri Botanical Garden, 86:590-643.

Polcyn, M.J., Tchernov, E., and Jacobs. L.L. 1999. The Cretaceous biogeography of the eastern Mediterranean with a description of a new basal mosasauroid from 'Ein Yabrud, Israel. National Science Museum, Tokyo, Monograph, 15:259-290.

Winkler, D.A., Gomani, E.M., and Jacobs, L.L. 2000. Comparative taphonomy of an Early Cretaceous sauropod quarry, Malawai, Africa. Paleontological Society of Korea, Special Publication, 4:99-114.

Tchernov, E., Rieppel, O., Zaher, H., Polcyn, M.J., Jacobs, L.L. 2000. A fossil snake with legs. Science, 287:2010-2012.

Kobayashi, Y., Winker, D.A., and Jacobs, L.L. 2002. Origin of the tooth replacement pattern in therian mammals: Evidence from a 110-million-year-old fossil. Proceedings of the Royal Society of London B, 269:369-373.

Polcyn, M.J., Jacobs, L.L., Rogers, J.V. II, and Kobayashi, Y. 2002. Computed Tomography of an *Anolis* lizard in Dominican amber: Systematic, taphonomic, biogeographic, and evolutionary implications. Paleontologica Electronica, 5(1):13 pp, 5.6 MB, http://palaeo-electronica.org/paleo/2002_1/amber/issue1_02.htm.

Polcyn, M.J., Winkler, D.A., Jacobs, L.L., and Newman, K. 2002. Fossil occurrences and structural disturbance in the Triassic Chinle Formation at North Stinking Springs Mountain near St. Johns, Arizona. New Mexico Museum of Natural

History Bulletin, 21:43-49.

Flynn, L.J., Winkler, A.J., Jacobs, L.L., and Downs, W.R. 2003. Tedford's gerbils from Afghanistan. American Museum of Natural History Bulletin, 279:603-624.

Polcyn, M.J., Tchernov, E., and Jacobs, L.L. 2003. *Haasiasaurus* gen. nov., A new generic name for the basal mosasauroid *Haasia*, Polycn, et al., 1999. Journal of Vertebrate Paleontology, 23(2):476.

Polcyn, M.J., Jacobs, L.L., and Haber, A. 2005. A morphological model and CT assessment of the skull of *Pachyrhachis problematicus* (Squamata: Serpentes): A 98 million-year-old snake with legs from the Middle East. Palaeontologica Electronica, 8(1): http://palaeo-electronica.org.

Jacobs, L.L., Winkler, D.A., Newman, K.D., Gomani, E., and Deino, A. 2005. Therapsids from the Permian Chiweta Beds and the age of the Karoo Supergroup in Malawi. Palaeontologica Electronica, 8(1):http://palaeo-electronica.org.

Jacobs, L.L., Ferguson, K. Polcyn, M.J., and Rennison, C. 2005. Cretaceous $\delta^{13}C$ stratigraphy and the age of dolichosaurs and early mosasaurs. Netherlands Journal of Geosciences, 84:257-268.

Jacobs, L.L., Polcyn, M.J., Taylor, L.H., and Ferguson, K. 2005. Sea-surface temperatures and palaeoenvironments of dolichosaurs and early mosasaurs. Netherlands Journal of Geosciences, 84:269-281.

Jacobs, L.L., and Flynn, L.J. 2005. Of mice … again: The Siwalik rodent record, murine distribution, and molecular clocks. In Leiberman, D.E., Smith, R.J., and Kelley, J. (eds.), Interpreting the past: Essays on human, primate, and mammal evolution in honor of David Pilbeam. Brill Academic Publishers, Inc., Boston, Pp. 63-80.

Jacobs, L.L., Mateus, O., Polcyn, M.J., Schulp, A.S., Antunes, M.T., Morais, M.L., and Tavares, T. da S. 2006. The occurrence and geological setting of Cretaceous dinosaurs, mosasaurs, plesiosaurs, and turtles from Angola. Journal of the Paleontological Society of Korea, 22(1):91-110.

Polcyn, M. J., L.L. Jacobs, and Lü J.C. 2006. Unravelling distortion: Techniques for reconstructing a flattened 98 million-year-old snake skull. In Lü, J.C., Kobayashi, Y., Huang, D., and Lee, Y.N. (eds.), Papers from the 2005 Heyuan International Dinosaur Symposium. Geological Publishing House, Beijing, pp. 205-215.

Schulp, A.S., Polcyn, M.J., Mateus, O., Jacobs, L.L., Morais, M.L., and Tavares, T. da S. 2006. New mosasaur material from the Maastrichtian of Angola, with notes on the phylogeny, distribution and paleoecology of the genus *Prognathodon*. Maastricht Museum, Publicaties van het Natuurhistorisch Genootschap in Limburg, 45(1):57-67.

Taylor, L. H., Jacobs, L.L. and Downs, W.R. 2006. A review of the Cretaceous-Paleogene Boundary in the Nanxiong Basin: Where is it? In Lü, J.C., Kobayashi, Y., Huang, D., and Lee, Y.N. (eds.), Papers from the 2005 Heyuan International Dinosaur Symposium. Geological Publishing House, Beijing, pp. 39-59.

Jacobs, L.L., Fiorillo, A., Gangloff, R., and Pasch, A. 2007. Desmostylian remains from Unalaska Island, Aleutian Chain, Alaska. In Beard, C., and Luo, Z.X. (eds.), Mammalian Paleontology on a Global Stage: Papers in Honor of Mary R. Dawson. Bulletin of the Carnegie Museum of Natural History, 39:189-202.

Flynn, L.J., and Jacobs, L.L. 2008. Castoroidea. In Janis, C.M, Gunnell, G.F., and Uhen, M.D. (eds.), Evolution of Tertiary Mammals of North America. Cambridge University Press, pp. 391-405.

Flynn, L.J., and Jacobs, L.L. 2008. Aplodontoidea. In Janis, C.M, Gunnell, G.F., and Uhen, M.D. (eds.), Evolution of Tertiary Mammals of North America. Cambridge University Press, pp. 377-390.

Robbins, J., Ferguson, K., Polcyn, M., and Jacobs, L.L. 2008. Application of stable carbon isotope analysis to mosasaur ecology. Proceedings of the Second Mosasaur Meeting, Hays, Kansas:123-130.

Schulp, A.S., Polcyn, M.J., Mateus, O., Jacobs, L.L., and Morais, M.L. 2008. A new species of *Prognathodon* (Squamata, Mosasauridae) from the Maastrichtian of Angola, and the affinities of the mosasaur genus *Liodon*. Proceedings of the Second Mosasaur Meeting, Hays, Kansas:1-12.

Jacobs, L.L., Fiorillo, A.R., Nishida, Y., and Fitzgerald, E.M.G. 2009. Mid-Cenozoic marine mammals from Alaska. In Papers on Geology, Vertebrate Paleontology, and Biostratigraphy in Honor of Michael O. Woodburne. Museum of Northern Arizona Bulletin, 64:171-184.

Jacobs, L.L., Mateus, O., Polcyn, M.J., Schulp, A.S., Scotese, C.R., Goswami, A., Ferguson, K.M., Robbins, J.A., Vineyard,

D.P., and Neto, A.B. 2009. Cretaceous paleogeography, paleoclimatology, and amniote biogeography of the low and mid-latitude South Atlantic Ocean. Bulletin of the Geological Society of France, 180(4):333-341.

Mateus, O., Jacobs, L.L., Polcyn, M.J., Schulp. A.S., Vineyard, D.P., Antunes, M.T., and Neto, A.B. 2009. The oldest African eucryptodiran turtle from the Cretaceous of Angola. Acta Paleontologica Polonica, 54:581-588.

Adams, T.L., Strganac, C., Polcyn, M.J., and Jacobs, L.L. 2010. High resolution three- dimensional laser-scanning of the type specimen of *Eubrontes* (?) *glenrosensis* Shuler,1935, from the Comanchean (Lower Cretaceous) of Texas: Implications for digital archiving and preservation. Palaeontologica Electronica, http://palaeo-electronica.org/2010_3/226/index.html.

Fiorillo, A.R., McCarthy, P.J., Flaig, P.P., Brandlen, E., Norton, D., Zippi, P., Jacobs, L., and Gangloff, R.A. 2010. Paleontology and paleoenvironmental interpretation of the Kikak- Tegoseak Quarry (Prince Creek Formation: Late Cretaceous), Northern Alaska: A multi-disciplinary study of a high-latitude ceratopsian dinosaur bonebed. In Ryan, M.J, Chinnery-Allgeier, B.J., and Eberth, D.A., (eds.), New Perspectives on Horned Dinosaurs. Indiana University Press, Bloomington, pp. 456-477.

Polcyn, M.J., Jacobs, L.L., Schulp, A.S., and Mateus, O. 2010. The North African mosasaur *Globidens phosphaticus* from the Maastrichtian of Angola. Historical Biology, 22(1-3):175-185.

Lee, Y.-N., and Jacobs, L.L. 2010. The platacanthomyine rodent *Neocometes* from the Miocene of South Korea and its paleobiogeographical implications. Acta Paleoaeontologica Polonica, 55(4):581-586.

Jacobs, L.L., Strganac, C., and Scotese, C.R. 2011. Plate motions, Gondwana dinosaurs, Noah's Arks, Ghost Ships, and Beached Viking Funeral Ships. Anais da Academia Brasileira de Ciências, 83(1):3-22.

Mateus, O., Jacobs, L.L., Schulp. A.S., Polcyn, M.J., Tavares, T.S., Neto, A.B., Morais, M.L., and Antunes, M.T. 2011. *Angolatitan adamastor*, a new sauropod dinosaur and the first record from Angola. Anais da Academia Brasileira de Ciências, 83(1):221-233.

Lindgren, J., Uvdal, P., Engdahl. A., Lee, A.H., Alwmark, C., Bergquist, K.-E., Nilsson, E., Ekström, Rasmussen, M., Douglas, D.A., Polcyn, M.J., and Jacobs, L.L. 2011. Microspectroscopic evidence of Cretaceous bone proteins. PloS One, 6(4):e19445. Doi:10.1371/journal.pone.0019445.

Adams, T. L., Polcyn, M. J., Mateus, O., Winkler, D. A. and Jacobs, L. L. 2011. First occurrence of the long-snouted crocodyliform *Terminonaris* (Pholidosauridae) from the Woodbine Formation (Cenomanian) of Texas. Journal of Vertebrate Paleontology, 31(3):712-716.

Myers, T.S., Tabor, N.J., and Jacobs, L.L. 2011. Late Jurassic paleoclimate of central Africa. Palaeogeography, Palaeoclimatology, Palaeoecology, 311:111-125.

Winkler, D.A., Jacobs, L.L., Kobayashi, Y., and Polcyn, M.J. 2011. CT Reconstructions and relationships of the Early Cretaceous tribosphenidan mammal, *Slaughteria eruptens* (Trinity Group, Texas, USA). Palaeontologica Electronica, 14(3):http://palaeo-electronica.org.

Parham, J.F., Donoghue, P.C., Bell, C.J., Calway, T.D., Head, J.J., Holroyd, P.A., Inoue, J.G., Irmis, R.B., Joyce, W.G., Ksepka, D.T., Patané, J.S.L., Smith, N.D., Tarver, J.E., van Tuinen, M., Yank, Z., Angielczyk, K.D., Greenwood, J.M., Hipsley, C.A., Jacobs, L., Makovicky, P.J., Müller, J., Smith, K.T., Theodor, J.M., Warnock, R.C.M., and Benton, M.J. 2012. Best practices for justifying fossil calibrations. Systematic Biology, 61:1-14.

Jacobs, L.L., Vogel, P., and Lewis, J. 2012. Jacob Boll, Robert T. Hill and the early history of vertebrate paleontology in Texas. Historical Biology, 24(4):341-348.

Myers, T.S., Tabor, N.J., Jacobs, L.L., and Mateus, O. 2012. Estimating soil *p*CO2 using paleosol carbonates: Implications for the relationship between primary productivity and faunal richness in ancient terrestrial ecosystems. Paleobiology, 38(4):585-604.

Myers, T.S., Tabor, N.J., Jacobs, L.L., and Mateus, O. 2012. Palaeoclimate of the Late Jurassic of Portugal: Comparison with the Western United States. Sedimentology, 59:1695-1717.

Mateus, O., Polcyn, M.J., Jacobs, L.L., Araújo, R., Schulp, A.S., Marinheiro, J., Pereira, B., and Vineyard, D. 2012.

Cretaceous amniotes from Angola: Dinosaurs, pterosaurs, mosasaurs, plesiosaurs, and turtles. V Jornadas Internacionales sobre Paleontología de Dinosaurios y su Entorno, 75-105, Salas de los Infantes, Burgos.

Kimura, Y., Jacobs, L.L., Cerling, T.E., Uno, K.T., Ferguson, K.M., Flynn, L.J., and Patnaik, R. 2013. Fossil mice and rats show isotopic evidence of niche partitioning and change in dental ecomorphorphogy related to dietary shift in Late Miocene of Pakistan. PloS One, 8(8):e69308. Doi:10.1371/journal.pone.0069308.

Kimura, Y., Jacobs, L.L., and Flynn, L.J. 2013. Lineage-specific responses of tooth shape in murine rodents (Murinae, Rodentia) to Late Miocene dietary change in the Siwaliks of Pakistan. PloS One, 8(10):e76070. Doi:10.1371/journal.pone.0076070.

Schulp, A.S., Polcyn, M.J., Mateus, O., and Jacobs, L.L. 2013. Two rare mosasaurs from the Maastrichtian of Angola and the Netherlands. Netherlands Journal of Geosciences, 92(1):3-10.

Winkler, D.A., Polcyn, M.J., and Jacobs, L.L. 2013. New sauropod dinosaur material from Jones Ranch: a large Comanchean nonmammalian tetrapod from Texas. Earth and Environmental Science Transactions of the Royal Society of Edinburgh, 103:1-11.

Polcyn, M.J., Jacobs, L.L., Schulp, A.S., Mateus, O. 2014. Physical drivers of mosasaur evolution. Palaeogeography, Palaeoclimatology, Palaeoecology, 400:17-27.

Strganac, C., Jacobs, L.L., Ferguson, K.M., Polcyn, M.J., Mateus, O., Schulp, A.S., Morais, M.L., Tavares, T. da S., Gonçalves, A.O. 2014. Carbon isotope stratigraphy, magnetostratigraphy, and $^{40}Ar/^{39}Ar$ age of the Cretaceous South Atlantic coast, Namibe Basin, Angola. Journal of African Earth Sciences, http://dx.doi.org/10.1016/j.jafrearsci.2014.03.003

Strganac, C., Jacobs, L.L., Polcyn, M.J., Ferguson, K.M., Mateus, O., Gonçalves, A.O., Morais, M-L., and Tavares, T. da S. 2014.Geological setting and paleoecology of the Upper Cretaceous Bench 19 marine vertebrate bonebed at Bentiaba, Angola. Netherlands Journal of Geosciences – Geologie en Mijnbouw, doi:10.1017/njg.2014.32

Araújo, R., Polcyn, M.J., Schulp, A.S., Mateus, O., Jacobs, L.L., Gonçalves, A.O., and Morais, M.-L. 2015. A new elasmosaurid from the early Maastrichtian of Angola and the implications of girdle morphology on swimming style in plesiosaurs. Netherlands Journal of Geosciences – Geologie en Mijnbouw, DOI:10.1017/njg.2014.44

Araújo, R., Polcyn, M.J., Lindgren, J., Jacobs, L.L., Schulp, A.S., Mateus, O., Gonçalves, A.O., and Morais, M.-L. 2015. New aristonectine elasmosaurid plesiosaur specimens from the Lower Maastrichtian of Angola and comments on paedomorphism in plesiosaurs. Netherlands Journal of Geosciences – Geologie en Mijnbouw, 94(1):93-108, DOI:10.1017/njg.2014.43.

Wichura, H., Jacobs, L.L., Lin, A., Polcyn, M.J., Manthi, F.K., Winkler, D.A., Strecker, M.R., and Clemens, M. 2015. A 17 million year old whale constrains onset of uplift and climate change in East Africa. Proceedings of the National Academy of Sciences, 112(13):3910-3915. www.pnas.org/cgi/doi/10.1073/pnas.1421502112.

Chiba, K., Fiorillo, A.R., Jacobs, L.L., Kimura, Y., Kohno, N., Kobayashi, Y., Nishida, Y., Polcyn, M.J., and Tanaka, K. 2015 (online; 2016 print). A new desmostylian mammal from Unalaska (USA), and the robust Sanjussen jaw from Hokkaido (Japan), with comments on feeding in derived desmostylids. Historical Biology, 28(1-2):289-303. http://dx.doi.org/10.1080/08912963.2015.1046718.

Colleary, C., Dolocan, A., Gardner, J., Singh, S., Wuttke, M., Rbenstein, R., Habersetzer, J., Schaal, S., Feseha, M., Clemens, M., Jacobs, B.F., Currano, E.D., Jacobs, L.L., Sylvestersen, R.L., Gabbott, S.E., and Vinther, J. 2015. Chemical, experimental, and morphological evidence for diagenetically altered melanin in exceptionally preserved fossils. Proceedings of the National Academy of Sciences, 112(41):12592-12597. www.pnas.org/cgi/doi/10.1073/pnas.1509831112.

Jacobs, L. L., Flynn, L. J., Kimura, Y., Kobayashi, Y., Wang, X., Qiu, Z., Jin, C., Zhang, Y., Taylor, L.H., Kohno, N., and Winkler, A.J. 2015 (online; 2016 print). Contributions to vertebrate palaeontology in honour of Yukimitsu Tomida. Historical Biology, DOI:10.1080/08912963.2015.1049839.

Kimura, Y., Hawkins, M.T.R., McDonough, M.M., Jacobs, L.L., and Flynn, L.J. 2015. Corrected placement of *Mus-Rattus*

fossil calibration forces precision in the molecular tree of rodents. Scientific Reports, 5(1):1-9. DOI:10.1038/srep14444.

Kimura, Y., Flynn, L.J., and Jacobs, L.L. 2015 (online; 2016 print). A paleontological case study for species delimitation in diverging fossil lineages. Historical Biology. DOI: 10.1080/08912963.2015.1022175.

Kruger, A., Rubidge, B.S., Abdala, F., Chindebvu, E.G., and Jacobs, L.L. 2015. *Lende chiweta*, a new therapsid from Malawi, and its influence on burnetiamorph phylogeny and biogeography. Journal of Vertebrate Paleontology, 35(6), p.e1008698. http://dx.doi.org/10.1080/02724634.2015.1008698.

Strganac, C., Jacobs, L.L., Polcyn, M.J., Ferguson, K.M., Mateus, O., Gonçalves, A.O., Morais, M-L., and Tavares, T. da S. 2015. Stable oxygen isotope chemostratigraphy and paleotemperature regime of mosasaurs at Bentiaba, Angola. Netherlands Journal of Geosciences – Geologie en Mijnbouw, DOI:10.1017/njg.2015.1

Carabajal, A.P., Lee, Y.-N., Jacobs, L.L. 2016. Endocranial morphology of the primitive nodosaurid dinosaur *Pawpawsaurus campbelli* from the Early Cretaceous of North America. PloS One, 11(3):e0150845. Doi:10.1371/journal.pone.0150845.

Myers, T.S., Tabor, N.J., Jacobs, L.L., and Brussert, R. 2016. Effects of different organic-matter sources on estimates of atmospheric and soil *p*CO2 using pedogenic carbonate. Journal of Sedimentary Research, 86:800-812. DOI: http://dx.doi.org/10.2110/jsr.2016.52.

Jacobs, L.L., Polcyn, M.J., Mateus, O., Schulp, A.S., Gonçalves, A.O., and Morais, M.-L. 2016. Post-Gondwana Africa and the vertebrate history of the Angolan Atlantic coast. Memoires of Museum Victoria, 74:343-362; http://museumvictoria.com.au?about/books- and-journals/journals/memoirs-of-museum-victoria/

Mateus, O., Marzola, M. Schulp, A.S., Jacobs, L.L., Polcyn, M.J., Pervov, V., Goncalves, A.O., Morais, M.L. 2017. Angolan ichnosite in a diamond mine shows the presence of a large terrestrial mammaliamorph, a crocodylomorph, and sauropod dinosaurs in the Early Cretaceous of Africa. Palaeogeography, Palaeoclimatology, Palaeoecology, 471: 220-232.

Myers, T.S., Polcyn, M.J., Mateus, O., Vineyard, D.P., Goncalves, A.O., and Jacobs, L.L. 2017. A new durophagous stem cheloniid turtle from the Lower Paleocene of Cabinda, Angola. Papers in Palaeontology, 2017:1-16.

Kimura, Y., Flynn, L.J., and Jacobs, L.L. 2017. Early late Miocene murine rodents from the upper part of the Nagri Formation, Siwalik Group, Pakistan, with a new fossil calibration point for the tribe Apodemurini (*Apodemus*/*Tokudaia*). Fossil Imprint, 73:197-212.

Graf, J., Tabor, N.J., Ferguson, K., Winkler, D.A., Lee, Y-N., May, S., and Jacobs, L.L. 2018. Diagenesis of dinosaur eggshell from the Gobi Desert, Mongolia. Palaeogeography, Palaeoclimatology, Palaeoecology, 494:65-74.

Lee, H.-J., Lee, Y-N., Adams, T.L., Currie, P.J., Kobayashi, Y., Jacobs, L.L., and Koppelhus, E.B. 2018. Theropod trackways associated with a *Gallimimus* foot skeleton from the Nemegt Formation, Mongolia. Palaeogeography, Palaeoclimatology, Palaeoecology, 494:160-167.

Flynn, L.J., Jacobs, L.L., Kimura, Y., and Lindsay, E.H. 2019. Rodent Suborders. Fossil Imprint, 75(3-4):292-298.

Andrzejewski, K.A., Winkler, D.A., and Jacobs, L.L. 2019. A new basal ornithopod (Dinosauria: Ornithischia) from the Early Cretaceous of Texas. PloS One, 14(8):e0207935.

Andrzejewski, K.A., Winkler, D.A., and Jacobs, L.L. 2019. Correction: A new basal ornithopod (Dinosauria: Ornithischia) from the Early Cretaceous of Texas. PloS One, 14(8):e0217232.

Andrzejewski, K.A., Polcyn, M.J., Winkler, D.A., Chindebvu, E.G., and Jacobs, L.L. 2019. The braincase of *Malawisaurus dixeyi* (Sauropoda: Titanosauria): A 3D reconstruction of the brain endocast and inner ear. PloS One, 14(8): e0211423.

Mateus, O., Callapez, P.M., Polcyn, M.J., Schulp, A.S., Gonçalves, and Jacobs, L.L. 2019. The Fossil Record of Biodiversity in Angola Through Time: A Paleontological Perspective. Biodiversity of Angola, 53:76.

Mateus, O., Callapez, P.M., Polcyn, M.J., Schulp, A.S., Gonçalves, and Jacobs, L.L. 2019. O registo rocod da biodiversidade em Angola ao longo do tempo: uma perspectiva paleontológica. Biodiversidade de Angola: Ciência e Conservação-

Uma Sintese Moderna.

Flynn, L.J., Kimura, Y., and Jacobs, L.L. 2020. The murine cradle. In Prasad, G.V.R., and Patnail, R. (eds), Biological Consequences of Plate Tectonics: New Perspectives on Post-Gondwanaland Break-up – A tribute to Ashok Sahni, Springer Nature, Switzerland, pp. 347-362.

Taylor, L.H., Flynn, L.J., Jacobs, L.L., and Baskin, J.A. 2020. James Gilbert Honey. Paludicola, 12(4):171-174.

Flynn, L.J., Jacobs, L.L Taylor, L.H., and Tomida, Y. 2020. Siwalik fossil Soricidae: A calibration point for the molecular phylogeny of *Suncus*. Paludicola, 12(4):247-258.

Kimura, Y., Flynn, L.J., and Jacobs, L.L. 2021. Tempo and mode: Evidence on a protracted split from a dense fossil record. Frontiers in Ecology and Evolution, 9:642814. Doi:10.3389/fevo.2021.642814.

Marx, M.P., Mateus, O., Polcyn, M.J., Schulp, A.S., Gonçalves, A. O., Jacobs, L.L. 2021. The cranial anatomy and relationships of *Cardiocorax mukulu* (Plesiosauria: Elasmosauridae) from Bentiaba, Angola. PLoS ONE 16(8): e0255773. https://doi.org/10.1371/journal.pone.0255773

Park, J.-Y., Lee, Y.-N., Kobatashi, Y., Jacobs, L.L., Barsbold, R., Lee, H.-J., Kim, N., Song, K.Y., and Polcyn, M.J. 2021. A new ankylosaurid from the Upper Cretaceous Nemegt Formation of Mongolia and implications for paleoecology of armoured dinosaurs. Scientific Reports, 11:2298. https://doi.org/10.1038/s41598-021-02273-4.

Augusta, B.G., Zaher, H., Polcyn, M.J., Fiorillo, A.R., Jacobs, L.L. 2022. A review of non-mosasaurid (dolichosaur and aigialosaur) mosasaurians and their relationships to snakes. In Gower, D.J., and Zaher, H. (eds.), The Origin and Early Evolutionary History of Snakes. Cambridge University of Press, Cambridge, UK., pp. 157-179.

Fernandes, A.E., Mateus, O., Andres, B., Polcyn, M.J., Schulp, A.S., Gonçalves, A.O., and Jacobs, L.L. 2022. Pterosaurs from the Late Cretaceous of Angola. Diversity, 14, 741. https:/doi.org/10.3390/d14090741.

Araújo, R., Macungo, Z., Fernandez, V., Chindebvu, E.G., and Jacobs, L.L. 2022. *Kembawacela yajuwayeyi* n. sp., a new cistecephalid species (Dicynodontia: Emydopoidea) from the Upper Permian of Malawi. Journal of African Earth Sciences, 196, 104726. https://doi.org/10.1016/j.jafrearsci.2022.104726.

Kim, S.-H., Lee, Y.-N., Park, J.-Y., Lee, S., Winkler, D.A., Jacobs, L.L., and Barsbold, R. 2022. A new species of Osteoglossomorpha (Actinopterygii: Teleostei) from the Upper Cretaceous Nemegt Formation of Mongolia: Paleobiological and paleogeographic implications. Journal of Cretaceous Research, 135, 105214. https://doi.org/10.1016/j.cretres.2022.105214.

Jacobs, L.L. and Flynn, L.J. 2022. Forward. In Bibi, F, Kraatz, B., Beech, M, and Hill, A. (eds.), Sands of Time: Ancient Life in the Late Miocene of Abu Dhabi, United Arab Emirates. pp. vii-viii, Springer, Cham, Switzerland.

May, S.R., Bader, K.S., Boucher, L.D., Jacobs, L.L., Lively, J.R., Myers, T.S., and Polcyn, M.J. 2023. A record of Late Jurassic vertebrates from Texas. Rocky Mountain Geology, 58(1):19-37.

Jacobs, L.L., Schröder, S., Sousa, N. da, Dixon, R. Fiordalisi, E., Marechal, A., Mateus, O., Nsungani, P.C., Polcyn, M.J., Pereira, G. do C. R., Rochelle-Bates, N., Schulp, A.S., Scotese, C.r., Sharp, I., Silvano, C.G., Swart, R., and Vineyard, D.P. Submitted. The Atlantic jigsaw puzzle and the geoheritage of Angola. Geological Society of London, Special Publication 2022-301, Geology's Significant Sites and their Contributions to Geohistory.

Chindebvu, E.G., Jacobs, L.L., Juwayeyi, Y.M., Perez, M.L., Polcyn, M.J., Simfukwe, H.H., Vineyard, D.P., and Winkler, D.A. Submitted. The Mwesia Beds of Northern Malawi in relation to the Tanganyika Problem. Geological Society of London, Special Publication 2022-301, Geology's Significant Sites and their Contributions to Geohistory.

Polcyn, M.J., McPherson, A.B., White, C, Irwin, K., Martin, J.E., Hargrave, J.E., Tykoski, R.S., Kinsland, G.L., and Jacobs, L.L. Submitted. Louisiana's Cretaceous Sea Monsters, Its Paleocene Mammal Fossil, and the Ghost Maker Megaripples. Vertebrate Paleontology of Louisiana: Papers in Honor of Judith A. Schiebout. Louisiana State Museum Museum Publication.

Comments, Replies, Letters (exclusive of newspapers), Field Guides, Magazine Articles

Jacobs, L.L. 1978. Pakistan and fossils: an introduction. Plateau, 51(1):4-17.

Pilbeam, D., and Jacobs, L.L. 1978. Changing views of human origins. Plateau, 51(1):18-31.

Jacobs, L.L. 1981. The setting: geology and fossils of the Verde Valley, Arizona. Plateau, 53(1):2-5.

Jacobs, L.L., and Flynn, L.J. 1981. Development of the modern rodent fauna of the Potwar Plateau, northern Pakistan. Neogene/Quaternary Boundary Field Conference, India, 1979, Proceedings, 1981, pp. 79-81.

Lindsay, E.H., Butler, R.F., Johnson, N.M., and Jacobs, L.L. 1979. Reply to comment by Alvarez and Vann on "Biostratigraphy and magnetostratigraphy of Paleocene terrestrial deposits, San Juan Basin, New Mexico." Geology, 7(2):68-69.

Lindsay, E.H., Butler, R.F., Johnson, N.M. and Jacobs, L.L. 1979. Reply to comment by Fasset on "Biostratigraphy and magnetostratigraphy of Paleocene terrestrial deposits, San Juan Basin, New Mexico." Geology, 7(2):70-71.

Luckett, W.P., and Jacobs, L.L. 1980. Proposed fossil tree shrew genus *Palaeotupaia*. Nature, 288:104.

Jacobs, L.L. 1981. (Louis Leakey and the lions.) Swara (East African Wildlife Society), 4(4):22.

Jacobs, L.L. 1984. Rodentia: Extraordinary diversification of a morphologically distinctive and stereotyped order. In Broadhead, T.W. (ed.), Mammals: Notes for a short course. Univ. Tennessee, Studies in Geology (Geological Society of America Short Course), 8:155-166.

Jacobs, L.L. 1985. Small vertebrates from the Chinle Formation (Triassic) near St. Johns, Arizona. National Geographic Society, Research Reports, 20:417-419.

Winkler, D.A., Murry, P.A., and Jacobs, L.L. 1989. Vertebrate paleontology of the Trinity Group, Lower Cretaceous of Central Texas. ISEM, 22 pp.

Jacobs, L.L. 1990. Malawi or Malawi? National Geographic Research, 6(3):260.

Jacobs, L.L. The Evolutionary Clock. 1991. McGraw-Hill Yearbook of Science and Technology, pp. 320-322.

Jacobs, L.L., Winkler, D.A., and Downs, W.R. 1992. Malawi's paleontological heritage. Occasional Papers of Malawi. Department of Antiquities, 1:5-23.

Jacobs, L.L. 1993. An African Jurassic Park. Oil Progress, 43, Fall: 9-15.

Jacobs, L.L. 1993. The first dinosaur from Arabia. In Reed, D.W. (ed.), Spirit of Enterprise: The 1993 Rolex Awards, pp. 229-231.

Winkler, D.A., Jacobs, L.L., Lee, Y.-N., and Murry, P.A. 1995. Sea level fluctuation and terrestrial faunal change in North-Central Texas. In Ailing Sun and Yuanging Wang (eds.), Sixth Symposium on Mesozoic Terrestrial Ecosystems and Biota, Short Papers, pp. 175-177.

Jacobs, L.L. 1997. Dinosaur trackmakers in the Cretaceous of central Texas. In Hastings, R.J., Jacobs, L.L., and Clarke, R.T. (eds.), Dinosaur tracks in the Cretaceous Glen Rose Formation of central Texas. Field Trip Guide 3, 1997 Annual Meeting American Association of Petroleum Geologists.

Jacobs, L.L. 1997. Dinosaurs of Africa. In P.J. Currie and K. Padian (eds.), Encyclopedia of Dinosaurs. Academic Press, San Diego, pp. 2-4.

Jacobs, L.L. 1997. A global view of Early Cretaceous dinosaurs. Paleontological Society of Korea, Special Publication 2:67-75.

Jacobs, L.L. 1997. The making of Dinosaur Valley State Park, Glen Rose, Texas. The International Dinosaur Symposium for the Uhangri Dinosaur Center and Theme Park in Korea, 226-232.

Jacobs, L.L., L.J. Flynn, Y. Tomida, and L.H. Taylor. 1998. Everett Harold Lindsay: An appreciation of the Doc. In Tomida, Y., Flynn, L.J., and Jacobs, L.L. (eds.), Advances in Vertebrate Paleontology and Chronology in honor of Everett H. Lindsay. National Science Museum, Tokyo, Monograph 14:1-11.

Jacobs, L.L., Hastings, R.J., and Clarke, R.T. 2004. Dinosaur tracks in the Cretaceous Glen Rose Formation of Central Texas. Dallas Geological Society Field Trip #3 Guidebook, American Association of Petroleum Geologists 2004 Annual Convention, Dallas, Texas, 61 pp.

Badgley, C., Flynn, L.J., Jacobs, L.L., and Taylor, L.H. 2004. A consideration of the paleontological contributions of Will Downs with a general correlation of Chinese Neogene localities. Vertebrata PalAsiatica, 42:340-344.

Jacobs, L.L. 2005. Preface. In Lü, J.C., Oviraptorid Dinosaurs from Southern China. Geological Publishing House, Beijing. In English and Chinese.

Jacobs, L.L., Polcyn, M.J., Poff, K., and Poff, N. 2005. Ocean Dallas. National Earth Science Teachers Association Field Trip Guide.

Jacobs, L.L. 2006. In memoriam … Victor Oppenheim. GeoSpectrum, American Geological Institute, 5(2):21.

Lindsay, E., L.L. Jacobs, and N. Tessman. 2006. Vertebrate fossils from Yepómera, Chihuahua, Mexico – The University of Arizona connection. In Carranza-Casteñada, Óscar, and Lindsay, E.H. (eds.), Advances in late Tertiary vertebrate paleontology in Mexico and the Great American Biotic Interchange. Universidad Nacional Autónoma de México, Instituto de Geologia and Centro de Geosciencias, Publicación Especial, 4:19-32.

Jacobs, L.L., Polcyn, M.J., Winkle, D.A., Myers, T.S., Kennedy, J.G., and Wagner, J.B. 2013. Late Cretaceous strata and vertebrate fossils of North Texas, in Hunt, B.B., and Catlos, E.J., eds., Late Cretaceous to Quaternary Strata and Fossils of Texas: Field Excursions Celebrating 125 Years of GSA and Texas Geology, GSA South-Central Section Meeting, Austin, Texas, April 2013: Geological Society of America Field Guide 30:1-13, doi:10.1130/2013.0030(01).

Jacobs, L. L. 2013. Multidisciplinary and interdisciplinary uses and approaches to vertebrate biostratigraphy. Ciências da Terra (UNL), 18:81-84.

Jacobs, L.L. 2013. African dinosaurs and museums. Hwaseong International Dinosaurs Expedition Symposium, Korea-Mongolia International Dinosaur Expedition, December 4-6, 2013, Hwaseong City, Gyeonggi Province, Korea, 34-37.

Busbey, A., Fiorillo, A.R., Jacobs, B.F., Jacobs, L.L.,Nestell, M., Peppe, D., Polcyn, M.J., Tykoski, R.S., Walter, C., and Winkler, D.A. 2016. The Dallas Paleontological Society and the North Texas paleontological nexus. Dallas Paleontological Society Guide to Fossil Collecting. Maxey, G., and Farish, R. (editors). Pp. 3-1 – 3-21.

Abstracts

Jacobs, L.L., 1973. Small mammals of the Quiburis Formation, southeastern Arizona. Abs., 17th Annual Mtg., Arizona Acad. Sci. Journal of the Arizona Academy of Science, Proceedings Supplement, pp. 45-46.

Jacobs, L.L., 1974. Additional rodent material from the Redington fauna, Pliocene of Arizona. Abs., 18th Annual Mtg., Arizona Acad. Sci. Journal of the Arizona Academy of Science, Proceedings Supplement, p. 35.

Butler, R.F., Lindsay, E.H., and Jacobs, L.L., 1976. Paleomagnetic stratigraphy through the Cretaceous-Tertiary boundary, San Juan Basin, New Mexico. EOS, American Geophysical Unnion Transactions, 57(12):902.

Butler, R.F., Lindsay, E.H., Jacobs, L.L., and Johnson, N.M., 1976. Preliminary report on magnetic stratigraphy of the Cretaceous-Paleocene continental deposits in the San Juan Basin, New Mexico. EOS, American Geophysical Union, Transactions, 57(4):238.

Butler, R.F., Lindsay, E.H., Jacobs, L.L., and Johnson, N.M., 1976. Magnetostratigraphy through the Cretaceous-Tertiary boundary, San Juan Basin, New Mexico. Società Geologica Italiana, Memorie, 15:69-72.

Jacobs, L.L. 1978. Homology of tooth cusps in murid rodents based on Miocene fossils from Pakistan. Second International Theriological Congress, Brno, Czechoslovakia, Abs., p. 68.

Jacobs, L.L., and Lindsay, E.H., 1978. Small mammal fossils from Pliocene deposits in Chihuahua. Geological Society of America, 74th Annual Meeting, Cordilleran Section, Abstracts, p. 110.

Jacobs, L.L., 1982. The beginning of the Age of Murids in Africa. Third International Theriological Congress, Helsinki, Finland, Abs.:114.

Jacobs, L.L., Fejfar, O., Flynn, L.J., Kretzoi, M., and Downs, W.R., 1985. Small mammal composition of Rudabanya, Hungary: Comparison to Siwalik and African faunas, Abs., VIIIth Congress of the Regional Committee on Mediterranean Neogene Stratigraphy, p. 274.

Jacobs, L.L., Flanagan, K.M., Dejax, J., and Brunet, M.,1986. Dinosaur footprints from the Lower Cretaceous of Cameroun,

West Africa. First International Symposium on Dinosaur Track and Traces, Abs., 16.

Winkler, D.A., Murry, P.A., Downs, W.R., and Jacobs, L.L., 1987. Paleoecology of the Proctor Lake dinosaur locality. Geological Society of America, Abstracts with Programs, 19(3):180.

Winkler, D.A., Jacobs, L.L., Congleton, J.D. and Downs, W.R., 1987. Taphonomy and paleontology of the Navajo Sandstone. Journal of Vertebrate Paleontology, Abstracts, 7(3):29A.

Jacobs, L.L., Flynn, L.J., and Downs, W.R., 1988. Patterns of change in the Siwalik muroid record. Journal of Vertebrate Paleontology, Supplement to number 3, 18A.

Winkler, D.A., Jacobs, L.L., Downs, W.R., and Congleton, J.D., 1988. The Dinosaur Beds of Northern Malawi, African Journal of Vertebrate Paleontology, Supplement to number 3, 29A.

Murry, P.A., Winkler, D.A., and Jacobs, L.L., 1989. Small tetrapods from the Comanchean (Early Cretaceous) of Central Texas. Journal of Vertebrate Paleontology 9, Suppl. 3, 33A.

Winkler, D.A., Murry, P.A., and Jacobs, L.L., 1989. Ornithopod dinosaurs from the Lower Cretaceous Trinity Group, Central Texas. Journal of Vertebrate Paleontology, Suppl., 3, 45A.

Jacobs, L.L., Winkler, D.A., and Murry, P.A., 1989. On the Age of Trinity Mammals. Journal of Vertebrate Paleontology, Suppl. 3, 26A.

Jacobs, L.L., Murry, P.A., and Winkler, D.A., 1989. The Paluxian Land Mammal Age. GSA, Abstracts.

Jacobs, L.L., 1990. The nonmarine Cretaceous of Malawi. International Geological Congress Program 245, Nonmarine Cretaceous Correlations, African working Group. West Berlin.

Jacobs, L.L., Winkler, D.A., Downs, W.R., and Gomani, E., 1991. The dinosaurs of Africa: sauropods from the Early Cretaceous of Malawi. Journal of Vertebrate Paleontology II (Suppl. To 3), 38A.

Jacobs, L.L., and Janis, C. 1992. Patterns of Evolution in North American Neogene Mammals. NAPC V, Abstracts, 146.

Flynn, L.J., Barry, J.C., Morgan, M.E., Pilbeam, D., Jacobs, L.L., and Lindsay, E.H. 1992. Neogene Siwalik mammalian lineages: species longevities, rates of change, and modes of speciation. NAPC V, Abstracts, 101.

Barry, J.C., Morgan, M.E., Flynn, L.J., Jacobs, L.L., and Lindsay, E.H. 1992. Patterns of faunal turnover and diversity in the Siwalik Neogene record in relation to regional and global events. NAPC V, Abstracts, 18.

Jacobs, L.L., 1992. Biostratigraphy of Lower Cretaceous Terrestrial deposits, Texas. Petroleum Research Fund, 36th Annual Report on Research, 480.

Jacobs, L.L., and Downs, W.R., 1992. The evolution of murid rodents in Asia. 29th International Geological Congress, Workshop, Rodent Families of Asian Origins and Dioversification, p. 30.

Winkler, D.A., Murry, P.A., and Jacobs, L.L., 1992. Differentiating adult and juvenile ornithischian dinosaurs in the Early Cretaceous. Journal of Vertebrate Paleontology, 52nd Annual Meeting, Abstracts, 60A.

Winkler, A. J., and Jacobs, L.L., 1993. The fossil mammals of Africa. Sixth International Theriological Congress, Abstracts, Sydney, Australia.

Rennison, C.J., Jacobs, L.L., Ferguson, K.M., and Gregory, R.T., 1995. Terrestrial faunal change and carbon isotope variation in the Texas mid-Cretaceous. Geological Society of America, Annual Meeting, New Orleans, Abstracts, p. A-387.

Jacobs, L.L., 1996. The pattern of terrestrial faunal change in the mid-Cretaceous of North America. Sixth North American Paleontological Convention, Smithsonian Institution, Abstracts.

Tchernov, E., Polcyn, M.J., and Jacobs, L.L., 1996. Snakes with legs: The Cenomanian fauna of Ein Yabrud, Israel. Journal of Vertebrate Paleontology, Volume 16, Supplement to Number 3, 68A.

Winkler, D.A., Jacobs, L.L., and Murry, P.A. 1997. Jones Ranch: An early Cretaceous sauropod bone-bed in Texas. Journal of Vertebrate Paleontology, 17 (Supplement to 3): 85A.

Winkler, D.A., Murry, P.A., and Jacobs, L.L. 1998. The new ornithopod dinosaur from Proctor Lake, Texas, and the deconstruction of the family Hypsilophodontidae. Journal of Vertebrate Paleontology, 18 (Supplement to 3): 87A.

Polcyn, M.J., Tchernov, L., and Jacobs, L.L. 1999. Application of computed tomography in the morphological interpretation of *Pachyrhachis problematicus*, a snake with legs from the Cretaceous of Israel. 31st International Geological congress,

Rio de Janeiro, Brazil.

Polcyn, M.J., Tchernov, L., and Jacobs, L.L. 999. The northern edge of Gondwana in Africa and Europe. 31st International Geological congress, Rio de Janeiro, Brazil.

Polcyn, M.J., Jacobs, L.L., Rogers, J.V. II, and Kobayashi, Y. 2001. A third *Anolis* lizard in Dominican amber: Application of computer tomography. Journal of Vertebrate Paleontology, 21(3) Abstracts:89A-90A.

Tchernov, E., Polcyn, M.J., and Jacobs, L.L. 2001. Application of computed tomography to *Pachyrhachis problematicus*, a snake with legs from the Cretaceous of Israel. Journal of Vertebrate Paleontology 21(3) Abstracts:107A.

Winkler, D.A., Kobayashi, Y., and Jacobs, L.L. 2001. Ultra-high-resolution CT images reveal replacement dentition in *Slaughteria eruptens*, an Early Cretaceous mammal from Texas. Journal of Vertebrate Paleontology 21(3) Abstracts: 115A.

Winkler, D.A., and Jacobs, L.L. 2003. Review of Early Cretaceous (Aptian/Albian) boreasphenidan mammals from Texas. Journal of Vertebrate Paleontology, 23(3):111A.

Jacobs, L.L., D.A. Winkler, E. Gomani, K. Newman. 2004. A new burnetiamorph therapsid from the Permian Chiweta Beds, Malawi. Journal of Vertebrate Paleontology, 24 (3):75A.

Jacobs, L.L., Polcyn, M.J., Ferguson, K., Rennison, C., and Taylor, L.H. 2004. Age, environment, and habitat of dolichosaurs and primitive mosasauroids. 1st International Mosasaur Conference, Abstract, Maastricht, The Netherlands.

Lindsay, E., L.L. Jacobs, and N. Tessman. 2005. Vertebrate fossils from Yepómera, Chihuahua, Mexico – The University of Arizona connection. Guidebook to Yepomera (Hemphillian and Blancan), Chihuahua, Mexico Fieldtrip, Society of Vertebrate Paleontology, 65th Annual Meeting, Mesa, Arizona.

Jacobs, L.L., and M.J. Polcyn. 2005. CT analysis of a 98 million-year-old snake. 2005 Heyuan International Dinosaur Symposium, Abstract.

Jacobs, L.L. 2005. Marine mammals from Unalaska Island, Alaska. All the World is a Stage for Evolution. Carnegie Museum, Pittsburgh.

Jacobs, L.L. 2005. Teaching evolution at the undergraduate level. Journal of Vertebrate Paleontology, 25(3):74A.

Jacobs, L.L., Morais, M.L., Schulp, A.S., Mateus, O., Polcyn, M.J. 2006. Systematic position and geological context of *Angolasaurus* (Mosasauridae) and a new sea turtle from the Cretaceous of Angola. Journal of Vertebrate Paleontology, 26, Supplement to Number 3:81A.

Mateus, O., Morais, M.L., Schulp, A.S., Jacobs, L.L., Polcyn, M.J. 2006. The Cretaceous of Angola. Journal of Vertebrate Paleontology, 26, Supplement to Number 3:96A.

Schulp, A.S., Mateus, O., Polcyn, M.J., Jacobs, L.L. 2006. A new *Prognathodon* (Squamata: Mosasauridae) from the Cretaceous of Angola. Journal of Vertebrate Paleontology, 26, Supplement to Number 3:81A.

Jacobs, L.L. 2007. Large scale tectonic and paleogeographic determinants of biogeography: The Angola example. Ecosystem evolution of Baikalian region and adjacent areas in context of global change: Past, present, future. Siberian Branch, Russian Academy of Sciences, Irkutsk, Baikal, Bol'shie Koty, Russia.

Jacobs, L.L. 2007. Desmostylians in Alaska. Ecosystem evolution of Baikalian region and adjacent areas in context of global change: Past, present, future. Siberian Branch, Russian Academy of Sciences, Irkutsk, Baikal, Bol'shie Koty, Russia.

Fiorillo, A.R., McCarthy, P.J., Brandlen, E., Flaig, P.P., Norton, D., Jacobs, L., Zippi, P., and Gangloff, R.A. 2007. Paleontology, sedimentology, paleopedology, and palynology of the Kikak-Tegoseak Quarry (Prince Creek Formation: Late Cretaceous), Northern Alaska. Royal Terrell Museum, Ceratopsian Symposium, 2007.

Nishida, Y., Polcyn, M.P., Jacobs, L.L., and Fiorillo, A. 2007. A juvenile desmostylid dentary from Unalaska Island, Alaska, and an application of three-dimensional laser scanning. Journal of Vertebrate Paleontology, 27 Supplement to number 3:124A.

Polcyn, M.P., Jacobs, L.L., Schulp, A., and Mateus, O. 2007. *Halisaurus* (Squamata: Mosasauridae) from the Maastrichtian of Angola. Journal of Vertebrate Paleontology, 27 Supplement to number 3:130A.

Robbins, J., Ferguson, K., Polcyn, M., Jacobs, L., and Rick, T. 2007. Application of stable carbon isotope analysis to mosasaur

ecology. Second International Mosasaur Meeting, Hays, Kansas.

Robbins, J., Ferguson, K., Polcyn, M., Jacobs, L., and Rick, T. 2007. Life history patterns of mosasaurs inferred from stable carbon isotopes. Journal of Vertebrate Paleontology, 27 Supplement to number 3:135A.

Jacobs, L.L., Polcyn, M.J., Mateus, O., Schulp, A., and Strganac, C. 2008. Adaptations in the Cretaceous marine amniote fauna of Angola. Fifth Conference on Secondary Adaptation of Tetrapods to Life in Water, June 9-13, 2008, Tokyo, Japan.

Jacobs, L.L., Polcyn, M.J., Nishida, Y., and Fiorillo, A.R. 2008. Fossil marine mammals of the Aleutian Islands and Gulf of Alaska. Fifth Conference on Secondary Adaptation of Tetrapods to Life in Water, June 9-13, 2008, Tokyo, Japan.

Lee, Y.-N., Barsbold, R., Jacobs, L.L., and Currie, P. 2008. A short report of Korea-Mongolia International Dinosaur Project (1st and 2nd year). Journal of Vertebrate Paleontology, 28 Supplement to Number 3:104A.

MacPhee, R., Reguero, M., Strganac, C., Nishida, Y., and Jacobs, L.L. 2008. Out of Antarctica: Paleontological reconnaissance of Livington Island (South Shetlands) and Seymour Island (James Ross Group). Journal of Vertebrate Paleontology, 28 Supplement to Number 3:110A.

Strganac, C., Nishida, Y., Jacobs, L.L., Hooker, J., and MacPhee, R.D.E. 2008. Cretaceous carbon isotope values from the Cerro Negro Formation, Antarctica. Journal of Vertebrate Paleontology, 28 Supplement to Number 3:64A.

Mateus, O., Jacobs, L.L., Polcyn, M.J., Schulp, A.S., Neto, A.B.,and Antunes, M.T. 2008. Dinosaur and turtles from the Turonian of Iembe, Angola. III Congreso Latinoamericano de Paleontología de Vertebrados – Neuquén, Patagonia, Argentina, p. 156.

Jacobs, L.L., Polcyn, M.J., Mateus, O., Schulp, A., Neto, A.B. 2009. The Cretaceous Skeleton Coast of Angola. Abstract, SVP Annual Meeting, Bristol, UK.

Jacobs, L.L., Polcyn, M.J., Mateus, O., Strganac, C., Jacobs, B.F., Schulp, A., Morais, M.L., Neto, A.B. 2009. The Skeleton Coast Desert, southwest Africa, from Cretaceous to Recent Times. Abstract, GSA Annual Meeting, Portland, Oregon.

Polcyn, M.J., Jacobs, L.L., Schulp, A.S., and Mateus, O. 2009. The North African mosasaur *Globidens phosphaticus* from the Maastrichtian of Angola. Symposium on North African Vertebrate Paleontology.

Vineyard, D.P., and Jacobs, L.L. 2009. A new eucryptodiran turtle from the Mid-Cretaceous Glen Rose Formation of Texas. Eugene Gaffney Turtle Symposium, Royal Tyrrell Museum.

Vineyard, D.P., Jacobs, L.L., Polcyn, M.J., Mateus, O., Schulp, A.S., and Strganac, C. 2009. *Euclastes* from the Maastrichtian of Angola and the distribution of the Angolachelonia. Eugene Gaffney Turtle Symposium, Royal Tyrrell Museum.

Adams, T.L., Strganac, C., Polcyn, M.J., and Jacobs, L.L. 2009. High resolution three- dimensional laser-scanning of the type specimen of *Eubrontes* (?) *glenrosensis* Shuler, 1935, from the Comanchean (Lower Cretaceous) of Texas: Implications for digital archiving and preservation. Geological Society of America.

Adams, T., Polcyn, M., Mateus, O., Winkler, D., and Jacobs, L. 2010. New occurrence of the long-snouted crocodyliform, *Terminonaris* cf. *T. robusta*, from the Woodbine Formation (Cenomanian) of Texas. Society of Vertebrate Paleontology 70th Annual Meeting.

Araújo, R., Jacobs, L., Polcyn, M., Mateus, O., and Schulp, A. 2010. Plesiosaurs from the Maastrichtian of Bentiaba, Namibe Province, Angola. Abstract, Society of Vertebrate Paleontology 70th Annual Meeting.

Chiba, K., Jacobs, L.L., Kobayashi, Y., Ando, T., Sawamura, H., Adams, T., T.L. 2010. The North Pacific and Panthalassic distribution of ichthyosaurs.Paleontological Society of Japan, 159th Annual Meeting, A20.

Jacobs, L., Polcyn, M., Araújo, R., Strganac, C., Mateus, O., Schulp, A. 2010. Physical drivers of evolution and the history of the marine tetrapod fauna of Angola. Abstract, Society of Vertebrate Paleontology 70th Annual Meeting.

Jacobs, L.L., Polcyn, M.J., Araújo, R., Strganac, C., Mateus, O., Schulp, A.S., Jacobs, B.F., Morais, M.L. 2010. Tectonic drift, climate, and paleoenvironment of Angola since the Cretaceous. Abstract, American Geophysical Union.

Jacobs, L.L., Nishida, Y., Polcyn, M.J., Fiorillo. A.R., Kobayashi, Y., Ando, T., Sawamura, H., Adams, T., Kimura, Y. 2010. Desmostylian and other marine mammal fossils from AlaskaPaleontological Society of Japan, 159th Annual

Meeting, A10.

Myers, T.S., Tabor, N., and Jacobs, L.L. 2010. Correlated faunal richness and primary productivity in Late Jurassic terrestrial environments. Geological Society of America Abstracts with Programs, 42(5).

Robbins, J., Polcyn, M., Ferguson, K., and Jacobs, L. 2010. Stable carbon isotope values in mosasaur tooth enamel reflect niche differentiation. Abstract, Society of Vertebrate Paleontology 70th Annual Meeting.

Strganac, C., Jacobs, L.L., MacPhee, R.D.E., Fiorillo, A.R., Ferguson, K., Hooker, J.J., Nishida, Y., and Flemming, C. 2010. Latitudinal variation in δ13C derived from terrestrial plants during the Cretaceous. Abstract, American Geophysical Union.

Jacobs, L.L., Polcyn, M.J., Mateus, O., Schulp, A., and Arauja, R. 2011. African upwelling and the Neogene Whales of Angola. Abstracts of the Sixth Triennial Conference on Secondary Adaptations of Tetrapods to Life in Water, San Diego.

Jacobs, L.L. 2011. Jacob Boll, Robert T. Hill, Edward Drinker Cope, and the Early History of Vertebrate Paleontology in Texas. Abstracts of 12th International Symposium on Early and Lower Vertebrates, Ichthyolith.

Araújo, R., Jacobs, L.L., Polcyn, M.J., Mateus, O., and Schulp, A. 2011. Plesiosaur structural extreme from the Maastrichtian of Angola. Abstract, Society of Vertebrate Paleontology 71st Annual Meeting.

Graf, J., Jacobs, L.L., Polcyn, M.J., Mateus, P., and Schulp, A. 2011. New fossil whales from Angola. Abstract, Society of Vertebrate Paleontology 71st Annual Meeting.

Lee, H.-J., Lee, Y.-N., Adams, T., Kobayashi, Jacobs, L.L. 2011. Theropod trackways associated with ornithomimid skeletons from the Nemegt (Maastrichtian) at Bugin Tsav, Mongolia. Abstract, Society of Vertebrate Paleontology 71st Annual Meeting.

Lee, Y.-N., and Jacobs, L.L. 2011. The platacanthomyine rodent *Neocometes* from the Miocene of South Korea and its paleobiogeographical implications. Abstract, Society of Vertebrate Paleontology 71st Annual Meeting.

Jacobs, L.L., Polcyn, M.P., Schulp, A.S., and Vaz Pinto, P. 2012. An experience of the national natural heritage study of Angola. The Turkmen Nature: Undiscovered miracles of the Koytendag. Abstracts of reports of the International Scientific Conference (May 23-29, 2012).

Jacobs, L.L. 2012. Tectonic drift as a driver of Gondwanan vertebrate evolution. Keynote address, Section 23.5 Session 3 – Gondwanan Mesozoic Vertebrates, 34th International Geological Congress, Brisbane, Australia.

Jacobs, L.L., Strganac, C., Rooney, T., Goncalves, A.O., Morais, M.L., Polcyn, M.J., Mateus, O., Schulp. A.S., and Myers, T.S. 2012. Implications of geochemical and paleontological results from Cretaceous rocks of the South Atlantic margin, Angola. XI Congresso de Geochemíca dos Países de Língua Portuguesa, Luanda, Angola.

Strganac, C., Ferguson, K.M., Jacobs, L.L., Polcyn, M.J., Mateus, O. 2012. Age and paleoecology of mosasaurs from the Late Cretaceous South Atlantic margin at Bentiaba, Angola. Society of Vertebrate Paleontology, 72nd Annual Meeting.

Vineyard, D.P., Mateus, O., Jacobs, L.L., Polcyn, M.J., and Schulp, A.S. 2012. A new marine turtle from the Maastrichtian of Angola. Society of Vertebrate Paleontology, 72nd Annual Meeting.

Jacobs, L.L. 2013. Notes on the history of vertebrate paleontology in Texas from the Archives of the DeGolyer Library, Southern Methodist University. South-Central Geological Society of America Section Meeting, 2013 Abstract Program.

Polcyn, M.J., Jacobs, L.L., Schulp, A.S., and Mateus, O. 2013. The mosasaurs of Angola: An update. In Polcyn, M.J., and Jacobs, L.L. (eds.), 4th Triennial International Mosasaur Meeting, Program and Abstracts. Southern Methodist University.

Strganac, C., Jacobs, L.L., Polcyn, M.J., Ferguson, K.M., Mateus, O., and Schup, A.S. 2013. Chronostratigraphy of marine sediments at Bentiaba, Angola, and mosasaur niche partitioning at the South Atlantic margin. In Polcyn, M.J., and Jacobs, L.L. (eds.), 4th Triennial International Mosasaur Meeting, Program and Abstracts. Southern Methodist University.

Jacobs, L.L., and Polcyn, M.J. 2013. Upper Cretaceous marine amniote-bearing rocks of the East Texas Basin. In Polcyn, M.J.,

and Jacobs, L.L. (eds.), 4th Triennial International Mosasaur Meeting, Program and Abstracts. Southern Methodist University.

Jacobs, Louis L. 2013. Multidisciplinary and interdisciplinary uses and approaches to vertebrate biostratigraphy. Abstracts, Strati 2013, First International Congress on Stratigraphy, Lisbon, 1-7 July 2013.

Araúja, R., Lindgren, J., Polcyn, M.J., Jacobs, L.L., Schulp, A.S., and Mateus, O. 2013. A new elasmosaurid plesiosaur from Angola and the effects of paedomorphism in plesiosaurs. Society of Vertebrate Paleontology, 73rd Annual Meeting, Los Angeles, CA, Abstracts.

Chiba, K., Kobayashi, Y., Jacobs, L.L., Tanaka, K., and Graf, J. 2013. A robust desmostylid from Kokkaido, Japan, and the feeding style of desmostylids. Society of Vertebrate Paleontology, 73rd Annual Meeting, Los Angeles, CA, Abstracts.

Jacobs, L.L., Myers, T.S., Gonçalves, A.O., Graf, J., Jacobs, Bonnie, F., Kappelman, J.W., Jr., Mateus, O., Polcyn, M.J., Rasbury, E. T., and Vineyard, D. 2013. Cabinda revisited: Age and environment of new Cenozoic vertebrate fossils from northern Angola. Geological Society of America, 125th Annual Meeting Abstracts. Geological Society of America, 125th Annual Meeting, Denver, CO, Abstracts.

Lin, A., Jacobs, L.L., Wichura, H., Polcyn, M.J., Manthi, F.K., and Winkler, D.A. 2013. Miocene beaked whale from West Turkana, Kenya, and paleoelevation of the northern Kenya Rift. Geological Society of America, 125th Annual Meeting, Denver, CO, Abstracts.

Polcyn, M.J., Jacobs, L.L., Mateus, O., Schulp, A.S., Strganac, C., Araúja, R., Graf, J., Vineyard, D., and Myers, T.S. 2013. A marine vertebrate assemblage from the Campanian- Maastrichtian boundary at Bentiaba, Angola. Geological Society of America, 125th Annual Meeting, Denver, CO, Abstracts.

Strganac, C., Jacobs, L.L., Ferguson, K.M., Polcyn, M.J., Mateus, O., Schulp, A.S., Morais, M.L., Tavares, T., and Gonçalves, A.O. 2013. Late Cretaceous marine reptiles and cooling at the South Atlantic coast inferred through stable oxygen isotopes of *Inoceramus* from the Namibe Basin, Angola. Geological Society of America, 125th Annual Meeting, Denver, CO, Abstracts.

Graf, J., Polcyn, M.J., and Jacobs, L.L. 2014. Mobile scanning of large and rare specimens. North American Paleontological Convention. Gainesville, FL, 15-18 February, Abstracts, 171-172.

Jacobs, L.L., Wichura, H., Lin, A., Polcyn, M.J., Manthi, F.K., Winkler, D.A, Strecker, M.R. and Clemens, M. 2014. The Miocene Kenyan beaked. SecAd (Secondary Adaptations to Life in Water) 2014, George Mason University, Fairfax, VA, Abstracts.

Polcyn, M.J., Jacobs, L.L., Strganac, C., Mateus, O., Myers, T.S., May, S., Araúja, R., Schulp, A.S., Morais, M.L. 2014. Geological and paleoecological setting of a marine vertebrate bonebed from the Lower Maastrichtian at Bentiaba, Angola. SecAd (Secondary Adaptations to Life in Water) 2014, George Mason University, Fairfax, VA, Abstracts.

Kimura, Y., Casanova-Vilar, I., Cerling, T., Jacobs, L., Flynn, L., Lindsay. E., Pilbeam, D., Alba, D. and Moyà-Solà, S. 2014. Dietary plasticity of muroid rodents for continental-scale comparisons of carbon isotopes in the Late Miocene of Pakistan and Spain. Geological Society of America, 126th Annual Meeting, Denver, CO, Abstracts, 289-10.

Wichura, H., Jacobs, L.L., Lin, A., Polcyn, M.J., Manthi, F.K., Winkler, D.A., Strecker, M.R., and Clemens, M. 2014. Onset of uplift and environmental change in East Africa: Paleoaltimetry constraints from a 17 Ma beaked whale fossil from northern Kenya. Abstract, American Geophysical Union.

Carabajal, A.P., Lee, Y.-N., Jacobs, L.L., Kobayashi, Y., and Currie, P.J. 2014. Comparison of the endocranial morphology of the nodosaurid *Pawpawsaurus* and ankylosaurids from North America and Mongolia, with comments on the presence of the flocculus in the brain of non-theropod dinosaurs. Society of Vertebrate Paleontology, 74th Annual Meeting, Abstracts, November 4-8, 2014, Berlin.

Jacobs, L.L., Polcyn, M.J., Mateus, O., Myers, T.S., Gonçalves, A.O., Morais, M.L. 2014. Cenozoic vertebrates of coastal Angola. Society of Vertebrate Paleontology, 74th Annual Meeting, Abstracts, November 4-8, 2014, Berlin.

Kimura, Y., Flynn, L.J., and Jacobs, L.L. 2014. Classical murine lineages have been misused as a fossil-based calibration point

of molecular phylogeny. Society of Vertebrate Paleontology, 74th Annual Meeting, Abstracts, November 4-8, 2014, Berlin.

Marzola, M., Mateus, O., Schulp, A.S., Jacobs, L.L., Polcyn, M.J., Pervov, V. 2014. Early Cretaceous tracks of a large mammaliamorph, a crodylomorph, and dinosaurs with skin impressions from an Angolan Diamond mine. Society of Vertebrate Paleontology, 74th Annual Meeting, Abstracts, November 4-8, 2014, Berlin

Polcyn, M.J., Jacobs, L.L., Strganac, C., Mateus, O., Myers, T.S., May, S., Araúja, R., Schulp, A.S., Morais, M.L. 2014. Geological and paleoecological setting of a marine vertebrate bonebed from the Lower Maastrichtian of Angola. Society of Vertebrate Paleontology, 74th Annual Meeting, Abstracts, November 4-8, 2014, Berlin.

Wichura, H., Jacobs, L.L., Strecker, M.R., Lin, A., Polcyn, M.J., Manthi, F.K., Winkler, D.A., and Clemens, M. 2015. A 17 million year old whale constrains onset of uplift and climate change in East Africa. European Geosciences Union, Vienna, Austria, 12-17 April.

Jacobs, L.L., Fiorillo, A., Adams, T.L., Polcyn, M.J., Winkler, D.A., Newman, K., Baichtal, J.F. 2015. Looping the Alaska (Vertebrate) highway. Geological Society of America, Cordilleran Section Meeting, 47(1):21.

Polcyn, M.J., Jacobs, L.L., Schulp. A., Mateus, O. 2015. Trolling the Late Cretaceous seas: Marine amniotes of two West Coast margins.. Geological Society of America, Cordilleran Section Meeting, 47(1):21.

Marzola, M., Mateus O., Schulp, A.S., Jacobs, L.L., Polcyn, M.J., Pervov V., Gonçalves, A.O., and Morais, M.L. (2015). Comparative anatomy and systematics of Cretaceous mammal tracks of Angola. In Jagt, J.W.M., Hebda, G., Mitrus, S., Jagt-Yazykova, E., Bodzioch, A., Konietzko-Meier, D., Kardynal, K., and Gruntmejer, K. (eds.). 13th Annual Meeting of the European Association of Vertebrate Paleontologists, Opole, Poland, 8-12 July 2015 – Abstracts, p. 35

Clemens, M., Jacobs, L. L., Jacobs, B. B., Currano, E. D., Feseha, M. 2015. A new pipid frog from the Miocene of Ethiopia. Abstracts, 75th Annual Meeting, Society of Vertebrate Paleontology, October 13-17, 2015, Dallas, Texas.

Graf, J., Tabor, N., Ferguson, K., Jacobs, L. L., Winkler, D., Lee, Y., May, S. R. 2015. Stable isotope geochemistry of dinosaur eggshell from the Gobi Desert, Mongolia. Abstracts, 75th Annual Meeting, Society of Vertebrate Paleontology, October 13-17, 2015, Dallas, Texas.

Kimura, Y., McDonough, M. M., Hawkins, M. T., Jacobs, L. L., Flynn, L. J., Tomida, Y. 2015. Enhanced fossil calibration points for molecular clocks of muroid rodents. Abstracts, 75th Annual Meeting, Society of Vertebrate Paleontology, October 13-17, 2015, Dallas, Texas.

Kohno, N., Fiorillo, A. R., Jacobs, L. L., Chiba, K., Kimura, Y., Kobayashi, Y., Nishida, Y., Polcyn, M. J.,Tanaka, K. 2015. Desmostylian remains from Unalaska (USA). Abstracts, 75th Annual Meeting, Society of Vertebrate Paleontology, October 13-17, 2015, Dallas, Texas.

Manthi, F., Jacobs, L. L., Polcyn, M. J., Winkler, D. A., Scotese, C. R. 2015. CT assessment and phylogenetic relationships of a Miocene beaked whale from Kenya. Abstracts, 75th Annual Meeting, Society of Vertebrate Paleontology, October 13-17, 2015, Dallas, Texas.

Mateus, O., Jacobs, L. L., Polcyn, M. J., Myers, T. S., Schulp, A. S. 2015. The fossil record of testudines from Angola from the Turonian to Oligocene. Abstracts, 75th Annual Meeting, Society of Vertebrate Paleontology, October 13-17, 2015, Dallas, Texas.

Polcyn, M. J., Jacobs, L. L., Schulp, A. S., Mateus, O., Araújo, R. 2015. Tethyan and Weddellian biogeographic mixing in the Maastrichtian of Angola. Abstracts, 75th Annual Meeting, Society of Vertebrate Paleontology, October 13-17, 2015, Dallas, Texas.

Winkler, D. A., Ruoff, K., Clemens, M., Jacobs, L. 2015. Changes in small tetrapod faunas during the Early to Late Cretaceous transition in North Central Texas. Abstracts, 75th Annual Meeting, Society of Vertebrate Paleontology, October 13-17, 2015, Dallas, Texas.

Jacobs, L. L., Polcyn, J., Mateus, O., Schulp, A.S., Goncalves, A.O., and Morais, M.L. 2015. Long-term, multi-scale plate and geotectonic influences on primate paleoenvironments in West Africa. Geological Society of America 2015 Annual Meeting, Abstracts.

Polcyn, M.J., Bardet, N., Amaghzaz, M., Gonçalves, O.A., Jourani, E., Kaddumi, H.F., Lindgren, J., Mateus, O., Meslouhf, S., Morais, M.L., Pereda-Suberbiola, X., Schulp, A.S., Vincent, P., and Jacobs, L.L. 2016. An extremely derived plioplatecarpine mosasaur from the Maastrichtian of Africa and the Middle East. 5th Triennial Mosasaur Meeting – a global perspective on Mesozoic marine amniotes. May 16-20, 2016. Museum of Evolutiom, Uppsala University, Uppsala, Sweden.

Augusta, B.G., Polcyn, M.J., Zaher, H., and Jacobs, L.L. 2016. A gravid coniasaur (*Coniasaurus* sp.) female from the Upper Cretaceous of Texas (USA) and the development of dolichosaurs. 5th Triennial Mosasaur Meeting – a global perspective on Mesozoic marine amniotes. May 16-20, 2016. Museum of Evolutiom, Uppsala University, Uppsala, Sweden.

Jacobs, Louis L., Polcyn, M.J., Mateus, O., Schulp, A.S., Gonçalves, and Morais, M.L., and Myers, T.S. 2016. Angolan fossil vertebrates and geotectonic influences inform Cretaceous and Cenozoic paleoenvironments of Africa. 35th International Geological Congress, Cape Town, South Africa.

Jacobs, Louis L., Polcyn, M.J., Winkler, D.A., and Manthi, F.A. 2016. Redescripton of a Miocene beaked whale fossil from the Turkana Basin, Kenya. Symposium on the Evolution of Marine Mammals Honoring Gurum Mchedlidze. Georgia National Museum, Tbilisi.

Jacobs, Louis L., Polcyn, M.J., Mateus, O., Gonçalves, Schulp, A.S., and Morais, M.L. 2016. Projecto PaleoAngola and the Neogene record of whales in Angola. Symposium on the Evolution of Marine Mammals Honoring Gurum Mchedlidze. Georgia National Museum, Tbilisi.

Kimura, Y., Lindsay, E., Jacobs, L.L., and Flynn, L.J. 2016. Isotopic dietary response to interspecific competition between murine and cricetid rodents in the Early Miocene of Pakistan. Society of Vertebrate Paleontology, 76th Annual Meeting, Abstracts.

Myers, T.S., Mateus, O., Polcyn, M.J., Vineyard, D., and Jacobs, L.L. 2016. A new turtle from the Paleocene of Cabinda, Angola. Society of Vertebrate Paleontology, 76th Annual Meeting, Abstracts.

Chindebvu, E.G., Andrzejewski, K., Polcyn, M.J., Winkler, D.A., and Jacobs, L.L. 2017. 3D reconstruction of the brain endocast and inner ear of *Malawisaurus dixeyi* (Sauropoda: Titanosauria). Society of Vertebrate Paleontology, 77th Annual Meeting, Abstracts.

Clemens, M., Winkler, D.A., and Jacobs, L.L. 2017. A nodosaurid (Ornithischis, Ankylosauria) from the Lower Eagle Ford Group of North Central Texas. Society of Vertebrate Paleontology, 77th Annual Meeting, Abstracts.

Perez, M., Chindebvu, E.G., Simfukwe, H., Vineyard, D.P., Polcyn, M.J., Winkler, D.A., and Jacobs, L.L. 2017. *Eunotosaurus* from the Middle Permian of the Republic of Malawi. Society of Vertebrate Paleontology, 77th Annual Meeting, Abstracts.

Andrzejewski, K., Tabor, N.J., and Jacobs, L.L. 2018. Paleoenvironmental and paleoclimatic reconstruction of Cretaceous terrestrial formations of Texas and Oklahoma using pedogenic minerals. GSA Annual Meeting.

Meyers, T.S., Tabor, N.J., Eagle, R., Bateman, J.B., May, S., Jacobs, L.L., and Weil, A. 2018. Paleoclimate of the Upper Jurassic Morrison Formation in Oklahoma and Texas. GSA Annual Meeting, Indianapolis, Indiana.

Schulp, A.S., Mateus, O., Polcyn, M.J., Jacobs, L.L. 2019. Angola and its role in the paleobiogeography of Africa. Society of Vertebrate Paleontology, Annual Meeting, Abstracts.

Jacobs, L.L., Sousa, N., Goncalves, A.O., Mateus, O., Polcyn, M.J., and Schulp, A.S. 2020. Projecto PaleoAngola: Geoheritage and conservation paleobiology as science for development in Angola. American Geophysical Union, Meeting Abstracts.

Jackson, Y., Economos, R., Mateus, O., and Jacobs, L.L. 2021. When dinosaurs walked through diamonds: Constraining the age of Early Cretaceous footprints in volcanic crater sediments. SMU Journal of Undergraduate Research, 6(1): 1.

Schulp, A.S., Mateus, O., Polcyn, M.J., Goncalves, A.O., Sousa, N., Jacobs, L.L. 2021. Cretaceous marine tetrapods from Bentiaba, Angola. SECAD, 2021.

Sousa, N., Mateus, O., Schulp, A.S., Polcyn, M.J., Goncalves, A.O., and Jacobs, L.L. 2021. The Atlantic puzzle: a contribution

from Angola to global geoheritage. X International Online ProGEO Symposium, Spain, 7-10th June, 2021

Books and Editorships

Jacobs, L.L. (ed.), 1980. Aspects of vertebrate history: Essays in honor of Edwin Harris Colbert.

Museum of Northern Arizona Press, Flagstaff, 407 p.

Winkler, D.A., Murry, P.A., and Jacobs, L.L. (eds.), 1989. Field guide to the vertebrate paleontology of the Trinity Group, Lower Cretaceous of Central Texas. ISEM, 33 pp.

Jacobs, L.L., 1993. Quest for the African Dinosaurs: Ancient Roots of the Modern World. Villard Books, New York, 330 pp.

Jacobs, L.L., 1993. Cretaceous airport: the surprising story of real dinosaurs at DFW. Institute for the Study of Earth and Man, 24 pp.

Jacobs, L.L., 1995. Lone Star Dinosaurs. Texas A&M University Press, 160 pp.

Tomida, Y., L.J. Flynn, and L.L. Jacobs (eds.) 1998. Advances in Vertebrate Paleontology and Geochronology in honor of Everett H. Lindsay. National Science Museum, Tokyo, 292 pp.

Janis, C.M., K.M. Scott, and Louis L. Jacobs, (eds.). 1998. Evolution of Tertiary mammals of North America. Volume I: Terrestrial carnivores, ungulates, and ungulatelike mammals. Cambridge University Press, 691 pp.

Jacobs, L.L. 2000. Quest for the African dinosaurs, with a new introduction by the author. The Johns Hopkins University Press.

Badgley, C., Flynn, L.J., Jacobs, L.L., and Taylor, L.H. (guest editors). 2005. Paleontology from China, Pakistan and around the world in honor of Will Downs. Palaeontologica Electronica, 8(1):http://palaeo-electronica.org.

Taylor, L.H., Jacobs, L.L., and Bell, C.J. (guest editors). 2011. Papers in honor of Charles A. Repenning. Palaeontologica Electronica, 14(3):http://palaeo-electronica.org.

Polcyn, M.J., and Jacobs, L.L. (editors). 2013. 4th Triennial International Mosasaur Meeting, Program and Abstracts. Southern Methodist University.

Kimura, Y., Flynn, L.J., and Jacobs, L.L. (guest editors). 2015. Contributions to vertebrate palaeontology in honour of Yukimitsu Tomida. Historical Biology, on-line publication; 2016, hard copy publication.

Jacobs, L.L., Polcyn, M.J., Mateus, O., Schulp, A. Under contract. Projecto PaleoAngola. Springer.

Louis Leo Jacobs III

Louis H. Taylor, Lawrence J. Flynn, and Michael J. Polcyn

4931 W. Rowland Avenue, Littleton, Co 80128. loutaylor44@aol.com
Department of Human Evolutionary Biology, Harvard University, Cambridge, MA 02138. ljflynn@fas.harvard.edu
Roy M. Huffington Department of Earth Sciences, Southern Methodist University, Heroy Hall, PO Box 750385, Dallas, TX 75275-0395.
mpolcyn@smu.edu

Louis the Vertebrate Paleontologist

Louis L. Jacobs III received the Society of Vertebrate Paleontology Joseph T. Gregory Award in 2005. His acceptance speech demonstrated his humility: "I am Louis Jacobs. I am a vertebrate paleontologist. Thank you for this honor." Those of us who know him understand that Louis Jacobs is not only a vertebrate paleontologist but a scientist without academic or geographic limits, a teacher and mentor, and a friend to all who meet him.

This man who has contributed so much to the science of vertebrate paleontology was born on August 27, 1948, in Syracuse, New York. Louis spent much of his early life in Louisiana, graduating from DeRidder High School in DeRidder, Louisiana. He earned a B.S. from the University of Southwestern Louisiana (now the University of Louisiana at Lafayette) in 1970. While an undergraduate, Louis was employed as part of an offshore seismic crew in the Gulf of Mexico and briefly served in the United States Merchant Marine.

As a graduate student mentored by Everett Lindsay and George Gaylord Simpson at the University of Arizona, he began his vertebrate paleontology research by investigating Miocene (Hemphillian) rodents from Arizona. That research later expanded to include studies of rodent evolution and migration in Pakistan that have continued throughout his career. The Pakistan research began as part of an ongoing project directed by Dr. David Pilbeam. Louis' research resulted in, among other discoveries, *Antemus*, a new genus at the base of murid rodents.

As a University of Arizona student, Louis was a prominent contributing member of the informal seminar group known as The Red Fireballs. RFB members attended a weekly lunch with Drs. Lindsay and Simpson. Occasionally, they were joined by Dr. Laurence McKinley Gould, the first geologist to work in Antarctica. The lunch and brief seminar that followed allowed the students to discuss vertebrate paleontology and geology with their mentors in an informal setting.

Upon receipt of the Ph.D. in 1977, Louis accepted a position at the Museum of Northern Arizona, where he continued his informal education by working with Edwin H. (Ned) Colbert. It was at MNA that Louis developed a working relationship with his long-time field partner, Will Downs. They spent many years together working in Asia, Africa, and elsewhere around the world.

Following short stints as a USGS geologist and a lecturer at The University of Arizona, Louis accepted a position as Head of the Division of Paleontology at the Kenya National Museum in 1981, working under director Richard E. Leakey.

Louis became a faculty member in the Department of Geological Sciences at Southern Methodist University in Dallas, Texas, in 1983. At that time, he became affiliated with the Shuler Museum of Paleontology, ultimately serving as its director from 1987 to 2000.

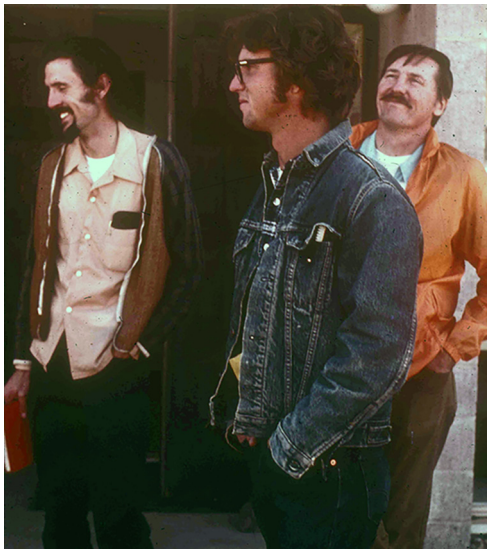

Photo 1. (L-R) Jim Honey, Louis Jacobs, and Everett Lindsay at the home of Ned Colbert, ~1976. Credit: Lou Taylor
Photo 2. Louis Jacobs in Bentiaba, Angola, 2010. Credit: Kalunga Lima.
Photo 3. Everett Lindsay greeting Louis Jacobs at Lindsay's 90th Birthday Party, June 2021. Jessica Harrison in the background. Credit: Kurt Lindsay
Photo 4. Louis and Bonnie Jacobs holding Louis' SVP Joseph T. Gregory award plaque. 2005 SVP annual meeting Mesa, Arizona. Credit: Lou Taylor. When he received the Gregory Award, he said, "My name is Louis Jacobs. I am a vertebrate paleontologist. Thank you for this honor."

Outside of his faculty duties, Louis was appointed *ad interim* museum director of the Dallas Museum of Natural History and also president of the Institute for the Study of Earth and Man (ISEM) at SMU, an organization "focused on interdisciplinary research and related education." Louis continues as President of ISEM to this day, in addition to his ongoing paleontological research in *Projecto PaleoAngola* (a collaboration with colleagues from SMU, Angola, the Netherlands, and Portugal) and as emeritus professor at SMU.

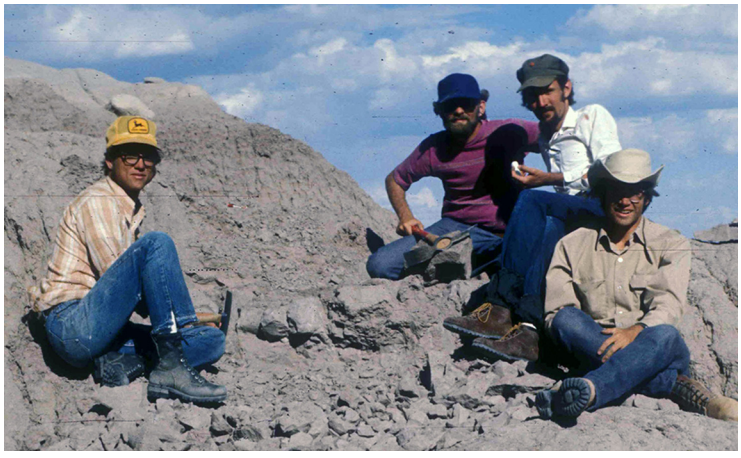

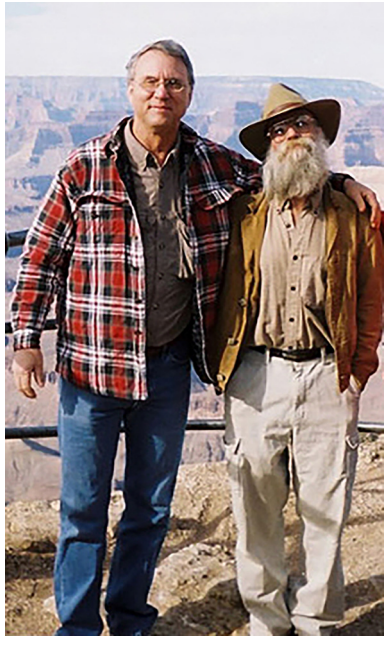

Photo 5. (L-R) Louis Jacobs, Lou Taylor, and Jim Honey in the Paleocene Nacimiento Formation, San Juan Basin, New Mexico, June 1975. Credit: Larry Flynn

Photo 6. Louis Jacobs and Nancy Stevens working on the humerus of *Angolatitan adamastor* in Iemba, Angola, 2006. Credit: Mike Polcyn or Octavio Mateus.

Photo 7. (L-R) Louis Jacobs, Fred Cropp, George Gaylord Simpson at Simpson's home for the annual Darwin's Day party, Tucson, Arizona, ~1976. Credit: Lou Taylor

Photo 8. Louis Jacobs and Will Downs at the Grand Canyon, Arizona, December 2005. Credit: Bonnie Jacobs

Photo 9. (L-R) Louis Jacobs, Mary Taylor, Will Downs, and Lou Taylor. Louis Jacobs and friends viewing *Malawisaurus*; Dallas, Texas, 1998, Credit: Bonnie Jacobs

Photo 10. Louis and Bonnie Jacobs on the occasion of Louis' 50th Birthday, 1998. Credit: unknown

Photo 11. (L-R) Everett Lindsay, Jim Honey, Larry Flynn, Yuki Tomida, Dick Haskin, Louis Jacobs, Lou Taylor. Red Fireballs after one of their weekly luncheons at the panda restaurant, Tucson, Arizona, ~1975. Credit: unknown

Louis, the vertebrate paleontologist, has been honored by ten patronymns (Appendix 1), the most recent of which was the oviraptorid dinosaur *Corythoraptor jacobsi*. It was described through the collaboration of three former students: the late Junchang Lü of China, Yuong-Nam Lee of Korea, and Yoshitsugu Kobayashi of Japan.

Louis the Man

In addition to his scientific and professional accomplishments, some of us have been fortunate to know Louis' generous spirit, manifested in his personal relationships as a husband, father, friend, colleague, teacher, and mentor.

Louis Jacobs and Bonnie Fine were married in Tucson on November 22, 1980. Their wedding was a vertebrate paleontology festival. Not only did the Red Fireballs attend, but also the Simpsons and Colberts. Louis continues to collaborate with Bonnie, a paleobotanist and SMU emeritus professor. Louis and Bonnie are the proud and doting parents of their son Matthew and their daughter Melissa, and they are thrilled to have two grandchildren.

Louis has maintained old friendships and created new friends throughout his time as a vertebrate paleontologist. Many of the Red Fireballs still meet annually or more often to work together or to celebrate special events in each other's lives. They often

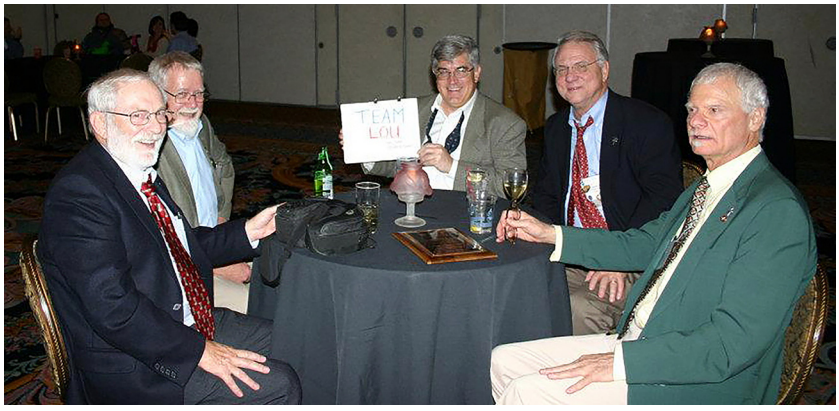

Photo 12. (L-R) Oldrich Fejfar, Emmie Ericson, Everett Lindsay, Tushi Fejfar, Charles "Rep" Repenning, Louis Jacobs, Dale Winkler, Lou Taylor, and Mary Taylor. The Repenning home, Lakewood, Colorado, 2004. Credit: Shiela Stephens

Photo 13. (L-R) Lou Taylor, Gary Johnson, Ted Vlamis, Louis Jacobs, and Steven Cohen at the 2011 SVP Annual Meeting, Las Vegas, Nevada. Credit: Rebecca Hunt-Foster

can be seen together at the Society of Vertebrate Paleontology annual meetings. Louis is one of the first to join any effort to honor a friend or colleague. He has been involved in a number of festschrifts as well as articles honoring historical figures and events.

Louis is also well known to be quick to support the profession through public outreach and professional service. As an active and contributing member of the Society of Vertebrate Paleontology, Louis has served the society through various committees and as president for two years, beginning in 1996. He remains active as co-chair of SVP's Steven Cohen Award for Student Research Committee. Louis has been instrumental in producing two videos for SVP. He and his colleagues produced the video *We Are SVP* to provide stories of vertebrate paleontologists from around the world and to present their research and fieldwork. The video also emphasized the value of vertebrate paleontology as a science and particularly as one of the avenues by which children are introduced to the world of science. They also produced a documentary on the development of the SVP logo by artist Margaret Colbert, wife of vertebrate paleontologist Ned Colbert, and the daughter of another, William Diller Matthew. For his service to the Society of Vertebrate Paleontology, Louis has been awarded the Joseph T. Gregory Award (2005) and Honorary Membership (2012). He aided the science community of Dallas in 1999 as director *ad*

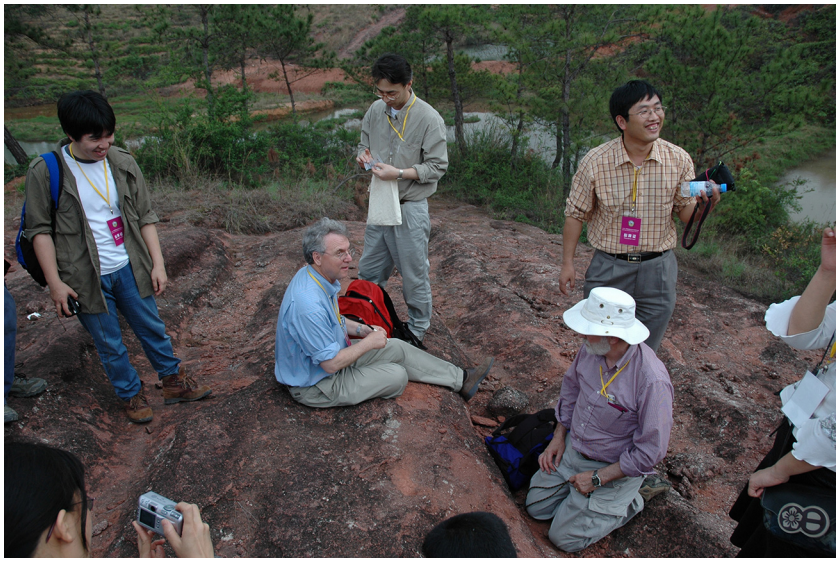

Photo 14. (L-R) Katsuhiro Kubota, Louis Jacobs, Yuong-Nam Lee, Lou Tayor, Junchang Lü at the Heyuan dinosaur egg site, Heyuan, China, April 2005. Credit: unknown

Photo 15. (L-R) Yuong-Nam Lee, Louis Jacobs, Rinchen Barsbold, Yoshitsugu Kobayashi, Philip Currie, Anthony Fiorillo at Ulaan Khushuu base camp, Mongolia, September 2006. Credit: Namsoo Kim

Photo 16. (L-R) Louis Jacobs, Yuong-Nam Lee, Yoshitsugu Kobayashi, Junchang Lü at Tarchia tumanovae digging site at Hermiin Tsav, Mongolia, September 2008. Credit: Michael Ryan

interim of the Dallas Museum of Natural History. To this day, he serves as a professional advisor to the Dallas Paleontological Society.

Louis the Educator

Throughout his years at SMU, Louis continued his research as a paleomammalogist, but also stretched his research to include other aspects of vertebrate paleontology, particularly dinosaurs and marine reptiles, and how they can be applied to answering questions about the Earth and the history of life on it.

He has eagerly included fellow faculty members and graduate students in vertebrate paleontology studies in Texas, Arizona,

Photo 17. Group photo at Rolling Hills Hotel for 2013 Hwaseong International Dinosaurs Expedition Symposium, South Korea, December 2013. Credit: unknown

Alaska, Mexico, Cameroon, Malawi, Mozambique, Yemen, Israel, Antarctica, and, most recently, in Angola through *Projecto PaleoAngola*.

Projecto PaleoAngola research has resulted in not only vertebrate paleontological discoveries but also provides great insight into the opening and effects of the opening of the South Atlantic Ocean. A collaboration among scientists from the U.S.A., Portugal, Finland, Sweden, The Netherlands, and Angola, this project has profited from contributions by many other colleagues and students.

SMU students and staff members, under Louis' leadership, created and constructed an exhibit highlighting the results of research in Angola. The exhibit, a long-term temporary installation at the Smithsonian National Museum of Natural History in Washington, DC., is designed to travel to other venues.

Louis has been an extraordinary "paleontological father" and is now a "paleontological grandfather." His research contributions, and those of the students he has trained and junior colleagues he has mentored, are impactful at a global level. His program has attracted 28 graduate students from around the world (Appendix 2). Not only has he mentored and trained new vertebrate paleontologists, but he has also encouraged them to apply their expertise to develop their own academic programs, create museums, and serve their respective communities as scientists and good citizens.

Louis has also mentored undergraduate students and generously donated time through science outreach to interested amateur fossil enthusiasts and educators around North Texas. For his contributions to education, Louis has been honored by Texas Tech University with the Skoog Cup, which is "presented to higher education faculty members in appreciation for their outstanding contributions to the development of quality science education."

Louis, Our Friend

We have been honored to have been colleagues and friends of Louis L. Jacobs as he studied and fostered vertebrate paleontology around the globe. He included us and so many of his students in the research, enriching everyone involved.

He has spent a career not only adding to the body of vertebrate paleontology knowledge but also as a mentor to us all. Rarely does anyone encounter Louis and not come away with some new knowledge or a question to think about.

We are all fortunate to know Louis Jacobs.

APPENDIX 1. Patronymns

Apatosciuravus jacobsi Flanagan, 1986, Vertebrates, Phylogeny, and Philosophy: Contributions to Geology, University of Wyoming, Special Paper 3, p. 204.

Jacobsomys verdensis Czaplewski, 1987, Journal of Vertebrate Paleontology, 7(2), p. 191.

Hadromys loujacobsi Musser, 1987, American Museum Novitates, 2883, p. 12.

Chinleogomphius jacobsi (Murry, 1987), Journal of Paleontology, 61(4), p. 773.

Chardinomys louisi Zhou, 1988, Vertebrata PalAsiatica, 26(3), p. 189.

Microsteiromys jacobsi Walton, 1990, Ph.D. Thesis, Southern Methodist University.

Mus jacobsi Kotlia, 1992, Neues Jahrbuch für Geologie und Paläontologie, 184(3):348.

Karnimata jacobsi Winkler, 2003, Lothagam: The Dawn of Humanity in Eastern Africa, Columbia University Press, p. 180.

Paronychomys jacobsi Kelly, 2013, Paludicola, 9(2)70-96.

Corythoraptor jacobsi Junchang Lü et al., 2017, Scientific Reports, 7(6393) DOI:10.1038/s41598-017-05016-6

APPENDIX 2. Student Advisees

Anne Walton (Ph.D. 1990), USA
Alisa Winkler (Ph.D. 1990), USA
John Congleton (M.S. 1990), USA
Xiaofeng Xu (Ph.D. 1995), CHINA
Yuong-Nam Lee (Ph.D. 1995), SOUTH KOREA
Christine Rennison (M.S. 1996), USA
Jerry Harris (M.S. 1997), USA
Jack Whittles (M.S. 1997), USA
Elizabeth Gomani Chindebvu (M.S. 1993, Ph.D. 1999), MALAWI
Jack Rogers (M.S. 2000), USA
Jason Head (M.S. 1997, Ph.D. 2002), USA
Yoshitsugu Kobayashi (M.S. 1998, Ph.D. 2004), JAPAN
Junchang Lü (Ph.D. 2004), CHINA
Peter Rose (M.S. 2004), USA
Annat Haber (M.S. 2005), ISRAEL
John Robbins (co-advisor, Ph.D. 2007), USA

Timothy Scott Myers (Ph.D. 2009), USA
Diana Vineyard (M.S. 2009), USA
Yosuke Nishida (M.S. 2009), JAPAN
Martha Carolina Aguillon (M.S. 2010), MEXICO
Thomas Adams (M.S. 2008, Ph.D. 2011), USA
Ricardo Araújo (Fulbright Scholar, Ph.D. 2013), PORTUGAL
Yuri Kimura (M.S. 2009, Ph.D. 2013), JAPAN
Chris Strganac (M.S. 2008, Ph.D. 2014), USA
John Graf (Fulbright Scholar, Ph.D. 2016), USA
Kate Andrzejewski (Ph.D. 2018), USA
Matthew Clemens (M.S. 2014, Ph.D. 2018), USA
Juror for Emanuel Tschopp (Universidade Novo de Lisboa, Ph.D. 2014), PORTUGAL

WINDOWS INTO SAUROPSID AND SYNAPSID EVOLUTION
Essays in honor of Prof. Louis L. Jacobs, pp. 1–65, 2023

NOVEL ANATOMY AND PALEOBIOLOGICAL INSIGHTS ON *CISTECEPHALUS MICRORHINUS* (SYNAPSIDA: DICYNODONTIA)

Z. MACUNGO[1,2,*], R. ARAÚJO[1,3,*], C. BROWNING[4], R. M. H. SMITH[2,4], R. DAVID[5], K. D. ANGIELCZYK[6], A. MASSINGUE[1], S. FERREIRA-CARDOSO[7], and D. J. P. KORTJE[4]

[1]Museu Nacional de Geologia, Maputo, Mozambique
[2]Evolutionary Studies Institute, University of the Witwatersrand, Johannesburg, South Africa
[3]Instituto de Plasmas e Fusão Nuclear, Universidade de Lisboa, Portugal
[4]Iziko South African Museum, Cape Town, South Africa
[5]Natural History Museum, London, United Kingdom
[6]Negaunee Integrative Research Center, Field Museum of Natural History, 1400 South DuSable Lake Shore Drive, Chicago, Illinois, 60605, USA
[7]Institut des Sciences de l'Evolution de Montpellier (ISEM), CNRS, IRD, EPHE, Université de Montpellier, Montpellier, France

ABSTRACT Although *Cistecephalus microrhinus* is a well-researched dicynodont taxon, our study using bone-by-bone manual segmentation of micro-computed tomography scans has unveiled a plethora of new insights into its paleobiology, anatomy, and variation. We detail the neuroanatomy of two South African *Cistecephalus* specimens, SAM-PK-K6814 and SAM-PK-011474, and shed light on the internal three-dimensional structures of the *Cistecephalus* skull. Our findings also clarify previously ambiguous bone contacts in serial-sections and highlight external morphological features previously obscured by the species' small size, taphonomic deformation, overpreparation, or matrix obstructions. We specifically studied the evolution of the postfrontal in emydopoids and propose that it may have resulted from co-ossification with the postorbital, rather than element deletion. Our examination of the inner ear anatomy allowed the calculation of the thermo-motility index, which suggests that cistecephalids, including *Kawingasaurus*, and other dicynodonts, were likely ectotherms — a stance that challenges a recent hypothesis based on the angle between semicircular canals. Both *Cistecephalus* and its close relative *Kawingasaurus*, were found to have typical angles between these canals. This result emphasizes the significance of considering the utricular section of the canal when measuring angles and making paleobiological inferences. Additional evidence supporting the ectothermic nature of cistecephalids, despite their atypical brain morphology, comes from propagation phase-contrast synchrotron tomography scans. These scans did not reveal mammal-like complex turbinals; instead, these structures appear to be the result of sediment infilling. When the physiological inferences are contextualized within the Permian Karoo paleoclimate, it is plausible that *Cistecephalus* underwent brumation in winter, aligning with its fossorial traits.

KEYWORDS Dicynodonts, Cistecephalids, Thermo-motility index, Ectothermy, Semicircular canals, Postfrontal

INTRODUCTION

Cistecephalus, recognized as one of the most disparate dicynodont species, was promptly designated a new genus in Owen's (1876) catalogue. Remarkably, some features highlighted by Richard Owen remain pertinent today, such as the "singular proportions of the skull, which is broader than long" and the "box-like shape of the skull" (Owen, 1876, p. 63), the latter giving the genus its name (*Kiste* from the Ancient Greek for box). The genus' unique anatomy and abundant specimens led Broom (1906) to acknowledge its biostratigraphic value, which persists through to the present as the *Cistecephalus* Assemblage Zone (Kitching 1970, Smith and Keyser 1995, Smith 2020). Various paleobiological hypotheses have been proposed for *Cistecephalus*, including (semi)aquatic (Broom 1948, Brink 1950), scansorial (McRae 1999), and arboreal (Keyser 1973) lifestyles. However, due to its robust forelimbs, which are analogous to those of moles, its bone microstructure, and compact skull anatomy, *Cistecephalus* is currently viewed as an obligate fossorial dicynodont, embodying some of the most extreme fossorial adaptations among dicynodonts (Keyser 1973, Cluver 1978, Lungmus and Angielczyk 2021, Kammerer 2021, Macungo et al. 2022).

*Corresponding and co-first author

The prevalence of *Cistecephalus* is so notable that Keyser (1965, 1973) utilized serial-sectioning on one specimen to reveal more detailed anatomy than external morphology alone could provide. Since then, Keyser's (1973) work has served as a reference for the anatomy of cistecephalids and has been utilized in a comparative framework for other emydopoids and Permian dicynodonts in general (e.g., Kammerer et al. 2011, Angielczyk et al. 2019, 2023). Given its significance, *Cistecephalus* warrants further reanalysis utilizing contemporary technology, specifically micro-computed tomography. This technology enables a detailed examination of osteohistology and internal cranial anatomy, as well as meticulous bone contact analysis in multiple anatomical planes, and generates three-dimensional endocasts of volumes once occupied by soft tissue.

In this study, we conduct bone-by-bone segmentation of a *Cistecephalus* specimen (SAM-PK-6814), supplemented, when necessary, with segmentation of an additional specimen (SAM-PK-K011474). This work complements Keyser's (1973) description and provide new details on the neuroanatomy, as well as inner ear and maxillary antrum morphology in this species. We also reanalyze some characters in a phylogenetic context, propose an evolutionary hypothesis for loss of the postfrontals in emydopoids, calculate the thermomotility index for *Cistecephalus* — indicating it was most likely an ectotherm, refute previous suggestions that the angle between semicircular canals was unusual, confirm the absence of turbinals, and contextualize cistecephalids and other dicynodonts within their Permian Karoo paleoclimate. The latter work suggests that these animals likely engaged in brumation during the colder season, consistent with their fossorial adaptations.

MATERIALS AND METHODS

Specimen SAM-PK-K6814 is a well-preserved, complete *Cistecephalus microrhinus* skull with articulated lower jaw and partial postcranial skeleton (Fig. 1), and SAM-PK-K011474 is a well-preserved *Cistecephalus microrhinus* specimen with complete, but disarticulated lower jaw and partial postcranial skeleton (Fig. 2). Both specimens were mechanically prepared in the Karoo Palaeontology laboratory of Iziko South African Museum using a compressed-air driven air-scribe and consolidated using Paraloid B72 diluted with acetone. SAM-PK-K6814 was prepared by Annelise Crean Georgina Skinner and SAM-PK-K011474 was prepared by Jay Van den Berg. Based on their size (Nasterlack et al. 2012), the specimens represent adults, with basal skull lengths of 53,3 and 47 mm, and maximum skull widths of 61,6 and 62,4 mm for SAM-PK-K6814 and SAM-PK-K011474, respectively.

Institutional Abbreviations

BP, Evolutionary Studies Institute (Johannesburg, South Africa); BSP, Bayerische Staatssammlung für Paläontologie und Historische Geologie, Munich, Germany; GPIT, Institut und Museum für Geologie und Paläontologie der Eberhard-Karls-Universität Tübingen, Germany; NHCC, National Heritage Conservation Commission (Lusaka, Zambia); PK, Karoo Palaeontology Collection; PPM, Projecto PaleoMoz, Museu Nacional de Geologia (Maputo, Mozambique); SAM; Iziko South African Museum, Cape Town, South Africa.

Geological setting

Specimen SAM-PK-K6814 was found by Annelise Crean and collected by R.M.H. Smith in 1995 on the farm Good Luck (Matjesfontein 412) in the Namakwa District, Northern Cape Province, South Africa (Fig. 3). It was found in the late Permian (~259.9-254.17 Ma; Rubidge et al. 2013) Steenkampsvlakte Member of the Teekloof Formation (Beaufort Group, Adelaide Subgroup, Karoo Supergroup) in strata assigned to the uppermost *Cistecephalus* Assemblage Zone (Smith 2020, Fig. 3). Specimen SAM-PK-K011474 was collected by A.T. Bremner in 1978 from the farm Doornplaats (Rust 126) near Graaff-Reinet in the Eastern Cape Province, South Africa. It was also found in the upper *Cistecephalus* Assemblage Zone strata.

Micro-computed tomography scanning

The *Cistecephalus microrhinus* specimens were imaged at Stellenbosch University's Central Analytical Facility (CAF) using a walk-in microfocus X-ray μCT scanner (General ElectricPhoenixV|Tome|XL24 with NF180). A 0.2 mm Cu filter was used in both scans to reduce the potential effect of beam hardening artifacts. For SAM-PK-K6814, a total of 3500 slices were generated in coronal planes with the following metrics: resolution = 2024 pixels, isotropic voxel size = 0.04500001 mm, magnification ratio = 4.44444352, voltage = 180 kV, current = 120 μA. A total of 3500 slices were generated in coronal planes for SAM-PK-K011474, with the

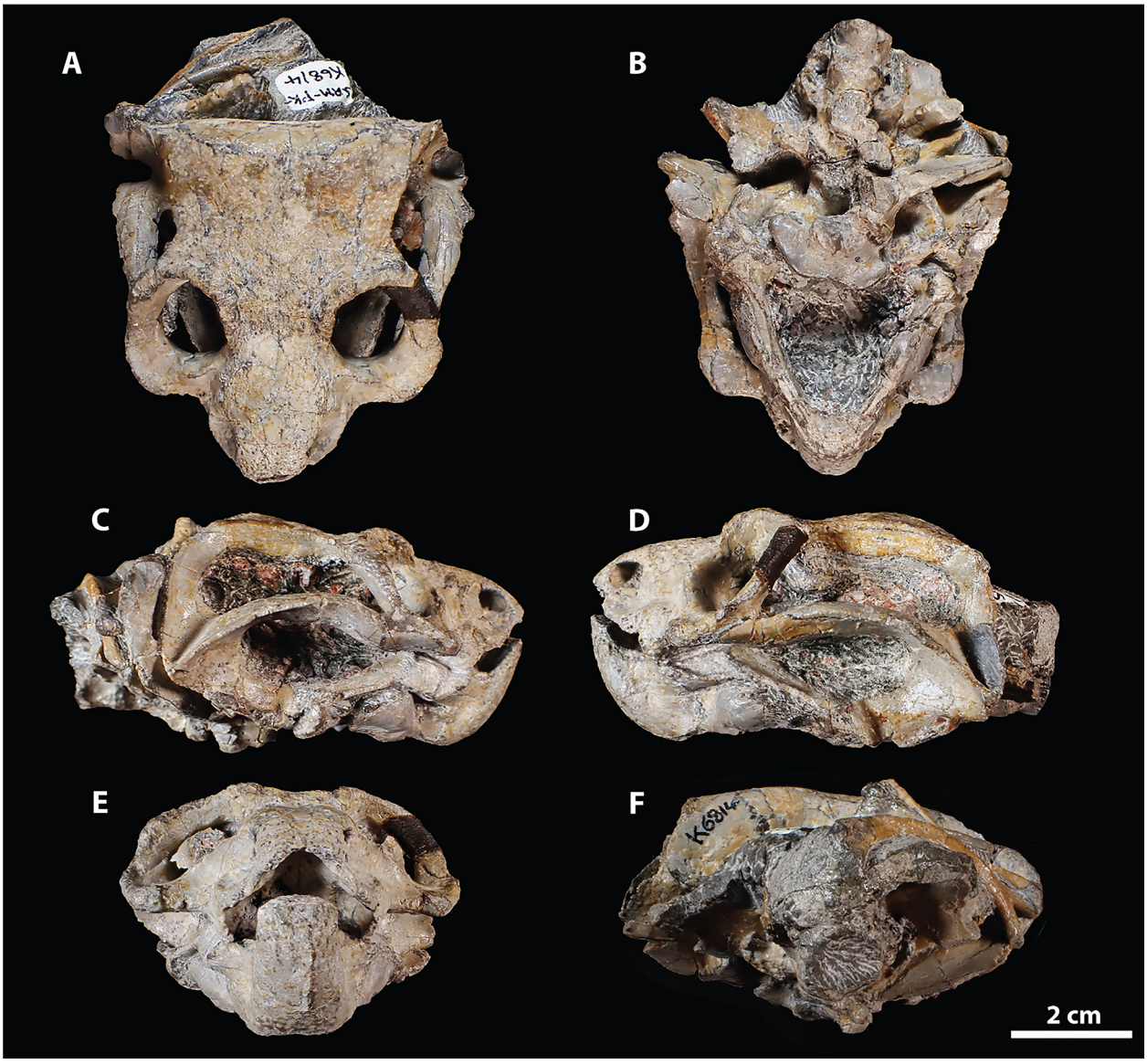

FIGURE 1. Photographs of *Cistecephalus microrhinus* specimen SAM-PK-K6814 in A, dorsal; B, ventral; C, right lateral; D, left lateral; E, anterior; and F, posterior view.

following metrics: resolution = 2024 pixels, isotropic voxel size = 0.03000001 mm, magnification ratio = 6.66666528, voltage = 245 kV, current = 120 lA. The acquired projection images were reconstructed using system-supplied Datos reconstruction software. Three-dimensional reconstructions and visualization of CT data of specimens were generated using Avizo 9.0 (FEI VSG, Hillsboro, OR, USA). Morphological structures (i.e., cranial bones and the endocasts of the brain, maxillary canal, and inner ear) were manually segmented using the same software to produce three-dimensional renderings that were measured virtually following a similar protocol used in Macungo et al. (2022). Raw CT data sets are stored at the Iziko South African Museum and are available upon request to the authors by email: cbrowning@iziko.org.za. Bone-by-bone segmentation of SAM-PK-K6814 and SAM-PK-K011474 resulted in full three-dimensional renderings of the entire skull (Fig. 4), including the skull roof (Fig. 5), palate (Fig. 6), internal cranial bones (Fig. 7), braincase (Fig. 8), stapes (Fig. 9), and various endocasts, such as the brain, endosseous labyrinth and maxillary antrum (Fig. 10). All 3D renderings are available in Morphobank project # 4895, and can be opened and visualized with 3D

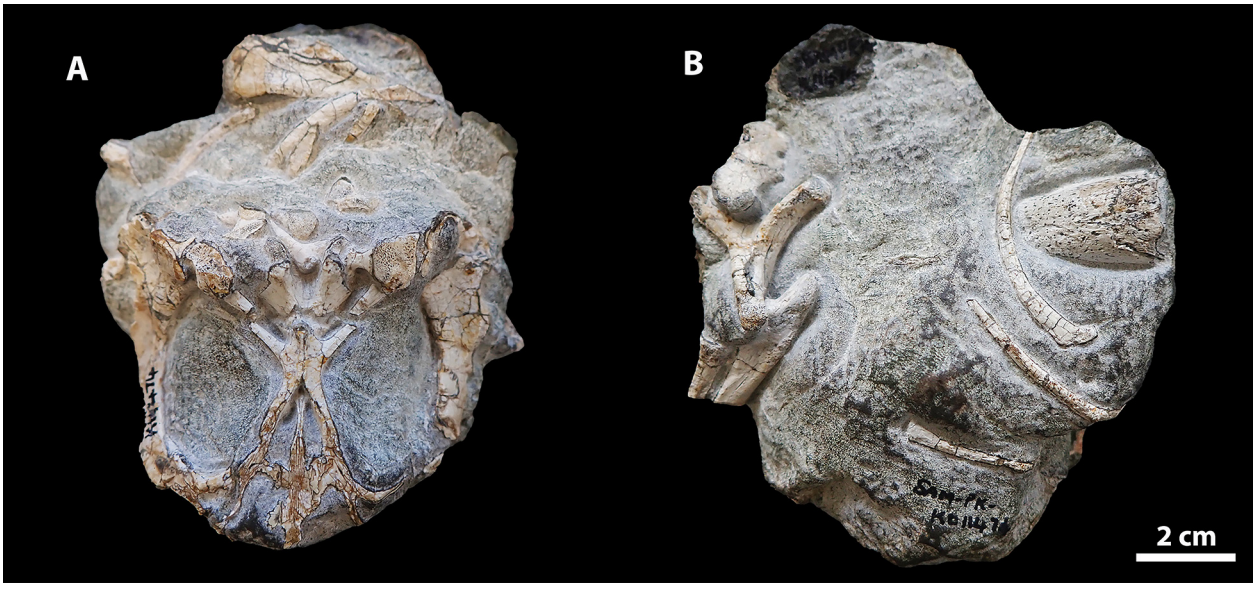

FIGURE 2. Photographs of *Cistecephalus microrhinus* specimen SAM-PK-K011474 in A, ventral and B, dorsal view.

object software (e.g., Meshlab).

In addition to the *Cistecephalus* specimens, µCT data for several other dicynodont specimens was used in our examination of postfrontal morphology. These specimens were all scanned a the University of Chicago's PaleoCT facility using a GE v|tome|x s 240 µCT scanner. The *Compsodon helmoedi* specimen NHCC LB14 was scanned with a 0.5mm Sn filter, using a voltage of 200 kV and 210 µA current, resulting in an isotropic voxel size of 64.90 µm. The *Kembawacela kitchingi* specimen NHCC LB18 was scanned with a 0.5 mm Sn filter, using a voltage of 120 kV and 380 µA current, resulting in an isotropic voxel size of 46.63 µm. NHCC LB37, a specimen representing a new lystrosaurid taxon, with a 0.5 mm Sn filter, using a voltage of 200 kV and 200 µA current, resulting in an isotropic voxel size of 107 µm. The *Dicynodontoides* sp. NHCC LB117 skull NHCC LB117 was scanned with a 0.5 mm Sn filter, using a voltage of 210 kV and 210 µA current, resulting in an isotropic voxel size of 68.87 µm. The *Abajudon kaayai* specimen NHCC LB314 was scanned with a 0.5 mm Sn filter, using a voltage of 120 kV and 660 µA current, resulting in an isotropic voxel size of 80.11 µm. The *Oudenodon bainii* specimen NHCC LB631 was scanned with a 0.5 mm Sn filter, using a voltage of 220 kV and 260 µA current, resulting in an isotropic voxel size of 87.04 µm.

Kawingasaurus fossilis GPIT-PV-117032 (formerly GPIT/RE/9272) was scanned at the propagation phase-contrast synchrotron tomography facilities at the European Synchrotron Radiation Facility in Grenoble, France, at the BM05 beamline. Voxel resolution was 27 µm. The *Kawingasaurus* was analyzed using propagation phase contrast X-ray synchrotron micro-Computed Tomography (PPC-SRµCT). The beam setup included: (1) a white beam filtered through 10 mm of aluminium and 3 mm of copper, (2) a resulting total detected energy of 107 keV. The imaging details were as follows: (1) an indirect detector with a 750 µm thick LuAG scintillator was used, (2) the detector had 2x magnification using Hasselblad lenses, (3) it utilized a sCMOS PCO.edge 5.5 camera (from PCO, Kelheim, Germany) with a USB3 camera link, (4) the detector was positioned 2250 mm beyond the sample in the X-ray path for PPC-SRµCT, (5) the X-ray beam dimensions on the sample were 29.72 mm horizontally and 4.25 mm vertically. Due to the sample's size exceeding the field of view: (1) he rotation axis of the sample stage was first shifted by about 8 mm, following the half acquisition protocol by Carlson et al (2011). This produced tomograms measuring 45.63 mm in diameter (or 3441 pixels). Next, 20 acquisitions were made, moving the specimen 2.12 mm vertically each time. This created a 50% overlap between consecutive datasets. Each acquisition had 8000 projections, each lasting 40 milliseconds. This high number of projections compensated for camera noise since frame averaging was not available then. For the white field image (beam image without a sample), 101 images were taken and a median image was produced. For the darkfield (capturing camera noise without

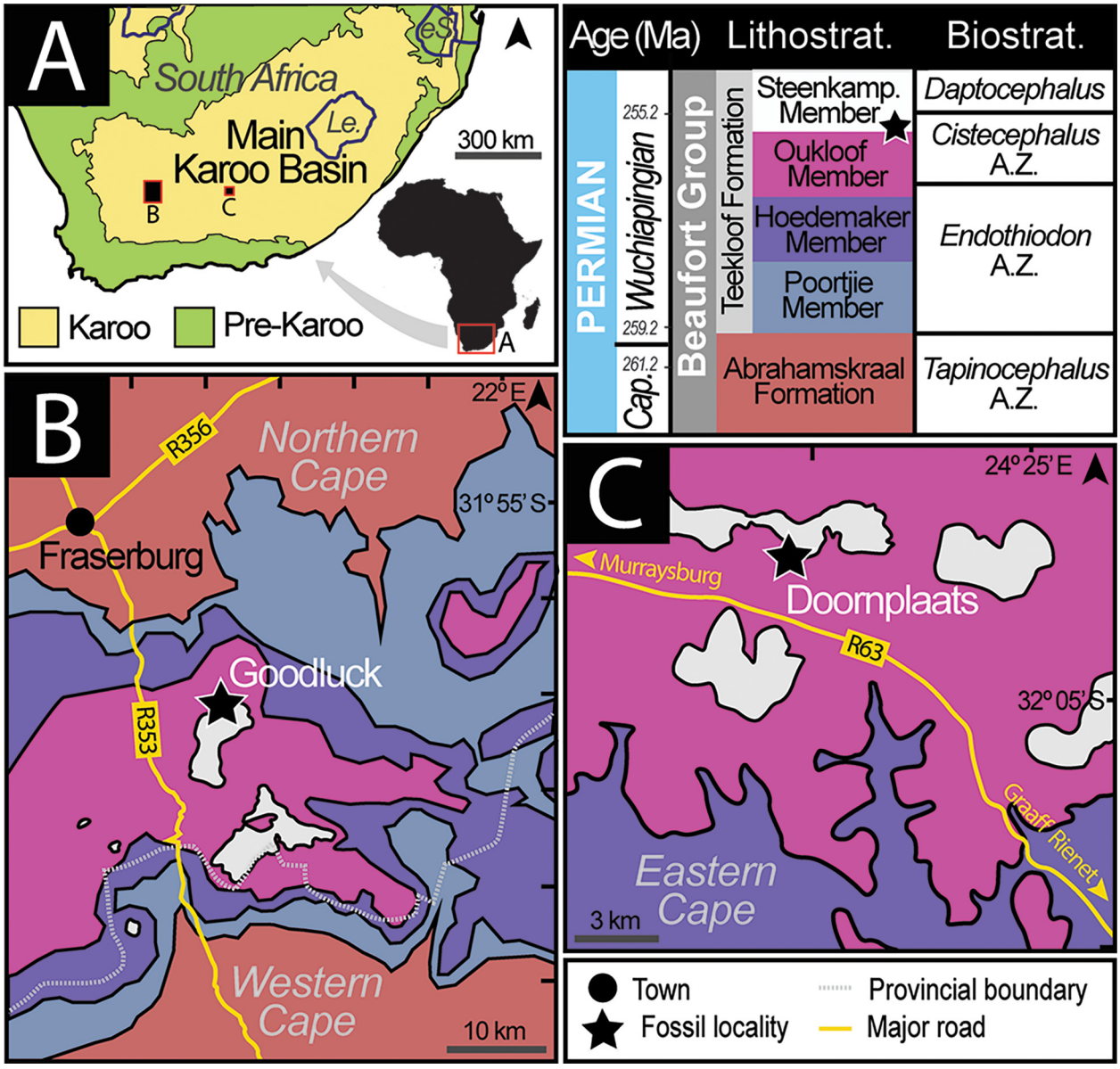

FIGURE 3. (A) Simplified stratigraphic context and geological map indicating the location of the study areas (insets B and C) within the Main Karoo Basin, South Africa. Detailed geological maps of the (B) Good Luck and (C) Doornplaats fossil localities indicating where *Cistecephalus microrhinus* specimens were collected. Specimen SAM-PK-K6814 was collected from Good Luck and specimen SAM-PK-K011474 was collected from Doornplaats. Both specimens were found in the lower Steenkampsvlakte Member (upper *Cistecephalus* Assemblage Zone). Abbreviations: Cap. = Capitanian, Steenkamp. = Steenkampsvlakte Member, A.Z. = Assemblage Zone. Lithostrat. = Lithostratigraphy. Biostrat. = Biostratigraphy.

the beam), 40 images were averaged. The tomographic reconstruction process involved: (1) using PyHST2 (as per Mirone et al. 2014) with the single distance phase retrieval method (Paganin et al. 2002), (2) setting the δ/β parameter to balance noise reduction and avoid blurring, (3) other steps included adjusting the bit depth from 32 to 16 bits based on the 3D histogram by PyHST2, applying ring correction as per Lyckegaard et al 2011, and cropping the volume, (4) lastly, a 2x2x2 binning was done to enhance the signal-to-noise ratio and minimize data size for segmentation.

Phylogenetic analysis

The phylogenetic analysis reflects the new additions and revisions of the most recent analyses of dicynodonts, namely

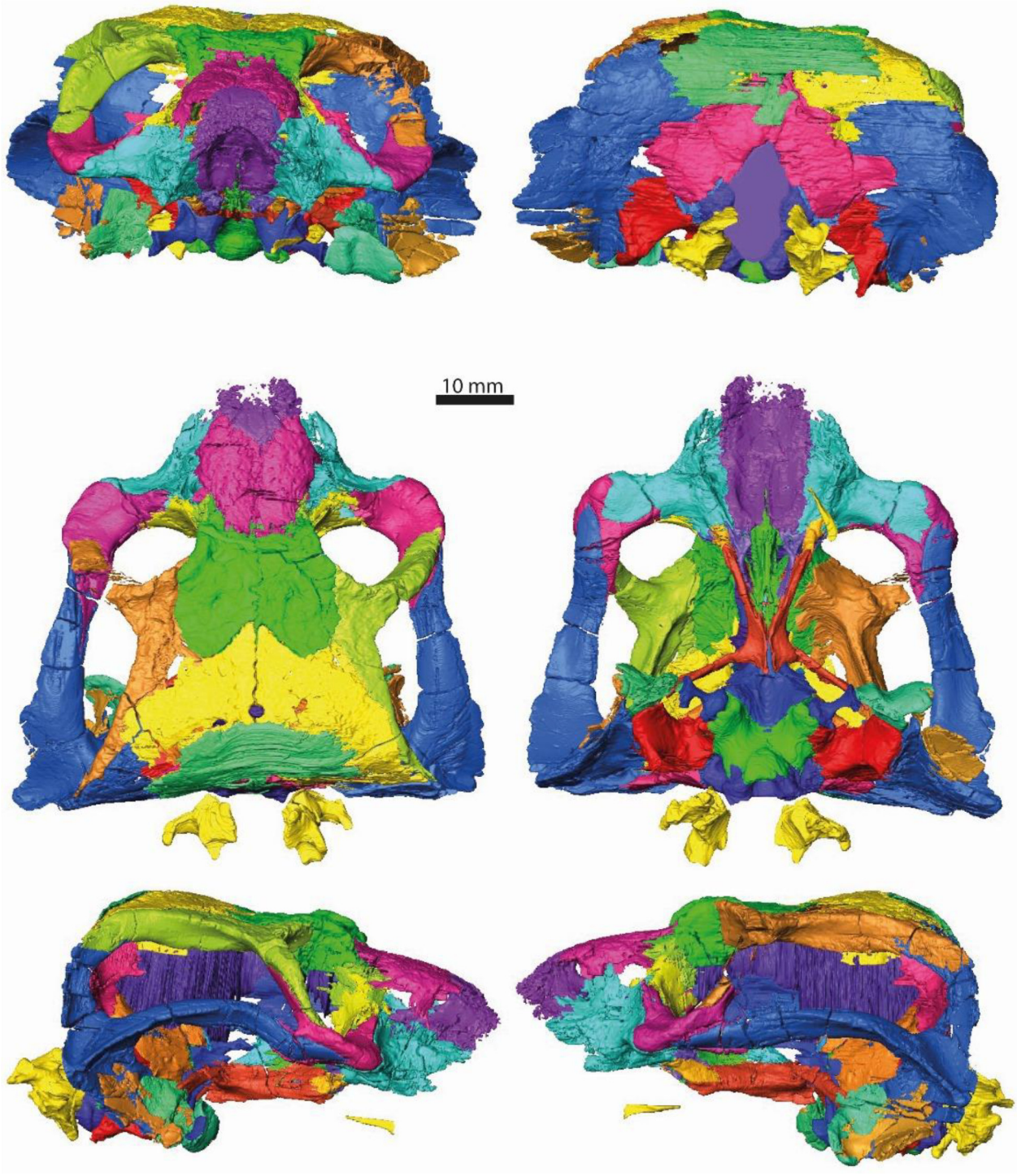

FIGURE 4. Segmentated three-dimensional rendering of *Cistecephalus microrhinus* (SAM-PK-K6814) in anterior, posterior, dorsal, ventral, right lateral and left lateral views.

from Kammerer & Ordoñez (2021), Angielczyk et al. (2021), Liu (2021, 2022), Araújo et al. (2022b), Macungo et al. (2022), Shi & Liu (2023), Szczygielski & Sulej (2023), Escobar et al. (2023) and Angielczyk et al. (2023). We also added some Mozambican specimens that will be described in detail elsewhere (PPM2019-38Z, PPM2019-106R, PPM2019-46R and PPM2019-96R).

We added 10 new discrete characters to the 190 characters

proposed by Macungo et al. (2022), resulting in 200 discrete characters and 23 continuous characters. Some of these characters cannot be visualized without micro-computed tomography (e.g., characters 193-195), but they represent an initial effort to incorporate observed interspecific variation.

Character 191: The mean position of the transverse axis of the frontal margin is far from the ascending process of the premaxilla (0), closely approaches the ascending process of the premaxilla (1). This character can be assessed, in most cases, by observing the external surface of the skull. Basal non-bidentalian and kannemeyeriform taxa have a small ascending process of the premaxilla (e.g., *Niassodon*), whereas - for instance - the geikiid *Bulbasaurus* has a long ascending process of the premaxilla such that it nearly touches the frontal (Kammerer & Smith 2017).

Character 192: Postorbital: The articular surface with the jugal located along the posterior aspect of the descending process of the postorbital (0), the articular surface with the jugal located medially (1). This character can be assessed by observing the postorbital bar. It may represent the structural importance of the jugal dorsal process in lieu of the postorbital descending process, and vice-versa. Whereas in some taxa the descending process of the postorbital completely obscures the postorbital (e.g., *Diictodon*, see Supplementary Information), in others the dorsal process of the jugal is well-exposed posteriorly (e.g., *Cistecephalus*).

Character 193: Mesethmoid: Horizontal plate present (0), horizontal plate absent (1). Macungo et al. (2022) observed a horizontal plate on the anterodorsal section of the orbito-sphenoid in their segmented specimens *Myosaurus* and *Pristerodon*, whereas this plate is absent in *Diictodon* (Supplementary Information). For more information, on the homologies of the ethmoid, or 'anterior plate' (Cluver 1971), please refer to the description of the ethmoid below.

Character 194: Mesethmoid: Dorsal fossa present (0), dorsal fossa absent (1). The horizontal plate dorsal fossa is clearly defined in *Myosaurus*, whereas *Pristerodon* does not have any depression on its dorsal surface (Macungo et al. 2022).

Character 195: Presphenoid: The vertical process is far from reaching the palate (0), the vertical process reaches the palate or nearly touches it (1). This condition can be assessed only by micro-computed tomography or serially-ground sections. The character states differentiate between morphologies observed in *Myosaurus* and *Diictodon* (Supplementary Information, Macungo et al. 2022), in which the orbitosphenoid does not contact any palatal element (Macungo et al. 2022), and *Cistecephalus* where the orbitosphenoid nearly contacts the parasphenoid.

Character 196: Quadrate: lateral condyle shorter medio-laterally or similar in size relative to the medial condyle (0), lateral condyle significantly longer than the medial condyle (1). This condition can be assessed by observing the ventral surface of the skull. Whereas *Eosimops* has the lateral condyle significantly longer than the medial condyle (Angielczyk et al. 2013), in *Cistecephaloides* the medial condyle is similar in size to the lateral condyle (Cluver 1974a).

Character 197: Quadrate: posterior quadrate crest absent (0), posterior quadrate crest present (1). This condition can be contrasted between *Niassodon*, which has a simple dorsal process of the quadrate, and *Ciscecephalus,* which has a small, anterolaterally-directed, infolding posteriorly (this paper).

Character 198: Quadrate: quadrate notch visible (i.e., at the intersection of the lateral condyle and dorsal plate there is a noticeable notch posteriorly) (1), quadrate notch not visible (0). Whereas in basal anomodonts (e.g., *Patranomodon*) this region of the quadrate is straight, in *Cistecephalus* (this paper), for instance, it has an obvious recess.

Character 199: Quadratojugal twisted (1), quadratojugal does not twist (0). These character states can be contrasted between *Niassodon*, in which the quadratojugal twists counterclockwise (Castanhinha et al. 2013), and *Cistecephalus* where the quadratojugal is flat (this paper).

Character 200: Supraoccipital transverse crest present (1), supraoccipital transverse crest absent (0). The supraoccipital transverse crest can be seen on the anterior surface of the bone, thus, it can only be seen using micro-computed tomography scanning. This condition can be contrasted between *Niassodon* and *Cistecephalus* (Castanhinha et al. 2013, this paper), which do not possess this crest, and *K. yajuwayeyi*, which has a horizontal crest arising from the median section of the supraoccipital (Araújo et al. 2022b).

We also revised some character codings to reflect our observations. Discrete Character 22 was rescored as polymorphic for *Dicynodontoides* because some specimens possess a tusk and others possess only an edentulous caniniform process (e.g., NHCC LB117). Similarly, *Prosictodon* (e.g. BP/1/7190), *Diictodon*, *Brachyprosopus*, *Pristerodon*, *Abajudon*, *Tropidostoma*, *Australobarbarus*, *Odontocyclops*, and *Emydops* spp. were coded as polymorphic for Discrete Character 22

because tusked and tuskless adult specimens are known for these taxa. The original codings for *Compsodon* and *Colobodectes* were kept because ontogeny should be avoided as a confounding factor when assessing the presence of tusks in the data matrix (Angielczyk and Rubidge 2009, Angielczyk et al. 2023). The situation for *Robertia* and *Digalodon* is uncertain because some specimens are badly preserved in this region (Angielczyk & Rubidge 2013, Kammerer et al. 2015), and the original codings was left unchanged.

We changed Discrete Character 51 to '?' for *Rastodon* because the holotype appears to be dorsoventrally compressed, making the original orientation of the postorbital uncertain. The morphology of the temporal portion of the postorbital in *Dicynodontoides* is difficult to accommodate in the current character-state scheme as the postorbital is sub-vertical medially and then curves towards a more horizontal position laterally, with some variation in the extent of this shape changing between specimens. Therefore, we coded this character as polymorphic (i.e., [0,1]) to accommodate this variability, but we note that is will be important to clearly tackle this issue at the specimen level in the future as part of on-going revisions to the species taxonomy of *Dicynodontoides*.

For Discrete Character 66, *Rastodon* was rescored as '?' as the area for the sutural contact of the maxilla and squamosal is badly damaged.

We changed Discrete Character 72 for *Rastodon* from '1' to '0' because the mid-ventral plate of vomers does not show a notable expanded area posterior to the junction with premaxilla, just as in *Dicynodontoides*. We also changed Discrete Character 73 for *Rastodon* from '1' to '0', because the mid-ventral plate of vomers is relatively wide in ventral view, as in *Dicynodontoides*. However, for Discrete Character 72 and 73 a segmentation of this part of the skull in *Rastodon* would help to be more confident in these character state codings.

We changed Discrete Character 91 for *Rastodon* to '?' as the surface of the anterior region of the pterygoids is poorly preserved.

We changed Discrete Character 112 for *Rastodon* and *Dicynodontoides* to '1' (i.e., presence of a lateral edge of paroccipital process drawn into sharp posteriorly-directed process that is distinctly offset from the surface of the occipital plate), because despite being damaged in some specimens (e.g., UNI-PAMPA 317, NHCC LB117) the base of the 'tympanic process' is still visible.

We recoded Discrete Character 114 for *Rastodon* as '?' because it is not clear whether the mandibular fenestra is present from available data (Boos et al. 2016, Simão-Oliveira et al. 2020).

We also changed Discrete Character 128 for *Rastodon* to '1' because a groove is visible on the anterodorsal edge of the lateral dentary shelf.

We recoded Discrete Character 183 for *Rastodon* to '?' because the posterior surface of the supraoccipital is poorly preserved.

We were able to observe in some micro-computed data and specimens of *Dicynodontoides* that the pilaantotica is narrow and rod-like, which led us to code Discrete Character 185 as '1'. Also, we recoded Discrete Character 190 for *Dicynodontoides* as '1' because the full extent of the exoccipital is visible in NHCC LB117, showing that it reached approximately half the height of the foramen magnum.

We analyzed two versions of the data matrix, one with *Kunpania* and another excluding it, using TNT 1.5 June 2021 version with no taxon limit for Windows (Goloboff & Catalano, 2016). Discrete-state characters 58, 61, 79, 140, 150, 151 and 166 were ordered. The analysis used the 'new technology search' algorithms to find the most parsimonious trees. Once the shortest tree length was hit 20 independent times using 'xmult' plus ten cycles of tree-drifting cycles (Goloboff, 1999), the strict consensus tree was drawn by collapsing the tree using tree bisection-reconnection and respective node supports. Synapomorphies common to the one most parsimonious tree are shown in the Supplementary Information. Absolute and relative Bremer supports were calculated for the nodes using tree bisection-reconnection by swapping the trees (Bremer, 1994; Goloboff & Farris, 2001). We also used resampling to assess node support, which was calculated by doing 10000 replications of symmetric resampling (Goloboff et al., 2003), analyzing each data set with a single random addition sequence plus tree bisection-reconnection and then collapsing the resulting tree (Goloboff & Farris, 2001). The phylogenetic matrix with named discrete characters which can be opened in Mesquite and the matrix with continuous and discrete characters which can be run in TNT, as well as the complete retrieved phylogenetic tree, with Bremer support and resampling values can be downloaded from the Morphobank project # 4895.

Node calibration and last appearance datum for *Cistecephalus*

Node calibration is necessary to attribute the appropriate branch lengths (in Ma) to the trees to calculate the thermo-motility indices for *Cistecephalus*. The oldest well-documented cistecephalid is *Cistecephalus microrhinus*, which first appears in the upper *Tropidostoma-Gorgonops* Subzone of the *Endothiodon* Assemblage Zone of the Karoo Basin (Day & Smith 2020). This assemblage zone is bracketed by radiometric dates of 259.26 Mya and 256.25 Mya (Day et al. 2015). The undescribed Mid-Zambezi Basin cistecephalid (see Angielczyk et al. 2019) may be older, but its age is very poorly constrained (Barbolini et al. 2016). Therefore, we calibrate this node at 259.26 Mya. The last appearance datum for *Cistecephalus microrhinus* is at the top of the *Cistecephalus* Assemblage Zone, which has been radiometrically dated at 255.2 Mya (Smith 2020 and references therein).

RESULTS

Thermo-motility indices

Following the methods described in Araújo et al. (2022a), we computed the thermo-motility index of *Cistecephalus* and obtained a value of 1.18, corresponding to an endothermy probability of 47%, which is interpreted as ambiguous. Additionally, we combined our *Cistecephalus* data with previously published data for *Kembawacela* (48%) and *Kawingasaurus* (27%, Araújo et al. 2022), and obtained endothermy probabilities of 23 and 40%, respectively, at the node (*Cistecephalus*, *Kawingasaurus*, *Kembawacela*) and for the average of these species. These values are lower than 47%, which has been shown to be the threshold below which ectothermy can be interpreted with more than 95% accuracy in extant species (Araújo et al. 2022a). Taken together, these values are lower than 47%, which has been shown to be the threshold below which ectothermy can be interpreted with more than 95% accuracy in extant species (Araújo et al. 2022a).

Semicircular canal orientations

Applying equations of semicircular duct biomechanics to landmark sets placed along each semicircular canal torus, including the utricular parts, we were able to measure functional semicircular canal plane orientations in *Kawingasaurus* and *Cistecephalus* (Fig. 11). Results are presented in Table 1, along with 95% confidence intervals for angular values observed across 57 amniote species.

Cistecephalus falls within 95% C.I. for extant amniote variation for all angles. *Kawingasaurus* falls within 95% C.I. for extant amniote variation for most angles, except for the angles between the anterior and posterior semicircular canals, and the angles the anterior and posterior semicircular canals form with the horizontal plane.

COMPARATIVE ANATOMICAL DESCRIPTION

Keyser's (1965, 1973) provided the most recent detailed description of *Cistecephalus*, including information from serially-sectioned specimens. However, these works focused on the contacts between bones and omitted various details, particularly when full three-dimensional views of the bone or anatomical structure were required. Our comparative description utilizes μCT data to update and expand on Keyer's important contribution.

Skull

Premaxilla

Despite being at a right angle in relation to the antero-posterior axis of the skull at its base (Keyser 1965), the ascending process of the premaxilla (appmx, median spine of the premaxilla; "median spine" of Keyser 1965) deflects abruptly posteriorly at its midheight. The ascending process

TABLE 1. Semicircular canal angular relationships

	A^P	A^L	L^P	A^S	A^C	A^H	P^S	P^C	P^H	L^S	L^C	L^H
Kawingasaurus	82	76	82	40	51	81	42	52	76	82	90	8
Cistecephalus	87	85	82	41	49	89	47	44	83	88	90	4
Amniote 95C.I.	86:105	73:94	82:99	32:50	41:58	85:106	34:54	37:56	80:97	78:99	90	-3:11

Angles in degrees. A: Anterior semicircular canal, P: Posterior semicircular canal, L: Lateral semicircular canal, S: Sagittal plane, C: Coronal plane, H: Horizontal plane, ^: Angle between.

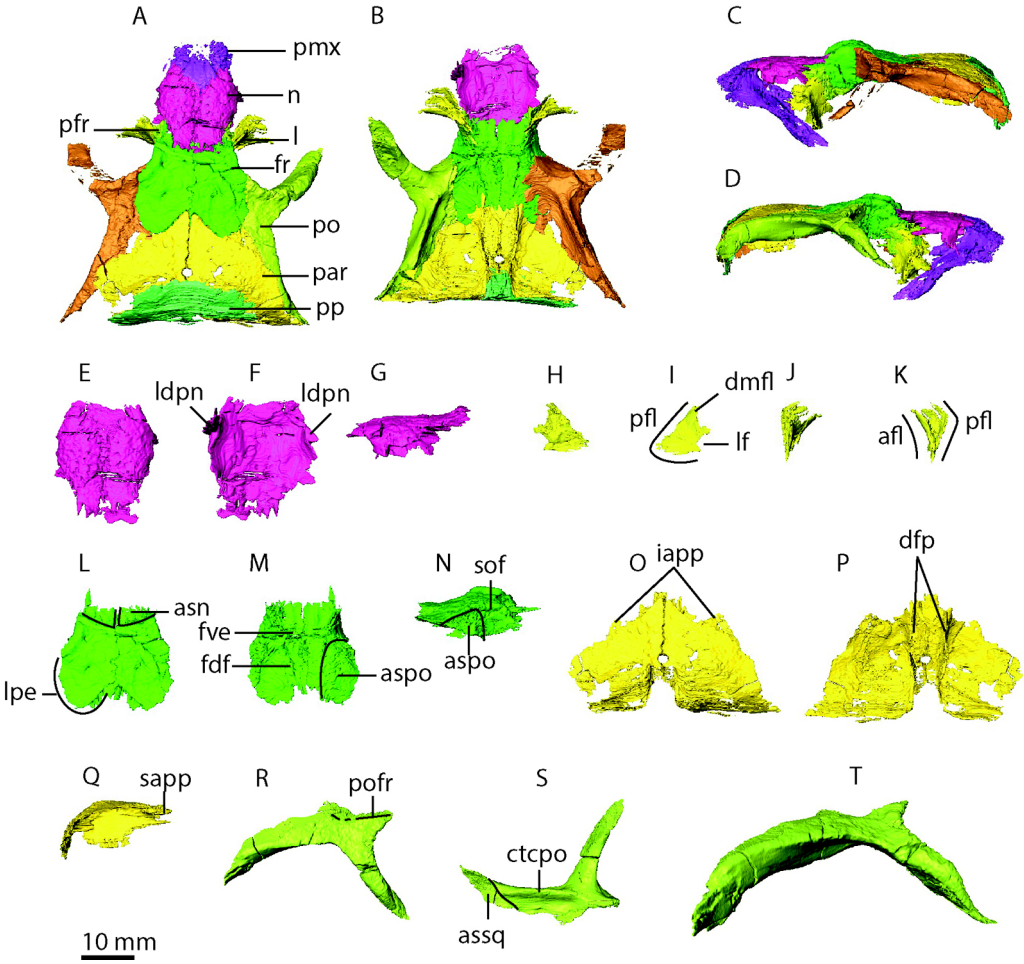

FIGURE 5. Skull roof of SAM-PK-K6814. A, dorsal view of the skull roof; B, ventral view of the skull roof; C, left lateral view of the skull roof; D, right lateral view of the skull roof; E, dorsal view of the nasals; F, ventral view of the nasals; G, lateral view of the nasals; H, anterior view of the left lacrimal; I, posterior view of the left lacrimal; J, dorsal view of the right lacrimal; K, ventral view of the right lacrimal. Abbreviations: afl, anterior flange of the lacrimal; asn, articular surface of the nasal; aspo, articular surface of the postorbitals; assq, articular surface of the squamosal; ctcpo, crest of the temporal component of the postorbital; dfp, descending flanges of the parietal; dmfl, dorsomedial foramen of the lacrimal; fdf, frontal descending flanges; fr, frontals; fve, frontal ventral excavations; iapp, internal anterior process of the parietal; n, nasals; l, lacrimal; ldpn, lateral descending process of the nasal; lf, lacrimal foramen; lpe, lobate posterior extension of the frontal; par, parietal; pfr, prefrontals; pfl, posterior flange of the lacrimal; pmx, premaxilla; po, postorbital; pofr, postorbital-frontal ridge; pp, postparietal; sapp, short anterior projections of the parietal; sof, supraorbital ridges of the frontal.

does not extend far between the nasals, and it tapers to a broad subtriangular apex, unlike the significantly more acute apex of *Compsodon* (Angielczyk and Kammerer 2017). The ascending process of the premaxilla clasps the anteriormost process of the nasal, becoming exposed dorsally. There are various nutritive foramina on the dorsal surface of the ascending process that continue posteriorly as furrows that are likely associated with the presence of a keratinous rhamphotheca (Benoit et al. 2018). As in *K. kitchingi* (Angielczyk et al. 2019), the frontal does not closely approach the ascending process of the premaxilla and there is no longitudinal ridge on its anterior surface.

The palatal surface of the maxilla is cupped and the premaxilla forms most of the secondary palate. As *Kembawacela kitchingi* (Angielczyk et al. 2019), the cutting edge of the premaxilla is badly preserved in SAM-PK-K6814, but it seems to have formed a thin, narrow anterior edge (not a downturned rim as most dicynodonts). In *K. kitchingi* the cutting edge of the premaxilla is arched in anterior view, with the palatal rim having a more anteriorly-facing edge, in

Cistecephalus it has a more ventrally-facing cutting edge. Although Keyser (1965, 1973) describes a squared ridge on the ventral surface of the premaxillaries, it is rather a bifurcating ridge that smoothly opens into a slit from about midlength in SAM-PK-K6814 (pmrpmx, posterior median ridge of the premaxilla, Fig. 6). However, it is important to note that this morphology for *Cistecephalus* is unusual, and could be either the true morphology or the result of slight taphonomic displacement. The two small foramina on the anterior part of the palate observed in SAM-PK-K150 by Keyser (1965, 1973) were not observed in SAM-PK-K011474 and SAM-PK-K6814. Unfortunately, it is not possible to confirm this character by physical inspection of the specimens because the anterior part of the palate is not visible in either specimen as it is covered in matrix. However, physical inspection of other specimens (e.g., SAM-PK-K11187) reveals the presence of these foramina. As mentioned by Keyser (1965), the premaxillae form the small medial portion of the anterior border of the choanae (cho, Fig. 6), and laterally is the articular surface for the palatine (aspal, Fig. 6). There is a posterior median palatal ridge (pmrpmx, Fig. 6), no anterior median palatal ridges but lateral palatal ridges are present (lpr, Fig. 6). The lateral palatal ridges border the premaxilla laterally and are significantly thicker than the posterior median palatal ridge. Between the lateral anterior palatal ridges, the surface of the secondary palate is deeply domed, similar to the morphology present in *Compsodon* (Angielczyk and Kammerer, 2017). As in other dicynodonts (e.g., *K. kitchingi*, *Compsodon*), the lateral palatal ridge marks the border with the maxilla. The posterior median palatal ridge can be regarded as the ventral thickening of the nasal septum. Specifically, the ridge is formed by the portion of the premaxilla that covers the vomerine septum in this region of the secondary palate. Unlike *Compsodon*, the height of the median palatal ridge is constant anteroposteriorly. As in *Kembawacela* (Angielczyk et al. 2019, Araújo et al. 2022b), there is an oval depression (odpmx, Fig. 6) between the lateral ridge and the posterior median palatal ridge. This depression is an elongated ellipse (groove-like depressions according to Angielczyk & Kammerer 2017) in *Compsodon*.

Unlike *K. kitchingi* in which the premaxilla forms the anterior and dorsal margin of the external nares (Angielczyk et al. 2019), in *Cistecephalus* the premaxilla only forms the anterior margin, whereas the dorsal margin is entirely formed by the nasal. The short nasal septum, "internasal septum" following Keyser's (1965, 1973) nomenclature, is formed by a single crest anteriorly, that diverges into two posteriorly pointing processes (ppns, pointed processes of the nasal septum), which then slope ventrally to form two subparallel low crests for the remaining half of the premaxilla (lcns, low crests of the nasal septum).There are also two short crests, that terminate in short pointed processes unsupported by the palatal surface of the premaxilla, that run parallel to the nasal septum and are separated by a shallow concavity (pscns, parallel short crests of the nasal septum).

Septomaxilla

The septomaxilla is not observable in the segmented specimens (SAM-PK-K011474 and SAM-PK-K6814). Despite the excellent quality of the scan and contrast between rock matrix and bone, the septomaxilla does not seem to be preserved in the specimen, apparently due to erosion. However, if preserved, along the posterior border of the external nares, it is indistinguishable in the trabecular structure with the surrounding bone, hence, extremely co-ossified and remodeled. It is important to note that the broad, recurved base of the premaxilla ascending process visible near the anterior border of the external nares could be confounded with the septomaxilla.

Maxilla

The maxilla is formed by the posterolateral ramus (plrmx, Fig. 6), the palatal component (pcmx, Fig. 6) and the facial component (fcpmx, Fig. 6). The posterolateral ramus is broad anteroposteriorly, in contrast to *K. kitchingi* (Angielczyk et al. 2019). There is a double embayment on the ventral aspect of the palatal component of the maxilla (demx, Fig. 6). The anterior embayment is anterior to the caniniform process, as seen in many emydopoids, whereas the more incipient posterior embayment is aligned with and slightly posterior to the caniniform process. On the ventral side of the posterolateral ramus, there is a round fossa (rfmx, Fig. 6) pierced by a small foramen at the intersection with the facial component of the maxilla, an autapomorphy of *Cistecephalus*. The angle formed by the lateral border of the facial component of the maxilla and the anterior border of the posterolateral ramus is slightly obtuse. The postcaniniform keel is laterally convex. A secondary lateral crest forms forms a horizontal slot joint with the suture with the premaxilla (lcmx, Fig. 6), and represents the maxillary contribution to the palatal rim. On its dorsal surface the maxilla forms the median and ventral

walls of the maxillary antrum, as well as part of the anteromedial wall. The triradiate crest dividing the maxillary antrum and the nasal cavity on the dorsal side of the maxilla is here referred to as the dorsal vertical crest of the maxilla (dvcmx, Fig. 6). Keyser (1965, 1973) mentioned a groove near the dorsal vertical crest, but its exact location is not clear from his description. At the intersection between the secondary crest and dorsal vertical crest of the maxilla in SAM-PK-6814 there is a well-delimited groove on the dorsal floor of the maxilla lateral to the crest. This crest continues into a canal anteriorly, forming part of the cast of the infraorbital/maxillary canal [see Keyser (1965, 1973) description]. This canal exits on the facial side of the maxilla. It seems that Keyser (1965, 1973) misinterpreted the labial fossa as the posterior opening of the maxillary antrum. Indeed, the maxillary antrum is not exposed ventrally, being surrounded by the maxilla and lacrimal only. The labial fossa as described by Ewer (1961) and Cluver & King (1983), being surrounded by the palatine, jugal and maxilla is not present.

Nasal

Expanding on Keyser's (1965, 1973) description, we note that the anterior portion of the nasals is overlapped by the premaxilla (i.e., there is an internal continuation of the nasals that extends anteriorly beyond their anterior edge on the external surface of the skull roof). Likewise, there is a posterior extension of the nasals that overlaps the frontals. Indeed, both the nasal and the frontal have expanded sutural surfaces such that the two bones interlock. The frontal underplates the nasal medially, whereas the nasal is under the frontal more laterally. The ventral surface of the nasal is flat, except laterally where it forms a short descending irregularly-shaped descending process (ldpn, lateral descending process of the nasal, Fig. 5). As typical for other dicynodonts, the nasals are covered in minute foramina on their dorsal surface.

Prefrontal

The prefrontal-lacrimal-maxilla-jugal region of the skull is particularly complex as several bones intersect with inter-digitating sutures, making clear segmentation of the elements difficult. Nevertheless, segmentation in both specimens (SAM-PK-6814 and SAM-PK-K011474) resulted in similar morphology. In dorsal view, the prefrontal is a simple subtriangular, plate-like bone with a somewhat hyperbolic shape. The dorsal half is thicker than the ventral half and most of the prefrontal is covered by the lacrimal. Medial to the orbital exposure of the lacrimal, the prefrontal forms a small part of the orbital wall lateral to the frontal contribution. The dorsal exposure of the prefrontal is minimal, making it easy to confuse with surrounding bones in less well-preserved specimens.

Lacrimal

The lacrimal is composed of a short anterior flange (afl, Fig. 5) and the larger posterior flange (pfl, Fig. 5) that forms part of the anterior margin of the orbit. The anterior and posterior flanges are united dorsally. Our segmentation indicates that the lacrimal is contacted by the jugal laterally, but not ventrally (as mentioned by Keyser 1965, 1973). The maxilla forms the entire ventral floor of the lacrimal. As segmented, our assessment also differs from Keyser's on account of the lack of contact between the lacrimal and the nasal/frontal. The lacrimal nearly touches the frontal, but it is separated by the thin prefrontal. However, this contact is seen in other specimens (e.g., BSP 1932-I-502, BPS 1932-I-56). The lacrimal converges posteriorly with medial borders of the palatal component of the maxilla. In addition to the lacrimal foramen, there is a small foramen in the dorsomedial corner of the lacrimal (dmfl, Fig. 5). Keyser (1965, 1973) describes most important information about the lacrimal foramen (lf, Fig. 5). Our main new observations are that the lacrimal foramen connects to the maxillary antrum internally and is located on the ventromedial corner of the bone, forming a semicircular notch.

Jugal

The jugal is formed by three anatomical subunits: the 'anterior' process ('a'pj, Fig. 8), the posteroventral process (pvpj) and the ascending process (aspj). The ascending process is lanceolate, the posteroventral process is subtriangular, and the 'anterior' process is semilunate and is one of the most distinguishing features of *Cistecephalus*. Indeed, the 'anterior' process is a medial deflection from the conjunction of the posteroventral and ascending processes, such that it does not develop anteriorly, but rather medially. This condition is distinct from *Kembawacela* sp. (Angielczyk et al. 2019, Araújo et al. 2022b) because the foot-like anterior process develops anteriorly and smoothly turns medially. In *Cistecephalus*, the 'anterior' process sharply turns medially, and this inflection contributes to the frontation of the orbits

especially in larger specimens. It also differs from *Compsodon*, *Digalodon* or *Emydops* (Fröbisch & Reisz 2008, Kammerer et al. 2015, Angielczyk & Kammerer 2017) where there is little lateral exposure of the anterior process of the jugal, which instead mostly forms the floor of the mostly orbit. The 'anterior' process is thickened along its anteriormost border. Anteromedially, the jugal forms the lateral and most of the anterior wall of the maxillary antrum (medial jugal excavation; mje). The ascending process is oriented posteriorly when compared to other cistecephalid taxa, with the jugal notch (jn, Fig. 8) forming a rounded acute angle (~60º) between the ascending process and the posteroventral process. The articular surface with the squamosal (assq, Fig. 8) on the posteroventral process is lanceolate.

Frontal

The midfrontal suture is highly interdigitated with complex corrugations along its anteroposterior length. Similarly, the articular surface of the nasal (asn, Fig. 5) leaves a subtriangular imprint on the dorsal surface of the frontal, as segmented, but the contact between the two bones is highly interdigitated as described by Kammerer (2021). The orbital surface of the frontal is concave. The anterior third of the lateral surface of the frontal contributed to the orbit and is ornamented by the supraorbital ridges of the frontal dorsally (sof, Fig. 5), whereas the posterior two-thirds form the lateral contact with the postorbital. Keyser (1973) offered little insight on the nature of the frontal-postorbital suture, referring to an "uneven suture". At the midlength of the frontal part of the supraorbital ridge, the postorbital interdigitates with the frontal leaving a subtriangular articular surface when viewed from the lateral side (aspo, Fig. 5). However, the lobate posterior extension of the frontal (lpe, Fig. 5) overlaps a significant portion of the anteromedial portion of the postorbital in a tight interdigitating suture. More medially, the ventral surface of the frontals is marked by the posteriorly-converging descending flanges (fdf, frontal descending flanges, Fig. 5) that continue onto the parietal. Medial to the descending flanges the frontals are excavated ventrally to form the dorsal enclosure of the olfactory tract (fve, frontal ventral excavations, Fig. 5), which becomes shallower posteriorly. The sutural contact between the frontal and prefrontal is consistent in general shape, yet difficult to precisely delineate due to co-ossification, in both specimens (SAM-PK-K011474 and SAM-PK-K6814) resulting in some asymmetry. The anteroventral corner of the frontal interdigitates and co-ossifies in some places with the posterior and dorsal borders of the prefrontal.

Postfrontal

A distinct postfrontal could not be identified. Similar to the situation in *K. kitchingi* (see below), it is not clear whether a primordial postfrontal ossification center fuses with the postorbital early in ontogeny, or if the element is deleted completely.

Parietal

Keyser (1965, 1973) described the parietal as being shaped like a right-angled triangle. However, its shape is rather chevron-like with the anterior border having a short projection near the midline of the skull (sapp, short anterior projections of the parietal, Fig. 5). Lateral to the short anterior projections there is an internal anterior process (iapp, Fig. 5) near the junction between the frontal, postorbital and parietal. The contact with the frontals is interdigitating medially, but becomes a simple butt joint laterally. Posteriorly, the parietals are overlapped by the postparietal, such that the parietals develop a deep central invagination in their posterior margin that accepts an anterior process of the postparietal. In ventral view, the descending flanges of the parietals (dfp, Fig. 5) are convex laterally and extend the entire length of the elements. The descending flanges arise from the near-vertical section of the parietal near the dorsal portion of the foramen magnum. Moving anteriorly, the descending flanges diverge and then smoothly curve medially to become subparallel. The canal passing though the parietals to form the pineal foramen is hourglass-shaped.

Postorbital

The postorbital is significantly better preserved in SAM-PK-K6814 when compared to the specimen examined by Keyser (1965, 1973), providing additional anatomical information. The postorbital receives the frontal dorsally forming a biconcave suture (see frontal description), delimited by a thin ridge (pofr, postorbital-frontal ridge, Fig. 5). The transition between the dorsal and ventral surfaces of the temporal component of the postorbital forms an acute crest (ctcpo, crest of the temporal component of the postorbital, Fig. 5), resulting in the bi-planar appearance typical of most emydopoids. Posteriorly, this crest along the temporal component of the

postorbital is faceted to produce a lanceolate articular surface for the squamosal (assq, Fig. 5) with the acute angle pointing anteriorly. As in *K. kitchingi*, the articular surface for the jugal is located on the posterior aspect of the descending process of the postorbital, unlike *K. yajuwayeyi* where it is on the medial surface (Discrete Character 192). The postorbital bulge, visible in ventral view, is a flat subtriangular projection anteriorly that continues as a straight ventral crest along the temporal component of the postorbital, similar to that observed in *K. yajuwayeyi* (Araújo et al. 2022b), in that it is a flat subtriangular region anteriorly that continues as a straight ventral crest along the temporal component of the postorbital.

Squamosal

The four anatomical subunits of the squamosal are: the zygomatic process (zpsq, Fig. 8), the dorsal process (dpsq, Fig. 8), the ventral process (vpsq, Fig. 8) and the lateral process (lpsq, Fig. 8). The zygomatic process bows dorsally, and its anteriormost tip sharply pointed. There is a strong lateral crest along the lateral aspect of the zygomatic process of the squamosal. At its anterior end, the cross-section of the zygomatic process is crescentic with the concavity pointing dorsomedially; at midlength it becomes an isosceles triangle, with the obtuse angle located dorsomedially; and near the lateral process it becomes aerofoil shaped with the trailing edge pointing laterally. The connection of the zygomatic process of the squamosal with the posterior region of the bone is made by the lateral process, which is subtriangular in posterior view.

The termination of the zygomatic process of the squamosal continues posteriorly as a vertical buttress along the anterior aspect of the dorsal process of the squamosal (avbdpsq, anterior vertical buttress of the dorsal process of the squamosal), which bends medially at its dorsal end. Medial to the vertical buttress there is a broad recess, somewhat ovoid, and delimited medially by the medial border of the dorsal process of the squamosal (mardpsq, medioanterior recess of the dorsal process of the squamosal). Lateral to the anterior vertical buttress, there is a subrectangular flange (lfdpsq, lateral flange of the dorsal process of the squamosal), which is significantly mediolaterally narrower than the medioanterior recess of the dorsal process of the squamosal. The dorsal process of the squamosal is subrectangular but with the dorsal portion bent medially, in posterior view. In lateral view, there is a conspicuous anterior deflection of the dorsal process of the squamosal.

Keyser (1965, 1973) described the quadrate recess (qr, Fig. 8) and the crests delimiting it, but there are various anatomical details that were missing in his description. The quadrate recess is oval, being laterally and medially delimited by the lateral and medial crest of the squamosal's quadrate recess (lcsqr, mcsqr Fig. 8), respectively. The lateral crest is vertically-oriented, straight, and thinner but more pronounced than the medial crest. The medial crest is dorsomedially convex and extends more dorsally than the lateral crest. The ventralmost border of the squamosal in the quadrate recess area terminates abruptly and this region is posteriorly convex. The tympanic process (*sensu* Cox, 1959) is entirely formed by the opisthotic (*contra* Keyser 1965, 1973).

Vomer

Keyser (1965, 1973) claimed that the vomers are paired, but we do not find any sutural markings internally. Importantly, the images that allegedly show the separation between the vomers either point to a coronal section without the vomer (fig. 17, Keyser 1973), or show only a single median bone with no suture visible (fig. 20, Keyser 1973). In the specimens described here (SAM-PK-K6814 and SAM-PK-K011474), the median anterior projection of the vomer fits in between the premaxilla, and there is no anterior separation with the bone. The cultriform process of the vomer (cpv, Fig. 6) is subtrapezoidal in lateral view, with the ventral border substantially thinner than the dorsal region. The ventral exposure of the vomer has subparallel crests that open and curve slightly posteriorly. The subtriangular mid-ventral vomerine plate (mvvp, Fig. 6) terminates posteriorly as two processes that form the ventral crests of the vomer (vcv, Fig. 6). In between the ventral crests of the vomer is the interpterygoid vacuity (iptv, Fig. 6), which, despite the name of the structure, is closed entirely by the cultriform process except for a small ventroposterior portion. This differs from *K. yajuwayeyi* where the vacuity seems to be mostly covered by the parasphenoid (Araújo et al. 2022b). Thus, the vestigial interpterygoid vacuity remains as a narrow cleft. Irrespective of the bones involved, the closure of the interpterygoid vacuity is a prevalent cistecephalid feature (Broili & Schröder 1935; Cox 1972; Keyser 1973; Cluver 1974a). On the dorsal aspect of the cultriform process of the vomer there are two dorsal crests that taper into acute

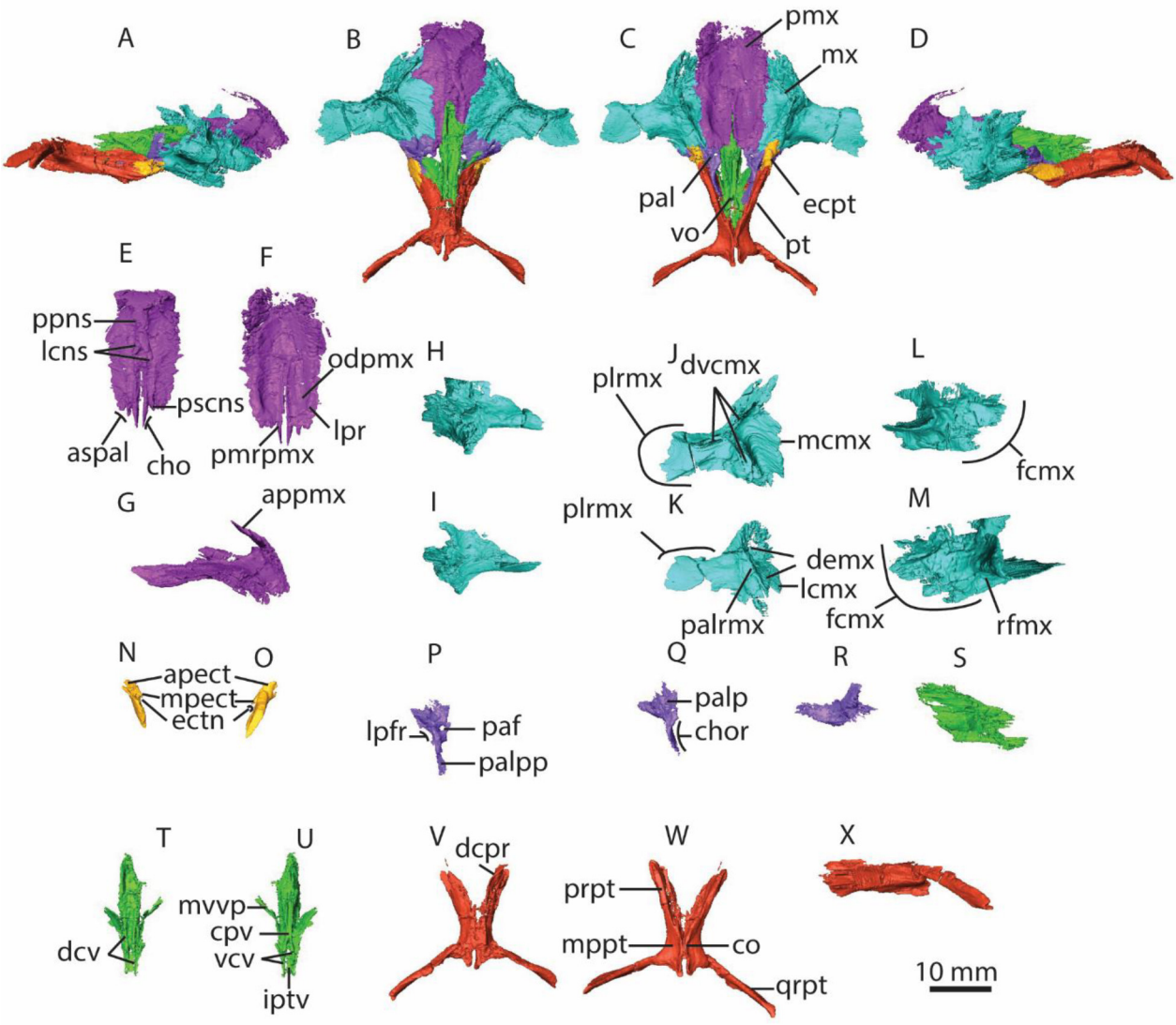

FIGURE 6. Palatal elements of SAM-PK-6814. A, right lateral view; B, dorsal view; C, ventral view; D, left lateral view; E, premaxilla in dorsal view; F, premaxilla in ventral view; G, premaxilla in lateral view; H, anterior view of the left maxilla; I, posterior view of the right maxilla; J, dorsal view of the right maxilla; K, ventral view of the right maxilla; L, lateral view of the left maxilla; M, lateral view of the left maxilla; N, left ectopterygoid in dorsal view; O, right ectopterygoid in dorsal view; P, left palatine in dorsal view; Q, right palatine in ventral view; R, right palatine in lateral view; S, vomer in lateral view; T, vomer in dorsal view; U, vomer in ventral view; V, pterygoid in dorsal view; W, pterygoid in ventral view; X, pterygoid in lateral view. Abbreviations: apect, anterior process of the ectopterygoid; appmx, median spine of the premaxilla; aspal, articular surface for the palatine; cho, choana; chor, choana recess; co, crista oesophagea; cpv, cultriform process of the vomer; dcpr, dorsal crest of the palatal ramus of the pterygoid; dcv, dorsal crests of the vomer; demx, double embayment of the palatal component of the maxilla; dvcmx, dorsal vertical crest of the maxilla; ecpt, ectopterygoid; ectn, ectopterygoid notch; fcmx, facial component of the maxilla;iptv, interpterygoid vacuity; lcmx, lateral crest of the maxilla; lcns, low crests of the nasal septum; lpr, lateral palatal ridges; lpfr, lateral palatal foramen recess; mcmx, medial crest of the maxilla; mpect, medial process of the ectopterygoid; mppt, median pterygoid plate; mvvp, mid-ventral vomerine plate; mx, maxilla; odpmx, oval depression of the premaxilla; paf, palatine foramen; pal, palatine; palp, palatine pad; palpp, palatine posterior process; palrmx, palatal rim of the maxilla; pmx, premaxilla; ppns, pointed processes of the nasal septum; plrmx, posterolateral ramus of the premaxilla; plrmx, posterolateral ramus of the maxilla; prpt, palatal ramus of the pterygoid; pscns, parallel short crests of the nasal septum; pt, pterygoid; qrpt, quadrate ramus of the pterygoid; rfmx, round fossa of the maxilla; vcv, ventral crests of the vomer; vo, vomer.

processes (dcv, Fig. 6), which resemble *K. yajuwayeyi* (Araújo et al. 2022b).

Palatine

The palatines do not extend beyond the choanae anteriorly (*contra* Keyser 1965), but terminate at the level of the choanae (chor, choanal recess of the palatine, Fig. 6). The ventral surface of the palatine pad (palp, Fig. 6) is smooth, lacking the rugosity seen in most bidentalians. The palatine foramen perforates the anterior portion of the palatine pad along an anteriorly-angled path. On the lateral aspect of the palatine between the pad-like anterior region and the posterior process there is a slight excavation to form the lateral palatal foramen (lpfr, lateral palatal foramen recess, Fig. 6), which is slit-like and easily distinguishable from the subcircular palatine foramen. The medial face of the palatine is concave and forms the walls of the choanae together with the vomer. The palatine posterior process forms a distinct crest (palpp, Fig. 6), unlike *Kembawacela* sp. (Angielczyk et al. 2019, Araújo et al. 2022b) where the palatine has a relatively flat posterior process.

Ectopterygoid

The ectopterygoid is rhomboidal in lateral view, and is mediolaterally as thick as the anteriormost portion of the palatal ramus of the pterygoid. There is a short anterior projection (apect, anterior process of the ectopterygoid; Fig. 6) overlapping the posteriormost portion of the palatal component of the maxilla. Along the anteroventral border of the ectopterygoid there is a short posteriorly-oriented medial process (mpect, medial process of the ectopterygoid) that has a notch posteriorly that forms the lateral wall of the palatal foramen (ectn, ectopterygoid notch).

Pterygoid

The pterygoid is formed by the palatal ramus anteriorly (prpt, Fig. 6), and the quadrate ramus posteriorly (qrpt, Fig. 6), which contact each other medially at the median pterygoid plate (mptp, Fig. 6). The palatal ramus is thinner ventrally than dorsally, and bows laterally in dorsal view, whereas in ventral view it is straight. The medial surfaces of the palatal rami suture dorsally with the mid-ventral vomerine plate along most of the latter's anteroposterior extension, and the dorsal half of the palatal ramus sutures with the palatine posterior process ventrally, approaching the median pterygoid plate. The mid-ventral vomerine plate is flush with the dorsal crest of the palatal ramus (dcpr, Fig. 6). There is no distinct ventral keel of the pterygoid as in *K. yajuwayeyi* (Araújo et al. 2022b).

The cristae oesophagea (co, Fig. 6) do not meet medially, forming a slit that closes more dorsally by the medial interdigitation of the pterygoids. The cristae slightly diverge anteriorly, nearly touch at midlength and then diverge slightly posteriorly again. The cristae are thicker posteriorly, and form blunt and short posterior processes, which are distinct from the acute posterior processes of *K. yajuwayeyi* (Araújo et al. 2022b). The cristae are also thicker ventrally forming a distinct rim from the lateral ala of the median pterygoid plate.

In posterior view, the ventral border between the quadrate ramus of the pterygoid and the median plate of the pterygoids is sigmoidal. In cross-section, the quadrate ramus is teardrop-shaped anteriorly with the apex pointed dorsally, and becomes reniform posteriorly, with the concavity oriented posteriorly throughout. Similar to *Myosaurus*, most of the parasphenoid rostrum forms an anteriorly projecting process that overhangs the pterygoids but it is not exposed ventrally as in *K. yajuwayeyi* (see Araújo et al. 2022b). The pterygoid suture with the basisphenoid slopes posteriorly and is co-ossified to some extent (Fig. 4), as in *K. kitchingi* (Angielczyk et al. 2019). Additionally, it is interesting to note that the anteriormost extension of the basisphenoid overhangs the dorsal surface of the pterygoids, without any contact.

Our observations differ from Keyser's (1965, 1973) description of the interpterygoid vacuity: "the two pterygoids approach one another closely, but are separated by a thin vertical plate extending ventrally from the basisphenoid, thus forming a rudimentary interpterygoid vacuity" (page 52, Keyser 1973). Furthermore, Keyser's Plate XVI does not pass through the interpterygoid vacuity. Our observations indicate that the interpterygoid vacuity is bordered posteriorly only by a small segment of the crista oesophagea. Predominantly, the vacuity is flanked by two gently diverging ventral crests of the vomer (see Vomer). Interestingly, there is a large canal passing through the pterygoids medially between the crista and dorsal contact between these bones.

Epipterygoid

In SAM-PK-6814 only a small sliver of the ascending ramus of the left epipterygoid is preserved. The right

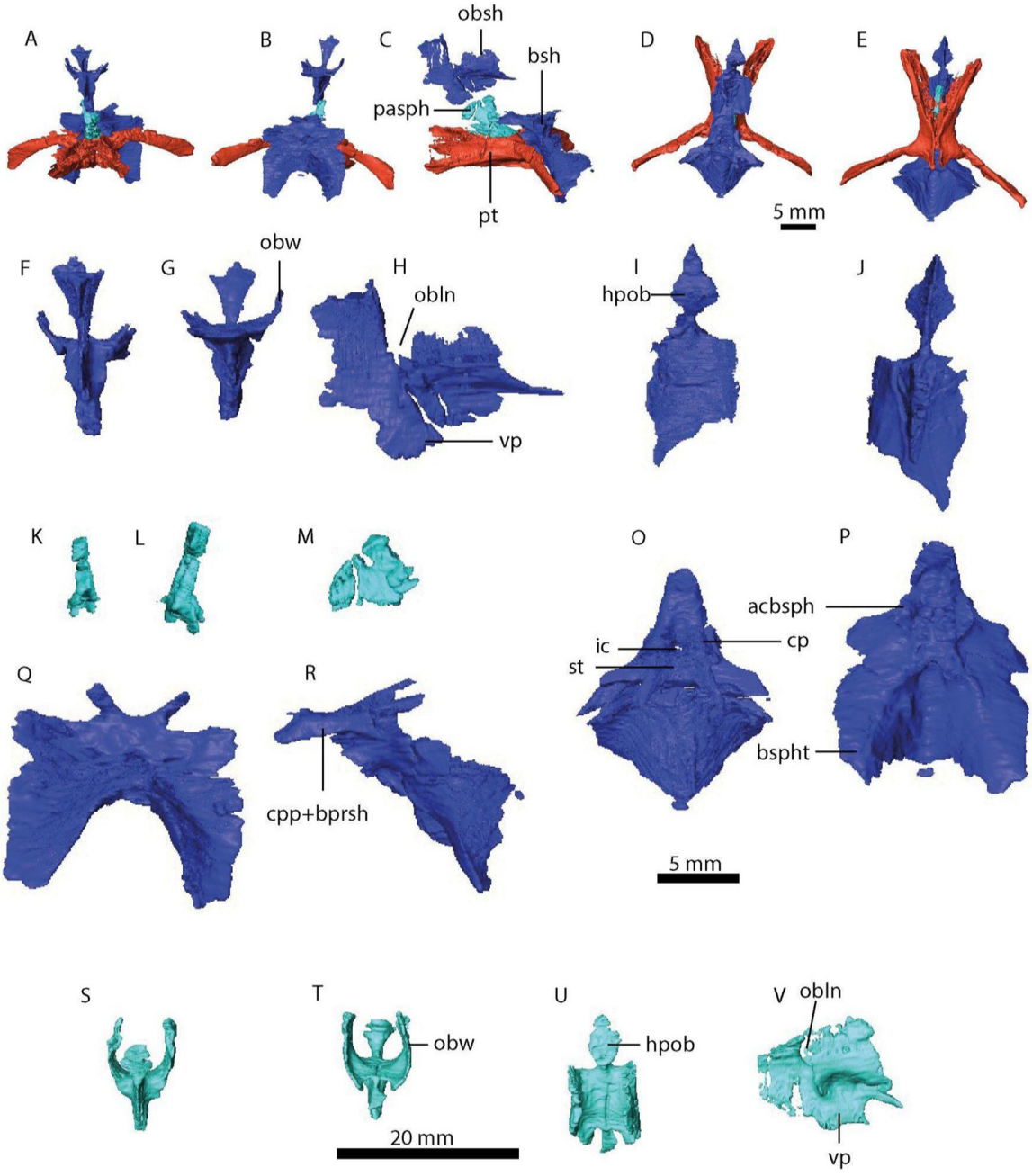

FIGURE 7. Internal cranial bones of SAM-PK-K6814 and SAM-PK-K011474. A, internal cranial bones of SAM-PK-K6814 in anterior view; B, internal cranial bones of SAM-PK-K6814 in posterior view; C, internal cranial bones of SAM-PK-K6814 in left lateral view; D, internal cranial bones of SAM-PK-K6814 in dorsal view; E, internal cranial bones of SAM-PK-K6814 in ventral view; F, SAM-PK-K6814 orbitosphenoid in anterior view; G, SAM-PK-K6814 orbitosphenoid in posterior view; H, SAM-PK-K6814 orbitosphenoid in lateral view; I, SAM-PK-K6814 orbitosphenoid in dorsal view; J, SAM-PK-K6814 orbitosphenoid in posterior view; K, SAM-PK-K6814 orbitosphenoid in ventral view; L, SAM-PK-K6814 orbitosphenoid in dorsal view; M, SAM-PK-K6814 orbitosphenoid in lateral view; O, SAM-PK-K6814 basisphenoid in dorsal view; P, SAM-PK-K6814 basisphenoid in ventral view; Q, SAM-PK-K6814 basisphenoid in posterior view; R, SAM-PK-K6814 basisphenoid in lateral view; S, SAM-PK-K011474 orbitosphenoid in anterior view; T, SAM-PK-K011474 orbitosphenoid in posterior view; U, SAM-PK-K011474 orbitosphenoid in dorsal view; V, SAM-PK-K011474 orbitosphenoid in lateral view. Abbreviations: acbsph, anterior crest of the basisphenoid; bsh, basisphenoid; bspht, basisphenoidal tubera; cp, clinoid process; cpp+bprsh, cultriform process of the parasphenoid and basipresphenoid; ic, internal carotid foramen; hpob, horizontal plate of the orbitosphenoid; obln, orbitosphenoid lateral notch; obsh, orbitosphenoid; obw, orbitosphenoid wings; pasph, parasphenoid; pt, pterygoid; st, sella turcica; vp, vertical process of the orbitosphenoid.

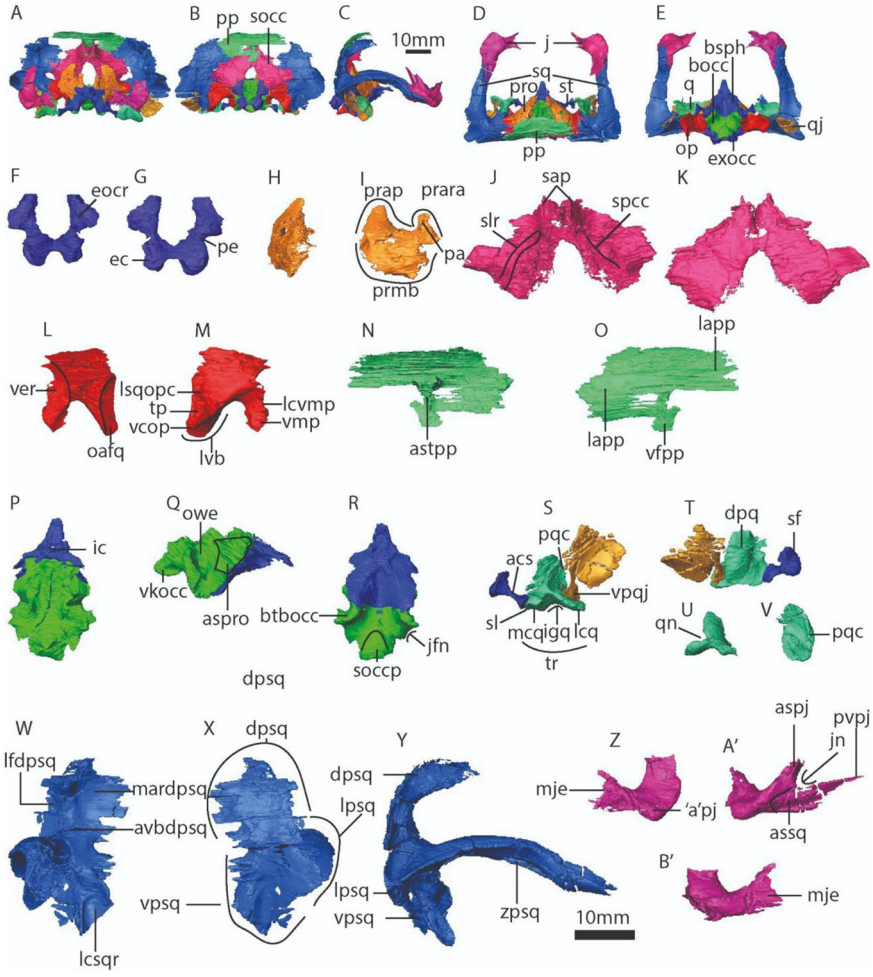

FIGURE 8. Braincase elements and jugal of SAM-PK-K6814. A, anterior view of the articulated braincase and jugal ; B, posterior view; C, lateral view, D, dorsal view, E, ventral view, F, exoccipital in anterior view, G, exoccipital in posterior view; H, prootic in anterior view; I, prootic in lateral view; J, supraoccipital in anterior view; K, supraoccipital in posterior view; L, opisthotic in anterior view; M, opisthotic in posterior view, N, postparietal in anterior view; O, postparietal in posterior view; P, basisphenoid and basioccipital in dorsal view; Q, basisphenoid and basioccipital in lateral view; R, basisphenoid and basioccipital in ventral view; S, quadrate, quadratojugal and stapes in anterior view; T, quadrate, quadratojugal and stapes in dorsal view; U, quadrate in posterior view; U, quadrate in lateral view; V, right squamosal in anterior view; X, right squamosal in posterior view; Y, right squamosal in lateral view; Z, left jugal in anterior view; A', left jugal in lateral view; B', left jugal in posterior view. Abbreviations: acs, anterior crus of the stapes; 'a'pj, 'anterior' process pof the jugal; aspj, ascending process of the jugal; assq, articular surface with the squamosal; aspro, basioccipital articular surface for the prootic; astpp, anterior subtriangular tuberosity of the postparietal; avbdpsq, anterior vertical buttress of the dorsal process of the squamosal; bocc, basioccipital; bsph, basisphenoid; btbocc,basal tuber of the basioccipital; dpq, dorsal process of the quadrate; dpsq, dorsal process of the squamosal; ec, exoccipital condyle; eocr, exoccipital descending crest; exocc, exoccipital; ic, internal carotid foramen; igq, intercondylar groove of the quadrate; j, jugal; jn, jugal notch; jnf, jugal foramen notch; lapp, lateral alae of the postparietal; lcsqr, lateral crest of the squamosal's quadrate recess; lcq, lateral condyle of the quadrate; lcvmp, lateral crest of the opisthotic ventromedial process; lfdpsq, lateral flange of the dorsal process of the squamosal; lpsq, lateral process of the squamosal; lsqopc, lateral squamosal-opisthotic crest; lvb, lateral vertical buttress; mardpsq, medioanterior recess of the dorsal process of the squamosal; mje, medial jugal excavation; mcq, medial condyle of the quadrate; mcsqr, medial crest of the squamosal's quadrate recess; oafq, opisthotic articular facet; op, opisthotic; owe, oval window excavation; pa, pila antotica; pe, pedicle; pp, postparietal; pqc, posterior quadrate crest; prap, prootic alar process; prmb, prootic main body; pro, prootic; pvpj, posteroventral process of the jugal; q, quadrate; qj, quadratojugal; qn, quadrate notch; sap, supraoccipital anterior processes; sf, stapedial footplate; sl, stapedial lip; slr, supraoccipital-opisthotic lateral recess; socc, supraoccipital; soccp, semioval occipital condyle prominence; spcc, supraoccipital-prootic coronal crest; sq, squamosal; st, stapes; ver, vestibular recess; vcop, ventral crest of the opisthotic; vfpp, ventral flange of the postparietal; vkocc, ventral knob of the occipital condyle; vmp,ventromedial process of the opsithotic; vpqj, ventral process of the quadratojugal; vpsq, ventral process of the squamosal; tr, trochlea; tp, tympanic process; zpsq, zygomatic process of the squamosal.

epipterygoid has a longer portion preserved but it is very damaged and fragmented (see Supplementary Information).

Parabasisphenoid

The thin plate of bone composing the parasphenoid, also described by Keyser (1965, 1973), is subtriangular and lies dorsal to the anteriormost portion of the parasphenoid rostrum. This thin plate is clearly distinguishable from the surrounding bones, but there is no separation between the cultriform process of the parasphenoid and the basipresphenoid (cpp + bprsh, Fig. 7, 8). Contrary to Keyser (1965, 1973), we can clearly observe the separation between the basipostsphenoid and the basioccipital in the tomographic slices, but we agree that there is no unossified zone between these bones. The basisphenoidal tubera are formed by a hyperbolic-shaped plate of bone and are subtriangular in lateral view. The anterior surface of the basisphenoidal tubera (bspht, Fig. 7, 8) develops two converging crests that form an X-pattern at the junction with the cultriform process (acbsph, anterior crest of the basisphenoid). These crests form the sutural contact with the pterygoid. The sutural contact with the prootic follows the lateral flanges of the basisphenoidal tubera, which deflect medially. However, the sutural contact with the prootic also continues farther medially as two posterior processes (the clinoid processes; cp, Fig. 7, 8). extending from the crests lateral to the sella turcica (st, Fig. 7, 8) A single carotid foramen is observed on the dorsal aspect of the basipostsphenoid, near the contact with the pterygoid. Internally the single branch bifurcates into two canals for the cerebral carotids, which then exit via paired carotid foramina on the ventral surface of basipostpshenoid as in other specimens such as SAM-PK-K10554 and as mentioned by Broili & Schröder (1936).

Ethmoid

The ethmoid, or 'anterior plate', anatomy is complex and its homologies with extant mammal are not trivial (Cluver 1971). Here, we follow the three-bone homology scheme provided by Crompton et al. (2017), which can be easily identified in *Cistecephalus*. The most anterior element is the mesethmoid, which coossifies to the fused orbitosphenoid (the wings) and presphenoid (the vertical process). Few additional anatomical observations are possible for this element in SAM-PK-6814 because the orbitosphenoid wings and mesethmoid posterior wall are damaged. However, the ethmoid of SAM-PK-K011474 is nearly complete. There is an orbitosphenoid lateral notch (obln, Fig. 7), but it is indented as in *Kawingasaurus* or *Myosaurus* and unlike *Pristerodon*, which possesses an anteroposteriorly-elongated notch (Macungo et al. 2022). There is a horizontal plate of the mesethmoid (hpmsth, Fig. 7) as in *Pristerodon* (Character 193), and no dorsal fossa as in *Myosaurus* (Character 194). The presphenoid vertical process or septum (cf. Keyser 1965, 1973) is anteroposteriorly short when compared to *Kawingasaurus*, but similar to *Pristerodon* (Macungo et al. 2022). The presphenoid vertical process reaches (psph, Fig. 7) the ventral aspect of the palate contacting the parasphenoid, unlike *Myosaurus* (Character 195).

Basioccipital

The ventral knob of the occipital condyle (vkocc, Fig. 8), the basioccipital condyle, is semilunate in shape in posterior view, and it is clearly demarcated from the rest of the bone by a semi-oval prominence ventrally (soccp, Fig. 8), as in *Compsodon* (Angielczyk & Kammerer 2017). The contact with the exoccipital is teardrop-shaped. Anterior to the basioccipital condyle is an excavation that forms the ventral floor of the jugular foramen (jfn, jugal foramen notch, Fig. 8). This structure is marked posteriorly by the posterior crest delimiting the oval window (btbocc, basal tuber of the basioccipital, Fig. 8), which is somewhat conical with the apex pointing ventrally. The prootic contact is subtrapezoidal (aspro, Fig. 8) and is located anteriorly relative to the oval window (owe, oval window excavation, Fig. 8), despite being oriented dorsolaterally. What Keyser (1965, 1973) considered the internal acoustic meatus is essentially the vestibule for the inner ear, which opens dorsal to the oval window excavation (see Endosseous Labyrinth).

Stapes

As segmented, both right and left stapes of SAM-PK-K6814 do not have a fully-enclosed stapedial foramen. Figure 10 in Keyser (1973) does show the stapedial foramen, but not the posterior crus as in SAM-PK-K6814 described here (as for most dicynodonts, see Angielczyk 2007). However, the posterior crus is preserved in SAM-PK-K011474, demonstrating the presence of a completely enclosed stapedial foramen in that specimen (sfor, Fig. 9). In both specimens the stapes has a dumbbell shape, although the right stapes in SAM-PK-K011474 is damaged, with the stapedial head being significantly

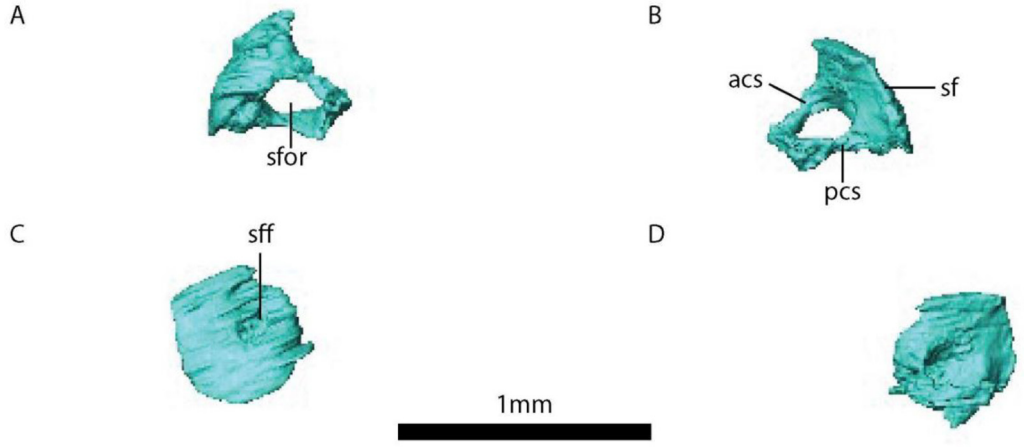

FIGURE 9. Stapes of SAM-PK-K011474. A, Dorsal view, B, ventral view, C, medial view, D, lateral view. Abbreviations: acs, anterior crus of the stapes; pcs, posterior crus of the stapes; sf, stapedial footplate, sff, stapedial footplate foramen; sfor, stapedial foramen.

smaller than the footplate (sf, Fig. 8, 9). As in *Kawingasaurus* and *K. kitchingi* (Laaß 2015, Angielczyk et al. 2019), there is a central concavity in the stapedial footplate, where a small foramen pierces through (stapedial footplate foramen, sff, Fig. 9). Similarly, the stapedial head is concave but is teardrop-shaped with the apex pointing posteriorly in SAM-PK-K6814. The anterior border of the anterior crus (acs, anterior crus of the stapes, Fig. 8, 9) is concave, and the posterior border is semicircular to accommodate the stapedial artery. The dorsal region of the stapedial footplate is thinner dorsally where it forms a distinct laterally-oriented rim. Additionally, there is no distinct dorsal process of the stapes, as in *Kombuisia* (Fröbisch 2007).

Quadrate

As typical for dicynodonts, the trochlea (tr, Fig. 8) is formed by two easily distinguishable condyles, but it differs from *Cistecephaloides* and *Kawingasaurus,* in which the condyles are reduced in size.

The trochlea is as robust as in *K. yajuwayeyi*, but less developed than in *Niassodon*. The lateral condyle (lcq, Fig. 8) is flat and angles ventrolaterally, whereas it is gently ventrally concave in *Niassodon* and *K. yajuwayeyi*, but convex in *Compsodon* (Angielczyk & Kammerer 2017). The lateral condyle is significantly longer anteroposteriorly than the medial condyle (mcq, Fig. 8) as in *Compsodon* (Angielczyk & Kammerer 2017), whereas this difference is smaller in *Niassodon* (Character 196). The lateral and medial condyle angle is approximately 100° (as *K. yajuwayeyi*), whereas *Niassodon* is ~93°. The medial condyle has the typical subrectangular shape, but its dorsal border forms a well-delimited crest that continues dorsally to form the dorsal plate anterior border (dpq, Fig. 8). There is an indistinct stapedial lip (sl, Fig. 8) on the medialmost aspect of the quadrate to accommodate the stapes. The dorsal plate is medially convex, and at the intersection with the lateral condyle there is a noticeable notch posteriorly (qn, quadrate notch), representing the medial and ventral margins of the quadrate foramen. The posterior border of the quadrate forms a distinct rim as the margin of the dorsal plate curls anterolaterally (pqc, posterior quadrate crest). The quadrate notch and posterior quadrate crest (Discrete Character 197 and 198, respectively) are also visible in *K. yajuwayeyi,* but not in *Kawingasaurus* (Laaß 2015).

Quadratojugal

The dorsal portion of the quadratojugal is subrectangular and expands dorsally to fit the anterior aspect of the squamosal, but it tapers ventrally into a crest-like ventral process (vpqj, Fig. 8). The quadratojugal is mostly posteriorly convex and is relatively flat as in *Kawingasaurus* (Laaß 2015), unlike the twisted morphology of *Niassodon* or *K. yajuwayeyi* (Castanhinha et al. 2013, Araújo et al. 2022b; Discrete Character 199). However, the exact shape and dimension of the quadratojugal are hard to appreciate in these specimens (SAM-PK-K6814 and SAM-PK-K011474) because they have several fractures, and the quadratojugal is significantly co-ossified with the squamosal.

Postparietal

Keyser (1965, 1973) had difficulties delineating the suture between the postparietal and the squamosal, but our segmentation elucidates this contact. The postparietal contacts the dorsal process of the squamosal along an interdigitating suture where the postparietal mostly overlaps the squamosal. More dorsally, despite some interdigitation the suture mostly becomes a scarf joint. The lateral alar regions (lapp, lateral alae of the postparietal) are difficult to delineate due to preservation, but seem to be subtrapezoidal. There is no evidence for the tabulars, which is important because there has been uncertainty about their presence in *Cistecephalus* (Angielczyk et al. 2019). Maybe due to preservation, SAM-PK-K6814 does not have a nuchal crest, although this structure was mentioned by Keyser (1965, 1973): "On the ventral border of the interparietals along the suture between them, a ridge overlapping the supraoccipital is formed". SAM-PK-K1187 does have a nuchal crest, but it is more strongly developed on the supraoccipital, with a low swelling continuing onto the ventral process of the postparietal; most of the postparietal is smooth, lacking a crest completely. Notably, in SAM-PK-K6814, the postparietal overlaps the supraoccipital posteriorly with a short ventral flange (vfpp, ventral flange of the postparietal). Unlike *Kembawacela* spp. (Angielczyk et al. 2019, Araújo et al. 2022b), there are no paired ellipsoidal foramina between the suture of the postparietal and the supraoccipital.

Given the overall excellent preservation of the specimen, it is possible to describe the anterior surface of the postparietal. This face presents a central subtriangular tuberosity (astpp, anterior subtriangular tuberosity of the postparietal) that is trapezoidal with flat lateral surfaces and a slightly concave dorsal surface. Ventrally, the tuberosity slots into a groove on the dorsal surface of the supraoccipital. Except for the tuberosity, the anterior surface of the postparietal is smooth and concave.

Supraoccipital

Given the complexity of this bone, especially its anterior aspect, various details were not described by Keyser (1965, 1973) that we expand on here. Each side of the dorsolateral borders of the supraoccipital are concave, forming two conspicuous lateral alae, which resembles the condition in *Kawingasaurus* (Macungo et al. 2022). However, these lateral alae are thin and do not possess the dorsal crests of the supraoccipital alae seen in *Kawingasaurus*. There is no evidence of a nuchal crest on the supraoccipital in SAM-PK-K6814, unlike for other specimens. The anterior surface of the supraoccipital is, as usual, where most of the anatomical information is contained. There are no supraoccipital transverse crests as in *K. yajuwayeyi* (Discrete Character 200), but the supraoccipitalprootic coronal crest is present (spcc, Fig. 8). Posterior to the latter structure is the prootic-supraoccipital recess, which forms a ventrally-descending excavation. However, the supraoccipital-opisthotic lateral recess (slr, Fig. 8) is shallow when compared to that of *K. yajuwayeyi* (Araújo et al. 2022b). The supraoccipital anterior processes (sap, Fig. 8) of the median lobe are somewhat triangular in lateral view, slightly converge dorsally, and become thinner anteriorly. The anteroventral corner of the anterior process is more prominent than the remaining anterior border, which is gently anteriorly convex. The floccular fossa is hemispherical but shallower when compared to other taxa, such as *Niassodon* or *K. yajuwayeyi* (Castanhinha et al. 2013, Araújo et al. 2022b). The posterior half of the floccular fossa is formed by the supraoccipital, whereas the anterior half is formed by the prootic, a common feature among emydopoids (Macungo et al. 2022).

Exoccipital

The exoccipital condyles (ec, Fig. 8), which form the dorsolateral portions of the occipital condyle, are reniform with the convexity oriented laterally. The thin pedicle (pe, Fig. 8) linking the occipital portion of the exoccipital and the exoccipital condyle is angled approximately 70° with the horizontal plane, and contrasts with the robust pedicle in *Myosaurus* and *Pristerodon* (Macungo et al. 2022). The exoccipital contribution to the occipital plate is subtriangular in posterior view, most similar to the condition in *K. yajuwayeyi* (Araújo et al. 2022b), and clearly different from the subrectangular morphology in *Myosaurus* (Macungo et al. 2022). The dorsal contact with the supraoccipital is oval. The exoccipital descending crest is most prominent ventrally (eocr, Fig. 8) and obliquely oriented at an angle of approximately 45° relative to the sagittal axis. A similar crest is also present in *Kawingasaurus* and *Myosaurus*, but absent in *Pristerodon*, whose exoccipital dorsal component is poorly developed (Macungo et al. 2022). This crest forms the dorsal border of the jugular foramen. The anterior contact with the basioccipital is subtriangular with rounded edges and with the apex

pointing ventrally.

Opisthotic

Although the opisthotic and prootic are co-ossified, we were able to separate them through segmentation. This was possible because the two distinct ossification centers produced different internal trabeculae orientations, enabling us to distinguish and separate the bones. The posterior surface of the opisthotic is flat and does not possess the opisthotic posterior crests and opisthotic posterior depression seen in *K. yajuwayeyi* (Macungo et al. 2022). The 'tympanic process' (tp, *sensu* Cox, 1959) points posteroventrally and it is marked by a lateral crest resulting from the squamosal contact (lsqopc, lateral squamosal-opisthotic crest) and a faint crest that follows the ventral border of the opisthotic (vcop, ventral crest of the opisthotic, Fig. 8). The anterolateral surface of the opisthotic is broadly concave forming the articular facet for the quadrate (oafq, opisthotic articular facet). The anteromedial region of the opisthotic hosts part of the vestibule. Keyser (1973) referred to this structure as the "sacculo-cochlear recess", but we avoid using this term because neither the saccule nor the cochlea are identifiable structures within the vestibule, and this region contains other structures such as the utriculus. Instead we refer to this region as the vestibular recess (ver, Fig. 8, for the concavity in the bone) or vestibule (for the void formed by the bony concavity). The ventromedial process of the opisthotic (vmp, Fig. 8) is excavated by the lagenar recess. The ventromedial process is subtriangular in cross-section and bears a prominent lateral crest (lcvmp, lateral crest of the opisthotic ventromedial process). The ventromedial process has variable morphology among kistecephalians: it may be absent in *Kawingasaurus* or subquadrangular in posterior view as in *Myosaurus* (Macungo et al. 2022). In *Cistecephalus*, the ventromedial process is semilunate in posterior view. Such variation seems to have taxonomic relevance.

Keyser (1965, 1973) referred to the small anteroventral process in the lateralmost region of the opisthotic as the quadrate process, which is poorly developed to absent in cistecephalids (Macungo et al. 2022). According to Keyser (1965, 1973), the 'mastoid process' is the region that contacts the squamosal. However, not only is the homology of this structure with the mastoid process of mammals is difficult to verify; the contact occurs mostly in the lateral region and it is unlikely that the process served for the attachment of the atlantoccipital musculature in *Cistecephalus*. Therefore, we prefer to designate the entire descending region of the opisthotic as the lateral vertical buttress (lvb, Fig. 8) following Macungo et al. (2022).

Prootic

The prootic is composed by the main body (prmb, prootic main body, Fig. 8), which includes the alar process (prap, prootic alar process, Fig. 8), and the anterior ascending ramus (praar, prootic anterior ascending ramus, Fig. 8), which includes the pila antotica (pa, Fig. 8). The anteroventral process of Keyser (1965, 1973) is the same as the anterior ascending ramus in Macungo et al. (2022), whereas the anterodorsal process (Olson 1944, Keyser 1965, 1973) corresponds to the dorsal process of the prootic alae in Macungo et al. (2022). There is no sign of the prootic sinus described by Laaß & Kaestner (2017), nor the pila antotica ellipsoidal depression, nor the prootic anterior bulge seen in *Kawingasaurus* (Macungo et al. 2022). The prootic main body is sickle-shaped, with the alar process being blunt dorsally, and the contact with the opisthotic-supraoccipital is formed by a smooth, well-delineated, posteriorly-convex border. The general shape of the prootic main body, surprisingly, more closely resembles the condition in *Pristerodon* and *Diictodon*, rather than the more quadrilateral shape of *Myosaurus* or *Kawingasaurus,* or the subtriangular shape of *Niassodon* and *K. yajuwayeyi* (Castanhinha et al. 2013, Macungo et al. 2022, Araújo et al. 2022b, Supplemental Information). The pila antotica is short and blunt, and devoid of the anterodorsally-directed ridges and corresponding median excavation present in *Kawingasaurus* (Macungo et al. 2022). An interesting anatomical region where there seems to be considerable variation is the supraoccipital lateral recess and the corresponding supraoocipital-prootic coronal crest (Macungo et al. 2022, Araújo et al. 2022b). The supraoocipital-prootic coronal crest is noticeably pronounced and smoothly posteriorly convex, with a uniformly wide supraoccipital lateral recess in *Niassodon* (Castanhinha et al. 2013). A uniformly wide supraoccipital lateral recess is also present in *Pristerodon*, but with a low supraoocipital-prootic coronal crest (Macungo et al. 2022). However, in *Cistecephalus* the supraoocipital-prootic coronal crest is low and fades ventrally onto the main body of the prootic, whereas the supraoccipital lateral recess is significantly wider ventrally than dorsally, as in *K. yajuwayeyi* and *Kawingasaurus* (Macungo et al. 2022,

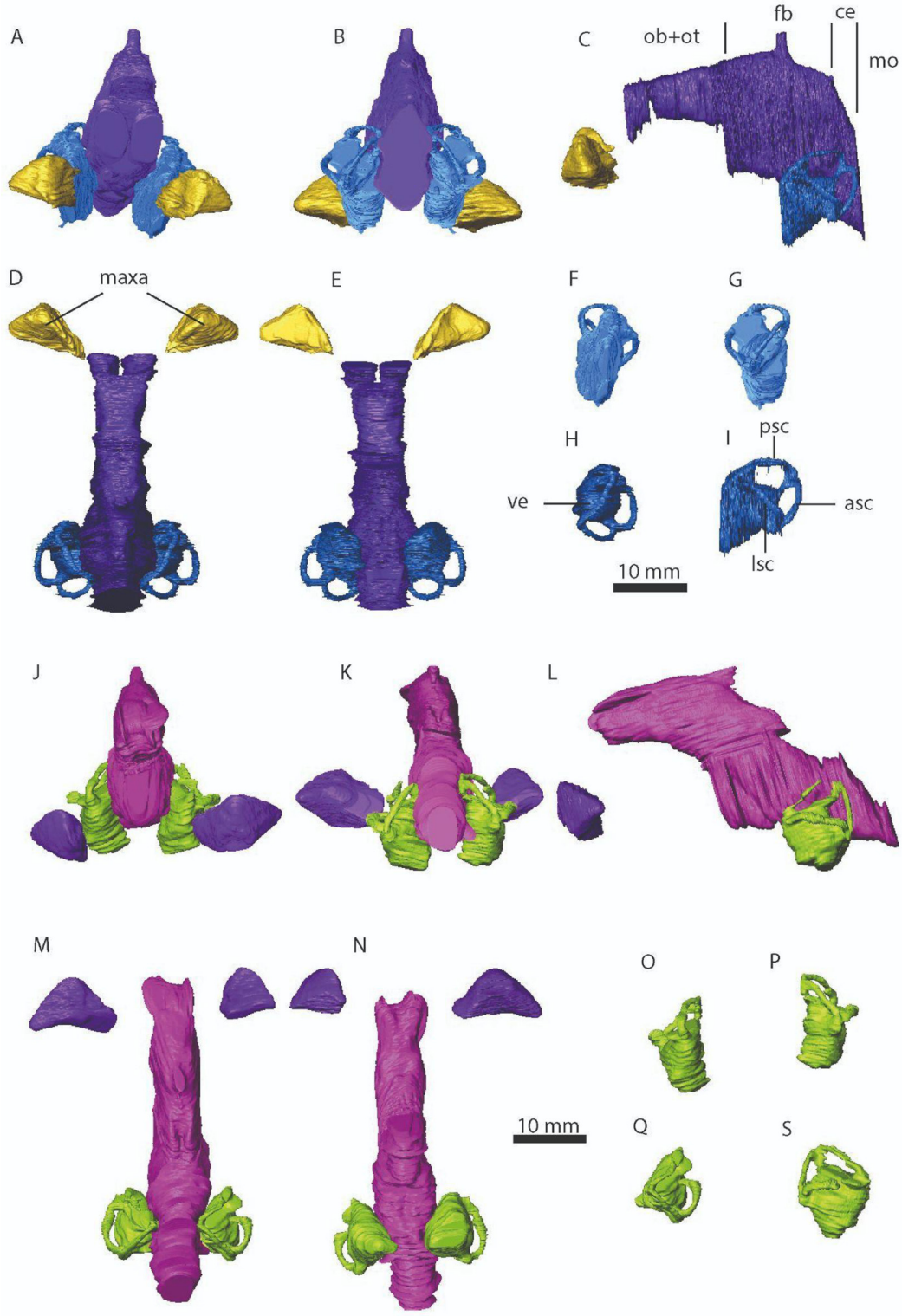

FIGURE 10. Endocasts of SAM-PK-K6814 and SAM-PK-K011474. A, anterior view, B, posterior view, C, lateral view, D, dorsal view, E, ventral of SAM-PK-K6814 endocasts. E, ventral view, G, posterior view, H, dorsal and, I, lateral view of SAM-PK-K6814 endosseous labyrinth endocasts. J, anterior view, K, posterior view, L, lateral view, M, dorsal view, N, ventral of SAM-PK-K011474 endocasts. O, ventral view, P, posterior view, Q, dorsal and, R, lateral view of SAM-PK-K011474 endosseous labyrinth endocasts. Abbreviations: ob+ot, olfactory bulbs and olfactory tracts; fb, forebrain; ce, cerebellum; mo, edulla oblongata; maxa, maxillary antrum; ve, vestibulum; psc, posterior semicircular canal; asc, anterior semicircular canal; lsc, lateral semicircular canal.

Araújo et al. 2022b).

Endosseous labyrinth

The prootic envelops the anterior halves of the anterior and lateral semicircular canals, the opisthotic envelops the posterior half of the lateral semicircular canal and the ventral half of the posterior semicircular canal, and the supraoccipital envelops the dorsal portion of the anterior and posterior semicircular canal. The dorsal component of the exoccipital also contributes to form the medial enclosure of the posterior semicircular canal. This arrangement is similar to what has been reported for the pylaecephalid *Diictodon* and the emydopoids *Myosaurus* and *Kawingasaurus*, but the exoccipital of *Pristerodon* is not pierced by the bony labyrinth (Macungo et al. 2022, see Supplementary Information). The bony enclosure for the endosseous labyrinth is also different in *Niassodon* (Castanhinha et al. 2013), in which the posterior semicircular canal is entirely enveloped by the supraoccipital, the opisthotic only envelops the posterior half of the semicircular canal, and the exoccipital does not contribute to the endosseous labyrinth. Whether this anatomical arrangement has phylogenetic significance needs to be confirmed in other endothiodontid and eumantelliid dicynodonts. However, given the high degree of fusion between the occipital and braincase bones in *Niassodon* and the lack of anatomical information about this region at the time *Niassodon* was described, uncertainty exist about the accuracy of some of those sutures presented in Castanhinha et al. (2013).

All three semicircular canals are ellipsoidal (Fig. 10), as is typical in non-mammaliaform synapsids (Araújo et al. 2022b). Among the three canals, the lateral is the thickest in cross section, followed by the posterior semicircular canal. The crus communis is short and opens dorsally in a triangular fashion as the vertical semicircular canals diverge, somewhat resembling the condition in *Endothiodon* cf. *bathystoma* (Araújo et al. 2018). There are no visible vertical semicircular canal ampullae, as in *Endothiodon* and *Niassodon* (Castanhinha et al. 2013, Araújo et al. 2018). The ampulla for the lateral semicircular canal is slightly developed, contrasting with that of *Kawingasaurus*, *Emydops* and *Eodicynodon* which are well-delimited (Araújo et al. 2022b).

In *Cistecephalus*, the lateral enclosure of the vestibule is formed by the ventromedial process of the opisthotic, whereas it is the prootic and the basioccipital that form the anterior and medial wall, respectively. In *Niassodon* and *Diictodon* the basisphenoid and the basipostsphenoid form the anterior and posterior walls of the lagena, respectively (Castanhinha et al. 2013, see Supplementary Information). The vestibule is subtriangular and not as inflated as those observed in *Kawingasaurus* and *K. yajuwayeyi* (Araújo et al. 2022b).

Brain endocast

The *Cistecephalus* brain endocast in both specimens (SAM-PK-K6814 Fig. 10 and SAM-PK-K011474 Fig. 10) is remarkably similar to other cistecephalid endocasts and distinct from other dicynodonts, following the pattern mentioned in Araújo et al. (2022b). Specifically, the forebrain and cerebellum are significantly shortened, and the post-olfactory tract brain section is dorsoventrally bulky. The extreme modifications of the brain endocast anatomy cannot be solely explained by verticalization of the occipital plate seen in cistecephalids because there are other dicynodonts in which the occiput does not slope forward very strongly, and yet do not have such brain endocast organization (e.g., *Lystrosaurus*). Cistecephalids seem to have undergone an additional, substantial posterior telescoping of the skull that is presumably related to broadening the back of the skull and more closely aligning the posterior part of the temporal fenestra with the occipital plate. Other dicynodonts (e.g., *Compsodon*, *Oudenodon*, *Geikia*) have more emarginated temporal fenestrae that extend posteriorly beyond the plane of the occipital plate. The location of the pineal foramen can be used as a landmark for recognizing this telescoping: typically it is located towards the middle of the intertemporal bar, whereas in cistecephalids it is very close to the posterior edge of the intertemporal bar (e.g., *Cistecephalus*) or right at the posterior edge of the intertemporal bar (e.g., *Kembawacela* spp., *Cistecephaloides*). Therefore, cistecephalids appear to have reorganized the portion of the skull roof that is typically posterior to the pineal foramen. There are other non-cistecephalid dicynodonts that have their pineal foramen located posteriorly on the skull roof (e.g., *Niassodon*), but in those cases it is never as far posteriorly as in cistecephalids, and the occipital plate often has some anterior angulation that helps to accommodate a more typical, elongated dicynodont brain endocast (Laaß et al. 2010, Castanhinha et al. 2013, Simão-Oliveira et al. 2020). In sum, cistecephalids were not only making their occipital plate more vertical, they also reorganized the entire post-pineal portion of the skull anteriorly,

requiring a compact brain to accommodate these changes.

The frontal covers the dorsal surface of the olfactory tract and bulbs, whereas the parietal covers the dorsal surface of the forebrain including the epiphyseal nerve endocast, and the supraoccipital covers the dorsal surface of the cerebellum and the inception of the medulla oblongata, similar to the the condition in *K. yajuwayeyi* (Araújo et al. 2022b). The ventral and lateral aspects of the olfactory tract and bulbs are bounded by the orbitosphenoid. The ventrolateral aspect is bounded by the prootic, whereas the ventral aspect by the basisphenoid anteriorly and the basicoccipital posteriorly.

The anterior region of the brain endocast is not especially expanded laterally compared to the posterior region, despite the latter being more enlarged in this dimension. The floccular process is reduced and barely perforates the anterior semicircular canal. The epiphyseal nerve is developed into a relatively long, straight, vertical cylinder that reaches the skull roof at nearly mid-length of the forebrain. The olfactory tracts and bulbs are separated by a median septum of the mesethmoid, which unlike other cistecephalid specimens (Laaß & Kaestner 2017, Araújo et al. 2022b), physically divides the two tracts. Interestingly, the olfactory tracts in cistecephalids (Laaß & Kaestner 2017, Araújo et al. 2022b) seem to be dorsoventrally taller than in other dicynodonts (Laaß 2010, Castanhinha et al. 2013, Simão-Oliveira et al. 2020). The brain endocast of SAM-PK-6814 brain has a volume of ~2340 mm^3 including the olfactory bulbs, and ~1030 mm^3 without the olfactory bulbs, measured using Amira software.

Maxillary antrum and lacrimal gland endocast

The maxillary antrum is enveloped by the maxilla anteriorly, the jugal laterally, and the lacrimal posteriorly. A small portion of the medialmost aspect of the maxillary antrum is enveloped by the palatine. The anatomy and variation of the maxillary antrum rarely has been described in dicynodonts. Therefore, we give further detail to begin building a database that could be useful for future taxonomic studies. Contrary to *K. yajuwayeyi* (Araújo et al. 2022b), there is no separation between the maxillary antrum and the lacrimal gland endocast, resulting in a single structure. The maxillary antrum can be described as an isosceles triangle pyramid (Fig. 10). The base of the triangle forming the ventral face of the pyramid is on the posterior side, which forms an angle with the lateral face of ~50°, and ~65° with the medial face in SAM-PK-1174 (in SAM-PK-K6814 ~47° and ~42°, respectively). The angle between the lateral and medial face is ~85°, despite being significantly more rounded in SAM-PK-1174 (in SAM-PK-K6814 is ~89)° . Whereas the lateral aspect of the maxillary antrum tapers into a point, the medial aspect forms an edge. The intraspecific variation of this structure is negligible, except for the angle between the lateral posterior and lateral edge of the ventral face of the maxillary antrum, despite there being taphonomic preservation differences between specimens (i.e., SAM-PK-1174 vs. SAM-PK-6814). This suggests that the maxillary antrum may have utility for taxonomic purposes.

DISCUSSION

Semicircular canal biomechanics and cistecephalid ectothermy

A recent paper hypothesized that endothermy could have evolved in cistecephalids, independently from its evolution along the mammalian lineage (Laaß & Kaestner 2023). These results are mainly based on data from *Kawingasaurus*, and seemingly contradict results obtained from the analysis of the semicircular canals of this species, which had a probability for endothermy of 27% (Araújo et al. 2022a). They also contradict results obtained in the present study, where we found an endothermy probability of 23-40% for cistecephalids, and interpret them as most likely ectotherms. Laaß & Kaestner (2023) asked "whether the approach of Araújo et al. (2022a) can be applied to *Kawingasaurus* and other burrowing dicynodonts to infer their metabolic status." They argued that *Kawingasaurus* was fossorial, and like other fossorial species, has semicircular canal planes deviating from an ideal configuration (i.e., orthogonal semicircular canals), illustrated by an angle of 53° they measured between the anterior and lateral canals (Laaß 2015). Furthermore, they explained that "the sense of balance is less important for burrowers, due to the restricted head rotations and the decreased requirements for motor coordination underground", and that "such behaviour requires less sensitivity of the semicircular canals (Berlin et al. 2013), which might be an indication of a degenerated sense of balance".

There are several issues with these claims. First, fossorial mammals do not have a diminished sense of balance. On the contrary, studies on the biomechanics of the membranous semicircular ducts of *Cryptomys*, *Spalax* and *Talpa* showed

that, when compared to *Rattus* and after body mass correction, the three fossorial species showed increased semicircular duct sensitivity (Lindenlaub et al. 1995, McVean 1999), not decreased semicircular duct sensitivity (*contra* Berlin et al. 2013). This is particularly true of the lateral semicircular ducts, and was interpreted as providing improved sensory cues for navigation, which depends on semicircular duct function (Fitzpatrick et al. 2006).

Second, classical anatomical measurements of semicircular canal planes are generally based on the slender portion of the canals and omit the utricular part of the streamline trajectory. This is likely what happened with the measurement of the angle between the anterior and posterior semicircular canals presented for *Kawingasaurus*. Taking the full streamline torus, and applying biomechanical equations for the maximal response plane (Rabbitt et al. 2004), we find an angle of 76° between these two canals, a value that fall within extant amniote variation and that is much closer to the ideal angle of 90° than the 53° reported in Laaß (2015). The same is true for *Cistecephalus*, a closely related cistecephalid, which also shows an angle between anterior and lateral semicircular canals that falls within extant amniote variation. Thus, it is important to note that when one aims to derive functional interpretations, maximal response planes are the only relevant planes to be compared to an "optimal" configuration (Rabbitt et al. 2004).

Third, it should be stressed that the thermo-motility index is based on two main terms derived from anterior semicircular canal biomechanics, only one of which, the sensitivity, is affected by the orientation of maximal response planes. In this context, the anterior semicircular canals of *Kawingasaurus* make an angle of 40° with the midsagittal plane, and of 51° with the coronal plane, the two major planes of head motion relevant for these canals. When compared with optimal angles of 45°, it appears that the spatial orientation of the anterior semicircular canals of *Kawingasaurus* are thus fairly normal and fall well within extant amniote variation. The same is true for *Cistecephalus*. Importantly though, even if these angles fell at the edge of extant amniote distribution, this fact would not prevent use of the thermo-motility index to predict the corresponding thermal regime. The reason for this is simple: although canal plane orientation was not taken into account by Araújo et al. (2022a) when developing models correlating the thermo-motility index to body temperature and endothermic regime, the extant vertebrate species used in their study show variation in the spatial orientation of their semicircular canals. Hence, if this variation was large enough to affect the thermo-motility index, it would contribute to its residual variation, which is taken into account when computing 95% confidence intervals on body temperature of fossil species.

Nevertheless, as indicated in Araújo et al. (2022a) and as mentioned in Laaß & Kaestner (2023), the use of the thermo-motility index is indeed less suited to predicting the metabolic status of a single species. Furthermore, while unlikely, unforeseen modifications of some functional parameters (e.g., endolymph viscosity) cannot be ruled out in clades branching off from the main lineage leading to mammals. In this context, the 95% C.I. for the body temperature of cistecephalids, predicted from the thermo-motility Index of three species and taking into account uncertainty linked to uncontrolled parameters, ranges between 24.0-35.4 °C, with 30.5% chance of being higher than 31°C, the lowest body temperature found in extant endotherms.

Fossoriality as a thermoregulatory strategy in *Cistecephalus* and other dicynodonts

Cistecephalus and other cistecephalids are at an extreme point on the spectrum of fossorial anatomical specialization among dicynodonts (Macungo et al. 2022). Features such as skull telescoping (this paper), verticalization of the occipital plate (Araújo et al. 2022b), high nasofrontal suture complexity (Kammerer 2021), development of the atlantoccipital musculature and basicranial co-ossification (this paper, Macungo et al. 2022), compact bone histology (Nasterlack et al. 2012), and robust limb morphology (Cox 1972, Cluver 1978, Lungmus & Angielczyk 2021) provide evidence for an obligate fossorial lifestyle for *Cistecephalus*, despite the lack of direct ichnological evidence (Smith et al. 2021). Living as an obligate fossorial animal is known to provide significant thermoregulatory benefits due to relatively constant temperatures and humidity in burrows, which led to a notable reversal to ectothermy among fossorial mammals such as naked mole-rats (e.g., Buffenstein et al. 1991, Martinez et al. 2023). However, it seems that fossoriality demonstrated by *Cistecephalus* and other cistecephalids has deeper origins among dicynodonts. Various lines of evidence from preserved burrow structures (Smith 1987, King & Cluver, 1991; Bordy et al., 2011; Botha-Brink, 2017; Smith et al., 2021) to postcranial adaptations (Smith, 1987; Sullivan et al., 2002; Ray &

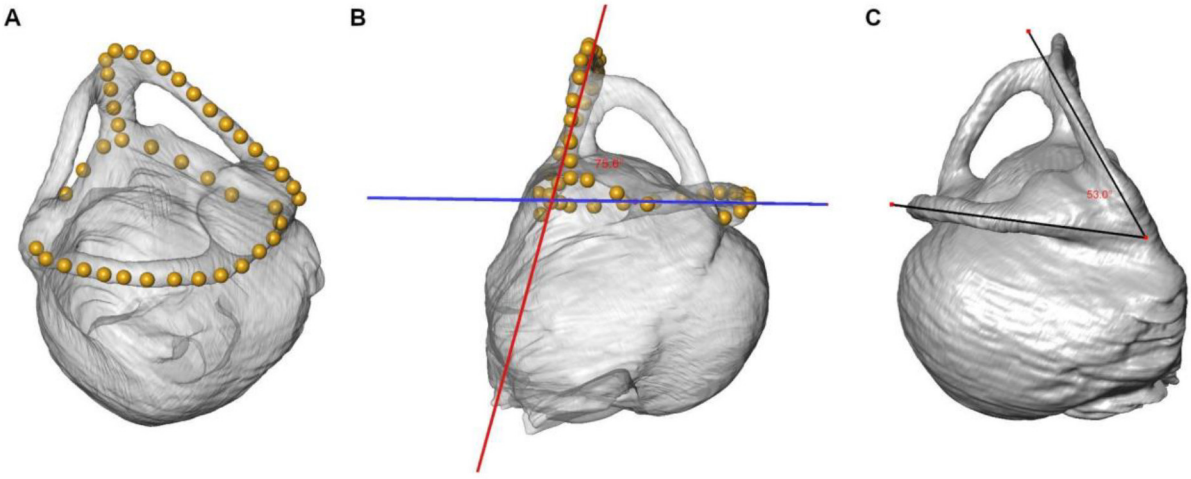

FIGURE 11. Semicircular canal planes of *Kawingasaurus*. A, Landmarks used to compute the functional planes of the anterior and posterior canals. Note that landmarks were placed in the vestibule where the anterior utriculus is supposed to be. B**,** Angle between functional planes of the anterior (red) and lateral (blue) semicircular canals. C, Angle between anatomical planes of the anterior and lateral semicircular canals when measured "classically". Note that the angle obtained using anatomical planes (53°) differs greatly from the angle obtained using functional planes (75.6°).

Chinsamy, 2003; Smith et al., 2022) indicate that non-cistecephalid dicynodonts burrowed to some extent, perhaps to shelter from harsh paleoenvironmental conditions and/or rear young.

To provide a broader context, it is important to consider the paleoecological scenario that cistecephalids and other Permian dicynodonts were experiencing. In particular, it is significant that unlike today, terrestrial tetrapod communities were dominated by ectotherms. Recent evidence indicates that synapsid endothermy likely originated in mammaliamorphs in the early Late Triassic (Araújo et al. 2022a). This finding is supported by other lines of evidence, such as brain enlargement (Benoit et al., 2023) or the evolution of vibrissae (Rowe et al. 2011, Benoit et al. 2016, 2023, Crompton et al. 2017), which seem to also occur at this time. The corollary of this result is that during the Permian all tetrapods were ectothermic, because other purported endothermic clades such as dinosaurs or pterosaurs had not yet originated (Benton et al. 2021). Visualizing a scenario wherein intricate trophic hierarchies exist, involving terrestrial megafauna that are physiologically restricted by ectothermy poses a significant challenge when viewed from the perspective of modern, largely endotherm-dominated ecosystems. Ectotherms have restricted annual and diurnal activity patterns and/or heightened reliance on behavioral thermoregulation for routine daily activities (e.g., Pianka 1986). Thus, ectothermic Permian and Early to Middle Triassic synapsids include top-predators such as gorgonopsians, and megaherbivores like large herbivorous dicynodonts. Following this line of thought, synapsids could not engage in long aerobic terrestrial migrations to escape the harsh Karoo winter in the Permian, similar to most modern terrestrial ectotherms (Southwood & Avens 2010). The cosmopolitan presence of some dicynodont species demonstrates long distance dispersal (e.g., Angielczyk & Sullivan 2008), yet presumably over timescales that were longer than seasonal/yearly. Nevertheless, the middle-late Permian Karoo, given its paleolatitude, is predicted to have been a warm temperate climate (Köppen equivalent: CSa, CSb) according to Boucout et al. (2013), to a boreal/subartic climate (Köppen equivalent: Dfc, Dwc, Dsc, Dfb, Dwb) according to Rees et al. (2002) and Rey et al. 2016), to a cold steppe/cold desert type (Köppen equivalent: BSk, Bwk) according to Roscher et al. (2011). Regardless of the exact Köppen climate type or specimen age range and associated paleolatitude range, the Permian Karoo region would have night and winter temperatures that would be difficult for modern ectotherms to tolerate (Araújo et al. 2022a). For instance, *Clemmys guttata*, *Alligator sinensis* or *Phrynosoma mcalli* start to brumate when environmental temperatures drop ~20°C below their preferential temperature (Yagi & Litzgus 2013, Zhang et al. 2021, Mayhew 1965). Indeed, gorgonopsians and Permian dicynodonts show a probability of >0.7 of brumating during the winter

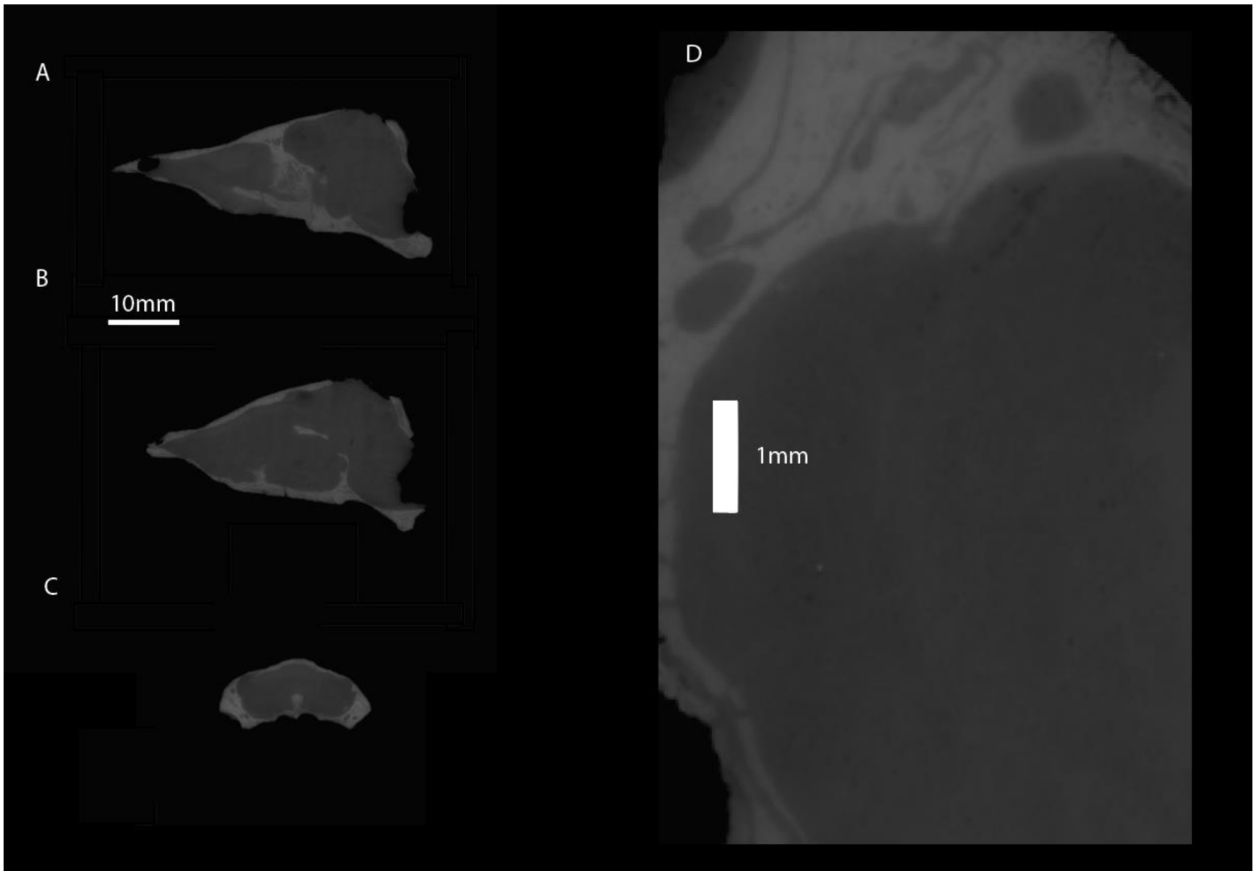

FIGURE 12. Propagation phase-contrast synchrotron micro-tomography sections equivalent to those depicted in Laaß & Kaestner (2023) showing no evidence for turbinals in *Kawingasaurus fossilis* (GPIT-PB-117032). A, midstagittal section, B, sagittal section section left from the midline, C, coronal section at the level of the nasal cavity, D, close-up on C.

and >0.76 of being diurnal (Araújo et al. 2022a). In other words, the hypothesis that gorgonopsians were obligatorily diurnal is derived from their estimated body temperature, taking into account the paleotemperature at their paleolatitude, which is in line with previous studies (Angielczyk & Schmitz 2014). Essentially, drawing upon knowledge from contemporary reptiles, the nights (and the winters) would have been too cold for gorgonopsians and dicynodonts to function effectively, considering their thermo-motility index. The profusion of burrow structures discovered within the Permian Karoo ecosystems (Smith et al. 2021), provides compelling evidence supporting the imperative requirement for shelter during the winter period while undergoing brumation. This would result in a stark winter landscape in the Karoo during the middle-late Permian. During the hot seasons, synapsids would be expected to resort to intermittent locomotion (Kramer & McLaughlin 2001) like modern lizards, and/or long periods of rest and behavioral thermoregulation punctuated by short periods of activity (Hertz et al. 1988). Consequently, diurnal gorgonopsians (P = 0.7, P refers to probability) and, potentially diurnal Permian therocephalians (P = 0.63), likely were ambush predators using cryptic camouflage, or would pursue prey for short anaerobic bursts, like terrestrial tetrapod ectotherms do today (Hertz et al. 1988). Middle-late Permian dicynodonts are predicted to brumate during the winter and to also be diurnal (P = 0.8, P = 0.79, respectively), and the sampled cistecephalids are no exception (*Kawingasaurus,* diurnal P = 0.79, winter brumation, P = 0.77; *Kembawacela kitchingi*, diurnal P = 0.92, winter brumation P = 0.84), irrespective of their fossorial status.

Turbinates and thermoregulation

Despite the exceptional preservation of the *Cistecephalus* specimens studied here, none presented structures resembling turbinals or evidence of ridges where they could attach if cartilaginous. Recent developments in understanding the

function, anatomy and physiology of turbinates seem to be progressively dismantling their relationship with the origin and evolution of endothermy. Martinez et al. (2023) found no relationship between the relative surface area of the maxilloturbinal and the corrected basal metabolic rate, body temperature, or the different forms of torpor (short- or long-term torpor) for >300 mammalian species. Furthermore, for >100 species from Martinez et al. (2020, 2023), they demonstrated an absence of trade-off between the size-corrected surface area of the maxillo- and the nasoturbinal, suggesting that their results on the maxilloturbinal may be correctly extended to the mammalian respiratory turbinals. These results are particularly relevant in the context of synapsid evolution because complex turbinals have been proposed as a hallmark for endothermy (e.g., Hillenius 1992, 1994, Ruben et al. 2012, Owerkowicz et al. 2015) and subsequently claimed as evidence of endothermy in some non-mammaliamorph synapsid species (Hillenius 1994, Laaß et al. 2010, Laaß & Kaestner 2023). However, Martinez et al. (2023) seriously questions the role of turbinals for body temperature regulation because regardless of the complexity of maxilloturbinals, there is no effect on thermal biology. For instance, the rodents *Psammomys obesus* and *Massoutiera mzabi* have some of the lowest maxilloturbinal relative surface areas, whereas other rodents such as *Blarinomys breviceps* have high relative surface areas. Perhaps surprisingly, the platypus, which is among the mammals with lowest body temperatures, has some of the highest maxilloturbinal surface areas. Indeed, the simplicity of the turbinals in multiple endothermic mammals parallels that of ectothermic diapsids (Bourke & Witmer 2023). Furthermore, it was found that airflow patterns are very similar irrespective of turbinal complexity and thermal regime (Bourke & Witmer 2023). Importantly, the authors found that soft-tissue reconstruction of the nasal cavity is crucial for assessing airflow patterns, because simple cartilaginous turbinals have similar overall effects when compared to more complex and ossified turbinals (Bourke & Witmer 2023). It is thus reasonable to hypothesize that the known thermoregulatory and moisture conservation effects of turbinals (e.g., Schmidt-Nielsen et al. 1970) are by-products of the turbinal anatomy, a structure primarily serving for olfaction. Indeed, it has been proposed that turbinals can be modeled after a gas chromatograph (Mozell 1970, Schoenfeld & Cleland 2005), in which odorants are heterogeneously distributed through the turbinals olfactory epithelia during respiration. To conclude, reported structures such as those observed in *Kawingasarus* (Laaß & Kaestner 2023) likely are not be indicative of endothermy in cistecephalids and probably represent lines left by sediment infilling of the skull cavity (Fig. 12, Fernandez et al. 2013). We could not replicate the observations of the presence of turbinals based on a 27µm-voxel propagation phase-contrast scan of the same specimen of *Kawingasaurus fossilis*.

Evolution of the postorbital-postfrontal complex in dicynodonts

Postfrontal bones are ancestrally present in anomodonts, as evidenced by their ubiquity among non-dicynodont anomodonts for which the relevant region of the skull is preserved (e.g., Brinkman 1981; Ivakhnenko 1996; Rubidge and Hopson 1996; Rybczynski 2000; Liu et al. 2010; Cisneros et al. 2015). Among dicynodonts, the postfrontal (when present) usually is a relatively small, wedge-shaped element that is sandwiched between the frontal and postorbital and contributes to the posterior margin of the orbit. The postfrontal has been lost in a number of dicynodont taxa, and the presence or absence of postfrontals has been used frequently as a character in phylogenetic analyses of dicynodonts (e.g., Maisch 2001, 2002; Maisch and Gebauer 2005; Angielczyk 2007; Fröbisch 2007; Kammerer et al. 2011 and the many subsequent derivatives of that dataset). However, patterns of variation in the presence or absence of this element are more complex than they might first appear, and there are inconsistencies in the literature concerning which taxa lack the postfrontal. For example, Broili and Schröder (1936) and Angielczyk (2007) tentatively reported the presence of postfrontals in *Endothiodon*, whereas Cox (1964), Ray (2000), and Cox and Angielczyk (2015) stated that they were absent; Macungo et al. (2020) did not note their presence in the specimens from Mozambique that they studied. Similarly, Cluver and King (1983) reported that postfrontals were absent in *Rhachiocephalus*, but Keyser (1975), Maisch, (2000), and Angielczyk (2002) stated that they were present in that taxon. There is also evidence of ontogenetic variation in the presence of the element (Kammerer and Smith 2017; Olroyd et al. 2018, Kammerer et al., 2022), and some taxa, especially some Permian basal dicynodontoids, reduce the exposure of the element on the skull roof to a thin strip but retain it as a distinct element seemingly throughout ontogeny (e.g., Kammerer et al. 2011). Of particular relevance to the current paper is the fact that

loss of the postfrontal is widespread among emydopoids. Stemward taxa such as *Emydops* and *Compsodon* retain a postfrontal (Fröbisch and Reisz 2007; Angielczyk and Kammerer 2017), but it is absent in kistecephalians, including all kingoriids (Cox 1959; Fröbisch 2007; Fröbisch et al. 2010; Kammerer 2019) and cistecephalids described to date (Broili and Schröder 1935; Brink 1950; Cox 1972; Keyser 1973; Cluver 1974a; Kammerer et al. 2016; Angielczyk et al. 2019; Araújo et al. 2022b) (also see Cluver 1974b; Kammerer et al. 2015).

Despite being a widespread phenomenon in dicynodonts, the mechanism by which the loss of the postfrontal occurs has received little attention. Passing comments in the literature regarding ontogenetic variation in the presence of the element suggest that at least in some cases its loss stems from fusion of the postfrontal with the postorbital during ontogeny, as opposed to the complete loss of a postfrontal ossification center (Kammerer and Smith 2017; Olroyd et al. 2018). Olroyd et al. (2018) hypothesized that this fusion begins near the dorsal surface of the skull and proceeds ventrally. We examined micro-computed tomography data for a selection of dicynodont taxa to provide a preliminary test of the hypotheses that loss of the postfrontal in dicynodonts typically occurs via fusion of the element with the postorbital, and whether this process begins near the dorsal surface of the skull.

Although it falls in a somewhat nested phylogenetic position, within the dicynodont clade Bidentalia, a specimen of the Permian cryptodont *Oudenodon bainii* from the Luangwa Basin, Zambia (NHCC LB631) provides a useful starting point for comparison as it retains a relatively broad exposure of the postfrontal on the dorsal surface of the skull roof (Fig. 13A). Near its anterior edge, at the posterior margin of the orbit, the postfrontal of *Oudenodon* is relatively wide on the skull roof, and a transverse section through the skull at this level shows that the bone is of a fairly uniform mediolateral width throughout its thickness. Moving posteriorly, the exposure of the postfrontal on the skull roof narrows, but a transverse section near the mid-width of the postorbital bar reveals that the rate of narrowing is not uniform throughout the thickness of the bone. Instead, the dorsal edge of the element narrows more rapidly than the more ventral portions of the bone, giving the postfrontal a greater width within the thickness of the skull roof than on its dorsal surface. Posterior to the level of the postorbital bar, the postfrontal returns to having a more consistent width throughout the thickness of the skull roof, but it takes on a complex sigmoid shape in transverse section to interdigitate with the frontal and the temporal portion of the postorbital. Sutures between the postfrontal, the frontal, and the postorbital are generally consistent in their visibility from the dorsal surface to the ventral surface of the skull roof, suggesting that no fusion of the elements was taking place.

Two other bidentalians that have reduced the exposure of the postfrontal on the skull roof to a narrow strip appear to have done so in a manner resembling the anterior-posterior trend observed in *Oudenodon*. NHCC LB736 consists of the anterior portion of a skull of the geikiid *Aulacephalodon* sp. from the Luangwa Basin that was naturally broken near the level of the postorbital bar, exposing a transverse section of the skull roof in this region (Fig. 13B). The dorsal exposure of the postfrontal in this specimen is extremely narrow. At the posterior margin of the orbit, the postfrontal makes a small, triangular contribution of the orbital rim, but moving posteriorly very little of the postfrontal is visible. Near the mid-width of the postorbital bar, parts of the postfrontal are visible within the thickness of the postorbital–frontal suture, but near the posterior edge of the postorbital bar there is no exposure of the postfrontal visible. However, the broken surface shows that the internal extent of the postfrontal is quite large. Its dorsal surface curves laterally and is extensively overlapped by the frontal, such that only a narrow bit of the bone actually reaches the dorsal surface of the skull roof. As with the *Oudenodon* specimen, the internal sutures bounding the postfrontal are well-marked throughout the thickness of the skull roof, suggesting that fusion was not actively occurring despite the highly reduced exposure of the element on the skull roof.

NHCC LB37 represents a new, undescribed Permian lystrosaurid from the Luangwa Basin whose dorsal exposure of the postfrontal also consists of a narrow strip between the postorbital and frontal (Fig. 13C). Anteriorly, the postfrontal is visible on the anterior surface of the postorbital bar, but it has an extremely narrow exposure on the dorsal surface of the skull roof. A transverse section at this level shows that the postfrontal is broad ventrally, but is extensively overlapped by the postorbital laterally and the frontal medially. A thin triangular process extends dorsally from the approximate midpoint of the postfrontal, but only the narrow apex of this process reaches the skull roof. Closer to the mid-width of the

postorbital bar, the postfrontal is narrower and of a more consistent width across its height. However, its medial surface angles laterally and is overlapped by the frontal, resulting in a narrow exposure on the skull roof. Posterior to the level of the postorbital bar, the postfrontal takes on a more triangular shape in transverse section, with its widest portion dorsally. Its lateral and medial margins in this area are relatively straight, and it does not extend through the whole thickness of the skull roof. The sutures between the postfrontal, the frontal, and the postorbital are well marked throughout the thickness of skull roof. Therefore, areas on the skull roof where the postfrontal is difficult to discern stem more from overgrowth of the bone by the frontal and/or postorbital instead of the obliteration of the sutures separating the elements. The margins of the bone also are straight posteriorly, indicating that it did not interdigitate with the postorbital and the frontal to the degree seen in *Oudenodon.*

As noted above, Olroyd et al. (2018) stated that a distinct postfrontal was visible in some specimens of the Permian basal endothiodont *Abajudon kaayai*, and μCT data are available for one of the specimens that possesses the element (NHCC LB314) from the Mid-Zambezi Basin of Zambia (Fig. 13D). These data facilitate a test of Olroyd et al.'s (2018) hypothesis that the postfrontal began to fuse with the postorbital near the dorsal surface of the skull, and with the bidentalian data described above they provide a useful phylogenetic bracket for members of Emydopoidea that lack a postfrontal. The morphology of the postfrontal on the skull roof of *Abajudon* generally resembles that of *Oudenodon*, consisting of a wider section near the posterior margin of the orbit that then narrows posteriorly. A transverse section through the skull roof at this level also reveals a generally similar internal anatomy, although the postfrontal of *Abajudon* extends farther medially and underplates the frontal more extensively than in *Oudenodon*. Moving posteriorly, to near the mid-width of the postorbital bar, the exposure of the postfrontal on the skull roof is narrower, and its dorsal margin takes on a stepped appearance internally. Medially, a vertical process of the postfrontal extends between the frontal and postorbital to reach the external surface of the skull roof, but laterally the dorsal surface of the postfrontal is horizontal and extensively overlapped by the postorbital. The ventral exposure of the element remains quite wide at this level. Farther posteriorly, near the posterior margin of the postorbital bar, the postfrontal becomes very narrow and takes on a triangular shape (apex oriented ventrally) in transverse section. As a result, the dorsal exposure of the element is its widest portion at this level, and its lateral and medial margins are straight, indicating that it did not interdigitate with the frontal and postorbital. The sutures bounding the postfrontal generally are well-marked throughout the skull roof. Near the dorsal margin of the skull, the sutures are sometimes slightly fainter than is the case farther ventrally, but it is somewhat uncertain if this is a real feature because the effect is subtle and inconsistent from slice to slice in the μCT image stack.

Taken together, the specimens that we examined that phylogenetically bracket Emydopoidea suggest that the reduction of the size of this element on the skull roof in these taxa is largely achieved by increasing the degree to which the postorbital and/or the frontal overlap the postfrontal dorsally, such that the dorsal exposure is narrow but the internal size of the element remains large, especially in the vicinity of the orbit and the postorbital bar. There is limited evidence that fusion of the the postorbital proceeds from dorsal to ventral in *Abajudon*, as suggested by Olroyd et al. (2018), but more investigation is needed to confirm that this is the case.

The situation is quite different in the emydopoids we considered that lack external evidence of a postfrontal. For example, in a specimen of *Dicynodontoides* sp. (NHCC LB117; Fig. 13E) and the holotype of *Kembawacela kitchingi* (NHCC LB18; Fig. 13F), both from the Luangwa Basin, there is no evidence internally of a discrete postfrontal. Instead, the suture between the postorbital and the frontal is well-marked, but no sutures delimiting a postfrontal are visible, and there are also no obvious discontinuities in the internal structure of the postorbital that would suggest the location of a postfrontal early in ontogeny. The *Dicynodontoides* specimen is especially interesting because the portion of the postorbital near the posteromedial margin of the orbit (i.e., the area that would be occupied ancestrally by the postfrontal) has an external appearance that strongly resembles the shape of the postfrontal of taxa in which the element is present. Based on this appearance, it is very easy to imagine a distinct postfrontal ossification being present initially in ontogeny that later fused with the postorbital while retaining its basic shape. However, if this did occur in NHCC LB117, it happened at a sufficiently early stage in ontogeny that all evidence of the sutures bounding the postfrontal were obliterated, and the internal structure of the resulting single

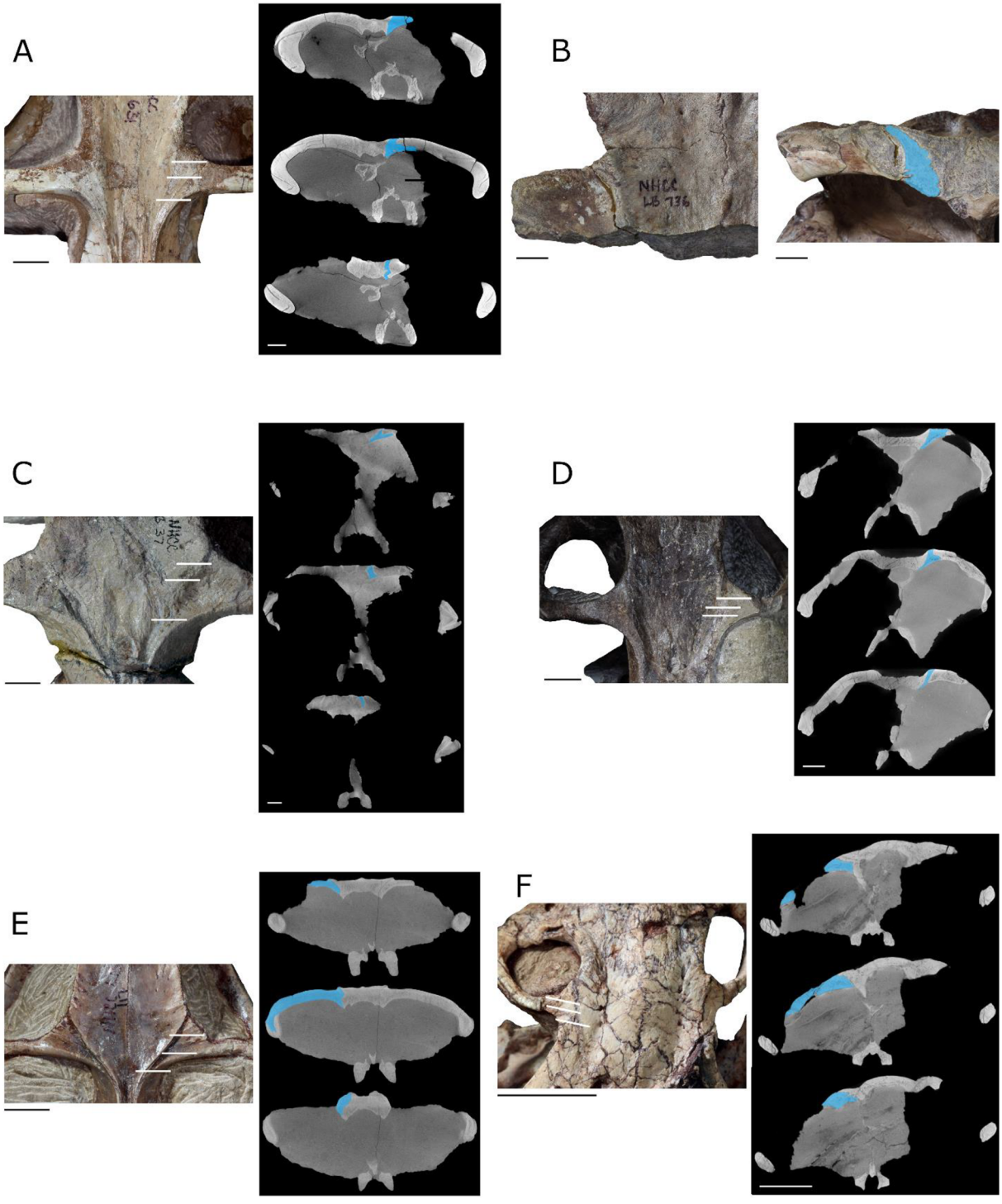

FIGURE 13. Comparisons of the postfrontal in dicynodonts. A, Photograph of the interorbital skull roof (left) and example micro-computed tomography slices (right) of *Oudenodon bainii* (NHCC LB631). B, Photographs of the left side of the interorbital skull roof (left) and the broken posterior surface of the skull roof (right) of *Aulacephalodon* sp. (NHCC LB736). C, Photograph of the interorbital skull roof (left) and example μCT slices (right) of an undescribed lystrosaurid (NHCC LB37). D, Photograph of the interorbital skull roof (left) and example μCT slices (right) of *Abajudon kaayai* (NHCC LB314). E, Photograph of the interorbital skull roof (left) and example μCT slices (right) of *Dicynodontoides* sp. (NHCC LB117). E, Photograph of the interorbital skull roof (left) and example μCT slices (right) of *Kembawacela kitchingi*. White lines in the photographs indicate the approximate planes shown in the μCT slices. The most anterior slice is at the top of each stack. The postfrontal is highlighted in blue in the μCT slices and on the broken surface of NHCC LNB736. Scale bars are 1 cm.

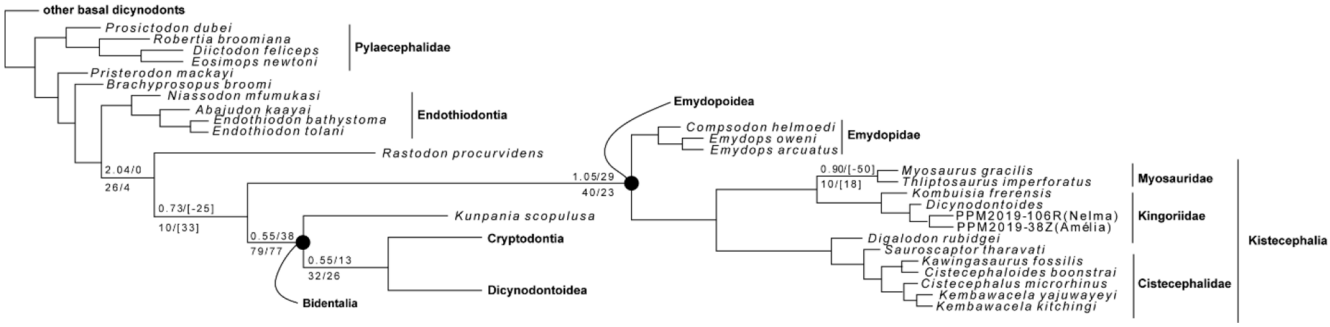

FIGURE 14. Phylogenetic analysis topology and branch support for a section of the tree. Bremer support and relative Bremer support above the tree branches, and symmetric resampling and GC values below the branches, based on 10k replications. Note the relatively strong support for the position of *Kunpania* as a basal bidentalian, whereas the position of *Rastodon* is particularly poorly supported. *Rastodon* can be retrieved as an emydopoid closely related to *Dicynodontoides* in some test analysis with different coding for some characters or outside Emydopoidea as shown above.

element was sufficiently remodeled to remove any discontinuities in its internal structure. A small piece of bone on the left side of the *Kembawacela* specimen, just behind the posterior margin of the orbit, is somewhat suggestive of perhaps representing the remains of a postfrontal element, but based on comparisons with the better-preserved right side, we think this more likely represents a broken fragment of bone that is delimited by cracks in the skull roof.

In summary, the emydopoids that lack a postfrontal appear to reduce this element in a notably different way compared to the endothiodont and bidentalians. Instead of reducing the exposure of the postfrontal on the skull roof by increasing the degree to which the postorbital and frontal overlap the postfrontal and maintaining a relatively large internal extent of the bone, the emydopoids show no evidence of a postfrontal ossification internally or externally. Our current dataset is too limited to determine whether the morphology in emydopoids reflects a fusion of the postorbital and postfrontal very early in ontogeny, or the actual loss of a postfrontal ossification center altogether, but further investigation of this previously unappreciated aspect of variation clearly is warranted.

Phylogenetic analysis

The results from the phylogenetic analysis shown in Fig. 14 largely align with earlier versions of the dataset (Kammerer et al. 2011, Macungo et al. 2022, Araújo et al. 2022b, Angielczyk et al. 2021, 2023). However, there are some significant changes in the topology that deserve attention: (1) *Rastodon* is now positioned as the basalmost member of Therocelonia; (2) *Kunpania* is identified as the basalmost member of Bidentalia; (3) *Thliptosaurus* is a sister-taxon to *Myosaurus*.

Regarding *Rastodon*'s position, its detailed character recoding and its similarities to *Dicynodontoides* suggest a more basal position, placing it outside of Emydopoidea. This result is in contrast to what Macungo et al. (2022) proposed, but we acknowledge that a better understanding of the palate and basicranial anatomy may produce different results. Hence, micro-computed tomography and bone-by-bone segmentation may elucidate many characters for this important taxon. Interestingly, when we adjusted the analysis by coding Discrete Character 41 (related to the presence of the postfrontal, as discussed earlier) as present for both *Dicynodontoides* and *Rastodon* (based on Boos et al. 2016) and removed the less complete taxon *Kunpania* (referenced in Angielvzyk et al. 2021), *Rastodon* emerged as a sister-taxon to *Dicynodontoides*. This finding underscores the significance of the postfrontal's evolution in emydopoids. It also hints at potential broader implications for understanding the evolutionary relationships among therochelonians. Following the most parsimonious tree, *Rastodon* is excluded from the bidentalian because: the relatively wide median pterygoid plate compared to basal skull length (Continuous Character 8), and we consider that the mid-ventral plate of the vomer has an overall shape comparable to other emydopoids despite considerable taphonomic deformation (Discrete Character 72, 73 and 74).

Kunpania is identified as the basalmost bidentalian, which represents a notably more basal position than what Angielczyk et al. (2021) suggested. They recovered it as a basal dicynodontoid and a sister-taxon to *Sintocephalus*. The structure of our tree

aligns more closely with the topology presented by Kammerer et al. (2011) than with the dicynodontoid arrangements of Liu (2021) and Angielczyk et al. (2023). In our tree, there is a sequence of stem-dicynodontoids, such as *Taoheodon* (as the basalmost dicynodontoid), *Repelinosaurus*, and *Dicynodon* spp. (Supplementary Information in Morphobank). These taxa provide the foundation for lystrosaurids and a clade that includes species like *Daptocephalus* spp. and *Turfanodon* spp. Importantly, several characteristics solidify *Kunpania*'s position as a bidentalian, specifically the height of anterior pterygoid keel in lateral view relative height of non-keel ramus (Continuous Char. 7); the length of the deltopectoral crest relative to the total humerus length (Continuous Char. 18); the presence of a distinct lateral caniniform buttress (Discrete Character 29); the absence of a keel-like extension of the palatal rim posterior to the caniniform process (Char. 30); the strong lateral bend of the jaw ramus (Discrete Character 115); the presence of an up-turned beak and scooped-out depression on the lower jaw as in most bidentalians (Discrete Character 121); the presence of a curved ridge that follows the profile of the symphysis present on the edge between the anterior and lateral surfaces of the dentary as in most bidentalians and unlike emydopoids and endothiodonts (Discrete Character 122); presence of a long, narrow and deep post-dentary sulcus, unlike emydopoids (Discrete Character 125); and the insertion of the latissimus dorsi is extended into a dorsoventrally flattened pinna-like process, unlike non-bidentalian dicynodonts (Discrete Character 152). The more basal position of *Kunpania* in the current analysis would also fit well with its potential middle Permian age (Angielczyk et al., 2021).

In contrast to the findings of Macungo et al. (2022), which placed Kingoriidae near the base of Emydopoidea, we obtained a more conventional arrangement as in Kammerer et al. (2011) and Angielczyk et al. (2023). In their work, Emydopidae was positioned at the base of Emyopoidea, followed by Kistecephalia. In our analysis, *Thliptosaurus* is identified as closely related to *Myosaurus*, with their relationship unified by a single synapomorphy: the development of the ventromedial process of the opisthotic into a robust, tuber-like knob (Discrete Character 181). However, it is important to note that the current topology should be considered tentative until a comprehensive bone-by-bone segmentation of *Myosaurus* and *Thliptosaurus* is conducted.

ACKNOWLEDGMENTS

We thank the PaleoMoz Project, FCT and AGA KHAN grant (333206718), National Geographic Society (CP-109R-17). We also thank Christian Kammerer and Julien Benoit for their insightful reviews.

REFERENCES

Angielczyk, K. D. (2002). Redescription, phylogenetic position, and stratigraphic significance of the dicynodont genus *Odontocyclops* (Synapsida: Anomodontia). *Journal of Paleontology*, 76, 1047–1059.

Angielczyk, K. D. (2007). New specimens of the Tanzanian dicynodont *"Cryptocynodon" parringtoni* von Huene, 1942 (Therapsida, Anomodontia), with an expanded analysis of Permian dicynodont phylogeny. *Journal of Vertebrate Paleontology*, 27, 116–131.

Angielczyk, K. D. & Sullivan, C. (2008). *Diictodon feliceps* (Owen, 1876), a dicynodont (Therapsida, Anomodontia) species with a Pangaean distribution. *Journal of Vertebrate Paleontology*, 28(3), 788-802.

Angielczyk, K. D. & Rubidge, B. S. (2013). Skeletal morphology, phylogenetic relationships and stratigraphic range of *Eosimops newtoni* Broom, 1921, a pylaecephalid dicynodont (Therapsida, Anomodontia) from the Middle Permian of South Africa. *Journal of Systematic Palaeontology*, 11(2), 191-231.

Angielczyk, K. D. & Schmitz, L. (2014). Nocturnality in synapsids predates the origin of mammals by over 100 million years. *Proceedings of the Royal Society B: Biological Sciences*, 281(1793), 20141642.

Angielczyk, K. D. & Kammerer, C. F. (2017). The cranial morphology, phylogenetic position and biogeography of the upper Permian dicynodont *Compsodon helmoedi* van Hoepen (Therapsida, Anomodontia). *Papers in Palaeontology*, 3(4), 513-545.

Angielczyk, K. D., Benoit, J., & Rubidge, B. S. (2021). A new tusked cistecephalid dicynodont (Therapsida, Anomodontia) from the upper Permian upper Madumabisa Mudstone formation, Luangwa Basin, Zambia. *Papers in Palaeontology*, 7(1), 405-446.

Angielczyk, K. D., Liu, J., & Yang, W. (2021). A redescription of *Kunpania scopulusa*, a bidentalian dicynodont (Therapsida, Anomodontia) from the ?Guadalupian of northwestern China. *Journal of Vertebrate Paleontology*, 41(1), e1922428.

Angielczyk, K. D., Brandon R. Peecook, & Roger M. H. Smith (2023). The mandible of *Compsodon helmoedi* (Therapsida: Anomodontia), with new records from the Ruhuhu Basin, Tanzania. *Palaeontologia Africana*, 56, 88–102.

Araújo, R., Fernandez, V., Rabbitt, R. D., Ekdale, E. G., Antunes, M. T., Castanhinha, R., Fröbisch, J., & Martins, R. M. (2018). *Endothiodon* cf. *bathystoma* (Synapsida: Dicynodontia) bony labyrinth anatomy, variation and body mass estimates. *PLoS one*, 13(3), e0189883.

Araújo, R., David, R., Benoit, J., Lungmus, J. K., Stoessel, A., Barrett, P. M., Maisano, J. A., Ekdale, E., Orliac, M., Luo, Z. X., & Martinelli, A. G. (2022a). Inner ear biomechanics reveals a Late Triassic origin for mammalian endothermy. *Nature*, 607(7920), 726-731.

Araújo, R., Macungo, Z., Fernandez, V., Chindebvu, E. G., & Jacobs, L.

L. (2022b). *Kembawacela yajuwayeyi* n. sp., a new cistecephalid species (Dicynodontia: Emydopoidea) from the Upper Permian of Malawi. *Journal of African Earth Sciences*, 196, 104726.

Barbolini, N., Smith, R. M. H., Tabor, N. J., Sidor, C. A., & Angielczyk, K. D. (2016). Resolving the age of Madumabisa fossil vertebrates. Palynological evidence from the Mid-Zambezi Basin of Zambia. *Palaeogeography, Palaeoclimatology, Palaeoecology*, 457, 117-128.

Benoit, J., Manger, P. R., & Rubidge, B. S. (2016). Palaeoneurological clues to the evolution of defining mammalian soft tissue traits. *Scientific Reports*, 6, 25604.

Benoit, J., Angielczyk, K. D., Miyamae, J. A., Manger, P., Fernandez, V., & Rubidge, B. (2018). Evolution of facial innervation in anomodont therapsids (Synapsida): Insights from X-ray computerized microtomography. *Journal of Morphology*, 279(5), 673-701.

Benoit, J., Dollman, K. N., Smith, R. M. H., & Manger, P. R. (2023). At the root of the mammalian mind: the sensory organs, brain, and behavior of pre-mammalian synapsids. In T. Calvey, A. A. de Sousa, & A. A. Baudet (Eds.), *Fossils to Mind* (pp. 25-72). *Progress in Brain Research*, 275.

Benton, M. J. (2021). The origin of endothermy in synapsids and archosaurs and arms races in the Triassic. *Gondwana Research*, 100, 261-289.

Berlin, J. C., Kirk, E. C., & Rowe, T. B. (2013). Functional implications of ubiquitous semicircular canal non-orthogonality in mammals. *PLoS One*, 8(11), e79585.

Boos, A. D., Kammerer, C. F., Schultz, C. L., Soares, M. B., & Ilha, A. L. (2016). A new dicynodont (Therapsida: Anomodontia) from the Permian of southern Brazil and its implications for bidentalian origins. *PLoS One*, 11(5), e0155000.

Boucot, A. J., Chen, X., Scotese, C. R., & Morley, R. J. (2013). *SEPM Concepts in Sedimentology and Paleontology*, Vol. 11, SEPM.

Bourke, J. M. & Witmer, L. M. (2023). Soft tissues influence nasal airflow in diapsids: Implications for dinosaurs. *Journal of Morphology*, 284(9), e21619.

Brink, A. S. (1950). On a new species of *Cistecephalus* Owen. *Annals & Magazine of Natural History*, Series 12, 985–997.

Brinkman, D. (1981). The structure and relationships of the dromasaurs (Reptilia; Therapsida). *Breviora*, 465, 1–34.

Broili, F. & Schröder, J. (1935). Beobachtungen an Wirbeltieren der Karrooformation. VI. Über den Schädel von *Cistecephalus* Owen. *Sitzungsberichte der Bayerischen Akademie der Wissenschaften Mathematisch-Naturwissenschaftliche Abteilung*, 1935, 1–20.

Broili, F. & J. Schröder. (1936). Beobachtunger an Wirberltieren der Karrooformation. XVI. Beobachtungen am Schädel von *Emydochampsa* Broom. *Sitzungberichte der Bayerischen Akademie der Wissenschaften Mathematisch-naturwissenschaftliche Abteilung*, 1936, 21–44.

Broom, R. (1906). On the Permian and Triassic faunas of South Africa. *Geological Magazine New Series*, 5, 29-30.

Bremer, K. (1994). Branch support and tree stability. *Cladistics*, 10, 295–304.

Buffenstein, R. & Yahav, S. (1991). Is the naked mole-rat *Hererocephalus glaber* an endothermic yet poikilothermic mammal? *Journal of Thermal Biology*, 16, 227–232.

Carlson, K. J., Stout, D., Jashashvili, T., De Ruiter, D. J., Tafforeau, P., & Berger, L. R. (2011). The endocast of MH1, *Australopithecus sediba*. *Science*, 333, 1402-1407.

Castanhinha, R., Araújo, R., Junior, L. C., Angielczyk, K. D., Martins, G. G., Martins, R. M., Chaouiya, C., Beckmann, F., & Wilde, F. (2013). Bringing dicynodonts back to life: paleobiology and anatomy of a new emydopoid genus from the Upper Permian of Mozambique. *PLoS One*, 8(12), e80974.

Cisneros, J. C., Abdala, F., Jashashvili, T., de Oliveira Bueno, A., & Dentzien-Dias, P. *Tiarajudens eccentricus* and *Anomocephalus africanus*, two bizarre anomodonts (Synapsida, Therapsida) with dental occlusion from the Permian of Gondwana. *Royal Society Open Science*, 2(7), 150090.

Cluver, M. A. (1971). The cranial morphology of the dicynodont genus *Lystrosaurus*. *Annals of the South African Museum*, 56, 155–274.

Cluver, M. A. (1974a). The skull and mandible of a new cistecephalid dicynodont. *Annals of the South African Museum*, 67, 7–23.

Cluver, M. A. (1974b). The cranial morphology of the Lower Triassic dicynodont *Myosaurus gracilis*. *Annals of the South African Museum*, 66, 35–54.

Cluver, M. A. (1978). The skeleton of the mammal-like reptile *Cistecephalus* with evidence for a fossorial mode of life. *Annals of the South African Museum*, 76, 213–246.

Cluver, M. A. & King, G. M. (1983). A reassessment of the relationships of Permian Dicynodontia (Reptilia, Therapsida) and a new classification of dicynodonts. *Annals of the South African Museum*, 91, 195–273.

Cox, C. B. (1959). On the anatomy of a new dicynodont genus with evidence of the position of the tympanum. *Procedings of the Zoological Society of London*, 132, 321–367.

Cox, C. B. (1964). On the palate, dentition, and classification of the fossil reptile *Endothiodon* and related genera. *American Museum Novitates*, 2171, 1–25.

Cox, C. B. (1972). A new digging dicynodont from the Upper Permian of Tanzania. In T. S. Kemp (Ed.), *Studies in vertebrate evolution* (pp. 73–189). Edinburgh: Oliver and Boyd.

Cox, C. B. & Angielczyk, K. D. (2015). A new endothiodont dicynodont (Therapsida, Anomodontia) from the Permian Ruhuhu Formation (Songea Group) of Tanzania and its feeding system. *Journal of Vertebrate Paleontology*, 35, e935388.

Crompton, A. W., Owerkowicz, T., Bhullar, B. A., & Musinsky, C. (2017). Structure of the nasal region of non-mammalian cynodonts and mammaliaforms: speculations on the evolution of mammalian endothermy. *Journal of Vertebrate Paleontology*, 37(1), e1269116.

Day, M. O. & Smith, R. M. H. (2020). Biostratigraphy of the *Endothiodon* Assemblage Zone (Beaufort Group, Karoo Supergroup), South Africa. *South African Journal of Geology*, 123(2), 165–180.

Escobar, J. A., Martinelli, A. G., Ezcurra, M. D., Fiorelli, L. E., Von Baczko, M. B., Novas, F. E., & Desojo, J. B. (2023). A Reassessment of the Mandibular Anatomy of *Dinodontosaurus brevirostris* (Synapsida, Dicynodontia) from the Ladinian–Early Carnian Chañares Formation (Northwestern Argentina), and Its Taxonomic and Phylogenetic Significance. *Ameghiniana*, 60(2), 178–201.

Ewer, R. F. (1961). The anatomy of the anomodont *Daptocephalus leoniceps* (Owen). *Proceedings of the Zoological Society of London*, 136(3), 375-402.

Fitzpatrick, R. C., Butler, J. E., & Day, B. L. (2006). Resolving head rotation for human bipedalism. *Current Biology*, 16, 1509–1514.

Fröbisch J. (2007). The cranial anatomy of *Kombuisia frerensis* Hotton (Synapsida, Dicynodontia) and a new phylogeny of anomodont therapsids. *Zoological Journal of the Linnean Society*, 150, 117–144.

Fröbisch, J. & Reisz, R. R. (2008). A new species of *Emydops*

(Synapsida, Anomodontia) and a discussion of dental variability and pathology in dicynodonts. *Journal of Vertebrate Paleontology*, 28(3), 770-787.

Fröbisch, J., Angielczyk, K. D., & Sidor, C. A. (2010). The Triassic dicynodont *Kombuisia* (Synapsida, Anomodontia) from Antarctica, a refuge from the terrestrial Permian-Triassic mass extinction. *Naturwissenschaften*, 97, 187–196.

Goloboff, P. A. (1999). Analyzing large data sets in reasonable times: solutions for composite optima. *Cladistics*, 15, 415–428.

Goloboff, P. A. & Farris, J. S. (2001). Methods for quick consensus estimation. *Cladistics*, 17, S26–S34.

Goloboff, P. A., Farris, J. S., Källersjö, M., Oxelman, B., Ramírez, M. J., & Szumik, C. A. (2003). Improvements to resampling measures of group support. *Cladistics*, 19, 324–332.

Goloboff, P. A. & Catalano, S. A. (2016). TNT version 1.5, including a full implementation of phylogenetic morphometrics. *Cladistics*, 32, 221–238.

Hertz, P. E., Huey, R. B., & Garland Jr, T. (1988). Time budgets, thermoregulation, and maximal locomotor performance: are reptiles olympians or boy scouts? *American Zoologist*, 28(3), 927-938.

Hillenius, W. J. (1992). The evolution of nasal turbinates and mammalian endothermy. *Paleobiology*, 18(1), 17–29.

Hillenius, W. J. (1994). Turbinates in therapsids: evidence for Late Permian origins of mammalian endothermy. *Evolution*, 48(2), 207-229.

Ivakhnenko, M. F. (1996). Primitive anomodonts, venyukoviids, from the Late Permian of Eastern Europe. *Paleontological Journal*, 30, 575–582.

Kammerer, C. F. (2019). A new dicynodont (Anomodontia: Emydopoidea) from the terminal Permian of KwaZulu-Natal, South Africa. *Palaeontologia africana*, 53, 179–191.

Kammerer, C. F. & Smith, R. M. S. (2017). An early geikiid dicynodont from the *Tropidostoma* Assemblage Zone (late Permian) of South Africa. *PeerJ*, 5, e2913.

Kammerer, C. F., Angielczyk, K. D., & Fröbisch, J. (2011). A comprehensive taxonomic revision of *Dicynodon* (Therapsida, Anomodontia) and its implications for dicynodont phylogeny, biogeography, and biostratigraphy. *Society of Vertebrate Paleontology Memoir*, 11, 1–158.

Kammerer, C. F. (2015). Redescription of *Digalodon rubidgei*, an emydopoid dicynodont (Therapsida, Anomodontia) from the Late Permian of South Africa. *Fossil Record*, 18(1), 43-55.

Kammerer, C. F., S. Bandyopadhyay, & S. Ray. (2016). A new taxon of cistecephalid dicynodont from the Upper Permian Kundaram Formation of India. *Papers in Palaeontology*, 2, 589–594.

Kammerer, C. F., R. Araújo, K. Cumbane, Z. Macungo, R. M. H. Smith, & K. D. Angielczyk. (2021). New material of *Dicynodon angielczyki* (Synapsida: Anomodontia) from Mozambique and Zambia with biostratigraphic implications for African Permo-Triassic basins. *Journal of Vertebrate Paleontology*, 41(6). DOI: 10.1080.02724634.2021.2041652.

Kammerer, C. F. (2021). Elevated cranial sutural complexity in burrowing dicynodonts. *Frontiers in Ecology and Evolution*, 9, 674151.

Keyser, A. W. (1965). The morphology of the anomodont genus *Cistecephalus* Owen (1876). (M.Sc. thesis, University of Pretoria.)

Keyser, A. W. (1973). A preliminary study of the type area of the *Cistecephalus* Zone of the Beaufort Series, and a revision of the anomodont family Cistecephalidae. *Geological Survey of South Africa*, 62, 1–71.

Keyser, A. W. (1975). A reevaluation of the cranial morphology and systematics of some tuskless Anomodontia. *Geological Survey of South Africa Memoir*, 67, 1–110.

Kitching, J. W. (1970). A short review of the Beaufort zoning in South Africa in *Second Gondwana Symposium- Proceedings and Papers*. Council for Scientific and Industrial Research, Pretoria, 309–312.

Kramer, D. L. & McLaughlin, R.L. (2001). The behavioral ecology of intermittent locomotion. *American Zoologist*, 41(2), 137-153.

Laaß, M., Hampe, O., Schudack, M., Hoff, C., Kardjilov, N., & Hilger, A. (2010). New insights into the respiration and metabolic physiology of *Lystrosaurus*. *Acta Zoologica*, 92, 363–371.

Laaß, M. (2015). Bone-conduction hearing and seismic sensitivity of the late Permian anomodont *Kawingasaurus fossilis*. *Journal of Morphology*, 276(2), 121–143.

Laaß, M. & Kaestner, A. (2023). Nasal turbinates of the dicynodont *Kawingasaurus fossilis* and the possible impact of the fossorial habitat on the evolution of endothermy. *Journal of Morphology*, 284(9), e21621.

Lyckegaard, A., Johnson, G., & Tafforeau, P. (2011). Correction of ring artifacts in X-ray tomographic images. *International Journal of Tomography and Statistics*, 18, 1-9.

Lindenlaub, T., Burda, H., & Nevo, E. (1995). Convergent evolution of the vestibular organ in the subterranean mole-rats *Cryptomys* and *Spalax*, as compared with the aboveground rat, *Rattus*. *Journal of Morphology*, 224, 303–311.

Liu, J., B. Rubudge, & J. Li. (2010). A new specimen of *Biseridens qilianicus* indicates its phylogenetic position as the most basal anomodont. *Proceedings of the Royal Society B*, 277, 285–292.

Liu, J. (2021). The tetrapod fauna of the upper Permian Naobaogou Formation of China: 6. *Turfanodon jiufengensis* sp. nov. (Dicynodontia). *PeerJ*, 9, e10854.

Liu, J. (2022). On kannemeyeriiform dicynodonts from the *Shaanbeikannemeyeria* Assemblage Zone of the Ordos Basin, China. *Vertebrata Palasiatica*, 60(3), 212-248.

Lungmus, J. K. & Angielczyk, K. D. (2021). Phylogeny, function and ecology in the deep evolutionary history of the mammalian forelimb. *Proceedings of the Royal Society B*, 288, 20210494.

Macungo, Z., Loide, I., Zunguza, S., Nhamutole, N., Maharaj, I. E. M., Mugabe, J., Angielczyk, K. D., & Araújo, R. (2020). *Endothiodon* (Therapsida, Anomodontia) specimens from the middle/late Permian of the Metangula Graben (Niassa Province, Mozambique) increase complexity to the taxonomy of the genus. *Journal of African Earth Sciences*, 163, 103647.

Macungo, Z., Benoit, J., Fernandez, V., & Araújo, R. (2022). X-ray microcomputed and synchrotron tomographic analysis of the basicranial axis of emydopoid dicynodonts: implications for fossoriality and phylogeny. *Zoological Journal of the Linnean Society*, 198(1), 1-46.

Maisch, M. W. (2001). Observations on Karoo and Gondwana vertebrates. Part 2: a new skull-reconstruction of *Stahleckeria potens* von Huene, 1935 (Dicynodontia, Middle Triassic) and a reconsideration of kannemeyeriiform phylogeny. *Neues Jahrbuch für Geologie und Paläontologie Abhandlungen*, 220, 127–152.

Maisch, M. W. & Gebauer, E. V. I. (2005). Reappraisal of *Geikia locusticeps* (Therapsida: Dicynodontia) from the Upper Permian of Tanzania. *Palaeontology*, 48, 309–324.

Martinez, Q., Clavel, J., Esselstyn, J. A., Achmadi, A. S., Grohé, C., Pirot, N., & Fabre, P. H. (2020). Convergent evolution of olfactory

and thermoregulatory capacities in small amphibious mammals. *Proceedings of the National Academy of Sciences*, 117(16), 8958-8965.

Martinez, Q., Okrouhlík, J., Šumbera, R., Wright, M., Araújo, R., Braude, S., Hildebrandt, T. B., Holtze, S., Ruf, I., & Fabre, P. H. (2023). Mammalian maxilloturbinal evolution does not reflect thermal biology. *Nature Communications*, 14(1), 4425.

Mayhew, W. W. (1965). Hibernation in the horned lizard, *Phrynosoma m'calli*. *Comparative Biochemistry and Physiology*, 16(1), 103-119.

McVean, A. (1999). Are the semicircular canals of the European mole, *Talpa europaea*, adapted to a subterranean habitat?. *Comparative Biochemistry and Physiology Part A: Molecular & Integrative Physiology*, 123(2), 173-178.

Mirone, A., Brun, E., Gouillart, E., Tafforeau, P., & Kieffer, J. (2014). The PyHST2 hybrid distributed code for high-speed tomographic reconstruction with iterative reconstruction and a priori knowledge capabilities. *Nuclear Instruments and Methods in Physics Research Section B: Beam Interactions with Materials and Atoms*, 324, 41-48.

Mozell, M. M. (1970). Evidence for a chromatographic model of olfaction. *Journal of General Physiology*, 56, 46–63.

Nasterlack, T., Canoville, A., & Chinsamy, A. (2012). New insights into the biology of the Permian genus *Cistecephalus* (therapsida, dicynodontia). *Journal of Vertebrate Paleontology*, 32(6), 1396–1410.

Olroyd, S. L., Sidor, C. A., & Angielczyk, K. D. (2018). New materials of the enigmatic dicynodonts *Abajudon kaayai* (Therapsida, Anomodontia) from the lower Madumabisa Mudstone Formation, middle Permian of Zambia. *Journal of Vertebrate Paleontology*, 37(6). DOI: 10.10180/02724634.2017.1403442.

Owerkowicz, T., Musinsky, C., Middleton, K. M., & Crompton, A. W. (2015). Respiratory turbinates and the evolution of endothermy in mammals and birds. In K. P. Dial, N. Shubin, & E. L. Brainerd (Eds.), *Great Transformations in Vertebrate Evolution* (pp. 143–165). University of Chicago Press.

Paganin, D., Mayo, S., Gureyev, T. E., Miller, P. R., & Wilkins, S. W. (2002). Simultaneous phase and amplitude extraction from a single defocused image of a homogeneous object. *Journal of Microscopy*, 206, 33-40.

Pianka, E. R. (1986). *Ecology and natural history of desert lizards: analyses of the ecological niche and community structure.* Princeton University Press.

Plessis, A., le Roux, S. G., & Guelpa, A. (2016). The CT Scanner Facility at Stellenbosch University: An open access X-ray computed tomography laboratory. *Nuclear Instruments & Methods in Physics Research. Section B, Beam Interactions with Materials and Atoms*, 384, 42–49. DOI: 10.1016/j.nimb.2016.08.005.

Rabbitt, R., Damiano, E., & Grant, J. (2003). Biomechanics of the vestibular semicircular canals and otolith organs. In: *The Vestibular System*, edited by Highstein SM, Popper A, Fay R. New York: Springer.

Ray, S. (2000). Endothiodont dicynodonts from the Late Permian Kundaram Formation, India. *Palaeontology*, 43, 375–404.

Rees, P. M. et al. (2002). Permian phytogeographic patterns and climate data/model comparisons. *Journal of Geology*, https://doi.org/10.1086/324203.

Rey, K. et al. (2016). Global climate perturbations during the Permo-Triassic mass extinctions recorded by continental tetrapods from South Africa. *Gondwana Research*, 37, 384–396.

Roscher, M., Stordal, F., & Svensen, H. (2011). The effect of global warming and global cooling on the distribution of the latest Permian climate zones. *Palaeogeography Palaeoclimatology Palaeoecology*, 309, 186–200.

Rowe, T. B., Macrini, T. E., & Luo, Z.-X. (2011). Fossil evidence on origin of the mammalian brain. *Science*, 332, 955–957.

Rubidge, B. S. & Hopson, J. A. (1996). A primitive anomodont therapsid from the base of the Beaufort Group (Upper Permian) of South Africa. *Zoological Journal of the Linnean Society*, 117, 115–139.

Rubidge, B. S., Erwin, D. H., Ramezani, J., Bowring, S. A., & de Klerk, W. J. (2013). High-precision temporal calibration of Late Permian vertebrate biostratigraphy: U-Pb zircon constraints from the Karoo Supergroup, South Africa. *Geology*, 41, 363-366.

Ruben, J. A., Hillenius, W. J., Kemp, T. S., & Quick, D. E. (2012). The evolution of mammalian endothermy. In A. Chinsamy (Ed.), *Forerunners of Mammals: Radiation, Histology, Biology* (pp. 273–286). Indiana University Press.

Rybczynski, N. (2000). Cranial anatomy and phylogenetic position of *Suminia getmanovi*, a basal anomodont (Amniota: Therapsida) from the Late Permian of Eastern Europe. *Zoological Journal of the Linnean Society*, 130, 329–373.

Schmidt-Nielsen, K., Hainsworth, F. R., & Murrish, D. E. (1970). Counter-current heat exchange in the respiratory passages: Effect on water and heat balance. *Respiratory Physiology*, 9, 263–276.

Schoenfeld, T. A. & Cleland, T. A. (2005). The anatomical logic of smell. *Trends in Neurosciences*, 28(11), 620-627.

Shi, Y. T. & Liu, J. (2023). The tetrapod fauna of the upper Permian Naobaogou Formation of China: 10. *Jimusaria monanensis* sp. nov. (Dicynodontia) shows a unique epipterygoid. *PeerJ*, 11, e15783.

Simão-Oliveira, D., Kerber, L., & Pinheiro, F. (2020). Endocranial morphology of the Brazilian Permian dicynodont *Rastodon procurvidens* (Therapsida: anomodontia). *Journal of Anatomy*, 236(3), 384-397.

Smith, R. M. H. & Keyser, A. W. (1995). Biostratigraphy of the Cistecephalus Zone. In B. S. Rubidge (Editor), *Biostratigraphy of the Beaufort Group (Karoo Supergroup)*, S.A.C.S. Biostratig. Series 1, 23-28.

Smith, R. M. H. (2020). Biostratigraphy of the *Cistecephalus* Assemblage Zone (Beaufort Group, Karoo Supergroup), South Africa. *South African Journal of Geology*, 123(2), 181-190.

Smith, R. M., Angielczyk, K. D., Benoit, J., & Fernandez, V. (2021). Neonate aggregation in the Permian dicynodont *Diictodon* (Therapsida, Anomodontia): evidence for a reproductive function for burrows?. *Palaeogeography, Palaeoclimatology, Palaeoecology*, 569, 110311.

Southwood, A. & Avens, L. (2010). Physiological, behavioral, and ecological aspects of migration in reptiles. *Journal of Comparative Physiology B*, 180, 1-23.

Szczygielski, T. & Sulej, T. (2023). *Woznikella triradiata* n. gen., n. sp. – a new kannemeyeriiform dicynodont from the Late Triassic of northern Pangea and the global distribution of Triassic dicynodonts. *Comptes Rendus Palevol*, 22(16), 279-406.

Yagi, K. T. & Litzgus, J. D. (2013). Thermoregulation of spotted turtles (*Clemmys guttata*) in a beaver-flooded bog in southern Ontario, Canada. *Journal of Thermal Biology*, 38*(5), 205-213.

Zhang, J., Cai, R., Liang, J., et al. (2021). Molecular mechanism of Chinese alligator (*Alligator sinensis*) adapting to hibernation. *Journal of Experimental Zoology (Molecular and Developmental Evolution)*, 336, 32–49.

SUPPLEMENTARY INFORMATION – COMPUTED TOMOGRAPHY-BASED RE-DESCRIPTION OF THE SKULL AND MANDIBLE OF THE MID-PERMIAN DICYNODONT *DIICTODON FELICEPS* SPECIMEN GPIT-PV-60758.

INTRODUCTION

Anomodontia was first described by Richard Owen (1859) and was one of the most speciose tetrapod clades during the Permian and Triassic (Fröbisch, 2008; Kammerer et al., 2011). Anomodonts were herbivorous non-mammalian therapsids that dominated terrestrial habitats, ranging from small burrowers (e.g., Castanhinha et al., 2013) to hippopotamus-sized grazers (e.g., Sulej and Niedzwiedzki, 2019). Most of anomodont diversity is represented by the largest anomodont sub-clade, Dicynodontia (Owen, 1859). Initially, many new specimens were allocated to the genus *Dicynodon*, which was originally described to group newly discovered reptiles with some mammal-like features (Owen, 1845). This practice persisted through most of the first half of the 20th century, making it a taxonomic wastebasket and resulting in the grouping of several species with unclear affinities (Broom, 1911).

The chaotic state of taxonomy within *Dicynodon* led to an extensive revision of the genus (Kammerer et al., 2011). *Dicynodon megalorhinus*, one of the 168 species ascribed to this genus (Kammerer et al., 2011), is a good representation of its contorted taxonomic history. It was first described based on a skull from the middle Permian, *Tapinocephalus* Assemblage Zone of South Africa (SAM-PK-640; Broom, 1904). SAM-PK-640 was ascribed to the genus *Oudenodon*, which was later synonymized with *Dicynodon* by the same author (Broom, 1913). The specimen was later assigned to the genus *Orophicephalus* (Van Hoepen, 1934) and subsequently re-erected as *D. megalorhinus* (Toerien, 1953; Haughton and Brink, 1954; King, 1988). *Dicynodon megalorhinus* was considered as a synonym of *Diictodon feliceps*, but the *D. megalorhinus* holotype lacks synapomorphies of all species to which it has been ascribed (Kammerer et al., 2011). The external anatomy of SAM-PK-640 is poorly preserved and its lack of preparation keeps several traits unrevealed (Kammerer et al., 2011). Nevertheless, Kammerer et al. (2011) identified this specimen as falling within *Emydops* based on the shape of the palatal rim, the occiput, the width of the intertemporal region, and the broad exposition of the parietals. Therefore, since the specimen described here, GPIT-PV-60758, was referred to *D. megalorhinus*, and SAM-PK-640 — the holotype of *D. megalorhinus* — is still identified as *Emydops* sp. to date (Kammerer et al. 2011), this specimen does not impact the nomenclatural status of the taxon. Indeed, Brink (1986) had already listed by GPIT-PV-60758 as *Diictodon feliceps*, and subsequent authors maintained this ascription (Kammerer et al. 2011, 2020).

GPIT-PV-60758 was a specimen found near Abrahamskraal (South Africa) originally described by von Huene (1931), consisting of a complete skull and mandible (Fig. 1). The abundance of *Diictodon* while being a key species among dicynodonts justify anatomical description using computed tomography. X-ray micro-computed tomography (μCT) has become an increasingly important tool to paleontologists (e.g., Castanhinha et al., 2013; Laaß, 2015). We describe the internal and external anatomy of GPIT-PV-60758, including the bony labyrinths and the braincase endocast. Our phylogenetic analysis recovers this specimen as a sister taxon to *Diictodon feliceps,* providing support to the current ascription (e.g., Brink 1986, Kammerer et al. 2020). *Diictodon feliceps* has a Pangean distribution, spanning from middle to late Permian (Angielczyk and Sullivan 2008). We analyze and discuss the differences between GPIT-PV-60758 and other *Di. feliceps* specimens. We discuss the range of variation within *Di. feliceps* and the relevance of ontogenetically variable traits in the occipital and cranial vault regions of dicynodonts.

MATERIALS AND METHODS

X-ray μ-CT scanning and segmentation

GPIT-PV-60758 (Figs. 1, 2) consists of a complete skull and partially preserved lower jaws collected near Blaauw Krantz, close to Abrahamskraal, in South Africa (von Huene, 1931). The specimen is housed at the Institut für Geowissenschaften der Universität Tübingen, Paläontologische Sammlung (Germany). Von Huene (1931) reported that GPIT-PV-60758 was collected in strata assigned to the *Tapinocephalus* Assemblage Zone

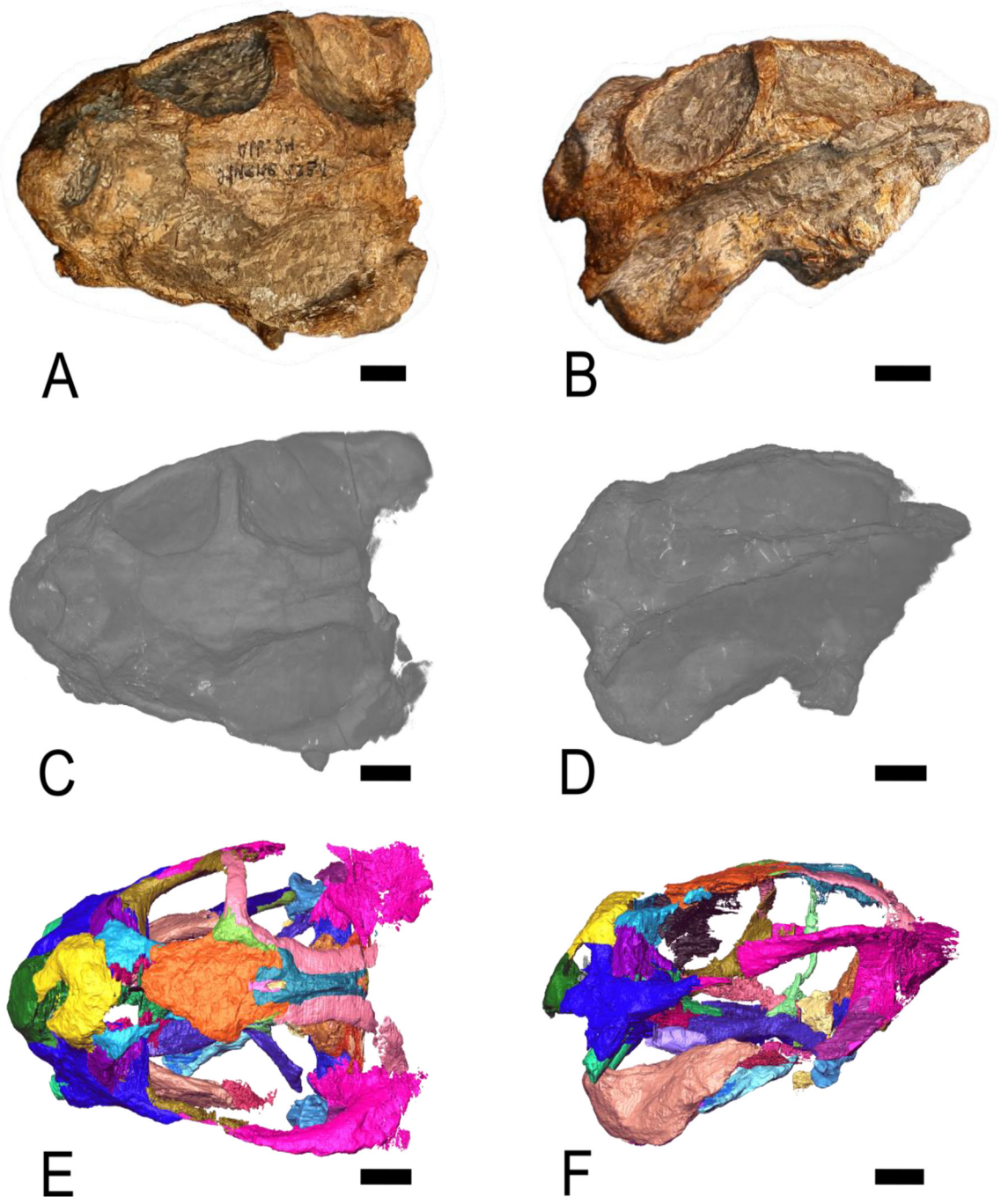

FIGURE 1. Dorsal (A, C, E) and lateral (B, D, F) views of GPIT-PV-60758. The specimen is on top (A, B), the volume rendering of the µ-CT scan is on the middle (C, D), and the 3D segmentation with colors representing different bones is on the bottom (E, F). Scale bar = 10 mm.

(van der Walt et al., 2010). These sediments date from the middle Permian, with more than 261Ma (Rubidge et al., 2013). Von Huene (1922) described the external anatomy of the relatively well-preserved and well-prepared GPIT-PV-60758 and ascribed it to *Dicynodon megalorhinus*. The most recent publication including this specimen grouped it with many other specimens in the species *Diictodon feliceps* (Kammerer et al. 2020).

We used Propagation Phase Contrast Synchrotron Radiation-based (PPC-SR) micro-Computed Tomography (µCT) to scan

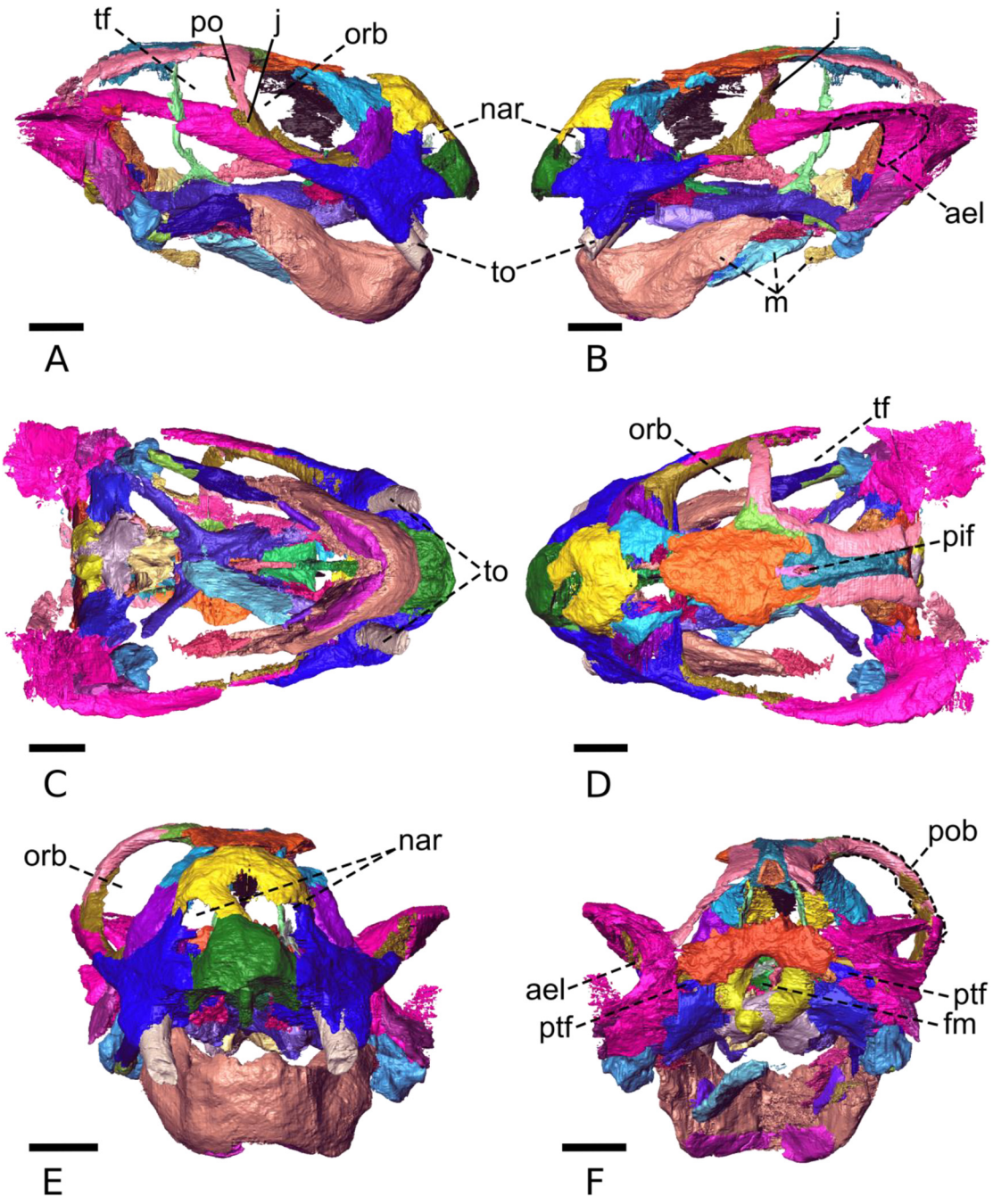

FIGURE 2. 3D segmentation of GPIT-PV-60758, with different colors corresponding to different bones. The skull is shown in right and left lateral views (A, B), ventral (C), dorsal (D), anterior (E) and posterior (F) views. ael - origin of the *adductor externus lateralis*; fm - foramen magnum; j - jugal; m - maxilla; nar - naris; orb - orbit; pif - pineal foramen; po - postorbital; pob - postorbital bar; ptf - posttemporal fenestra; t - tooth; tf - temporal fenestra. Dashed lines point anatomical structures. Scale bar = 10 mm.

GPIT-PV-60758 at the European Synchrotron Radiation Facility (ESRF, Grenoble, France). The setup was the same as that reported in Araújo et al. (2017). The resulting scan was composed of 1285 tomograms, with a voxel size of 46.57 µm. Projections were assembled and the scan reconstructed using PyHST2 software (Paganin et al., 2002; Mirone et al., 2014), with the same parameters as in Araújo et al. (2017).

The GPIT-PV-60758 scan was binned (resolution reduced

by half) in order to facilitate the manipulation of the file. Avizo 8.1 (FEI Vizualization Sciences Group, Mérignac, France) was used to perform the segmentation of the binned version of the scan. Because of the poor contrast between bone and sediment, most of the segmentation was done manually, with the "brush" tool (Fig. 2). Whenever a structure cross-section presented a regular shape, the area of interest was selected every five slices and the final volume was obtained using the "Interpolate" function. The olfactory bulbs, dorsal, and basicranial/occipital regions of the endocast were manually segmented. The cartilaginous lateral walls of the braincase are not preserved in GPIT-PV-60758, making the exact shape of the endocast is impossible to derive. Therefore, the median and ventral regions between the posterior limit of the olfactory bulbs and the epipterygoid bones were interpolated. The bony labyrinths were manually segmented. If semicircular canals were damaged, the segmentation was performed only if the shape was predictable from the preserved parts. All length measurements were performed with the "Measure" tool in the surface viewer menu of Avizo 8.1. Endocranial volumes were calculated with the "Material statistics" function.

ANATOMICAL DESCRIPTION

Palate

Premaxilla

The premaxilla is the most anterior element of the snout, forming the round apex of the keratinous beak (Figs. 2, 3). In GPIT-PV-60758, the premaxilla is a single bone with no visible suture separating the two paired elements found in some other specimens (Sullivan & Reisz, 2005). As in almost all other dicynodonts there are no premaxillary teeth. The premaxilla is bordered by the nasals dorsally, the maxillae posterolaterally and by the vomer posteriorly (Fig. 2). The premaxilla anterior surface slopes posterodorsally towards the nasals and its lateral expansions confer a triangular shape in anterior view (Fig. 2E). Ventrally, the bone is subrectangular (Fig. 3D), becoming more triangular as it narrows towards its contact with the vomer, finishing in an ascending process that projects dorsoventrally, forming a well-defined median ridge (Fig. 3D). The premaxilla has a considerable palatal contribution and it forms the anteroventral margin of the internal nares, along with the maxilla (Figs. 2A,B, 3A,B). The premaxilla-maxilla suture extends from the palate to the ventral margin of the naris. Ventrally, this suture extends to the the level of the posterior edge of the latter. The contact between premaxilla and vomer occurs along the sagittal skull midline, with the vomer projecting anteriorly to lie just dorsal to the ascending process of the premaxilla, reaching close the midpoint of the nasal cavity (Fig. 3C). The badly preserved dorsal process of the premaxilla in GPIT-PV-60758 does not allow identification of its forked insertion into the nasal boss or the precise shape of the dorsal margin of the external nares. In palatal view, the anterior ridges of the premaxilla are badly preserved, only allowing identification of the worn right anterior ridge (Fig. 3D). However, it is possible to identify the depression between both anterior ridges (Fig. 3D). The posterior projection of the left anterior ridge appears to converge towards the anterior part of the median posterior ridge, despite being severely worn (Fig. 3D). Two well-defined depressions (Sullivan & Reisz, 2005) flank the posterior ridge (Fig. 3D). The left depression is better preserved, displaying a small vascular groove just lateral to the posterior ridge (Fig. 3D). The lateral eminences that run along the suture with the maxillae, in palatal view, can be easily identified both in the 3D reconstruction (Fig. 3D).

Septomaxilla

Only the left bone is partially preserved in GPIT-PV-60758, and it is a small and delicate bone located in the nasal cavity, close to the posteroventral part of the naris (Fig. 3A-C). The septomaxilla can be divided in two flattened processes. The ventral process contacts the premaxilla and the dorsal process contacts the maxilla on the lateral margin of the nostril (Fig. 3C). The ventral process is mediolaterally elongated and its suture with the premaxilla extends from the posterior margin of the ascending process of the premaxilla (medially) to near the premaxilla-maxilla suture (laterally; Figs. 3A & S1). The dorsal process is dorsoventrally elongated, with its dorsal extremity contacting the maxilla close to the nasomaxillary suture whereas its ventral tip reaches just posteriorly to the most ventrolateral margin of the left nostril (Fig. S1). The cross-section of the septomaxilla is subtriangular due to the secondary contact between the distal tips of both processes (Fig. S1).

Maxilla

The anterior and anterodorsal portions of the paired maxillae are poorly preserved (Figs. 2, 3). The maxilla bears one caniniform tooth and comprises the anterolateral part of the face. The maxilla borders the premaxilla anteriorly and medially, the nasal anterodorsally, the lacrimal dorsolaterally, the jugal posterolaterally, both the jugal and the squamosal along the medial surface of the zygomatic process of the maxilla, the ectopterygoid posterolaterally and the palatine posteroventrally (Figs. 2, 3). The ventral aspect of the maxilla is subtriangular. Its medial margin contacts the premaxilla along an interdigitating subtriangular suture. At mid-length of its anteroposterior axis, the maxilla displays an anteroventrally projecting caniniform process. Dorsal to the caniniform teeth, the maxilla does not display a maxillary antrum. The caniniform tooth is ankylosed to the alveolar bone, i.e., there is no space filled with matrix between the caniniform tooth and the enveloping maxilla alveolar bone (Fig. S2). This space is typically filled by the periodontal ligament in life and its absence in GPIT/RE/'9275 is similar to the condition observed in other *Diictodon* specimens (LeBlanc et al. 2018; Whitney et al. 2021). More posteriorly, the ectopterygoid projects anteriorly to form an interdigitating suture with the maxillary posteromedial margin. The posterior portion of the medial margin of the maxilla contacts the palatine bone along a large interdigitating suture. The palatine prevents the contact of the medial part of the maxilla with the vomer (Fig. 3C). Anterodorsally, the maxilla forms the posterior margin of the nares and contacts the nasal dorsally to form its posterodorsal margin (Fig. 2A, B, E). The posterodorsal margin of the maxilla forms a fossa where the large lacrimal bone is embedded, preventing the maxilla from contacting the prefrontal (Figs. 2-4A, B). The lateral surface of the maxilla is flat anteriorly, but its posterior margin bulges to form the caniniform process (Figs. 2A, B, 3A, B). The caniniform process extends dorsally to the mid-height of the maxilla. The posteromedial surface of the maxilla is horizontally flat near the contacts with the jugal and the lacrimal (Figs. 2D, 3A, B, C). Posteriorly, the zygomatic process of the maxilla projects smoothly from the caniniform process and nearly reaches the postorbital process of the jugal (Fig. 2C). The zygomatic process of the maxilla sharpens posteriorly, and borders the lateral surface of the jugal anteriorly, and the anterior process of the squamosal posteriorly (Fig. 2C, D).

Vomer

The vomers are coossified at the midline of the nasal cavity to form the internarial septum (Fig. 3C, D). Although the vomers coossify anteriorly, the intervomeral suture is visible in cross-section, posterior to the internal nares (Fig. S3). The vomer contacts the premaxilla anteriorly, the palatine laterally, the cultriform process of the parabasisphenoid posteriorly, the pterygoids posteriorly, and the ethmoid posterodorsally (Fig. 3). The vomer is composed of two major anatomical subunits: the internarial septum and the mid-ventral plate. The internarial septum lays along the dorsal edge of the posterior ridge of the premaxilla (Fig. 3C). The vomer receives the anterior part of the cultriform process of the parabasisphenoid posterodorsally. These two bones form the insertion area of the ventral portion of the sphenethmoid (Fig. 3A, B). Ventral to its contact with the sphenethmoid, the vomer presents its maximum height, dividing the choanae posteriorly (Fig. 3D). The vomers project laterally to contact the palatines at the posteriormost part of the internarial septum (Fig. 3C). These vomerine lateral projections form a plate-like coronal section (mid-ventral plate) that constitute the roof of the choanae (Fig. 3D). Posteriorly, the mid-ventral plates of the vomer are two symmetric subtriangular processes that project along the suture with the palatines. The mid-ventral plates of the vomer frame the interpterygoid vacuity anteriorly and laterally. The mid-ventral plates contact with the pterygoid posteriorly, thus excluding the palatines from the margins of the interpterygoid vacuity.

Ethmoid

The sphenethmoid is a median ossification that consists of a sheet-like septum, the mesethmoid, ventrally and anteriorly (lateral wall *sensu* Araújo et al., 2017) and a semi-tubular region, the orbitosphenoid, posterodorsally which descends into to form the presphenoid (Fig. 3). The lateral wall of the ethmoid contacts the vomer and the cultriform process of the parabasisphenoid ventrally, the frontal dorsally, and it might have contacted the nasal, but the latter is badly preserved in GPIT-PV-60758 (Fig. S3). In lateral view, the ethmoid is narrow ventrally and widens towards the top (Fig. 3A, B). Its dorsalmost part contacts the descending process of the frontal and contributes to the ventral part of the sagittal septum that divides the olfactory bulbs (Fig. 2A, B). This anterodorsal part of the ethmoid appears to be homologous to the *crista*

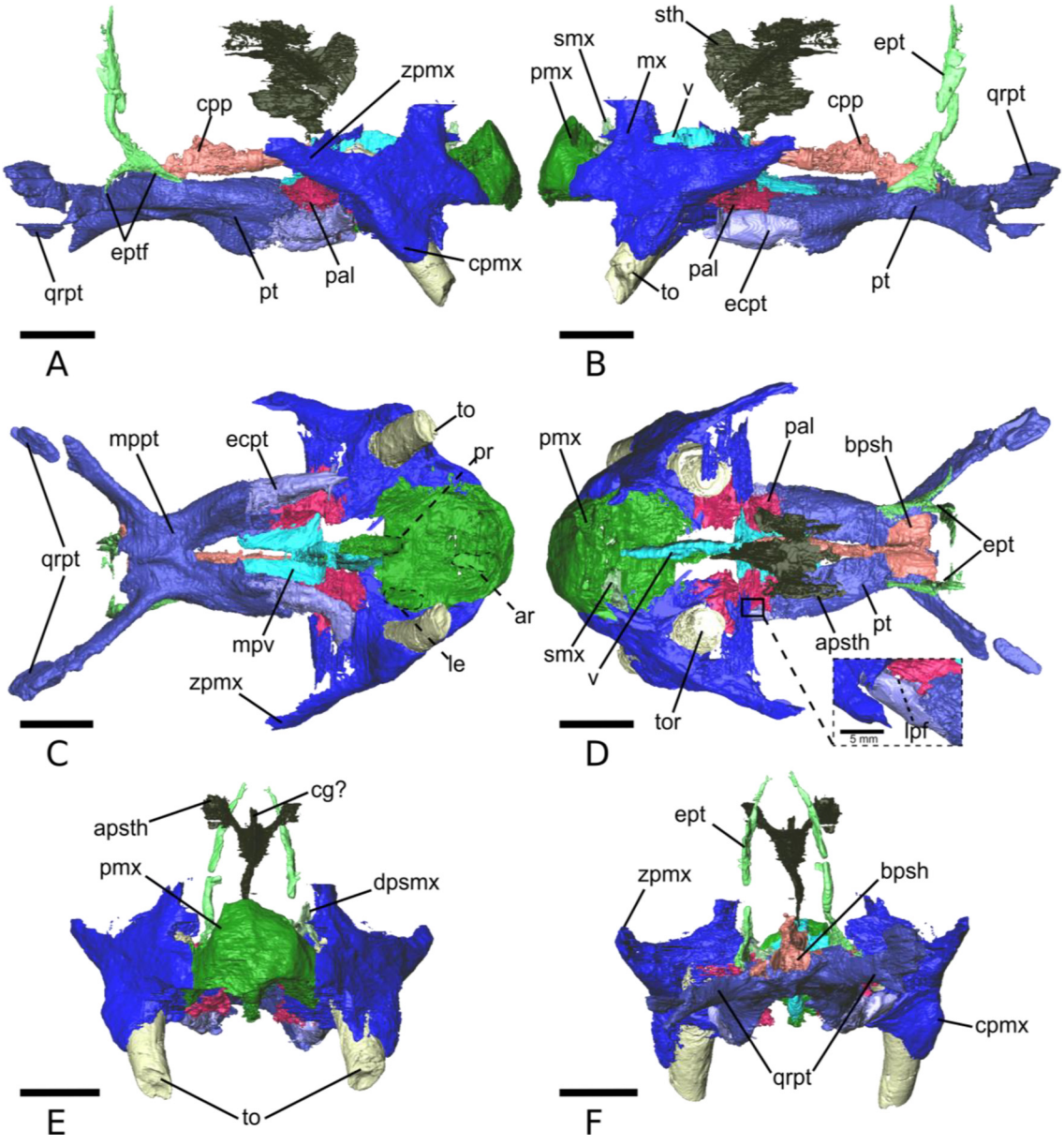

FIGURE 3. Palate and lateral wall. Lateral right and left (A, B), dorsal (C), and ventral (D) views. apsth - ascending process of the sphenethmoid; bsph - basipresphenoid; cpmx - caniniform process of the maxilla; cg - mesethmoid, or "*crista galli*?"; cpp - cultriform process of the parasphenoid; ecpt - ectopterygoid; ept - epipterygoid; eptf - epipterygoid foot; mppt - median plate of the pterygoid; mvp - mid-ventral plate of the vomer; mx - maxilla; pal - palatine; pmx - premaxilla; qrpt - quadrate process of the pterygoid; smx - septomaxilla; sth - sphenethmoid; to - tooth; tor - tooth root; v - vomer. Dashed lines point anatomical structures. Scale bar = 10 mm.

galli of the mammalian ethmoid (Bird et al., 2014). The semi-tubular region of the ethmoid forms a vacuity that housed the olfactory tract (Figs. 3 and 7). It consists of two ascending processes that project laterally to contact the frontal (Figs. 2A, B, and 3). In contrast with the ascending processes in *Niassodon mfumukasi* (Castanhinha et al., 2013), those in GPIT-PV-60758 are not inflected dorsomedially.

Palatine

The palatine can be divided in two anatomical subunits (Fig. 3C): the anterior section (maxillary flanges) and the posterior section (palatine pad *sensu* Castanhinha et al., 2013). The palatines do not contact in the midline due to the presence of the vomer (Fig. 3C, D). They contact the maxilla anteriorly, the ectopterygoid and pterygoid laterally and

posteriorly, and the vomer medially. The maxillary flanges are wider dorsally than ventrally and present a medial concavity that forms the lateral walls of the choanae (Figs. 3C, D and S4C). They are comparatively wider than the palatine pad. Laterally, the palatine presents a subtriangular dorsolateral projection (Figs. 3C and S4A, B). The anterior margin of the maxillary flange of the palatine receives the medial processes of the maxilla (Fig. 3D). The anterior contact between the palatine and the premaxillae is prevented by these medial processes. In lateral view, the posterior portion of the maxillary flange transitions to the palatine pad. The palatine pad contacts the ectopterygoid laterally. It displays a dorsolaterally projecting shelf that is limited anteriorly by the maxilla, and medially by the vomer. The lateral palatal foramen (lpf) is present between the palatal pad and the ectopterygoid suture, just posterior the triple junction between the maxilla, the palatine and the ectopterygoid (Fig 3F). In dorsal view, the pterygoid invaginates the margin of the palatine, forming a hemicircular suture. A posterior projection of the palatine borders the anteromedial margin of the pterygoid (Fig. 3C, D). Medially, the palatines contact the vomer along a scarf joint.

Ectopterygoid

The ectopterygoids are relatively small elements that connect the palatal processes of the pterygoid to the maxilla (Fig. 3). They also contact the palatine dorsolaterally and anterodorsally. The ectopterygoids are ellipsoidal in cross-section, being broadest posteriorly at the contact with the pterygoid. In ventral view, the ectopterygoids are thinnest anteriorly, having a similar shape to the pterygoid at the its suture. The right ectopterygoid presents a small keel along the posterior half of its ventral margin that is contiguous with a similar structure on the ventral surface of the pterygoid (Fig. 3D). In other dicynodonts (e.g., Castanhinha et al., 2013; Sullivan and Reisz, 2005), an elongated lateral palatal foramen is present between the ectopterygoid and the palatine. However, this perforation is not preserved in GPIT-PV-60758.

Pterygoid

The pterygoid is composed of three distinct parts: the anteriorly projecting palatal rami, the median plate, and the posteriorly projecting quadrate rami (Fig. 3). The pterygoid contacts the ectopterygoids anteriorly, the palatine anterodorsally, and the vomer anteromedially, the parabasisphenoid posteriorly and dorsally at the median plate of the parabasisphenoid cultriform process, the epipterygoids dorsally at nearly midpoint of the anteroposterior extension of the bone, and the quadrate, the squamosal, and the opisthotic posteriorly (Figs. 2 and 3). The palatal rami of the pterygoid are robust and increase slightly in height and width anteriorly. They project anterolaterally, making an angle of ~26º with the median plate, giving a V-shape to the anterior part of the pterygoid (Fig. 3D). The palatal processes of the pterygoid contacts the palatines anterodorsally, whereas the ventral part of its anterior portion interdigitates with the ectopterygoid. The ventral edge of the palatal processes bears the pterygoid keel that is continuous with the ectopterygoid (Fig. 3D). Two ventral ridges extend posteriorly from the pterygoid keels, converging at the anterior margin of the median plate to form the *crista oesophagea* (Fig. 3D). The palatal ramus of the pterygoid contacts the vomer dorsomedially, along the anterior half of the interpterygoid vacuity. The palatal processes and the median plate of the pterygoid frame the remaining posterior half of the interpterygoid vacuity. This vacuity narrows posteriorly, as the palatal rami converge towards the median plate, forming a somewhat elliptical posterior half. The median plate is relatively short, representing about one third of the total length of the pterygoid. Posteriorly, most of the median plate dorsal surface is covered by the anterior flange of the parabasisphenoid . The epipterygoids rest along the dorsolateral edge of the median plate and the dorsal margin of the anteriormost part of the quadrate rami of the pterygoid. Posteriorly, the quadrate rami are mediolaterally compressed and project posterolaterally, making an angle of approximately 40º with the median plate. They reach the posteriormost region of the skull, wedging between the medial surface of the quadrates, the ventrolateral margin of the opisthotics, and the ventromedial edges of the ventral processes of the squamosal.

Epipterygoid

The epipterygoids are paired elements consisting of a rod (ascending ramus) and a footplate that connects the pterygoid to the descending flange of the parietal (Figs. 2 and 3). Ventrally, the epipterygoid consists of a footplate that originates at the level of the most anterior point of the pterygoid-basipresphenoid suture and extends posteriorly, resting on the posterior quadrate rami of the pterygoid (Fig. 3A, B). In lateral view, the footplate is C-shaped, presenting a flattened

portion anteriorly (Fig. 3A, B). The rod-like ascending ramus of the right epipterygoid has a posterior inclination (~53°) near its junction with the footplate, but then becomes more vertical. The left epipterygoid is closer to vertical for its entire length.

Cultriform process of the parasphenoid and basipresphenoid

The cultriform process is elongated and mediolaterally compressed, and it contacts the vomer anteriorly, the ethmoid anterodorsally, and the basipresphenoid posteriorly (Fig. 3). The cultriform process is tall as it projects from its insertion on the basipresphenoid, but becomes progressively lower anteriorly. The dorsal groove of the vomer receives the anterior projection of the cultriform process. A groove opens on the dorsal surface of the cultriform process near its midlength and continues to the contact with the vomer, corresponding to the vidian canal. In our specimen, the anteriormost part of this groove receives the sphenethmoid. The remaining space is probably for the insertion of the anterior braincase wall (e.g., possibly the unpreserved orbitosphenoid). Posteriorly, the cultriform process (parasphenoid) coossifies with the broad basispres-phenoid (Fig. 3C, F; Fig. S5). The basipresphenoid is rectangular in dorsal view, being housed on a deep concavity on the dorsal surface of the median plate of the pterygoid (Fig. 3C). The basipresphenoid is anterodorsally thick and presents a spongious internal structure (Fig. S5). Posteriorly, it contacts the parabasisphenoid (parasphenoid + basipres-phenoid) and contributes to the anterior margin of the internal carotid canal.

Skull roof

Nasal

The nasals are located anterodorsally in the skull (Figs. 2, 4), but are poorly preserved in GPIT-PV-60758. The nasal is a dome-shaped bone that contacts its counterpart in the sagittal midline, the premaxilla and the maxilla ventrally, and the prefrontal posterolaterally. The ventral part of the left nasal is not preserved. The posterodorsal portion and most of the midline of both nasals are also not preserved. The most posterior part of the internasal suture presents an interdigitating pattern (Fig. S6). In lateral view, the anterior margin is flat, with a small boss anterodorsally (Fig. 4A).

Prefrontal

The prefrontals form the anterodorsal part of the orbital margin and part of the orbital wall between the lacrimal and the frontal (Fig. 4). The left prefrontal is poorly preserved in this specimen, consisting only of the anteriormost part of the lacrimal and nasal contacts and a small fragment of its posterior contact with the frontal (Fig. 4C). The right prefrontal is more complete and contacts the nasal anteriorly, the lacrimal anteroventrally, the frontal posteriorly and the anterior tip of the dorsolateral wing of the sphenethmoid just ventral to the anterior margin of the frontal (Fig. 2B). The prefrontal is a small element that is widest near the contact with the lacrimal and tapers posterodorsally. A small dorsomedial projection of the bone is present, but it is worn, as is most of the dorsal surface between the frontal and the nasal. In cross-section, the prefrontal is thin medially and ventrally, thickening dorsolaterally at its contribution to the orbital margin (Fig. S7). This section reveals a concavity on the medial surface, with the dorsomedial projection forming an angle of about 90° with the lateral part of the bone. (Fig. S7).

Lacrimal

Both lacrimals are present in this specimen, but only the right element presents a well-preserved external surface (Fig. 4). The lacrimal abuts on the anterodorsal part of the maxilla, slightly dorsal to the caniniform process (Fig. 2A, B). The lacrimal also contacts the jugal posteroventrally along a mediolaterally-oriented suture, the prefrontal dorsally, and the nasal anterodorsally. The lacrimal is the anteriormost element of the orbital wall and orbital margin. In lateral view, it presents a subtriangular shape, with a slightly concave and anteriorly-inclined posterior margin (Fig. 2A, B). The lateral surface of the lacrimal presents a small posterior ridge, oriented dorsoventrally, that corresponds to the orbital rim (Fig. 2A, B). Anteriorly, the lacrimal makes a small contribution to the lateral surface of the snout. The posterior surface of the lacrimal extends from the lateral edge of the orbit to its medialmost extension. It displays a relatively large lacrimal foramen (1.3 mm diameter) just medial to its lateral margin (Fig. 4C). The dorsomedial surface of the lacrimal is the roof of a large maxillary sinus. This sinus is connected to the orbit by the lacrimal duct that opens into the lacrimal foramen.

Frontals

The frontal is a flat bone that is elongated anteroposteriorly, and represents 40% of the condylobasal length and about 50% of the skull width (Fig. 4). It contacts the prefrontals anteriorly, the sphenethmoid anteroventrally, the postfrontal posterolaterally, and the postorbital, the prepariental, and the parietal posteriorly (Figs. 2, 4). The anterior part of the frontal is not preserved in this specimen and, therefore, the contact with the nasal is not present. In dorsal view, the frontal is roughly rectangular, being slightly expanded at its midlength. The dorsal surface presents no ornamentation, although this might be due to preservation. The frontal anterolateral margins form the dorsal part of the orbital edge, being limited anteriorly by the prefrontal. The posterior portion of the frontal is split in two halves that receive the prepariental and partially overlap its anterior end. The posterior margin of the two portions of the frontal that encircle the prepariental are bordered by the anterior margin of the parietal (Fig. 4C). Anteriorly, the ventral surface of the frontal presents a shallow excavation limited anteriorly by a median descending process that delimits the dorsal part of the olfactory tract (dpf, Fig. 4B). The descending process of the frontal contacts with the most dorsal projection of the sphenethmoid (Fig. 2).

Postfrontals

The postfrontal is well preserved on the right side of the skull roof (Fig. 4). This bone is triangular in dorsal view (Fig. 4C). The postfrontal contacts the frontal medially, the postorbital laterally, and presents a narrow contact with the parietal posteriorly (Fig. 4C). Its wider anterior margin contributes to the dorsal part of the orbital margin, filling the small gap between the frontal and the postorbital bar (Fig. 4B, C). The postfrontal narrows from the orbit to the frontal-postorbital contact, posteriorly.

Prepariental

The prepariental is a narrow, anteroposteriorly elongated bone bordered by the frontal anteriorly and laterally, and by the parietal posteriorly (Fig. 4). In dorsal view, the prepariental is subrectangular and its surface is flush with the dorsal surface of the frontal and the parietal. Its anterior margin is roughly rectangular and is covered by the frontal. In dorsal view, the exposed anterior margin of the prepariental is ellipsoidal whereas the posterior margin bifurcates (Fig. 4C). It surrounds the anterior and lateral margins of an ellipsoidal pineal foramen. The prepariental bifurcations fused with the parietal, hindering the observation of the simple butt joint with the parietal. In lateral view, the prepariental thickens anteroposteriorly. The dorsal surface of the prepariental is flat and does not form a pineal boss (Fig. 4C). In ventral view, the prepariental develops considerably under the frontal (Fig. 4B).

Parietal

The parietal is a subrectangular bone with concave edges that forms a narrow and crest-like temporal bar (Fig. 4). It is bordered anteriorly by the frontal and the prepariental, laterally by the postorbital and postfrontal, ventrally by the epipterygoids, and posteriorly by the squamosal and the postparietal (Fig. 2). It likely would have contacted the tabulars as well (Sullivan and Reisz, 2005), but they are not preserved . The narrow dorsal exposure of the parietals presents two temporal lines forming a small crest along the interparietal suture (Fig. 4C). This crest is wide anteriorly and sharpens posteriorly, flattening anteriorly to the contact with the postparietal bone (Fig. 4C). The ventral surface of the parietals presents two median ridges that originate from posterior margins of the pineal foramen (Fig. 4B). These ridges project ventrolaterally in a more posterior position, forming the descending flanges of the parietals (Fig. 4A). The lateral surface of the descending flange corresponds to the attachment area of the temporal musculature. The two median ridges converge into a single median structure posterior to the contact with the epipterygoids (Fig. 2A, B). Posteriorly, the ridge bifurcates and projects laterally as the descending processes of the parietal, bordering the ventrolateral surface of the postparietal (Fig. 4B, C). Internally, the parietals bear thin laterally-projecting shelves that are overlain by the temporal portions of the postorbital. Two slender posteroventrally-projecting processes probably contacted the squamosal posteromedially, although the processes are badly preserved. Medially, the postparietal lies on the posterior portion of the parietal (Fig. 4B, C). The cross section of the parietals presents a flat dorsal surface anteriorly, and the descending flanges are close to perpendicular to the shelves that underlie the postorbitals. At the level of the epipterygoid contact, the cross section of the parietal presents a broad ridge dorsally and the descending flanges describe an angle of approximately 53^{o} with the skull roof (Fig. S6B, C). At the posterior end of the parietal, the skull roof component thickens and the attachment area for the temporal

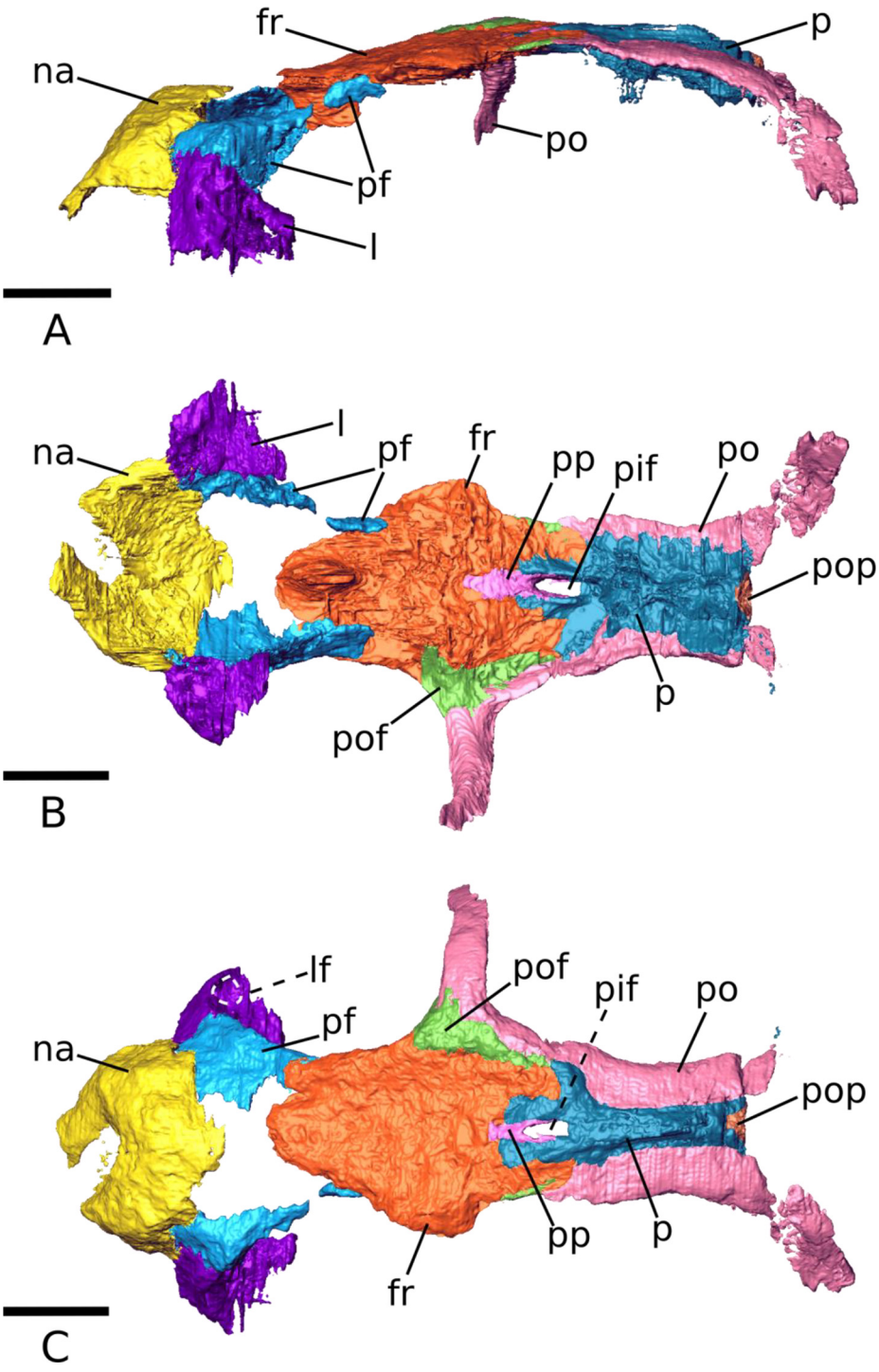

FIGURE 4. Skull roof. Lateral left (A), ventral (B), and dorsal (C) views. fr - frontal; l - lacrimal; lf - lacrimal foramen; na - nasal; p - parietal; pf - prefrontal; pif - pineal foramen; po - postorbital; pof; postfrontal; pop - postparietal; pp - preparietal. Dashed lines point anatomical structures. The lacrimal foramen is outlined in dashed white. Scale bar = 10 mm.

musclulature becomes rounder, with the descending flanges describing an angle of approximately 58°. The cross sections show the interdigitating suture between the left and right parietal along its anteroposterior length.

Postparietal

The postparietal is a small wedge-like element on the posterior part of the skull roof (Fig. 4). It is harboured by a concavity formed on the posterior margin of the paired parietals, just posterior to the interparietal suture (Fig. 4B, C). The postparietal likely contacted most of the supraoccipital ventrally, and the dorsal tips of the tabulars (e.g., Sullivan & Reisz, 2005). The preserved bone is subtriangular in dorsal view (Fig. 4C). It is anteroposteriorly short and its height is similar to that of the parietals.

Postorbitals

The right postborbital is almost completely preserved in GPIT-PV-60758 (Fig. 4). The anterior postorbital process of the left side bone is not preserved, although its most posterior tip is better preserved than on its right side. The postorbital consists of two parts, the thin postorbital process and a posterior sheet that overlays on the lateral shelf of the parietal, reaching the squamosal posteriorly. The postorbital process is curved and concave medially (Fig. 4C). The postorbital contacts the dorsal process of the jugal ventrally, overlapping its lateral surface (Fig. 2A, B). The postorbital also contacts the postfrontal dorsally, thus connecting the skull roof with the subtemporal bar. The dorsal part of the postorbital presents a long sheet-like posterior projection that borders the lateral edge of the postfrontal. A contact between the postorbital and the frontal is prevented by the narrow posterior extension of the prefrontal and the anterolateral projection of the parietal (Fig. 4B, C). The temporal portion of the postorbital rests on the lateral shelves of the parietal and borders the dorsal exposure of the parietal medially (Fig. 4B, C). The temporal portion of the postorbital is thin medially and increases in thickness laterally. Posteriorly, the temporal portion of the postorbital reaches the dorsal process of the squamosal, and it also likely contacted the tabular (Sulivan and Reisz, 2005).

Occipital and zygomatic regions

Jugal

The jugal can be divided into a broad anterior part and a narrower posterior process that contributes to the zygomatic arch (Fig. 2). Here, we focus on the right jugal due to its better-preserved anatomy (Fig. 2D). The bone contributes to the lateral border of the orbital wall anteriorly, where it broadly contacts the lacrimal dorsally and the maxilla medially and laterally (Fig. 2D). A small ventral contact with the ectopterygoid is also present, and the jugal contacts the postorbital dorsomedially. The posterior process of the jugal forms much of the medial surface of the zygomatic arch and contacts the anterior process of the squamosal along a scarf joint (Fig. 2D). The anterior portion of the jugal presents a medial projection, overlapping the dorsal contribution of the maxilla to the orbital wall (Fig. 2D). On the right side, the CT scan sections show the jugal contribution to the posterolateral wall of the caniniform alveolus. Anterior to this region, the jugal is hollow until it forms the medial surface of the compact suborbital bar. The suborbital bar is subcylindrical in section posteriorly, becoming elliptical as it approaches the postorbital bar, where the major axis is almost aligned with the sagittal plane. Here the bone becomes broader, with a transversely compressed dorsal process contributing to the ventromedial part of the postorbital bar that is complemented, dorsolaterally, by the descending process of the postorbital (Fig. 2D). A badly preserved posterior process extends posteriorly from the medially concave posterior ramus of the jugal to join the anterior process of the squamosal, forming the subtemporal bar (Sullivan & Reisz, 2005).

Squamosal

The squamosal has a complex shape consisting of dorsal, zygomatic, and ventral processes (Fig. 5). It contacts the parietal and the postorbital dorsally, the jugal anterodorsally, the maxilla anteriorly, the supraoccipital and the opisthotic medially, and the quadrate-quadratojugal complex ventrally (Fig. 2, 5). The zygomatic process of the squamosal consists of an anteriorly projecting zygomatic/anterior branch that articulates with the lateral surface of the jugal and is overlain laterally by the zygomatic process of the maxilla just anterior to the postorbital bar (Figs. 2 and 5A-D). Dorsally, the anterior process contacts the descending flange of the postorbital. The zygomatic process widens posteriorly, forming the flat and wide dorsal surface of the ventral process. Ventrally, the strongly concave lateral surface of the ventral process of the squamosal represents the origin of the lateral external adductor musculature (Fig. 2A, B, 5A, B, King, 1989). The medialmost part of the dorsal process probably contacted the tabular (Sullivan & Reisz 2005), although the latter element is not preserved in our specimen. The dorsal process of the

squamosal contacts the supraoccipital ventromedial to the parietal flange (Fig. 5F). The squamosal narrows ventrally and acquires a more columnar shape in the transition between the dorsal and the ventral process of the bone (Fig. 5E). At mid-height, the squamosal contributes to the lateral margin of the posttemporal fenestra, with the supraoccipital limiting the fenestra dorsomedially and the opisthotic forming its ventromedial corner (Fig. 5E, F). The squamosal widens to form the ventral process that contacts the opisthotic medially and presents a concavity anterolaterally that receives the quadrate-quadratojugal complex (Fig. 5E). Ventrally, the squamosal narrows in medial view, presenting a flattened posterior surface. Anteriorly, the ventral margin of the ventral process projects slightly anteriorly and presents a fossa that receives the dorsal process of the quadrate. The lateral surfaces of both right and left squamosals are badly weathered (Fig. 5C, D). The dorsal process of the squamosal contacts a thin posteroventral projection of the parietal and the overlying posterior process of the postorbital.

Quadratojugal

The quadratojugal is a sheet-like bone that covers the lateral surface of the ventral process of the squamosal (Fig. 5 A, B). Ventrally, this element contacts the lateral margin of the dorsal process of the quadrate, which is best preserved on the right side of GPIT-PV-60758. The medial surface of the ventral portion of the quadratojugal, which is preserved on the left side only, forms the lateral margin of the quadrate foramen. In lateral view, the quadratojugal is subrectangular, being wider dorsally.

Quadrate

The quadrate is characterized by a large dorsal process and two ventral articular condyles, one projecting medially and the other projecting laterally (Fig. 5). The quadrate contacts the squamosal dorsally and dorsomedially, the quadratojugal dorsolaterally, and the quadrate ramus of the pterygoid dorsomedially. The quadrate receives the posterior portion of the articular process on an anteroposteriorly-oriented articular facet. In lateral view, the quadrate is subrectangular, with its anterodorsal surface being posteriorly inclined in relation to the coronal plane. The posterior part of the quadrate is characterized by an oval-shaped dorsal process presenting a flat posterior surface (Fig. 5E). In dorsal view, the dorsal process of the quadrate slants laterally, with its medial and posterior surfaces articulating with the squamosal. The lateral surface of the dorsal process of the quadrate is overlain by the ventral portion of the quadratojugal (Fig. 5E). The anterior aspect of the dorsal process of the quadrate presents an anterolaterally-facing concavity (Fig. 5E). The lateral edge of this concavity and the dorsal edge of the lateral articular condyle contribute to the medial margin of the quadrate foramen (Fig. 5E). The medial articular condyle is antero-posteriorly longer than the lateral one. The latter presents a slightly grooved posterior surface that forms the lower ventral surface of the quadrate foramen.

Parabasisphenoid (parasphenoid+basipostsphenoid)

The parabasisphenoid comprises the floor of the braincase between the pterygoid and the basioccipital, as well as the anterodorsally projecting cultriform process (Figs. 3 and 5). As in other dicynodonts (Castanhinha et al., 2013), the posterior portion of the parasphenoid and the basipost-sphenoid are fused (Araújo et al. 2017). Here these two structures are referred to as a single coossified element, the parabasisphenoid (Fig. 3 and 5). We make an anatomical distinction with the more anterior cultriform process and basipresphenoid, despite resulting developmentally from the fusion of the basipresphenoid to the parasphenoid (Araújo et al. 2017). The parabasisphenoid contacts the pterygoid and the basipresphenoid anteriorly, the basioccipital posteriorly, and the prootics posteroventrally. In ventral view, the para-basiphenoid is subtriangular, having a wide posterior margin and tapering anteriorly (Fig. 5C). Its ventral margin is characterized by the presence of two lateral buttresses that form the anterior part of the ventrolaterally projecting tubera, together with the ventrolateral projections of the basioccipital. The tubera present laterally exposed stapedial facets. The tubera flank a medial flat surface and their anterior edges form anterodorsally-sloping ridges, creating a medial excavation that continues anteriorly to the base of the cultriform process (Fig. 5C). The ventral surface of the parabasisphenoid slopes anteriorly, from a highpoint on the tubera to the median pterygoid plate (Fig. 5C). The parabasisphenoid dorsal surface bears two depressions adjacent to the suture with the basioccipital (Fig. 5D). These depressions are anteromedial to the foramen ovale and are separated by a small crest that extends from the contact with the basioccipital to near the midpoint of the parabasisphenoid (Fig. 5D). Laterally, the parabasisphenoid presents two anteromedially converging

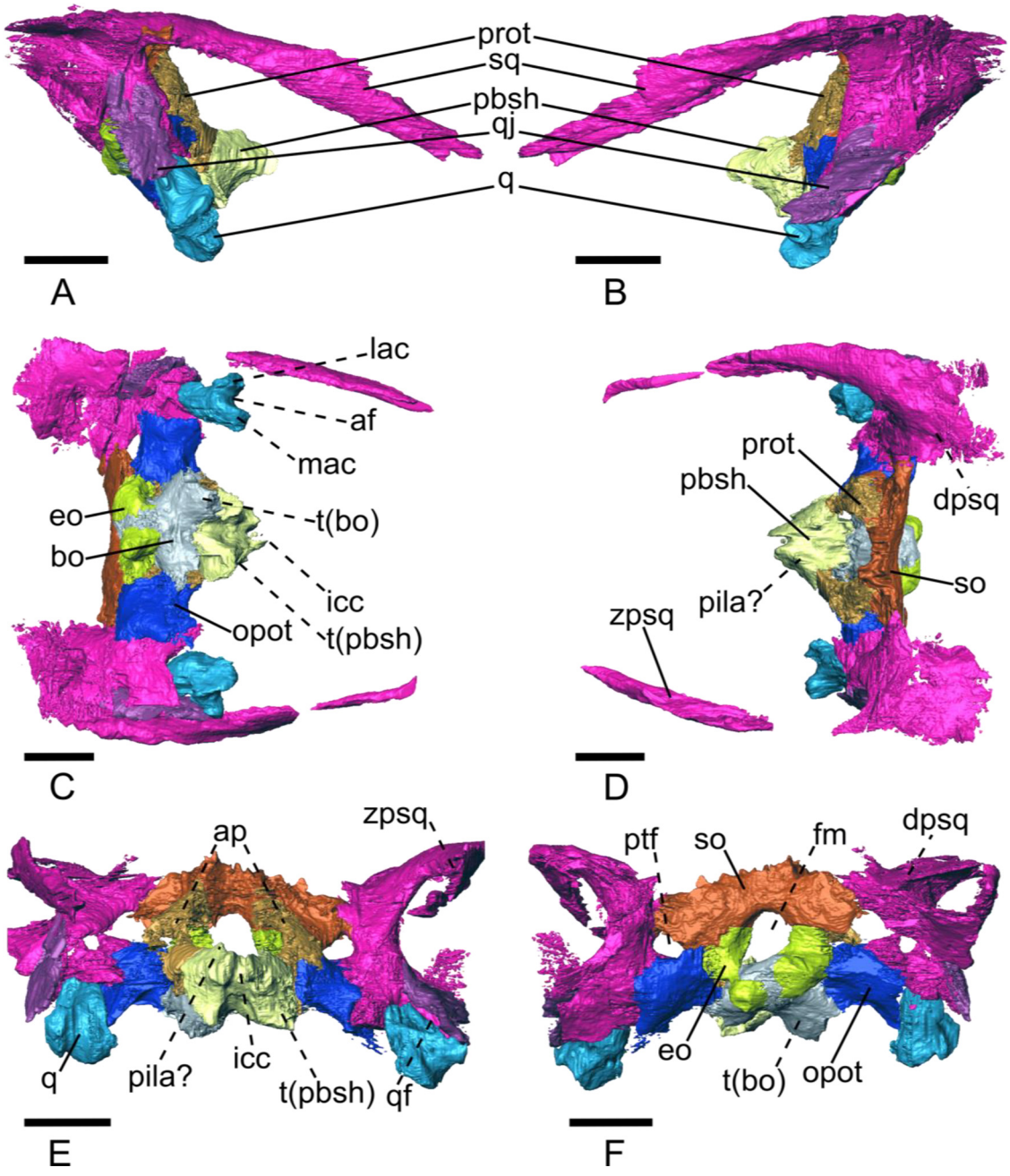

FIGURE 5. Occipital and zygomatic regions.The skull is shown in right and left lateral views (A, B), ventral (C), dorsal (D), anterior (E) and posterior (F) views. Af - articular facet; ap - ascending process of the prootic; bo - basioccipital; dpsq - dorsal process of the squamosal; eo - exoccipital; fm - foramen magnum; icc - internal carotid canal; lac - lateral articular condyle; mac - medial articular condyle; opot - opisthotic; pila - *pila antotica*; prot - prootic; pbsh - parabasisphenoid; ptf - posttemporal fenestra; q - quadrate; qf - quadrate foramen; qj - quadratojugal; sq - squamosal; t - tuber; zpsq - zygomatic process of the squamosal. Dashed lines point anatomical structures. Scale bar = 10 mm.

crests that appear to correspond to the parabolic crests (Araújo et al., 2017). The parabolic crests are continuous with the anterior projections of the prootics, and the ossification of the *pila antotica* might have rested on their anterior portions (Fig. 5D). The parabolic crests flatten out just posterior to the suture with the pterygoid, where they abut the basipresphenoid. The internal carotid foramen opens on the median part of the parabasisphenoid-basipresphenoid

suture (Fig. 5C, D). Ventrally, the internal carotid canal bifurcates (see "Brain Endocast").

Basioccipital

The basioccipital is the ventral element composing the posteriormost part of the braincase floor (Fig. 5). The basioccipital contacts the exoccipitals dorsolaterally, the opisthotics laterally and the parabasisphenoid anteriorly. This bone makes up the ventral part of the foramen magnum and presents a posteriorly-projected protuberance, part of the occipital condyle. The occipital condyle is typically composed of a median knob, located ventrally and formed by the basioccipital, and paired lateral knobs that flank it dorsally (Sullivan and Reisz 2005). The condyle in GPIT-PV-60758 is damaged: only the central portion of the basioccipital knob is preserved, the right exoccipital knob is mostly present, and only a fragment of the left exoccipital knob remains. Anteriorly, the ventral surface of the basioccipital presents two ventral tuberosities that fuse with the posterior part of the parabasisphenoid tubera. These tuberosities project ventrolaterally and partially enclose the *fenestra ovalis*. We follow Sullivan and Reisz (2005) and call these prominences the "ventrolateral tubera". The basioccipital contacts the opisthotics along the dorsal margins of the tubera ventrolateral to the jugular foramen. Medial to the ventrolateral tubera, the basioccipital presents a flat region that continues anteriorly to the parabasisphenoid. The basioccipital contributes to the posterior margin of the *fenestra ovalis*, with the anterior margin being composed by the parabasisphenoid, to which both bones contribute in equal proportions, with the opisthotic contributing to a small portion of the margin dorsolaterally (Fig 5C, F). The basioccipital also contributes to the lateral and dorsal margin of the jugular foramen.

Interparietal + tabular

The occipital region of GPIT-PV-60758 is damaged, as indicated by the absence of the dorsalmost part of the supraoccipital and the posterior part of the right postorbital (Fig. 2). Because of this damage, the interparietal and the tabulars are not preserved in this specimen.

Supraoccipital

The supraoccipital is badly preserved in GPIT-PV-60758, with most of its dorsal and anterodorsal parts broken off (Fig. 5C-F). The supraoccipital delimits the foramen magnum dorsally, and it is bordered by the squamosals laterally. It also contacts the prootics anteroventrally, and the exoccipitals posteroventrally. Dorsally, a gap between the supraoccipital and the parietals represents the space for the interparietal and the tabulars, with the supraoccipital originally contacting these dorsally (Sullivan and Reisz, 2005). Anterodorsally, the supraoccipital preserves a small flange on the right side that appears to contribute to the lateral wall of the braincase, and it encloses the bony labyrinth dorsally. The external surface of the supraoccipital is better preserved on the left side of the skull, where it contacts the ventralmost portion of the squamosal dorsal process laterally and the exoccipital ventrally. The supraoccipital lateral extensions contribute to the dorsomedial margins of the posttemporal fenestra (Fig. 5F).

Exoccipital

The exoccipitals are two small elements that contribute to the lateral margins of the foramen magnum (Fig. 5C, F). They are bordered by the supraoccipital dorsally, the prootics anteriorly, the opisthotic ventrolaterally and the basioccipital ventromedially. In GPIT-PV-60758, the left exoccipital is better preserved than the right. Our segmentation shows that the exoccipitals contribute to the dorsolateral swelling of the occipital condyle, which is visible only on the left side of the specimen because the right side of the occipital condyle is not preserved. The exoccipital contributes to the dorsal margin of the jugular foramen, which is located between the exoccipital, the basioccipital ventromedially and the opisthotic ventrolaterally. The anterodorsal surface of the exoccipital contributes to the wall of the floccular fossa.

Opisthotic

The opisthotics form the ventrolateral part of the braincase and are subrectangular in posterior view (Fig 5). The left opisthotic is better preserved in GPIT-PV-60758, and it will be the focus of this description. The opisthotic forms the paroccipital process between the occipital complex and the squamosal, and it also bears an anterior projection that reaches the posterolateral portion of the parabasispenoid and contacts the ventral margin of the prootic (Fig. 5C, D). The opisthotic and the prootic are strongly coossified and their suture is hard to trace (Fig. 5E). The opisthotic also contacts the supraoccipital dorsally (Fig. 5F). The opisthotic contributes to the lateral margin of the *fenestra ovalis* ventromedially, and it makes up the lateral margin of the jugular foramen

medially. Our description matches that of Sullivan & Reisz (2005), which defines the jugular foramen as being located between the opisthotic, the exoccipital and the lateral knob of the occipital condyle. The opisthotic also contributes to the ventral margin of the posttemporal fenestra (Fig. 5E, F). The contact between the opisthotic and the squamosal is large, covering the entire medial surface of the squamosal ventral to the posttemporal foramen. Medially, the opisthotic forms the lateral wall of the otic capsule, enclosing the lagena of the inner ear.

Prootic

The prootics are paired elements located anterolateral to the foramen magnum (Fig. 5A, B, D, E). They enclose the semicircular canals and compose the anterior, dorsal and lateral walls of the recesses that house the lobes of the floccular complex of the cerebellum (fcl; fcl fossae). The prootic contacts the parabasisphenoid anteroventrally, the opisthotic ventrolaterally, the supraoccipital posteriorly, and the exoccipital posteroventrally. The sutures with the opisthotic and the supraoccipital are particularly well-resolved, and correspond to most of the sutural area of these bones. The prootic is subtriangular in lateral view. The anterior margin of the prootic is slightly curved, reflecting the shape of the anterior semicircular canal that it encloses. The ascending process of the prootic likely fuses with the epiotic, a bone that usually coossifies with the prootic at the level of the suture with the supraoccipital (Jollie, 1960). The epiotic could not be discriminated as a distinct element. The prootic (+epiotic) and the opisthotic are part of the periotic complex, a group of structures homologous to the petrosal of modern mammals. In dicynodonts, including other specimens of *Diictodon*, the prootics normally present a pila antotica anteriorly, an element that projects dorsally and that is part of the braincase wall. However, this element is not preserved in GPIT-PV-60758. The medial surface of the left prootic presents a large fossa that housed the floccular complex lobe, posteriorly. This structure is not preserved on the right element.

Mandible

Dentary

The dentary is the largest and best-preserved element of the mandible, although the anteriormost tip is relatively worn compared to the rest of the bone (Fig. 6). In lateral aspect, the dentary presents a rounded upturned beak at the level of the symphysis (Fig. 6A, B, C). The bone increases in height as the anterior margin descends steeply (53^{o} with the occlusal plane). The dentary reaches its maximum height at approximately one third of its total length. It then gradually becomes slender posteriorly. The ventral margin of the dentary is convex anteriorly, just posterior to the symphysis, but becomes slightly concave anterior to the ascending ramus (Fig. 6A, B). The dentary does not present a strong lateral dentary shelf, but a shallow trough running posterodorsally-anteroventrally (oblique line) marks the anterior border of a blunt dentary swelling (dsw, Fig. 6A, B). In dorsal view, the hemimandibles diverge at an angle of 47^{o}, measured from the anteriormost part of the beak to the posteriormost part of the rami. The anterior part of the dentary is characterized by the up-turned symphysis (Fig. 6C). The anterior edge of the dentaries presents two small swellings that form dorsal bony protrusions (bp, Fig 6C), each of which continue posteriorly as a ridge (dentary blades) that borders the dentary table medially. The dentary blades (dbl, Fig. 6C) are antero-posteriorly oriented, parallel to the dentary tables (dta, Fig. 6C). The latter are transversely excavated and present foramina that appear to connect to the mandibular canal (Fig. S8). These structures appear to resemble the *dorsal canaliculi* described in mammals (Ferreira-Cardoso et al., 2019). In GPIT-PV-60758, the dentary table is continuous posteriorly with the small shallow posterior dentary sulcus (pds, Fig. 6C). The posterior part of the dentary blades preoject medially forming small round medial dentary shelves (mds; Fig. 6C). These shelves limit the longitudinal extent of the horizontal ramus, dorsally. The ascending rami project posterolaterally, forming a 40^{o} angle with the anteroposterior axis of the dentary tables (Fig. 6C, D). They narrow posteriorly and their medial surface presents a furrow that houses the anterior part of the surangular (Fig. 6B, D).

Splenial

The splenial is a flattened and elongated bone that covers the ventral part of the dentary medial surface along its entire length (Fig. 6D). Anteriorly, it consists of a medial projection that contacts its bilaterally symmetric counterpart. The intersplenial suture is small but visible (Fig. S9A) on a small ventral concavity on the lingual surface of the dentary symphysis (Fig. 6D). The splenial broadens and thickens

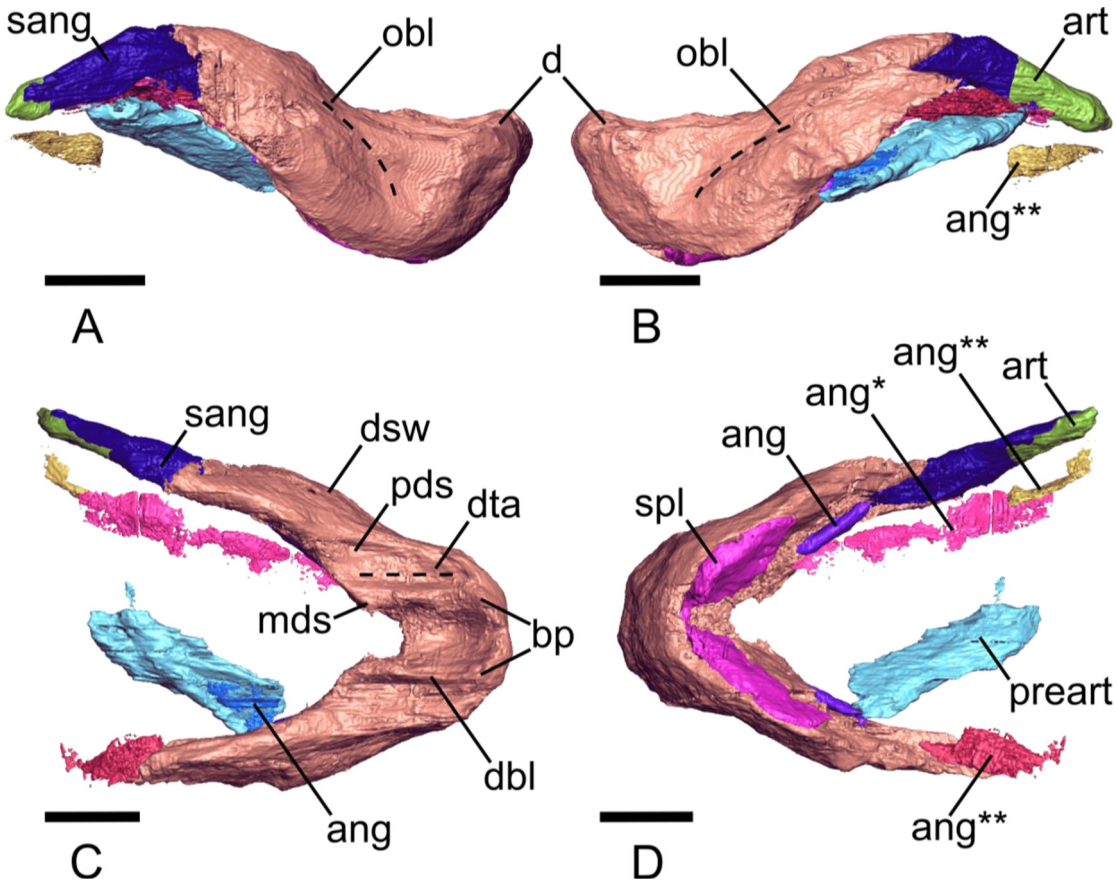

FIGURE 6. Mandible. Lateral right (A), lateral left (B), dorsal (C), and ventral (D) views. * - putative fragments of the angular; ang - angular; art - articular; bp - bony protrusions; d - dentary; dbl - dentary blade; dsw - dentary swelling; dta - dentary table; mds - medial dentary shelf; obl - oblique line; preart - prearticular; sang - surangular; spl - splenial. Dashed lines point anatomical structures. Scale bar = 10 mm.

posteriorly for a short length. Apart from its anterior symphyseal part, the spenial has an elliptical shape in medial/lateral view. The bone is housed by a broad medial dentary recess. At its round posterior margin, the splenial likely contacted the anterior parts of both the angular and prearticular, but they are not well-preserved in our specimen.

Angular

Both angulars are extremely damaged in GPIT-PV-60758 (Fig. 6B-D). The anterior part of the left and right angulars are still attached to the ascending ramus of the dentary, posterodorsal to the splenial (ang, Fig. 6D). In addition to the dentary, the angular probably contacted the splenial, the surangular, and the prearticular. Our reconstruction shows a badly weathered part of the right angular bone attached to the anterolateral surface of the disarticulated prearticular (ang*; Fig. 6D). Several unidentifiable elements putatively belonged to the angular bones (ang**, ang***, ang****; Fig. 6D).

Surangular

The surangular contacts the dentary anteriorly, the articular posteriorly, and in other *Diictodon* specimens, it contacts the angular ventrally (Sullivan & Reisz, 2005). This element forms the dorsal edge of the posterior portion of the mandible (Fig. 6). The right surangular is better preserved whereas the left is a badly preserved fragment located near its articulation with the dentary. The right surangular has a wide V-shape with a ventrally-opening angle. The anterior portion of the surangular rests in a relatively deep descending furrow on the medial surface of the dentary. The anterior half of the surangular is three times longer than high and has a subrectangular anterior tip. The posterior half of the surangular appears to be damaged, as well as the articular-prearticular complex to which it attaches.

Articular-prearticular complex

The articular-prearticular complex is highly damaged in GPIT-PV-60758 (Fig. 6B, D). The articular surface of the left articular bone is preserved. It contacts the medial surface of the posterior part of the surangular. Posteriorly, the articular forms a knob that articulates with the intercondylar groove of the quadrate. The prearticular of GPIT-PV-60758 is represented by the right element only (Fig. 6). It is disarticulated from all the remaining elements of the mandible, except for a badly preserved part of the angular on its medial surface (Fig 6D). The prearticular is a broad, flattened, and anteroposteriorly elongated bone. The poor preservation of the posterior elements of the mandible prevents an accurate description of these bones.

Braincase endocast and bony labyrinth

Brain endocast

The brain endocast is subtriangular in lateral view, with a narrower forebrain anteriorly and a broader hindbrain posteriorly (Fig. 7). The endocast is limited anteriorly by the sphenethmoid and the frontal, with both bones contributing to the olfactory dorsal and ventral walls, respectively. The olfactory bulbs (*sensu* Mammalia) are relatively small, practically nonexistent, and consist of two large-diamter nerves at the most anterior part of the endocast. Posteriorly, these nerves are fused in a mass that corresponds to the olfactory tract (Fig. 7). The olfactory tract and posterior part of the bulbs are wrapped by the ascending processes of the sphenethmoid ventrally and laterally (broadly analogous to the cribriform plate in mammals; Bird, 2014, 2018; Martinez et al., 2020). Posterior to this region, the dorsal surface of the endocast projects dorsally as an elongated and mediolaterally narrow protuberance that corresponds to the pineal foramen (Fig. 7A, B). The ventral part of the endocast between the sphenethmoid and the posterior margin of the pineal foramen is interpolated, as there is no preserved osseous element delimiting the brain in this region. The lateral wall was probably composed of cartilage associated with the *pila metotica* anteriorly and the *pila antotica* posteriorly (Novacek, 1993; Rieppel, 1993; Paluh & Sheil, 2013). Ventrally, the midbrain presents a large hypophysis, which is anteriorly limited by the cultriform process of the parasphenoid (Fig. 7A, C). The ventral margin of the hypophysis presents a projecting cylindrical structure that corresponds to the internal carotid canal (icc, Fig. 7A, C). The internal carotid canal is wide dorsally but splits in two smaller structures on its most ventral part (Fig. 7C). Posterior to the level of the pineal foramen, the dorsal margin of the hindbrain is inclined ventrally, mirroring the orientation of the parietal. Laterally, the width of the endocast is limited by the epipterygoids and the descending flanges of the anterior part of the parietal. Ventrally, the hindbrain is delimited by the basisphenoid anteriorly and the basioccipital posteriorly. The posterior part of the endocast consists of a badly preserved cerebellum, delimited posteriorly by the supraoccipital and the exoccipitals at the posterior portion of the floccular fossae. Laterally, the cerebellum is delimited by the prootics, which form almost the entirety of the walls of the floccular complex lobe (fcl) fossae (e.g., Ferreira-Cardoso et al., 2017). Only the right floccular fossa is well preserved. Cranial nerve V (and the *vena capitis medialis*) can be identified anteroventrally to the floccular complex lobe (e.g., Laaß, 2015). The most posterior portion of the endocast consists of the medulla oblongata and is delimited by the foramen magnum, framed by the supraoccipital dorsally and the basioccipital ventrally. The cast of the cranial nerves IX-XI is present on the ventral part of the hindbrain.

Bony labyrinth

The bony labyrinth houses the vestibular organ dorsally and the vestibule ventrally (Fig. 7). In GPIT-PV-60758, the left bony labyrinth is better preserved, with all three semicircular canals represented. Both vertical semicircular canals are elliptical and equally thick. In dorsal view, the circumference of the anterior semicircular canal (ascc) faces anteromedially, with the canal projecting laterally from the *crus communis* to form an angle of about 38° with the sagittal plane of the skull (Fig 7). The ascc encloses the largest area, with the floccular complex of the cerebellum protruding through it. The ascc presents an ampula anteriorly. This semicircular canal is enclosed by the prootic. The posterior semicircular canal (pscc) projects posterolaterally from the *crus communis* with an anteriorly opening angle of approximately 113° relative to the sagittal plane of the skull. The pscc is enclosed by the exoccipital medially and by the supraoccipital on its most lateral part. The *crus communis* is filled with dense sediment, making it hard to reconstruct. Only the most dorsal and most ventral parts of this structure are preserved. The horizontal semicircular canal (hscc) is subcircular, and its

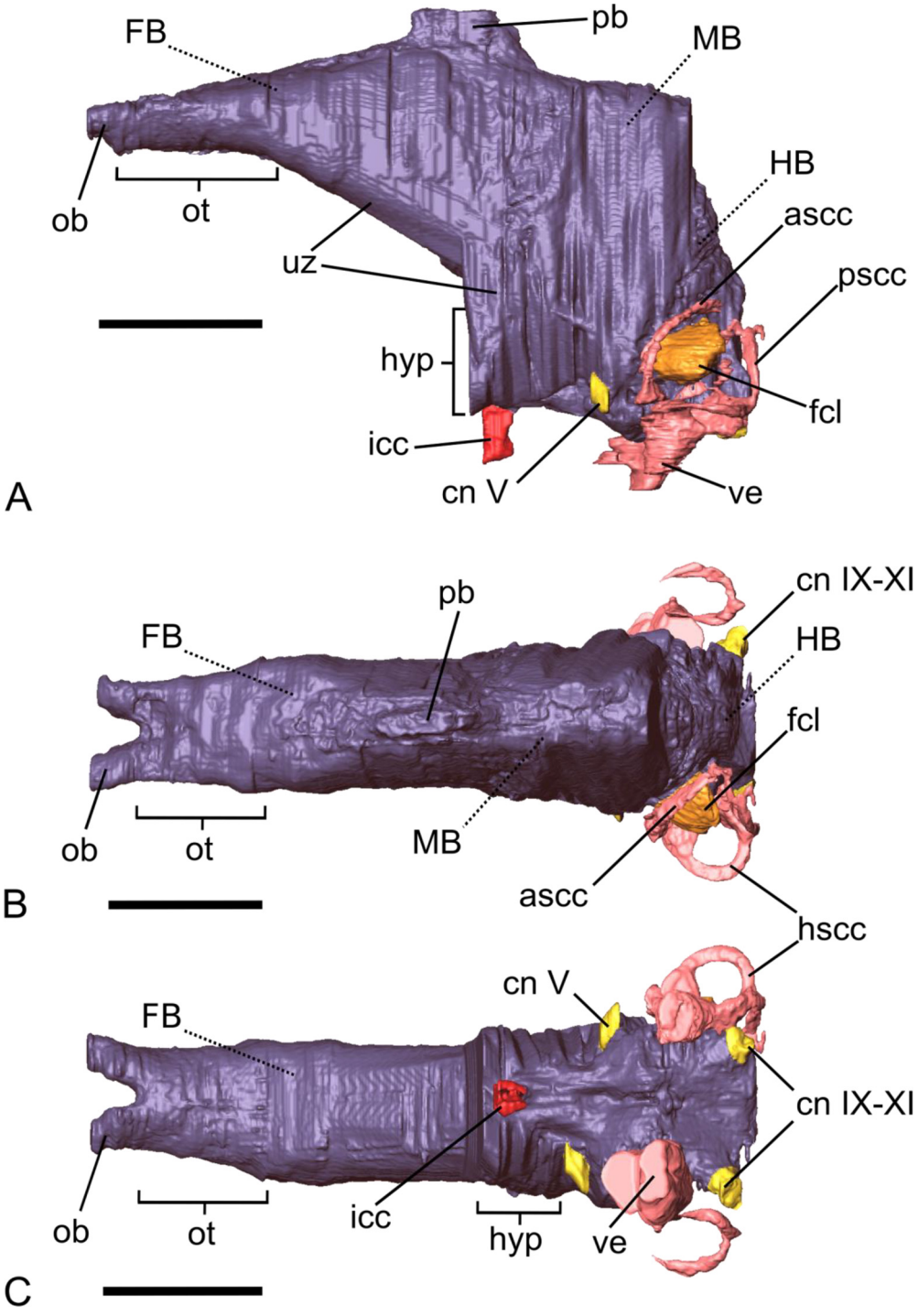

FIGURE 7. Braincase endocast and bony labyrinth. Lateral left (A), dorsal (B), and ventral (C) views. ascc - anterior semicircular canal; cn - cranial nerve(s); fcl - floccular complex lobe; hyp - hypophysis; horizontal semicircular canal; icc - internal carotid canal; ob - olfactory bulb; ot - olfactory tract; pb - pineal body; pscc - posterior semicircular canal; uz - unossified zone; ve - vestibule; FB - forebrain; HB - hindbrain; MB - midbrain. Scale bar = 10 mm.

posterior ampulla merges with the ampulla of the pscc, forming a ventral projection and concave internal surface between the latter and the vestibule. The anterior ampulla of the hscc is large and merges with the ampulla of the ascc,

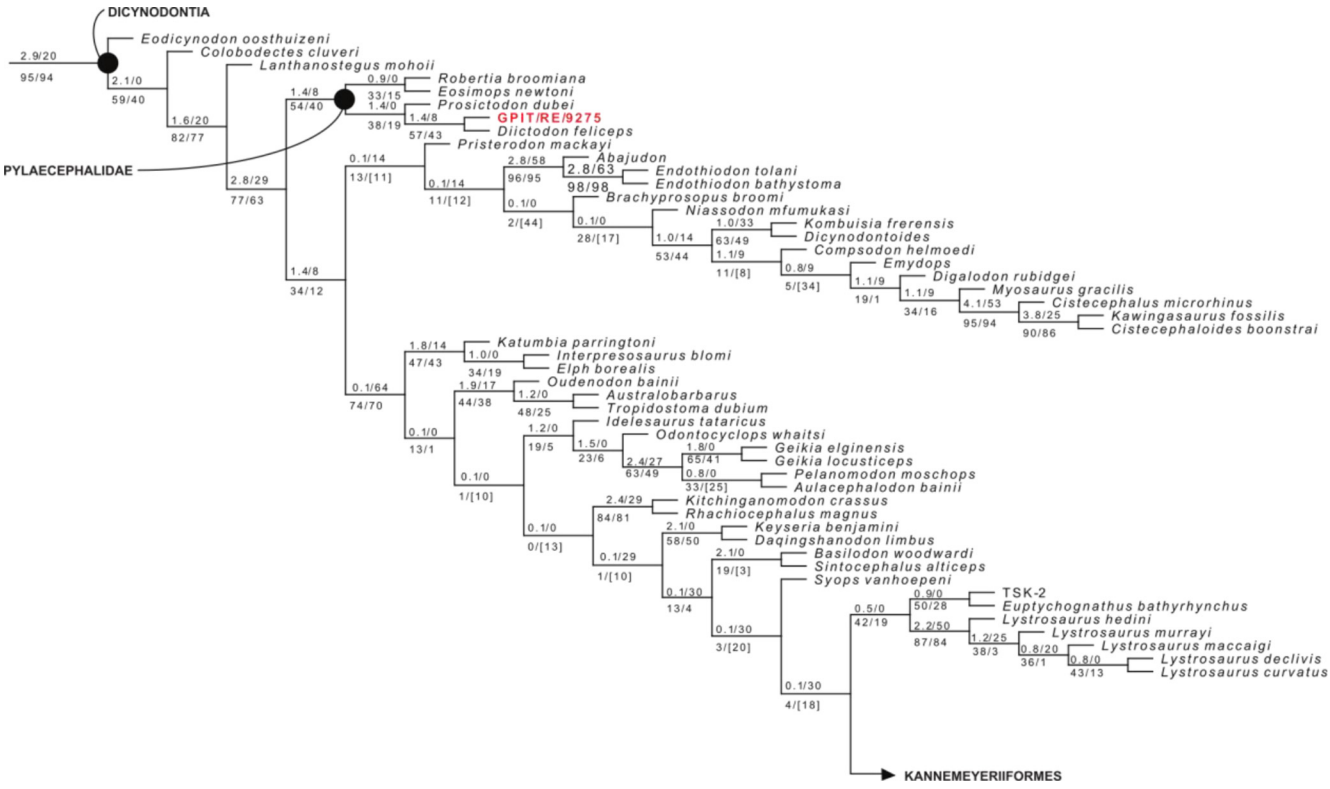

FIGURE 8. Region of interest of the most parsimonious cladogram from the phylogenetic analysis. Scores: 1135.549 steps, consistency index = 0.240, retention index = 0.718. Numbers at nodes represent Bremer supports (left/top), relative Bremer supports (right/top), symmetric resampling (left/bottom), and the percentage of suboptimal trees in which the node is resolved. GPIT-PV-60758 in red.

forming a wide surface in dorsal view (Fig. 7). The hscc is enclosed anteriorly by the prootic and posteriorly by the opisthotic. The sacculus and utriculus are not distinguishable in the vestibule. The vestibule projects ventrally with a slight anterior inclination. This structure has an elliptical cross-section with a mediolaterally oriented major axis. The lagena forms the ventral part of the cast of the bony labyrinth and is limited by the aperture of the fenestra ovalis on the tubera formed by the basioccipital and the parabasisphenoid.

Phylogenetic analysis

The phylogenetic analysis retained a single most parsimonious tree with a tree length of 1135.549 steps (Fig. 8; CI = 0.240; RI = 0.718), resulting from 5,892,799,471 rearrangements. GPIT-PV-60758 was recovered as the sister taxon of *Diictodon feliceps,* a moderately supported node (Bremer support = 1.379). The symmetric resampling value for the GPIT-PV-60758-*Di. Feliceps* node was 43. This relationship is supported by four discrete-state unambiguous synapomorphies: presence of a posterior median ridge on the palatal surface of the premaxilla without a flattened, expanded anterior area (5[2]); posterior process of the premaxilla with a non-bifurcated posterior tip (10[0]); presence of a distinct lateral caniniform buttress (29[1]); ventral edge of the caniniform process anterior to the anterior orbital margin (32[0]). The analysis places GPIT-PV-60758 and *D. feliceps* within the Pylaecephalidae, grouped with *Eosimops newtoni*, *Robertia broomiana*, and *Prosictodon dubei*. The symmetric resampling value corresponding to this node is 40. The Pylaecephalidae node is supported by the following diagnostic traits: presence of lateral anterior palatal ridges (3[1]); posterior process of the premaxilla with a bifurcated posterior tip (10[1]); caniniform depression with the form of a notch in the palatal rim anterior to caniniform process (28[2]); ventral edge of the caniniform process at the same level or slightly posterior to the anterior orbital margin (32[1]); presence of a tall, dorsally-convex cutting blade on medial edge of dorsal surface of dentary (126[1]); presence of a cleithrum (144[1]); procoracoid foramen or notch formed by the contributions of the procoracoid and scapula in lateral view (148[1]); presence

of an ectepicondylar foramen on the humerus (154[0]). GPIT-PV-60758 presents two character state reversals (10[1->0] and 32[1->0]) compared to the plesiomorphic condition in the Pylaecephalidae.

DISCUSSION

Phylogeny

The phylogenetic analysis allowed us to show that GPIT-PV-60758 falls within the Pylaecephalidae (Figs. 8 and S10). The specimen was retrieved as a sister taxon to *Di. feliceps*, which lends support to the referral of this specimen proposed by various authors including Brink (1986) or Kammerer et al. (2011, 2020). Our specimen showed four unambiguous synapomorphies, including two reversals that contrast with the emended diagnosis proposed here for the genus *Diictodon*. In addition, *Di. feliceps* presents an unambiguous synapomorphy (102[2]) that is not shared by GPIT-PV-60758. Nevertheless, we maintain the previous hypothesis that GPIT-PV-60758 should be considered as a *Di. feliceps*, and that the results from our phylogenetic analyses (including a relatively low resampling value) reflect intraspecific variation within *Di. feliceps*, previously studied by Sullivan & Reisz (2005). Perhaps, these results justify a more in depth revision of the genus *Diictodon*. Phylogenetic affinities within the Pylaecephalidae are the same as those in the trees recently published by Olroyd et al. (2017) and Kammerer et al. (2019).

Internal anatomy of the skull in GPIT-PV-60758

Our description provides the first digital reconstructions of the endocast and inner ear of *Diictodon*. Only a few dicynodonts have had their brain endocast anatomy reconstructed based on µ-CT scanning, including the endothiodontid *Niassodon mfumukasi* (Castanhinha et al., 2013), the eumantellid *Pristerodon mackayi* (Laaß, 2015), the cistecephalid *Kawingasaurus fossilis* (Laaß, 2014), and the basal bidentalian *Rastodon procurvidens* (Simão-Oliveira et al. 2019). GPIT-PV-60758 endocast presents the typical general shape known from other early therapsids, with a distinctive thin tubular forebrain and a more dorsoventrally and mediolaterally expanded mid- and hindbrain (see 'Anatomical description'). The olfactory tract in GPIT-PV-60758 is relatively shorter when compared to those in *N. mfumukasi*, *P. mackayi*, and *R. procurvidens*. It resembles the condition in *Dicynodon* (Lehman, 1961), which presents a short olfactory tract and dorsoventrally high mid- and hindbrains. As other dicynodonts, the GPIT-PV-60758 endocast falls in the description of the first stage of mammalian brain evolution and is comparable to that of nonmammalian cynodonts (Kemp, 2009). Kemp (2009) associates the development of the mid- and hindbrains to a development of movement coordination and proprioception. The large hindbrain presents a small lateral projection (flocculus) that protrudes through the anterior semicircular canal (Fig. 7). Although the flocculus is prominent in *N. mfumukasi* (Castanhinha et al., 2013) and *P. mackayi* (Laaß, 2015), this structure is much less pronounced in *R. procurvidens* (Simão-Oliveira et al., 2019), which is likely a result of the architecture of the braincase and a well-developed hindbrain in the former species (Walsh *et al.*, 2013; Ferreira-Cardoso et al., 2017). Similar to the remaining dicynodonts, the relatively small forebrain presents weakly developed olfactory bulbs, suggesting that olfaction was not as well-developed as seen in more recent cynodonts and modern mammals (Rowe et al., 2011). The short forebrain is directly related to the antero-posteriorly short ethmoid in GPIT-PV-60758 (Fig. 3).

Boonstra (1968) described the braincase of *Dicynodon* (considered as *Diictodon* by Simão-Oliveira et al., 2019). Our description matches the observations in Boonstra (1968), including the presence of a relatively shallow sella turcica that housed an equally small hypophysis (pituitary gland). Similar to other dicynodonts (Boonstra, 1968; Castanhinha et al., 2013; Laaß, 2015; Simão-Oliveira, 2019), the sella turcica structure was not delimited by a bony dorsum sella, given that the prootics do not meet at the midline to form the posterior wall of the hypophyseal fossa, such as in *Dimetrodon* (Romer & Price, 1940), dinocephalians (Boonstra, 1968), and gorgonopsians (Araújo et al., 2017). Instead, a blunt "dorsum sella" is present on the basioccipital, just posterior to the parabasisphenoid-basioccipital suture (Fig. 5D). Although the GPIT-PV-60758 "dorsum sella" is structurally analogous to that of other synapsids (limiting the hypophyseal fossa posteriorly), it has a distinct developmental origin, the basioccipital ossification center. This condition contrasts with that described in *Dicynodon*/*Diictodon* (Boonstra, 1968), in which the ventral part of the dorsum sella is formed by the parabasisphenoid.

The lack of long and prominent *pilae antoticae* delimiting the anterolateral part of the hypophysis in GPIT-PV-60758 contrasts with the condition usually found in other dicynodonts (Castanhinha et al., 2013; Laaß, 2015, Simão-Oliveira et al.,

2019). While Boonstra (1968) makes no reference to the pila antotica in *Dicynodon*/*Diictodon*, this structure only ossifies as a small anterior process of the prootic in *D. feliceps*, making its contribution to the lateral wall of the braincase extremely reduced (Sullivan & Reisz, 2005). In our specimen, a small triangular anterior process (putative part of the prootic) is indistinctly fused to the parabasisphenoid (Fig. 5). Such ossification on the parabasisphanoid is found, for instance, on the braincase of the cynodont *Diarthrognathus* (Olson, 1944; Presley & Steel, 1976).

The reconstruction of the internal anatomy of the GPIT-PV-60758 did not allow the identification of many relevant details concerning vascularization with the exception of the internal carotid canal (icc; Figs. 7). Similar to previous descriptions of *Diictodon* (Boonstra, 1968; Sullivan & Reisz, 2005) the internal carotid canal bifurcates ventrally. This condition resembles that in other dicynodonts such as *N. mfumukasi* (Castanhinha et al., 2013) and *P. mackayi* (Laaß, 2015). However, for most of its length, the internal dorsal canal in GPIT-PV-60758 consists of a single and relatively large cavity, similar to that in *R. procurvidens* (Simão-Oliveira et al., 2019). While Boonstra (1968) and Sullivan & Reisz (2005) described the internal carotid canals as enclosed by the parabasisphenoid, in GPIT/RE9275 their anterior part of margins consist of the pterygoid and the cultriform process (parasphenoid).

Internal anatomy of the mandible in GPIT-PV-60758

Most of the posterior elements of the mandible were badly preserved in GPIT-PV-60758 (see 'Anatomical description'). Nevertheless, the dentary was generally well preserved, including the dentary tables (Fig. 6). In *Diictodon*, these structures present a perforated surface (Sullivan & Reisz, 2005; Fig. 11E, Angielczyk & Rubidge, 2013). Vascular foramina are typically associated with the presence of a keratinous covering, not only in dicynodonts (e.g., Jasinoski & Chinsamy-Turan, 2012; Castanhinha et al., 2013), but also across a wide range of vertebrates such as ceratopsian dinosaurs (e.g., Bell et al., 2012), birds (Stidham, 1998), or mammals (Csorba et al., 2004). However, the perforations on the dentary table of *Diictodon* are relatively large in diameter. Despite the numerous scan artifacts and bad contrast in GPIT-PV-60758 internal mandibular structures, a close examination of the coronal slices of the specimen allowed us to identify these structures, as well as the corresponding canals (Fig. S8). Ferreira-Cardoso et al. (2019) associated similar structures (dorsal canaliculi) with vestigial tooth loci in some placental mammals such as anteaters, armadillos, or aardvarks. They discussed that the presence of dorsal canaliculi might be related to an exaptation of tooth nerve and vessel networks to innervate and vascularize keratinous structures (Ferreira-Cardoso et al., 2019). The presence of dorsal canaliculi in *Diictodon* and GPIT-PV-60758 suggest that vestigial tooth development might have occured in early ontogenetic stages (Ferreira-Cardoso et al., 2019 and reference therein). Further assessment of the internal mandibular anatomy of dicynodonts (including a three-dimensional reconstruction of a well preserved *Diictodon* specimen) is necessary to confirm this hypothesis.

CONCLUSION

Here we have used µ-CT scanning technology to re-describe a historical specimen from the South African Karoo (GPIT-PV-60758). In addition to a detailed description of its external morphology, we described for the first time the internal anatomy of GPIT-PV-60758, including the brain endocast and the left bony labyrinth. We also showed previously undescribed details such as the presence of dorsal canaliculi in the mandible, and the ossification of the anterior part of the braincase floor. Our phylogenetic analysis showed that GPIT-PV-60758 is, as noted by other authors, a *Diictodon feliceps* specimen. We hypothesize that autapomorphies recovered for GPIT-PV-60758 can be attributed to either ontogeny or to a stratigraphic variation within the genus *Diictodon*.

BIBLIOGRAPHY

Araújo, R., Fernandez, V., Polcyn, M. J., Fröbisch, J., & Martins, R. M. (2017). Aspects of gorgonopsian paleobiology and evolution: insights from the basicranium, occiput, osseous labyrinth, vasculature, and neuroanatomy. *PeerJ*, 5, e3119.

Araújo, R., Fernandez, V., Rabbitt, R. D., Ekdale, E. G., Antunes, M. T., Castanhinha, R., & Martins, R. M. (2018). *Endothiodon* cf. *Bathystoma* (Synapsida: Dicynodontia) bony labyrinth anatomy, variation and body mass estimates. *PLoS One*, 13(3), e0189883.

Angielczyk, K. D. & Rubidge, B. S. (2013). Skeletal morphology, phylogenetic relationships and stratigraphic range of Eosimops newtoni Broom, 1921, a pylaecephalid dicynodont (Therapsida, Anomodontia) from the Middle Permian of South Africa. *Journal of Systematic Palaeontology*, 11(2), 191–231.

Bell, P. R., Fanti, F., Currie, P. J., & Arbour, V. M. (2014). A mummified duck-billed dinosaur with a soft-tissue cock's comb. *Current Biology*, 24(1), 70-75.

Brink, A. S. (1986). Illustrated bibliographic catalogue of the Synapsida. Parts 1 and 2. Department of Mineral and Energy Affairs, Pretoria, Handbook 10, 540 pp.

Broom, R. (1911). On some new South African Permian reptiles. *Proceedings of the Zoological Society of London*, 1911: 1073–1082.

Broom, R. (1904). On a new species of *Oudenodon (O. megalorhinus)* from the Gough, S. Africa. *Records of the Albany Museum*, 1: 180–181.

Broom, R. (1913). On four new fossil reptiles from the Beaufort Series, South Africa. *Records of the Albany Museum*, 2, 397–401.

Csorba, G., Buzás, B., & Farkas, B. (2004). A previously undescribed skull of Steller's sea cow, *Hydrodamalis gigas* (Mammalia: Sirenia: Dugongidae) in the Hungarian Natural History Museum. In Annales historico-naturales Musei nationalis hungarici (Vol. 96, pp. 317–320). Hungarian Natural History Museum, Budapest.

Ferreira-Cardoso, S., Delsuc, F., & Hautier, L. (2019). Evolutionary tinkering of the mandibular canal linked to convergent regression of teeth in placental mammals. *Current Biology*, 29(3), 468–475.

Fröbisch, J. (2008). Global taxonomic diversity of anomodonts (Tetrapoda, Therapsida) and the terrestrial rock record across the Permian-Triassic boundary. *PLoS One*, 3(11), e3733.

Haughton, S. H. & Brink, A. S. (1954). A bibliographical list of Reptilia from the Karroo beds of Africa. *Palaeontologia Africana*, 2: 1–187.

Hoepen, E. C. N. van (1934). Oor die indeling van die Dicynodontidae na aanleiding van nuew vorme. *Paleontologiese Navorsing van die Nasionale Museum*, 2: 67–101.

Goloboff, P. A., Farris, J. S., & Nixon, K. C. (2008) TNT, a free program for phylogenetic analysis. *Cladistics*, 24: 774–786.

Jasinoski, S. C. & Chinsamy-Turan, A. (2012). Biological inferences of the cranial microstructure of the dicynodonts *Oudenodon* and *Lystrosaurus*. Forerunners of Mammals. *Radiation, Histology, Biology*, 148–176.

Jollie, M. T. (1960). The head skeleton of the lizard. *Acta Zoologica*, 41(1-2), 1-64.

Kammerer, C. F., Angielczyk, K. D., & Fröbisch, J. (2011). A comprehensive taxonomic revision of *Dicynodon* (Therapsida, Anomodontia) and its implications for dicynodont phylogeny, biogeography, and biostratigraphy. *Journal of Vertebrate Paleontology*, 31(sup1), 1-158.

Kammerer, C. F., Deutsch, M., Lungmus, J. K., & Angielczyk, K. D., (2020). Effects of taphonomic deformation on geometric morphometric analysis of fossils: a study using the dicynodont *Diictodon feliceps* (Therapsida, Anomodontia). *PeerJ*, 8, p.e9925.

King, G. M. (1988). Anomodontia. In P. Wellnhofer (Ed.), Handbuch der Paläoherpetologie, 17 C. Gustav Fischer Verlag, Stuttgart, 174 pp.

Novacek, M. J. (1993). Patterns of diversity in the mammalian skull. In J. Hanken & B. K. Hall (Eds.), The skull vol. 2 (pp. 438–545). University of Chicago Press.

Laaß, M. (2015). Virtual reconstruction and description of the cranial endocast of *Pristerodon mackayi* (Therapsida, Anomodontia). *Journal of morphology*, 276(9), 1089-1099.

LeBlanc, A. R., Brink, K. S., Whitney, M. R., Abdala, F., & Reisz, R. R. (2018). Dental ontogeny in extinct synapsids reveals a complex evolutionary history of the mammalian tooth attachment system. *Proceedings of the Royal Society B*, 285, 20181792.

Owen, R. (1845). Report on the Reptilian Fossils of South Africa. Part I. — Description of certain fossil crania, discovered by A. G. Bain, Esq., in sandstone rocks at the south-eastern extremity of Africa, referable to different species of an extinct genus of Reptilia (Dicynodon), and indicative of a new Tribe or Sub-order of Sauria. *Transactions of the Geological Society of London*, 2nd Series, 7, 59–84.

Paluh, D. J. & Sheil, C. A. (2013). Anatomy of the fully formed chondrocranium of *Emydura subglobosa* (Chelidae): a pleurodiran turtle. *Journal of Morphology*, 274(1), 1-10.

Presely, R. & Steel, F. L. (1976). On the homology of the alisphenoid. *Journal of Anatomy*, 121(Pt 3), 441.

Rieppel, O. (1993). Patterns of diversity in the reptilian skull. In *The Skull*, 2, 344-390.

Sidor, C. A., Hopson, J. A., & Keyser, A. W. (2004). A new burnetiamorph therapsid from the Teekloof Formation, Permian, of South Africa. *Journal of Vertebrate Paleontology*, 24(4), 938-950.

Stidham, T. A. (1998). A lower jaw from a Cretaceous parrot. *Nature*, 396(6706), 29–30.

Sulej, T. & Niedźwiedzki, G. (2019). An elephant-sized Late Triassic synapsid with erect limbs. *Science*, 363(6422), 78-80.

Toerien, M. J. (1953). The evolution of the palate in South African Anomodontia and its classificatory significance. *Palaeontologia Africana*, 1, 49–117.

Tschopp, E., Mateus, O., & Benson, R. B. (2015). A specimen-level phylogenetic analysis and taxonomic revision of Diplodocidae (Dinosauria, Sauropoda). *PeerJ*, 3, e857.

Whitney, M. R., Angielczyk, K. D., Peecook, B. R., & Sidor, C. A. (2021). The evolution of the synapsid tusk: insights from dicynodont therapsid tusk histology. *Proceedings of the Royal Society B*, 288(1961), 20211670.

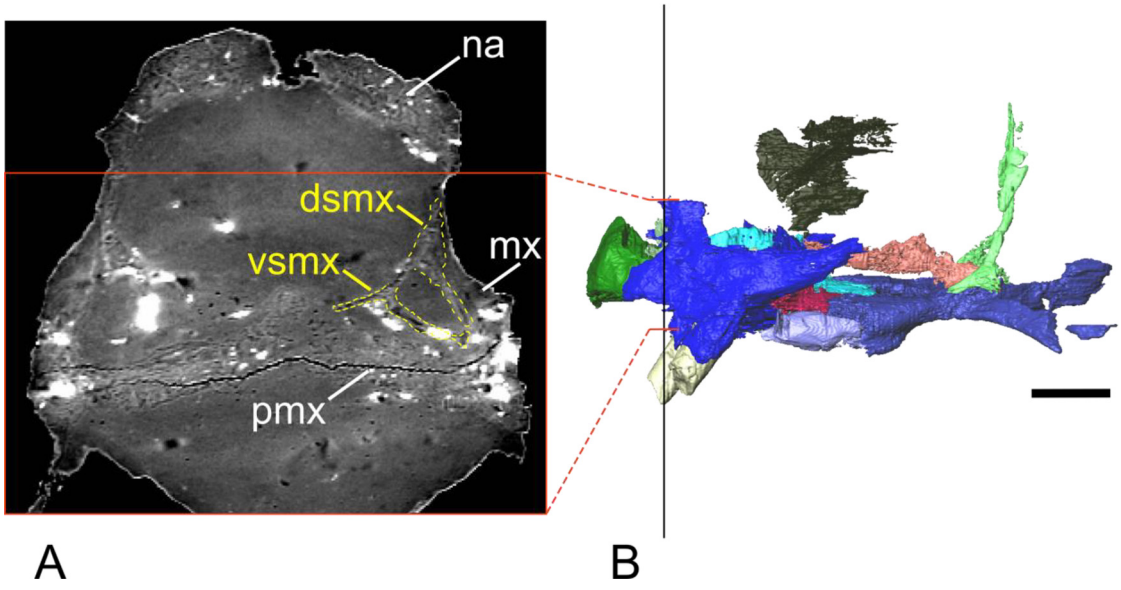

FIGURE S1. Cross-section of the septomaxilla. µCT scan coronal slice (A) and correspondent location (black line) shown on a lateral view of a 3D reconstruction (B). The orange rectangle and lines mark the region of interest. The septomaxilla is shown with a dashed yellow outline. dsmx - dorsal process of the septomaxilla; mx - maxilla; na - nasal; pmx - premaxilla. The cross-section is not to scale. Scale bar = 10 mm.

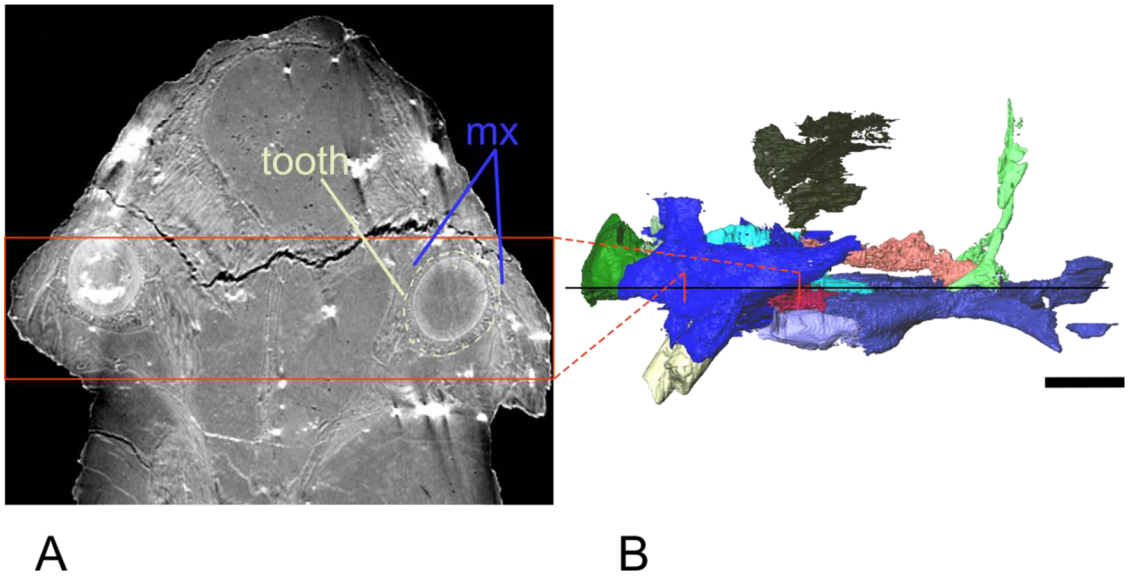

FIGURE S2. Transverse section of the tooth region. µCT scan transverse slice (A) and correspondent location (black line) shown on a lateral view of a 3D reconstruction (B). The orange rectangle and lines mark the region of interest. The tooth is shown with a dashed outline. mx - maxilla. The transverse section is not to scale. Scale bar = 10 mm.

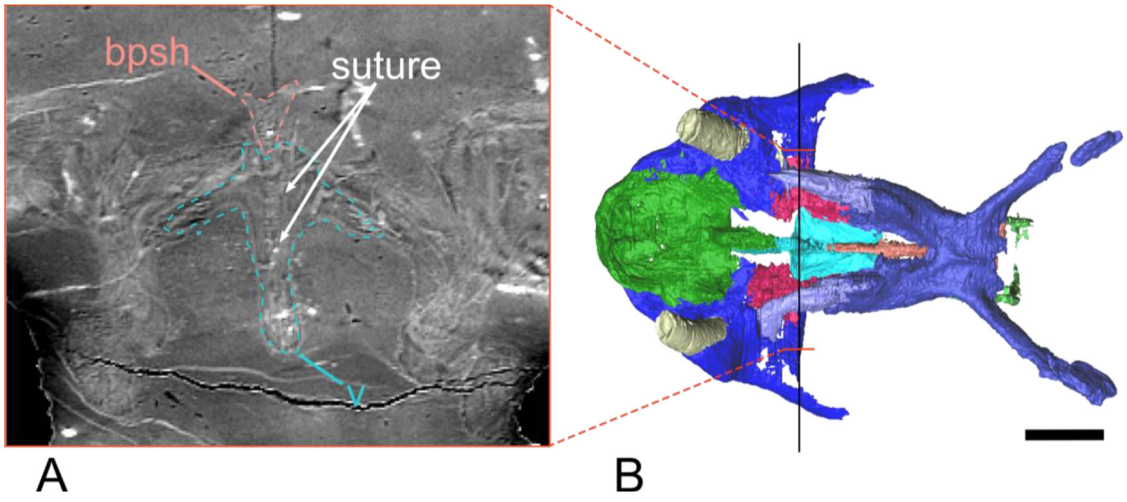

FIGURE S3. Cross-section of the vomer. µCT scan coronal slice (A) and correspondent location (black line) shown on a lateral view of a 3D reconstruction (B). The orange rectangle and lines mark the region of interest. The vomer and the cultriform process of the basiparasphenoid are shown with dashed cyan and coral outlines, respectively. The arrows point to the intervomerine suture. psh - cultriform process of the parabasisphenoid; v - vomer. The cross-section is not to scale. Scale bar = 10 mm.

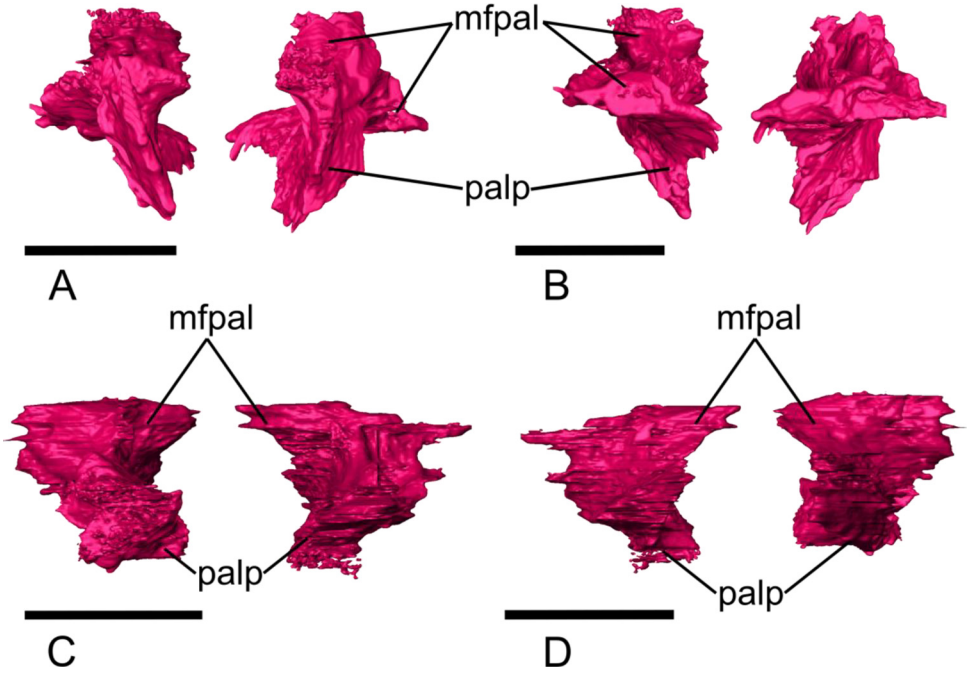

FIGURE S4. Palatine. Ventral (A), dorsal (B), anterior (C), and posterior (D) views. Mfpal - maxillary flanges of the palatine; palp - palatine pads. Scale bar = 10 mm.

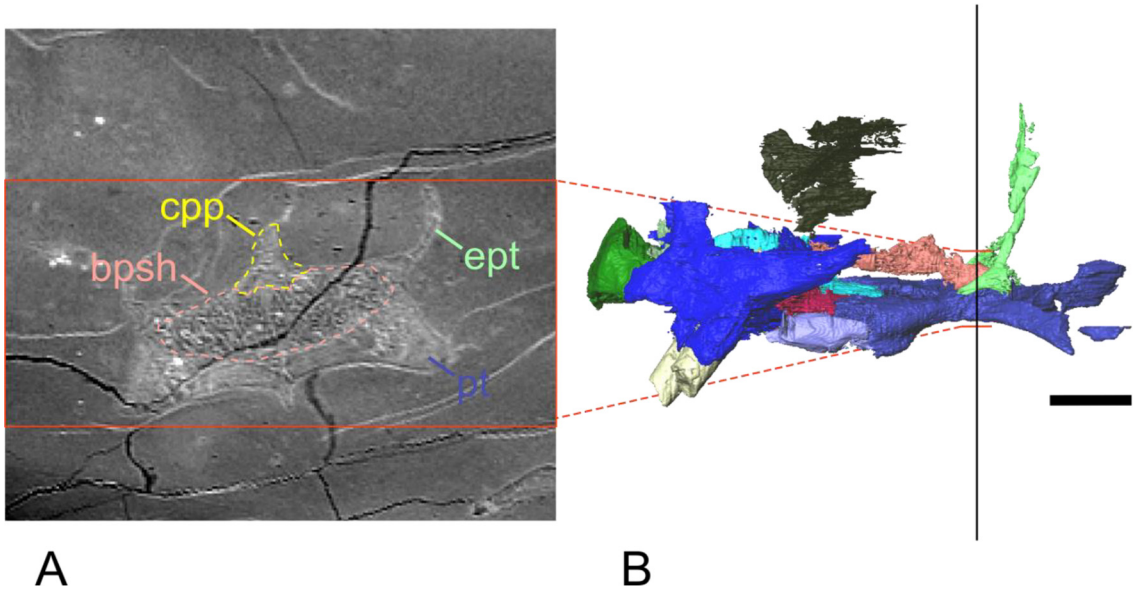

FIGURE S5. Cross-section of the basipresphenoid. µCT scan coronal slice (A) and correspondent location (black line) shown on a lateral view of a 3D reconstruction (B). The orange rectangle and lines mark the region of interest. The basipresphenoid and the cultriform process of the parasphenoid are shown with dashed coral and yellow outlines, respectively. bpsh - basipresphenoid; cpp - cultriform process of the parasphenoid; ept - epipterygoid; pt - pterygoid. The cross-section is not to scale. Scale bar = 10 mm.

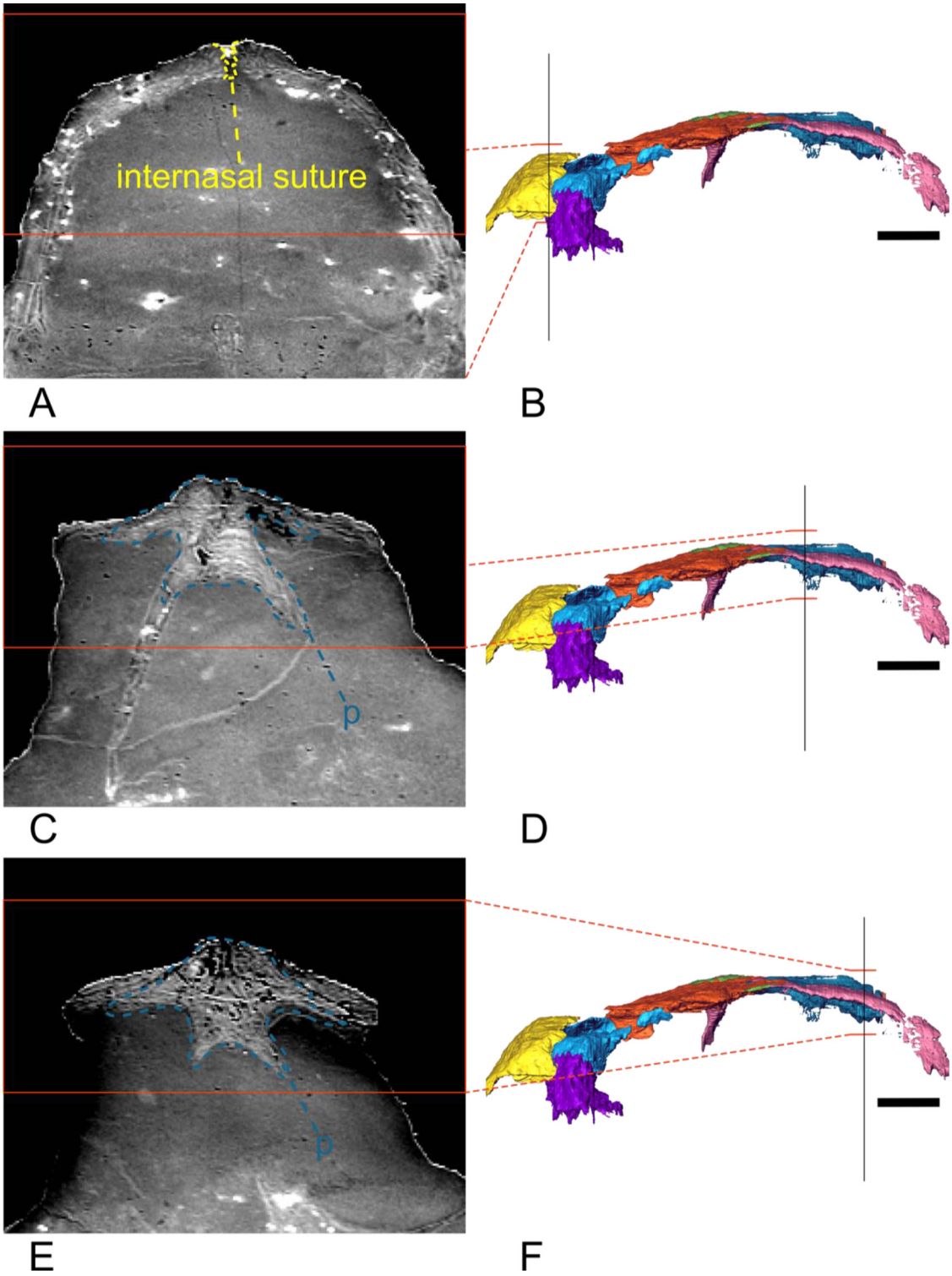

FIGURE S6. Cross-sections of the nasal and parietal. µCT scan coronal slice (A, C, E) and correspondent location (black line) shown on a lateral view of a 3D reconstruction (B, D, F). The orange rectangle and lines mark the region of interest. The internasal suture and the parietal are shown with dashed yellow and dark green outlines. p - parietal. The cross-sections are not to scale. Scale bar = 10 mm.

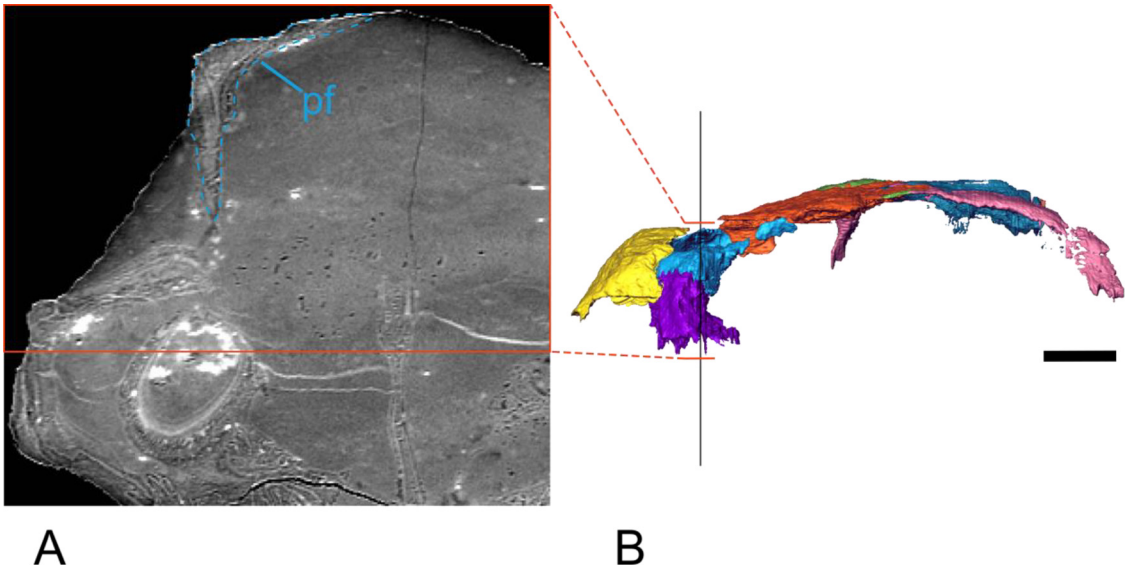

FIGURE S7. Cross-section of the prefrontal. µCT scan coronal slice (A) and correspondent location (black line) shown on a lateral view of a 3D reconstruction (B). The orange rectangle and lines mark the region of interest. The prefrontal is shown with a dashed blue outline. pf - prefrontal. The cross-section is not to scale. Scale bar = 10 mm.

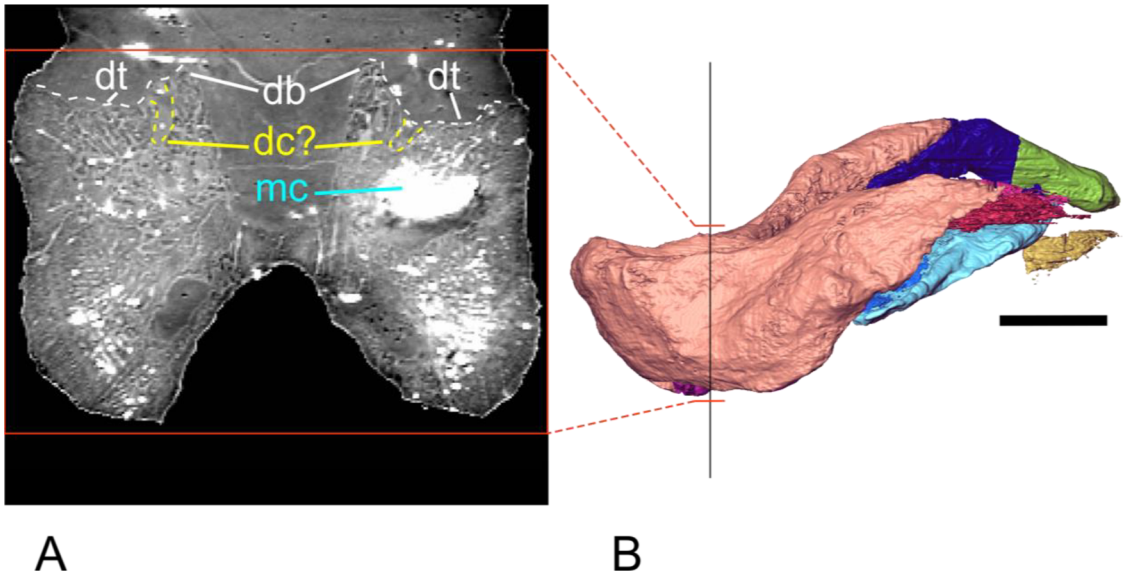

FIGURE S8. Cross-section of the dentary. µCT scan coronal slice (A) and correspondent location (black line) shown on a lateral view of a 3D reconstruction (B). The orange rectangle and lines mark the region of interest. Putative dorsal canaliculi and the dentary table are shown with dashed yellow and white outlines, respectively. db - dentary blade; dc - dorsal canaliculi; dt - dentary table; mc - mandibular canal. The cross-section is not to scale. Scale bar = 10 mm.

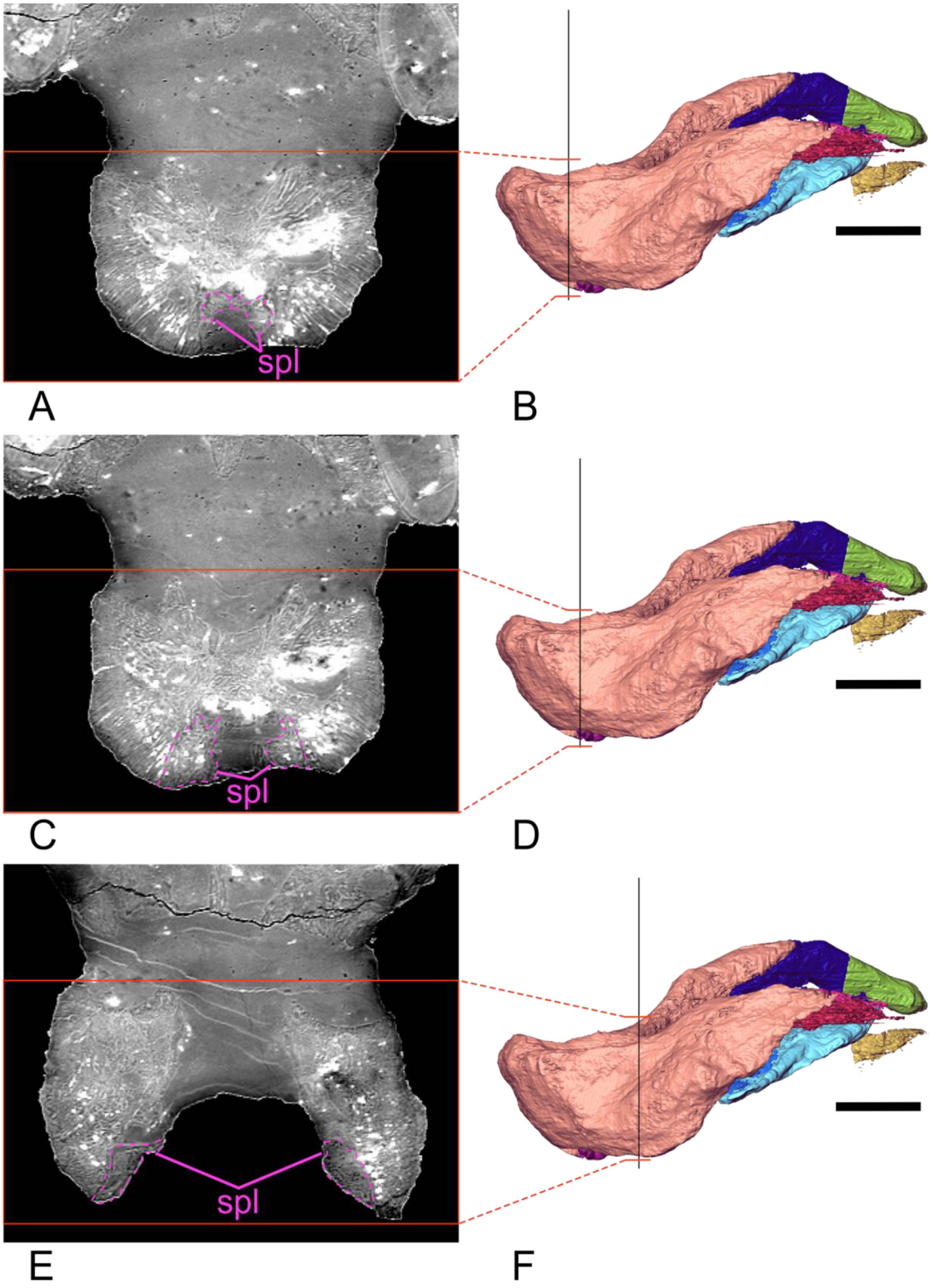

FIGURE S9. Cross-sections of the splenial. µCT scan coronal slice (A, C, E) and correspondent location (black line) shown on a lateral view of a 3D reconstruction (B, D, F). The orange rectangle and lines mark the region of interest. The splenial is shown with a dashed pink outline. spl - splenial. The cross-section is not to scale. Scale bar = 10 mm.

WINDOWS INTO SAUROPSID AND SYNAPSID EVOLUTION
Essays in honor of Prof. Louis L. Jacobs, pp. 66–98, 2023

REMARKABLY WELL-PRESERVED *IN-SITU* GUT-CONTENT IN A SPECIMEN OF *PROGNATHODON KIANDA* (SQUAMATA: MOSASAURIDAE) REVEALS MULTISPECIES INTRAFAMILIAL PREDATION, CANNIBALISM, AND A NEW MOSASAURINE TAXON

Michael J. Polcyn[1,3,*], Anne S. Schulp[2,3], and António Olímpio Gonçalves[4]

[1]Roy M. Huffington Department of Earth Sciences, Southern Methodist University, Dallas, Texas, USA, mpolcyn@smu.edu
[2]Naturalis Biodiversity Center, Leiden, The Netherlands
[3]Utrecht University, Utrecht, The Netherlands
[4]Departamento de Geologia, Faculdade de Ciências, Universidade Agostinho Neto, Luanda, Angola

ABSTRACT In this contribution we report a spectacularly well-preserved, semi-articulated specimen of *Prognathodon kianda* containing three partial mosasaurs in its stomach region. The discovery is from the lower Maastrichtian (~71.5Ma) "Bench 19 Bonebed" at Bentiaba, Angola. Each of the three mosasaurs found in the gut region is a unique taxon, one being the first documented occurrence of cannibalism in mosasaurs, and another representing a new mosasaurine genus and species, *Bentiabasaurus jacobsi* gen. et sp. nov., a taxon closely related to *Mosasaurus*. Trophic interactions at the "Bench 19 Bonebed" locality appear to be controlled in part by relative size of the predator and the prey, all prey taxa falling between 43 and 57% of the predator's body length. Prey items are all dismembered to some degree and individual parcels approach the estimated maximum sizes that can pass the gullet. Tooth and bone modification, and other aspects of prey processing are discussed. Though the sample is small, the observed range of modalities suggests prey processing, digestive biology, and methods of elimination in mosasaurs was diverse.

KEYWORDS Predator, Prey, Mosasaurid, Gut-content, Regurgitaliths, Cannibalism, Feeding ecology

INTRODUCTION

Mosasaurs are marine-adapted lizards that occupied the top predator niche in many marine ecosystems towards the end of the late Cretaceous. There are numerous reports of mosasaur predation on invertebrates such as cephalopods, pteriomorphian bivalves, and echinoderms (e.g., Dollo, 1913; Kauffman, 2004; Martin and Fox, 2007; Konishi et al., 2011; Neumann and Hampe, 2018), and also of predation and consumption of vertebrates, including fishes, plesiosaurs, turtles, and birds (e.g., Dollo, 1887; Williston, 1899; Sternberg, 1922; Camp, 1942; Martin and Bjork, 1987; Everhart, 2004a; Einarsson et al., 2010; Konishi et al, 2011, 2014). However, there are few reports of mosasaur-on-mosasaur predation. Furthermore, evidence of trophic interactions between mosasaurs is relatively rare and mostly in the form of trauma inflicted by other mosasaurs (Everhart, 2008; Bastiaans et al., 2020; Tykoski and Polcyn, 2023).

Longrich et al. (2022) recently presented a number of mosasaurid specimens displaying varying degrees of erosion and decalcification of teeth and bones, which they interpreted as disgorged stomach content, hypothesizing these were in fact mosasaur gastric pellets, or regurgitaliths (see also Cooper et al., 2022). Furthermore, Longrich et al. (2022) argued the maker of the pellets was likely *Thalassotitan atrox,* a gigantic predatory mosasaurid nested among *Prognathodon* in their phylogenetic analysis. Additionally, Martin and Bjork (1987) interpreted large masses of commutated fish material, in one case containing ammonite "hash", and in another putative plesiosaur gastroliths, as possibly representing mosasaur coprolites, though qualifying their interpretations as "somewhat conjectural". In light of the interpretations of Longrich et al. (2022), the coprolites reported by Martin and Bjork (1987) may also represent regurgitaliths.

Direct evidence of mosasaur-on-mosasaur predation, in the form of *in-situ* gastric content, is exceedingly rare. Russell

*Corresponding author

(1967, p. 69) citing Anonymous (1962, p. 5), briefly mentioned "possible cannibalism reported from Canada where fragments of a small mosasaur were found mixed with the skeleton of a larger one", but that occurrence has not been described. There are two reports of predation of mosasaurs by the mosasaur genus *Tylosaurus* (Martin and Bjork, 1987; Bell and Barnes, 2007). The gut-content reported by Martin and Bjork (1987) contained a mix of taxa, including parts of the mosasaur *Latoplatecarpus* sp., fishes, and the sea bird *Hesperornis* sp., consumed by a *Tylosaurus proriger*. In a conference abstract, Bell and Barnes (2007) reported portions of the mosasaur *Plesioplatecarpus planifrons* and the durophagous shark *Ptychodus mortoni* in the gut region of a specimen of *Tylosaurus nepaeolicus*. Strganac et al. (2015a) briefly reported two occurrences of mosasaur stomach content, one in the gut region of a specimen of *Prognathodon kianda* (Fig. 1), and the other as an isolated multi-taxon mass of partially decalcified bones, interpreted as disgorged stomach content. Since that report, one of those specimens has been prepared for study and is the subject of this contribution.

The occurrences briefly reported by Strganac et al. (2015a) come from the Lower Maastrichtian (~71.5 Ma) locality of Bentiaba, Namibe Province, Angola, which was located at approximately 24°S paleolatitude (Jacobs et al., in press) at that time, placing it in a highly productive upwelling zone, analogous to that seen along the west coast of Africa between 15° and 30°S latitude today, an area known as one of the world's most productive fisheries. The sediments at the locality were deposited relatively nearshore on a narrow continental shelf, in waters approximately 50-100 meters deep, and a water temperature of ~18°C (Strganac et al., 2015b). All of these are contributing factors to the high concentration of vertebrate fossils found at the locality today, which has produced a large number of marine amniote specimens, including mosasaurs (Schulp et al., 2008; Schulp et al, 2013; Polcyn et al., 2010), plesiosaurs (Araújo et al., 2015a; 2015b; Marx et al., 2022), and marine turtles (Mateus et al, 2012). Many of the fossils collected at Bentiaba show evidence of scavenging in the form of tooth marks on various elements of mosasaur, plesiosaur, and turtle carcasses left by the teeth of the anacoracid shark *Squalicorax pristodontus* and to a lesser extent, *Cretalamna* sp. (Fig. 2; see also Strganac et al., 2015a).

We report here a remarkable example of well-preserved, in-situ mosasaur gut-content, containing three partial mosasaurs, each a unique taxon, one being the first documented instance of cannibalism in mosasaurs, and another representing a new genus and species closely related to *Mosasaurus*. We first provide a brief overview of the gut-content association, then address each of the prey taxa systematically, including the naming, describing, and diagnosing the new mosasaurine taxon, and close with a discussion of feeding and digestive biology of mosasaurs.

METHODS

Specimen preparation — The specimen MGUAN PA183 (and associated materials) was excavated with power and hand tools, and removed in seven plaster jackets and numerous hand samples. It was prepared at SMU with air-scribes and hand tools, and bones were treated with PVA. Once taken to the preparation stage shown in Fig. 1, the specimen was molded and cast in polyurethane resin. The resin casts were scanned with an Artec Leo (Artec Inc., Luxembourg) to generate 3d surface models, which were rendered in Lightwave 3D 2020 (Lightwave Digital, Stevenage, UK) to produce Fig. 1. Subsequent to mold making, the blocks were prepared further removing bones from matrix for study.

CT scanning — CT scanning was performed at the University of Texas high-resolution X-ray computed tomography facility in Austin, Texas, USA, producing 3 scan data sets used for study and to produce Figs. 6, 7, 9, and 12. The scans were processed in Amira 6.3 (ThermoFisher Scientific, Waltham, Massachusetts, USA).

Institutional Abbreviations — **MGUAN PA**, Projecto PaleoAngola collection in the Museum of Geology, Universidade Agostinho Neto, Luanda, Angola; **MHNM**, Museum of Natural History of Marrakech at Cadi Ayyad University, Morocco; **NDGS**, North Dakota Geological Survey, Bismarck, ND, USA; **SMU**, Southern Methodist University Shuler Museum of Paleontology, Dallas, TX, USA; **YPM**, Yale Peabody Museum, New Haven, CT, USA.

RESULTS

The specimen MGUAN PA183 is a semi-articulated skeleton of an adult *Prognathodon kianda* (Schulp et al., 2008), missing most of the tail due to recent erosion, and most of the ribs, limbs, and girdles due to ancient scavenging

(Fig. 1A). The vertebral column is nearly completely articulated, with four trunk vertebrae just posterior to the cervical series, and the articulated series of the last thirteen trunk vertebrae slightly displaced. Proximal portions of ribs are found on both sides of the vertebral column in the cervical and thoracic region but more posteriorly, they appear to have been completely removed by scavengers, except for a few small fragments. The skeleton of the predator is well preserved, but postdepositional cracking and displacement is common (Fig. 2A).

Teeth and bone surfaces of the predator (MGUAN PA183) are well preserved, showing no sign of erosion; however, some skull elements and ribs preserve signs of predation by sharks, including fine parallel grooves such as those made by the serrated teeth of *Squalicorax pristodontus* (Fig. 2B-D), as well as punctures and isolated grooves, likely inflicted by *Cretalamna* sp. (Fig. 2E-G) suggesting the missing elements including the ribs, girdles, and limbs were likely removed by large scavengers such as these. Numerous remains of bony fishes of different sizes, a single sawfish rostral tooth, and shed mosasaur teeth attributable to *Prognathodon kianda*, were collected on and around the carcass in the field and during laboratory preparation of the field jackets (cataloged as MGUAN PA183A 1-n), but show no evidence of acid etching or other indication of travel through the digestive tract and are interpreted as a time-averaged sample of additional scavengers and/or background attrition. The locality is extremely fossiliferous, and thus the recovery of fishes and mosasaur remains in the sediments underlying, overlying and surrounding the carcass are expected. There are only a small number of examples of fish remains that were found in close association with the bone layer, but again, none of these are acid etched or worn in such a way as to indicate they were ingested. More likely, they were attrition of the scavenging community that developed around this carcass.

The carcass of the predator (MGUAN PA183) is lying upside down, and based on the pattern of rib preservation, its visceral cavity was apparently opened and facing up, prior to burial. Remains of three other mosasaurs are lying primarily on the left side of the carcass, roughly parallel to the vertebral column (Fig. 1A and B), spanning trunk vertebra three through 15, an area approximately one meter long and half a meter wide, the details of which are shown in Fig. 1B. These remains are identified as gut-content based on the pattern of bone and tooth erosion, the physical arrangement of individuals and elements, and their relationship to the articulated predator's body, preserved in the region known to house the stomach in extant lizards (Srichairat et al., 2018). The preservation of the gut-content is generally good, and it appears digestion was halted relatively soon after the meal was taken, preserving large portions of the individual elements of the prey items. There is no evidence of shark scavenging on the prey items; however, it is possible that some prey items were lost due to scavenging, complete digestion, or non-fossilization.

Although some mixing has occurred, the prey items are largely segregated taxonomically in the sequence in which they were consumed (Fig. 1B). In the most posterior part of the stomach mass are portions of the skull and mandible of a *Gavialimimus* sp. (MGUAN PA 183B). There are also portions of the snout and the left squamosal of the mosasaurine that is largely preserved in the most anterior part of the gut (MGUAN PA183D), but those are situated and preserved in such a way that they were likely transported there once the visceral cavity of the consumer was breached. What are now recognized as gut-content, were largely covered in matrix at the time of the field excavation, and were not recognized as such. Consequently, the area containing the gut-content was taken as two blocks (Fig. 1B), and the anterior portion of the snout of a *Prognathodon kianda* (MGUAN PA 183C) was found while trenching, between the main concentrations of the two other taxa. Thus, there is not the same level of detail in mapping these elements as the remainder of the specimen (Fig. 1A, B). In the most anterior part of the stomach region is a partial skull, mandibles, and some postcrania of a small mosasaurine (MGUAN PA183D), which represents a new taxon, which is named, diagnosed, figured, and described in the present contribution.

SYSTEMATIC PALEONTOLOGY

Order SQUAMATA Oppel, 1811
Family MOSASAURIDAE Gervais, 1852
Subfamily PLIOPLATECARPINAE Dollo, 1884
Genus *GAVIALIMIMUS* Strong et al., 2020
GAVIALIMIMUS sp.

Referred specimen — MGUAN PA 183B (Fig. 3A, B)

Locality, Horizon, and Age — The specimen was collected

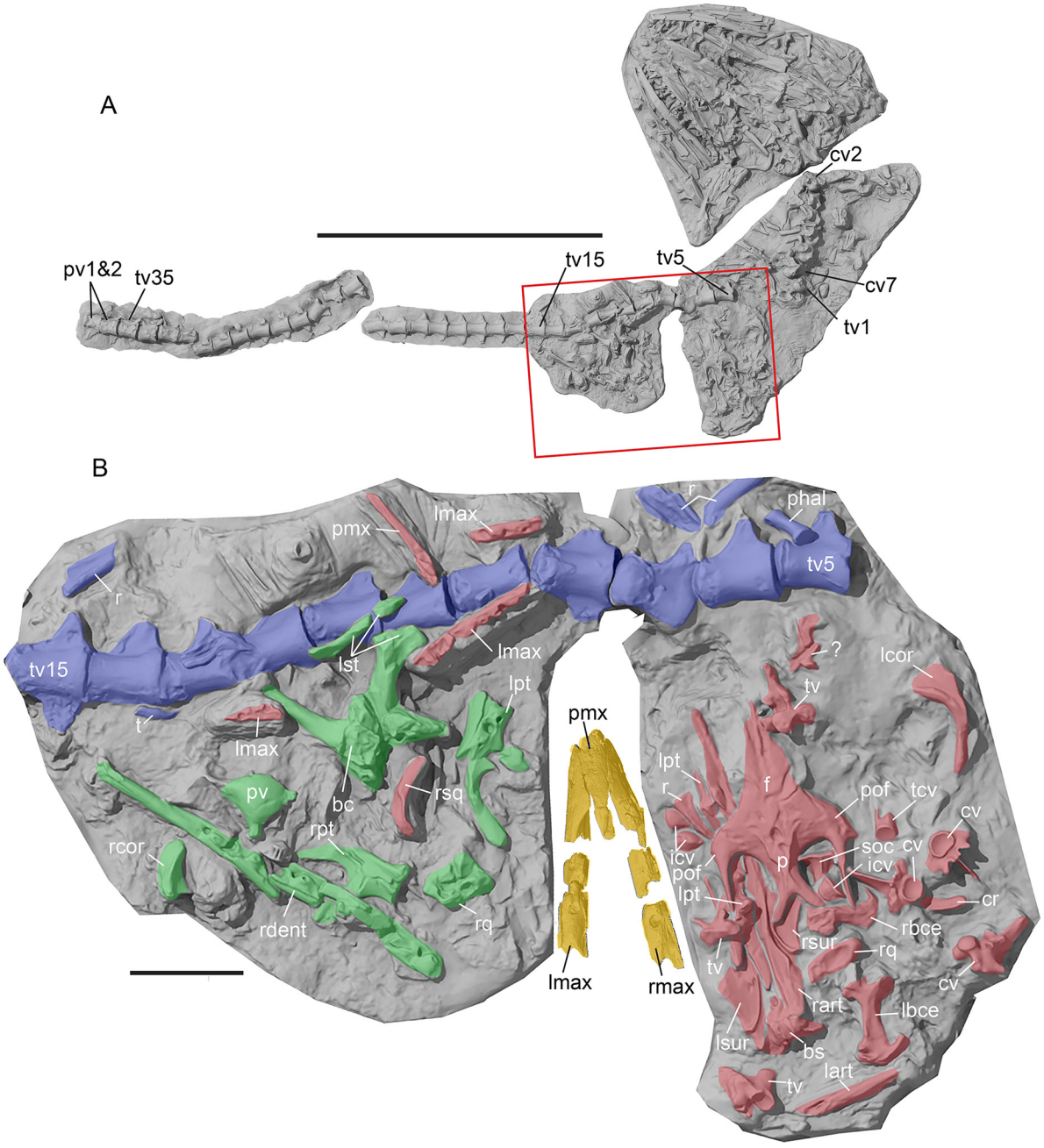

FIGURE 1. Overview of preservation orientation of predator and prey items. **A**, position of the primary field jackets of a semi-articulated skeleton *Prognathodon kianda* (MGUAN PA183) with rectangle denoting location of prey items; **B**, detail of stomach region with prey items. Bones colored blue are those of the predator *Prognathodon kianda* (MGUAN PA183). Prey items are *Gavialimimus* sp. (MGUAN PA183B) identified by green shading, *Prognathodon kianda* (MGUAN PA183C) in yellow, and *Bentiabasaurus jacobsi* gen. et sp. nov. (MGUAN P183D) in red. Note that disarticulated elements of MGUAN PA183C were removed in the field as hand samples while separating the two main blocks containing the gut-content, and therefore the position of the rearticulated elements as shown is conjectural. Additional elements of MGUAN PA183 (e.g., premaxilla, palatines, rib fragments, trunk vertebrae 2-4, 2 pygal vertebrae) were collected in the field as hand samples and smaller blocks and are not shown in this figure. **Abbreviations: cv**, cervical vertebra; **bc**, braincase; **bs**, basisphenoid; **f**, frontal; **icv**, indeterminate caudal vertebra; **lart**, left articular; **lbce**, left braincase elements; **lcor**, left coronoid; **lmax**, left maxilla; **lpt**, left pterygoid; **lst**, left supratemporal; **lsur**, left surangular; **p**, parietal; **pmx**, premaxilla; **phal**, phalanx; **pv**, pygal vertebra; **r**, rib; **rart**, right articular; **rbce**, right braincase elements; **rcor**, right coronoid; **rdent**, right dentary; **rmax**, right maxilla; **rpt**, right pterygoid; **rq**, right quadrate; **rsq**, right squamosal; **rsur**, right surangular; **soc**, supraoccipital; **t**, tooth; **tcv**, terminal caudal vertebra; **tv**, trunk vertebra. Scale bars equal 1 m for A and 10 cm for B.

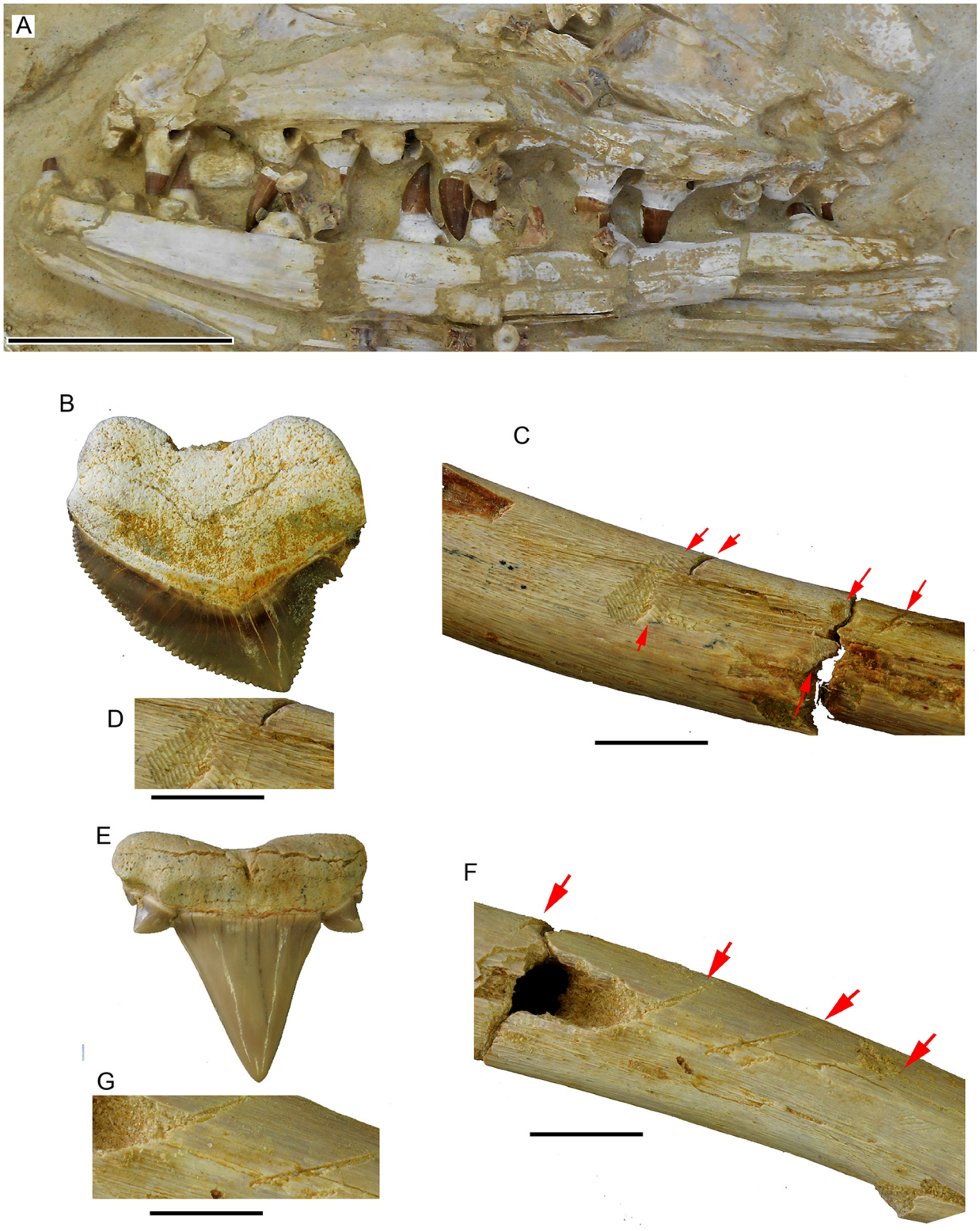

FIGURE 2. Typical preservation of the predator, *Prognathodon kianda* (MGUAN PA183) with examples of taphonomic modifications. **A**, detail of right maxilla and dentary showing preservation of bone and tooth surfaces; **B**, tooth of *Squalicorax pristodontus;* **C**, typical scavenging marks on rib section of predator by *Squalicorax pristodontus*; **D**, detail of same; **E**, tooth of *Cretalamna* sp.; **F**, typical scavenging marks on rib section of predator by *Cretalamna* sp.; **G**, detail of same. Arrows point to scavenger marks. Scale bar for A equals 10 cm, and for B-F scale bar equals 1 cm.

at Bentiaba, Angola, approximately one meter above "Bench 19" of Strganac et al. (2015a), falling within magnetochron 32n, a period of about 240 kyr, between 71.40 and 71.64 Ma (Strganac et al., 2014; 2015a).

DESCRIPTION

Preservation

The specimen MGUAN PA 183B, here identified as *Gavialimimus* sp., is the most posterior of the three concentrations of bone found in the stomach region of the predator. It preserves parts of the skull and right mandible, including the fragmentary right quadrate, dentary, squamosal, the articulated braincase, the left coronoid, both pterygoids, and a single anterior caudal vertebra. Once prepared to the point seen in Fig. 1, the orientation of all of the elements was captured with photography, silicone mold making and casting, and 3d scanning, and subsequently, the individual elements were removed and prepared for study. All of the elements referred to this taxon were found in close proximity to one another (Fig. 1B, highlighted in green). There are no repeating elements, and most of those preserved are positioned relative to one another approximately as they would have been in life, though there is anterior displacement of the quadrate and anterior and rightward displacement of the coronoid. Taking the orientation of the braincase as defining the midline, the right and left elements are largely preserved on their respective sides. We therefore interpret the skull elements and mandible parts are a single individual; however, the unexpected association of the anterior caudal (pygal) vertebra with the skull elements cannot rule out that it is a remnant of another meal, so our acceptance of it here as being part of this animal is tentative.

Skull

Braincase — The braincase is largely complete, but cracked and component elements displaced, and some postdepositional crushing is apparent. The occipital condyle makes up most of the vertebral articulation, with the otooccipitals contributing minimally. The basal tubera are more or less ventrally oriented in posterior view and tall and narrow in lateral view. Their posterior lateral surface is largely covered with the inferior process of the otoccipital. Their anterior faces are extensively overlapped by the posterior parts of the basisphenoid.

The basisphenoid is somewhat crushed and broken but complete. In ventral view, it is broad posteriorly where it articulates with and overlaps the basioccipital, and narrows substantially anteriorly. The basipterygoid processes are short and narrow and directed anterolaterally and trend anteroventrally. On the ventral surface, between the basipterygoid processes, is a groove and within it a low narrow ridge originates, continuing anteriorly along the centerline of the convex ventral surface of the parasphenoid rostrum. Above, the parasphenoid rostrum is concave, its edges converging anteriorly to form a point. Further posterior, the sella turcica is not well preserved and is damaged posteriorly, exposing an internal canal for the so-called basilar artery, behind which is the floor of the medullary cavity, suggesting it would have possessed a relatively short dorsum sellae. The exits for the carotid and cerebral carotid arteries are not discernable.

The otooccipitals, prootics, and supratemporals are in articulation but slightly cracked and displaced. The inferior process of the otoccipital forms a crista tuberalis posterolaterally, medial to which there is a recess for the foramina for nerves X, XI, and XII, similar to the condition in *Platecarpus* (Russell, 1967). Anteriorly the oval and round windows are obscured. The prootics are nearly complete, but again, broken and some fragments displaced. There is a large anterior notch for nerve V, overhung by a long anterodorsal process. Nerve VII appears to exit on the posterior part of the lateral face of the inferior process of the prootic, and runs anteroventrally in a shallow groove. The supraoccipital forms a relatively flat surface posteriorly and rises anteriorly, but preservation limits further description. Both the right and left supratemporals are present but broken, but the left is relatively complete. The anteroventral part of the supratemporal is deeply sandwiched between the paroccipital processes medially and the posterodorsal ramus of the prootic laterally. Proximally, in lateral view the supratemporal expands and is somewhat T-shaped. The dorsal part forms an anteriorly trending raised ridge.The ventral part is flat, forming a large posteroventral process, below which is part of the ventrally facing articulation for the quadrate. Though broken and displaced slightly (Fig. 1B), the anteromedial process of the supratemporal that articulates with the parietal is preserved. This process is rod-like, but distally, it thins and expands laterally, and would have inserted between the horizontally bifurcated distal parietal ramus (MJP personal observation). Additionally, raised edges lateral to the articulating surface limit angular motion at this joint, rendering it akinetic. This novel supratemporal-parietal articulation

appears to be unique to this taxon.

Squamosal — The posterior part of the right squamosal was recovered below the braincase during removal of the elements from the field jacket. It is somewhat hatchet-shaped with a short dorsal process and a broad, distally expanding ventral process that articulates with the quadrate. The dorsal slot-like articulation for the posterior ramus of the postorbitofrontal terminates anterior to the quadrate articulation.

Quadrate — The right quadrate is more complete than the one described by Strong et al. (2020), but the surface is somewhat decalcified, and it is missing the alar rim. The basal portion, including the mandibular condyle, is badly eroded. The suprastapedial process is long, about two-thirds the total height of the quadrate. The dorsal part of the suprastapedial process has nearly parallel sides, and it broadens distally reaching its maximum breadth where it meets the so-called infrastapedial process. The stapedial pit is broadly oval and inclined posterodorsally, and lies between the narrow dorsal medial ridge anterodorsally, and partly overlying the auditory meatus (stapedial notch of Strong et al., 2020). There is a marked posterodorsal inflection of the narrow medial ridge at the level of the stapedial pit. A deep sulcus originates just below the stapedial pit, trending posteroventrally while broadening, and terminating at the level of the juncture of the suprastapedial and infrastapdial processes. The comparable aspects of the quadrate are nearly identical to those of Strong et al. (2020, their figure 8).

Pterygoids — The main body of the pterygoid is flat and broad and the tooth row lies slightly medially, and does not extend posteriorly beyond the posterior margin of the ectopterygoid process. The ectopterygoid process is obscured by the dentary above, but has a broad base and extends laterally. In ventral view, there is an incomplete ectopterygoid, displaced slightly from its extensive sutural articulation with the ectopterygoid process. Posteromedially, a thin, slightly oval, rod-like basisphenoid process leaves the main body of the pterygoid and a more robust quadrate ramus posterolaterally. Neither are complete distally. Both pterygoids appear to have been truncated anteriorly, each preserving only three tooth positions. Other pterygoid specimens of this taxon from the locality are also incomplete anteriorly, but demonstrate a minimum of 5 tooth positions (MGUAN PA 551).

Dentary — The posterior dentary bears a long edentulous portion about five tooth positions long, and the dentigerous part preserves space for 10 tooth positions, but there are portions where the alveolus is completely eroded. It is not clear if it is complete anteriorly. Teeth are completely eroded to their bases and there are no preserved replacement teeth. The most posterior eroded tooth bases are elongate, suggesting laterally compressed dentition whereas the more anterior ones are more nearly oval to circular. Resorption pits are present posteromedial to eroded tooth bases. There are clear accommodation pits (interdental pits of Strong et al., 2020) anterolateral to the third from last and the fifth from last tooth positions. The medial parapet is taller than the lateral wall of the dentary.

Coronoid — Only the anterior part of the coronoid is preserved. There is no anterior bifurcation in dorsal view. In lateral view, the dorsal margin rises quickly, suggesting a tall, short coronoid such as that seen in *Selmasaurus johnsoni* (Polcyn and Everhart, 2008). The ventral articulation with the surangular is only slightly concave.

Taxonomic remarks — Based on comparison with the holotype material (MHNM.KHG.1231), the specimen (MGUAN PA183B) can be confidently referred to the genus *Gavialimimus* (Strong et al., 2020) on the basis of the long edentulous posterior portion of the dentary, presence of accommodation pits anterolateral to tooth positions, the tall medial parapet, the positionally controlled geometry of teeth, and tentatively, the reconstructed tooth count. This referral is also supported by characters of the quadrate, including the distally expanded suprastapedial process.

Subfamily MOSASAURINAE Gervais, 1852
Tribe GLOBIDENSINI Bell, 1997
PROGNATHODON KIANDA Schulp et al. 2008

Referred specimen — MGUAN PA 183C (Fig. 3C-J, see also Strganac et al., 2015).

Locality, Horizon, and Age — As for MGUAN PA183B above.

DESCRIPTION

Preservation

The preserved portion of the skull is represented by the anterior part of the premaxilla and portions of both maxillae. The external surfaces are badly decalcified, removing the anterior end of premaxilla, much of the cortical bone of all elements, and the tooth crowns. Conversely, the internal

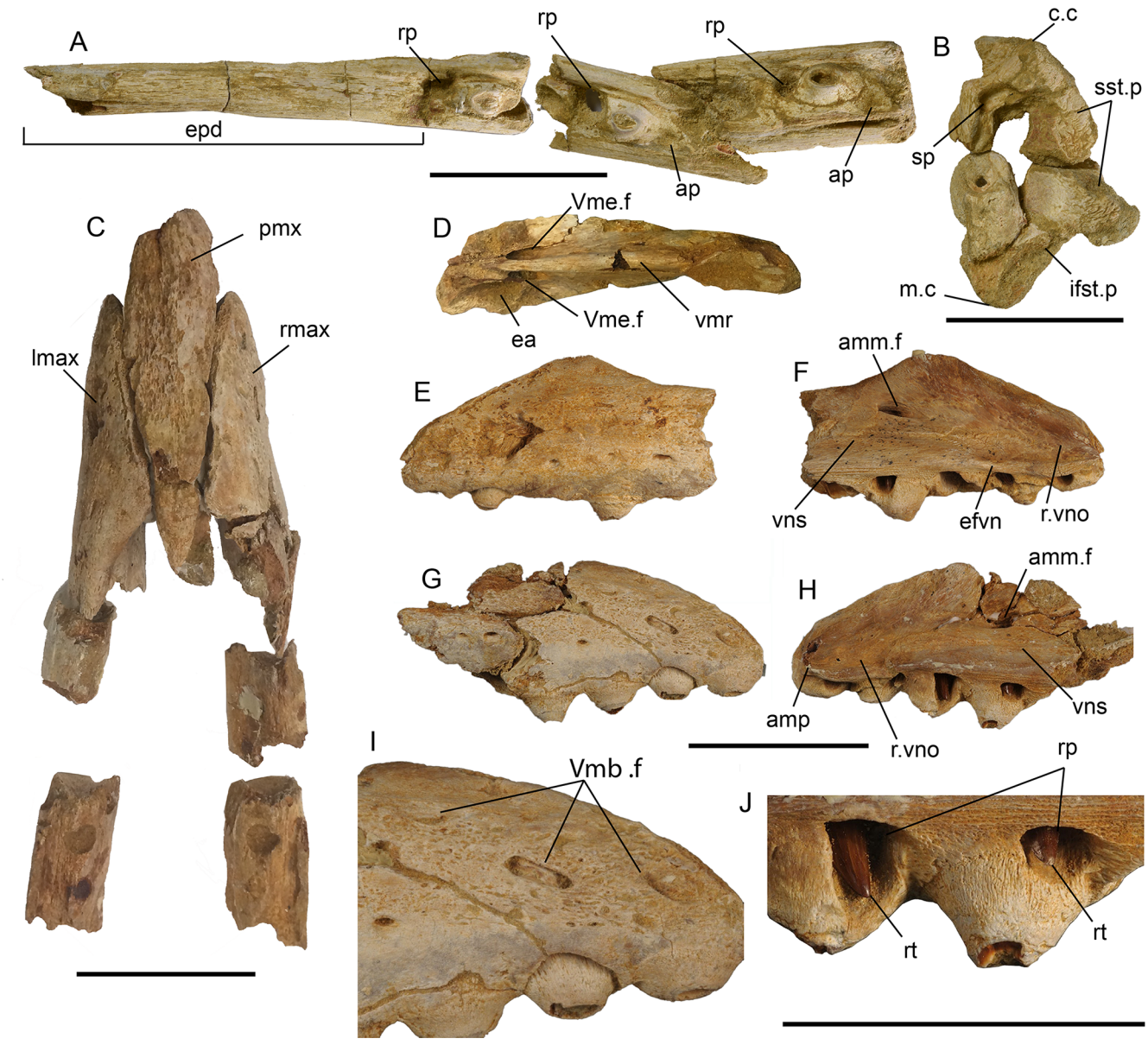

FIGURE 3. Preservation of prey items *Gavialimimus* sp. (MGUAN PA 183B) and *Prognathodon kianda* (MGUAN PA183C). **A**, *Gavialimimus* sp. (MGUAN PA183B) posterior right dentary in dorsal view; **B**, right quadrate of the same in medial view; **C**, *Prognathodon kianda* (MGUANPA183C), rearticulated snout fragments in dorsal view; **D**, premaxilla of same in ventral view; **E**, anterior left maxilla fragment of same in lateral and **F**, medial views; right maxilla fragment of same in **G**, lateral and **H**, medial views; **I**, details of anterior part of right maxilla fragment in lateral view; **J**, detail of posterior part of right maxilla fragment in medial view. **Abbreviations: amm.f**, anteromedial maxillary foramen; **amp**, anteromedial process; **ap**, accommodation pit; **c.c**, cephalic condyle; **efvn**, emargination for the fenestra vomeronasalis; **epd**, edentulous posterior dentary; **lmax,** left maxilla; **ifst.p**, infrastapedial process; **m.c**, manibular condyle; **pmx**, premaxilla; **rmax**, right maxilla; **rp**, resorption pit; **rt**, replacement tooth; **r.vno**, recess for vomeronasal organ; **sp**, stapedial pit; **sst.p**, suprastapedial process; **Vmb.f**, foramen for maxillary branch of trigeminal nerve; **Vme.f**, foramen for medial ethmoidal branch of trigeminal nerve; **vns**, vomeronasal sulcus. Scale bars equal 5 cm.

surfaces, including the maxillary premaxillary articulation surfaces, are well preserved and show no damage, suggesting the anterior snout was still intact during digestion.

Skull

Premaxilla — The premaxilla is badly decalcified anteriorly, missing the rostrum and the anterior tooth positions, but

retaining portions of the resorption pits for those (Fig. 3). The posterior alveoli are empty, their anterior walls trending anteroventrally, and their lateral walls breached by erosion (Fig. 3C, D). The posterior teeth were apparently in late stage replacement as the teeth were not ankylosed within the alveoli and there is no sign of resorption pits. Medially, between the posterior tooth positions, is the remnant of an elevated incisive process, bearing a central groove lateral to which are parasagittal ridges. The parasagittal ridges of the process trend posteriorly, terminating just at the anterior rim of the foramen for the medial ethmoidal nerve. The ventral medial ridge begins between the parasagittal ridges, just medial to the center of the posterior tooth positions and just below the level of the incisive process. The foramina for the medial ethmoidal nerve are far anterior, just posteromedial to the posterior tooth positions, in the posterior wall of the dentigerous portion of the premaxilla. The foramina are separated by a relatively low ventral medial ridge, posterior to which the ridge protrudes from the apex of a somewhat triangular cross section of the posterior process. On either side of the posterior process are well preserved maxillary articulation surfaces showing fine ridges and textures associated with soft tissues. The posterior process protrudes about 2 cm into the internarial space but is eroded and missing posterior to this. In dorsal view, the cortical bone is mostly gone, exposing trabecular bone, except for some small patches on the anterior right side (Fig. 3C).

Maxillae — Each maxilla, though fragmentary and badly eroded, preserves ten tooth positions. The anterior part of both maxillae is well-preserved medially, but their external surfaces are badly eroded. Anteriorly, at the ventral part of the medial parapet, the anteromedial process is preserved on the left maxilla. Posterior to that, there is an emargination for the fenestra vomeronasalis, running posteriorly to a point one-third of the third tooth position. Dorsal to this emargination is a recess for the vomeronasal organ, and at a point dorsal to the posterior terminus of the emargination, a sulcus we term the "vomeronasal sulcus", which originates on the posterior border of the recess for the vomeronasal organ, and runs posteriorly, trending slightly laterally. Dorsal to the posterior half of the recess for the vomeronasal organ is another small sulcus we take to receive the lateral part of the septomaxilla or associated soft tissue. The maximum height of the maxilla is dorsal to a point between the third and fourth tooth positions, posterior to which lies a well-defined narial emargination. Above the fourth tooth position, near the narial emargination, is the anteromedial maxillary foramen, homologous with the dorsal maxillary foramen of Bahl (1937). As with the premaxilla, the external surfaces of the maxillae are badly eroded (Fig. 3E, G), and significant portions of the cortical bone are missing. Interestingly, the area just above the teeth and just anterior to the external nares, preserves the cortical bone, possibly indicative of thicker and/or more resistant soft tissue in those areas. The lateral central part of both maxillae is eroded, exposing trabecular bone. The foramina for the maxillary branch of trigeminal nerve are eroded and opened to reveal the underlying canals (Fig. 3I). The erupted and ankylosed marginal teeth are all eroded, but replacement teeth are perfectly preserved within the resorption pits. Judging from the eroded tooth bases, the anterior tooth cross sections are nearly circular and more posterior teeth increasingly laterally compressed.

Taxonomic remarks — The specimen is confidently referred to *Prognathodon kianda* by comparison with other individuals in the MGUAN PA collection (e.g., MGUAN PA 129 [holotype], PA 25, PA 183, PA 271). These specimens were all collected within a limited geographic area and at essentially the same stratigraphic level (Strganac et al., 2015a) and no other *Prognathodon* species have been recovered at the locality. The far anterior position of the ethmoidal foramina, the position and nature of the external nares, the dorsal shape of the premaxilla, the nature of the tooth implantation and replacement pattern, are all identical to the comparative specimens. Nonetheless, the individual described here (MGUAN PA 183C) is smaller than the holotype and referred specimens of *P. kianda*, and some ontogenetic differences are apparent. For instance, the slope of the anterior maxillary premaxillary suture is relatively low compared to larger individuals of *P. kianda*. We quantify this by measuring the relative height of the anterior snout (distance on lateral side from its tallest anterior point to the ventral margin) compared to the distance between the centers of the bases of the first four teeth (Fig. 4). The larger individuals all range between ~0.9 and ~1.0, whereas PA 183C is ~0.7. An individual of intermediate size between PA 183C and PA 183, is ~0.8. There is a general trend toward a relatively taller, higher sloped suture through the ontogeny of *P. kianda*, but with a downward shift in the ratio for the largest individual (PA 271) at ~0.9. However, that individual has 12 tooth positions, versus 13 in the rest of the sample of

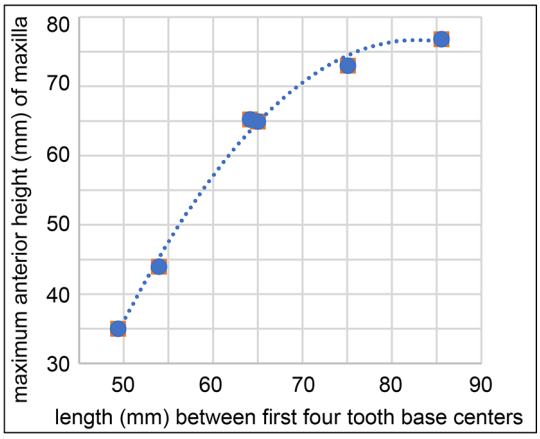

specimen	length	height	ratio	tooth count
PA183C	49.47	35.00	0.71	?
PA25	53.93	43.95	0.81	13
PA13	64.97	64.92	1.00	13
PA183	64.11	65.22	1.02	13
PA129	75.05	73.00	0.97	13
PA271	85.53	76.83	0.90	12

FIGURE 4. Ontogenetic maxillary growth. All measurements in millimeters. Curve fit is second order polynomial.

complete maxillae, and thus changes in tooth spacing may in part account for this difference in the ratio. In any event, when plotted (Fig. 4), these data can be interpreted as allometric growth, with height increasing faster than length, and the relative increase in height slowing as the individual ages. Another example of ontogenetic change, taken from the specimen described here, can be seen in the ventral medial ridge. While the ridge is low and robust in PA 183C, in the larger specimens that preserve it (PA 183, PA 129), it is increasingly thinner and their height correlates with the relative height increase of the snout in older (larger) individuals. A third but related example, is the increased distance between the level of the ethmoidal foramina entrances and the level of the incisive process, as the premaxilla grows taller. Though preliminary, these observations demonstrate the potential of the Projecto PaleoAngola collection for the understanding of ontogenetic change in at least *Prognathodon kianda*, which will be addressed elsewhere. Notwithstanding the ontogenetic differences noted above, we consider MGAUN PA 183C a relatively young individual of *Prognathodon kianda*, and thus the first report of cannibalism in mosasaurs.

Tribe PLOTOSAURINI Bell 1997

BENTIABASAURUS JACOBSI gen. et sp. nov.

(Figs. 1,5,6,7,8,9,10,11,12, and 13)

Syntypes — MGUAN PA 183D, recovered from the most anterior part of the gut-content, and thus the predators last meal, includes a partial skull, partial mandibles, four cervical vertebrae, two cervical ribs, six trunk vertebrae, and five caudal vertebrae; MGUAN PA554, partial mandibles and quadrates.

Referred specimens — MGUAN PA 282, MGUAN PA 283, and MGUN PA 284, all partial right quadrates.

Locality and horizon — All of the specimens except MGUAN PA 554 were collected within the first two meters above "Bench 19" of Strganac et al. (2015). The exception, MGUAN PA 554, was collected approximately 10-12 meters above "Bench 19", but included in the interval which is constrained to magnetochron 32n, a period of about 240 kyr, between 71.40 and 71.64 Ma (Strganac et al., 2014; 2015a).

Etymology — The genus name is a combination of Bentiaba, for the locality that produced the specimens, and to honor the people of Bentiaba, Angola, and the Greek "*saurus*" for lizard. The species epithet is in honor of Louis L. Jacobs for his many contributions to African vertebrate paleontology. He is the consummate vertebrate paleontologist, explorer, ambassador, teacher, mentor, and friend.

Diagnosis — A gracile mosasaurine of the tribe plotosaurini possessing the following unique combination of characters: premaxilla with foramen for medial ethmoidal nerve enters posterior process between the second and third maxillary tooth position, minimum of 15 maxillary teeth (14 present and one additional posterior tooth estimated), a distinct ventromedial facing groove on the medial side of maxilla parapet, frontal subtriangular and narrow with concave lateral margins, frontal posterior parasagittal tabs closely embrace a relatively large pineal foramen, anterior parietal table elongate and triangular with posterior margins that diverge sharply, postorbitofrontal-parietal suture angular and z-shaped, prootic with cranial nerve VII exit on lateral surface of inferior process, quadrate laterally narrow, blunt poster-oventral ascending rim, well developed alar groove, distinct vertical groove on anteromedial quadrate face at mid-height, pterygoid tooth row on straight elevated process, dentary with 15 or 16 tooth positions (13 present and room for two

or three additional estimated), surangular with high coronoid buttress, retroarticular projects posteriorly without ventral or medial deflection, coronoid with posterior notch in medial flange, medial flange only slightly deeper than lateral flange and does not contact angular, marginal dentition symmetrically bicarinate, laterally compressed, with smooth enamel surface, zygosphenes-zygantra present through at least thoracic vertebrae, and fused hemal arches on caudal vertebrae.

Taxonomic comments — *Bentiabasaurus jacobsi* gen. et sp. nov. can be differentiated from all other mosasaurs by the unique combination of characters noted in the diagnosis. It can be confidently referred to mosasaurinae by possession of a narrow, straight and elevated pterygoid tooth row, coronoid concave above with greatly expanded posterior wing, rapidly rising high thin surangular-coronoid buttress, anterior vertebral condyles nearly circular and essentially equidimensional, and fused caudal hemal arches. Though it retains some relatively plesiomorphic mosasaurine characters (e.g., smooth, symmetrically bicarinate and laterally compressed teeth; narrow triangular frontal; and well-developed zygosphenes and zygantra in trunk vertebrae), it can be referred to the tribe Plotosaurini (*sensu* Bell, 1997) by possession of a prominent medial maxillary groove, large parasagittal frontal tabs embracing pineal foramen, and a quadrate with deep alar groove and accessory medial ridge. The mosaic of plesiomorphic and derived characters present in *Bentiabasaurus jacobsi* gen. et sp. nov. separate it from other known Plotosaurini.

Furthermore, the position of the exit for cranial nerve VII in *Bentiabasaurus jacobsi* gen. et sp. nov. is unique among Plotosaurini with a single exception, a specimen referred to *Mosasaurus dekayi* (Bronn, 1838) by Russell (1967 p. 138). That specimen (YPM 1582), preserves a tooth, the posterior part of the parietal, and a fragmentary left prootic, which bears a similar position of the exit for cranial nerve VII. However, in that specimen, the preserved tooth, though "more or less" symmetrically bicarinate, is significantly more robust and highly faceted, and the margins of parietal surface slightly converge at their posterior termination. These two latter characters are unlike the morphology of *Bentiabasaurus jacobsi* gen. et sp. nov. (MGUAN PA 183D) and thus any relationship with *M. dekayi* is rejected.

Two of the characters noted above, the prominent medial maxillary groove and the accessory medial ridge of the quadrate, have not been previously used to diagnose Plotosaurini. Both characters are present in the holotype and referred specimens of *Mosasaurus hoffmanni,* referred specimens of *Mosasaurus* cf. *M. conodon* (e.g., SMU 76348, SMU 76836), and verified in CT data of the holotype of *Plotosaurus bennisoni* (DigiMorph.org). The medial maxillary groove has not been verified in the holotype of *Mosasaurus missouriensis*, but that specimen does possess the accessory medial ridge of the quadrate, although it is slightly damaged. It is present in referred specimens of that taxon (Konishi et al., 2014; their figure 5). Neither character is present in *Clidastes* or *Prognathodon* and related forms (MJP personal observations), and thus appear to be useful to diagnose Plotosaurini.

Recently, Zietlow et al. (2023) described *Jormungandr walhallaensis* (NDGS 10838) from the middle Campanian of North Dakota, which also possesses a mosaic of plesiomorphic and derived mosasaurine characters, including some it shares with later diverging plotosaurins, including the medial maxillary groove, and the deep alar groove of quadrate, but is unlike that of *Bentiabasaurus jacobsi* gen. et sp. nov. in that its quadrate does not possess any posterior projection of the infrastapedial process, nor does it possess an accessory medial ridge, but uniquely possesses a deep posteroventral medial sulcus (Zietlow et al., 2023, their figure 24).

DESCRIPTION

Specimens and preservation

Bentiabasaurus jacobsi gen. et sp. nov. is described primarily from MGAUN PA 183D, with supplementary description of the quadrate, dentary, coronoid, and marginal dentition from MGUAN PA 554. Additional data is also derived from quadrate specimens MGUAN PA 282, MGUAN PA 283, and MGUAN PA 284. The largest concentration of MGUAN PA 183D is in the anterior part of the gut of a specimen of *Prognathodon kianda* (MGUAN PA 183), and probably represents the last meal of the predator. The left squamosal, premaxilla and maxillae fragments are displaced posteriorly in the region of MGUAN PA 183B (hindgut) with the premaxilla and maxillary fragments lying upon and adjacent to the vertebrae of the predator (Fig. 1B). The frontal, parietal, and postorbitofrontals are in articulation, the braincase and quadrates disarticulated but in close proximity, and the left pterygoid and partial mandibles, lying below the bone mass. Mixed with this concentration are both trunk and caudal vertebrae, and the cervical vertebrae and additional trunk and caudal vertebrae were recovered in close proximity.

The partial quadrates and mandibles of MGUAN PA 554 were recovered about two hundred meters from MGUAN PA 183 and about ten meters higher in the section. The specimen suffered severe weathering at the surface, with significant bone loss and breakage, but is included here as the primary source of data on the dentaries and marginal dentition. The partial quadrates (MGUAN PA 282, MGUAN PA 283, and MGUAN PA 284) were isolated finds at the weathered surface and all within the first two meters above Bench 19.

Skull

Premaxilla — The nearly complete premaxilla is present (Fig. 5A-F). Its dorsal and dentigerous sections are partially digested, but the post-dentigerous ventral part is well preserved, suggesting it may have been protected from stomach acids by soft tissue or was in articulation with the maxillae for some time after ingestion. In dorsal view (Fig. 5A), most of the cortical bone is missing. The dentigerous part is eroded to the point that the bases of the anterior alveoli are exposed. The lateral margins of the posterior process are nearly parallel, gradually diverging slightly posteriorly. Nothing can be said of the suture with the maxilla due to decalcification. In ventral view, the anterior and posterior tooth bases and resorption pits can be seen, and tooth bases suggest they supported laterally compressed crowns. The vomer processes are prominent and there is a deep groove between them that extends anteriorly, its margins converging. The medial ethmoidal nerve enters on the ventral posterior process at approximately the second or third maxillary tooth position. A narrow, prominent ventral medial ridge originates at or near the posterior base of the dentigerous portion, extending posteriorly and deepening slightly.

Maxilla — The left maxilla is present, but broken into three pieces (Fig. 5G-K, Q). There is a small fragment of the anterior part of the right maxilla (Fig. 5L-P). Judging by comparison with complete and better-preserved specimens of *Mosasaurus* and related forms, nearly the entire length of the left maxilla is present, missing only a small posterior portion. There are 14 tooth positions, and room for at least one more in the missing posterior section. There is a prominent groove or gutter on the medial side of the parapet, which runs from about the fifth to about the 11^{th} or 12^{th} tooth position becoming shallower and less distinct at the anterior terminus of the palatine articulation on the posterior fragment (Fig. 4G). The palatine articulation is a thin blade-like process that projects dorsomedially high on the posterior parapet, rising at about the 12^{th} or 13^{th} tooth position. All eroded tooth bases in the maxilla suggest the crowns were laterally compressed. There are two replacement teeth preserved in the anterior maxillae fragments. They are laterally compressed and possess smooth enamel surfaces with no fluting or facets, and their tips are digested.

Frontal — The frontal is heavily decalcified dorsally, but preserves the overall shape and is mostly complete, except for the very anterior part (Fig. 6). It is subtriangular and narrow, measuring ~113 mm midline length and ~84 mm between the posterolateral alae (L:W=1.35). The lateral margins are slightly concave, arcuate posteriorly. Anteriorly, the margins appear to step in medially, then converge slightly. Though eroded, there is a remnant of an anterior median ridge preserved. The posterior parasagittal tabs of the frontal are large and triangular, together are 34.6 mm wide, occupying about 41% the posterior width between the posterolateral alae. They closely embrace a relatively large pineal foramen medially, and only a narrow band of bone on the parietal that surrounds the pineal foramen, is exposed between them. The broadly triangular posterolateral alae trend more lateral than posterior. Posteriorly, the posterior margin of the posterolateral ala and the lateral margin of the parasagittal tab, meet at an angle of about 110^{o}. Ventrally, most of the frontal is obscured by overlying bone (Fig. 7), exposing only the anterior part. The surface preservation is good and shows no sign of erosion. The olfactory canal is relatively broad anteriorly, bounded by descending processes that are parallel anteriorly and converge posteriorly. The ventral rim of the posterior part of the descending process thins to a crest, and then expands slightly and bears a sulcus, interpreted here as the solium supraseptale. Anteriorly the descending processes are broad and rounded over, and they also slope down to meet the ventral surface of the frontal anteriorly, and bear longitudinal striations. There is no evidence of an anterior ventral medial ridge within the olfactory canal.

Parietal — The parietal is complete, but the dorsal surface partially digested. A pit to the right of and posterolateral to the pineal foramen is field damage that occurred during excavation. The posterolateral rami, and portions below the parietal table and within the supratemporal fenestrae are well preserved with no erosion, and were likely protected from stomach acids by muscle and connective tissue. Anteriorly, a large, slightly elongate pineal foramen is closely embraced by

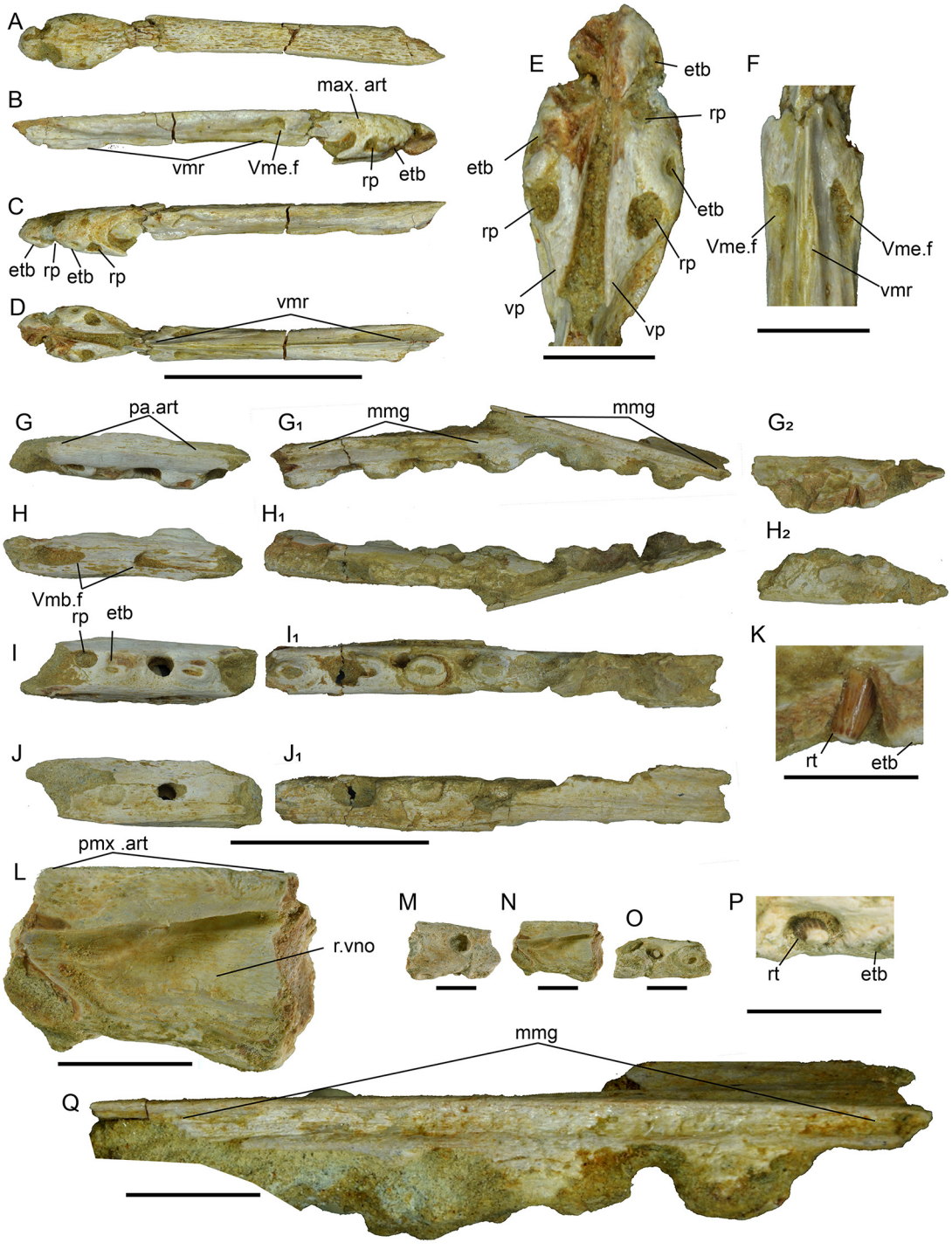

FIGURE 5. Snout elements of *Bentiabasaurus jacobsi* gen. et sp. nov. (MGUAN P183D). **A**, premaxilla in dorsal, **B**, right lateral, **C**, left lateral, and **D**, ventral views; **E**, ventral detailed view of dentigerous part of premaxilla; **F**, ventral detailed view of post-dentigerous part of premaxilla; **G**, left maxilla in medial, **H**, lateral, **I**, ventral, and **J**, dorsal views; **K**, detail of replacement tooth in G_2; **L**, anterior fragment of right maxilla in medial view; **M**, same in dorsal, **N**, medial and **O**, ventral views. **P**, detail of replacement tooth in O; **Q**, detail of anterior part of G_1 showing prominent medial groove. **Abbreviations: etb**, eroded tooth base; **max.art**, maxillary articulation; **mmg**, medial maxillary groove; **pa.art**, palatine articulation; **pmx.art**, premaxillary articulation; **rp**, replacement tooth; **r.vno**, recess for vomeronasal organ; **Vmb.f**, foramen for maxillary branch of trigeminal nerve; **Vme.f**, foramen for medial ethmoidal branch of trigeminal nerve; **Vme.f**, foramen for medial ethmoidal branch of trigeminal nerve; **Vmr**, ventral median ridge; **Vp**, vomer process. Scale bars equal 5 cm for A-D, and G-J. Scale bars for all others equals 1 cm.

FIGURE 6. Main skull block of *Bentiabasaurus jacobsi* gen. et sp. nov. (MGUAN P183D) from above. **A**, skull roof, palatal elements, partial mandibles, braincase elements, and quadrate from above; **B**, same, rendered isosurface model derived from threshold-segmented of CT scan data. **Abbreviations: ct.f**, foramen for the chorda tympani; **f**, frontal; **lart**, left articular; **lsur**, left surangular; **p**, parietal; **pof**, postorbitofrontal; **rart**, right articular; **rbce**, right braincase elements; **rcor**, right coronoid; **rpt**, right pterygoid; **rq**, right quadrate; **rsur**, right surangular; **soc**, supraoccipital; **tcv**, terminal caudal vertebra; **tv**, trunk vertebra. Scale equals 10 cm.

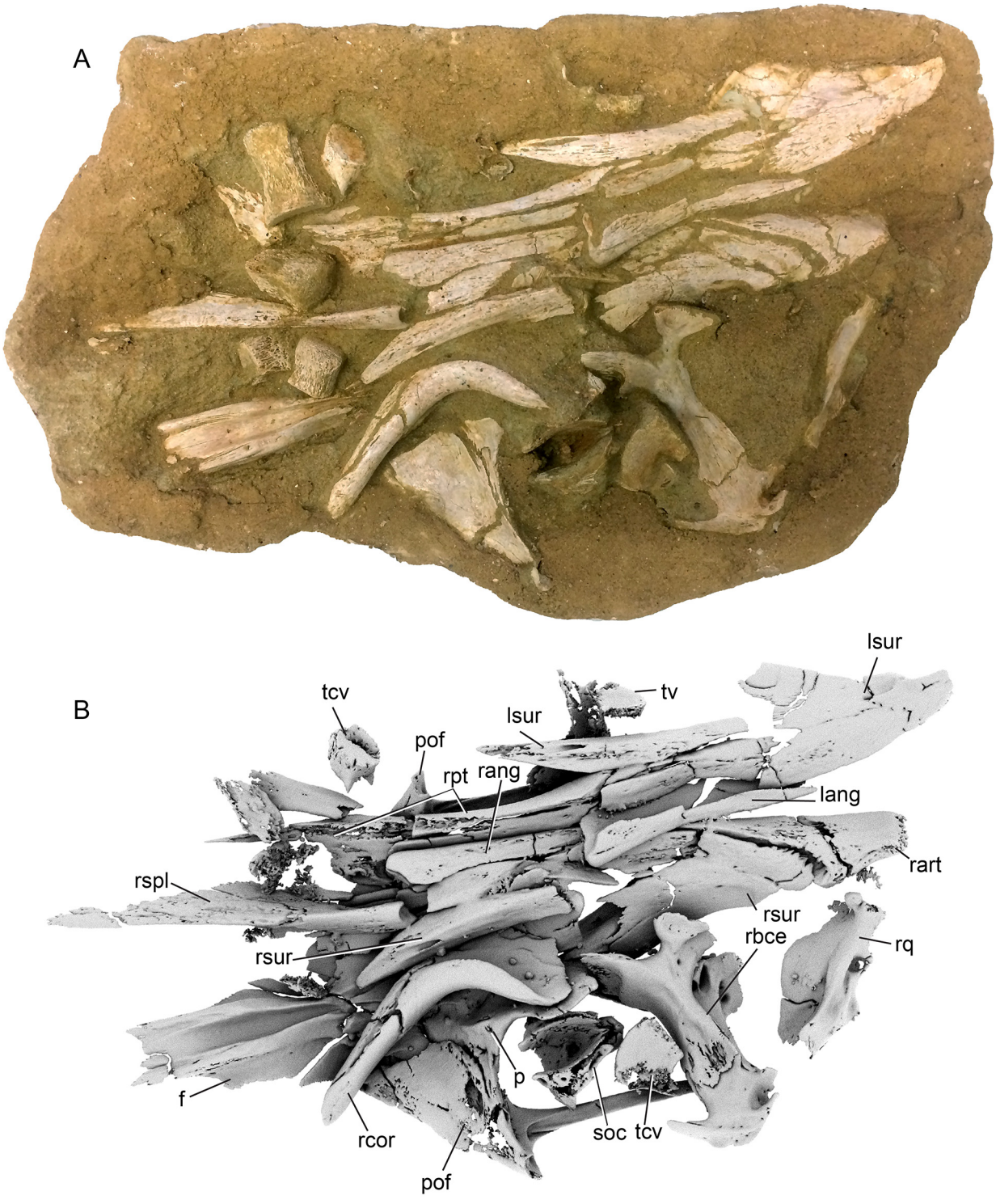

FIGURE 7. Main skull block of *Bentiabasaurus jacobsi* gen. et sp. nov. (MGUAN P183D) from below. **A**, skull roof, palatal elements, partial mandibles, braincase elements, and quadrate from below; **B**, same, rendered isosurface model derived from threshold-segmented of CT scan data. **Abbreviations:** as in Figure 5. Scale equals 10 cm.

parasagittal posterior tabs from frontal. The foramen is completely within the parietal. Laterally, the parietal meets the postorbitofrontal in an angular, z-shaped suture, inset medially from the posterolateral alae. The parietal is ~61 mm long measured along the midline from the anterior margin of the pineal foramen. In dorsal view, the anterior lateral margins of the triangular parietal table are nearly straight, converging posteriorly, and reaching their narrowest point at the anterior terminus of the posteromedial fossa, or about 71% posterior midline length of the parietal (measuring ~43 mm from anterior pineal foramen to narrowest point). The lateral margins then diverge posteriorly, bounding the posteromedial fossa, and blend into the dorsal surface of the posterolateral rami. The posteromedial fossa is shallow and featureless. On the posterior face, just behind the posteromedial fossa are two parasagittal depressions nearly meeting one another medially, separated by a narrow ridge. The posterolateral rami are relatively short, and horizontally bifurcated distally, to receive the parietal process of the supratemporal. The descending processes are deep and well developed.

Postorbitofrontals — The postorbitofrontals are in articulation with the frontal and parietal. They are well preserved, but there is some dorsal erosion or possible field damage on the dorsal surface of the right one. They broadly underlay the frontal, but significantly less-so, the parietal (Fig. 7). In dorsal view, the element is only visible anterolaterally a short distance before disappearing under the frontal. Examination of the articulation surfaces of the postorbitofrontals and frontal in CT data, indicates the (missing) prefrontal would have contacted the postorbitofrontal, excluding the frontal from the supraorbital margin. Posteromedially, the postorbital meets the parietal in an angular, z-shaped suture, and is inset medially, and thus borders the posterolateral frontal alae posteriorly. The jugal process projects posterolaterally and ventrally, and bears a weak ridge along its anterolateral margin, diminishing anteriorly on the dorsal facing surface of the postorbitofrontal. The distal part of the jugal process is convex anteriorly in cross-section, nearly u-shaped, and slightly curved anteriorly near its distal terminus in lateral view. It is concave posteriorly to receive the dorsal jugal. Ventrally, a strong ridge runs from just medial to the jugal articulation, trending medially, and terminating in an interfingered articulation with the parietal. Posteriorly, the postorbitofrontal gives rise to the blade-like squamosal process. It is thin and dorsoventrally narrow. It appears the squamosal would have articulated with this process far anterior, the sutural contact trending anteroventrally in lateral view.

Squamosal — The right squamosal is preserved and relatively complete, missing a portion of its dorsal process and it is broken and incomplete anteriorly (Fig. 8G-J). The top of the anterolateral wall (lateral ridge of Street and Caldwell, 2016), is relatively straight anteriorly, and at a point parallel to the anterior terminus of the supratemporal articulation on the medial side, forms a crest that slopes posteroventrally, terminating in a sharp point at the convergence of the dorsal, medial, and ventral surfaces. The medial wall is slightly lower than the lateral wall and posteriorly forms the ventral margin of the supratemporal articulation. The articulation for the supratemporal is roughly triangular, its apex directed posteroventrally. In dorsal view, the squamosal bears a deep groove to receive the supratemporal. The quadrate articular facet is well defined and narrow, about one-third the posterior ventral width of the element, and lacks any anteroventral elongation. In dorsal view, the groove to receive the postorbitofrontal is open posteriorly.

Quadrate — The left quadrate of MGUAN PA 183D is complete (Fig. 8A-F) and the right damaged dorsally, missing most of suprastapedial process (Fig. 6A, B). The specimen MGUAN PA 554 (Fig. 10D-J) preserves both quadrates, but they are missing their distal ends, the distal suprastapedial processes, and the alar rims are somewhat weathered, but a segment of the alar groove survives on the left quadrate. Three isolated partial right quadrates were also recovered, MGUAN PA 282 and MGUAN PA 283, missing their distal ends, and MGUAN PA 284, missing the dorsal portion and alar rim.

In lateral view, the suprastapedial extends ventrally to almost mid-height, and nearly touches the quadrate shaft, creating a small auditory meatus, but some of this may be due to taphonomy. The alar cavity (conch) is relatively shallow. The alar groove is deep, and the laterally facing part of the alar rim forms a somewhat wider band of bone posterior to the groove, widening anterodorsally. The posteroventral ascending rim is poorly developed, but steep and blunt. Just medial to the posteroventral ascending rim and just below the suprastapedial process is a well-developed infrastapedial process. Ventrally, the condylar bone is well

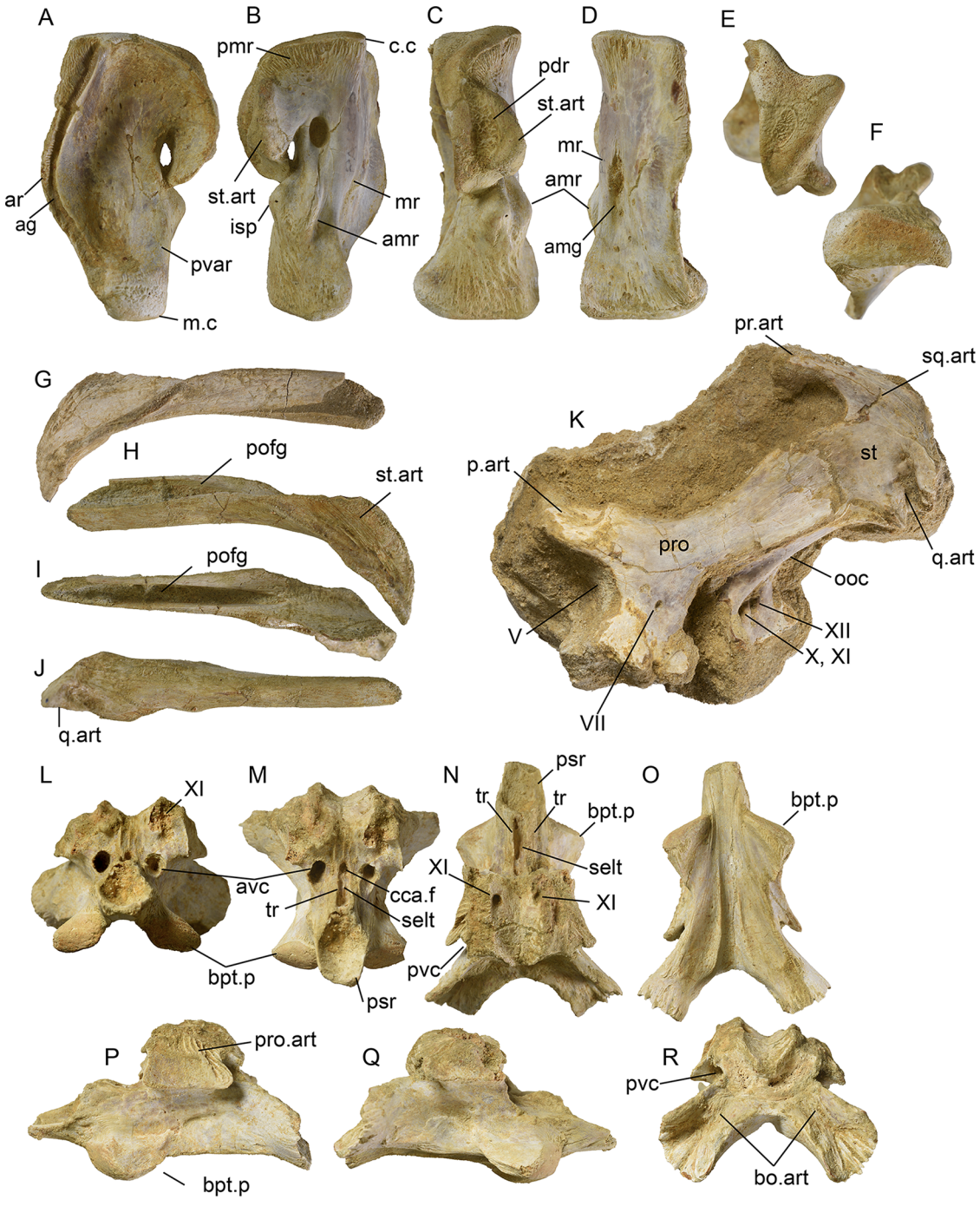

FIGURE 8. Quadrate, suspensorium, and braincase of *Bentiabasaurus jacobsi* gen. et sp. nov. (MGUAN P183D). **A**, left quadrate in lateral view; **B**, same in medial, **C**, posterior, **D**, anterior, **E**, dorsal, and **F**, ventral views; **G**, right squamosal in lateral view; **H**, same in medial, **I**, dorsal, and **J**, ventral views; **K**, articulated left braincase elements in lateral view; **L**, basisphenoid in anterior view; **M**, same in anterodorsal, **N**, dorsal, **O**, ventral, **P**, left lateral, **Q**, right lateral, and **R**, posterior views. **Abbreviations: amg**, anteromedial groove; **amr**, accessory medial ridge; **ar**, alar rim; **avc**, anterior vidian canal; **bpt.p**, pbasipterygoid process; **bo.art**, basioccipital articulation; **cca.f**, foramen for the cerebral carotid artery; **isp**, infraspedial process; **c.c**, cephalic condyle; **m.c**, mandibular condyle; **mr**, medial ridge; **ooc**, otoccipital; **pdr**, posterodorsal rugosity; **pmr**, postermedial rugosity; **pro**, prootic; **pro.art**, prootic articulation; **pvc**, posterior vidian canal; **p.art**, parietal articulation; **pr.art**, parietal ramus articulation; **psr**, parasphenoid rostrum; **pvar**, posteroventral ascending rim; **q.art**, quadrate articulation; **selt**, sella turcica; **st**, supratemporal; **tr**, trabecula; **V**, trigeminal nerve; **VI**, abducens nerve; **VII**, facial nerve; **X**, vagus nerve; **XI**, accessory nerve; **XII**, hypoglossal nerve. Scale bar equals 5 cm.

exposed below the alar cavity, covering the ventrolateral surface.

In medial view the suprastapedial process bears a tall narrow medial boss that inserts in the quadrate articulation of the supratemporal. Anterodorsal to this boss is a depressed area, bearing slight rugosities and well-defined striae dorsally. This area lies adjacent to and largely covers the supratemporal, but does not contact it, suggesting extensive soft tissue between them in life. Ventral to this is the stapedial pit, which is broadly oval, and taller than wide. Just below the stapedial pit, a small ridge rises, extending gradually posteroventrally to a point about one-third the quadrate height terminating just below the level of the infrastapedial process and near the posterior margin of the quadrate shaft. We term this structure the accessory medial ridge. The juncture of the medial surface and the anterior surface forms the medial ridge. This ridge terminates at the cephalic condyle dorsally, below which it becomes increasingly blunt and rounded-over to about mid quadrate height, below which it narrows, its ventral part forming a thin anteromedially directed flange just above the mandibular condyle. Cortical bone covers the ventromedial face of the quadrate shaft to nearly its ventral margin where the cartilage-covered bone of the condyle is minimally exposed.

In posterior view, the suprastapedial process bears an elongate rugose area that separates the supratemporal articulation from the lateral part of the process. The infrastapedial process is visible just below the suprastapedial process, below which the posteroventral face of the quadrate shaft is rugose and weakly striated. The quadrate shaft broadens significantly ventrolaterally and to a lesser degree ventromedially, and the ventral margin formed by the mandibular condyle is flat. Little condylar bone is exposed in posterior view.

In anterior view, the quadrate is tall and laterally narrow, expanding ventrally as described above. On the anterior face is a narrow vertical groove, inset slightly from the medial ridge, its well-defined dorsal terminus slightly above mid-height, and its ventral part forming the apex of a triangular shaped field of bone bounded by the anteriorly expanded alar rim and the medial and ventral margins. We term this "the anteromedial groove".

Braincase

The braincase elements are reasonably well-preserved and only the basioccipital is missing (Figs. 8K-R, 9A-J). The otooccipitals, prootics, and supratemporals are preserved in articulation on both the right and left side, but disarticulated from the basicranial elements and the supraoccipital. The right braincase elements and supraoccipital were left in the block containing the skull roof and partial mandibles (Figs. 6, 7). The left braincase elements and basisphenoid were removed and prepared and scanned separately (Figs. 8, 9).

Prootic — In lateral view (Fig. 9A), the prootic is triradiate, with an anterodorsal process articulating with the supraoccipital and parietal, an inferior process articulating with the basisphenoid and otooccipital, and a posterodorsal process articulating with both the supraoccipital above and the otoccipital medially. The relatively short anterodorsal process bears a deep facet that receives the anteroventral part of the descending process of the parietal, the anterodorsal part of the descending process articulating with the supraoccipital. A large trigeminal notch separates the anterodorsal process from the inferior process. Posterior to the trigeminal notch, the exit for cranial nerve VII is nearly centered on the lateral face of the inferior process, at the dorsal terminus of a sulcus. The ridge forming the anterior margin of the sulcus is homologous with the so-called otosphenoidal crest. The posterodorsal process overlays the otoccipital's posterodorsal process, exposing only the posteroventral part of that element.

Anteromedially, the articulation for the supraoccipital is bipartite, the dorsal portion bearing vertical interdigitating sutures and the ventral part smooth (Fig. 9D). Within the latter, the anterior semicircular canal and the anterior half of the utriculus are visible (Fig. 9E). Slightly anteroventral to the utriculus are the entrances for cranial nerves VII and VIII within a shallow recess. Ventromedially, the inferior process or the prootic articulates with the basisphenoid, bearing vertical interdigitating sutures.

Otoccipital — In lateral view, a portion of the posteroventral part of the otoccipital is visible beneath the prootic ventral margin, its posterodorsal part mostly covered by the supratemporal (Fig. 9A, B). Viewed from behind and left (Fig. 9B, C), an array of external openings is visible. At the anteroventral terminus of a shallow stapedial groove, the round fenestra vestibuli is formed with nearly equal contribution of the prootic. Slightly posterior, the vertically elongate oval fenestra rotunda is separated from the fenestra vestibuli by a narrow crista interfenestralis. On the middle part of the anterior wall of the fenestra rotunda is a foramen for cranial nerve IX. Posteriorly, is a long slit-like foramen which

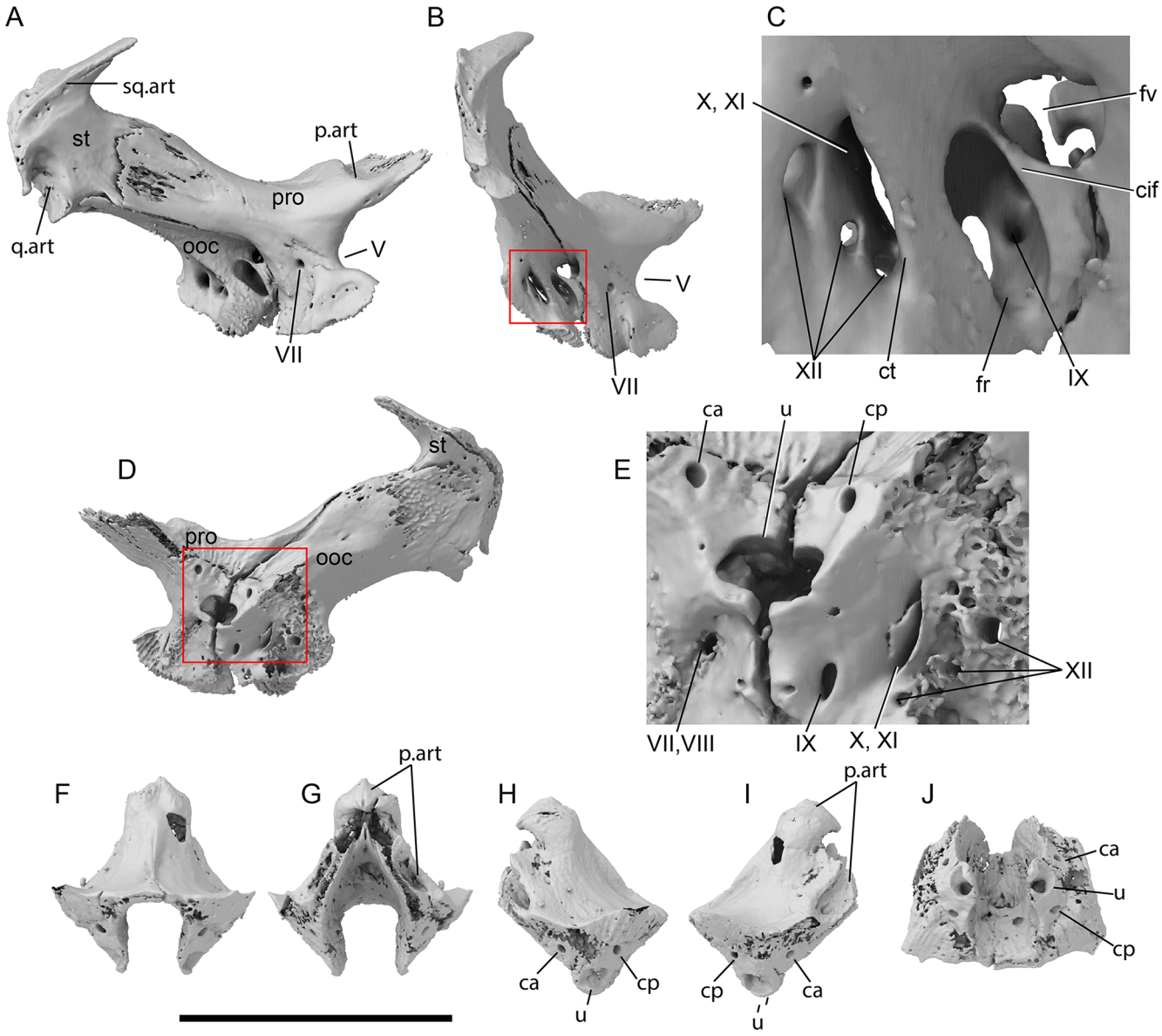

FIGURE 9. Braincase elements of *Bentiabasaurus jacobsi* gen. et sp. nov. (MGUAN PA 183D). **Abbreviations: ca**, anterior vertical semicircular canal; **cif**, crista interfenestralis; **cp**, posterior vertical semicircular canal; **ct**, crista tuberalis; **fr**, fenestra rotunda; **fv**, fenestra vestibuli; **j.f**, jugular foramen; **sq.art**, squamosal articulation; parietal articulation; **q.art**, quadrate articulation; **u**,utriculus; **V**, trigeminal nerve; **VII**, facial nerve; **VIII**, acoustic nerve; **IX**, glossopharyngeal nerve; **X**, vagus nerve; accessory nerve; **XII**, hypoglossal nerve. Scale equals 5 cm.

carried cranial nerves X and XI. This foramen is also thought to have carried the "posterior cerebral branch of the internal jugular vein, and the occipital branch of the internal carotid artery to the lateral surface of the braincase." (Russell, 1967, p. 38). In the posteroventral part of this foramen are two smaller foramina, and a third posterodorsal to those, which carry cranial nerve XII. Posteroventral to these foramina is a small condylar surface (Fig. 8K).

Anteromedially, the otoccipital articulation with the supraoccipital is similar to that described for the prootic, but contributes only about a quarter of the articulating surface area with that element (Fig. 9D, E). The smooth ventral portion preserves the posterior semicircular canal and posterior half of the utriculus. Posteroventrally, the foramen for cranial nerve IX is visible. Posterior to that, is a slit-like foramen carrying cranial verves X and XI, and posterior to

that, the three foramina for cranial nerve XII are present on the broken surface. Posteromedially, the medial surface of the posterodorsal process expands distally, and covers much of the supratemporal (Fig. 9D). The ventral margin curves distally, buttressing the medial part of the quadrate articulation with the supratemporal.

Supratemporal — In lateral view, the supratemporal can be divided into three regions; the articulation for the squamosal dorsally, the articulation for the quadrate medial suprastapedial process ventrally, and between those a large featureless subrectangular area that would have been medial to the dorsal part of the main body of the quadrate in life (Fig. 9A). The squamosal articulation is roughly triangular, a narrow ridge beginning near its posterior apex and trending anterodorsally. This ridge sits within a conjugate groove on the medial surface of the squamosal. The articulation for the quadrate is deep and receives a process on the posteromedial suprastapedial process, separated from the suprastapedial part of the alar rim, by a vertically elongate posterodorsal rugosity. The tight articulation of the supratemporal around this process, rendered the quadrate immobile rostrocaudally, but may have allowed lateral translation of the mandibular joint. In dorsal view, the supratemporal expands anteriorly, articulating with the squamosal posteriorly and the parietal anteriorly.

Basisphenoid — The basisphenoid is relatively complete and well preserved (Fig. 8L-R) with minor only breakage in the anterodorsolateral right part, exposing the path of cranial nerve VI dorsally. Anteriorly the parasphenoid rostrum is a relatively short, shallow u-shaped structure, but may be incomplete anteriorly. The posterior part of the u-shaped rostrum terminates on a posterior wall, with medially sloping lateral margins and a relatively straight dorsal margin, which is the anterior terminus of the sella turcica. The sides of the sella turcica are bound by low thin walls, the trabeculae, which run parallel posteriorly and terminate at the posterior wall, below the dorsum sellae. Slightly above the level of the floor of the sella turcica, on the posterior wall, is a single foramen for the cerebral carotid, which in turn gives rise to the basilar artery. The cerebral carotid branches medially from the internal carotid within the vidian canal. The posterior wall of the sella turcica is vertical and tall, the dorsum sellae slightly concave. The floor of the medullary cavity is nearly perpendicular to the posterior wall of the sella turcica. Lateral to the sella turcica are the anterior openings of the vidian canals anterior to which a shallow sulcus runs anteriorly, lateral to the trabeculae. The posterior opening of the vidian canal is relatively far posterior, but anterior to the basioccipital articulation, hidden below the posteroventral part of the prootic articulation in lateral view (Fig. 8P), but visible in posterior view (Fig. 8R). Dorsal to the anterior opening of the vidian canal is the exit for cranial nerve VI. The entrance for cranial nerve VI is on the lateral margin of the floor of the medullary cavity, one quarter its length posteriorly. The articulation for the basioccipital occupies most of the posterior surface, with long posterolateral processes which would have wrapped around the anterior basal tubers. Anteroventrally, the short subtriangular basipterygoid process, bears an anteroventrally and a slightly laterally directed articular surface (Fig. 8M-Q). In ventral view, there is a ventral median groove whose posterolateral margins are more defined and diverge posteriorly.

Supraoccipital — The supraoccipital is complete (Fig. 9F-J). In posterior view, the supraoccipital is trapezoidal, its sides converging dorsally. Its posterior margin is relatively straight, its medial part forming the top of the foramen magnum. A thin median ridge rises from near the dorsal border of the foramen magnum and trends anterodorsally, and diminishes dorsally. Anterodorsally, the supraoccipital articulated with the parietal in a poorly defined knuckle. Anterolaterally, there are prominent sulci to receive the posterior descending processes of the parietal (Fig. 9G, I). The ventral part forms conjugate articulation with the otoccipital and the prootic, and corresponding openings of the semicircular canals and utriculus.

Pterygoid — The right pterygoid is present but largely obscured, broken, and partially digested. Some tooth bases are visible anteriorly and just anterior to the incomplete ectopterygoid process, set on a high thin ridge, but an accurate count cannot be made. Anteriorly, there is a long thin process visible posterior to which the element widens substantially, together forming the articulation with the palatine. The base of the laterally directed ectopterygoid process anterior margin curves anteromedially, meeting the main body of the pterygoid. The tooth row is taphonomically folded over, almost touching the ectopterygoid process. Posteriorly, in line with the tooth row, there is a broad, transversely concave, quadrate ramus. The basisphenoid process is broken and displaced slightly.

Mandible

The right posterior mandible of MGUAN PA 183D is nearly complete and largely articulated, but the anterodorsal part is broken and slightly displaced along with the coronoid (Figs. 6, 7). The right splenial is closely associated and appears to be in articulation with the prearticular though broken and twisted (Fig. 7B). The left posterior mandible preserves the surangular and angular in close proximity to one another, but the articular is displaced from the bone mass and fragmentary. The left coronoid was also displaced, but well preserved (Fig. 1B). No dentaries are preserved with MGUAN PA 183. Partial dentaries and marginal dentition are preserved in MGUAN PA 554 (Fig. 10). The preserved parts of the quadrates, coronoid, and splenial of this specimen are nearly identical to those in MGUAN PA 183D, and thus confidently identified as *Bentiabasaurus jacobsi* gen. et sp. nov. and used here to describe the dentaries and marginal dentition.

Dentary — The dentaries are badly weathered, fragmentary, and their anterior parts missing (Fig. 10A-C, M, Q, S). There are 11 tooth positions preserved in right dentary and 13 in left, but along with additional isolated and fragmentary alveoli and tooth root parts, the tooth count was at least 15 and possibly higher. The medial parapet is as high as the lateral wall, though it is taphonomically displaced dorsally in the left dentary. In lateral view, the base of attachment is elevated, and in dorsal view, resorption pits are relatively small and visible posteromedial to tooth positions. The posterodorsal edentulous region is about one and a half tooth positions long. The broken tooth bases, the teeth in place, and the isolated teeth are all more or less symmetrically bicarinate, laterally compressed, and slightly recurved posteriorly and medially, and have smooth enamel surfaces (Figs. 10, 11). The teeth vary somewhat in recurvature along the tooth row. The carinae bear no serrations.

Splenial — The right splenial is nearly complete in MGUAN PA 183D, but the anterior part is broken and rotated out of position (Figs. 7B, 12A-D). A fragmentary right splenial is preserved in MGUAN PA 554 (Fig. 10K, L). In dorsal view, the body of the splenial gives rise to a short lateral and a taller medial dorsal lamina that would have received the prearticular between them posteriorly. There are two small foramina in the posterior floor, anterior to which the internal opening of the large anterior mylohyoid foramen is visible piercing the medial wall. In lateral view the posterior border is gently arcuate, the dorsal part extending slightly more posterior than the ventral (Fig. 12B). The dorsal and ventral margins are nearly parallel posteriorly, and the dorsal margin quickly slopes anteriorly beginning at the level of the anterior mylohyoid foramen, and is narrow anteriorly. In medial view, the posterior margin is embayed at about mid-height (Figs. 10K, 12D), the dorsal and ventral parts extending posterior about equally. The medial lamina rises near the posterior margin, sloping gradually antero-dorsally reaching its apex at about one-third the preserved length of the splenial. The emargination for the anterior inferior alveolar foramen is visible on the dorsal margin between the anterior margin of the anterior mylohyoid foramen and the apex. Anterior to the apex, the dorsal margin slopes gradually anteroventrally, the anterior two-thirds of the preserved splenial forming a roughly triangular shape. In posterior view the central part of the splenial is shallowly recessed, the dorsomedial part more recessed and meeting the dorsal surface of the splenial (Fig. 12C).

Angular — The right and left angulars are preserved in MGUAN PA 183D, the right still in articulation with the surangular and articular (Figs. 7, 12E-J). It is relatively narrow in anterior view, the anterior medial flange extending more anterior than the lateral, and forming a shallow dorsal triangular depression between them. In medial view, the posterior margin is only slightly posterodorsally oriented and slightly concave (Fig. 12H). In lateral view, the posterior margin rises at a shallow angle posterodorsally, then turns posterior at the suture with the surangular, narrowing slightly posteriorly (Fig. 12F, I). The posterior mylohyoid foramen is obscured, but can be seen in cutaway views (Figs. G-G_2) relatively low on the medial side. The posterior part is not visible.

Surangular-Articular — The right surangular and articular are broken, but largely in articulation in MGUAN PA 183D (Figs. 6, 7). In lateral view, the anterior part of the surangular is narrow, its ventral margin sloping posteroventrally at a shallow angle to meet the angular at a point below the middle of the coronoid facet. The anterior surangular foramen lies relatively far posteriorly, dorsal to a point near the anterior terminus of the angular. The coronoid articulation is long and buttressed posteriorly by the anterodorsal sloping dorsal margin of the surangular that rapidly rises just anterior to the glenoid. The glenoid is formed about equally by the articular and surangular and bears a prominent anteromedial foramen.

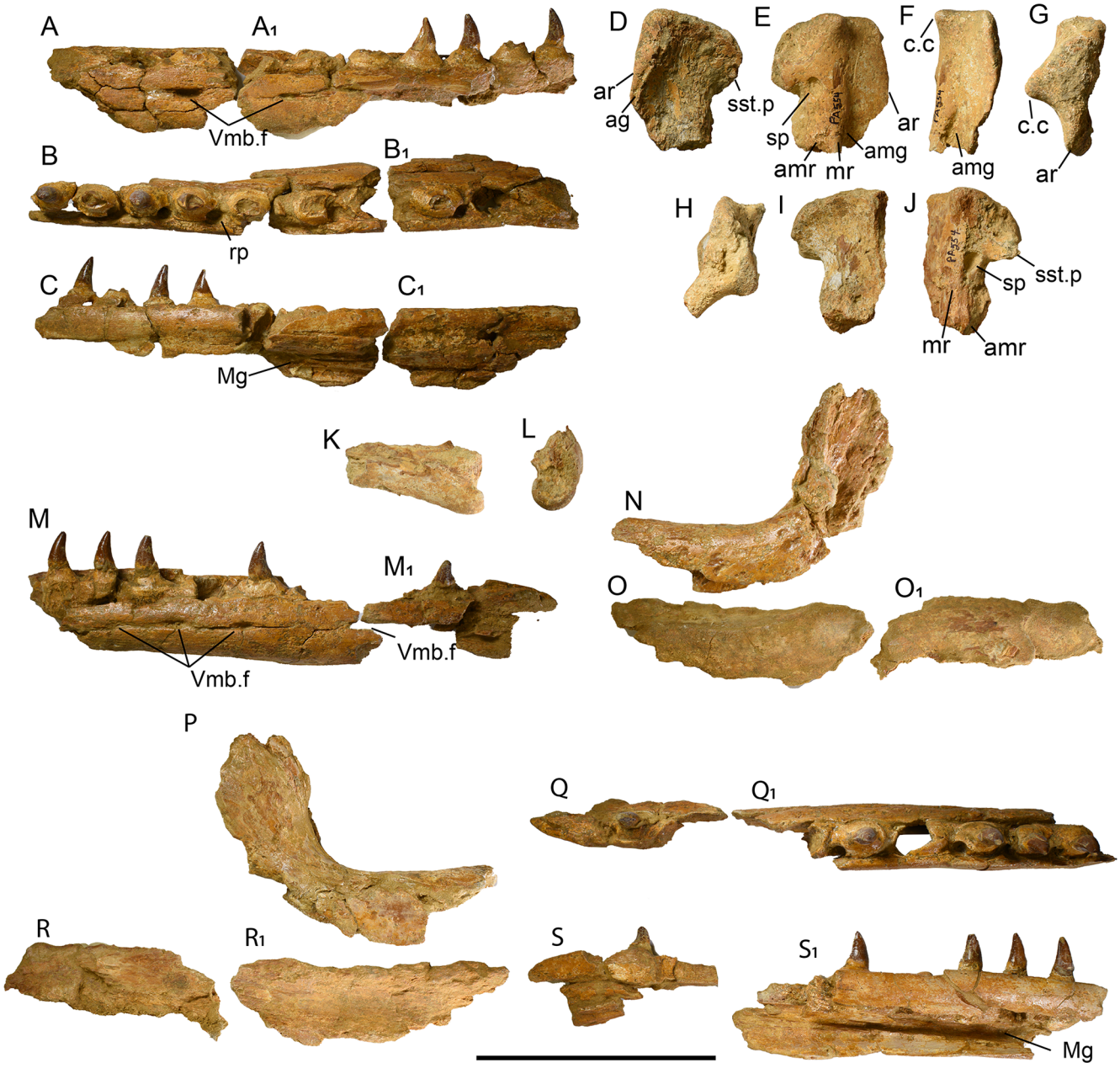

FIGURE 10. *Bentiabasaurus jacobsi* gen. et sp. nov. (MGUAN PA 554) partial mandibles and quadrates. **A**, posterior partial right dentary in lateral, **B**, dorsal, and **C**, medial views; **D**, left quadrate in lateral, **E**, medial, **F**, anterior, and **G**, dorsal view; **H**, right quadrate in dorsal, **I**, lateral, and **J**, medial views; **K**, posterior fragment of right splenial in medial, and **L**, posterior views; **M**, posterior partial left dentary in lateral, **Q**, dorsal, and **S**, medial views. **N**, left coronoid in lateral, and **P**, medial views. **O**, fragmentary left surangular in lateral and **R**, medial views. **Abbreviations: ar**, alar rim; **ag**, alar groove; **amg**, anteromedial groove; **amr**, accessory medial ridge; **c.c**, cephalic condyle; **lc**, left coronoid; **ldent**, left dentary **lq**, left quadrate; **lsur**, left surangular; **Mg**, Meckelian groove; **mr**, medial ridge; **rp**, resorption pit; **rs**, right splenial; **rt**, replacement tooth; **rq**, right quadrate; **sp**, stapedial pit; **sst.p**, suprastapedial process; **Vmb.f**, foramen for mandibular branch of trigeminal nerve. Scale bars equals 5 cm.

In lateral view, the surangular-articular suture begins at the posterior glenoid, then slopes posteroventrally a short distance, then turns and slopes gently anteroventrally. The retroarticular is broadly trapezoidal and projects posteriorly without significant medial deflection. In medial view, near the center of the retroarticular, is a single small foramen for the chorda

FIGURE 11. *Bentiabasaurus jacobsi* gen. et sp. nov. (MGUAN PA 554) marginal dentition. **A**, anterior portion of preserved posterior right dentary in dorsal view; **B**, fragment of left dentary in dorsal view; **C**, anterior portion of preserved posterior left dentary in dorsal view. **D**, disarticulated, associated marginal tooth in medial, **E**, lateral, **F**, posterior, **G**, anterior, and occlusal **H**, views; a second disarticulated, associated marginal tooth crown in medial, **E**, lateral, **F**, anterior, **G**, posterior, and occlusal **H**, views; **I**, left dentary fragment in posterolateral view. **Abbreviations: rp**, resorption pit; **rt**, replacement tooth. Scale bars equal 5 cm.

tympani. The surangular-articular suture begins at the antero-medial part of the glenoid, and slopes gently anteroventrally and then horizontally more anteriorly, medial to which is a large mandibular fossa.

Coronoid — Both coronoids are present with MGUAN PA 183D (Fig. 7) and the left is preserved with MGUAN PA 554 (Fig. 10N, P). In lateral view, the lateral face of the coronoid is arcuate, the horizontal ramus longer than the vertical, the two rami diverging at about 115°. The anterior end of the lateral face is pointed, the dorsal and ventral margins diverging gently posteriorly, then turning postero-dorsally and narrowing again, converging and meeting posterodorsally in a

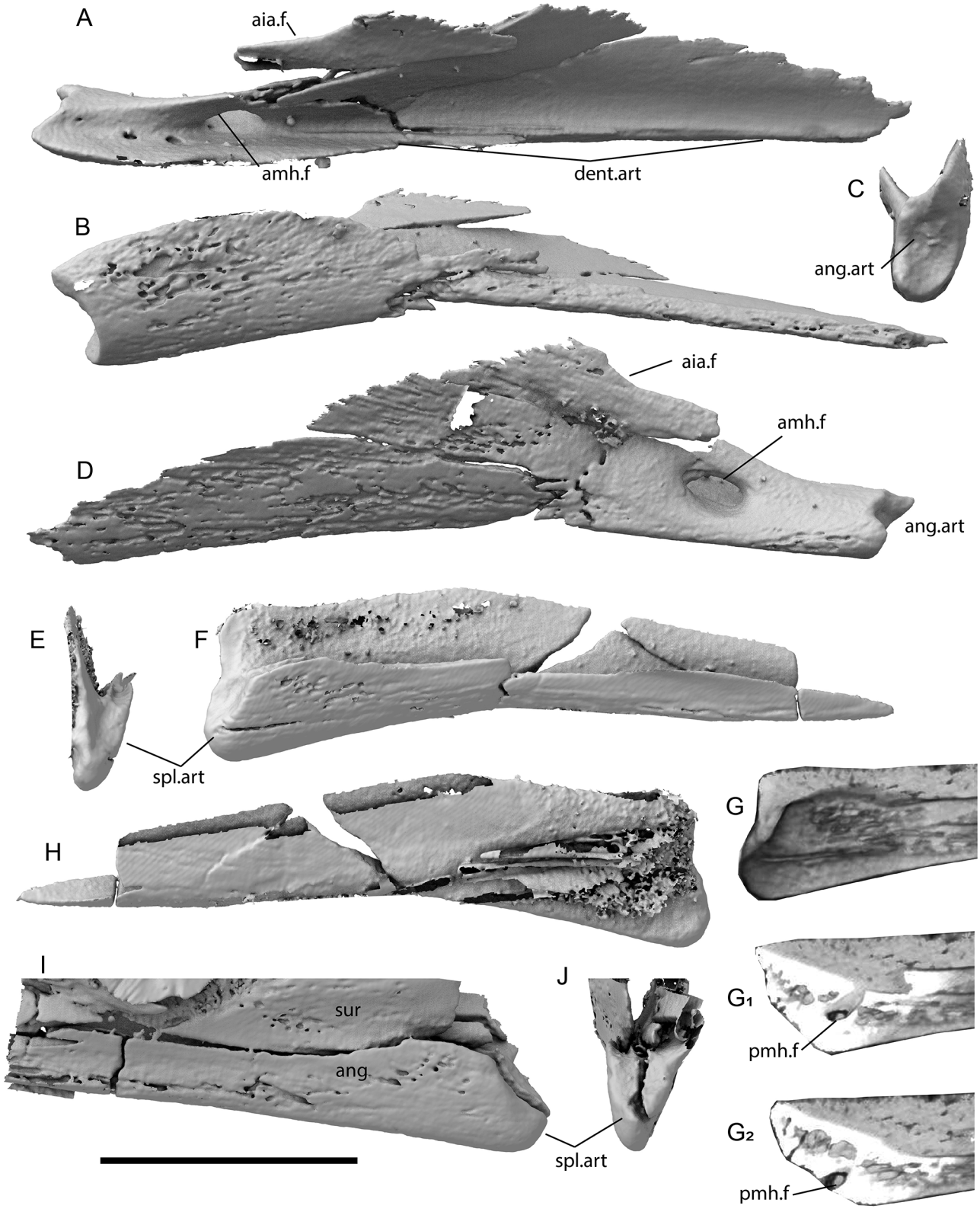

FIGURE 12. Splenial and angular of *Bentiabasaurus jacobsi* gen. et sp. nov. (MGUAN PA 183D). Right splenial in **A**, dorsal, **B**, lateral, **C**, posterior, and **D**, medial views; **Abbreviations: aia.f,** margin of anterior inferior alveolar foramen; **amh.m**, anterior mylohyoid foramen; **ang**, angular; **ang.art**, angular articulation; **dent.art**, dentary articulation; **pmh.f**, posterior mylohyoid foramen; **spl.art**, splenial articulation; **sur**, surangular. Scale equals 3 cm.

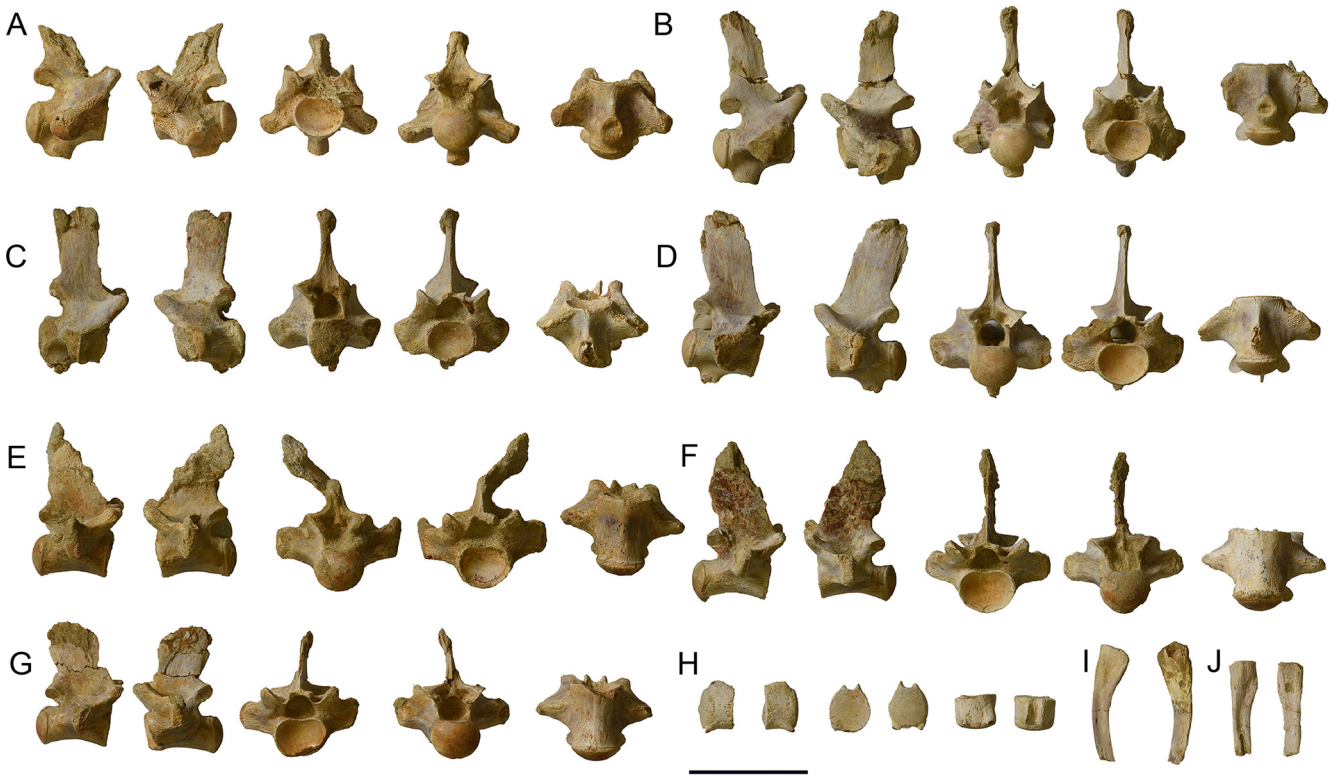

FIGURE 13. Representative vertebrae of *Bentiabasaurus jacobsi* gen. et sp. nov. (MGUAN PA 183D). **A**, cervical vertebra three; **B**, cervical vertebra five; **C**, cervical vertebra six; **D**, cervical vertebra seven; **E-G**, thoracic trunk vertebrae; **H**, terminal caudal vertebra; **I**, **J**, cervical ribs. All vertebrae arranged from left to right in right lateral, left lateral, anterior, posterior, and ventral views. Scale equals 5 cm.

point. In lateral view, the medial face of the posteromedial process is visible, and bears a large contact area where it would have been overlain by the anterior part of the surangular buttress. The posteroventral vertical ramus bears a deep groove for insertion of the adductor musculature. In medial view, the medial ventral margin is only slight deeper than the lateral and would not meet the angular. The posterior margin of the medial ventral flange is notched, posterior to which the coronoid medial face broadens posteriorly, its posteroventral part overlapping the medial surangular and its dorsal part bearing striations. In dorsal view, there is no evidence of an anterior cleft.

Postcrania

Cervical vertebrae — There are four cervical vertebrae preserved with MGUAN PA 183D (Fig. 13A-D), which we interpret as representing positions C3, and C5-C7 based on development of synapophyses and hypapophyseal peduncles. No hypapophyses are preserved. Articular surfaces are nearly circular, with some dorsal emargination below the neural canal anteriorly and slightly progressively more depressed posteriorly. The dorsolateral trending contact of the zygopophyses is about 45 degrees. Though missing due to breakage C3 and C5, well-developed zygosphenes and zygantra are present on others. The rib facet on C3 is small and slightly oval, becoming more vertically elongate posteriorly. C3, and C5 bear well preserved peduncles, broken in C6, and C7 does not bear an articular facet for the hypapophysis. The anterior margin of the peduncles is drawn out anteriorly, making the articular surface weakly teardrop shaped. None of the neural spines are complete, but the above the level of the postzygapophyses, C3 is posteriorly broad, forming a somewhat triangular cross-section, the posterior width diminishing in more posterior vertebrae. Anteriorly the preserved parts of the neural spines are narrower in lateral view, and become broader in the more posterior ones.

Trunk vertebrae — There are six trunk vertebrae and three of those free of matrix and well preserved enough for description and interpreted as coming from the thoracic region based on their relatively deep synapophyses (Fig. 13E-

G). The articular surfaces are nearly circular, but appear more depressed than the cervicals, due to increased flattening of the dorsal rim, beneath the neural canal. The dorsolaterally trending contact of the zygopophyses is about 45°. All elements in which the area is preserved bear well-developed zygosphenes and zygantra. Although they are broken distally, the preserved parts of the neural spines are similar to C7, broad and trending posterodorsally.

Caudal vertebrae — There are five caudal vertebrae, only two of which are free of matrix and of those, one well preserved well-enough to be described (Fig. 13H). It is partially digested, the neural and hemal spines reduced to their bases, and the cortical bone partially decalcified. It is identified as a terminal caudal by lack of transverses processes on its lateral sides. The articular surfaces are slightly taller than wide (1.07:1), the ventral part is arcuate, forming a semicircle, and the dorsolateral margins slightly flatter and converge with the dorsal margin which is embayed beneath the neural canal. The articular surfaces are only minimally curved. The centrum is relatively short compared to its articular height (0.64:1).

DISCUSSION

The remarkable specimens reported here provide a unique snapshot of ancient trophic interactions that took place in a highly productive upwelling zone along the west coast of Africa approximately 71.5 Mya. The fossil reveals aspects of the feeding behavior of *Prognathodon kianda* including prey selection, acquisition, processing, and digestive biology. Furthermore, the fossil provides an empirical basis to discuss the relationship of tooth morphology and prey processing, and also allows comparison with other putative gut-content occurrences. In the following paragraphs, we provide additional context for the locality and the range of trophic interactions preserved there. We then discuss size relationships of the predator and prey items, prey completeness and prey processing.

The "Bench 19 Bonebed" — The fossils described herein were collected from a horizon that preserves an extra-ordinarily dense concentration of marine amniote fossils, referred to as the "Bench 19 Bonebed" located at Bentiaba, Namibe Province, Angola (Strganac et al., 2015a). The bonebed is restricted to outcrops in erosional channels and hillsides, all within a very small area (100,000 m^2) and a stratigraphically restricted horizon (~10 m). The greatest concentration of bone falls within the first few meters above Bench 19, the topmost of a series of resistant sandstone benches exposed on the sea cliffs adjacent to the site. The bonebed preserves two plesiosaur taxa, four turtle taxa, and at least seven mosasaur taxa (Strganac et al., 2015a). There are also numerous fishes, pterosaurs, and occasionally dinosaurian elements found. The density of preserved vertebrate marine life has been explained as the result of attritional accumulation in a highly productive upwelling area (Jacobs et al, 2009), occurring within a relatively short time-frame (240 kyr) falling within magnetochron 32n.1n, and dated at 71.40-71.64 Ma (Strganac et al., 2014; Jacobs et al., 2016). The continental shelf is quite narrow along that part of the coast and together with the sedimentology at the site indicates the locality of Bentiaba was deposited in a relatively nearshore, cold water paleoenvironment (Strganac et al., 2015a; 2015b).

Paleo-foraging-area — Strganac et al. (2015a) inferred foraging area preferences for select marine amniotes in the Bench 19 fauna at Bentiaba using stable carbon isotopes. Of those taxa analyzed, two of them (*Halisaurus* and *Gavialimimus*) were found to exclusively occupy the nearshore foraging area (about −7 $\delta^{13}C$), while a third (*Prognathodon kianda)* occupied the widest range of foraging areas, including the nearshore (−7 to −15 $\delta^{13}C$). *Bentiabasaurus jacobsi* was not included in that analysis; however, large *Mosasaurus* cf. *M. hoffmanni*, were included and were found to occupy an offshore foraging area (−10 to −13 $\delta^{13}C$), consistent with the absence of body fossils of that taxon at the locality, known only from a few isolated shed teeth, suggesting it only occasionally visited the nearshore environment. The taxa *Gavialimimus* sp. and *Prognathodon kianda* found in the gut of MGUAN PA 183, along with those taxa plus parts of multiple individuals of *Halisaurus* sp. in MGUAN PA 25, the isolated regurgitalith reported in Strganac et al (2015a), and *Bentiabasaurus jacobsi* are all represented by body fossils at the locality. Thus, it is likely that all of the prey items and their predator died and were preserved were they foraged.

Trophic interactions — Although shark scavenging on the marine amniote skeletons is common at the locality (Fig. 2), the only evidence of trophic interactions among the marine amniotes are the remains of the *Prognathodon kianda* (MGUAN PA 183) and its associated gut-content described herein and one other bone mass, interpreted as a regurgitalith (MGUAN PA 25), and briefly mentioned by Strganac et al.

(2015a). The latter is undergoing preparation and will be addressed in detail elsewhere, but also contains the remains of *Gavialimimus* sp., *Prognathodon kianda,* and *Halisaurus* sp. The size of the regurgitalith would have been impossible to pass through the small gape presented by the elasmosaurid plesiosaurs known from the site. A large offshore foraging predator like *Mosasaurus* cf. *M. hoffmanni,* known to be transient at the locality, may have been the maker of the regurgitalith. However, given that the size, taxonomic composition, and morphology of the regurgitalith is quite similar to that seen in MGUAN PA 183, and *P. kianda* is the most common large predator preserved at the site, it is most likely attributed to *P. kianda*. There is no evidence of predation by mosasaurs on any of the plesiosaur material recovered.

The predator — *Prognathodon kianda* (MGUAN PA 183) has a reconstructed skull length of about 713 mm measured at the midline and a snout-vent length of about 3.64 m approximating the vent at the start of the caudal series. Head to body length proportions for select mosasaur taxa and estimated lengths for others was provided by Russell (1967, p. 208-210) and using the skull measurements of the predator, we estimate the animal was about 6.5-7 meters long in life. In PA 183 some of the anterior teeth are broken and missing but there is no sign of apical wear on those that remain. More posterior well-preserved teeth present in the maxillae (position 7+) and dentaries (position 8+), show no signs of apical wear (Fig. 2A). The first tooth in the right dentary and corresponding premaxillary tooth do show conjugate tooth-on-tooth wear anterolateral on the dentary tooth and posteromedially on the premaxillary tooth. Anterior teeth are nearly circular at their bases and with a high base to length aspect ratio in the first few positions, but become increasingly laterally compressed posteriorly. All marginal teeth are bicarinate, with slightly greater contribution of the lingual surface, and posteriorly carinae are sharp and well developed, and the crowns slightly recurved posteriorly. These posterior teeth fall within the "cut guild" of Massare (1987), for which she predicts prey items to include large fish and reptiles. They are also consistent with the "flesh cutter guild" of Fischer et al. (2022). However, *Prognathodon kianda*, like many members of globidensini, possesses a highly heterodont tooth row. The anterior teeth in *P. kianda* are prognathous and conical, seemingly better suited for gripping or manipulating prey than cutting flesh. Additionally, and as with many globidensins, *P. kianda* possesses a tall anterior premaxilla in the part of the tooth row containing the prognathous dentition. The beam strength of a given thickness of bone increases at the square of its height, suggesting the anterior part of the snout in this group may have been adapted to dealing with higher compressional stresses in the sagittal plane than those taxa in the narrower low-snouted Plotosaurini. In any event, the more posterior teeth were clearly suited to "flesh cutting" and together with the anterior teeth, and large recurved pterygoid teeth (Schulp et al., 2008), were likely used in a repertoire of actions for prey prehension, processing, and ingestion.

Preservation and taphonomy of prey items — Differences in tissue cover, and the degree of articulation at time of ingestion and throughout digestion, are reflected in the relative decalcification and erosion of bone surfaces. Differential digestion likely indicates durability and/or thickness of soft tissue covering. For instance, the inferred attachment area for temporal musculature of the parietal is pristine, and bone surfaces on the pterygoid and posterior mandible which would have anchored large muscle masses such as the pterygoideus are also well preserved. Conversely, areas directly exposed to stomach acids such as tooth crowns are nearly completely eroded. Those areas with presumably thin soft tissue cover, such as the snout and skull roof are significantly decalcified.

There are also some differences in preservation of those elements in the hindgut versus those in the foregut. Some of the best-preserved elements are present in the foregut region, near the back of the skull of MGUAN PA 183D (Figs. 8, 9). These elements show little or no erosion, suggesting they had not been subjected to the full strength of and/or long exposure to the stomach acids, compared to those elements in the hindgut. Contrast this with the preservation of MGUAN PA 183B, in which large portions of the dentary and quadrate have been digested. No tooth crowns are present, including replacement teeth, though anterior portions of the snout of MGUAN PA 183D found in the hindgut do preserve replacement teeth, but as noted above, these elements may have been transported. Nonetheless, even in the hindgut, durability of the soft tissue appears to have protected large parts of the braincase and pterygoids.

The degree of digestion in the stomach content of MGUAN PA 183 is generally greater than seen in the examples presented by Longrich et al. (2022). In those, eroded teeth

ranging from slight enamel damage to complete erosion of the crown are present. However, the erosion of the bone surfaces in those same specimens does not appear to be as great. These differences between the Moroccan and Angolan samples may simply be due the amount of time the food parcel was in the stomach prior to egestion. In the case of MGUAN PA 183, there is differential erosion of elements found in the hindgut compared to the foregut, demonstrating at least a qualitative difference is degree of digestion due to resident time. It may also indicate taxonomic differences in digestive biology or possibly differences in digestion efficiency as a function of temperature. Mosasaurs did have high metabolic rates, with estimated body temperatures ranging from ~35° to ~39° reported by Bernard et al. (2010) and ~33°C to ~36°C reported by Harrell et al. (2016), or between ~2°C and ~8°C above ambient sea temperature. However, mosasaurs may not have been homeothermic, their body temperature influenced by ambient temperature (Bernard et al., 2010). In the case of the Moroccan sample, sea surface waters were relatively warm in the Maastrichtian, approximately 27°C (Lécuyer et al., 1993) compared to Bentiaba which was about 18°C (Strganac et al., 2015a). If body temperature does covary with sea temperatures, and digestive efficiency is a function of temperature, this may account for some differences in the level of decalcification seen in the two samples.

Estimated size of prey items — In the case of the fossils here, all of the inferred food parcels are of a relatively small size and include discontinuous portions of the prey items body in some cases, suggesting some level of dismemberment prior to ingestion. With few exceptions, most individual bones appear to have been complete at the time of ingestion, and do not show any apparent trauma, including longer dentigerous elements. Intuitively, physical constraints, such as the size and elasticity of the esophagus would be a major factor in limiting the maximum prey parcel size that could be ingested.

The length of preserved dentary preserved with *Gavialimimus* sp. (MGUAN PA 183B) is ~375 mm long, and is the longest individual element among the gut-content. The articulated braincase preserved with that specimen, if uncrushed, is estimated to have had a minimum diameter of ~200 mm at the time of ingestion, and is the largest diameter parcel taken. Scaled to the dentary, the skull would have been an estimated at 532 mm in length at midline. Although *Gavialimimus* sp. is a plioplatecarpine, it has an unusually long and narrow skull (Strong et al., 2020), and the measurements and estimates given by Russell (1967, p. 208-210) are for short faced plioplatecarpines such as *Platecarpus* and *Plioplatecarpus*. We therefore instead use an average of his estimates for the elongate skulled *Tylosaurus,* yielding a total body length of about 4 meters, or approximately 57% the body length of the predator.

Judging by the lack of decalcification of the internal surfaces, the isolated snout elements of *Prognathodon kianda* (MGUAN PA 183C) were likely in articulation at the time of ingestion. There are no prefrontals or palatal elements recovered, and there is no evidence of truncation; however, the most posterior parts of both maxillae were not recovered. The articulated snout would have had a maximum posterior diameter of about ~100 mm and a length of ~220 mm. Comparing the size of the snout with more complete specimens, the skull is estimated to be ~470 mm midline length and would have had a maximum diameter of ~285 mm. Again, using the methods of Russell (1967, p. 208-210) the animal is estimated to have been about 4.6 m total length, or approximately 66% the size of the predator.

The most complete and smallest specimen is *Bentiabasaurus jacobsi* gen. et sp. nov. (MGUAN PA 183D). The mandible length is estimated to be ~400 mm and the skull ~365 mm midline length. The skull and mandibles, if articulated when consumed, would have measured ~150 mm maximum diameter and ~400 mm in length, and would have represented the largest single food parcel volumetrically. Given that this appears to be a gracile form, the body length was estimated using the data give by Russell (1967) for *Clidastes liodontus*, in which the head is 12.1% of total body length. This would suggest MGUAN PA 183D would have been just over three meters in length. However, if we use the proportions given by Russell (1967) on *Mosasaurus hoffmanni* it could have been as long as 3.7 meters. This gives a range of between 47-53% the body length of the predator.

Fischer et al. (2022) used interglenoid distance as an estimate of gullet diameter, and thus the limiting factor for ingestion of food parcels. The reconstructed interglenoid distance in MGUAN PA 183 is ~270 mm. Given the largest food parcel diameter noted above was the braincase of the *Gavialimimus* sp. at about 200 mm, there would be no issue with ingestion even with other elements such as the pterygoids and mandibular parts adherent. However, an articulated and uncrushed skull and mandibles of a *Gavialimimus* scaled to the size of the dentary present, would approach the upper

limits of what the gullet could pass. The maximum diameter of an uncrushed and articulated skull of *Prognathodon,* scaled to the preserved snout, would have been ~285 mm and thus would have exceeded the diameter of the gullet. So, in the case of the *Gavialimimus* and *Prognathodon* skull parts, some level of dismemberment was required, at least for a predator the size of MGAUN PA 183, while a smaller complete skull and mandibles such as those of *Bentiabasaurus jacobsi* gen. et sp. nov. would not.

All of the prey items were considerably smaller than the predator in life, ranging from 43-57% the body length of the predator. In an analysis of prey size taken by marine predators, Costa (2014) found "that larger predators increase the maximum size of the prey that they consume while also increasing minimum prey size". In the case presented here, the predator appears to be taking prey sizes up to the limits of its ability to pass through its gullet, but no smaller prey items have been identified. That is also the case with the undescribed regurgitalith (MGUN PA 25). This may be an artifact of the availability of large prey items in this rich ecosystem, maximizing calorie intake for a given feeding bout.

A cannibal headhunter? — Curiously, most of the prey items in the stomach of MGUAN PA 183 are cranial elements. Two of the prey species likely carried with them all or parts of the adductor mandibulae and the pterygoideus. These large muscles would of course provide some needed calories, but the cost of acquisition seems inefficient for an active predator, raising the possibility these are scavenged meals. The paleoproductivity evident at the locality in the form of the dense concentration of marine amniote carcasses supports this speculation, providing ample opportunity for free or cheap meals. Additionally, the second regurgitalith reported by Strganac et al. (2015a) does contain a substantial number of vertebrae of a small halisaurine taxon along with the skull parts of at least three individuals of this taxon. However, no ribs or limbs are present, suggesting these elements were removed by others predators and/or scavengers prior to being eaten by the regurgitalith maker. It would not appear that *Prognathodon kianda* was an obligate scavenger given its morphology, and was more likely an opportunist, and like many carnivorous animals, taking a free meal when available and hunting when necessary.

Though unusual, this is not the first report of headhunting nor cannibalism in the fossil record, both being reported in a semi-aquatic reptile from the lower cretaceous of China (Wang et al., 2005). In that case, seven skulls of juvenile *Monjurosuchus splendens* were found in the abdominal cavity of an adult of the species. In fact, it appears that cannibalism is relatively common in extant reptiles (Mitchell, 1986), and although the data presented terse, it appears it is not uncommon for juveniles and subadults to be preyed upon, at least occasionally, by conspecific adults. This is also supported by data-oriented surveys, such as that of Mateo and Pleguezuelos (2015) that accessed the prevalence of cannibalism through collection and analysis of a large number of fecal pellets of the lacertid *Gallotia caesaris*. The diet of *Gallotia* is mainly herbivorous, secondarily insectivorous, and vertebrates constitute a minor component. In that taxon they found only males preyed on conspecifics, in line with their sexually dimorphic large size, and cannibalism was seasonally linked to the species reproduction cycle, yielding young prey availability during the summer and fall. Nonetheless, cannibalism was only detected in about 0.7% of the 11,651 fecal pellets examined, suggesting overall, cannibalism is relatively rare in this species. Cannibalism has also previously been reported in primarily carnivorous monitor lizards (Shine et al., 1996; King and King, 2004; Stanner, 2004; Géczy, 2009) but those instances are isolated captive or field observations, so it is unclear how common this behavior is in natural populations.

Comparisons with other reports — There are few examples of mosasaur gut-content and those containing other mosasaurs are even more rare. The only published, peer reviewed reports of mosasaur-on-mosasaur predation are those of Martin and Bjork (1987) and Strganac et al. (2015a) while others remain undescribed (Anonymous, 1962; Bell and Barnes, 2007). The report by Martin and Bjork (1987) was "a mat of bones that is partially mixed yet retains some order", which we assume meant the remains were somewhat taxonomically segregated like that described herein. However, unlike our specimen, the mass reported by Martin and Bjork (1987) was a mix of fish, bird, and mosasaur remains, and was found in the pelvic and prepelvic region of the body, presumably near the cloaca, and had therefore presumably passed through the intestines. This is similar to the position of the gut-content preserved with a specimen of *Prognathodon overtoni* (Konishi et al., 2011), which is also located in the hind quarters near the pelvis. In the latter case, the vertebrate gut-content included turtle and fish remains.

Mosasaur-on-mosasaur predation has also been inferred

from disgorged regurgitaliths (Strganac et al., 2015a; Longrich et al., 2022). In both cases, the modifications to remains are nearly identical to that seen in the gut-content MGUAN PA183. Both possess similar patterns of tooth crown erosion, bone decalcification, the presence of anatomical associations, and similar patterns of parcel size, and dismemberment. Comparison with the in-situ preservation reported here, it is reasonable to interpret those reported by Longrich et al. (2022) as regurgitaliths. However, their attribution to *Thalassotitan atrox* may not be warranted as other large mosasaurid predators are also present in the fauna (Bardet et al., 2015). Interestingly, the regurgitalith examples given by Longrich et al. (2022) are mostly portions of mosasaurid skulls and mandibles, but some also contains turtle and fish material as well, whereas the example of Strganac et al. (2015a) also includes significant postcranial elements of one of the preserved taxa and is exclusively mosasaurids. In any event, the preservation of in-situ gut content as reported here, the cololites reported by (Martin and Bjork, 1987; Konishi et al., 2011), and the regurgitaliths reports (Strganac et al., 2015a; Longrich et al., 2022), suggests digestive biology and methods of elimination in mosasaurs was diverse.

CONCLUSION

We reported here a semiarticulated specimen of *Prognathodon kianda* containing well-preserved in situ-gut-content from the "Bench 19 Bonebed" locality at Bentiaba, Angola. We described the preservation and morphology of the gut content and assigned it to three different mosasaurid species including *Gavialimimus* sp., *Prognathodon kianda*, and a new mosasaurine taxon *Bentiabasaurus jacobsi* gen. et sp. nov. The new taxon is related to *Mosasaurus* and *Plotosaurus* but retains a mosaic of plesiomorphic and derived characters. The diversity present in the gut-content represents taxa consumed in their preferred foraging area as evidenced by stable carbon isotopes. The presence of a subadult *Prognathodon kianda* in the stomach of a mature individual of the same species represents the first documented case of cannibalism in mosasaurs. Trophic interactions at the "Bench 19 Bonebed" locality appear to be controlled in part by relative size, with all prey taxa at roughly half of the predator's body length and food parcels approaching the estimated maximum sizes that can pass the gullet. Prey items were all apparently reduced in size through dismemberment prior to ingestion of individual parcels, though details of that process are unknown. Though the sample is quite small, the observed range of modalities suggests prey processing, digestive biology, and methods of elimination in mosasaurs was diverse.

ACKNOWLEDGMENTS

We are thankful to the organizers of this Festschrift for allowing us to honor our friend and colleague Louis L. Jacobs with this contribution. His career has taken him around the world, to all continents, exploring many periods of Earth history and numerous taxonomic groups. We, as members of Projecto PaleoAngola, are thankful for being a part of one leg of his journey. Our work in Angola has been supported by National Geographic, the Petroleum Research Fund of the American Chemical Society, LS filmes, Luanda, Angola, the Dutch Embassy in Angola, ISEM at SMU, and many friends and colleagues in Angola, and we are thankful to all of them. We thank the dozens of SMU students that helped with the conservation of MGUAN PA183 and its final meals. We thank the volunteers, staff, and SMU alumni that helped with preparation including Tyler Nelson, Connor Flynn, Rocky Manning, and Larry Bell. Diana Vineyard, Wayne Furstenwerth, and Bill Stenberg. We are especially indebted to Bill Johnson, who saw the project through from opening of field jacket number one to helping build the mounts and reproductions of the specimens for public display. Finally, we thank Nick Longrich and Amelia Zietlow for their constructive reviews of the manuscript.

AUTHOR CONTRIBUTIONS

MJP and AAS designed the project, OG facilitated field work and project logistics in Angola, MJP drafted the manuscript and figures, MJP and AAS analyzed the data and all authors contributed to refining and editing the manuscript.

LITERATURE CITED

Anonymous. 1962. Reptiles of Saskatchewan's ancient seas. *Saskatchewan Museum of Natural History, popular series* 1, 12 pp.

Araújo, R., Polcyn, M. J., Schulp, A. S., Mateus, O., Jacobs, L. L., Gonçalves, A. O., & Morais, M.-L. (2015a). A new elasmosaurid from the early Maastrichtian of Angola and the implications of girdle morphology on swimming style in plesiosaurs. *Netherlands Journal of Geosciences – Geologie en Mijnbouw*, 94, 109–120. https://doi.org/10.1017/njg.2014.44

Araújo, R., Polcyn, M. J., Lindgren, J., Jacobs, L. L., Schulp, A. S., Mateus, O., Gonçalves, A. O., & Morais, M.-L. (2015b). New aristonectine elasmosaurid plesiosaur specimens from the Lower Maastrichtian of Angola and comments on paedomorphism in plesiosaurs. *Netherlands Journal of Geosciences – Geologie en Mijnbouw*, 94, 93–108. https://doi.org/10.1017/njg.2014.43

Bardet, N., Houssaye, A., Vincent, P., Suberbiola, X. P., Amaghzaz, M., Jourani, E., & Meslouh, S. (2015). Mosasaurids (Squamata) from the Maastrichtian phosphates of Morocco: biodiversity, palaeobiogeography and palaeoecology based on tooth morphoguilds. *Gondwana Research*, 27(3), 1068–1078.

Bastiaans, D., Kroll, J. J., Cornelissen, D., Jagt, J. W. M., & Schulp, A. S. (2020). Cranial palaeopathologies in a Late Cretaceous mosasaur from the Netherlands. *Cretaceous Research*, 112, 104425. https://doi.org/10.1016/j.cretres.2020.104425

Bell Jr., G. L. & Barnes, K. R. (2007). First record of stomach contents in *Tylosaurus nepaeolicus* and comments on predation among mosasauridae *Second Mosasaur Meeting Abstract Booklet and Field Guide, Sternberg Museum of Natural History, Hays Kansas*, pp. 9–10.

Bernard, A., Lécuyer, C., Vincent, P., Amiot, R., Bardet, N., Buffetaut, E., Cuny, G., Fourel, F., Martineau, F., Mazin, J-M., & Prieur, A. (2010). Regulation of body temperature by some Mesozoic marine reptiles. *Science*, 328(5984), 1379-1382.

Camp, C. L. (1942). California mosasaurs. *Memoirs of the University of California 13, vi + 1–67.*

Cooper, S. L., Marson, K. J., Smith, R. E., & Martill, D. (2022). Contrasting preservation in pycnodont fishes reveals first record of regurgitalites from the Upper Cretaceous (Maastrichtian) Moroccan phosphate deposits. *Cretaceous Research*, 131, 105111. https://doi.org/10.1016/j.cretres.2021.105111

Dollo, L. (1913). Globidens Fraasi, Mosasaurien Mylodonte Nouveau du Maestrichtien (Crétacé Supérieur) du Limbourg et l'éthologie de la Nutrition chez les Mosasauriens. *Archives de Biologie*, 28, 609–626.

Dollo, L. (1887). Le hainosaure et les nouveaux vertébrés fossiles du Musée de Bruxelles. *Revue des Questions Scientifiques*, 21, 504–539.

Einarsson, E., Lindgren, J., Kear, B. P., & Siverson, M. (2010). Mosasaur bite marks on a plesiosaur propodial from the Campanian (Late Cretaceous) of southern Sweden. *GFF*, 132(2), 123–128.

Everhart, M. J. (2002a). Remains of immature mosasaurs (Squamata; Mosasauridae) from the Niobrara Chalk (Late Cretaceous) argue against nearshore nurseries. *Journal of Vertebrate Paleontology*, 22 (Suppl. to 3), 52A.

Everhart, M. J. (2002b). New data on cranial measurements and body length of the mosasaur *Tylosaurus nepaeolicus* (Squamata: Mosasauridae), from the Niobrara Formation of Western Kansas. *Transactions of the Kansas Academy of Science*, 105, 33–43.

Everhart, M. J. (2004a). Plesiosaurs as the food of mosasaurs; new data on the stomach contents of a *Tylosaurus proriger* (Squamata; Mosasauridae) from the Niobrara Formation of western Kansas. *The Mosasaur*, 7, 41–46.

Everhart, M. J. (2004b). Late Cretaceous interaction between predators and prey. Evidence of feeding by two species of shark on a mosasaur. *PalArch*, 1, 1–6

Everhart, M. J. (2007). Remains of young mosasaurs from the Smoky Hill Chalk (Upper Coniacian-Lower Campanian) of western Kansas. In M. J. Everhart (Ed.), *Second Mosasaur Meeting Abstract Booklet and Field Guide* (pp. 2–6). Sternberg Museum of Natural History, Hays, Kansas.

Everhart, M. J. (2008). A bitten skull of *Tylosaurus kansasensis* (Squamata: Mosasauridae) and a review of mosasaur-on-mosasaur pathology in the fossil record. *Transactions of the Kansas Academy of Science*, 111(3), 251–262.

Fernandes, A. E., Mateus, O., Andres, B., Polcyn, M. J., Schulp, A. S., Gonçalves, A. O., & Jacobs, L. L. (2022). Pterosaurs from the Late Cretaceous of Angola. *Diversity*, 14(9), 741.

Fischer, V., Bennion, R. F., Foffa, D., MacLaren, J. A., McCurry, M. R., Melstrom, K. M., & Bardet, N. (2022). Ecological signal in the size and shape of marine amniote teeth. *Proceedings of the Royal Society B*, 289(1982), p. 20221214. https://doi.org/10.1098/rspb.2022.1214

Fisher, D. C. (1981). Crocodilian scatology, microvertebrate concentrations, and enamel-less teeth. *Paleobiology*, 7(2), 262–275.

Géczy, C. (2009). Cannibalism in captive *Varanus timorensis*. *Biawak*, 3(2), 61-63.

Harrell Jr, T. L., Pérez-Huerta, A., & Suarez, C. A. (2016). Endothermic mosasaurs? Possible thermoregulation of Late Cretaceous mosasaurs (Reptilia, Squamata) indicated by stable oxygen isotopes in fossil bioapatite in comparison with coeval marine fish and pelagic seabirds. *Palaeontology*, 59(3), 351-363.

Jacobs, L. L., Mateus, O., Polcyn, M. J., Schulp, A. S., Antunes, M. T., Morais, M.-L., & Tavares, T. da S. (2006). The occurrence and geological setting of Cretaceous dinosaurs, mosasaurs, plesiosaurs, and turtles from Angola. *Journal of the Paleontological Society of Korea*, 22(1), 91–110.

Jacobs, L. L., Polcyn, M. J., Mateus, O., Schulp, A. S., Gonçalves, A. O., & Morais, M.-L. (2016). Post-Gondwana Africa and the vertebrate history of the Angolan Atlantic coast. *Memoirs of Museum Victoria*, 74, 343–362.

Jacobs, L. L., Mateus, O., Polcyn, M. J., Schulp, A. S., Scotese, C. R., Goswami, A., Ferguson, K. M., Robbins, J. A., Vineyard, D. P., & Neto, A. B. (2009). Cretaceous paleogeography, paleoclimatology, and amniote biogeography of the low and mid-latitude South Atlantic Ocean. *Bulletin of the Geological Society of France*, 180(4), 333–341.

Jacobs, L. L., Schröder, S., da Sousa, N., Dixon, R., Fiordalisi, E., Marechal, A., Mateus, O., Nsungani, P. C., Polcyn, M. J., do Couto, G., Pereira, R., Rochelle-Bates, N., Schulp, A. S., Scotese, C. R., Sharp, I., Gaudari Silvano, C., Swart, R., & Vineyard, D. P. (in press). The Atlantic jigsaw puzzle and the geoheritage of Angola. In R. M. Clary, E. J. Pyle, & W. M. Andrews (Eds.), *Geology's Significant Sites and their Contributions to Geoheritage.* Geological Society, London, Special Publications.

Kauffman, E. G. (2004). Mosasaur predation on Upper Cretaceous nautiloids and ammonites from the United States Pacific Coast. *Palaios*, 19(1), 96–100.

King, D. R. & King, R. A. (2004). *Varanus rosenbergi*. In E. R. Pianka & D. R. King (Eds.), *Varanoid Lizards of the World* (pp. 438–450). Indiana University Press, Bloomington, Indiana.

Konishi, T., Brinkman, D., Massare, J. A., & Caldwell, M. W. (2011). New exceptional specimens of *Prognathodon overtoni* (Squamata, Mosasauridae) from the upper Campanian of Alberta, Canada, and the systematics and ecology of the genus. *Journal of Vertebrate Paleontology*, 31(5), 1026–1046.

Konishi, T., Newbrey, M. G., & Caldwell, M. W. (2014). A small, exquisitely preserved specimen of *Mosasaurus missouriensis* (Squamata, Mosasauridae) from the upper Campanian of the

Bearpaw Formation, western Canada, and the first stomach contents for the genus. *Journal of Vertebrate Paleontology*, 34(4), 802–819.

Lécuyer, C., Grandjean, P., O'Neil, J. R., Cappetta, H., & Martineau, F. (1993). Thermal excursions in the ocean at the Cretaceous—Tertiary boundary (northern Morocco): $\delta^{18}O$ record of phosphatic fish debris. *Palaeogeography, Palaeoclimatology, Palaeoecology*, 105(3-4), 235-243.

Longrich, N. R., Jalil, N. E., Khaldoune, F., Yazami, O. K., Pereda-Suberbiola, X., & Bardet, N. (2022). *Thalassotitan atrox*, a giant predatory mosasaurid (Squamata) from the upper Maastrichtian phosphates of Morocco. *Cretaceous Research*, 140, 105315.

Martin, J. E. & Bjork, P. P. (1987). Gastric residues associated with a mosasaur from the Late Cretaceous (Campanian) Pierre Shale in South Dakota. In J. E. Martin & G. E. Ostrander (Eds.), *Papers in Vertebrate Paleontology in honor of Morton Green* (pp. 68-72). Dakoterra, 3.

Martin J. E. & Fox J. E. (2007). Stomach contents of *Globidens*, a shell-crushing mosasaur (Squamata), from the late Cretaceous Pierre Shale, big bend area of the Missouri River, central South Dakota. In J. E. Martin & D. C. Parris (Eds.), *Geology and Paleontology of the Late Cretaceous Marine Deposits of the Dakotas* (pp. 167-176). Geological Society of America, Special Paper, 427.

Marx, M. P., Mateus, O., Polcyn, M. J., Schulp, A. S., Gonçalves, A. O., & Jacobs, L. L. (2021). The cranial anatomy and relationships of *Cardiocorax mukulu* (Plesiosauria: Elasmosauridae) from Bentiaba, Angola. *PLoS ONE*, 16(8), e0255773.

Massare, J. A. (1987). Tooth morphology and prey preference of Mesozoic marine reptiles. *Journal of Vertebrate Paleontology*, 7(2), 121-137.

Mateo, J. A. & Pleguezuelos, J. M. (2015). Cannibalism of an endemic island lizard (genus *Gallotia*). *Zoologischer Anzeiger-A Journal of Comparative Zoology*, 259, 131-134.

Mateus, O., Callapez, P. M., Polcyn, M. J., Schulp, A. S., Gonçalves, A.O., & Jacobs, L. L. (2019). The Fossil Record of Biodiversity in Angola Through Time: A Paleontological Perspective. In B. J. Huntley et al. (Eds.), *Biodiversity of Angola*, (pp. 53–76). https://doi.org/10.1007/978-3-030-03083-4_4

Mateus, O., Marzola, M. Schulp, A. S., Jacobs, L. L., Polcyn, M. J., Pervov, V., Goncalves, A. O., & Morais, M.-L. (2017). Angolan ichnosite in a diamond mine shows the presence of a large terrestrial mammaliamorph, a crocodylomorph, and sauropod dinosaurs in the Early Cretaceous of Africa. *Palaeogeography, Palaeoclimatology, Palaeoecology*, 471, 220–232.

Mateus, O., Jacobs, L. L., Polcyn, M. J., Schulp. A. S., Vineyard, D. P., Antunes, M. T., & Neto, A. B. (2009). The oldest African eucryptodiran turtle from the Cretaceous of Angola. *Acta Palaeontologica Polonica*, 54, 581–588.

Mateus, O., Jacobs, L. L., Schulp. A. S., Polcyn, M. J., Tavares, T. S., Neto, A. B., Morais, M. L., & Antunes, M. T. (2011). *Angolatitan adamastor*, a new sauropod dinosaur and the first record from Angola. *Anais da Academia Brasileira de Ciências*, 83(1), 221–233.

Mateus, O., Polcyn, M. J., Jacobs, L. L., Araújo, R., Schulp, A. S., Marinheiro, J., Oereira, B., & Vineyard, D. (2012). Cretaceous amniotes from Angola: Dinosaurs, pterosaurs, mosasaurs, plesiosaurs, and turtles. *V Jornadas Internacionales sobre Paleontología de Dinosaurios y su Entorno*, 75–105, Salas de los Infantes, Burgos.

McBrayer, L. D. & Reilly, S. M. (2002). Prey processing in lizards: behavioral variation in sit-and-wait and widely foraging taxa. *Canadian Journal of Zoology*, 80(5), 882–892.

Mitchell, J. C. (1986). Cannibalism in Reptiles: A Worldwide Review. *Herpetological circular No. 15. Society for the Study of Amphibians and Reptiles*, Lawrence, Kansas.

Myers, T. S., Polcyn, M. J., Mateus, O., Vineyard, D. P., Gonçalves, A. O., & Jacobs, L. L. (2017). A new durophagous stem cheloniid turtle from the Lower Paleocene of Cabinda, Angola. *Papers in Palaeontology*, 2017, 1–16.

Neumann, C. & Hampe, O. (2018). Eggs for breakfast? Analysis of a probable mosasaur biting trace on the Cretaceous echinoid *Echinocorys ovata* Leske, 1778. *Fossil Record*, 21(1), 55–66.

Polcyn, M. J., Jacobs, L. L., Schulp, A. S., & Mateus, O. (2014). Physical drivers of mosasaur evolution. *Palaeogeography, Palaeoclimatology, Palaeoecology*, 400, 17–27.

Polcyn, M. J., Jacobs, L. L., Schulp, A. S., & Mateus, O. (2010). The North African mosasaur *Globidens phosphaticus* from the Maastrichtian of Angola. *Historical Biology*, 22(1–3), 175–185.

Robbins, J. A., Ferguson, K. M., Polcyn, M. J., & Jacobs, L. L. (2008). Application of stable carbon isotope analysis to mosasaur ecology. In M. J. Everhart (Ed.), *Proceedings of the Second Mosasaur Meeting, Hays, Kansas* (pp. 123–130).

Russell, D. A. (1967). Systematics and morphology of American mosasaurs. *Peabody Museum of Natural History, Yale, Bulletin*, 23, 1–241.

Schulp, A. S., Polcyn, M. J., Mateus, O., Jacobs, L. L., Morais, M.-L., & Tavares, T. da S. (2006). New mosasaur material from the Maastrichtian of Angola, with notes on the phylogeny, distribution and paleoecology of the genus *Prognathodon*. *Publicaties van het Natuurhistorisch Genootschap in Limburg*, 45(1), 57–67.

Schulp, A. S., Polcyn, M. J., Mateus, O., Jacobs, L. L., & Morais, M.L. (2008). A new species of *Prognathodon* (Squamata, Mosasauridae) from the Maastrichtian of Angola, and the affinities of the mosasaur genus *Liodon*. In M. J. Everhart (Ed.), *Proceedings of the Second Mosasaur Meeting, Hays, Kansas* (pp. 1–12).

Schulp, A. S., Polcyn, M. J., Mateus, O., & Jacobs, L. L. (2013). Two rare mosasaurs from the Maastrichtian of Angola and the Netherlands. *Netherlands Journal of Geosciences*, 92(1), 3–10.

Shine, R., Harlow, P. S., & Keogh, J. S. (1996). Commercial harvesting of giant lizards: the biology of water monitors *Varanus salvator* in southern Sumatra. *Biological Conservation*, 77(2-3), 125−134.

Sternberg, C. H. (1922). Explorations of the Permian of Texas and the chalk of Kansas, 1918. *Kansas Academy of Science, Transactions*, 30/1, 119–120.

Srichairat, N., Taksintum, W., & Chumnanpuen, P. (2018). Gross morphological structure of digestive system in water monitor lizard *Varanus salvator* (Squamata: Varanidae). *Walailak Journal of Science and Technology (WJST)*, 15(3), 245–253.

Stanner, M. (2004). *Varanus griseus*. In E. R. Panaka & D. R. King (Eds.), *Varanoid Lizards of the World* (pp. 104−132). Indiana University Press, Bloomington, Indiana.

Strganac, C., Salminen, J., Jacobs, L. L., Polcyn, M. J., Ferguson, K. M., Mateus, O., Schulp, A. S., Morais, M.-L., Tavares, T. da S., & Gonçalves, A. O. (2014). Carbon isotope stratigraphy, magneto-stratigraphy, and $^{40}Ar/^{39}Ar$ age of the Cretaceous South Atlantic coast, Namibe Basin, Angola. *Journal of African Earth Sciences*, 9, 452–462. https://doi.org/10.1016/j.jafrearsci.2014.03.003

Strganac, C., Jacobs, L. L., Polcyn, M. J., Ferguson, K. M., Mateus, O., Gonçalves, A. O., Morais, M.-L., & Tavares, T. da S. (2015a). Geological setting and paleoecology of the Upper Cretaceous Bench 19 marine vertebrate bonebed at Bentiaba, Angola. *Netherlands*

Journal of Geosciences – Geologie en Mijnbouw, 96(1), 29–33. https://doi.org/10.1017/njg.2014.32

Strganac, C., Jacobs, L. L., Polcyn, M. J., Ferguson, K. M., Mateus, O., Gonçalves, A. O., Morais, M.-L., & Tavares, T. da S. (2015b). Stable oxygen isotope chemostratigraphy and paleotemperature regime of mosasaurs at Bentiaba, Angola. *Netherlands Journal of Geosciences – Geologie en Mijnbouw,* https://doi.org/10.1017/njg.2015.1

Strong, C. R., Caldwell, M. W., Konishi, T., & Palci, A. (2020). A new species of longirostrine plioplatecarpine mosasaur (Squamata: Mosasauridae) from the Late Cretaceous of Morocco, with a re-evaluation of the problematic taxon *'Platecarpus' ptychodon*. *Journal of Systematic Palaeontology*, 18(21), 1769–1804.

Street, H. P. & Caldwell, M. W. (2017). Rediagnosis and redescription of *Mosasaurus hoffmannii* (Squamata: Mosasauridae) and an assessment of species assigned to the genus *Mosasaurus*. *Geological Magazine*, 154(3), 521–557.

Schwenk, K. (2000b). Feeding in lepidosaurs. In K. Schwenk (Ed.), *Feeding* (pp. 175−291). Academic Press, New York.

Tykoski, R. S. & Polcyn, M. J. (2023). "Tis but a scratch!" Said the Black Knight; Severe Craniofacial Pathologies in a *Tylosaurus* from the Ozan Formation (Campanian) of Northeast Texas. *Journal of Vertebrate Paleontology, Program and Abstracts*, 2023, 428L.

Wang, X., Miao, D., & Zhang, Y. (2005). Cannibalism in a semi-aquatic reptile from the Early Cretaceous of China. *Chinese Science Bulletin*, 50, 281−283.

Williston, S. W. (1899). Some additional characters of mosasaurs. *Kansas University Quarterly*, 8, 39–41.

Zietlow, A. R., Boyd, C. A., & Van Vranken, N. E. (2023). A new mosasaurine from the Pierre Formation (Pembina Member: Campanian) of North Dakota. *Bulletin of the American Museum, New York, New York*, 464, 1−82.

WINDOWS INTO SAUROPSID AND SYNAPSID EVOLUTION
Essays in honor of Prof. Louis L. Jacobs, pp. 99–119, 2023

PALEODIVERSITY AND NICHE PARTITIONING OF CROCODYLIFORMS FROM THE WOODBINE GROUP (LATE CRETACEOUS: CENOMANIAN)

THOMAS L. ADAMS[1,*], STEPHANIE K. DRUMHELLER[2], and CHRISTOPHER R. NOTO[3]

[1]Witte Museum, San Antonio, TX, 78209, U.S.A., thomasadams@wittemuseum.org;
[2]Department of Earth and Planetary Sciences, University of Tennessee, Knoxville, Tennessee 37996, U.S.A., sdrumhel@utk.edu;
[3]Department of Biological Sciences, University of Wisconsin-Parkside, P.O. Box 2000, Kenosha, Wisconsin 53141, U.S.A., noto@uwp.edu

ABSTRACT Excavations at the mid-Cretaceous Arlington Archosaur Site (AAS) of north-central Texas has produced a diverse assemblage of terrestrial and coastal vertebrates including sharks, bony fishes, lungfish, amphibians, turtles, snakes, crocodyliforms, ornithopod and theropod dinosaurs, and mammals. Within this unique fauna, fossils of crocodyliforms remain the most common resident of this ancient ecosystem. Prior to work at AAS, the only two taxa recognized from the Woodbine Group were *Terminonaris* and *Woodbinesuchus*. Both these taxa are longirostrine pholidosaurs, occupying marginal to fully marine paleoenvironments. At the Arlington Archosaur Site, located within the upper strata of the Woodbine Group, at least five crocodyliform taxa have been identified, with the possibility of as many as six taxa, based on numerous cranial and post-cranial remains. The dominant constituent of the assemblage is represented by an ontogenetic series attributable to the large neosuchian crocodyliform *Deltasuchus motherali*. Several fragmentary cranial remains and isolated teeth are assigned to *Terminonaris* sp. *Scolomastax* represents a small-bodied and durophagus taxon that lived alongside larger, more generalized forms indicating that a broad taxonomic and ecological diversity of crocodyliforms existed in mid-Cretaceous Appalachia. Eusuchian crocodyliforms are represented by cranial material (including a second heterodont form), isolated teeth, procoelous vertebrae, and numerous osteoderms. The presence of such a diverse assortment of crocodyliforms at the Arlington Archosaur Site suggests individuals exhibiting widely disparate body plans and size ranges were occupying separate niches within a marginal marine ecosystem.

KEYWORDS Crocodyliformes, Woodbine Group, Cenomanian, Neosuchia, Late Cretaceous

INTRODUCTION

The mid-Cretaceous (Aptian to Cenomanian) of North America saw a major turnover within the dominant terrestrial clades as the Western Interior Seaway (WIS) spread, dividing the continent into two landmasses: Laramidia to the west and Appalachia to the east. However, understanding the exact timing and tempo of these faunal shifts is complicated by significant taphonomic biases. Fossil-bearing sites are comparatively rare from the mid-Cretaceous (Jacobs and Winkler, 1998; Weishampel et al., 2004; Zanno and Makovicky, 2013), and the best-known and -sampled localities are concentrated in the west (Ullmann et al., 2012; Krumenacker et al., 2016; Prieto-Márquez et al., 2016). The few Appalachian sites often contain poorly preserved isolated remains, which nevertheless provide tantalizing clues as to the communities present on the eastern landmass (Adams et al., 2017; Brownstein, 2018; Adrian et al., 2019; Noto et al., 2019; Drumheller et al., 2021; Noto et al., 2022).

Fossils from the Woodbine Group of north-central Texas, U.S.A., preserve a coastal ecosystem from the Cenomanian of Appalachia (Powell, 1968; Dodge, 1969; Kennedy and Cobban, 1990; Emerson et al., 1994; Lee, 1997; Jacobs and Winkler, 1998; Gradstein et al., 2004). Most Woodbine deposits yield poorly preserved, scattered fossils from a mixture of terrestrial, freshwater, and marine organisms (Lee, 1997; Head, 1998; Jacobs and Winkler, 1998; Adams et al., 2011). The Arlington Archosaur Site (AAS) represents an unusual outlier, a Woodbine deposit that is rich in well-preserved fossils (Adams et al., 2017; Adrian et al., 2019; Noto et al., 2019; Drumheller et al., 2021, Noto et al., 2022; 2023a). The AAS has produced a wide diversity of coastal taxa, including several new species (Adams et al., 2017; Main et al., 2011; Adrian et al., 2019; Noto et al., 2019;

*Corresponding author

Adrian et al., 2021; Adrian et al., 2023). Analyses of these groups suggests a complex biogeographic pattern was at play during the mid-Cretaceous transition in Appalachia, with more stereotypically Early and Late Cretaceous groups coexisting within this one ecosystem (Drumheller et al., 2021; Noto et al., 2022; 2023a).

Crocodyliforms are particularly common within the AAS, representing a wide range of body sizes and ecomorphotypes (Noto et al., 2012; Adams et al., 2017; Noto et al., 2019; Drumheller et al., 2021). Here we document all crocodyliforms present within the AAS and then discuss the factors leading to the high diversity of sympatric crocodyliforms present in this single ecosystem.

Anatomical Abbreviations — **ang**, angular; **anr**, angular ridge; **aps**, ascending process of the surangular; **bo**, basioccipital; **den**, dentary; **fio**, foramen intermandibularis oralis; **f**, frontal; **j**, jugal; **mx**, maxilla; **mxp**, posterior maxillary process; **na**, nasal; **oto**, otoccipital (opisthotic-exoccipital); **pal**, palatine; **par**, parietal; **pmx**, premaxilla; **po**, postorbital; **pob**, postorbital bar; **pop**, postorbital process; **q**, quadrate; **qd**, quadrate dorsal process; **sp**, splenial; **sq**, squamosal; **sur**, surangular; **sym**, mandibular symphysis.

Institutional Abbreviation — **AMNH**, The American Museum of Natural History, New York; **DMNH**, Perot Museum of Nature and Science (formerly the Dallas Museum of Natural History), Dallas, Texas, USA; **SMNH**, Royal Saskatchewan Museum (formerly the Saskatchewan Museum of Natural History), Regina; **WM**, Witte Museum, San Antonio, Texas, USA.

AGE AND GEOLOGIC SETTING

The Woodbine Group is the oldest Upper Cretaceous unit on the Gulf Coastal Plain, representing primarily terrigenous, near shore, and shallow marine depositional systems, including shelf, deltaic, and fluvial environments (Fig. 1; Hedlund 1966; Oliver, 1971; Trudel, 1994; Ambrose et al., 2009; Hentz et al., 2014). Originally called the Woodbine Formation by geologist R.T. Hill during his geological survey from Big Bend to North Texas, it is named for the town of Woodbine in Cooke County, Texas. Surface outcrops of the Woodbine Group are exposed in a narrow, irregular band, stretching from central Texas into southern Oklahoma (Dodge 1969; Johnson 1974; Oliver 1971; Trudel 1994). Two units are currently recognized based on sequence stratigraphic and biostratigraphic criteria: the lower Dexter Formation representing marginal and marine environments (Bergquist 1949; Dodge 1952; 1968; 1969; Johnson 1974; Oliver 1971) and the overlying Lewisville Formation, which represents a low-lying coastal plain (Oliver 1971; Powell 1968). In the study area the Woodbine Group sits unconformably over the Grayson Marl (Washita Group) and is separated by another unconformity from the overlying Eagle Ford Group. The Woodbine Group is separated by a period of marine deposition lasting at least ten million years from the older terrestrial units that distinguish the Lower Cretaceous Trinity Group (Winkler et al., 1995).

Sequence stratigraphic and chronostratigraphic studies suggest a maximum age of middle-early Cenomanian for the Woodbine Group (Adams and Carr 2010; Ambrose et al. 2009; Donovan et al. 2015; Vallabhaneni et al. 2016). The presence of the ammonite *Conlinoceras tarrantense*, a zonal marker for the base of the middle Cenomanian, in the Lewisville Formation provides an age estimate no younger than early middle Cenomanian (approximately 96 Ma) (Kennedy and Cobban, 1990; Emerson et al., 1994; Lee, 1997; Jacobs and Winkler, 1998; Gradstein et al., 2004). However, Ambrose et al. (2009) suggests the Lewisville Formation may be as young as late Cenomanian, with overall deposition of the Woodbine Group ending around 92 Ma.

The AAS consists of a 200 meter long, 5-meter-thick outcrop belt that includes the primary fossil quarry and isolated patches of fossiliferous exposure. Fossils are found in deposits interpreted as terrestrial, freshwater, and marine (Noto, 2015; Noto et al., 2012, 2019, 2022, 2023b; Adams et al., 2017). The main quarry contains four lithofacies (A-D) that indicate increasing marine influence through time (Noto, 2015; Adams et al., 2017). Fossils are largely concentrated in the lowermost facies (A), a dark brown, sandy siltstone that transitions upwards into a dark gray, carbonaceous sandy siltstone (Adams et al., 2017). These layers are rich in plant macrofossils, palynomorphs, invertebrates, and well-preserved but disarticulated vertebrate remains (Noto, 2015; Noto et al., 2012; Main et al., 2014; Adams et al., 2017). Facies A represents a low-energy freshwater or brackish coastal wetland proximal to the ancient coastline (Noto, 2015; Noto et al., 2012; Adams et al., 2017).

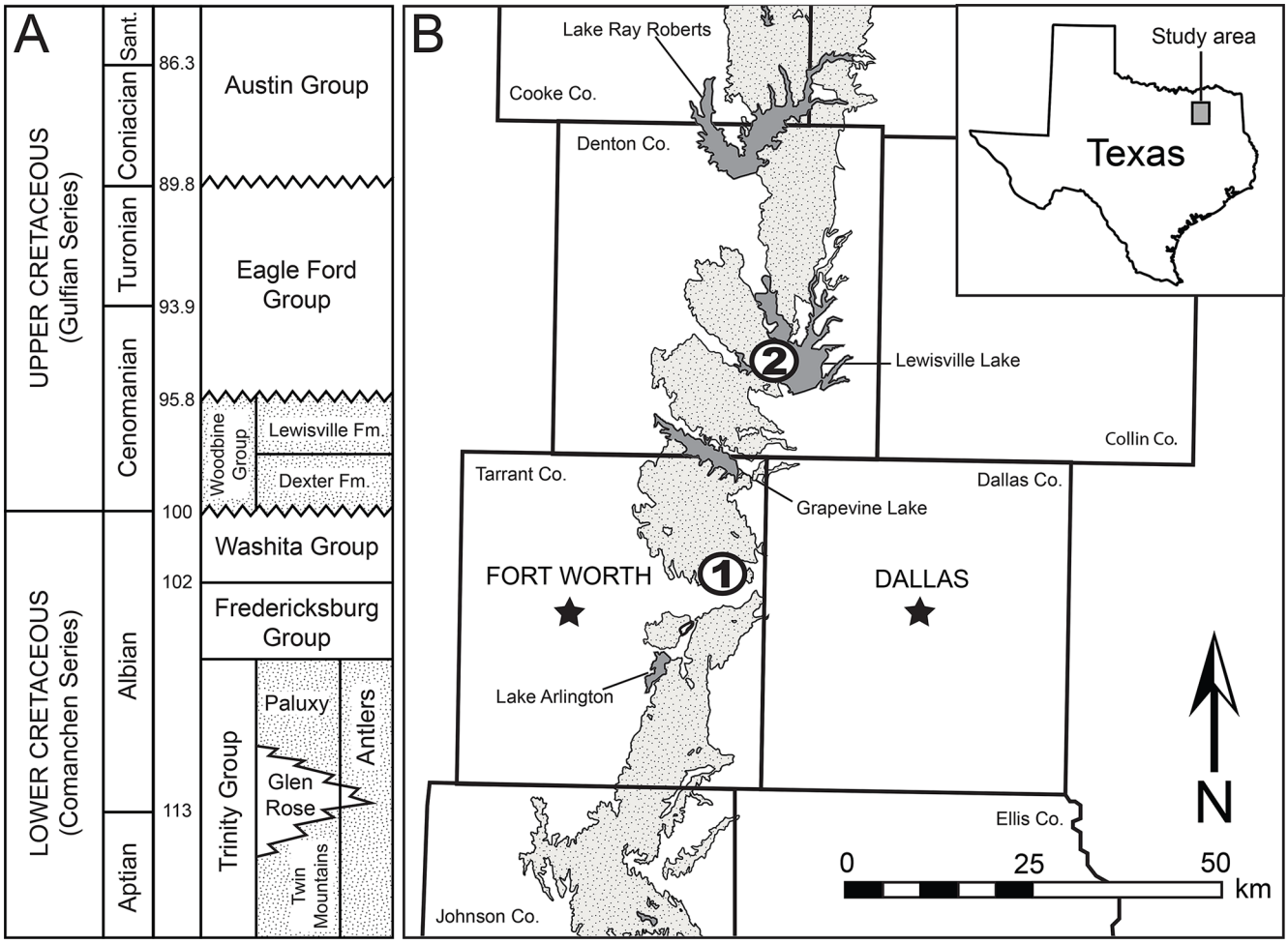

FIGURE 1. Location and geologic setting of the Arlington Archosaur Site (AAS). **A**, stratigraphic column for the Upper Cretaceous of north-central Texas showing the position of the Woodbine Group relative to timescale and adjacent geologic units. Stippled intervals represent terrestrial deposits. Time scale based on Gradstein et al. (2004). **B**, Generalized map of geologic units in the Fort Worth Basin, showing enlarged area from white box of inset map of Texas. Location of AAS, **1**; location of Lewisville Lake (*Terminonaris* localities), **2**. Modified from Barnes et al. (1972), Strganac (2015), Noto et al. (2021).

MATERIALS AND METHODS

3D Modeling — 3D digital modeling and reconstructions on numerous fossils from AAS was conducted using a variety of technologies and software. Digital scanning of individual elements was done with NextEngine™ HD Desktop 3D scanner and ScanStudio™ HD PRO software (NextEngine™, 2008) and with Revopoint™ POP 2 3D scanner and Revo Scan software (Revopoint 3D Technologies, 2014). Reconstruction and rendering of 3D models were completed using Blender 3D creation suite version 2.8 (Blender Foundation, 2002). In the case of damaged or missing elements, the 3D digital model of the opposing elements was digitally mirrored and used in skull reconstructions.

The holotype of *Scolomastax sahlsteini* (DMNH 2013-07-1256) was microCT scanned at the Microscopy and Imaging Facility in the American Museum of Natural History using a GE Phoenix v|tome|x s 240 high resolution scanner. The scan utilized a voltage of 180 kV and current of 180 mA; 1,200 images were collected at a voxel size of 0.0837 mm. Original scan files and models for this specimen are available at Morphosource.org (Project P605). CT images were post processed with 3D Slicer v 4.11 (Fedorov et al., 2012). The specimen was first segmented using the threshold function, then the paint tool was used to manually segment the individual alveoli, which were each rendered in a color according to tooth position (incisiform, caniniform, 'premolariform', molariform) with a surface smoothing factor of 0.5.

SYSTEMATIC PALEONTOLOGY AND DESCRIPTIONS

CROCODYLIFORMES Hay, 1930
MESOEUCROCODYLIA Whetstone and Whybrow, 1983
NEOSUCHIA Benton and Clark, 1988
PALUXYSUCHIDAE Drumheller et al., 2021
DELTASUCHUS Adams et al., 2017
DELTASUCHUS MOTHERALI Adams et al., 2017
(Fig. 2)

Holotype — DMNH 2013-07-0001, partial skull and mandible

Referred Material — DMNH 2013-07-1859, partial skull and mandible; DMNH 2014-06-01, partial mandible; DMNH 2013-07-0079, right dentary and maxilla; DMNH 2013-07-0297, left premaxilla, right premaxilla; DMNH 2013-07-1888, right dentary; DMNH 2013-07-0239, left dentary; DMNH 2013-07-0218, right dentary; DMNH 2013-07-1984, right dentary; DMNH 2013-07-0240, left dentary; DMNH 2013-07-0322, left dentary; DMNH 2013-07-0228, left dentary; DMNH 2013-07-0312, right dentary; DMNH 2013-07-0802, right dentary; DMNH 2013-07-0219, left maxilla; DMNH 2013-07-1404d, left prefrontal; DMNH 2013-07-0733, left quadrate; DMNH 2013-07-0084, left lacrimal; DMNH 2013-07-1871, frontal; DMNH 2013-07-1992, left and right quadratojugals, left and right quadrates; DMNH 2013-07-1993, left lacrimal; DMNH 2013-07-1994, partial right exoccipital; DMNH 2013-07-1995, right prefrontal; DMNH 2013-07-0004, left otoccipital and right surangular; DMNH 2013-07-1997, right quadrate; DMNH 2013-07-1975, right prefrontal, left jugal; DMNH 2013-07-0178, 2013-07-0164, 2013-07-0043, 2013-07-0165, 2013-06-04 teeth; SMU 76810, articulated right surangular and angular; WM 2019-15 Ga, left premaxilla; WM 2019-15 Gb, tooth.

Description

The holotype of *Deltasuchus motherali* (DMNH 2013-07-0001) includes associated, but disarticulated craniomandibular elements ascribable to a large, adult neosuchian crocodyliform with a robust, broadly triangular snout (Adams et al., 2017; Fig. 2A, B). The specimen is incomplete, including both premaxillae, maxillae, and nasals, a left postorbital, a left jugal, a right squamosal, both quadrates, a right otoccipital, the basioccipital, both ectopterygoid, and fragments of the pterygoids and dentaries. Based on a reconstructed cranial length of 800 mm, the total body length of the holotype animal is estimated at between 5.6 and 6 meters in length (Drumheller et al., 2021).

Multiple smaller-bodied individuals are also known from AAS and ascribable to *D. motherali*, based on the following combination of characters: more robust, widely-triangular snout shape; paired pseudocanines in the maxilla (m4 and m5); paired pseudocanines in the dentary (d3 and d4); ventrally directed premaxilla; posterior process of the premaxilla overlaps anterodorsal surface of the maxilla anterolaterally, then transition to a butt joint articulation posteromedially; anterior process of the frontal extends anterior to the tip of the prefrontal; frontal excluded from the orbital margin; and enlarged supratemporal fenestrae, as well as the associated bulging of the lateral margins of the maxilla which accommodate that enlarged dentition (Adams et al., 2017; Drumheller et al., 2021). The most complete specimen of these smaller individuals when articulated (DMNH 2013-07-1859) had a cranial length of 440 mm (measured from the anteriormost tip of the premaxilla, along the midline, to the posteriormost margin of the skull table), roughly half the size of the holotype (Drumheller et al., 2021; Fig. 2C, D).

Remarks

Based on a total of 14 individuals of *Deltasuchus* are recognized from AAS, ranging in size from just under 1.5 meters long to roughly 6 meters in total length; and the assemblage provides a unique ontogenetic sampling across much of the group (Drumheller et al., 2021). *Deltasuchus motherali* (DMNH 2013-07-0001) is easily differentiated from the other two large crocodyliforms known from the Woodbine Group of Texas; *Woodbinesuchus byersmauricei* (Lee, 1997) and *Terminonaris robusta* (Adams, et al. 2011). Both of these taxa are longirostrine neosuchians with tubular snouts, while *D. motherali* has a broad platyrostral rostrum.

CROCODYLIFORMES Hay, 1930
MESOEUCROCODYLIA Whetstone and Whybrow, 1983
NEOSUCHIA Benton and Clark, 1988
PARALLIGATORIDAE Konzhukova, 1954
SCOLOMASTAX Noto et al., 2019
SCOLOMASTAX SAHLSTEINI Noto et al., 2019
(Fig. 3)

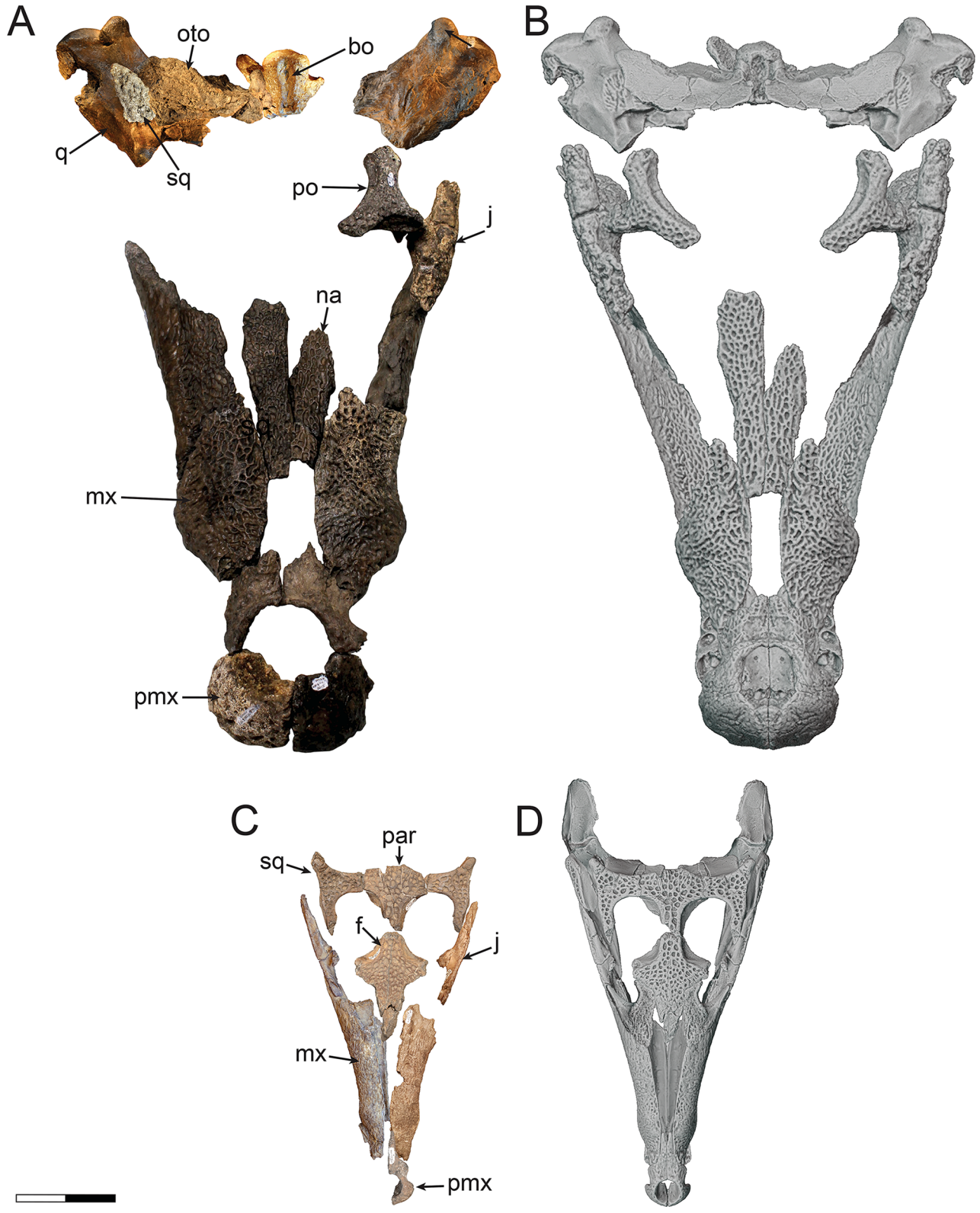

FIGURE 2. Adult skull of *Deltasuchus motherali* (DMNH 2013-07-0001; holotype), **A**, articulation of cranial elements in dorsal view; **B**, orthographic image of 3D digital reconstruction of adult skull in dorsal view. Subadult of *Deltasuchus motherali* (DMNH 2013-07-1859), **C**, cranial elements in dorsal view; **D**, orthographic image of 3D digital reconstruction of subadult skull in dorsal view. See text for anatomical abbreviations. Scale bar equals 10 cm. Modified from Adams et al. (2017) and Drumheller et al. (2021).

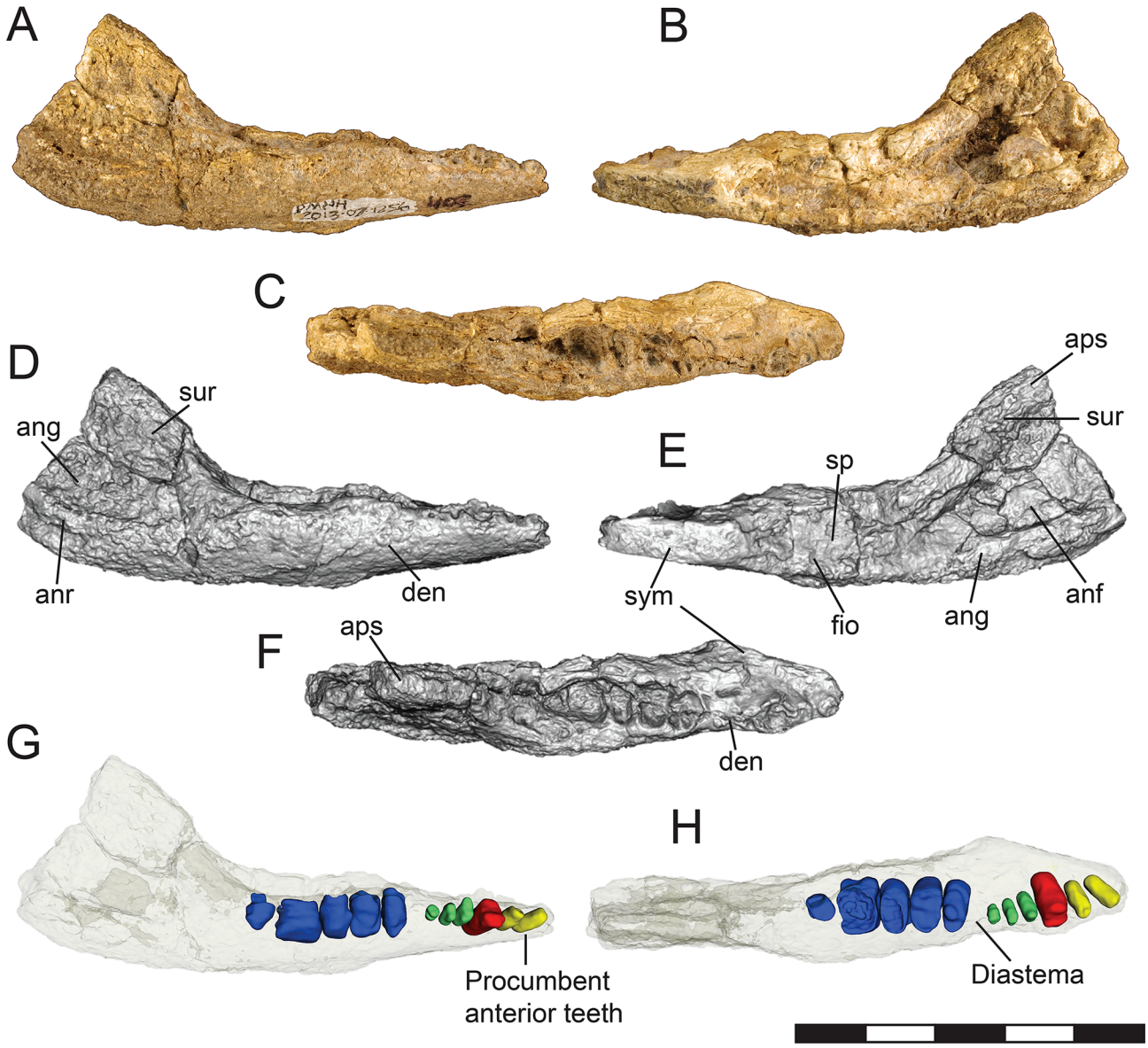

FIGURE 3. Right hemimandible of DMNH 2013-07-1256, *Scolomastax sahlsteini* in **A**, Lateral, **B**, medial, and **C**, dorsal views. CT model of DMNH 2013-07-12562 in **D**, Lateral, **E**, medial, and **F**, dorsal views. 3D Slicer images of 2013-07-12562 in **G**, Lateral and **H**, dorsal views. Incisiform in yellow, caniniform in red, 'premolariform' in green, molariform in blue. See text for anatomical abbreviations. Scale bar equals 5 cm.

Holotype — DMNH 2013-07-1256, partial right mandibular ramus.

Description

The holotype of *Scolomastax* (DMNH 2013-07-1256) is a right, lower mandible, comprising the dentary, splenial, and partial angular and surangular (Noto et al., 2019; Fig. 3A-F). Surface preservation is poor so that sutural contacts and other fine surficial details are obscured. The mandibular symphysis incorporates both the dentary and the splenial and is very elongate, extending over one-third the total length of the dentary. The dentary tapers anteriorly and expands posteriorly with two waves of prominent festooning, with associated alveolar enlargement at the third and tenth alveoli. Eleven dental alveoli are present, though none retain observable teeth. The alveoli range significantly in size, with small, procumbent alveoli in the anteriormost portion of the dentary, transitioning to significantly larger, more rectangular shaped

alveoli in the posteriormost portion of the jaw. There is a diastema between the 6th and 7th alveoli. There is no external mandibular fenestra, as the dentary is sutured to the angular and surangular. The right splenial participates in the posterior third of the mandibular symphysis. Only the anterior portion of the surangular is preserved, but what remains expands in a stepwise fashion into an unusually tall ascending, coronoid-like process. This element is mediolaterally compressed. Most of the angular is present, forming the posteroventral surface of the mandible (Noto et al., 2019).

Remarks

The partial mandible comes from a small individual and is distinguished by its low tooth count (11 alveoli; Fig. 3G-H), elongate symphysis with splenial participation, no external mandibular fenestra, a dorsally-expanded surangular forming a coronoid-like process, and an angular possessing a dorsoventral ridge. When reconstructed with the left ramus, the complete mandible would have been V-shaped in ventral view with a convex ventral margin in lateral view. The shortened toothrow and small number of enlarged posterior teeth suggests a more durophagus, or possibly omnivorous, diet. The phylogenetic position of the mandible was recovered within Paralligatoridae, although it shares characteristics with multiple mesoeucrocodylian clades (Noto et al., 2019).

CROCODYLIFORMES Hay, 1930
MESOEUCROCODYLIA Whetstone and Whybrow, 1983
NEOSUCHIA Benton and Clark, 1988
PHOLIDOSAURIDAE Zittel and Eastman, 1902
TERMINONARIS Osborn, 1904 sensu Wu et al., 2001

cf. *TERMINONARIS* sp.
(Fig. 4)

Referred Material — DMNH 2013-07-1071, left postorbital; DMNH 2013-07-1885, left postorbital; DMNH 2013-07-1868, left postorbital; DMNH 2013-07-1873, right postorbital; DMNH 2013-07-0086, right postorbital; DMNH 2013-07-0331, right postorbital; DMNH 2013-07-0225, left frontal; DMNH 2013-07-1863, parietal; DMNH 2013-07-1286, parietal; DMNH 2013-07-0049a,b, left and right squamosals; DMNH 2013-07-0168, DMNH 2013-07-0171, teeth.

Description

Terminonaris from AAS is represented by disarticulated elements found within the same bedding horizon, in close association. All elements are densely ornamented with rounded pits along the dorsal, dermal surface. The postorbitals (DMNH 2013-07-0331, DMNH 2013-07-0086, DMNH 2013-07-1071, DMNH 2013-07-1868, DMNH 2013-07-1873, DMNH 2013-07-1885; Fig. 4A-J) display a prominent anterolateral process giving a strong Y-shape to the element in dorsal view. This anterolateral process extends anterolaterally past the postorbital bar to contribute to the posteroventral border of the orbit. It projects ventrally below the level of the intertemporal bar, tapering to a point at the anteriormost projection. The projection has a smooth and shallow, concave lateral surface. The medial and posterior processes of the postorbitals form the anteromedial corner of the supratemporal fenestra. The medial process is not preserved in DMNH 2013-07-033, DMNH 2013-07-0086, DMNH 2013-07-1071, and DMNH 2013-07-1885. The descending process of the postorbital bar is smooth and short. It articulates with the ascending process of the jugal posteromedially at the dorsoventral midpoint of the postorbital bar.

The partial frontal (DMNH 2013-07-0225) is a flat element missing the anterior process that would have contacted the nasals (Fig. 4K). Only a small portion of the orbital margin is preserved. Posteriorly, the supratemporal fossa of the frontal forms the anteromedial corner of the supratemporal fenestra.

The parietals (DMNH 2013-07-1863, DMNH 2013-07-1286) are unpaired and dorsally flat elements (Fig. 4L, M). The anterior projection is very narrow, forming the dorsomedial border of the supratemporal openings. Within the supratemporal fossa, fragments of the left dorsal process of the quadrate remain in articulation on both specimens. DMNH 2013-07-1286 was exposed on the surface and has undergone weathering so that the anteriormost projection has been rounded. It does not preserve the posterior portion of the element. The posterior margin of DMNH 2013-07-1863 is broken and missing, so it is not possible to determine if the posterior margin overhangs the occiput as described by Wu et al., 2001.

Like the frontal, the squamosals (DMNH 2013-07-0049a,b) are dorsoventrally flat elements (Fig. 4N, O). In dorsal view,

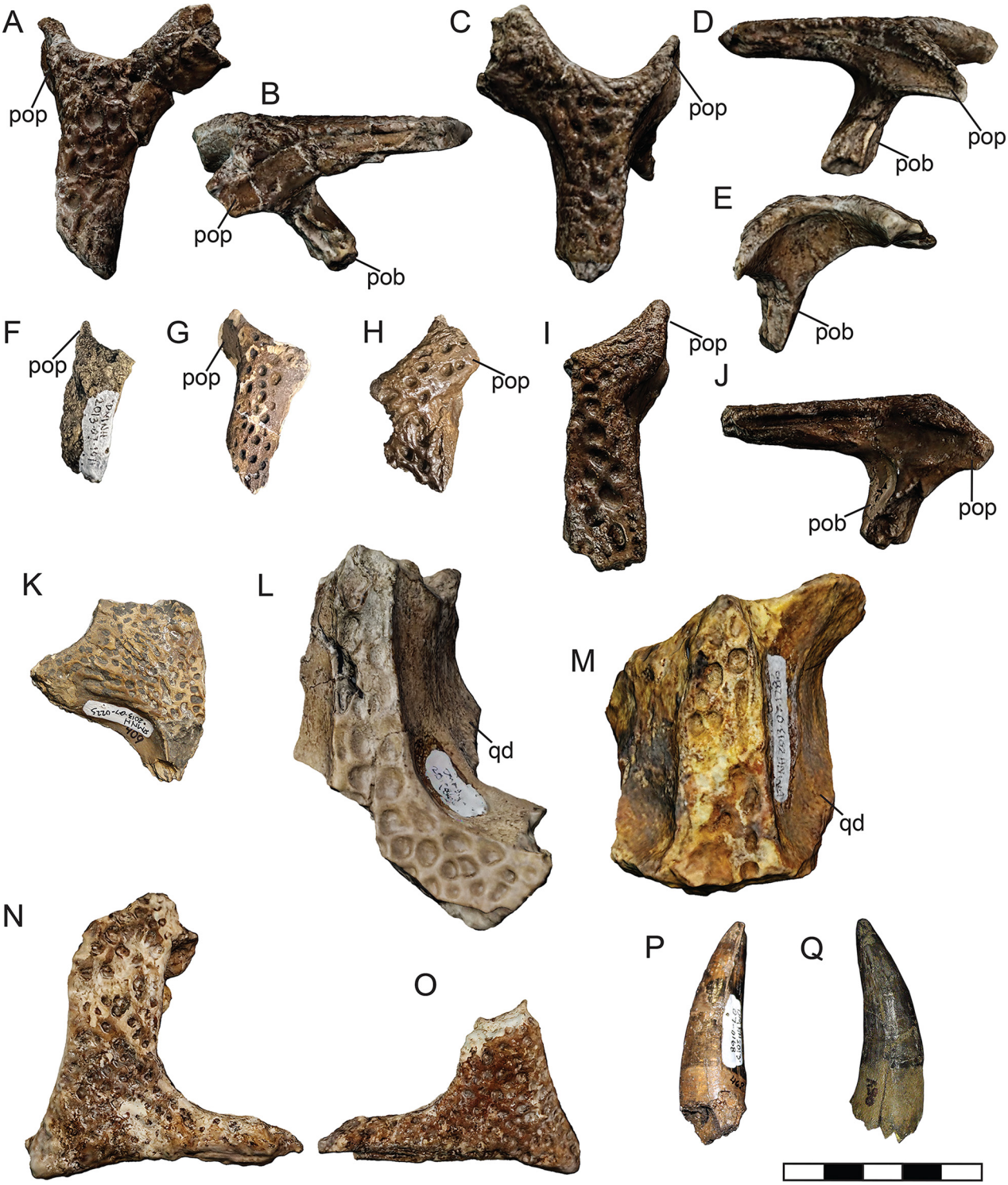

FIGURE 4. Cranial elements of cf. *Terminonaris* sp. Left postorbital DMNH 2013-07-1868 in **A**, dorsal, **B**, lateral views; right postorbital DMNH 2013-07-1873 in **C**, dorsal, **D**, lateral, and **E,** anterior views; **F**, left postorbital DMNH 2013-07-1071 in dorsal view; **G**, left postorbital DMNH 2013-07-1885 in dorsal view; **H**, right postorbital DMNH 2013-07-0331 in dorsal view; right postorbital DMNH 2013-07-0086 in **I**, dorsal, **J**, lateral views; **K**, parietal DMNH 2013-07-1286 in dorsal view; **L**, parietal DMNH 2013-07-1863 in dorsal view; **M**, left frontal DMNH 2013-07-0225 in dorsal view; **N**, **O**, left and right squamosals, DMNH 2013-07-0049a,b in dorsal view; Teeth DMNH 2013-07-0168, **P** and DMNH 2013-07-0171, **Q** labiolingual views. See text for anatomical abbreviations. Scale bar equals 5 cm.

the triangular posterolateral process extends posterolaterally beyond the level of the anterior and medial processes. Posterior to the supratemporal fenestra, the medial process is much narrower than the anterior process. In occipital view, DMNH 2013-07-0049a has a pronounced ventral projection extending from the posterolateral process. Remnants of this same projection can be seen in DMNH 2013-07-0049b.

The teeth (DMNH 2013-07-0168, DMNH 2013-07-0171) are long, slender, conical and recurved (Fig. 4P, Q; Appendix 1). The enamel is smooth, with fine, basiapical striations occurring along the surface. Smooth carina without denticles are present along the mesial and distal surfaces. The upper apical region of DMNH 2013-07-0171 has a slight sigmoidal curve but may be a result of wear at the apex. In cross-section, the teeth have a circular base.

Remarks

The presence of *Terminonaris* is well established within the middle Cenomanian (96 Ma) Woodbine Group due to multiple individuals recovered from deposits of the upper Lewisville Formation at Lewisville Lake in Denton County, Texas (Adams et al., 2011). However, the Lewisville Lake material is represented by only rostral and postcranial elements. Excluding the teeth, no direct comparison is possible with that of the AAS fossils. However, the AAS cranial material described above can be tentatively assigned to *Terminonaris* due to strong similarities to that of the type specimen (AMNH 5850) and SMNH P2411.1 of *T. robusta* (Mook, 1934; Wu et al., 2001). Specifically, the anterolaterally directed anterolateral process on the postorbital, not presence in *Deltasuchus motherali* (Adams et al., 2017). The teeth can be distinguished from the teeth of *D. motherali*, which have broader, conical crowns with closely spaced basiapical ridges that terminate shortly before the apex of the crown (Adams et al., 2017). The teeth can also be distinguished from those of *Woodbinesuchus*, which are more lingually curved, possess strong, basiapical ridges, and a subcircular to ovoid base in cross-sectional view (Lee, 1997). Postorbitals DMNH 2013-07-1868 and DMNH 2013-07-1873 most likely represent the left and right elements for a single individual. Similarly with the squamosals DMNH 2013-07-0049a and 2013-07-0049b. Based on the postorbitals, the minimum number of individual *Terminonaris* is 3, and potentially 5 when considering the size differences between them (Fig. 4A-J). This suggests another potential ontogenetic group from AAS.

CROCODYLIFORMES Hay, 1930
MESOEUCROCODYLIA Whetstone and Whybrow, 1983
NEOSUCHIA Benton and Clark, 1988
EUSUCHIA Huxley, 1875

EUSUCHIA indet.
(Fig. 5)

Referred Material — DMNH 2013-07-1066, DMNH 2013-07-2085, dentary; DMNH 2013-07-2058, DMNH 2013-07-2059, DMNH 2013-07-2060, DMNH 2013-07-2061, DMNH 2013-07-2062, teeth; DMNH 2013-07-1779, cervical vertebra; DMNH 2013-07-0537, DMNH 2013-07-0713, DMNH 2013-07-0714, DMNH 2013-07-0718, DMNH 2013-07-2064, DMNH 2013-07-2066, DMNH 2013-07-2073, dorsal vertebra; DMNH 2013-07-0056, DMNH 2013-07-0715, DMNH 2013-07-0716, DMNH 2013-07-1665, DMNH 2013-07-2068, DMNH 2013-07-2069, caudal vertebra; DMNH 2013-07-0020, DMNH 2013-07-0035, DMNH 2013-07-0037, DMNH 2013-07-1065, DMNH 2013-07-1269, DMNH 2013-07-1270, DMNH 2013-07-1271, DMNH 2013-07-1272, DMNH 2013-07-1273, DMNH 2013-07-1274, DMNH 2013-07-1276, DMNH 2013-07-1277, DMNH 2013-07-1280, DMNH 2013-07-1281, DMNH 2013-07-1283, DMNH 2013-07-1439, DMNH 2013-07-1474, DMNH 2013-07-1477, DMNH 2013-07-1509, DMNH 2013-07-1539, DMNH 2013-07-1562, DMNH 2013-07-1662, DMNH 2013-07-1946, DMNH 2013-07-2057, DMNH 2013-07-2065, DMNH 2013-07-2078, DMNH 2013-07-2079, DMNH 2013-07-2080, DMNH 2013-07-2081, DMNH 2013-07-2082, DMNH 2013-07-2083, DMNH 2013-07-2067, DMNH 2013-07-2071, DMNH 2013-07-2072, DMNH 2013-07-2074, DMNH 2013-07-2075, DMNH 2013-07-2076, DMNH 2013-07-2077, DMNH 2013-07-2086, DMNH 2013-07-2087, osteoderms.

Description

At the Arlington Archosaur Site, two partial dentaries (DMNH 2013-07-1066 and DMNH 2013-07-2085) have been recovered and assigned to Eusuchia (Fig. 5A, B; Appendix 1). DMNH 2013-07-1066 possesses alveoli positioned along the labial edge with raised margins. The alveoli are oval and separated by distinct grooves. Alveoli changes from oval to more circular in DMNH 2013-07-2085, suggesting a heterodont dentition. DMNH 2013-07-1066 preserves a single tooth that is triangular in outline in lingual/labial view and is medio-

laterally compressed. There are smooth mesial and distal carinae. A constriction separates the tooth crown from the root. The surface ornamentation consists of thin parallel longitudinal ridges that converge towards the apex on both lingual and labial surfaces.

Additionally, Five isolated teeth (DMNH 2013-07-2058, DMNH 2013-07-2059, DMNH 2013-07-2060, DMNH 2013-07-2061, DMNH 2013-07-2062) representing two distinct morphotypes have also been recovered (Fig. 5C-G). DMNH 2013-07-2060 and DMNH 2013-07-2061 are small, lanceolate teeth with a pointed apex, labio-lingually compressed, and a weak mesiodistal constriction at the base of the crown. They have smooth carinae and weak basiapical striations. The second morphotype (DMNH 2013-07-2058, DMNH 2013-07-2059, DMNH 2013-07-2062) is also lanceolate, but shorter with a more rounded apex. It is also labio-lingually compressed, with distinct carinae, weak basiapical striations, and a constricted base.

Fourteen isolated procoelous vertebrae have been recovered from AAS, of which 10 are isolated centra, disassociated from their neural arches (Appendix 1). All possess a cup-shaped anterior cotyle and a low, rounded condyle surrounded by a smooth shelf posteriorly. DMNH 2013-07-1779 represents the only cervical vertebra recovered, thus far (Fig. 5H). The centrum is unfused to the neural arch. It represents a more posterior cervical, due to the position of the diapophysial and parapophysial processes, and the lack of a hypapophysial process. The anterior and posterior articular surfaces of the centrum are circular and roughly equal in height and width. In lateral view, the centrum is spool-shaped and is smooth along the ventral surface. The parapophyses are situated dorsoventrally at the centrum's anterior margin. The diapophyses project laterally along the length of the dorsolateral margin of the centrum.

DMNH 2013-07-2066 is an anterior dorsal vertebra unfused from its neural arch (Fig. 5I). In posterior view, the articular surface of the centrum is wider, extending laterally beyond the centrum's anterior margin. In lateral view, the centrum is spool-shaped, and the wall of the centrum is concave. A deep hypapophysial process and keeled ridge extend anteroposteriorly along the ventral surface. DMNH 2013-07-0718 and DMNH 2013-07-1665 are also anterior dorsal vertebrae unfused from their neural arches. There is no indication of a hypapophysial process, but the lateral surface of the centra are concave giving a pinched shape to the ventral surface. DMNH 2013-07-0537 is a mid-dorsal vertebra which includes a centrum and associated, unfused neural arch. The centrum is anteroposteriorly long, being nearly twice as long as high. The neurocentral sutures are rugose and extend the length of the centra. There is no indication of a hypapophysial processes or keels on the ventral surface. The unfused neural arch is nearly complete, missing the prezygapophyses and portions of the neural spine. The transverse processes are located on the neural arch at the level of the neural canal. The neural canal is large, similar in size to the anterior articular surface of the centrum. Its shape is sub-circular, being wider dorsally at the position of the transverse processes. DMNH 2013-07-0713 (Fig. 5J), DMNH 2013-07-0714, DMNH 2013-07-2064, and DMNH 2013-07-2073 represent more posterior dorsal vertebrae. Much like DMNH 2013-07-0537, they are anteroposteriorly twice as long as high. DMNH 2013-07-0714 is the only one to have had a fused neural arch but is broken at the dorsal surface of the centrum.

DMNH 2013-07-0715 is a more proximal caudal vertebra (Fig. 5K). The base of the transverse process extends halfway along the anteroposterior length of the centrum. Although the neural arch is not preserved, the rough, broken dorsal surface indicates that the neural arch was fused to the centrum. The anterior and posterior articular surfaces are circular and roughly equal in shape and size. DMNH 2013-07-0716, DMNH 2013-07-2068, and DMNH 2013-07-2069 are mid-caudal vertebra with elongated centra in lateral view with fused neural arches, although much of the neural spine are missing for DMNH 2013-07-2068 and DMNH 2013-07-2069 (Fig. 5L, M). The articular facets of the prezygapophyses are positioned lower than that of the postzygapophyses. The base of the neural arch for DMNH 2013-07-0716 extends along the anteroposterior length of the centrum.

Forty isolated osteoderms have been collected from the AAS, 38 of which can be classified into four general morphotypes; 15 belonging to morphotype 1, 13 to morphotype 2, 8 to morphotype 3, and 2 to morphotype 4 (Fig. 5N-Z; Appendix 1).

Morphotype 1 — these osteoderms are rectangular to subrectangular in shape, being longer anteroposteriorly than they are mediolaterally wide (Fig. 5N-P). Their average width-to-length ratio is approximately 0.78. They are devoid of a dorsal keel or an anterolateral process. Dorsally, they exhibit a well-defined, convex articular facet, representing

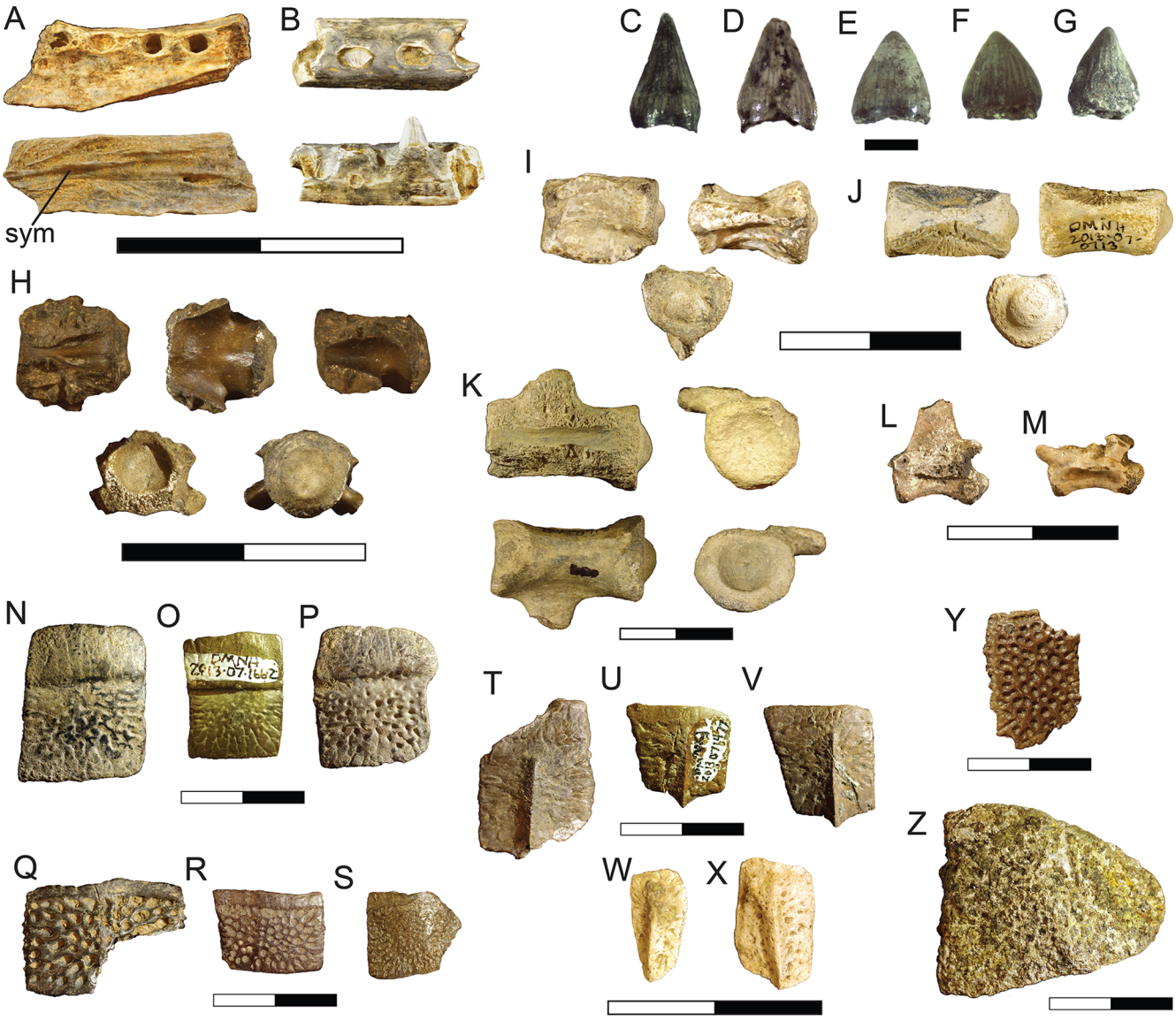

FIGURE 5. Isolated cranial and postcranial elements of Eusuchia indet. Dentary DMNH 2013-07-2085, **A**, in dorsal and medial views; dentary DMNH 2013-07-1066, **B**, in dorsal and medial views; teeth **C**, DMNH 2013-07-2061, **D**, DMNH 2013-07-2060, **E**, DMNH 2013-07-2058, **F**, DMNH 2013-07-2062, and **G**, DMNH 2013-07-2059, in mesial or distal views; cervical vertebra DMNH 2013-07-1779, **H**, in dorsal, ventral, lateral, anterior, and posterior views; dorsal vertebra DMNH 2013-07-2066, **I**, in lateral, ventral, and posterior views; dorsal vertebra DMNH 2013-07-0713, **J**, in dorsal, lateral, and posterior views; caudal vertebra DMNH 2013-07-0715, **K**, in dorsal, anterior, ventral, and posterior views; caudal vertebra DMNH 2013-07-0716, **L**, and DMNH 2013-07-2068, **M**, in lateral views; morphotype 1 osteoderms, DMNH 2013-07-1274, **N**, DMNH 2013-07-1662, **O**, DMNH 2013-07-1273, **P**, in dorsal views; morphotype 2 osteoderms, DMNH 2013-07-0035, **Q**, DMNH 2013-07-2076, **R**, DMNH 2013-07-2077, **S**, in dorsal views; morphotype 3 osteoderms, DMNH 2013-07-0020, **T**, DMNH 2013-07-1477, **U**, DMNH 2013-07-2067, **V**, in dorsal views; morphotype 4 osteoderms, DMNH 2013-07-1065, **W**, DMNH 2013-07-2071, **X**, in dorsal views; osteoderm DMNH 2013-07-0037, **Y**, in dorsal view; osteoderm DMNH 2013-07-1562, **Z**, in dorsal view. See text for anatomical abbreviations. Scale bar for **C-G** equals 1 mm, all others equal 2 cm.

approximately 40% of the anteroposterior length. This suggests a deep, imbricating articulation to the posterior edge of the next anterior osteoderm. The dorsal surface is ornamented by small, shallow pits or grooves. The ventral surface is smooth with small neurovascular foramina across the ventral surface. These are the most common of the eusuchian osteoderms from AAS and correspond to more medial, paravertebral osteoderms of the dermal shield (Hill, 2010).

Morphotype 2 — like morphotype 1, these are rectangular to subrectangular in shape, but are mediolaterally wider than the anteroposterior length (Fig. 5Q-S). The average width-to-length ratio is approximately 1.25. DMNH 2013-07-2065 and DMNH 2013-07-2074 demonstrate very shallow keels down the midline, while all others show no indication of a dorsal keel or anterolateral process. They have a smooth, narrow anterior margin for an imbricating articulation with the next anterior osteoderm. The dorsal surface is ornamented with deep, circular pits. DMNH 2013-07-2077 is strongly concave, giving the osteoderm a nearly 100^{o} bend in axial view. Similar to morphotype 1, the ventral surface is smooth with neurovascular foramina. Like morphotype 1, these characterize paravertebral osteoderms with DMNH 2013-07-2077 positioned at the most-lateral boundary along the dermal shield (Hill, 2010).

Morphotype 3 — these are subrectangular being longer anteroposteriorly than they are mediolaterally wide (Fig. 5T-V). They bear a slightly offset, parasagittally oriented keel. The keels are relatively low and extend posteriorly beyond the posterior osteoderm margin to form a distinct point. Much like morphotype 2, they also have a narrow anterior margin. In axial view, they are concave. The ventral surface is also smooth. Morphotype 3 best represents more laterally positioned dorsal, accessory osteoderm, appendicular osteoderms, or possibly caudal osteoderms (Hill, 2010).

Morphotype 4 — DMNH 2013-07-1065 and DMNH 2013-07-2071 are oval to subrectangular in shape with an obliquely oriented midline keel (Fig. 5W, X). There is no indication of an anterior margin for articulation with the next anterior osteoderm. They are most similar to morphotype 3 in also being concave. These represent the smallest identified osteoderms yet found in the AAS and are most likely appendicular osteoderms associated with the limbs (Hill, 2010).

DMNH 2013-07-0037 does not fit into any of the four morphotypes described above. It is rectangular in shape, being longer anteroposteriorly than they are mediolaterally wide (Fig. 5Y). However, it differs from the morphotype 1 in that it has a very narrow and slightly upturned, anterior articular margin. It is dorsoventrally flat and plate-like, with its dorsal surface ornamented with deep, circular pits. The left and right margins possess sutural articulation for the osteoderm directly medial and lateral to it. Its position along the osteodermal shield is unknown.

DMNH 2013-07-1562 also differs from the others significantly (Fig. 5Z). It has undergone surface exposure and weathering, so that surface ornamentation and the presence of an articular margin is difficult to discern. It is D-shaped in dorsal view, with a broken, straight medial border and a convex lateral margin. An obliquely oriented keel trends laterally to the posterior border. It is strongly concave in axial view. DMNH 2013-07-1562 corresponds to a nuchal osteoderm (Hill, 2010).

Remarks

Outside of *Deltasuchus motherali*, numerous small, isolated elements assigned to Eusuchia are among some of the most common elements recovered from the AAS assemblage. Both dentaries described above differ from *Scolomastax* (DMNH 2013-07-1256) in the shape and position of alveoli, symphyseal morphology, and parallel margins (Noto et al., 2019). The five isolated teeth demonstrate an atoposaurid-like dentition with lanceolate shaped teeth characteristic of taxa similar to *Theriosuchus pusillus* Owen, 1879. The dentaries and teeth are consistent with taxa such as *Theriosuchus* and *Wannchampsus* (Adams, 2014), suggesting this material may belong to a basal eusuchian, marking the presence of another taxon of small-bodied, heterodont crocodyliform in the Woodbine Formation.

Procoelous vertebrae, in which the anterior end is concave, and the posterior end is convex, are characteristic of members of Eusuchia. Neurocentral fusion occurs in a predictable pattern across crocodyliforms, with neonates exhibiting a lack of fusion along their entire vertebral column and sutural fusion progressing from caudal to cranial elements, with complete fusion of the cervical vertebrae used as an indicator of skeletal maturity (Brochu, 1996). The lack of fusion exhibited in most AAS eusuchian vertebrae suggests that these specimens were all immature individuals.

The osteoderms are identified as belonging to Eusuchia based on the following characteristics: small and rectangular to semi-rectangular in outline; keeled; imbricating leading edge; lacking the anterolateral process as seen in non-eusuchian neosuchians, such as goniopholidids and pholidosaurids.

CROCODYLIFORMES Hay, 1930

CROCODYLIFORMES indet.

(Fig. 6)

Referred Material — DMNH 2013-07-0018, left maxilla and palate

Description

DMNH 2013-07-0018 is a nearly complete left maxillae and palate (Fig 6; Appendix 1). Preservation quality is poor due to heavy gypsum invasion and weathering of the skull. As a result, neurovascular foramina and surface texture are not clearly visible. Even with the poor surface preservation, there is no indication of deep pitting or a strongly rugose surface texture. The maxilla is crushed dorsoventrally, and the posterior maxillary process and palate are fused and separated from the main body of the maxilla. In dorsal view, the lateral border of the maxilla is medially curved anteriorly and becomes straighter posteriorly (Fig 6A, C). There is a slight bulge at the level of the third maxillary tooth. The premaxilla-maxilla suture is obliquely oriented. The maxilla has edge-to-edge contact with the nasal along its straight dorsomedial margin. Posteriorly to this, the medial margin trends obliquely away from the midline. The secondary palate is well preserved with crushing of the palatal shelves medial to the alveolar margin. The palate is fused to the maxilla in the posteriorly extended secondary palate (Fig 6B, D). It extends posteriorly between the suborbital fenestrae, forming a narrow palatine bar with a straight lateral margin. The palatine bar is part of the medial border of the suborbital fenestra, with the posterior maxillary process forming the lateral border.

Eight tooth positions are present in the maxilla, with 5 teeth preserved in situ (Fig. 6B; Appendix 1). The alveoli increase in size from the first alveolus to the third, which is the largest in the maxilla and results in a slight lateral bulge in the maxillary margin. Four alveoli are preserved in the posterior maxillary process, with only one tooth in situ (Fig. 6D). The alveoli again decrease in size after the third. The posterior- most alveoli are not well preserved due to transverse crushing. The gap between the maxilla and the posterior maxillary process is indeterminate, so the total number of tooth positions for this taxon is unknown. The teeth are poorly preserved and have conical-shaped crowns with no indication of carinae or striations.

Remarks

Despite the poor preservation, reconstructing the rostrum of DMNH 2013-07-0018 suggests it was platyrostral in shape. It can be distinguished from *Deltasuchus motherali* whose maxilla tapers anteriorly to a narrow rostral constriction that is slightly upturned dorsally (Adams et al., 2017; Drumheller et al., 2021; Fig. 7). DMNH 2013-07-0018 also does not share the paired pseudocanines in the maxilla (m4 and m5) that help diagnose *D. motherali*. It is also discernable from the longirostrine taxa *Woodbinesuchus* and *Terminonaris* with their tubular snouts. Unlike *Scolomastax*, the teeth of DMNH 2013-07-0018 suggest a homodont dentition (Noto et al., 2019). The presence of an enlarged third maxillary tooth is a feature shared with *Wannchampsus kirpachi* from the Early Cretaceous of Texas and with the clade Paralligatoridae (Adams 2014).

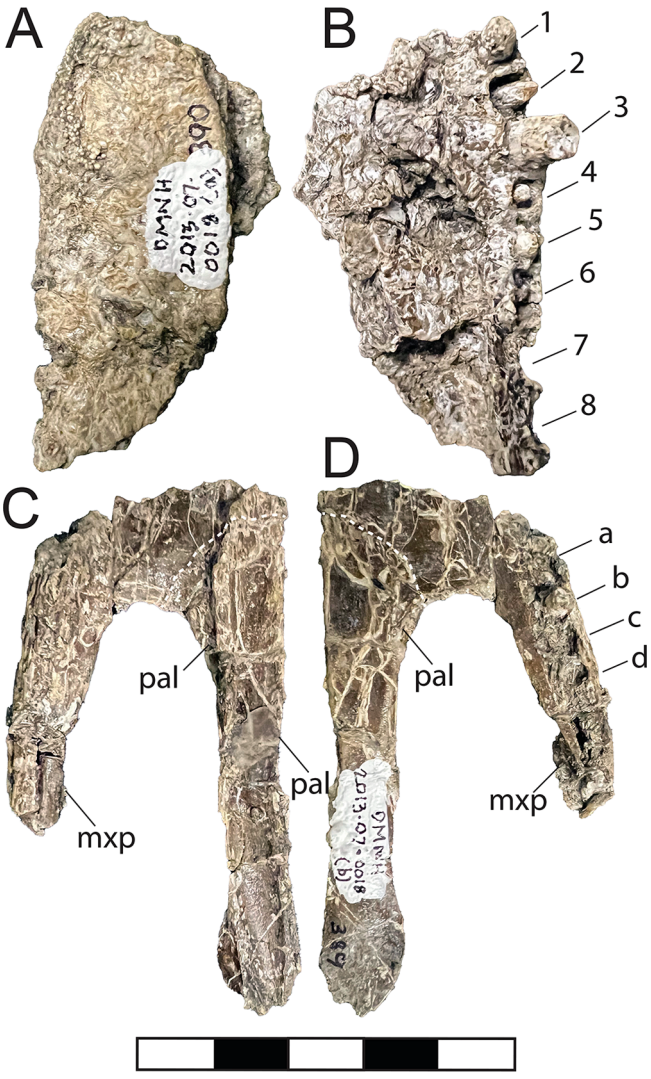

FIGURE 6. Left maxilla and palate of Crocodyliformes indet. DMNH 2013-07-0018 in dorsal, **A** and **C**, and ventral **B** and **D**, views. See text for anatomical abbreviations. Scale bar equals 5 cm.

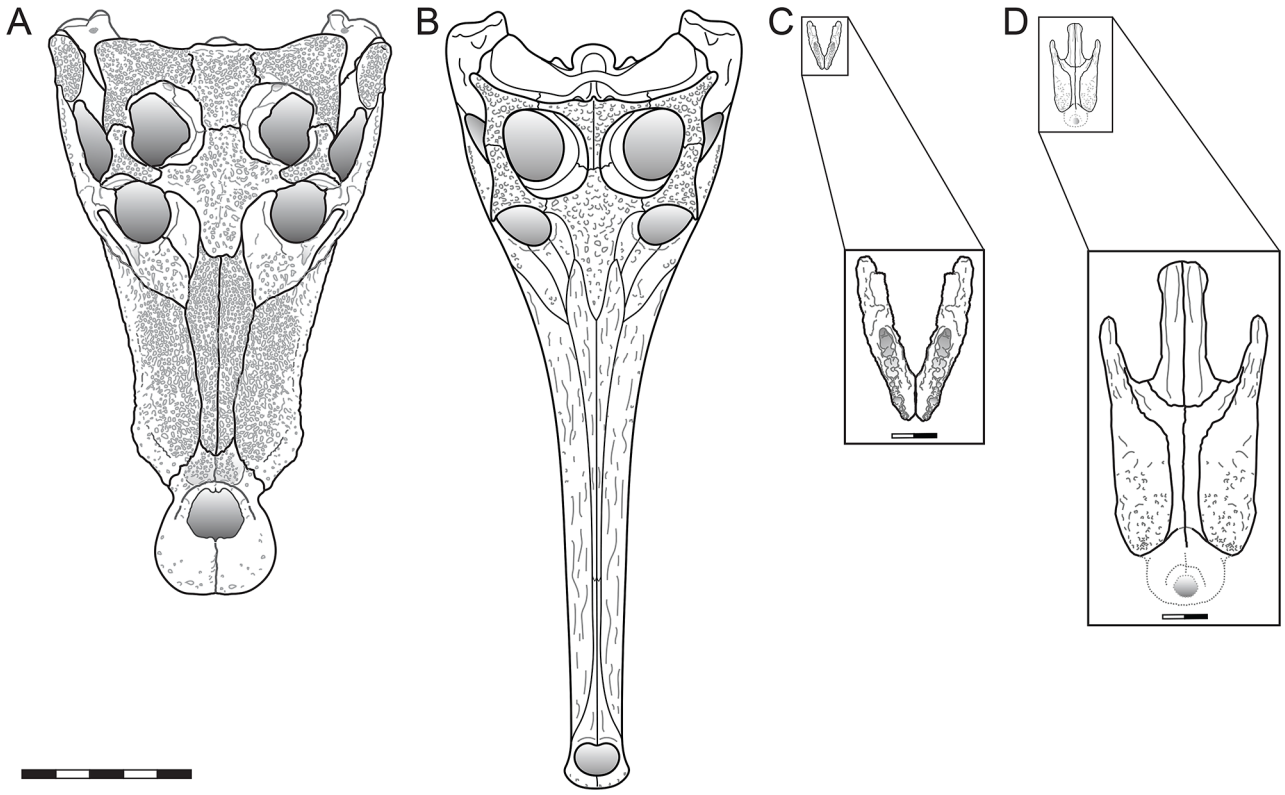

FIGURE 7. Comparisons of identifiable AAS Crocodyliformes. **A**, reconstruction of the skull of *Deltasuchus motherali*, modified after Adams et al. (2017); **B**, reconstruction of the skull of *Terminonaris robusta*, modified after Wu et al. (2001); **C**, reconstruction of the lower jaw of *Scolomastax sahlsteini*, modified after Noto et al. (2019); **D**, reconstruction of maxilla and palate of Crocodyliformes indet. (DMNH 2013-07-0018) Scale bar equals 50 cm. Scale bar in the inset boxes equals 2 cm.

DISCUSSION

Extant, sympatric crocodylians ecologically partition their habitats to reduce direct competition for resources (Drumheller and Wilberg, 2020). This often takes the form of dietary niche partitioning, which is itself reflected in variation of maximum body size, snout shape (Brochu, 2001; Drumheller and Wilberg, 2020), and dental morphologies (D'Amore et al., 2019). While modern crocodylian diversity within any single habitat rarely exceeds two or three sympatric species (Brochu, 2001), fossil assemblages across crocodyliformes can reach as high as seven morphologically and ecologically distinct species (Salas-Gismondi et al., 2015). This increased intra-site diversity is often seen during high stands in global crocodyliform diversity (Markwick, 1998a), often driven by a combination of favorable climatic conditions (Markwick, 1998b) and ecomorphological niche occupation well outstripping that seen in the present day (Brochu, 2001; Drumheller and Wilberg, 2020).

However, these patterns of dietary niche occupation among crocodyliforms often focus on only the adult morphotypes, with less attention given to juveniles (Drumheller et al., 2021), despite the fact that extreme changes in body size and corresponding shifts in snout shape and dietary preferences are observed among extant members of the clade (e.g. McIlhenny, 1935; Ross and Magnusson, 1989; Gignac and O'Brien, 2016; Gignac et al., 2019).

The AAS supported at least five crocodyliform taxa, and possibly as many as six (Fig. 7). These groups exhibit a range in snout shapes and body sizes, suggesting dietary partitioning is driving this high diversity (Adams et al., 2017; Noto et al., 2019; Drumheller et al., 2021) Additionally, these groups are often represented by multiple individuals sampling much of their ontogenetic variation, especially *Deltasuchus* (Drumheller et al., 2021) and *Terminonaris*. Partnered with the low transport seen in the fossil assemblage (Adams et al., 2017; Noto et al., 2019; Drumheller et al., 2021), this suggests that juveniles and adults were not separating out geographically

but were instead living and dying in the same area. This means that potential dietary competition and niche partitioning must be addressed across the full range of these groups' body sizes (Drumheller et al., 2021).

By far, the most common crocodyliform present in the AAS ecosystem was *Deltasuchus*. As adults, members of these groups had a broadly triangular snout with sturdy, conical teeth, morphologies which are consistent with a generalist feeding strategy (D'Amore et al., 2019; Drumheller and Wilberg, 2020; Fig 2A, D and Fig. 7A). This interpretation is further bolstered by the presence of bite marks attributable to *Deltasuchus* on smaller turtles ranging through subadult dinosaurs (Noto et al., 2012). However, the youngest and correspondingly smallest individuals known from this clade had comparatively slender dentition and narrower snouts, which pushes them more into an ecomorphotype consistent with targeting smaller, more compliant prey (Gignac and O'Brien, 2016; Drumheller and Wilberg, 2020; Drumheller et al., 2021 (Fig. 2C, D). This aligns with ecological observations among modern, generalist groups, in which juveniles often target small invertebrates, fish, and amphibians, while adults diverge into larger-bodies, more durable prey types (e.g., McIlhenny, 1935; Ross and Magnusson, 1989).

However, as slender as the snouts of these juvenile *Deltasuchus* were relative to adult members of their species, they never reached a degree of snout-elongation and narrowing comparable to *Terminonaris* (Adams et al., 2011; Fig 2C, D and Fig. 7B). This ecomorphotype is correlated with a preference for smaller-bodied, more compliant prey across ontogeny, even among very large-bodied individuals (Drumheller and Wilberg, 2020), which aligns with the slender dentition also seem in members of both clades (D'Amore et al., 2019). The overlap in this morphotype between relatively large-bodied species suggests significant competition might have been an issue, but the more longirostrine *Terminonaris* tends to be found in more coastal, marine environments (Jouve and Jalil, 2020; Jouve et al., 2021). Given that the AAS itself was deposited in a coastal system, the assemblage includes freshwater, brackish, marine, and terrestrial input associated with small-scale fluctuations in sea level throughout the facies present in the site (Adams et al., 2017; Noto et al., 2023b). This suggests that actual interactions between members of these species might have been minimal, given their differing salinity preferences, and both would have been ecomorphologically distinct from the similarly large-bodied, but generalist *Deltasuchus*.

Scolomastax represents a third major ecomorph in the AAS, a small-bodied taxon with strongly heterodont dentition (Noto et al., 2019; Fig 3 and Fig. 7C). This combination of snout and tooth shape is correlated with preferential consumption of harder food items, i.e. durophagy (Drumheller and Wilberg, 2020). Partnered with the deep, short snout, it is likely that this species was omnivorous or even herbivorous, especially if the short-crowned, button-shaped teeth observed in other Woodbine localities turn out to be associated with this taxon (Noto et al., 2019). Additional eusuchian dentaries differ in overall shape and tooth positioning to suggest a second morphotype of small, heterodont crocodyliforms was also present in the AAS. However, these elements are highly fragmentary, inhibiting more detailed analysis of phylogenetic relationships or ecomorphological classifications.

A fifth ecomorphotype is present at the site, but again, the identity of the species (DMNH 2013-07-0018) is not straightforward. It includes a small maxilla, palatine, and in situ dentition. The snout is blunter and more U-shaped in profile than *Deltasuchus*, potentially suggesting a more macro-generalist or durophagous ecomorphotype (Drumheller and Wilberg, 2020; Fig. 6 and 7D). The specimen also lacks the enlarged, paired pseudocanines seen in *Deltasuchus*, and instead has more conical dentition along the entire toothrow. It lacks the rostral shortening and low, anvil-shaped dentition seen in more hard-prey specialists (D'Amore et al., 2019), excluding obligate durophagy or other evidence of dietary specialization. Taken together, this indicates that this animal was some kind of macro-generalist, meaning that it was able to take prey items as big or even bigger than itself (Drumheller and Wilberg, 2020). Unfortunately, the specimen is also poorly preserved, with extensive crushing and flattening obscuring other, more diagnostic characteristics. We are unable to identify it beyond the level of Crocodyliformes, nor are we able to meaningfully comment on the ontogenetic stage this animal represents. However, we can say that it represents the only crocodyliform with this particular ecomorphotype in the Woodbine Group.

The remaining crocodyliform material from the AAS is even more ambiguous. The disassociated teeth, vertebrae, and osteoderms attributable to Eusuchia may represent elements from *Scolomastax*, the only eusuchian currently known from the site, or they might represent evidence of one or more unidentified eusuchian taxa, such as that represented by the

partial dentaries. More complete material is required to make this determination.

Woodbinesuchus byersmauricei Lee, 1997 has tentatively been identified within the AAS assemblage based on isolated teeth (Noto et al., 2019). Further investigation has shown that there is significant overlap between subadult *Deltasuchus* teeth described by Drumheller et al. (2021) and those described for *Woodbinesuchus* by Lee (1997). The holotype (SMU 74626) of *Woodbinesuchus* was recovered from the lower Dexter Formation (formerly Rush Creek Member). Its presence in the upper Lewisville Formation would extend the range of this taxa through the Woodbine Group. Currently, *Woodbinesuchus* is only known from lower jaw and postcrania (Lee, 1997). It is possible that some of the disarticulated cranial material described from AAS in this study could come from this clade. Again, without more complete material, it is impossible to determine which elements might be related to *Woodbinesuchus* and whether any of them instead represent other poorly known or even wholly unknown taxa.

Taking a broader perspective, the crocodyliform material from the AAS described here supports the record of faunal turnover and large-scale continental interchange through the 'mid' Cretaceous interval. This record supports hypotheses of widespread mid-Mesozoic cosmopolitanism and lower biodiversity that gave way to increased endemism and diversification during the Cretaceous (Zanno & Makovicky, 2011; Suarez et al., 2021; Buscalioni et al., 2011; Montefeltro et al., 2013; Turner, 2004). While this pattern is reciprocated in Woodbine Group crocodyliforms, it differs from other vertebrate groups in a few key respects. First, the named taxa *Deltasuchus*, *Scolomastax*, and *Terminonaris* are all members of lineages with distributions across Gondwana and/or Laurasia; part of the dominant, cosmopolitan fauna that persisted through the Early Cretaceous. Second, these lineages appeared to respond differentially during the transition. For example, the Paluxysuchidae, which includes *Deltasuchus* and *Paluxysuchus*, began to diverge from other neosuchians to form an endemic crocodyliform assemblage at the beginning of the Early Cretaceous, prior to many other vertebrate groups, implying the transition from Early to Late Cretaceous may have been more gradual for at least some crocodyliform clades (Drumheller et al., 2021). On the other hand, current phylogenetic analysis finds the sister taxa of *Scolomastax* in Asia, which suggests a more recent (and short-term) biogeographic connection with southern Appalachia, requiring significant interchange between these distant and periodically isolated areas in the Aptian-Albian or early Cenomanian prior to completion of the Western Interior Seaway (Noto et al., 2022). Third, members of these formerly cosmopolitan groups, a few endemic clades, and more recent immigrants combined to form a distinctive local fauna on the southwestern coast of Appalachia. The extraordinary diversity observed in the AAS and throughout Woodbine exposures was likely supported by the paleoenvironmental heterogeneity of the vast and complex coastal, delta plain, and shallow shelf ecosystems (Noto et al., 2022; 2023b). The Woodbine Group fossil assemblage represents an early stage of the transition during the emergence of later Late Cretaceous faunal assemblages, as 'mid' Cretaceous ecosystems evolved in response to major faunal interchange, sea level, and climate change, creating unique communities that in turn enhanced taxonomic diversity and endemism.

ACKNOWLEDGMENTS

We dedicate this paper to Dr. Louis L. Jacobs in recognition of his support and guidance, as a teacher, mentor, and colleague, which has been a great source of inspiration for so many. We thank the Huffines family and R. Kimball of Johnson Development, who provided access to the property on which the AAS is situated. A. Sahlstein, P. Kirchoff, and B. Walker first discovered the site, and a dedicated team of volunteers helped excavate and prepare much of the material over the past ten years. Thanks to the Perot Museum of Nature and Science, Southern Methodist University, and the Witte Museum for access to research collections. We thank H. Maddox for her assistance in production of orthographic models. We thank A. R. Fiorillo and A. K. Hastings for their valuable comments that helped improve this manuscript. This study was supported by funding from the National Geographic Society Conservation Trust grant #C325-16 to C. Noto, National Science Foundation DUE-IUSE GP-IMPACT grant #1600376 to L. McKay and S. Horn, as well as our contributors on Experiment.com.

LITERATURE CITED

Adams, R. L. & Carr, J. P. (2010). Regional depositional systems of the Woodbine, Eagle Ford, and Tuscaloosa of the U.S. Gulf Coast. *Gulf Coast Association of Geological Societies Transactions*, 60, 3–27.

Adams T. L. (2014). Small crocodyliform from the Lower Cretaceous

(Late Aptian) of Central Texas and its systematic relationship to the evolution of Eusuchia. *Journal of Paleontology*, 88, 1031–1049.

Adams, T. L., Noto, C. R., & Drumheller, S. K. (2017). A large neosuchian crocodyliform from the Upper Cretaceous (Cenomanian) Woodbine Formation of North Texas. *Journal of Vertebrate Paleontology*, 37(4), e1349776.

Adams, T. L., Polcyn, M. J., Mateus, O., Winkler, D. A., & Jacobs, L. L. (2011). First occurrence of the long-snouted crocodyliform *Terminonaris* (Pholidosauridae) from the Woodbine Formation (Cenomanian) of Texas. *Journal of Vertebrate Paleontology*, 31, 712–716.

Adrian, B., Smith, H. F., Noto, C. R., & Grossman, A. (2019). A new baenid,"*Trinitichelys*" maini sp. nov., and other fossil turtles from the Upper Cretaceous Arlington Archosaur Site (Woodbine Formation, Cenomanian), Texas, USA. *Palaeontologia Electronica*, 22, 1–29.

Adrian, B., Smith, H. F., Noto, C. R., & Grossman A. (2021). An early bothremydid from the Arlington Archosaur Site of Texas. *Scientific Reports*, 11, 9555. 10.1038/s41598-021-88905-1

Adrian, B., Smith, H., & Noto, C. R. (2023). A revision of "*Trinitichelys*" *maini* (Testudines: Baenidae) and additional material of its new genus from the Lewisville Formation (Woodbine Group, Cenomanian), Texas, USA. *Palaeontologia Electronica*, 26(2), a28. https://doi.org/10.26879/1266

Ambrose, W. A.,Hentz, T. F., Bonnaffe, F., Loucks, R. G., Brown Jr, L. F., Wang, F. P., & Potter, E. C. (2009). Sequence-stratigraphic controls on complex reservoir architecture of highstand fluvial-dominated deltaic and lowstand valley-fill deposits in the Upper Cretaceous (Cenomanian) Woodbine Group, East Texas field: regional and local perspectives. *AAPG Bulletin*, 93, 231–269.

Benton, M. J. & Clark, J. M. (1988). Archosaur phylogeny and the relationships of the Crocodylia. In M. J. Benton (Ed.), The *Phylogeny and Classification of the Tetrapods Volume 1*: Amphibians, Reptiles, Birds (pp. 295–338). Clarendon Press, Oxford.

Bergquist, H. R. (1949). Geology of the Woodbine Formation of Cooke, Grayson, and Fannin Counties, Texas. 1: 63,360. U. S. Geological Survey. Oil and Gas Investigations Map OM-98.

Blender Foundation, (2002). Blender 3D creation suite version 2.8. Stichting Blender Foundation, Amsterdam, the Netherlands.

Brochu, C. A. (1996). Closure of neurocentral sutures during crocodilian ontogeny: implications for maturity assessment in fossil archosaurs. *Journal of Vertebrate Paleontology*, 16(1), 49–62.

Brochu, C. A. (2001). Crocodylian snouts in space and time: phylogenetic approaches toward adaptive radiation. *American Zoologist*, 41, 564–585.

Brownstein, C. D. (2018). The biogeography and ecology of the Cretaceous non-avian dinosaurs of Appalachia. *Palaeontologia Electronica*, 21(1), 1–56.

Buscalioni, A. D., Piras, P., Vullo, R., Signor, M., & Barber, C. (2011). Early eusuchia crocodylomorpha from the vertebrate-rich Plattenkalk of Pietraroia (Lower Albian, southern Apennines, Italy). *Zool J Linn Soc*, 163, S199-S227.

D'Amore, D. C., Harmon, M., Drumheller, S. K., & Testin, J. J. (2019). Quantitative heterodonty in Crocodylia: assessing size and shape across modern and extinct taxa. *PeerJ*, 7, e6485.

Dodge, C. F. (1952). Stratigraphy of the Woodbine Formation in the Arlington area. *Tarrant County, Texas: Field and Laboratory*, 20(2), 66–78.

Dodge, C. F. (1968). Stratigraphic Nomenclature of the Woodbine Formation Tarrant County, Texas. In C. F. Dodge (Ed.), *Field trip Guidebook, South Central Section, Stratigraphy of the Woodbine Formation, Tarrant County, Texas* (pp. 107–125). Geological Society of America.

Dodge, C. F. (1969). Stratigraphic nomenclature of the Woodbine Formation Tarrant County, Texas. *Texas Journal of Science*, 21, 43–62.

Donovan, A. D., Gardner, R. D., Pramudito, A., Staerker, T. S., Wehner, M., Corbett, M. J., Lundquist, J. J., Romero, A. M., Henry, L. C., & Rotzien, J. R. (2015). Chronostratigraphic relationships of the Woodbine and Eagle Ford Groups across Texas. *GCAGS Journal*, 4, 67–87.

Drumheller, S. K. & Wilberg, E. W. (2020). A synthetic approach for assessing the interplay of form and function in the crocodyliform snout. *Zoological Journal of the Linnean Society*, 188(2), 507–521.

Drumheller, S. K., Adams, T. L., Maddox, H., & Noto, C. R. (2021). Expanded sampling across ontogeny in *Deltasuchus motherali* (Neosuchia, Crocodyliformes) revealing ecomorphological niche partitioning and Appalachian endemism in Cenomanian crocodyliforms. Cambridge University Press.

Emerson, B. L., Emerson, J. H., Akers, R. E., & Akers, T. J. (1994). *Texas Cretaceous ammonites and nautiloids.* Houston Gem & Mineral Society, Houston, Texas, 439 pp.

Fedorov, A., Beichel, R., Kalpathy-Cramer, J., Finet, J., Fillion-Robin, J. C., Pujol, S., Bauer, C., Jennings, D., Fennessy, F., Sonka, M., & Buatti, J. (2012). 3D Slicer as an image computing platform for the Quantitative Imaging Network. Magnetic Resonance Imaging, 30(9), pp. 1323–1341.

Gignac, P. & O'Brien, H. (2016). Suchian feeding success at the interface of ontogeny and macroevolution. *Integrative and Comparative Biology*, 56(3), 449–458.

Gignac, P. M., Santana, S. E., & O'Brien, H. D. (2019). Ontogenetic inertia explains Neosuchian giants: a case study of *Sarcosuchus imperator* (Archosauria: Suchia). *Journal of Morphology*, 280, S65–S66.

Gradstein, F. M., Ogg, J. G., & Smith, A. G. (Eds.). (2004). A Geologic Time Scale 2004. Cambridge University Press, Cambridge, 500 pp.

Hay, O. P. (1930). Second Bibliography and Catalogue of the Fossil Vertebrata of North America, Volume 1. Carnegie Institution of Washington Publication 390, 990 pp.

Head, J. (1998). A new species of basal hadrosaurid (Dinosauria, Ornithischia) from the Cenomanian of Texas. *Journal of Vertebrate Paleontology*, 18, 718–738.

Hedlund, R. W. (1966). Palynology of the Red Branch Member of the Woodbine Formation (Cenomanian), Bryan County, Oklahoma. *Oklahoma Geological Survey Bulletin*, 112, 1-69.

Hentz, T. F., Ambrose, W. A., & Smith, D. C. (2014). Eaglebine play of the southwestern East Texas basin: stratigraphic and depositional framework of the Upper Cretaceous (Cenomanian-Turonian) Woodbine and Eagle Ford Groups. *AAPG Bulletin*, 98, 2551–2580.

Hill, R. V. (2010). Osteoderms of *Simosuchus clarki* (Crocodyliformes: Notosuchia) from the Late Cretaceous of Madagascar. *Journal of Vertebrate Paleontology*, 30, 154–176.

Huxley, T. H. (1875). On *Stagonolepis robertsoni*, and on the evolution of the Crocodilia. *Quarterly Journal of the Geological Society*, 31, 423–438.

Jacobs, L. L. & Winkler, D. A. (1998). Mammals, archosaurs, and the Early to Late Cretaceous transition in north-central Texas. In Y. Tomida, L. J. Flynn, & L. L. Jacobs (Eds.), *Advances in Vertebrate*

Paleontology and Geochronology (pp. 253–280). National Science Museum, Tokyo.

Johnson, R. O. (1974). Lithofacies and depositional environments of the Rush Creek Member of the Woodbine Formation (Gulfian) of North Central Texas, University of Texas, Arlington, 158 pp.

Jouve, S. & Jalil, N. E. (2020). Paleocene resurrection of a crocodylomorph taxon: biotic crises, climatic and sea level fluctuations. *Gondwana Research*, 85, 1–18.

Jouve, S., de Muizon, C., Cespedes-Paz, R., Sossa-Soruco, V., & Knoll, S. (2021). The longirostrine crocodyliforms from Bolivia and their evolution through the Cretaceous-Palaeogene boundary. *Zoological Journal of the Linnean Society*, 192(2), 475–509.

Kennedy, W. J. & Cobban, W. A. (1990). Cenomanian ammonite faunas from the Woodbine Formation and lower part of the Eagle Ford Group, Texas. *Palaeontology*, 33, 75–154.

Konzhukova, E. D. (1954). [New fossil crocodilian from Mongolia] (in Russian). *Trudy Paleontologicheskogo Instituta ANSSSR*, 48, 171-194.

Krumenacker, L. J., Simon, D. J., Scofield, G., & Varricchio, D. J. (2016). Theropod dinosaurs from the Albian-Cenomanian Wayan Formation of eastern Idaho. *Historical Biology*, 29(2), 170–186.

Lee, Y.-N. (1997). Archosaurs from the Woodbine Formation (Cenomanian) in Texas. *Journal of Paleontology*, 71, 1147–1156.

Main D. J., Parris, D. C., Grandstaff, B. G., & Carter, B. (2011). A new lungfish (Dipnoi; Ceratodontidae) from the Cretaceous Woodbine Formation, Arlington Archosaur Site, North Texas. *Texas Journal of Science*, 63, 283–298.

Main D. J., Noto, C. R., & Weishampel, D. B. (2014). Postcranial anatomy of a basal hadrosauroid (Dinosauria: Ornithopoda) from the Cretaceous (Cenomanian) Woodbine Formation of North Central Texas. In D. A. Eberth & D. C. Evans (Eds.), *Hadrosaurs* (pp. 77–95). Bloomington, IN: Indiana University Press.

Markwick, P. J. (1998a). Crocodilian diversity in space and time: the role of climate in paleoecology and its implication for understanding K/T extinctions. *Paleobiology*, 24(4), 470–497.

Markwick, P. J. (1998b). Fossil crocodilians as indicators of Late Cretaceous and Cenozoic climates: implications for using palaeontological data in reconstructing palaeoclimate. Palaeogeography, Palaeoclimatology. *Palaeoecology*, 137(3-4), 205–271.

McIlhenny EA. (1935). The alligator's life history. Boston: Christopher Publishing House.

Montefeltro, F. C., Larsson, H. C. E., de França, M. A. G., & Langer, M. C. (2013). A new neosuchian with Asian affinities from the Jurassic of northeastern Brazil. *Naturwissenschaften*, 100, 835-841.

Mook, C. C. (1934). A new species of *Teleorhinus* from the Benton Shales. *American Museum Novitates*, 702, 1–11.

NextEngine™, Inc. (2008). HD Desktop 3D scanner and ScanStudio™. NextEngine™, Incorporated, Santa Monica, California.

Noto, C. R. (2015). Archosaur Localities in the Woodbine Formation (Cenomanian) of North-Central Texas. In C. R. Noto (Ed.), *Early- and Mid- Cretaceous Archosaur Localities of North-Central Texas, Fieldtrip Guidebook for the 75th Annaul Meeting of the Society of Vertebrate Paleontology, Dallas, Texas* (pp. 38–51).

Noto, C. R., Main, D. J., & Drumheller, S. K. (2012). Feeding traces and paleobiology of a Cretaceous (Cenomanian) Crocodyliform: example from the Woodbine Formation of Texas. *Palaios*, 27, 105–115.

Noto, C. R., Adams, T. L., Drumheller, S. K., & Turner, A. H. (2019). A small enigmatic neosuchian crocodyliform from the Woodbine Formation of Texas. The Anatomical Record: ar.24174

Noto, C. R., D'Amore, D., Drumheller, S., & Adams, T. (2022). A newly recognized theropod assemblage from the Lewisville Formation (Woodbine Group; Cenomanian) and its implications for understanding Late Cretaceous Appalachian terrestrial ecosystems. *PeerJ*, 10, e12782.

Noto, C., Drumheller, S., Adams, T., Adrian, B., Smith, H., Tykoski, R., & Flaig, P. (2023a). Faunal composition, distribution, and paleobiogeography of fossil vertebrates from the Lewisville Formation (Woodbine Group, Cenomanian). 14th Symposium on Mesozoic Terrestrial Ecosystems and Biota. *Anatomical Record*, 306, 203–206. https://doi.org/10.1002/ar.25219

Noto, C., Flaig, P., Contreras, D., Zippi, P., Lorente, M., Andrzejewski, K., & Tykoski, R. (2023b). Deciphering the Woodbine Group (Late Cretaceous; Cenomanian) outcrops of the Dallas-Ft. Worth Metroplex: new data and new horizons. 14th Symposium on Mesozoic Terrestrial Ecosystems and Biota. *Anatomical Record*, 306, 206–208. https://doi.org/10.1002/ar.25219

Oliver, W. B. (1971). Depositional systems in the Woodbine Formation (Upper Cretaceous), northeast Texas. The University of Texas at Austin, Bureau of Economic Geology, Report of Investigations 73, 28 pp.

Osborn, H. F. (1904). *Teleorhinus browni*—A Teleosaur in the Fort Benton. *Bulletin of the American Museum of Natural History*, 20, 239–240.

Owen, R. (1879). Monograph on the fossil Reptilia of the Wealden and Purbeck formations. Supplement IX, Crocodilia (*Goniopholis*, *Brachydectes*, *Nannosuchus*, *Theriosuchus*, and *Nuthetes*). *Palaeontographical Society of London Monograph*, 33, 1–19.

Powell, J. D. (1968). Woodbine-Eagle Ford transition, Tarrant Member. In F. Dodge (Ed.), *Stratigraphy of the Woodbine Formation: Tarrant County, Texas*. *Field Trip Guidebook* (pp. 27–43). Geological Society of America, South Central Section, Denver.

Prieto-Márquez, A., Erickson, G. M., & Ebersole, J. A. (2016). Anatomy and osteohistology of the basal hadrosaurid dinosaur *Eotrachodon* from the uppermost Santonian (Cretaceous) of southern Appalachia. *PeerJ*, 4, e1872.

Revopoint 3D Technologies, Inc. (2014). Revopoint POP2 3D scanner and Revo Scan. Revopoint 3D Technologies, Incorporated, Shenzhen, China.

Ross, C. A. & Magnusson, W. E. (1989). Living Crocodiles. Crocodiles And Alligators., 58–73 pp.

Salas-Gismondi, R., Flynn, J. J., Baby, P., Tejada-Lara, J. V., Wesselingh, F. P., & Antoine, P. O. (2015). A Miocene hyperdiverse crocodylian community reveals peculiar trophic dynamics in proto-Amazonian mega-wetlands. *Proceedings of the Royal Society B: Biological Sciences*, 282(1804), 20142490.

Suarez C. A., Frederickson, J., Cifelli, R. L., Pittman, J. G., Nydam, R. L., Hunt-Foster, R. K., & Morgan, K. (2021). A new vertebrate fauna from the Lower Cretaceous Holly Creek Formation of the Trinity Group, southwest Arkansas, USA. *PeerJ*, 9, e12242. 10.7717/peerj. 12242

Trudel, P. (1994). Stratigraphic sequences and facies architecture of the Woodbine-Eagle Ford interval, Upper Cretaceous, North Central Texas. unpublished Master's thesis, Tarleton State University, 105 pp.

Turner, A. H. (2004). Crocodyliform biogeography during the Cretaceous: evidence of Gondwanan vicariance from biogeographical analysis. *Proc R Soc Lond B Biol Sci*, 271, 2003–2009.

Ullmann, P. V., Varricchio, D. J., & Knell, M. J. (2012). Taphonomy and taxonomy of a vertebrate microsite in the mid-Cretaceous (Albian-Cenomanian) Blackleaf Formation, southwest Montana. *Historical Biology*, 24, 311–328.

Vallabhaneni, S., Olszewski, T. D., Pope, M. C., & Heidari, Z. (2016). Facies and stratigraphic interpretation of the Eaglebine Play in Central Texas. *GCAGS Journal*, 5, 25–46.

Whetstone, K. & Whybrow, P. (1983). A 'cursorial' crocodilian from the Triassic of Lesotho (Basutoland), southern Africa. *Occasional Publications of the Museum of Natural History of the University of Kansas*, 106, 1–37.

Weishampel, D. B., Barrett, P. M., Coria, R. A., Le Loeuff, J., Xing, X., Xijin, Z., Sahni, A., Gomani, E. M. P., & Noto, C. R. (2004). Dinosaur Distribution. In D. B. Weishampel, P. Dodson, & H. Osmólska (Eds.), *The Dinosauria, second edition* (pp. 517–606).

Winkler, D., Jacobs, L., Lee, Y., & Murry, P. (1995). Sea level fluctuation and terrestrial faunal change in North-Central Texas. In A. Sun & Y. Wang (Eds.), *Sixth Symposium on Mesozoic Terrestrial Ecosystems and Biota, Short Papers* (pp. 175–177). China Ocean Press, Beijing.

Wu, X.-C., Russell, A. P., & Cumbaa, S. L. (2001). *Terminonaris* (Archosauria: Crocodyliformes): new material from Saskatchewan, Canada, and comments on its phylogenetic relationships. *Journal of Vertebrate Paleontology*, 21, 492–514.

Zanno, L. E. & Makovicky, P. J. (2011). On the earliest record of Cretaceous tyrannosauroids in western North America: implications for an Early Cretaceous Laurasian interchange event. *Historical Biology*, 23, 317–325. 10.1080/08912963.2010.543952

Zanno, L. E. & Makovicky, P. J. (2013). Neovenatorid theropods are apex predators in the Late Cretaceous of North America. *Nature Communications*, 4, 2827.

Zittel, K. A. & Eastman, C. R. (1902). *Text Book of Palaeontology.* Macmillan and Co., London, 283 pp.

APPENDIX 1. Cranial

Specimen #	Element	Max Length	Max Width	Max Height	Taxa
2013-07-0018a	Maxilla	55.21	29.25	10.46	Crocodyliform indet.
2013-07-0018b	Palate	75.05	40.80	9.64	Crocodyliform indet.
2013-07-1066	Dentary	12.46	4.56	4.9	eusuchian indet.
2013-07-2085	Dentary	17.83	6.53	5.6	eusuchian indet.
2013-07-0171	Tooth	37.61	15.69		Terminonaris sp.
2013-07-0168	Tooth	38.01	15.29		Terminonaris sp.

APPENDIX 2. Alveoli diameters

Specimen #	Alveolus position	Length (mm)	*measured anteroposteriorly*
2013-07-0018a	M-1	4.53	
	M-2	4.47	
	M-3	6.22	
	M-4	3.81	
	M-5	4.36	
	M-6	3.8	
	M-7	4.04	
	M-8	4.49	
2013-07-0018b	M-a	3.84	
	M-b	4.25	
	M-c	3.32	
	M-d	2.8	

APPENDIX 3. Vertebrae

Specimen #	Element	Max Length	Max Width	Max Height	Notes
2013-07-1779	Cervical	9.61	8.01	7.28	
2013-07-0537	Dorsal	14.36	8.09	6.46	height of neural arch 13.71
2013-07-0713	Dorsal	21.22	12.31	11.65	
2013-07-0714	Dorsal	13.45	7.55	6.86	
2013-07-0718	Dorsal	12.35	7.72	7.23	
2013-07-2064	Dorsal	15.05	7.53	8.35	
2013-07-2066	Dorsal	14.05	9.63	10.03	deep ventral keel
2013-07-2073	Dorsal	18.53	10.27	8.71	
2013-07-0056	Caudal	16.29	7.94	7.75	
2013-07-0715	Caudal	30.10	16.12	13.51	
2013-07-0716	Caudal	12.10	5.02	12.38	height of centrum 4.68
2013-07-1665	Caudal	11.05	6.68	5.73	
2013-07-2068	Caudal	13.24	6.04	8.07	
2013-07-2069	Caudal	11.07	3.16	6.76	

APPENDIX 4. Osteoderms

Specimen #	Morphotype	AP Length	ML Width	AM length	Depth	W/L ratio	AM/AP	Notes
2013-07-1269	1	19.57	16.35	7.48	5.34	0.84	0.38	
2013-07-1270	1	18.96	16.21	8.53	3.31	0.85	0.45	
2013-07-1272	1	16.63	13.15	6.36	2.69	0.79	0.38	
2013-07-1273	1	24.32	21.95	9.70	2.71	0.90	0.40	
2013-07-1274	1	27.23	21.02	9.98	3.36	0.77	0.37	
2013-07-1276	1	20.18	15.04	9.98	2.59	0.75	0.49	
2013-07-1277	1	19.61	16.45	8.39	4.59	0.84	0.43	
2013-07-1280	1	19.09	14.72	8.29	3.70	0.77	0.43	
2013-07-1283	1	24.77		10.45	3.35	0.00	0.42	Fragmentary
2013-07-1662	1	21.93	16.45	9.91	3.16	0.75	0.45	
2013-07-1946	1	19.61	19.37	7.38	3.29	0.99	0.38	
2013-07-2079	1	16.64	15.80	6.12	1.92	0.95	0.37	
2013-07-2083	1	16.77	16.24	7.18	2.60	0.97	0.43	
2013-07-2086	1	25.28	20.93	9.51	2.72	0.83	0.38	
2013-07-2087	1	26.98	20.57	11.47	4.60	0.76	0.43	
2013-07-0035	2	20.77	28.52		2.91	1.37		
2013-07-1271	2	7.62	10.41		1.97	1.37		
2013-07-1281	2	17.11	18.73		4.20	1.09		
2013-07-1439	2	9.22	14.13		1.76	1.53		
2013-07-1474	2	30.94	30.94		4.98	1.00		
2013-07-1509	2	9.31	13.67		1.79	1.47		Fragmentary
2013-07-2057	2	12.07	11.12		1.36	0.92		Fragmentary
2013-07-2065	2	19.10	22.48		3.15	1.18		shallow keel
2013-07-2074	2	8.10	12.31		1.09	1.52		shallow keel
2013-07-2075	2	10.64	12.56		1.46	1.18		Fragmentary
2013-07-2076	2	14.28	19.92		1.74	1.39		
2013-07-2077	2	14.80	15.05		1.42	1.02		strongly concave
2013-07-2080	2	15.72	18.94		2.00	1.20		
2013-07-0020	3	27.26	19.71		4.25	0.72		keel; concave
2013-07-1477	3	17.27	18.03		2.04	1.04		keel; concave
2013-07-1539	3	17.39	11.68		2.09	0.67		keel; concave; Fragmentary
2013-07-2067	3	21.00	18.91		2.57	0.90		keel; concave
2013-07-2072	3	13.19	6.89		1.09	0.52		keel; concave; Fragmentary
2013-07-2078	3	20.87	14.91		2.87	0.71		keel; concave
2013-07-2081	3	19.18	14.86		2.00	0.77		keel; concave
2013-07-2082	3	20.32	16.21		2.30	0.80		keel; concave
2013-07-1065	4	10.29	5.48		0.98	0.53		keel; concave
2013-07-2071	4	12.03	7.39		1.20	0.61		keel; concave
2013-07-0037		16.45	24.09		2.00	1.46		no keel; no art. Margin
2013-07-1562		32.74	36.28		6.91	1.11		strongly concave; keel; rounded edge

WINDOWS INTO SAUROPSID AND SYNAPSID EVOLUTION
Essays in honor of Prof. Louis L. Jacobs, pp. 120–129, 2023

LATE CARNIVOROUS DINOSAURS: HAND MODIFICATIONS, EVOLUTION, AND ECOLOGY

RINCHEN BARSBOLD*

Institute of Paleontology, Mongolian Academy of Sciences, Ulaanbaatar 15160, Mongolia; maspaleo@gmail.com

ABSTRACT Late theropods are distinguished by a variety of hand structures, divided into grasping and non-grasping types, easily identified and distinguished from each other. Both types were self-sufficient ecomorphological structures, and an ability to grasping-non-grasping is established without difficulty and unambiguously. The grasping hand is predetermined by predation, while functions of a non-grasping hand often remain undefined, retaining its evolutionary and ecological significance. A three-digited grasping hand is an exemplary grasping pattern in dromaeosaurids with a fixed pulley-like structure limiting dislocation and "late basal" oviraptorosaurs. The absence of a pulley-like joint in a non-grasping hand increased mobility and risk of dislocation. The fused pulley-like joint indicates its ultimate fixation. Two-and single-digited hands testify in favor of its non-grasping ability. Transformation of food preferences seems acceptable as a direction for interpreting the functions of giant hands that fall out of regularity in theropod evolution, suggesting the appearance and evolution of "terrible-handed" dinosaurs. Hand modifications reached different levels of completeness, perfection, and distribution in the late theropods of North America, China, and Mongolia; some examples of the latter were almost exemplary. Hand modifications were more likely the "last" innovations in the theropod evolution, and the non-predatory theropods probably opened the way to unpredictable relationships in the late dinosaur communities, but the "great extinction" ended their history as a whole.

KEYWORDS Late theropods, Hand modifications, Grasping, Non-grasping ability, Food preferences

INTRODUCTION

During the Cretaceous time, the carnivorous dinosaurs, so-called the late theropods, underwent various morphological changes, which reached a high level in the second half of the period. Here only the modifications of their hand (manus) are touched upon, which became more diverse, highly specialized, and therefore more narrowly functional. At first glance, the hand structures seem to be only a small part of their morphology, which had no special significance in the historical development of their bearers. However, the modifiable hand outlines some regularities in the morphological evolution of theropods. The regularities are formulated as follows: modifications signify an evolution and, with a high probability, reflect an ecology that is generally accepted, although, in reality, it is far from being known. Thus, hand modification and diversity are significant to a certain extent, as they were an indicator of both phenomena – evolution and ecology. The question seems inevitable – is it necessary to consider hand modification if it already indicates both of them? At the same time, it would be too simple if the ecology of the environment and organisms were revealed so easily. Modifications only generally indicate the probability of environmental differences without disclosing their content. These issues and related details are considered below.

The mentioned regularities reflect the following directions in the evolution of carnivorous dinosaurs: first, a mosaic combination of more generalized and more specialized characters; second, a transformation of food preferences. Regularities reached varying degrees of completeness, perfection, and distribution among the late theropods of North America, China, and Mongolia. Sometimes Mongolian samples were more indicative and often used here as the most illustrative examples (Barsbold, 2019). However, traditional understanding of functional morphology often remained limited due to a lack of knowledge.

DROMAEOSAURID HAND

The theropod hand was defined almost from the beginning,

*Corresponding author

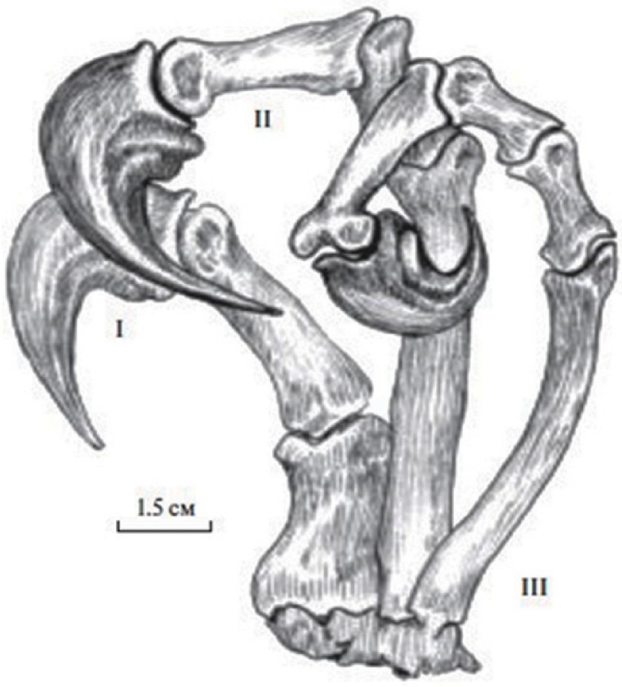

FIGURE 1. *Velociraptor*: left hand, exemplary-grasping type in flexor view. I-II-III - digits and metacarpals.

as grasping (Fig. 1), in contrast to the herbivore hand, whose actions are still little known. The ability of the hand to grasp objects is easily recognized by its structure. Morphological innovations of the theropod hands reaching their highest level by the second half of the Cretaceous were most likely the "last" in their evolution, representing samples of an even narrower specialization. The functional features of the late theropod hand became widely known, first of all, on an example of *Deinonychus* (Ostrom, 1969), the third in a row member of the dromaeosaurid family. Its first two species remained for almost half a century without movement and in full obscurity in the museum collections. Based on the first three co-family species, it was possible to identify and recreate the previously unknown structures and their functional capabilities across the whole family.

Most remarkably, interpretations of the possible functions of the hand (and foot) as a weapon of attack and defense were fully confirmed definitely by the uniquely interpreted location of these structures in dromaeosaurid *Velociraptor* Osborn 1923, one of the first theropods discovered in Mongolian Gobi, and one of two participants in the unique find of the "Fighting Dinosaurs" (Fig. 2). This happy confirmation is an almost impossible, unheard-of phenomenon in the history of vertebrate paleontology, as is the uniqueness of the "Fighting Dinosaurs" (Barsbold, 1974, 1988) so far. In this remarkable find, the hands of the carnivore *Velociraptor* (in addition to the highly specialized feet) demonstrated their functional role as effective organs for capturing a victim/enemy (Ostrom, 1969). The hand with an extremely high degree of grasping and pointed claws pierced the tissues, firmly holding the *Protoceratops* head from both sides, leaving the victim no hope of escaping from the deadly embrace of a predator. So, the weapon functions of dromaeosaurids were firstly determined in *Deinonychus* (Ostrom, 1969), but without the "Fighting Dinosaurs," these functional interpretations could turn out to be only rather successful conclusions, having remained largely speculative and divorced from a reality. Fortunately, this not happened.

Here there is no need to touch further on the various weaponry structures of the dromaeosaurids, which are beyond the scope of this consideration. Further, only the late theropod hand is touched upon, which, first, retained the "late basal" structure in more generalized groups and, second, in the specialized branches, was subject to significant shifts of changes. These more basal and equally advanced traits also fall under the two evolutionary lines outlined above (here briefly named) - a mosaic of features and transformation of food. The different mosaic features (previously known) and the transformation of food (known recently) are more concerned with the variability of the hand and its possible adaptations to the changeable environment. The established hand modifications are narrowly specialized, while other branches retain signs of more generalization, named further "late basal." This hand development is a natural consequence of morphological evolution and, more importantly, corresponds to changes in ecology in niches presented, which are not always accurately defined. Hand modifications are directly related to evolution, which is definitely and often obvious, and to the ecology of the environment, which is most indefinite and not obvious at all, considered below.

Thus, in the late theropods, thanking the example of the "Fighting Dinosaurs," a more generalized hand in a typical form represents a three-digited structure (I-II-III), which is capable of significant bending (providing a better "girth"), which created a powerful grasping effect, further enhanced by curved pointed claws. The ability of the hand to grasp objects is easily recognized by its structure. The hand has been specially adapted to perform the function of a strong

FIGURE 2. "Fighting Dinosaurs": *Velociraptor* (on the right) vs. *Protoceratops*. Predator uses its exemplary-grasping hands (along with the attacking means of the feet).

grip on the victim/enemy, thereby significantly limiting its possible counteraction. The further fate of the victim/enemy was indeed in the clutches of the predator, wonderfully demonstrated by the "Fighting Dinosaurs."

OVIRAPTOROSAURID HAND

The probable capacity for similar functions of the similarly built three-digited hand in other groups of carnivorous dinosaurs becomes high and is illustrated by the number of their branches. Among the late theropods, the hands of oviraptorosaurs (Oviraptorosauria) were the most illustrative, showing not only a typical three-digited grasping type in the "late basal" branch but also represented, in contrast to dromaeosaurids, a complete loss of the grasping ability in their advanced lines attributed to the family Ingeniidae (Barsbold, 1981, 1983). Hand modifications of the flight and swim-oriented dromaeosaurids (Lü and Brusatte, 2015; Cau et al., 2017), not considered here, were independent groups and represented, especially, in the first case, the most radical variability to conquer a special environment sphere. Perhaps, the swimming group needs more confirmation.

The grasping manus of dromaeosaurids (Ostrom, 1969) and more generalized "late basal" oviraptorosaurs (Clark et al., 2001) are practically indistinguishable from each other, being, perhaps, the highest expression of the grasping function and both representing an exemplary - grasping pattern. Dromaeosaurids and generalized oviraptorosaurs should probably be attributed to the niche of the typical attacking predators (remember "Fighting Dinosaurs," even if it was an accident).

The "late basal" oviraptorosaurs include relatively large and small forms, respectively, almost a third more (*Citipati*) and half less than dromaeosaurids (ingeniids). Small oviraptorosaurs were formerly assigned to Ingenia and Ingeniidae (Barsbold, 1981,1983), among which both more generalized (Fig. 3) and more specialized (Figs. 4, 5) forms are distinguished. Perhaps, the classification of ingeniids needs to be revised. The clear difference in the structure of an unmodified and modified hand indicates an equal difference in their functions: in the first case, the hand corresponds to the grasping, preserving

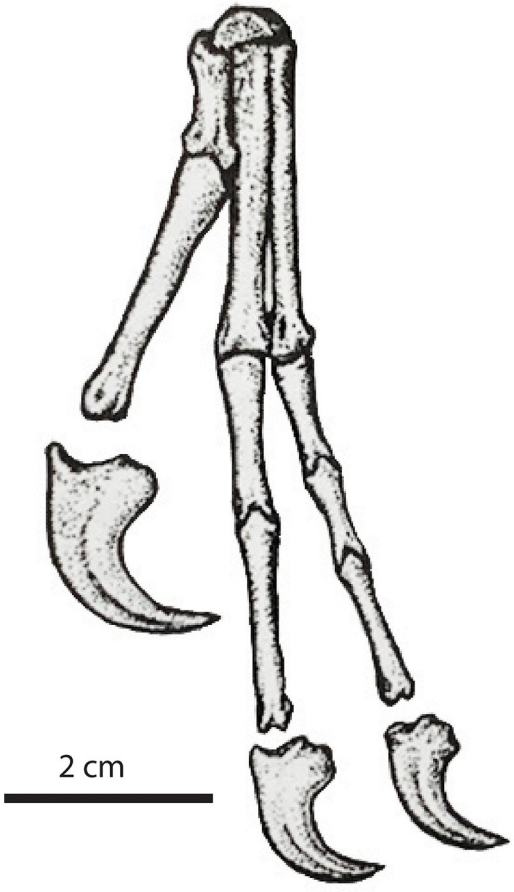

FIGURE 3. Unknown sp. of the small "late basal" Oviraptorosauria: right manus in dorsal view. Digits and their ungual phalanges are typical for a grasping hand. Assigned to Ingenia, most likely belongs to yet unidentified genus. The scale bar equals 2 cm (from Osmólska et al., 2004, fig. 8.4).

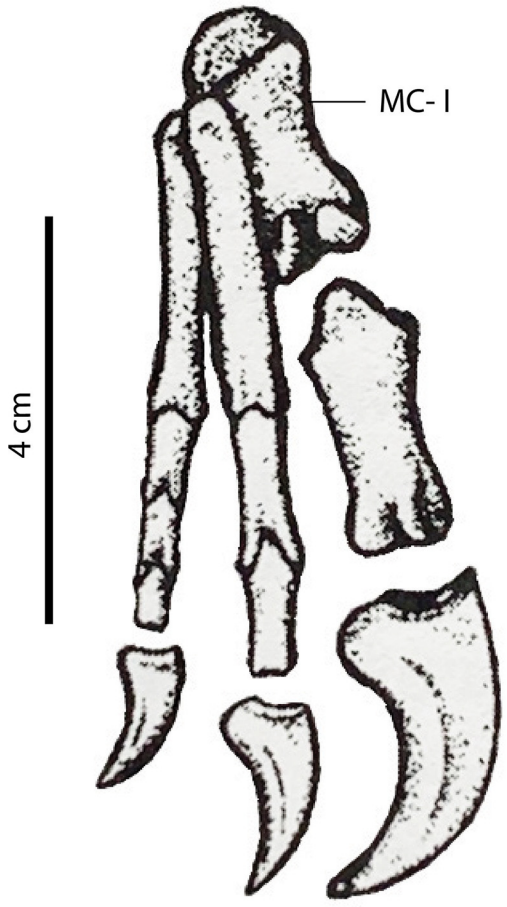

FIGURE 4. Ingeniid sp. (advanced Oviraptorosauria): right manus not grasping in dorsal view; mc I -metacarpal I. Lateral digits (II, III) are reduced (length almost equal to the first I), their ungual phalanges on straightening. The scale bar equals 4 cm (from Osmólska et al., 2004, fig. 8.3)

the main features of this type - inequality in the size of the first and two lateral digits, all with the certain signs of grasping ability. In the second, the hand is completely incapable of grasping: the hand is reduced, digit I is largest, the other two are almost equal in size, their ungual phalanges reduced and straightened. The clear difference in the structure of an unmodified and modified hand indicates an equal difference in their functions: in the first case, the hand probably possesses sufficient grasping ability, albeit inferior to larger oviraptorosaurs, like *Citipati*. In the second, the hand is completely incapable of grasping. Hence the first conclusion is: that there are at least two types of hand structure – grasping (Figs. 1, 3) and non-grasping (Figs. 4, 5). The functions of the grasping type are thoroughly defined above in dromaeosaurids (and "late basal" oviraptorosaurs, both large and small), including most clearly visible in the repeatedly mentioned "Fighting Dinosaurs."

FUNCTION OF NON-GRASPING HAND

An inevitable question - what are the functions of a non-grasping type? Various options are possible here, including those that depend to a certain extent on the imagination of researchers. There may be several acceptable real options, in case not so many. What follows are three main points regarding possible functions. First, in almost all variants, the functions of a non-grasping hand often remain indeterminate, and its actions are often not recognizable exactly. Although, for the interests of the case, an acceptable definition of the functions is certainly desirable. Second, the presence or

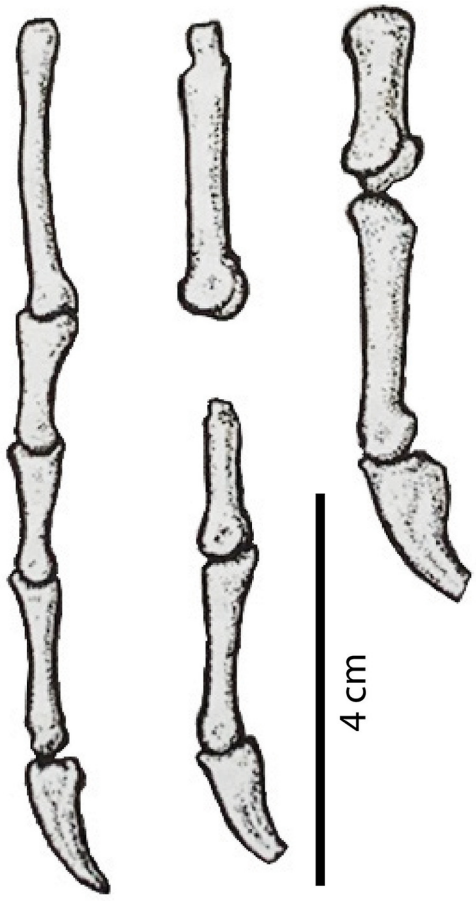

FIGURE 5. *Conchoraptor* (family Ingeniidae, advanced Oviraptorosauria): right hand not grasping, in medial view, metacarpals and digits reduced in size, thinned, ungual phalanges straightened. The scale bar equals 3 cm (from Osmólska et al., 2004, fig. 8.4).

absence of grasping ability in the vast majority is easily and accurately established: the size and shape of the hand, as a whole, then, digits and ungual phalanges, their mutual proportions make it possible to quickly and unambiguously determine whether the hand is grasping, or not. Third, for all the functional uncertainty of the non-grasping hand, its evolutionary and ecological significance does not underestimate. In ecology, much remains uncertain, although precisely this uncertainty serves (for researchers) as a warning sign of possible changes in the newly opened niches presented to the dinosaurs. Basal oviraptorosaurs with a well-pronounced grasping hand did not change the general type of feeding. The absence of teeth and the development of a horny beak may reflect the transformation of the food spectrum, but the methods of obtaining it can be variable. For example, modern flying theropods - birds of prey are equipped with a hook-shaped beak, being the predators. The "late basal" oviraptorosaurs had a massive beak, and usual grasping hands, that were probably adapted to the predation (Barsbold, 1983). The advanced branch (twice - three times smaller in size, as mentioned) with a less massive beak had a modified hand incapable of grasping. The structure of such a hand could suggest the development of a leathery (swimming) membrane. Of course, this is only one of the shaky assumptions, but consisting of the elongation of the spinal processes of the caudal vertebrae, which turns the tail into a swimming organ. Didn't specialized ingeniids feed on mollusks not capable of active resistance and living in abundance in the Late Cretaceous lakes (Martinson, 1982; Barsbold, 1983), thereby changing their habitat and preserving the predator lifestyle, but adapted to the new conditions? Basal oviraptorosaurs with a well-pronounced grasping hand did not change the general type of feeding. The hand modifications' examples of narrow specialization potentially contain supposed orientations in these conditions. In addition to the typical three-digited hand in theropods, another phenomenon of variability, as a reduction of the digit number took place-to two digits in tyrannosaurids and advanced oviraptorosaurs and, at least, in one alvarezsaurid (Bonaparte, 1991) species to one. Previously, these characters were known in tyrannosaurids at first, and later the examples of reduction gradually increased. The well-known two-digited hand in tyrannosaurids usually not raised any questions, although so far, the functions of their greatly reduced and shortened forelimbs have not found an acceptable explanation. The grasping ability of the two-digited hand was fully lost, being usually accepted even without taking into account its structure, which really hardly contained this ability with such a reduction in the forelimbs. Maybe, the loss of grasping and reduction of the forelimbs indicated a transition of the tyrannosaurids into the niche of scavenger predators (Edwin Colbert's remark that a tyrannosaurid was a mouth set on its hindlimbs). It is only about the main direction of their adaptation, but tyrannosaurid's food preferences could include dead animals and food objects caught by them, which is typical of the recent predators (Farlow & Holtz, 2002).

In the exemplary - grasping hand in dromaeosaurids, the numerically reduced carpal elements formed with metacarpals a "pulley"-like connection (Ostrom, 1969), which simplified and "modernized" this important joint allowing both mobility freedom of the hand and its strong fixation. This joint

protected the predator's hand from dislocation due to sudden movements of the prey/enemy in order to free themselves from the deadly embrace of the predator. On the contrary, the extended participation of carpal elements (often up to 5, what's a typical "non-pulley" structure) in this joint forms a connection of the non-grasping hand with more freedom of mobility, more disorderly and much less fixation, and therefore more prone to dislocation (Barsbold, 1983). Such a joint is observed in Mongolian ornithomimids and tyrannosaurids (*Tarbosaurus*), which had a non-grasping ("non-pulley") hand, although in earlier works non-Mongolian ornithomimids, as a rule, were traditionally called grasping, and reconstructed, as grabbing their food objects, which now seems hardly acceptable. In extreme cases, their hand could occupy an intermediate position; however, this option has not yet been met; perhaps, they preserved (in vivo?) rarely, being probably maladaptive.

DISCUSSION

Approximately a dozen scattered remains of carpometacarpals found in a large area of Nemeget deposits in the Gobi, forming the completely fused pulley-like structure (Fig. 6), eliminating any mobility at this point of the hand. At first glance, such an unusually strong fusion, not seen before, suggested teratology in the hand of its bearers. However, the multitude of these remains testified with a greater probability that this fusion was not accidental and most likely represented the creation of a monolithic unity of metacarpal-carpal elements, which increased fixation to the complete exclusion of any mobility in the former joint. In this way, the possibility of any dislocations in the grasping hand was excluded since the articular connection was no longer in reality. With the resistance of the victim/enemy, the bones of the hands and forelimbs would be more likely to be broken than these monolithic joints dislocated.

It can be assumed that in a lifetime, this small but important region of the hand joint was often subjected to dislocations, which could serve as a challenge to strengthen this weak point, which would be a significant win for the predator. Doesn't this testify in favor of the fact that the grasping hand, as a weapon of attack and defense, often came into action, and the victim/enemy captured by it in the category of size and weight was at least not inferior to the predator, capable of active resistance and in attempts to free

FIGURE 6. Unidentified small "late basal" oviraptorosaur: metacarpals and carpals (medial-dorsal view) were completely fused, greatly restricting mobility freedom and protecting against dislocation in the joint. MC I - metacarpal I; pulley-like joint shown by arrow.

itself had a strong impact on the grasping hands up to dislocating or breaking off its weak point? An increase in the fixation of this point towards solidity and hardening was noted above in the pulley structures of dromaeosaurids. However, the structures of the hand considered here are more similar to those of specialized oviraptorosaurs (Ingenia) mentioned above, which could suggest that the hand was oriented towards a very strong, immovable connection in some of them (Barsbold, 1981). Unfortunately, the digits and ungual phalanges have not been preserved, so the question of the grasping - non-grasping in this curious case remains open. It seems unlikely this is a mass disease within one species over such a wide area. In any case, with or without grasping ability, this phenomenon could be a clear sign of a probable radical modification of the hand in one of the still-unknown late theropods.

Other apparently radical modifications include unusual

FIGURE 7. *Therizinosaurus*: ungual phalange probably of digit I, medial view about 0.7 m long (Maleev, 1954).

hand structures (and forelimbs) in *Therizinosaurus* and *Deinocheirus* (Rozhdestvenskiy, 1970; Barsbold, 1974; Lee et al., 2014), from the very beginning, separately assigned to independent families of therizinosaurids and deinocheirids correspondingly (Maleev, 1954; Osmólska and Roniewicz, 1970). Their hands were distinguished by gigantism, which was not previously found in theropods but differed sharply from each other (Figs. 7, 8). The former had laterally flattened ungual phalanges up to 0.7 m long, while the latter was half as large and very massive. One glance is enough that these hands are completely outside the grasping ability: their general structure, dimensions, shape, and proportions of the digits and ungual phalanges, in particular, clearly indicate an impossibility of any form of grasping or, holding a food object with the help of digits and claws, and even more so actively counteracting enemy.

For many decades these unusual giants remained the most mysterious Mongolian dinosaurs, although *Deinocheirus* (but not *Therizinosaurus*), now represented by almost complete skeletal material (Lee et al., 2014), went through its second discovery and its long-distinguished position was assigned to ornithomimosaurs. The first discoverers (H. Osmólska, personal communication) also suggested a possible assignment of *Deinocheirus* to ornithomimosaurs, the most numerous part of which (actually ornithomimids) are probable herbivores (Kobayashi et al., 1999; Chinzorig et al., 2017), in any case reflecting changes in the environment, and likely related approaches to the consumption of its resources. Stomach stones have been found in ornithomimids, and deinocheirids were not bypassed by this, being related to ornithomimosaurs. This adaptation is considered an indicator of herbivory, even though the recent crocodiles, which can hardly be classified as vegetarians, and some birds of prey are found to have stomach stones (according to Y.-N. Lee, stomach stones are also found in Mongolian *Tarbosaurus*). Perhaps, the presence of stomach stones is not so simple a phenomenon unequivocally deciding the food preferences, which seem to have led some late theropods into vegetarian niches. The reasons are unknown; one can name the increased competition for consumption (old-fashioned fight for food), an abundance and variety of plant foods, and the emergence of new resources (for example, angiosperms). Whatever the reasons

FIGURE 8. *Deinocheirus*: both forelimbs and right manus (front left) with the massive ungual phalanges. The first ungual phalange (shown by arrow) is about 35 cm long.

for the appearance of these strange reptiles, such an unusual developmental path only emphasizes the evolutionary and ecological potential of the late theropods and is an indicative sign of hand modifications in general. The gigantic size and theropod appearance of these "terrible-handed" theropods probably served as self-defense for them. Consumption of plant foods, if it was in reality, should have led to considerable changes in their digestive system (almost imperceptible in the fossil state) and other, taphonomically more accessible parts of their morphology (Xu et al., 2002; Zhou & Zhang, 2002; Barrett, 2005; Barrett & Rayfield, 2006; Chinzorig et al., 2017). However, the hand functions of both giants remain unshakably undefined, especially in *Therizinosaurus* ("Lizard mowing the grass," Maleev, 1954).

More than a decade ago, the classification, possible family ties, and ecological features of these dinosaurs were raised based on incoming new material in search of a way out of established ideas led to the most successful path - to a new approach in the evolutionary orientation of "terrible-handed" dinosaurs, exemplified the transformation of food preferences (Paul, 1984; Kirkland & Wolfe, 2001; Zhang et al., 2001; Li et al., 2007; Zanno, 2010) – mainly from carnivore to herbivore (Russel & Russel, 1993; Zanno et al., 2009; Zanno, Makovicky, 2011). The variety of vegetation could also suggest its differences, as food for "terrible-handed." But the most important is the transformation of food (Lautenschlager et al. 2013; Lautenschlager 2014), which serves as an acceptable explanation for the appearance of such unusual modifications of the hand (and how this food is consumed): it completely loses its no longer necessary grasping and acquires non-grasping function in probable accordance with the class of vegetable food and possible ways of its consumption. Some Mongolian examples (advanced oviraptorosaurs, as mentioned) may suggest a food change within predation (eating mollusks). Hand modifications demonstrate a simple and revealing approach to some peculiarities of the late ecosystems, whose dinosaur communities are now well known in contrast to many features of their ecology, consumption of the food resources, and environment as a whole.

Such a radical change outlines a way out of a hopeless situation for decades. Although the hand functions are not really defined, this uncertainty indicates the presence of a non-grasping hand, as established in all the above examples, and appears to be equally significant and self-sufficient in an evolutionary and ecological sense (Weishampel & Norman, 1989; Russell & Russell 1993; Kirkland et al., 2005), of course, being not free from the inherent problems of the non-grasping hand.

CONCLUSION

Late theropods are distinguished by a variety of hand structures, divided into grasping and non-grasping types, easily identified and distinguished from each other. Both types appear to be self-sufficient ecomorphological structures, the first fully adapted for grasping, the second for non-grasping. The ability to grasping-non-grasping is established without difficulty and unambiguously. The functions of the grasping hand are predetermined by predation, while those of the non-grasping hand most often remain completely undefined, nevertheless retaining its evolutionary and ecological significance. Like most other modifications, these reflect the movement of evolution, which is certain and obvious, and the ecology, which is often indefinite, indefinable, and therefore not obvious. The three-digited grasping hand is an exemplary-grasping pattern (as in dromaeosaurids and "later basal" oviraptorosaurs). In the exemplary-grasping hand, the carpal elements are reduced to two, constituting the pulley-like structure of the fixed connection, limiting the risk of dislocation. An increase in the number of carpal elements expands the freedom of movement in the joint, thereby increasing the risk of dislocation. The complete fusion of the metacarpal-carpal elements in the pulley joint indicates its ultimate fixation. The two- and single-digited hand correspondingly with a change in the remaining digits also testifies to its non-grasping ability. The transformation of food preferences seems acceptable as a general direction for interpreting the functions of giant and unusual hands, presumably indicating an infrequent and rather strange orientation that falls out of regularity in the late theropod evolution. This orientation suggests the possible consequences of the appearance and evolution of "terrible-handed" dinosaurs in the communities by the end of the Cretaceous. Perhaps, an intensification of the food competition and an abundance of diverse vegetation (including angiosperms) created favorable conditions for entry into the new consumer's spheres, formerly predatory groups, but capable of radical changes, which developed relationships never existed before in the late organic communities.

Manual structures and their significant and varied modifiability (in balance with all other features) outlined two established directions of the theropod evolution: a mosaic of more generalized and specialized features and a transformation of food preferences. All these features reached different levels of completeness, perfection, and distribution among the late theropods of North America, China, and Mongolia, some of which were almost exemplary. Much later, the evolutionary hand transformations are determined by their ecomorphology, primarily indicating a change in ecology and clearly stated in the evolution of the late theropods. Much later, it was discovered that hand modifications are the simple way of an attempt to define the late ecosystems, the dinosaur communities of which became now well known (like other organic groups), being more refined over time, but unlike many specific conditions of the environment.

The hand structure reached its development to a modifiable ecomorphological pattern, evolutionarily fixed in the late theropods, the functions of which were determined initially. Freedom from locomotion opened the way to diversity in structure, among which the non-grasping modifications were developed in various ways, leading to deviations in the evolution and ecology of their bearers. These modifications showed significant innovations, probably almost the "last" in the evolution of the late theropods. The appearance of probable non-predatory theropods of various, especially gigantic sizes, and generally retaining a theropod appearance could open the way to unpredictable relationships in the late dinosaur communities if not for the "great extinction" that ended the Cretaceous period and an entire Mesozoic history of the dinosaur evolution.

LITERATURE CITED

Barsbold, R. (1981). Toothless carnivore dinosaurs of Mongolia. Proceedings of Soviet-Mongolia Joint Expedition. *Nauka*, 15, 28–39. (in Russian).

Barsbold, R. (1983). Carnivorous dinosaurs of the Cretaceous of Mongolia. Proceedings of Soviet-Mongolia Joint Expedition. *Nauka*, 19, 1–120. (in Russian).

Barsbold, R. (2016). "The fighting dinosaurs ": The position of their bodies before and after death. *Paleontological Journal*, 50(12),

1412–1417.

Barsbold, R. (2019). On the evolutionary morphology of the Cretaceous carnivorous dinosaurs of Mongolia (Dinosauria, Theropoda). *Journal of General Biology*, 80(4), 297–306. (in Russian).

Barrett, P. M. & Rayfield, E. J. (2006). Ecological and evolutionary implications of dinosaur feeding behaviour. *Trends in Ecology & Evolution*, 21(4): 217–224.

Bonaparte, J. P. (1991). Fossil vertebrates of the Rio Colorado Formation, from the city of Neuquen and surroundings, Late Cretaceous, Argentina. *Magazine of the Argentine Museum of Natural Sciences "Bernardino Rivadavia"*, 4, 15–123.

Cau, A., Beyrand, V., Voeten, D. F. A. E., Fernandez, V., Tafforeau, P., Stein, K., Barsbold, R., Tsogtbaatar, K., Currie, P. J., & Godefroit, P. (2017). Synchrotron scanning reveals amphibious ecomorphology in a new clade of bird-like dinosaurs. *Nature*, 552, 395–399.

Chinzorig, T., Kobayashi, Y., Tsogtbatar, K., Currie, P. J., Takahashi, R., Tanaka, T., Iijima, M., & Barsbold, R. (2017). Onithomimosaurs from the Nemegt Formation of Mongolia: Manus morphological variation and diversity. *Palaeogeography Palaeoclimatology Palaeoecology*, 494, 91–100.

Clark, J. M., Norell, M. A., & Barsbold, R. (2001). Two new (Theropoda: Oviraptorosauria), Upper Cretaceous Djadokhta Formation, Ukhaa Tolgod, Mongolia. *Journal of Vertebrate Paleontology*, 21(2), 209–213.

Farlow, J. O. & Holtz, T. R., Jr. (2002). The fossil record of predation in dinosaurs. *Paleontological Society Papers*, 8, 251–265.

Kirkland, J. I. & Wolfe, D. (2001). First definitive therizinosaurid (Dinosauria: Theropoda) from North America. *Journal of Vertebrate Paleontology*, 21, 410–414.

Kirkland, J. I., Zanno, L. E., Sampson, S. D., Clark, J. M., & DeBliex, D. D. (2005). A primitive therizinosauroid dinosaur from the Early Cretaceous of Utah. *Nature*, 435, 84–87.

Kobayashi, Y., Lü, J.-C., Dong, Z.-M., Barsbold, R., Azuma, Y., & Tomida, Y. (1999). Herbivorous diet in an ornithomimid dinosaur. *Nature*, 402, 480–481.

Lautenschlager, S. (2014). Morphological and functional diversity in therizinosaur claws and the implications for theropod claw evolution. *Proceedings of the Royal Society of London, Series B*, 281, 2014.0497.

Lautenschlager, S., Witmer, L. M., Perle, A., & Rayfield, E. J. (2013). Edentulism, beaks, and biomechanical innovations in the evolution of theropod dinosaurs. *PNAS*, 110, 657–662.

Lee, Y-N., Barsbold, R., Currie, P. J., Kobayashi, Y., Lee, H.-J., Godefroit, P., Escullie, F., & Chinzorig, T. (2014). Resolving the long-standing enigmas of a giant ornithomimosaur *Deinocheirus mirificus*. *Nature*, 515, 257–260.

Lü, J. & Brusatte, S. L. (2015). A large, short-armed, winged dromaeosaurid (Dinosauria: Theropoda) from the Early Cretaceous of China and its implications for feather evolution. *Scientific Reports*, 5, 11775.

Maleev, E. A. (1955). Giant carnivorous dinosaurs of Mongolia. *Report Academy of Sciences of the USSR*, 104(4), 634–637.

Matthew, W. D. & Brown, B. (1922). The family Deinodontidae, with notice of a new genus from the Cretaceous of Alberta. *Bulletin of American Museum of Natural History*, 46(6), 367–385.

Osborn, H. F. (1905). *Tyrannosaurus* and other Cretaceous carnivorous dinosaurs. *Bulletin of American Museum of Natural History*, 21, 259–265.

Osmólska, H. & Roniewicz E. (1970). Deinocheiridae, a new family of theropod dinosaurs. *Paleontologia Polonica*, 21, pp. 5–19.

Paul, G. S. (1984). The segnosaurian dinosaurs: Relics of the prosauropod-ornithischian transition? *Journal of Vertebrate Paleontology*, 4, 507–515.

Rozhdestvenskiy, A. K. (1970). On the gigantic ungual phalanges of the enigmatic reptiles of the Mesozoic. *Paleontologicheskii Zhurnal*, 1, 131–141.

Russell, D. A. & Russell, D. E. (1993). Mammal–dinosaur convergence. Evolutionary convergence between a mammalian and dinosaurian clawed herbivore. *Research and Exploration*, 9, 70–79.

Weishampel, D. B. & Norman, D. B. (1989). Vertebrate herbivory in the Mesozoic: Jaws, plants, and evolutionary metrics. In J.O. Farlow (Ed.), *Paleobiology of the dinosaurs* (pp. 87-100). Geological Society of America Special Paper 238.

Xu, X., Norel, M. A., Wang, X. L., Makovicky, P. J., & Wu, X. C. (2002). A basal troodontid from the Early Cretaceous of China. *Nature*, 415, 780–784.

Zanno, L. E., Gillette, D. D., Albright, L. B., & Titus, A. L. (2009). A new North American therizinosaurid and the role of herbivory in 'predatory' dinosaur evolution. *Proceedings of the Royal Society of London, Series B*, 276, 3505–3511.

Zanno, L. E. & Makovicky P. J. (2011). Herbivorous ecomorphology and specialization patterns in theropod dinosaur evolution. *PNAS*, 108, 232–237.

Zanno, L. E., Tsogtbaatar, K. Chinzorig, T., & Gate, T. A. (2016). Specializations of the mandibular anatomy and dentition of *Segnosaurus galbinensis* (Theropoda: Therizinosauria). *PeerJ*, 4, e1885.

Zhang, X.-H., Xu, X., Sereno, P., Kuang, X.-W., & Tan L. (2001). A long-necked Therizinosauroid dinosaur from the Upper Cretaceous Iren Dabasu Formation of Nei Mongol, People's Republic of China. *Vertebrata PalAsiatica*, 39, 282–290.

Zhou, Z. & Zhang, F. (2002). Largest bird from the Early Cretaceous and its implications for the earliest avian ecological diversification. *Naturwissenschaften*, 90, 220–225.

WINDOWS INTO SAUROPSID AND SYNAPSID EVOLUTION
Essays in honor of Prof. Louis L. Jacobs, pp. 130–139, 2023

FIRST RECORD OF AN ABELISAURID (DINOSAURIA, THEROPODA) NATURAL ENDOCAST, AND COMMENTS ON SKULL ROOF ORNAMENTATION

ARIANA PAULINA-CARABAJAL[1,*], KAREN ULLOA-GUAIQUÍN[1], LEONARDO S. FILIPPI[2], ARIEL H. MÉNDEZ[3], and YUONG-NAM LEE[4]

[1]Instituto de Investigaciones en Biodiversidad y Medioambiente (CONICET-Universidad Nacional del Comahue), S. C. de Bariloche (8400), Argentina, a.paulinacarabajal@conicet.gov.ar; ulloaka@comahue-conicet.gob.ar;
[2]CONICET-Museo Municipal "Argentino Urquiza", Chos Malal 1277, 8319, Rincón de los Sauces, Neuquén, Argentina, lsfilippi@gmail.com;
[3]Instituto Patagónico de Geología y Paleontología (CCT CONICET-CENPAT), Bv. Brown 2915, 9120, Puerto Madryn, Chubut, Argentina, amendez@cenpat-conicet.gob.ar;
[4]School of Earth and Environmental Sciences, Seoul National University, Seoul 08826, South Korea

ABSTRACT We present here a natural cranial endocast assigned to an abelisaurid theropod found in Cretaceous rocks of the outcropping Bajo de la Carpa Formation (Santonian) in Neuquén Province, Northern Patagonia, Argentina. The specimen was found in association with fragmentary braincase remains, which include an otic capsule and part of the skull roof. These fragments bear abelisaurid features that support the taxonomic assignment. The general shape of the endocast is similar to that in other abelisaurids, being anteroposteriorly elongated with long and robust olfactory tract and olfactory bulbs, rounded cerebral hemispheres, and pronounced and triangular dural peak. It is the second natural endocast described for a dinosaur in Argentina and the first for a theropod. The comparison with other Patagonian abelisaurids indicates the endocast belonged to a small to mid-sized specimen that highly resembles that of *Viavenator* and *Llukalkan*. However, the skull roof ornamentation is markedly different, and comments are made on certain features of the ornamentation of the frontal in the new specimen and other close relatives.

KEYWORDS Paleoneurology, Abelisauridae, Argentina

INTRODUCTION

Natural cranial endocasts (*Steinkern*) are rare in the fossil record of vertebrates in general but are even rarer for terrestrial taxa, especially for reptiles (e.g., Hopson, 1979; Jerison, 2009; Dozo et al., 2023 and references therein). This particular kind of endocast corresponds to physical casts of the endocranial cavity (the space occupied in life by the brain and related soft tissues), which were formed naturally during the taphonomic process. Isolated natural endocasts result when the sediment filling the endocranial cavity is lithified, becoming hard enough to survive the erosion of the surrounding skull bones. However, in the face of the systematic and widespread absence of natural endocasts, paleoneurologists have been constructing physical endocasts for well over a century (e.g., *Stegosaurus*, Marsh 1880; *Iguanodon*, Andrews 1897; *Tyrannosaurus*, Osborn 1912). These early endocasts were initially cast using plaster first, and later took advantage of latex and silicone as casting materials. It was Othniel C. Marsh, a pioneer worker in dinosaur paleoneurology, who studied around a dozen of dinosaur cranial endocasts, including sauropods, theropods, and ornithischians from North America (e.g., Marsh, 1881, 1884a,b, 1890,1894, 1896). Nowadays, digital techniques, such as computed tomography, allow paleontologists to construct digital 3D models that, in turn, can be made into physical objects using 3D printing--regardless of whether or not the endocranial cavity is filled with sediment.

Today, the neuroanatomy of more than 150 dinosaur taxa have been studied using both natural and artificial (physical or digital) endocasts (see an actualized list of studied dinosaur endocasts in Paulina-Carabajal et al., 2023; Burch et al., in press). Natural endocasts, however, represent less than 5 percent of the total sample, and thus, paleoneurology

*Corresponding author

studies based on natural endocasts of dinosaurs are remarkably few. These include the ceratopsian *Anchiceratops* (Brown, 1914), two iguanodontids (Serrano Barañas et al., 2006; Brasier et al., 2016), the duckbill *Edmontosaurus* (Jerison, 2009), the partially exposed dorsal cerebrum of the ornithopod *Leaellynasaura amicagraphica* (Rich and Rich, 1989), an indeterminate dicraeosaurid sauropod (Paulina-Carabajal et al., 2018), and the theropods *Allosaurus* (Rogers, 1998) and *Ceratonykus oculatus* (Alifanov and Barsbold, 2009).

Here, we present the first record of a natural cranial endocast of a representative of the abelisaurid family found in the Cretaceous rocks of North Patagonia, Argentina (Fig. 1). The specimen comes from an area near the city of Rincón de los Sauces, where an elevated number of dinosaur braincase remains have been recovered from the Bajo de la Carpa Formation, and from the underlying sedimentary rocks (i.e., the titanosaurids *Narambuenatitan* and *Pitekunsaurus* from the Anacleto Formation). This "hot spot", known as Cerro Overo-La Invernada, has provided from Bajo de la Carpa Formation only, braincase remains of four abelisaurids (the complete braincases of *Llukalkan aliocranianus* (Gianechini et al., 2021), *Viavenator exxoni* (Filippi et al., 201), MAU-Pv-LI-582 (Méndez et al., 2021), the fragmentary fused frontals of MAU-Pv-LE-620, and three titanosaurid sauropods (MAU-Pv-LI-595, Mau-Pv-CO-687 and MAU-Pv-CO-688) (Fig. 2).

The comparison of the new specimen, MAU-Pv-CO-725, with the abelisaurids mentioned above — in particular, the isolated skull roof MAU-Pv-LE-620 — shed some light on our understanding of the morphological disparity within the clade and the possibile presence of an unknown group.

MATERIAL AND METHODS

The specimen MAU-Pv-CO-725 was collected from continental deposits of the Bajo de la Carpa Formation (Santonian, Upper Cretaceous; Garrido 2010), which outcrops at the Cerro Overo locality, 50 km west of the city of Rincón de los Sauces, Neuquén Province, Argentina (Fig. 1). It corresponds to a fragmentary skull roof (preserving a pair of frontals), the right otic capsule (formed by a partial prootic and opisthotic), and a natural cranial endocast that is missing the anterior end of the forebrain and most of the hindbrain mostly at the brainstem region. Thus, the endocast does not preserve most of the cranial nerves (V-XII). The natural endocast is made of very fine clastic material (only single crystals) cemented by calcium carbonate.

The specimen fragments (bone and endocast) exhibit considerable damage produced by erosion, indicating that they have been fractured and exposed, probably for a long time (can be years in a desert climate as in North Patagonia). As a result, the endocast exhibits several small punctuations on its surface produced by friction with surrounding rocks.

Comparisons of this natural endocast were made with the digital endocasts of other studied abelisaurids collected from Argentina, including *Aucasaurus garridoi* (Paulina-Carabajal and Succar, 2015), *Carnotaurus sastrei* (Cerroni and Paulina-

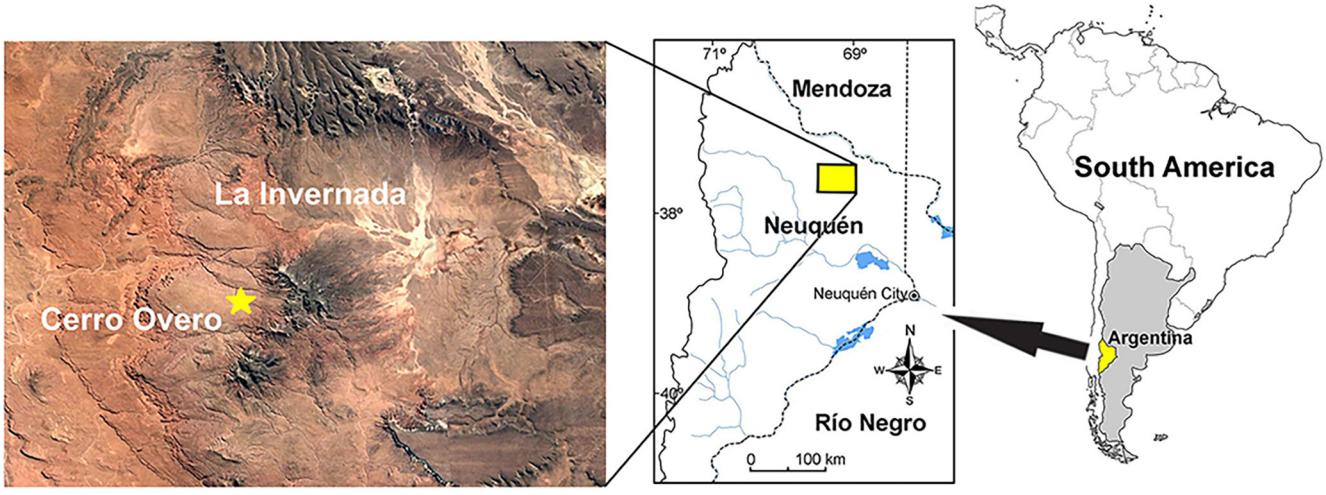

FIGURE 1. Location map. The star indicates the fossil site at the Cerro Overo locality that yielded the specimen MAU-Pv-CO-725. [planned for column]

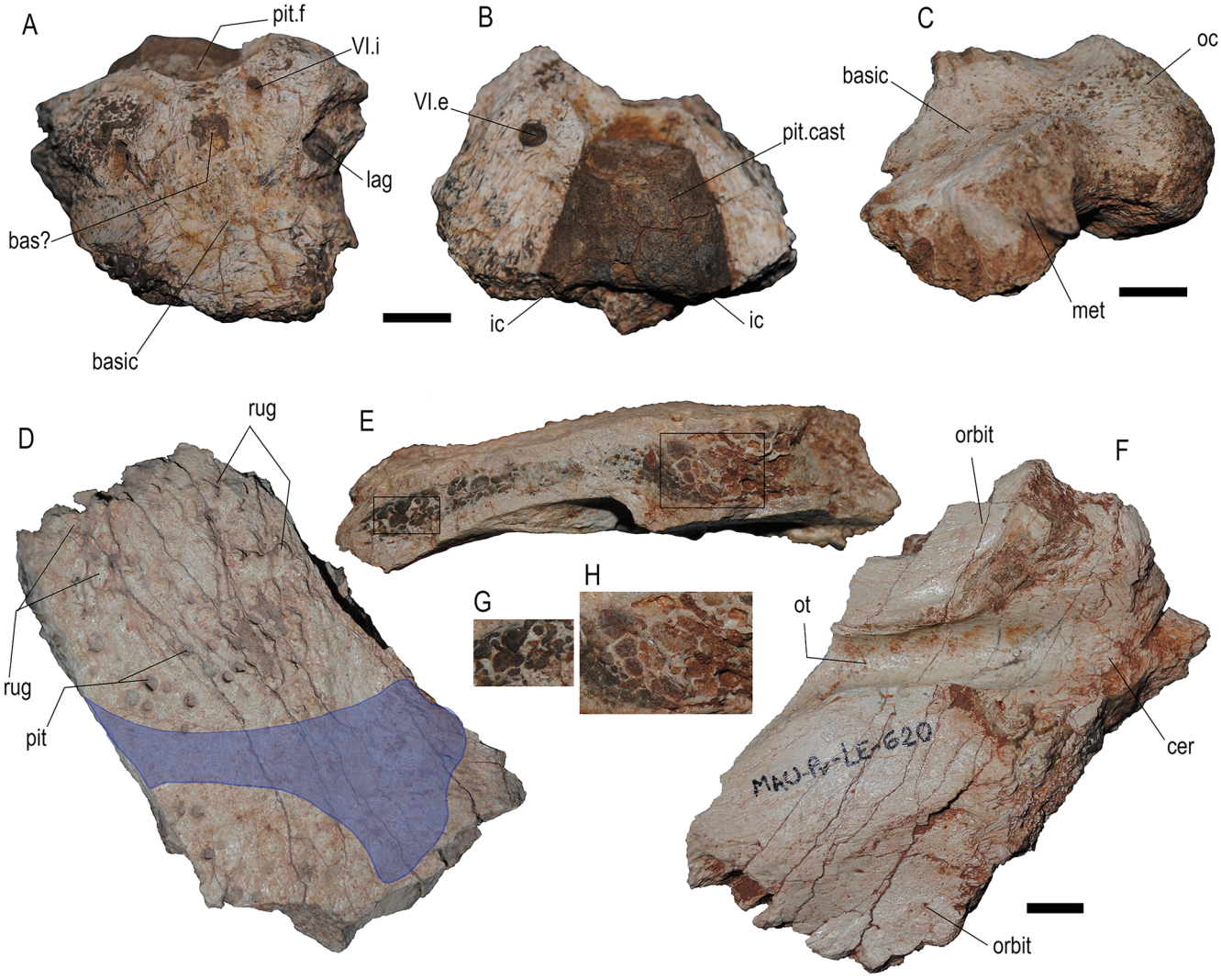

FIGURE 2. Previously unpublished dinosaur braincase remains from Cerro Overo-La Invernada sites (Bajo de la Carpa Formation). These materials include the titanosaurid basicrania MAU-Pv-CO-687 (A, B) and MAU-Pv-CO-688 (C), and the abelisaurid theropod skull roof MAU-Pv-LE-620 (D-F). A and D) dorsal view, B) anterior view, C) left lateroventral view, F) ventral view. E) transverse fracture along the right frontal and details (G, H) of the internal pneumaticity. The impression of the forebrain is on the ventral side of the frontals. To facilitate the orientation of the fragmentary skull roof, a blue shade indicates the forebrain size and position in a dorsal view of the frontals. Abbreviations: **bas**?, basilar artery; **basic**, basicranium (floor of the endocranial cavity); **cer**, osteological correlate of the cerebral hemisphere; **ic**, cerebral branch of the internal carotid artery; **lag**, lagena (section); **met**, metotic passage (for CN IX-XI and jugular vein); **oc**, occipital condyle; **orbit**, orbital part of the frontal; **ot**, osteological correlate of the olfactory tract; **pit**, blind circular pits on dorsal surface of the frontals (ornamentation); **pit.cast**, pituitary cast; **pit.f**, pituitary fossa. **II**, Cranial Nerve II. Scale bar equals 10 mm. [planned for page width]

Carabajal, 2019), *Guemesia ochoai* (Agnolín et al., 2022), *Llukalkan* (Gianechini et al., 2021), *Niebla antiqua* (Aranciaga Rolando et al., 2021), *Viavenator* (Paulina-Carabajal and Filippi, 2018), and an indeterminate abelisaurid MAU-Pv-Ll-582 (Méndez et al., 2021), as well as *Majungasaurus crenatissimus* (Sampson and Witmer, 2007) from Madagascar.

The natural specimen was photographed using a Nikon D3000 camera, and the figures were created using Adobe Photoshop (PS 2020). Photos were used to create a PDF 3D model of the natural endocast using the photogrammetry software Agisoft PhotoScan (see Supplementary information).

Institutional Abbreviations — **MAU**, Museo Municipal Argentino Urquiza, Rincón de los Sauces, Argentina.

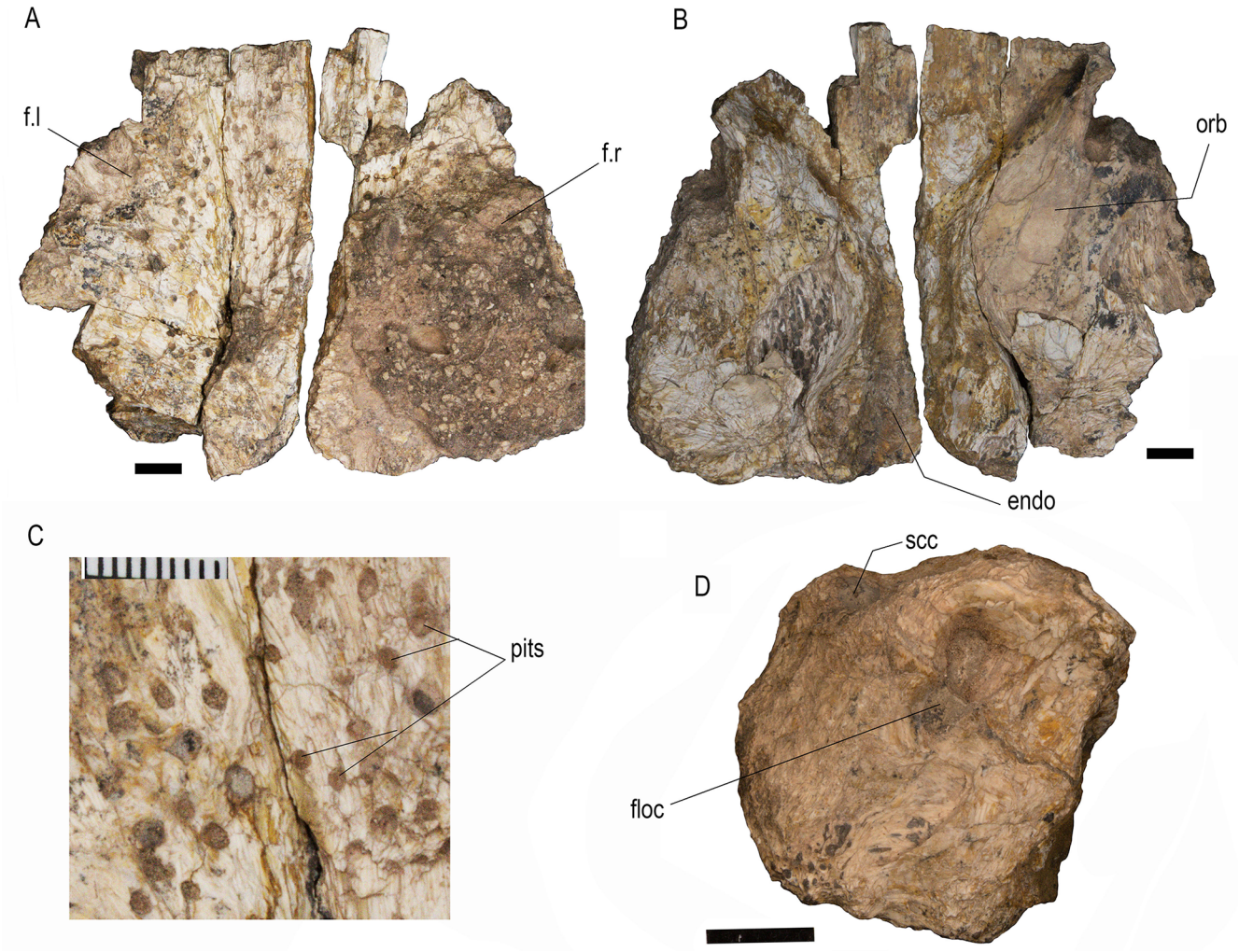

FIGURE 3. MAU-Pv-CO-725, frontals (A-C), and right otic capsule (D), in dorsal (A), ventral (B), and medial (D) views. (E) detail of the frontal ornamentation formed by pits. Abbreviations: **endo**, endocranial cavity (osteological correlates of olfactory apparatus and anterior region of the cerebrum); **f.l,** left frontal; **f.r**, right frontal; **floc**, floccular recess; **orb**, orbital part of the frontal; **ssc**, semicircular canal of the inner ear, in section (probably anterior semicircular canal). Scale bar equals 10 mm. [planned for page width]

DESCRIPTION

Skull roof

Both frontals were recovered (Figs. 3A, B). They form a flat plate approximately 120 mm wide, 90 mm long, and 21 mm in maximum thickness. Unlike most abelisaurids, the frontals in the specimen MAU-Pv-CO-725 are not especially dorsoventrally tall and exhibit a low degree of ornamentation. This particular ornamentation is formed not by grooves, crests, and rugosities as in most abelisaurids (e.g., *Abelisaurus*, *Aucasaurus*, *Carnotaurus*, *Viavenator*; Bonaparte 1985; Tykoski and Rowe 2004; Paulina-Carabajal 2011a, b), but formed by sparcely spaced circular pits distributed on an almost flat surface (Figs. 3A, C).

On the ventral surfaces of the frontals, osteological correlates of the olfactory tracts and olfactory bulbs are preserved (Fig. 3B). This anatomical information completes the missing anterior region of the natural endocast, allowing a complete reconstruction of the brain in dorsal view.

Cranial endocast

The natural cranial endocast is missing the anterior region of the forebrain (olfactory tract and bulbs), the distal end of the hindbrain, and the pituitary ventrally. Small fragments of supraoccipital/parietal and orbitosphenoid/mesethmoid bones are still attached to the posterodorsal and ventromedial sides,

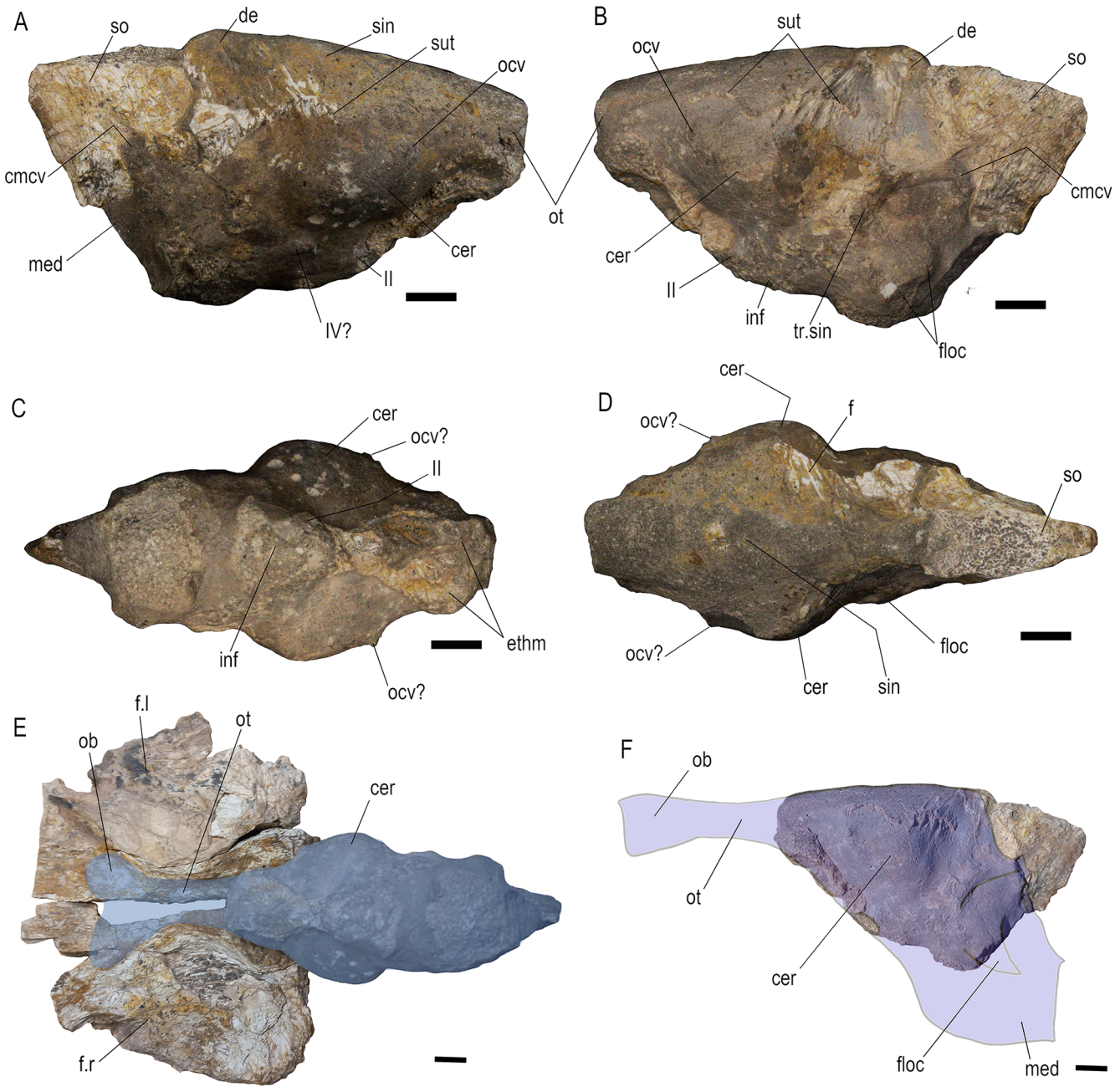

FIGURE 4. MAU-Pv-CO-725 natural cranial endocast (A-D) in right lateral (A), left lateral (B), ventral (C), and dorsal (D) views. Reconstructions (blue shades) of the complete endocast in ventral (E) and left lateral (F) views. Abbreviations: **de**, dorsal expansion or dural peak; **cer**, cerebral hemisphere; **cmcv**, caudal middle cerebral vein; **f**, frontal fragments; **f.l**, left frontal; **f.r**, right frontal; **floc**, base of flocculus of cerebellum; **inf**, proximal section of the infundibulum; **med**, medulla oblongata; **ob**, olfactory bulb; **ocv**, orbitocerebral vein; **ot**, olfactory tract; sin, dorsal longitudinal venous sinus; **so**, supraoccipital fragment; **sut**, suture marks between frontal and laterosphenoid-prootic; **tr.sin**, transverse venous sinus. Scale bar equals 10 mm. [planned for page width]

respectively (Figs. 4A-D). The osteological correlates of the olfactory tract and bulbs are preserved on the ventral surface of the frontals, allowing the reconstruction of the complete forebrain morphology (Fig. 4E).

The general shape of the endocast is reminiscent of that of other basal theropods, being anteroposteriorly long, with elongate olfactory tract and bulbs, the maximum transverse width lying across the cerebral hemispheres, and a pronounced

and triangular dorsal expansion (dural peak) dorsoposteriorly overlying the hindbrain. The angles between the forebrain, midbrain, and hindbrain result in a sigmoid shape in the lateral view (Fig. 4F).

Forebrain — The natural endocast is missing the anterior region. However, osteological correlates of the olfactory tract and bulbs on the ventral surface of the frontals allow the reconstruction of the olfactory region (Figs. 3B, 4E).

The olfactory tract is approximately 30 mm long and 15 mm transversely wide, resulting in a relatively robust structure, as is a common feature among abelisaurids (e.g., Sampson and Witmer, 2007; Paulina-Carabajal and Succar, 2015; Paulina-Carabajal and Filippi, 2018, and references therein) and carcharodontosaurids (Larsson, 2001; Paulina-Carabajal and Canale, 2010; Paulina-Carabajal and Nieto, 2020). The olfactory bulbs are relatively large, oval, and markedly divergent from the midline, as in other abelisaurids (e.g., *Majungasaurus*, *Viavenator*) (Figs. 3B, 4E). The Olfactory Ratio (OR) for MAU-Pv-CO-725 is approximately 58%, similar to that of *Viavenator* (57%, Paulina-Carabajal and Filippi, 2018), while *Majungasaurus* OR is 48.3% (Sampson and Witmer, 2007; Cerroni and Paulina-Carabajal, 2019). The OR is calculated by comparing the size of the olfactory bulb with the size of the cerebral hemisphere, a measurement that can be used with body size to estimate olfactory acuity (Zelenitzky et al., 2009). The body mass of MAU-Pv-CO-725 remains unknown, thus preventing further calculation of olfactory acuity.

The cerebral hemispheres are well marked, rounded, and laterally expanded, as in other abelisaurids (Figs. 4A-D). The lateral border of the cerebral hemisphere is rounded.

Based on known abelisaurid neuroanatomy, the entire endocast of MAU-Pv-CO-725 would have had a length of approximately 130 mm from the tip of the olfactory bulbs to the end of the medulla oblongata (Fig. 4F).

Midbrain — The only structures that can be observed in non-avian dinosaur brains are the optic lobes and cranial nerves III and IV (Franzosa, 2004). As in other non-coelurosaur theropods, the optic lobes of MAU-Pv-CO-725 are not visible in the endocast. As for the roots of CNs III and IV, they are not preserved in the endocast, except for a possible short passage for CN IV observed on the right side of the endocast (Fig. 4A).

Hindbrain — A part of the cerebellum (i.e., the floccular process) and the proximal part of the medulla oblongata are observed in the endocast. The main body of the cerebellum, located just posterior to the optic lobes, is obscured on the endocast by the dorsal longitudinal venous system, which covers the dorsal surface and forms a dorsal expansion in this region (Fig. 4B). This dural expansion, located above the anterior margin of the floccular process, does not project over the dorsal surface of the forebrain, as in *Viavenator* and *Llukalkan* (Fig. 4D). In contrast, the dural expansion is more anteriorly placed in MAU-Pv-LI-582 and *Majungasaurus*, level with the root of the trigeminal nerve (CN V) and resulting in a different sigmoidal shape of the endocast.

The floccular process of the cerebellum is broken at the base on both sides, so its complete length and shape remain unknown. The proximal section of the flocculus is oval and markedly lateromedially compressed (Fig. 4B), as in other abelisaurids. Moreover, the right otic capsule exhibits the floccular recess on the anterior surface of the vestibular eminence, which is figure eight-shaped (Fig. 3D), similar to that described in *Aucasaurus* (Paulina-Carabajal and Succar, 2015). Nevertheless, the figure eight-shaped floccular recess is not limited to abelisaurids among theropods (i.e., the tyrannosaurid *Daspletosaurus*; Paulina-Carabajal et al., 2021)

The medulla oblongata is partially preserved. Unfortunately, the brainstem region is missing, preventing the preservation of the roots of the remaining cranial nerves (CNs V-XII). The caudal middle cerebral vein is the only blood vessel observed in this region (Figs. 4A, B). This large passage projects posterodorsally from the intersection with the transverse sinus to exit the braincase posteriorly. The caudal middle cerebral vein has a larger diameter proximally than distally, where the passage becomes more flattened. The impression left on the supraoccipital indicates that the exit foramen for this vein was near the midline, separated from its counterpart by a vertical crest, as commonly observed in other abelisaurids (e.g., *Aucasaurus, Niebla*).

DISCUSSION

Endocast and bone features supporting abelisaurid designation

The general shape of the natural endocast from the Cerro Overo site resembles most non-maniraptoran theropods, being longer than wide and lacking observable anatomical definition from the optic lobes and the cerebellum. The

markedly elongated and robust olfactory tracts and bulbs are typical features of ceratosaurs and carcharodontosaurids (e.g., Larsson, 2001; Sanders and Smith, 2005; Sampson and Witmer, 2007; Paulina-Carabajal and Canale, 2010; Paulina-Carabajal and Filippi, 2018).

The general morphology of the endocast of MAU-Pv-CO-725 largely resembles that of *Viavenator* and *Llukalkan* but not that of MAU-Pv-LI-582, which shares more similarities with *Majungasaurus*. MAU-Pv-CO-725 also represents a smaller specimen than *Viavenator* and slightly smaller than *Llukalkan* and *Niebla*.

Luckily, the endocast was recovered with fragmentary but very informative bones. Thus, extra data supports the taxonomic assignment of this specimen and includes the morphology of the frontals and otic capsule (e.g., the shape of the floccular recess).

The frontals of MAU-Pv-CO-725 are transversely wider than longer, not particularly thick at the midline (frontals of abelisaurids are, in general, markedly engrossed at the midline, Tykoski and Rowe, 2004). More recently, relatively low frontals have been described for the small taxon *Guemesia*, and the basal abelisaurid *Spectrovenator* from Brazil (Zaher et al ., 2020), but not for *Niebla*, suggesting that this feature is not directly related to body size. Internally the frontals in MAU-Pv-CO-725 exhibit some degree of pneumaticity, as observed through fractures, a feature also present in MAU-Pv-LE-620 and observed through CT scans in *Guemesia* (Agnolín et al., 2022).

The frontals exhibit an ornamented surface, a characteristic feature of the abelisaurid skull roof, although much less developed in MAU-Pv-CO-725 than in most other representatives of this clade. Moreover, the ornamentation in this specimen is particular regarding both, the large amount of pits and its irregular distribution on the surface of the frontals. In this regard, the particular type of ornamentation present in MAU-Pv-CO-725 is also observed in MAU-Pv-LE-620 (another skull roof from Bajo de la Carpa Formation) and in the non-Patagonian abelisaurid *Guemesia*, which exhibit a lower number of pits near the midline and some rugosities laterally, near the orbital rim. The complete lack of ornamentation is observed in the Jurassic taxon *Eoabelisaurus*, and the early Cretaceous *Spectrovenator*, which suggests that the reduction of ornamentation in derived late Cretaceous forms may represent the retention of a primitive character in adult specimens or possibly a younger ontogenetic stage.

The isolated right otic capsule exhibits on the anterior surface of the vestibular eminence a figure eight-shaped floccular recess. A similar morphology has been described for *Aucasaurus* (Paulina-Carabajal, 2009; Paulina-Carabajal and Succar, 2015), although it is observed in non-ceratosaurian theropods as well (Paulina-Carabajal, 2009; Paulina-Carabajal et al., 2021).

Comparisons with other abelisaurids of the Bajo de la Carpa Formation

The abelisaurids collected from sites near Cerro Overo that preserve braincases are *Llukalkan*, *Viavenator*, MAU-Pv-Ll-582, and MAU-Pv-LE-620, the latter corresponding to a previously unpublished isolated skull roof. *Llukalkan*, *Viavenator*, and MAU-Pv-Ll-582 are mid-to-large-sized abelisaurids, with *Viavenator* being the largest. The surface of the bone in the skull roof of the three specimens has been damaged by erosion, obscuring the nature of the ornamentation. However, fragments of skull roof preserved in each specimen indicate the presence of “normal” abelisaurid ornamentation, this is, the presence of well-marked grooves and rugosities, in *Llukalkan* and MAU-Pv-LI-582, and most likely also in *Viavenator*. Other abelisaurids with marked ornamentations (and even with cornual structures) are *Abelisaurus comahuensis* (Bonaparte and Novas, 1985), *Aucasaurus garridoi* (Coria et al., 2002), *Carnotaurus sastrei* (Bonaparte, 1985), *Ekrixinatosaurus novasi* (Calvo et al., 2004), *Niebla antiqua* (Aranciaga-Rolando et al., 2020), *Skorpiovenator bustingorryi* (Canale et al., 2008) from Argentina, *Majungasaurus crenatissimus* from Madagascar (Sampson et al., 1998), *Arcovenator escotae* from France (Tortosa et al., 2014), and the Indian *Indosaurus matleyi* and *Rajasaurus narmadensis* (Huene and Matley, 1933; Wilson et al., 2003; Carrano and Sampson, 2008).

Guemesia and *Niebla* are the smaller abelisaurids with preserved braincases from the Upper Cretaceous of Northwestern Argentina and Patagonia, respectively, followed by *Llukalkan*, also from Patagonia. *Niebla* and *Llukalkan*, however, have an engrossed skull roof with marked ornamentation formed by grooves and rugosities, whereas *Guemesia* has a non-engrossed frontal and exhibits a low degree of ornamentation formed by few pits near the midline and “normal” ornamentation (grooves and rugosities) near the orbital rim. The holotype of *Niebla* also is considered an adult specimen (Aranciaga Rolando et al., 2020). The isolated braincase of *Guemesia,* however, bears no evidence

enough to discard it as a juvenile individual, and therefore is not possible to associate its small size to any ontogenetic state. Regarding skull roof morphology, the Jurassic abelisaurid *Eoabelisaurus* has a skull roof that is not markedly engrossed and has no ornamentation (Pol and Rauhut, 2012). This suggests that the lack of ornamentation represents a primitive character within the clade Abelisauridae. So far, the secondary reduction of the ornamentation in the Cretaceous abelisaurid forms described here, seem to be related to body size. Also, although it is difficult to determine if *Guemesia*, MAU-Pv-LE-620, and MAU-Pv-CO-725 represent juvenile specimens, the lack of ornamentation may represent a paedomorphic character.

Finally, MAU-Pv-LE-620 and MAU-Pv-CO-725, although from different sites (apart 13 km away from each other), are from the same geological formation and share a relatively small size and the reduction of ornamentation, suggesting that both specimens belong to the same unknown taxon.

CONCLUSION

The endocast and the associated braincase fragments bear features that support the taxonomical assignment of the specimen to Abelisauridae. The endocranial morphology of the abelisaurids from Cerro Overo-La Invernada sites indicates the presence of two morphotypes, with *Viavenator*, *Llukalkan*, and the natural endocast MAU-Pv-CO-725 sharing the same general morphology. The relative size of the latter is interpreted here as similar to that of *Llukalkan*. The marked reduction of ornamentation in MAU-PV-CO-725 and MAU-Pv-LE-620 (the two isolate skull roofs) is, however, a distinctive pattern that differentiates them from *Llukalkan* and *Viavenator*, which exhibit well-developed ornamentation formed by grooves and rugosities.

The natural endocast and skull roof described here correspond to a small-sized individual, but due to its incompleteness, it is impossible to rule out that it may be a juvenile. Are MAU-Pv-CO-725 and MAU-Pv-LE-620 juvenile specimens or representatives of sexual dimorphism of known taxa? Or do they represent an unknown group of small-sized abelisaurids characterized by the reduction of the skull roof sculpturing? Further findings and studies are needed to answer these questions.

ACKNOWLEDGMENTS

We thank Secretaría de Cultura of Neuquén Province for authorizing the fieldwork and the field owner (Mr. Cofre) who allowed entrance to his land. Geologist F. Bechis for helping determine specimen composition. We thank the reviewers, Amy Balanoff and Mauricio Cerroni for their corrections and comments, which improved the first version of this manuscript. This research was supported by CONICET PIP 2021-2023 11220200101108CO (AHM), PICT-2021-0024 (AHM), PICT-2021-I-INVI-00513 (LSF), PICT 2021-1053 (APC), and NRF 2022R1I1A2060919 (Y-NL).

AUTHOR CONTRIBUTIONS

APC designed the project and drafted the manuscript; LF and KUG took photographs; APC created the illustrations, and KUG made the 3D photogrammetry model. All authors analyzed the data and edited the manuscript.

SUPPLEMENTARY INFORMATION

Supplemental-3D model (photogrammetry) of natural enocast.pdf

LITERATURE CITED

Agnolín, F. L., Cerroni, M. A., Scanferla, A., Goswami, A., Paulina-Carabajal, A., Halliday, T., Cuff, A. R., & Reuil, S. (2022). First definitive abelisaurid theropod from the Late Cretaceous of Northwestern Argentina. Journal of Vertebrate Paleontology. DOI: 10.1080/02724634.2021.2002348.

Alifanov V. & Barsbold R. (2009). *Ceratonykus oculatus* gen. et sp. nov., a new dinosaur (?Theropoda, Alvarezsauria) from the Late Cretaceous of Mongolia. *Paleontological Journal*, 43, 94–106.

Aranciaga Rolando, M. A., Cerroni, M. A., García Marsà, J. A., Motta, M. J., Rozadilla, S., Brissón Eglí, F., & Novas, F. E. (2021). A new medium-sized abelisaurid (Theropoda, Dinosauria) from the late cretaceous (Maastrichtian) Allen Formation of Northern Patagonia, Argentina. *Journal of South American Earth Sciences*, 105, 102915.

Bonaparte, J. F. (1985). A horned Cretaceous carnosaur from Patagonia. *National Geographic Research*, 1, 149–151.

Bonaparte, J. F. & Novas, F. (1985). *Abelisaurus comahuensis* n. gen. n. sp. Carnosauria del cretácico superior de Patagonia. *Ameghiniana*, 21, 259–265.

Brasier M. et al. (2016). Remarkable preservation of brain tissues in an Early Cretaceous iguanodontian dinosaur. *Geological Society, London, Special Publications* (2017), 448(1), 383.

Burch, S. H., Paulina-Carabajal, A., O'Connor, P., & Hieronymous, T. (in press). *Dinosaur soft tissues*. In D. B. Weishampel, M. Carrano, P. Barret, & P. Makovicky (Eds.), *The Dinosauria, 3rd edition.* Cambridge University Press.

Calvo, J. O., Rubilar-Rogers, D., & Moreno, K. (2004). A new Abelisauridae (Dinosauria: Theropoda) from northwest Patagonia. *Ameghiniana*, 41, 555–563.

Cerroni, M. A. & Paulina-Carabajal, A. (2019). Novel information on the endocranial morphology of the abelisaurid theropod Carnotaurus sastrei. *Comptes Rendus Paleovol*, 18(8), 985–995.

Coria, R. A., Chiappe, L. M., & Dingus, L. (2002). A new close relative of *Carnotaurus sastrei* Bonaparte 1985 (Theropoda: Abelisauridae) from the Late Cretaceous of Patagonia. *Journal of Vertebrate Paleontology*, 22, 460–465.

Dozo, T., Paulina-Carabajal, A., Macrini, T. y Walsh, S. (2023). *Paleoneurology of Amniotes*. Springer.

Franzosa, J. W. (2004). Evolution of the brain in Theropoda (Dinosauria) (unpublished PhD Thesis). The University of Texas at Austin, Austin, 357 pp.

Gianechini, F. A., Méndez, A. H., Filippi, L. S., Paulina-Carabajal, A., Juárez-Valieri, R., & Garrido, A. C. (2021). A new furileusaurian abelisaurid from La Invernada (Upper Cretaceous, Santonian, Bajo De La Carpa Formation), Northern Patagonia, Argentina. *Journal of Vertebrate Paleontology*, e1877151.

Hopson, J. A. (1979). Paleoneurology. In C. Gans, R. G. Northcutt, & P. Ulinski (Eds.), *Biology of the Reptilia*, vol. 9 (pp. 39–146). London and New York, Academic Press.

Huene, F. v. & Matley, C. A. (1933). The Cretaceous Saurischia and Ornithischia of the Central Provinces of India. Memoirs of the Geological Survey of India. *Palaeontologica Indica*, 21, 1–72.

Jerison (2009). Dinosaur Brains. In L. R. Squire (Ed.), *Encyclopedia of neuroscience.* Elsevier.

Jirak, D. & Janacek, J. (2017). Volume of the crocodilian brain and endocast during ontogeny. *PLoS ONE*, 12(6), e0178491.

Larsson, H. C. E. (2001). Endocranial anatomy of *Carcharodontosaurus saharicus* (Theropoda: Allosauroidea) and its implications for theropod brain evolution. In D. H. Tanke & K. Carpenter (Eds.), *Mesozoic Vertebrate Life* (pp. 19–33). Indiana University Press.

Marsh, O. C. (1890). Additional characters of the Ceratopsidae, with notice of the new Cretaceous dinosaurs. *Am J Sci*, 39, 418–426.

Marsh, O. C. (1891). The gigantic Ceratopsidae, or horned Dinosaurs, of North America. *Am J Sci*, 41, 168–178.

Marsh, O. C. (1893). The skull and brain of *Claosaurus*. *Am J Sci*, 3(265), 83–86.

Marsh, O. C. (1894). The typical Ornithopoda of the American Jurassic. *Am J Sci*, 48, 85–90.

Marsh, O. C. (1896). The dinosaurs of North America. United States Geological Survey, sixteenth annual report, 1894–95, 133–244.

Marsh, O. C. (1879). Principal characters of American Jurassic dinosaurs. Part II. *Am J Sci*, 3(17), 86–92.

Marsh, O. C. (1880). Principal characters of American Jurassic dinosaurs. Part III. *Am J Sci*, 19, 253–259.

Marsh, O. C. (1881). Principal characters of American Jurassic dinosaurs. Part IV. *Am J Sci*, 122, 167–170.

Marsh, O. C. (1884a). Principal characters of American Jurassic dinosaurs. Part VII. On the Diplodocidae, a new family of the Sauropoda. *Am J Sci*, 27, 161–168.

Marsh, O. C. (1884b). Principal characters of American Jurassic dinosaurs. Part VIII. The order Theropoda. *Am J Sci*, 27, 329–340.

Marsh, O. C. (1889). The skull of the gigantic Ceratopsidae. *Am J Sci*, 228, 501–506.

Méndez, A., Gianechini F. A., Paulina-Carabajal A. et al. (2021). New furilesaurian remains from La Invernada (northern Patagonia, Argentina): A site of unusual abelisaruids abundance. *Cret Res*, 129, 104989. https://doi.org/10.1016/j.cretres.2021.104989.

Paulina-Carabajal, A. (2009). El neurocráneo de los dinosaurios Theropoda de la Argentina: osteología y sus implicancias filogenéticas. Unpublishe Thesis, Universidad Nacional de La Plata. (available at:http://naturalis.fcnym.unlp.edu.ar/id/20120126000947).

Paulina Carabajal, A. (2011). The braincase anatomy of *Carnotaurus sastrei* (Theropoda: Abelisauridae) from the Upper Cretaceous of Patagonia. *Journal of Vertebrate Paleontology*, 31, 378–386.

Paulina Carabajal, A. (2011b). Braincases of abelisaurid theropods from the upper Cretaceous of north Patagonia. *Palaeontology*, 54, 793–806.

Paulina Carabajal, A. & Canale, J. I. (2010). Cranial endocast of the carcharodontosaurid theropod *Giganotosaurus carolinii*. *Neues Jahrbuch für Geologie und Paläontologie*, Abhandlungen, 258, 249–256.

Paulina-Carabajal, A. & Filippi, L. (2018). Neuroanatomy of the abelisaurid theropod *Viavenator*: the most complete reconstruction of cranial endocast and inner ear for a South American representative of the clade. *Cret Res*, 83, 84–94.

Paulina-Carabajal, A. & Succar, C. (2015). Endocranial morphology and inner ear of the theropod *Aucasaurus garridoi*. *Acta Palaeontol Pol*, 60(1), 141–144.

Paulina-Carabajal, A., Coria, R. A., Currie, P. J. et al. (2018a). A natural cranial endocast with possible dicraeosaurid (Sauropoda, Diplodocoidea) affinities from the Lower Cretaceous of Patagonia. *Cret Res*, 84, 437–441.

Paulina-Carabajal, A., Currie, P. J., Dungeon, T. W., Larsson, H. C. E., & Miyashita, T. (2021). Two braincases of Daspletosaurus (Theropoda: Tyrannosauridae): anatomy and comparison. *Canadian Journal of Earth Sciences*, 58. https://doi.org/10.1139/cjes-2020-0185.

Pol, D. & Rauhut, O. W. M. (2012). A Middle Jurassic abelisaurid from Patagonia and the early diversification of theropod dinosaurs. *Proceedings of the Royal Society B: Biological Sciences*, 279(1741), 3170–3175.

Rich, T. & Rich, P. (1989). Polar dinosaurs and biotas of the Early Cretaceous of southeastern Australia. *Nat Geograp Res*, 5(1), 15–53.

Rogers, S. W. (1998). Exploring dinosaur neuropaleobiology: computed tomography scanning and analysis of an *Allosaurus gracilis* endocast. *Neuron*, 21, 673–679.

Sampson, S. D. & Witmer, L. M. (2007). Craniofacial anatomy of *Majungasaurus crenatissimus* (Theropoda: Abelisauridae) from the Late Cretaceous of Madagascar. S*ociety of Vertebrate Paleontology Memoirs*, 8, 32–102.

Serrano-Brañas, C. I., Hernández-Rivera, R., Torres-Rodríguez, E. et al. (2006). A natural hadrosaurid endocast from the Cerro del Pueblo Formation (Upper Cretaceous) of Coahuila, Mexico. In S. G. Lucas & R. M. Sullivan (Eds.), *Late Cretaceous Vertebrates from the Western Interior* (pp. 317–321). *Bull N M Mus Nat Hist Sci*, 35.

Tortosa, T., Buffetaut, E., Vialle, N., Dutour, Y. aTurini, E., & Cheylan, G. (2014). A new abelisauri dinosaur from the Late Cretaceous of southern France: Palaeobiogeographical implications. *Annales de Paleontologie*, 100, 63-86.

Tykoski, R. S. & Rowe, T. (2004). Ceratosauria. In D.B. Weishampel, P. Dodson & H. Osmolska (Eds.), *The Dinosauria* (2nd edition) (pp.

47–70). Berkeley: University of California Press.

Zaher, H., Pol, D., Navarro, B. A., Delcourt, R., & Carvalho, A. B. (2020). An Early Cretaceous theropod dinosaur from Brazil sheds light on the cranial evolution of the Abelisauridae. *Comp Ren Palevol*, 19, 101-115.

Zelenitsky, D. K., Therrien, F., & Kobayashi, Y. (2009). Olfactory acuity in theropods: palaeobiological and evolutionary implications. *Proc R Soc B*, 276, 667–673.

Osborn, H. F. (1912). Crania of *Tyrannosaurus* and *Allosaurus*. *Mem Am Mus Nat Hist*, 1, 1–97.

WINDOWS INTO SAUROPSID AND SYNAPSID EVOLUTION
Essays in honor of Prof. Louis L. Jacobs, pp. 140–150, 2023

NEW INSIGHTS ON THE FRILL ORNAMENTATIONS OF PROTOCERATOPSIDS

KENTARO CHIBA[1,*], MICHAEL J. RYAN[2,3], MOTOTAKA SANEYOSHI[1], SATOSHI KONISHI[1], YUDAI YAMAMOTO[1], DAVID C. EVANS[4,5], TSOGTBAATAR CHINZORIG[6,7,8], PUREVDORJ KHATANBAATAR[8], ZORIGT BADAMKHATAN[8], BUUVEI MAINBAYAR[8], and KHISHIGJAV TSOGTBAATAR[8]

[1]Department of Biosphere-Geosphere Science, Okayama University of Science, Okayama, Okayama 700-0005, Japan, chiba@ous.ac.jp, saneyoshi@ous.ac.jp, g15g053ks@ous.jp, g18gm13yy@ous.jp;
[2]Department of Earth Sciences, Carleton University, Ottawa, Ontario K1S 5B6, Canada,
[3]Department of Palaeobiology, Canadian Museum of Nature, Ottawa, Ontario K1P 6P4, Canada, michaelj.ryan@carleton.ca;
[4]Department of Natural History, Royal Ontario Museum, Toronto, Ontario M5S 2C6, Canada,
[5]Department of Ecology and Evolutionary Biology, University of Toronto, Toronto, Ontario M5S 3B2, Canada, davide@rom.on.ca;
[6]Paleontology Research Lab, North Carolina Museum of Natural Sciences, Raleigh, North Carolina 27601, United States of America;
[7]Department of Biological Sciences, North Carolina State University, Raleigh, North Carolina 27607, United States of America, ctsogtb@ncsu.edu;
[8]Institute of Paleontology, Mongolian Academy of Sciences, Ulaanbaatar 15160, Mongolia, ambaajaa52@gmail.com, badmaa@mas.ac.mn, Mainbayarb@mas.ac.mn, tsogtbaatar@mas.ac.mn

ABSTRACT *Protoceratops andrewsi* is a small-bodied, non-ceratopsoid ceratopsian dinosaur found in the Upper Cretaceous Djadokhta Formation in Mongolia. Although it has a well-developed parietosquamosal frill, the frill margin has been thought to be unadorned, unlike ceratopsids. On ceratopsids, especially centrosaurines, the subadult frill margin in dorsal view is typically undulated, with the apex of each undulation providing a locus onto which an epiparietal can potentially fuse and mature into a frequently modified shape that can aid in the identification of species. This study explicitly notes that the frill margin of *P. andrewsi* frill is undulated. Although virtually all *P. andrewsi* and a limited number of specimens of other protoceratopsids examined in this study have frill margin undulations, their development is variable and generally quite subtle; the size, number, and position of the processes are highly plastic among individuals and do not exhibit a consistent pattern related to the size of individuals. There is no sign that the undulations of *P.* andrewsi were associated with epiossifications. Due to the subtlety and inconsistency of the frill undulations, the potential functions of the frill margin undulations are currently not obvious. We also report several previously underappreciated protoceratopsid features that may have taxonomic utility within marginocephalians and important implications for understanding the evolution of the integumentary structures within Ceratopsia.

KEYWORDS Dinosauria, Marginocephalia, Ceratopsia, *Protoceratops*, Parietosquamosal

INTRODUCTION

Protoceratops is a non-ceratopsoid ceratopsian and one of the most abundant taxa found in the Upper Cretaceous Djadokhta Formation and contemporaneous strata distributed in the Gobi Desert of Mongolia and Inner Mongolia, China. Hundreds of specimens of this genus have been collected since its discovery in 1922 (Granger and Gregory, 1923), and new specimens are still being collected (Chen, 2017; Ishigaki et al., 2018; Chen et al., 2022). The huge sample size presented by the *Protoceratops* specimens has allowed for the investigations of morphological variations, growth, sexual dimorphism, and ecology in this genus (e.g., Brown and Schlaikjer, 1940; Dodson, 1976; Fastovsky et al., 1997, 2011; Hone et al., 2014, 2016; Maiorino et al., 2015; Fostowicz-Frelik and Słowiak, 2018), with implications for its function and the selection pressures related to its evolution (e.g., Brown and Schlaikjer, 1940; Kurzanov, 1972; Dodson, 1976; Maiorino et al., 2015; Hone et al., 2016; Knapp et al., 2021). The parietosquamosal frill of *Protoceratops* is well developed compared to other non-ceratopsoid ceratopsians but has generally been thought to be unadorned (Gregory and Mook, 1925; Brown and Schlaikjer, 1940), unlike ceratopsids whose parietosquamosal frills can have processes composed of either the frill margin, epiossifications, or both (Sampson et al., 1997; Ryan et al., 2001; Mallon et al., 2023). The initial

*Corresponding author

suggestion that *Protoceratops* has frill margin undulations (Sereno, 2000) was later questioned, with the putative undulations being instead considered to be preservational artifacts (Makovicky, 2002). Here we report data supporting the presence of the frill undulations in *Protoceratops* along with some underappreciated anatomical features of *Protoceratops* that may have implications for the evolution of the ceratopsian frill.

MATERIALS AND METHODS

We examined 62 *Protoceratops* specimens housed in the American Museum of Natural History, the Institute of Paleontology of the Mongolian Academy of Sciences, and the former Hayashibara Museum of Natural Sciences. There are two known *Protoceratops* species, *P. andrewsi* and *P. hellenikorhinus*; the former is only known from Mongolia, and the latter from Inner Mongolia, China. Only Mongolian specimens were examined due to logistical constraints, and, therefore, we could not examine *P. hellenikorhinus* specimens.

Most of the specimens examined here are from two localities: Bayn Dzag, the type locality of *P. andrewsi* (Granger and Gregory, 1923), and Tugrikin Shire, where the famous "Fighting Dinosaurs" (*P. andrewsi* MPC-D 100/512 and *Velociraptor mongoliensis* MPC-D 100/25) were found (Kielan-Jaworowska and Barsbold, 1972). We also examined specimens of *P. andrewsi* and *Protoceratops* sp. from Udyn Sayr (Handa et al., 2012), *Protoceratops* sp. from the adjacent locality of Bor Tolgoi (Saneyoshi et al., 2010; Tsogtbaatar and Chinzorig, 2010) and *Bagaceratops* sp. from Udyn Syar (Czepiński, 2020).

Additionally, we briefly describe MPC-D 100/555, a nearly complete articulated skeleton of *Protoceratops* (field number 949726 TSGT-Ts-IV), which was found at Tugrikin Shire during the Hayashibara Museum of Natural Sciences-Mongolian Paleontological Center Joint Paleontological Expedition in 1994. Unfortunately, the specimen was damaged during preparation, so our observations of this specimen are based on the original specimen stored at IP-MAS and from photographs taken in the field during the collection of the specimen.

Institutional Abbreviations — AMNH, American Museum of Natural History, New York, United States; HMNS, Hayashibara Museum of Natural Sciences, Okayama, Japan; IP-MAS; the Institute of Paleontology, Mongolian Academy of Sciences, Ulaanbaatar, Mongolia; MPC, Mongolian Paleontological Center, Ulaanbaatar, Mongolia (currently IP-MAS)

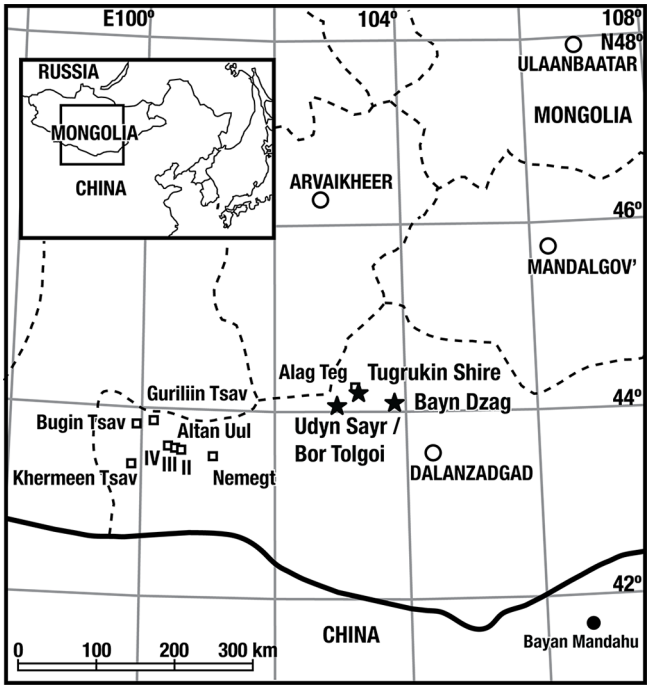

FIGURE 1. Locality map of central and western Gobi Desert. Stars represent the localities yielding *P. andrewsi*, a black circle indicates the locality of *P. hellenikorhinus*, and open squares indicate representative dinosaur fossil localities of this area. The map was modified from Watabe et al. (2010).

RESULTS

Description of MPC-D 100/555

MPC-D 100/555 was, when collected, a well-preserved, nearly completely articulated skeleton (Fig. 2A), but it was extensively damaged during preparation. The skull was almost complete but lacked the right posterior bar of the parietal when found (Fig. 2B and C). Although small fragments of the frill are still available, it is impossible to know their relative original positions in the frill. A well-defined, dorsally convex longitudinal ridge on the lateral surface of the maxilla, the curved anterior margin of the predentary, and the curved ventral edge of the dentaries all indicate that this specimen belongs to *Protoceratops andrewsi* rather than to *P. hellenikorhinus* (Lambert et al., 2001). This is congruent with

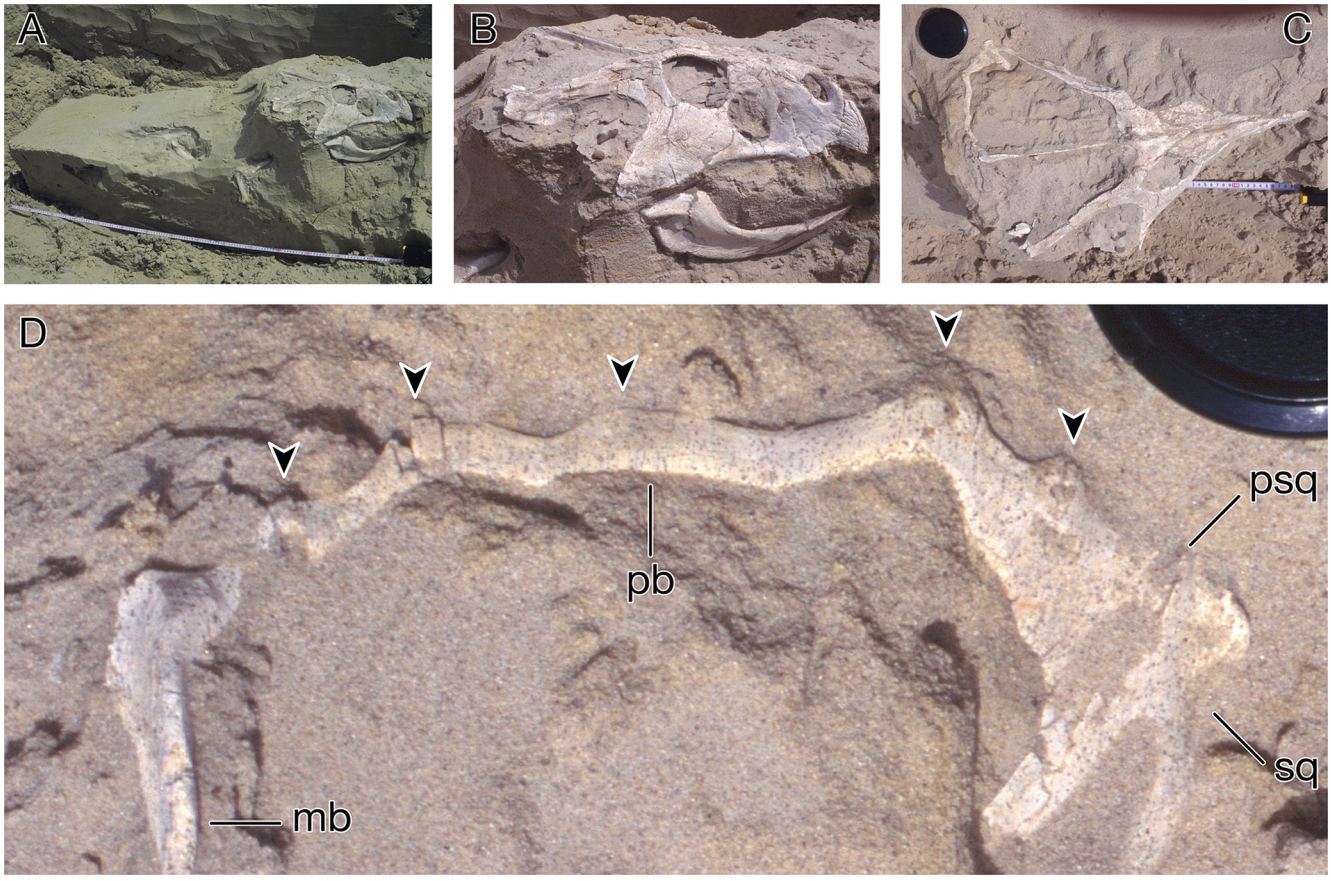

FIGURE 2. Field photographs of MPC-D 100/555, a *Protoceratops andrewsi* specimen with strong undulations. **A**, right lateral view of the whole skeleton in sediments; **B**, right lateral view of the skull; **C**, dorsal view of the skull; **D**, close-up of the posterior portion of the parietosquamosal frill in the dorsal view. Black arrows indicate the processes. **Abbreviations**: **mb**, midline bar of parietal; **pb**, posterior bar of parietal; **psq**, parietal-squamosal contact; **sq**, squamosal.

the fact that, to date, only *P. andrewsi* has been reported from the locality. Based on the field photographs and the fragmented specimen, the total (390 mm) and basal (250 mm) skull lengths, frill length (160 mm), and half-width (123 mm) can be reliably estimated. The basal skull length is approximately 70% of the longest reported *Protoceratops andrewsi* basal skull length (AMNH 6466, 357 mm; Dodson, 1976; Maiorino et al., 2015; Hone et al., 2016). The field photographs clearly show that the frill margin of this specimen is strongly undulated compared to typical *Protoceratops* specimens (Fig. 2D), although none of the frill fragments in the collection preserve the undulated frill margin. There appear to be five processes located on the convex posterior margin of the parietal. The size and shape of the processes are not consistent, and they are unevenly distributed; the second and third processes lateral to the midline bar have wide bases, but the first, fourth, and fifth processes have relatively narrower bases, giving the latter three more triangular-shaped. There are no episossifications associated with the processes or indications that they were ever present.

Additional Protoceratopsid Specimens with Undulated Frill Margins

Undulated *Protoceratops* frill margins were noted by Sereno (2000), who included "low tab-shaped processes on the frill margin (three on the squamosal and four or five on the parietal)" as one of the potential autapomorphies of *P. andrewsi*, and illustrated by drawings of AMNH 6408 (Sereno 2000: Fig. 25.6). Four tab-shaped flanges on the left and five on the right posterior parietal bar are indicated in the figure, but processes on the squamosals are not indicated. AMNH 6408 is currently on display but inaccessible for

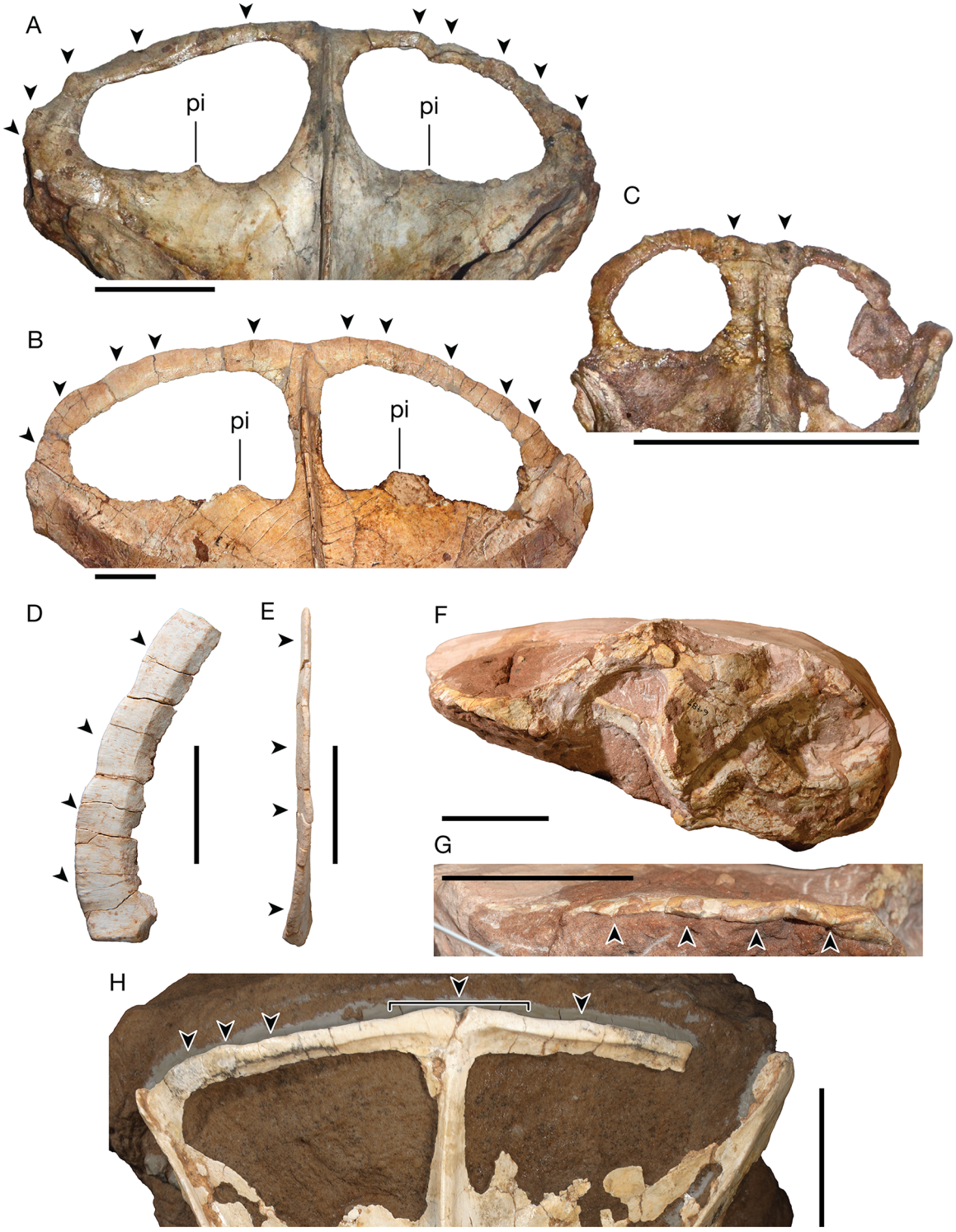

FIGURE 3. *Protoceratops andrewsi* specimens showing frill margin undulations. **A**, dorsal view of AMNH 6408 parietosquamosal frill; **B**, dorsal view of AMNH 6466 parietosquamosal frill; **C**, dorsal view of AMNH 6419 parietosquamosal frill; **D**, dorsal view of MPC-D 100/554; **E**, lateral view of MPC-D 100/554, right side of the photograph is dorsal side; **F**, right lateral view of AMNH 6487 (a partial skull); **G**, ventral oblique posterolateral view of right posterior parietal bar of AMNH 6487; **H**, dorsal view of MPC-D 100/537 parietosquamosal frill. Note that the matrix and modeling clays supporting some parts of this specimen are shaded since the color of the clay obscures the frill margin. **Abbreviation**: **pi**, process projecting inward to the parietal fenestra. Black arrows indicate the processes. Scale bars equal 5 cm. Scale bars of A-C are produced based on the frill width reported in Hone et al. (2016).

TABLE 1. Summary of measurements and degrees of undulation development of selected protoceratopsid specimens in this study. * indicates the measurements are estimated. **Abbreviations**: **TSL**, total skull length; **BSL**, basal skull length; **FL**, frill length; **FHW**, frill half-width.

Specimen number	Taxon	Locality	TSL	BSL	FL	FHW	Source of measurement	Development of undulations	Figure numbers
AMNH 6419	*Protoceratops andrewsi*	Bayn Dzag	115	76	52	34	Hone et al. (2016)	moderately	Fig. 3C
AMNH 6487	*Protoceratops andrewsi*	Bayn Dzag	-	149*	97*	-	this study	moderately	Fig. 3F and G
MPC 100/534	*Protoceratops andrewsi*	Tugrikin Shire	222	157	153	144	this study	slightly	Fig. 8 in Hone et al. (2014)
MPC-D 100/537	*Protoceratops andrewsi*	Udyn Sayr	274*	168*	163	119	this study	slightly	Fig. 3G
AMNH 6408	*Protoceratops andrewsi*	Bayn Dzag	314	235	152	121	Hone et al. (2016)	moderately	Fig. 3A
MPC-D 100/555	*Protoceratops andrewsi*	Tugrikin Shire	360*	250*	160*	123*	this study	highly	Fig. 2D
MPC-D 100/554	cf. *Protoceratops andrewsi*	Bayn Dzag	-	-	-	160*	this study	moderately	Fig. 3D and E
AMNH 6425	*Protoceratops andrewsi*	Bayn Dzag	469	313	264	236	Hone et al. (2016)	slightly	not figured
AMNH 6466	*Protoceratops andrewsi*	Bayn Dzag	491	357	262	233	Hone et al. (2016)	moderately	Fig. 3B
MPC-D 100/540	*Protoceratops* sp.	Udyn Sayr	-	-	-	338	this study	slightly	Fig. 4A and B
MPC-D 100/551	*Bagaceratops* sp.	Udyn Sayr	140*	230*	90	146	this study	slightly	Fig. 4C

close observation; however, at least some of the processes are visible (Fig. 3A). Based on the figure in Sereno (2000) and observation of the displayed specimen, the lateralmost processes are the most prominent. Although the squamosal frill margin is not preserved on the right, the left squamosal seems to have at least two processes. AMNH 6466, also on display, also appears to have frill margin undulations, although their development is less pronounced (Fig. 3B). The shapes of these processes are more elliptical in dorsal view than those of AMNH 6408. There seem to be five processes on both sides, but their relative positions do not seem to be symmetrical. The squamosal frill margins of AMNH 6466 also have slightly developed processes, three on the right and at least one on the left. Another gallery specimen, AMNH 6419, with a basal skull length of only 76 mm (Table 1), also appears to have weakly developed processes including at least one process close to the midline on both sides of the posterior parietal bar (Fig. 3C). Although it is difficult to confirm, the frill margin undulations of these three AMNH gallery specimens appear to be real features of the frill and can not be attributed to breakage or postmortem modification by scavenging by insects or mammals, the latter frequently observed on *Protoceratops* specimens from the aeolian Djadokhta and Barun Goyot formations (Kirkland and Bader, 2010; Matsumoto and Saneyoshi, 2010; Saneyoshi et al., 2011).

Frill undulations were also observed on MPC-D 100/554 from Bayn Dzag (field number IPG-OUS18Sep-038, Ishigaki et al., 2018) that we tentatively assign to cf. *Protoceratops andrewsi* based on the shape of the parietal (Makovicky and Norell, 2006; Chinnery and Horner, 2007). The specimen preserves four processes (Fig. 3D). The lateralmost process is associated with short ridges that run perpendicular to the outer margin of the frill. Although it is very subtle, these processes appear to be imbricated (Fig. 3E), a feature that is characteristic of Centrosaurinae (Dodson et al., 2004). The imbrication of the processes is also seen on AMNH 6487, a partial skull preserving a partial right parietal and a right squamosal (Fig. 3F and G). The degree of imbrication tends to be most pronounced on the lateralmost processes.

Three specimens of *P. andrewsi* have been observed to have a process spanning the posterior margin of the midline

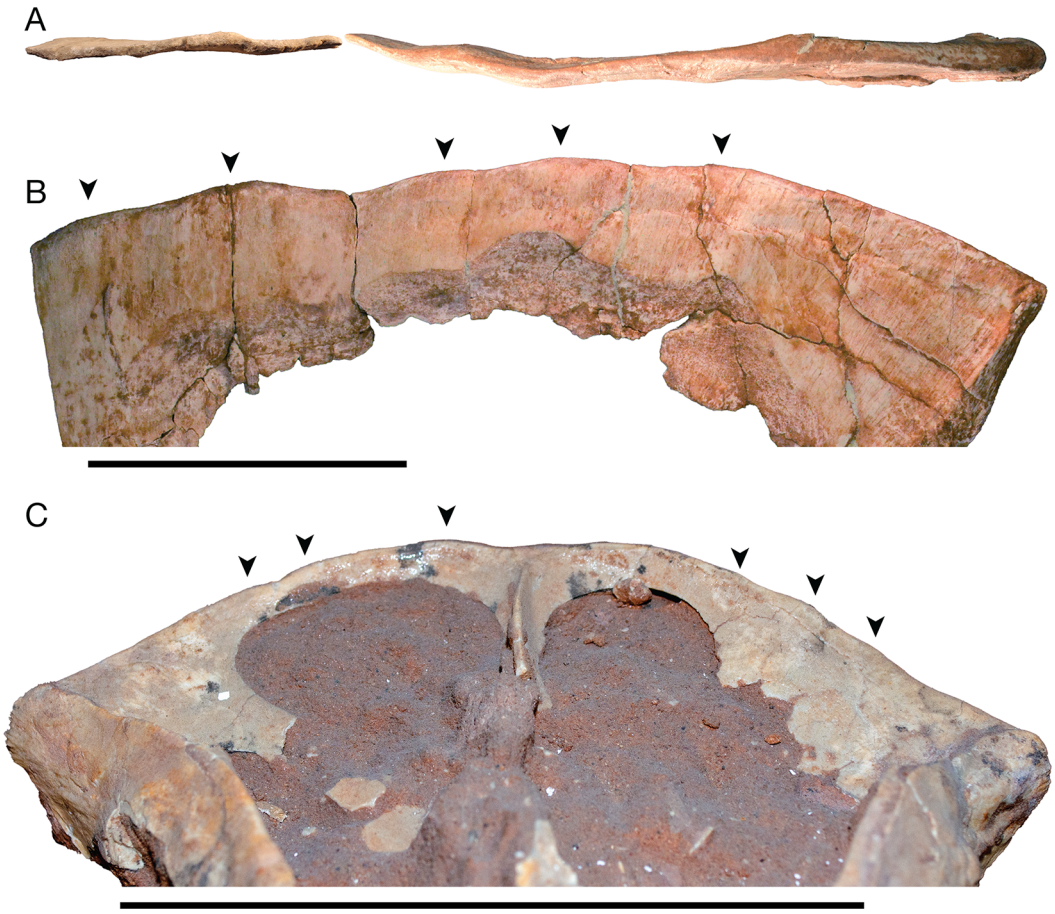

FIGURE 4. Protoceratopsid specimens showing frill margin undulations. **A**, *Protoceratops* sp., MPC-D 100/540 parietosquamosal frill in posterolateral view; **B**, in dorsal view; **C**, *Bagaceratops* sp., MPC-D 100/506, parietosquamosal frill in anterodorsal view. Black arrows indicate the processes. Scale bars equal 10 cm.

parietal bar (Fig. 3H). It is distinct on MPC-D 100/537 from Udyn Sayr (Handa et al., 2012) but only subtly developed on MPC-D 100/534, an almost complete skeleton and skull from Tugrikin Shire (Hone et al., 2014). AMNH 6425, an almost complete skull (Brown and Schlaikjer, 1940), is also interpreted as having this feature, but its identification is equivocal due to the poor preservation of this portion of the skull.

The undulations along the posterior parietal margins are also present on protoceratopsid specimens that are not assigned to *P. andrewsi*. MPC-D 100/540, a partial skull of *Protoceratops* sp., includes the left half of the parietal (Handa et al., 2012) that has at least five imbricated processes along the posterior margin (Fig. 4B and C). Although the specimen is fragmentary, the surface preservation is pristine, and there are no signs of postmortem damage along the posterior margin of the parietal, allowing us to confidently identify this feature. The *Bagaceratops* sp. parietal (MPC-D 100/551, mislabeled as MPC-D 100/551B in Czepiński, 2020) also has at least three processes, but their development is quite subtle (Fig. 4C).

Additional Observations on Protoceratopsid Frills

Several protoceratopsid specimens show a region of rugose texture and eminences on the lateral side of the squamosals (Fig. 5A) adjacent to the dorsoposterior margin of the infratemporal fenestra. Both rugosities and eminences co-occur in many individuals, but one feature or the other can be variably expressed. The rugosity on the squamosal is like the texture developed on the posterior part of the jugals and the postorbitals of some *Protoceratops* specimens, typically near the posterodorsal margin of the orbit (Fig. 5B). The eminences are typically expressed as elongated bumps. When multiple bumps co-occur, they are aligned in parallel.

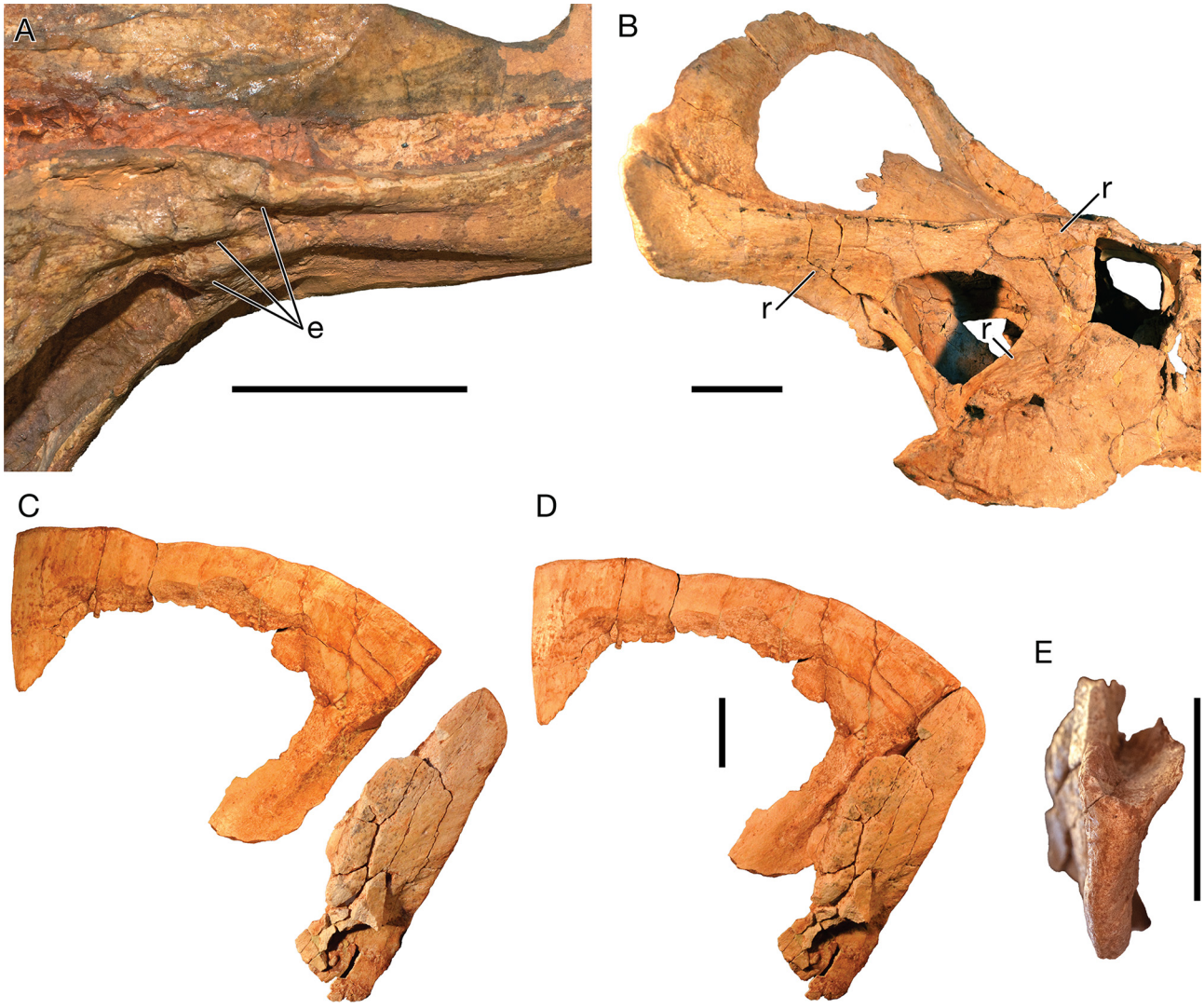

FIGURE 5. Protoceratopsid specimens showing some anatomical features that have been underappreciated in previous studies. **A**, dorsally obliqued anterolateral view of ridges on the lateral surface of left squamosal of AMNH 6433, *P. andrewsi*, note the posterior parts of squamosal including ridges are not preserved and sculpted; **B**, right lateral view of the skull of MPC-D 100/530, *P. andrewsi* showing rugosity on squamosal, postorbital, and jugal; C-E, parietosquamosal frill of MPC-D 100/540; **C**, disarticulated parietal and squamosal; **D**, articulated parietal and squamosal; **E**, posterior view of squamosal, showing deeply concaved parietal contact. **Abbreviations**: **e**, eminence; **r**, rugosity Scale bars equal 5 cm.

Although the superb articulated preservation of many *Protoceratops* specimens allows for the detailed investigation of their anatomy, the information on the articular surface of individual skull bones is poorly understood. The disarticulated partial skull of MPC-D 100/540 (*Protoceratops* sp.) presents the unique opportunity to observe the parietosquamosal contact of this genus in detail, revealing that the convex parietal inserts into the deeply concave articulating surface of the squamosal (Fig. 5C-E).

DISCUSSION

Evolution of Frill Margin Undulations of Protoceratopsids

In this study, we confirm the presence of marginal frill undulations in *Protoceratops andrewsi*, a feature that is common in ceratopsids. This feature on *P. andrewsi* was first noted by Sereno (2000) but subsequently discounted by Makovicky (2002). The presence of frill margin undulations on *Protoceratops* sp. and *Bagaceratops* sp. suggests that the

undulated frill margin is not an autapomorphy of *P. andrewsi* as suggested by Sereno (2000) but is rather potentially a synapomorphy for Protoceratopsidae. In Ceratopsoidea, a similar feature was reported by Nessov (1995) on a squamosal of *Turanoceratops* with a "slightly serrated or unserrated along the posterolateral margin". Unfortunately, the squamosal is now missing (Sues and Averianov, 2009), so its presence cannot be confirmed. A frill margin undulation has not been reported in *Zuniceratops* (Wolfe et al., 2010); however, the frill margin is poorly represented in the known specimens. Additional frill specimens of non-ceratopsid ceratopsoids will be critical to our understanding of the evolution of frill margin undulations and their associated ornamentations.

Although the protoceratopsid frill itself likely functioned as a display structure either intra-, interspecifically or both (Dodson, 1976; Maiorino et al., 2015; Hone et al., 2016; Knapp et al., 2021), the subtlety of undulations and the lack of systematic patterns relative to size increase or sexual dimorphism in the undulation morphology among the examined individuals (Table 1) do not provide unequivocal support for the hypothesis that the undulations contributed to a display function in this group. This interpretation could be rejected if the processes were in some way exaggerated by soft tissues. However, we did not find any signs of epiossifications on the examined protoceratopsid specimens or evidence (e.g., neurovascular grooves) for attachment points for overlying cornified sheaths (Hieronymus et al., 2009), although rugose texturing or small bumps were occasionally observed on some processes, which cannot be discounted as being associated with overlying soft tissues. Even if the undulations were not associated with enlarged soft tissue structures, they may still have been covered with pronounced scales as suggested by bumps on parietal midline bars, squamosals, and supraorbital regions as well as epiparietals and episquamosals of centrosaurines (Hieronymus et al., 2009). Further detailed observations on the surface texture and osteohistological analyses of protoceratopsid parietosquamosal frills that are beyond the scope of this study are necessary to elucidate the possible presence of soft tissue on these processes during life. Based on the dataset of VanBuren et al. (2015), the ratio of total skull length/basal skull length of *P. andrewsi* is exceptionally high among non-ceratopsid ceratopsians and within the range of ceratopsids (*P. andrewsi* 2.13; non-ceratopsid ceratopsians except *P. andrewsi* 1.01-1.32; ceratopsids 1.87-2.56). Our observations, therefore, suggest that frill undulations occur when the frill is enlarged in the ceratopsian evolution, such as seen in *Protoceratops*.

The imbrications of parietal frill margin undulations have been regarded as a synapomorphy of centrosaurines (e.g., Dodson et al., 2004). Although the imbricated processes seen on some protoceratopsid specimens are generally very subtle compared to centrosaurines, the pattern of the imbrications (the anterior margins of processes shift ventrally, and the posterior margins dorsally) is the same as that observed in centrosaurines, suggesting that the frill margin undulations in these clades are not independently acquired, but are homologous.

Chiba et al. (2017) suggested that epiparietal morphology was highly plastic in non-eucentrosauran centrosaurines (e.g., *Xenoceratops* [Ryan et al., 2012] and *Wendiceratops* [Evans and Ryan, 2015]) and became relatively fixed in eucentrosaurans. The degree of plasticity seen in the morphology, number, and location of protoceratopsid frill processes is even higher than that of non-eucentrosauran centrosaurines, suggesting that the plasticity of this feature was present in the common ancestor of Coronosauria and decreased during the evolution of Ceratopsoidea.

As frill margin imbrications are potentially a shared feature between protoceratopsids and centrosaurines, the morphology of the parietosquamosal contact of protoceratopsids is also similar to that of centrosaurines. The parietosquamosal contact is a buttress-like structure made of the convex contact surface of the parietal and the concave squamosal contact. Chasmosaurines differ from centrosaurines in having a contact that is relatively flat in cross-section (Ryan and Russell, 2005; Longrich, 2013). The parietosquamosal contact of *Protoceratops* was previously coded as the chasmosaurine-like condition (Ryan and Russell, 2005), but our observations clearly indicate that protoceratopsids have a deeply concaved centrosaurine-type parietosquamosal contact (Fig. 5E). Additionally, some *Protoceratops andrewsi* have a short process projecting posteriorly from the anterior margin of the parietal fenestra (e.g., AMNH 6466 and AMNH 6408 in Fig. 3A and B) which has been listed as one of three diagnostic characters for *Protoceratops andrewsi* (Makovicky, 2002). However, similar processes are reported in many centrosaurine specimens (e.g., Holmes et al., 2019; Brown et al., 2020), suggesting that this structure may also be a shared feature between protoceratopsids and centrosaurines.

Comments on the Cranial Features Shared within Marginocephalia

In reference to the bumps or ridges on the lateral surface of *Protoceratops* squamosals, similar structures are often reported in centrosaurines (Penkalski and Dodson, 1999; Sampson et al., 2013; Rivera-Sylva et al., 2016; Chiba et al., 2017) and have been suggested to be associated with overlying scales (Hieronymus et al., 2009). Similar structures to the eminences and rugosities on squamosals, postorbitals or jugals seen on protoceratopsids can also be seen on these elements of basal ceratopsians such as *Yinlong* (Xu et al., 2006; Han et al., 2015), *Archaeoceratop*s (You and Dodson, 2003), and *Auroraceratops* (Morschhauser et al., 2019). Furthermore, the similarities have been pointed out between the nodes on supraorbitals, postorbitals, and squamosals of pachycephalosaurs and the bumps in corresponding locations of centrosaurines (Hieronymus et al., 2009). Although the homology of ornamentations on the circumorbital regions and the lateral surface of squamosals have not been thoroughly investigated, the potential integumentary traces on *Protoceratops* squamosals imply the deeply nested homology of facial integumentary structures in various marginocephalians.

CONCLUSION

We regard that undulated frill margins exist in virtually all examined protoceratopsid specimens unless the feature has been taphonomically altered. The location of each process is variable within an individual bilaterally and among individuals. The degree of undulations is also variable among the specimens examined and does not appear to exhibit a systematic pattern relative to size increase or sexual dimorphism. Our examination of *Protoceratops andrewsi* and protoceratopsid frills has brought insights regarding the morphology and evolutionary implications of frill margin undulations in Ceratopsia. Our findings indicate that *P. andrewsi* has frill margin undulations, contrary to most of the previous studies. Furthermore, the undulated frill margin is not a unique characteristic of *P. andrewsi* but may be a shared feature in protoceratopsids or even Coronosauria. Frill margin undulations seem to have evolved when the frill itself was enlarged in the ceratopsian evolutionary history. Due to the subtlety of the frill undulations in protoceratopsids, it is plausible that these undulations, first a by-product of an enlarged frill, were later augmented by epiossifications in the ceratopsids for signaling functions. Several other anatomical features, such as imbrications of frill margins and the parietal contact of the squamosals, highlight the similarity between protoceratopsids and centrosaurines that have not been previously documented. Detailed observations, including osteohistological analyses of frill and other skull elements on other non-ceratopsid ceratopsians, as well as discoveries of more non-ceratopsid ceratopsoid specimens, will be critical to further elucidating the frill and facial integumentary structures in the ceratopsian evolution.

ACKNOWLEDGMENTS

We are thankful to Y.-N. Lee for giving us an opportunity to contribute to this book honoring Louis L. Jacobs and for handling the manuscript. We would like to thank Y. Matsumoto at HMNS for sharing the specimen information and the field photographs of MPC-D 100/555 when we initiated this project. We would also like to thank S. Suzuki, M. Watabe, Y. Matsumoto (HMNS), M. Norrell and K. Mehling (AMNH), and S. Ulziitseren at IP-MAS for specimen access. We also thank Y. Matsumoto (HMNS), P. J. Currie (University of Alberta), and K. S. Brink (University of Manitoba) for discussions. We are thankful to A. R. Fiorillo and A. A. Farke for their constructive suggestions as reviewers. This research was funded, in part, by the Private University Research Branding Project (Okayama University of Science) for KC, MS, SK, and YY provided by the Ministry of Education, Culture, Sports, Science and Technology, Japan, and the Grant-in-Aid for Early-Career Scientists (Project no. 19K14831) for KC by the Japan Society for the Promotion of Science. Lastly, we would like to show our gratitude to Louis L. Jacobs for his tremendous contributions to various aspects of our society and also being our great friend, colleague, and academic grandfather.

AUTHOR CONTRIBUTIONS

KC and MJR designed the project and drafted the manuscript. KC, YY, and SK gathered and interpreted the data. All authors edited the manuscript.

LITERATURE CITED

Brown, B. & Schlaikjer, E. M. (1940). The structure and relationships of *Protoceratops*. *Annals of the New York Academy of Sciences*, 40(3),

133–266. https://doi.org/10.1111/j.1749-6632.1940.tb57047.x

Brown, C., Holmes, R., & Currie, P. (2020). A subadult individual of *Styracosaurus albertensis* (Ornithischia: Ceratopsidae) with comments on ontogeny and intraspecific variation in *Styracosaurus* and *Centrosaurus*. *Vertebrate Anatomy Morphology Palaeontology*, 8(1), 67–95. https://doi.org/10.18435/vamp29361

Butler, R. J., Upchurch, P., & Norman, D. B. (2008). The phylogeny of the ornithischian dinosaurs. *Journal of Systematic Palaeontology*, 6(1), 1–40. https://doi.org/10.1017/s1477201907002271

Chen, X. (2017). The discovery and significance of the protoceratopsid dinosaur from the Lower Cretaceous of Ordos region, Inner Mongolia. *Acta Geoscientica Sinica*, 1–5. https://doi.org/10.3975/cagsb.2017.02.08

Chen, X., Tan, K., Lu, L., & Ji, S. (2022). Occurrence of *Protoceratops hellenikorhinus* (Ceratopsia: Protoceratopsidae) in Alxa region, western Inner Mongolia, China. *Acta Geologica Sinica*, 96(11), 3722–3732. https://doi.org/10.19762/j.cnki.dizhixuebao.2022302

Chiba, K., Ryan, M. J., Fanti, F., Loewen, M. A., & Evans, D. C. (2017). New material and systematic re-evaluation of *Medusaceratops lokii* (Dinosauria, Ceratopsidae) from the Judith River Formation (Campanian, Montana). *Journal of Paleontology*, 92(2), 272–288. https://doi.org/10.1017/jpa.2017.62

Chinnery, B. J. & Horner, J. R. (2007). A new neoceratopsian dinosaur linking North American and Asian taxa. *Journal of Vertebrate Paleontology*, 27(3), 625–641. https://doi.org/10.1671/0272-4634(2007)27[625:anndln]2.0.co;2

Czepiński, Ł. (2020). New protoceratopsid specimens improve the age correlation of the Upper Cretaceous Gobi Desert strata. *Acta Paleontologica Polonica*, 65. http://www.app.pan.pl/article/item/app007012019.html

Dodson, P. (1976). Quantitative aspects of relative growth and sexual dimorphism in *Protoceratops*. *Journal of Paleontology*, 50(5), 929–940.

Dodson, P., Forster, C. A., & Sampson, S. D. (2004). Ceratopsidae. In D. B. Weishampel, P. Dodson, & H. Osmólska (Eds.), *The Dinosauria* (pp. 494–513). University of California Press. https://doi.org/10.1525/9780520941434-029

Evans, D. C. & Ryan, M. J. (2015). Cranial anatomy of *Wendiceratops pinhornensis* gen. et sp. nov., a centrosaurine ceratopsid (Dinosauria: Ornithischia) from the Oldman Formation (Campanian), Alberta, Canada, and the evolution of ceratopsid nasal ornamentation. *PLOS ONE*, 10(7), e0130007. https://doi.org/10.1371/journal.pone.0130007

Fastovsky, D. E., Badamgarav, D., Ishimoto, H., Watabe, M., & Weishampel, D. B. (1997). The paleoenvironments of Tugrikinshireh (Gobi Desert, Mongolia) and aspects of the taphonomy and paleoecology of *Protoceratops* (Dinosauria: Ornithischia). *PALAIOS*, 12(1), 59–70. https://doi.org/10.2307/3515294

Fastovsky, D. E., Weishampel, D. B., Watabe, M., Barsbold, R., Tsogtbaatar, K. H., & Narmandakh, P. (2011). A nest of *Protoceratops andrewsi* (Dinosauria, Ornithischia). *Journal of Paleontology*, 85(6), 1035–1041. https://doi.org/10.1666/11-008.1

Fostowicz-Frelik, L. & Słowiak, J. (2018). Bone histology of *Protoceratops andrewsi* from the Late Cretaceous of Mongolia and its biological implications. *Acta Palaeontologica Polonica*, 63(3), 503–517. https://doi.org/10.4202/app.00463.2018

Granger, W. & Gregory, W. K. (1923). *Protoceratops andrewsi*, a preceratopsian dinosaur from Mongolia. *American Museum Novitates*, 72, 1–9.

Gregory, W. K. & Mook, C. C. (1925). On *Protoceratops*, a primitive ceratopsian dinosaur from the Lower Cretaceous of Mongolia. *American Museum Novitates*, 156, 1–9.

Han, F.-L., Forster, C. A., Clark, J. M., & Xu, X. (2015). Cranial anatomy of *Yinlong downsi* (Ornithischia: Ceratopsia) from the Upper Jurassic Shishugou Formation of Xinjiang, China. *Journal of Vertebrate Paleontology*, 36(1), e1029579. https://doi.org/10.1080/02724634.2015.1029579

Handa, N., Watabe, M., & Tsogtbaatar, K. (2012). New specimens of *Protoceratops* (Dinosauria: Neoceratopsia) from the Upper Cretaceous in Udyn Sayr, southern Gobi area, Mongolia. *Paleontological Research*, 16(3), 179–198. https://doi.org/10.2517/1342-8144-16.3.179

Hieronymus, T. L., Witmer, L. M., Tanke, D. H., & Currie, P. J. (2009). The facial integument of centrosaurine ceratopsids: morphological and histological correlates of novel skin structures. *The Anatomical Record*, 292(9), 1370–1396. https://doi.org/10.1002/ar.20985

Holmes, R. B., Persons, W. S., Rupal, B. S., Qureshi, A. J., & Currie, P. J. (2019). Morphological variation and asymmetrical development in the skull of *Styracosaurus albertensis*. *Cretaceous Research*, 104308. https://doi.org/10.1016/j.cretres.2019.104308

Hone, D. W. E., Farke, A. A., Watabe, M., Shigeru, S., & Tsogtbaatar, K. (2014). A new mass mortality of juvenile *Protoceratops* and size-segregated aggregation behaviour in juvenile non-avian dinosaurs. *PLOS ONE*, 9(11), e113306. https://doi.org/10.1371/journal.pone.0113306

Hone, D. W. E., Wood, D., & Knell, R. J. (2016). Positive allometry for exaggerated structures in the ceratopsian dinosaur *Protoceratops andrewsi* supports socio-sexual signaling. *Palaeontologia Electronica*, 19(1), 1–13. http://palaeo-electronica.org/content/2016/1369-sexual-selection-in-ceratopsia

Ishigaki, S., Tsogtbaatar, K., Toyoda, S., Mainbayar, B., Noumi, Y., Takahashi, A., Buyantegsh, B., Byambaa, P., Zorig, E., Bayardorj, C., Ochirjantsan, E., Saneyoshi, M., Hayashi, S., & Chiba, K. (2018). Report of the Okayama University of Science – Mongolian Institute of Paleontology and Geology Joint Expedition in 2018. *Bulletin of Research Institute of Natural Sciences, Okayama University of Science*, 44, 19–32.

Kielan-Jaworowska, Z. & Barsbold, R. (1972). Narrative of the Polish-Mongolian Palaeontological Expeditions 1967-1971. *Palaeontologia Polonica*, 27, 5–13.

Kirkland, J. I. & Bader, K. (2010). Insect trace fossils associated with *Protoceratops* carcasses in the Djadokhta Formation (Upper Cretaceous), Mongolia. In M. J. Ryan, B. J. Chinnery-Allgeier, & D. A. Eberth (Eds.), *New Perspectives on Horned Dinosaurs: The Royal Tyrrell Museum Ceratopsian Symposium* (pp. 509–519). Indiana University Press.

Knapp, A., Knell, R. J., & Hone, D. W. E. (2021). Three-dimensional geometric morphometric analysis of the skull of *Protoceratops andrewsi* supports a socio-sexual signalling role for the ceratopsian frill. *Proceedings of the Royal Society B: Biological Sciences*, 288(1944), 20202938. https://doi.org/10.1098/rspb.2020.2938

Kurzanov, S. M. (1972). Sexual dimorphism in protoceratopsians. *Palaeontological Journal*, 1, 91–97.

Lambert, O., Godefroit, P., Li, H., Shang, C.-Y., & Dong, Z.-M. (2001). A new species of *Protoceratops* (Dinosauria, Neoceratopsia) from the Late Cretaceous of Inner Mongolia (P. R. China). *Bulletin de l'Institut royal des Sciences naturelles de Belgique. Sciences de la Terre*, *Supplement* 71, 5–28.

Maiorino, L., Farke, A. A., Kotsakis, T., & Piras, P. (2015). Males

resemble females: re-evaluating sexual dimorphism in *Protoceratops andrewsi* (Neoceratopsia, Protoceratopsidae). *PLOS ONE*, 10(5), e0126464-22. https://doi.org/10.1371/journal.pone.0126464

Makovicky, P. (2002). *Taxonomic revision and phylogenetic relationships of basal Neoceratopsia (Dinosauria: Ornithischia)*. Columbia University.

Makovicky, P. J. & Norell, M. A. (2006). *Yamaceratops dorngobiensis*, a new primitive ceratopsian (Dinosauria: Ornithischia) from the Cretaceous of Mongolia. *American Museum Novitates*, 3530, 1–42. https://doi.org/10.1206/0003-0082(2006)3530[1:ydanpc]2.0.co;2

Mallon, J. C., Holmes, R. B., & Rufolo, S. J. (2023). Development and homology of the medial parietal ornamentation in centrosaurine ceratopsids (Dinosauria, Ornithischia). *Journal of Vertebrate Paleontology*, 42(5), e2211637. https://doi.org/10.1080/02724634.2023.2211637

Matsumoto, Y. & Saneyoshi, M. (2010). Bored dinosaur skeletons. *The Journal of the Geological Society of Japan*, 116(1), I–II. https://doi.org/10.5575/geosoc.116.1.i_ii

Morschhauser, E. M., Li, D., You, H., & Dodson, P. (2019). Cranial anatomy of the basal neoceratopsian *Auroraceratops rugosus* (Ornithischia: Ceratopsia) from the Yujingzi Basin, Gansu Province, China. *Journal of Vertebrate Paleontology*, 38(sup1), 36–68. https://doi.org/10.1080/02724634.2017.1399136

Nessov, L. A. (1995). *Dinozavry Severnoy Yevrazii: novyye dannyye o sostave kompleksov, ekologii i paleobiogeografii* [Dinosaurs of Northern Eurasia: New data on the composition of assemblages, ecology, and paleobiogeography]. Izdatelstvo Sankt-Peterburgskogo universiteta, St.-Petersburg.

Ryan, M. J., Evans, D. C., & Shepherd, K. M. (2012). A new ceratopsid from the Foremost Formation (middle Campanian) of Alberta. *Canadian Journal of Earth Sciences*, 49(10), 1251–1262. https://doi.org/10.1139/e2012-056

Ryan, M. J., Russell, A. P., Eberth, D. A., & Currie, P. J. (2001). The taphonomy of a *Centrosaurus* (Ornithischia: Ceratopsidae) bone bed from the Dinosaur Park Formation (Upper Campanian), Alberta, Canada, with comments on cranial ontogeny. *PALAIOS*, 16, 482–506. https://doi.org/10.2307/3515564

Sampson, S. D., Ryan, M. J., & Tanke, D. H. (1997). Craniofacial ontogeny in centrosaurine dinosaurs (Ornithischia: Ceratopsidae): taxonomic and behavioral implications. *Zoological Journal of the Linnean Society*, 121(3), 293–337. https://doi.org/10.1111/j.1096-3642.1997.tb00340.x

Saneyoshi, M., Watabe, M., Suzuki, S., & Tsogtbaatar, K. (2011). Trace fossils on dinosaur bones from Upper Cretaceous eolian deposits in Mongolia: Taphonomic interpretation of paleoecosystems in ancient desert environments. *Palaeogeography, Palaeoclimatology, Palaeoecology*, 311(1–2), 38–47. https://doi.org/10.1016/j.palaeo.2011.07.024

Saneyoshi, M., Watabe, M., Tsubamoto, T., Tsogtbaatar, K., Chinzorig, T., & Suzuki, S. (2010). Report of the HMNS-MPC Joint Paleontological Expedition in 2007. In T. Tsubamoto (Ed.), *Hayashibara Museum of Natural Sciences Research Bulletin Vol. 3* (pp. 19–28). Hayashibara Museum of Natural Sciences.

Sereno, P. C. (2000). The fossil record, systematics and evolution of pachycephalosaurs and ceratopsians from Asia. In M. J. Benton, M. A. Shishkin, D. M. Unwin, & E. N. Kurochkin (Eds.), *The age of dinosaurs in Russia and Mongolia* (pp. 480–516). Cambridge University Press.

Sues, H.-D. & Averianov, A. (2009). *Turanoceratops tardabilis*—the first ceratopsid dinosaur from Asia. *Naturwissenschaften*, 96(5), 645–652. https://doi.org/10.1007/s00114-009-0518-9

Tsogtbaatar, K. & Chinzorig, T. (2010). Fossil specimens prepared in Mongolian Paleontological Center: 2002–2008. In T. Tsubamoto (Ed.), *Hayashibara Museum of Natural Sciences Research Bulletin Vol. 3* (pp. 155–166). Hayashibara Museum of Natural Sciences.

VanBuren, C. S., Campione, N. E., & Evans, D. C. (2015). Head size, weaponry, and cervical adaptation: Testing craniocervical evolutionary hypotheses in Ceratopsia. *Evolution*, 69(7), 1728–1744. https://doi.org/10.1111/evo.12693

Watabe, M., Tsogtbaatar, K., Suzuki, S., & Saneyoshi, M. (2010). Geology of dinosaur-fossil-bearing localities (Jurassic and Cretaceous: Mesozoic) in the Gobi Desert: Results of the HMNS-MPC Joint Paleontological Expedition. In T. Tsubamoto (Ed.), *Hayashibara Museum of Natural Sciences Research Bulletin Vol. 3* (pp. 41–118). Hayashibara Museum of Natural Sciences.

Wolfe, D. G., Kirkland, J. I., Smith, D., Poole, K., Chinnery-Allgeier, B., & McDonald, A. (2010). *Zuniceratops christopheri*: the North American ceratopsid sister taxon reconstructed on the basis of new data. In M. J. Ryan, B. J. Chinnery-Allgeier, & D. A. Eberth (Eds.), *New perspectives on horned dinosaurs: The Royal Tyrrell Museum Ceratopsian Symposium* (pp. 91–98). Indiana University Press.

Xu, X., Forster, C. A., Clark, J. M., & Mo, J. (2006). A basal ceratopsian with transitional features from the Late Jurassic of northwestern China. *Proceedings of the Royal Society B: Biological Sciences*, 273(1598), 2135–2140. https://doi.org/10.1098/rspb.2006.3566

You, H. L. & Dodson, P. (2003). Redescription of neoceratopsian dinosaur *Archaeoceratops* and early evolution of Neoceratopsia. *Acta Palaeontologica Polonica*, 48(2), 261–272.

WINDOWS INTO SAUROPSID AND SYNAPSID EVOLUTION
Essays in honor of Prof. Louis L. Jacobs, pp. 151–165, 2023

A NEW LATE CRETACEOUS LEPTOCERATOPSID (DINOSAURIA: CERATOPSIA) FROM THE OLDMAN FORMATION (CAMPANIAN) OF ALBERTA, CANADA

MICHAEL J. RYAN[1,*], LOGAN MICUCCI[1], HANIKA RIZO[1], CORWIN SULLIVAN[2,3], YUONG-NAM LEE[4], and DAVID C. EVANS[4,5]

[1]Department of Earth Sciences, Ottawa-Carleton Geoscience Centre, Carleton University, Ottawa, ON Canada, MichaelJRyan@cunet.carleton.ca, LoganMicucci@cmail.carleton.ca, HanikaRizo@cunet.carleton.ca
[2]Department of Biological Sciences, University of Alberta, Edmonton, AB, Canada, corwin1@ualberta.ca
[3]Philip J. Currie Dinosaur Museum, Wembley, AB, Canada, corwin1@ualberta.ca
[4]School of Earth and Environmental Sciences, Seoul National University, Seoul 08826, South Korea, ynlee@snu.ac.kr
[5]Department of Natural History, Royal Ontario Museum, Toronto, ON, Canada, d.evans@utoronto.ca
[6]Department of Ecology and Evolutionary Biology, University of Toronto, Toronto, ON, Canada, d.evans@utoronto.ca

ABSTRACT Leptoceratopsid ceratopsians are poorly known from the Upper Cretaceous fossil record of the Western Interior of North America. The description of two leptoceratopsid frontals, ROMVP 66302, a left frontal from the holotype *Prenoceratops* bonebed in the Two Medicine Formation of Montana and TMP 2011.053.0027, a right leptoceratopsid frontal from the lower unit of the Oldman Formation (~77 Ma) of Alberta allows for the re-evaluation of potentially informative frontal phylogenetic characters. Straightness of the anterior margin of the frontal depression has been used to help distinguish *Cerasinops* and *Prenoceratops* from other leptoceratopsids in which the margin is rostrally convex. While the margin can indeed be considered straight in the holotype and previously referred specimens of *Prenoceratops*, this feature is distinctly crescentic in the slightly smaller ROMVP 66302. The apparent ontogenetic variability within *Prenoceratops* suggests that the condition of the margin should be carefully coded using only adult specimens. The right leptoceratopsid frontal TMP 2011.053.0027 has several unique features, including the presence of a transverse ridge that extends perpendicularly across the dorsal surface from the medial margin to the anterodorsal border of the orbit. The transverse ridge is separated from the crescentic anterior border of the frontal depression by a narrow band of smooth bone. The transverse ridge and raised anterior margin of the frontal depression both diverge from the same point on the slightly raised medial frontal margin. No other leptoceratopsid frontal presents this combination of features, leading us to assign the specimen to the new taxon *Gremlin slobodorum*.

KEYWORDS Ceratopsia, Leptoceratopsidae, Campanian, Alberta

INTRODUCTION

Leptoceratopsidae consists of non-ceratopsid, typically small-bodied neoceratopsians that are largely restricted to the Upper Cretaceous of western North America (Fig. 1) and Asia. However, a leptoceratopsid maxilla fragment (YPM-PU 24964) has been collected from the Campanian Tar Heel Formation (Black Creek Group) of North Carolina (Longrich 2016) and leptoceratopsid-like teeth and vertebrae have been found in the lower Campanian of the Kristianstad Basin of southern Sweden (Lindgren et al. 2007).

In North America, Maastrichtian strata have been the richest source of leptoceratopsids, including *Leptoceratops gracilis* Brown 1914 from the Lancian North American Land Vertebrate Age (NALVA) and *Montanoceratops cerorhynchus* Brown and Schlaikjer 1942 from the Edmontonian NALVA. *Leptoceratops* is known in Alberta from several partial or complete skeletons (i.e., AMNH 5205, CMN 8887, CMN 8888, CMN 8889) from the lower Scollard Formation (Eberth et al. 2013); in Montana from a partial skull from the upper half of the Hell Creek Formation in eastern Carter County ((UWGM-200) and an isolated tooth from ~75 m below the K-Pg boundary (UWGM-2), also from the Hell Creek Formation (Ott 2007); and in Wyoming from a partial skeleton (PU 18133) from the Lance Formation of the Bighorn Basin (Ostrom 1978) and an isolated tooth (AMNH

*Corresponding author

2571; McKenna and Love 1970) from the Pinyon Conglomerate in the Jackson Hole area. *Montanoceratops* is known in Alberta from a braincase (AMNH 5244), from the upper Tolman Member of the Horseshoe Canyon Formation (Makovicky 2001), and in Montana from the holotype skeleton (AMNH 5464) and a referred partial skeleton (MOR 542; Chinnery and Weishampel (1998)), both from the same locality in the St Mary River Formation. A partial skeleton from the Maastrichtian lower Willow Creek Formation of Alberta (TMP 1988.011.0001) that was previously referred to *Montanoceratops* by Ryan and Currie (1998) based on its field identification, needs re-evaluation. *Ferrisaurus sustutensis* Arbour and Evans 2019 is known from a single partial skeleton (RBCM P900) from British Columbia. Although its exact stratigraphic position is unknown, it has been identified as coming from the Tatlatui Member of the Tango Creek Formation that straddles the Campanian-Maastrichtian boundary in this part of the Sustut Basin (Arbour et al. 2020).

Campanian-aged leptoceratopsids from the Judithian NALVA include *Cerasinops hodgskissi* Chinnery and Horner 2007, *Prenoceratops pieganensis* Chinnery 2004 and *Unescoceratops koppelhusae* Ryan, Evans, Currie, Brown, and Brinkman 2012. *Cerasinops* from the lowermost Two Medicine Formation of Montana (Fig. 2) is known from the holotype (MOR 300) consisting of an associated skull and skeleton from Teton County and two partial skeletons (USNM 13863 and USNM 13864) from Pondera County (Chinnery and Horner 2007). *Prenoceratops* is known from four partial skeletons collected from a bonebed from the upper Two Medicine Formation of Montana on the Blackfeet Reservation, Pondera County (Fig. 2) and acquired by Canada Fossils (CF). Some of this material was incorporated into the composite mounts MNHM 000573-00000 and TCM 2001.96.4, the latter of which includes the holotype fused articular and surangular. The remaining Montanan *Prenoceratops* material was acquired by the Royal Ontario Museum, Ontario, before Canada Fossils went out of business. The isolated frontal TMP 1987.089.0008 collected from the upper unit (Dinosaur Park Formation equivalent) of the Oldman Formation has been referred to *Prenoceratops* sp. (Miyashita et al. 2010). *Unescoceratops* is known from the Campanian middle Dinosaur Park Formation (DP Fm) from the holotype dentary (TMP 1995.012.0006) collected from Bonebed 55, Steveville region of Dinosaur Provincial Park (DPP), Alberta (Fig. 2), and a partial dentary (TMP 1974.010.031) also collected from the DP Fm of DPP.

The oldest known leptoceratopsid is *Gryphoceratops morrisoni* Ryan, Evans, Currie, Brown, and Brinkman 2012, a species only represented by the holotype dentary (ROMVP 56635) collected from the Santonian of the Deadhorse Coulee Member of the Milk River Formation, Black Coulee, Warner County, Alberta (Fig. 2).

Multiple Asian leptoceratopsid taxa are also known. *Ischioceratops zhuchengensis* He, Makovicky, Wang, Chen, Sullivan, Han, and Xu, 2015 and *Zhuchengceratops inexpectus* Xu, Wang, Zhao, Sullivan, and Chen, 2010 are both known from partially articulated skeletons from the Maastrichtian Xingezhuang Formation of Shandong, China. Taxa from outside China include the large-bodied *Udanoceratops tschizhovi* Kurzanov 1992 (Djadokhta Formation; Campanian), known from a relatively complete skull from Mongolia.

In the southern hemisphere, the problematic taxon *Serendipaceratops arthurcclarkei* is based on an isolated ulna from the Aptian Wonthangii Formation and a referred ulna from the Aptian-Albian Eumaralla Formation of Australia. These ulnae have been reported to have leptoceratopsid-like affinities (Rich and Vickers-Rich 2003), although this has been challenged (Agnolin et al. 2010).

Here we describe the new leptoceratopsid frontals TMP 2011.053.0027 (Fig. 3A-C) from the lower Oldman Formation (upper Campanian) in southern Alberta and ROMVP 66302 (Fig. 4I-K) from the *Prenoceratops* bonebed in Montana. These specimens provide us with an opportunity to re-evaluate frontal characters previously considered taxonomically informative for leptoceratopsids. The recognition of TMP 2011.053.0027 as representing a new taxon also helps to narrow the temporal gap between *Gryphoceratops* and *Unescoceratops* in Alberta.

LOCALITIES

TMP 2011.053.0027 was collected from the Herronton SS zone, within 15 m of the top of the Taber Coal zone underlying the lower unit of the Campanian Oldman Formation (Fig. 1) in southern Alberta at 49°04'43"N 110°51'19"W (Fig. 2). The locality is along a southern tributary of the Milk River located on the southern Pinhorn Grazing Reserve adjacent to the Montana border (Fig. 2).

ROMVP 66302 was collected from the *Prenoceratops* bonebed in the Two Medicine Formation on the Blackfeet Indian Reservation in Pondera County, Montana (Fig. 2),

approximately 50 m below the Bearpaw-Two Medicine contact (Fig. 1) (Chinnery 2004).

REGIONAL GEOLOGY

The Upper Cretaceous Belly River Group of southern Alberta is composed of, in ascending stratigraphic succession, the conformable Foremost, Oldman, and Dinosaur Park formations (Fig. 1). The Dinosaur Park Formation (76.7-74.3 Ma; Ramezani et al., 2022) preserves a transgressive sequence of up to 70 m in Dinosaur Provincial Park of channel sandstones and overbank mudstones capped by a series of coals (Lethbridge Coal Zone) that grade into the overlying marine Bearpaw Formation (Eberth 2005). The Oldman (76.7 Ma; Ramezani et al., 2022 to ~77 Ma) and Foremost (~77 to ~80.2 Ma) formations are, respectively, up to 100 and 170 m in thickness (Eberth 2005) (Fig. 1). The Oldman Formation is informally divided into the upper, middle (Comrey Sandstone) and lower units. The upper unit, as exposed in southeastern Alberta, is time equivalent to the lower Dinosaur Park Formation in Dinosaur Provincial Park (Eberth and Hamlin 1993). Overall, the middle and lower units comprise lightly colored sandstones and mudstones deposited in a regressive setting, whereas the upper unit documents the beginning of a transgressive cycle that ended with the Bearpaw Sea covering much of southeastern Alberta (Eberth 2005). The lower unit represents a time of high basin-ward extension of the sediments that make up the Belly River Group, indicating a continuing regression of the nearby Western Interior Seaway, a trend that had begun as the upper Foremost Formation was being deposited (Eberth 2005).

Many fewer diagnostic dinosaur specimens are known from the Oldman Formation than from the Dinosaur Park Formation, partly due to the fact that the former has received much less prospecting attention (Evans and Ryan, 2015). While the upper unit of the Oldman Formation preserves taxa also found in the lower Dinosaur Park Formation of Dinosaur Provincial Park, only the tyrannosaurid *Daspletosaurus torosus* Russell 1970 and the hadrosaurine hadrosaurids *Brachylophosaurus canadensis* Sternberg 1953 and *Maiasaura* sp. (McFeeters et al. 2021) are known from skeletal material from the Comrey Sandstone, and only the centrosaurine ceratopsids *Albertaceratops nesmoi* Ryan 2007 and *Wendiceratops pinhornensis* Evans and Ryan 2015, the hadrosaurine *Gryposaurus* sp. (Scott et al. 2022), and the pachycephalosaur cf. *Stegoceras* Sternberg 1945 (Scott et al. 2022), are known from diagnostic, non-tooth skeletal remains from the lower unit.

The Campanian Two Medicine Formation (82.4 to ~75.2 Ma; Ramezani et al., 2022) in northwestern Montana is time equivalent to portions of the Belly River Group of Alberta (Fig. 1). The formation can be informally split into three portions. The lower portion is about 100 m thick, records a brief transgression of the Western Interior Seaway (Rogers et al. 1993), and overlies the Virgelle Sandstone which is composed of nearshore sandstone deposits (Trexler 2001). The middle portion is approximately 225 m thick and was deposited during a transgression of the Bearpaw Sea (a portion of the Western Interior Seaway). It is characterized by siltstones and mudstones with occasional sandstone inclusions (Rogers et al. 1993). The upper portion composes about half of the entire formation, being approximately 275 m thick (Rogers et al. 1993).

The Two Medicine Formation is well known for containing a large and diverse suite of fossil taxa (You and Dodson 2004), including the leptoceratopsid ceratopsians *Cerasinops hodgskissi* Chinnery and Horner 2007 and *Prenoceratops pieganensis* Chinnery 2004, and the centrosaurine ceratopsids *Achelousaurus horneri* Sampson 1995, *Einiosaurus procurvicornis* Sampson 1995, *Stellasaurus ancellae* Wilson, Ryan and Evans 2020, and *Styracosaurus ovatus* Gilmore 1930. In the context of this study, it is notable that *Prenoceratops* was described based on material collected from the uppermost portion of the Two Medicine Formation (Chinnery 2004) (Fig. 1), approximately time equivalent to the Bearpaw Formation in Alberta. The holotype and referred specimens of *Cerasinops* were collected from the lowermost Two Medicine Formation beds that are not far above the 80 Ma ash layer reported by Chinnery (2004) (Fig. 1), and approximately time equivalent to the Foremost Formation of the Belly River Group in Alberta.

MATERIALS AND METHODS

TMP 2011.053.0027 and ROMVP 66302 were photographed using an Apple iPhone 10, measured with a standard 30-cm ruler and Vernier 150 mm digital calipers, and described following standard anatomical terminologies for ceratopsians (e.g., You and Dodson 2004; Miyashita et al. 2010). Comparative measurements for other leptoceratopsid specimens were

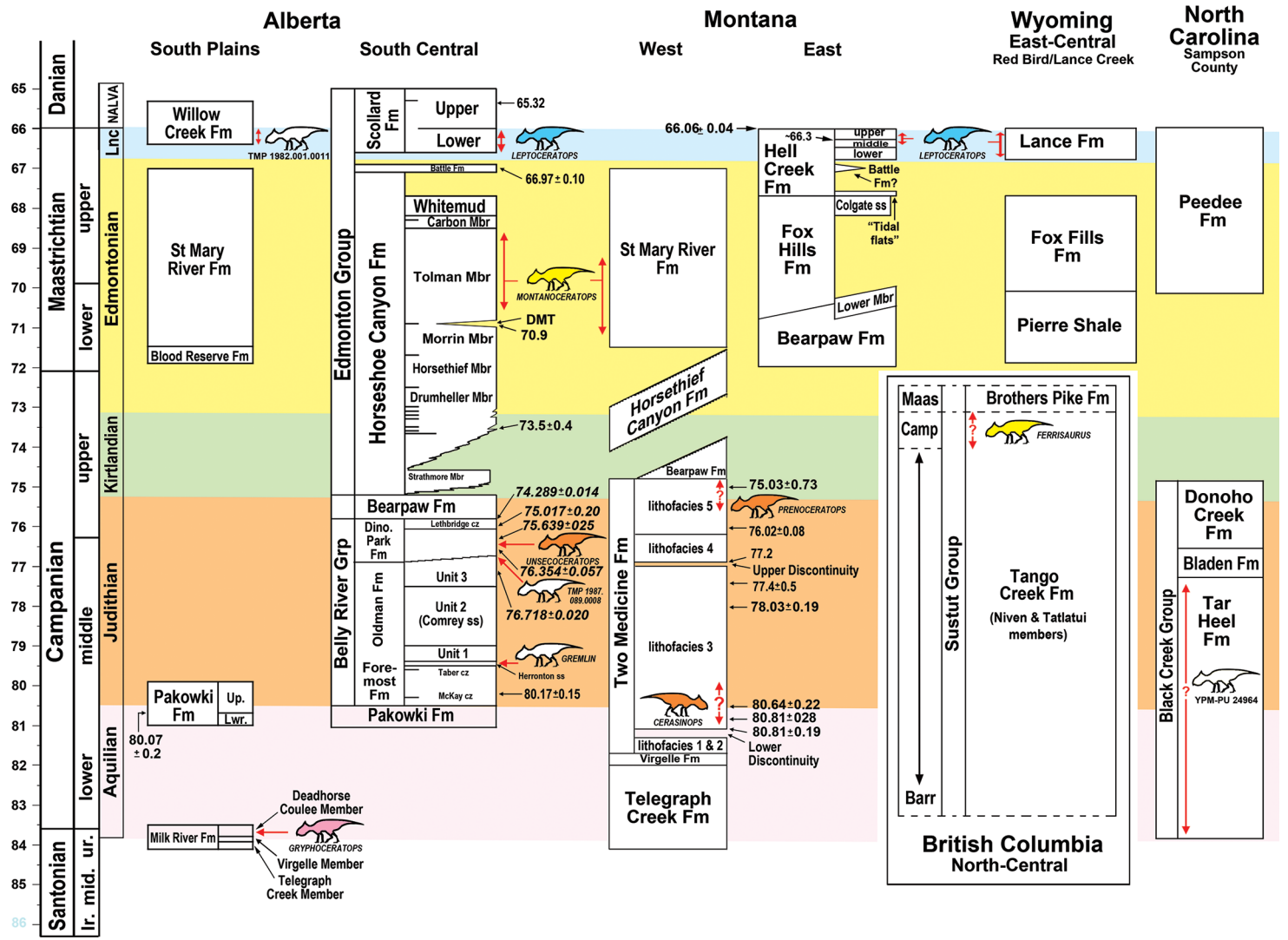

FIGURE 1. Stratigraphic and geographic distribution of North American leptoceratopsids. Chart and dates are adapted from Fowler (2017), except the British Columbia column that is adapted from Arbour et al. (2019); dates in italics for the Belly River Group of Alberta are from Ramezani et al. (2022). Note that Ramezani et al. (2022) report a more recent date from near the base of the Two Medicine Formation (CB061417-1) of ~82.42 Ma. Red arrows with question marks indicate that the range of a taxon is uncertain or that more than one specimen is known from a given formation. Note that the stratigraphic column for British Columbia (BC) is shown in an inset with its own time scale; see Evenchick and Thorkelson (2005) and Arbour et al. (2020) for discussion of the age and boundaries of the Sustut Group of BC. **Abbreviations**: **Barr**, Berriasian; **Camp**, Campanian; **cz**, coal zone; **Fm**, Formation; **Lnc**, Lancian; **lr**, lower; **Maas**, Maastrichtian; **mbr**, member; **mid**, middle; **ss**, sandstone; **ur**, upper

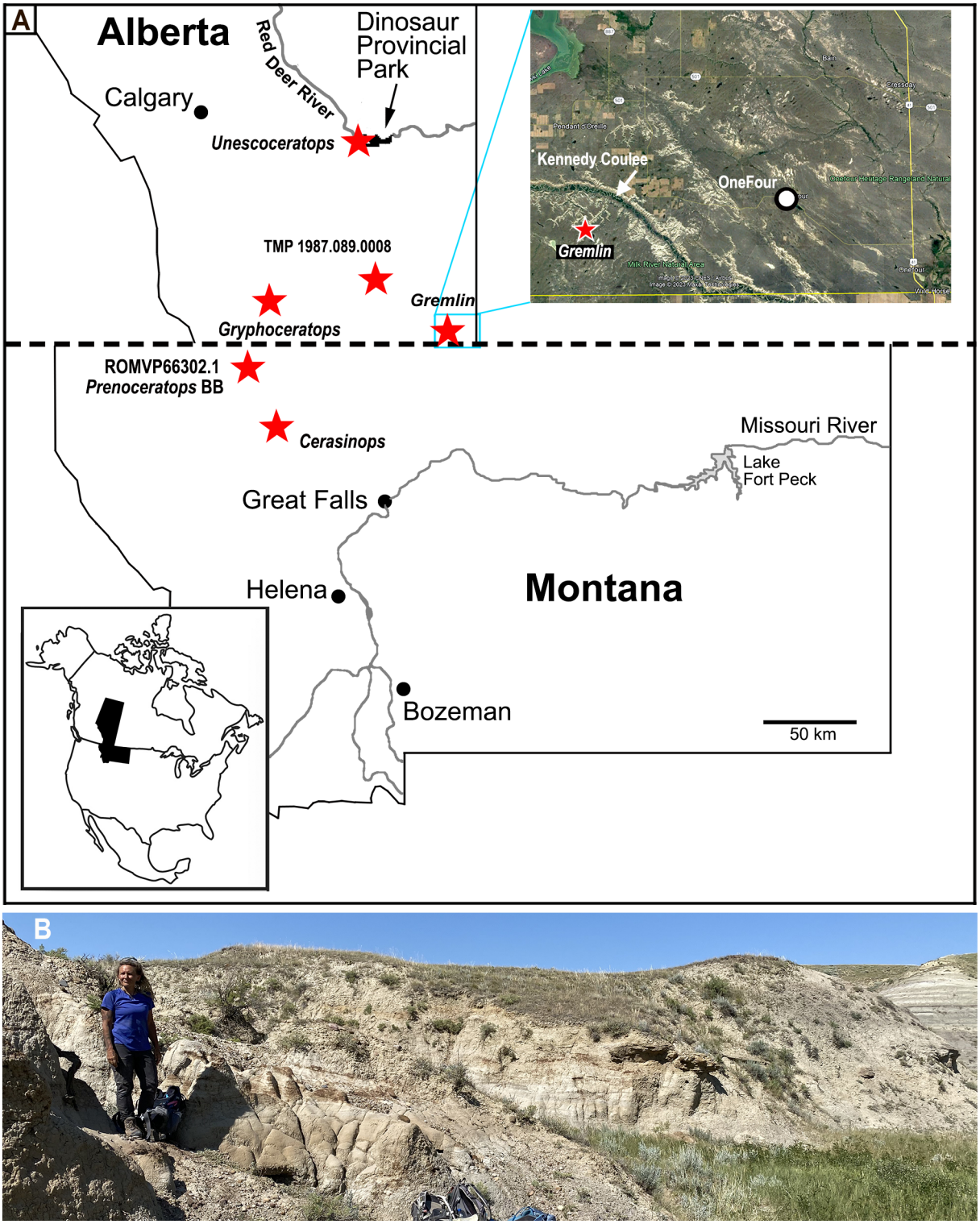

FIGURE 2. **A**, Locality map for *Cerasinop*s from Teton County, MT; *Unescoceratops* from Dinosaur Provincial Park, AB; ROMVP 66302 from the holotype *Prenoceratops* bonebed, Blackfoot Reservation, Pondera County, MT; TMP 2011.053.0027 from the South Pinhorn Grazing Reserve, AB; TMP 1987.089.0008 from Devil's Coulee, AB; and *Gryphoceratops* from Black Coulee, AB. **B**, photograph of the *Gremlin* locality with collector, Wendy Sloboda, standing where she found TMP 2011.053.0027. Map modified from Ryan et al. (2012). Southern Alberta municipal districts and counties inset photograph: Google, image © 2023 Maxar Technologies; image © 2023 CNES/ Airbus; accessed March 24, 2023.

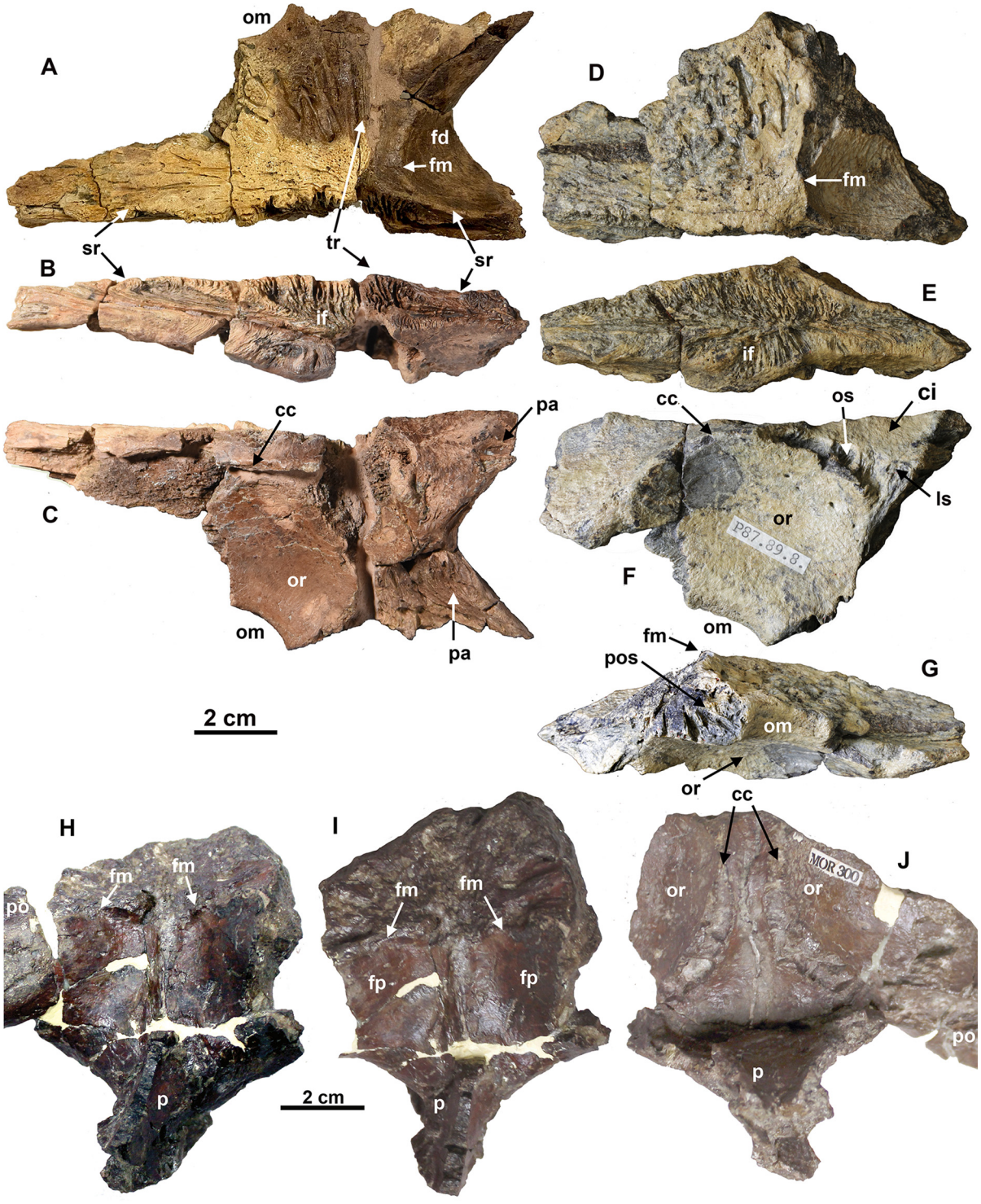

FIGURE 3. Leptoceratopsid frontals. *Gremlin slobodorum* (holotype) TMP 2011.053.0027 right frontal in **A**, dorsal; **B**, medial; and **C** ventral views. TMP 1987.089.0008 right frontal in **D**, dorsal; **E**, medial; **F**, ventral; and **G**, lateral views. *Cerasinops hodgskissi* (holotype) MOR 300 frontals in **H**, dorsal; **I**, anterodorsal; and **J**, ventral views. **Abbreviations**: **cc**, crista cranii; **ci**, impression of cerebrum; **fd**, frontal depression; **fm**, anterior margin of frontal depression; **if**, interfrontal suture; **ls**, laterosphenoid suture; **om**, orbital margin; **or**, roof of orbit; **os**, orbitosphenoid suture; **p**, parietal; **pa**, parietal suture; **po**, postorbital; **pos**, postorbital suture; **sr**, sagittal ridge; **tr**, transverse ridge.

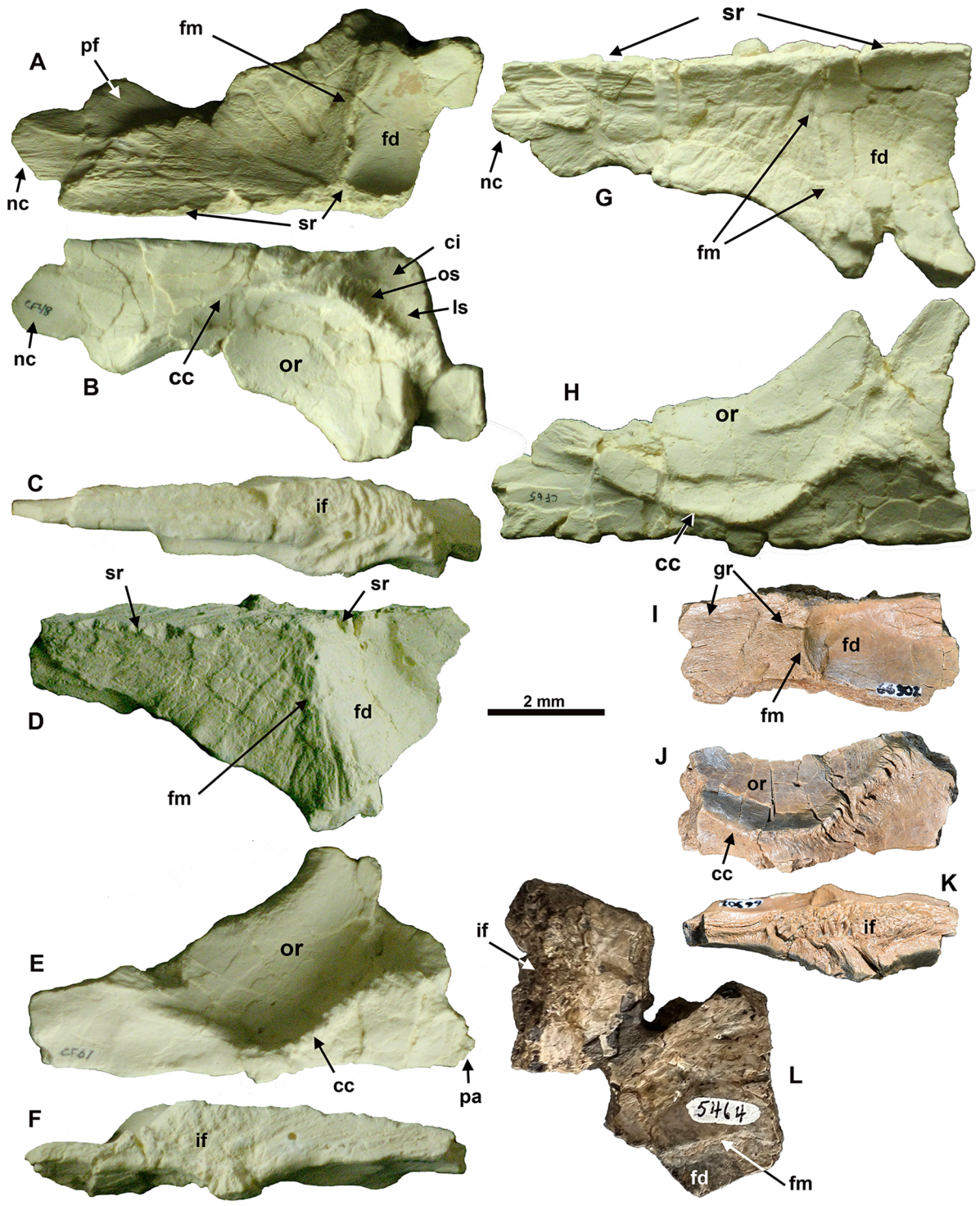

FIGURE 4. Leptoceratopsid frontals. *Prenoceratops pieganensis* CF48 (cast) right frontal in **A**, dorsal; **B**, ventral; and **C**, medial views. CF61 (cast) left frontal in **D**, dorsal; **E**, ventral; and **F**, medial views. CF65 (cast) left frontal in **G**, dorsal; and **F**, ventral views. The original frontals were incorporated into the composite mounts MNHM 000573-00000 and TCM 2001.96.4, but it is unknown which mount has which elements. ROMVP 66302 left frontal in **I**, dorsal; **J**, ventral; and **K**, medial views. *Montanoceratops cerorhynchus* (holotype) AMNH 5464 frontal in **L**, dorsal view. **Abbreviations**: **cc**, crista cranii; **ci**, impression of cerebrum; **fd**, frontal depression; **fm**, anterior margin of frontal depression; **gr**, groove; **if**, interfrontal suture; **ls**, laterosphenoid suture; **nc**, nasal contact; **or**, roof of orbit; **os**, orbitosphenoid suture; **pa**, parietal suture; **pf**, prefrontal articulation; **sr**, sagittal ridge.

obtained from the collections of the Canadian Museum of Nature, a cast of a *Leptoceratops* frontal (ROMVP 64223), and the literature. A phylogenetic analysis was conducted using the in the data matrix of Arbour and Evans (2019) with the TNT software package (Goloboff and Morles 2023).

Institutional Abbreviations — **AMNH**, American Museum of Natural History, New York, New York; **CF**, Canada Fossils, Calgary, Alberta; **CMN**, Canadian Museum of Nature, Ottawa, Ontario; **MOR**, Museum of the Rockies, Bozeman, Montana; **MNHM**, Mokpo Natural History Museum, South Korea; **PU**, Princeton University, Princeton, New Jersey; **ROM**, Royal Ontario Museum, Toronto, Ontario; **TCM**, Children's Museum of Indianapolis, Indiana; **TMP**, Royal Tyrrell Museum of Palaeontology, Drumheller, Alberta; **USNM**, Smithsonian Institution, Washington, D.C; **UWGM**, University of Wisconsin-Madison, Madison, Wisconsin; **YPM-PU**, Yale Peabody Museum, Princeton University collection, New Haven, Connecticut.

PERMITS — TMP 2011.053.0027 was collected following the Historical Resources Act of Alberta (Canada) under the Government of Alberta Permits to Excavate Palaeontological Resources Nos. 3951-E03 (DCE) and 3950-R03 (MJR).

NOMENCLATURAL ACTS

This published work and the nomenclatural acts it contains have been registered in ZooBank, the online registration system for the ICZN. The ZooBank LSIDs (Life Science Identifiers) can be resolved and the associated information is viewed through any standard web browser by appending the LSID to the prefix "http://zoobank.org/".

SYSTEMATIC PALAEONTOLOGY

Dinosauria Owen, 1842

Ornithischia Seeley, 1887

Ceratopsia Marsh, 1890

Neoceratopsia Sereno, 1986

Leptoceratopsidae Makovicky, 2001

Gremlin gen. nov.

urn:lsid:zoobank.org:act:74B2D4AC-09A7-49EB-A2E6-18CDB59BF738

Diagnosis. Monotypic, as for species.

Gremlin slobodorum, gen. et. sp. nov.

urn:lsid:zoobank.org:act:698361A5-68ED-474D-91E5-6AC0D24950B0

(Fig. 3A-C)

Type and only species — *Gremlin slobodorum*

Holotype — TMP 2011.053.0027, an incomplete frontal lacking a portion of the anterolateral margin (Fig. 3A-C).

Etymology — The generic name refers to a small, troublesome, imaginary creature blamed by early 20th century aviators for mysterious mechanical faults (Massinger 1944). The specific epithet honors Ed and Wendy Sloboda for their contributions to Albertan palaeontology, and Wendy for having discovered the holotype.

Diagnosis — Leptoceratopsid ceratopsian that exhibits the following features, each of which is autapomorphic within Leptoceratopsidae: transverse ridge of the frontal that extends across the dorsal surface from the medial margin to the anterodorsal border of the orbit; the transverse ridge is separated from the raised, crescentic anterior border of the frontal depression by a narrow band of smooth bone that continues as the smooth surface of the depression; transverse ridge and anterior margin of the frontal depression both diverge from the same point on the slightly raised medial frontal margin. No other leptoceratopsid has a transverse ridge developed separately from the margin of the frontal depression. In all other leptoceratopsids, the dorsum of the frontal either has a rugose portion that contacts the margin the frontal depression (*Cerasinops*, *Prenoceratops*), or is relatively smooth (*Leptoceratops*, *Montanoceratops*).

Locality, Horizon and Age — TMP 2011.053.0027 was collected from an outcrop of the lower unit of the middle Campanian Oldman Formation (Fig. 1), located in southern Alberta at 49°04'43"N 110°51'19"W (Fig. 2).

DESCRIPTIONS

TMP 2011.053.0027

TMP 2011.053.0027 (Fig. 3A-C) is an isolated right frontal. Portions of the anterolateral margin have been lost to erosion. A mediolaterally oriented gap immediately posterior to the transverse ridge has been infilled with epoxy putty, but very little bone has been lost. As preserved, the frontal is approximately triangular in dorsal outline, with the deep,

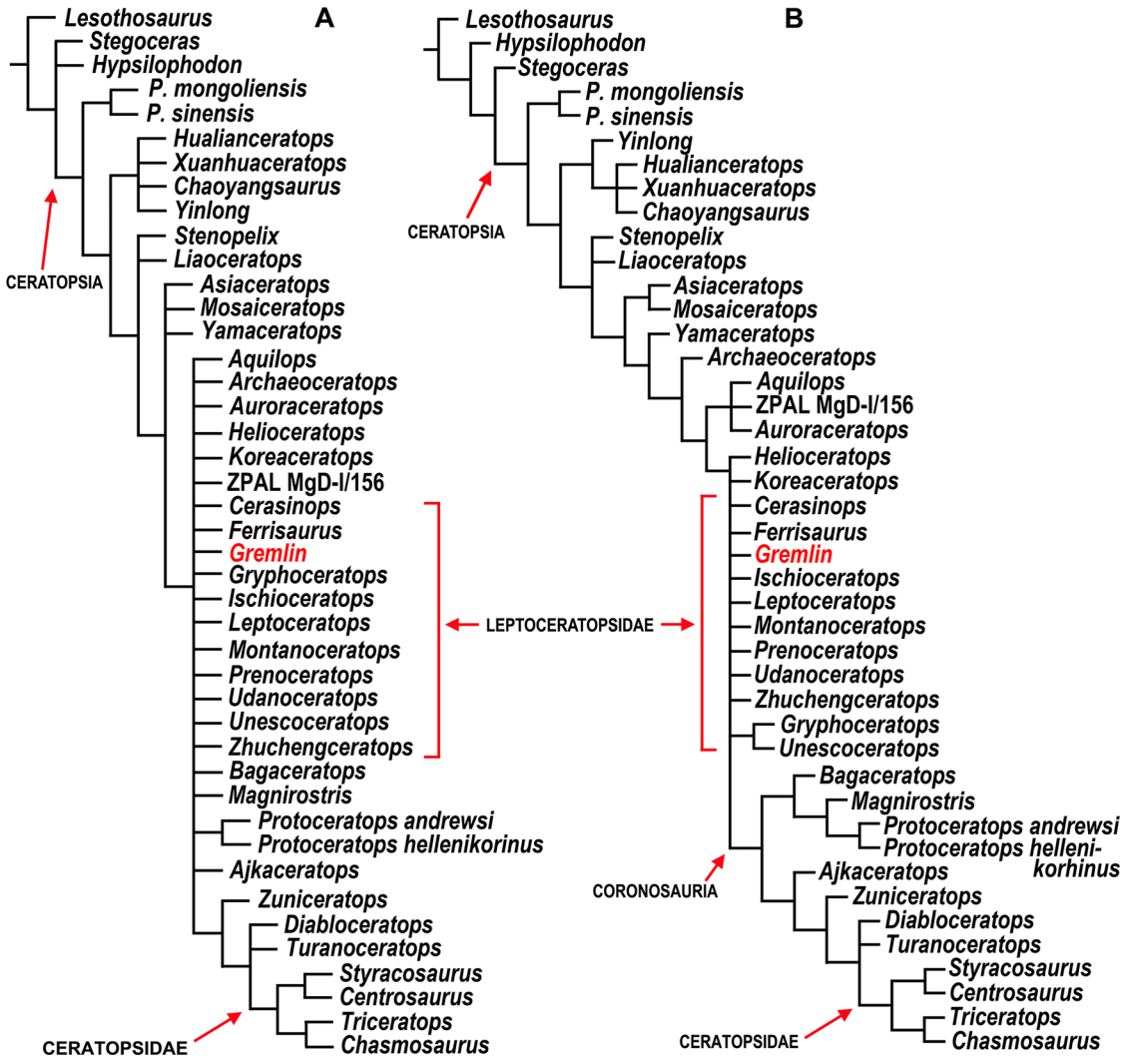

FIGURE 5. Results of a phylogenetic analysis of Ceratopsia using a matrix modified from Arbour and Evans (2019) to test rescored characters discussed in this paper. **A**, strict consensus cladogram of 746 most parsimonious trees, with a best tree length of 688 steps; consistency index (CI) of 0.45, and retention index (RI) 0.67; **B**, 50% majority rule cladogram. The taxa traditionally comprising Leptoceratopsidae are indicated in red brackets, but were not recovered as a monophyletic clade in this analysis.

almost sagittally oriented crenulated area for the left frontal. The frontal would have contacted the nasal anteriorly, the left frontal medially, the parietal posteriorly, the postorbital posterolaterally, and the prefrontal anterolaterally. The frontal forms approximately one-half of the dorsal orbital margin, as it does in *Leptoceratops* (Sternberg 1951).

The maximum preserved length of TMP 2011.053.0027 is approximately 120 mm and the maximum thickness is 24.1 mm, occurring at the medial margin of the transverse ridge. A fan of grooves and pits emanates from this high point to cover the dorsal surface of the bone, except for the frontal depression and a 10 mm-wide band of smooth bone along the depressions crescentic anterior margin. A portion of the orbital rim (Fig. 3A) emargination is visible, and the well-preserved roof of the orbit forms the adjacent part of the ventral surface (Fig. 3C).

The frontal depression occupies approximately the posterior third of the preserved length of the element's dorsal surface. The medial and anterior margins of the depression are formed by a crescentic raised, smoothly rounded rim, which diminishes in prominence posterolaterally. The interior of the depression is smooth.

The subtle transverse ridge and the anterior margin of the frontal depression both arise in a bifurcation of the medial

margin.

The dorsal surface is slightly deflected dorsally at the midline, and when in articulation with the left frontal would have contributed to a weak sagittal crest which would have continued onto the parietal. The otherwise vertical medial sutural surface for the left frontal is laterally deflected in dorsal view in the region of the transverse ridge which would have resulted in the sagittal ridge being asymmetrical; a similar asymmetry is seen in most articulated leptoceratopsid skulls.

Much of the ventral surface is occupied by the smooth roof of the orbital cavity. This is bordered medially by the crista cranii, most of which is broken away. The posteromedial and posterolateral corners of the frontal bear sutural surfaces for contact with overlapping processes of the parietal. In most leptoceratopsid frontals the sutural areas for the laterosphenoid and orbitosphenoid, as well as the impression of the olfactory bulb, and the nasal cavity are all clearly seen, but the present specimen is broken in the regions where those features would be expected. However, an ovoid cerebral fossa is present anterior to the posteromedial contact area for the parietal.

ROMVP 66302

ROMVP 66302 (Fig. 4I-K) is a fragment of an isolated left *Prenoceratops* frontal from a small individual based on its estimated original length (110 mm; approximately 75% of the estimated reconstructed length of TMP 2011.053.0027). Much of the lateral and anterior margins have been lost to breakage. Its preserved maximum length is approximately 44 mm, and it has a maximum thickness of 14 mm measured at the anteromedial margin of the frontal depression. From this point, the frontal thins gradually in the anterior direction and more sharply in the posterior direction. The dorsal surface, excluding the frontal depression, is ornamented with small, closely packed pits which give way to shallow, narrow grooves on the anteriormost preserved part of the frontal. In the region where the pits begin their transition into grooves, the dorsal surface is marked by an approximately transverse fracture that appears to be the result of dorsoventral crushing. The crescentic, slightly elevated anterior margin of the smooth frontal depression is accentuated in its lateralmost preserved portion by a narrow depression (approximately 0.5 cm in anteroposterior width) adjacent to its anterior edge. The dorsal surface of the frontal has a lightly inscribed groove, possibly a vascular impression, that extends anteriorly from the margin of the depression to the preserved anterior margin of the element.

The frontal depression occupies slightly more than one-half of the anteroposterior length of the dorsal surface of the preserved part of the frontal and thins to a minimum thickness of 4 mm at its posterior margin. The morphology of the medial surface of the bone indicates the sutural surface that would have formed an interdigitating contact with the right frontal, and the contact does not appear to be asymmetrical in dorsal view as it is in other *Prenoceratops* frontals (Fig. 4A-H) from the same bonebed. As in TMP 2011.053.0027, the medial margin of the frontal is deflected slightly dorsally, reaching its maximum height where it intersects the anteromedial margin of the frontal depression, and would have contributed to a very low sagittal ridge.

The ventral surface of the frontal preserves the smooth roof of the orbital cavity. The sutural surface for the orbitosphenoid is preserved, unlike in TMP 2011.053.0027, but that for the laterosphenoid is not.

PHYLOGENETIC ANALYSIS

To date, only three phylogenetically informative characters have been identified for the leptoceratopsid frontal: Ch 97, large caudolateral process on the frontal: absent (0), present (1); Ch 98, degree of incisure of frontal fossae/parieto-frontal contact: incisures absent (0), shallow (1), deeper (2); fronto-parietal depression present (3); invaginated by fontanelle, secondary skull roof present (4); and Ch 99 (rostral border of frontal depression: rostrally convex (0), transversely straight (1) (Morschhauser et al. 2019). Based on observations discussed below, we rescored two taxa for one character each (*Montanoceratops* Ch 98 (? → 0) and *Prenoceratops* Ch 99 (0 → 0&1)) in the matrix of Arbour and Evans (2019) derived from Morschhauser (2019) with the addition of *Ferrisaurus*, and we used this modified matrix with the inclusion of *Gremlin* to reanalyze phylogenetic relationships within Ceratopsia. The final matrix contained 44 taxa and 256 characters. *Lesothosaurus* was set as the outgroup taxon. A cladistic parsimony analysis was run under the Traditional Search option in TNT v1.5 (Goloboff and Morles 2023), using the tree bisection reconnection swapping algorithm with 1,000 replications. All characters were treated as unordered and of equal weight. Branches were collapsed if their minimum

length equalled zero.

A total of 746 most parsimonious trees were obtained, each having a best tree length of 688 steps; consistency index (CI) of 0.45 and a retention index (RI) of 0.67. In the strict consensus of those trees, relationships among ceratopsians basal to Ceratopsoidea were poorly resolved, and leptoceratopsid taxa formed an unresolved polytomy outside Ceratopsoidea. A 50% majority rule tree did recover a monophyletic Coronosauria, but leptoceratopsids, together with the closely related *Helioceratops* and *Koreaceratops*, were unresolved, although *Gryphoceratops* and *Unescoceratops* were posited as sister taxa.

DISCUSSION

Our phylogenetic analysis of Ceratopsia using the matrix of Arbour and Evans (2019), with leptoceratopsid taxa rescored for one frontal character each and the inclusion of *Gremlin* yielded a similar result to that obtained by Arbour and Evans (2019). Neither the strict consensus or the 50% majority rule tree recovered Leptoceratopsidae as a monophyletic clade. Such results were not unexpected due to a large number of missing data in the matrix.

The isolated frontal TMP 2011.053.0027 is the first leptoceratopsid element to have been recovered from the lower unit of the Oldman Formation of southern Alberta. Although the frontal was clearly not coossified to its counterpart at the time of death, this condition does not necessarily indicate ontogenetic immaturity. In most dinosaurs, the interfrontal suture does close with age; however, in ceratopsians it is common for the suture to remain unfused, even in mature individuals (You and Dodson 2004).

The taxon represented by TMP 2011.053.0027 shares the general morphology characteristic of all leptoceratopsids. The only other catalogued leptoceratopsid element from the formation is also a frontal, TMP 1987.089.0008, referred to *Prenoceratops* sp. (Miyashita et al. 2010) that was collected from the upper unit of the Oldman Formation of southeastern Alberta where this unit is time equivalent to the lower Dinosaur Park Formation in Dinosaur Provincial Park.

TMP 2011.053.0027 is very similar to TMP 1987.089.0008, but differs from the latter in two features. First, the anterior margin of the frontal depression of TMP 2011.053.0027 is anteriorly convex, rather than straight. Second, TMP 2011.053.0027 has a low, narrow transverse ridge that extends across the dorsal surface of the bone from the medial margin to the dorsolateral edge of the orbit. This transverse ridge and the raised anterior margin of the frontal depression both branch off the raised medial margin of the frontal. The transverse ridge marks the posterior limit of strong rugose texturing on the dorsum of the frontal, and is separated from the raised margin of the smooth frontal depression by a narrow (approximately 10 mm wide) band of smooth bone that follows the margin of the depression. No other known leptoceratopsid has this transverse ridge situated at the posterior edge of the rugose part of the dorsum that is separated from the smooth frontal depression by a strip of smooth bone. Except for TMP 2011.053.0027, the dorsum of the leptoceratopsid frontal either bears rugose texturing that terminates only at the margin of the frontal depression (in *Cerasinops* and *Prenoceratops*) or has a relatively smooth texture that continues uninterrupted onto the surface of the depression (in *Leptoceratops* and *Montanoceratops*). It should be noted that *Leptoceratops* displays some variation in frontal texture, in that the partial skull UWGM-200 bears some radiating, groove-like, presumably vascular striations that originate at the center of each frontal. Even in this specimen, however, the dorsum cannot be characterized as rugose, and the *Leptoceratops* skeletons CMN 8887 and CMN 8889 each have smooth frontals.

The transverse ridge of TMP 2011.053.0027 also marks the frontal's point of maximum thickness, from which the frontal tapers slightly anteriorly and sharply posteriorly across the frontal depression. The maximum thickness of the frontal coincides with the anterior margin of the frontal depression in all other leptoceratopsids that have well-developed dorsal rugosites. In the stratigraphically youngest taxon, *Leptoceratops*, maximum frontal thickness occurs at approximately the same position as TMP 2011.053.0027, but *Leptoceratops* lacks a discernable transverse ridge or well-developed dorsal rugose texturing.

ROMVP 66302 is a fragment of a small frontal from the holotype *Prenoceratops* bonebed in the Two Medicine Formation of Montana. It resembles the holotype *Prenoceratops* frontals described by Chinnery and Horner (2007) and the referred specimen of Miyashita et al. (2010) in all its preserved features, apart from lacking the degree of rugose texturing seen in other *Prenoceratops* frontals and having a rostrally convex, not straight, anterior margin of the frontal depression. The crescentic form of the margin of ROMVP

66302 suggests that this character is variable in *Prenoceratops*. Given that ROMVP 66302 is approximately 25% smaller than the holotype and referred frontals (CF48, Fig. 4A-C; CF61, Fig. 4D-F; and CF65, Fig. 4G-H) and lacks the rugose texture of those specimens, it is likely that both the level of dorsal rugosity and the curvature of the anterior margin of the frontal depression changed during ontogeny.

Comments on variation in the anterior border of the frontal depression

Character 99, the straight anterior margin of the frontal depression previously has been considered a synapomorphy of *Cerasinops* and *Prenoceratops* (Morschhauser et al. 2019) However, in describing the frontals of *Cerasinops* (Fig. 3H-I), Chinnery and Horner (2007:629) described the holotype MOR 300 as having "a low ridge, curving caudolaterally [that] delineates the dorsal surface from the frontal depression." In redescribing the holotype of *Montanoceratops* (AMNH 5464), Makovicky (2010) noted that the anterior margin of its frontal depression (his supraorbital depression) was curved, and we confirm that here (Fig. 4L), but apparently this character was not coded for *Montanoceratops* in Morschhauser et al. (2019). Our observations of the fused frontals of MOR 300 indicate that the actual shape of the margin is difficult to assess. The margin appears to be rostrally convex when viewed dorsally (Fig. 3H), but when viewed anterodorsally the same margin appears to be straight (Fig. 3I), suggesting that even under optimal conditions this character is difficult to code.

Regarding the frontals of *Prenoceratops*, it should be noted that the condition of the anterior margin of the frontal depression has been described in at least two related, but slightly different ways. Chinnery (2004) defined the margin as a "straight, transverse border" for the *Prenoceratops* bonebed specimens that she described and they are accordingly coded as having a straight margin in the character matrix of Morschhauser et al. (2019). By contrast, Miyashita et al. (2010) renamed it as the "transverse postorbital ridge" (i.e., a straight anterior margin of the frontal depression). We confirm the presence of a straight margin on three of the *Prenoceratops* frontals (Fig. 4A-H; casts) described by Chinnery (2004). Given that the margin is clearly curved in the smaller ROMVP 66302, we propose that this character varies ontogenetically, at least within *Prenoceratops*. Until more leptoceratopsid specimens of different size classes can be evaluated, we advocate caution when coding this character in ceratopsian phylogenetic analyses.

Taxonomic assignment of ROMVP 66302, TMP 1987.089.0008, and TMP 2011.053.0027.

ROMVP 66302 — This specimen can be unequivocally assigned to *Prenoceratops hodgskissi* based on having been collected from the *Prenoceratops* bonebed that produced the holotype specimen, and the fact that no other ceratopsian taxa were found associated with the *Prenoceratops* material collected. The specimen is morphologically compatible with other *Prenoceratops* material, and we believe that it is likely that the noted differences are ontogenetic in nature given the specimen's small size.

TMP 1987.089.0008 — Miyashita et al. (2010) referred this specimen to *Prenoceratops* sp. based on what they considered to be autapomorphies for *Prenoceratops* (citing Chinnery 2004): "(1) transversely straight postorbital ridge, (2) frontal depression that is deeper than one-third the thickness of the frontal, and (3) crista cranii that coincides with the interfrontal suture" Miyashita et al. (2010:88).

Chinnery (2004) did not comment on the crista cranii of *Prenoceratops*, so it is unclear where Miyashita et al. (2010) derived the coding for this feature. Examination of TMP 1987.089.0008 and the casts of the frontals show that the crista cranii does not coincide with the interfrontal suture in the sense of being positioned at the medial edge of the frontal, but rather is stepped back from the margin by several millimetres, except for a small (~5 mm) portion anteromedial to the sutural area for the orbitosphenoid on TMP 1987.089.0008. The mediolateral position of this part of the crista cranii is rarely remarked on in ceratopsians as most described specimens are based on articulated skulls where the ventral surface of the frontal is not visible, thus its utility as a diagnostic character is questionable.

Moreover, the frontal depression's being deeper than one-third the thickness of the frontal is not a character Chinnery (2004) used in her phylogenetic analysis or her taxon diagnosis of *Prenoceratops*. A non-qualitative version of the character was used by Morschhauser (2018; Ch 98) and Arbour and Evans (2019; Ch 98), but was coded as state 2 (deeper for all leptoceratopsids in which it could be coded at all (*Cerasinops*, *Leptoceratops*, *Montanoceratops* and *Prenoceratops*), and thus was not phylogenetically informative within the clade.

Our re-evaluation of TMP 1987.089.0008 did not produce

any potentially diagnostic characters beyond those listed by Miyashita et al. (2010). We agree that the anterior margin of the frontal depression of TMP 1987.089.0008 is straight, as in the putatively mature *Prenoceratops* frontals described by Chinnery and Horner (2007) (Fig. 4A-H), and does, indeed, closely resemble them in all frontal depression features, including shape and depth. The *Cerasinops* frontals (MOR 300) can also be argued to have a similarly straight anterior frontal margin, suggesting that this character is a synapomorphy for *Cerasinops* and *Prenoceratops*. Thus, although TMP 1987.089.0008 may be referable to one of those two taxa, based on its stratigraphic position we suggest that it is probably best left referred to *Prenoceratops* sp.

Another consideration is that TMP 1987.089.0008 was found in the upper unit of the Oldman Formation of southern Alberta in strata equivalent in time to the lower part of the Dinosaur Park Formation in Dinosaur Provincial Park. Given that the two sediments packages are known to share dinosaur taxa (e.g., *Centrosaurus* (Chiba et al. 2015)), and that the leptoceratopsid *Unescoceratops* is known from the middle portion of the Dinosaur Park Formation., it is also possible that TMP 1987.089.0008 may eventually prove referrable to *Unescoceratops* which is known only from partial dentaries (Ryan et al. 2012).

TMP 2011.053.0027 — Based on the data presented here, we make TMP 2011.053.0027 the holotype of the new taxon, *Gremlin slobodorum*. The recognition of *Gremlin* increases the number of dinosaur genera known from the lower unit of the Oldman Formation of southern Alberta from non-tooth skeletal material to five, with *Gremlin* joining the centrosaurine ceratopsids *Albertaceratops nesmoi* Ryan, 2007 and *Wendiceratops pinhornensis* Evans and Ryan, 2015, the hadrosaurine hadrosaurid *Gryposaurus* sp., and a pachycephalosaurid, cf. *Stegoceras*. To date, these ceratopsids are only known from this unit and geographic region, offering circumstantial stratigraphic support for the hypothesis that *Gremlin* represents a distinct new taxon within Alberta.

CONCLUSIONS

Analysis demonstrates that TMP 2011.053.0027 is a leptoceratopsid frontal that can be referred to the new taxon *Gremlin slobodorum* based, in part, on the presence of a transverse ridge that marks the posterior limit of rugose ornamentation on the dorsal surface and is separated from the margin of the frontal depression by a narrow band of smooth bone. *Gremlin slobodorum* helps to fill in a significant temporal gap in the Albertan leptoceratopsid record between *Gryphoceratops* from the Santonian Milk River Formation and *Unescoceratops* from the upper Campanian Dinosaur Park Formation. Examination of TMP 2011.053.0027, and the *Prenoceratops* frontal ROMVP 66302, and reevaluation of TMP 1987.089.0008 indicate that the shape of the anterior margin of the frontal depression varies ontogenetically in at least some leptoceratopsids.

ACKNOWLEDGMENTS

Thanks to S. Rufolo and M. Currie (CMN) for specimen access and help with loan transfers. K. Seymour (ROM) provided loans. B. Strilisky (Royal Tyrrell Museum of Palaeontology) facilitated the transfer of the loan of TMP 2011.053.0027 to the CMN. I. Morrison (ROM) expertly prepared ROMVP 66302. J. Scannella and E. Metz (Museum of The Rockies) provided photographs of MOR 300. P. Makovicky (University of Minnesota) and J. Mallon (CMN) provided photographs of AMNH 5464. A. Farke provided photographs of the *Prenoceratops* frontal casts CF48, 61 and 65. Danielle Dufault (ROM) photographed ROMVP 66302. Thanks to V. Arbour, D. Brinkman, T. Cullen, R. Holmes, J. Mallon, and T. Miyashita for providing data and helpful discussions. W. Sloboda discovered and collected TMP 2011.053.0027 while part of the 2011 field crew of the Southern Alberta Dinosaur Project jointly run and funded by DEC and MJR. We thank Rob Holmes and an anonymous reviewer, and the editor for their constructive suggestions that improved the manuscript during the review process. A Natural Sciences and Engineering Research Council of Canada Discovery Grant to DCE (NSERC Grant File Number: RGPIN 355845) supported this research, and CS acknowledges NSERC Discovery Grants RGPIN-2017-06246 and RGPIN-2023-04916.

AUTHOR CONTRIBUTIONS

MJR and DCE designed the project. LM and MJR gathered and analyzed the data. MJR and LM drafted the manuscript. All authors edited the manuscript.

LITERATURE CITED

Agnolin, F. L., Ezcurra, M. D., Pais, D. F., & Salisbury. S. W. (2010). A reappraisal of the Cretaceous non-avian dinosaur faunas from Australia and New Zealand: evidence for their Gondwanan affinities. *Journal of Systematic Palaeontology*, 8(20), 257–300.

Arbour, V. M. & Evans, D. C. (2019). A new leptoceratopsid dinosaur from Maastrichtian-aged deposits of the Sustut Basin, northern British Columbia, Canada. *PeerJ*, 7, e7926. Doi: 10.7717/peerj.7926.

Arbour, V. M., Evans, D. C., Simon, D. J., Cullen, T. M., & Braman, D. (2020). Cretaceous flora and fauna of the Sustut Group near the Sustut River, northern British Columbia, Canada. *Canadian Journal of Earth Sciences*, 57, 671–680.

Brinkman, D. B. (1990). Paleoecology of the Judith River Formation (Campanian) of Dinosaur Provincial Park, Alberta, Canada: Evidence from vertebrate microfossil localities. *Palaeogeography, Palaeoclimatology, Palaeoecology*, 78, 37–54. https://doi.org/10.1016/0031-0182(90)90203-j.

Brown, B. (1914). *Leptoceratops*, a new genus of Ceratopsia from the Edmonton Cretaceous of Alberta. *Bulletin of the American Museum of Natural History*, 33, 567–580.

Brown, B. & Schlaikjer, E. M. (1942). The skeleton of *Leptoceratops* with the description of a new species. *American Museum Novitates*, 1169, 2–15.

Chiba, K., Ryan, M. J., Braman, D. R., Eberth, D. A., Scott, E. E., Brown, C. M., Kobayashi, Y., & Evans, D. C. (2015). Taphonomy of a monodominant *Centrosaurus apertus* (Dinosauria: Ceratopsia) bonebed from the upper Oldman Formation of southeastern Alberta. *Palaios*, 30, 655–667.

Chinnery, B. & Weishampel, D. B. (1998). *Montanoceratops cerorhynchus* (Dinosauria: Ceratopsia) and relationships among basal neoceratopsians. *Journal of Vertebrate Paleontology*, 18(3), 569–585.

Chinnery, B. (2004). Description of *Prenoceratops pieganensis* gen. et sp. nov. (Dinosauria: Neoceratopsia) from the Two Medicine Formation of Montana. *Journal of Vertebrate Paleontology*, 24(3), 572–590.

Chinnery, B. J. & Horner, J. R. (2007). A new neoceratopsian dinosaur linking North American and Asian taxa. *Journal of Vertebrate Paleontology*, 27(3), 625–641.

Eberth, D. A. & Hamblin, A. P. (1993). Tectonic, stratigraphic, and sedimentologic significance of a regional discontinuity in the upper Judith River Group (Belly River Wedge) of southern Alberta, Saskatchewan, and Northern Montana. *Canadian Journal of Earth Sciences*, 30(1), 174–200. https://doi.org/10.1139/e93-016.

Eberth, D. A. (2005). Geology. In P. J. Currie, & E. B. Koppelhus (Eds.), *Dinosaur Provincial Park: A Spectacular Ancient Ecosystem Revealed* (pp. 54–82). Indiana University Press.

Eberth, D. A., Evans, D. C., Brinkman, D. B., Therrien, F., Tanke, D. H., & Russell, L. S. (2013). Dinosaur Biostratigraphy of the Edmonton Group (Upper Cretaceous), Alberta, Canada: Evidence for climate influence. *Canadian Journal of Earth Sciences*, 50(7), 701–726. https://doi.org/10.1139/cjes-2012-0185.

Evans, D. C. & Ryan, M. J. (2015). Cranial anatomy of *Wendiceratops pinhornensis* gen. et sp. nov., a centrosaurine ceratopsid (Dinosauria: Ornithischia) from the Oldman Formation (Campanian), Alberta, Canada, and the evolution of ceratopsid nasal ornamentation. *PLOS One*, 10(7), e0130007. https://doi.org/10.1371/journal.pone.0130007.

Evenchick, C. A. & Thorkelson, D. J. (2005). Geology of the Spatsizi River map area, north-central British Columbia. *Geological Survey of Canada Bulletin*, 557, 1–276.

Fowler, D. W. (2017). Revised geochronology, correlation, and dinosaur stratigraphic ranges of the Santonian-Maastrichtian (Late Cretaceous) formations of the Western Interior of North America. *PloS One*, 12, e0188426.

Gilmore, C. W. (1930). On dinosaurian reptiles from the Two Medicine Formation of Montana. *Proceedings of the US National Museum*, 77, 1–39. doi:10.5479/si.00963801.77-2839.1.

Goloboff, P. A. & Morales, M. E. (2023). TNT version 1.6, with a graphical interface for MacOS and Linux, including new routines in parallel. *Cladistics*, 39, 144–153.

He, Y., Makovicky, P. J., Wang, K., Chen, S., Sullivan, C., Han, F., & Xu, X. (2015). A new leptoceratopsid (Ornithischia, Ceratopsia) with a unique ischium from the Upper Cretaceous of Shandong Province, China. *PLoS One*, 10(12), e0144148. https://doi.org/10.1371/journal.pone.0144148.

Kurzanov, S. M. (1992). A giant protoceratopsid from the Upper Cretaceous of Mongolia. *Paleontological Journal*, 3, 81–93.

Lindgren, J., Currie, P., Siverson, M., Rees, J., Cederström, P., & Lindgren, F. (2007). The first Neoceratopsian dinosaur remains from Europe. *Palaeontology*, 50(4), 929–937.

Longrich, N. R. (2016). A ceratopsian dinosaur from the late Cretaceous of Eastern North America, and implications for dinosaur biogeography. *Cretaceous Research*, 57, 199–207.

Makovicky, P. J. (2001). A *Montanoceratops cerorhynchus* (Dinosauria: Ceratopsia) braincase from the Horseshoe Canyon Formation of Alberta, In D. H. Tanke & K. Carpenter (Eds.), *Mesozoic Vertebrate Life* (pp. 243–262). Indiana University Press.

Makovicky, P. J. (2010). A redescription of the *Montanoceratops cerorhynchus* holotype, with a review of referred material. In M. J. Ryan, B. J. Chinnery-Allgeier, & D. A. Eberth, (Eds.), *New Perspectives on Horned Dinosaurs: The Royal Tyrrell Museum Ceratopsian Symposium* (pp. 68–82). Indiana University Press.

Marsh, O. C. (1890). Additional characters of the Ceratopsidae, with notice of new Cretaceous dinosaurs. *American Journal of Science*, 39, 418–26.

Massinger, C. (1944). The gremlin myth. *The Journal of Educational Sociology*, 17(6), 359–367. https://doi.org/10.2307/2262351.

McFeeters, B. D., Evans, D. C., Ryan, M. J., & Maddin, H. C. (2021). First occurrence of *Maiasaura* (Dinosauria, Hadrosauridae) from the Upper Cretaceous Oldman Formation of Southern Alberta, Canada. *Canadian Journal of Earth Sciences*, 58(3), 286–296.

McKenna, M. C. & Love, J. D. (1970). Local stratigraphic and tectonic significance of *Leptoceratops*, a Cretaceous dinosaur in the Pinyon Conglomerate, northwestern Wyoming. *United States Geological Survey, Professional Paper*, 700D, 55–61.

Miyashita, T., Currie, P. J., & Chinnery-Allgeier, B. J. (2010). First basal neoceratopsian from the Oldman Formation (Belly River Group), Southern Alberta. In Ryan, M. J., Chinnery-Allgeier, & B. J., Eberth, D. A. (Eds.), *New Perspectives on Horned Dinosaurs: The Royal Tyrrell Museum Ceratopsian Symposium* (pp. 83–90). Indiana University Press.

Morschhauser, E. M., You, H., Li, D., & Dodson, P. (2019). Phylogenetic history of *Auroraceratops rugosus* (Ceratopsia: Ornithischia) from the Lower Cretaceous of Gansu Province, China. *Journal of Vertebrate Paleontology*, 38(supl), 117–147.

Ostrom, J. H. (1978). *Leptoceratops gracilis* from the "Lance" Formation of Wyoming. *Journal of Paleontology*, 52, 697–704.

Ott, C. J. (2007). Cranial anatomy and biogeography of the first

Leptoceratops gracilis (Dinosauria: Ornithischia) specimens from the Hell Creek Formation, Southeast. In K. Carpenter (Ed.). *Horns and Beaks: Ceratopsian and Ornithopod Dinosaurs* (pp. 213–233). Indiana University Press.

Owen, R. (1842). Report on British Fossil Reptiles. Part II. *Report of the Eleventh Meeting of the British Association for the Advancement of Science*, 1841, 66–204.

Ramezani, J., Beveridge, T. L., Rogers, R. R., Eberth, D. A., & Roberts, E. M. (2022). Calibrating the zenith of dinosaur diversity in the Campanian of the Western Interior Basin by CA-ID-TIMS U-Pb geochronology. *Scientific Reports*, 12, 16026.

Rich, T. H. & Vickers-Rich, P. (2003). Protoceratopsian? ulnae from Australia. *Records of the Queen Victoria Museum*, 113, 1-12.

Rogers, R. R., Swisher, C. C., & Horner, J. R. (1993). $^{40}Ar/^{39}Ar$ age and correlation of the nonmarine Two Medicine Formation (Upper Cretaceous), northwestern Montana, USA. *Canadian Journal of Earth Sciences*, 30, 1066–1075.

Russell, D. A. (1970). Tyrannosaurs from the Late Cretaceous of western Canada. *Publications in Palaeontology*, 1, 1–34.

Ryan, M. J. & Currie, P. J. (1998). First report of protoceratopsians (Neoceratopsia) from the late cretaceous Judith River Group, Alberta, Canada. *Canadian Journal of Earth Sciences*, 35, 820–826. https://doi.org/10.1139/e98-033.

Ryan, M. J. (2007). A new basal centrosaurine ceratopsid from the Oldman Formation, Southeastern Alberta. *Journal of Paleontology*, 81(2), 376–396.

Ryan, M. J., Evans, D. C., Currie, P. J., Brown, C. M., & Brinkman, D. (2012). New leptoceratopsids from the Upper Cretaceous of Alberta, Canada. *Cretaceous Research*, 35, 69–80.

Sampson, S. D. (1995). Two new horned dinosaurs (Ornithischia: Ceratopsidae) from the Upper Cretaceous Two Medicine Formation, Montana, USA. *Journal of Vertebrate*, 15(4), 743–760.

Scott, E. E., Chiba, K., Fanti, F., Saylor, B. Z., Evans, D. C., & Ryan, M. J. (2022). Taphonomy of a monodominant *Gryposaurus* sp. bonebed from the Oldman Formation (Campanian) of Alberta, Canada. *Canadian Journal of Earth Sciences*, 59, 6, 389–405.

Seeley, H. G. (1887). On the classification of the fossil animals commonly named Dinosauria. *Proceedings of the Royal Society of London*, 43, 165–71.

Sereno, P. C. (1986). Phylogeny of the bird-hipped dinosaurs (Order Ornithischia). *National Geographic Research*, 2, 234–56.

Sternberg, C. M. (1945). Pachycephalosauridae proposed for dome-headed dinosaurs, *Stegoceras lambei*, n. sp., described. *Journal of Paleontology*, 19(5), 534–538.

Sternberg, C. M. (1951). Complete Skeleton of *Leptoceratops gracilis* Brown from the Upper Edmonton Member on Red Deer River, Alberta. *National Museum of Canada Bulletin, Annual Report*, 123, 225–255.

Sternberg, C. M. (1953). A new hadrosaur from the Oldman Formation of Alberta: Discussion of nomenclature. *Canadian Department of Resource Development Bulletin*, 128, 1–12.

Trexler, D. (2001). Two Medicine Formation, Montana: geology and fauna. In D. H. Tanke, & K. Carpenter (Eds.), *Mesozoic Vertebrate Life* (pp. 298–309). Indiana University Press.

Wilson, J. P, Ryan. M. J., & Evans, D. C. (2020). A new, transitional centrosaurine ceratopsid from the Upper Cretaceous Two Medicine Formation of Montana and the evolution of the '*Styracosaurus*-line' dinosaurs. *Royal Society Open Science*, 7, 200284. http://dx.doi.org/10.1098/rsos.200284.

You, H. & Dodson, P. (2004). Basal Ceratopsia. In D. B. Weishampel, P. Dodson, & H. Osmâolska (Eds.), *The Dinosauria* (pp. 478–493). University of California Press.

Xu, X., Wang, K., Zhao, X., Sullivan, C., & Chen, S. (2010). A new leptoceratopsid (Ornithischia: Ceratopsia) from the Upper Cretaceous of Shandong, China, and its implications for Neoceratopsian Evolution. *PLoS One*, 5(11), e13835. https://doi.org/10.1371/journal.pone.0013835.

WINDOWS INTO SAUROPSID AND SYNAPSID EVOLUTION
Essays in honor of Prof. Louis L. Jacobs, pp. 166–175, 2023

A JUVENILE HADROSAUR MAXILLA FROM THE DINOSAUR PARK FORMATION (CAMPANIAN) OF DINOSAUR PROVINCIAL PARK (ALBERTA, CANADA)

Philip J. Currie[1,*], Junchang Lü (deceased), and Yan-Yin Wang[2]

[1]University of Alberta, pjcurrie@ualberta.ca;
[2]University of Alberta

ABSTRACT A nicely preserved right maxilla of a juvenile lambeosaurine hadrosaur was found by Junchang Lü from the Dinosaur Park Formation (Campanian) of Dinosaur Provincial Park, Alberta, Canada. It came from the *Centrosaurus-Corythosaurus* Assemblage Zone (probably equivalent to Megaherbivore Assemblage Zone 1b), suggesting that it is likely referable to either *Corythosaurus* or *Lambeosaurus*. An X-ray Computed Tomography helical scan revealed 23 tooth families of up to four teeth per family. The number of tooth families and number of teeth per family increase during ontogeny in hadrosaurids, and this number is approximately what is expected for either a lambeosaurine, or any other subfamily of the Hadrosauridae for a specimen of this size. A second maxilla with teeth of approximately the same size can be identified as a right maxilla of a hadrosaurine based on the nature of the premaxillary contact. UALVP60543 and UALVP62346 have approximately equivalent tooth row lengths with a similar number of tooth families (22-23). Because it has been established that Lambeosaurines and hadrosaurines can have radically different tooth counts at maturity, these specimens indicate that tooth counts in these two clades were similar at hatching, but rapidly diverged during ontogeny.

KEYWORDS Dinosaur, Hadrosaur, Maxilla, Dinosaur Provincial Park, Late Cretaceous, Campanian

INTRODUCTION

As part of the volume honoring the long career of Louis Jacobs, it seems appropriate to also recognize the all-too short career of one of his star students – Junchang Lü (Conniff 2018; Guangzhou Daily 2021). I originally met Junchang in Beijing in the late 1980s when we were doing the Sino-Canadian Dinosaur Project (CCDP) and he was a student working at the Institute of Vertebrate Paleontology and Paleoanthropology. Over the years I had the pleasure of working with Junchang (both in in the field and on research papers) many times in China and Mongolia. In 2015, three palaeontologists (Junchang Lü, Yoshi Kobayashi and Yuong-Nam Lee) who had been graduate students of Louis Jacobs joined a University of Alberta field party in Dinosaur Provincial Park (referred to henceforth as DPP). On June 17, 2015, Junchang found a nicely preserved, juvenile hadrosaur maxilla with most of the teeth intact.

The bones of small dinosaurs are rare in DPP, where there was a preservational bias that commonly led to the complete disarticulation and/or loss of small animal remains (Dodson 1975, Brown et al. 2013). This includes baby or juvenile dinosaurs, the articulated or associated remains of which are hard to find in Dinosaur Provincial Park. However, disarticulated, isolated bones of juvenile dinosaurs are not uncommon (Tanke and Brett-Surman 2001). Nevertheless, disarticulated maxillae and dentaries of juveniles are rarely complete and almost never include teeth. For these reasons, the discovery of UALVP60543 was noteworthy in that it is one of the smallest (Table 1) and most complete hadrosaur maxillae with teeth known from DPP. Smaller hadrosaur maxillae with teeth have, of course, been recovered from other sites, including those of embryonic skeletons from Devil's Coulee (Oldman Formation; Horner and Currie 1994), which is approximately 300 km south of DPP.

The specimen (UALVP60543, field number DPP2015.248) was found in a coarse-grained fluvial sandstone. Over the years, several attempts have been made to find associated parts of the skeleton in the vicinity of the discovery site (12U 0465413E, 5621217N), but no other bones have been

*Corresponding author

Table 1. Measurements in mm of various small hadrosaur maxillae. Information on CMN 8917 from Sternberg (1956), Warnock-Juteau 2023, and Warnock-Juteau et al. 2023; on MOR 548 from Brink et al. 2011; on MPC-D100/764 by Dewaele et al., 2015; on RAM 14000 from Farke et al., 2013; on TMP 87.79.286 from Tanke and Brett-Surman (2001); on TMP 94.385.1 from Brink et al. 2011; on YPM-PU 22400 from Prieto-Márquez and Guenther (2018); on ROM specimens from Evans 2010. Abbreviations: e, estimate that is approximate only; H, height at jugal suture; L, length; +/-, estimate is close to what the measurement probably was

Specimen #	Skull L	Maxilla L	Tooth Row L	Maxilla H	# tooth families
AMNH 5461			162		
CMN 2247	362		149		
CMN 8917		57.5	46e	–	15
MOR 548		69			
MPC-D100/764		20.6			5-7
RAM 14000	246		117.7		20
ROM 759			187		
ROM 758	384		184		
TMP 81.22.6					
TMP 82.16.177					
TMP 87.79.286		45	–	–	12
TMP 88.36.4					
TMP 89.79.52		40e	35e	9.5e	10e
TMP 94.385.1		158			31
YPM-PU 22400		60	–	20	15
UALVP 60543		139	124.5+/-	57	23
UALVP 62346		124	110.8		22

recovered that can be associated with the maxilla. The specimen was found at elevation 688masl in the Dinosaur Park Formation (DPF), and the closest measured contacts with the underlying Oldman Formation (OF) are 0.7 to 1.2 km from the site, mostly on a west to north arch. The elevation of the contacts range from 660 masl to 672 masl, and the average is 668 masl. The specimen was, therefore, recovered approximately 20 m above the OF/DPF contact, which suggests it is part of the *Corythosaurus-Centrosaurus* assemblage zone (75.77-76.47 Ma) (Ryan and Evans 2005, Eberth et al. 2023), or Megaherbivore Assemblage Zone 1b (MAZ-1b) of Mallon et al. (2012). Hadrosaur species reported from this interval include *Corythosaurus intermedius*, *Gryposaurus notabilis*, *Lambeosaurus* (*L. clavinitialis* and *L. lambei* are both in MAZ-1b) and *Parasaurolophus walkeri*. However, the specimen was also found only 73m to the NE of Q213, where a *Prosaurolophus maximus* skeleton was collected (TMP 1993.081.0001) only 10 m higher in section in MAZ-2a. Although the elevation of the excavation site of UALVP60543 probably came from MAZ-1b, there is enough uncertainty that hadrosaur species from MAZ-1a and MAZ-2a need to be considered as possible identifications of UALVP60543.

The second specimen (UALVP) was found when this paper on UALVP60543 was nearing completion. It was also recovered from the *Corythosaurus-Centrosaurus* Assemblage Zone, but was found in Bonebed BB150 at the northwest end of DPP. This specimen had only been prepared from the medial side by the time this paper was written. Its morphology suggests it is probably a hadrosaurine, and its most likely identification is *Gryposaurus*.

Institutional Abbreviations — CMN, Canadian Museum of Nature, Ottawa, Ontario, Canada; MOR, Museum of the Rockies, Bozeman, Montana, USA; MPC-D, Mongolian Paleontological Center, Dinosaur Collection (of the Institute

of Paleontology, Mongolian Academy of Sciences), Ulaanbaatar, Mongolia; RAM, Raymond M. Alf Museum of Paleontology, Claremont, California, USA; TMP, Royal Tyrrell Museum of Palaeontology, Drumheller, Alberta, Canada; UALVP, University of Alberta Laboratory of Vertebrate Palaeontology, Edmonton, Alberta, Canada; YPM-PU, Yale Peabody Museum (collection that was formerly in the Museum of Natural History, Princeton University), New Haven, Connecticut, USA.

METHODOLOGY

An X-ray Computed Tomography (XCT) helical scan of the maxilla (UALVP60543) was taken at the Permafrost Archives Science (PACS) lab at the University of Alberta using a Nikon XT H 225 ST Industrial CT Scanner. The scan used a beam energy of 220 kV, current of 191 μA, and exposure of 4 fps with 8 frames averaging and a total of 5591 projections (3132 per rotation). A 36 μm effective pixel size was achieved. A 3mm copper filter was also attached to the target head to reduce artefact effects caused by higher-density minerals.

Primary images were reconstructed through Nikon's CT 3D Pro software, where minor beam hardening effects were applied and volume files were exported to be used for visual analysis in ORS Dragonfly 4.0, and were polished using Zbrush 2018.

Acknowledgements — Like so many vertebrate palaeontologists, the first author owes a great debt of gratitude to Dr. Louis Jacobs (Southern Methodist University, Dallas, Texas). In addition to being a great scholar with broad-based experiences in collecting and researching fossil vertebrates, Lou has been a great teacher and friend to many, has a great sense of humour, and is a tireless supporter of the Society of Vertebrate Paleontology. UALVP60543 was found by Junchang Lü on June 17, 2015, and was collected by the first author on June 22, 2015. Further searching in the same area both that day and over subsequent years failed to turn up any additional associated material that can be attributed to this individual. It was prepared by Susan Kagan in the UALVP. UALVP62346 was found by Colton Coppock in 2023 and was prepared initially by the first author. We thank Duane Froese, Joel Pumple, and Jordan Harvey of the PACs CT Lab at the University of Alberta for CT scanning and imaging. Many thanks to Jordan Mallon (Canadian Museum of Nature, Ottawa, Canada) and Trystan Warnock-Juteau (Carleton University) for providing unpublished information on (and a cast of) CMN8917, and to Brandon Strilisky (Royal Tyrrell Museum of Palaeontology) and to Howard Gibbons (University of Alberta Laboratory of Vertebrate Palaeontology) for their assistance in finding specimens and cataloguing data in the collections of their respective institutions. Finally the authors would like to thank the reviewers (Phil Bell and Michael Ryan) for many good suggestions that improved the quality and readability of the paper.

SYSTEMATIC PALAEONTOLOGY

Dinosauria Owen, 1842
Ornithischia Seeley, 1887
Ornithopoda Marsh, 1881
Iguanodontia Dollo, 1888
Hadrosauridae Cope, 1870
Lambeosaurinae Parks, 1923

Comparative Material

CMN 8917 is a partial skull collected by G.E. Lindblad in 1953 from what is now Dinosaur Provincial Park. It has recently been CT-scanned and redescribed by Warnock-Juteau (2023), who suggests that it probably represents *Gryposaurus notabilis*. The locality suggests it was recovered from the Dinosaur Park Formation.

MPC-D 100/764 are *Saurolophus angustirostris* perinates from Mongolia that were described by Dewaele et al (2015). Presumably they were collected from the Nemegt Formation.

TMP 1989.079.0052 is an embryonic skull of *Hypacrosaurus stebingeri* described by Horner and Currie (1994). It is from time-equivalent (Oldman Formation) sediments of Devil's Coulee, which is some 300 km south of Dinosaur Provincial Park. Other Tyrrell Museum specimens from Dinosaur Provincial Park and Devil's Coulee have also been referred to.

UALVP62346 (Figs. 1E and 3E, F) is a right maxilla with an intact tooth bank of a juvenile hadrosaur found at the base of the Dinosaur Park Formation in BB150 in Dinosaur Provincial Park by Colton Coppock in June, 2023. The specimen was still in preparation at the time of writing.

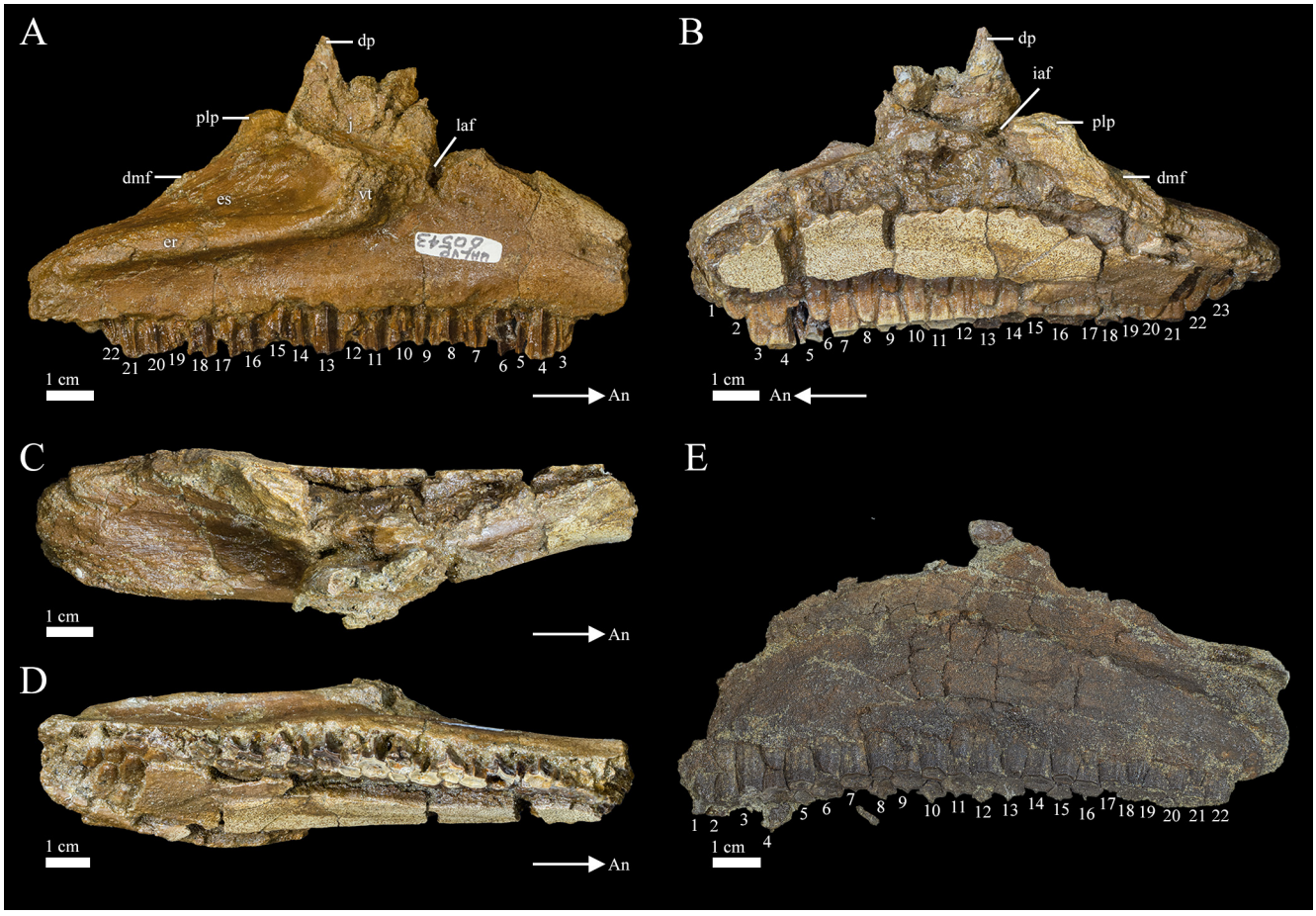

FIGURE 1. Right maxilla (UALVP60543) in right lateral (A), medial (B), dorsal (C) and ventral (D) views. E, right maxilla (UALVP62346) in medial view. **Abbreviations: dmf**, dorsomedial flange; **dp**, dorsal process; **er**, ectopterygoid ridge; **es**, ectopterygoid shelf; **if**, internal antorbital fenestra; **laf**, maxillary foramen; **plp**, palatine process; **vt**, ventral jugal tubercle.

YPM-PU 22400 is a single number that includes perinatal specimens of *Maiasaura peeblesorum* from Egg Mountain (Two Medicine Formation; Montana) and includes six left maxillae, eight right maxillae and three maxillary fragments (Prieto-Marquez and Gunther 2018). The most complete maxilla is 60mm long.

DESCRIPTION

UALVP60543 (Fig. 1) is an almost complete right maxilla (lacking small fragments around the periphery of the bone that were lost to erosion before the specimen was found). It is 124.9 mm long as preserved, and the height between the alveolar margin and the top of the dorsal process is 55.3mm. The tooth row seems to be complete (judging from the arch of "special foramina", Fig. 1B) and is 124.5 mm long. It includes alveoli for 23 tooth families, which is in the range of other hadrosaur juveniles of similar size (Table 1). The edentulous anteroventral process was lost to erosion. It can compose about 11% of the maxillary length (Wagner and Lehman 2010). However, the process can also be much longer in some specimens, and in "*Tetragonosaurus*" is 17% the length of the tooth row (Evans et al., 2005). Using the more conservative estimate of 11%, the total estimated length of the maxilla of UALVP60543 is 139 mm.

Like all hadrosaur maxillae, the outline of UALVP60543 is triangular in lateral view (Figs. 1, 2, 3). The angle between the alveolar margin and the premaxillary shelf is 33 degrees, whereas that between the alveolar margin and the ectopterygoid shelf is 30 degrees. The angles are higher in neonate specimens of *Hypacrosaurus stebingeri* (Horner and Currie 1994, Warnock-Juteau 2023) and other younger hadrosaurids,

which is a consequence of their relatively shorter, deeper preorbital regions. The alveolar margin is essentially straight in lateral view, and the dorsal process is centered above the midpoint of the bone. Although the apex was lost to erosion, the dorsal process clearly tapered into a pointed dorsal termination as in all lambeosaurines. Even so, the dorsal process is still taller than it is anteroposteriorly long, which is characteristic of lambeosaurines (Horner et al. 2004). The roughly rhomboidal sutural surface for the jugal has a sharply-defined anteroventral margin. There is a well-defined ventral jugal tubercle on the lateral surface of the dorsal process below the ventral limit of the jugal suture. It is separated by a gap from the straight, well-developed ectopterygoid ridge (Figs. 1, 2). Posterior to the base of the dorsal process is the mediolaterally widest part of the maxilla. Here the medial edge rises into a prominent palatine process that is separated from the dorsal process by a trough-like longitudinal groove that extends from what is sometimes referred to as the internal antorbital fenestra to the back of the palatine process (Fig. 1B). The palatine process is continuous with the dorsomedial flange that slopes posteroventrally until it disappears into the posteromedial surface of the ectopterygoid shelf. There is a weak suggestion of a pterygoid flange projecting posteriorly from the back of the dorsomedial flange. The medial surface has a dorsally arched row of alveolar ("special") foramina as in other hadrosaurids. Although the margins of some of the foramina were destroyed by erosion, the number of foramina correlates with the low number of alveoli and consists of only about 20 preserved openings.

Unfortunately, the anterior edge of the dorsal process is broken at the base, thereby obscuring the details of the foramina that are normally present in this area of hadrosaurid maxillae (Warnock-Juteau 2023). As noted by Evans (2010), the number, sizes and positions of these foramina are highly variable in lambeosaurines. Nevertheless, the posteroventral edge of a large foramen is visible. It is possible that the opening was closed anteriorly and dorsally by the premaxilla, but it is more likely that it was entirely surrounded by the maxilla. The opening is equivalent to what some workers (Xing et al. 2017) have termed the internal antorbital fenestra. Horner et al. (2004) stated that this maxillary foramen is not homologous to the antorbital fenestra because less derived taxa like *Iguanodon* possess both an antorbital fenestra and a maxillary foramen. Galton (1973), Horner et al. (2004) and Warnock-Juteau (2023) suggest that foramina in this region may have transmitted vasculature or the maxillary branches of the trigeminal nerve. However, CT scans suggest that a foramen entered the bone level with the maxillary foramen, and continued forward within the main body of the maxilla as a long channel. The course of this channel does not provide evidence as to whether it was either for vascularizing or innervating musculature, skin, or teeth. These functions were more likely attributable to a second, narrow canal that extends mediodorsally from the maxillary foramen across a ridge and then joins a broad, longitudinal groove that extends between the medial wall of the dorsal process and the lateral surface of the palatine process. As in other lambeosaurines, the maxillary foramen presumably led anterodorsally into a groove on the premaxilla. No other foramina are evident on the lateral surface of the maxilla.

The "special foramina" (Edmund 1957) between the medial dental plate and the main body of the maxilla form an arch of twenty or more foramina (erosional damage to the medial surface of the maxilla left only the lower margins of the foramina, making an exact count uncertain). The most posterior three alveoli were exposed by loss of the front part of the medial dental plate.

The apex of the dorsal process is at mid-length of the maxilla, although the center of the base (between the maxillary foramen and the front of the ectopterygoid shelf) is anterior to the midpoint of the bone (as expected in lambeosaurines). There is a deep depression on the lateral surface of the dorsal process for the contact with the jugal. It is sharply defined ventrally and posteroventrally by a ridge. The surface of the maxilla has the texturing expected of juvenile, rapidly growing hadrosaurs. The dorsal surface of the anterior maxillary process is broad (for contact with the premaxilla), shallowly concave (mediolaterally), relatively smooth (although there are weak longitudinal ridges), and preserves the base of the anteromedial process found in lambeosaurines. At its broadest point the premaxillary contact is 41mm mediodorsally to lateroventrally. It is underlain laterally by a strong longitudinal ridge that is 16mm above the alveolar margin. The lateral surface of the dorsal process is deeply excavated by the suture for the anterior process of the jugal. The concave sutural surface is roughened by ridges and channels for a strong contact.

UALVP62346 (Figs. 1E and 3E, F) is the right maxilla of a juvenile hadrosaur with an intact tooth bank. It was found

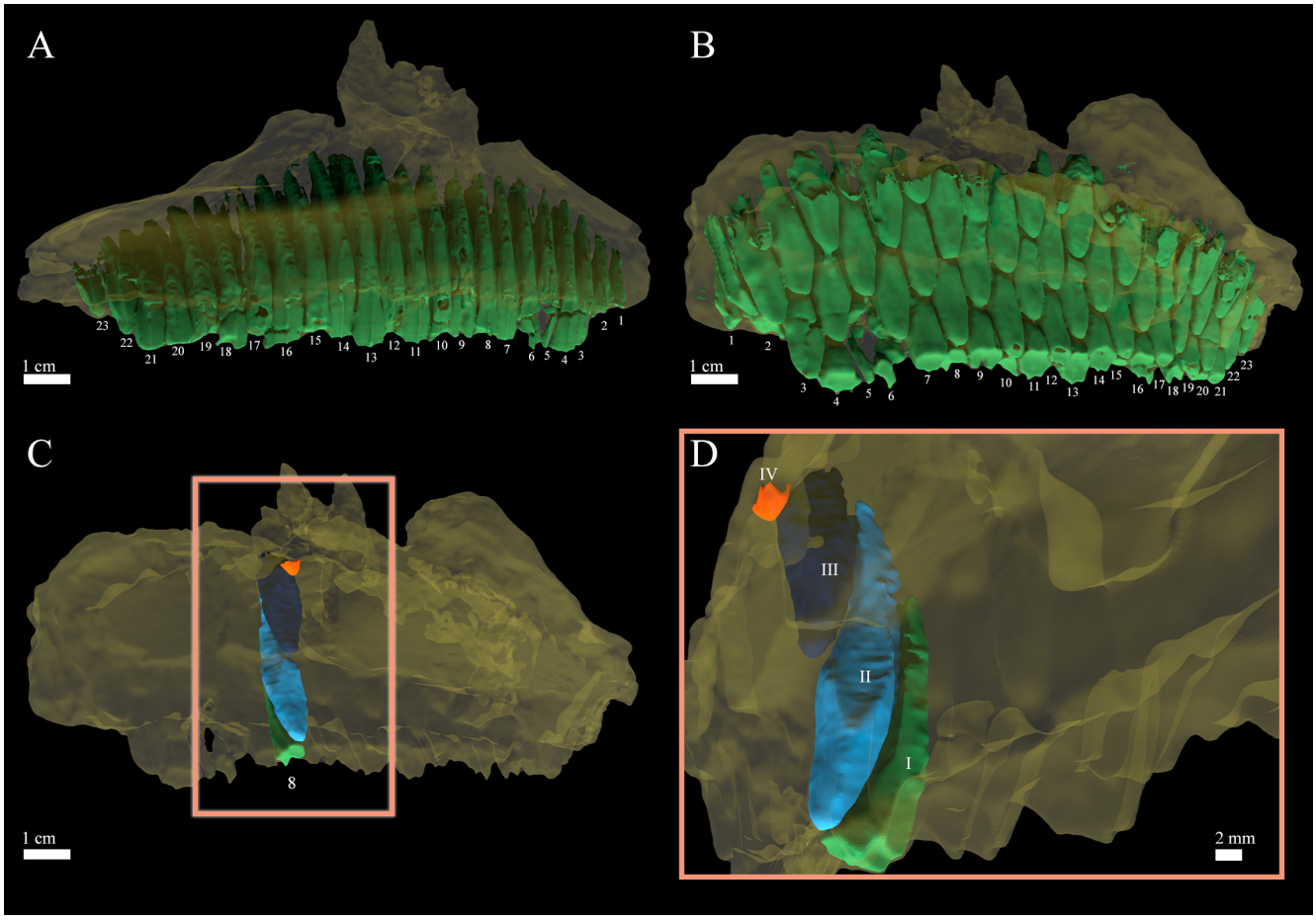

FIGURE 2. Rendered CT Images of UALVP60543 in lateral (A) and ventromedial (B) views. C, D, tooth family 8 showing worn, erupted tooth (I, green), an unerupted tooth (II, light blue), the crown and developing root of another tooth (III, dark blue) and the tip of a newly developing crown (IV, red)

at the base of the Dinosaur Park Formation in Bonebed BB150. The specimen was still in preparation at the time of writing. The fact that it has a separate anterior process medial to the posteroventral process of the maxilla that forms part of the medial floor of the external naris shows that this is a hadrosaurine (Horner et al., 2004). Other characters that support the hadrosaurine identification include the maxillary apex being low and gently rounded, and positioned behind the centre of the maxilla; and, the poor development of the ectopterygoid ridge.

Teeth — Twenty-three tooth families are preserved in the maxillary tooth battery (Fig. 1B), held to each other by periodontal ligaments (LeBlanc et al. 2016; Bramble et al. 2017). There are three teeth in the tooth family of the third alveolus (Fig. 2B). However, the CT scans show that there are as many as four teeth in tooth families of the larger alveoli (Fig. 2C, 2D). Each erupted tooth shows tooth wear on its apex, and the presence in each tooth of enamel, orthodentine, mantle dentine and coronal cementum maintained a suitably rough occlusal surface (Erickson et al. 2012). The presence of these tissues can be seen as elevated ridges for enamel, mantle dentine and coronal cementum in worn occlusal surfaces (Figs. 3A, 3B, 3D) whereas orthodentine can be identified by its basin-like wear (Fig. 3D) and radiating lines from the center of the tooth (Figs. 3A, 3B). There is a strong medial, longitudinal ridge on the lateral surface of each (Figs. 1, 2, 3). There do not appear to be any secondary longitudinal (vertical ridges), but that may be because it is difficult to see the enameled surfaces in most teeth, and the CT scanned cross-sections may not be at the right levels. The anterior and posterior rims of the enameled

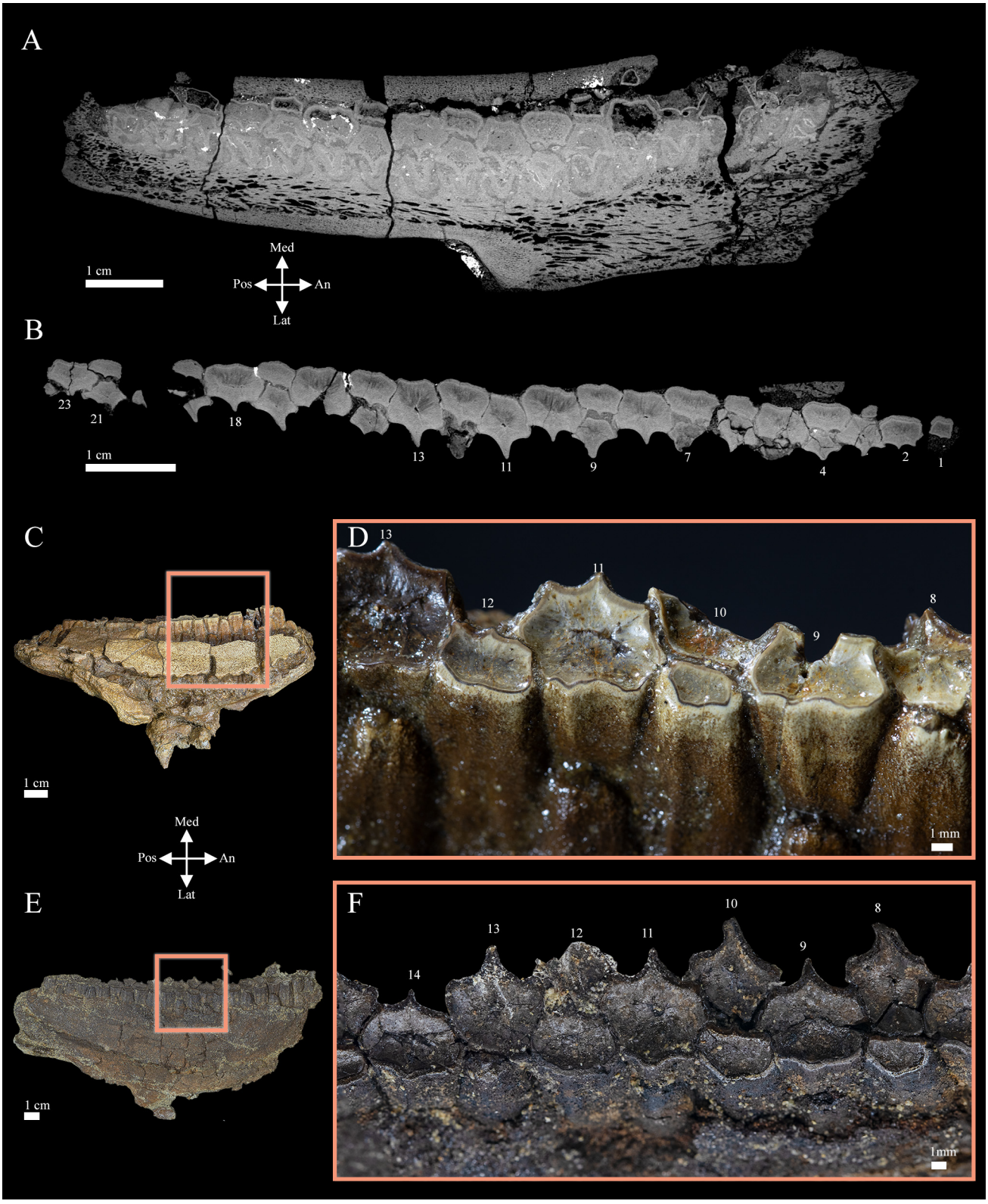

FIGURE 3. Anteroposterior CT scans (A, B) and photographs (C, D, E, F) of UALVP60543 (C, D) and UALVP62346 (E, F). A, Slice 782 of 1880. B, Slice 220 of 1880. C, medial photograph of the central part (tooth positions 8 to 13) of the tooth battery of UALVP60543. D, Occlusal surface of tooth battery (tooth positions 8 to 13). E, medial photograph of tooth positions 8 to 14. F, occlusal surface of tooth battery (tooth positions 8 to 14).

parts of the teeth are all smooth, and there is no evidence of denticulation (Fig. 1A). The unenameled medial surfaces of many of the teeth also seem to have each had a weak medial ridge (Figs. 3B, 3D). The tooth crowns are largest at mid-length of the maxilla (the anteroposterior lengths of the twelfth and fourteenth maxillary teeth are the largest teeth, but decrease progressively in size towards the front and back of the tooth row (Figs. 2A, 2B).

The maxillary teeth are typical of lambeosaurines in that each unworn crown has a dorsoventrally elongate, lanceolate (diamond-shaped) enameled labial surface. Each alveolus has a stack (family) of three to four developing and functional teeth (Fig. 3), two of which generally take part in the ventromedially inclined occlusal surface as in other, similar-sized lambeosaurine taxa (Farke et al. 2013). In contrast, only a single tooth in each family forms the occlusal surface in embryonic and hatchling tooth batteries (Horner and Currie 1994, Erickson and Zelenitsky 2014), each of which wears into a simple basin-like structure. The complex ridge and basin occlusal surfaces of subadult and adult hadrosaur teeth (Fig. 3A) are produced by different hardness values of the enamel and multiple types of dentine (Erickson et al. 2012; Erickson and Zelenitsky 2014). The enameled labial surface with its prominent, straight vertical carina (central in its anteroposterior position) was covered by the root of the previous tooth in the stack (Fig. 3A). However, the worn stubs of the roots of the most mature teeth of many of the tooth families were not preserved in UALVP60543, and presumably had fallen out before burial and fossilization of the specimen. Therefore, the edge of the dental battery is more jagged than it would have been in the living animal, and the longitudinal ridges are visible in many of the maxillary teeth (Figs. 1A, 3B). The largest teeth are in the centre of the tooth battery, but decrease in size towards the front and the back (Lambe 1920; Lull and Wright 1942, Ostrom 1961; LeBlanc et al. 2016). This is true in all subfamilies of hadrosaurids.

DISCUSSION AND CONCLUSIONS

UALVP60543 is one of the smallest hadrosaur maxillae with teeth presently known from DPP, and can be identified as belonging to one of the many lambeosaurine species known from the Dinosaur Park Formation. At this level (the *Corythosaurus-Centrosaurus* Assemblage Zone), it is likely from either *Corythosaurus* or *Lambeosaurus*. UALVP62346 is from about the same level in the DPF, but is relatively deeper, has a relatively lower but anteroposteriorly more elongate dorsal process, and is more likely identifiable as *Gryposaurus*.

Hadrosaurid teeth went through many changes in ontogeny, including the presence or absence of secondary ridges, denticulation of the margins of the lanceolate enameled surfaces of the crowns, orientations of the occlusal surfaces, height to width ratios of crowns, and even tissue compositions of the teeth themselves. The number of tooth families also increases dramatically with body size (Horner and Currie 2004, Suzuki et al. 2004, Warnock-Juteau 2023), as does the number of teeth that make up each tooth family. These changes have been hypothesized as evidence of ontogenetic and interspecific differences in dietary preferences, which may have allowed for more efficient niche partitioning (Hall 1993, Erickson et al. 2012, Erickson and Zelenitsky 2014, Mallon et al. 2022, Wyenberg-Henzler 2022, Warnock-Juteau 2023).

Estimates of tooth growth, wear and replacement rates (Erickson 1996, Horner et al. 2000) for hadrosaurs this small range between 0.24 mm to 0.40 mm per day. Warnock-Juteau (2023) calculated that a single tooth crown in CMN8917 was worn out between 27 to 45 days, whereas young *Maiasaura peeblesorum* wore out their teeth in 46 days, but adults of the same taxon had to replace their teeth in 58 days (Erickson 1996)

The absence of a pronounced anterodorsal process, and the proportions of the dorsal process that is taller than antero-posteriorly long, identify UALVP60543 as a lambeosaurine. Several species of *Corythosaurus* and *Lambeosaurus* are present in the *Corythosaurus-Centrosaurus* assemblage zone (75.77-76.47 Ma) (Ryan and Evans 2005, Eberth et al. 2023), or Megaherbivore Assemblage Zone 1b (MAZ-1b). However, there are currently no characters known in the maxilla to refine the identification of UALVP60543. As pointed out by Warnock-Juteau (2023), dental characters like secondary ridges and denticulation are no longer considered variable enough to identify the teeth to subfamily level.

UALVP60543 and UALVP62346 have tooth row lengths that are roughly equivalent, and even though the specimens represent two different subfamilies that can have radically different tooth counts at maturity, they have equivalent numbers of tooth families at this size. These specimens indicate that

tooth counts in these two clades were similar at hatching, but rapidly diverged during ontogeny. The juveniles of both subfamilies presumably had similar diets, but the morphological divergences during ontogeny suggests there were fundamental differences in the diets of the adults. It is beyond the scope of this paper to determine whether those differences were because of dietary differences, because of differences in how they processed the food, or differences in both.

REFERENCES

Bell, P. R. (2011). Cranial osteology and ontogeny of *Saurolophus angustirostris* from the Late Cretaceous of Mongolia with comments on *Saurolophus osborni* from Canada: Acta Palaeontologica Polonica, v. 56, p. 703–722. doi: 10.4202/app. 2010.0061.

Bramble, K., LeBlanc, A. R. H., Lamoureux, D. O., Wosik, M., & Currie, P. J. (2017). Histological evidence for a dynamic dental battery in hadrosaurid dinosaurs. *Scientific Reports*, 7, 15787. doi: 10.1038/s41598-017-16056-3.

Brink, K. S., Zelenitsky, D. K., Evans, D. C., Horner, J. R., & Therrien, F. (2014). Cranial morphology and variation in *Hypacrosaurus stebingeri* (Ornithischia: Hadrosauridae). In D. A. Eberth & D. C. Evans (Eds.), *Hadrosaurs* (pp. 245–265). Indiana University Press, Bloomington, Indiana, USA.

Brown, C. M., Evans, D. C., Campione, N. E., O'Brien, L. J., & Eberth, D. A. (2013). Evidence for taphonomic size bias in the Dinosaur Park Formation (Campanian, Alberta), a model Mesozoic terrestrial alluvial-paralic system. *Palaeogeography, Palaeoclimatology, Palaeoecology*, 372, 108–122. doi: 10.1016j,palaeo.2012.06.027.

Conniff, R. (2018). Death of a fossil hunter. Scientific American Blog Network, Oct. 17, 2018.

Dewaele, L., Tsogtbaatar, K., Barsbold, R., Garcia, G., Stein, K., Escuillié, F., & Godefroit, P. (2015). Perinatal specimens of *Saurolophus angustirostris* (Dinosauria: Hadrosauridae), from the Upper Cretaceous of Mongolia. *PLoS One*, 10(10), e0128806. doi: 10.1371/journal.pone.0138806.

Dodson, P. (1975). Taxonomic implications of relative growth in lambeosaurine hadrosaurs. *Systematic Zoology*, 24, 37-54.

Eberth, D., Evans, D. C., Jahan, R., Kamo, S., Brown, C., Currie, P. J., & Braman, D. R. (2023). Calibrating geologic strata, dinosaurs, and other fossils at Dinosaur Provincial Park (Alberta, Canada) using a new CA-ID-TIMS U-Pb geochronology. Canadian Journal of Earth Sciences 60: 000-000. https://doi.org/10.1139/cjes-2023-0037

Edmund, A. G. (1957). On the special foramina in the jaws of many ornithischian dinosaurs. *Contributions of the Royal Ontario Museum Division of Zoology and Paleontology*, 48, 3–14.

Erickson, G. M. (1996). Incremental lines of von Ebner in dinosaurs and the assessment of tooth replacement rates using growth line counts. *Proceedings of the National Academy of Sciences of the United States of America*, 93, 14623–14627.

Erickson, G. M., Krick, B. A., Hamilton, M., Bourne, G. R., Norell, M. A., Lilleodden, E., & Sawyer, W. G. (2012). Complex dental structure and wear biomechanics in hadrosaurid dinosaurs. *Science*, 338, 98–101.

Erickson, G. M. & D. Zelenitsky. (2014). Osteohistology and occlusal morphology of *Hypacrosaurus stebingeri* teeth throughout ontogeny with comments on wear-induced form and function. In D. A. Eberth & D. C. Evans (Eds.), *Hadrosaurs* (pp. 422–432). Indiana University Press, Bloomington, Indiana, USA.

Evans, D. C. (2010). Cranial anatomy and systematics of *Hypacrosaurus altispinus*, and a comparative analysis of skull growth in lambeosaurine hadrosaurids (Dinosauria: Ornithischia). *Zoological Journal of the Linnean Society*, 159, 398–434.

Evans, D. C., Forster, C. A., & Reisz, R. R. (2005). The type specimen of *Tetragonosaurus erectofrons* (Ornithischia: Hadrosauridae) and the identification of juvenile lambeosaurines. In P. J. Currie & E. B. Koppelhus (Eds.), *Dinosaur Provincial Park, a Spectacular Ancient Ecosystem Revealed* (pp. 349-366). Indiana University Press, Bloomington, Indiana.

Farke, A. A., Chok, D. J., Herrero, A., Scolieri, B., & Werning, S. (2013). Ontogeny in the tube-crested dinosaur *Parasaurolophus* (Hadrosauridae) and heterochrony in hadrosaurids. *PeerJ*, e182, doi: 10.7717/peerj.182.

Galton, P. M. (1973). The cheeks of ornithischian dinosaurs. *Lethaia*, 6, 67–89.

Guangzhou Daily, 2021-10-26, www.laitimes.com/en/article/crw_csq.html.

Hall, J. P. (1993). A juvenile hadrosaurid from New Mexico. *Journal of Vertebrate Paleontology*, 13, 367–369. doi: http://dx.doi.org/10.1080/02724634.1993.10011516.

Horner, J. R. & Currie, P. J. (1994). Embryonic and neonatal morphology and ontogeny of a new species of *Hypacrosaurus* (Ornithischia, Lambeosauridae) from Montana and Alberta. In K. Carpenter, K. F. Hirsch, & J. R. Horner (Eds.), *Dinosaur Eggs and Babies* (pp. 312–336). Cambridge University Press, Cambridge, England.

Horner, J. R., Weishampel, D. B., & Forster, C. A. (2004). Hadrosauridae. In D. B. Weishampel, P. Dodson, & H. Osmólska (Eds.), *The Dinosauria, 2nd edition* (pp 438–463). University of California Press, Berkeley and Los Angeles, California, USA.

Lambe, L. M. (1920). The hadrosaur *Edmontosaurus* from the upper Cretaceous of Alberta. *Geological Survey of Canada Memoir*, 120, 1-79.

LeBlanc, A. R. H., Reisz, R. R., Evans, D. C., & Bailleul, A. M. (2016). Ontogeny reveals function and evolution of the hadrosaurid dinosaur dental battery. *BioMed Central BMC Evolutionary Biology*, 16, 152. doi: 10.1186/s12862-016-0721-1.

Lull, R. S. & Wright, N. E. (1942). Hadrosaurian dinosaurs of North America. *Geological Society of America Special Paper* 40, 242 pp.

Mallon, J. C., Evans, D. C, Ryan, M. J., & Anderson, J. S. (2012). Megaherbivorous dinosaur turnover in the Dinosaur Park Formation (upper Campanian) of Alberta, Canada. *Palaeogeography, Palaeoclimatology, Palaeoecology*, 350-352, 125–138.

Mallon, J. C., Evans, D. C., Zhang, Y., & Xing, H. (2022). Rare juvenile material constrains estimation of skeletal allometry in *Gryposaurus notabilis* (Dinosauria: Hadrosauridae). *The Anatomical Record*, 306, 1646−1668. doi: 10.1002/ar.25021.

Ostrom, J. H. (1961). Cranial Morphology of the hadrosaurian dinosaurs of North America. *American Museum of Natural History*, *Bulletin*, 122(2), 39-186.

Parks, W. A. (1923). *Corythosaurus intermedius*, a new species of trachodont dinosaur. University of Toronto Studies, *Geological Series*, 15, 1-57.

Prieto-Márquez A. (2011). Cranial and appendicular ontogeny of *Bactrosaurus johnsoni*, a hadrosauroid dinosaur from the Late Cretaceous of northern China. *Palaeontology*, 54, 773–792. doi:

10.1111/j.1475-4983.2011.01053.

Prieto-Márquez, A. (2014). A juvenile *Edmontosaurus* from the late Maastrichtian (Cretaceous) of North America: implications for ontogeny and phylogenetic inference in saurolophine hadrosaurids. *Cretaceous Research*, v. 50, p. 282–303. doi: 10.1016/j.cretres.2014.05.003.

Prieto-Márquez, A. & Guenther, M. F. (2018). Perinatal specimens of *Maiasaura* from the Upper Cretaceous of Montana (USA): insights into the early ontogeny of saurolophine hadrosaurid dinosaurs. *Peer J*, 6. doi: 10.7717/peerj.4734.

Ryan, M. J. & Evans, D. C. (2005). Ornithischian dinosaurs. *In* Dinosaur Provincial Park, a Spectacular Ancient Ecosystem Revealed. *Edited by* Philip J. Currie and Eva B. Koppelhus. Indiana University Press, Bloomington, Indiana. Pp. 312–348.

Sternberg, C. M. (1956). A juvenile hadrosaur from the Oldman Formation of Alberta. Annual Report of the National Museum for the fiscal year 1953–54. *National Museum of Canada Bulletin*, 136, 120–122.

Suzuki, D., Weishampel, D. B., & Minoura, N. (2004). *Nipponosaurus sachalinensis* (Dinosauria; Ornithopoda): anatomy and systematic position within Hadrosauridae. *Journal of Vertebrate Paleontology*, 24, 145–164. doi: 10.1671/A1034-11.

Tanke, D. H. & Brett-Surman, M. K. (2001). Evidence of hatchling-nestling-size hadrosaurs (Reptilia: Ornithischia) from Dinosaur Provincial Park (Dinosaur Park Formation: Campanian), Alberta. In D. H. Tanke & K. Carpenter (Eds.), *Mesozoic Vertebrate Life*, *New Research Inspired by the Paleontology of Philip J. Currie* (pp. 206-214). NRC Research Press, Indiana University Press, Bloomington & Indianapolis.

Wagner, J. & Lehman, T. M. (2009). An enigmatic new lambeosaurine hadrosaur (Reptilia: Dinosauria) from the Upper Shale member of the Campanian Aguja Formation of Trans-Pecos Texas. *Journal of Vertebrate Paleontology*, 29(2), 605–611. doi: 10.1671/039.029.0208.

Warnock-Juteau, T. M. (2023). Redescription of a juvenile hadrosaurid skull from the Upper Cretaceous of Alberta using Computed Tomography. Unpublished BSc Thesis, Department of Earth Sciences, Carleton University (Ottawa). 85 pp.

Warnock-Juteau, T. M., Ryan, M. J., Patterson, R. T., & Mallon, J. C. (2023). Redescription of a juvenile hadrosaurid from the Upper Cretaceous of Alberta using computed tomography. CSVP Program with Abstracts. *VAMP*, 11, 36.

Wyenberg-Henzler, T., Patterson, R. T., & Mallon, J. C. (2022). Ontogenetic dietary shifts in North American hadrosaurids (Dinosauria: Ornithischia). *Cretaceous Research*, 135, 105177. https://doi.org/10.1016/j.cretres.2022.105177.

Xing, H., Mallon, J. C., & Currie, M. L. (2017). Supplementary cranial description of the types of *Edmontosaurus regalis* (Ornithischia: Hadrosauridae), with comments on the phylogenetics and biogeography of Hadrosaurinae. *PLoS ONE*, 12(4), e175253. https://doi.org/10.1371/journal.pone.0175253.

WINDOWS INTO SAUROPSID AND SYNAPSID EVOLUTION
Essays in honor of Prof. Louis L. Jacobs, pp. 176–210, 2023

DESCRIPTION AND REVIEW OF NON-AVIAN DINOSAUR EGGS FROM CRETACEOUS DEPOSITS OF THE MONGOLIAN GOBI DESERT

KOHEI TANAKA[1,*], DARLA K. ZELENITSKY[2], FRANÇOIS THERRIEN[3], YUONG-NAM LEE[4], KATSUHIRO KUBOTA[5], YOSHITSUGU KOBAYASHI[6], GREGORY F. FUNSTON[7], and KHISHIGJAV TSOGTBAATAR[8]

[1]Faculty of Life and Environmental Sciences, University of Tsukuba, Tsukuba, Ibaraki 305-8572, Japan, koheitanaka@geol.tsukuba.ac.jp;
[2]Department of Geoscience, University of Calgary, Calgary, Alberta T2N 1N4, Canada, dkzeleni@ucalgary.ca;
[3]Royal Tyrrell Museum of Palaeontology, Drumheller, Alberta T0J 0Y0, Canada, francois.therrien@gov.ab.ca;
[4]School of Earth and Environmental Sciences, Seoul National University, Seoul 08826, South Korea, ynlee@snu.ac.kr;
[5]Museum of Nature and Human Activities, Hyogo, Sanda, Hyogo 669-1546, Japan, kubota@hitohaku.jp;
[6]Hokkaido University Museum, Sapporo, Hokkaido 060-0801, Japan, ykobayashi@museum.hokudai.ac.jp;
[7]Department of Natural History, Royal Ontario Museum, Toronto, Ontario M5S 2C6, Canada, greg.funston@rom.on.ca;
[8]Institute of Paleontology, Mongolian Academy of Sciences, Ulaanbaatar 15160, Mongolia, tsogtbaatar@mas.ac.mn

ABSTRACT Mongolia has a long history of discoveries and research related to dinosaur eggs. Since the first scientific discoveries in the early 1920s, numerous eggs, eggshells, and nests have been collected by various international expeditions and have contributed significantly to our understanding of reproductive traits in dinosaurs. In this study, we report on non-avian dinosaur egg remains that were collected as part of the Korean-Mongolia International Dinosaur Expeditions and the joint expeditions between Japan and Mongolia. This research includes the first detailed descriptions of six ootaxa (*Collacoidoolithus* oosp., *Dendroolithus* oosp., *Macroelongatoolithus* oosp., *Paraspheroolithus irenensis*, cf. *Protoceratopsidovum minimum,* and cf. *Spheroolithus maiasauroides*) from Upper Cretaceous localities (Altan Uul I, Altan Uul IV, Bayanshiree, Shine Us Khudag and Shiluut Uul) in order to provide a current summary of dinosaur ootaxa and egg-producing localities from the Gobi Desert of Mongolia. A compilation of locality and formation data for these and other ootaxa from Mongolia reveals the egg-bearing Upper Cretaceous formations, except the Javkhlant Formation, have each yielded ten or more non-avian dinosaur ootaxa (Baruungoyot, Bayanshiree, Djadokhta, and Nemegt formations). Mongolia is thus among the richest countries with respect to abundance and diversity of dinosaur eggs.

KEYWORDS Upper Cretaceous, Gobi Desert, Mongolia, Dinosaur, Egg, Eggshell

INTRODUCTION

The first scientific discoveries of dinosaur eggs from Mongolia occurred nearly a century ago in Cretaceous strata of the Gobi Desert. During the Central Asiatic Expeditions, dinosaur egg remains were uncovered in the early 1920s by the American Museum of Natural History, which led to the sudden realization that dinosaurs had laid eggs (Andrews, 1932). Subsequent significant collections of dinosaur eggs, eggshells and nests were made during the Mongolian Paleontological Expeditions of the USSR Academy of Science (1946-1949), the Polish-Mongolian Paleontological Expeditions (1963-1971), and the Joint Soviet (Russian)-Mongolian Palaeontological and Geological Expeditions (since 1969) (see Mikhailov, 2000 for the summary). Importantly, these expeditions found additional egg-producing localities and increased the known diversity of dinosaur eggs in Cretaceous rocks of the southern Gobi Desert. From the 1990s onwards, Mongolian-international joint expeditions with the United States (American Museum of Natural History), South Korea (Korea-Mongolia International Dinosaur Expedition), and Japan (Hayashibara Museum of Natural Sciences expeditions, Hokkaido University Museum expeditions, etc.) continued to collect dinosaur eggs/nests from the Gobi Desert, yielding some remarkable discoveries. Such specimens include embryos in ovo, egg clutch-adult skeleton associations, and fossilized soft-shelled eggs, which have contributed significantly to our understanding of various nesting and reproductive traits (e.g.,

*Corresponding author

eggshell types, nest types, egg pigmentation, brood-like behavior) within the dinosaur-bird lineage (e.g., Norell et al., 1995, 2001, 2018, 2020; Clarke et al., 1999; Weishampel et al., 2008; Fanti et al., 2012; Tanaka et al., 2015; Erickson et al., 2017; Wiemann et al., 2018).

This study focuses on the description of non-avian dinosaur egg remains that were collected as part of the Korean-Mongolia International Dinosaur Expeditions (KID) and the joint expeditions between Japan (Hokkaido University Museum) and Mongolia (Institute of Paleontology, Mongolian Academy of Sciences, MPC). The first detailed descriptions of all egg taxa (i.e., ootaxa) found at various localities are conducted in order to provide a summary of dinosaur ootaxa and egg-producing localities from the Gobi Desert of Mongolia, thus updating prior reviews (e.g., Sochava, 1969; Mikhailov, 1991, 2000; Sabath, 1991; Mikhailov et al., 1994).

REVIEW OF NON-AVIAN DINOSAUR EGGS FROM MONGOLIA

Some of the earliest discovered dinosaur eggs from Mongolia were studied by van Straelen (1925) and Brown and Schlaikjer (1940), the former of whom adopted light microscopy to describe the eggshell microstructures. After decades of collecting by various expeditions, dinosaur egg remains from Mongolia were described and classified, contributing to the development of a parataxonomy based on macro-features and microstructures of the eggs (e.g., Sochava, 1969; Mikhailov, 1991, 1994a, 1994b).

To date, more than twenty ootaxa are known from 46 localities in the Gobi Desert of southern Mongolia (Fig. 1 and see Appendix Table 1 for the list of egg-producing localities in Mongolia). Eight formations have produced these localities, most of which are Late Cretaceous in age with few (<10%) dating to the Early Cretaceous. To our knowledge, dinosaur egg sites have not been discovered in either Triassic or Jurassic deposits of Mongolia.

Eight egg families (i.e., oofamilies) have been recognized from Mongolia (Fig. 2 and see Appendix Table 2 for the measurements and outer surface morphology of non-avian dinosaur eggs in Mongolia). Eggs assignable to Dendroolithidae, Ovaloolithidae, Spheroolithidae, Elongatoolithidae, and Prismatoolithidae are common, whereas those attributable to Dictyoolithidae, Faveoloolithidae, and Stalicoolithidae are relatively rare (Mikhailov, 2000).

Dictyoolithidae eggs are relatively well documented from sites in China but are rarely reported from Mongolian sites. Eggs assigned to *Dictyoolithus* oosp. were identified from two localities, Nogoon Tsav and Algui Ulan Tsav (Ariunchimeg, 2000), although these specimens have not been described in detail.

Dendroolithidae eggs are commonly found in Upper Cretaceous formations of southern Mongolia, where two egg species, *Dendroolithus microporosus* and *D. verrucarius*, are currently recognized. Both of these oospecies are only known from Mongolia, and they can be differentiated from one another based on egg size and eggshell thickness (Appendix Table 2; Mikhailov, 1994b). Several egg clutches assignable to Dendroolithidae were reported at a single site in the Javkhlant Formation, from which colonial nesting and nest attendance behaviors in a possible therizinosaurian theropod have been inferred (Tanaka et al., 2019).

Faveoloolithidae eggs are found at several Upper Cretaceous localities in the Gobi Desert, notable for their large size and spherical shape. Although only a single oospecies, *Faveoloolithus ningxiaensis*, was recognized from Mongolia initially (Mikhailov, 1994b), it has been suggested that some of these eggs from the Algui Ulan Tsav locality are attributable to *Parafaveoloolithus* oosp., an oogenus known from Zhejiang and Henan provinces, China (Zhang, 2010).

Ovaloolithidae eggs are represented by two oospecies, *Ovaloolithus chinkangkouensis* and *O. dinornithoides*, from Upper Cretaceous deposits of Mongolia, the latter of which occurs only in Mongolia. These two oospecies differ with respect to eggshell thickness (primary range) and outer surface morphology (Appendix Table 2; Mikhailov, 1994b). An eggshell fragment assigned to *O. chinkangkouensis* along with embryonic remains (only possible metatarsals identified) adhered to the inner surface were described by Sochava (1972). The author suggested these few bones were similar to those of ceratopsian dinosaurs such as *Leptoceratops* and *Protoceratops*, but a recent study revealed that *Protoceratops* laid soft-shelled eggs (Norell et al., 2020) and not hard-shelled eggs like *Ovaloolithus*.

Spheroolithidae eggs are known from most Upper Cretaceous formations in Mongolia (Bayanshiree, Djadokhta, Baruungoyot, and Nemegt formations). Three oospecies, *Paraspheroolithus irenensis*, *Spheroolithus tenuicorticus* and *Sp. maiasauroides* have been recognized in Mongolia, but our analysis finds that *Sp. tenuicorticus* is a junior synonym of *Pa. irenensis* (see

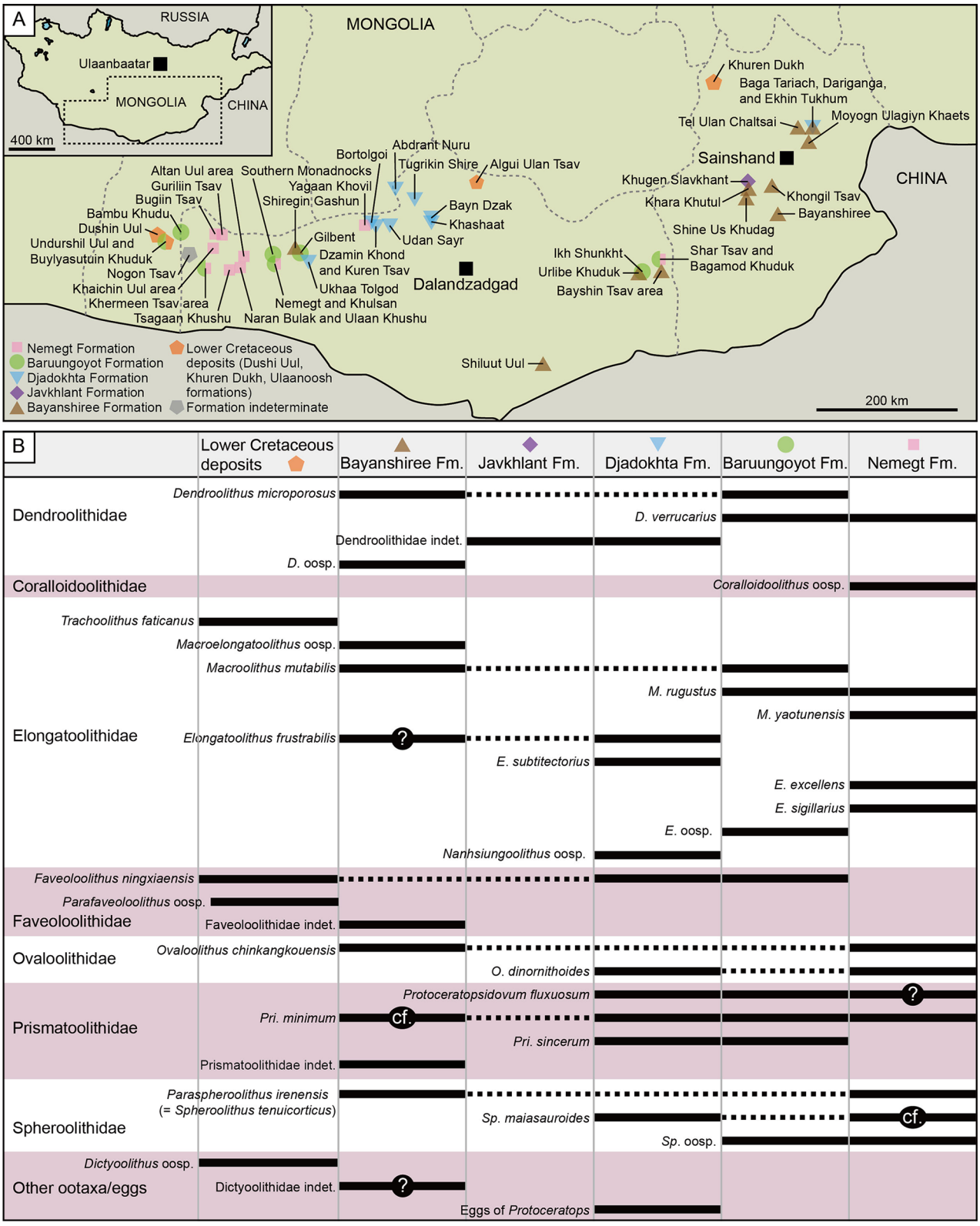

FIGURE 1. Summary of non-avian dinosaur egg localities and formations from Mongolia. **A**, approximate locations of fossil egg, eggshell and nest sites in Mongolia, based on Carpenter and Alf (1994), Mikhailov (2000), Watabe and Suzuki (2000a), Suzuki and Narmandakh (2004), Watabe and Tsogtbaatar (2004), Watabe et al. (2010a), Ishigaki et al. (2016), Saneyoshi et al. (2010); **B**, stratigraphic distribution of ootaxa (solid bars, ootaxon present; dashed bars, ootaxon currently absent). See Appendix Table 1 for the dataset of this figure.

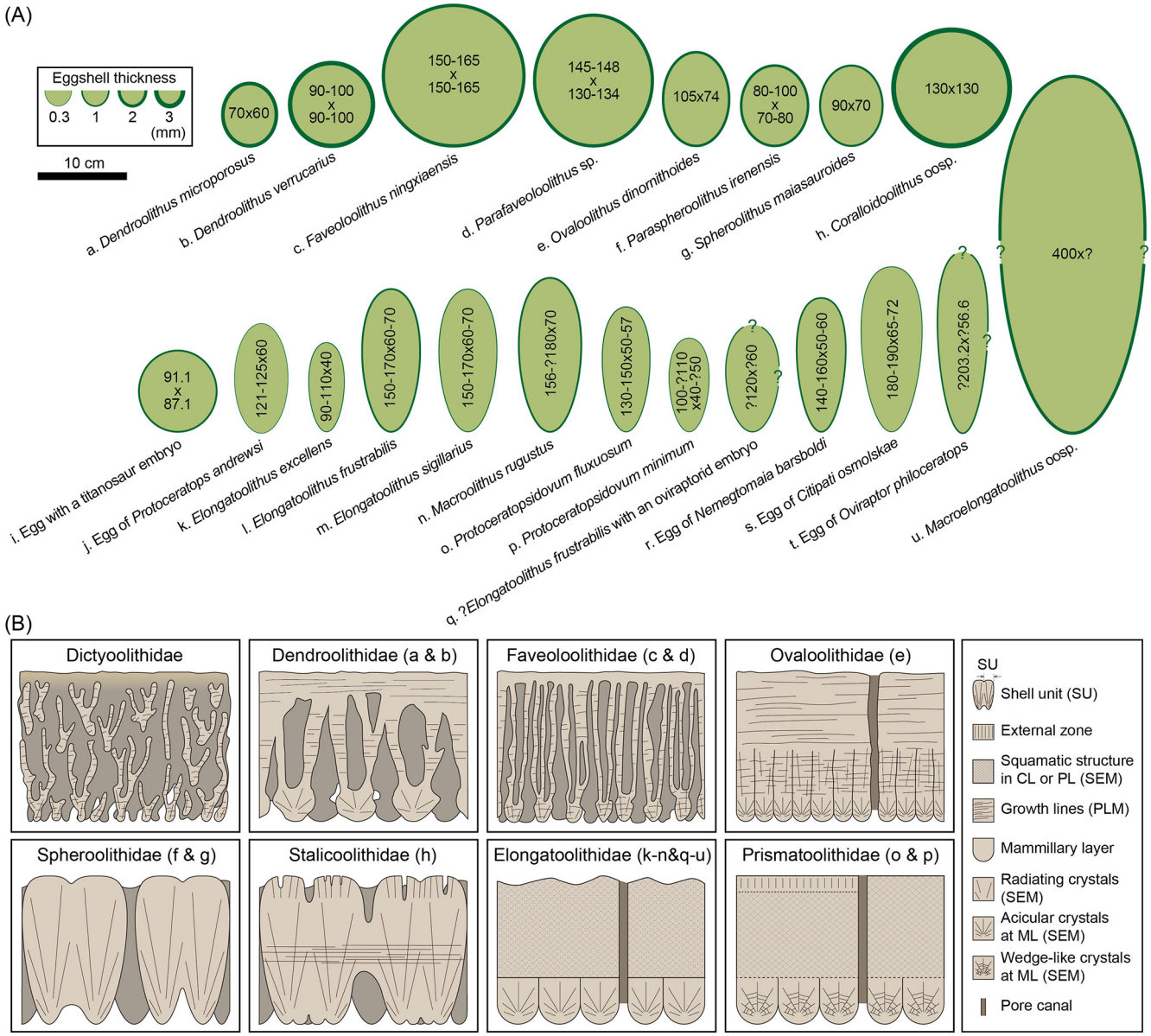

FIGURE 2. Comparisons of non-avian dinosaur eggs from Mongolia. **A**, comparison of egg size, shape, and eggshell thickness among ootaxa (size-known ootaxa only); **B**, schematic illustrations of eggshell microstructure (radial view) among oofamilies. Letters in parentheses for each oofamily correspond to letters (for ootaxa) in A. Note that *Protoceratopsidovum fluxuosum* and *Pro. sincerum* may be assignable to Elongatoolithidae and Montanoolithidae, respectively, rather than to Prismatoolithidae (Choi et al., 2022). See Appendix Table 2 for the dataset of this figure.

Systematic Paleontology). Although the egg sizes and eggshell thicknesses are similar, *Pa. irenensis* and *Sp. maiasauroides* can be differentiated based on the outer surface morphology (i.e., generally no ornamentation for *Pa. irenensis,* whereas prominent sagenotuberculate ornamentation for *Sp. maiasauroides*: Appendix Table 2). In the Altan Uul area, a perinatal *Saurolophus angustirostris* was found in association with *Spheroolithus* eggshells (Dewaele et al., 2015).

Stalicoolithidae eggs were not recognized in Mongolia until recently. Wang et al. (2012a) pointed out that some dendroolithid eggshells previously reported in Mongolia belong to Stalicoolithidae. Our study confirms the occurrence of Stalicoolithidae (*Coralloidoolithus*) in the Nemegt Formation of Mongolia (see Systematic Paleontology).

Elongatoolithidae is the most diverse oofamily known from strata of the Gobi Desert, and account for about half of the

ootaxa known from Mongolia. Whereas *Trachoolithus faticanus* is restricted to Lower Cretaceous deposits, *Elongatoolithus*, *Macroolithus*, *Macroelongatoolithus*, and *Nanhsiungoolithus* are all known from Upper Cretaceous formations. These ootaxa have been differentiated from one another based on egg size, eggshell thickness, spacing of ridges on the outer surface, and/or relative thickness of the mammillary layer to the continuous layer (Mikhailov, 1994a). Specimens of eggs associated with skeletal remains from Mongolia were the first to provide conclusive evidence that elongatoolithid eggs were laid by oviraptorosaur theropods (Norell et al., 1994, 1995).

Prismatoolithidae eggs are documented from many Upper Cretaceous localities of the Gobi Desert. *Protoceratopsidovum* and *Prismatoolithus* are currently recognized from Mongolia; three oospecies have been identified within *Protoceratopsidovum* (Mikhailov, 1994a), including: *Pro*. *fluxuosum* that has linearituberculate ornamentation, and *Pro*. *minimum* and *Pro*. *sincerum* that both have a smooth eggshell surface. Choi et al. (2022) argue that *Pro*. *minimum* and *Pro*. *sincerum* can be distinguished from one another based on the ultrastructure of the mammillary layer (i.e., wedge-like crystals in *Pro*. *minimum*, but acicular crystals in *Pro*. *sincerum*). They also argue that *Pro*. *fluxuosum* could be reassigned to the Elongatoolithidae and *Pro. sincerum* to Montanoolithidae based on microstructure and crystallography. Prismatoolithid eggs/eggshells from Mongolia are reported to have been found associated with troodontid skeletons (Grellet-Tinner, 2005; Pei et al., 2017).

In addition to the wide diversity of ootaxa listed above, in-ovo dinosaur embryos are known for fossilized soft-shelled eggs from Mongolia which have not been classified using the parataxonomy. A clutch of eggs and embryos of *Protoceratops andrewsi* was reported from Ukhaa Tolgod (Erickson et al., 2017; Norell et al., 2020) for which geochemical analyses revealed that these eggs were soft-shelled.

MATERIALS AND METHODS

Over 300 eggshell fragments and partial eggs recovered from the areas of Altan Uul (Altan Uul I and IV), Bayanshiree, Shine Us Khudag, and Shiluut Uul were examined. The original egg diameter of *Coralloidoolithus* oosp. was estimated from the curvature of the partially-preserved egg, following Ribeiro et al. (2014). Eggshell thickness was measured with either a digital caliper (Mitutoyo CD-15CPX, precision of ±0.02 mm) or a digital micrometer (Mitutoyo CPM30-25 MJ, precision of ±2 μm). Macro- and microscopic structures of eggshell fragments were examined via scanning electron microscopy (SEM: Hitachi TM1000 and TM3000) and polarized light microscopy (PLM: Nikon Eclipse 50iPOL) instruments housed at the Royal Tyrrell Museum of Palaeontology, Drumheller, Canada, the Nagoya University Museum, Nagoya, Japan, and Sapporo Medical University, Sapporo, Japan. Descriptive terminology for eggshell generally follows Mikhailov (1991). Although Mikhailov (1997) considered *Paraspheroolithus* synonymous with *Spheroolithus*, we use the term '*Paraspheroolithus*' following the argument of Shen et al. (2023) (see discussions therein).

Institutional Abbreviations — **DNHM**, Dalian Natural History Museum, Dalian, China; **IVPP**, Institute of Vertebrate Paleontology and Paleoanthropology, Chinese Academy of Sciences, Beijing, China; **KID**, Korean-Mongolia International Dinosaur Expeditions; **MPC**, Institute of Paleontology, Mongolian Academy of Sciences, Ulaanbaatar, Mongolia; **PIN**, Paleontological Institute, Russian Academy of Sciences, Moscow, Russia; **PMRE**, Beijing Museum of Natural History, Beijing, China; **TMNH**, Tianjin Museum of Natural History, Tianjin, China.

SYSTEMATIC PALEONTOLOGY

Oofamily SPHEROOLITHIDAE Zhao, 1979

Oogenus *PARASPHEROOLITHUS* Zhao, 1979 emend. Zhao et al., 2015

PARASPHEROOLITHUS IRENENSIS (Young, 1954, 1965; Zhao and Jiang, 1974) Zhao, 1979 emend. Zhao et al., 2015

(Figs. 3A-C and 4A-E)

Holotype — The holotype specimen was not originally designated but selected as TMNH No. 40.095 by Zhao et al. (2015), which included four complete eggs and two egg impressions from a partial clutch collected from Shandong Province, China (Upper Cretaceous Jiangjunding Formation).

Referred Specimens — Partially preserved eggs from two clutches (eight and three eggs, respectively: MPC-D uncatalogued) and isolated eggshell fragments [MPC-D 100/1065 (n = 11) and MPC-D 100/1066 (n = 42)]. *Spheroolithus tenuicorticus* from Shiluut Uul (PIN 4476-4: Mikhailov, 1994b) is herein

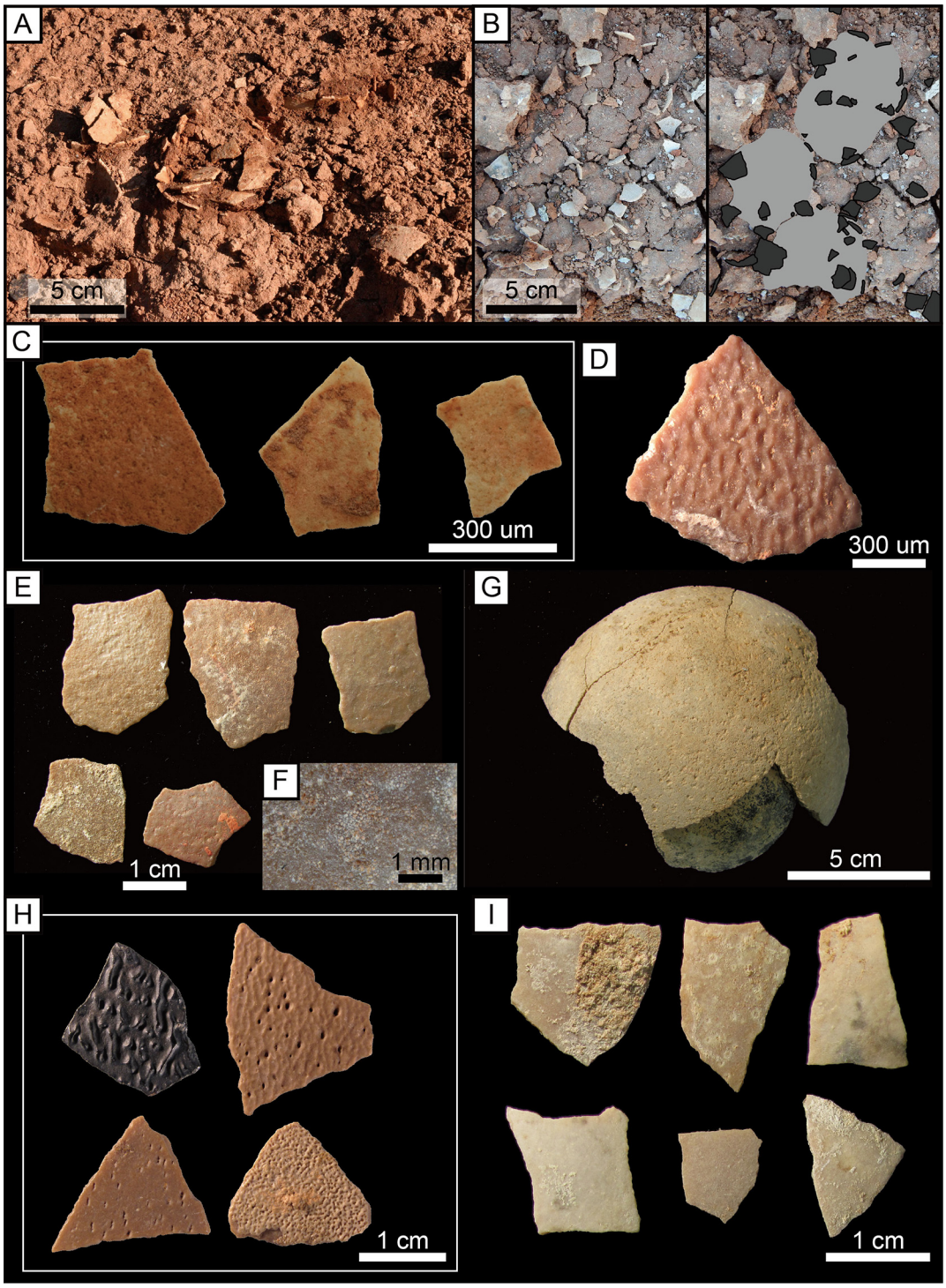

FIGURE 3. Selection of fossil eggs and eggshells examined in this study. **A**, partial clutch of *Paraspheroolithus irenensis* from Shiluut Uul, containing eight eggs and embryonic bones (only three eggs are visible in photograph whereas embryos are not visible); **B**, scattered eggshell fragments on a partial clutch of three *Pa. irenensis* eggs (left: original photograph, right: original photograph with light gray shadows of three eggs and darker shadows of eggshell fragments) from Shiluut Uul; **C**, rough outer surface of *Pa. irenensis* (MPC-D 100/1065); **D**, reticulated outer surface of cf. *S. maiasauroides* from Altan Uul IV (MPC-D 100/1060); **E**, rough outer surface of *Dendroolithus* oosp. from Bayanshiree (MPC-D 100/1063); **F**, magnification of outer surface of E; **G**, partial egg of *Coralloidoolithus* oosp. from Altan Uul I (MPC-D 100/1045); **H**, linearituberculate to smooth outer surface of *Macroelongatoolithus* oosp. from Bayanshiree (MPC-D 100/1064); **I**, smooth outer surface of cf. *Protoceratopsidovum minimum* from Bayanshiree (MPC-D 100/1062).

considered a junior synonym of *Pa. irenensis*.

Locality, Horizon, and Age — Egg and eggshell specimens examined in this study were recovered from a red-brown mudstone layer at the Shiluut Uul locality (N42.17.160; E105.44.604), a site located approximately 80 km southeast of Nomgon in Ömnögovi Aimag, Mongolia. The mudstone layer is part of the red beds of the Upper Cretaceous (Cenomanian to early Santonian?) Bayanshiree Formation.

Description — At least two clutches of *Paraspheroolithus irenensis* have been recovered from Shiluut Uul, containing at least eight and three eggs each (Fig. 3A, B); the larger clutch contains some embryonic remains (which will be described in a future study). The eggs are spherical to subspherical (diameter ~70-80 mm) in shape. All eggs were missing their upper halves due to erosion, whereas the lower halves were still imbedded in the mudstone layer. Abundant scattered eggshell fragments were found in the same horizon as the eggs, and were usually small in size (<20 mm in length).

Eggshell thickness ranges from 0.94 to 1.56 mm with a mean value of 1.25 mm (n = 52). The outer surface of the eggshell is smooth to rough and lacks a conspicuous ornamentation pattern (Fig. 3C). Round to oval pore openings are present on the outer surface. The eggshell consists of a single layer of closely-spaced fan-shaped shell units each made up of densely-packed acicular crystals (prolatospherulitic shell units: Fig. 4A-C). In radial thin section, the shell unit margins are poorly defined in the upper three-quarters to one-half of the eggshell. A sweeping extinction pattern and subhorizontal growth lines are visible through the shell units under PLM (Fig. 4B). The shell unit bases, which are composed of acicular crystals radiating from the core, are finger-like in shape and densely packed with little to no space between them (Fig. 4A-C). Pore canals appear irregular in shape along their length and are unbranching (assigned to prolatocanaliculate) (Fig. 4D). They vary in diameter and cross-sectional shape, from round to oval or somewhat irregular, with relatively smooth pore walls (Fig. 4E).

Comparisons — The eggs and eggshells (MPC-D 100/1065 and 100/1066 and uncatalogued specimens) are assignable to the oofamily Spheroolithidae based on the presence of prolatospherulitic shell units, but lack sagenotuberculate ornamentation (Table 1). Of the two oogenera within the oofamily Spheroolithidae, *Paraspheroolithus* and *Spheroolithus*, the specimens examined are attributable to *Paraspheroolithus* because of a scarcity of interstices between the finger-shaped bases of the shell units. These specimens are assignable to *Pa. irenensis* because all attributes of eggshell morphology are shared with this ootaxon, and the egg width and eggshell thickness are within the ranges of *Pa. irenensis*. Currently, *Paraspheroolithus* has only one valid oospecies, *Pa. irenensis* (see the review of *Paraspheroolithus* in Shen et al., 2023).

Remarks — Only a single spheroolithid ootaxon, *Spheroolithus tenuicorticus* had been reported previously from the Shiluut Uul locality (Mikhailov, 1994b). Although described as oval in shape [elongation index (100 × egg width / egg length): 71.43 - 76.92?] with weak sagenotuberculate ornamentation or a smooth outer surface (Mikhailov, 1994b), the ootaxon presently lacks sufficient description or illustration of the eggshell microstructure. The microstructure of *Sp. tenuicorticus*, according to Mikhailov (1994b), is similar to that of *Pa. irenensis*; the only differences noted between the two oospecies are a more elongate egg and thinner eggshell in *Sp. tenuicorticus*. Because egg shape and eggshell thickness of *Sp. tenuicorticus* are shown to largely overlap with these ranges for *Pa. irenensis* (Fig. 5), we consider *Sp. tenuicorticus* to be a junior synonym of *Pa. irenensis*. Thus, a single spheroolithid ootaxon (*Pa. irenensis*) is currently known from the Shiluut Uul locality.

The egg remains (MPC-D 100/1065 and 100/1066) were likely laid by hadrosaurs as embryonic and neonatal bones of these dinosaurs have been found in close association with spheroolithid eggs from sites in China, Mongolia, and the USA (Horner and Makela, 1979; Hirsch and Quinn, 1990; Horner, 1999; Dewaele et al., 2015; Xing et al., 2022). From the Bayanshiree Formation of Mongolia, the non-hadrosaurid hadrosauroid *Gobihadros mongoliensis* has been reported from skeletal remains (Tsogtbaatar et al., 2019) and is thus a potential candidate for the producer of these eggs.

Oogenus *SPHEROOLITHUS* Zhao, 1979 emend. Zhao et al., 2015

SPHEROOLITHUS cf. *S. MAIASAUROIDES* Mikhailov, 1994b

(Figs. 3D and 4F-H)

Holotype — PIN 4228-2, compressed egg from Baga Tariach, Mongolia (middle Campanian Djadokhta Formation).

Referred Specimens — An isolated eggshell fragment (MPC-D 100/1060).

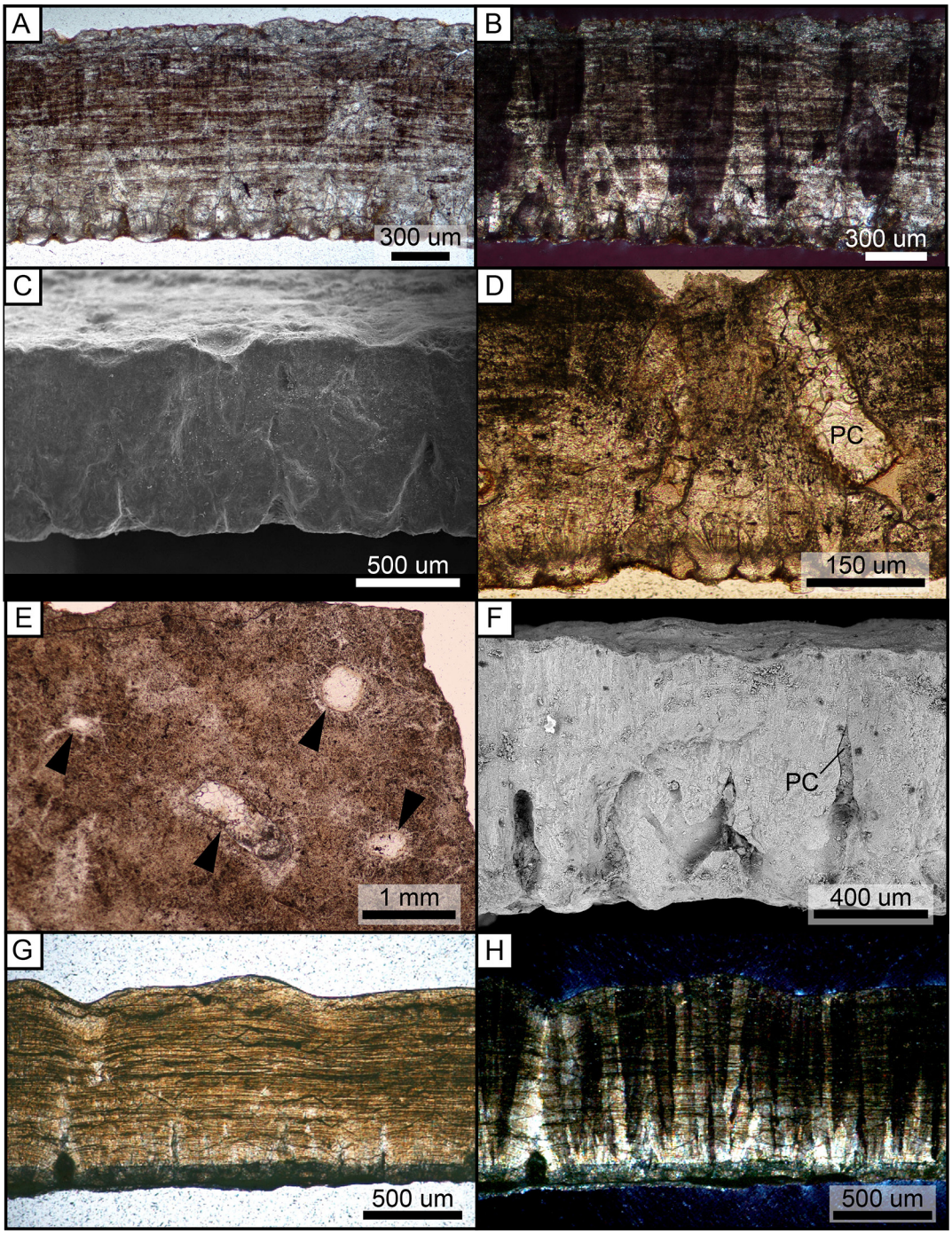

FIGURE 4. Photomicrographs of spheroolithid eggshells (A-E, *Paraspheroolithus irenensis*, MPC-D 100/1065; F-H, *Spheroolithus* cf. *S. maiasauroides*, MPC-D 100/1060). **A**, radial thin section of eggshell under polarized light, showing single layer of fan-shaped shell units with subhorizontal growth lines; **B**, radial thin section of A under cross-polarized light, showing sweeping extinction pattern; **C**, radial view of eggshell under SEM, showing fan-shaped shell units; **D**, radial thin section of eggshell under polarized light, showing oblique pore canal; **E**, tangential thin section of eggshell under polarized light, showing round to irregular pore canals with relatively smooth pore walls (black arrows); **F**, radial view of eggshell under SEM, showing single layer of fan-shaped shell units; **G**, radial thin section of eggshell under polarized light, showing fan-shaped shell units with subhorizontal growth lines; **H**, radial thin section of G under cross-polarized light, showing sweeping extinction pattern.

TABLE 1. Comparison of spheroolithid and related ootaxa. References: [1]this study; [2]Moreno-Azanza et al. (2014a); [3]Hirsch and Quinn (1990); [4]Zelenitsky and Hills (1997); [5]Sellés et al. (2014); [6]Xue et al. (1996); [7]Zhu et al. (2022); [8]Mikhailov (1994b); [9]Shen et al. (2023); [10]Young (1954); [11]Young (1965); [12]Zhao and Jiang (1974); [13]Zhao et al. (2015); [14]Bureau of Geology and Mineral Resources of Jilin Province (1992); [15]Jackson and Varricchio (2010); [16]Liu et al. (2013); [17]Chow (1951); [18]Mikhailov (2000); [19]Dawaele et al. (2015); [20]Xing et al. (2022). *Ootaxa that have been recently reassigned to *Stromatoolithus* by Zhao et al. (2015) and/or Zhu et al. (2022). **Incomplete egg. Parentheses include mean values or main ranges

Ootaxon	Egg length (mm)	Egg width (mm)	Mean EI	Eggshell thickness (mm)	Surface texture	Locality	Formation
Shiluut Uul *Paraspheroolithus irenensis*	?	70.00-80.00[1]	?	1.25[1]	Smooth[1]	Shiluut Uul, Mongolia[1]	Upper Cretaceous (Cenomanian to lower Santonian?) Bayanshiree Formation[1]
Altan Uul *Spheroolithus* cf. *S. maiasauroides*	?	?	?	0.97[1]	Prominent sagenotuberculate ornamentation[1]	Altan Uul IV, Mongolia[1]	Upper Cretaceous (upper Campanian to lower Maastrichtian) Nemegt Formation[1]
*Guegoolithus turolensis**	?	?	?	0.42-1.50 (0.815)[2]	Prominent sagenotuberculate ornamentation[2]	Teruel, Spain[2]	Lower Cretaceous (lower Barremian) Blesa, Camarillas, Upper El Castellar, and Mirambel formations[2]
Spheroolithus albertensis (egg of *Maiasaura peeblesorum*)*	100.00-120.00[3]	70.00-90.00[3]	72.73[3]	1.00-1.20[3]; 0.96-1.46 (0.98-1.22)[4]	Sagenotuberculate ornamentation[4]	Montana, USA[3] and Alberta, Canada[4]	Upper Cretaceous (Campanian) Two Medicine Formation (Montana)[3] and Upper Cretaceous (Campanian) Oldman and Dinosaur Park formations (Alberta)[4]
*Spheroolithus europaeus**	?	?	?	1.04-1.11 (1.07)[5]	Sagenotuberculate ornamentation[5]	Lleida, Spain[5]	Upper Cretaceous (upper Maastrichtian) Tremp Formation[5]
*Spheroolithus lamelliformae**	?	?	?	1.20-1.46 (1.33)[6]	'spots and curved strips' (prominent sagenotuberculate ornamentation)[6,7]	Shanyang, Shaanxi Province, China[6]	Upper Cretaceous Shanyang Formation[6]
*Spheroolithus maiasauroides**	90.00[8,**]	70.00[8,**]	77.78[8,**]	1.00-1.60 (1.20-1.50)[8]	Prominent sagenotuberculate ornamentation[8]	Baga Tariach and Bayn Dzak, Mongolia[8]	Upper Cretaceous (middle Campanian) Djadokhta Formation[8]
Paraspheroolithus irenensis, including *Paraspheroolithus jilinensis*	83.74[9]; 83.00-91.00 (87.00)[10]; 88.00-105.00 (93.73)[11]; 84.00-91.00 (86.75, 90.30)[12]; 83.00-99.00 (84.00)[13]; 87.00[14]	66.58[9]; 71.00-77.00 (73.75)[10]; 72.00-88.00 (78.91)[11]; 67.00-75.40 (68.25, 75.40)[12]; 67.00-88.00 (70.00)[13]; 81.50[14]	79.51[9]; 81.11, 86.10[10]; 84.19[11]; 83.50, 78.79[12]; 83.33[13]; 93.67[14]	1.05[9]; 1.10-2.60 (1.50-2.20), 1.10-3.00 (1.50-2.22)[10]; 1.50-2.20 (1.80)[12,13]; 2.00[14]	Smooth to rough and a very weak reticulate ornamentation (sagenotuberculate ornamentation)[9,10]	Gongzhuling of Jilin, Changtu of Liaoning, Erlian of Neimongolia, Laiyang of Shangdong, Xichuan and Xixia of Henan, Yunxian of Hubei, and Jinqu and Tiantai of Zhejiang, China[9]	Upper Cretaceous (Cenomanian) Quantou Formation (Jilin and Liaoning), Upper Cretaceous Earlian Formation (Neimongolia), Upper Cretaceous (Coniacian-Santonian) Jiangjunding Formation (Shangdong), Upper Cretaceous (Cenomanian-Turonian) Gaogou (or Zoumagang) Formation and (Coniacian-Santonian) Majiacun (or Zhaoying) Formation (Henan), Upper Cretaceous (Cenomanian-Turonian) Gaogou Formation (Hubei), and Upper Cretaceous Quixian and Chichengshan formations (Zhejiang)[9]

TABLE 1. Continued

Ootaxon	Egg length (mm)	Egg width (mm)	Mean EI	Eggshell thickness (mm)	Surface texture	Locality	Formation
Spheroolithus chiangchiungtingensis	81.00[12]	77.00[12]	95.06[12]	2.20[12]	Generally smooth but small nodes observed under microscopy[10,12]	Laiyang, Shangdong, China[12]	Upper Cretaceous (Coniacian-Santonian) Jiangjunding Formation[12]
Spheroolithus choteauensis	110.00[15,**]	95.00[15,**]	?	0.66-0.94[15]	Relatively smooth to ramotuberculate[15]	Montana, USA[15]	Upper Cretaceous (Campanian) Two Medicine Formation[15]
Spheroolithus quantouensis	90.00[16]	80.00[16]	88.90[16]	4.80-5.22[15]; 4.80-5.70[12]	Smooth[16]	Changtu, Liaoning, China[16]	Upper Cretaceous (Cenomanian) Quantou Formation[16]
Spheroolithus spheroides	68.00-81.00 (79.00)[10]; 81.00[12]; 74.00-90.00 (80.00)[13,16]	55.00-71.00 (64.67)[10]; 77.00[12]; 57.00-67.00 (62.33)[15]; 68.00[13]	81.94[10]; 95.06[12]; 78.51[15]; 85.00-90.50[13]	1.40-3.00[10]; 2.80-3.10[15]; 2.40-3.20[13]	Smooth[1,17]	Changtu, Liaoning and Laiyang, Shangdong, China[16]	Upper Cretaceous (Cenomanian) Quantou Formation (Liaoning) and Upper Cretaceous (Coniacian-Santonian) Jiangjunding Formation[16]
Spheroolithus tenuicorticus (= *Pa. irenensis*)	?	?	71.43-76.92?[8]	0.80-1.80 (1.00-1.30)[18]	No ornamentation or weak sagenotuberculate pattern[8]	Shiluut Uul, Mongolia[8]	Upper Cretaceous (Cenomanian to lower Santonian?) Bayanshiree Formation[1]
Spheroolithus eggshell of *Saurolophus angustirostris*	?	?	?	1.80[19]	Ramotuberculate or sagenotuberculate ornamentation[19]	Dragon's Tomb dinosaur locality, Mongolia[19]	Upper Cretaceous (upper Campanian to lower Maastrichtian) Nemegt Formation[19]
Spheroolithid egg of Lambeosaurinae	?	?	?	0.32-0.42[20]	?	Jiangxi, China[20]	Upper Cretaceous Hekou Formation[20]

TABLE 2. Comparison of egg size and eggshell thickness in Stalicoolithidae. Parentheses indicate mean values.

Ootaxon	Egg length (mm)	Egg width (mm)	Eggshell thickness (mm)	Reference
Coralloidoolithus oosp.	130.0	130.0	2.53-3.95 (3.24)	This study
Coralloidoolithus shizuiwanensis	93.6	81.9	1.80-2.60	Wang et al. (2012a)
Shixingoolithus erbeni	105.0-125.0	99.0-123.0	2.30-2.60	Zhao et al. (1991)
Stalicoolithus shifengensis	95.4	88.9	3.90-4.00	Wang et al. (2012a)

Locality, Horizon, and Age — The single eggshell fragment was recovered from the Altan Uul IV locality (N43.36.101; E100.27.102), which is located approximately 58 km northwest of Gurvantes in Ömnögovi Aimag, Mongolia. The exposures belong to the Upper Cretaceous (upper Campanian to lower Maastrichtian) Nemegt Formation.

Description — The outer eggshell surface exhibits a reticulated pattern of ridges (sagenotuberculate ornamentation), with an average width of 0.4 mm (Fig. 3D). The eggshell is 1.05 mm thick when the ornamentation height is included, and 0.97 mm with the ornamentation excluded. Oval pore openings are visible between the ridges on the outer surface. The eggshell consists of adjacent fan-shaped shell units (prolatospherulitic) that interlock at one-third to three-fifth of the eggshell thickness (Fig. 4F-H). Under SEM, acicular crystals are observed to radiate from the bases and occur throughout the shell units (Fig. 4F). In radial thin section, a sweeping extinction pattern is visible under PLM through the slender wedges that comprise the shell units (Fig. 4G, H). Multiple growth lines that roughly parallel the outer surface are also visible (Fig. 4G). Pore canals are non-branching, but their diameter varies throughout the length (prolatocanaliculate pore system) (Fig. 4F).

Comparisons — The eggshell microstructure of MPC-D 100/1060 is comparable to that of *Stromatoolithus* as well as to those of other spheroolithid ootaxa with a prominent sagenotuberculate ornamentation (e.g., *Guegoolithus turolensis*, *Spheroolithus lamelliformae*, *Sp. albertensis*, *Sp. europaeus*, and *Sp. maiasauroides*: Table 1). These ornamented spheroolithid ootaxa were recently transferred to the oogenus *Stromatoolithus* because of morphological similarities (Zhu et al., 2022). According to Zhu et al. (2022), the (remaining) spheroolithids, which lack prominent ornamentation, differ from ornamented spheroolithids (i.e., *Stromatoolithus*) in that they have irregular pores in cross-section (i.e., unevenly pinched by surrounding shell units) and less conspicuous growth lines. However, Shen et al. (2023) more recently found that non-ornamented spheroolithid eggs could also possess features characteristic of ornamented spheroolithids (e.g., some pores are circular to sub-circular in cross section, subhorizontal to undulating growth lines continue through adjacent spherulitic shell units), suggesting that such features are transitional or shared between ornamented and non-ornamented spheroolithid ootaxa. Because of this, we presently consider *G. turolensis*, *Sp. lamelliformae*, *Sp. albertensis*, *Sp. europaeus*, and *Sp. maiasauroides* as distinct ootaxa, rather than synonyms of *Stromatoolithus*, until further investigations are conducted.

Compared to ornamented spheroolithid ootaxa, MPC-D 100/1060 has the most apparent differences with the ootaxon *G. turolensis* (ornamentation is significantly higher at one-fifth to one-third of the eggshell thickness: Moreno-Azanza et al., 2014a), whereas more subtle differences occur with *Sp. albertensis* (Zelenitsky and Hills, 1997), *Sp. europaeus* (Sellés et al., 2014), *Sp. maiasauroides* (Mikhailov, 1994b), and *Sp. lamelliformae* (Xue et al., 1996). These *Spheroolithus* oospecies are difficult to differentiate from one another as they are all characterized by sagenotuberculate ornamentation (which is extremely variable) and have similar eggshell thicknesses. The ornamentation ridges in MPC-D 100/1060 are wider than those of *Sp. europaeus* (180 μm in width), but similar measurement data are not provided for other oospecies. According to Mikhailov (1994b), *Sp. maiasauroides* eggshell from Mongolia has finer ornamentation than eggshells of the hadrosaur *Maiasaura peeblesorum* from North America (eggshells of *Maiasaura* were assigned to the oospecies *Sp. albertensis*: Zelenitsky, 2000), which also appears to be the case for MPC-D 100/1060. Although *Sp. maiasauroides* and *Sp. lamelliformae* (from Shaanxi Province of China: Xue et al., 1996) appear very similar, we tentatively assign MPC-D 100/1060 to *Sp. maiasauroides* due to geographic and stratigraphic considerations, as well as the fact that *Sp. maiasauroides* would be the senior synonym if these two oospecies cannot be differentiated.

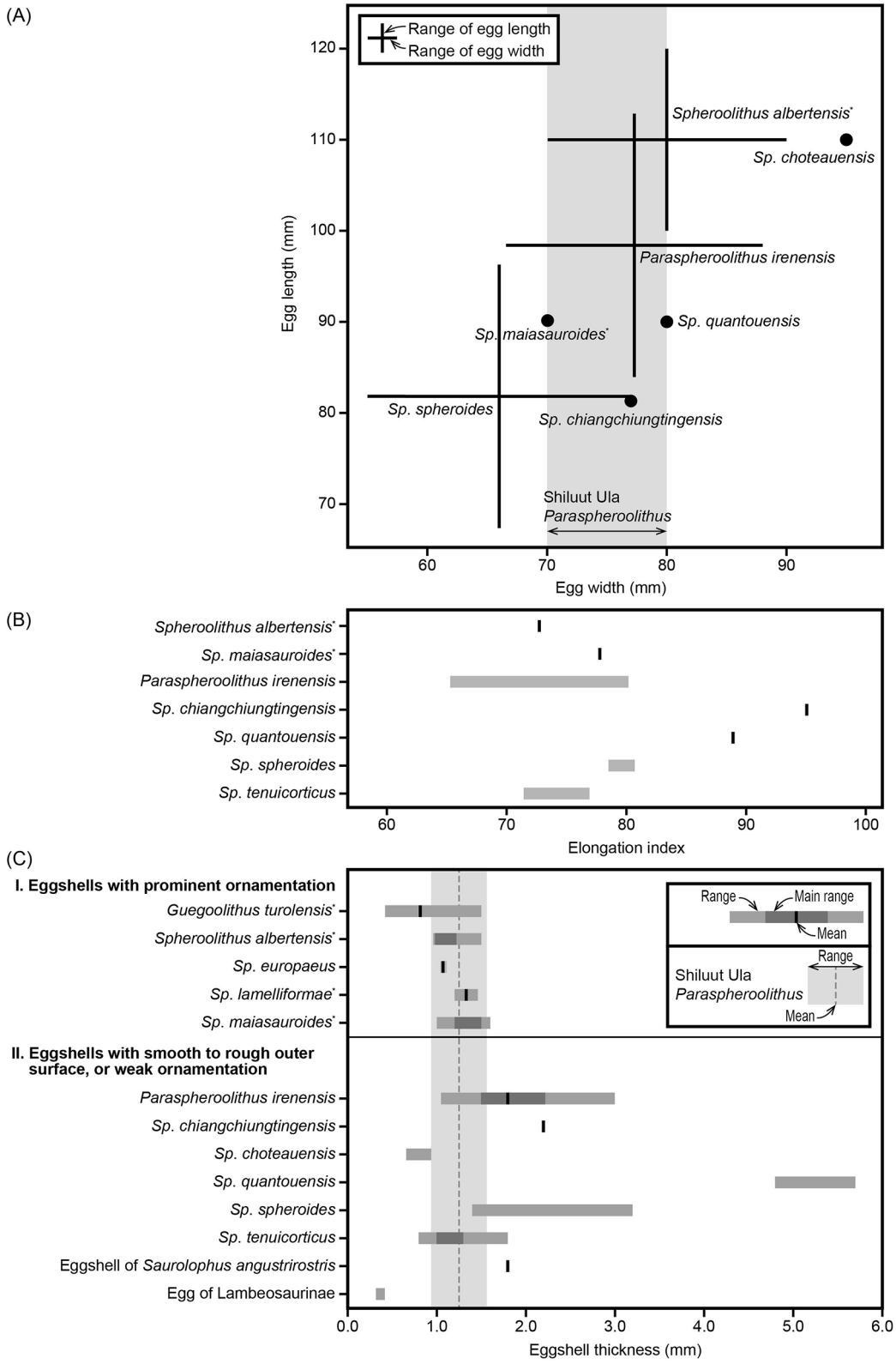

FIGURE 5. Comparisons of spheroolithid eggs. **A**, bivariate plot of egg length vs. egg width. Grey shaded area shows egg width of Shiluut Uul *Paraspheroolithus irenensis*; **B**, comparison of egg elongation index [100 × egg width (mm)/egg length (mm)] among ootaxa; **C**, comparison of eggshell thickness among ootaxa. Grey shaded area shows eggshell thickness of Shiluut Uul *Pa. irenensis* (MPC-D 100/1065 and MPC-D 100/1066).

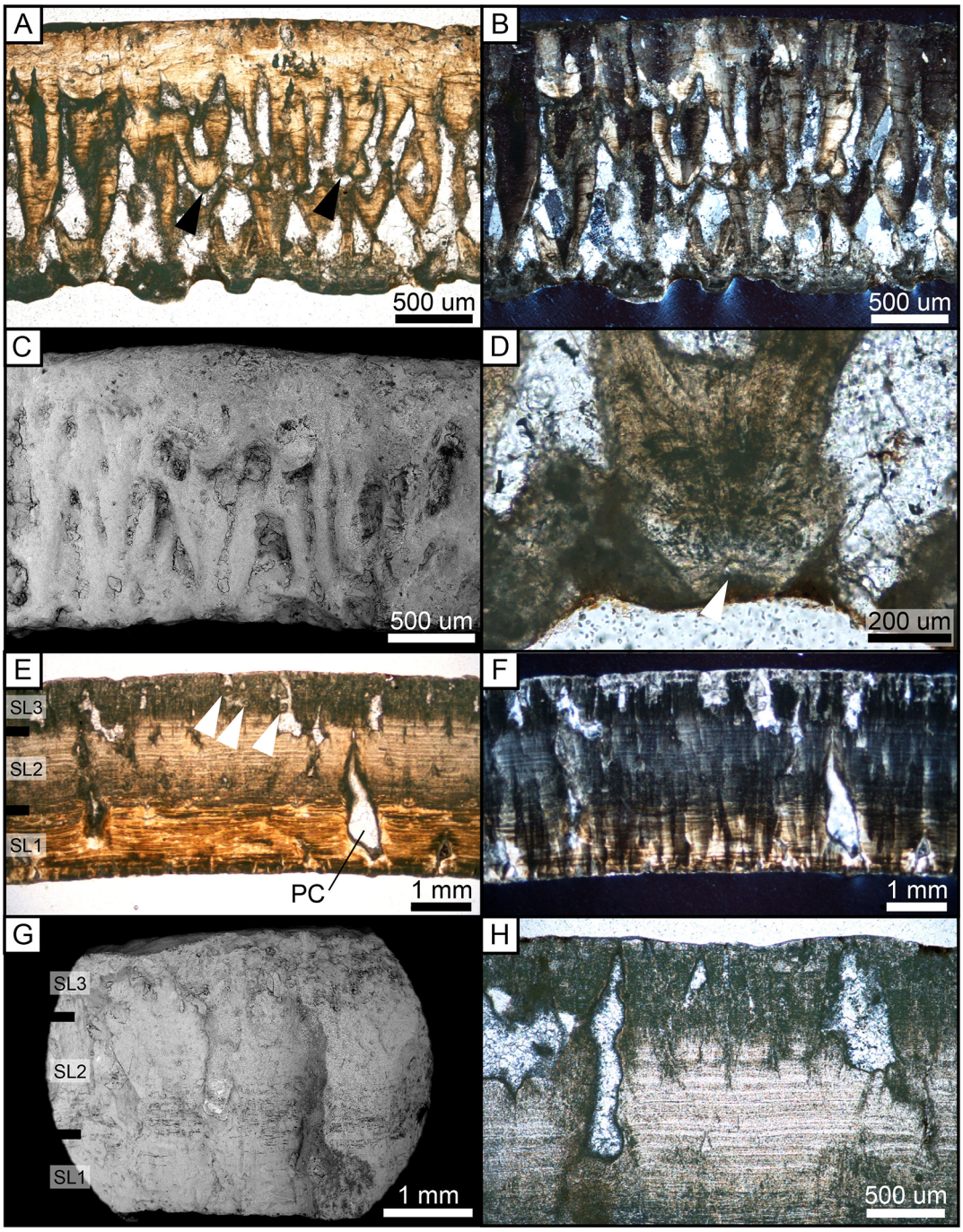

FIGURE 6. Photomicrographs of *Dendroolithus* oosp., MPC-D 100/1063 (A-D) and *Coralloidoolithus* oosp., MPC-D 100/1045 (E-H). **A**, radial thin section of eggshell under polarized light, showing shell units branching at mid-thickness of eggshell (black arrows); **B**, radial thin section of A under cross-polarized light, showing sweeping extinction pattern; **C**, radial view of eggshell under SEM, showing branched shell units; **D**, radial thin section of base of shell unit under polarized light, showing organic core (white arrow); **E**, radial thin section of eggshell under polarized light, showing three sublayers (SL1-3); **F**, radial thin section of E under cross-polarized light, showing narrow, columnar extinction pattern; **G**, radial view of eggshell under SEM, showing very porous layer in lower part of sublayer 2; **H**, radial thin section of upper part of eggshell under polarized light, showing narrow wedge-like structure with irregular aerial spaces.

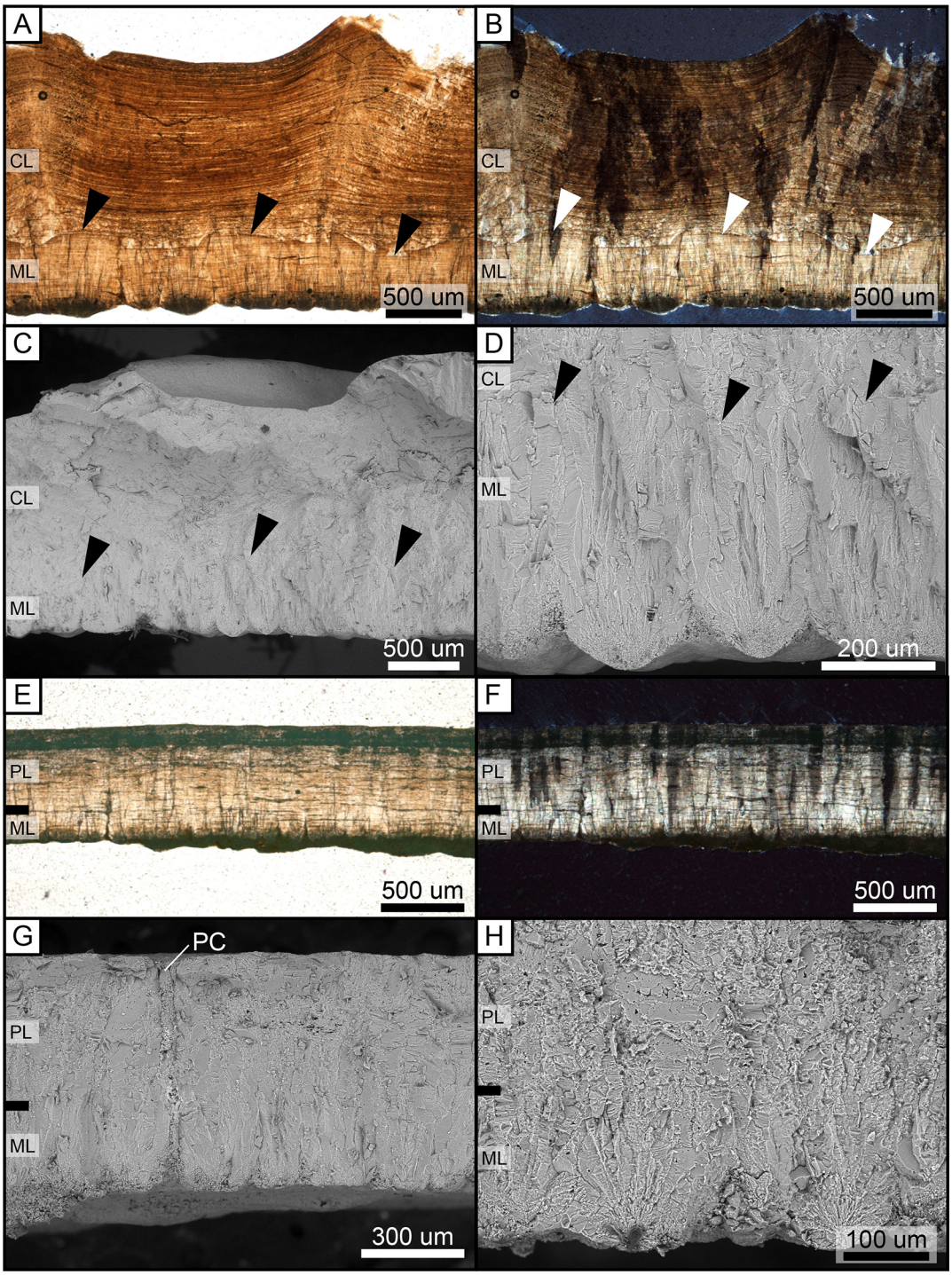

FIGURE 7. Photomicrographs of *Macroelongatoolithus* oosp., MPC-D 100/1064 (A-D) and *Protoceratopsidovum* cf. *Pro. minimum*, MPC-D 100/1062 (E-G) and MPC-D 100/1061 (H). **A**, radial thin section of eggshell under polarized light, showing two layers (ML and CL) delimited by undulating boundary (black arrows); **B**, radial thin section of A under cross-polarized light, showing undulating boundary between ML and CL (white arrows) and irregular extinction pattern; **C**, radial view of eggshell under SEM, showing two layers (ML and CL) delimited by undulating boundary (black arrows); **D**, radial view of ML under SEM, showing tall mammillae with overlying CL and CL boundary (black arrows); **E**, radial thin section of eggshell under polarized light, showing two layers (ML and PL) delimited by gradual boundary; **F**, radial thin section of E under cross-polarized light, showing prismatic extinction pattern; **G**, radial view of eggshell under SEM, showing straight, tubular pore canal (PC); **H**, radial view of ML, showing wedge-like crystals, and lower PL, showing squamatic structure, under SEM.

Remarks — As for the spheroolithid *Pa. irenensis*, MPC-D 100/1060 was likely laid by a hadrosaurid. Perinatal remains of the hadrosaurids *Maiasaura peeblesorum* (from Montana) and *Saurolophus angustirostris* (from Mongolia) have been discovered in association with *Spheroolithus* eggshell (Horner and Makela, 1979; Dewaele et al., 2015).

Oofamily DENDROOLITHIDAE Zhao and Li, 1988, emend. Zhao et al., 2015

Oogenus DENDROOLITHUS Zhao and Li, 1988, emend. Zhao et al., 2015

DENDROOLITHUS oosp.

(Figs. 3E, F and 6A-D)

Referred Specimens — Isolated eggshell fragments (MPC-D 100/1063: n = 7).

Locality, Horizon, and Age — Eggshell specimens were recovered from the Bayanshiree type locality (N44.16.426; E109.54.373), which is located approximately 70 km south-southwest of Sainshand in Dornogovi Aimag, Mongolia. The exposures are part of the Upper Cretaceous (Cenomanian to lower Santonian?) Bayanshiree Formation.

Description — Eggshell thickness ranges from 1.55 to 2.04 mm with a mean value of 1.73 mm (n = 7). The outer surface of the eggshell is rough or shagreen. The eggshell is porous and abundant circular pore openings form honeycomb-like structures on the outer surface in places (Fig. 3E, F). Fan-shaped shell units that comprise the eggshell are sub-symmetrical and bifurcate at the base with further branching in the upper part of the shell units (dendrospherulitic shell units: Fig. 6A-D). It appears that shell units occasionally originated around mid-thickness of the eggshell and overlie the primary (lower) shell units (Fig. 6A), although these structures are likely just truncated branches of the primary shell units rather than additional shell units. The primary shell units have a core (which is integral to a shell unit) at the base near the inner shell surface (Fig. 6D), whereas the structures that appear to emanate near mid-thickness lack evidence of a core. This structure is similar to the secondary origin of extra-spherulites that lack organic cores (Moreno-Azanza et al., 2016). In the upper one-fifth of the shell thickness, the shell units are fused together forming a dense layer (Fig. 6A, B). Under PLM, a sweeping extinction pattern and subhorizontal growth lines were visible in radial view (Fig. 6B), and pore canals are irregular and branching (prolatocanaliculate pore system).

Comparisons — The eggshells MPC-D 100/1063 are comparable to those of other dendroolithid eggs, including *Dendroolithus* and *Placoolithus*. These specimens are assignable to *Dendroolithus* due to the presence of symmetrical shell units that bifurcate near the base (Zhao et al., 2015); *Placoolithus* has symmetrical or asymmetrical shell units that usually bifurcate around mid-thickness of the eggshell (Zhang et al., 2018). Most oospecies of *Dendroolithus* are between 1.5 and 2.5 mm in eggshell thickness (i.e., *D. dendriticus*, *D. microporosus*, *D. wangdianensis*, and *D. xichuanensis*), and few fall outside of this range (only *D. verrucarius* of 2.6-3.3 mm eggshell: Mikhailov, 1994b). Due to morphological similarities (including eggshell thickness) among oospecies, we assign MPC-D 100/1063 to *Dendroolithus* oosp.

Remarks — Embryonic remains discovered inside putative dendroolithid eggs from China and Portugal indicate that Dendroolithidae was likely laid by megalosauroids and therizinosaurs (Manning et al., 1997; Kundrát et al., 2008; Araujo et al., 2013; Ribeiro et al., 2014; Kundrát and Cruickshank, 2021). Attribution of MPC-D 100/1063 to therizinosaurs is more likely because megalosauroids are not found in Upper Cretaceous deposits of Mongolia.

Oofamily STALICOOLITHIDAE Wang et al., 2012a

Oogenus CORALLOIDOOLITHUS Wang et al., 2012a

CORALLOIDOOLITHUS oosp.

(Figs. 3G and 6E-H)

Referred Specimens — A partial egg and isolated eggshell fragments (MPC-D 100/1045: n = 694).

Locality, Horizon, and Age — Egg and eggshell specimens were recovered from the Altan Uul I locality (N43.34.881; E100.38.156), located approximately 52 km northwest of Gurvantes in Ömnögovi Aimag, Mongolia. The exposures belong to the Upper Cretaceous (upper Campanian to lower Maastrichtian) Nemegt Formation.

Description — Based on the curvature, the partially preserved egg was originally spherical with a diameter of approximately 13 cm (Fig. 3G). Eggshell thickness ranges from 2.53 to 3.95 mm with a mean value of 3.24 mm (n = 257). The outer surface of the eggshell is rough or shagreen and lacks conspicuous ornamentation. The eggshell consists of narrow, interlocking fan-shaped shell units (possibly prolatospherulitic) that often contain irregular fissures (Fig.

6E-G). At least three sublayers are recognizable within the eggshell, which are delimited by gradational boundaries. The inner sublayer is about 1.10 mm thick and includes the lower half of the shell units. The base of the shell units (0.20 mm thick) consists of an accumulation of cone-shaped spherites with radiating crystals. Overlying the shell unit bases, radiating crystals are visible under SEM and well-developed subhorizontal growth lines are visible under PLM. The middle sublayer has a lower (0.60 mm thick) very porous interval consisting of fine subhorizontal laminations (Fig. 6G) that gradually transitions into a denser, upper interval (0.85 mm thick). The upper sublayer (0.75 mm thick) consists of narrow, wedge-like structures with numerous irregular voids (Fig. 6H). Small globular structures (i.e., the 'secondary shell units' of Wang et al., 2012a) are occasionally visible within these voids (Fig. 6E). Regardless of structural differences between sublayers, a narrow columnar extinction pattern is observed throughout the eggshell under PLM (Fig. 6F). Pore canals are irregular in shape, and the diameter changes through the eggshell thickness (possibly prolatocanaliculate pore system) (Fig. 6E).

Comparisons — The spherical egg shape, thick eggshell (≥2.4 mm), and presence of at least three eggshell sublayers indicate that MPC-D 100/1045 belongs to Stalicoolithidae, an oofamily that contains three oogenera (i.e., *Coralloidoolithus*, *Shixingoolithus*, and *Stalicoolithus*). MPC-D 100/1045 differs from these oogenera with respect to egg size and eggshell thickness (Table 2). The microstructure, however, is comparable to that of *Coralloidoolithus* in that globular structures occur within the upper sublayer (Wang et al., 2012a), so we assign MPC-D 100/1045 to *Coralloidoolithus* oosp.

Remarks — Stalicoolithid eggs are mainly known from Lower and Upper Cretaceous deposits of China. As suggested by Wang et al. (2012a), some eggshells from Mongolia assigned to Dendroolithidae by Mihailov (1991, 1994b) may actually belong to Stalicoolithidae because they have the characteristic eggshell sub-layers (see Plate 24.7 of Mikhailov, 1991; Figure 7.6D of Mikhailov et al., 1994). The producer of stalicoolithid eggs has yet to be identified.

Oofamily ELONGATOOLITHIDAE Zhao, 1975
Oogenus MACROELONGATOOLITHUS Li et al., 1995
emend. Simon et al., 2019
MACROELONGATOOLITHUS oosp.
(Figs. 3H and 7A-D)

Referred Specimens — Isolated eggshell fragments (MPC-D 100/1064: n = 114).

Locality, Horizon, and Age — Bayanshiree type locality (N44.16.277; E109.54.530), which is located approximately 70 km south-southwest of Sainshand in Dornogovi Aimag, Mongolia. The exposures belong to the Upper Cretaceous (Cenomanian to lower Santonian?) Bayanshiree Formation.

Description — The outer surface texture of the eggshell is highly variable; eggshells exhibiting prominent short ridges and nodes (linearituberculate, ramotuberculate and dispersituberculate ornamentation) are common (74% of 113 fragments), whereas those exhibiting coarse ridges (14%), fine reticulate ridges (0.9%) or a smooth surface (11%) are relatively uncommon (Fig. 3H). With the ornamentation height included, eggshell thickness ranges from 1.31 to 2.90 mm with a mean value of 1.90 mm (n = 112). Excluding the ornamentation height, eggshell thickness ranges from 1.22 to 2.39 mm with a mean value of 1.68 mm (n = 113). Two microstructural layers are visible in radial section, regardless of the outer surface texture: an inner mammillary layer (ML) and an outer continuous layer (CL), delimited by an abrupt undulatory boundary (Fig. 7A-C). The ML consists of cone-shaped mammillae and forms one-seventh to one-third of the eggshell thickness (Fig. 7D). Possible squamatic structures with small vesicles are present in the CL. Observations from PLM reveal a blocky to irregular extinction pattern and multiple fine growth lines that parallel the outer surface (Fig. 7B). Pore canals are straight and tubular (angusticanaliculate pore system).

Comparisons — Among elongatoolithids, both *Macroelongatoolithus* (1.11-3.23 mm) and *Macroolithus* (0.71-1.88 mm) have eggshells with a thickness of 1.6 mm (Tanaka et al., 2018). However, the relative thickness of the ML tends to be thinner in *Macroelongatoolithus* eggshell (ML : CL thickness ratio of 1 : 2-1 : 8: Simon et al., 2019) and thicker in *Macroolithus* eggshell (1 : 3: Zhao et al., 2015), indicating a *Macroelongatoolithus* affinity for MPC-D 100/1064.

Furthermore, *Macroelongatoolithus* eggs and eggshell fragments have been reported previously from the Bayanshiree locality (Iijima et al., 2011, 2012). The two eggs recovered are approximately 40 cm in length (Iijima et al., 2012), and significantly larger than other elongatoolithid ootaxa (Tanaka et al., 2018). MPC-D 100/1064 specimens are comparable to previously-described Bayanshiree *Macroelongatoolithus* eggshell, which has linearituberculate, ramotuberculate, and dispersituberculate ornamentation and a mean eggshell thickness of

2.04 mm (Iijima et al., 2011, 2012).

Remarks — *Macroelongatoolithus* eggs are known to have been laid by large species of caenagnathid oviraptorosaur, based on the discovery of several eggs associated with a perinatal skeleton from Henan Province, China (Pu et al., 2017). Fused dentaries belonging to a large species of unnamed caenagnathid are also known from the Tsagaan Teg locality of the Bayanshiree Formation (Tsuihiji et al., 2015), and could be the producer of *Macroelongatoolithus* eggs from the formation.

Oofamily PRISMATOOLITHIDAE Hirsch, 1994 emend. Moreno-Azanza et al., 2014b

Oogenus PROTOCERATOPSIDOVUM Mikhailov, 1994b

PROTOCERATOPSIDOVUM cf. *Pro. MINIMUM* Mikhailov, 1994b

(Figs. 3I and 7E-H)

Holotype — PIN 4228-1, four incomplete eggs of a partial clutch from Baga Triach, Mongolia (middle Campanian Djadokhta Formation).

Referred Specimens — Isolated eggshell fragments from the localities of Shine Us Khudag (MPC-D 100/1061: n = 24) and Bayanshiree (MPC-D 100/1062: n = 22).

Locality, Horizon, and Age — Eggshell specimens were recovered from the Bayanshiree type locality (N44.16.426; E109.54.373) and the Shine Us Khudag locality (N44.22.857; E109.18.720), which are located approximately 70 km south-southwest and 87 km southwest, respectively, of Sainshand in Dornogovi Aimag, Mongolia. Outcrops at these localities belong to the Upper Cretaceous (Cenomanian to lower Santonian?) Bayanshiree Formation.

Description — The outer surface of the eggshell is smooth with scattered circular pore openings (Fig. 3I). Eggshell thickness ranges between 0.34 and 0.68 mm (mean value of 0.54 mm) for the Shine Us Khudag specimens (MPC-D 100/1061: n = 24) and between 0.34 to 0.80 mm (mean value of 0.61 mm) for the Bayanshiree specimens (MPC-D 100/1062: n = 22). The eggshell is composed of interlocking columnar shell units and consists of two structural layers, an inner ML and an outer prismatic layer (PL), delimited by a gradual boundary (Fig. 7E-G). The ML, representing one-quarter to one-third of the eggshell thickness, is composed of wedge-like crystals radiating from a core, whereas the PL is composed of well-developed squamatic structure with tiny vesicles (Fig. 7H). The uppermost part of the PL is dark in color under PLM, but no microstructural differences were identified under SEM, indicating a lack of an external zone or layer in these specimens, PLM also reveals a narrow columnar extinction pattern within the shell units (Fig. 7F). Pore canals are narrow, tubular and straight (angusticanaliculate pore system) (Fig. 7G).

Comparisons — MPC-D 100/1061 and MPC-D 100/1062 have a smooth outer surface and relatively thin eggshell (around 0.5-0.6 mm in thickness), features that are comparable to four prismatoolithid oospecies, including: *Prismatoolithus hirschi*, *Pri. tenuis*, *Protoceratopsidovum sincerum* and *Pro. minimum*. Particular characteristics of our specimens differ from those in the following oospecies: *Pri. tenuis* has a relatively thinner ML (ML : PL = 1 : 6: Vianey-Liaud and Crochet, 1993), *Pri. hirschi* has narrower and taller mammillae (ML : PL = 1 : 2-1 : 2.5: Jackson and Varricchio, 2010), and *Pro. sincerum* has acicular mammillae and an abrupt boundary between the ML and PL (Choi et al., 2022). With respect to *Pro. minimum*, although Choi et al. (2022) indicate the ML to PL boundary seems abrupt, other features (e.g., wedge-like crystals of the mammillae) are comparable to MPC-D 100/1061 and MPC-D 100/1062; we thus tentatively assign these specimens to *Pro. minimum*.

Remarks — Although a troodontid affinity is known for the oospecies *Prismatoolithus levis* (Varricchio et al., 2002), the taxonomic affinities of other ootaxa within the Prismatoolithidae are uncertain. Troodontid skeletons are apparently associated with prismatoolithid eggs/eggshells from Mongolia (Grellet-Tinner, 2005; Pei et al., 2017), although the oogenera and oospecies of these remains are unknown. The taxonomic affinity of *Protoceratopsidovum* eggs is also uncertain as no associated perinatal remains have been discovered with this ootaxon. The name *Protoceratopsidovum*, meaning eggs of *Protoceratops*, is clearly a misnomer as *Protoceratops* eggs are soft-shelled (Norell et al., 2020) and *Protoceratopsidovum* eggs share many characteristics (e.g., elongate eggs, asymmetrical egg shape, two microstructural layers) with known maniraptoran (e.g., oviraptorosaurs and deinonychosaurs) eggs (e.g., Zelenitsky and Therrien, 2008; Varricchio and Barta, 2014; Choi et al., 2022). Based on the variation in characteristics among *Protoceratopsidovum* oospecies (Varricchio and Barta, 2014; Choi et al., 2022), it is possible that the known *Protoceratopsidovum* oospecies are attributable to different maniraptoran clades (e.g., oviraptorosaur, dromaeosaurid, and troodontid).

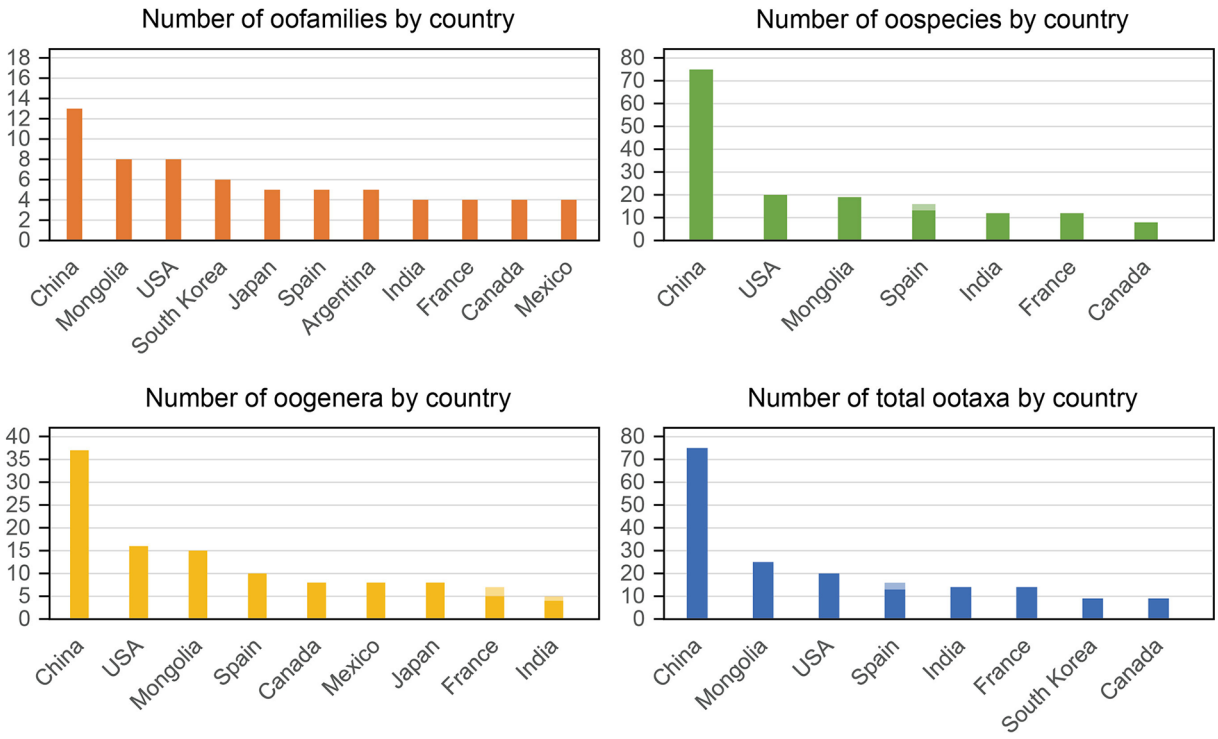

FIGURE 8. Numbers of non-avian dinosaur oofamilies, oogenera, and oospecies and the total numbers of non-avian dinosaur ootaxa recognized in various countries. Only egg specimens that were parataxonomically classified were included. See Appendix Table 3 for the dataset of this figure.

DISCUSSION

Fossil eggshells described in this study reveal new occurrences of ootaxa at several localities in the Gobi Desert, providing further insight into the diversity of non-avian dinosaur eggs from Mongolia. Six ootaxa, *Coralloidoolithus* oosp., *Dendroolithus* oosp., *Macroelongatoolithus* oosp., *Paraspheroolithus irenensis*, cf. *Protoceratopsidovum minimum,* and *Spheroolithus* cf. *S. maiasauroides*, were identified among eggshell specimens recovered at five localities, including Altan Uul I, Altan Uul IV, Bayanshiree, Shine Us Khudag and Shiluut Uul, during joint Mongolian expeditions with Korea (KID) and with Japan (Hokkaido University Museum expedition). Although eggs from these localities were described/reported previously (e.g., Mikhailov, 1994b; Mikhailov et al., 1994; Ariunchimeg, 2000; Iijima et al., 2011, 2012), the current study recognizes at least one new ootaxon from each locality, except at Bayanshiree. A compilation of locality and formation data for these and other ootaxa from Mongolia reveals the egg-bearing Upper Cretaceous formations, except for the Javkhlant Formation, have each yielded ten or more non-avian dinosaur ootaxa (Baruungoyot, Bayanshiree, Djadokhta, and Nemegt formations) (Fig. 1). Whereas each of these latter formations has produced several eggshell localities, only one eggshell locality is known from the Javkhlant Formation explaining the small number of ootaxa known from this formation. Lower Cretaceous deposits in Mongolia also have few localities and ootaxa compared to Upper Cretaceous deposits, a trend also found in strata of China (Wang et al., 2012b).

China and Mongolia are among the richest places with respect to abundance and diversity of dinosaur eggs (Fig. 8). Each country has produced more than twenty ootaxa attributable to non-avian dinosaurs. Abundant dinosaur eggs have been collected from individual basins in China (e.g., Laiyang or Jiaolai Basin of Shandong Province, Xixia Basin of Henan Province, Tiantai Basin of Zhejiang Province, and Heyuan and Nanxiong basins of Guangdong Province: Dong, 2005; Wang et al., 2012b), although skeletal remains of dinosaurs are usually uncommon in such egg-rich strata. Mongolia is unique in that it preserves both egg and skeletal remains in the same formations. The Upper Cretaceous Bayanshiree, Djadokhta, Baruungoyot, and Nemegt formations each have produced more than ten ootaxa (Fig. 1), as well as skeletons of more

than ten species of dinosaurs (e.g., Weishampel et al., 2004; Tanaka et al., 2021). For each formation, the taxonomic affinities of the ootaxa present are generally consistent with the known dinosaur taxa. For example, sauropods, therizinosaurs, and deinonychosaurs are known from the Bayanshiree Formation as are ootaxa attributed to these clades, including faveoloolithids, dendroolithids, and prismatoolithids, respectively. Finally, many significant discoveries of dinosaur eggs (several with closely associated skeletal remains) in Mongolia have shed light on nesting behaviors and other reproductive traits of particular dinosaurs.

ACKNOWLEDGMENTS

We would like to thank field crews of the joint Mongolian expeditions with Korea (KID) and with Japan (Hokkaido University Museum expedition), including Professor Louis L. Jacobs. We thank staff at MPC, Natsuko Takagi at the Nagoya University Museum, Chisako Sakata at the National Museum of Nature and Science in Tokyo, Daisuke Suzuki at Hokkaido Chitose College of Rehabilitation, and Kosuke Nakamura at Hokkaido University for their technical support. We also thank Daniel Barta and Seung Choi for their constructive reviews. Japan Society for the Promotion of Science [22K14133] to K.T. and Basic Science Research Program through the National Research Foundation of Korea (NRF), funded by the Ministry of Education (grant number 2022R1I1A2060919) to Y.-N.L. supported this research.

AUTHOR CONTRIBUTIONS

KT, FT, DKZ, YNL, KK, YK, GFF, TK. KT and DKZ designed the project, YNL, YK, and TK organized the fieldworks, KT, FT, DKZ, YNL, KK, and GFF collected specimens, TK prepared specimens, KT, YNL, KK, YK, and GFF gathered the data, KT conducted the analyses, KT, FT, and DKZ drafted the manuscript. All authors edited the manuscript.

LITERATURE CITED

Andrews, R. C. (1932). *The New Conquest of Central Asia*. New York, American Museum of Natural History.

Araujo, R., Castanhinha, R., Martins, R. M. S., Mateus, O., Hendrickx, C., Beckmann, F., Schell, N., & Alves, L. C. (2013). Filling the gaps of dinosaur eggshell phylogeny: Late Jurassic theropod clutch with embryos from Portugal. *Scientific Reports 3*, 1924. https://doi.org/10.1038/srep01924

Ariunchimeg, Y. (2000). Results of studies of dinosaur eggshells (in Abstract of Report Meeting of the Japan-Mongolia Joint Paleontological Expedition). *Hayashibara Museum of Natural Sciences Research Bulletin*, 1, 131–132.

Brown, B. & Schlaikjer, E. M. (1940). The structure and relationships of *Protoceratops*. *Transactions of the New York Academy of Sciences*, 2, 99–100.

Bureau of Geology and Mineral Resources of Jilin Province. (1992). *Paleontological Atlas of Jilin China*. Changchun, Jilin Science and Technology Press.

Carpenter, K. & Alf, K. (1994). Global distribution of dinosaur eggs, nests, and babies. In K. Carpenter, K. F. Hirsch, & J. R. Horner (Eds.), *Dinosaur Eggs and Babies* (pp. 15–30). Cambridge, Cambridge University Press.

Choi, C., Barta, D. E., Moreno-Azanza, M., Kim, N.-H., Shaw, C. A., & Varricchio, D. J. (2022). Microstructural description of the maniraptoran egg *Protoceratopsidovum*. *Papers in Palaeontology 8*, e1430. https://doi.org/10.1002/spp2.1430

Chow, M. M. (1951). Notes on the Late Cretaceous dinosaurian remains and the fossil eggs from Laiyang Shantung. *Bulletin of the Geological Society of China*, 31, 89,96.

Clark, J. M., Norell, M. A., & Chiappe, L. M. (1999). An oviraptorid skeleton from the Late Cretaceous of Ukhaa Tolgod, Mongolia, preserved in an avianlike brooding position over an oviraptorid nest. *American Museum Novitates*, 3265, 1–35.

Dewaele, L., Tsogtbaatar, K., Barsbold, R., Garcia, G., Stein, K., Escuillie, F., & Godefroit, P. (2015). Perinatal specimens of *Saurolophus angustirostris* (Dinosauria: Hadrosauridae), from the Upper Cretaceous of Mongolia. *PLoS One*, 10, e0138806. https://doi.org/10.1371/journal.pone.0138806

Dong, H. (2005). Brief introduction to vertebrate fossils from the Heyuan Basin, Guangdong Province. In J. Lü, Y. Kobayashi, D. Huang, & Y.-N. Lee (Eds.), *Papers from the 2005 Heyuan International Dinosaur Symposium* (pp. 1–9). Beijing, Geological Publishing House.

Erickson, G. M., Rogers, C. K., Varricchio, D. J., Norell, M. A., & Xu, X. (2007). Growth patterns in brooding dinosaurs reveals the timing of sexual maturity in non-avian dinosaurs and genesis of the avian condition. *Biology Letters*, 3(5), 558–561. https://doi.org/10.1098/rsbl.2007.0254

Erickson, G. M., Zelenitsky, D. K., Kay, I., & Norell, M. A. (2017). Dinosaur incubation periods directly determined from growth-line counts in embryonic teeth show reptilian-grade development. *Proceedings of the National Academy of Sciences*, 114, 540–545. https://doi.org/10.1073/pnas.1613716114

Fanti, F., Currie, P. J., & Badamgarav, D. (2012). New specimens of *Nemegtomaia* from the Baruungoyot and Nemegt formations (Late Cretaceous) of Mongolia. *PLoS One*, 7, e31330. https://doi.org/10.1371/journal.pone.0031330

Funston, G. F., Currie, P. J., Eberth, D. A., Ryan, M. J., Chinzorig, T., Badamgarav, D., & Longrich, N. R. (2016). The first oviraptorosaur (Dinosauria: Theropoda) bonebed: evidence of gregarious behaviour in a maniraptoran theropod. *Scientific Reports*, 6, 35782. https://doi.org/10.1038/srep35782

Graf, J., Tabor, N. J., Ferguson, K., Winkler, D. A., Lee, Y. N., May, S., & Jacobs, L. L. (2018). Diagenesis of dinosaur eggshell from the Gobi Desert, Mongolia. *Palaeogeography, Palaeoclimatology,*

Palaeoecology, 494, 65–74. https://doi.org/10.1016/j.palaeo.2017.11.011

Grellet-Tinner, G. (2005). *A phylogenetic analysis of oological characters: a case study of saurischian dinosaur relationships and avian evolution*. [Unpublished Ph.D. Thesis]. University of Southern California.

Grellet-Tinner, G., Chiappe, L., Norell, M., & Bottjer, D. (2006). Dinosaur eggs and nesting behaviors: a paleobiological investigation. *Palaeogeography, Palaeoclimatology, Palaeoecology*, 232, 294–321. https://doi.org/10.1016/j.palaeo.2005.10.029

Grellet-Tinner, G., Sim, C. M., Kim, D. H., Trimby, P., Higa, A., An, S. L., Oh, H. S., Kim, T., & Kardjilov, N. (2011). Description of the first lithostrotian titanosaur embryo in ovo with neutron characterization and implications for lithostrotian Aptian migration and dispersion. *Gondwana Research*, 20, 621–629. https://doi.org/10.1016/j.gr.2011.02.007

Hirsch, K. F. (1994). Upper Jurassic eggshells from the Western Interior of North America. In K. Carpenter, K. F. Hirsch, J. R. Horner (Eds.), *Dinosaur eggs and babies* (pp. 137–150). Cambridge, Cambridge University Press.

Hirsch, K. F. & Quinn, B. (1990). Eggs and eggshell fragments from the Upper Cretaceous Two Medicine Formation of Montana. *Journal of Vertebrate Paleontology*, 10, 491–511. http://doi.org/10.1080/02724634.1990.10011832

Horner, J. R. (1999). Egg clutches and embryos of two hadrosaurian dinosaurs. *Journal of Vertebrate Paleontology*, 19, 607–611. https//doi.org/10.1080/02724634.1999.10011174

Horner, J. R. & Makela, R. (1979). Nest of juveniles provides evidence of family structure among dinosaurs. *Nature*, 282, 296–298. https//doi.org/10.1038/282296a0

Iijima, M., Sato, T., Watabe, M., Tsogtbaatar, K., & Ariunchimeg, Y. (2011). Bone bed of baby oviraptorosaur and hadrosauroid dinosaurs from the Bayanshiree Formation (Late Cretaceous) in southern Mongolia. *Journal of Vertebrate Paleontology*, 32(Supplement 2), 130.

Iijima, M., Tamura, S., Suwa, S., Sato, T., Watabe, M., Tsogtbaatar, K., & Ariunchimeg, Y. (2012). Dinosaur bones (Caenagnathoidea indet., Hadrosauroidea indet.) and eggs (*Macroelongatoolithus* sp.) from Bayanshiree Formation (Late Cretaceous), southeastern Mongolia. *Abstracts with Programs of the 161st Regular Meeting of the Palaeontological Society of Japan*, 52.

Ishigaki, S., Tsogtbaatar, K., Saneyoshi, M., Mainbayar, B., Aoki, K., Ulziitseren, S., Imayama, T., Takahashi, A., Toyoda, S., Bayardorj, C., Buyantegsh, B., Batsukh, J., Purevsuren, B., Asai, H., Tsutanaga, S., & Fujii, K. (2016). Report of the Okayama University of Science-Mongolian Institute of Paleontology and Geology Joint Expedition in 2016. *The Bulletin of Research Institute of Natural Sciences, Okayama University of Science*, 42, 33–46.

Jackson, F. D. & Varricchio, D. J. (2010). Fossil eggs and eggshell from the lowermost Two Medicine Formation of western Montana, Sevenmile Hill locality. *Journal of Vertebrate Paleontology*, 30, 1142–1156.

Kundrát, M. & Cruickshank, A. R. (2022). New information on multispherulitic dinosaur eggs: Faveoloolithidae and Dendroolithidae. *Historical Biology*, 34(6), 1072–1084. https://doi.org/10.1080/08912963.2021.1961764

Kundrát, M., Cruickshank, A. R. I., Manning, T. W., & Nudds, J. (2008). Embryos of therizinosauroid theropods from the Upper Cretaceous of China: diagnosis and analysis of ossification patterns. *Acta Zoologica*, 89, 231–251. https://doi.org/10.1111/j.1463-6395.2007.00311.x

Kurzanov, S. M. & Mikhailov, K. E. (1989). Dinosaur eggshells from the Lower Cretaceous of Mongolia. In D. D. Gillette, & M. G. Lockley (Eds.), *Dinosaur Tracks and Traces* (pp. 109–113). New York, Cambridge University Press.

Lee, H., Lee, Y.-N., Kobayashi, Y., & Tsogtbaatar, K. (2017). A preliminary report of unusual dinosaur nesting ground, eastern Gobi, Mongolia. *Society of Vertebrate Paleontology 77th Annual Meeting Program and Abstracts,* 149.

Li, Y., Yin, Z., & Liu, Y. (1995). The discovery of a new genus of dinosaur egg from Xixia, Henan, China. *Journal of Wuhan Institute of Chemical Technology*, 17, 38–40.

Liu, J. Y., Wang, Q., Zhao, Z., Wang, X. L., Gao, C. L., & Shen, C. Z. (2013). A parataxonomic revision of spheroolithid eggs from the Upper Cretaceous Quantou Formation in Changtu, Liaoning. *Vertebrata PalAsiatica*, 51, 278–288.

Manning, T. W., Joysey, K. A., & Cruickshank, A. R. I. (1997). Observations of microstructures within dinosaur eggs from Henan Province, Peoples' Republic of China. In D. L. Wolberg, E. Stump, & R. D. Rosenberg (Eds.), *Dinofest International: Proceedings of a Symposium Held at Arizona State University* (pp. 287–290). Philadelphia, Academy of Natural Sciences.

Mikhailov, K. E. (1991). Classification of fossil eggshells of amniotic vertebrates. *Acta Palaeontologica Polonica*, 36, 193-238.

Mikhailov, K. (1994a). Theropod and protoceratopsian dinosaur eggs from the Cretaceous of Mongolia and Kazakhstan. *Paleontological Journal*, 28, 101-120.

Mikhailov, K. E. (1994b). Eggs of sauropod and ornithopod dinosaurs from the Cretaceous deposits of Mongolia. *Paleontological Journal*, 28, 141-159.

Mikhailov, K. E. (1997). Fossil and recent eggshell in amniotic vertebrates: fine structure, comparative morphology and classification. *Special Papers in Palaeontology*, 56, 1-80.

Mikhailov, K. E. (2000). Eggs and eggshells of dinosaurs and birds from the Cretaceous of Mongolia. In M. J. Benton, M. A. Shishkin, D. M. Unwin, & E. N. Kurochkin (Eds.), *The Age of Dinosaurs in Russia and Mongolia* (pp. 560–572). Cambridge: Cambridge University Press.

Mikhailov, K. E. (2014). Eggshell structure, parataxonomy and phylogenetic analysis: some notes on articles published from 2002 to 2011. *Historical Biology*, 26, 144–154. http://dx.doi.org/10.1080/08912963.2013.829824

Mikhailov, K. E., Sabath, K., & Kurzanov, S. (1994). Eggs and nests from the Cretaceous of Mongolia. In K. Carpenter, K. F. Hirsch, & J. R. Horner (Eds.), *Dinosaur Eggs and Babies* (pp. 88–115). Cambridge, Cambridge University Press.

Moreno-Azanza, M., Canudo, J. I., & Gasca, J. M. (2014a). Spheroolithid eggshells in the Lower Cretaceous of Europe. Implications for eggshell evolution in ornithischian dinosaurs. *Cretaceous Research*, 51, 75–87. https://doi.org/10.1016/j.cretres. 2014.05.017

Moreno-Azanza, M., Canudo, J. I., & Gasca, J. M. (2014b). Unusual Theropod Eggshells from the Early Cretaceous Blesa Formation of the Iberian Range, Spain. *Acta Palaeontologica Polonica*, 59, 843–854. http://www.bioone.org/doi/full/10.4202/app.2012.0069

Moreno-Azanza, M., Bauluz, B., Canudo, J. I., Gasca, J. M., & Fernández-Baldor, F. T. (2016). Combined use of electron and light microscopy techniques reveals false secondary shell units in Megaloolithidae eggshells. *PLoS ONE*, 11(5), e0153026. https://doi.org/10.1371/journal.pone.0153026

Noda, M. & Hayashi, S. (2021). Classification of fossil dinosaur eggshells from the Upper Cretaceous Bayanshiree Formation, Gobi Desert of Mongolia. *The Bulletin of Institute of Paleontology and Geochronology, Okayama University of Science*, 1, 42–43. [in Japanese]

Norell, M. A., Balanoff, A. M., Barta, D. E., & Gregory, M. E. (2018). A second specimen of *Citipati osmolskae* associated with a nest of eggs from Ukhaa Tolgod, Omnogov Aimag, Mongolia. *American Museum Novitates*, 3899, 1–44. http://orcid.org/0000-0002-2453-0220

Norell, M., Clark, J. M., & Chiappe, L. M. (2001). An embryonic oviraptorid (Dinosauria: Theropoda) from the Upper Cretaceous of Mongolia. *American Museum Novitates*, 3315, 1–17. https://doi.org/10.1206/0003-0082(2001)315<0001:AEODTF>2.0.CO;2

Norell, M. A., Clark, J. M., Chiappe, L. M., & Demberelyin, D. (1995). A nesting dinosaur. *Nature*, 378, 774–776. https://doi.org/10.1038/378774a0

Norell, M. A., Clark, J. M., Demberelyin, D., Rhinchen, B., Chiappe, L. M., Davidson, A. R., Mckenna, M. C., Altangerel, P., & Novacek, M. J. (1994). A theropod dinosaur embryo and the affinities of the Flaming Cliffs dinosaur eggs. *Science*, 266, 779–782.

Norell, M. A., Wiemann, J., Fabbri, M., Yu, C., Marsicano, C. A., Moore-Nall, A., Varricchio, D.J., Pol, D., & Zelenitsky, D. K. (2020). The first dinosaur egg was soft. *Nature*, 583, 406–410. https://doi.org/10.1038/s41586-020-2412-8

Pei, R., Norell, M. A., Barta, D. E., Bever, G. S., Pittman, M., & Xu, X. (2017). Osteology of a new Late Cretaceous troodontid specimen from Ukhaa Tolgod, Ömnögovi Aimag, Mongolia. *American Museum Novitates*, 3889, 1–47. https://doi.org/10.1206/3889.1

Pu, H., Zelenitsky, D. K., Lü, J., Currie, P. J., Carpenter, K., Xu, L., Koppelhus, E. B., Jia, S., Xiao, L., Chuang, H., Li, T., Kundrát, M., & Shen, C. (2017). Perinate and eggs of a giant caenagnathid dinosaur from the Late Cretaceous of central China. *Nature Communications*, 8, 14952. https://doi.org/10.1038/ncomms14952

Ribeiro, V., Mateus, O., Holwerda, F., Araújo, R., & Castanhinha, R. (2014). Two new theropod egg sites from the Late Jurassic Lourinhã Formation, Portugal. *Historical Biology*, 26(2), 206–217. https://doi.org/10.1080/08912963.2013.807254.

Sabath, K. (1991). Upper Cretaceous amniotic eggs from the Gobi Desert. *Acta Palaeontologica Polonica*, 36, 151–192.

Saneyoshi, M., Watabe, M., Tsubamoto, T., Tsogtbaatar, K., Chinzorig, T., & Suzuki, S. (2010). Report of the HMNS-MPC Joint Paleontological Expedition in 2007. *Hayashibara Museum of Natural Sciences Research Bulletin*, 3, 19–28.

Sellés, A. G., Via B., & Galobart, À. (2014). *Spheroolithus europaeus*, oosp. nov. (late Maastrichtian, Catalonia), the youngest oological record of hadrosauroids in Eurasia. *Journal of Vertebrate Paleontology*, 34, 725–729. http://dx.doi.org/10.1080/02724634.2013.819360

Shen, C.-Z., Tanaka, K., Zelenitsky, D. K., Gao, C.-L., Zhang, F.-J., & Lü, J. (2023). A probable ornithopod egg from a historic collection of dinosaur eggs recovered from the Upper Cretaceous of Liaoning Province, China. *Historical Biology.* https://doi.org/10.1080/08912963.2023.2201929

Simon, D. J., Varricchio, D. J., Jin, X., & Robison, S. F. (2019). Microstructural overlap of *Macroelongatoolithus* eggs from Asia and North America expands the occurrence of colossal oviraptorosaurs. *Journal of Vertebrate Paleontology*, 38, e1553046. https://doi.org/10.1080/02724634.2018.1553046

Sochava, A. V. (1969). Dinosaur eggs from the Upper Cretaceous of the Gobi Desert. *Paleontological Journal*, 4, 517–527.

Sochava, A. V. (1972). The skeleton of an embryo in a dinosaur egg. *Paleontological Journal*, 4, 527–531.

Suzuki, S. & Narmandakh, P. (2004). Change of the Cretaceous Turtle faunas in Mongolia. *Hayashibara Museum of Natural Sciences Research Bulletin*, 2, 7–14.

Suzuki, S. & Watabe, M. (2000a). Report on the Preliminary Joint Field Excursion to the Gobi desert, 1992. *Hayashibara Museum of Natural Sciences Research Bulletin*, 1, 13–16.

Suzuki, S. & Watabe, M. (2000c). Report on the Japan-Mongolia Joint Paleontological Expedition to the Gobi desert, 1995. *Hayashibara Museum of Natural Sciences Research Bulletin*, 1, 45–57.

Suzuki, S. & Watabe, M. (2000b). Report on the Japan-Mongolia Joint Paleontological Expedition to the Gobi desert, 1998. *Hayashibara Museum of Natural Sciences Research Bulletin*, 1, 83–98.

Suzuki, S., Watabe, M., & Tsogtbaatar, K. (2010). Report of the HMNS-MPC Joint Paleontological Expedition in 2004. *Hayashibara Museum of Natural Sciences Research Bulletin*, 3, 1–9.

Tanaka, K., Anvarov, O. U. O., Zelenitsky, D. K., Ahmedshaev, A. S., & Kobayashi, Y. (2021). A new carcharodontosaurian theropod dinosaur occupies apex predator niche in the early Late Cretaceous of Uzbekistan. *Royal Society Open Science*, 8, 210923. https://doi.org/10.1098/rsos.210923

Tanaka, K., Zelenitsky, D. K., Therrien, F., Ikeda, T., Kubota, K., Saegusa, H., Tanaka, T., & Ikuno, K. (2020). Exceptionally small theropod eggs from the Lower Cretaceous Ohyamashimo Formation of Tamba, Hyogo Prefecture, Japan. *Cretaceous Research*, 114, 104519. https://doi.org/10.1016/j.cretres.2020.104519

Tanaka, K., Kobayashi, Y., Zelenitsky, D. K., Therrien, F., Lee, Y. N., Barsbold, R., Kubota, K., Lee, H.-J., Chinzorig, T., & Idersaikhan, D. (2019). Exceptional preservation of a Late Cretaceous dinosaur nesting site from Mongolia reveals colonial nesting behavior in a non-avian theropod. *Geology*, 47, 843–847. https://doi.org/10.1130/G46328.1

Tanaka, K., Zelenitsky, D. K., Lü, J., DeBuhr, C. L., Yi, L., Jia, S., Ding, F., Xia, M., Liu, D., Shen, C., & Chen, R. (2018). Incubation behaviours of oviraptorosaur dinosaurs in relation to body size. *Biology Letters*, 14, 20180135. https://doi.org/10.1098/rsbl.2018. 0135

Tanaka, K., Zelenitsky, D. K., & Therrien, F. (2015). Eggshell porosity provides insight on evolution of nesting in dinosaurs. *PLoS One*, 10, e0142829. https://doi.org/10.1371/journal.pone.0142829

Tsogtbaatar, K., Weishampel, D. B., Evans, D. C., & Watabe, M. (2019). A new hadrosauroid (Dinosauria: Ornithopoda) from the Late Cretaceous Baynshire Formation of the Gobi Desert (Mongolia). *PLoS ONE*, 14, e0208480. https://doi.org/10.1371/journal.pone.0208480

Tsuihiji, T., Watabe, M., Barsbold, R., & Tsogtbaatar, K. (2015). A gigantic caenagnathid oviraptorosaurian (Dinosauria: Theropoda) from the Upper Cretaceous of the Gobi Desert, Mongolia. *Cretaceous Research*, 56, 60–65. https://doi.org/10.1016/j.cretres. 2015.03.007

van Straelen, V. (1925). The microstructure of the dinosaurian egg-shells from the Cretaceous beds of Mongolia. *American Museum Novitates*, 173, 1–4.

Varricchio, D. J. & Barta, D. E. (2014). Revisiting Sabath's "larger avian eggs" from the Gobi Cretaceous. *Acta Palaeontologica Polonica*, 60(1), 11–25. https://doi.org/10.4202/app.00085.2014

Varricchio, D. J., Horner, J. R., & Jackson. F. D. (2002). Embryos and eggs for the Cretaceous theropod dinosaur *Troodon formosus*. *Journal of Vertebrate Paleontology*, 22, 564–576.

Vianey-Liaud, M. & Crochet, J. (1993). Dinosaur eggshells from the late

Cretaceous of Languedoc (southern France). *Revue de Paleobiologie*, 7, 237–249.

Wang, Q., Wang, X., Zhao, Z., & Jiang, Y. (2012a). A new oofamily of dinosaur egg from the Upper Cretaceous of Tiantai Basin, Zhejiang Province, and its mechanism of eggshell formation. *Chinese Science Bulletin*, 57, 3740–3747. https://doi.org/10.1007/s11434-012-5353-2

Wang, X., Wang, Q., Jiang, S., Cheng, X., Zhang, J., Zhao, Z., & Jiang, Y. (2012b). Dinosaur egg faunas of the Upper Cretaceous terrestrial red beds of China and their stratigraphical significance. *Journal of Stratigraphy*, 36(2), 400–416. https://doi.org/10.19839/j.cnki.dcxzz.2012.02.017

Watabe, M. (2004). New dinosaur ovifauna from the Upper Cretaceous vertebrate fossil locality, Abdrant Nuru, Central part of the Gobi desert, Mongolia. *Hayashibara Museum of Natural Sciences Research Bulletin*, 2, 15–27.

Watabe, M. & Suzuki, S. (2000a). Report on the Japan-Mongolia Joint Paleontological Expedition to the Gobi desert, 1993. *Hayashibara Museum of Natural Sciences Research Bulletin*, 1, 17–29.

Watabe, M. & Suzuki, S. (2000b). Report on the Japan-Mongolia Joint Paleontological Expedition to the Gobi desert, 1994. *Hayashibara Museum of Natural Sciences Research Bulletin*, 1, 30–44.

Watabe, M. & Suzuki, S. (2000c). Report on the Japan-Mongolia Joint Paleontological Expedition to the Gobi desert, 1996. *Hayashibara Museum of Natural Sciences Research Bulletin*, 1, 58–68.

Watabe, M. & Suzuki, S. (2000d). *Hayashibara Museum of Natural Sciences Research Bulletin*, 1, 69–82.

Watabe, M., Suzuki, S., Tsogtbaatar, K., Tsubamoto, T., & Saneyoshi, M. (2010b). Report of the HMNS-MPC Joint Paleontological Expedition in 2006. *Hayashibara Museum of Natural Sciences Research Bulletin*, 3, 11–18.

Watabe, M. & Tsogtbaatar, K. (2004). Report on the Japan-Mongolia Joint Paleontological Expedition to the Gobi desert, 2000. *Hayashibara Museum of Natural Sciences Research Bulletin*, 2, 45–67.

Watabe, M., Tsogtbaatar, K., & Japan-Mongolia Joint Paleontological Expedition crew. (1998). First reports of fossil dinosaur eggs and nests from Bayanshiree (Upper Cretaceous Bayanshiree Formation), eastern Gobi desert, Mongolia. *Abstracts with Programs of the 1998 Annual Meeting of the Palaeontological Society of Japan*, 51. [in Japanese]

Watabe, M., Tsogtbaatar, K., Suzuki, S., & Saneyoshi, M. (2010a). Geology of dinosaur-fossil-bearing localities (Jurassic and Cretaceous: Mesozoic) in the Gobi Desert: results of the HMNS-MPC Joint Paleontological Expedition. *Hayashibara Museum of Natural Sciences Research Bulletin*, 3, 41–118.

Watabe, M., Tsogtbaatar, K., Uranbileg, L., & Gereltsetseg, L. (2004). Report on the Japan-Mongolia Joint Paleontological Expedition to the Gobi desert, 2001. *Hayashibara Museum of Natural Sciences Research Bulletin*, 2, 69–96.

Weishampel, D. B., Barrett, P. M., Coria, R. A., Loeuff, J., Xu, X., Xijin, Z., Sahni, A., Gomani, E. M. P., & Noto, C. R. (2004). Dinosaur distribution. In D. B. Weishampel, P. Dodson, & H. Osmólska (Eds.), *Dinosauria, 2nd Ed.* (pp. 517–606). Barkeley and Los Angeles, University of California Press.

Weishampel, D. B., Fastovsky, D. E., Watabe, M., Varricchio, D., Jackson, F., Tsogtbaatar, K., & Barsbold, R. (2008). New oviraptorid embryos from Bugin-Tsav, Nemegt Formation (Upper Cretaceous), Mongolia, with insights into their habitat and growth. *Journal of Vertebrate Paleontology*, 28(4), 1110–1119. https://doi.org/10. 1671/0272-4634-28.4.1110

Wiemann, J., Yang, T. R., & Norell, M. A. (2018). Dinosaur egg colour had a single evolutionary origin. *Nature*, 563(7732), 555–558. https://doi.org/10.1038/s41586-018-0646-5

Xing, L., Niu, K., Yang, T., Wang, D., Miyashita, T., & Mallon, J. (2022). Hadrosauroid eggs and embryos from the Upper Cretaceous (Maastrichtian) of Jiangxi Province, China. *BMC Ecology and Evolution*, 22, 60. https:// 10.1186/s12862-022-02012-x

Xue, X., Zhang, Y., Bi, Y., Yue, L., & Chen, D. (1996). *The Development and Environmental Changes of the Intermontane Basins in the Eastern Part of Qinling Mountains*. Beijing, Geological Publishing House.

Young, C. C. (1954). Fossil reptilian eggs from Laiyang, Shantung, China. *Acta Palaeontologica Sinica*, 34, 371–388.

Young, C. C. (1965). Fossil eggs from Nanhsiung, Kwangtung and Kanchou, Kiangsi. *Vertebrata PalAsiatica*, 9, 141–170.

Zelenitsky, D. K. & Hills, L. V. (1997). Normal and pathological eggshells of *Spheroolithus albertensis*, oosp. nov., from the Oldman Formation (Judith River Group, late Campanian), southern Alberta. *Journal of Vertebrate Paleontology*, 17, 167–171.

Zelenitsky, D. K. & Therrien, F. (2008). Phylogenetic analysis of reproductive traits of maniraptoran theropods and its implications for egg parataxonomy. *Palaeontology*, 51(4), 807–816. https://doi.org/10.1111/j.1475-4983.2008.00770.x

Zhang, S.-K. (2010). A parataxonomic revision of the Cretaceous faveoloolithid eggs of China. *Vertebrata PalAsiatica*, 48, 203–219.

Zelenitsky, D. K. (2000). Dinosaur eggs from Asia and North America. *Paleontological Society of Korea Special Publication*, 4, 13–26.

Zhang, S., Yang, T.-R., Li, Z., & Hu, Y. (2018). New dinosaur egg material from Yunxian, Hubei Province, China resolves the classification of dendroolithid eggs. *Acta Palaeontologica Polonica*, 63(4), 671–678. https://doi.org/10.4202/app.00523.2018

Zhao, Z. K. (1975). Microstructures of dinosaurian eggshells of Nanxiong, Guangdong, and the problem in egg classification. *Vertebrata PalAsiatica*, 13, 105–117.

Zhao, Z. (1979). Progress in the research of dinosaur eggs. In Institute of Vertbrate Paleontology, Paleoanthoropology and Nanjing Institute of Paleontology (Eds.), *Mesozoic and Cenozoic Red Beds of South China Selected Papers from the "Cretaceous-Tertiary Workshop, Nanxiong, Guangdong Province"* (pp. 330–340). Beijing, Science Press.

Zhao, Z. & Jiang, Y. (1974). Microscopic studies on the dinosaurian eggshells from Laiyang, Shantung Province. *Scientica Sinica*, 17, 73–83.

Zhao, Z. & Li, R. (1988). A new structural type of the dinosaur eggs from Anlu Country, Hubei Province. *Vertebrata PalAsiatica*, 26, 107–115.

Zhao, Z., Wang, Q., & Zhang, S. (2015). *Dinosaur Eggs. Paleovertebrata Sinica II Fascicle 7 (Serial no. 11)*. Beijing, Science Press.

Zhao, Z., Ye, J., Li, H., Zhao, Z., & Yan, Z. (1991). Extinction of the dinosaurs across the Cretaceous-Tertiary boundary in Nanxiong Basin, Guangdong Province. *Vertebrata PalAsiatica*, 29, 1–20.

Zhu, X., Wang, Q., & Wang, X. (2022). Restudy of the original and new materials of *Stromatoolithus pinglingensis* and discussion on some Spheroolithidae eggs. *Historical Biology*, 34(2), 283–297. https://doi.org/10.1080/08912963.2021.1910817

APPENDIX TABLE 1. List of non-avian dinosaur egg localities in Mongolia. **Ovaloolithus chinkangkouensis* has been divided into three oospecies: *O. mixtistriatus*, *O. monostriatus*, and *O. tristriatus* by Zhao (1979a). †Choi et al. (2022) indicate that *Protoceratopsidovum fluxuosum* and *Pro. sincerum* are maniraptoran eggs and could belong to Elongatoolithidae and Montanoolithidae, respectively. ‡Zhang (2010) suggested that some eggs of *Faveoloolithus ningxiaensis* from Algui Ulan Tsav are actually *Parafaveoloolithus* oosp. Abbreviations of 'Fm.' column: BG, Baruungoyot Formation; BS, Bayanshiree Formation; Dj, Djadokhta Formation; Du, Dushi Uul (/Doshuul/ Dushihin/ Duhih Ula) Formation; J, Javkhlant Formation; KD, Khuren Dukh Formation; N, Nemegt Formation; UN, Ulaanoosh Formation (formerly known as Barunbayan Formation)

Locality	Fm.	Dendroolithidae	Elongatoolithidae	Ovaloolithidae	Prismatoolithidae	Spheroolithidae	Other ootaxa/eggs
Abdrant Nuru[1-4]	Dj	Dendroolithidae indet.	*Elongatoolithus* oosp.			Spheroolithidae indet.	
Altan Uul area[5-15]	N	Dendroolithidae indet.	Elongatoolithidae indet.	*Ovaloolithus dinornithoides*	*Protoceratopsidovum minimum*	*Spheroolithus* cf. *S. maiasauroides*; *Spheroolithus* oosp. with perinatal *Saurolophus angustirostris*	*Coralloidoolithus* oosp.
Baga Tariach[6-8,12,16]	Dj				*Protoceratopsidovum minimum*	*Spheroolithus maiasauroides*	
Bagamod Khuduk[6]	BG						Dinosaur egg indet. (?*Protoceratopsidovum minimum*)
Bambu Khudu[6]	BG						Dinosaur egg indet.
Bayan Dzak (Bayan Zag)[5-8,12,16-21]	Dj		*Elongatoolithus frustrabilis*; ootaxonomically unassigned clutch associated with a skeleton of *Oviraptor philoceratops*		*Protoceratopsidovum fluxuosum*†; *Protoceratopsidovum sincerum*†	*Spheroolithus maiasauroides*	*Faveoloolithus ningxiaensis*‡
Bayanshiree[2,6,9,12,15,22-25]	BS	*Dendroolithus* oosp. (and/or Dictyoolithidae indet.)	*Macroelongatoolithus* oosp.; *Macroolithus mutabilis*		cf. *Protoceratopsidovum minimum*		Faveoloolithidae indet.
Baynshin Tsav area[6,9,12,23]	BS	*Dendroolithus microporosus*	Elongatoolithidae indet.				
Bortolgoi[12,21]	Dj		Elongatoolithidae indet.			Spheroolithidae indet.	
Bugiin Tsav[1,9-12,20,26]	N	*Dendroolithus verrucarius*	*Elongatoolithus sigillarius*; ootaxonomically unassigned eggs with oviraptorid embryos		*Protoceratopsidovum* oosp.	Spheroolithidae indet.	
Buylyasutuin Khuduk[6,8,27]	Du		*Trachoolithus faticanus*				

APPENDIX TABLE 1. Continued

Locality	Fm.	Dendroolithidae	Elongatoolithidae	Ovaloolithidae	Prismatoolithidae	Spheroolithidae	Other ootaxa/eggs
Dariganga[7]	BS			*Ovaloolithus chinkangkouensis**			
Dushin Uul[6]	Du						Dinosaur egg indet.
Dzamin Khond[1,9,10,12,20,28]	Dj		Elongatoolithidae indet. (including ?*Elongatoolithus subtitectorius*)			Spheroolithidae indet.	
Ekhin Tukhum (Ikh Eren?)[6]	BS						Dinosaur egg indet.
Gilbent[6]	BG	*Dendroolithus microporosus*					*Faveoloolithus ningxiaensis*‡
Guriliin Tsav[6-9,11,20]	N	Dendroolithidae indet.	*Elongatoolithus sigillarius*; *Macroolithus rugustus*; *Macroolithus yaotunensis*			*Paraspheroolithus irenensis*	
Ikh Shunkht[6-8,12,16,30]	BG	*Dendroolithus verrucarius*	*Macroolithus mutabilis*		*Protoceratopsidovum minimum*; *Protoceratopsidovum sincerum*†	*Spheroolithus* oosp.	*Faveoloolithus ningxiaensis*‡
Khaichin Uul area[6,8,11,12,20,30]	N	*Dendroolithus* oosp.	*Elongatoolithus* oosp.; ?*Macroolithus rugustus*				
Khara Khutul[6]	BS						Dinosaur egg indet.
Khashaat[5,20]	Dj		Elongatoolithidae indet.		*Protoceratopsidovum fluxuosum*†		
Khermeen Tsav area[1,5-9,11,12,15,16]	BG/N	*Dendroolithus microporosus; Dendroolithus verrucarius*	*Macroolithus rugustus*		*Protoceratopsidovum minimum*; *Protoceratopsidovum fluxuosum*†; *Protoceratopsidovum sincerum*†	*Spheroolithus maiasauroides*	?*Coralloidoolithus*; *Faveoloolithus ningxiaensis*‡
Khongil Tsav[1,9,31]	BS		*Macroolithus mutabilis*		Prismatoolithidae indet.		Dinosaur egg indet.
Khugen Slavkhant[32]	J	Dendroolithidae indet.					
Khulsan[6-8,16]	BG	*Dendroolithus microporosus; Dendroolithus verrucarius*			*Protoceratopsidovum minimum*; *Protoceratopsidovum fluxuosum*†		*Faveoloolithus ningxiaensis*‡

APPENDIX TABLE 1. Continued

Locality	Fm.	Dendroolithidae	Elongatoolithidae	Ovaloolithidae	Prismatoolithidae	Spheroolithidae	Other ootaxa/eggs
Khuren Dukh[7]	KD						*Faveoloolithus ningxiaensis*‡
Kuren Tsav[6]	?						Dinosaur egg indet.
Moyogn Ulagiyn Khaets (Mogoin Ulaagiin Hets / Mogoin Bulak?)[6,7]	BS			*Ovaloolithus chinkangkouensis**			
Naran Bulak[6,12]	N						Dinosaur egg indet.
Nemegt[5,7,9,10,12,33,34]	BG/N	*Dendroolithus verrucarius*	*Elongatoolithus* oosp.; ootaxonomically unassigned clutch with a brooding *Nemegtomaia barsboldi*	*Ovaloolithus dinornithoides*	*Protoceratopsidovum fluxuosum*†		
Nogon Tsav[9,10,12]	?		?*Elongatoolithus* oosp.				*Dictyoolithus* oosp.; Faveoloolithidae indet.
Algui Ulan Tsav (= Ologoy Ulaan Tsav)[1,7,12,19,30,35,36]	UN						*Dictyoolithus* oosp.; *Parafaveoloolithus* oosp.‡; ootaxonomically unassigned egg with a possible titanosaur embryo
Shar Tsav[2,12,37]	N	Dendroolithidae indet.	Elongatoolithidae indet.			Spheroolithidae indet.	
Shiluut Uul (Shiljust Ula)[3,6,7,15]	BS	*Dendroolithus microporosus*				*Paraspheroolithus irenensis* (= *Spheroolithus tenuicorticus*)	
Shine Us Khudag[9,15]	BS			*Ovaloolithus chinkangkouensis**	*Protoceratopsidovum* cf. *Pro. minimum*		
Shiregin Gashun[6]	BS					*Spheroolithus* oosp.	
Southern Monadnocks[1]	BG						Dinosaur egg indet.
Tel Ulan Chaltsai (Tel Ulan Ula)[1,6,7,9,10,12,38]	BS		?*Elongatoolithus frustrabilis*	*Ovaloolithus chinkangkouensis** with a partial embryo			
Tsagaan Khushu[3,5-12,16]	N	Dendroolithidae indet.	*Elongatoolithus excellens*; *Macroolithus rugustus*	Ovaloolithus dinornithoides	?*Protoceratopsidovum fluxuosum*†	*Spheroolithus* oosp.	

APPENDIX TABLE 1. Continued

Locality	Fm.	Dendroolithidae	Elongatoolithidae	Ovaloolithidae	Prismatoolithidae	Spheroolithidae	Other ootaxa/eggs
Tugrikin Shire (Toogreek) [1,6,8,9,12,16,20,28]	Dj		*Elongatoolithus frustrabilis*; ?*Elongatoolithus subtitectorius*		*Protoceratopsidovum minimum*; *Protoceratopsidovum sincerum*†		
Udan Sayr[6-9,12,16,19-21,23,28]	Dj		*Elongatoolithus subtitectorius; Nanhsiungoolithus* oosp.	*Ovaloolithus dinornithoides*	*Protoceratopsidovum* oosp.		
Ukhaa Tolgod[39-47]	Dj		?*Elongatoolithus frustrabilis* (with a *Citipati osmolskae* embryo); clutch (?*Elongatoolithus frustrabilis*) with brooding *Citipati osmolskae*		*Prismatoolithus* oosp. (associated with a skeleton of *Almas ukhaa*); ootaxonomically unassigned eggs with a juvenile *Byronosaurus jaffei*		ootaxonomically unassigned clutch with embryos of *Protoceratops andrewsi*
Ulaan Khushu[9,10]	N	*Dendroolithus verrucarius*					
Undurshil Uul[6]	BG		*Elongatoolithus* oosp.				
Urlibe Khuduk[48,49]	BS	Dendroolithidae indet.	Elongatoolithidae indet.		Prismatoolithidae indet.		
Yagaan Khovil[12,20,21,28]	N?	Dendroolithidae indet.	Elongatoolithidae indet.			Spheroolithidae indet.	

References: 1, Watabe and Suzuki (2000b); 2, Watabe and Suzuki (2000c); 3, Watabe and Suzuki (2000d); 4, Watabe (2004); 5, Sabath (1991); 6, Carpenter and Alf (1994); 7, Mikhailov (1994b); 8, Mikhailov (1994a); 9, Ariunchimeg (2000); 10, Watabe and Suzuki (2000a); 11, Watabe et al. (2010b); 12, Watabe et al. (2010a); 13, Dewaele et al. (2015); 14, Graf et al. (2018); 15, this study; 16, Mikhailov et al. (1994); 17, van Straelen (1925); 18, Brown and Schlaikjer (1940); 19, Suzuki and Watabe (2000a); 20, Suzuki and Watabe (2000b); 21, Saneyoshi et al. (2010); 22, Watabe et al. (1998); 23, Suzuki and Watabe (2000c); 24, Iijima et al. (2012); 25, Iijima et al. (2012); 26, Weishampel et al. (2008); 27, Kurzanov and Mikhailov (1989); 28, Watabe and Tsogtbaatar (2004); 29, Suzuki et al. (2010); 30, Sochava (1969); 31, Lee et al. (2017); 32, Tanaka et al. (2019); 33, Fanti et al. (2012); 34, Funston et al. (2016); 35, Grellet-Tinner et al. (2011); 36, Kundrát and Cruickshank (2021); 37, Watabe et al. (2004); 38, Sochava (1972); 39, Clark et al. (1999); 40, Norell et al. (1994); 41, Norell et al. (2001); 42, Norell et al. (2018); 43, Norell et al. (2020); 44, Grellet-Tinner (2005); 45, Grellet-Tinner et al. (2006); 46, Erickson et al. (2017); 47, Pei et al. (2017); 48, Ishigaki et al. (2016); 49, Noda and Hayashi (2021)

APPENDIX TABLE 2. List of non-avian dinosaur eggs known from Mongolia. *Ootaxa known also from outside of Mongolia but data presented here are based on Mongolian specimens. †Eggshell thickness excluding the height of ornamentation. Parentheses indicate mean values or main ranges. Abbreviations: L, egg length; ST, eggshell thickness; W, egg width.

Oofamily	Ootaxon/ taxon	L (mm)	W (mm)	ST (mm)	Outer surface morphology	Reference of egg
Dendroolithidae	*Dendroolithus microporosus*	70.0	60.0	1.5-3.0 (2.0-2.7)	Primarily unsculptured	Mikhailov (1994b)
	Dendroolithus verrucarius	90.0-100.0	90.0-100.0	1.8-4.3 (2.6-3.3)	Rough and nodose, lacking any clear ornamentation (eroded by numerous ravines surrounding wartlike projections of repeated spherulites)	Mikhailov (1994b)
Dictyoolithidae	*Dictyoolithus* oosp.*	?	?	?	?	Ariunchimeg (2000)
Elongatoolithidae	*Elongatoolithus excellens*	90.0-110.0	40.0	0.3-0.9 (0.4-0.7)†	Linearituberculate ornamentation	Mikhailov (1994a)
	Elongatoolithus frustrabilis	150.0-170.0	60.0-70.0	0.8-1.5 (1.1-1.3)†	Linearituberculate ornamentation	Mikhailov (1994a)
	Elongatoolithus sigillarius	150.0-170.0	60.0-70.0	0.3-1.1 (0.4-0.8)†	Linearituberculate ornamentation	Mikhailov (1994a)
	Elongatoolithus subtitectorius	?	?	0.5-0.9 (0.7-0.8)†	Linearituberculate ornamentation	Mikhailov (1994a)
	Macroelongatoolithus oosp.*	400.0	?	~2.9 (2.0)	Linearituberculate ornamentation	Iijima (2012)
	Macroolithus mutabilis	>170.0?	?	1.3-2.0 (1.5-1.8)†	Linearituberculate ornamentation	Mikhailov (1994a)
	*Macroolithus rugustus**	165.0-?180.0	70.0	0.8-1.5 (1.1-1.3)†	Linearituberculate ornamentation	Sochava (1969); Mikhailov (1994a, 2000)
	Macroolithus yaotunensis	?	?	?	?	Ariunchimeg (2000)
	Nanhsiungoolithus oosp.*	?	?	?	?	Ariunchimeg (2000)
	Trachoolithus faticanus	?	?	0.3-0.5	Linearituberculate ornamentation	Mikhailov (1994a)
	Clutch with the holotype skeleton of *Oviraptor philoceratops*	203.2?	56.6?	1	Linearituberculate ornamentation	van Straelen (1925); Andrews (1932); Brown and Schlaikjer (1940); Norell et al. (2018)
	Clutches (?*Elongatoolithus frustrabilis*) with brooding *Citipati osmolskae*	180.0-190.0	65.0-72.0	0.5-0.6	Linearituberculate ornamentation	Clark et al. (1999); Grellet-Tinner et al. (2006); Norell et al. (2018)
	Clutch with a brooding *Nemegtomaia barsboldi*	140.0-160.0	50.0-60.0	1.0-1.2	Linearituberculate ornamentation	Fanti et al. (2012)

APPENDIX TABLE 2. Continued

Oofamily	Ootaxon/ taxon	L (mm)	W (mm)	ST (mm)	Outer surface morphology	Reference of egg
	Egg (?*Elongatoolithus frustrabilis*) with an oviraptorid embryo	120.0?	60.0?	0.5-1.0	Linearituberculate ornamentation	Norell et al. (1994, 2001); Mikhailov (2014)
	Eggs with oviraptorid embryos	?	?	0.7-1.0 (0.9)	Linearituberculate ornamentation	Weishampel et al. (2008)
Faveoloolithidae	*Faveoloolithus ningxiaensis*	150.0-165.0	150.0-165.0	1.8-2.6	Smooth or rough	Mikhailov (1994b)
	Parafaveoloolithus oosp.	145.0-148.0	130.0-134.0	1.8-2.5	Smooth	Sochava (1969); Mikhailov (1994b)
Ovaloolithidae	*Ovaloolithus chinkangkouensis**	?	70.0-80.0	1.4-3.0 (2.2-3.0)	Fine-corrugated ornament of sagenotuberculate ornamentation	Mikhailov (1994b)
	Ovaloolithus dinornithoides	105.0	74.0	1.3-1.6 (1.5-1.8)	No ornamentation or weak sagenotuberculate ornamentation at poles	Mikhailov (1994b)
	Eggshell (*Ovaloolithus chinkangkouensis*) with a partial indeterminate embryo	?	?	2.2-2.8	Small tubercles	Sochava (1972); Mikhailov (1994b)
Prismatoolithidae	*Protoceratopsidovum fluxuosum*	130.0-150.0	50.0-57.0	0.3-1.4 (0.6-0.7)	Lineartuberculate ornamentation	Mikhailov (1994a)
	Protoceratopsidovum minimum	100.0-?110.0	40.0-?50.0	0.3-0.7	Smooth	Mikhailov (1994a)
	Protoceratopsidovum sincerum	?	?	0.4-1.2 (0.6-0.7)	Smooth	Mikhailov (1994a)
	Clutch with juveniles of *Byronosaurus jaffei*	?	?	0.5	Smooth	Grellet-Tinner (2005)
	Prismatoolithus oosp. with the holotype skeleton of *Almas ukhaa*	?	?	0.4	Smooth	Pei et al. (2017)
Spheroolithidae	*Paraspheroolithus irenensis* (including *Spheroolithus tenuicorticus*)*	80.0-100.0	70.0-80.0	0.8-2.2 (1.0-2.0)	Smooth to rough, or weak sagenotuberculate ornamentation at poles	Mikhailov (1994b, 2000)
	Spheroolithus maiasauroides	90.0	70.0	1.0-1.6 (1.2-1.5)	Sagenotuberculate ornamentation	Mikhailov (1994b)
	Eggshells (*Spheroolithus* oosp.) with perinatal *Saurolophus angustirostris*	?	?	1.6-2.0 (1.8)	Between ramotuberculate and sagenotuberculate ornamentation	Dewaele et al. (2015)
Stalicoolithidae	*Coralloidoolithus* oosp.*	130.0	130.0	2.5-4.0 (3.2)	Rough or shagreen	This study
Other eggs	Clutch with *Protoceratops andrewsi* embryos	121.0-125.0	60.0	0.3	?	Erickson et al. (2017); Norell et al. (2020)
	Brooding troodontidae	?	?	?	?	Erickson et al. (2007)
	Egg with a titanosaur embryo	91.1	87.1	1.0-1.4	Eroded but occasionally nodes	Grellet-Tinner et al. (2011)

APPENDIX TABLE 3. List of non-avian dinosaur ootaxa in each country. Only egg specimens that were parataxonomically classified were included. **Subtiliolithus hyogoensis* is considered as a non-avian theropod eggshell (see Tanaka et al., 2020)

Region	Country	Oofamily	Oogenus	Oospecies
Africa	Morocco	Megaloolithidae	*Megaloolithus*	*Megaloolithus magharebiensis*
Africa	Morocco		*Pseudomegaloolithus*	*Pseudomegaloolithus atlasi*
Africa	Morocco	Prismatoolithidae	*Prismatoolithus*?	
Africa	Tanzania	Megaloolithidae		
Asia	China	Dendroolithidae	*Dendroolithus*	*Dendroolithus alimiaoensis*
Asia	China			*Dendroolithus dendriticus*
Asia	China			*Dendroolithus furcatus*
Asia	China			*Dendroolithus sanlimiaoensis*
Asia	China			*Dendroolithus wangdianensis*
Asia	China			*Dendroolithus xichuanensis*
Asia	China		*Phaceloolithus*	*Phaceloolithus hunanensis*
Asia	China		*Placoolithus*	*Placoolithus taohensis*
Asia	China			*Placoolithus tiantaiensis*
Asia	China			*Placoolithus tumiaolingensis*
Asia	China	Dictyoolithidae	*Dictyoolithus*	*Dictyoolithus hongpoensis*
Asia	China		*Paradictyoolithus*	*Paradictyoolithus xiaxishanensis*
Asia	China			*Paradictyoolithus zhuangqianensis*
Asia	China		*Protodictyoolithus*	*Protodictyoolithus jiangi*
Asia	China			*Protodictyoolithus neixiangensis*
Asia	China	Dongyangoolithidae	*Dongyangoolithus*	*Dongyangoolithus nanmaensis*
Asia	China		*Multifissoolithus*	*Multifissoolithus megadermus*
Asia	China			*Multifissoolithus chianensis*
Asia	China	Elongatoolithidae	*Elongatoolithus*	*Elongatoolithus andrewsi*
Asia	China			*Elongatoolithus elongatus*
Asia	China			*Elongatoolithus magnus*
Asia	China			*Elongatoolithus taipinghuensis*
Asia	China			*Elongatoolithus yuanshutensis*
Asia	China		*Heishanoolithus*	*Heishanoolithus changii*
Asia	China		*Lepidotoolithus*	*Lepidotoolithus guofenglouensis*
Asia	China		*Macroelongatolithus*	*Macroelongatolithus xixiaensis*
Asia	China		*Macroolithus*	*Macroolithus rugustus*
Asia	China			*Macroolithus yaotunensis*
Asia	China		*Nanhsiungoolithus*	*Nanhsiungoolithus chuetienensis*
Asia	China		*Paraelongatoolithus*	*Paraelongatoolithus reticulatus*
Asia	China		*Undulatoolithus*	*Undulatoolithus pengi*
Asia	China	Faveoloolithidae	*Duovallumoolithus*	*Duovallumoolithus shangdanensis*
Asia	China		*Faveoloolithus*	*Faveoloolithus ningxiaensis*
Asia	China			*Faveoloolithus zhangi*
Asia	China		*Hemifaveoloolithus*	*Hemifaveoloolithus muyushanensis*

APPENDIX TABLE 3. Continued

Region	Country	Oofamily	Oogenus	Oospecies
Africa	Morocco	Megaloolithidae	*Megaloolithus*	*Megaloolithus magharebiensis*
Africa	Morocco		*Pseudomegaloolithus*	*Pseudomegaloolithus atlasi*
Africa	Morocco	Prismatoolithidae	*Prismatoolithus*?	
Africa	Tanzania	Megaloolithidae		
Asia	China	Dendroolithidae	*Dendroolithus*	*Dendroolithus alimiaoensis*
Asia	China			*Dendroolithus dendriticus*
Asia	China			*Dendroolithus furcatus*
Asia	China			*Dendroolithus sanlimiaoensis*
Asia	China			*Dendroolithus wangdianensis*
Asia	China			*Dendroolithus xichuanensis*
Asia	China		*Phaceloolithus*	*Phaceloolithus hunanensis*
Asia	China		*Placoolithus*	*Placoolithus taohensis*
Asia	China			*Placoolithus tiantaiensis*
Asia	China			*Placoolithus tumiaolingensis*
Asia	China	Dictyoolithidae	*Dictyoolithus*	*Dictyoolithus hongpoensis*
Asia	China		*Paradictyoolithus*	*Paradictyoolithus xiaxishanensis*
Asia	China			*Paradictyoolithus zhuangqianensis*
Asia	China		*Protodictyoolithus*	*Protodictyoolithus jiangi*
Asia	China			*Protodictyoolithus neixiangensis*
Asia	China	Dongyangoolithidae	*Dongyangoolithus*	*Dongyangoolithus nanmaensis*
Asia	China		*Multifissoolithus*	*Multifissoolithus megadermus*
Asia	China			*Multifissoolithus chianensis*
Asia	China	Elongatoolithidae	*Elongatoolithus*	*Elongatoolithus andrewsi*
Asia	China			*Elongatoolithus elongatus*
Asia	China			*Elongatoolithus magnus*
Asia	China			*Elongatoolithus taipinghuensis*
Asia	China			*Elongatoolithus yuanshutensis*
Asia	China		*Heishanoolithus*	*Heishanoolithus changii*
Asia	China		*Lepidotoolithus*	*Lepidotoolithus guofenglouensis*
Asia	China		*Macroelongatolithus*	*Macroelongatolithus xixiaensis*
Asia	China		*Macroolithus*	*Macroolithus rugustus*
Asia	China			*Macroolithus yaotunensis*
Asia	China		*Nanhsiungoolithus*	*Nanhsiungoolithus chuetienensis*
Asia	China		*Paraelongatoolithus*	*Paraelongatoolithus reticulatus*
Asia	China		*Undulatoolithus*	*Undulatoolithus pengi*
Asia	China	Faveoloolithidae	*Duovallumoolithus*	*Duovallumoolithus shangdanensis*
Asia	China		*Faveoloolithus*	*Faveoloolithus ningxiaensis*
Asia	China			*Faveoloolithus zhangi*
Asia	China		*Hemifaveoloolithus*	*Hemifaveoloolithus muyushanensis*

APPENDIX TABLE 3. Continued

Region	Country	Oofamily	Oogenus	Oospecies
Asia	China		*Parafaveoloolithus*	*Parafaveoloolithus guoqingsiensis*
Asia	China			*Parafaveoloolithus macroporus*
Asia	China			*Parafaveoloolithus microporus*
Asia	China			*Parafaveoloolithus pingxiangensis*
Asia	China			*Parafaveoloolithus tiansicunensis*
Asia	China			*Parafaveoloolithus xipingensis*
Asia	China			*Parafeveoloolithus fengguangcunensis*
Asia	China	Ovaloolithidae	*Ovaloolithus*	*Ovaloolithus huangtulingensis*
Asia	China			*Ovaloolithus laminadermus*
Asia	China			*Ovaloolithus mixtistriatus*
Asia	China			*Ovaloolithus monostriatus*
Asia	China			*Ovaloolithus nanxiongensis*
Asia	China			*Ovaloolithus sangequanensis*
Asia	China			*Ovaloolithus shitangensis*
Asia	China			*Ovaloolithus tristriatus*
Asia	China			*Ovaloolithus weiqiaoensis*
Asia	China	Polyclonoolithidae	*Polyclonoolithus*	*Polyclonoolithus yangjiagouensis*
Asia	China	Prismatoolithidae	*Laiyangoolithus*	*Laiyangoolithus lixiangensis*
Asia	China		*Prismatoolithus*	*Prismatoolithus tiantaiensis*
Asia	China			*Prismatoolithus gebiensis*
Asia	China			*Prismatoolithus heyuanensis*
Asia	China			*Prismatoolithus hukouensis*
Asia	China	Similifaveoolithidae	Similifaveoloolithus	*Similifaveoloolithus gongzhulingensis*
Asia	China			*Similifaveoloolithus shuangtangensis*
Asia	China		*Wormoolithus*	*Wormoolithus luxiensis*
Asia	China	Spheroolithidae	*Paraspheroolithus*	*Paraspheroolithus irenensis*
Asia	China		*Spheroolithus*	*Spheroolithus chiangchiungtingensis*
Asia	China			*Spheroolithus quantouensis*
Asia	China			*Spheroolithus spheroides*
Asia	China	Stalicoolithidae	*Coralloidoolithus*	*Coralloidoolithus chichengshanensis*
Asia	China			*Coralloidoolithus shizuiwanensis*
Asia	China		*Shixingoolithus*	*Shixingoolithus erbeni*
Asia	China		*Stalicoolithus*	*Stalicoolithus shifengensis*
Asia	China			*Stalicoolithus spheroides*
Asia	China	Umbellaoolithidae	*Umbellaoolithus*	*Umbellaoolithus xiuningensis*
Asia	China	Youngoolithidae	*Youngoolithus*	*Youngoolithus xipingensis*
Asia	China	(Oofamily incertae sedis)	*Mosaicoolithus*	*Mosaicoolithus zhangtoucaoensis*
Asia	China		*Parvoblongoolithus*	*Parvoblongoolithus jinguoensis*
Asia	China		*Stromatoolithus*	*Stromatoolithus pinglingensis*
Asia	China		*Taoyuanoolithus*	*Taoyuanoolithus dontingensis*

APPENDIX TABLE 3. Continued

Region	Country	Oofamily	Oogenus	Oospecies
Asia	India	Elongatoolithidae	*Ellipsoolithus*	*Ellipsoolithus khedaensis*
Asia	India		*Trachoolithus*	
Asia	India	Fusioolithidae	*Fusioolithus*	*Fusioolithus baghensis*
Asia	India	Megaloolithidae	*Megaloolithus*	*Megaloolithus cylindricus*
Asia	India			*Megaloolithus dholiyaensis*
Asia	India			*Megaloolithus dhoridungriensis*
Asia	India			*Megaloolithus jabalpurensis*
Asia	India			*Megaloolithus khempurensis*
Asia	India			*Megaloolithus matleyi*
Asia	India			*Megaloolithus megadermus*
Asia	India			*Megaloolithus mohabeyi*
Asia	India			*Megaloolithus padiyalensis*
Asia	India			*Megaloolithus walpurensis*
Asia	India	Spheroolithidae	*Spheroolithus?*	
Asia	Japan	Dongyangoolithidae	*Multifissoolithus*	*Multifissoolithus shimonosekiensis*
Asia	Japan	Elongatoolithidae	*Elongatoolithus*	
Asia	Japan	Prismatoolithidae	*Prismatoolithus*	
Asia	Japan		*Ramoprismatoolithus*	*Ramoprismatoolithus okurai*
Asia	Japan	Spheroolithidae	*Spheroolithus*	
Asia	Japan	Laevisoolithidae	*Subtiliolithus*	*Subtiliolithus hyogoensis**
Asia	Japan	(Oofamily incertae sedis)	*Himeoolithus*	*Himeoolithus murakamii*
Asia	Japan		*Nipponoolithus*	*Nipponoolithus ramosus*
Asia	Kazakhstan	Elongatoolithidae		
Asia	Kazakhstan	Spheroolithidae		
Asia	Mongolia	Dendroolithidae	*Dendroolithus*	*Dendroolithus microporosus*
Asia	Mongolia			*Dendroolithus verrucarius*
Asia	Mongolia	Dictyoolithidae	*Dictyoolithus*	
Asia	Mongolia	Elongatoolithidae	*Elongatoolithus*	*Elongatoolithus excellens*
Asia	Mongolia			*Elongatoolithus frustrabilis*
Asia	Mongolia			*Elongatoolithus sigillarius*
Asia	Mongolia			*Elongatoolithus subtitectorius*
Asia	Mongolia		*Macroelongatoolithus*	
Asia	Mongolia		*Macroolithus*	*Macroolithus mutabilis*
Asia	Mongolia			*Macroolithus rugustus*
Asia	Mongolia			*Macroolithus yaotunensis*
Asia	Mongolia		*Nansiungoolithus*	
Asia	Mongolia		*Trachoolithus*	*Trachoolithus faticanus*
Asia	Mongolia	Faveoloolithidae	*Faveoloolithus*	*Faveoloolithus ningxiaensis*
Asia	Mongolia		*Parafaveoloolithus*	
Asia	Mongolia	Ovaloolithidae	*Ovaloolithus*	*Ovaloolithus chinkangkouensis*

APPENDIX TABLE 3. Continued

Region	Country	Oofamily	Oogenus	Oospecies
Asia	Mongolia			*Ovaloolithus dinornithoides*
Asia	Mongolia			*Ovaloolithus turpanensis*
Asia	Mongolia	Prismatoolithidae	*Prismatoolithus*	
Asia	Mongolia		*Protoceratopsidovum*	*Protoceratopsidovum fluxuosum*
Asia	Mongolia			*Protoceratopsidovum minimum*
Asia	Mongolia			*Protoceratopsidovum sincerum*
Asia	Mongolia	Spheroolithidae	*Paraspheroolithus*	*Paraspheroolithus irenensis*
Asia	Mongolia		*Spheroolithus*	*Spheroolithus maiasauroides*
Asia	Mongolia	Stalicoolithidae	*Coralloidoolithus*	
Asia	Russia	Prismatoolithidae	*Prismatoolithus*	*Prismatoolithus ilekensis*
Asia	Russia	Spheroolithidae		
Asia	South Korea	Dendroolithidae		
Asia	South Korea	Dictyoolithidae	*Protodictyoolithus*	*Protodictyoolithus neixiangensis*
Asia	South Korea	Elongatoolithidae		
Asia	South Korea			*Macroelongatoolithus goseongensis*
Asia	South Korea	Faveoloolithidae	*Faveoloolithus*	
Asia	South Korea		*Propagoolithus*	*Propagoolithus widoensis*
Asia	South Korea	Ovaloolithidae		
Asia	South Korea	Spheroolithidae	*Spheroolithus*	
Asia	South Korea	(Oofamily incertae sedis)		*Reticuloolithus acicularis*
Europe	UK	Faveoloolithidae (or Dictyoolithidae)		
Europe	UK	Ovaloolithidae		
Europe	UK	Megaloolithidae		
Europe	France	Cairanoolithidae	*Cairanoolithus*	*Cairanoolithus dughii*
Europe	France		*Dughioolithus*	*Dughioolithus roussentensis*
Europe	France	Megaloolithidae	*Megaloolithus*	*Megaloolithus aureliensis*
Europe	France			*Megaloolithus mammillare*
Europe	France			*Megaloolithus microtuberculata*
Europe	France			*Megaloolithus petralta*
Europe	France			*Megaloolithus pseudomamillare*
Europe	France			*Megaloolithus siruguei*
Europe	France	Montanoolithidae	*Montanoolithus*	*Montanoolithus labadousensis*
Europe	France	Prismatoolithidae	*?Pseudogeckoolithus*	
Europe	France		*Prismatoolithus*	*Prismatoolithus carboti*
Europe	France			*Prismatoolithus matellensis*
Europe	France			*Prismatoolithus tenuis*
Europe	France	(Oofamily incertae sedis)	cf. *Ageroolithus*	
Europe	Portugal	Phaceloolithidae		
Europe	Portugal	Prismatoolithidae	*Preprismatoolithus*	

APPENDIX TABLE 3. Continued

Region	Country	Oofamily	Oogenus	Oospecies
Europe	Romania	Megaloolithidae	*Megaloolithus*	*Megaloolithus siruguei*
Europe	Spain	Cairanoolithidae	*Dughioolithus*	*Dughioolithus* cf. *roussetensis*
Europe	Spain	Fusioolithidae	*Fusioolithus*	*Fusioolithus baghensis*
Europe	Spain	Megaloolithidae	*Megaloolithus*	?*Megaloolithus pseudomamillare* (or *M. petralta*)
Europe	Spain			Maybe *Megaloolithus mammillare*
Europe	Spain			*Megaloolithus aureliensis*
Europe	Spain			*Megaloolithus petralta*
Europe	Spain			*Megaloolithus siruguei*
Europe	Spain	Prismatoolithidae	*Prismatoolithus*	aff. *Prismatoolithus matellensis*
Europe	Spain			*Prismatoolithus tenuis*
Europe	Spain			*Prismatoolithus trempii*
Europe	Spain		*Pseudogeckoolithus*	*Pseudogeckoolithus nodosus*
Europe	Spain		*Sankofa*	*Sankofa pyrenaica*
Europe	Spain		*Trigonoolithus*	*Trigonoolithus amoae*
Europe	Spain	Spheroolithidae	*Guegoolithus*	*Guegoolithus turolensis*
Europe	Spain		*Spheroolithus*	*Spheroolithus europaeus*
Europe	Spain	(Oofamily incertae sedis)	*Ageroolithus*	*Ageroolithus fontllongensis*
North America	Canada	Arriagadoolithidae	*Triprismatoolithus*	
North America	Canada	Montanoolithidae	*Montanoolithus*	*Montanoolithus strongorum*
North America	Canada	Prismatoolithidae	*Prismatoolithus*	*Prismatoolithus levis*
North America	Canada	Spheroolithidae	*Spheroolithus*	*Spheroolithus albertensis*
North America	Canada			*Spheroolithus* cf. *S. choteauensis*
North America	Canada	(Oofamily incertae sedis)	*Continuoolithus*	*Continuoolithus canadensis*
North America	Canada		*Porituberoolithus*	*Porituberoolithus warnerensis*
North America	Canada		*Reticuloolithus*	*Reticuloolithus hirschi*
North America	Canada		*Tristraguloolithus*	*Tristraguloolithus cracioides*
North America	Mexico	Prismatoolithidae	*Pseudogeckoolithus*	
North America	Mexico	Prismatoolithidae	*Prismatoolithus*	
North America	Mexico	Spheroolithidae	*Spheroolithus*	
North America	Mexico	Tubercuoolithidae	*Tubercuoolithus*	
North America	Mexico	(Oofamily incertae sedis)	*Disperituberoolithus*	
North America	Mexico		*Continuoolithus*	
North America	Mexico		*Porituberoolithus*	
North America	Mexico		*Tristraguloolithus*	
North America	USA	Arriagadoolithidae	*Triprismatoolithus*	*Triprismatoolithus stephensi*
North America	USA	Belonoolithidae	*Belonoolithus*	*Belonoolithus garbani*
North America	USA	Elongatoolithidae	*Macroelongatoolithus*	*Macroelongatoolithus carlylei*
North America	USA		*Spongioolithus*	*Spongioolithus hirschi*
North America	USA	Montanoolithidae	*Montanoolithus*	*Montanoolithus strongorum*

APPENDIX TABLE 3. Continued

Region	Country	Oofamily	Oogenus	Oospecies
North America	USA	Ovaloolithidae	*Ovaloolithus*	*Ovaloolithus tenuisus*
North America	USA			*Ovaloolithus utahensis*
North America	USA	Prismatoolithidae	*Preprismatoolithus*	*Preprismatoolithus coloradensis*
North America	USA		*Prismatoolithus*	*Prismatoolithus hirschi*
North America	USA			*Prismatoolithus jenseni*
North America	USA			*Prismatoolithus levis*
North America	USA		*Spheruprismatoolithus*	*Spheruprismatoolithus condensus*
North America	USA		*Tetonoolithus*	*Tetonoolithus nelsoni*
North America	USA	Spheroolithidae	*Spheroolithus*	*Spheroolithus albertensis*
North America	USA			*Spheroolithus choteauensis*
North America	USA	Tubercuoolithidae	*Dimorphoolithus*	*Dimorphoolithus bennetti*
North America	USA		*Tubercuoolithus*	*Tubercuoolithus tentonensis*
North America	USA	(Oofamily incertae sedis)	*Continuoolithus*	*Continuoolithus canadensis*
North America	USA		*Porituberoolithus*	*Porituberoolithus warnerensis*
North America	USA		*Stillatuberoolithus*	*Stillatuberoolithus storrsi*
South America	Argentina	Arriagadoolithidae	*Arriagadoolithus*	*Arriagadoolithus patagoniensis*
South America	Argentina	Faveoloolithidae		
South America	Argentina	Fusioolithidae	*Fusioolithus*	*Fusioolithus berthei*
South America	Argentina			*Fusioolithus baghensis*
South America	Argentina	Megaloolithidae		
South America	Argentina	Prismatoolithidae		
South America	Brazil	Elongatoolithidae?		
South America	Brazil	Megaloolithidae	*Megaloolithus*	*Megaloolithus pseudomamillare*
South America	Peru	Megaloolithidae	*Megaloolithus*	*Megaloolithus pseudomamillare*
South America	Uruguay	Faveoloolithidae	*Sphaerovum*	*Sphaerovum erbei*
South America	Uruguay	(Oofamily incertae sedis)	*Tacuarembovum*	*Tacuarembovum oblongum*

WINDOWS INTO SAUROPSID AND SYNAPSID EVOLUTION
Essays in honor of Prof. Louis L. Jacobs, pp. 211–221, 2023

ON THE SIGNIFICANCE OF A LATE CRETACEOUS TYRANNOSAUR TRACK FROM ANIAKCHAK NATIONAL MONUMENT (CHIGNIK FORMATION, CAMPANIAN – MAASTRICHTIAN), SOUTHWESTERN ALASKA

ANTHONY R. FIORILLO[1,*], YOSHITSUGU KOBAYASHI[2], PAUL J. MCCARTHY[3], LAURA STELSON[4], and EMILY SCHWING[1,5]

[1]New Mexico Museum of Natural History & Science, 1801 Mountain Road, NW, Albuquerque, New Mexico, 87104, USA, anthony.fiorillo@dca.nm.gov;
[2]Hokkaido University Museum, Hokkaido University, Sapporo, Hokkaido, 060-0810, Japan, ykobayashi@museum.hokudai.ac.jp;
[3]Department of Geosciences, University of Alaska, Fairbanks, Alaska, 99775, USA, pjmccarthy@alaska.edu;
[4]Katmai National Park and Preserve, 1000 Silver Street, Building 603, King Salmon, AK, 99613, USA, lfs20@psu.edu;
[5]New Mexico Museum of Natural History & Science, 1801 Mountain Road, NW, Albuquerque, New Mexico, 87104, USA, emilyschwing@gmail.com

ABSTRACT Here we report on the new discovery of a large track, attributed to a tyrannosaur, from Aniakchak National Monument in southwestern Alaska. The track is from the Late Cretaceous (Campanian: Maastrichtian) Chignik Formation, a cyclic sequence of rocks, approximately 500-600 m thick, representing shallow marine to nearshore marine environments in the lower part and continental alluvial and coastal plain environments in the upper part of the section. The track is from within rocks representing estuarine settings. The Chignik Formation is part of the Peninsular Terrane and paleomagnetic reconstructions based on the volcanic rocks of this terrane suggest that the rock unit was deposited near its current latitude of almost 57° N. This track adds to the biodiversity of the ichnofauna known from this rock unit, and the size of the track adds to our understanding of adaptation by high-latitude tyrannosaurs throughout the region.

KEYWORDS Footprint, Theropoda, High-latitude, Biogeography, Dinosauria, *Nanuqsaurus*

INTRODUCTION

In 2001, an inventory and monitoring program initiated by the United States National Park Service, Alaska Region, resulted in the first discovery of Cretaceous dinosaurs in southwestern Alaska, in Aniakchak National Monument (Fiorillo and Parrish, 2004). Further, this discovery was the first documentation of any dinosaur record in any Alaska National Park (Fiorillo and Parrish, 2004). Subsequent work at Aniakchak has shown that the Cretaceous Chignik Formation has an abundant and diverse record of dinosaur footprints (Fiorillo et al., 2018a, 2019).

These fossil vertebrate occurrences are approximately correlative with the famous fossil bone deposits of the Prince Creek Formation of the North Slope of Alaska (e.g., Parrish et al., 1987; Gangloff and Fiorillo, 2010; Fiorillo, 2018), which are located approximately 1500 kilometers north of this study area on the Alaska Peninsula. Together these discoveries demonstrate that terrestrial ecosystems could support dinosaurs across a vast geographic region in ancient high-latitude Alaska.

This study documents the occurrence of a previously unrecognized large theropod track, attributable to a tyrannosaur larger than any previously encountered in the Upper Cretaceous Chignik Formation of southwestern Alaska. The track was discovered during the 2022 field season. This report serves two purposes. First, it expands the known vertebrate ichnotaxonomic biodiversity within this rock unit, by adding a large, 55 cm long tyrannosaur track to the previously documented dinosaur fauna. Secondly, the discovery of a large tyrannosaur track, approximately 60% larger than previously recorded from theropod tracks from the study area in southwestern Alaska adds to our understanding of the adaptative pressures faced by high-latitude tyrannosaurs throughout the region.

Lastly, we are pleased to contribute this work to a volume celebrating the career of Dr. Louis Jacobs. In his role as a bold scientist, explorer, and mentor at Southern Methodist

*Corresponding author

University, Professor Jacobs has inspired a force of new paleontologists who, through their own efforts, have furthered our understanding of the history of life on this planet. As Aniakchak National Monument is one of the least visited National Park units within the United States, it is fitting to contribute this work to a volume dedicated to a paleontologist who has made a career of exploring places where few had gone before him.

METHODS

Photographic data of the tyrannosaur track described here were obtained using a digital camera in the field. A three-dimensional model of the track was created using the software Agisoft Metashape Standard v1.7.3. In the software, sixty photos from different angles were added, aligned, and used to build a dense cloud with texture. The trimmed data of the 3D model was exported and saved as an obj. file. This obj. file was then imported into another software, CloudCompare v2.13 alpha, to create a heat map of the track.

GEOGRAPHIC AND GEOLOGIC BACKGROUND

Aniakchak National Monument and Preserve (ANIA), comprises approximately 240,000 hectares and is one of the least-visited parks within the United States National Park Service system (Fig. 1). Established in 1978, the park is centered around the massive Aniakchak Caldera, a circular volcanic feature approximately 10 kilometers wide with walls ranging from a few hundred meters to over a thousand meters in height. Much of the landscape seen today has been shaped by Holocene-era volcanic activity that included the collapse of the magma chamber beneath the caldera around 3,590 cal. B.P., along with ten other volcanic events that occurred between 7,000 BP and 1931 (Hubbard, 1931; Jaggar, 1932; Miller and Smith, 1987; Beget et al., 1992; Bacon et al., 2014). Aside from the Holocene volcanic deposits and the Pleistocene sedimentary deposits, sedimentary rocks within Aniakchak National Monument range in age from the Upper Jurassic (Naknek Formation) to Eocene

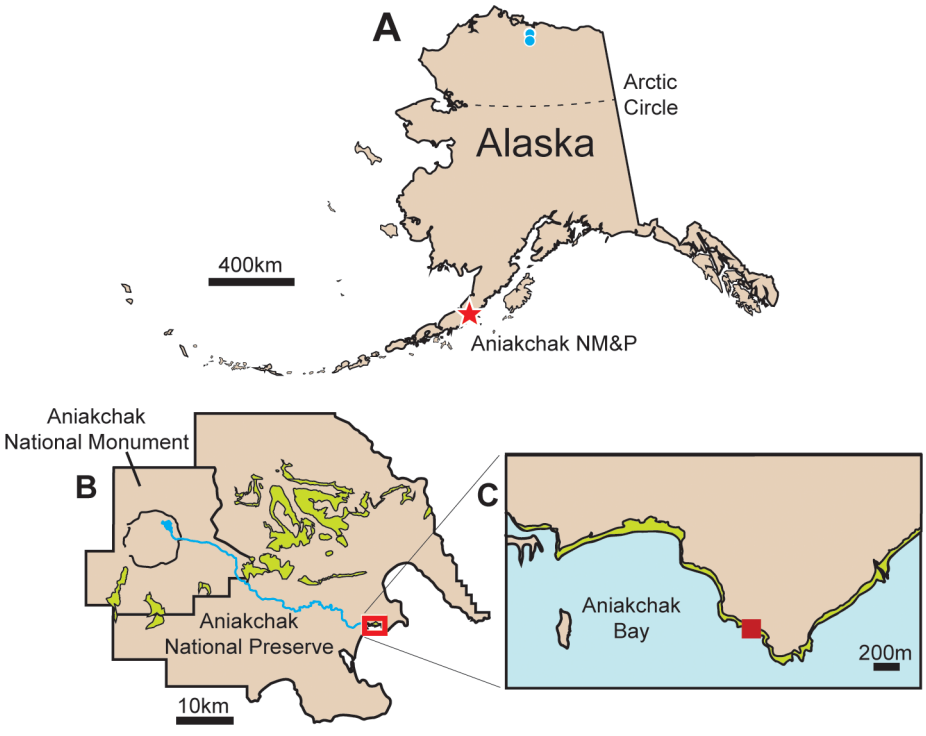

FIGURE 1. Location of Aniakchak National Monument, the study area for this report. Blue dots in **A** represent locations of primary bonebeds in correlative Prince Creek Formation. The green band in **B** represents coastal exposures of Chignik Formation. Red square in **C** represents the location where the track was found.

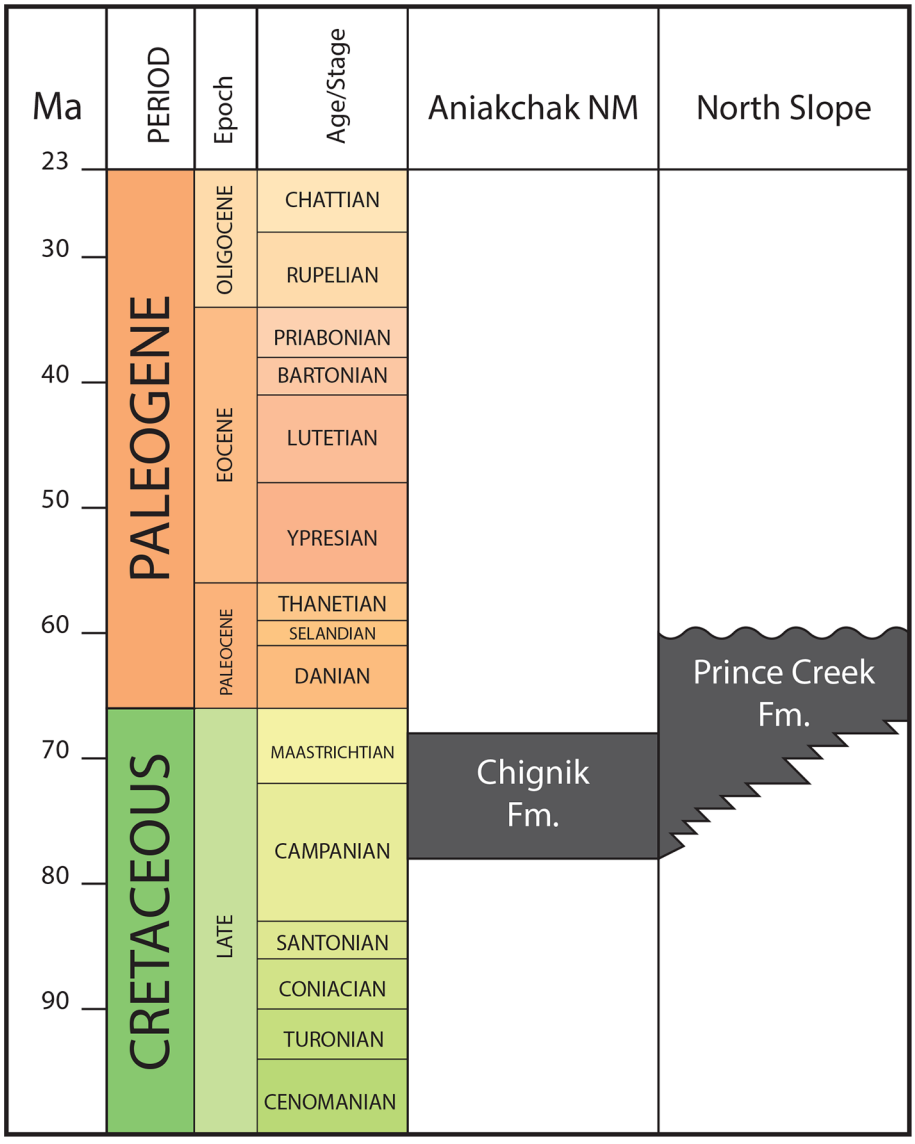

FIGURE 2. Stratigraphic correlation of Chignik and Prince Creek formations (modified from Fiorillo, 2018).

(Tolstoi Formation) and are also preserved in the park (Detterman et al., 1981; Wilson et al., 1999).

These Mesozoic and younger rocks are part of the Peninsular Terrane, a structural unit encompassing much of southwestern Alaska. Paleomagnetic reconstructions based on the Upper Cretaceous and Lower Tertiary volcanic rocks of this terrane suggest that the sediments of the Chignik Formation were initially deposited at nearly their current latitude of approximately 57° North (Hillhouse and Coe, 1994). The Chignik Formation was named by Atwood (1911) for rocks exposed in the vicinity of Chignik Lagoon, approximately 75 kilometers southwest of our study site in Aniakchak Bay. The formation has a maximum stratigraphic thickness of approximately 600 m in the type area of Chignik Bay (Detterman et al., 1996). Outside of the type area, deposit thicknesses start to change significantly, thinning rapidly to the northeast and southwest (Detterman et al., 1996).

Based on the presence of marine bivalves, the age of the Chignik Formation was interpreted as late Campanian to early Maastrichtian (Detterman et al., 1996). These data suggest then, that the Chignik Formation exposed in Aniakchak Bay is approximately correlative with dinosaur-bearing sections in the Prince Creek Formation along the

FIGURE 3. Annotated outcrop photograph illustrating the depositional settings for where the track in this report was found.

Colville River of northern Alaska (Fig. 2, Fiorillo, 2018).

Fiorillo and Parrish (2004) originally measured a 280 m section of the Chignik Formation in the study area in Aniakchak Bay. Their documentation was later expanded by extending this section to encompass slightly more of the local marine context and adding additional details of the sedimentology (Fiorillo et al., 2019). Detailed sedimentological work on the upper 300 m of the section indicates that the entire section represents a tidally influenced estuary-fill. Marine shoreface deposits are incised by a thick sandstone package interpreted as a multi-story, meandering fluvial channel valley-fill. This is overlain by outer estuary deposits, containing two thick red paleosols, culminating in estuary mouth sands with disarticulated bivalve shells. This succession is overlain by an inner estuarine succession containing weakly developed paleosols, tidal channels, tidal flats, and thin coals, overlain by a tidally influenced alluvial succession containing small meandering fluvial channels, floodplain successions, and thin, grey and red paleosols (Fiorillo et al., 2019, 2022). The tyrannosaurid track was found in a large block (approximately 60 cm by 75 cm) on a prominent point along the coast (Fig. 3). Based on size and lithological characteristics, the block is likely derived from a 4 m-thick, multi-story channel sandstone that overlies a thick, red, upper estuarine paleosol. Sand and mud tidal flats and splay deposits overlie and interfinger with the other facies in this vicinity.

TRACK DESCRIPTION

A single large tridactyl, mesaxonic track was found in 2022 which is preserved in epirelief (Fig. 4). The digits are long and linear, and the preserved digits taper to points. Digits III and IV are well preserved, while digit II is incomplete. In addition to the sharply terminated distal end, digit III also has a slight sinusoidal curve. The length of the track is 55 cm, with the lengths of digits II, III, and IV are respectively, 26 cm, 55 cm, and 35 cm. The outer digits (digits II and IV) are diverged to 27 and 26 degrees from digit III, respectively. The morphology of this track allows attribution as a large

non-avialan theropod.

Given the track length of 55 cm, using an equation of 4X the track length as an estimate of hip height, and 3.75X the hip height as an estimate of body length (Alexander, 1976; Henderson, 2003; Fiorillo and Tykoski, 2016), this track was made by a non-avialan theropod approximately 825 cm in length, or over 8 meters. Such a body length is approximately 60% larger than previously recognized from this ichnofauna (Fiorillo et al., 2019). There are a great number of tridactyl non-avian theropod ichnotaxa. It is not the purpose of this paper to review all of the nuances distinguishing these various taxa and debates on ichnotaxon validity such as the discussions surrounding *Buekeburgichnus* and *Megalosauripus* (e.g., Thulborn, 2001; Castenera et al., 2014; Razzolini et al., 2017).

A similarly aged theropod track, *Bellatoripes*, warrants some discussion as it was described from Wapiti Formation (upper Campanian – lower Maastrichtian) in northeastern British Columbia (McCrea et al., 2014). The diagnosis for this taxon is generally broad for individual tracks, with characters such as longer than wide, and digits that are thick proximally but taper strongly digitally. The diagnosis includes pace length, stride length, pace angulation and trackway width. The track described here, though most similar to *Bellatoripes* in a very broad sense (Fig. 4), is isolated rather than part of a trackway so a fuller, more detailed, comparison with this ichnotaxon is not available. Further, as northern theropod footprints, though it is tempting that these tracks may be the same ichnogenus, it remains that there is approximately 2000 km between northeastern British Columbia and southwestern Alaska, and it would be unwise to invoke a geographic justification for attribution.

Instead, we focus instead on a subjective comparison of this track to two of the more commonly discussed theropod ichnotaxa, *Grallator* and *Eubrontes*. Several authors have quantified the differences between these two ichnogenera (Weems, 1992; Olson et al., 1998; Smith and Farlow, 2003). In general, the most significant aspect distinguishing these two ichnogenera is the relative length of digit III in relation to digits II and IV, and the track length as a whole. Smith and Farlow (2003) relied more on simple ratios between digits III and II, and digits III and IV which allowed them to distinguish the two ichnotaxa by *Grallator* having a proportionately longer digit III than *Eubrontes*. Because of the incomplete nature of digit II in the specimen described here, we only compare the simple ratios for digits III and IV (Table 1) for *Grallator* and *Eubrontes* with the track described here. Comparison of the digit III/IV length ratio for the Aniakchak track described here with those provided by Smith and Farlow (2003) shows the Alaska track to have a greater affinity with *Grallator* than with *Eubrontes*.

TABLE 1. Average ratios of digit lengths for *Grallator* and *Eubrontes* based on original sample data (17 and 16 tracks, respectively) from Smith and Farlow [54], as well as the ratios for the Aniakchak track (ANIA) described here. Note that the ratios indicate that digit III is proportionately longer in *Grallator* than in *Eubrontes*. Based on these ratios, the Aniakchak track is assigned to the ichnogenus *Grallator*

Taxon	III:IV
Grallator	1.22
Eubrontes	0.93
Grallator (ANIA)	1.57

DISCUSSION

The paleontological survey work in Aniakchak National Monument continues to increase the dinosaur track record from the Alaska Peninsula and provide new insights into high-latitude dinosaur biodiversity and adaptation to life in the North. The discovery of dinosaurs in the high latitudes initially puzzled researchers and one of the early ideas to explain these discoveries in such extremely seasonal latitudes was that these Arctic dinosaurs must have undergone large-scale migrations to cope with the extreme nature of the ancient high-latitude environment (Fiorillo, 2018). While it is no longer thought that dinosaurs survived the winter using seasonal migrations like caribou (Fiorillo and Gangloff, 2001; Chinsamy et al., 2012; Fiorillo et al., 2014), evidence does suggest that dinosaurs migrated between what is now modern Asia and North America through Alaska during the Cretaceous (Russell, 1993; Cifelli et al., 1997; Sereno, 2000; Fiorillo, 2008; Zanno, 2010; Fiorillo and Adams, 2012; Fiorillo et al., 2018b; Kobayashi et al., 2019). The fossil records of Alaska and eastern Asia show some of the most robust evidence for this dispersal route with the close phylogenetic relationship between *Edmontosaurus* and *Kamuysaurus* (Kobayashi et al., 2019), as well as with the enigmatic theropods, the Therizinosauridae (Fiorillo et al., 2018b).

Late Maastrichtian tridactyl tracks measuring over 70-80

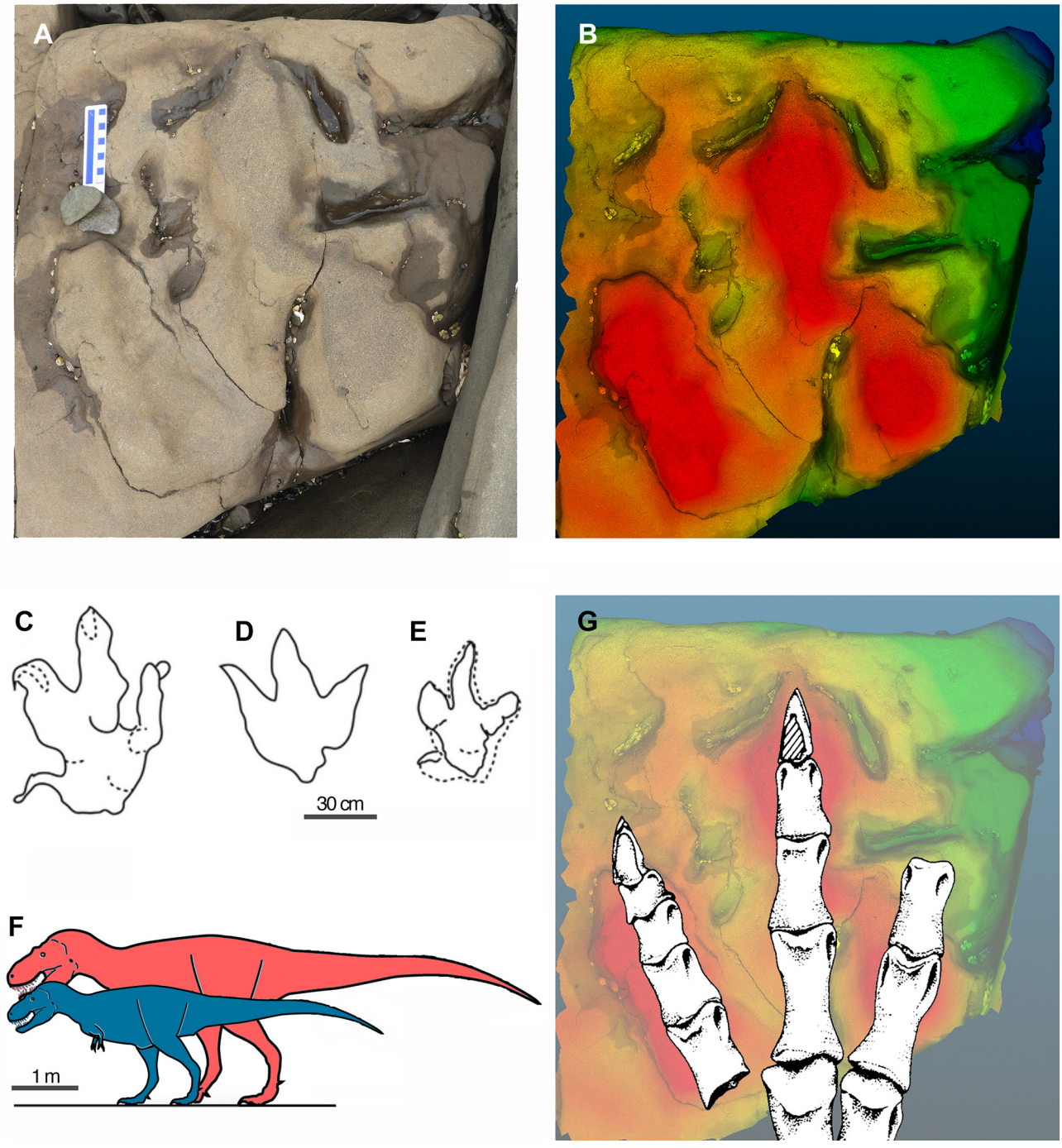

FIGURE 4. Composite track figure. **A**. Tyrannosaur track as found in the field. **B**. Heat map which illustrates the general morphology of the track. **C – E**. Track outlines from Razzolini (2016) of ichnogenera *Tyrannosauripus*, *Bellatoripes*, *Bueckeburgichnus*, respectively. **F**. Comparison of body size between *Nanuqsaurus* and *Albertosaurus* (modified from Fiorillo & Tykoski, 2014). The larger *Albertosaurus* serves as a proxy for the trackmaker in this study. G. Pes of *Albertosaurus* (Molnar, 1980) overlain on Aniakchak footprint to illustrate the compatibility between track and skeletal structure of large theropod.

cm (approximately 68% larger than the track described here), *Tyrannosauripus* (Lockley and Hunt, 1994), have been attributed to the apex tyrannosaur, *Tyrannosaurus rex* (Lockley and Hunt, 1994; Manning et al., 2008). However, based on biostratigraphy, it has been shown that the Chignik Formation is older and is likely late Campanian to early Maastrichtian

in age (Detterman et al., 1981; Fiorillo and Parrish, 2004; Fiorillo et al., 2019). Based on comparisons of its lengths with similar tridactyl tracks (e.g., Enriquez et al., 2022) from correlative ages, the track described here represents a full-sized (i.e., adult) tyrannosaur for its geologic age. So far, at least one hundred tracks of herbivorous dinosaurs, dominated by hadrosaurs, have been recorded from the section at this park (Fiorillo et al., 2019). This is the second definitive non-avian theropod track, suggesting a general rareness of carnivory in the estuarine environment of this region during the latest Cretaceous.

The well-known dinosaur remains in the Prince Creek Formation, approximately 1,500 kilometers farther north in Alaska, overlap in age with the dinosaur discoveries in the Chignik Formation (Fiorillo and Parrish, 2004; Flaig et al., 2014; Fiorillo, 2018). Considering recent work by others (Druckenmiller et al., 2021), we first review the study of the correlative tyrannosaur, *Nanuqsaurus* (Fiorillo and Tykoski, 2014). We then briefly review biogeographic patterns in body size changes in insular populations that are observed in modern vertebrates. We conclude by discussing the implications for the track described in this study.

Without providing the typical details of methods used to measure tooth crown height, and why taxa were chosen for comparisons, Druckenmiller et al. (2021) challenged the assertion that the tyrannosaurid, *Nanuqsaurus* (Fiorillo and Tykoski, 2014), described from the Kikak-Tegoseak Quarry in the Prince Creek Formation was of a diminutive nature. In the absence of such details in methodologies and practices, it is challenging to provide any in-depth understanding of any presented counter points from that study. What is of interest from the work by Druckenmiller et al. (2021) is the mention of additional, yet undescribed and unfigured, tyrannosaurid material from the Prince Creek Formation. But these specimens were collected across an approximately 20 km transect and therefore are unassociated and perhaps taxonomically distinct from each other. Further, even with the shallow dips of the strata that occur across the river exposures of the Prince Creek Formation (Flaig et al., 2011), given the range of radiometric dates reported through the formation (Phillips, 2003; Flaig et al., 2014) there is likely some significant geologic time represented over this transect, of the scale of 10^6 years, and of the scale of taxonomic turnover in dinosaurs (Dodson, 1990). Until such details are presented for critique, we instead focus here on the details presented in Fiorillo and Tykoski (2014) regarding an associated set of bones from a single quarry.

Though the skeletal remains are limited, *Nanuqsaurus* was diagnosed on characters such as thin, rostrally forked, spur of the fused parietals on the dorsal skull roof that overlaps and separates the frontals within the sagittal crest; a frontal with a long, rostrally pointed process separating the prefrontal and lacrimal facets; and the first two dentary teeth/alveoli much smaller than the remaining dentary teeth (Fiorillo and Tykoski, 2014). Despite the high percentage of missing skeletal data, Bremer support for this taxon and its taxonomic relationships to other tyrannosaurs was higher than Bremer support amongst more basal tyrannosaurs with more complete skeletal material (Fiorillo and Tykoski, 2014), indicating that despite the incomplete nature of the type material, the necessary skeletal remains for understanding the distinctiveness of the taxon were present for *Nanuqsaurus*. Further, the type material for *Nanuqsaurus* included the presence of a robust peg-in-socket articulation between the maxillae and nasals and was interpreted as a characteristic of a mature individual as it is a character shared by other tyrannosaurs (Fiorillo and Tykoski, 2014). From these data, Fiorillo and Tykoski (2014) estimated a skull length of approximately 60-70 cm and a body length of approximately 6 meters, suggesting an animal approximately half the body length of a full-sized *Tyrannosaurus rex* from the latest Maastrichtian and approximately two-thirds the body length of a correlative *Albertosaurus*.

The evolution of body size changes within insular populations have been studied extensively across a variety of taxa (e.g., Van Valen, 1973; Heaney, 1978; Lomolino, 1985; 2005; Anderson and Handley, 2002; Pafilis et al., 2009; Lomolino et al., 2013, McFadden and Meiri, 2021; van der Geer et al., 2016; Stadler et al., 2022; Hayashi et al., 2023). It is widely recognized that the causes of these changes in body size within insular populations are the result of a combination of selective forces that include geographic characters as well as climate parameters (Heaney, 1978; Lomolino, 1985; 2005; Anderson and Handley, 2002; Lomolino et al., 2012, van der Geer et al., 2016), though there has been some challenges to the broader recognized patterns from some studies of mammalian carnivores and reptiles (Meiri et al., 2005; 2007; Itescu et al., 2018). Fiorillo and Tykoski (2014), followed the broader patterns recognized, and largely attributed the diminutive size of the high-latitude *Nanuqsaurus* when compared to correlative lower-latitude tyrannosaurs to the

FIGURE 5. Reconstruction comparing potential prey sizes, hadrosaurs, and the relative sizes of Aniakchak tyrannosaur (left), and *Nanuqsaurus* (right) in their respective environments. Artwork by Masato Hattori.

isolated depositional setting of the Prince Creek Formation, to the rising Brooks Range in northern Alaska, and suggested this mountain range may have largely separated this section of coastal plain from other parts of North America, and therefore functionally making it serve as an island.

Further, in the modern Arctic there are profound seasonal changes in light regime and such changes affect biological productivity and thus highly impact seasonal resource availability (Blix, 2005, 2016). It has been interpreted that a similarly varying light regime was present in the Cretaceous (e.g., Fiorillo, 2018). These inferred light conditions similarly created limited food resource availability for mega-herbivores, namely the hadrosaurs.

In a recent study (Fiorillo et al., 2022) compared paleoclimate conditions between the Cretaceous of northern Alaska which was at approximately 71°-85°N paleolatitude and the Cretaceous of southern Alaska which had a paleolatitude of approximately 57°N paleolatitude. Fiorillo and others (2022) demonstrated there was some variation in climate parameters, and that differences in conditions were different between northern and southern Alaska during the Cretaceous. Specifically, both mean annual temperature (~5-13°C) and mean annual precipitation (~661- ~1250 mm/year) varied across the region.

The track size of the predatory dinosaur described here contrasts with the projected body size of the diminutive *Nanuqsaurus*. In terms of interpreted body size from track length, the track length of 55 cm for the Aniakchak footprint provides an estimate of body length of greater than 8 meters (see above). This interpreted body length is consistent with the body length of correlative theropods, such as *Albertosaurus*, further to the south. *Albertosaurus* is known from several nearly complete specimens from the Red Deer River area of southern Alberta, Canada, and has a body length of approximately 9 m. This contrast in body size between the far northern tyrannosaur, *Nanuqsaurus*, and the tyrannosaur reported here from Aniakchak National Monument (Fig. 5), suggests a combination of geographic and climatic factors produced different selective pressures on the Tyrannosauridae between the northern and southern extremes of Alaska.

CONCLUSIONS

There are a growing number of records of dinosaurs from Cretaceous rocks around the state of Alaska. Nevertheless, very few fossil records of terrestrial vertebrates are known from the Mesozoic rocks of the southwestern part of the state. With the documentation of a large tyrannosaur track (55 cm long), this study adds new information on the dinosaur footprint record preserved in the Cretaceous Chignik Formation in Aniakchak National Monument of the Alaska Peninsula. This rock unit was deposited at approximately its current latitude of almost 57°N and thus the dinosaurs living in the region were living in the high latitudes.

The track size of the predatory dinosaur described here contrasts with the body size of the diminutive *Nanuqsaurus*, the tyrannosaurid known from bones from the approximately correlative Prince Creek Formation on the North Slope, some

1500 km further north in Alaska. This contrast in body size between the far northern tyrannosaur, and the tyrannosaur reported here suggests that the adaptative pressures of the very far north were different than those experienced in the lower high latitudes.

ACKNOWLEDGMENTS

We thank the National Park Service for their support in all phases of this project. We gratefully thank Troy Hamon of the National Park Service for his enthusiastic support of our work and coordinating critical logistics that have been invaluable to our success. We also thank Dr. Yuong-Nam Lee for the invitation to contribute to a special volume honoring our friend and colleague, Dr. Louis Jacobs. Drs. Ryuji Takasaki and Junki Yoshida provided very helpful reviews which greatly improved this manuscript.

Funding for this field work was graciously and enthusiastically provided by the Friends of Alaska Paleontology. We also thank ISEM at Southern Methodist University for additional support for our project.

AUTHOR CONTRIBUTIONS

ARF, YK, and PJM designed the project. ARF drafted the initial manuscript. All authors contributed to the data gathering, data analysis, and edited the manuscript.

LITERATURE CITED

Alexander, R. McN. (1976). Estimates of speeds of dinosaurs. *Nature*, 261, 129–130.

Anderson, R. P. & Handley Jr, C. O. (2002). Dwarfism in insular sloths: biogeography, selection, and evolutionary rate. *Evolution*, 56(5), 1045–1058.

Atwood, W. W. (1911). Geology and mineral resources of parts of the Alaska Peninsula. *United States Geological Survey Bulletin*, 467, 1–137.

Bacon, C. R., Neal, C. A., Miller, T. P., McGimsey, R. G., & Nye, C. J., (2014). Postglacial eruptive history, geochemistry, and recent seismicity of Aniakchak volcano, *Alaska Peninsula. United States Geological Survey Professional Paper* 1810, 1–74. http://dx.doi.org/10.3133/pp1810.

Beget, J., Mason, O., & Anderson, P. (1992). Age, extent, and climatic significance of the c. 3400 BP Aniakchak tephra, western Alaska, USA. *The Holocene*, 2, 51–56.

Blix, A. S. (2005). *Arctic animals and their adaptations to life on the edge*. Tapir Academic Press.

Blix, A. S. (2016). Adaptations to polar life in mammals and birds. *Journal of Experimental Biology*, 219(8), pp. 1093–1105.

Chinsamy, A., Thomas, D. B., Tumarkin-Deratzian, A. R., & Fiorillo, A. R. (2012). Hadrosaurs were perennial polar residents. *The Anatomical Record*, 295, 610–614.

Cifelli, R. L., Kirkland, J. I., Weil, A., Deino, A. L., & Kowallis, B. J. (1997). High-precision 40Ar/39Ar geochronology and the advent of North America's Late Cretaceous terrestrial fauna. *Proceedings of the National Academy of Sciences*, 94, 11,163–11,167. https://doi.org/10.1073/pnas.94.1.

Detterman, R. L., Miller, T. P., Yount, M. E., & Wilson, F. H. (1981). Geologic map of the Chignik and Sutwik Island Quadrangles, Alaska. 1:250,000. *United States Geological Survey Miscellaneous Investigations Series*, Map I-1229.

Detterman, R. L., Case, J. E., Miller, J. W., Wilson, F. H., & Yount, M. E. (1996). Stratigraphic framework of the Alaska Peninsula. *United States Geological Survey Bulletin*, 1969-A, 1–74.

Dodson, P. (1990). Counting dinosaurs: how many kinds were there? *Proceedings of the National Academy of Sciences*, 87(19), 7608–7612.

Druckenmiller, P. S., Erickson, G. M., Brinkman, D., Brown, C. M., & Eberle, J. J. (2021). Nesting at extreme polar latitudes by non-avian dinosaurs. *Current Biology*, 31(16), pp. 3469–3478.

Enriquez, N. J., Campione, N. E., White, M. A., Fanti, F., Sissons, R. L., Sullivan C, Vavrek, M. J., & Bell, P. R. (2022). The dinosaur tracks of Tyrants Aisle: An Upper Cretaceous ichnofauna from Unit 4 of the Wapiti Formation (upper Campanian), Alberta, Canada. *PLOS ONE* 17(2): e0262824. https://doi.org/10.1371/journal.pone.0262824

Fiorillo, A. R. (2008). Cretaceous dinosaurs of Alaska: Implications for the origins of Beringia. In R. B. Blodgett & G. Stanley (Eds.), *The Terrane Puzzle: New perspectives on paleontology and stratigraphy from the North American Cordillera* (pp. 313–326). Geological Society of America Special Paper 442. Boulder: Geological Society of America.

Fiorillo, A. R. (2018). *Alaska Dinosaurs: an Ancient Arctic World*. CRC Press, Boca Raton.

Fiorillo, A. R. & Gangloff, R. A. (2001). The caribou migration model for Arctic hadrosaurs (Dinosauria: Ornithischia): A reassessment. *Historical Biology*, 15, 323–334.

Fiorillo, A. R. & Parrish, J. T. (2004). The first record of a Cretaceous dinosaur from western Alaska. *Cretaceous Research*; 25, 453–458.

Fiorillo, A. R. & Adams, T. L. (2012). A therizinosaur track from the Lower Cantwell Formation (Upper Cretaceous) of Denali National Park, Alaska. *PALAIOS*, 27, 395–400.

Fiorillo, A. R. & Tykoski, R. S. (2014). A diminutive new tyrannosaur from the top of the world. *PLOS ONE*, 9(3), p.e91287. https://doi.org/10.1371/journal.pone.0091287

Fiorillo, A. R., Hasiotis, S. T., & Kobayashi, Y. (2014). Herd structure in Late Cretaceous polar dinosaurs: a remarkable new dinosaur tracksite, Denali National Park, Alaska, USA. *GEOLOGY*, 42, 719–722.

Fiorillo, A. R. & Tykoski, R. S. (2016). Small hadrosaur manus and pes tracks from the lower Cantwell Formation (Upper Cretaceous), Denali National Park, Alaska: Implications for locomotion in juvenile hadrosaurs. *PALAIOS*, 31, 479–482.

Fiorillo, A. R., McCarthy, P. J., Kobayashi, Y., & Tanaka, T. (2018). Duck-billed Dinosaurs (Hadrosauridae), Ancient Environments, and Cretaceous Beringia in Alaska's National Parks. *Alaska Park Science*, 17, 20–27.

Fiorillo, A. R., McCarthy, P. J., Kobayashi, Y., Tomisch, C. S., Tykoski, R. S., Lee, Y.-N., Tanaka, T., & Noto, C. R. (2018) An unusual

association of hadrosaur and therizinosaur tracks within Late Cretaceous rocks of Denali National Park, Alaska. *Scientific Reports* 8; https://doi.org/10.1038/s41598-018-30110-8 PMID: 30076347

Fiorillo, A. R., Kobayashi, Y., McCarthy, P. J., Tanaka, T., Tykoski, R. S., Lee Y.-N., Takasaki, R., & Yoshida, J. (2019). Dinosaur ichnology and sedimentology of the Chignik Formation (Upper Cretaceous), Aniakchak National Monument, southwestern Alaska; Further insights on habitat preferences of high-latitude hadrosaurs. *PLOS ONE* 14(10): e0223471. https://doi.org/10.1371/journal.pone.0223471

Fiorillo, A. R., McCarthy, P. J., Kobayashi, Y., & Suarez, M. B. (2022). Cretaceous Dinosaurs across Alaska Show the Role of Paleoclimate in Structuring Ancient Large-Herbivore Populations. *Geosciences* 12(4), 161, https://doi.org/10.3390/geosciences12040161.

Flaig, P. P., McCarthy, P. J., & Fiorillo, A. R. (2011). A tidally influenced, high-latitude coastal plain: the Upper Cretaceous (Maastrichtian) Prince Creek Formation, North Slope, Alaska. In S. Davidson, S. Leleu, & C. North (Eds.), *From River to Rock Record: the Preservation of Fluvial Sediments and their Subsquent Interpretation* (pp. 233–264). Tulsa, SEPM (Society for Sedimentary Geology), Special Publication 97.

Flaig, P. P., Fiorillo, A. R., & McCarthy, P. J. (2014). Dinosaur-bearing hyperconcentrated flows of Cretaceous Arctic Alaska: recurring catastrophic event beds on a distal paleopolar coastal plain. *PALAIOS*, 29, 594–611.

Gangloff, R. A. & Fiorillo, A. R. (2010). Taphonomy and paleoecology of a bonebed from the Prince Creek Formation, North Slope, Alaska. *PALAIOS*, 25(5), 299–317.

Hayashi, S., Kubo, M.O., Sánchez-Villagra, M.R., Taruno, H., Izawa, M., Shiroma, T., Nakano, T., & Fujita, M. (2023). Variation and process of life history evolution in insular dwarfism as revealed by a natural experiment. *Frontiers in Earth Science*, 11: 1095903. doi: 10.3389/feart.2023.1095903

Heaney, L. R. (1978). Island area and body size of insular mammals: evidence from the tri-colored squirrel (*Calliosciurus prevosti*) of Southeast Asia. *Evolution*, 32, 29–44.

Henderson, D. (2003). Footprints, trackways, and hip heights of bipedal dinosaurs—testing hip height predictions with computer models. *Ichnos*, 10, 99–114.

Hillhouse, J. W. & Coe R. S. (1994). Paleomagnetic data from Alaska. In G. Plafker & H. C. Berg (Eds.), *Geology of Alaska* (pp. 797–812). The Geology of North America, G-1. Boulder: Geological Society of America.

Hubbard, B. R. (1931). A world inside a mountain, the new volcanic wonderland of the Alaska Peninsula, is explored. *National Geographic Society* 60, 319–345.

Itescu, Y., Schwarz, R., Donihue, C. M., Slavenko, A., Roussos, S. A., Sagonas, K., Valakos, E. D., Foufopoulos, J., Pafilis, P., & Meiri, S. (2018). Inconsistent patterns of body size evolution in co-occurring island reptiles. *Global Ecology and Biogeography*, 27(5), 538–550.

Jaggar, T. A. (1932). *The Volcano Letter*, 375, 1–3.

Kobayashi, Y., Nishimura, T., Takasaki, R., Chiba, K., Fiorillo, A. R., Tanaka, K., Chinzorig, T., Sato, T., & Sakurai, K. (2019). A new hadrosaurine (Dinosauria: Hadrosauridae) from the marine deposits of the Late Cretaceous Hakobuchi Formation, Yezo Group, Japan. *Scientific Reports*, 9(1), p. 12389. https://doi.org/10.1038/s41598-019-48607-1

Lockley, M. G. & Hunt, A. P. (1994). A track of the giant theropod dinosaur *Tyrannosaurus* from close to the Cretaceous/Tertiary boundary, northern New Mexico. *Ichnos*, 3(3), 213–218.

Lomolino, M. V. (1985). Body size of mammals on islands: the island rule re-examined. *The American Naturalist*, 125, 310–316.

Lomolino, M. V. (2005). Body size evolution in insular vertebrates: generality of the island rule. *Journal of Biogeography*, 32, 1683–1699.

Lomolino, M. V., van der Geer, A. A., Lyras, G. A., Palombo, M. R., Sax, D. F., & Rozzi, R. (2013). Of mice and mammoths: generality and antiquity of the island rule. *Journal of Biogeography*, 40, 1427–1439.

Manning, P. L., Ott, C., & Falkingham, P. L. (2008). A probable tyrannosaurid track from the Hell Creek Formation (Upper Cretaceous), Montana, United States. *PALAIOS*, 23(10), 645–647.

McCrea, R. T., Buckley, L. G., Farlow, J. O., Lockley, M. G., Currie, P. J, Matthews, N. A., & Pemberton, S. G. (2014). A 'Terror of Tyrannosaurs': The first trackways of tyrannosaurids and evidence of gregariousness and pathology in Tyrannosauridae. *PLOS ONE*, 9(7), e103613. doi:10.1371/journal.pone.0103613

McFadden, K. W. & Meiri, S. (2012). Dwarfism in insular carnivores: a case study of the pygmy raccoon. *Journal of Zoology*, 289(3), 213–221.

Meiri, S., Dayan, T., & Simberloff, D. (2005). Area, isolation and body size evolution in insular carnivores. *Ecology Letters*, 8(11), 1211–1217.

Meiri, S. (2007). Size evolution in island lizards. *Global Ecology and Biogeography*, 16(6), 702–708.

Miller, T. P. & Smith, R. L. (1987). Late Quaternary caldera-forming eruptions in the eastern Aleutian arc, Alaska. *GEOLOGY*, 15, 434–438.

Molnar, R. E. (1980). An albertosaur from the Hell Creek formation of Montana. *Journal of Paleontology*, 54, 102–108.

Olsen, P. E., Smith, J. B., & McDonald, N. G. (1998). Type material of the type species of the classic theropod footprint genera *Eubrontes*, *Anchisauripus*, and *Grallator* (Early Jurassic, Hartford and Deerfield basins, Connecticut and Massachusetts, U.S.A.). *Journal of Vertebrate Paleontology*, 18, 586–601.

Pafilis, P., Meiri, S., Foufopoulos, J., & Valakos, E. (2009). Intraspecific competition and high food availability are associated with insular gigantism in a lizard. *Naturwissenschaften*, 96(9), 1107–1113.

Parrish, J. M., Parrish, J. T., Hutchison, J. H., & Spicer, R. A. (1987). Late Cretaceous vertebrate fossils from the North Slope of Alaska and implications for dinosaur ecology. *PALAIOS*, 2, 377–389.

Phillips, R. L. (2003). Depositional environments and processes in Upper Cretaceous nonmarine and marine sediments, Ocean Point dinosaur locality, North Slope, Alaska. *Cretaceous Research*, 24(5), 499–523.

Razzolini, N. L., Oms, O., Castanera, D., Vila, B., Santos, V. F. D., & Galobart, À. (2016). Ichnological evidence of megalosaurid dinosaurs crossing Middle Jurassic tidal flats. *Scientific Reports*, 6(1), p. 31494.

Razzolini, N. L., Belvedere, M., Marty, D., Paratte, G., Lovis, C., Cattin, M., & Meyer, C. A. (2017) *Megalosauripus transjuranicus* ichnosp. nov. A new Late Jurassic theropod ichnotaxon from NW Switzerland and implications for tridactyl dinosaur ichnology and ichnotaxomy. *PLOS ONE* 12(7): e0180289. https://doi.org/10.1371/journal.pone. 0180289.

Russell, D. A. (1993). The role of central Asia in dinosaurian biogeography. *Canadian Journal of Earth Sciences*, 30, 2002–2012.

Sereno, P. C. (2000). The fossil record, systematics, evolution of pachycephalosaurs and ceratopsians from Asia. In M. J. Benton, M.

A. Shishkin, D. M. Unwin, & E. N. Kurochkin (Eds.), *The age of dinosaurs in Russia and Mongolia* (pp. 480–516). Cambridge: Cambridge University Press.

Smith, J. B. & Farlow, J. O. (2003). Osteometric approaches to trackmaker assignment for Newark Supergroup ichnogenera *Grallator*, *Anchisauripus*, and *Eubrontes*. In P. M. LeTourneau & P. E. Olsen (Eds.) *The Great Rift Valleys of Pangea in Eastern North America, Vol. 2: Sedimentology, Stratigraphy, and Paleontology* (pp. 273–292). Columbia University Press, New York.

Stadler, S. R., Brock, K. M., Bednekoff, P. A., & Foufopoulos, J. (2022). More and bigger lizards reside on islands with more resources. *Journal of Zoology*, 319(3), pp. 163–174.

Thulborn, T. (2001). History and nomenclature of the theropod dinosaur tracks *Bueckeburgichnus* and *Megalosauripus*. *Ichnos*, 8, 207–222.

van der Geer, A. A., van den Bergh, G. D., Lyras, G. A., Prasetyo, U. W., Due, R. A., Setiyabudi, E., & Drinia, H. (2016). The effect of area and isolation on insular dwarf proboscideans. *Journal of Biogeography*, 43(8), pp.1656–1666.

Van Valen, L. (1973). Pattern and the balance of nature. *Evolutionary Theory*, 1, 31–49.

Weems, R. E. (1992). A re-evaluation of the taxonomy of Newark Supergroup saurischian dinosaur tracks, using extensive statistical data from a recently exposed tracksite near Culpeper, Virginia: Richmond. *Virginia Division of Mineral Resources*, 119, 113–127.

Wilson, F. H., Detterman, R. L., & DuBois, G. D. (1999). Digital data for geologic framework of the Alaska Peninsula, southwest Alaska,and the Alaska Peninsula terrane. *United States Geological Survey, Open-File Report*, OFR 99–317.

Zanno, L. E. (2010). A taxonomic and phylogenetic re-evaluation of Therizinosauria (Dinosauria: Maniraptora). *Journal of Systematic Palaeontology*, 8, 503–543.

WINDOWS INTO SAUROPSID AND SYNAPSID EVOLUTION
Essays in honor of Prof. Louis L. Jacobs, pp. 222–232, 2023

INSIGHT ON INTERACTIONS AMONG CLIMATIC, BIOTIC, AND ATMOSPHERIC PROCESSES DURING THE MID-CRETACEOUS USING TERRESTRIAL DEPOSITS IN TEXAS AND OKLAHOMA

KATE A. ANDRZEJEWSKI[1,*], ANDREAS MÖLLER[2], and CHRISTOPHER R. NOTO[3]

[1]Kansas Geological Survey, University of Kansas, Lawrence, Kansas, 66047, U.S.A., geokate@ku.edu;
[2]Department of Geology, University of Kansas, Lawrence, Kansas, 66045, U.S.A., amoller@ku.edu;
[3]Deparment of Biological Sciences, University of Wisconsin-Parkside, Kenosha, Wisconsin, 53141, U.S.A., noto@uwp.edu

ABSTRACT Chemical, mineralogical, and stable isotopic proxies are applied to reconstruct paleoclimatic and paleoatmospheric conditions during the Mid-Cretaceous (Aptian-Cenomanian) using terrestrial deposits from fossil localities in north-central Texas and southern Oklahoma. These results in conjunction with analyses of the $\delta^{13}C$ of plant organic material at each locality are compared to investigate interactions between biotic responses in plant organic matter to changes in paleoprecipitation and paleoatmospheric pCO_2. Results show a strong correlation between mean annual precipitation (MAP) and the $\delta^{13}C$ of plant organic matter. Localities reporting low paleoprecipitation estimates correlate with more positive $\delta^{13}C$ organic matter values, consistent with modern observations. Less understood and constrained is the influence of changes in pCO_2 levels on $\delta^{13}C$ of plant organic matter. Using paleosol carbonates, we show a decrease in $\delta^{13}C$ of occluded organic matter associated with increases in estimated atmospheric pCO_2 levels, with an estimated pCO_2 effect of -0.9‰ ± -0.5‰ per 100 ppmV on the $\delta^{13}C$ values of organic matter collected from two localities with similar paleoprecipitation estimates. U-Pb dating of zircon collected from the Jones Ranch locality indicates a maximum depositional age of 113.1 ± 1.5 Ma (n=4). This provides the first reported absolute age for the Twin Mountains Formation and is a valuable time constraint for a reported increase in atmospheric pCO_2 occurring at the Aptian/Albian boundary and at the onset of the OAE1b interval. Together these data exhibit how deep time proxies from terrestrial deposits can contribute to our knowledge and understanding of interactions among biotic, climatic, and atmospheric processes while also providing crucial paleoclimatic and paleoatmospheric data for periods of greenhouse climate conditions.

KEYWORDS Cretaceous, Paleoclimate, Paleosols, Stable Isotopes, Maximum depositional age

INTRODUCTION

The transition from Lower to Upper Cretaceous deposits in Texas and Oklahoma captures significant changes in the biologic, climatic, and geographic spheres at both regional and global scales. Regionally, this includes dynamic evolutionary changes with major faunal turnover events among archosaurs and mammals, the rise of angiosperms, and the first appearance of snakes and marsupial taxa (Jacobs and Winkler, 1998; Winkler et al., 2015). Additionally, these biotic changes occur during intervals of major paleogeographic changes with a transgression of the Glen Rose Sea onto the Texas craton around the Aptian/Albian boundary, followed by the formation and completion of the Western Interior Seaway (Haq et al., 1987; Kauffman and Caldwell, 1993; Slattery et al., 2015). Globally, this time frame (Aptian-Cenomanian) also encompasses several major perturbations in the global carbon cycle, which are associated with the widespread development of anoxic-euxinic conditions in the ocean basins, known as Ocean Anoxic Events (OAE's; Schlanger and Jenkyns 1976; Jenkyns, 1980, 2010; Arthur et al. 1987; Schlanger et al.; 1987). These include the Early Albian OAE1b (Jenkyns, 2010), the Albian-Cenomanian OAE1d (Gröcke et al., 2006; Richey et al., 2018), and the mid-Cenomanian Event (MCE; Coccioni and Galeotii, 2001). Several studies have attempted to place these events in the context of abiotic and biotic factors including regional paleogeographic changes with the formation and completion of the Western Interior Seaway (Jacobs and Winkler 1998, Winkler et al., 2015) and changes in paleoclimate (Andrzejewski & Tabor, 2020).

*Corresponding author

Deciphering the influence of regional and global changes in deep time is difficult given numerous factors including incomplete sedimentary records, uncertainty in stratigraphic correlation, and varied sample preservation. Paleosols constitute a large part of the terrestrial sedimentary record and thus provide a wealth of information regarding Earth history (Retallack, 1986). Paleosols capture slices of geologic time and provide a unique interface where biotic, climatic, and atmospheric processes interact. This allows paleosols to record important factors that can be used to reconstruct paleoenvironment and estimate paleotemperature, paleoprecipitation, terrestrial organic matter carbon values, paleoatmospheric pCO_2 levels, and absolute geologic age (e.g. Sheldon and Tabor, 2009; Tabor and Myers, 2015, Tabor et al., 2017; Smith et al., 2017; Joeckel et al., 2023). Given the preservation of paleosols in terrestrial units during the transition from Lower to Upper Cretaceous in Texas and Oklahoma, we apply current methodologies and developed proxies to investigate the possible influences of regional and global paleoprecipitation and paleoatmospheric pCO_2 on changes in the $\delta^{13}C$ of terrestrial organic matter.

GEOLOGICAL SETTING

This study analyzes data collected from 5 localities, spanning the Lower to Upper Cretaceous (Aptian-Cenomanian) stratigraphy of north-central Texas and southern Oklahoma. This includes two fossil localities from the Twin Mountains Formation in north-central Texas: Proctor Lake (PL) and Jones Ranch (JR), one locality in the Antlers Formation of southern Oklahoma: (CR), and two localities in the Woodbine Group in north-central Texas: the Arlington Archosaur Site (AAS), and Acme Brick Pit (ABP) (Fig. 1). Correlation of these localities is difficult as the succession includes the time-transgressive progradational-retrogradational sequence of the Western Interior Seaway. However, the stratigraphic analysis by Jacobs and Winker, (1998) provides sufficient constraints to place these localities within a framework that ensures chronological order, albeit without chronometric dates (Fig. 1). Andrzejewski and Tabor, (2020) and Andrzejewski et al., (2022) report data from paleosols sampled at these localities including paleo-precipitation, paleotemperature, and atmospheric pCO_2 estimates which will be referenced herein.

The Twin Mountains Formation represents the lowest Cretaceous deposits in north-central Texas and lies unconformably upon Pennsylvanian and Permian strata (Young, 1967). The overlying Glen Rose Formation contains ammonite faunas used to define the Aptian-Albian boundary indicating the Twin Mountains Formation is Aptian in age (Young, 1967; Scott, 1940; Young, 1974; Young 1986). Exposures of the Twin Mountains Formation have been interpreted as sedimentary deposits of meander belt fluvial systems transitioning stratigraphically upward to marginal marine deposits (Hall, 1976). The Proctor Lake locality lies approximately 17 m above the Pennsylvanian contact and 35 m below the Glen Rose Formation contact. The Jones Ranch fossil locality occurs stratigraphically higher in the Twin Mountains Formation, occurring approximately 9.7 m below the Glen Rose Formation contact. Morphology and data produced from the paleosols sampled from these localities are described in Andrzejewski and Tabor (2020) and Andrzejewski et al. (2022).

The marine-dominated Glen Rose Formation pinches out to the north, juxtaposing the terrestrial-dominated Twin Mountains and Paluxy Formations which combine to form the Antlers Formation (Fig. 1). The Antlers Formation contains claystone layers with unconsolidated sandstone lenses and carbonate concretions that have been interpreted as fluvial, deltaic, and strandplain settings (Winkler et al.1990; Hobday et al. 1981). The absence of the Glen Rose Formation as a biostratigraphic marker makes it difficult to determine precise stratigraphic positions of localities within the Antlers Formation. Locality CR sampled in southern Oklahoma is stratigraphically equivalent with the fossil locality OMNH V706, which is considered to be located in the middle of the Antlers Formation, approximately 87 m above the base and stratigraphically above the PL and JR localities (Cifelli et al., 1997).

The Woodbine Group has a long history of revisions in stratigraphic subdivision and nomenclature based on differing interpretations of surface exposures versus subsurface drill cores and wireline logs (Ambrose et al. 2009; Berquist, 1949; Dodge 1952; Dodge 1968; Hentz et al. 2014; Johnson, 1974; Murlin, 1975; Oliver, 1971; Trudel, 1994). Current stratigraphic subdivision recognizes two units: the Dexter and Lewisville Formations. The lower Dexter Formation represents marginal and marine environments (Berquist, 1949; Dodge, 1952; Dodge 1968; Dodge, 1969; Johnson, 1974; Oliver, 1971) while the overlying Lewisville Formation represents a low-lying coastal plain (Main, 2009; Oliver, 1971; Powell, 1968). Both the Arlington Archosaur Site and Acme Brick Pit localities occur in the middle to upper Lewisville Formation.

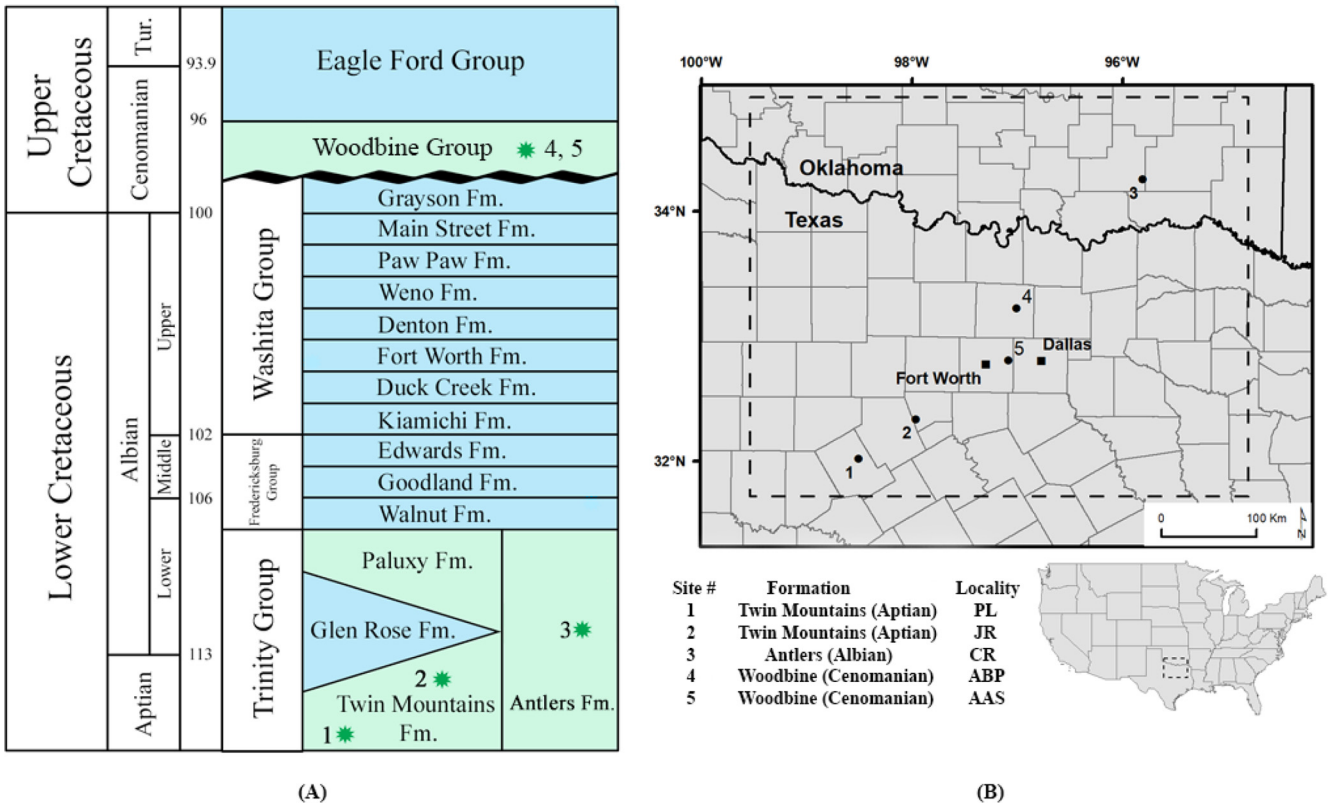

FIGURE 1. Regional stratigraphic column and map of study area: (A) lithostratigraphic units spanning the Early to Late Cretaceous interval of north-central Texas and southern Oklahoma (modified from Jacobs and Winkler, 1998). (B) map displaying the study area with localities correlating to the site number listed with collected samples: 1 = Proctor Lake locality (PL), 2 = Jones Ranch locality (JR), 3 = Cross locality (CR), 4 = Acme Brick Pit (ABP), 5 = Arlington Archosaur Site (AAS).

Due to lack of surface exposures and chronostratigraphic constraint exact stratigraphic relationship between the two localities cannot be determined. The presence of the ammonite *Conlinoceras tarrantense* has been used to indicate an early middle Cenomanian age (~96 Ma) for Lewisville Formation strata (Kennedy and Cobban, 1990; Emerson et al., 1994; Lee, 1997a, b; Jacobs and Winkler; 1998; Gradstein et al., 2004). However, Ambrose et al., (2009) suggest that upper portions of the Lewisville Formation were deposited during the late Cenomanian, with overall deposition of the Woodbine Group ending around 92 Ma. Andrzejewski and Tabor, (2020) contains descriptions of the Arlington Archosaur Site and Acme Brick Pit, including detailed descriptions of the sampled paleosols.

METHODS

Bulk paleosol samples were collected approximately every 10 cm from the measured section at the Arlington Archosaur Site. Two bulk samples were collected at the Acme Brick Pit site, one from the paleosol B horizon and one 15 cm above the B horizon. New $\delta^{13}C$ values for bulk sedimentary organic matter reported from the Woodbine Group were produced at the Keck Palaeoenvironmental and Environmental Stable Isotope Lab at the University of Kansas. Samples were powdered with mortar and pestle to generate approximately 1 g of powder. Samples were then decarbonated with 0.5 M hydrochloric acid for at least 24 h or until samples no longer reacted with fresh acid. Samples were then rinsed with deionized water by centrifugation and decanting until no longer acidic. Rinsed samples were then dried at 50°C. Approximately 0.3-2 mg per sample were combusted with a Costech elemental analyzer, with the resulting CO_2 analyzed with a ThermoFinnigan MAT 253 continuous-flow isotope ratio mass spectrometer. All samples are reported relative to V-PDB, with accuracy monitored by analysis of internal

standards IAEA-600 and USGS 24 to within 0.1‰. Methodology for previously reported chemical, mineralogical, and stable isotopic analyses can be found in Andrzejewski and Tabor, (2020) and Andrzejewski et al. (2022).

A 5 cm interval of bulk paleosol sample collected approximately 50 cm below the top of the B horizon from the Jones Ranch Quarry was selected for detrital zircon U-Pb geochronology. Zircon grains were separated from bulk paleosol material at the University of Kansas Isotope Geochemistry Laboratories by a combination of chemical and physical disaggregation and heavy-mineral separation techniques including a disk mill, ultrasonic bath (Hoke et al. 2014), Frantz^{TM} isodynamic magnetic separator, and heavy liquids (methylene iodide). At least 175 grains were handpicked under a binocular microscope and mounted on double sided tape. The purpose of the investigation is determination of the age of deposition based on the premise that mature paleosols may be cryptotephra, as they can capture volcanic zircons during the time period of soil formation (Smith et al., 2017 Joeckel et al., 2023). During grain picking preference was therefore given to euhedral, unabraded, colorless, zircons to maximize the chance to find the youngest, non-detrital zircons. Results for older, detrital grains are therefore not providing an unbiased sample of the entire detrital population, but only a qualitative example of older populations, and should not be used in statistical comparisons and likeness tests. U-Pb zircon ages were determined by laser ablation inductively coupled plasma mass spectrometry (LA-ICP-MS) using a Photon Machines Analyte G2 193 nm ArF excimer laser ablation system coupled with a Thermo Scientific Element2 ICP-MS. Circular 15 µm spots were ablated with the laser at 1.3 J/cm^2 fluence with a 10 Hz repetition rate for 25 seconds, and ablated material was carried to the ICP-MS in helium gas with a 1 L/min combined flow rate. Downhole elemental and isotopic fractionation and calibration drift were corrected by bracketing measurements of unknowns with zircon reference materials using the IOLITE software package (Paton et al., 2011) and the VizualAge data reduction scheme (Petrus and Kamber, 2012). Zircon GJI (Jackson et al., 2004) was used for calibration, the zircon reference materials Plesovice (Sláma et al., 2008), Fish Canyon Tuff (FCT, Wotzlaw, 2013), Duluth Gabbro (FCSZ, Paces and Miller, 1993) were used to validate the calibration. All reference materials matched the published ages within 1% uncertainty. Analytical results are presented using Isoplot (Vermeesch, 2018). The maximum age of deposition was determined from the youngest population of grains. Kernel density estimates (KDEs) were produced using DensityPlotter 7.1 (Vermeesch 2012).

RESULTS

The $\delta^{13}C$ of bulk sedimentary organic matter collected from two localities in the Woodbine Group ranged from −22.2 to −26.1‰ with an average of −24.6‰ reported from 23 samples (Table 1). The $\delta^{13}C$ values reported for organic matter in the Woodbine Group are consistent with C3 vegetation shown to dominate the Cretaceous landscape (Koch, 1998). These reported values are combined with previous analyses of organics occluded in paleosol carbonate nodules from Andrzejewski et al. (2022) and shown in Fig. 2(A). While comparing the $\delta^{13}C$ of plant organic matter, we note that results from Myers et al. (2016) indicate an ~1‰ offset between average $\delta^{13}C$ values of bulk and occluded organic matter; however, this offset is far less than the overall range $\delta^{13}C$ values of plant organic matter reported at the localities and does not affect the results of the produced chemostratigraphic profile. Results from this combined chemostratigraphic profile show a sharp decrease of ~3.0‰ in the mean $\delta^{13}C$ of organic matter from the Proctor Lake locality to the Jones Ranch locality in the Twin Mountains Formation. This is followed by a smaller decrease in the mean $\delta^{13}C$ of organic matter of ~0.6‰ from the Jones Ranch locality in the Twin Mountains formation to the Oklahoma localities in the Antlers Formation. The mean $\delta^{13}C$ of organic matter between localities in the Antlers Formation and the Woodbine Group appear to be fairly consistent with their mean values overlapping.

Results showing the concordia ages of the 4 youngest concordant zircon grains from a total population of 175 zircon grains analyzed from the Jones Ranch locality in the Twin Mountains Formation are shown in Figs. 3 and 4. The youngest four overlapping zircon U-Pb results from this population (2.3% of total) yield a maximum depositional age of 113.1 ± 1.5 Ma. Microscope images of these four euhedral zircon grains are shown in Fig. 3, indicating minimal detrital transport of these grains. This age fits within the span of the Aptian/Albian stage boundary and is consistent with previously reported age estimates of the locality based on stratigraphic relationship and overlying biostratigraphic markers in the Glen Rose Formation (Young, 1967; Scott, 1940; Young,

TABLE 1. Measured $\delta^{13}C$ of organic matter ($\delta^{13}C_{OM}$ ‰ VPDB), of acid-treated bulk paleosol samples from the Woodbine Group (Cenomanian)

Location	Sample	Formation (Age)	$\delta^{13}C_{om}$ (‰ VPDB)
Arlington Archosaur Site	15CS717-1	Woodbine Group (Cenomanian)	-24.15
	15CS717-2		-26.09
	15CS717-3		-23.58
	15CS717-4		-25.19
	15CS717-5		-22.22
	15CS717-6		-24.98
	15CS717-7		-24.21
	15CS717-8		-25.42
	15CS717-9		-23.62
	15CS717-10		-24.58
	15CS717-11		-24.08
	15CS717-15		-23.28
	15CS717-17		-24.24
	15CS717-18		-25.01
	15CS717-19		-24.69
	15CS717-20		-25.03
	15CS717-21		-25.73
	15CS717-9 proximal end		-23.44
	15CS717-9 middle		-24.00
	15CS717-9 distal end		-23.69
	AA1		-25.59
Acme Brick Pit		Woodbine Group (Cenomanian)	
	Above ABP		-25.92
	ABP B Horizon		-25.83

1974; Young, 1986). These results provide the first absolute age determined for the upper Twin Mountains Formation and the Jones Ranch fossil locality.

DISCUSSION

The $\delta^{13}C$ or plant organic matter is thought to be influenced by several factors, the most influential being mean annual precipitation (Swap et al., 2004; Schulze et al., 1998). Modern studies show C_3 plants that are water stressed and receive lower amounts of mean annual precipitation correlate with more positive $\delta^{13}C$ values (Kohn, 2010; Ma et al., 2012). The Cretaceous record in Texas and Oklahoma is consistent with this relationship, as shown by the $\delta^{13}C$ of organic matter results of this study and Andrzejewski et al. (2022) in relation to paleoprecipitation estimates produced by Andrzejewski and Tabor (2020) (Fig. 2). The PL locality recorded the most positive $\delta^{13}C$ organic matter values, averaging −21.3‰ which correlate to the lowest MAP estimates averaging 331 ± 110 mm/yr. Localities in the Antlers Formation and Woodbine Group with significantly higher MAP estimates ranging from 952 ± 110 to 1486 ± 110 mm/yr contain more negative $\delta^{13}C$ organic matter values ranging from −23.3 to −26.1‰. These periods of higher estimated mean annual precipitation correspond to and are likely driven by various transgressions onto the Texas craton during sea level

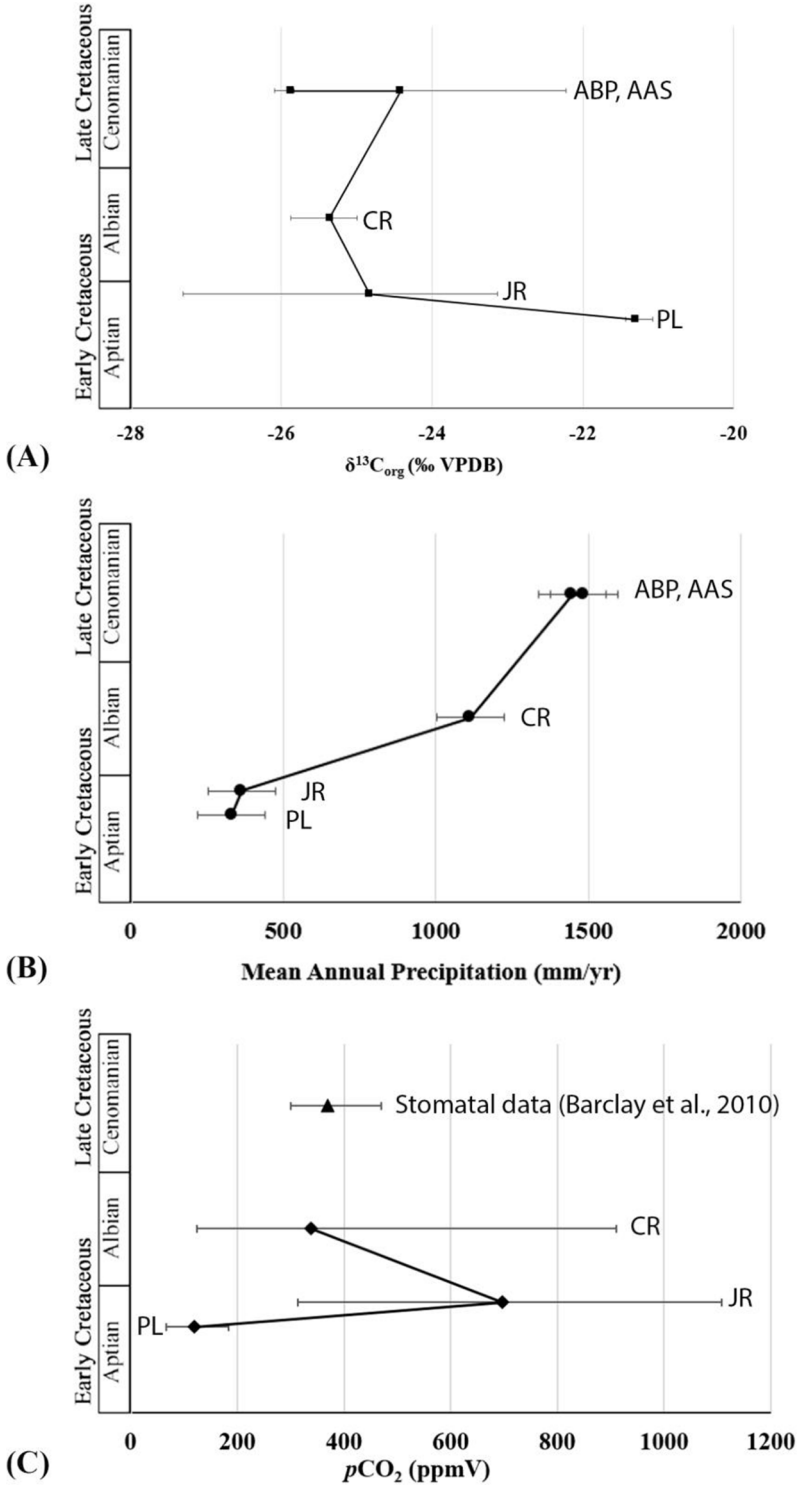

FIGURE 2. (A) Measured $\delta^{13}C$ of organic matter from this study and Andrzejewski et al. (2022). Squares represent the mean $\delta^{13}C$ of organic matter of each locality and error bars show minimum and maximum values recorded. (B) Mean annual precipitation estimates for each locality produced from weathering proxies of bulk paleosol material (Andrzejewski and Tabor 2020). Circles represent estimated value with a reported error of ±110 mm/yr. (C) Atmospheric pCO_2 estimates produced from paleosol carbonates at localities PL, JR, and CR with mean estimates represented as diamonds and error bars showing minimum and maximum estimated values (Andrzejewski et al. 2022). Atmospheric pCO_2 estimates produced from stomatal data from Cenomanian deposits in Utah with mean estimate represented as triangle with error bars showing minimum and maximum estimated values (Barclay et al., 2010).

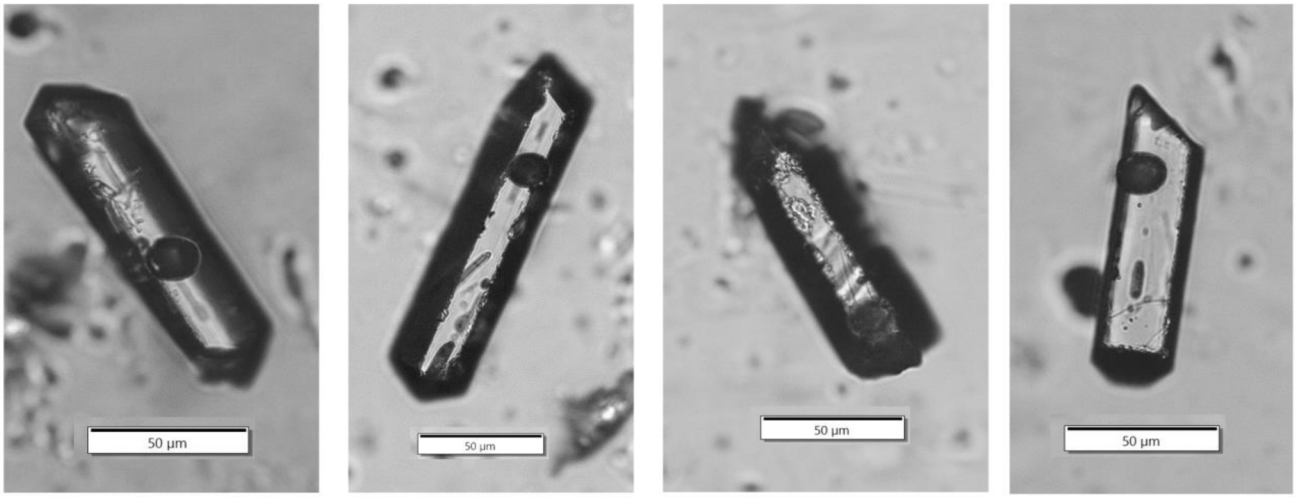

FIGURE 3. Microscopic images of the youngest population of zircon grains analyzed from the Jones Ranch locality in the Twin Mountains Formation. Note circles on the grains where laser ablation sample was targeted. Scale bar equals 50 µm.

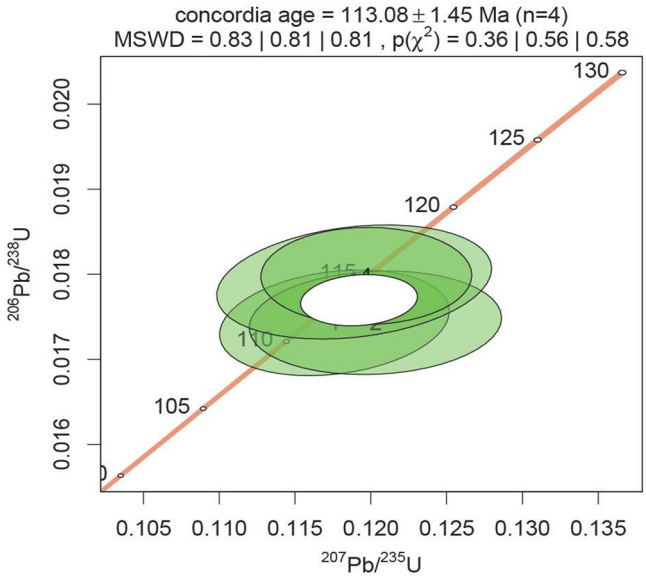

FIGURE 4. Concordia plot of youngest population of zircon grains (n = 4) collected from the Jones Ranch locality in the Twin Mountains Formation. Analysis reveals an age of 113.1 ± 1.45 MA.

highstands, which provided new moisture sources (Andrzejewski and Tabor, 2020). However, mean annual precipitation does not explain the significant decrease in the $\delta^{13}C$ of organic matter between the PL and JR localities in the Twin Mountains Formation as both exhibit similar MAP estimates of 331 ± 110 and 365 ± 100 mm/yr respectively.

The lack of consistency between precipitation and the $\delta^{13}C$ of plant organic matter when comparing the PL and JR localities leads to the less understood and constrained influence that changes in atmospheric pCO_2 levels have on the $\delta^{13}C$ of plant organic matter. While the relationship between fluctuating atmospheric pCO_2 levels and the $\delta^{13}C$ of plant organic matter is still debated, two recent studies have shown a negative correlation, with increased atmospheric pCO_2 levels corresponding to more negative $\delta^{13}C$ signatures in plant organic matter (Breecker, 2017; Hare et al. 2018). A study by Hare et al. (2018) found a pCO_2 effect on the $\delta^{13}C$ of organic matter in gymnosperms of −1.4 ± 1.2‰ per 100ppmV during the last deglaciation using ice cores and fossil plant materials. Results from Breecker (2017) found a pCO_2 effect on the $\delta^{13}C$ of organic matter of −1.6 ± 0.3‰ per 100 ppmV (1σ) during the Quaternary using data collected from speleothems. Atmospheric pCO_2 estimates produced in Andrzejewski et al. (2022) using paleosol carbonates show a significant increase between the PL and JR localities in the Twin Mountains Formation with atmospheric pCO_2 from locality PL ranging from 67-183 ppmV to locality JR ranging from 313-1108 ppmV (Fig. 2). Given that both the PL and JR localities have similar paleoprecipitation estimates yet show a negative shift of ~3.5‰ in the $\delta^{13}C$ of organic matter it provides an opportunity to estimate the influence of changes in atmospheric pCO_2 levels on the $\delta^{13}C$ of organic matter during the Early Cretaceous. When the average pCO_2 estimates from the PL and JR localities are combined with the negative 3.5‰ shift

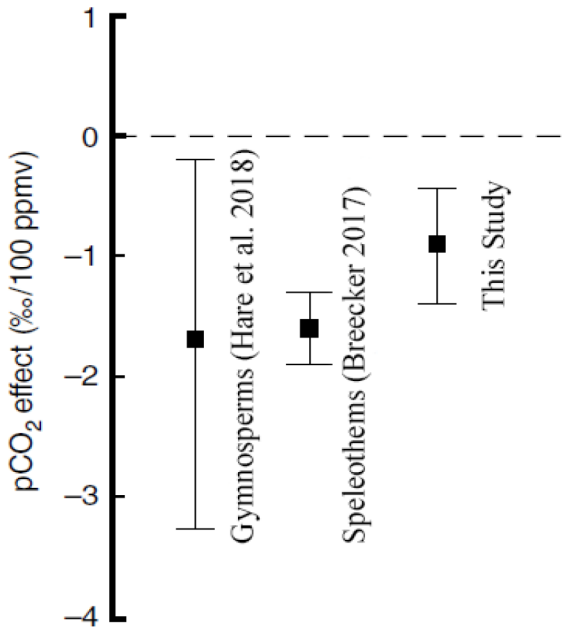

FIGURE 5. Effect of atmospheric pCO_2 on mean stable carbon isotope composition of plant organic matter (modified from Hare et al., 2018). Estimate from Hare et al. (2018) include data produced from gymnosperms from the last deglaciation. Estimate from Breecker (2017) include data from speleothems from the Quaternary. Estimate from this study include data from paleosol carbonates during the Aptian/Albian.

in organic carbon values it reveals a pCO_2 effect on the $\delta^{13}C$ of organic matter of −0.9 ± 0.5‰ per 100ppmV (Fig. 5). This range appears consistent with the studies conducted by Hare et al. (2018) and Breecker (2017). Notably, these results confirm the direct influence of global atmospheric processes on terrestrial organic carbon in deep time.

To further investigate the significant increase in atmospheric pCO_2 a bulk paleosol sample was collected from the JR locality to extract and date zircon grains by the U-Pb method. Paleosols have been shown to be a great source for volcanic zircon, yielding U-Pb ages close to the age of deposition (e.g. Smith et al. 2017). Many paleosols can be referred to as cryptotephras. While they may not stand out as immediately recognizable volcanic ash deposition in the field like white bentonite clay layers, they may contain microscopic fragments from volcanic tephra deposits that can be separated and analyzed using technical laboratory techniques (Davies, 2015; Joeckel et al., 2023). Results from the analyzed 175 zircon grains in this study revealed a youngest population consisting of 4 grains to produce a maximum depositional age of 113.1 ± 1.5 Ma. This age provides the first absolute age for this important fossil locality and confirms its geochronological position near the Aptian/Albian boundary. Furthermore, it confirms a rapid rise in atmospheric pCO_2 near the onset of ocean anoxic event 1b (OAE1b: 113-109 Ma; Leckie et al. 2002). Several black-shales have been identified and described as events within OAE1b including the 113/Jacob (Aptian), the Kilian (Aptian-Albian boundary), the Paquier (Albian), and the Lenhardt (Albian) (Leandro et al. 2022). While the current sample set of one zircon U-Pb maximum depositional age does not provide the resolution needed to correlate the changes in atmospheric pCO_2 with any of these specific events, future work including extraction of zircon from multiple samples from the remaining fossil localities and increasing precision of the dates using the CA-ID-TIMS dating techniques would provide the clarity needed to understand climatic and atmospheric shifts and their association with global carbon events. Increased age resolution could also be provided by improving stratigraphic coverage through obtaining and analyzing core samples in the study area. Together, the presented dataset confirms how deep time proxies from paleosols can contribute to our understanding of climatic, atmospheric, and biological processes during earth's history including critical periods where greenhouse climatic conditions persisted and highlight the necessity for continued study.

CONCLUSION

Data produced from chemical, mineralogical, and stable isotopic analyses from Mid-Cretaceous (Aptian-Cenomanian) paleosols sampled from fossil localities in north-central Texas and southern Oklahoma reveal insight into the biotic response of the $\delta^{13}C$ of plant organic matter to changes in estimated mean annual precipitation and atmospheric pCO_2. Localities reporting low paleoprecipitation estimates correlate with more positive $\delta^{13}C$ organic matter values while localities reporting high paleoprecipitation estimates correlate with more negative $\delta^{13}C$ organic matter values which is consistent with observations in modern systems. The changes in estimated mean annual precipitation appear to be related to regional transgressive/regressive events, with higher mean annual precipitation estimates occurring due to new moisture sources provided by various transgressions onto the Texas craton during sea level highstands. To understand and constrain the influence of changes in atmospheric pCO_2 levels on the

$\delta^{13}C$ of plant organic matter, paleosol carbonates from two localities (Proctor Lake and Jones Ranch) with consistent mean annual precipitation estimates but significant differences in estimated atmospheric pCO_2 estimates were used to estimate a pCO_2 effect of −0.4 to −1.4‰ per 100 ppmV on the $\delta^{13}C$ values of organic matter. U-Pb dating of zircon collected from the Jones Ranch locality indicates a maximum depositional age of 113.1 ± 1.5 Ma (n = 4, Figs. 3, 4). This provides the first reported absolute age dating for the Twin Mountains Formation and is a valuable time constraint for a reported increase in atmospheric pCO_2 occurring at the Aptian/Albian boundary and near the onset of the OAE1b interval suggesting a global influence on the $\delta^{13}C$ of terrestrial plant organic matter. Together these data exhibit how deep time proxies from paleosols can contribute to our knowledge and understanding of interactions among biotic, climatic, and atmospheric processes occurring at both regional and global scales while also providing crucial paleoclimatic, paleoatmospheric, and geochronological data for periods where greenhouse climate conditions persisted. Future work to constraint geochronology of the remaining fossil localities and increase stratigraphic coverage will continue to provide more resolution into the complex interaction of regional and global changes occurring during the Mid-Cretaceous transition in Texas and Oklahoma.

ACKNOWLEDGMENTS

We thank B. Barnett and M. Suarez for access to the Keck Palaeoenvironmental and Environmental Stable Isotope Lab at the University of Kansas and analyses of organic carbon samples. We thank L. Jacobs for his contributions and support for this research in addition to his exceptional mentoring over the years. This research was supported by NSF FRES 2121594 (CO2PIP Community Project) and funds from the Kansas Geological Survey.

AUTHOR CONTRIBUTIONS

KAA designed the project, compiled data, analyzed data, and drafted the manuscript, AM gathered data and analyzed data, and CRN collected samples. All authors edited the manuscript.

LITERATURE CITED

Ambrose, W. A., Hentz, T. F., Bonnaffe, F., Loucks, R. G., Brown, L. F. Jr., Wang, F. P., & Potter, E. C. (2009). Sequence-stratigraphic controls on complex reservoir architecture of highstand fluvial-dominated deltaic and lowstand valley-fill deposits in the Upper Cretaceous (Cenomanian) Woodbine Group, East Texas field: Regional and local perspectives. *AAPG Bulletin*, 93(2), 231–269. DOI 10.1306/09180808053.

Andrzejewski, K. A. & Tabor, N. J. (2020). Paleoenvironmental and paleoclimatic reconstruction of Cretaceous (Aptian-Cenomanian) terrestrial formations of Texas and Oklahoma using phyllosilicates. *Palaeogeography, Palaeoclimatology, Palaeoecology,* 543, 109491.

Andrzejewski, K. A., Tabor, N. J., Winkler, D., & Myers, T. S. (2022). Atmospheric pCO_2 reconstruction of Early Cretaceous terrestrial deposits in Texas and Oklahoma using pedogenic carbonate and occluded organic matter. *Geosciences*, 12, 148.

Arthur, M. A., Schlanger, S. O., & Jenkyns, H. C. (1987). The Cenomanian-Turonian oceanic anoxic event II, paleoceanographic controls on organic matter production and preservation. In J. Brooks & A. Fleet (Eds.), *Marine petroleum source rocks* (pp. 399–418), Geological Society Special Publication, 4. Oxford, UK: Blackwell.

Berquist, H. R. (1949). Geology of the Woodbine Formation of Cooke, Grayson and Fannin counties, Texas. In *Oil and Gas Investigations Map OM-98*. Reston: U.S. Geological Survey.

Breecker, D. O. (2017). Atmospheric pCO_2 control on speleothem stable carbon isotope compositions. *Earth and Planetary Science Letters*, 458, 58–68.

Cifelli, R. L., Gardner, J. D., Nydam, R. L., & Brinkman, D. L. (1997). Additions to the vertebrate fauna of the Antlers Formation (Lower Cretaceous), southeastern Oklahoma. *Oklahoma Geology Notes*, 57, 124–131.

Coccioni, R. & Galeotti, S. (2001). The mid-Cenomanian Event: the Prelude to the OAE2. *AGU Fall Meeting Abstracts* Vol. 2001.

Davies, S. M. (2015). Cryptotephras: The revolution in correlation and precision dating. *Journal of Quaternary Science*, 30(2), 114–130.

Dodge, C. F. (1952). Stratigraphy of the Woodbine Formation in the Arlington area. Tarrant County, TX. *Field and Laboratory*, 20, 66–78.

Dodge, C. F. (1968). Stratigraphic nomenclature of the Woodbine Formation Tarrant County, Texas. In C. F. Dodge (Eds.), *Field trip guidebook, south central section, stratigraphy of the Woodbine Formation, Tarrant County, Texas* (pp. 107−125). Geological Society of America.

Dodge, C. F. (1969). Stratigraphic nomenclature of the Woodbine Formation Tarrant County, Texas. *Texas Journal of Science*, 21, 43–62.

Emerson, B. L., Emerson, J. H., Akers, R. E., & Akers, T. J. (1994). *Texas Cretaceous Ammonites and Nautiloids*. Houston, Texas: Houston Gem and Mineral Society.

Gradstein, F. M., Ogg, J. G., & Smith, A. G. (2004). *A geologic time scale 2004*. UK: Cambridge University Press.

Gröcke, D. R., Ludvigson, G. A., Witzke, B. L., Robinson, S. A., Joeckel, R. M., Ufnar, D. F., & Ravn, R. L. (2006). Recognizing the Albian-Cenomanian (OAE1d) sequence boundary using plant carbon isotopes: Dakota Formation, Western Interior Basin, USA. *Geology*, 34(3), 193–196.

Hall, W. D. (1976). Hydrogeologic significance of depositional systems and facies in Lower Cretaceous sandstones, north-central Texas. *University of Texas, Austin, Bureau of Economic Geology Circular*, 76−1.

Haq, B. V., Hardenbol, J., & Vail, P. R. (1987). Chronology of fluctuating sea levels since the Triassic. *Science*, 235, 1159−1167.

Hare, V. J., Loftus, E., Jeffrey, A., & Ramsey, C. B. (2018). Atmospheric CO_2 effect on stable carbon isotope composition of terrestrial fossil archives. *Nature Communications*, 9(1), 1−8.

Hentz, T. F., Ambrose, W. A., & Smith, D. C. (2014). Eaglebine play of the southwestern East Texas basin: stratigraphic and depositional framework of the Upper Cretaceous (Cenomanian-Turonian) Woodbine and Eagle Ford Groups. *AAPG Bulletin*, 98(12), 2551−2580.

Hobday, D., Woodruff, C., & McBride., M. (1981). Paleotopographic and structural controls on non-marine sedimentation of the lower Cretaceous Antlers Formation and correlatives North Texas and Southeastern Oklahoma. *University of Texas, Austin, Bureau of Economic Geology Circular*, 71−87.

Hoke, G. D., Schmitz, M. D., & Bowring, S. A. (2014). An ultrasonic method for isolating non-clay components from clay-rich material. *Geochemistry, Geophysics, Geosystems*, 15, 492−498.

Jackson, S. E., Pearson, N. J., Griffin, W. L., & Belousova, E. A. (2004). The application of laser ablation-inductively coupled plasma-mass spectrometry to in situ U-Pb zircon geochronology. *Chemical geology*, 211(1-2), 47−69.

Jacobs, L. L. & Winkler, D. A. (1998). Mammals, archosaurs, and the Early to Late Cretaceous transition in north-central Texas. In Y. Tomida., L. J. Flynn, and L. L. Jacobs (Eds.), *Advances in vertebrate paleontology and geochronology* (pp. 253−280). National Science Museum, Tokyo.

Jenkyns, H. C. (1980). Cretaceous anoxic events: From continents to oceans. *Journal of Geological Society*, 137, 171-188. https://doi.org/10.1144/gsjgs.137/2/0171.

Jenkyns, H. C. (2010). Geochemistry of oceanic anoxic events. *Geochemistry Geophysics Geosystems*, 11, Q03004. https://doi.org/10.1029/2009GC002788

Joeckel, R. M., Suarez, C. A., Mclean, N. M., Möller, A., Ludvigson, G. A., Suarez, M. B., Kirkland, J. I., Andrew, J., Kiessling, S., & Hatzell, G. A. (2023). Berriasian-Valanginian geochronology and carbon-isotope stratigraphy of the Yellow Cat member, Cedar Mountain Formation, eastern Utah, USA. *Geosciences*, 13, 32. https://doi.org/10.3390/geoscienes13020032.

Johnson, R. O. (1974). *Lithofacies and depositional environments of the Rush Creek Member of the Woodbine Formation (Gulfian) of North Central Texas* [Unpublished M.S. thesis]. University of Texas.

Kauffman, E. G. & Caldwell, W. G. E. (1993). The Western Interior Basin in space and time. In: *Evolution of the Western Interior Basin: Geological Association of Canada*, [Special Paper]. 39, 1−30.

Kennedy, W. J. & Cobban, W. A. (1990). Cenomanian ammonite faunas from the Woodbine Formation and lower part of the Eagle Ford Group, Texas. *Palaeontology*, 33, 75−154.

Koch, P. L. (1998). Isotopic reconstruction of past continental environments. *Annual Review of Earth and Planetary Sciences*, 26(1), 573−613.

Kohn, M. J. (2010). Carbon isotope compositions of terrestrial C_3 plants as indicators of (paleo) ecology and (paleo) climate. *Proceedings of National Academy of Sciences*, 107(46), 19691−19695.

Lee, Y-N. (1997a). The archosauria from the Woodbine Formation (Cenomanian) in Texas. *Journal of Paleontology*, 71, 1147−1156. DOI 10.1017/S0022336000036088.

Lee, Y-N. (1997b). Bird and dinosaur footprints in the Woodbine Formation (Cenomanian). *Texas Cretaceous Research*, 18(6), 849−864. DOI 10.1006/cres.1997.0091.

Leandro, C. G., Savian, J. F., Kochhann, M. V. L., Franco, D. R., Coccioni, R., Frontalini, F., Gardin, S., Jovane, L., Figueiredo, M., Tedeschi, L. R., & Janikian, L. (2022). Astronomical tuning of the Aptian stage and its implications for age recalibrations and paleoclimate events. *Nature Communications*, 13(1), 2941.

Leckie, R. M, Bralower, T. J., & Cashman, R. (2002). Ocean anoxic events and plankton evolution: Biotic response to tectonic forcing during the mid-Cretaceous. *Paleoceanography*, 17(3), 13−1.

Ma, J. Y., Sun, W., Liu, X. N., & Chen, F. H. (2012). Variations in the stable carbon and nitrogen isotope composition of plants and soil along a precipitation gradient in northern China. *PloS One*, 7(12), e51894.

Main, D. J. (2009). Delta plain environments and ecology of the Cretaceous (Cenomanian) Woodbine Formation at the Arlington Archosaur Site, North Texas. *Geological Society of America, Abstracts with Programs*, 41, 103.

Murlin, J. R. (1975). *Stratigraphy and depositional environments of the Arlington Member, Woodbine Formation (Upper Cretaceous), Northeast Texas* [Unpublished M.S. Thesis]. University of Texas at Arlington, Arlington, TX, USA.

Myers, S. T., Tabor, N. J, Jacobs, L. L., & Bussert, R. (2016). Effects on different organic-matter sources on estimates of atmospheric and soil pCO_2 using pedogenic carbonate. *Journal of Sedimentary Research,* 86, 800−812.

Oliver, W. B. (1971). Depositional systems in the Woodbine Formation (Upper Cretaceous), northeast Texas: the University of Texas at Austin. *Bureau of Economic Geology Report of Investigations,* 73, 28. DOI 10.23867/RI0073D

Paces, J. B. & Miller Jr, J. D. (1993). Precise U-Pb ages of Duluth complex and related mafic intrusions, northeastern Minnesota: Geochronological insights to physical, petrogenetic, paleomagnetic, and tectonomagmatic processes associated with the 1.1 Ga midcontinent rift system. *Journal of Geophysical Research: Solid Earth*, 98(B8), 13997−14013.

Paton, C., Hellstrom, J., Paul, B., Woodhead, J., & Hergt, J. (2011). Iolite: Freeware for the visualization and processing of mass spectrometric data. *Journal of Analytical Atomic Spectrometry*, 26(12), 2508−2518.

Petrus, J. A. & Kamber, B. S. (2012). VizualAge: A novel approach to laser ablation ICP-MS U-Pb geochronology data reduction. *Geostandards and Geoanalytical Research*, 36(3), 247−270.

Powell, J. D. (1968). Woodbine-Eagle Ford transition, Tarrant Member. In C. F. Dodge (Eds.), *Stratigraphy of the Woodbine Formation: Tarrant County, Texas Field Trip Guidebook* (pp. 27–43). Geological Society of America, South Central Section.

Retallack, G. J. (1986). The fossil record of soils. In V. P. Wright (Eds.), *Paleosols: Their Recognition and Interpretation* (pp. 1–57). Blackwell Scientific Publications, Oxford.

Richey, J. D., Upchurch, G. R., Montañez, I. P, Lomax, B. H., Suarez, M. B., Crout, N. M. J., Joeckel, R. M., Ludvigson, G. A., & Smith, J. J. (2018). Changes in CO_2 during Ocean Anoxic Event 1d indicate similarities to other carbon cycle perturbations. *Earth and Planetary Science Letters*, 491, 172−182.

Schlanger, S. O. & Jenkyns, H. C. (1976). Cretaceous anoxic events: Causes and consequences. *Geologie et Mijnbouw*, 55, 179−184.

Schlanger, S. O., Arthur, M. A., Jenkyns, H. C., & Scholle, P. A. (1987).

The Cenomanian-Turonian Oceanic Anoxic Event, I. Stratigraphy and distribution of organic carbon-rich beds and the marine $\delta^{13}C$ excursion. In J. Brooks & A. J. Fleet (Eds.) *Marine petroleum source rocks*, *Geological Society Special Publication*, 26, 371-399. Oxford, UK: Blackwell. https://doi.org/10.1144/GSL.Sp.1987.026.01.24.

Schulz, E. D., Williams, R. J., Farquhar, G. D., Schulze, W., Langridge, J., Miller, J. M., & Walker, B. H. (1998). Carbon and nitrogen isotope discrimination and nitrogen nutrition of trees along a rainfall gradient in northern Australia. *Functional Plant Biology*, 25(4), 413–425.

Scott, C. (1940). Cephalopods from the Cretaceous Trinity Group of the south-central United States. *The University of Texas Bulletin*, 3945, 969–1125.

Sheldon, N. D. & Tabor, N. J. (2009). Quantitative paleoenvironmental and paleoclimatic reconstruction using paleosols. *Earth Science Reviews*, 95, 1–52.

Sláma, J., Košler, J., Condon, D. J., Crowley, J. L., Gerdes, A., Hanchar, J. M., & Whitehouse, M. J. (2008). Plešovice zircon: a new natural reference material for U-Pb and Hf isotopic microanalysis. *Chemical Geology*, 249(1-2), 1–35.

Slattery, J. S., Cobban, W. A., McKinney, K. C., Harries, P. J., & Sandness, A. L. (2015). Early Cretaceous to Paleocene paleogeography of the Western Interior Seaway: the interaction of eustasy and tectonism. In M. Bingle-Davis (Ed.), *Wyoming Geological Association Guidebook* (pp. 22–60). Casper, Wyoming.

Smith, J. J., Ludvigson, G. A., Layzell, A., Möller, A., Harlow, R. H., Turner, E., Platt, B., & Petronis, M. (2017). Discovery of Paleogene depostits of the central High Plains aquifer in the western Great Plains, USA. *Jounral of Sedimentary Resaerch*, 87(8), 880–896.

Swap, R. J., Aranibar, J. N., Dowty, P. R., Gilhooly, W. P., & Macko, S. A. (2004) Natural abundance of ^{13}C and ^{15}N in C_3 and C_4 vegetation of southern Africa: patterns and implications. *Global Change Biology*, 10, 350–358.

Tabor, N. J. & Myers, T. S. (2015). Paleosols as indicators of paleoenvironment and paleoclimate. *Annual Review Earth Planetary Sciences*, 43, 333–361.

Tabor, N. J., Myers, T. S., & Michel, L. A. (2017). Sedimentologist's guide for recognition, description, and classification of paleosols. In *Terrestrial depositional systems*. Elsevier. 165–208.

Trudel, P. (1994). *Stratigraphic sequences and facies architecture of the Woodbine-Eagle Ford interval, Upper Cretaceous, North Central Texas* [M.S. thesis] Tarleton State University, Stephenville, TX, USA.

Vermeesch, P. (2012). On the visualization of detrital age distributions. *Chemical Geology*, 312-313, 190–194.

Vermeesch, P. (2018). IsoplotR: A free and open toolbox for geochronology. *Geoscience Frontiers*, 9(5), 1479–1493.

Winkler, D. A., Murry, P. A., & Jacobs, L. L. (1990). Early Cretaceous (Comanchean) vertebrates of central Texas. *Journal of Vertebrate Paleontology*, 10, 95–116.

Winkler, D. A., Ruoff, K. A., Clemens, M. C., & Jacobs, L. L. (2015). Changes in small tetrapod faunas during the Early to Late Cretaceous transition in north-central Texas. *SVP Annual Meeting Program*. p. 239.

Wotzlaw, J. F., Schaltegger, U., Frick, D. A., Dungan, M. A., Gerdes, A., & Günther, D. (2013). Tracking the evolution of large-volume silicic magma reservoirs from assembly to supereruption. *Geology*, 41(8), 867–870.

Young, K. (1967). Comanche series (Cretaceous), south central Texas. Comanchean (Lower Cretaceous) Stratigraphy and Paleontology of Texas. *Permian Basin Section, Society of Economic Paleontologists and Mineralogists*, 67, 9–29.

Young, K. (1974). Lower Albian and Aptian (Cretaceous) ammonites of Texas. *Geoscience and Man*, 8, 175–228.

Young, K. (1986). Cretaceous, marine inundations of the San Marcos platform, Texas. *Cretaceous Research*, 7(2), 117–140.

WINDOWS INTO SAUROPSID AND SYNAPSID EVOLUTION
Essays in honor of Prof. Louis L. Jacobs, pp. 233–251, 2023

NARRATIVE OF THE KOREA-MONGOLIA INTERNATIONAL DINOSAUR EXPEDITIONS (KID) 2006-2010 WITH SCIENTIFIC RESULTS

YUONG-NAM LEE[1,*], LOUIS L. JACOBS[2], PHILIP J. CURRIE[3], and RINCHEN BARSBOLD[4]

[1]School of Earth and Environmental Sciences, Seoul National University, Seoul 08826, South Korea
[2]Roy M. Huffington Department of Earth Sciences, Southern Methodist University, Dallas, TX 75275, USA
[3]Department of Biological Sciences, University of Alberta, Edmonton, Alberta T6G 2E9, Canada
[4]Institute of Paleontology, Mongolian Academy of Sciences, Ulaanbaatar 15160, Mongolia

ABSTRACT The Korea-Mongolia International Dinosaur Expeditions (KID) were initiated by the discovery of the most significant dinosaur egg site known in South Korea, and as one project associated with the construction of a new dinosaur museum at Hwaseong City. It ran for five years (2006-2010) and involved 33 researchers from eleven countries supported by twenty-seven Mongolian staff. Since the American Museum of Natural History expeditions in 1923-1930, they were the first multi-international dinosaur expedition in Mongolia, and the first international dinosaur expedition organized by Korea. These expeditions worked mainly in Upper Cretaceous formations, including the Bayanshiree and Javkhlant formations in the eastern Gobi and the Baruungoyot and Nemegt formations in the southwestern Gobi. The KID expeditions succeeded by collecting 694 cataloged specimens and produced meaningful paleontological research on *Bagaceratops*, *Deinocheirus*, *Gobiraptor*, *Harenaichthys, Natovenator*, *Nemegtonykus*, *Prenocephale*, *Talarurus*, and *Tarchia*. In addition, comprehensive stratigraphic correlations were completed in the famous dinosaur localities in eastern and southern Gobi. The KID expeditions successfully promoted international research cooperation, built valuable collections, fostered the education of graduate students, and accelerated the development of a museum in South Korea.

KEYWORDS KID expedition, Hwaseong City, Dinosaurs, Gobi Desert, Mongolia

INTRODUCTION

The largest dinosaur egg site known in the Korean Peninsula was discovered in 1999 at Hwaseong City, Gyeonggi Province, near Seoul. To date, more than 200 dinosaur eggs of four different kinds (dongyangoolithid, elongatoolithid, faveoloolithid, and stalicoolithid), including 29 clutches, have been discovered in the reddish conglomeratic sandstone beds (Early Cretaceous, Sihwa Formation) of nine small islands in a salt marsh, indicating the first discovery of dinosaur colonial nesting ground in Asia (Lee, 2003). Because of this locality's unique setting and scientific importance, the Korean government designated 1.5 km^2 as a National Monument in 2000. And Hwaseong City began planning for the construction of a new dinosaur museum with extensive collections and research facilities. Therefore, Hwaseong City sponsored Y.-N. Lee for five years to carry out the Korea-Mongolia International Dinosaur Expeditions (nicknamed the KID expeditions). After KIGAM (Korea Institute of Geoscience and Mineral Resources, where Y.-N. Lee worked) entered into an official research agreement with the Institute of Geology of Mongolian Academy of Sciences in 2006, KIGAM additionally made a research partnership with Southern Methodist University (Louis L. Jacobs), USA, and the University of Alberta (Philip J. Currie), Canada. The KID expeditions ran for about 40 days in the Gobi Desert between August and September every year from 2006 to 2010. The team crew was augmented each year by additional researchers from various countries including Argentina, Australia, Canada, China, Denmark, Japan, Portugal, Slovenia, and the USA. Consequently, this project was the first large multi-international dinosaur expedition in the Gobi since the famous Roy Chapman Andrews' expeditions of the American Museum of Natural History (AMNH) from 1923-1930. Each year, the KID crew consisted of around 15 researchers on average, with ten Mongolian staff, including drivers and cooks (Appendix 1). We neither hired laborers nor medical doctors. Three Russian military trucks (models GAZ-66, KAMAZ-43114, ZIL-131),

*Corresponding author

jeeps, and mini-vans were usually used for transportation. The purpose of this expedition was to discover, collect and study scientifically important dinosaurs from the Gobi Desert in Mongolia, which is one of the most important dinosaur areas in the world, and to collect displayable specimens for the new dinosaur museum at Hwaseong City.

The KID expeditions were carried out in famous localities known from American, Mongolian, Polish, and Soviet expeditions. Except for the first half of the second expedition in the eastern Gobi in 2007, the rest of the expeditions worked in the southwestern Gobi, where we explored Altan Uul, Bugiin Tsav, Guriliin Tsav, Hermiin Tsav, Khuree Tsav, Nemegt, Nogoon Tsav, Tsagaan Khushuu, and Ulan Khushuu (Table 1, Fig. 1). From these regions, we discovered a variety of dinosaur fossils and other vertebrate fossils from the Baruungoyot and Nemegt formations (middle Campanian? to early Maastrichtian). In the eastern Gobi in 2007, the Bayanshiree and Javkhlant formations (Cenomanian to Santonian?) were explored at Bayan Shiree, Khar Khutul, and Shine Us Khudag. These localities also produced a rich assemblage of vertebrate fossils, especially dinosaurs.

Here, we briefly describe each expedition by year for the journey, the localities we explored, discoveries, and scientific results.

TABLE 1. The dates and localities of the KID expedition

	Date	Localities
1st	2006.08.30 - 10.03	Altan Uul I-IV, Ulaan Khushuu, Bugiin Tsav, Guriliin Tsav, Nemegt
2nd	2007.08.16 - 09.21	Shine Us Khudag, Khar Khutul, Bayan Shiree, Hermiin Tsav, Nogoon Tsav
3rd	2008.08.15 - 09.24	Hermiin Tsav, Bugiin Tsav, Altan Uul II, III, Nemegt
4th	2009.08.03 - 09.09	Bugiin Tsav, Tsagaan Khushuu, Altan Uul, Nemegt
5th	2010.08.23 - 10.01	Bugiin Tsav, Guriliin Tsav, Khuree Tsav, Nogoon Tsav, Altan Uul, Nemegt

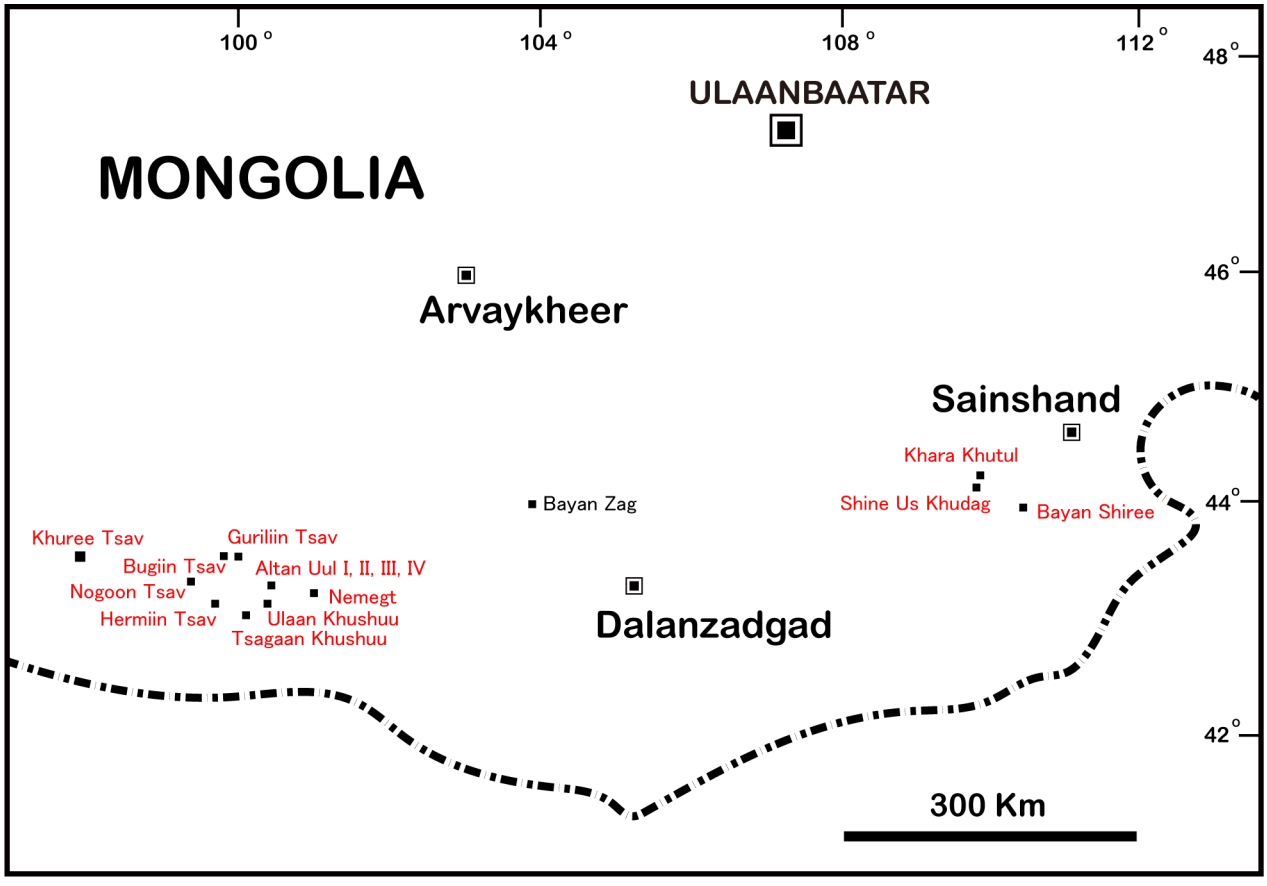

FIGURE 1. Explored localities (red color) in the eastern and southern Gobi (modified from Watabe and Suzuki, 2000, fig. 1).

2006 EXPEDITION

The first KID expedition was carried out over a period of 35 days between August 30 and October 3. The field crew comprised 24 people (15 researchers and nine Mongolian staff, including the field manager, six drivers, and two cooks) (Appendix 1). On August 21, the field gear for the Korean group was sent by DHL from Seoul to Ulaanbaatar. From August 30, all field equipment with food was prepared and loaded into the two GAZ trucks by the Korean and Mongolian contingents. All other researchers arrived in Ulaanbaatar on September 1 and 2 from Canada, Japan, and the USA. The flight of Lü was delayed for 14 hours in Beijing due to strong winds at the Chinggis Khaan International Airport, and he arrived one day later than the original schedule. Official meetings in which a detailed expedition plan was finalized were held in the Paleontological Center between September 1 and 3. Altan Uul, Bugiin Tsav, Guriliin Tsav, and Ulaan Khushuu were selected as destinations for prospecting the Nemegt Formation. The main target was the Altan Uul (I, II, III, IV) area. All foreign researchers applied for visa extensions at the Mongolian Immigration Agency so that they could stay more than one month.

Two GAZ trucks left on September 3, which was one day earlier than the field crew. On September 4, the rest of the expedition members left in one jeep and three vans for Arvaykheer, the last big central city before entering the Gobi region. In the afternoon, we caught up with one of our trucks, which had broken down on the road approximately 200 km from Ulaanbaatar. The front wheel bearings needed to be replaced. Ligden Barsbold, the field manager, went back to Ulaanbaatar to get new bearings, and we kept moving forward after moving the broken truck's load to another truck. Ligden returned with new parts the next day, and the Mongolian mechanics fixed the truck. We passed Arvaykheer in the afternoon and camped north of Guchin Us on September 5. It snowed that night, when Ligden went back to Arvaykheer to buy truck parts. On September 6, the same truck broke down again 32 km before reaching Bogd. We left the truck, moved to the Shireegiin Gashuun Basin, and camped at the east end of Nemegt Mountain. The broken truck came to our camp in the evening, and Mongolian mechanics worked on fixing the truck all night. The next day, we passed a narrow gorge between Gilbent and Nemegt mountains and passed into the southern Gobi region. We rented a ger from a nomadic family and finally arrived at Ulaan Khushuu during the afternoon on September 7. The base camp was set up after spending four days on the road-twice as long as expected because of mechanical problems.

On September 8, we began prospecting at Altan Uul III. We found many isolated bones, various dinosaur teeth, and eggshells. Nine specimens were cataloged on the first day. Interestingly, we found a microvertebrate site near the base camp, containing many isolated fish vertebrae and dinosaur teeth. Compared with abundant dinosaur faunas, fish fossils (other than isolated centra) are scarce in the Nemegt Formation. All fish material from Altan Uul, Bugiin Tsav, Hermiin Tsav, and Ulaan Khushuu collected during the KID expeditions was identified as a new species of Osteoglossomorpha now known as *Harenaichthys lui*, which is the first and only reported fish taxon of the Nemegt Formation (Kim et al., 2022). We collected sauropod teeth and a *Tarbosaurus* coracoid and lacrimal at Altan Uul III the next day. By 2006, the poaching of dinosaur skeletons had become a significant problem. Its effects were visible throughout the field area. We determined that the origin of *Raptorex kriegsteini* is the Nemegt Formation, and may even have come from one of the poached quarries that we saw (Kim et al., 2022).

On September 10, an articulated *Tarbosaurus* pelvic girdle (with an ilium length of 112 cm) with all sacral and eight proximal caudal vertebrae (KID 022) was found at Altan Uul IV. Although we encountered many *Tarbosaurus* remains, mainly at poached quarries in various localities, it was the first major excavation of a *Tarbosaurus* specimen in 2006. We spent five days on the excavation because it was in hard sandstone. On September 15, all *Tarbosaurus* plaster jackets were moved to the camp except for the biggest one. On the same day, a poached quarry was found in another canyon (sayr) at Altan Uul IV, where ilia with dorsal and sacral vertebrae (MPC-D 100/128) were found scattered across a slope. Because the ilium shape and long neural spines of dorsal and sacral vertebrae were quite different from those of other dinosaurs, we tentatively identified it as a "therizinosaur," speculating that it would be *Therizinosaurus*, a mysterious dinosaur mostly known from giant arms with elongate claws.

On September 16, we headed to Bugiin Tsav in reconnaissance for the next expedition. The landscape of Bugiin Tsav consists mainly of low rounded exposures that are very different from the deep gorges of Altan Uul. Turtle shells are abundant, but are often associated with isolated skulls. The next day, a few

FIGURE 2. A jacket of *Tarbosaurus* (ilia with sacral vertebrae) on the top of the hill at Altan Uul IV (KID 022) was being dragged down to the hill only by human resources with ropes on September 18, 2006.

bones were collected at Ulaan Khushuu. On September 18, we went back to the top of the hill at Altan Uul IV to collect the largest plaster jacket (weighing more than 500 kg) of the *Tarbosaurus* (ilia with sacral vertebrae). We dragged it down the hill and loaded into the truck using only human power and ropes (Fig. 2). Ironically, we subsequently learned that our quarry was close to where the Polish-Mongolian Paleontological Expedition had collected the holotype of *Opisthocoelocaudia* in 1965, and they had dragged the jackets down the same trail and loaded them onto trucks in the same area (which they called "the Café"). Polish graffiti still adorns the sandstone walls of the canyon where the specimens were crated.

A beautifully preserved, articulated tail was also excavated at the "therizinosaur" site on the same day. Subsequently, this specimen was identified as a subadult *Deinocheirus* (Lee et al., 2014).

On September 19, we visited the "Dragon's Tomb" at Altan Uul II, which is a bonebed of the giant hadrosaurine, *Saurolophus angustirostris*. Although the Soviet expeditions of the 1940s had excavated many articulated specimens, we collected mostly skin impressions that had been left behind. Those specimens were used to standardize the terminology of hadrosaurid skin impressions (Bell, 2012).

The next day, we visited Altan Uul I, which has fewer and smaller outcrops, and more shallow gorges than other Altan Uul localities. Nevertheless, we found that bones and eggs were abundant. We collected a *Gallimimus* postcranial skeleton containing a complete tail at a poached quarry. At the camp, we met Barsbold and the American group (Fiorillo, Jacobs, and Newman), who arrived three days late after waiting for lost luggage to show up at the airport.

On September 21, the expedition team, which gained new vitality by the addition of the American group, headed for Altan Uul III again. In an abandoned quarry, Y.-N. Lee found a juvenile *Tarbosaurus* skeleton (KID 069). Although some bones, including the skull, had been taken by poachers, many postcranial elements were left untouched in the blocks. They

included 14 articulated vertebrae (posterior dorsals, sacrals, and proximal caudals), a left manus, an articulated pelvic girdle, both femora, an incomplete tibia and fibula, right distal tarsals, phalanges, and complete gastralia. Eighteen segments of gastralia are preserved in life position. Inside the left side of the gastral basket, fossilized stomach contents were found for the first time in *Tarbosaurus*. This specimen is now under study.

A new ornithomimid skeleton (KID 101) was also found on the same day near the camp. It was almost a complete skeleton, including the braincase. Based on the unique manual claws, it differs from *Anserimimus* and *Gallimimus,* which are the only known ornithomimids from the Nemegt Formation. Consequently, it may be a new taxon of ornithomimids. These two were the most exciting specimens discovered, along with the *Deinocheirus* (MPC-D 100/128), that were found in 2006.

From September 22 to 23, all team members excavated KID 069 and KID 101 during the day and made plaster jackets in the evening at the camp. The American group collected dinosaur eggshells and carbonate nodules to test for paleoenvironmental and paleoecological parameters important in dinosaur evolution. They were studied by examining diagenesis using light microscopy, SEM, and cathodoluminescence with $\delta^{13}C$ and $\delta^{18}O$ values (Graf et al., 2018). On September 24, all members worked at the mud-dominant Guriliin Tsav, where many turtles (mainly *Mongolemys*) were found along with *Saurolophus* and *Tarbosaurus* at poached quarries. The next day, we finished excavating KID 069 and KID 101.

On September 26, the Canadian group returned to Ulaanbaatar, and the American group headed to Nemegt for reconnaissance. The rest of the team disassembled the camp, packed the specimens, and loaded 65 plaster jackets in 36 boxes into the trucks. Two trucks left for Ulaanbaatar the next day, and the team returned to Ulaanbaatar on September 29 via Bayan Zag.

2007 EXPEDITION

The second KID expedition lasted 38 days, from August 16 to September 21. The field crew comprised 27 people (17 researchers and ten Mongolian staff) (Appendix 1). Through official meetings in the Paleontological Center, Shine Us Kudag in the eastern Gobi and Hermiin Tsav in the southern Gobi were picked for exploration. Before heading to the first base camp at Shine Us Kudag on August 20, all members from Canada, Japan, Korea, Portugal, and the USA arrived in Ulaanbaatar. Martin Kundrát from Slovakia joined our expedition at Barsbold's request. Like last year, two trucks (GAZ, ZIL) hauling a big water bowser left one day earlier than the rest of the team. Therrien and Zelenitsky were left behind because their luggage did not arrive until the departure day. On August 20, we met our trucks at Sainshand in the evening, moved 200 km further, and arrived in Shine Us Khudag at 11:00 PM.

On the first working day, all members visited the sauropod quarry found by Kobayashi's group near the base camp two years previously. Several cervical and caudal vertebrae had already been collected on a small hill, and were stored in the Paleontological Center. We decided to excavate this animal (KID 106) because sauropods are rare in the Bayanshiree Formation. *Erketu* was the only known sauropod in the Bayanshiree Formation (Ksepka and Norell, 2006; 2010), and had been found in Bor Guvé, 23 km from the KID 106 site.

Two formations are distributed in the vicinity of Shine Us Kudag: the Bayanshiree Formation (280 m thick) and the Javkhlant Formation (380 m thick). The Javkhant Formation is broadly exposed in Shine Us Kudag and Khar Khutul, and consists of massive red siltstones. The stratigraphic relationship between these two formations was uncertain, but it was clarified through detailed fieldwork this year (Eberth et al., 2009) that the Javkhant Formation conformably overlies the Bayanshiree Formation. The Shine Us Kudag area is relatively flat with low hills, so outcrops are distributed as patches.

Therrien and Zelenitsky arrived at the camp in the evening of August 21. On August 22, one group began excavating the sauropod using two jackhammers and shovels to remove the overburden, while the other group searched for fossils in the Bayanshiree Formation, where they found a therizinosaurid femur (KID 113). The next day, it rained in the morning, and there was a sandstorm in the afternoon. On August 24, the sauropod quarry was getting too large, and many bones needed to be excavated in a few days to finish. Nishida found and kept digging an ankylosaur (KID 155) containing the pelvic girdle, dorsal vertebrae, and hindlimbs. The following day, Y.-N. Lee and Lidgen visited a uranium mining company nearby to rent an excavator. Many significant sandstone-hosted uranium occurrences have been found in the eastern Gobi in proximal Cretaceous sedimentary basins. Very low radioactivity can be detected in dinosaur bones collected in

FIGURE 3. Excavating a sauropod (KID 106) at Shine Us Kudag on August 31, 2007.

this area. The manager of the uranium company promised to help us the next day. At the sauropod quarry, pelvic girdles were newly exposed with dorsal vertebrae and ribs. On August 26, the excavator arrived at the quarry in the morning and began to remove the overburden. With the help of the excavator, 62 bones were located within 117 m^2, which include almost all postcranial elements except for the proximal cervical and distal caudal vertebrae, the manus, and the pes.

On August 27, the plaster jacketing began for some isolated bones while the main block was excavated in a sauropod quarry. Two small ceratopsians (KID 148, 150), probably *Yamaceratops*, were collected in the Javkhlant Formation. The next day, most of the crew went to the type section of the Bayanshiree Formation at Bayanshiree, 50 km from the base camp. A microsite was found there, containing ankylosaurid, ornithopod, and theropod teeth and claws, an ornithomimid phalanx, fish vertebrae, crocodyliform teeth and scutes, turtle bones, and eggshell fragments (KID 139). On August 29, Lidgen left for Ulaanbaatar to pick up Currie, Koppellhus, and Ryan and to get food, plaster, and acetone. Four plaster jackets were made for the ankylosaur body (KID 155). Mapping was finished at the sauropod quarry before everything was encased in plaster jackets. From August 30 to 31, the Canadian group searched for fossils and investigated the stratigraphy and geology in the Bayanshiree Formation distributed in the Black Mountain area of Khar Khutul. Twelve jackets were made at the sauropod quarry (Fig. 3).

On September 1, while four more jackets were made at the sauropod quarry, Kobayashi, Mateus, Therrien, and Zelenitsky visited Bayanshiree and found two *Talarurus* skulls (MPC-D 100/1354, 1355). Although *Talarurus plicatospineus* was reported by Maleev (1952), the holotype skull only includes part of the back of the skull. Therefore, the new skulls provided new details of the cranial osteology of *Talarurus* (Park et al., 2020). Thanks to the well-preserved braincase, the detailed endocranial morphology of *Talarurus* was also revealed for the first time (Paulina-Carabajal et al., 2018). Currie's contingent arrived at the camp in the evening without the truck (GAZ), which was stuck in the mud 20 km from Sainshand. After dinner, Ligden and two drivers returned to Sainshand with another truck (ZIL) for towing. The next day, jacketing of the sauropod blocks continued while the Canadian contingent worked at Khar Khutul.

However, Ligden did not come back to the camp until the morning. Y.-N. Lee, Chenbur, Kundrát, and Lkhaasuren drove to Sainshand to find our two trucks. On the way, we met our GAZ being towed. Ligden drove back to Ulaanbaatar to get truck parts with Kundrát, and we returned to the camp with two trucks. With plaster loaded in a towed truck, we kept making jackets.

On September 3, one group excavated the two *Talarurus* skulls at Bayanshiree while the other group continued to make plaster jackets for the sauropod. Ligden returned to the camp with truck parts and worked the whole afternoon on repairing the GAZ. The next day, the sauropod quarry was closed with 30 plaster jackets removed. The Canadian contingent plus Mateus collected one more *Talarurus* skull (MPC-D 100/1356) at Bayanshiree. Because the GAZ was not ready to move, we emptied the ZIL so that we could load all jackets in it. On the morning of September 5, Y.-N. Lee and the Mongolian staff went to the mining company with the ZIL full of plaster jackets collected in Shine Us Kudag. We asked the company to store our jackets while we continued our expedition to the southern Gobi. After dissembling the camp, we finally moved out at 3:00 PM. However, the GAZ stopped after a short distance because of a defective camshaft and we were forced to spend the night in the middle of nowhere. Lidgen called the Paleontological Center to bring another truck to Dalanzadgad. The next day, we moved to Mandakh with one jeep, three vans, and the ZIL towing the GAZ. At Mandakh, a small village, there was one old GAZ that was not working. Lidgen bought its engine from the owner, and used it to replace the engine in ours. The drivers worked for the next six hours to switch the engines. We were all amazed that it was possible for the drivers to exchange the truck engines under such primitive conditions, and at 10:30 PM, the expedition left town. We stopped to camp at 11:30 PM between Mandkh and Manlai, but had only progressed 140 km from our camp of the previous night.

On September 7, we did not arrive in Dalanzadgad until 6:00 PM. After buying some supplies and food, and having supper in a local restaurant, we finally checked into a ger hotel at midnight. We got an early start the next morning, but because of continued vehicle problems, we did not arrive at Hermiin Tsav until the afternoon of September 10. Song found a concretion containing a partial skull and body of *Bagaceratops* (KID 196) in the Baruunyogot Formation near camp. Although *Bagaceratops* is well known for skulls of various ontogenetic stages, the description of the postcranial skeleton of this specimen was the first for *Bagaceratops* (Kim et al., 2019). The lower Nemegt and Baruungoyot formations are widely distributed at Hermiin Tsav (Eberth, 2018). Prospecting the next day produced a nest of dinosaur eggs with embryos (KID 202) in the Nemget Formation, and a few *Gobipteryx* eggs in the Barrungoyot Formation.

Prospecting continued on September 12, and produced a *Tarbosaurus* maxilla (KID 206) and a crocodyliform skull (KID 205) from the Nemegt Formation. The next day, while Kobayashi, Therrien, and Zelenitsky excavated the nest of eggs (KID 202), most of the crew left in the early morning to prospect at Nogoon Tsav, which was 55 km in a direct line from camp. We had to make a major detour to get around the vast, low sandy region at the center of the basin, and did not arrive at Nogoon Tsav until 3:00 PM. We only had time to look around for an hour, but found natural casts of theropod and hadrosaur footprints, and many turtle shells. The lithology and fossils were similar to those of Guriliin Tsav. Because it was getting late, we took a different road north from Nogoon Tsav that the drivers thought was a shortcut. However, this turned out to be a terrible mistake. In the evening, we passed by the south escarpment of Hermiin Tsav, only 14 km from camp, but there was no road down into the canyon. As darkness fell, we were forced south along a narrow mountain road. We climbed to the top the mountain 45 km south of the camp at midnight, and almost ran out of gas. Fortunately, we found a ger at 1:00 AM, where we asked for help. Thankfully, a young nomad riding a motorbike guided us to our camp, where we arrived at 4:15 AM. We had basically been lost for 15 hours and drove 345 km! After a quick “supper” we went to bed at 5:00 AM. In the meantime though, there were three trucks out looking for us that got lost in the bottom of the basin, and did not return to camp until 7:30 AM.

After a short sleep, we began to make jackets and pack fossils while the Canadian contingent relocated an ankylosaur specimen that the Joint Soviet-Mongolian Paleontological Expedition had abandoned in 1972 or 1973. It was encased in a wooden crate covered by loose boards. Although the skull was missing, the body (MPC-D 100/1359) was in good condition, especially with in situ dermal scutes. We decided to excavate it next year. This specimen has the most complete postcranial skeleton of an ankylosaurid from the Baruungoyot Formation, and seemed to support the possibility that

ankylosaurids practiced digging behavior (Park et al., 2021a). We also found many sauropod footprints beneath an overhanging cliff.

September 15 was our last day in the field. We continued to search for fossils when we were not packing those we had already collected. We found the 1973 Russian-Mongolian quarry for *Tarchia gigantea* (PIN 3142/250). We started our return to Ulaanbaatar the next day. It was also a difficult trip because of many vehicle problems, such as flat tires, overheated engines, leaking radiators, and broken axle, so it was not until 8:00 PM on September 18 that we arrived in Ulaanbaatar.

2008 EXPEDITION

The third KID expedition lasted 40 days between August 15 and September 24, 2008. The field crew included 28 people (16 researchers and twelve Mongolian support staff) (Appendix 1). In addition, we were joined for the whole period by the MBC documentary team (4 people) from Korea to make a film. Because of the vehicle difficulties in 2007, Hwaseong City donated a used six-wheel truck (KAMAZ) to the Paleontological Center. We used two jeeps, six vans, and three trucks for this expedition. Therefore, the expedition was the largest among the five expeditions. Meetings at the Paleontological Center selected Altan Uul, Bugiin Tsav, Hermiin Tsav, and Nemegt for the 2008 field program. The base camp was to be set up at Hermiin Tsav, the primary target.

The Korean contingent plus Currie, Jacobs, Koppelhus, Polcyn, and Sissons arrived in Ulaanbaatar on August 15, after attending a workshop in Hwaseong City in Korea. The next day, the MBC documentary team arrived in Ulaanbaatar. Two more days were spent in Ulaanbaatar applying for visa extensions, preparing supplies and food, and arranging a hot air balloon for aerial cinematography (because cinematic drones were unavailable at that time).

On August 19, two trucks (KAMAZ and ZIL) left before dawn, and the team started with eight vehicles at 8:15 AM. Gas prices had suddenly increased when Russia stopped exporting gasoline, and the Mongolians were seriously concerned about this matter. Consequently, this year an unpaved road was used to go to Arvaykheer, unlike in the past, because it was shorter than the paved road by about 100 km. Furthermore, the paved road was heavily damaged and was in worse shape than the unpaved road. This decision turned out to be very good in that the trip went smoothly except for one flat tire.

We set up the first camp beside the road at 7:30 PM, some 250 km from Ulaanbaatar. We arrived at Arvaykheer the next day at 3:00 PM, but the entire city was experiencing a blackout. After asking around, we found a gas station that pumped gasoline with a generator. The gas station already had many cars lined up for gas, but we filled up all our vehicles. It was 8:00 PM before we set up camp next to the road. We arrived the following morning at Baruunbayan, a small village, on August 21. Alluvial fans, dunes, rivers, and small lakes spread out from the distant mountains, almost looking like environments of the Cretaceous Period. A gas station at Baruunbayan was the last place to fill up the vehicles with gasoline and diesel before entering the southern Gobi. The village was also in a blackout, and we had to use our generator to run a gas pump at the station. One van broke down en route, and we took the road to Bayanlig instead of Bayangobi. It was a slightly larger village, and had a mechanic to fix the van. This village was also in a blackout. We stayed one night near the north slope of Gilbent Mountain. The following day, we realized that the axle bearing of the wagon with the water bowser was broken and left behind with the plan to pick it up later after setting up the base camp at Hermiin Tsav. We finally arrived inside the valley of Hermiin Tsav at 7:00 PM on August 22.

On the first day of the fieldwork, we visited the “Russian ankylosaur” (MPC-D 100/1359). Y.-N. Lee found a small lizard (KID 236), and Lü found a multituberculate skull (KID 238) from the Barrungoyot Formation. On August 24, the prospecting was difficult because of a strong sandstorm. Nevertheless, Jacobs and Polcyn found a *Bagaceratops* skull (KID 262) and excavated it; another *Bagaceratops* skull was found nearby the following day. Bell found an oviraptorid skeleton (KID 251). On August 26, three lizard skulls, *Gobipteryx* eggs, and various isolated dinosaur bones were collected. Sissons found a small theropod (MPC-D 102/114), which turned out to be a significant specimen for confirming the validity of Halszkaraptorinae and their semi-aquatic behavior. Named *Natovenator polydontus*, it had a streamlined body similar to those of modern diving birds with ribs that are angled toward its tail (Lee et al., 2022). This discovery was important because it proved that this new type of non-avian dinosaur could be semi-aquatic.

On August 27, we excavated and made jackets for the

oviraptorid skeleton (KID 251) that Bell had found, which contained some postcranial elements, including the pelvic girdle. Kobayashi found a big therizinosaurid manual claw, which reminded us that we were in the famous place where two giant arms of *Therizinosaurus* (MPC-D 100/15) were found in 1973 (Barsbold, 1976). We split the team the next day to explore Bugiin Tsav and the Nemegt Basin. The Canadian contingent stayed in the Nemegt Basin, and the remainder of the team worked in Bugiin Tsav for three days. Y.-N. Lee found a braincase of cf. *Prenocephale* (MPC-D100/1207), which helped to illusidate the ontogenetic variation of Nemegt pachycephalosaurs (Evans et al., 2018). Jacobs found a turtle bone bed, where many turtles (mainly *Mongoleyms*) were aggregated, suggesting a mass death in a turtle pond. H.-J. Lee collected a complete *Mongoleyms*, including a skull (KID 323).

The Bugiin Tsav camp awoke on August 29 to find that it had rained all night. Ligden told us at noon that we had to return to camp in Hermiin Tsav because the road we had to pass was filling with water; so everyone packed their tents and headed to the base camp. Fortunately, our vehicles passed the river despite two crises, and we safely returned to the base camp around 4:00 PM. The next day, the Canadian contingent returned to camp after having discovered six *Tarbosaurus* sites. Fieldwork in the Nemegt Basin had not been easy either because of rain.

On August 31, we began to excavate the "Russian ankylosaur" (MPC-D 100/1359) by saving the wooden crates of the monolith as historical items. We hardened the skeleton with PVA because the upper layer containing the skeleton was in loose muddy sandstone, while the lower layer was hard sandstone. Bell found an oviraptorid femur and protected it with a plaster jacket (KID 331). The next day, H.-J. Lee found a nest containing eight round eggs. The matrix was too hard to excavate the entire nest, and it took two days to collect three complete eggs.

On September 3, we headed to Altan Uul III and relocated and reopened the holotype quarry of *Deinocheirus*. Nearby, Lü found small theropod bones and made two plaster jackets. The excavation produced one new oviraptorid, *Gobiraptor minutus* (MPC-D 102/111), and three alvarezsaurids (MPC-D 100/203, 206, 207), including a new species, *Nemegtonykus citus* (Lee et al., 2019a, b). The mandibular morphology of *Gobiraptor* is unique among oviraptorids, which may have been an adaptation for hard foodstuffs, such as seeds or bivalves. The number and diversity of alvarezsaurids also suggested that these dinosaurs were more abundant during Nemegt times than the previous fossil had suggested (*Mononykus* was the only known species before).

The film crew had arranged for some aerial photography to be done from a hot air balloon, but it had not shown up on the agreed-upon date. On September 3, we met people on the road looking for our camp. They were in a small, broken-down truck loaded with the hot air balloon. They had repeatedly gotten lost and stuck on the sandy road for six days after leaving Ulaanbaatar. Our meeting them on the road by chance in the middle of the Gobi Desert was truly miraculous. We continued to base camp, initially with them. However, their truck kept causing problems, and because it was getting dark, we had to leave them to spend another night on the road. The following day, the MBC team with Ligden rescued the balloon truck.

September 4 also saw the discovery of another *Bagaceratops* (KID 381) and a lower jaw of *Tarbosaurus* (KID 378) by Sissons and Bell. A rib sticking out from an exposure that Kobayashi had found a few days before turned out to be an ankylosaur (MPC-D 100/1353). The well-preserved *Tarbosaurus* lower jaw was high on a vertical cliff, but led to the discovery of most of the skull and skeleton, and over the next few days during excavation, produced the left maxilla, lacrimal, nasal, parts of the back of the mandible, teeth, and the axis and 3rd cervical vertebra.

In the meantime, the American contingent kept excavating the ankylosaur (MPC-D 100/1353), and soon found the pelvic girdle. The front part of the body was scattered, but the back of the body, including the tail, was articulated *in situ*. The MBC team recorded the whole process of excavation of this animal by using a Jimmy Jib. However, they gave up the idea of doing aerial cinematography using the air balloon because of the strong winds at Hermiin Tsav.

On September 6, Lü returned to Ulaanbaatar with three Mongolian staff. We continued to excavate the ankylosaur (MPC-D 100/1353) and *Tarbosaurus* (KID 378) for two more days. During this period, we collected two more *Bagaceratops* skulls. On September 8, we found both the skull and tail club at the ankylosaur site. The skull was found upside down inside the basket-like ilia, and the tail that was normally stiffened with ossified tendons was bent and broken so that the tail club was lying on top of the ilia. This specimen turned out to be a new species, *Tarchia tumanovae*, and

FIGURE 4. *Tarchia tumanovae* (MPC-D 100/1353) was being excavated at Hermiin Tsav on September 10, 2008.

provided evidence of a dietary change from low-level bulk feeding to selective feeding during Baruungoyot and the Nemegt times. In addition, pathologies on the dorsosacral ribs and the tail provided evidence of the agonistic behavior of this animal (Park et al., 2021b).

The *Tarbosaurus* quarry was finished with the production of eight plaster jackets. MPC-D 100/1353 was mapped, and on September 9 we began to make plaster jackets. The tail and four ribs were separated from the main ankylosaur body the next day and jacketed. We decided to make one jacket for most of the body with the skull (Fig. 4), and the plaster and burlap jacket, weighing approximately two tonnes was ready to move by September 11.

In the meantime, the Canadian contingent had begun to excavate the "Russian ankylosaur" (MPC-D 100/1359). It was too big to include in one jacket, and was separating into three. This ankylosaur includes twelve dorsal vertebrae, ribs, pectoral girdles, forelimbs, pelvic girdles, hindlimbs, and free osteoderms, which presented the most complete postcranial skeleton of an ankylosaurid from the Baruungoyot Formation. Therefore, this articulated postcranial skeleton with in situ dermal scutes provided valuable insight into the postcranial evolution of ankylosaurids (Park et al., 2021a).

We spent the next three days loading the two giant ankylosaur specimens (MPC-D 100/1353, 1359) into the truck. After barely being able to flip the oversized ankylosaur jacket (MPC-D 100/1353), the truck winch dragged it to the top of the hill. We all pushed it up into the truck on wooden boards. At the "Russian ankylosaur" quarry, the heavy truck could not climb the sandy hill after loading the three jackets of MPC-D 100/1359. The winches on the other two trucks eventually pulled it up the hill. From September 14 to 16, the Canadian contingent and Kobayashi worked in Altan Uul, and the remainder of the expedition worked in Bugiin Tsav. The Canadian contingent collected *Saurolophus* skin impressions (KID 416) at Altan Uul II, and three gastralia with many bone fragments at the holotype quarry of *Deinocheirus* at Altan Uul III. Bite marks on two gastralia (MPC-D 100/126) were attributed to *Tarbosaurus* based on the presence of parallel, broadly U-shaped 0.5 mm diameter striae (Bell et al., 2012). At Bugiin Tsav, the American contingent began to make two jackets of aggregated turtles (KID 431). The Canadian contingent came back in a sandstorm to the Bugiin Tsav camp on the evening of September 16.

On September 17, because all supplies, especially food and water, were running out, we decided to return to Ulaanbaatar the next day, which was one day earlier than the original plan. Because we had run out of burlap, we finished making the plaster jackets for the two turtle blocks by cutting up T-shirts. We found a *Tarbosaurus* foot (KID 428) underneath a three meter thick sandstone block but decided to excavate it next year. On September 18, we left for Ulaanbaatar, where we arrived at 2:30 AM on September 20. The MBC documentary "Land of Dinosaurs" was first broadcast in Korea on January 18th, 2009.

2009 EXPEDITION

The fourth KID expedition lasted 38 days, from August 3 to September 9. The field crew comprised 24 people (13 researchers and eleven Mongolian support staff) (Appendix 1). We used two jeeps, three vans, and two trucks (ZIL and KAMAZ) for this expedition. At official meetings in the Paleontological Center, the field sites of Altan Uul, Bugiin Tsav, Nemegt, and Tsagaan Khushuu were picked as the focus for the 2009 expedition. The base camp was set up at Bugiin Tsav, the primary target. The Nemegt Formation at Bugiin Tsav is unlike the other sites because rather than being in canyons, the 80 m thick beds are distributed over a wide area of 8 km^2. The fossils include skeletons of *Gallimimus*, *Nomingia*, *Saurolophus*, and *Tarbosaurus*.

The Korean contingent arrived in Ulaanbaatar on August 3. After checking our field gear at the Paleontological Center on August 4, we returned to the hotel to discover that Graf from the USA was not checked in because nobody had picked him up at the airport. We rushed to the airport and found him in a panic because he had been abandoned for four hours on his first visit to Mongolia. In the afternoon, we went to the eastern lab, where supplies were loaded onto one truck (ZIL). The other truck (KAMAZ) was empty, and its cargo space had been replaced with a giant shipping container. By the next day, the two trucks left in the evening.

On August 6, the rest of the expedition left at 8:30 AM. Basbold was not able to attend this time due to a health problem. We caught up with the two trucks at Arvaykheer that afternoon. However, by the next day the KAMAZ repeatedly stopped every few kilometers because the engine was over-heating. The Mongolian drivers tried to fix a cracked gasket, but the problem was not solved. We got stuck on the road just 50 km south of Arvaykheer. During the disassembly of the engine, the drivers found that the upper part of the right 4^{th} cylinder sleeve was cracked. When they opened the engine bottom and pulled out the piston, Lidgen went to Arvaykheer to get an engine sleeve. He returned with the sleeve much earlier than we expected. On the way back to Arvaykheer, lucky enough, he met a KAMAZ truck driver with an extra sleeve of the same model. Because of the engine problems of the KAMAZ, we spent three days getting parts and fixing the truck. There was nothing for researchers to do because we were on the Mongolian steppe above the metamorphic rocks. On September 10, we moved again, but frustrating enough, the truck soon stopped with an overheated engine. Most of the expedition proceeded to the next village, Baruunbayan, and left the two trucks to make their way with frequent stops to cool down. As expected, there was no way to fix the truck because we could not get the necessary parts in the village. We moved the essential items to set up camp from the KAMAZ to the ZIL truck, and left KAMAZ with Jagaa at Baruunbayan. The four vehicles finally arrived at Bugiin Tsav at 4:00 PM on August 11. It had taken six days to reach the destination, which was four days more than expected. After setting up the base camp, Ligden returned to the Baruunbayan with a ZIL to fix the KAMAZ.

We split into two groups on August 12, the first day of fieldwork. One group visited the *Tarbosaurus* site that we found on the last day of the 2008 expedition. We tried to move the big block covering the *Tarbosaurus* (KID 428) down the hill, but it would not move. We were at Bugiin Tsav, notorious for high summer temperatures, and it was over 40°C with a bit of humidity. We drank much water, so we worried about the shortage of drinking water. The other contingent visited the Hayashibara base camp (Hayashibara Museum of Natural History Expedition, Japan) nearby and got information on fossil occurrences. A few isolated dinosaur footprint casts were found in an outcrop at the west end of the camp. After removing the big block with pry bars and car jacks at the *Tarbosaurus* site the next day, we found a lower hind limb but no more bones. The ZIL and KAMAZ arrived in camp in the afternoon. A severe sandstorm hit the camp at night.

On the morning of August 14, we fixed broken tents and rebuilt the camp. In the afternoon, we investigated an attractive bone bed of *Gallimimus* that we had found on the day we arrived. It included five holes that had been made by

poachers, which were subsequently covered with sand. By sweeping the sand from one of these holes, we found the horizon had 14 theropod trackways, and the skeleton of a *Gallimimus* foot (MPC-D 100F/17). The next day, we continued to uncover the *Gallimimus* track site. We studied the unusual association of dinosaur bones and footprints using taphonomic and sedimentologic data, and concluded that it was hard to prove that there was a direct association between the *Gallimimus* foot and the theropod trackways (Lee et al., 2018).

On August 16, while prospecting in the low hills northwest of Bugiin Tsav, H.-J. Lee and Y.-N. Lee discovered a large quarry that had been poached. The poached quarry was littered with broken bones, large sandstone blocks, empty Chinese superglue and vodka bottles, pieces of plaster, and other junk – clearly the work of unprofessional poachers. The articulated sacral and caudal vertebrae, pelvic girdle, and femur were identified in the sandstone blocks. We returned to the camp as the sun went down. The next day, all the crew went back to see the quarry. Currie told us it could be *Therizinosaurus* because the long neural spines and uniquely shaped pelvic girdle did not belong to *Tarbosaurus*. We all were delighted to think that we might have found *Therizinosaurus*, one of the mysterious dinosaurs of the Gobi. The poached quarry was easy to access by car, and the overburden was not too thick, so the work did not seem too difficult. However, it was judged that a full excavation would take at least ten days.

On August 18, trucks were loaded with excavation equipment, and all team members headed for the site. Except for the big blocks, we started to collect the broken and scattered bones. The cervical, sacral, and caudal vertebrae were collected with the femur, tibia, fibula, and phalanges (Fig. 5). Still, the pectoral girdle and forelimbs were desperately needed to confirm the identification of *Therizinosaurus*. Adams, Jacobs, and Kobayashi arrived at the camp at 11:30 PM that night. The next day was the most memorable of the KID expedition. The quarry was getting more and more interesting. A uniquely shaped pygostyle was found with many gastralia. In addition, more than 1100 rounded and polished gastroliths were recovered in the vicinity of the abdominal ribs. The vertebrae were pneumatic, with highly developed fossae and laminae, similar to those of sauropod dinosaurs. The identity of this dinosaur became more and more curious. At 3:30 PM, Y.-N. Lee finally identified a fused left coracoid and scapula on the block he was working on. It was none other than the scapulocoracoid of *Deinocheirus*. It was clearly not *Therizinosaurus*. He jumped up and shouted. “This is *Deinocheirus*. We found *Deinocheirus*.” Everyone cheered and rushed to see the bone. It was at that moment that we identified the dinosaur that had been a mystery for the past half-century. Y.-N. Lee pulled out Osmólska’s 1970 *Deinocheirus* paper in the evening in camp, and the scapulocoracoid drawings and photographs exactly matched the bones we found.

From August 20 to September 3, the last day in the field, the excavation and jacketing continued to get all bones of *Deinocheirus* from the quarry. Larger blocks were encased in plaster jackets and pulled sideways from the excavation. Further excavation was carried out in the newly exposed regions to reveal several cervical vertebrae, and a left humerus, ulna, and radius. The distal parts of the ulna and radius, and part of the metacarpus were found in the rubble left by the poachers. The left forearm was now complete except for the distal parts of the metacarpals and the phalanges. The poachers probably took the left hand. They probably also had collected the right forelimb and both feet (except for one pedal phalanx), and unfortunately, the skull was also missing. The fact that the axis of the cervical vertebrae was broken suggested that they had found the skull. In addition, the dorsal vertebrae with long neural spines were severely crushed and damaged, probably in the process of pulling out the skull underneath. This illegal activity had occurred after 2002, because Mongolian paper money issued in 2002 was left in the quarry, supposedly by the poachers, along with a bottle of vodka. Mongolians have a tradition of leaving a bottle of liquor and a small donation at Ovoo for safe travel.

Fish vertebrae were found along with gastroliths inside the gastralia. These bones had been corroded by gastric acid, which suggested that *Deinocheirus* ate fish. But over 1100 gastroliths found together suggest that *Deinocheirus* ate plants, too. *Deinocheirus* (MPC-D 100/127) was transported to Ulaanbaatar in 38 large and small plaster jackets and several wooden boxes. During the preparation in Korea, Y.-N. Lee noticed that the characteristics of the femoral head were similar to those of an unidentified specimen (MPC-D 100/128) collected in Altan Uul IV in 2006. This specimen was smaller than the Bugiin Tsav *Deinocheirus*, and included the dorsal and caudal vertebrae, pelvic girdle, femur, and tibia. Its femur had the same characteristics as *Deinocheirus*, which confirmed that it was the same species.

FIGURE 5. *Deinocheirus* (MPC-D 100/127) excavating site at Bugiin Tsav on August 18, 2009.

In June 2011, Pascal Godefroit of the Royal Belgian Institute of Natural Sciences contacted Currie to inform him that a European private collector owned the skull, left hand, and both feet of what might be *Deinocheirus*. These bones had been sold to a Japanese fossil collector, and then resold to a German fossil dealer. Y.-N. Lee, Currie, and Kobayashi visited Belgium to observe the fossils and immediately realized they were the missing parts of MPC-D 100/127. None of these bones had been found in the poached quarry, so there were no overlapping bones. We had found the proximal ones of the left metacarpus, but the European specimen had the distal ends of the same bones. Even the one foot bone that we had recovered from the quarry (a right pedal II-2) was missing from the poached specimen in Belgium. When the specimen was repatriated from Europe, the proximal articular facet of pedal phalanx II-2 that we had found fit perfectly with the distal articular facet of pedal phalanx II-1, and with an impression in matrix that had not been prepared. Finally, the last puzzle piece was put together. The long-standing enigmas of *Deinocheirus* for a half-century had been resolved at last (Lee et al., 2014).

In addition, the bone color and the matrix surrounding bones were the same as those of the bones we had excavated. The elongate skull of *Deinocheirus* had a broad snout like a duck-billed hadrosaur, but also had a large lower jaw and no teeth like an ornithomimid dinosaur. The robust feet of *Deinocheirus* were shaped to support weight instead of running rapidly, and the tips of their claws were blunt, which was a unique shape observed for the first time in theropod dinosaurs. Eventually, these fossils were repatriated to Mongolia on May 1, 2014. Soon after, Y.-N. Lee and Currie visited the Paleontological Center to study the skull.

During the final days of the 2009 expedition, the Canadian contingent visited Altan Uul and Nemegt to collect fossils (including a *Deinocheirus* metatarsus KID 452), and also pinpointed the site of the Polish-Mongolian Paleontological Expedition quarry for the holotype specimen from 1965 (Currie, 2016). They also collected a *Saurolophus* braincase

and crest (KID 476) at Bugiin Tsav.

The American contingent made four jackets of blocks containing theropod trackways and the foot at the *Gallimimus* track site, and made a short visit to Tsagan Khushuu on August 24. The collected fossils include articulated proximal caudal vertebrae of *Barsboldia* (KID 477, Prieto-Márquez, 2011) and a hadrosaur foot (KID 459), as well as natural footprint casts of small (KID 444) and large (KID 445) theropods, a big ornithopod (KID 446), and a big sauropod pes (KID 448) footprints. On September 4, we left for Ulaanbaatar and arrived at 6:30 PM on September 5.

2010 EXPEDITION

The last KID expedition lasted for 43 days between August 18 and October 1. The field crew comprised 27 people (18 researchers and nine Mongolian support staff) (Appendix 1). The Canadian contingent left for the Nemegt Basin on August 19, but most of the expedition did not leave until August 26. Three jeeps, four vans, and two trucks (ZIL and KAMAZ) were used for this expedition. In addition, the SBS documentary team (two people) from Korea joined us for a short period to make a film. Altan Uul, Bugiin Tsav, Guriliin Tsav, Khuree Tsav, Nemegt, and Nogoon Tsav were the planned expedition destinations. The first base camp was set up at Bugiin Tsav and moved to Khuree Tsav later.

As usual, purchase of supplies and loading of field gear took three days in Ulaanbaatar. The two trucks left in advance on August 25, and the rest left on the following day in three jeeps and one van. We met our trucks at Arvaykheer at 1:30 PM and went further south, although the KAMAZ had a little problem. On August 28, we arrived at Bugiin Tsav through Khaichin Uul in the afternoon. The Canadian contingent joined us in the evening with a baby *Gallimimus* (KID 499) that they had collected from the Nemegt Basin. We had to rebuild our camp the next day after it was damaged by strong wind overnight. A few bones were collected in the afternoon near the camp. On August 30, we headed to Guriliin Tsav but did not find good specimens except for isolated *Gallimimus*, *Saurolophus*, *Tarbosaurus*, and turtle bones. The next day, we excavated an oviraptorid pelvic girdle with hind limbs (KID 585). On September 1, Barsbold and Eberth returned to Ulaanbaatar. The next day, we made a reconnaissance at Khuree Tsav, 25 km west of the base camp. Khuree Tsav is a relatively unexplored area compared with other famous localities in the southern Gobi. We found many poached sites with some bones, implying that dinosaurs and turtles are abundant at this site. The two hind legs of the oviraptorosaur (KID 585) were buried vertically in the lower mud layer, suggesting it was mired in death. Unfortunately, the upper body was already weathered in the upper sandstone layer.

On September 4, we tried to reach Nogoon Tsav, where we got lost on the way back to Hermiin Tsav in 2008. The trip was not as bad as the last time, and we found many turtles, ankylosaurid dermal scutes, and sauropod skin impressions (KID 599). A giant sandstorm hit our camp in the evening. It rained the next day, so we spent time cataloging and sorting bones. On September 6, we took a jackhammer with a generator to excavate further at the *Deinocheirus* site (MPC-D 100/127) to see if additional bones might exist, but only found a few fragmentary bones and more gastroliths. Fiorillo, Graf, Jacobs, Lü, and two SBS film crew arrived at the camp in the afternoon. The next day, it kept raining, and a cook (Otgon) returned to Ulaanbaatar because her mother passed away. On September 8, we collected an ankylosaurid humerus (KID 630), an ornithopod pathologic fibula (KID 632), and a few isolated bones in Khuree Tsav.

On September 10, we plastered an oviraptorosaur (KID 585), and the American contingent found natural footprint casts at Guriliin Tsav. A freshwater clam was found on the bottom of one ornithopod footprint. Several oviraptorid nests were found at Bugiin Tsav, which might be the first discovery of a colonial nesting ground of oviraptorids (KID 652). We excavated the site the next day, but the clutches were incomplete, so we only collected eggshells. The excavation of a small complete theropod (KID 643) and a sauropod (KID 650) continued in Bugiin Tsav on September 12. The sauropod consisted of giant ilia with six sacral vertebrae. The American contingent visited Khaichin Uul and collected dinosaur eggshells, where the Eocene beds unconformably overlie the Cretaceous Nemegt Formation.

An exciting site was found in the afternoon of September 13 at Khuree Tsav, where articulated distal caudal vertebrae stuck out on a low hill. They continued to the inside of the bed. A pelvis was soon exposed by excavation, followed by the dorsal vertebrae. Even though we were all excited, we had to be careful because the matrix was soft, and the bones were fragile. The skull curved backward, with the neck bent over the dorsal vertebrae. It was a juvenile *Tarbosaurus* (KID 675). Because it was getting dark, we returned to the camp

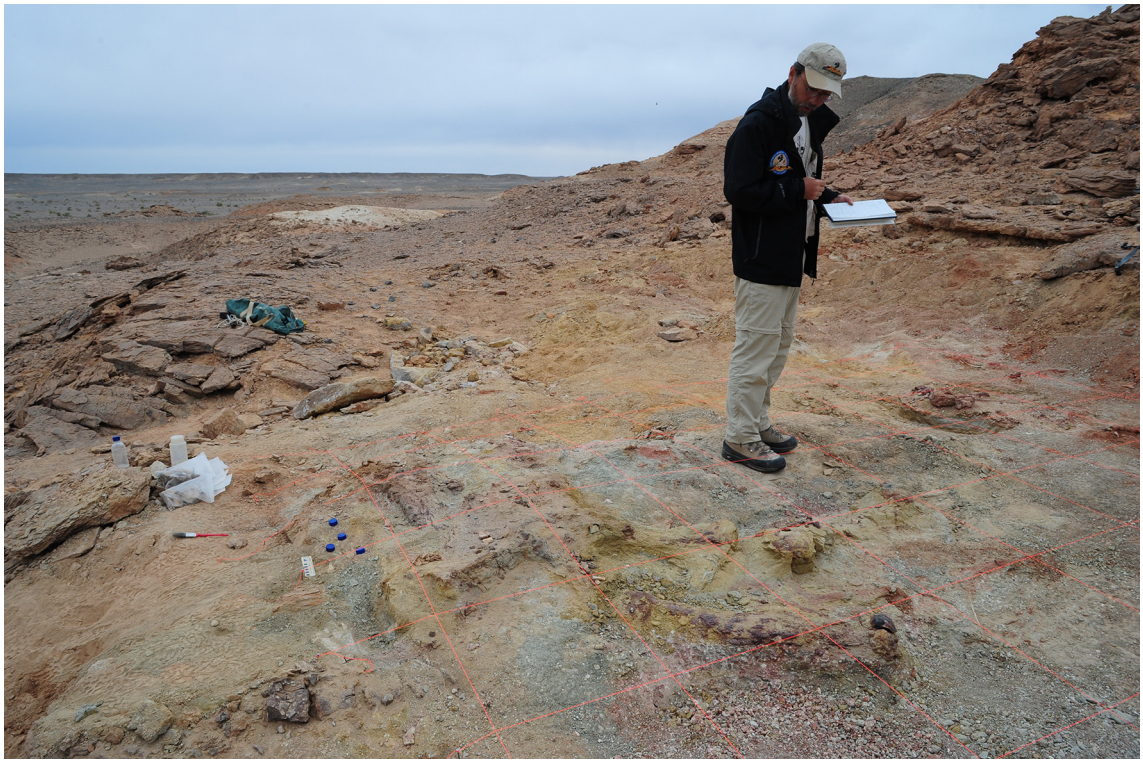

FIGURE 6. Mapping a juvenile *Tarbosaurus* (KID 675) at Khuree Tsav on September 20, 2010.

and discussed the specimen and moving the camp. However, before moving the camp to Khuree Tsav, we had to finish a big sauropod. While the Canadian contingent excavated it, the rest of the crew packed all collections on September 14. The Canadian contingent, Fiorillo, and two SBS producers left for Ulaanbaatar the next day. We finished closing the oversized jacket of the sauropod.

On September 16, we loaded the oversized sauropod jacket into the truck with 20 other plaster jackets and seven sample boxes. In the afternoon, two jeeps, three vans, and two trucks headed to Khuree Tsav and camped near the *Tarbosaurus* site. The next day, the American contingent returned to Bugiin Tsav and found twenty distal caudal vertebrae of *Barsboldia* (KID 477). The *Tarbosaurus* femur was inside a large concretion, and a well-preserved pubis was newly exposed. On September 18, we found another femur, pubis, the 3rd metatarsal, and phalanges. The next day, we found scattered gastralia and teeth in the dentary. We prepared the grid for mapping the next day. In the following two days, we made five jackets for the tail, limb bones, and isolated blocks except for the main body (Fig. 6).

On September 22, the skeleton that needed to be jacketed was cut down to $2 \times 1.5 \times 0.5$ m. Although the thick sandstone underneath the bone layer is too hard to dig out, we undercut the specimen as far as possible. After the jacket was completed (we had a shortage of burlap), we tried to flip it with a truck winch. The 500 kg jacket was slowly lifted and moved, but the center part had not separated from the sandstone layer below. The collapsed center was filled with plaster and sand and reinforced with pieces of wood. The skull part was secured with a separate jacket. This *Tarbosaurus* gave us a grand finale of five years of expeditions. Unfortunately, the specimens collected from the 2010 expedition have not been shipped to Korea due to new Mongolian custom regulations. They will be prepared and studied soon.

DISCUSSION

The greatest challenge for the KID expedition was the Russian military trucks, which were too old and frequently broke down. As a result, the exploration period was often shortened due to delays. If modern and sturdy 4-wheel drive trucks are used in the future, such problems are expected to decrease dramatically. This is also becoming less problematic

as the road system continues to be improved.

All the famous fossil localities that we visited had already been poached, and showed the magnitude of illegal activities. Although poaching has decreased somewhat due to the crackdown by the Mongolian government, it is not easy to manage such a vast area as the Gobi where even nomadic people are widely dispersed. Poachers often take only valuable parts of the skeleton, such as skulls, teeth or claws, and many large elements are left behind (or even destroyed) because they are too bulky. Therefore, we sometimes made astonishing discoveries by looking carefully at poached sites. This was the case with *Deinocheirus*. Due to continuous exploration and excavation since 1923, it is reasonable to say that there are almost no places in famous fossil sites where people have not been. Therefore, exploring unknown localities, even though small and unnamed, can be a way to find untouched fossil sites. Evidently, there are still many unexplored Cretaceous strata in the Gobi, such as Ukhaa Tolgod.

Although dinosaur footprints in the Gobi were relatively late to be discovered (Currie et al., 2003), they are now commonly found in many localities. They are found as impressions on bedding planes, but are more often as natural casts. These footprints are often preserved with sliding marks in three dimensions, so research on these footprint casts will continue to reveal information on how the animals were moving and interacting. Although many expeditions have visited the Gobi over the past 100 years, new fossils continue to be discovered every time. Undoubtedly the Gobi will always remain one of the most important areas for dinosaur fossils in the world.

CONCLUSION

After five years of KID expeditions, 267 plaster jackets and 125 boxes of specimens were transported to the Paleontological Center in Ulaanbaatar. Except for the 2010 collection, the specimens were then shipped to Hwaseong City, Korea, for preparation and research. The collection was cataloged as 694 specimens, including a variety of fossil assemblages such as plants, fishes, turtles, lizards, crocodyliforms, dinosaurs, birds, and mammals. In addition to bones, there were footprints, skin impressions, and eggs. These fossils prove again that the Gobi is the Mecca of Vertebrate Paleontology. Six people prepared all specimens shipped to Korea for six years at the Hwaseong dinosaur visitor center laboratory, and then all fossils were repatriated to Mongolia in April 2017.

All participating researchers of the KID expedition have been working on specimens for scientific papers together. Eighteen important paleontological papers have been published so far, and more articles are expected to be published soon. Besides its outstanding scientific achievement, the KID expedition promoted international cooperation, built collections for research, and fostered education by providing graduate students with opportunities to study valuable specimens. It was also a critical project for the museum of Hwaseong City, which is now constructing a “Dinosaur Science Center” at the dinosaur egg site that aims to be the top dinosaur research institute in Korea. The authorities of Hwaseong City recognize with confidence that this center associated with the KID expeditions will enhance the cultural attraction and promote ecotourism in Hwaseong City.

ACKNOWLEDGMENTS

We thank all members of the Korea-Mongolian International Dinosaur Expeditions (KID). The KID expedition was supported by a grant to Y.-N. Lee from Hwaseong City, Gyeonggi Province, South Korea. We appreciate Hwaseong City’s continuous support of the KID expeditions, fossil preparation, international dinosaur conferences, and the museum project. This research was supported by the Basic Science Research Program through the National Research Foundation of Korea (NRF), funded by the Ministry of Education (grant number 2022R1I1A2060919) to Y.-N.L.

LITERATURE CITED

Barsbold, R. (1976). “Новые данные о теризинозавре (Therizinosauridae, Theropoda)” [New data on Therizinosaurus (Therizinosauridae, Theropoda)]. In N. N. Kramarenko, B. Luvsandansan, Y. I. Voronin, R. Barsbold, A. K. Rozhdestvensky, B. A. Trofimov, & V. Y. Reshetov (Eds.), *Paleontology and Biostratigraphy of Mongolia* (pp. 76–92). The Joint Soviet-Mongolian Paleontological Expedition, Transactions (in Russian). Moscow: Nauka Press.

Bell, P. R. (2012). Standardized terminology and potential taxonomic utility for hadrosaurid skin impressions: a case study for *Saurolophus* from Canada and Mongolia. *PLoS ONE*, 7, e31295.

Bell, P. R., Currie, P. J., & Lee, Y.-N. (2012). Tyrannosaur feeding traces on *Deinocheirus* (Theropoda: ?Ornithomimosauria) remains from the Nemegt Formation (Late Cretaceous), Mongolia. *Cretaceous Research*, 37, 186–190.

Currie, P. J., Badamgarav, D., & Koppelhus, E. B. (2003). The first Late Cretaceous footprints from the Nemegt locality in the Gobi of

Mongolia. *Ichnos*, 10, 1–13.

Currie, P. J. (2016). Dinosaurs of the Gobi: following in the footsteps of the Polish-Mongolian Expedition. *Palaeontologia Polonica*, 67, 83–100.

Eberth, D. A. (2018). Stratigraphy and paleoenvironmental evolution of the dinosaur-rich Baruungoyot-Nemegt succession (Upper Cretaceous), Nemegt Basin, southern Mongolia. *Palaeogeography, Palaeoclimatology, Palaeoecology*, 494, 29–50.

Eberth, D. A., Kobayashi, Y., Lee, Y.-N. Mateus, O., Therrien, F., Zelenitsky, D. K., & Norell, M. A. (2009). Assignment of *Yamaceratops dorngobiensis* and associated redbeds at Shine Us Khudag (eastern Gobi, Dorngobi Province, Mongolia) to the redescribed Javkhlant Formation (Upper Cretaceous). *Journal of Vertebrate Paleontology*, 29, 295–302.

Evans, D. C., Hayashi, S., Chiba, K., Ryan, M. J., Lee, Y.-N., Currie, P. J., Tsogtbaatar, K., & Barsbold, R. (2018). Morphology and histology of new cranial specimens of Pachycephalosauridae (Dinosauria: Ornithischia) from the Nemegt Formation, Mongolia. *Palaeogeography, Palaeoclimatology, Palaeoecology*, 494, 121–134.

Graf. J., Tabor, N. J., Ferguson, K., Winkler, D. A., Lee, Y.-N., May, S., Barsbold, R., & Jacobs, L. L. (2018). Diagenesis of dinosaur eggshell from the Gobi Desert, Mongolia. *Palaeogeography, Palaeoclimatology, Palaeoecology*, 494, 65–74.

Kim, B, Yun, H., & Lee, Y.-N. (2019). The postcranial skeleton of *Bagaceratops* (Ornithischia: Neoceratopsia) from the Baruungoyot Formation (Upper Cretaceous) in Hermiin Tsav of southwestern Gobi, Mongolia. *Journal of the Geological Society of Korea*, 55, 179–190 (in Korean with English abstract).

Kim, S.-H., Lee, Y.-N., Park, J.-Y., Lee, S., Winkler, D. A., Jacobs, L. L., & Barsbold, R. (2022). A new species of Osteoglossomorpha (Actinopterygii: Teleostei) from the Upper Cretaceous Nemegt Formation of Mongolia: paleobiological and paleobiogeographic implications. *Cretaceous Research*, 135, 105214.

Ksepka, D. T. & Norell, M. A. (2006). *Erketu ellisoni*, a long-necked sauropod from Bor Guvé (Dornogov Aimag, Mongolia). *American Museum Novitates*, 3508, 1–16.

Ksepka, D. T. & Norell, M. A. (2010). The illusory evidence for Asian Brachiosauridae: new material of *Erketu ellisoni* and a phylogenetic reappraisal of basal Titanosauriformes. *American Museum Novitates*, 3700, 1–27.

Lee, H.-J., Lee, Y.-N., Adams, T. L., Currie, P. J., Kobayashi, Y., Jacobs, L. L., & Koppelhus, E. B. (2018). Theropod trackways associated with a *Gallimimus* foot skeleton from the Nemegt Formation, Mongolia. *Palaeogeography, Palaeoclimatology, Palaeoecology*, 494, 160–167.

Lee, S., Lee, Y.-N., Chinsamy, A., Lü, J., Barsbold, R., & Tsogtbaatar, K. (2019a). A new baby oviraptorid dinosaur (Dinosauria: Theropoda) from the Upper Cretaceous Nemegt Formation of Mongolia. *PLoS ONE*, 14(2), e0210867.

Lee, S., Pak, J.-Y., Lee, Y.-N., Kim, S.-H., Lü, J., Barsbold, R., & Tsogtbaatar, K. (2019b). A new alvarezsaurid dinosaur from the Nemegt Formation of Mongolia. *Scientific Reports*, 9, 15493

Lee, S., Lee, Y.-N., Currie, P. J., Sissons, R., Park, J.-Y., Kim, S.-H., Barsbold, R., & Tsogtbaatar, K. (2022). A non-avian dinosaur with a streamlined body exhibits potential adaptations for swimming. *Communications Biology*, 5, 1185.

Lee, Y.-N. 2003. Dinosaur bones and eggs in South Korea. *Memoir of the Fukui Prefectural Dinosaur Museum*, 2, 113–121.

Lee, Y.-N., Barsbold, R., Currie, P. J., Kobayashi, Y., Lee, H.-J., Godefroit, P., Escuillie, F., & Chinzorig, T. (2014). Resolving the long-standing enigmas of the giant ornithomimosaur *Deinocheirus mirificus*. *Nature*, 515, 257–260.

Park, J.-Y., Lee, Y.-N., Currie, P.J., Kobayashi, Y., Koppelhus, E. B., Barsbold, R., Mateus, O., Lee, S., & Kim, S.-H. (2020). Additional skulls of *Talarurus plicatospineus* (Dinosauria: Ankylosauridae) and implications for paleobiogeography and paleoecology of armored dinosaurs. *Cretaceous Research*, 108, 104340.

Park, J.-Y., Lee, Y.-N., Currie, P. J., Ryan, M. J., Bell, P., Sissions, R., Koppelhus, E. B., Barsbold, R., Lee, S., & Kim, S.-H. (2021a). A new ankylosaurid skeleton from the Upper Cretaceous Baruungoyot Formation of Mongolia: its implications for ankylosaurid postcranial evolution. *Scientific Reports*, 11, 4101.

Park, J.-Y., Lee, Y.-N., Kobayashi, Y., Jacobs, L. L., Barsbold, R., Lee, H.-J., Kim, N., Song, K.-Y., & Polcyn, M. J. (2021b). A new ankylosaurid from the Upper Cretaceous Nemegt Formation of Mongolia and implications for paleoecology of armoured dinosaurs. *Scientific Reports*, 11, 22928.

Paulina-Carabajal, A., Lee, Y.-N., Kobayashi, Y., Lee, H.-J., & Currie, P. J. (2018). Neuroanatomy of the ankylosaurid dinosaurs *Tarchia teresae* and *Talarurus plicatospineus* from the Upper Cretaceous of Mongolia, with comments on endocranial variability among ankylosaurs. *Palaeogeography, Palaeoclimatology, Palaeoecology*, 494, 135–146.

Prieto-Márquez, A. (2011). A reappraisal of *Barsbolida sicinskii* (Dinosauria: Hadrosauridae) from the Late Cretaceous of Mongolia. *Journal of Paleontology*, 85(3), 468–477.

Watabe, M. & Suzuki, S. (2000). Cretaceous fossil localities and a list of fossils collected by the Hayashibara Museum of Natural Sciences and Mongolian Paleontological Center Joint Paleontological Expedition (JMJPE) from 1993 through 1998. *Hayashibara Museum of Natural Sciences Research Bulletin*, 1, 99–108.

APPENDIX 1. List of field crew (alphabetic last name order of researchers)

2006	2007	2008	2009	2010
Rinchen Barsbold	Rinchen Barsbold	Rinchen Barsbold	Thomas L. Adams	Victoria M. Arbour
Philip J. Currie	Philip J. Currie	Phil Bell	Philip J. Currie	Rinchen Barsbold
Anthony R. Fiorillo	David A. Eberth	Philip J. Currie	David A. Eberth	Philip J. Currie
Bayasgaa Ganzorig	Bayasgaa Ganzorig	Louis L. Jacobs	Bayasgaa Ganzorig	David A. Eberth
Louis L. Jacobs	Namsoo Kim	Bayasgaa Ganzorig	John Graf	Anthony R. Fiorillo
Namsoo Kim	Yoshitsugu Kobayashi	Namsoo Kim	Louis L. Jacobs	Bayasgaa Ganzorig
Yoshitsugu Kobayashi	Eva B. Koppelhus	Yoshitsugu Kobayashi	Namsoo Kim	John Graf
Eva B. Koppelhus	Martin Kundrát	Eva B. Koppelhus	Yoshitsugu Kobayashi	Louis L. Jacobs
Yuong-Nam Lee	Yuong-Nam Lee	Hang-Jae Lee	Eva B. Koppelhus	Namsoo Kim
B. Lkhaasuren	B. Lkhaasuren	Yuong-Nam Lee	Derek W. Larson	Yoshitsugu Kobayashi
Junchang Lü	Buuvei Mainbayar	B. Lkhaasuren	Hang-Jae Lee	Eva B. Koppelhus
Kent Newman	Octavio Mateus	Junchang Lü	Yuong-Nam Lee	Hang-Jae Lee
Michael J. Ryan	Michael J. Ryan	Michael J. Polcyn	B. Lkhaasuren	Yuong-Nam Lee
Kyo-Young Song	Kyo-Young Song	Michael J. Ryan	Ligden Barsbold	Allan Lindoe
Dale A. Winkler	François Therrien	Robin Sissions	Babi	B. Lkhaasuren
Ligden Barsbold	Yosuke Nisida	Kyo-Young Song	Turuu	Junchang Lü
Tsatsral	Dala K. Zelenitsky	Ligden Barsbold	Jagaa	Ariana Paulina-Carabajal
Batugii	Ligden Barsbold	Zorigoo	Darcha	W. Scott Persons IV
Batchuluun	Batugii	Turuu	Mungh	Ligden Barsbold
Gomvold	Divide	Jagaa	Baska	Babi
Chuluunjav	Darcha	Darcha	Mindae	Jagaa
Otogondauur	Chegai	Batochia	Otgon	Darcha
Narantsetseg	Chenbur	Bayaraa		Ji
Otgon	Mungrut	Amgalan		Mungh
	Batbagir	Mungh		Mindae
	Inghe	Baska		Otgon
	Chumong	Otgon		Nara
		Chuka		

APPENDIX 2. List of KID collections mentioned in the text

KID #	Date	Identification	Elements	Locality	Formation	GPS (North)	GPS (East)
KID022	2006-09-12	*Tarbosaurus*	pelvic girdle with proximal caudals	Altan Uul IV	Nemegt	43°36.113'	100°27.274'
KID069	2006-09-21	*Tarbosaurus*	postcranial skeleton with gastralia and stomach content	Altan Uul III	Nemegt	43°35.586'	100°29.760'
KID101	2006-09-25	ornithomimid	a complete skeleton	Ulaan Khushuu	Nemegt	43°30.162'	100°29.373'
KID106	2007-08-21	sauropod	postcranial skeleton without a skull	Shine Us Khudag	Bayanshiree	44°21.515'	109°21.168'
KID113	2007-08-22	therizinosaur	femur	Shine Us Khudag	Bayanshiree	44°20.249'	109°19.224'
KID139	2007-08-28	microsite	"various dinosaur teeth, scutes, claws"	Shine Us Khudag	Bayanshiree	44°16.307'	109°54.503'
KID148	2007-08-28	*Yamaceratops*	postcranial skeleton	Shine Us Khudag	Javkhlant	44°22.648'	109°18.785'
KID150	2007-08-28	*Yamaceratops*	postcranial skeleton	Shine Us Khudag	Javkhlant	44°22.706'	109°19.313'
KID155	2007-08-29	ankylosaur	pelvic girdle with hind limbs	Shine Us Khudag	Bayanshiree	44°21.870'	109°21.450'
KID196	2007-09-10	*Bagaceratops*	skeleton	Hermiin Tsav	Baruungoyot	43°29.636'	99°49.677'
KID202	2007-09-12	an egg nest	dinosaur eggs with embryos	Hermiin Tsav	Nemegt	43°27.990'	99°53.851'
KID205	2007-09-12	crocodyliform	skull	Hermiin Tsav	Nemegt	43°29.582'	99°51.503'
KID206	2007-09-12	*Tarbosaurus*	maxilla	Hermiin Tsav	Nemegt	43°29.571'	99°51.489'
KID236	2008-08-23	lizard	articulated pelvic girdle and hind limbs	Hermiin Tsav	Baruungoyot	43°28.753'	99°50.831'
KID238	2008-08-23	multituberculata	skull and cervicals	Hermiin Tsav	Baruungoyot	43°28.121'	99°50.870'
KID251	2008-08-24	oviraptorid	postcranial skeleton	Hermiin Tsav	Baruungoyot	43°28.037'	99°50.849'
KID262	2008-08-25	*Bagaceratops*	a partial skull	Hermiin Tsav	Baruungoyot	43°28.484'	99°50.228'
KID323	2008-08-30	*Mongoleyms*	skull and shell	Bugiin Tsav	Nemegt	43°50.365'	100°00.903'
KID331	2008-08-31	oviraptorid	femur	Hermiin Tsav	Nemegt	43°27.903'	99°50.039'
KID378	2008-09-04	*Tarbosaurus*	a partial skull with cervicals	Hermiin Tsav	Nemegt	43°27.917'	99°50.268'
KID381	2008-09-04	*Bagaceratops*	a partial skull	Hermiin Tsav	Baruungoyot	43°28.094'	99°50.207'
KID416	2008-09-16	*Saurolophus*	skin impressions	Altan Uul II	Nemegt	43°36.191'	100°33.663'
KID428	2008-09-17	*Tarbosaurus*	a lower hind leg with foot	Bugiin Tsav	Nemegt	43°49.665'	99°58.596'
KID431	2008-09-18	*Mongoleyms*	turtle aggregation	Bugiin Tsav	Nemegt	43°50.365'	100°00.948'
KID444	2009-08-14	theropod	footprint cast	Bugiin Tsav	Nemegt	43°50.037'	100°0.624'
KID445	2009-08-15	*Tarbosaurus?*	footprint cast	Bugiin Tsav	Nemegt	43°50.037'	100°0.624'
KID446	2009-08-15	*Saurolophus?*	footprint cast	Bugiin Tsav	Nemegt	43°49.514'	99°58.553'
KID448	2009-08-18	sauropod	pes footprint cast	Bugiin Tsav	Nemegt	43°53.286'	99°58.174'
KID459	2009-08-24	therizinosaur	foot	Tsagaan Khushuu	Nemegt	43°28.838'	100°21.139'
KID476	2009-09-01	*Saurolophus*	braincase and crest	Bugiin Tsav	Nemegt	43°51.983'	100°00.582'
KID477	2009-09-02	*Barsboldia*	articulated caudals	Bugiin Tsav	Nemegt	43°52.638'	99°58.901'
KID499	2010-08-23	Galimimus	juvenile skeleton	Nemegt	Nemegt	43°32.609'	101°01.927'
KID585	2010-08-29	oviraptorid	pelvic girdle with hind limbs	Bugiin Tsav	Nemegt	43°50.381'	100°02.258'
KID599	2010-09-04	sauropod	skin impression	Nogoon Tsav	Nemegt	43°37.798'	99°10.454'
KID630	2010-09-08	ankylosaurid	humerus	Khuree Tsav	Nemegt	43°44.230'	99°42.323'
KID632	2010-09-08	hadrosaurid	pathologic fibula	Khuree Tsav	Nemegt	43°43.985'	99°41.445'
KID643	2010-09-09	theropd	skeleton	Bugiin Tsav	Nemegt	43°52.400'	100°1.121'
KID650	2010-09-10	sauropod	pelvic girdle	Bugiin Tsav	Nemegt	43°52.257'	100°00.592
KID652	2010-09-12	oviraptorosaur	eggs in nest	Bugiin Tsav	Nemegt	43°50.933'	100°03.169'
KID675	2010-09-13	*Tarbosaurus*	skeleton	Khuree Tsav	Nemegt	43°46.145'	99°41.264'

WINDOWS INTO SAUROPSID AND SYNAPSID EVOLUTION
Essays in honor of Prof. Louis L. Jacobs, pp. 252–259, 2023

THE HOUSE WITH THE WEIRD ANIMAL: A BRIEF ACCOUNT OF THE ESTABLISHMENT OF KARONGA AND OTHER MUSEUMS IN MALAWI

YUSUF M. JUWAYEYI*

Department of Social Sciences, Long Island University, Brooklyn, New York, USA, Yusuf.juwayeyi@liu.edu

ABSTRACT "Will you put them on display?" A Malawian journalist asked Professor Louis Jacobs upon seeing the dinosaur bones for the first time. It struck him that the bones were like nothing he had ever seen before, not even like bones of the *Nswala,* (giraffe) nor the *Mphoyo,* (Wildebeest), two other large animals known to be extinct in Malawi. They belonged to an animal that must have looked weird, and no matter how well he had described the bones in the newspaper, he could not quite capture their essence. The better approach was for Malawians to see the bones for themselves — perhaps in a museum. And therein lay the problem: Malawi had no suitable museums. Today, these bones are exhibited in the Karonga museum, constructed using funds and labor mobilized from both private and public sources. This paper discusses the establishment of the Karonga and other museums in Malawi and the research in Karonga district that resulted in the excavation of the Museum's most prominent fossil — the dinosaur *Malawisaurus dixeyi*. The museum also houses the hominids *Homo rudolfensis* and *Paranthropus boisei*. But the future of museums in Malawi is bleak, as the preservation of the country's cultural and natural heritage does not appear to be a priority for government authorities. Thus, in a broader sense, this paper is an attempt to show how far Malawi has come in the preservation and exhibition of its artifacts, and an argument for why it must continue along the path it has taken.

KEYWORDS Karonga, Museum, Dinosaurs, *Malawisaurus*, Hominids

INTRODUCTION

Museums are a repository of a nation's cultural and natural heritage. There are two things about museums in Malawi that I must mention at the outset. Firstly, there is no vernacular word for museum. This is because a building of any size, irrespective of its use, is called *nyumba*, in the vernacular Chichewa. If it is not a residential building, additional words are added to specify its use, as in *nyumba ya*, house for…. Thus, a museum is *nyumba ya* followed by whatever the local community thinks is easily identifiable with the *nyumba.* Secondly, Malawians had no museum tradition. Museums were not a big part of most Malawians lived experience, which made it difficult for them to even conceptualize what a museum might look like or how it may function. So, for instance, the people of Karonga thought that a museum meant mosque. When they became aware of plans to build one in their area, many of them believed that "the mission of the whole project [was]to Islamise the people" (Gondwe, 2001: 6).

Unlike in neighboring Zimbabwe and Zambia where museums were established early in the colonial period, museums were introduced in Malawi by British settlers very late in the country's colonial period. Malawi, unlike Zimbabwe and Zambia, lacked important discoveries to warrant a museum. Zimbabwe had the famous Great Zimbabwe ruins, which sparked archaeological research as early as the 1890s (Bent, 1892; Randal-MacIver, 1971 Caton-Thompson, 1931). At Kabwe in Zambia, the discovery in 1921 of a hominid, *Homo sapiens rhodesiensis* (Clark, 1970), now referred to as *Homo heidelbergensis* (Klein, 1999), helped intensify research in that country. Not surprisingly, by 1922, Zimbabwe had built its fourth museum (https://naturalhistorymuseumzimbabwe.com/history-of-the-museum/), and Zambia had its first museum opened in 1934 (Mufuzi, 2011).

Awareness of the archaeological finds in Zimbabwe and Zambia encouraged the settlers in Malawi to emphasize archaeology in addition to ethnographic collections. Previously, the settlers had channeled their efforts to collecting from the local people objects of material culture, including current

*Corresponding author

utility materials. With no qualified archaeologists among them, however, they turned to some of those who had worked in Zimbabwe and Zambia. Thus, at various times between 1950 and the 1970s, J. Desmond Clark and R.R. Inskeep, both of whom worked at the Rhodes-Livingstone Museum in Zambia, and Keith R. Robinson of the National Monuments Commission in Zimbabwe did archaeological research in Malawi. While Inskeep (1965) excavated only one Late Iron Age site, Clark and Robinson continued to work in Malawi until the 1970s (Clark, 1956; 1973; Clark et al., 1967; Robinson, 1966, 1970, 1973; Robinson & Sandelowsky,1968). Their research yielded results that clearly indicated that humans had lived in Malawi continuously at least since the Middle Stone Age. These results delighted the settler community in Malawi, whose plans to establish a museum in Blantyre, Malawi's largest city at the time, were realized in 1957 (Clark, 1968). It was the seventh decade since Malawi became a colony and only seven years before the country gained its independence. As an elementary school pupil living in Blantyre in the early 1960s, I visited the museum repeatedly along with my equally curious friends. My interest was not in the objects of material culture; I saw plenty of those in my village. My interest was in the mounted stuffed wild animals.

THE POST-COLONIAL PERIOD

When Malawi gained independence in 1964, three things happened that are relevant to this discussion: first, the Malawi government passed a law in 1965 called the *Monuments Act.* Second, realizing that the new nation lacked expertise in managing cultural and natural heritage, the government sought the advice of UNESCO on how to proceed. UNESCO responded by sending a consultant, J. Desmond Clark, who by then was professor of Anthropology at the University of California, Berkeley, USA. Third, the government established the University of Malawi. This was critically important for a country that at the time of independence had only a handful of degree-level college educated individuals. It was clear to both the British and Malawi governments that there would be an attrition of European expatriates within a decade of gaining independence, and their positions would have to be filled by college-educated Malawians.

Among other things, the provisions in the *Monuments Act* were enacted to protect objects of archaeological and historical value, and places of natural beauty. Some of these objects and places would be declared national monuments. To achieve this, the law provided for the establishment of a Monuments Advisory Council to advise the government minister responsible for monuments on matters related to the declaration of various objects as national monuments (Laws of Malawi, Act no. 44, 1965).

Clark's UNESCO consultancy was important in that he was more aware than anybody else at the time of the poor state of cultural and natural heritage management in Malawi. His recommendations included revision of the just passed *Monuments Act.* He quickly noticed that the Malawi Department of Antiquities, which was created by the government in 1967, had been established independent of this law. In other words, the department had no legal basis, yet it was mandated to be responsible for national monuments. Revision was necessary to make the department legal. He also recommended that the exhibition and storage areas of the Museum of Malawi be expanded (Clark, 1968). On its establishment in 1957, the museum was on temporary premises. Unlike the Department of Antiquities, the museum was not a government department but a private entity, run by a board of trustees appointed from among the European settlers themselves. By 1960, the board, with the support of the Beit Trust had raised enough money to have a museum building erected (Clark, 1968). Its exhibition area, however, was only 565 square meters. Clearly, this was an insufficient size in view of the collections expected from both the Department of Antiquities, the museum itself, and the settler community.

Clark also recommended the training of Malawians in cultural heritage activities. This call was timely, considering that it came about a year before the graduation of the University of Malawi's first graduates in 1969. The first two directors of the Department of Antiquities were expatriates, and both were historians. With the assistance of professors at the University of Malawi, the directors identified local talent and prepared them for training abroad. Not surprisingly, and thanks to Clark himself, the first three students were enrolled at the University of California, Berkeley. Between 1973 and 1999, five Malawians obtained doctorate degrees. Three earned the degrees in African Archaeology at Berkeley--Gadi Mgomezulu, 1978; Yusuf Juwayeyi, 1981; and Zefe Kaufulu, 1983. The other two, Obryne Chipeta earned his in history in 1986 from Dalhousie University in Canada, and Elizabeth

Gomani earned hers in Paleontology in 1999 at Southern Methodist University, in Dallas, Texas. One other individual obtained a master's degree at the University of Chicago; and another, a bachelor's degree at the University of London. Further, the Department of Antiquities sent three technicians to the National Museums of Kenya to train in various aspects of preparing archaeological materials. Two others were sent respectively to Southern Methodist University, and to Hessisches Landesmuseum in Darmstadt, Germany, to train in preparing paleontological materials. One technician went to Italy for training in preserving prehistoric rock art.

Being a private entity, the Museum had a very slow start to the training of museum curators. Training professionals abroad was so expensive that the board of trustees probably did not consider it a priority. It was not until 1981, when the Malawi Government decided to take over the operations of the museums, that its graduate staff were sent to train at universities abroad. During the next several years, four individuals obtained graduate degrees at universities in Australia, South Africa, and the United Kingdom. Two individuals earned doctorate degrees, one in ornithology, and the other in zoology. The rest earned master's degrees, one in museum management and the other in zoology (Juwayeyi, 2011).

EXPANSION OF MUSEUMS IN MALAWI

Despite Clark's recommendations, the exhibition space in the museum in Blantyre was never expanded. Instead, the government embarked on establishing more small museums, two in southern Malawi, and one in northern Malawi. These were followed by a fourth museum established in Karonga, following the initiative of private individuals with the support of the Department of Antiquities.

In 1971, a building in the lakeshore town of Mangochi was acquired by the Society of Malawi, formerly called the Nyasaland Society. Its membership was drawn almost exclusively from the European settler community, and its goal was to promote interest in literary, historical, and scientific matters, especially as they pertained to Malawi. The building was converted into a museum — the Lake Malawi Museum — and it exhibits "cultural material related to life on Lake Malawi and its shore areas" (Juwayeyi, 2011: 791). Just as it did with the museum in Blantyre, the government eventually took over the operations of the Lake Malawi Museum. It has an exhibition space of only 386 square meters. Eight percent of this space is taken up by one exhibit — the hull of the Guendolen, a British gunboat that disabled the Herman Von Wissmann, a German gunboat, on Lake Malawi in what was "the first British-German maritime engagement of the first world war" (Juwayeyi, 2011: 791). The rest of the space is taken up by archaeological material excavated by various archaeologists in the southern Lake Malawi area.

In 1985, the Malawi government approved a plan to establish a museum in Mzuzu, the largest city in northern Malawi. It acquired rented space in a building with an exhibition area of 160 square meters. This museum opened to the public in 1990 and it exhibits the material culture of the people of northern Malawi. In the same year, the Mtengatenga Postal Hut Museum opened at Namaka, along the Blantyre-Zomba Road in Chiradzulu district. It exhibits postage stamps and material related to the history of postal services in the country. Mtengatenga means porter/carrier. In this case, it means postal mail carrier. The story goes that during the early colonial period, mail was carried by porters. The distance between Blantyre and Zomba, the then capital town, was forty-two miles. Namaka postal hut was located at the twenty-one-mile point, and this is where the Zomba and Blantyre-based porters turned back after exchanging mail bags. With only 16.5 square meters of exhibition space, the Mtengatenga Postal Hut Museum is the smallest of the public museums in Malawi.

I should also point out that there are some privately owned museums in Malawi. All but one of these are operated by Christian churches. Chamare Museum at Mua in Dedza district is owned by the Catholic Church. The Stone House Museum at Khondowe in Rumphi, is owned by the Livingstonia Synod of the Church of Central Africa Presbyterian (CCAP). And William Murray Museum at Nkhoma in Lilongwe is owned by Nkhoma Synod, also of the CCAP (Lusaka, 2023a). In Limbe, there is the Transport Museum owned by the Society of Malawi. While The Stone House and William Murray Museums are about the history of those respective synods, Chamare Museum has gone beyond church history to depict various aspects of Malawi culture. The transport museum on the other hand has photographic exhibits covering the period from 1867 to 1996 showing the various means of transportation that were used in Malawi during this period. (https://www.malawitourism.com/experiences/culture/museums-historical-sites/the-society-of-malawi/).

FIGURE 1. Karonga Museum.

THE CULTURAL AND MUSEUM CENTER KARONGA (CMCK)

The CMCK or simply the Karonga Museum (Fig. 1), is the home of the "weird animal," the dinosaur, *Malawisaurus dixeyi*. The background to its establishment is interesting. Karonga district, unlike any other rift valley area in Malawi, is so rich in fossils (Jacobs, 1993) that the town authorities have branded it the "fossil district of Malawi" (Lusaka, 2023b: 3). The formation of the rift valley began about 8 million years ago. Subsequent tectonic activities led to subsidence that resulted in the creation of a river system and a rift lake (Schrenk et al., 1993). The exposed geological features were first surveyed and described by the then director of the Malawi Department of Geological Survey, Frank Dixey (1927). The area was also mapped using air photographs by E.A. Stephens of the British Overseas Geological Survey in the early 1960s (Clark, et al. 1967). Dixey recognized the Plio-Pleistocene Chiwondo beds, which overlie the dinosaur beds, and the younger Chitimwe beds. Eventually, soil erosion exposed fossils in the older beds (Sandrock, et al. 2007) and archaeological material in the Chitimwe beds (Clark, et al. 1967; Wright, et al. 2014).

The first discovery of fossils in Karonga district was made by Henry Drummond, a Scottish theologian and scientist in 1883 (Jacobs, 1993). Between this date and the late 1920s, more fossils were found by a planter named Holt, who reported their existence to Dixey. In 1930, Dixey along with F.W.H. Migeod of the British Museum of Natural History, who at the time was leading dinosaur excavations at Tendaguru in Tanzania, made a brief side trip to Malawi, and discovered more fossils, some of which were of dinosaurs (Jacobs 1993). They were taken to the British Museum in London where for a long time no serious researcher examined them. In other words, the fossils were simply forgotten. Meanwhile in Malawi no researcher was interested in the dinosaur beds again until 1984 when Professor Louis Jacobs of Southern Methodist University arrived in Karonga.

Before his arrival, four research projects targeting the younger Chiwondo beds had been undertaken. The first project was led by J. Desmond Clark in 1965/66. His research team included a geologist, a paleontologist, two archaeologists, and five graduate students from the University of California, Berkeley (Clark et al., 1967). The goal was to investigate Pleistocene deposits in Karonga with the expectation of finding both hominids and Early Stone Age artefacts. While no artefacts were found in the Chiwondo beds, some were found in the Chitimwe beds. Clark and his team proceeded to excavate Middle Stone Age sites and others including the well-known elephant Butchery site at Mwanganda's village (Clark & Haynes, 1970; Wright, et al., 2014). About fifteen years later Zefe Kaufulu and T.D. White reinvestigated the Chiwondo beds, the results of which suggested potential for paleontological research (Kaufulu, et. al., 1981). A few years later, Juwayeyi excavated Mwimbi-2 site; results indicated that research must continue to locate artefacts in the Chiwondo beds (Juwayeyi & Betzler, 1995).

The last project is the Hominid Corridor Research Project (HCRP), and it is an ongoing long-term study dating back to 1983. It was initiated by Professors Friedemann Schrenk then of the Hessisches Landesmuseum and Timothy Bromage, then of Hunter College, City University of New York (CUNY). The project focused on understanding "the role of southeastern Africa in the origin and dispersion of Plio-Pleistocene fauna, including early hominids" (Schrenk, et al., 1993: 833). Besides finding a considerable amount of fauna, the project also found an early hominid mandible, *Homo rudolfensis* (UR 501) in Unit 3A within the Chiwondo Beds at Uraha and *Paranthropus boisei* (RC 911) at Malema dated to between 2.5 and 2.3 million years. (Schrenk et.al. 1993; Bromage et.al. 1995; Kullmer et al., 1999).

MALAWISAURUS DIXEYI

When Jacobs first arrived in Malawi in 1984 to look for dinosaur fossils, it was a century after Drummond made the first ever discovery of fossils in the country. On Jacob's third trip to Malawi in 1989, he camped at Ngara, where Migeod had landed over 90 years before. Finally, here was an expert fully dedicated to finding and studying the dinosaurs of Malawi. The dinosaur digs, however, were at the village of Mwakasyunguti (also spelt Mwakashunguti), eleven miles away from camp.

Jacobs organized several field seasons, and the Mwakasyunguti site did not disappoint. It yielded dinosaur bones belonging to five different species including those of *Malawisaurus dixeyi*, three different kinds of crocodiles and even frogs, all dating to at least 100 million years ago. The site had and still has bones in abundance waiting for future Malawian scientists to follow in Jacobs' steps. The most common fossils recovered at the site are those of sauropod dinosaurs of the group called brontosaurs, familiar to many people in western countries. Some of them were the largest animals ever to have lived on land and all were herbivorous (Jacobs, 1993). Some bones were recovered singly while others were articulated, indicating good preservation.

THE HOUSE WITH THE WEIRD ANIMAL

One day in early August 1990, I brought a group of journalists to Mwakasyunguti to see the excavations for themselves. I was then the head of the Department of Antiquities. This department, now redesignated the Department of Museums and Monuments, is the first stop for all visiting researchers of paleontology, archaeology, history, and other aspects of Malawi's cultural heritage. Besides being a member of Jacobs' team, I was also the official government contact point for researchers in these fields. I invited the journalists because both Jacobs and I felt that Malawians needed to know what the project was all about. The journalists were fascinated as many people are when they see an excavation for the first time. They asked familiar questions: How did the bones get here? How did we know the exact spot to dig? Finally, and importantly for this discussion: will we put the bones on display?

It was not possible to answer the last question with clarity in 1990. If the dinosaur and other bones were to be put on display, where would we do that? I have demonstrated above that the exhibition areas of Malawi's museums are very small. Perhaps, the Museum in Blantyre could mount *Malawisaurus* in the middle of its single exhibition room. As head of Antiquities, I had on several occasions attempted to show the Malawi Government that Lilongwe is incomplete as the capital city of the country without a national museum. As recently as 2022, when my wife and I went to present my book to President Dr. Lazarus Chakwera at Sanjika Palace, I recalled during our conversation the encouraging comments he had made about museums on his recent visit to Scotland.

I reminded him that we have no museum in Lilongwe. Sadly, it seems the idea of a museum, even if it is for the capital city, is not a priority for the government.

Prof. Schrenk (of HCRP) and I talked a great deal about building a museum in which *Malawisaurus* would be the prominent exhibit. We agreed to raise funds, but first we needed to agree where to build it because donors would want this information before agreeing to provide funds. Schrenk wanted it built in Karonga because that is where all the fossils had been found. I wanted it in either Lilongwe or Blantyre, the two largest cities in Malawi to ensure that the exhibit would be visited by many people (https://www.youtube.com/watch?v=j7cDh-x1HqQ). But the requirement by donors of community participation in granting funds meant that Karonga rather than Lilongwe or Blantyre would be the place for the Museum. Lusaka (2023b) reports that Karonga already has a well-known community-based Non-Governmental Organization (NGO) called Karonga Development Trust (KADET). It was formed in 1994 by retired elites who had worked in Malawi or abroad and were resident in Karonga town. KADET's goal was to address social and economic issues by improving agricultural productivity and fishing. It had nothing to do with museums. But a chance meeting between Schrenk and the committee of KADET at a lodge in Karonga where the Committee was discussing the possibility of opening a vocational training school (Lusaka, 2023b), changed everything. Members of KADET were informed of the CMCK project and the importance of community participation to receive funding for it. Before long, a meeting involving members of KADET, Schrenk himself, and the country representative of the European Commission took place in Lilongwe; and subsequently, the European Commission agreed to fund the project in the amount of 30 million Malawi Kwacha — U$276,000 (Müller, 2001; https://momaa.org/directory/cultural-museum-centre-karonga/). As community contribution, KADET provided 1.5 hectares of land in mid-town on which to build the museum (Müller, 2005). This is how the "house with the weird animal" came to be in Karonga. *Malawisaurus* and the hominids came home.

Karonga museum consists of the main exhibition area, an administration block, and a laboratory. Later, an amphitheater was added for live presentation of traditional dances and other performing arts. However, since one of the goals of museums is to disseminate knowledge as widely as can be done, I maintain that a disservice was done to Malawians at large and, if they could express themselves, to *Malawisaurus* and the hominids as well by building the museum in Karonga instead of Lilongwe or Blantyre.

FROM DINOSAURS TO DEMOCRACY

Construction of the museum was finalized in April 2004, and on 10th November of the same year, the then president of Malawi, Dr. Bingu wa Mutharika presided over the opening ceremony. The theme of the exhibits is "From Dinosaurs to Democracy" (Müller, 2005: 1). Between 1964, when Malawi became independent, and 1994, when a democratically elected government came to power, the country was run by a single party dictatorship with the man at the top, Dr. Hastings Kamuzu Banda, styling himself president for life. Had democratization delayed by three years, he would have been; but he died in 1997. Besides *Malawisaurus* and other fossils, the exhibits in the museum include Stone Age and Iron Age objects and cultural materials related to the slave trade, missionaries, colonialism, dictatorship, and democracy and multiparty politics (Müller, 2005). When one enters the museum, one immediately feels the dominance of *Malawisaurus*. It is Malawi's most prominently displayed scientific object. In general, the exhibits show profound creativity on the part of the museum staff. A good exhibition job was done here.

What remains to be sorted out at Karonga museum, however, is the issue of its ownership and management. In the year 2000, another community-based foundation, the Uraha Foundation Malawi (UFM) was registered as an NGO. Its goal was "to facilitate the implementation of the Cultural and Museum Centre, Karonga" (Müller, 2005: 5). According to Lusaka (2023b), the composition of the board members of UFM and KADET is such that the two organizations are essentially one. Since the European Commission gave the money to KADET, it turns out that KADET/UFM feel that they own the museum and should therefore manage and benefit from it. Meanwhile, the Malawi Department of Museums and Monuments believes that it owns the museum. After all, it was responsible for approving the projects that recovered the fossils, and some of its staff participated in the research. According to H. Simfukwe, a former chief historian at the museum, the department also pays the salaries of most of the staff (pers. communication, August 31, 2023). Thus, the issue of ownership has yet to be satisfactorily resolved.

However, as far as researchers are concerned, what matters most is that there is a museum in the fossil rich district and that they can still go about finding fossils. As for the public, well, *Malawisaurus* still reigns supreme at the Karonga museum.

CONCLUSION

The Karonga Museum, like the museum in Blantyre, is small by any standard. Malawi's establishment of museums started very late in the colonial period. Now that Malawi has dinosaurs, hominids and other materials, the Malawi Government should see the wisdom to prioritize construction of a new national museum in Lilongwe, for example. A large museum in a large city is warranted as it would benefit more Malawians than the Karonga site.

ACKNOWLEDGMENTS

I thank M. Juwayeyi for his useful comments on the first draft of this paper. H. Simfukwe for responding to a questionnaire timely, and reviewers M. Lusaka and L. Flynn for their helpful comments and suggestions.

REFERENCES

Bent, J. T. 1892. *The ruined cities of Mashonaland*. Longmans.

Bromage, T. G., Schrenk, F., & Zonneveld, F. W. (1995). Paleoanthropology of the Malawi rift: an early hominid mandible from the Chiwondo beds, northern Malawi. *Journal of Human Evolution*, 28(1).

Caton-Thompson, G. (1931). *The Zimbabwe Culture*, *ruins*, and *reactions*. Clarendon Press.

Clark, J. D. (1956). Prehistory in Nyasaland. *The Nyasaland Journal*, 9, 92-119.

Clark, J. D. (1968). *Malawi: Antiquities programme*, (Consultancy report no.872/BMS.RD/CLT). UNESCO.

Clark, J. D., Haynes, C. V., Mawby, J. E., & Gautier, A. (1967). Interim report on palaeo-anthropological investigations in the Lake Malawi rift. *Quaternaria,* 13, 305-354.

Clark, J. D. & Haynes, C. V. (1970). An elephant butchery site at Mwanganda's Village, Karonga, Malawi, and its relevance for Palaeolithic archaeology. *World Archaeology*, 1(3), 390–411. https://doi.org/10.1080/00438243.1970.9979455.

Clark, J. D. (1970). *The prehistory of Africa*. Praeger.

Clark, J. D. (1973). Archaeological investigations of a painted rockshelter at Mwana wa Chencherere, north of Dedza, central Malawi. *Society of Malawi Journal*, 26, 28–46.

Cultural & Museum Centre Karonga. (n.d.). Listing details: https://momaa.org/directory/cultural-museum-centre-karonga/

Dixey, F. (1927). The tertiary and post-tertiary lacustrine sediments of the Nyasan rift valley. *Quarterly Journal of Geological Society of London*, 83, 432–447.

Gondwe, M. (2001). CMCK undertakes surveys. *CMCK Newsletter,* 1(1), 1–8.

Inskeep, R. R. (1965). *Preliminary investigation of a proto-historic cemetery at Nkudzi Bay, Malawi.* The National Museums of Zambia.

Jacobs, L. (1993). *Quest for the African dinosaurs*. Willard books.

Juwayeyi, Y. M. & Betzler, C. (1995). Archaeology of the Malawi rift: the search continues for Early Stone Age occurrences in the Chiwondo beds, northern Malawi. *Journal of Human Evolution*, 28(1), 115-116. https://doi.org/10.1006/jhev.1995.1009

Juwayeyi, Y. M. (2011). Excavating the history of archaeology in Malawi. In L. Lozny, (Ed.), *Comparative archaeologies: a sociological view of the science of the past* (pp. 785–805). Springer.

Kaufulu, Z. M.,Vrba, E. S., & White, T. D. (1981). Age of the Chiwondo beds, northern Malawi. *Annals of the Transvaal Museum*, 33, 1–8.

Klein, R. (1999). *The human career: human biological and cultural origins*. University of Chicago Press.

Kullmer, O., Sandrock, O., Abel, R., Schrenk, F., Bromage, T. G., & Juwayeyi, Y. M. (1999). The first Paranthropus from the Malawi rift. *Journal of Human Evolution,* 37, 121-127. https://doi.org/10.1006/jhev.1999.0308

Laws of Malawi. Act no. 44, 1965.

Lusaka, M. (2023a). Curating the nation: collections, ethnographic representations and heritage production at Museum of Malawi. *Cogent Arts and Humanities*, 10(1), 1–18. https://doi.org/10.1080/23311983.2022.2160577

Lusaka, M. (2023b). Whose museum? Collaboration and contestation over heritage management at the Cultural and Museum Center Karonga in Malawi. *Cogent Arts & Humanities*, 10(1), 1–17. https://doi.org/10.1080/23311983.2023.2243714

Mufuzi, F. (2011). Establishment of the Livingstone Museum and its role in colonial Zambia, 1934–1964. *Historia*, 56(1).

Müller, S. (2001). Project information on CMCK activities, (File no A/11/5.12). Department of Antiquities. Unpublished document on file in the Department of Museums and monuments.

Müller, S. (2005). The Cultural & Museum Centre, Karonga. *The Society of Malawi Journal*, 58(1), 1-5.

Natural History Museum of Zimbabwe. (n.d.). History of the natural History Museum. https://naturalhistorymuseumzimbabwe.com/history-of-the-museum/

Randall-MacIver, D. (1971). *Mediaeval Rhodesia*. Cass, London.

Robinson, K. R. (1966). A Preliminary report on the recent archaeology of Ngonde, Northern Malawi. *The Journal of African History*, 7, 169–188. https://doi.org/ 10.1017/s0021853700006253.

Robinson, K. R. & Sandelowsky, B. (1968). The Iron Age of northern Malawi: recent work. *Azania: Archaeological Research in Africa*, 3, 107–146. https://doi.org/ 10.1080/00672706809511489.

Robinson, K. R. (1970). *The Iron Age of the southern Lake Malawi area*. Malawi Government Press.

Robinson, K. R. (1973). *The iron age of the upper and lower Shire Malawi.* Malawi Government Press.

Sandrock, O., Kullmer, O., Schrenk, F., Juwayeyi, Y. M., & Bromage, G. T. (2007). Fauna, taphonomy, and ecology of the Plio-Pleistocene Chiwondo Beds, northern Malawi. In R. Bobe, Z. Alemseged, & A. K. Behrensmeyer (Eds.). *Hominin environments in East African Pliocene: an assessment of the faunal evidence* (pp. 315–332), Springer.

Schrenk, F. (n.d.). Paleontologist: https://www.youtube.com/watch?v=

j7cDh-x1HqQ

Schrenk, F., Bromage, T. G., Betzler, C. G., Ring, U., & Juwayeyi, Y. M. (1993). Oldest Homo and Pliocene biogeography of the Malawi Rift. *Nature*, 365, 833–836.

The Society of Malawi. (n.d.). Malawi: https://www.malawitourism.com/experiences/culture/museums-historical-sites/the-society-of-malawi/

Wright, D. K., Thompson, J., Mackay, A., Welling, M., Forman, S. L., Price, G., Zhao, J., Cohen, A. S., Malijani, O., & Gomani-Chindebvu, E. (2014). Renewed geoarchaeological investigations of Mwanganda's (elephant butchery site), Karonga, Malawi. *Geoarchaeology*, 29(2), 98–120.

WINDOWS INTO SAUROPSID AND SYNAPSID EVOLUTION
Essays in honor of Prof. Louis L. Jacobs, pp. 260–263, 2023

OF MICE AND MEN REVISITED (AGAIN)

DAVID PILBEAM*

Department of Human Evolutionary Biology, Harvard University, Cambridge MA 02138, U.S.A. pilbeam@fas.harvard.edu

I've known Louis Jacobs for almost fifty years and have learned to greatly value his wit (by which I mean both his wonderfully unique sense of humor and his intelligent astuteness). It has been both pleasure and privilege. This brief contribution is an *Hommage*.

I first met Louis in Pakistan in 1975 at the Khaur Rest-House on the Potwar Plateau. Lou (I still think of him as such) was beginning his doctoral research as part of the Dartmouth-Peshawar research group, which soon began collaborating closely with a Yale-Geological Survey of Pakistan group which I was coordinating. In the following couple of years we began discussing the important role fossils play in calibrating "molecular clocks" (the now widely accepted proposal that genetic differences between species can be used to make reasonable predictions about speciation times). These discussions led to "Of mice and men" (Jacobs and Pilbeam, 1980) in which we urged closer collaboration between paleontologists and molecular systematists. We focused in particular on the important role of the increasingly abundant murid fossil record, particularly as it was then believed to document the divergence of *Mus* and *Rattus*.

When we were discussing and then sometime in 1979 writing the paper, the most common molecular approaches involved immunological comparisons, protein sequencing, and DNA-DNA hybridization. Each served as proxies for the genomic difference ("distance") between a pair of living species. One contribution was particularly interesting to us because it summarized the genetic distances, based on albumin immunological and DNA-DNA hybridization differences, both between *Mus* and *Rattus* and between *Homo* and *Pan* (Sarich, 1972). For the two proxies, *Mus-Rattus* differences were an order of magnitude greater than for *Homo-Pan*. At that time, most paleoanthropologists accepted a date of 14 Ma or more for the divergence of *Homo* and *Pan*, while Sarich and his colleague Allan Wilson (1967) proposed 5 Ma for the human chimpanzee divergence. For the *Mus-Rattus* divergence, Sarich (1972) inferred a date of 35 to 40 Ma, rather than the fossil-based 8 to 14 Ma estimated in Jacobs and Pilbeam (1980).

The genetic difference between genomes of two species will be an average of the range of coalescent times (ages of separation) of their different alleles (Edwards and Beerli, 2000), chromosomes (Patterson et al 2006), or arbitrarily-selected DNA sequence "windows (Foley et al, 2023). These times vary across the genome, so this average must be older than the age of the splitting or speciation of the descendant lineages (Patterson et al, 2006, well-explained in their Fig. 1). Over the past six or more decades, there has been considerable progress in understanding molecular evolutionary processes, and gene sequences are now available for many mammal species, along with a range of model approaches to using such data and generating phylogenetic frameworks with age estimates for splitting of ancestral lineages (for example, Foley et al, 2023).

An important paper from the 1970's (King and Wilson, 1975) emphasized that the genetic variation between sister species has two components: variation within their common ancestor before the lineages speciated; and a second portion, differences accumulated along the diverging lineages. This critical insight was developed more formally over the following quarter century (for example, Edwards and Beerli, 2000), emphasizing the difference between genomic divergence time and population divergence in speciation or splitting time. In a useful paper for paleontologists, Steiper and Young (2008) drew attention to the significance of these differences. Determining that a split has occurred requires recovering fossils preserving hard-tissue features with clear apomorphies showing a relationship to at least one of the lineages. Clearly, even the oldest plausible member of a lineage will be younger than split time, how much younger remaining

*Corresponding author

unclear and effectively indeterminate. This splitting time will of course also be younger than genomic divergence time.

The "earliest" acceptable fossil representative of a lineage is used in a "phylogenetic" approach to estimating mutation rates and speciation times. Formally, determining a mutation rate per time interval would require using the averaged genomic difference (distance) as numerator and the genomic divergence time as denominator. But because divergence time is unknown, the (unavoidably) younger population splitting times are used in calculations. The denominator must therefore be reduced and mutation rates over-estimated; they will be least over-estimated if there is reason to believe that the fossil record is a sufficiently reliable predictor of the splitting times used in calculations. Taking a "phylogenetic" approach, Nachman and Crowell (2000) used a range of fossil-based estimates for the splitting time of humans and chimps, along with estimates of ancestral effective population size (the fraction of population reproducing), and estimated a human mutation rate of $\sim 2.5 \times 10^{-8}$ mutations per nucleotide per generation.

An important recent contribution to estimating mutation rates has been the expanding use of "pedigree" studies in living species. These involve the "trio" method in which genomes of parents and offspring are sequenced to recognize new mutations in offspring, hence determining mutation rates per generation. Accumulating data, especially for primates, show that mutation rates vary across species, with variation based on different factors. The current consensus is that for primates estimated mutation rates are low, on the order of $\sim 10^{-8}$ per base pair per generation (Chintalapati and Moorjani, 2020). The best available data are for humans: $\sim 1.2 \times 10^{-8}$ base pairs per generation. Note that the phylogenetic approach of Nachman and Crowell (2000) estimated a human mutation rate twice as great. Using a human generation interval of ~30 years, Chintalapati and Moorjani (2020) estimated a human mutation rate of 0.4 to 0.5×10^{-9} per base pair per year.

While there is not yet a completely stable estimate for hominoid genomic divergence and populations splitting times, Moorjani et al (2016) and Chintalapati and Moorjani (2020) provide what are the current best estimates for the *Pan-Homo* clade: a *Pan/Homo* divergence date of ~12.1 Ma and a splitting time of 7.9 Ma (midpoint of estimate range from 9.3 to 6.5 Ma). Around 8 Ma for the split between *Pan* and *Homo* lineages is the best that can currently be offered, not least because the fossil record of early hominins is poor and contested. Murids present a clear contrast, with an outstanding fossil record.

Using the murid fossil record as documented and interpreted at the time, Jacobs and Pilbeam (1980) had proposed a *Mus-Rattus* divergence time of between 8 and 14 Ma, based on the assignment of species of *Progonomys* and *Karnimata* respectively to *Mus* and *Rattus* lineages. A recent phylogenetic analysis (Kimura et al, 2015) confirmed the *Progonomys-Mus* relationship, but revised that of *Karnimata* to support a link with *Arvicanthis* with *Rattus* now seen as more distantly related to *Mus* and *Arvicanthis*.

The several decade-long campaign of intense screen-washing by Lou and his colleagues (especially the late, greatly missed, Will Downs) in the fossiliferous Miocene sequence of the Potwar Plateau greatly expanded collections of small mammal fossils (Jacobs and Flynn, 2005, Flynn et al, 2023, Flynn et al, in prep.). Intense stratigraphic surveys and use of paleomagnetic analyses made it possible to place most small-mammal samples within 100,000 year-long bins (Flynn et al, 2023, Flynn et al, in prep.).

Sample sizes of murines in particular have steadily expanded, as have analyses by Lou and his students and colleagues: systematic, phylogenetic and functional analyses, along with those of morphometrics and carbon and oxygen stable isotopes of tooth enamel (Kimura et al, 2013a, 2013b, 2015, 2016, Aghova et al, 2018, Flynn et al, 2020, Kimura et al, 2021). For my purpose here the most relevant of these recent analyses for calibrating clocks involves the detailed documentation over several million years of the speciation of the murines *Progonomys* and *Karnimata*, especially the recent work of Dr. Yuri Kimura (Kimura et al, 2013a, 2016, Flynn et al 2020, Kimura et al 2021). The record is abundant with well-dated specimens under excellent stratigraphic control, detailed morphometric analyses making possible plausible systematic and phylogenetic inferences (This material is likely to be discussed in greater detail in other contributions to this Festschrift.).

Good samples of *Potwarmus* and *Antemus* specimens document the evolving stem lineage ancestral to *Progonomys* and *Karnimata*, with good records between 15 and 12.5 Ma and especially between 14.2 and 12.8 Ma; this is followed by a sampling gap until the next good murine localities ranging in age between 11.6 and 11.2 Ma, which specimens present a very interesting pattern (Kimura et al. 2021). The most likely interpretation is that a single species is represented, but one

that is intriguingly variable. First molar patterns show continuous variation but with end-members resembling respectively *Progonomys* and *Karnimata* morphs. Other molars do not show this pattern. Kimura et al, 2021, label this sample "Pre-*Progonomys*, Indeterminate *Progonomys-Karnimata* grade", reflecting its morphological complexity and intermediacy, and systematic ambiguity. Following the 11.2 Ma level there is another fossil-free interval until the next good samples starting at 10.5 Ma; by this time clear morphological differences of the *Progonomys* and *Karnimata* lineages are present which become even more marked by 9.2 Ma.

How is this interval between 12.5 and 10.5 Ma best interpreted, during which *Progonomys* and *Karnimata* lineages separated and then diverged? What might we be observing? The sequence appears to document an ancestral species and its subsequent split into descendant lineages. The separation of these had definitely happened by 10.5 Ma, but until the preceding 700 ka has been well sampled the best that can be said with confidence is that splitting happened between 11.2 and 10.5 Ma. What might explain the intriguing variation patterns seen in the "Pre-*Progonomys*, Indeterminate *Progonomys-Karnimata* grade" taxon? One plausible scenario is that speciation is being documented.

The first decades of this century saw continuing and expanding interest in the speciation process (Harrison, 2012). A very recent whole-genome analysis of 241 placental mammal genomes (Foley et al, 2023) showed that for many splitting events there was evidence of introgression (gene flow from hybridization) in the early stages of lineage divergence. (The phenomenon is also well-documented in plants as well as animals: an example being a recent study (Zhou et al, 2017) of introgression among Pine subspecies.) Conveniently for us, introgression can also be observed in the house mouse, *Mus musculus*, a well-studied model organism for phylogenetic studies and not just for biomedical research -- and the descendant of the *Progonomys* lineage.

The oldest specimen of the genus *Mus* recorded anywhere is from an 8.0 Ma Potwar locality (Flynn et al, in prep.). *Mus musculus* evolved over the last 3 million years (Lawal et al, 2022), giving rise during the most recent million years (White et al, 2009) to three primary subspecies: (*M. m. domesticus* native to Western Europe, *M. m. musculus* present across Eastern Europe and Siberia, and *M. m. castaneus* across South and Southeast Asia. (Lawal et al 2022). The subspecies are well-supported genetically, but show considerable introgression among them (Lawal et al 2022, White et al 2009). Of interest, given our necessary hard-tissue paleontological approach, morphological differences in dentitions across the subspecies are present (Darvish, 2008), offering an additional perspective on variation seen in "Pre-*Progonomys*, Indeterminate *Progonomys-Karnimata* grade".

Hence, one plausible hypothesis, as noted by Kimura et al. (2021) and Flynn et al (in prep.), is that the Potwar murine record between 12 and 11 mya records a species that is in the process of differentiating, subspecific lineages showing some differences in tooth morphology while continuing to introgress before the lineages "emerge" and differentiate as full species (no doubt continuing exchanging genes). It is worth noting that the degree of morphological differences between molars of *Mus musculus* subspecies (Darvish, 2008) are equivalent to those between the *Progonomys* and *Karnimata* morphs observed between 12 and 11 Ma (Flynn, pers comm.) It is unfortunate that there is still too little understanding of the genomic determinants of hard-tissue phenotypic features, or how these might be or might not be involved in the introgressed fraction of genomes.

The history of the *Progonomys* and *Karnimata* lineages provides one of highest quality mammalian fossil records currently available for recognizing and addressing divergence and split times; best estimates are a population separation/ splitting time around 11 Ma with a genomic divergence time (averaged across the genome) around 12 Ma.

More such high-quality records are needed.

ACKNOWLEDGMENT

As a final note, in recognition and thanks to Lou for his contribution to my Festschrift (Jacobs and Flynn, 2005) I echo and analogize the great American philosopher Lawrence Peter Berra: "Always go to other people's funerals; that way they'll come to yours."

LITERATURE CITED

Aghová, T., Kimura Y., Bryja, J., Dobigny, G., Granjon, L., & Kergoat, G. J. (2018). Fossils know it best: using a new set of fossil calibrations to improve the temporal phylogenetic framework of murid rodents (Rodentia: muridae). *Molecular Phylogenetics & Evolution*, 128, 98–111. doi: 10.1016/j.ympev.2018.07.017.

Chintalapati, M. & Moorjani, P. (2020). Evolution of the mutation rate across primates. *Current Opinion in Genetics and Development*, 62, 58–64. https://doi.org/10.1016/j.gde.2020.05.028.

Darvish, J. (2008). Biosystematic approach to geographic variations of house mouse group, *Mus musculus* L.1766. *Iranian Journal of Animal Biosystematics*, 4, 31–54.

Edwards, S. V. & Beerli, P. (2000). Perspective: gene divergence, population divergence, and the variance in coalescent time in phylogeographic studies. *Evolution*, 54, 1839–1854.

Foley, N. M., Mason, V. C., Harris, A. J., Bredemeyer, K. R., Damas, J., Lewin, H. A., Eizirik, E., Gatesy, J., Karlsson, E. K., Lindblad-Toh, K., Zoonomia Consortium, Springer, M. S., & Murphy, W. J. (2023). A genomic timescale for placental mammal evolution. *Science*, 380, eabl8189. DOI: 10.1126.

Flynn, L. J., Kimura, Y., & Jacobs, L. L. (2020). The murine cradle. In G. V. R. Prasad & R. Patnaik (Eds.), Biological Consequences of Plate Tectonics: New Perspectives on Post-Gondwanaland Break-Up (pp. 347–362). Springer, Ostende.

Flynn, L. J., Morgan, M. E., Barry, J. C., Mahmood Raza, S., Cheema, I. U., & Pilbeam, D. (2023). Siwalik rodent assemblages for NOW: Biostratigraphic resolution in the Neogene of South Asia. In I. Casanovas i Vilar, C. Janis, J. Saarinen, & L. van den Hoek (Eds.), The NOW database of fossil mammals. Springer, Ostende.

Flynn, L. J., Jacobs, L. L., Kimura, Y., Lindsay, E. H., Cheema, I. U. (In prep.) Siwalik Glires. In C. Badgley, M. E. Morgan, & D. Pilbeam (Eds.), *At the Foot of the Himalayas: Paleontology and Ecosystem Dynamics of the Siwalik Record of Pakistan*. Johns Hopkins University Press, Baltimore.

Harrison, R. G. (2012). The language of speciation. *Evolution*, 66, 3643–3657.

Jacobs, L. L. & Flynn, L. J. (2005). Of mice…..again: the Siwalik rodent record, murine distribution, and molecular clocks. In D. E. Lieberman, R. J. Smith, & J. Kelley (Eds.), *Interpreting the Past: Essays on Human, Primate, and Mammal Evolution in Honor of David Pilbeam* (pp. 63–80). American School of Prehistoric Research Monograph Series 5. Boston, MA: Brill Academic Publishers, Inc.

Jacobs, L. L. & Pilbeam, D. (1980). Of mice and men: fossil-based divergence dates and molecular "clocks". *Journal of Human Evolution*, 9, 551–555. doi: 10.1016/0047-2484(80)90062-7.

Kimura, Y., Flynn, L. J., & Jacobs, L. L. (2016). A palaeontological case study for species delimitation in diverging fossil lineages. *Historical Biology*, 28, 189–198.doi: 10.1080/08912963.2015.1022175.

Kimura, Y., Flynn, L. J., & Jacobs, L. L. (2021). Tempo and Mode: Evidence on a protracted split from a dense fossil record. *Frontiers in Ecology and Evolution*, 9, 642814. doi:10.3389/fevo.2021.642814.

Kimura, Y., Hawkins, M. T. R., McDonough, M. M., Jacobs, L. L., & Flynn, L. J. (2015). Corrected placement of *Mus-Rattus* fossil calibration forces precision in the molecular tree of rodents. *Scientific Reports*, 5, 14444. doi: 10.1038/srep14444.

Kimura, Y., Jacobs, L. L., Cerling, T. E., Uno, K. T., Ferguson, K. M., Flynn, L. J., & Patnaik, R. (2013a). Fossil mice and rats show isotopic evidence of niche partitioning and change in dental ecomorphology related to dietary shift in late Miocene of Pakistan. *PLOS One*, 8, e69308. doi: 10.1371/journal.pone.0069308.

Kimura, Y., Jacobs, L. L., & Flynn, L. J. (2013b). Lineage-specific responses of tooth shape in murine rodents (Murinae, Rodentia) to late Miocene dietary change in the Siwaliks of Pakistan. *PLoS One*, 8, e76070. doi: 10.1371/journal.pone.0076070.

King. M. C. & Wilson, A. C. (1975). Evolution at two levels in humans and chimpanzees. *Science*, 188, 107–116.

Lawal, R. A., Mathis, V. L., Barter, M. E., Charette, J. R., Garretson, A., & Dumont, B. L. (2022). Taxonomic assessment of two wild house mouse subspecies using whole-genome sequencing. *Scientific Reports*, 12, 20866 | https://doi.org/10.1038/s41598-022-25420-x.

Moorjani, P., Amorin, C. O. G., Arndt, P. F., & Przeworski, M. (2016). Variation in the molecular clock of primates. *PNAS*, 113, 10607–10612.

Nachman, M. W. & Crowell, S. L. (2000). Estimate of the mutation rate per nucleotide in humans. *Genetics*, 156, 297–304.

Patterson, N., Richter, D. J., Gnerre, S., Lander, E. S., & Reich, D. (2006). Genetic evidence for complex speciation of humans and chimpanzees. *Nature*, 441, 1103–1108. doi:10.1038/nature04789.

Sarich, V. M. (1972). Generation time and albumin evolution. *Biochemical genetics*, 7, 205–212.

Sarich, V. M. & Wilson, A. C. (1967). Immunological time scale for hominid evolution. *Science*, 158, 1200–1203.

Steiper, M. & Young, N. (2008). Timing primate evolution: lessons from the discordance between molecular and paleontological estimates. *Evolutionary Anthropology*, 17, 179–188. https://doi.org/10.1016/j.gde.2020.05.028.

White, M. A., Ané, C., Dewey, C. N., Larget, B. R., & Payseur, B. A. (2009). Fine-Scale phylogenetic discordance across the House Mouse genome. *PLOS Genetics*, 5(11), e1000729.

Zhou, Y., Duvaux, L., Ren, G., Zhang, L., Savolainen, O., & Liu, J. (2017). Importance of incomplete lineage sorting and introgression in the origin of shared genetic variation between two closely related pines with overlapping distributions. *Heredity*, 118, 211–220. doi:10.1038/hdy.2016.72.

WINDOWS INTO SAUROPSID AND SYNAPSID EVOLUTION
Essays in honor of Prof. Louis L. Jacobs, pp. 264–272, 2023

ONE MORE SIWALIK SURPRISE: THE OLDEST RECORD OF *MUS* (MAMMALIA, RODENTIA) FROM THE LATE MIOCENE OF NORTHERN PAKISTAN

LAWRENCE J. FLYNN[1,*] and YURI KIMURA[2]

[1]Department of Human Evolutionary Biology, Harvard University, 11 Divinity Avenue, Cambridge, MA 02138 USA, ljflynn@fas.harvard.edu
[2]Department of Geology and Paleontology, National Museum of Nature and Science, 4-1-1 Amakubo Tsukuba, Ibaraki 305-0005 Japan, ykimura.research@gmail.com

ABSTRACT Louis L. Jacobs developed the outlines of murine evolution through original fieldwork in the Siwalik Hills of the Potwar Plateau in northern Pakistan. His discovery of middle Miocene age *Antemus*, an early stem murine, unveiled the roots of the modern mouse radiation of the later Miocene. He developed a hypothesis on the early late Miocene divergence of extant murine lineages, and included fossil *Progonomys* in the modern *Mus* lineage. A younger Miocene Siwalik locality produced a species close to the living house mouse. Louis named it *Mus auctor* and, as an early record of ~6.5 Ma on the present time scale, it seemed to define the emergence of modern mice. Since then, we have explored more thoroughly the Siwalik sequence and studied its series of rodent assemblages, including newer collections that antedate *Mus auctor*. We were surprised to discover a very small species of *Mus* older than *Mus auctor* and falling into the interval of 7.2 to 8.0 Ma. Morphometric analysis established it as a member of the modern genus and, although preceding *Mus auctor*, the new species proved more derived in some characters. Jacobs' hypotheses that *Progonomys* is in the *Mus* lineage and that *Mus auctor* is readily transformed from *Progonomys* appear to be validated. However, before *Mus auctor* was in place, a derived species of *Mus*, formally named here, was present on the Potwar Plateau. The center of evolution of the genus *Mus* was likely in southeastern Asia, and from time to time the Potwar Plateau sampled the periphery of that evolution. It is Jacobs' vision that led to this discovery, and we take this opportunity to explore in his honor the phylogenetic context of this new species.

KEYWORDS Murines, *Mus*, Pakistan, Siwaliks, Miocene

INTRODUCTION

An outline of rodent evolution in South Asia was developed by Louis L. Jacobs through his groundbreaking work in the 1970s. He was part of a collaboration of scientists from several institutions that has studied the well-exposed Siwalik sequence of the Potwar Plateau over the last half century. With direction from then-major advisor Prof. Everett H. Lindsay of the University of Arizona, Louis explored the thick Neogene sequence of the Potwar Plateau in Pakistan. At first attracted by the riches of the Plio-Pleistocene, Louis soon saw that the real challenge lay in the systematic screening of superposed deposits to document the history of Siwalik small mammals, especially rodents. He opened his fossil-hunting campaign by screening productive horizons of the Chinji Formation (middle Miocene), the Dhok Pathan Formation (two late Miocene levels), and the Plio-Pleistocene of the Upper Siwaliks.

Louis discovered that small mammals were richly preserved in Siwalik rocks of various ages. Given the long succession of thousands of meters of sediment and application of magnetostratigraphic dating by Lindsay and coauthors (e.g., Opdyke et al. 1979), the ages of most sites could be estimated to an accuracy of ~100,000 years (ages recalculated by Barry et al. 2013). Louis unveiled a rich assemblage of diverse small mammals in the middle Miocene Chinji Formation. Among the rodents of age calculated at 13.6 Ma (Ma = mega-annum, million years), were primitive muroids (Jacobs 1977) that proved to be basal mice. Given their antiquity preceding modern rats and mice, these represented a stem murine that Louis named *Antemus chinjiensis*. Jacobs (1978) put forward the hypothesis that the roots of the modern mouse and rat tribes (exemplified today by *Mus* and *Rattus*) could be found in late Miocene

*Corresponding author

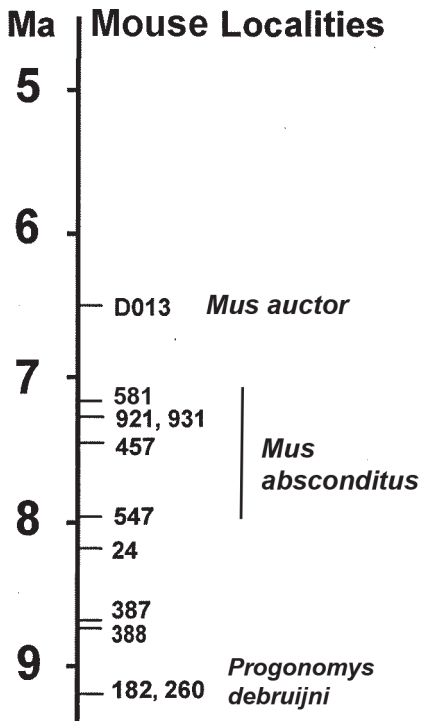

FIGURE 1. Temporal occurrence (stratigraphic order) of key small mammal sites of the Potwar Plateau that sample the *Mus* lineage. Locality Y182 at 9.2 Ma lacks *Mus* but records its predecessor *Progonomys debruijni*. *Progonomys* continues higher in the section into younger localities. Tiny *Mus absconditus* occurs at sites from 8.0 to 7.2 Ma. Younger D013 (6.5 Ma) has the different species *Mus auctor;* by then *Progonomys* is absent.

assemblages of the Dhok Pathan Formation on the Potwar Plateau. A productive horizon at 9.2 Ma (Y182) contained the distinct murine genera *Progonomys* and *Karnimata* that demonstrated diversification by that time, postdating *Antemus* (Jacobs and Pilbeam 1980). The hypothesis of Jacobs, placing the late Miocene murine *Progonomys* in the ancestry of living *Mus*, was buttressed by morphological features that seemed corroborated in a younger late Miocene Siwalik assemblage at 6.5 Ma. This assemblage contained the early mouse *Mus auctor* - by then *Progonomys* was gone.

It appeared that between 9.2 and 6.5 Ma *Progonomys* had disappeared and *Mus,* specifically *Mus auctor,* took its place. Our current work shows that the picture is not so simple. With Jacobs, Lindsay, and the late Will Downs, we continued to sample multiple horizons for small mammals, and developed over 100 productive Siwalik horizons yielding rodents. In the 1990s we concentrated on the late Miocene stratigraphy of the Hasnot area (for location see Barry et al. 2002, Winkler et al. 2011). Fossil murine rodents recovered there and from mid-Miocene deposits, formed the core of dissertation research including morphometric analysis by one of us (YK). Our samples include fossils from several horizons between 9.2 and 6.5 Ma (Fig. 1). These serve to test the simplistic hypothesis of gradual evolution and replacement of *Progonomys* by *Mus*, and the assumption that the transition was near 6.5 Ma. We find a more complex picture, with an unexpected record of the genus *Mus* preceding *Mus auctor.*

ABBREVIATIONS

D: designation for D013, a locality in the Dartmouth-Peshawar system that occurs high in the Dhok Pathan Formation on the Potwar Plateau, age estimated at 6.5 Ma. It is the type locality for *Mus auctor.*

M, **m**: prefix for molars followed by tooth position. M1, M2, M3 are upper molars; lower case signifies lower molars.

Y: prefix for localities in the Yale-Harvard locality system, e.g., Y024 through Y931.

YGSP: acronym for specimens in the Yale-Geological Survey of Pakistan catalogue of Siwalik fossils.

NOMENCLATURAL ACTS

This published work and the nomenclatural acts it contains have been registered in ZooBank. The ZooBank LSID number for this publication is urn:lsid:zoobank.org:act:48FF0897-D2EF-416F-8EBC-7495E9B550B0.

SYSTEMATICS

Family Muridae Illiger, 1811

Subfamily Murinae Illiger, 1811

Genus *Mus* Linnaeus, 1758

***Mus absconditus* sp. nov.**

Holotype — YGSP 52920, first upper molar, left M1, (Fig. 2A.

Etymology — From Latin *absconditus* for “hidden”. This species of *Mus* was hidden in the fossil record until a large array of fossil horizons was screened for small mammals.

Type Locality and Age — Y921, about 7.3 Ma based on current magnetostratigraphic interpolation (see for example

FIGURE 2. Upper molars of *Mus absconditus* sp. nov. from the Potwar Plateau Dhok Pathan Formation of northern Pakistan. Scale bar equals 1 mm, anterior is upward. **A**, left M1 (YGSP 52920, holotype); **B**, left M1 (YGSP 54354); **C**, right M2 (YGSP 54520, reversed); **D**, right M2 (YGSP 54523, reversed); **E**, left M3 (YGSP 54424); **F**, left M3 (YGSP 34477). SEM images were obtained with a Zeiss Gemini 360 SEM equipped with a variable pressure secondary electron (VPSE) detector at 50 Pa chamber pressure with 20 kV accelerating voltage in the VP mode.

Barry et al. 2013).

Referred Specimens — From Y457, 7.4 Ma, M1 YGSP 34473; M2 34468, 34492; M3, 34469, 34477; m1 34495, 52913, 52914; m3 34493. From Y547, 8.0 Ma, dentary with m1-m3 33322; m1 33307. From Y581, 7.2 Ma M1 52938; m1 52935. From Y921, M2 54290; m1 54292, 54293; m3 54291. From Y931, 7.3 Ma, M1 52972-52980, 54351-54355; M2 54519-54525; M3 54424, 54425; m1 54350, 54413-54422, m2 54526-54533; m3 54423. See Figs. 2, 3 and Tables 1, 2.

Diagnosis — Small species of *Mus*, of fossil species in southern Asia only *Mus narmadaensis* Kotlia et al., 2011 is as small; oldest record of the genus, 7.2 to 8.0 Ma. First molars narrow; M1 anterostyle pinched and posterior in position (posterior to double anterocone), variably reduced metacone, usually no vestige of a posterior cingulum; M2 with pinched anterostyle; m1 lacks tma or it is very weak, anterior four cusps of m1 form an 'x' pattern that is central or buccal to the midline in position, lingual anteroconid only slightly larger than labial anteroconid, labial cingulum weak; m2 with exceptionally small labial anteroconid and moderate labial cingulum with variable c1 and c3; m3 is relatively large (more reduced in size in other species of *Mus*; see Tables 2-4, Fig. 4).

Description — This small *Mus* is represented by one partial dentary with molars and by isolated teeth. Some of the teeth are broken but measurements of length or width can be tabulated (Table 1). Upper and lower first molars are narrow, width to length ratio being 0.595 for M1 and 0.610 for m1. Roots are generally broken but enamel is usually well-preserved.

The upper first molar has the apomorphic murine eight cusps. The double anterocone is large and the well-developed, oblique anterostyle is pinched so that its long dimension is anterobuccal-posterolingual. Shifted posteriorly, it lies lingual to the large protocone. The large enterostyle is linked to the posterolingual corner of the protocone. The hypocone is nearly as large as the protocone and both are larger than the paracone. The metacone is smaller and appressed to the hypocone, indistinct in some specimens. Unworn M1 may show an indistinct remnant of the posterior cingulum. The long slope of the anterocone is smooth but one tooth has a slight precingulum.

M2 is broader anteriorly than posteriorly. The straight anterior cingulum joins a large pinched anterostyle and a small buccal cusp, the "labial anterocone". The most prominent cusp, the protocone, is between a large paracone and the posteriorly turned enterostyle, which may reach the base of the hypocone but is not confluent with it. The hypocone is large and confluent with the smaller metacone. There is a small posterior cingulum.

The small M3 is dominated by one chevron, composed of a large protocone flanked by its enterostyle and paracone. It is triangular and tapers posteriorly more strongly than that of *Mus auctor*. At the anterolingual corner of the tooth is a

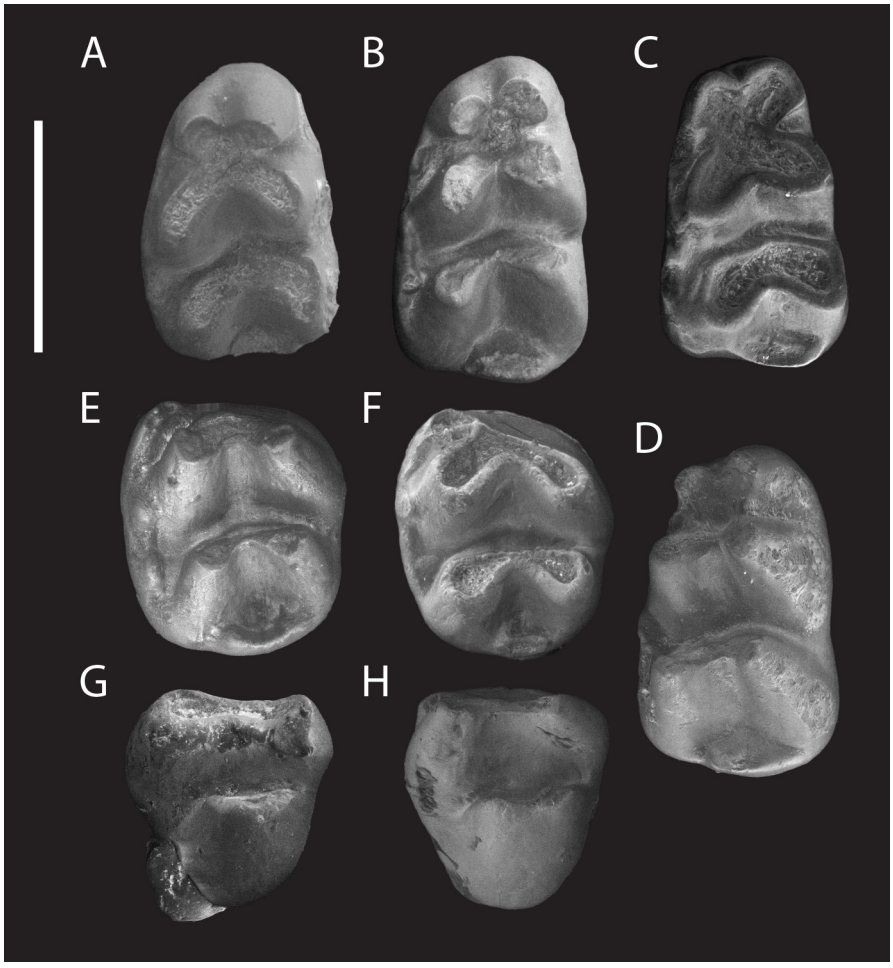

FIGURE 3. Lower molars of *Mus absconditus* sp. nov. Scale bar equals 1 mm, anterior is upward. **A**, right m1 (YGSP 52914, reversed); **B**, right m1 (YGSP 54421, reversed); **C**, left m1 (YGSP 54420); **D**, right m1 (YGSP 33307, reversed); **E**, left m2 (YGSP 52921); **F**, left m2 (YGSP 54531); **G**, left m3 (YGSP 52921); **H**, left m3 (YGSP 54423). Laser ablated craters on the lingual side of YGSP 52914 and 33307 are sites to obtain the stable carbon isotope values of Kimura et al. (2013a).

prominent anterostyle, opposed by a remnant "labial anterocone" at the opposite end of the anterior cingulum. The hypocone, not as large relatively as in *Mus auctor*, is fused with an indistinct metacone.

The narrow m1 (Fig. 3) has six major cusps. The anterior end of the tooth is dominated by four appressed cusps, the double anteroconid close to the protoconid and metaconid. The lingual anteroconid is slightly larger than the labial anteroconid unlike Upper Siwaliks *Mus flynni* Patnaik, 2001 or *M. jacobsi* Kotlia,1992, which have lingual anteroconid twice the size of the labial one. Wear lends an asymmetrical X-pattern with respect to the midline of the tooth, whereas in one specimen (YGSP 33307, Fig. 3D) the junction of the four cusps lies lingual to it. A deep transverse valley isolates the large hypoconid and entoconid. The strong posterior cingulum proceeds from the hypoconid, but develops an independent oval facet with wear (e.g., YGSP 54421). At the anterior end of the tooth there is no small medial anteroconid (tma). The labial cingulum is weak but usually bears a small c1 cusp, occasionally a minute c3.

Two transverse pairs of cusps dominate m2. The largest cusp, the protoconid, joins the metaconid near the midline of the tooth. A deep transverse valley separates them from the large hypoconid and the entoconid. Diagnostic for the species, a distinct labial anteroconid is present, and the posterior cingulum is a pinched oval as in m1. The labial cingulum is weak, but bears a small c3 and variably a c1.

The small, triangular m3 has a straight anterior connection

TABLE 1. Molar measurements of *Mus absconditus* sp. nov.

Locality	Specimen ID	Length	Width	Tooth position
Y457	34473	1.5	0.95	M1/
Y457	34468	1.25	1.05	M2/
Y457	34492	1.1	0.95	M2/
Y457	34469	0.6	0.8	M3/
Y457	34477	0.75	0.9	M3/
Y457	34495	NA	0.95	/m1
Y457	52913	1.4	0.95	/m1
Y457	52914	1.45	0.8	/m1
Y457	34493	NA	NA	/m3
Y547	33307	1.45	0.95	/m1
Y547	33322	1.5	0.95	/m1
Y547	33322	1.1	0.95	/m2
Y547	33322	0.85	0.75	/m3
Y581	52938	NA	1.05	M1/
Y581	52935	1.45	0.75	/m1
Y921	52920	1.44	0.79	M1/
Y921	54290	1	1.15	M2/
Y921	54292	1.4	0.9	/m1
Y921	54293	NA	0.8	/m1
Y921	54291	0.8	0.8	/m3
Y931	52972	1.61	0.92	M1/
Y931	52973	1.57	0.86	M1/
Y931	52974	1.54	0.96	M1/
Y931	52975	1.55	0.9	M1/
Y931	52976	1.57	0.88	M1/
Y931	52977	1.59	0.92	M1/
Y931	52978	1.61	0.91	M1/
Y931	52979	1.6	0.9	M1/
Y931	52980	1.67	0.89	M1/
Y931	54351	1.55	0.95	M1/
Y931	54352	NA	1.05	M1/
Y931	54353	NA	NA	M1/
Y931	54354	1.6	1.05	M1/
Y931	54355	NA	0.95	M1/
Y931	54519	1	0.85	M2/
Y931	54520	1.05	0.85	M2/
Y931	54521	1.1	0.85	M2/
Y931	54522	0.95	0.9	M2/
Y931	54523	1.05	0.85	M2/

TABLE 1. Continued

Locality	Specimen ID	Length	Width	Tooth position
Y931	54524	1.1	1.05	M2/
Y931	54525	1	0.9	M2/
Y931	54424	0.75	0.75	M3/
Y931	54425	0.85	0.8	M3/
Y931	54350	1.55	0.8	/m1
Y931	54413	NA	0.95	/m1
Y931	54414	NA	1	/m1
Y931	54415	1.35	0.85	/m1
Y931	54416	NA	NA	/m1
Y931	54417	1.3	0.75	/m1
Y931	54418	NA	NA	/m1
Y931	54419	NA	0.8	/m1
Y931	54420	1.25	0.8	/m1
Y931	54421	1.3	0.85	/m1
Y931	54422	NA	0.8	/m1
Y931	54526	0.9	0.85	/m2
Y931	54527	0.95	0.85	/m2
Y931	54528	0.95	0.85	/m2
Y931	54529	NA	NA	/m2
Y931	54530	0.9	0.85	/m2
Y931	54531	0.95	0.85	/m2
Y931	54532	1.05	1	/m2
Y931	54533	1.05	0.9	/m2
Y931	54423	0.85	0.8	/m3

between protoconid and metaconid. A reduced labial anteroconid is variable, usually present. The large, central hypoconid incorporates a remnant of the entoconid. There is no hint of a buccal cingulum.

Comparisons — Yuri Kimura studied the Potwar succession of murine rodents as part of her dissertation under Prof. Louis Jacobs. Her multifaceted work included morphometric analysis of dental morphology and firmly established by comparison with living mice that the mouse sample studied here represents a species of *Mus* (Kimura et al. 2013a, b). Kimura et al. (2015, 2016, 2021) further demonstrated that the older early late Miocene differentiation of the murine genera *Progonomys* and *Karnimata* witnessed in the Siwalik fossil record pertained respectively to the roots of the living *Mus* and *Arvicanthis* tribes. This was bolstered by consistent

TABLE 2. Dental measurements (in mm) and statistics for *Mus absconditus* sp. nov., see Table 1

Tooth position	Length					Width				
	n	min	mean	max	sd	n	min	mean	max	sd
M1	13	1.44	1.57	1.67	0.06	16	0.79	0.93	1.05	0.07
M2	10	0.95	1.06	1.25	0.08	10	0.85	0.94	1.15	0.11
M3	4	0.60	0.74	0.85	0.10	4	0.75	0.81	0.90	0.06
m1	11	1.25	1.40	1.55	0.09	17	0.75	0.86	1.00	0.08
m2	8	0.9	0.98	1.10	0.08	8	0.85	0.89	1.00	0.06
m3	3	0.8	0.83	0.85	0.03	3	0.75	0.78	0.80	0.03

TABLE 3. Length and width ratios of upper molars in *Mus* species. Data from Kotlia (2008), Kotlia et al. (2011), and references therein; original measurements in this study for *M. absconditus*. Note: *M. jacobsi* and *M. narmadaensis* do not appear in Fig. 4b since third molars are lacking

Genus	Species	Age	M3/M1		M3/M2	
			Length ratio	Width ratio	Length ratio	Width ratio
Mus	*absconditus*	7.5 Ma	0.47	0.87	0.70	0.86
Mus	*auctor*	6.5 Ma	0.37	0.80	0.60	0.84
Mus	*flynni*	2.5 Ma	0.41	0.76	0.74	0.85
Mus	*jacobsi*	2.4 Ma	NA	NA	NA	NA
Mus	*dhailai*	50 ka	0.33	0.55	0.51	0.65
Mus	*narmadaensis*	Upper Pleistocene	NA	NA	NA	NA
Mus	*dulamensis*	30 ka	0.38	0.53	0.65	0.62
Mus	*dunni*	Extant	0.34	0.56	0.65	0.65
Mus	*booduga*	Extant	0.32	0.62	0.62	0.68

TABLE 4. Length and width ratios of lower molars in *Mus* species. See Table 3 for notes

Genus	Species	Age	m3/m1		m3/m2	
			Length ratio	Width ratio	Length ratio	Width ratio
Mus	*absconditus*	7.5 Ma	0.56	0.91	0.80	0.88
Mus	*auctor*	6.5 Ma	0.49	0.78	0.65	0.73
Mus	*flynni*	2.5 Ma	0.39	0.62	0.71	0.71
Mus	*jacobsi*	2.4 Ma	0.34	0.54	0.48	0.57
Mus	*dhailai*	50 ka	0.41	0.67	0.59	0.64
Mus	*narmadaensis*	Upper Pleistocene	0.51	0.86	NA	NA
Mus	*dulamensis*	30 ka	0.41	0.68	0.58	0.64
Mus	*dunni*	Extant	0.43	0.67	0.69	0.69
Mus	*booduga*	Extant	0.39	0.78	0.60	0.67

molecular studies (e.g., Aghová et al. 2018) that found Tribe Rattini as sister to (outside) these murine groups after the earliest split of Tribe Phloeomyini. The early divergence of the Rattini is not recorded in dental morphological traits in the Siwalik record (Flynn et al. 2020).

Among murini *Progonomys* is primitive in most characters. Jacobs (1978) noted that the genus shows low crowned molars with low connections between cusps and undeveloped

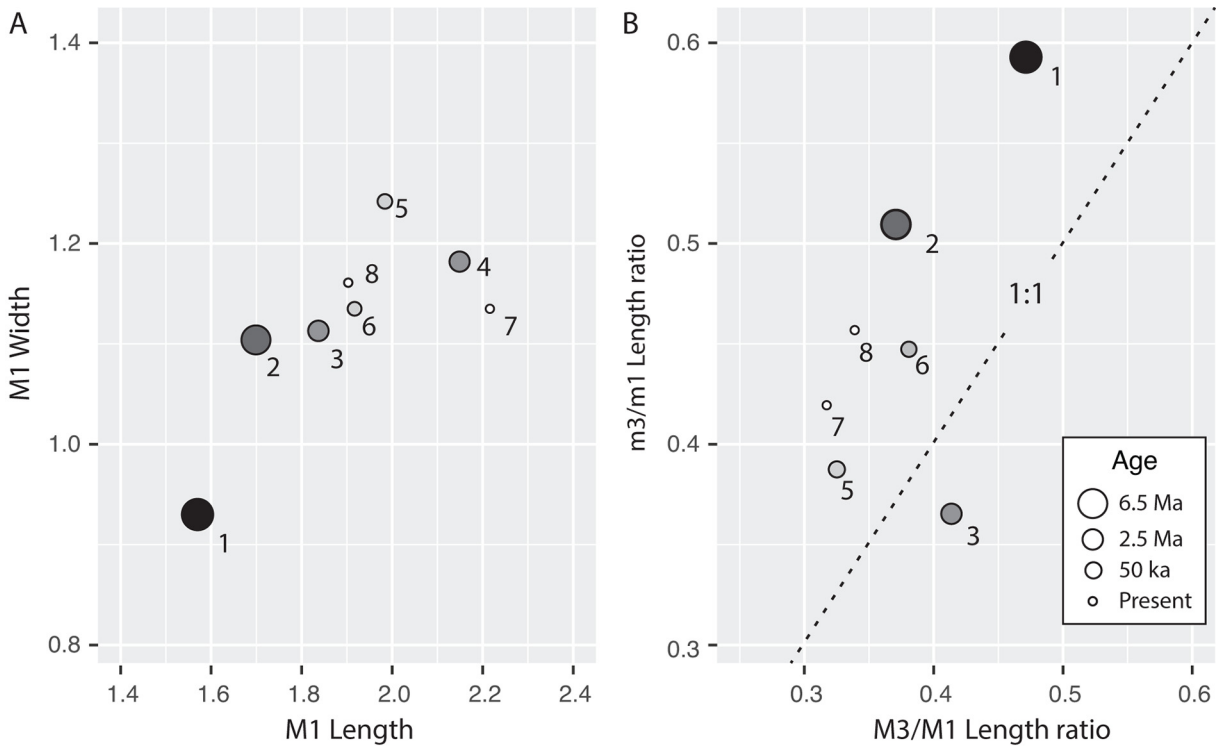

FIGURE 4. Scatter plots of tooth measurements in eight species of *Mus*, corresponding to Tables 2-4. **A**, M1 length vs. M1 width. **B**, M3/M1 length ratio vs. m3/m1 length ratio. **1**, *Mus absconditus* sp. nov.; **2**, *Mus auctor*; **3**, *Mus flynni*; **4**, *Mus jacobsi*; **5**, *Mus dhailai*; **6**, *Mus dulamensis*; **7**, *Mus dunni*; **8**, *Mus booduga*. Larger symbols represent older species. Dashed line on the right is 1:1 ratio.

stephanodonty. As a murin feature inherited by *Mus* the genus indicates a pinched anterostyle and enterostyle of M1, which is posterior in position. *Mus* is distinguished first by its small size. In contrast to *Progonomys*, the genus shows stronger transverse connections between cusps, a sloping anterocone on M1, reduced or absent posterior cingulum on M1, asymmetrical "X" on m1, and third molars proportionally reduced in size (Fig. 4). *Mus auctor* is little transformed from *Progonomys* in such features.

Mus absconditus of 8.0 to 7.2 Ma differs from younger *Mus auctor* in several key features. It is smaller, and its molars are relatively slenderer (width to length ratio = 0.65 in *Mus auctor*). Most *M. absconditus* M1 lack a precingulum, but at 6.5 Ma nearly half of the *Mus auctor* M1 has this structure, and its M1 metacone is usually distinct. The protrusion and degree of tapering of the anterior edge of the lingual anterocone on M1 compared to that of the labial anterocone is greater (derived) in *M. auctor* than in *M. absconditus* and even more significant in Pliocene-Pleistocene *M. jacobsi* and *M. flynni*. The "X" pattern of m1 is more anteriorly positioned in *M. absconditus* than *M. auctor*. The labial cingulum of m1 and m2 is less prominent in *M. absconditus*. *M. auctor* shares with extant *Mus* an anteriorly displaced lingual anteroconid on m1. In summary, whereas *M. auctor* is primitive for *Mus* in many but not all dental features, the size and morphology of *M. absconditus* molars is mostly advanced with respect to other *Mus*.

Mus auctor is the only other *Mus* known from the Miocene of southern Asia. Sen (1983), however, named the larger *Mus elegans* from the earliest Pliocene of Afghanistan. Its metacone on M1 is reduced and there is usually a precingulum. The labial cingulum on m1 and m2 is weak, less prominent than in *Mus auctor* (see Table 5).

Mus occurs in younger deposits of India. Both the Pliocene *Mus jacobsi* Kotlia, 1992 and *Mus flynni* Patnaik, 2001 are larger than the Potwar *Mus*. Their M1 anterostyle is less compressed and less deflected posteriorly, and the anterocone with precingulum is elongated. Two Pleistocene species in India (Kotlia 1995, 2008) are also large. *Mus dhailai* Kotlia, 1995 has simplified third molars and a less compressed anterostyle. *Mus dulamensis* Kotlia, 2008 has a strong M1 precingulum with accessory prestyles. Small *Mus narmadaensis*

TABLE 5. Key features of some South Asian Neogene species of *Mus*

Mus absconditus	Small size	Narrow molars	Weak M1 precingulum	Variable M1 posterior cingulum	Anterior X pattern on m1	Weak m1-2 labial cingulum
Mus auctor	Medium size	Wide molars	Usual precingulum	Posterior cingulum absent	X pattern not shifted anteriorly	Cingulum developed
Mus jacobsi	Large	Wide	Usual precingulum	Cingulum absent	Anterior X pattern	Weak labial cingulum
Mus flynni	Large	Wide	Strong	Absent	Not shifted	Weak
Mus dhailai	Large	Wide	Weak	Damaged	Not shifted	Weak
M. dulamensis	Large	Narrow	Strong	Absent	Anterior	Weak
M. elegans	Medium size	Narrow molars	Usual precingulum	Cingulum absent	Anterior m1 X pattern	Moderate cingulum

Kotlia et al. 2011 has compressed anteroconids on m1, and a strongly reduced posterior cingulum.

The latest Miocene and early Pliocene of Yushe Basin, Shanxi Province, northern China, does not record *Mus*, but has the closely related *Huaxiamys*. Those species are somewhat larger than Siwalik *Mus*, and are distinctive in stephanodonty. The compressed anterostyle on M1 of *Huaxiamys* is an oblique blade continuing through the lingual anterocone (Wu and Flynn 1992).

DISSCUSSION AND CONCLUSIONS

The Dhok Pathan Formation of the Potwar Plateau, Pakistan, records the rich history of Siwalik late Miocene mammalian assemblages. Low in the formation at locality Y182, Louis Jacobs (1978) found and named the murine rodents *Progonomys debruijni* and *Karnimata darwini*. In younger deposits he described the early mouse *Mus auctor*. Louis proposed that his *Progonomys* was close to *Mus* and evidenced that Tribe Murini had differentiated by the early late Miocene. More recently, Kimura et al. (2015, 2021) corroborated this, specifying that *Progonomys* and *Karnimata* represent the distinct murine tribes Murini and Arvicanthini, respectively. She could estimate the age limits on the *Progonomys*-*Mus* transition as well: Locality Y182 is about 9.2 Ma and D013 yielding *Mus auctor* dates to 6.5 Ma. *Mus* had appeared during the late Miocene in the fossil record of the Potwar Plateau.

Jacobs and Flynn (2005) saw some complexity in the origin of the genus and Kimura et al. (2016, 2021) recognized a small species of *Mus* preceding *Mus auctor*. It was clearly an unnamed member of the genus but more derived in some features than *Mus auctor*. Here we name this early *Mus* and distinguish its morphological features. It is small and derived in some characters such as reduced metacone, infrequent and low precingulum on M1, a weak labial cingulum on lower molars, lack of tma on m1. Meanwhile, *M. absconditus* possesses a basal trait in that its lingual anterocone is less protruded and less tapering than any other *Mus* species.

While *Mus auctor* may look like a diminutive *Progonomys debruijni*, *Mus absconditus* shows that the origin of the genus is complex. Evidently *Mus absconditus* evolved elsewhere in South Asia and its lineage immigrated to the Potwar Plateau. *Mus auctor* may also be an immigrant, arriving after *Mus absconditus*. It remains to be determined exactly the pattern of decline of *Progonomys* and rise of early *Mus*. Probably the evolution of modern Murini (*Mus* and close relatives) centered in southeastern Asia and the peripheral Potwar sampled the edges of that radiation.

As to the time of origin of extant Murini, the pattern and timing of the appearance of *Mus* provides a minimum age constraint. The fossil *Mus* recorded at locality Y547 is the oldest record of the genus and argues that its group was present by at least 8.0 Ma (Kimura et al. 2015, 2021). Future discoveries of *Mus* fossils will reveal the pattern of dispersal of the genus and provide a better temporal framework for molecular phylogeny.

Today we benefit from the labors of many and inherit a wealth of well-dated small mammal samples that were not previously available. It is the efforts of Louis Jacobs and

others that have built the Potwar record for us to read.

ACKNOWLEDGMENTS

Our biostratigraphic work was inspired by the energy and imagination of Louis L. Jacobs and our comrades in the field, the late Everett "Doc" Lindsay and Will Downs. Their combined efforts produced the rich Potwar record that we continue to study today. SEM viewing was performed with the able assistance of Timothy Cavanaugh at the Harvard University Center for Nanoscale Systems (CNS); a member of the National Nanotechnology Coordinated Infrastructure Network (NNCI), which is supported by the National Science Foundation under NSF award no. ECCS-2025158. Yuri Kimura was funded by JSPS KAKENHI Grant Number 21K15176. We appreciate evaluation of this work by reviewers and the editorial efforts of Yuong-Nam Lee.

REFERENCES

Aghová, T., Kimura, Y., Bryja, J., Dobigny, G., Granjon, L., & Kergoat, G. J. (2018). Fossils know it best: Using a new set of fossil calibrations to improve the temporal phylogenetic framework of murid rodents (Rodentia: Muridae). *Molecular Phylogenetics and Evolution* 128: 98-111. https://doi.org/10.1016/j.ympev.2018.07.017.

Barry, J. C., Behrensmeyer, A. K., Badgley, C., Flynn, L. J., Peltonen, H., Cheema, I. U., Pilbeam, D., Lindsay, E. H., Raza, S. M., Rajpar, A. R., & Morgan, M. E. (2013). The Neogene Siwaliks of the Potwar Plateau and other regions of Pakistan. In X. Wang, L. J. Flynn, & M. Fortelius (Eds.), *Fossil mammals of Asia: Neogene biostratigraphy and chronology* (pp. 373–399). Columbia University Press, New York.

Barry, J. C., Morgan, M. E., Flynn, L. J., Pilbeam, D., Behrensmeyer, A. K., Raza, S. M., Khan, I. A., Badgley, C., Hicks, J., & Kelley, J. (2002). Faunal and environmental change in the Late Miocene Siwaliks of Northern Pakistan. *Paleobiology Memoir*, 3, 1–71.

Flynn, L. J., Kimura, Y., & Jacobs, L. L. (2020). The Murine Cradle. In G. V. R. Prasad & R. Patnaik (Eds.), *Biological consequences of Plate Tectonics: New Perspectives on Post-Gondwana Break-up. A tribute to Ashok Sahni* (pp. 347–362). Cham: Springer

Jacobs, L. L. (1977). A new genus of murid rodent from the Miocene of Pakistan and comments on the origin of the Muridae. *Paleobios*, 25, 1–11.

Jacobs, L. L. (1978). Fossil rodents (Rhizomyidae and Muridae) from Neogene Siwalik deposits, Pakistan. *Museum of Northern Arizona Bulletin Series*, 52, 1–103.

Jacobs, L. L. & Flynn, L. J. (2005). Of Mice … Again: The Siwalik rodent record, murine distribution, and molecular clocks. In D.E. Lieberman, R. J. Smith, & J. Kelley (Eds.), *Interpreting the Past: Essays on Human, Primate, and Mammal Evolution in Honor of David Pilbeam* (pp. 63–80). American School of Prehistoric Research Monograph Series, Volume 5. Brill Academic Publishers, Inc., Boston.

Jacobs, L. L. & Pilbeam, D. (1980). Of mice and men: fossil-based divergence dates and molecular "clocks." *Journal of Human Evolution*, 9, 551–555.

Kimura, Y., Flynn, L.J., & Jacobs, L.L. (2016). A paleontological case study for species delimitation in diverging fossil lineages. *Historical Biology*, 28(1-2), 189–198.

Kimura, Y., Flynn, L. J., & Jacobs, L. L. (2021). Tempo and Mode: Evidence on a protracted split from a dense fossil record. In L.A Fostowicz-Frelik, D. Ge, & I. Ruf (Eds.), *Recent Advances in the Evolution of Euarchontoglires*, *Frontiers in Ecology and Evolution*, 9, 642814. https://doi.org/10.3389/fevo.2021.642814.

Kimura, Y., Hawkins, M. T. R., McDonough, M. M., Jacobs, L. L., & Flynn, L. J. (2015). Corrected placement of *Mus-Rattus* fossil calibration forces precision in the molecular tree of rodents. *Scientific Reports*, 5, 14444, 9 p., https://doi.org/10.1038/srep14444.

Kimura, Y., Jacobs, L. L., Cerling, T. E., Uno, K. T., Ferguson, K. M., Flynn, L. J., & Patnaik, R. (2013a). Fossil mice and rats show isotopic evidence of niche partitioning and change in dental ecomorphology related to dietary shift in late Miocene of Pakistan. *Plos One*, 8(8), e69308. https://doi.org/10.1371/journal.pone.0069308.

Kimura, Y., Jacobs, L. L., & Flynn, L. J. (2013b). Lineage-specific response of tooth shape in murine rodents (Murinae, Rodentia) to late Miocene dietary change in the Siwaliks of Pakistan. *Plos One*, 8(10), e76070. https://doi.org/10.1371/journal.pone.0076070.

Kotlia, B. S. (1992). Pliocene murids (Rodentia, Mammalia) from Kashmir Basin, northwestern India. *Neues Jahrbuch für Geologie und Paläontologie Abhandlungen*, 184, 339–357.

Kotlia, B. S. (1995). Upper Pleistocene Soricidae and Muridae from Bhimtal-Bilaspur deposits, Kumaun Himalaya, India. *Journal Geological Society of India*, 46, 177–190.

Kotlia, B. S. (2008). A new species of fossil *Mus* (Rodentia, Muridae) from the Indian Himalaya: Evolutionary and phylogenetic implications. *Palaeoworld*, 17, 47–56.

Kotlia, B. S., Joshi, M., & Joshi, L. M. (2011). A new species of fossil *Mus* (Muridae, Mammalia) from the Late Quaternary deposits of Narmada Valley, Central India. *Open Journal of Geology*, 1, 37–44.

Opdyke, N. D., Lindsay, E. H., Johnson, G. D., Johnson, N. M., Tahirkheli, R. A. K., & Mirza, M. A. (1979). Magnetic polarity stratigraphy and vertebrate paleontology of the Upper Siwalik Subgroup of Northern Pakisatan. *Palaeogeography, Palaeoclimatology, Palaeoecology*, 27, 1–34.

Patnaik, R. (2001). Late Pliocene micromammals from Tatrot Formation (Upper Siwaliks) exposed near Village Saketi, Himachal Pradesh, India. *Palaeontographica*, A261, 55–81.

Sen, S. (1983). Rongeurs et Lagomorphes du gisement pliocène de Pul-e Charkhi, bassin de Kabul, Afghanistan. *Bulletin du Museum national d'Histoire naturelle*, Paris, 5^{e} Séries, 5C(1), 33–74.

Winkler, A. J., Flynn, L. J., & Tomida, Y. (2011). Fossil lagomorphs from the Potwar Plateau, northern Pakistan. *Palaeontologia Electronica*, 14.3.38A, 16 p., http:palaeo-electronica.org/toc.htm

Wu W. & Flynn, L. J. (1992). New murid rodents from the Late Cenozoic of Yushe Basin, Shanxi. *Vertebrata PalAsiatica*, 30(1), 17-38, 2 pl.

WINDOWS INTO SAUROPSID AND SYNAPSID EVOLUTION
Essays in honor of Prof. Louis L. Jacobs, pp. 273–289, 2023

NEW MATERIAL OF *SAYIMYS* (RODENTIA, CTENODACTYLIDAE) FROM CHINA

LAWRENCE J. FLYNN[1,*], WENYU WU [2], LU LI [2, 3], ZHUDING QIU[2]

[1]Department of Human Evolutionary Biology, Harvard University, Cambridge MA 02138, USA, ljflynn@fas.harvard.edu;
[2]Institute of Vertebrate Paleontology and Paleoanthropology, Chinese Academy of Sciences, Beijing 100044, China;
[3]Key Laboratory of Vertebrate Evolution and Human Origins of Chinese Academy of Sciences, Institute of Vertebrate Paleontology and Paleoanthropology, Chinese Academy of Sciences, and CAS Center for Excellence in Life and Paleoenvironment, Beijing 100044, China

ABSTRACT We examine the fossil history as presently known in China of an obscure Neogene genus shared with the Siwaliks of the Indian subcontinent, the ctenodactylid *Sayimys*. *Sayimys* is a rodent distantly related to porcupines that was recognized last century from one area in China. Over the last 80 years, remains from several localities have emerged and these have proven sufficient to show that several species are represented among them. This enigmatic group has been neglected for too long. We take this opportunity to review what is known of *Sayimys* in China. The scattered remains of considerable age distribution include two new species named here; further analysis plus locality context enables validation of two other species that were previously described. In total, we find five species-level members of the genus *Sayimys* distributed across late early to middle Miocene deposits in China.

KEYWORDS *Sayimys*/Ctenodactylidae, Systematics, Biogeography, Miocene, China

INTRODUCTION

Sayimys is a genus of ctenodactylid rodents (Ctenohystrica) whose global record spans the Miocene Epoch. The geographical range of the genus is broad, from Jebel Zelten, Libya, in the west to Jiangsu province in eastern China and southward to the Indian subcontinent, with fossils locally distributed in Africa, Europe and Asia. Samples from most localities are small, exceptions being some from Pakistan and Turkey. Hinton (1933) noted the ctenodactylid family affinity of his Miocene Siwalik species *Pectinator sivalensis*. Wood (1937) saw hystricomorph affinity in his late Miocene *Sayimys perplexus* when he named the genus, and Bohlin (1946) saw similarity of his Chinese species *S. obliquidens* with the Siwalik lineage. It was Black (1972) who united the three in the same genus *Sayimys*. Late early Miocene species were included in *Sayimys* as work progressed. Sen and Thomas (1979) described *S. intermedius* from the Hofuf Formation, Saudi Arabia, and de Bruijn et al. (1981) added *Sayimys minor* from Pakistan.

Munthe (1980) studied a middle Miocene age sample of *Sayimys sivalensis* and proposed that *Sayimys perplexus* Wood, 1937 might be an end member, late Miocene synonym of *S. sivalensis* (Hinton, 1933). Baskin (1996) reviewed Siwalik ctenodactylids, retained *Sayimys perplexus*, and recognized the lineage to span the Miocene from the earliest Miocene *S. flynni* to the late Miocene *S. perplexus*.

A dozen species of *Sayimys* have been formally named: *S. baskini*, *S. minor*, *S*, *hintoni*, and *S. flynni* from the early Miocene in Pakistan, *S. giganteus* from the early Miocene in Turkey, *S. negevensis* from the early Miocene in Israel, *S. sihongensis* from the late early Miocene in China, *S. assarrarensis* from the late early Miocene in Saudi Arabia, *S. intermedius* from the early to middle Miocene in Saudi Arabia, Greece, Turkey and Pakistan, *S. sivalensis* and *S. chinjiensis* from the middle Miocene in Pakistan, *S. perplexus* (including *S. badauni*) from the late Miocene in India, and *S. obliquidens* from the middle Miocene in China (Hinton, 1933; Wood, 1937; Bohlin, 1946; Jaeger, 1971, 1977; Black, 1972; Sen and Thomas, 1979; Munthe, 1980; de Bruijn et al., 1981, 1989; Wessels et al., 1982, 2003; Vasishat, 1985; Flynn and Jacobs, 1990; Baskin, 1996; de Bruijn, 1999; Kordikova and de Bruijn, 2001; López-Antoñanzas and Sen, 2003, 2004; López-Antoñanzas et al., 2004, 2005, 2015, 2016; Qiu, 2017;

*Corresponding author

Hartman et al., 2019). There have been different opinions on the systematic position and validity of some species. *S. minor* and *S. intermedius* were considered synonyms (Wang, 1997; López-Antoñanzas and Sen, 2003, 2004; López-Antoñanzas et al. 2016), but Hartman et al. (2019) resurrected them as valid species. Munthe (1980) and López-Antoñanzas and Sen (2003) considered *S. perplexus* and *S. chinjiensis* to be junior synonyms of *S. sivalensis*, but Hartman et al. (2019) maintained *S. chinjiensis* and restricted the name of *S. sivalensis* to its holotype. De Bruijn et al. (1981), Wang (1997), and López-Antoñanzas and Sen (2003) accepted the Munthe (1980) suggestion that *S. perplexus* is a junior synonym of *S. sivalensis*, but de Bruijn et al. (1989) and Baskin (1996) rejected it. Hartman et al. (2019) synonymized *S. baskini* with *S. minor* from Pakistan, and *S. assarrarensis* with *S. intermedius* from Saudi Arabia. In addition, the primitive *Prosayimys* has been submerged as a junior synonym of *Sayimys* (Kordikova and de Bruijn, 2001; Hartman et al., 2019). *Akzharomys* Shevyreva, 1994 shares important features with *Sayimys* (see below). Obviously, much remains to be done and consensus on assignment of some species must await discovery and adequate study of new material.

We examine the slowly emerging fossil record of *Sayimys* in China since the first finding of *Sayimys*, *S. obliquidens* from Taben-Buluk, Gansu Province (Bohlin, 1946). After a hiatus of more than 30 years, remains of this genus were recovered in succession from other localities, including Fuhai in Junggar Basin, Xinjiang, Dongxiang, Guanghe in Linxia Basin and Qin'an in Gansu, Tongxin in Ningxia, Sihong in Jiangsu (Li et al., 1983; Cao et al., 1990; Wu et al., 1991, 1998; Ye et al., 2001a, b; Guo et al., 2002; Qiu et al., 2023). Figure 1 shows location of the six fossil localities producing Miocene *Sayimys* in China. All occur in North China, mainly concentrated along the Mongol-Xinjiang highland. Materials collected by screen-washing from Fuhai in Xinjiang and Linxia in Gansu are adequate, but from other localities are rather scarce. Of these samples, only a few specimens have been described in detail: one m2 assigned to an indeterminate species from the middle Miocene Dingshanyanchi Formation of Xinjiang and three cheek teeth identical as *S. sihongensis*

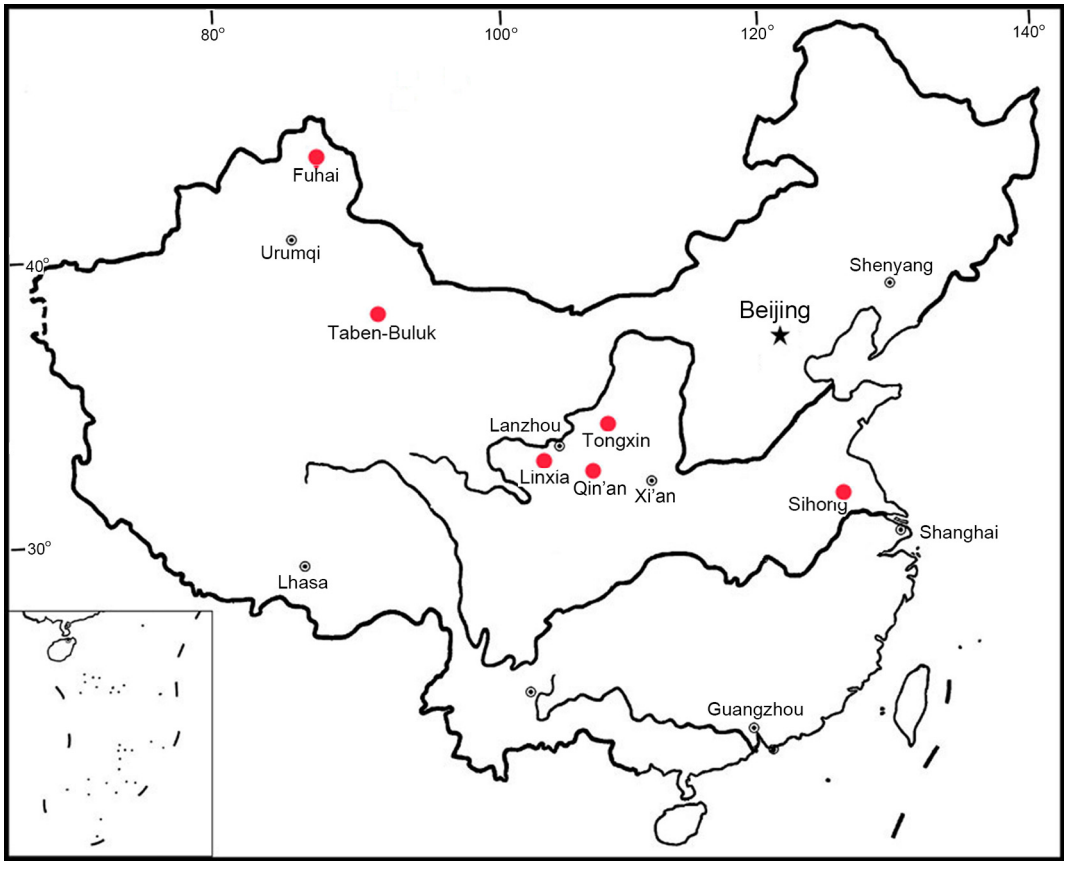

FIGURE 1. Geographical location of the fossil sites producing *Sayimys* in China.

from the early Miocene Xiacaowan Formation of Jiangsu (Wu et al. 2009; Qiu, 2017).

The aim of this work is to develop the systematics of *Sayimys* collected in the Miocene of China during the last decades. These samples document local evolution and seem to embrace several closely related species. For geological background, the reader is referred to Li et al. (1983) for Sihong localities, to Cao et al. (1990) and Qiu et al. (2023) for localities of Linxia in Gansu, to Wu et al. (1998) and Ye et al. (2001a, b) for localities of Fuhai in Xinjiang, to Guo et al. (2002) for Qin'an in Gansu.

This review celebrates the career of Louis L. Jacobs. One of the hallmarks of his work is advancing the study of rodents. In this, Louis has made many friends globally, and is welcome in China at the Institute of Vertebrate Paleontology and Paleoanthroplogy. We are pleased to dedicate this paper to an outstanding scientist, our friend Prof. Dr. Louis L. Jacobs.

MATERIAL AND METHODS

Most of the material is housed in the collections of the Institute of Vertebrate Paleontology and Paleoanthropology, Chinese Academy of Sciences in Beijing. The Shinanu fossils collected by Cao et al. (1990) are deposited in the collections of China University of Geosciences in Beijing. The dental morphological terminology used for description in the paper follows Hartman et al. (2019). To facilitate comparisons, some right-side teeth are figured as left ones (indicated as "reversed" in the illustration). Measurements (in millimeters with 0.01 mm precision for teeth and 0.1 mm for jaws) were made using a WILD microscope.

Abbreviations — **IVPP**, Institute of Vertebrate Paleontology and Paleoanthropology, Chinese Academy of Sciences; **CUGB**, China University of Geosciences (Beijing); **GV**, collection of vertebrates in CUGB; **LMS/A**, Chinese Land Mammal Stage/Age; **LX**, IVPP or XJ, IVPP localities in the Linxia Basin, Gansu, or Xinjiang Junggar Basin, respectively; **TB**, Taben Buluk collection; **V**, collection of vertebrates in IVPP.

SYSTEMATIC PALAEONTOLOGY

Family Ctenodactylidae Gervais, 1853

Subfamily Ctenodactylinae Hinton, 1933

Genus *Sayimys* Wood, 1937

***Sayimys obliquidens* Bohlin, 1946**

Holotype — TB 268, left lower jaw with incisor and p4-m1-3.

Paratype — TB 279, partial skull with cheek teeth.

Type Locality and Age — Tiejianggou Formation at Tiejianggou and Yandantugou, Aksay Kazakzu Zizhixian (Aksay Kazak Autonomous County, Gansu Province). Precise locality not recorded, although we confirm the general area; age, not well constrained, could be late Early Miocene or Middle Miocene (Shanwangian or Tunggurian LMS/A).

Characteristics — a large species of *Sayimys*, size overlapping with large *S. sivalensis* from the Indian subcontinent. High crowned, mesolophid retained on lower molars, transverse lower molar lophids are oblique.

***Sayimys fuhaiensis* sp. nov.**

(Fig. 2)

Holotype — IVPP V 27366.1, right maxillary fragment with P4-M3 (Fig. 2A-D).

Paratype — V 27366.2, right m2.

Etymology — Named after Fuhai, the county seat of the Xinjiang Uygur Autonomous Region.

Type Locality and Horizon — Duolebulejin (IVPP Loc. XJ 200910; 46°33'99.30"N, 87°46'96.50"E), Fuhai County, Xinjiang Uygur Autonomous Region; the lower Halamagai Formation (second sandstone layer from the top of the Suosuoquan Formation).

Age — Middle Miocene, early Tunggurian LMS/A.

Referred specimens — IVPP V 27368.1-8, 1 left maxillary fragment with P4-M3, 7 isolated cheek teeth (1 DP4, 1 M2, 2 dp4, 2 m1/2, 1 m3) from Loc. XJ 97008 (46°33'99.70"N, 87°48'29.80"E), and IVPP V 27367, 1 m3 from Loc. XJ 96004 (46°33'97.20"N, 87°47'05.00"E) at Duolebulejin, Fuhai, Xinjiang; the lower Halamagai Formation. IVPP V 27369.1-2, 2 P4 from Loc. XJ 200815 (46°24'28.10"N, 87°25'99.10"E) at 45 km mark of West Main Irrigation Canal (Xi-Gan-Qu), Southwest of Dingshan Salt Lake of (Dingshanyanchi), Fuhai, Xinjiang; upper muddy siltstone of Halamagai Formation (Tunggurian LMS/A).

Measurements (length × width) — Length of P4-M3 = 7.2, 6.6; DP4 = 1.85 × 1.65; P4 = 0.90 × 1.25, 1.00 × 1.65, 1.10 × 1.75,

1.00 × 1.50; M1 = 1.75 × 2.10, 1.80 × 2.15, M2 = 2.15 × 2.60, 2.00 × 2.55, 2.15 × 2.25; M3 = 2.10 × 2.70, 2.00 × 2.50; dp4 = 2.30 × 1.53, 2.20 × 1.30; m1/2 = 2.70 × 2.30, 2.54 × 2.20; m3 = 2.30 × 2.10, 2.60 × 2.30.

Diagnosis — Low crowned, moderate size to large *Sayimys* with zygomatic process extending laterally from the level of anterior margin of P4, and the incisive foramen reaching posteriorly to the level of the anterior root of M1. P4 with conical and isolated protocone, occasional anteroloph, short and thick endoloph, metaloph connecting the base of paracone, and two roots or single root with anterior perpendicular groove. Upper molars with distinct paraflexus and metaflexus in early stages of wear. dp4 with developed arc-shaped anteroconid almost contacting lingually the metaconid, no mesolophid. Lower molars with mesoflexid narrower but deeper than the metaflexid, lacking mesolophid, but having a broad metalophid-protoconid connection and an indistinct constriction of the posterolophid anterior to the triangular wear surface of the hypoconid.

Description — Both maxillae are damaged (Fig. 2A-E), the holotype shows the zygomatic process stretching out from the level of anterior margin of P4, the incisive foramen extending posteriorly to the level of the anterior root of M1. A distinct masseteric tubercle at the anteromesial corner of the zygomatic plate can be observed.

The DP4 is posterobuccally damaged (Fig. 2F). The protocone is slightly larger than the hypocone, and the paracone is anteroposteriorly compressed. The anteroloph is oblique and shows a thickening buccally. The slightly lingually constricted protoloph is almost parallel with the anteroloph. The metaloph turns backwards to meet the slightly anteriorly curved posteroloph. The narrow paraflexus extends to the mid-line of the tooth. The mesoflexus is prominent, bending posterolingually and extending lingually beyond the mid-line of the tooth. The hypoflexus is smaller but much deeper than the mesoflexus. The P4 is oval-shaped, with a conical and nearly isolated protocone, and a ridge-like paracone (Fig. 2G). Both protoloph and metaloph are transversely oriented, thin and low buccally, and connected by a short and thick medial crest (endoloph). An anteroloph is present in one of the four teeth. The metaloph joins the base of the paracone to enclose the mesoflexus. The hypoflexus is located posterolingually. A paraflexus is usually poorly developed. The tooth has two roots or one root with an anterior groove. The M1 and M2 (Fig. 2A, D, E) are similar in morphology, but M2 is larger than M1. Both molars have convex anterior margin, slightly wider anteriorly than posteriorly, straight and anterobuccally directed endoloph, and slightly wider and deeper paraflexus than metaflexus. In moderate stages of wear, the paraflexus and the metaflexus would be obliterated, with the former disappearing slightly earlier than the latter. The mesoflexus is broad and extends beyond the mid-line of the tooth, with its internal termination flexing posteriorly. The hypoflexus is deepest, but its extension does not reach the mid-line of the tooth, the external termination flexing anteriorly. M1 and M2 have 4 roots, a robust lingual root supporting the protocone, and a small lingual and two small buccal ones supporting the hypocone, paracone and metacone, respectively. The M3 resembles M1/2, except for the distinctly narrower and slightly concave posterior margin.

The elongated and brachydont dp4 has a large, isolated, kidney-shaped and slightly lingually positioned anteroconid (Fig. 2H-K). Both protoconid and hypoconid are anteroposteriorly compressed. A mesolophid (= metalophulid II of Baskin, 1996) is lacking. The metalophid is anterolingually stretched. The hypolophid is slightly anterobuccally directed, opposite to the hypoflexid. The posterolophid is constricted just before reaching the hypoconid. The ectolophid is curved, thicker anteriorly than posteriorly. All the flexids are very wide and become narrower with wear. The hypoflexid is the broadest and deepest. The posterobuccal cingulid is moderately developed. The subrectangular m2 is buccally slightly higher-crowned than lingually (Fig. 2L-O). The anterior face of the tooth is moderately concave. The metalophid is thick in the middle and tapers lingually and buccally. No mesolophid is present. The hypolophid extends obliquely and opposite to the protoconid. The posterolophid is slightly curved and the posterolophid-hypoconid connections are wide. The V-shaped mesoflexid is narrower but deeper than the metaflexid. The metaflexid extends mid-way or slightly beyond on the tooth. The hypoflexid is wider and deeper, and almost reaches the mid-line of the tooth. The posterobuccal cingulid is distinct. The m3 is identical to the m2 morphologically, except that it is much wider anteriorly than posteriorly, and its hypoflexid is more oblique, with the terminations of hypoflexid and metaflexid opposite each other (Fig. 2P-S). A slight constriction of the posterolophid occurs before reaching the hypoconid. The posterobuccal cingulid is weak.

Comparison and discussion — The described specimens from four different localities and horizons of the middle

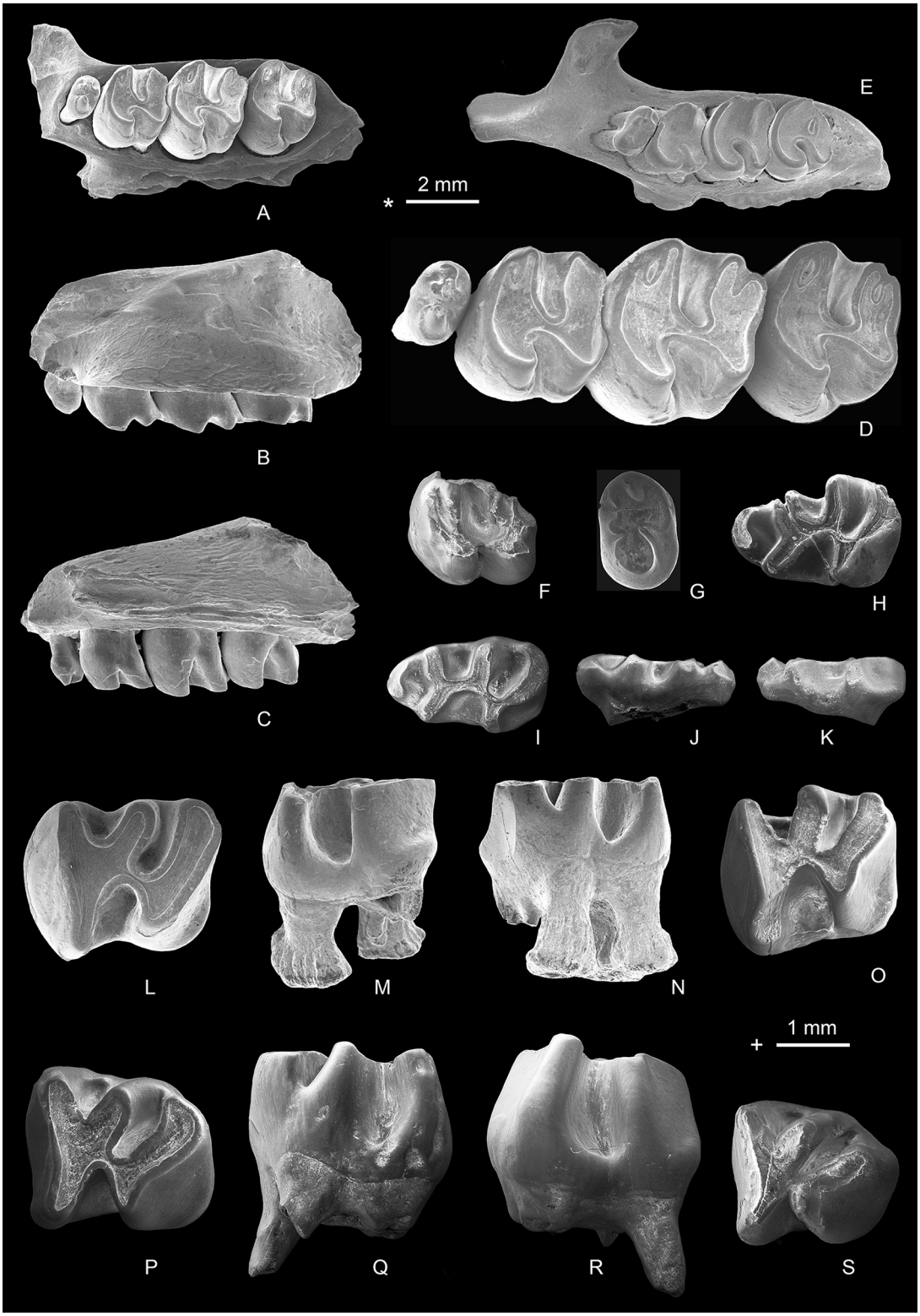

FIGURE 2. Maxillary fragments and cheek teeth of *Sayimys fuhaiensis* from Xinjiang. A-D. right maxillary fragment with P4-M3 (IVPP V 27366.1, holotype, reversed), E. left maxillary fragment with P4-M3 (IVPP V 27368.1), F. right DP4 (IVPP V 27368.2, reversed), G. right P4 (IVPP V 27369.1, reversed), H. left dp4 (IVPP V 27368.4), I-K. right dp4 (IVPP V 27368.5, reversed), L-N. right m2 (IVPP V 27366.2, paratype, reversed), O. left m2 (IVPP V 27368.6), P-R left m3 (IVPP V 27367), S. right m3 (IVPP V 27368.7, reversed); A, D-I, L, O, P, S. occlusal view, B, K, M, R. buccal view, C, J, N, Q. lingual view; * = scale for A-C, E, + = scale for D, F-S.

Miocene Halamagai Formation exhibit good homogeneity and represent the new species *Sayimys fuhaiensis*. They are characterized by relatively large dimension; P4 with conical and almost isolated protocone, and variable anteroloph; distinct paraflexus and metaflexus on upper molars; dp4 with developed arc-shaped anteroconid contacting lingually the metaconid; mesolophid on lower cheek teeth absent, but indistinct posterolophid-hypoconid constriction on lower molars present.

Sayimys fuhaiensis is smaller than *S. obliquidens*, and differs from the latter mainly in having comparatively lower-crowned cheek teeth, less unilateral hypsodonty of molars, and lacking mesolophid on lower molars. It is slightly larger than *S. sihongensis*, and differs in the absence of a mesolophid on dp4, and in its more curved upper molar crowns (indicating greater unilateral hypsodonty).

The new species can be distinguished from *Sayimys intermedius* from the type locality in Saudi Arabia mainly by dp4 with developed arc-shaped anteroconid contacting lingually the metaconid rather than a conical anteroconid joining the metalophid, and distinctly narrower mesoflexid than metaflexid on lower molars, and by the alternating hypoflexid (not opposite the hypolophid) of lower cheek teeth. While *S. intermedius* has been reported from Pakistan, Turkey and Greece (de Bruijn et al. 1989; López-Antoñanzas and Sen, 2004; López-Antoñanzas et al., 2004, 2005), likely some records are not so close morphologically. For example, the specimens of *S. intermedius* described by López-Antoñanzas et al. (2005) from Greece show distinct differences in morphology, and the specimens assigned to *S. intermedius* by de Bruijn (1989) from Pakistan display greatly variable morphology. The intraspecific variation of *S. intermedius* is yet to be documented, but *S. fuhaiensis* is distinguished by its P4 with isolated protocone and symmetrically arranged anteroloph and metaloph.

Sayimys fuhaiensis is about the size of *S. sivalensis* and the higher crowned *S. chinjiensis* but differs from them in lacking an anterolophulid in medial position on dp4, having more developed paraflexus and metaflexus on upper molars, and narrower mesoflexid than metaflexid on lower molars. It differs from small *Sayimys baskini* in having P4 with anteroloph connecting to the protoloph and two roots or one anteriorly grooved root (the latter has no anteroloph and only one root), its upper molar with developed paraflexus and metaflexus (the latter has narrow metaflexus and lacks paraflexus), and absence of mesolophid on dp4.

It differs from *S. badauni* = *S. perplexus* in having isolated protocone, more developed anteroloph and metaloph on P4, and distinct paraflexus and metaflexus on upper molars (the latter has neither paraflexus nor metaflexus). *S. perplexus* was proposed (Munthe, 1980) as a junior synonym of *S. sivalensis*.

Sayimys fuhaiensis is easily distinguishable from *S. giganteus* by its smaller size, absence of mesolophid on dp4, and presence of isolated protocone and symmetrically arranged anteroloph and posterolph on P4. It differs from *S. assarrarensis* in the absence of mesolophid on dp4, the presence of more obliquely extended hypolophid on lower molars, and the isolated protocone and symmetrically arranged anteroloph and metaloph on P4. The new species differs from *Sayimys negevensis* in the absence of mesolophid on lower molars, and the presence of much deeper metastriid but less reduced posteriorly on m3.

Sayimys fuhaiensis is easily distinguishable from small *S. flynni* by its lack of mesolophid but with a much deeper metastriid and thicker metalophid-protoconid connection on lower molars. It differs from *Sayimys mallos* in smaller size, having arc-shaped anteroconid isolated or connected low lingually with the metaconid on dp4, and in the absence of mesolophid on dp4 and lower molars.

Associated with *Sayimys fuhaiensis* are some remains of larger mammals. Wang et al. (2020) described a new species of basal hyaenid, *Tungurictis peignei* from localities XJ 200910 and XJ 200815, and considered the material about 17-14 Ma. *Tungurictis peignei*, the smallest and most primitive form of *Tungurictis*, preceded *T. spocki* Colbert, 1939 in the middle Miocene Tunggur Formation of Inner Mongolia. Thus, *T. peignei* should be older than *T. spocki* (middle Tungurian LMS/A), but younger than middle Shanwangian LMS/A.

Sayimys linxiacus sp. nov.

(Fig. 3, Table 1)

Sayimys cf. *obliquidens*: Cao et al., 1990, p. 21

Sayimys sp.: Qiu and Qiu, 1995, p. 62

Holotype — IVPP V 32330, right M1/2 (Fig. 3M).

Paratype — IVPP V 32331.1-52, 52 isolated cheek teeth (1 DP3, 1 DP4, 2 P4, 12 M1/2, 7 M3, 6 dp4, 3 p4, 14 m1/2, 6 m3).

Etymology — Named after Linxia Basin, Gansu, where the

holotype of this new species was found.

Type Locality and Horizon — Galijia (IVPP Loc. LX 201705; 35°34'58.98"N, 103°23'03.20"E), Dongxiang County, Linxia Prefecture, Gansu Province; the Dongxiang Formation.

Age — Middle Miocene, Tunggurian LMS/A.

Referred specimens — IVPP V 32332.1-16, 16 isolated cheek teeth (1 P4, 4 M1/2, 1 M3, 2 p4, 4 m1/2, 4 m3) from Galijia (IVPP Loc. LX 9801); IVPP V 32333, 1 mandibular fragment with damaged m1 and complete m2 from Yangwa (IVPP LX 201908), Dongxiang, Linxia, Gansu (the middle Miocene Dongxiang Formation). IVPP V 32334, 1 M1/2; CUGB GV 87008-87012, 1 maxillary fragment with M1-3, 4 mandibular fragments with p4-m3, p4-m2, m1-m3 and m2-m3, respectively from Shinanu (IVPP LX 201701), Guanghe, Linxia, Gansu (the middle Miocene Dongxiang Formation). IVPP V 27371, 1 m3 from QA-I Section (35°02'N, 105°27'E), Qin'an, Gansu (the middle Miocene). IVPP V 8860.1 and V8860.6, 1 m2 and 1 M1/2 from Baquan 7-11; IVPP V 8865, 1 damaged M1/2 from Xihuangjiashui 26; IVPP V 8864.1, 1 m2 from Huangjiashui 26; IVPP V 8866.1 and V 8867, 2 m1 from Yehulijuanzi 26, Tongxin, Ningxia (the middle Miocene Hongliugou Formation).

Measurements — See Table 1.

Diagnosis — Medium-sized species of *Sayimys* with distinct paraflexus and metaflexus in upper molars, narrower but deeper mesoflexid than metaflexid in lower molars. P4 without anteroloph, but metaloph joining the base of paracone. dp4 with a conical and isolated anteroconid and occasional

TABLE 1. Measurements of cheek teeth of *Sayimys linxiacus* from Gansu and Ningxia

Tooth	Length			Width		
	N	Mean	Range	N	Mean	Range
			Galijia			
DP3	1	-	0.75	1	-	0.70
DP4	1	-	1.75	1	-	1.50
P4	3	0.88	0.75-1.00	3	1.32	1.25-1.35
M1/2	12	2.05	1.65-2.55	12	2.02	1.70-2.30
M3	9	2.22	1.80-2.55	9	2.11	1.90-2.25
dp4	4	2.09	2.00-2.15	4	1.20	1.00-1.30
p4	5	1.04	1.00-1.10	5	1.00	0.90-1.05
m1/2	12	2.23	2.00-2.45	12	1.73	1.50-2.15
m3	12	2.41	2.30-2.50	12	1.98	1.85-2.05
			Shinanu			
M1	1	-	1.95	1	-	1.90
M2	1	-	2.00	1	-	2.20
M3	1	-	1.95	1	-	2.20
p4	2	1.13	1.05-1.20	2	1.18	1.05-1.30
m1	2	2.00	1.90-2.10	2	1.60	1.55-1.65
m2	4	2.31	2.10-2.30	4	1.98	1.80-2.15
m3	3	2.50	2.30-2.60	3	2.08	2.00-2.15
			Yangwa			
m2	1	-	2.40	1	-	2.25
			QA-I section			
m3	1	-	2.40	1	-	2.00
			Tongxin			
M1/2	1	-	2.10	2	2.20	2.10-2.30
m1/2	4	2.16	2.10-2.25	4	1.76	1.70-1.88

vestigial mesolophid; lower molars lacking mesolophid, but having a broad metalophid-protoconid connection and an indistinct constriction of the posterolophid at the triangular wear surface of the hypoconid.

Description — GV 87008 from Shinanu is a relatively well-preserved mandibular fragment with p4-m3 (Fig. 3D-F). The horizontal ramus of this specimen is thick, with a slightly concave lower border below the molars and a vertically concave medial surface. The height of the ramus beneath the m1 is 3.7 mm. The mandible diastema as preserved is longer than 4.5 mm, and would be shorter than the length of the cheek tooth row (7.6 mm). The lower masseteric ridge is rather prominent, particularly below m1-m2, and horizontally extends from beneath the anterior of m3 to below posterior of p4. An upper masseteric ridge is absent.

The DP3 is single rooted with a buccally located main cusp extending posterolingually as a loph, anterocone and a posterior cingulum are separated from the loph by a valley (Fig. 3G). The DP4 is subrectangular in occlusal outline (Fig. 3H). The apex of the protocone is located more buccally than the hypocone. The anteroloph is oblique, showing a thickening at the buccal portion. The protoloph is transverse and slightly constricted lingually. The metaloph is curved posteriorly to meet the hypocone. The posteroloph is slightly curved anteriorly. The straight paraflexus is longer, wider and slightly deeper than the metaflexus. The mesoflexus is prominent, bending posterolingually and extending lingually beyond the midline of the tooth. The hypoflexus, the deepest flexus on the tooth, is much smaller than the mesoflexus. There are three roots. The P4 is oval-shaped, with larger protocone than paracone (Fig. 3I). The protoloph and metaloph are both nearly transversely oriented, and connected by a short and thick medial crest. An anteroloph is lacking. The metaloph joins the base of the paracone to enclose the mesoflexus. The hypoflexus is located posterolingually. The tooth is single rooted, but with a groove on the anterior side. The M1/2 is subquadrate in occlusal outline with convex anterior margin, higher protocone and hypocone than the paracone and metacone (Fig. 3A, J-M). The protocone is strong, with its apex located slightly more lingually than that of hypocone. The protoloph is straight, its posterior rim confluent with the buccal margin of the oblique endoloph. The metaloph is connected to the hypocone or to the posteroloph (about halfway along it). The posteroloph is slightly curved in a little-worn specimen, and straight in the other worn specimens. In early stages of wear, the paraflexus and the metaflexus are similar in length, width and depth, but the paraflexus is more affected by wear than the metafexus, with more rapid shortening and obliteration than the metaflexus; in heavily worn specimens, the paraflexus and metaflexus are obliterated, and the protoloph and metaloph are fused with anteroloph and posteroloph, respectively; in late stages of wear, two fused lophs are present on the tooth, with the anterior wider than the posterior. The mesoflexus is larger and deeper than the paraflexus and metaflexus, and extends beyond the mid-line of the tooth, with its internal termination flexing posteriorly. The hypoflexus is the deepest, but does not reach the midline of the tooth, with its external termination flexing anteriorly. The four-rooted M1 and M2 are similar in morphology. Of these, smaller specimens are probably M1's and have lower crowns, with metaloph meeting posteroloph at a right angle and early disappearance of the paraflexus and metaflexus. The M3 is similar in morphology of the occlusal surface and in depth of flexi, but it has a relatively distinctly wider and smoother convex anterior margin than posterior margin (Fig. 3N, O). In addition, the metaloph always meets with the hypocone directly rather than halfway as in some M1/2, and the termination of hypoflexus and mesoflexus is less flexed. M3 has three roots.

The dp4 is low crowned and elongated in occlusal outline, with a conical and isolated anteroconid positioned on the mid-line of the tooth (Fig. 3P, Q). The protoconid is usually located slightly anterior to the metaconid. The anterior side of the metalophid is concave. A vestigial mesolophid is present in one of 6 specimens (Fig. 3P) and a small mesostylid is present in another. The strong hypolophid is slightly oblique or approximately transverse, joins a narrow ectolophid, and is opposite to the hypoflexid. The posterolophid is curved and rather prominent, but its connection with the hypoconid is slightly constricted. The mesoflexid is wider, but narrower than the metaflexid that extends to the tooth midline or beyond. The hypoflexid is the largest flexid of the tooth; it is deeper and wider than the mesoflexid, and extends to the midline of the tooth. The posterobuccal cingulid is weakly developed. The p4 is subquadrate (Fig. 3R). The protoconid and metaconid are distinct, but the entoconid, the anterior groove and the mesoflexid are variable in development. The metalophid connects at right angles to the posterior side of protoconid. A weak posterobuccal cingulid is present in all 3 specimens. The premolar is single rooted. The m1/2 is

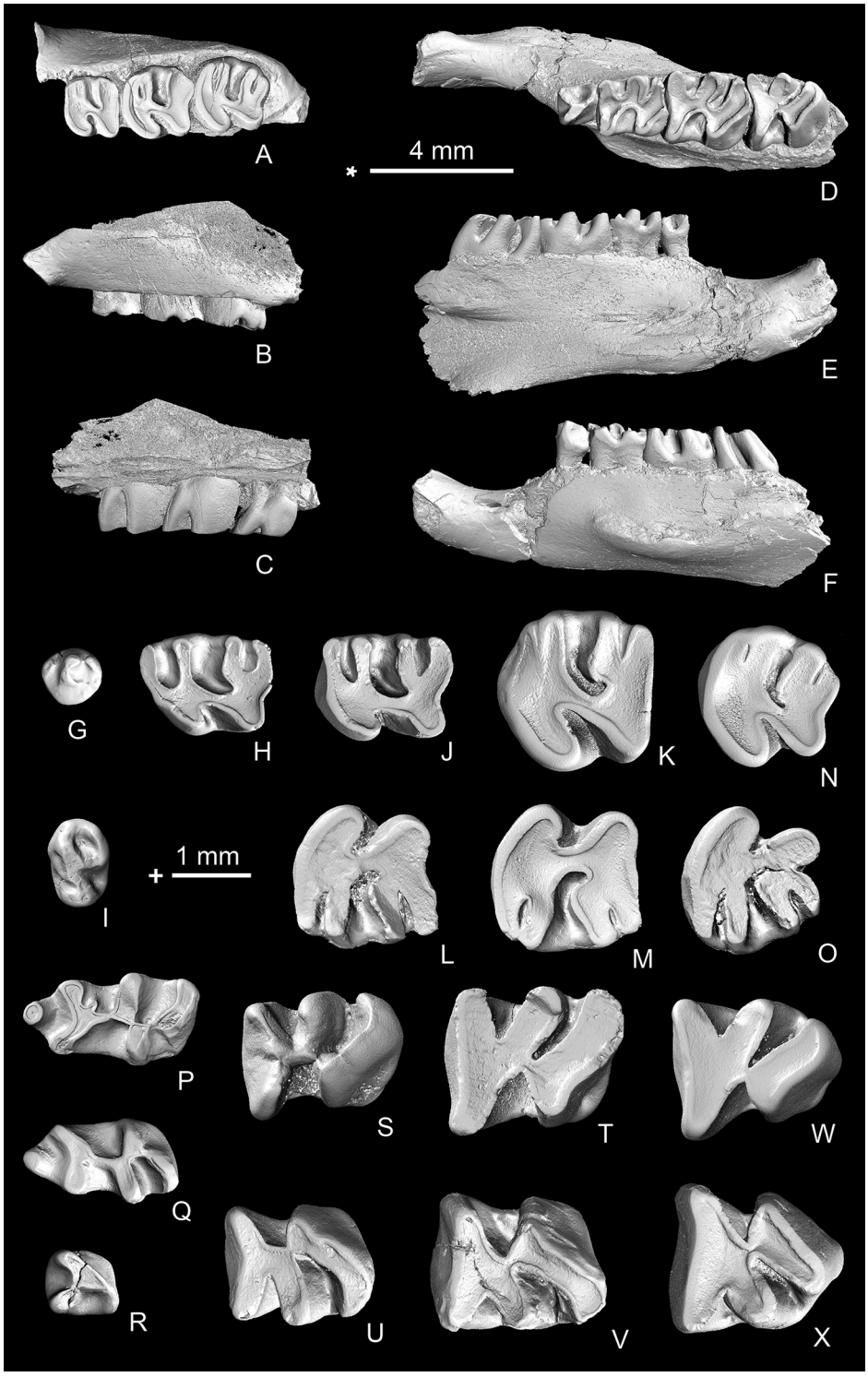

FIGURE 3. Jaw fragments and molars of *Sayimys linxiacus* from Gansu and Ningxia. A-C. right maxillary fragment with M1-3 (GV87012, reversed), D-F. right mandibular fragment with p4-m3 (GV87008, reversed), G. left DP3 (IVPP V 32331.1), H. left DP4 (IVPP V 32331.2), I. right P4 (IVPP V 32331.3, reversed), J. left M1/2 (IVPP V 32331.4), K. left M1/2 (IVPP V 32331.5), L. right M1/2 (IVPP V 32331.6), M. right M1/2 (holotype, IVPP V 32330), N. left M3 (IVPP V 32331.7), O. right M3 (IVPP V 32331.8), P. left dp4 (IVPP V 32331.9), Q. right dp4 (IVPP V 32331.10), R. right p4 (IVPP V 32331.11), S. left m1/2 (IVPP V 32331.12), T. left m1/2 (IVPP V 32331.13), U. right m1/2 (IVPP V 32331.14), V. right m1/2 (IVPP V 8864.1), W. left m3 (IVPP V 32331.15), X. right m3 (IVPP V 27371); A, D, G-X. occlusal view, B, F. buccal view, C, E. lingual view; scale: * = scale for A-F, + = scale for G-X.

subrectangular in occlusal outline, with anterior margin slightly concave or flat (Fig. 3S-V). The metalophid is broad at the protoconid-side and tapers lingually. The hypolophid is strong, and runs anterobuccal-posterolingually to connect the weakly developed ectolophid. The posterolophid is slightly curved at the early stage of wear. The posterolophid-hypoconid connections are wide. The mesoflexid is narrower but deeper than the metaflexid. The metaflexid reaches or extends slightly beyond the mid-line of the tooth. The hypoflexid is wider and deeper than the mesoflexid and metaflexid, and reaches the midline of the tooth. The posterobuccal cingulid is weakly developed. The m1 and m2 are similar in morphology, m1 smaller in size with lower crowns and the hypolophid being relatively transversely oriented and opposite the hypoflexid. In the possible m2 specimens, size is larger, crown is higher, and the hypolophid is distinctly oblique and partially aligned with the posterior arm of the protoconid. The m3 has a similar anterior margin as in m1/2, but the posterior margin is distinctly narrower (Fig. 3W, X). The hypolophid is oblique and completely confluent with the posterior arm of the protoconid. The mesoflexid is wider and deeper than the metaflexid, with the latter extending beyond the midline of the tooth. The hypoflexid is wider and deeper than the mesoflexid and metaflexid. The terminations of the hypoflexid and metaflexid are opposite each other. The posterobuccal cingulid is weak or absent.

Comparison and discussion — *Sayimys linxiacus* is a medium-sized species of the genus. It is smaller than *S. obliquidens*, *S. mallos*, *S. perplexus* and *S. giganteus*, roughly similar in size to *S. chinjiensis*, *S. intemedius*, *S. hintoni*, *S. sihongensis*, *S. fuhaiensis* and *S. minor*, but larger than *S. assarrensis*, *S. negenvensis* and *S. flynni*. Fig. 4 shows ranges of the dp4 and m3 length of some species of *Sayimys* based on data from literature.

Sayimys linxiacus differs from the early Miocene *Sayimys flynni* in the absence of anteroloph on P4 and mesolophid on lower molars, the presence of a broad metalophid-protoconid connection on lower molars, and in the greater height of the metaconid and entoconid above the enamel at their bases. *Sayimys obliquidens* and *S. giganteus* have a distinct mesolophid on the dp4 and a mesolophid on lower molars. In *S. obliquidens* a long mesolophid is present on m2 (Bohlin, 1946), and in *S. giganteus* a pronounced mesolophid is present on most dp4 (Hartman et al., 2019). In addition, the paraflexii and metaflexii on the upper molars of *S. linxiacus* are less developed than those in *S. obliquidens* and *S. giganteus*.

Sayimys linxiacus is slightly smaller than *S. fuhaiensis*, and differs from it in P4 having protocone connecting with paracone and lacking anteroloph, dp4 having a conical and isolated anteroconid and an infrequent vestigial mesolophid.

Sayimys linxiacus is similar to *S. intermedius* in its metaloph joining the protoloph on P4, in possessing relatively distinct paraflexus and metaflexus on upper molars, having a conical anteroconid on dp4, lacking mesolophid on lower molars; it differs from the latter in the absence of an anteroloph on P4, having an isolated anteroconid and vestigial mesolophid on dp4 occasionally, in the mesoflexid distinctly shorter but deeper than the metaflexid on lower molars, and in m1/2 lacking constriction of the posterolophid just before reaching the triangular wear surface of the hypoconid.

Sayimys linxiacus is slightly smaller than *S. sivalensis*/*chinjiensis* in size, and differs in dp4 lacking an anterolophulid in medial position and a confluent, long diagonal lophid formed by the protoconid, ectolophid, hypolophid and entoconid; upper molars have a more developed paraflexus and metaflexus, while lower molars have less oblique hypolophid.

Sayimys perplexus (= *badauni*) from the late Miocene of India is large-sized and similar to *S. sivalensis*/*chinjiensis*. Its P4 differs from *S. obliquidens* in having the paracone fused to the protocone, and the upper molars lacking the paraflexus and metaflexus.

Sayimys linxiacus is similar to *Sayimys minor*/*baskini* in size and in the absence of mesolophid on lower molars, but differs from them in lacking a well-developed or distinct mesolophid on the dp4. It is also close to *S. hintoni* in size, but the latter has an ovoid and elongate anteroconid on dp4, a prominent anteroloph on P4, a long and confluent diagonal lophid formed by protoconid, ectolophid, hypolophid and entoconid on the dp4 and lower molars.

Sayimys assarrarensis and *S. linxiacus* both have P4 with a metaloph joining the paracone, but *S. assarrarensis* is smaller and has a developed mesolophid on dp4 and an anteroloph on P4.

Sayimys linxiacus differs from *S. mallos* in its distinctly smaller size, the absence of an anteroloph on P4, in the presence of an isolated anteroconid and only rudimentary mesolophid on dp4, and in lack of mesolophid, but having

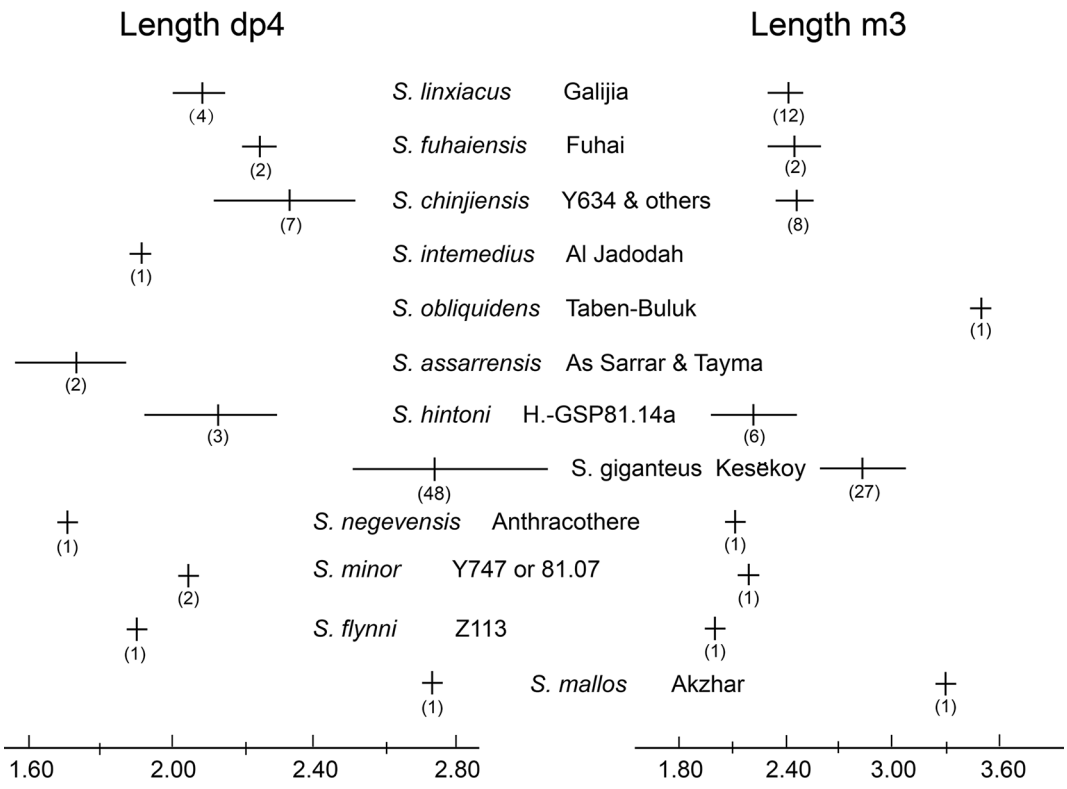

FIGURE 4. Ranges of the length of the dp4 and m3 for type specimens of some *Sayimys* based on published data.

narrower mesoflexid than metaflexid on m1/2.

While samples of *Sayimys negevensis* and *S. sihongensis* are limited, the new species differs from the former in the absence of a mesolophid on lower molars, and the m3 being less reduced posteriorly, and from the latter in having narrower mesoflexus and hypoflexus on upper molars, less persistent paraflexus and metaflexus on M1/2, less distinct mesolophid on dp4, and no vestigial mesolophid, less vertical striids on m1/2.

Sayimys linxiacus is mainly known from two localities, Galijia and Shinanu of the Linxia Basin, in Gansu. The Galijia Fauna and the Shinanu Fauna are roughly contemporaneous, and the two assemblages of *Sayimys* show similar dental morphology (Qiu et al., 2023). The collections, including isolated teeth of all tooth positions and fragments of jaws, and consisting of at least 9 individuals represent one of the larger samples of *Sayimys* known from China.

A single Xijiang m2 from the middle Miocene Dingshanyanchi Formation in Junggar Basin, represents an indeterminate species of *Sayimys* (Wu et al., 2009). The m2 shows similarities with *S. linxiacus* in lack of a mesolophid, mesoflexid shorter and deeper than the metaflexid, wide metalophid-protoconid connection and unconstricted posterolophid-hypoconid connection, and the oblique hypolophid partially aligned with the posterior arm of the protoconid. Nevertheless, it is larger than the corresponding tooth of *S. linxiacus*.

Evolutionary trends within *Sayimys* remain uncertain due to inadequate material from most fossil sites. In general, the evolution of the genus may include a tendency toward an increase in size and crown height, loss of mesolophid in dp4 and lower molars, appearance of anterolophulid in dp4, and simplified molars (reduced paraflexus and metafexus in uppers, development of a prominent diagonal ridge by the confluence of protoconid, ectolophid, hypolophid and entoconid in lower molars as well as in dp4) (de Bruijn et al., 1989; Hartman et al., 2019). The medium-sized teeth of *S. linxiacus* with moderately distinct paraflexus and metaflexus on upper molars, an isolated anteroconid and a rare vestigial mesolophid on dp4, and a prominent confluently diagonal ridge but no mesolophid on lower molars may represent intermediate evolutionary characters of *Sayimys*. This seems to suggest that *S. linxiacus* is more derived than earliest Miocene *S. flynni* or later *S. obliquidens*, *S. giganteus*, *S. minor*/*baskini*, *S. assarrarens* and *S. negevensis*, which have a distinct

mesolophid on dp4 or lower molars or both, but more primitive than middle to late Miocene *S. sivalensis*/*chinjiensis*, and *S. perplexus*, which have an anterolophulid on dp4, a prominent confluently ridge on dp4 and lower molars, and poorly developed or absent paraflexus and metaflexus on upper molars. *Sayimys linxiacus* seems closer to *S. intermedius* in evolutionary grade.

Sayimys mallos (Shevyreva, 1994)

(Fig. 5)

Akzharomys mallos: Shevyreva, 1994, p. 127

Asiazapus ingens: Lopatin and Zazahigin, 2000, p. 452

Material — IVPP V 27370.1-14, 14 isolated cheek teeth and fragments of cheek teeth (1 P4, 1 damaged M1/2, 1 damaged M3, 4 dp4, 1 p4, 1 m1, 2 fragments of dp4, 3 fragments of molars).

Locality and Horizon — Nan-Gan-Qu (South Main Irrigation Canal, Loc. XJ 200114), Fuhai County, Xinjiang Uygur Autonomous Region; the Suosuoquan Formation (late Early Miocene, Shanwangian LMS/A).

Measurements (length × width) — P4 = 1.00 × 1.45; M1/2 = 2.60 × 2.90; M3 = 2.90 × 2.50; dp4 = 2.70 × 1.60, 2.50 × 1.40, 2.60 × 1.40, 2.20 × 1.30; p4 = 1.70 × 1.90; m1/2 = 2.80 × 2.00.

Revised Diagnosis — Large species of *Sayimys*. P4 with anteroloph connecting to the protoloph, and metaloph with both labial and lingual branch connected to the protoloph by a thick longitudinal ridge. Upper molars with developed paraflexus and metaflexus, wider paraflexus than metaflexus, and wider mesoflexus than hypoflexus. dp4 with the anteroconid isolated or low on the lingual side of the metaconid, pronounced mesolophid, almost transverse hypolophid nearly opposite the hypoflexid, posterolophid constricted just before reaching the triangular hypoconid. Y-shaped p4 with posterolophid shorter than metalophid, without posterior spur. Rectangular m1/2 with developed mesolophid, equal extension of mesoflexid and metaflexid in width, narrow and perpendicular mesostriad and metastriad. Lower cheek teeth with marked posterobuccal cingulid.

Description — The P4 is oval-shaped, with a prominent protocone, a high paracone and a small hypocone (Fig. 5A). The anteroloph is complete and rapidly descends from the protocone to the base of paracone. The protoloph is curved and the long metaloph is nearly transversely oriented, descending from the hypocone to the base of paracone, both connected by a short medial crest. A hypocone spur is weakly developed. The hypoflexus is narrow and shallow. The M1/2, though damaged, show distinct unilateral hypsodonty; they narrow posteriorly, have a wider paraflexus than metaflexus, and mesoflexus extends beyond the midline of the tooth (Fig. 5B-D). Damaged M3 (Fig. 5E-G) has a narrow and concave posterior margin. In early wear, it shows a distinct metaflexus.

The dp4 has an ovoid and isolated anteroconid that contacts the metaconid lingually when heavily worn (Fig. 5H-K). The metalophid is straight or slightly curved. The developed mesolophid extends to the margin of the tooth or connects with the metaconid. The hypolophid is short, strong, and nearly opposite the hypoflexid. The posterolophid is prominent, being distinctly constricted just before reaching the hypoconid. The metaflexid extends beyond the midline of the tooth. The posterobuccal cingulum is developed in one specimen. The large p4 has Y-shaped occlusal surface (Fig. 5L-N). The protoconid, metaconid and entoconid are distinct and confluent. The mesoflexid and the posterobuccal cingulid are developed. The m1/2 is subrectangular in occlusal outline with anterior margin slightly concave (Fig. 5O-Q). The mesolophid is well developed and nearly perpendicular to the ectolophid. The hypolophid is short and strong, almost parallel to the mesolophid and opposite the hypoflexid. The posterolophid is marked and constricted before reaching the hypoconid. The mesoflexid is narrower but deeper than the metaflexid. The hypoflexid is wider and deeper than the mesoflexid and metaflexid, and reaches the mid-line of the tooth. The posterobuccal cingulid is developed.

Comparison and discussion — Based on a handful of isolated molars from the early Miocene Akzhar Formation of Zaisan Basin in Kazakhstan, Shevyreva (1994) assigned a ctenodactylid rodent to *Akzharomys mallos*. The taxon shows relatively quadrate outline of the occlusal surface, unilateral hypsodonty and subequal size of protocone(id) and hypocone(id) of molars, anteriorly directed hypoflexus of upper molars and posteriorly directed hypoflexid of lower molars, and well developed paraflexus and metaflexus in upper molars and mesoflexid and metaflexid in lower molars, which correspond to the diagnosis of *Sayimys* later emended by Baskin (1996). *Akzharomys* is here considered a synonym of *Sayimys*.

The described specimens from Fuhai in Junggar Basin are comparable to those of *Sayimys mallos* from Zaisan both in size and morphology. Zaisan Basin is close to the Junggar Basin geographically. Undoubtedly, these materials belong to

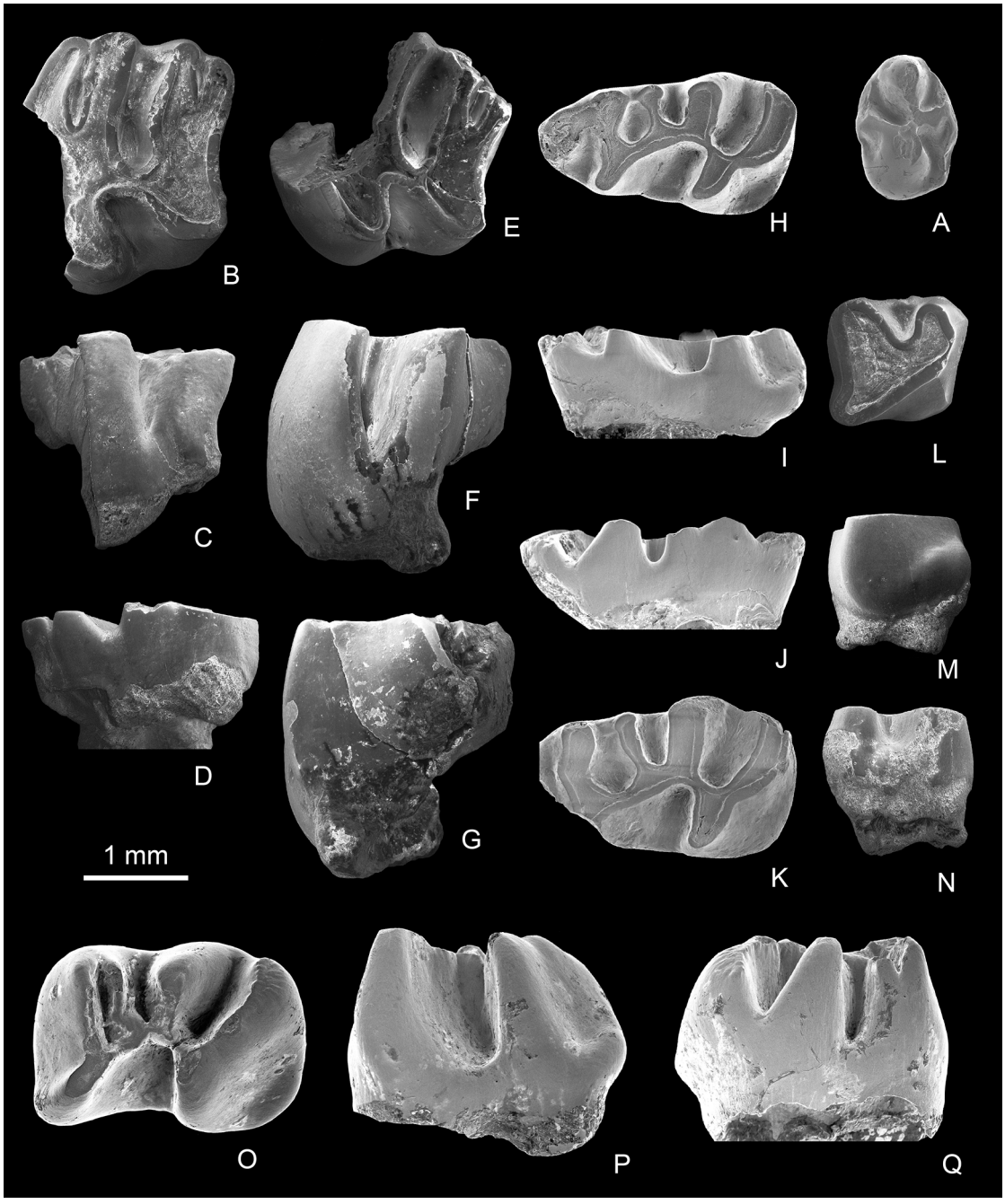

FIGURE 5. cheek teeth of *Sayimys mallos* from Xinjiang. left P4 (IVPP V 27370.1), B-D. right M1/2 (IVPP V 27370.2, reversed), E-G. left M3 (IVPP V 27370.3), H-J. left dp4 (IVPP V 27370.8), K. left dp4 (IVPP V 27370.6), L-N. left p4 (IVPP V 27370.12), O-Q. left m1/2 (IVPP V 27370.13); A, B, E, H, K, L, O. occlusal view, C, F, J, N, Q. lingual view, D, G, I, M, P. buccal view.

the same species of *Sayimys* and the premolars and lower deciduous teeth described here provide more morphological information for this species.

In addition, Lopatin and Zazhigin (2000) identified a tooth as m1 of their new zapodid (*Asiazapus ingens*) from the lower Miocene Akzhar Formationa of Eastern Kazakhstan-Batpaksunde Basin, the same basin and horizon where Shevyreva (1994) identified *Akzharomys mallos* (= *Sayimys mallos*). The "m1" was revised as a dp4 of *Sayimys* by López-Antoñanzas and Sen in 2004, and referred to *S. obliquidens* by López-Antoñanzas and Knoll in 2011. In fact, the dp4 described by Lopatin and Zazhigin (2000) falls

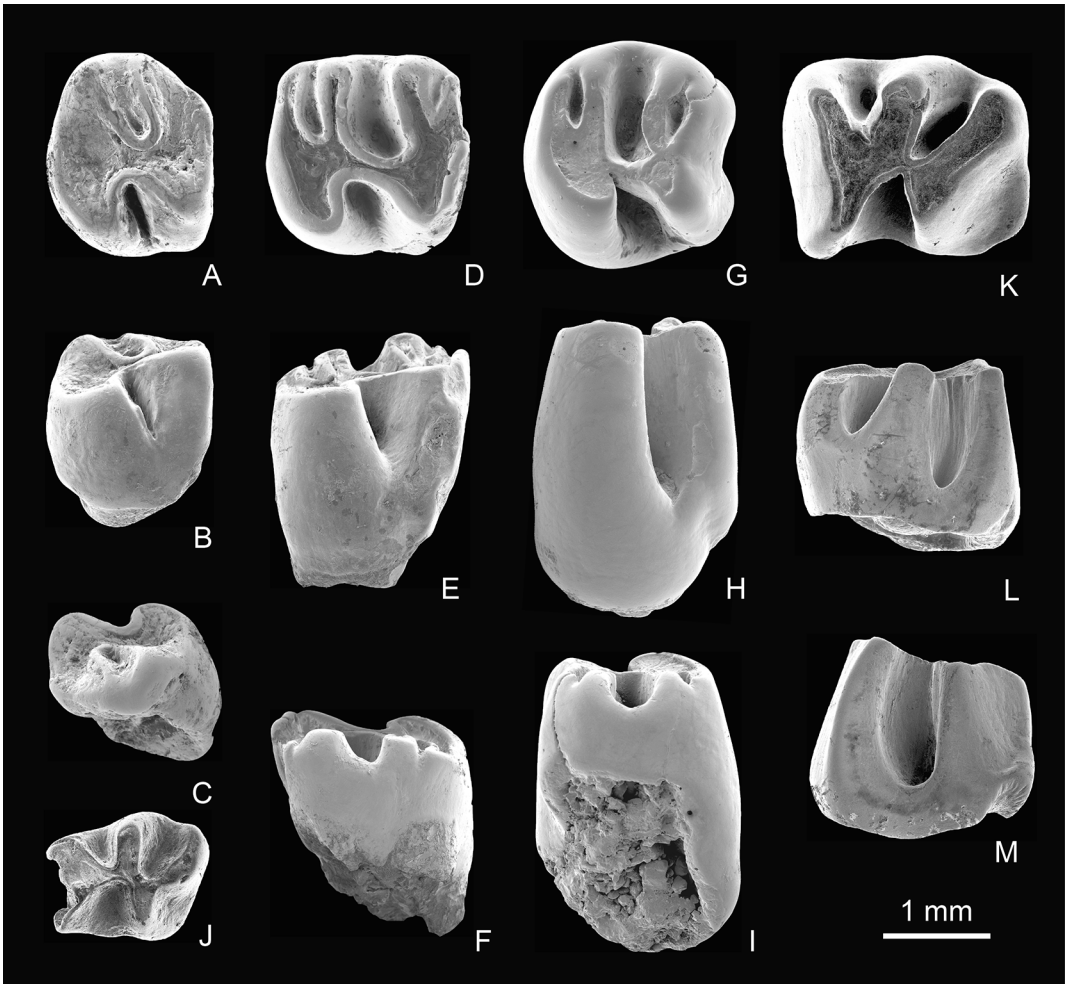

FIGURE 6. cheek teeth of *Sayimys sihongensis* from Jiangsu. A-C. right DP4 (IVPP V 23216, paratype, reversed), D-F. left M1 (V 23215, holotype), G-I. right M3 (V 23217, reversed), J. left dp4 (IVPP V 27373), K-M. l m1/2 (IVPP V 27372); A, D, G, J, K. occlusal view, B, E, H, L. lingual view, C, F, I, M. buccal view

within the range exhibited by the dp4 from Loc. XJ 200114 both as to size and pattern (dp4 of *S. obliquidens* should be smaller with higher crown). Thus, we treated this tooth as a dp4 of *S. mallos*.

Sayimys mallos can only match in size *S. giganteus* and is much larger than any other *Sayimys*. The pronounced mesolophid on lower cheek teeth seems to imply that *S. mallos* and *S. obliquidens* were closely allied.

Sayimys sihongensis Qiu, 2017

(Fig. 6)

Holotype — Left M1 (IVPP V 23215, from Zhengji, Sihong, Jiangsu Province).

New Material — IVPP V 27373, 1 damaged dp4 (from Zhengji), and IVPP V 27372, 1 m1/2 (Songlinzhuang).

Locality and Horizon — Zhengji and Songlinzhuang, Sihong County, Jiangsu Province; the Xiacaowan Formition (late Early Miocene, Shanwangian LMS/A).

Measurements (length × width) — dp4 => 1.60 × 1.30; m1/2 = 2.40 × 2.00.

Emended Diagnosis — Medium-sized species of *Sayimys*. DP4 with paraflexus and metaflexus quickly obliterated by occlusal wear, protoloph and metaloph longer than the anteroloph and posteroloph; M1 with slightly larger hypocone than protocone, relatively transverse and straight protoloph and metaloph, more persistent paraflexus and metaflexus, longer paraflexus than metaflexus; M3 with short paraflexus and metaflexus, wide and transverse mesoflexus. dp4 with mesolophid extending to metaconid, hypolophid opposite to

the posterior portion of hypoflexid, less transversely oriented posterolophid distinctly constricted before reaching hypoconid; m1/2 with narrow flexids and vertical striids, reduced mesolophid, and unconstricted posterolophid-hypoconid connection.

Description — The damaged dp4 (Fig. 6J) has a distinct mesolophid extending to the metaconid. The metaflexid and hypoflexid extend to the midline of the tooth. The m1/2 is subrectangular in occlusal outline with slightly concave front wall (Fig. 6K-M). The mesolophid is vestigial; the hypolophid extends slightly anterobuccal-posterolingually, almost in line with the triangular protoconid; the posterolophid is developed without a constricted posterolophid-hypoconid connection. The mesoflexid, metaflexid and hypoflexid are rather narrow and show an acute angle of termination; the metaflexid is opposite hypoflexid; the striids are vertical to the chewing surface of the tooth; there is a distinct posterobuccal cingulid on m1/2.

Remarks — *Sayimys sihongensis* was based on only three upper cheek teeth (Fig. 6A-I) from Zhengji and Songlinzhuang, Sihong, Jiangsu Province (Qiu, 2017). Songlinzhuang is less than 2 kms from the type locality Zhengji. The fossiliferous concentration of the two sites seems to be the same age. The described dp4 was collected from the same site as the type specimens from Zhengji and the m1/2 came from nearby Songlinzhuang (Li et al., 1983). The teeth added here match the type specimens in size, are treated as belonging to the same taxon, and broaden our knowledge of *S. sihongensis*.

Sayimys sihongensis is a relatively small species of the genus, characterized mainly by its moderate unilateral hypsodonty with relatively vertical tooth columns, the presence of narrow flexus(id)s and vertical stria(id)s on molars, upper molars with subquadrate occlusal surface and rather distinct paraflexus and metaflexus, marked mesolophid on dp4, vestigial mesolophid on m1/2, dp4 having posterolophid distinctly constricted

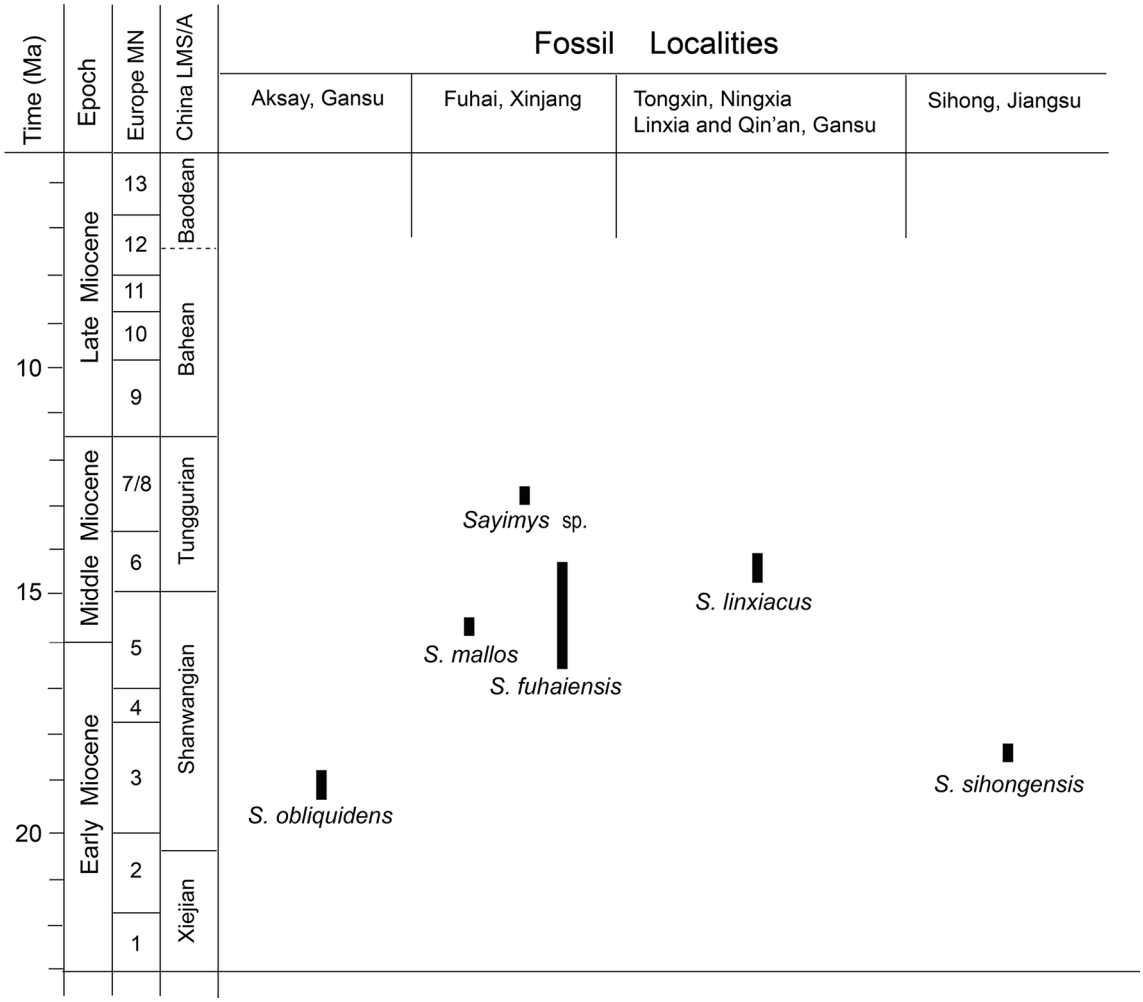

FIGURE 7. Age ranges and geographic distribution of *Sayimys* from China

before reaching hypoconid, m1/2 with unconstricted posterolophid-hypoconid connection. The species represents the most eastern occurrence of the genus.

DISCUSSION AND CONCLUSION

The early to mididle Miocene *Sayimys* from China includes 5 named species and one indeterminate species. Fig. 7 shows their occurrences and age ranges as presently understood.

Sayimys obliquidens has been known for almost 80 years. The original collection was well-studied (Bohlin, 1946; Baskin, 1996; López-Antoñanzas and Sen in 2004; Hartman et al., 2019), but its provenance has never been well-documented. *Sayimys*, subsequently found at several localities across China of different late early to middle Miocene ages, embraces more than one species in both morphology and size. There is enough material to distinguish five species in the Miocene of China, two of them newly described here. We hypothesize polarity in some variant features, consistent with the view that the species are not equivalent in age. *Sayimys obliquidens* is not a derived species and is reasonably considered of late early Miocene age. Given that the genus is well-represented in Pakistan and India, from earliest Miocene to late Miocene, the center of *Sayimys* evolution appears to be South Asia. Flynn and Wessels (2013) proposed a dispersalist scenario to explain the broad observed distribution of species of the genus. They noted in Pakistan that the earliest Miocene *Sayimys*, *S. flynni*, was followed by the late early Miocene *S.* cf. *intermedius,* and proposed that the genus dispersed westward to the Mediterranean area in the late early Miocene. *Sayimys intermedius* was first described from Saudi Arabia. The Chinese fossil record permitted a second phase of dispersal, eastward from the Mediterranean area and across Central Asia to account for the occurrence of *S. obliquidens* in China. Dispersal westward and then eastward in the early Miocene explained the far-flung distribution of the genus. This scenario is still viable although the fossil record as understood has become more complex.

For a time in the late early and middle Miocene, the modern ctenodactylid Subfamily Ctenodactylinae as represented by *Sayimys*, was widespread in China where it diversified at the species level. It is with improving knowledge of the chronology of fossil occurrences that the biogeographic history of such groups becomes known on a continental scale.

ACKNOWLEDGMENTS

We greatly appreciate the efforts by numerous members of the Xinjiang field team, of the colleagues from Bureau of Geology, Ningxia Hui Autonomous Region, who painstakingly accumulated the Xinjiang and Ningxia materials described in this paper. We thank the following individuals for their hard work in Gansu in amassing the collections under study: W.Q. Feng and C. Suo from the IVPP, S.Q. Chen and J.L. Li from Hezheng Paleozoological Museum (Gansu Province), Z.X. Cao and J. Cheng from CUGB. Many thanks are also due to J. Meng from the American Museum of Natural History (New York) and H.W. Si from IVPP for help with some photoshop manipulations of images. We wish to express our gratitude to Prof. B.Y. Wang who allowed us to study the material she collected from Galijia, Linxia. For financial support we thank the Chinese National Natural Science Foundation (40872032), National Basic Research Program of China (973 Program), and the Key project of Frontier Science Research of the Chinese Academy of Sciences (No. QYZDY-SSW-DQC002). We appreciate the attention to details by reviewers and an editor. Reviewers Jon Baskin and Yukimitsu Tomida offered perceptive and helpful suggestions and we appreciate the efforts of the editor.

LITERATURE CITED

Baskin, J. A. (1996). Systematic revision of Ctenodactylidae (Mammalia, Rodentia) from the Miocene of Pakistan. *Palaeovertebrata*, 25, 1–49.

Black, C. C. (1972). Review of fossil rodents from the Neogene Siwalik Beds of India and Pakistan. *Palaeontology*, 15, 238–266.

Bohlin, B. (1946). The fossil mammals from the Tertiary deposit of Taben-Buluk, western Kansu. Part 2: Simplicidentata, Carnivora, Artiodactyla, Perissodactyla, and Primates. *Palaeontologia Sinica New Ser C*, 8B, 1–259.

Cao, Z. X., Du, H. J., Zhao, Q. Q., & Cheng, J. (1990). Discovery of the Middle Miocene fossil mammals in Guanghe district, Gansu and their stratigraphic significance. *Geoscience*, 4(2), 16–29.

de Bruijn, H. (1999). Superfamily Ctenodactyloidea. In G. E. Rössner & K. Heissig (Eds.), *The Miocene Land Mammals of Europe* (pp. 263–266). München: Verlag Dr. Friedrich Pfeil Press.

de Bruijn, H., Boon, E., & Hussain, S. T. (1989). Evolutionary trends in *Sayimys* (Ctenodactylidae, Rodentia) from the Lower Manchar Formation (Sind, Pakistan). *Proceedings of the Koninklijke Nederlandse Akademie van Wetenschappen*, B92(3), 191–214.

de Bruijn, H., Hussain, S. T., & Leinders, J. J. M. (1981). Fossil rodents from the Murree Formation near Banda Daud Shah, Kohat, Pakistan. *Proceedings of the Koninklijke Nederlandse Akademie van Wetenschappen*, B84(1), 71–99.

Flynn, L. J. & Jacobs, L. L. (1990). Preliminary analysis of Miocene

small mammals from Pasalar, Turkey. *Journal of Human Evolution*, 19, 423–436.

Flynn, L. J. & Wessels, W. (2013). "Paleobiogeography and South Asian small mammals: Neogene latitudinal faunal variation." In X. Wang, L. J. Flynn, & M. Forteius (Eds.), *Fossil Mammals of Asia: Neogene Biostratigraphy and Chronology* (pp. 445-460). Columbia University Press, New York.

Guo, Z. T., Ruddiman, W. F., Hao, Q. Z., Wu, H. B., Qiao, Y. S., Zhu, R. X., Peng, S. Z., Wei, J. J., Yuan, B. Y., & Liu, T. S. (2002). Onset of Asian desertification by 22 Myr ago inferred from loess deposits in China. *Nature*, 416, 159–163.

Hartman, J., van de Weerd, A. A., de Bruijn, H., & Wessels, W. (2019). An exceptional large sample of the early Miocene ctenodactyline rodent *Sayimys giganteus*, specific variation and taxonomic implications. *Fossil Imprint*, 75(3-4), 359–382.

Hinton, M. (1933). Diagnosis of new genera and species of rodents from Indian Tertiary deposits. *Annals and Magazine of Natural History*, 72, 620–622.

Jaeger, J. J. (1971). Un cténodactylidé (Mammalia, Rodentia) nouveau, *Irhoudia bohlini* n. g., n. sp., du Pléistocène inférieur du Maroc. Rapports avec les formes actuelles et fossiles. *Notes du Service géologique, Maroc*, 31, 113–140.

Jaeger, J. J. (1977). Les rongeurs du Miocène moyen et supérieur du Maghreb. *Palaeovertebrata*, Montpellier, 8, 1–166.

Kordikova, E. G. & de Bruijn, H. (2001). Early Miocene rodents from the Aktau Mountains (South-Eastern Kazakhstan). *Senckenbergiana lethaea*, 81, 391–405.

Li, C. K., Lin, Y. P., Gu, Y. M., Hou, L. H., Wu, W. Y., & Qiu, Z. D. (1983). The Aragonian vertebrate fauna of Xiacaowan, Jiangsu. *Vertebrata PalAsiatica*, 21(4), 313–327.

Lopatin, A. V. & Zazhigin, V. S. (2000). The history of the Dipodoidea (Rodentia, Mammalia) in the Miocene of Asia: 2. Zapodidae. *Paleontological Journal*, 34(4), 449–454.

López-Antoñanzas, R. & Knoll, F. (2011). A comprehensive phylogeny of gundis (Ctenodactylinae, Ctenodactylidae, Rodentia). *Journal of Systematic Paleontology*, 9(3), 379–398.

López-Antoñanzas, R. & Sen, S. (2003). Systematic revision of Mio-Pliocene Ctenodactylidae (Mammalia, Rodentia) from the Indian subcontinent. *Ecl Geol Helv*, 96, 521–529.

López-Antoñanzas, R. & Sen, S. (2004). Ctenodactylids from the Lower and Middle Miocene of Saudi Arabia. *Palaeontology*, 47(6), 1477–1494.

López-Antoñanzas, R., Sen, S., & Saraç, G. (2004). A new large ctenodactylid species from the Lower Miocene of Turkey. *Journal of Vertebrate Paleontology*, 24(3), 676–688.

López-Antoñanzas, R., Sen, S., & Koufos, G. D. (2005). A ctenodactylid rodent (Mammalia: Rodentia) from the Middle Miocene of Chios Island (Greece). *Géobios*, 38, 113–126.

López-Antoñanzas, R., Knoll, F., Maksoud, S., & Azar, D. (2015). First Miocene rodent from Lebanon provides the missing link between Asian and African gundis (Rodentia: Ctenodactylidae). *Science Reports*, 5, 12871; doi: 10.1038/srep12871 PMID: 26250050.

López-Antoñanzas, R., Gutkin, V., Rabinovich, R., Calvo, R., & Grossman, A. (2016). A transitional gundi (Rodentia: Ctenodactylidae) from the Miocene of Israel. *PloS ONE*, 11(4), 1–16.

Munthe, J. (1980). Rodents of the Miocene Daud Khel Local Fauna, Mianwali District, Pakistan. Part 1. Sciuridae, Gliridae, Ctenodactylidae, and Rhyzomyidae. *Milwaukee Public Museum. Contributions in Biology and Geology*, 34, 1–36.

Qiu, Z. D. (2017). Several rarely recorded rodents from the Neogene of China. *Vertebrata PalAsiatica*, 55(2), 92–109.

Qiu, Z. X. & Qiu, Z. D. (1995). Chronological sequence and subdivision of Chinese Neogene mammalian faunas. *Palaeogeography Palaeoclimatology Palaeoecology*, 116, 41–70.

Qiu, Z. D., Wang, B. Y., & Li, L. (2023). Middle Cenozoic micromammals from Linxia Basin. Gansu Province, China, and their implications for biostratigraphy and palaeoecology. *Palaeogeography Palaeoclimatology Palaeoecology*. https://authors.elsevier.com/article/S0030182(23)00085-8.

Sen, S. & Thomas, H. (1979). Découvert de rongeurs dans le Miocène moyen de la Formation Holuf (Province du Hasa, Arabie Saoudite). *Comptes Rendus sommaires de la Societé géologique de France*, 1979(1), 34–37.

Shevyreva, N. S. (1994). A new ctenodactyloid (Rodentia, Mammalia) from the Neogene of the Zaysan Depression (Eastern Kazakhstan). *Paleontological Journal*, 28, 160–167.

Vasishat, R. N. (1985). Antecedents of early man in northwestern India: paleontological and paleoecological evidences. New Delhi: Inter-India Publications, 1–230.

Wang, B. Y. (1997). The Mid-Tertiary Ctenodactylidae (Rodentia, Mammalia) of eastern and central Asia. *Bulletin of the American Museum of Natural History*, 234, 1–88.

Wang, X., Tseng, Z. J., Wu, W. Y., Ye, J., Meng, J., & Bi, S. (2020). A new species of *Tunguractis* Colbert, 1939 (Carnivora, Hyaenidae) from the middle Miocene of Junggar Basin, northwestern China and the early divergence of basal hyaenids in East Asia. In L. de Bonis & L. Werdelin (Eds.), *Memorial to Stéphane Peigné: Carnivores (Hyaenodonta and Carnivora) of the Cenozoic* (pp. 29–45). *Geodiversitas*, 42(3). https://doi.org/10.5252/geodiversitas2020v42a3. http://geodiversitas.com/42/3

Wessels, W., De Bruijn, H., Hussain, S. T., & Leinders, J. J. M. (1982). Fossil rodents from the Chinji Formation, Banda Daud Shah, Kohat, Pakistan. *Proceedings of the Koninklijke Nederlandse Akademie van Wetenschappen* B, 85(3), 337–364.

Wessels, W., Fejfar, O., Peláez-Campomanes P., van der Meulen, A., & de Bruijn, H. (2003). Miocene small mammals from Jebel Zelten, Lybia. In N. López Martinez, P. Peláez-Campomanes, Hernández & M. Fernández (Eds.), *Entorno a Fósiles de Mamiferos: Datación, Evolución y Paleoaimbiente* (pp. 699–751). Coloquios de Paleontologia, Volumen Extraordinario, 1.

Wood, A. E. (1937). Fossil rodents from the Siwalik beds of India. *American Journal of Science*, 34, 64–76.

Wu, W. Y., Ye, J., Meng, J., Wang X. M., Liu, L. P., Bi, S. D., & Dong, W. (1998). Progress of the study of Tertiary biostratigraphy in North Junggar Basin. *Vertebrata PalAsiatica*, 36(1), 24–31.

Wu, W. Y., Meng, J., Ye, J., Ni X. J., Bi, S. D., & Wei, Y. P. (2009). The Miocene mammals from Dingshanyanchi Formation of North Junggar Basin, Xinjiang. *Vertebrata PalAsiatica*, 47(3), 208–233.

Wu, W. Y., Ye, J., & Zhu, B. C. (1991). On *Alloptox* (Lagomorpha, Ochotonidae) from the Middle Miocene of Tongxin , Ningxia Hui Autonomous Region, China. *Vertebrata PalAsiatica*, 29(3), 204–229

Ye, J., Wu, W. Y., & Meng, J. (2001a.) Tertiary stratigraphy in the Ulungur River Area of the northern Junggar Basin of Xinjiang. *Journal of Stratigraphy*, 25(3), 193–200.

Ye, J., Wu, W. Y., & Meng, J. (2001b). The age of Tertiary strata and mammal faunas in Ulungur River Area of Xinjiang. *Journal of Stratigraphy*, 25(4), 283–287.

WINDOWS INTO SAUROPSID AND SYNAPSID EVOLUTION
Essays in honor of Prof. Louis L. Jacobs, pp. 290–305, 2023

NEW RHIZOMYINE RODENT SPECIMENS FROM THE LATE PLIOCENE (UPPER SIWALIKS) OF INDIA: PHYLOGENETIC IMPLICATIONS

RAJEEV PATNAIK[1,*], LAWRENCE J. FLYNN[2], ROHIT KUMAR[1], BAHADUR SINGH[3,4], and KEWAL KRISHAN[3]

[1]Department of Geology, Panjab University, Chandigarh, 160 014, India, rajeevpatnaik@gmail.com
[2]Department of Human Evolutionary Biology, Harvard University, Cambridge, Massachusetts 02138, United States of America
[3]Department of Anthropology, Panjab University, Chandigarh 160014, India
[4]University School of Allied Health Sciences, Rayat-Bahra University, Kharar, Mohali, Punjab, India

ABSTRACT The ancestors of bamboo rats of south and south-east Asia and those of the root rats of Africa were quite common in the Middle and Late Miocene Siwalik deposits of India and Pakistan. However, their diversity dropped significantly in the Pliocene and Pleistocene. A derived late Pliocene form of the extinct rhizomyine genus *Rhizomyides* was recognized and named *Rhizomyoides saketiensis* based on two dentary fragments. This late rhizomyine has good provenance but appears to be a junior synonym of the species *Rhizomyides lydekkeri* from an unrecorded locality. We here report a partial skull (~ 2.6 Ma) and a palate (~ 3 Ma), plus a few molars of this species confirming the distinct nature of this species. Our phylogenetic analysis places *Rhizomyides lydekkeri* close to the Middle Siwalik *Rhizomyides sivalensis* and Afghan *Rhizomyides platytomeus* and *Rhizomyides carbonnelli,* implying late Neogene migration between Afghanistan and Indo-Pakistan. Micro-CT scanning allowed a better understanding of internal features, particularly assessing molar wear stages, without cutting the specimens. The skull features such as low skull profile, extremely elongated and gently curved snout, very long incisive foramina but strong incisors lead us to propose that *Rhizomyides lydekkeri* was most probably moderately fossorial.

KEYWORDS Upper Siwaliks, India, Rodents, Rhizomyinae, Phylogeny

INTRODUCTION

Professor Louis Jacobs' monograph on "Fossil rodents (Rhizomyidae and Muridae) from Neogene Siwalik deposits, Pakistan" published in 1978 has remained a benchmark contribution. This paper was one of the key motivations for one of us (RP) to undertake a Ph.D on the Siwalik muroid rodents. Professor Jacobs went on to publish many more interesting papers on these rodents (Jacobs et al., 1989;1990; Flynn and Jacobs, 1999) and remains active in this research (Kimura et al., 2013; 2017; 2021; Flynn et. al., 2020). As a tribute to his excellent contribution and keeping the legacy alive, an attempt has been made here to describe some new rhizomyine specimens from late Pliocene deposits exposed near Chandigarh, India. The paper also discusses phylogeny and paleobiogeography in the light of emerging hypotheses.

Today, the Bamboo Rat subfamily is confined to south, south-east Asia (tribe: Rhizomyini) and east Africa (tribe: Tachyoryctini) (Gogolevskaya et al., 2010), where they live a fully subterranean way of life. Living Asian bamboo rats include three species of *Rhizomys* and one species of *Cannomys*, while the African mole rats *Tachyoryctes*, comprise at least two extant species. Both the Asian *Rhizomys* (+ *Miorhizomys*) and the African *Tachyoryctes* have a long fossil record since they emerged in the Late Miocene, whereas there is no record of *Cannomys* fossils. Rhizomyines were widespread since the Late Oligocene. Over 30 fossil species belonging to 11 genera (*Prokanisamys, Kanisamys, Rhizomyides, Protachyoryctes, Tachyoryctes, Eicooryctes, Miorhizomys, Anepsirhizomys, Rhizomys* (*Brachyrhizomys*), *Pronakalimys* and *Nakalimys*) have been recorded from China, Thailand, India, Pakistan, Afghanistan and Africa (Black, 1972; Flynn, 1982, 1983; Vasishat, 1985; López-Antoñanzas et al., 2013, 2015).

Our rhizomyine specimens come from two rich Late Pliocene localities namely, Khetpurali and Kanthro (2.5 km

*Corresponding author

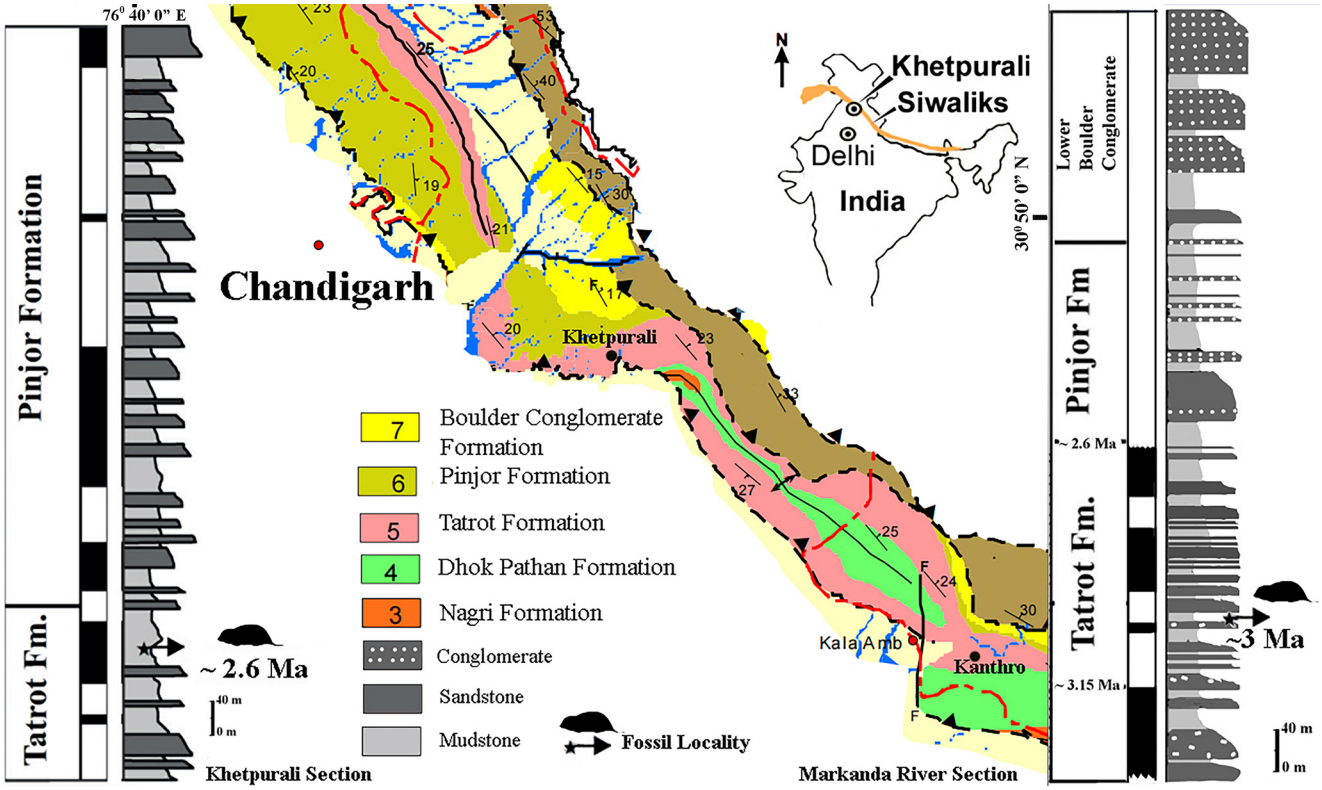

FIGURE 1. Geological map of the area (after Eliyas et al., 2017) showing the two fossil sites, palaeomagnetically dated section near Khetpurali (Tandon et al.,1984) and near Markanda River (Azzaroli and Napoleone, 1982).

north of Saketi) (Fig. 1). Both these sections have been tied to nearby paleomagnetic sections in stream-cut exposures (Tandon et al., 1984; Azzaroli and Napoleone, 1982). The Khetpurali locality has been estimated to be ~2.6 Ma and Kanthro locality would be ~3 Ma old.

MATERIAL AND METHODS

Materials

All the specimens described here come from field collections. The Khetpurali PU KPR-1 skull and the isolated teeth though from the same site were not found in association. The Kanthro (Saketi) PU KR-1 palate and the isolated teeth described earlier are also not associated. The isolated m3 and M3 were earlier assigned as *Rhizomyides* sp. and Cf. *Brachyrhizomys* by Patnaik (2001). One lower incisor described earlier from Kanthro (Patnaik, 2003) has also been included in this study. The two partial mandibles from Saketi on which the species *Rhizomyioides saketiensis* was erected by Gupta et al. (1978) are from a nearby locality and included in this study.

Methods

Micro-CT scanning of the partial skull PU KPR-1 and palate PU KR-1 was undertaken at the IIT, Mumbai X-Ray microscope facility using Zeiss, Xradia Versa 520. The fossils were also studied under Leica S8APO microscope. For photography and measurements Racold stereozoom microscope was used. Several images were taken using JEOL 6490 SEM housed at the Department of Geology, Panjab University. The dental terminology for *Rhizomyides* follows López-Antoñanzas et al. (2013) (Fig. 2).

Phylogenetic Analysis

The phylogenetic analysis of the morphological data was conducted using PAUP version 4.0a169 Swofford (2002) phylogenetic software package, employing the bootstrap method with heuristic search. The taxa were identified based on synapomorphic characters observed in specimens, published descriptions, and photographs. All the characters were given equal weight, and their order was not considered. Missing characters were denoted as "?" and gaps as "-". The text files were converted into NEXUS file formats using

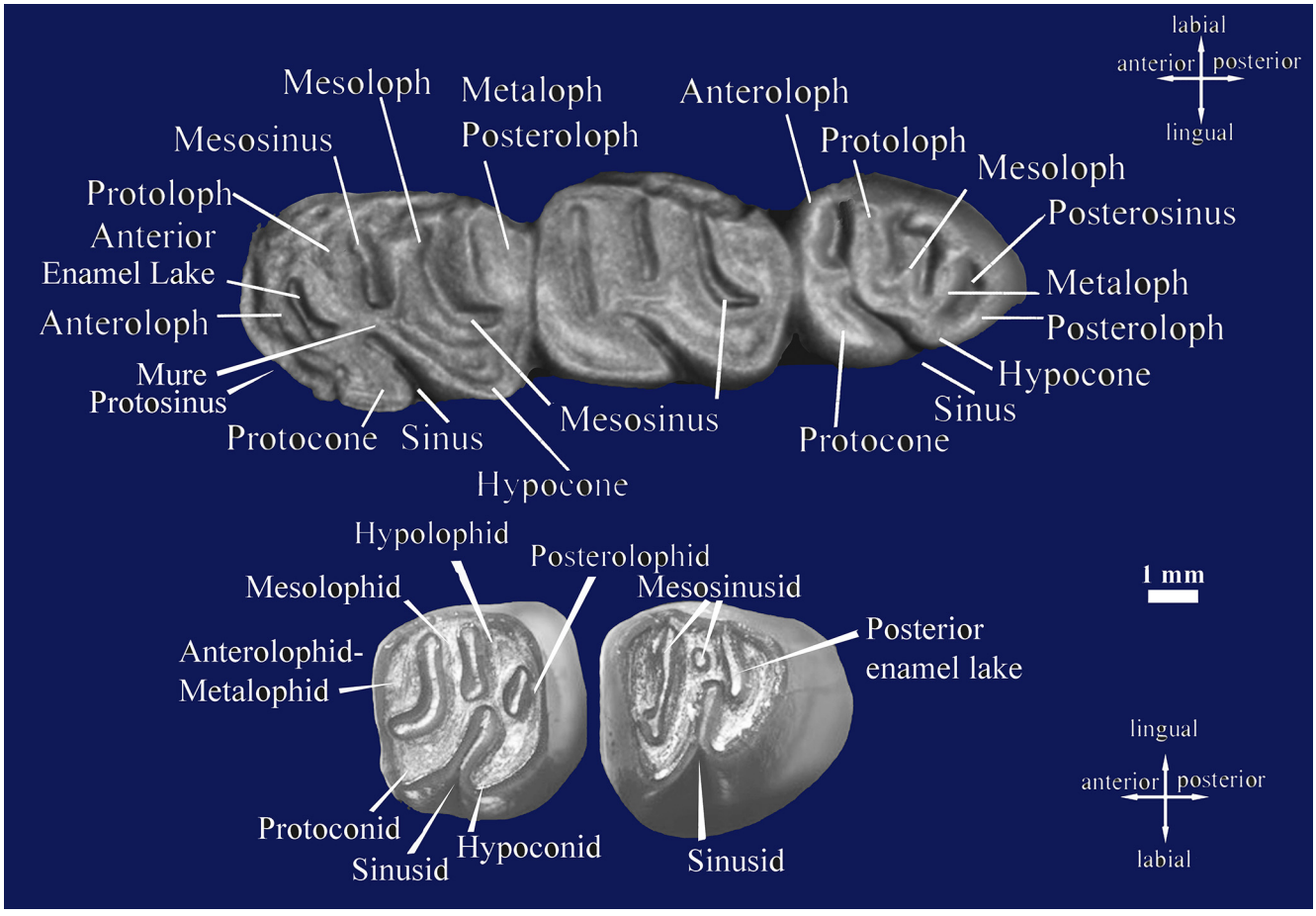

FIGURE 2. Dental terminology for *Rhizomyides* follows López-Antoñanzas et al. (2013). The upper molars are from the palate PU KPR-1, the left m2 is PU KPR-2 and left m3 is PU KPR-4.

Mesquite, version 3.5.1 (Madison and Madison, 2018). For this study, the parsimony optimality criterion was selected, and 50000 bootstrap replicates were performed, retaining 10 trees per replicate through the branch-swapping algorithm of the tree bisection-reconnection (TBR) method. A total of 5000 most parsimonious trees (Maxtrees) were retained. Branch support values for each tree were determined using the random addition sequence of taxa over 10000 replicates (Felsenstein, 1985). The 50% majority rule consensus tree was constructed based on the 5000 most parsimonious trees obtained in this study.

Abbreviations — PU KPR, Khetpurali rhizomyine and PU KR Kanthro rhizomyine, SM-Saketi Mammals; YGSP, Yale Geological Survey of Pakistan, DP, Darmouth Peshawar; NHMUK, Natural History Museum London, AMNH, American Museum of Natural History, GSI-Geological Survey of India; AFG-Afghanistan; BAM, Bamian, PEC, Pul-e Charkhi.

M1-First Upper Molar, M2-Second Upper Molar, M3-Third Upper Molar, m1 First Lower Molar, m2- Second Lower Molar, m3-Third Lower Molar.

SYSTEMATIC PALAEONTOLOGY

Family SPALACIDAE Gray, 1821

Subfamily RHIZOMYINAE Winge, 1887

Genus *RHIZOMYIDES* Bohlin, 1946

RHIZOMYIDES LYDEKKERI (Hinton, 1933)

Synonymy: 1972 *Rhizomyoides sivalensis* Black (in part), p. 249

1978 *Rhizomyoides saketiensis* Gupta et al., p. 112

(Fig. 3 A-J) (Table 1, 2)

Type Locality — Saketi and Kanthro, Himachal Pradesh

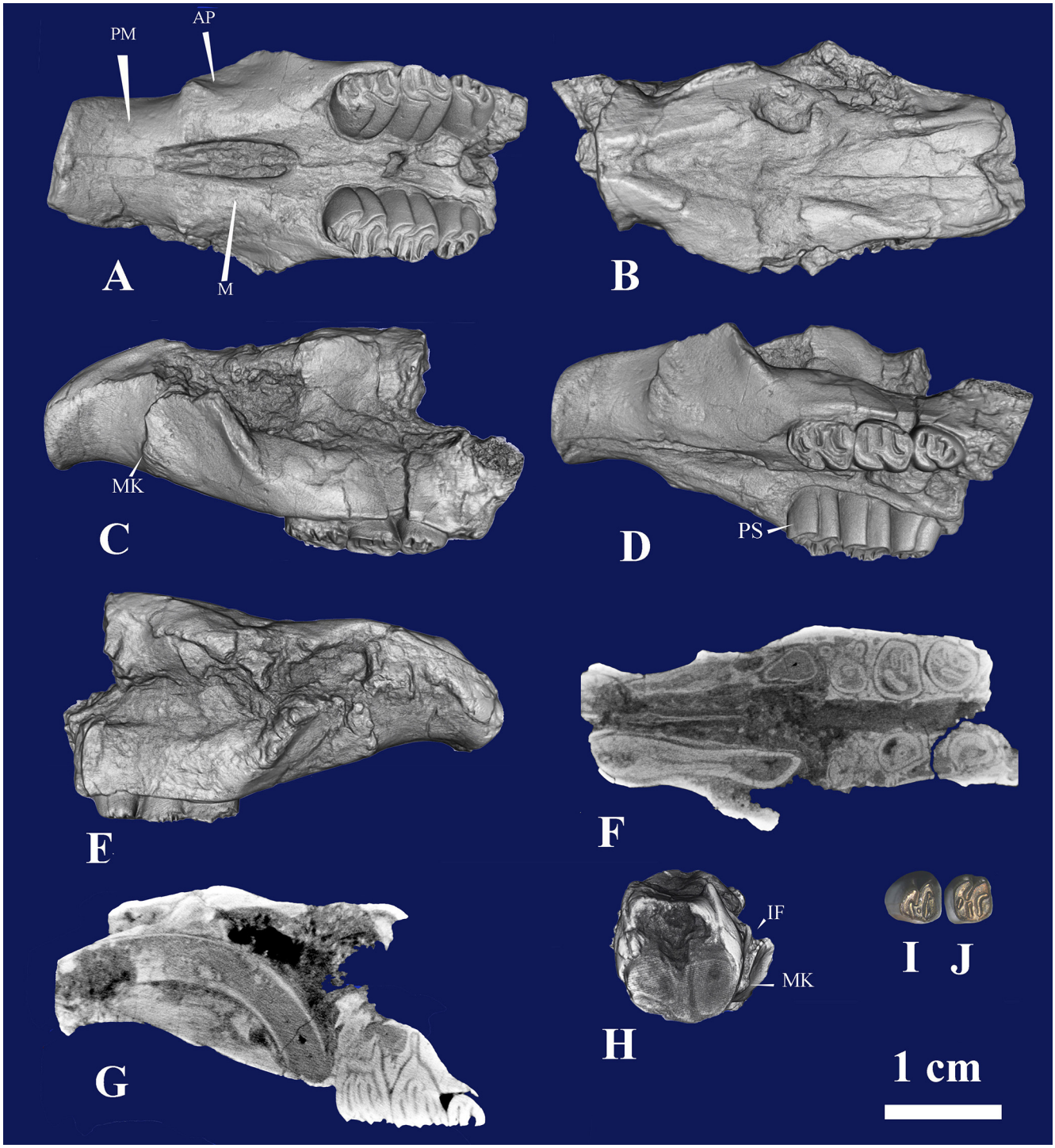

FIGURE 3. Upper and lower molars of *Rhizomyides lydekkeri* from Khetpurali. A-H: PU KPR-1, A, ventral view; B, dorsal view; C, lateral view (left side); D, skull tilted to show the occlusal surface of the left upper molars; E, lateral view (right side); F, micro-CT image at a depth parallel to the ventral surface; G, micro-CT image through left incisor and row of molars. H, frontal view showing nasal bones above broken incisors. I, isolated left m3 (PU KPR-2) and left m2 (PU KPR-3). PM-Pre-maxilla; AP-Anterior plate of the zygoma; IF-Infraorbital foramen; M-Maxilla; MK-Masseteric Knob; PS-Protosinus.

(India).

Referred Material — PU KPR-1 a partial skull with well-preserved palate; PU KPR-2, left m2; PU KPR-3, left m2; PU KPR-4 left m3. PU KR-1, palate with all the teeth preserved; GSI-19549 partial mandible with m2m3 and i1; GSI-19549 partial mandible with m3 and i1; VPL/RP-SM-79, isolated m3 and VPL/RP-SM-80, isolated M3 assigned earlier as *Rhizomyides* sp., cf. *Brachyrhizomys* sp., respectively (Patnaik, 2001); VPL/RP-SM-791, i1 isolated lower incisor considered *Rhizomyides* sp. (Patnaik, 2003).The type specimen of *R. lydekkeri* Hinton, 1933, NHMUK PV OR 15925.

Emended diagnosis — Skull and upper dentition of this large species of *Rhizomyides* were not known before. A robust skull having very long snout, long incisive foramina, an infraorbital foramen with a keyhole pattern, very large, hypsodont and lophodont molars showing a strong gradient of wear. Lingual sinus deep antero-labially oriented, mesoloph long and complete on M1M2M3; M1 three rooted with metaloph-posteroloph fused, posterior lake (posterosinus) retained on M3. Mandibles with strong masseteric crest anteriorly extended and inflated under m2; very large hypsodont lower m1, m2 and m3 with a mure lingual to a deep sinusid; large posterior enamel lake on m3, triangular lower incisors with a single, fine ridge.

Description — The partial skull of *Rhizomyides lydekkeri* has a low profile (about 18 mm from M2 occlusal surface to skull roof). The snout is slender (12 mm high and 10 mm wide at the incisive foramen) includes a very long diastema (22.5 mm) about twice the length of the tooth row (12.5 mm, Fig. 3D). Both the dorsal and ventral surfaces of the snout curve gently. The premaxillae and nasals reach posteriorly to join the frontals in an extremely jagged suture. The maxilla forms the narrow anterior root of the zygoma and the ascending zygomatic plate, which in turn encloses a myomorphous keyhole infraorbital foramen. A masseteric knob is also present at the anterior margin of the zygomatic plate. A slit-like infraorbital canal within the foramen shows a keyhole pattern (Fig. 3H). The maxilla-premaxilla suture lies right at the infraorbital foramen and zygomatic plate, and extends ventrally to intersect the anterior end of the incisive foramina. Incisive foramina are very long (12 mm) and broad (up to 3.5 mm), situated 2 mm anterior to M1 and 12 mm posterior to the robust I1. Nutritive foramina are located anteromedial to the internal root of M1. The I1 is strongly

TABLE 1. Measurements of upper and lower teeth of *Rhizomyides lydekkeri,* including holotype (estimate due to breakage) and those of other known fossil species from the region.

Tooth No.	Locus	Specimen No.	Length in mm	Width in mm
		Rhizomyides lydekkeri		
1	M1	PU KPR-1	4.8	3.5
2	M2	PU KPR-1	4.2	3.5
3	M3	PU KPR-1	3.5	3.4
4	m2	PU KPR-2	3.4	3.5
5	m2	PU KPR-3	3.5	3.5
6	m3	PU KPR-4	3.5	3.8
7	M1	PU KR-1	4.5	5.3
8	M2	PU KR-1	4.5	5.0
9	M3	PU KR-1	4.8	4.5
10	m2	GSI-19549	5.2	6
11	m3	GSI-19549	5	5
12	i1	GSI-19549	4.5	4.1
13	m3	GSI-19550	5	5
14	i1	GSI-19550	4.5	4.1
15	m3	SM-79	4.2	4.7
16	M3	SM-80	4.0	3.8
17	i1	SM-791	4.2	4.0
18	m1	NHMUK PV OR 15925	~5.5	4.2
19	m2	NHMUK PV OR 15925	5.0	5.5
20	m3	NHMUK PV OR 15925	6.0	~5.0
21	i1	NHMUK PV OR 15925	7.8	4.3
		R.sivalensis		
22	m2	GSI D97	5.46	5.06
23	m3	GSI D97	6.13	4.50
24	m2	GSI D276	5.25	4.31
25	m3	GSI D279	5.44	4.31
26	m2	YGSP 15319	4.00	4.94
27	m3	YGSP 15319	5.38	4.63
28	m3	DP 394	5.00	4.00
		R.punjabensis		
29	m2	AMNH 19762	2.75	2.75
30	m3	AMNH 19762	3.06	2.54
		R. carbonnelli		
31	m2	PEC 101	3.52	4.13
32	m3	PEC 101	3.96	4.01
		R. mirzadi		
33	M2	BAM 3	3.40	3.16
34	m1	BAM 1	3.93	2.59
35	m2	BAM 2	3.99	3.51
		R. platytomeaus		
36	m1	AFG 059	5.62	4.48
37	m2	AFG 059	5.25	5.38
38	m3	AFG 059	6.65	4.84
39	i1	AFG 059	4.42	3.78

TABLE 2. Measurements for the partial skull PU KPR-1 (*Rhizomyides lydekkeri*) compared with *Miorhizomys nagrii, Miorhizomys choristos* and *Kanisamys sivalensis* (data from Flynn, 1982; Flynn et al., 1990).

S.no	Cranial elements	*Rhizomyides lydekkeri*	*Miorhizomys nagrii*	*Miorhizomys choristos*	*Kanisamys sivalensis*
1.	Diastema length	22.5	17.3	18	15
2.	Snout height	12	9.5	13.7	9
3.	Snout width	10	10.8	13	10
4.	Incisive foramen length	12	5.9	7	6
4.	Incisive foramen width	3.5	-	3.6	2.5
4.	Incisive foramen-first molar distance	2.5	-	5	2.5
5.	Molar row length (upper)	12.5	9.0	12	7.4
6.	Palate width (outer margin at second molar)	17	13.4	14.6	-
7.	Distance between second molars (inner margin)	4.5	5.5	4.2	-
8.	Skull height (at and including second molar)	18	18.3	24.5	15
9.	Incisor cross section	4.0, 3.5	-	4.6,3.0	-

recurved and contained within the maxilla anterior to the molar row, but its capsule abuts the anterior side of the M1 root (Fig. 3F & G). The palatine foramina lie opposite the posterior end of M2. Posterior emargination of the palate extends anterior to the midline of M3. The robust incisors, low skull profile, very elongated and gently curved snout, and long incisive foramina may indicate that *Rhizomyides lydekkeri* was moderately fossorial.

The M1 (Fig. 2 and 3) occlusal outline is nearly rectangular in early wear but becomes squarish to round after moderate wear (Fig. 4). This tooth is three rooted with the anterolingual root the most developed (Fig. 3F). M1, somewhat larger than the M2 and M3, comprises four prominent transverse lophs (anteroloph, protoloph, mesoloph and metaloph-posteroloph). The anteroloph connects lingually to the protoloph through the protocone and labially to the protoloph, isolating an anterior enamel lake. The mesoloph, which is a long antero-labial continuation of the hypocone, joins labially the metaloph–posteroloph, isolating a posterior enamel lake (posterior mesosinus), which is larger than the anterior one. The M1 has a distinct deep lingual sinus directed strongly antero-labially towards the anterior lake. A faint protosinus is present at the antero-lingual border of the tooth (Fig. 3D). The M1 has a short mure.

The M2 (Figs. 2, 3) occlusal outline is nearly rectangular in early wear but appears squarish after moderate wear (Fig. 3) and somewhat rounded near the base as seen through the micro-CT image (Fig. 3F). M2 comprises four prominent transverse lophs (anteroloph, protoloph, mesoloph and metaloph-posteroloph). The anteroloph connects lingually to the protoloph through the protocone and labially to the protoloph, isolating an anterior enamel lake. The mesoloph is a long antero-labial continuation of the hypocone, joining labially with the metaloph-posteroloph to isolate a posterior enamel lake (posterior mesosinus), which is larger than the anterior one. The lingual sinus is deep and directed steeply anteriorly towards the anterior lake. The M2 has a short mure and is four rooted.

The occlusal outline of the M3 (Figs. 3, 4) is oval with its posterior part being narrower than the anterior. The outline becomes round at the base of the molar (Fig. 3F). It has five lophs, the posteroloph is the shortest. The lingual sinus is deep. In very late wear the protocone and hypocone are joined to enclose a large lingual lake (Fig. 4E). This is evident from the micro-CT scan image taken at the base of the molar (Fig. 3F). The anteroloph is a long and narrow continuation of the protocone. The protoloph and mesoloph extend from the middle of the tooth to the labial margin. In very early wear the mesoloph is divided with a buccal cusp (Fig. 3). The metaloph joins with the hypocone and with the lingual end of the posteroloph, forming a posterosinus. The M3 has a short mure and is three rooted.

The m1 of NHMUK PV OR 15925 is slightly damaged on the lingual side and anteriorly. The occlusal outline of the m1 is oval, with the anterior part being much narrower than posteriorly. The anteroconid is fused with the anterolophid

which in turn is attached to the metalophid lingually leaving a large anterosinusid. A protosinusid is present labially and the labial sinus is deep. Mesolophid is long and complete and joins the metalophid to enclose an anterior mesosinusid. It also joins lingually to the hypolophid enclosing the posterior mesosinusid. Posterolophid and hypolophid enlcose a large posterosinusid. The specimen shows a posterior metaconid-protoconid connection. The tooth has a midline mure.

The occlusal outline of m2 is squared (Fig. 3J). It has four major lophids: anterolophid-metalophid, mesolophid, hypolophid and long posterolophid (Figs. 2 and 3). The mesolophid extends labially from the protoconid. Hypoconid extends to posterolophid which in turn joins hypolophid lingually to form the posterior enamel lake. Lingual joining of anterolophid-metalophid and mesolophid leads to the formation of an anterior mesosinusid lake. A posterior mesosinusid lake is formed by the lingual joining of mesolophid and hypolophid. The sinusid is deep, but a central mure is present, very narrow in early wear. m2 is four rooted.

The m3 is hypsodont (occlusal measurement excludes the posteriorly flaring base) and has a triangular occlusal outline (Figs. 3 and 4). The main lophids are the anterolophid-metalophid, mesolophid shortened in early wear, hypolophid and posterolophid. The protoconid is V-shaped and its posterior arm (an abbreviated mesolophid in early wear) is broad and oblique. The hypolophid is directed lingually from the narrow mure that lies lingual to the deep sinusid. In later wear the mesolophid joins the hypolophid lingually to form a small lake (mesosinusid). Posterolophid and hypolophid join lingually to form a large posterior enamel lake. Root structure is not preserved.

Comparisons — The type species of *Rhizomyides* is *Rhizomyides sivalensis* (Lydekker, 1884). Bohlin (1946) had perceived that the fossil is distinct from any living species. *R. sivalensis* is a relatively common rhizomyine in the late Miocene of the Indian subcontinent. It is significantly larger than early Late Miocene *R. punjabiensis.* Gupta et al. (1978) realized that a yet larger form of the genus occurs in the Late Neogene of the subcontinent and distinguished Late Pliocene fossils as *R. saketiensis* (holotype GSI 19549). Their intuition was accurate, but Hinton (1933) had realized the same and named *R lydekkeri* based on two jaws (holotype, NHMUK PV OR 15925). Unfortunately, the locality was not recorded and Black (1972) preferred to synonymize them with *R. sivalen*sis. Renewed collecting with accurate locality information yields the new material described here and permits us to emend the diagnosis of this large rhizomyine.

The holotype of *Rhizomyides lydekkeri* is represented by a mandible with broken molars and incisor. The type of *R. saketiensis* (GSI 19549) was represented by two jaw fragments, one preserving m2-3, the other with broken m2. Table 1 includes estimated length and width of m1-3 in the holotype NHMUK PV OR 15925. The description above of the molars embraces both NHMUK PV OR 15925 and GSI 19549. These two specimens add to the impression that this late *Rhizomyides* has relatively broad molars. They also demonstrate a stout lower incisor (4.4 mm wide in NHMUK PV OR 15925) with enamel that is very gently rounded and bears a fine ridge. The dentary bone is not particularly deep.

The partial skull would be the largest among the Siwalik *Rhizomyides*, with the longest diastema and incisive foramina (Table 2). The partial skull of *Rhizomyides lydekkeri* may be compared with the skull of the early tachyoryctine *Kanisamys sivalensis* (Flynn, 1982) in having a low profile, a slender snout and a slit-like infraorbital canal within the foramen forming a keyhole constriction and a very longer incisive foramina compared to the modern burrowers *Rhizomys* and *Cannomys* with a stout skull, indicating less subterranean habits. In contrast the skulls of the bamboo rats *Miorhizomys nagrii* and *Miorhizomys choristos* (Flynn, 1982; Flynn et al., 1990) have solid incisors, short snouts and incisive foramina, all pointing towards a fossorial lifestyle (Table 2).

Rhizomyides lydekkeri molars are significantly larger than any known species of *Rhizomyides.* The upper and lower dentition of *Rhizomyides lydekkeri* differs from the Late Miocene (6.5-5.5 Ma) Siwalik species of *Rhizomyides sivalensis* being larger in size with a smaller posterior enamel lake on M3. The much smaller early Late Miocene (11.2-10.1 Ma) taxon *Rhizomyides punjabiensis* differs from the present species in having a shallow dentary, masseteric crest with a short anterior extension, and weak inflation; a short mesolophid on m2 and m3, a mesostyle on M1 and no posterior enamel lake on M3. The intermediate-size *Rhizomyoides carbonnelli* from the Late Miocene-Early Pliocene of Pul-e Charkhi, Kabul, Afghanistan (Brandy, 1979a, b, 1981) has short mesolophids on m2m3; an anterosinusid on m3; metaloph and posteroloph separate on M2, and no mesoloph on M3. *Rhizomyides platytomeus* from the Pliocene Sarobi Basin, Afghanistan (Flynn et al., 1983) rivals *R. lydekkeri* in size, but can be separated in having a constricted mure on m2 and a short

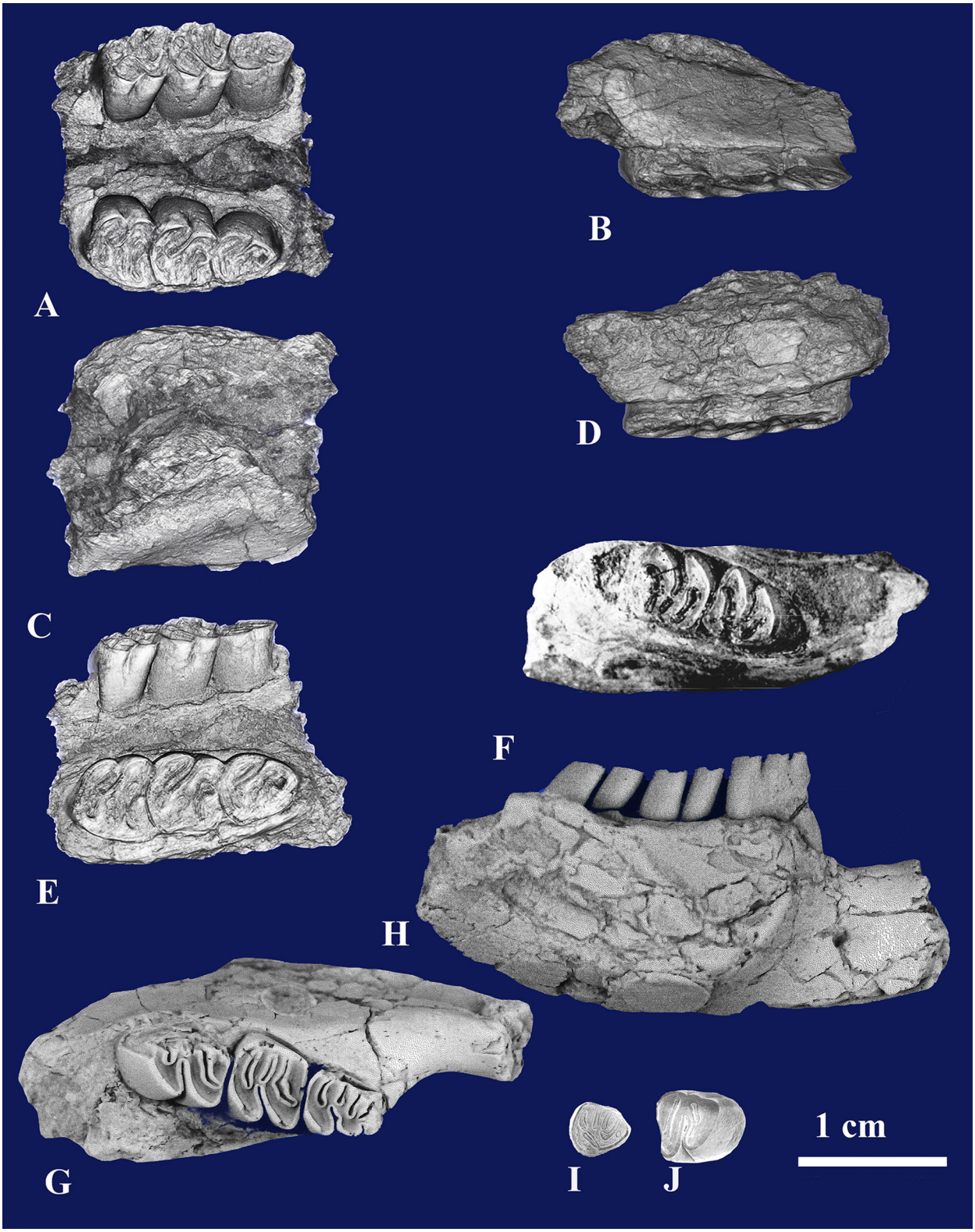

FIGURE 4. *Rhizomyides lydekkeri* from Kanthro and Saketi villages, Himachal Pradesh. A-E, PU KR-1, palate with all the teeth preserved; F, GSI-19549 partial mandible with m2m3 and i1, assigned as *R. saketiensis* (Gupta et al., 1978); G and H, occlusal and labial views of the mandible, the type specimen of *R. lydekkeri* NHMUK PV OR 15925; I, VPL/RP-SM-79, isolated M3 and J, VPL/RP-SM-80 isolated m3 formerly assigned respectively as *Rhizomyides* sp. and cf. *Brachyrhizomys* by Patnaik (2001).

mesolophid on m3. *Rhizomyides mirzadi* (Lang and Lavocat, 1968) a poorly-represented form from the Late Miocene of Afghanistan can be distinguished from *Rhizomyides lydekkeri* by its smaller size, short mesolophids on m2-3, and in having a masseteric crest with a short anterior extension but no inflation.

Rhizomyides lydekkeri differs from Middle Miocene *Kanisamys indicus* (16.8-11.4 Ma, Flynn et al., 2020) in having upper and lower molars with long and complete mesolophs/ mesolophids. Molars of *Kanisamys indicus*, *K. potwarensis,* and Late Miocene *K. sivalensis* are smaller, lower crowned and less lophodont than those of *Rhizomyides lydekkeri.* Among larger tachyoryctins from the Siwaliks (but smaller than *R. lydekkeri*) *Protachyoryctes tatroti* (Hinton, 1933) from the Latest Miocene (6.9-6.5 Ma) Dhok Pathan Formation (Flynn, 1982) has shallow sinusids. Compared to *Rhizomyides lydekkeri,* m2 of *Protachyoryctes tatroti* and Late Miocene *Eicooryctes kaulialensis* (Flynn, 1982) are more hypsodont. Lower molars of Plio-Pleistocene *Anepsirhizomys pinjoricus* are very hypsodont, have their lingual and labial sinusids open, and the mesolophids are short lying close to the hypolophids. The species of African *Tachyoryctes* have hypsodont teeth, lack a mesolophid on the m2 and m3 and protosinus on the M1.

The extinct bamboo rats (Rhizomyini) differ at the tribe level in many features. The molars of *Miorhizomys nagrii, Miorhizomys harii* and *Miorhizomys choristos* are smaller, with short mesolophs/mesolophids, no protosinus on M1, and lack ornamentation on i1 (Flynn, 1982, Patnaik, 2020). Species of the modern rhizomyines *Rhizomys* and *Cannomys* clearly differ dentally from the present species in having a mesolophid on m2 a long continuation of the protoconid, no mure on lower molars, no ornamentation on lower incisors.

Phylogenetic analysis of Rhizomyine rodents

A phylogenetic analysis was carried out to determine the affinity of *Rhizomyides lydekkeri.* For phylogenetic analysis we constructed a morphological character matrix of thirty-nine ingroup rhizomyine taxa with the early spalacid *Debruijnia arpati* as outgroup (Table 3). The most parsimonious tree was constructed based on a total of 44 morphological characters, all characters were parsimony informative.

López-Antoanzas et al. (2013) published a comprehensive cladistic study for spalacids. We placed *Rhizomyides lydekkeri* in the phylogenetic tree of rhizomyines based on the features they identified for upper and lower molars and incisors.

1. Hypsodonty: Crown height on at least one side of the tooth greater than length or width of the tooth. This character has been scored as (0) absent; (1) moderate; (2) high.
2. Size: Length of the m2: (0) 1.5-2.5 mm; (1) 2.5-3.5 mm; (2) 3.5-4.5 mm; (3) 4.5-5.5 mm; (4) >5.5 mm.
3. Lophodonty: (0) weak; (1) moderate; (2) high.
4. Masseteric crest: (0) with long anterior extension; (1) with short anterior extension; (2) without anterior extension.
5. Lower masseteric crest: (0) inflated under m2; (1) not inflated.
6. Dentary depth: (0) shallow; (1) moderate; (2) deep.
7. Infraorbital foramen: (0) with ventral slit; (1) with abbreviated ventral slit; (2) without ventral slit.
8. Longitudinal ornamentation on the i: (0) double ridge; (1) single ridge; (2) absent.
9. Anteroconid on the m1: (0) discernible); (1) absent (fused with the anterolophid).
10. Mure on the m1: (0) present; (1) constricted; (2) absent.
11. Labial anterolophid on the m1: (0) present; (1) absent.
12. Mesolophid on the m1: (0) long and complete and separated from the hypolophid; (1) short and well separated from the hypolophid; (2) short and migrated towards the hypolophid; (3) absent; (4) a long continuation of the protoconid.
13. Posterior protoconid–metaconid connection on the m1: (0) present; (1) absent.
14. Anterosinusid on the m1: (0) present; (1) absent.
15. Mure on the m2: (0) present; (1) constricted; (2) absent.
16. Mesolophid on the m2: (0) long and complete and separated from the hypolophid; (1) short and well separated from the hypolophid; (2) short and near the hypolophid; (3) absent; (4) a long continuation of the protoconid.
17. Labial anterolophid on the m2: (0) present; (1) absent.
18. Hypolophid on the m2: (0) not isolated; (1) isolated.
19. Protosinusid on the m2: (0) present; (1) absent.
20. Anterosinusid on the m2: (0) present; (1) absent.
21. m3: (0) reduced (shorter than the m2); (1) enlarged (equal or larger than the m2).
22. Labial anterolophid on the m3: (0) present; (1) absent.

23. Mure on the m3: (0) present; (1) absent.
24. Mesolophid on the m3: (0) long and complete, separated from the hypolophid; (1) short, well separated from the hypolophid; (2) short, near the hypolophid; (3) absent; (4) a long continuation of the protoconid.
25. Posterosinusid on the m3: (0) large; (1) small; (2) absent (posterolophid fused with hypolophid).
26. Entoconid on the m3: (0) not distinguished; (1) distinguishable.
27. Protosinusid on the m3: (0) present; (1) absent.
28. Anterosinusid on the m3: (0) present; (1) absent.
29. Roots on the M1: (0) three; (1) four; (2) Hypselodont. (four roots on M1 is a modern rhizomyin trait.)
30. Protosinus on the M1: (0) present; (1) absent.
31. Mesoloph on the M1: (0) absent; (1) short; (2) long and complete; (3) long and complete but divided with a buccal cusp.
32. Mesostyle on the M1: (0) may be present; (1) absent.
33. Ectoloph on the M1: (0) present; (1) absent.
34. Anterocone on the M1: (0) distinct; (1) fused with the anteroloph.
35. Metaloph on the M1: (0) present and distinct from the posteroloph; (1) fused with the posteroloph.
36. Posterosinus on the M1: (0) present; (1) absent.
37. Mesoloph on the M2: (0) absent; (1) short; (2) long and complete; (3) long and complete but divided with a buccal cusp.
38. Longitudinal crest on the M2: (0) present; (1) absent.
39. Ectoloph on the M2: (0) present; (1) absent.
40. Metaloph on the M2: (0) present and distinct from the posteroloph; (1) early fused with the posteroloph; (2) absent.
41. Posterosinus on the M2: (0) present; (1) absent.
42. Anterosinus on the M3: (0) open; (1) enclosed by anteroloph and paracone; (2) absent.
43. Mesoloph on the M3: (0) absent; (1) short; (2) long and complete; (3) long and complete but divided with a buccal cusp.
44. Posterior lake on the M3: (0) large; (1) small; (2) absent.

RESULTS AND DISCUSSION

Phylogenetic analysis produced 50% majority rule consensus of 43 trees (Fig. 5); this was supported by modest bootstrap values. The phylogenetic analysis shows that our specimens share closest affinity with *Rhizomyides.* Initial attempts to identify the evolutionary relationships between extinct and extant Rhizomyinae based on synapomorphies of many genera were carried out by Flynn (1990) and López-Antoanzas et al. (2013). According to López-Antoanzas et al. (2013), the Asian *Prokanisamys* is the most basal genus of the ingroup, followed by the East African *Nakalimys*; our phylogenetic study supports their findings. *Prokanisamys* is also the oldest known genus of a monophyletic Rhizomyinae subfamily supported by characters; short anterior extension of masseteric crest; mesolophid on the m2 short and well separated from the hypolophid; mesolophid on the m3 long and complete, separated from the hypolophid. *Pronakalimys* and *Nakalimys* are an early African branch followed by *Kanisamys* and supported by lower masseteric crest inflated under m2; moderate dentary depth; mesolophid of m2 short and migrated towards the hypolophid; open anterosinus on the M3. *Kanisamys* comprises a sequential array of Asian species; *K. indicus* is supported by mesolophid on the m1 long and complete, separated from the hypolophid; retained posterior protoconid-metaconid connection on the m1.

Kanisamys potwarensis and more derived taxa are supported by presence of ectoloph on the M1; metaloph on the M1 fused with the posteroloph; absence of posterosinus on the M1 and metaloph on the M2 early fused with the posteroloph. *Kanisamys nagrii* has greater lophodonty, labial anterolophid lost on m2 and m3 with protosinusid absent on m2 and m3. *Kanisamys sivalensis* supported by hypsodont uppers; short mesoloph on the M1; metaloph on the M1 present and distinct from the posteroloph; presence of posterosinus on the M1. Two Miocene species previously considered as congeners with *Rhizomyides sivalensis* plot next to primitive *Miorhizomys.* These are *Rhizomyides mirzadi* and *R. punjabensis,* their node supported by m1 mesolophid short and well separated from the hypolophid; presence of labial anterolophid on the m3. *Miorhizomys micrus* and other derived taxa show a large posterosinusid on the m3; large posterior lake on the M3. *Rhizomys shajius* and *Miorhizomys harii* node is supported by constricted mure on the m1 and m2; *M. blacki and M. nagrii* node is supported by the absence of anterosinusid on the m1; mesolophid on the m2, long and complete and separated from the hypolophid.

Protachyoryctes tatroti and *Tachyoryctes makooka* node is supported by short mesolophid migrated toward the

TABLE 3. Character coding matrix used in the study (as per López-Antoanzas et al., 2013)) for the relationships between *Rhizomyides saketiensis* and other extinct and extant rhizomyine rodents.

Taxa/Character	1	2	3	4	5	6	7	8	9	10	11	12	13	14	15	16	17	18	19	20	21	22	23	24	25	26	27	28	29	30	31	32	33	34	35	36	37	38	39	40	41	42	43	44
Rhizomyides lydekkeri	2	1&3	2	0	0	2	2	1	1	1	1	0	0	0	0	0	1	0	1	1	1	1	0	0	0	0	1	1	0	0	2	1	1	1	1	1	2	1	1	1	1	1	2&3	1&0
Debruijnia arpati	0	0	1	?	?	?	?	?	0	0	0	0	0&1	0	0	0	0	0	0	0	0	0	0	0	0	0	0	0	0	0	1	1	0	0	0	0	2	0	0	0	0	0	2	0
Rhizomys sumatrensis	2	4	2	2	1	2	2	2	1	2	1	4	1	1	2	4	1	1	1	0	1	1	1	4	2	1	1	1	1	1	3	1	1	1	1	1	3	1	1	1	1	2	3	2
Rhizomys sinensis	2	4	2	2	1	2	2	2	1	2	1	4	1	1	2	4	1	1	1	0	0	1	1	4	2	1	1	1	1	1	3	1	1	1	1	1	3	1	1	1	1	2	3	2
Rhizomys pruinosus	2	4	2	2	1	2	2	2	1	2	1	4	1	1	2	4	1	1	1	0	1	1	1	4	2	1	1	1	1	1	3	1	1	1	1	1	3	1	1	1	1	2	3	2
Rhizomys shansius	1	3	2	2	1	2	2	2	1	2	1	0	1	1	2	4	1	1	1	0	1	1	1	4	2	0	1	1	1	1	2	1	1	1	1	1	2	1	1	1	1	1	2	2
Rhizomys shajius	1	2	2	2	?	1	?	?	?	?	?	?	?	?	1	2	1	0	1	1	1	1	0	2	1	0	1	1	?	?	?	?	?	?	?	?	?	?	?	?	?	?	?	?
Cannomys badius	2	0&1	2	1	1	2	2	2	1	2	1	4	1	1	2	4	1	1	1	?	1	1	1	4	2	1	1	1	1	1	2	1	1	1	1	1	2	1	1	1	1	2	2	2
Miorhizomys nagrii	1	1&2	2	1	1	1	1	2	1	0	1	0&1	1	1	0	0	1	0	1	1	0	1	0	0&2	1	0	1	1	0	1	2&3	0	1	1	1	1	2	0	1	1	1	1	1&2	1
Miorhizomys micrus	1	1	2	1	1	1	?	2	1	0	1	0	1	0	0	2	1	0	1	0	1	1	0	2	1	0	1	0	?	?	?	?	?	?	?	?	?	?	?	?	?	?	?	?
Miorhizomys blacki	1	2	2	2	1	1	1	2	?	?	?	?	?	?	0	0	1	0	1	1	1	1	0	2	1	0	1	1	?	?	?	?	?	?	?	?	?	?	?	?	?	?	?	?
Miorhizomys pilgrim	1	3	2	2	1	1	1	2	?	?	?	?	?	?	2	4	1	0	1	1	1	1	1	4	1&2	0	1	1	?	?	?	?	?	?	?	?	?	?	?	?	?	?	?	?
Miorhizomys harii	1	2	2	1	1	?	?	2	1	1	1	0	1	0	1	1	0	0	1	1	?	?	?	?	?	?	?	?	?	?	?	?	?	?	?	?	?	?	?	?	?	?	?	?	?
Miorhizomys tetracharax	1	2&3	2	2	1	1	1	2	1	1	1	0	1	0	1	0	1	0	1	0	1	1	1	4	2	1	0	0	1	?	?	?	?	?	?	?	2	1	1	?	0	1	1	1
Miorhizomys choristos	1	2&3	2	2	1	1	1	2	1	1	1	0&1	1	1	2	4	1	0	1	1	1	1	1	4	2	1	1	1	1	1	0	1	1	1	1	1	3	1	1	1	1	0	1	1
Protachyoryctes tatroti	1	2	2	0	0	1	?	1	1	0	1	2	1	0	1	2	1	0	1	0	1	1	0	2	0	0	1	0	0	0	2	1	1	0	1	1	2	0	1	1	1	?	?	?
Tachyoryctes makooka	1	1&2	2	?	?	?	1	?	1	1	1	2	1	0	1	2	1	0	1	0	1	1	0	2	0	0	1	0	0	0	2	1	1	1	1	1	2	0	1	1	1	1	2	2
Tachyoryctes pliocaenicus	1	0&1	2	0	0	1	1	1	1	2	1	2	1	0	2	2&3	1	0	1	0	1	1	1	3	1	0	1	0	2	1	2	1	1	1	1	1	2	1	1	1	1	2	2	2
Tachyoryctes macrocephalus	2	2	2	0	0	1	1	1	1	2	1	3	1	0	2	3	1	0	1	1	1	1	1	3	2	0	1	1	2	1	2	1	1	1	1	1	2	1	1	1	1	2	2	2
Tachyoryctes splendens	2	0&1	2	0	0	1	1	1	1	2	1	3	1	0	2	3	1	0	1	1	1	1	1	3	2	0	1	1	2	1	2	1	1	1	1	1	2	1	1	1	1	2	2	2

TABLE 3. Continued.

Taxa/Character	1	2	3	4	5	6	7	8	9	10	11	12	13	14	15	16	17	18	19	20	21	22	23	24	25	26	27	28	29	30	31	32	33	34	35	36	37	38	39	40	41	42	43	44
Rhizomyides sivalensis	1	3	2	0	0	1	?	1	1	0	1	0	0	0	0	0	1	0	1	1	1	1	0	2	0	0	1	0	0	0	2	1	1	1	1	1	2	0	1	1	1	1	?	0
Rhizomyides punjabiensis	1	1	1	1	1	1	?	1	1	0	0	1	1	0	0	1&2	1	0	1	1	1	0	0	2	0	0	1	0	0	0&1	1&2	0	1	1	1	1	2	0	1	1	1	1	2	0
Rhizomyides carbonnelli	1	2	2	0	0	1	?	1	1	0	1	0	0	?	0	2	1	0	1	1	1	1	0	2	0	0	1	1	?	?	?	?	?	?	?	?	2	0	1	0	?	?	0	?
Rhizomyides playtomeus	1	3	2	0	0	1	?	1	1	0	1	0	0	?	1	0	?	0	1	1	1	?	?	2	0	?	1	1	?	?	?	?	?	?	?	?	?	?	?	?	?	?	?	?
Tachyoryctes konjiti	1	1	2	?	?	?	?	1	1	2	1	3	1	0	2	3	1	0	1	1	1	1	1	3	2	0	1	1	2	1	2	1	1	1	1	1	2	1	1	1	1	2	2	2
Kanisamys indicus	1	0	1	0	1	0	?	0	1	0	0&1	0	0&1	0	0	0	0	0	0	0	1	0	0	0	0	0	0	0	0	0	1	0	1	0	0	0	1&2	0	1	0	0	1	1	0
Kanisamys nagrii	1	0&1	2	0	1	0	1	1	1	0	0&1	0&2	1	0	0	2	1	0	1	0	1	0&1	0	2	0	0	1	0&1	0	0	1	0	1	0	0	0	2	0	1	0	0	1	1	0
Kanisamys sivalensis	1	1	2	0	1	0	1	1	1	0	0&1	0&2	1	0	0	2	1	0	1	0	1	1	0	2	0	0	1	0&1	0	0	1&2	0	1	0	1	1	2	0	1	0	0	1	1	0
Kanisamys potwarensis	1	0&1	1	0	1	0	?	1	1	0	1	1	0	0	0	0	0	0	0	0	1	0	0	0	0	0	0	0	0	0	1	0	0	0	1	1	2	0	1	1	0	1	1	0&1
Eicooryctes kaulialensis	2	1	2	1	0	1	?	1	1	1	1	2	0	1	1	2&3	1	0	1	1	1	1	0	3	0	0	1	1	2	1	2	1	1	1	1	1	2	1	1	1	1	?	?	?
Anepsirhizomys opdykei	2	4	2	2	1	1	?	?	1	1	1	0	0	?	2	0	1	0	1	0	?	?	?	?	?	?	?	?	?	?	?	?	?	?	?	?	?	?	?	?	?	?	?	?	?
Anepsirhizomys pinjoricus	2	3	2	0	?	1	?	1	1	?	1	0	0	1	2	0	1	0	1	1	1	1	1	0	2	0	1	?	?	?	?	?	?	?	?	?	?	?	?	?	?	?	?	?
Pronakalimys andrewsi	0	0	1	0	0	1	?	?	0	0	0	0	0	0	0	2	0	0	0	0	0	0	0	2	0	0	0	0	0	0	1	1	1	0	0	0	1	0	1	0	0	0	1	2
Nakalimys lavocati	0	1&2	1	0	0	1	?	1	1	0	0	1	0	0	0	2	0	0	0	0	1	0	0	0&1	0	0	0	0	0	0	1	1	1	0	0	0	0&1	0	1	0	0	0	1	0
Prokanisamys kowalskii	0	0	0	?	?	?	?	0	0	0	0	1	0	0	0	1	0	0	0	0	0	0	0	1	0	0	0	0	0	0	1	1	1	0	0	0	1	0	0	0	0	0	1	0
Prokanisamys arifi	0	0	0	?	?	?	?	0	0	0	0	0&1	0	0	0	1	0	0	0	0	0	0	0	1	0	0	0	0	0	0	1	1	0	0	0	0	0&1	0	0	0	0	1	1	0
Prokanisamys benjavuni	1	0	1	?	?	?	?	?	0	0	0	1	0	0	0	1	0	0	0	0	0	0&1	0	1&3	0	0	0	0	0	1	0&1	1	0	0	0	0	1	0	0	0	0	1	0&1	0
Prokanisamys major	0	0	0	1	1	0	?	?	0	0	0	1	0	0	0	1	0	0	0	0	1	0&1	0	0&1	0	0	0	0	0	0	1	1	0	0	0	0	1	0	0	0	0	1	1	0
Prokanisamys sp.	0	0	0	?	?	?	?	?	?	?	?	?	?	?	0	1	0	0	0	0	0	0	0	1	0	0	0	0	0	0	0&1	1	0	0	0	0	?	?	?	?	?	?	?	?	?
Rhizomyides mirzadi	1	1&2	2	1	1	?	?	?	1	0	1	1	0	0	0	2	1	0	1	1	?	?	?	?	?	?	?	?	?	?	?	?	?	?	?	?	2	0	1	1	?	?	?	?	?

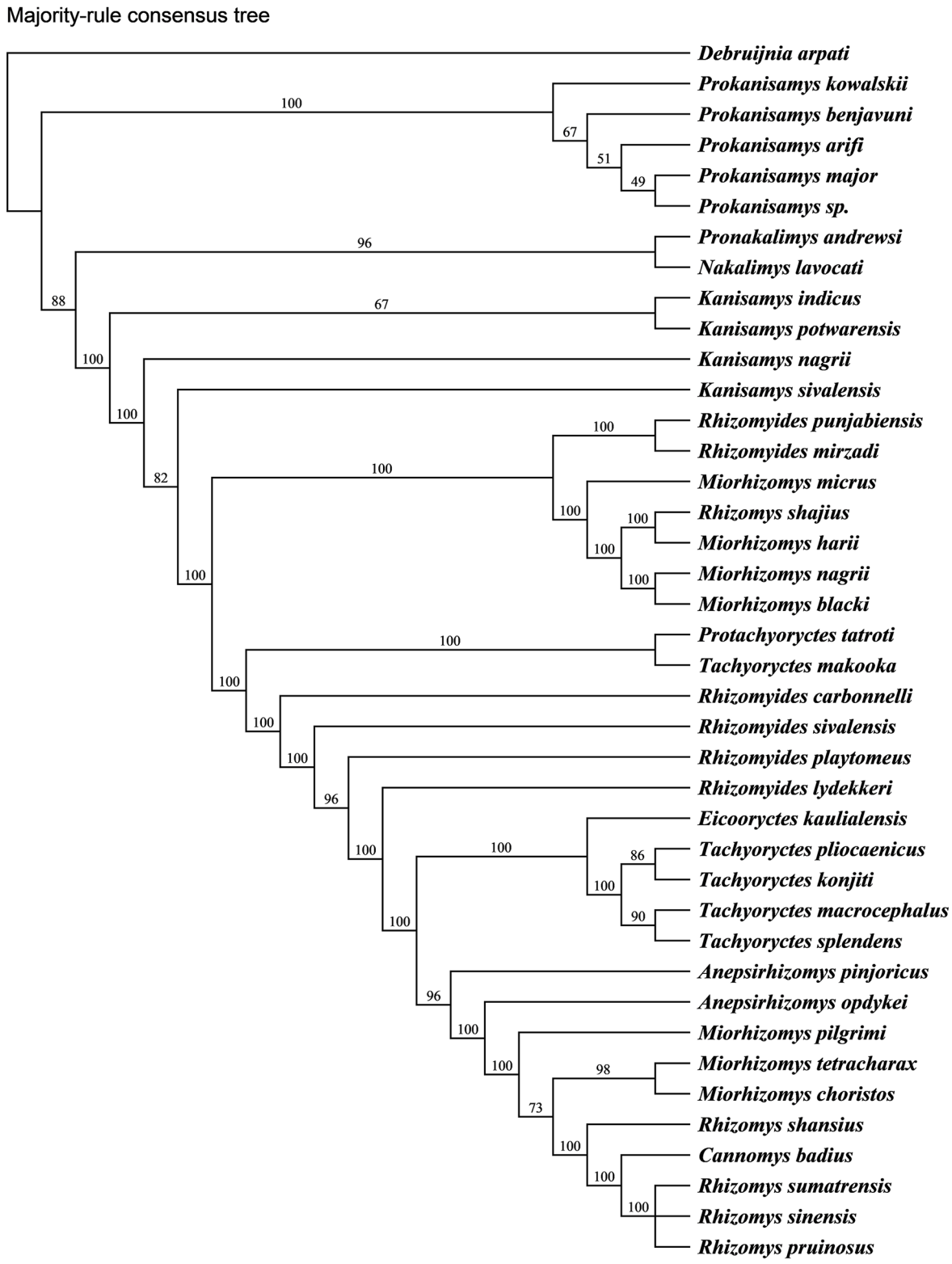

FIGURE 5. Cladogram illustrating the placement of *Rhizomyides lydekkeri* in relation to other fossil Rhizomyinae and their extant counterparts. 50% majority rule consensus of 49 trees shown above with bootstrap values assigned on branches. Branch swapping algorithm: tree bisection-reconnection (TBR) with reconnection limit = 8. Total number of rearrangements tried = 50000000, Score of best tree (s) found = 166. Number of trees retained = 49. Consistency index (CI) = 0.4398. Homoplasy index (HI) = 0.5602. Retention index (RI) = 0.8086. Rescaled consistency index (RC) = 0.3556.

hypolophid. The latter species represents an early expansion to East Africa. *Rhizomyides carbonnelli* and derived *R. sivalensis* and *R. platytomeus* are supported by lower masseteric crest inflated under m2; presence of posterior protoconid-metaconid connection on m1; length of m2 between 4.5 and 5.5 mm. *Rhizomyides lydekkeri* shows deeper dentary depth.

Eicooryctes kaulialensis is supported by length of m2 between 2.5 and 3.5 mm; and absence of mesolophid on m2. In this interpretation, it is at the base of a second expansion of tachyoryctines into East Africa: *Tachyoryctes macrocephalus* and derived *T. splendens, T. pliocaenicus* and *T. konjiti* are supported by absence of mure on m1; absence of posterior protoconid-metaconid connection on m1 and presence of anterosinusid on m1.

Anepsirhizomys is the first of the derived bamboo rats. *A. pinjoricus* and later derived taxa show a masseteric crest with reduced anterior extension. *A. opdykei* displays great hypsodonty and absence of posterior protoconid-metaconid connection on m1. *Miorhizomys pilgrimi* has mesolophid on m2 as a long continuation of the protoconid. *Miorhizomys tetracharax* and *M. choristos* lack mesoloph on the M1 but have short mesoloph on the M3 and small posterior lake on the M3. *Rhizomys shansius* shows entoconid as part of hypolophid on the m3; *Cannomys badius* and the extant *Rhizomys* species show incomplete mesoloph ending short of a buccal cusp on upper molars in early wear.

Flynn (1982, 1990) observed that, *Rhizomyides* and later *Kanisamys* shared many traits such as similar degree of hypsodonty, inclined masseteric crest, a strongly rounded I1, a large posterior enamel lake on M3. These observations led Flynn (1983) to suggest an earlier Miocene origin of *Rhizomyides* than reflected by its first occurrence in the fossil record and that it could have evolved from earlier *Kanisamys*. The fact that *Rhizomyides sivalensis* retained a strong mesolophid on the M2 (usually reduced in *K. sivalensis*) led Flynn (1982) to suggest that *R. sivalensis* may have evolved from *Kanisamys* outside Pakistan before the temporal range of *K. sivalensis* and later immigrated to the Potwar Plateau. The present partial skull displays several features similar to *Kanisamys* (Table 2). Our analysis is consistent with the hypothesis that *R. sivalensis* immigrated to the Indian subcontinent and supports affinity of Siwalik *R. sivalensis* with the Afghan *R. carbonnelli* and *R. platytomeus.* Further, our hypothesis also allows later interchange of the *Rhizomyides* lineage between Afghanistan and Indo-Pakistan.

Our results support the hypothesis by López-Antoanzas et al. (2013) and López Antoñanzas and Wesselman (2013) that the first dispersal of a tachyorhyctine (represented by Asian *Protachyoryctes tatroti*) to Africa (represented by *Tachyoryctes* (*Protachyoryctes*) *makooka*) likely happened in the Late Miocene, before the appearance of *Rhizomyides lydekkeri*. A second dispersal event to East Africa involving *Tachyoryctes pliocaenicus* could have taken place during the Pliocene (Fig. 5).

CONCLUSIONS

The distinct features of the newly discovered skull and palate support the definition of a large Plio-Pleistocene rhizomyine in northern India as perceived by Gupta et al. (1978) when they named *Rhizomyides saketiensis.* This form is a junior synonym of *R. lydekkeri,* which up to now had no locality context. We have included this species in a new phylogenetic analysis. Our phylogenetic analysis places *Rhizomyides lydekkeri* among the Late Miocene and Pliocene species of *Rhizomyides* of the Indian subcontinent and Afghanistan such as *R. sivalensis*, *R. carbonnelli*, and *R. platytomeus.* Further, the results are consistent with a dispersalist scenario between Afghanistan and Indo-Pakistan. The features of a low skull profile, extremely elongated and gently curved snout with very long incisive foramina, and strong incisors indicate that *Rhizomyides lydekkeri* was likely a moderately fossorial rodent.

ACKNOWLEDGMENTS

We would like to thank Yuong-Nam Lee for inviting us to contribute to this volume. We thank Science and Engineering Research Board, Government of India, grant number SERB-HRR/2018/000063 for the financial support. Rohit Kumar is thankful to UGC for providing fellowship (Senior Research Fellow) for pursuing his PhD. Kewal Krishan is supported by the UGC Centre of Advanced Study in Anthropology (CAS II), awarded to the Department of Anthropology, Panjab University, Chandigarh, India. We acknowledge the kind help by staff of NHMUK, who provided excellent photographs of the holotype of *Rhizomyides lydekkeri*. We would like to thank the reviewers for their constructive suggestions to improve the manuscript. We thank the reviewers Advait Jukar

and Mahmood Raza for their constructive comments and suggestions.

AUTHOR CONTRIBUTIONS

RP, KK and BS undertook the field study, RP and LJF designed the project and drafted the manuscript, RK and KK gathered and analysed the Phylogenetic data. All the authors edited the manuscript.

REFERENCES

Azzaroli, A. & Napoleone, G. (1982). Magnetostratigraphy investigation of the Upper Siwaliks near Pinjore, India. *Riv. Ital. Paleont. Stratigr*., 87, 739–762.

Black, C. C. (1972). Review of fossil rodents from the Neogene Siwalik Beds of India and Pakistan. *Palaeontology*, 15, 238–266.

Brandy, L. D. (1979a). Rongeurs nouveaux du Néogène d' Afghanistan. *C. R. Acad. Sci*., Sér. D 289, 81–83.

Brandy, L. D. (1979b). Etude de rongeurs muroïdés du Néogène supérieur et du quaternaire d Europe, d Afrique du nord et d'Afghanistan: évolution, biogéographie, correlations. PhD thesis, Universite´ des Sciences et Techniques du Languedoc.

Brandy, L. D. (1981). Rongeurs muroïdés du Néogène supérieur d'Afghanistan: évolution, biogéographie, corrélations. *Palaeovertebrata*, 11, 133–179.

Eliyas N., Khan, N. Kumar, D., Singh, P., & Prakash, S. (2017). Traverse mapping in gap areas with the help of photo interpreted maps and synthesis of STM data of the Siwalik Group in the states of Jammu and Kashmir, Punjab, Himachal Pradesh, Haryana and Uttarakhand. Item No. RP/NR/PHP/2016/002.

Felsenstein, J. (1985). Confidence limits on phylogenies: an approach using the bootstrap. *Evolution*, 39(4), 783–791.

Flynn, L. J. (1982). Systematic revision of Siwalik Rhizomyidae (Rodentia). *Geobios*, 15, 327–389.

Flynn, L. J. (1983). Sur l âge de la faune de Vertébrès du bassin de Bamian, Afghanistan. *C. R. Acad. Sci.* II 297, 687–690.

Flynn, L. J. (1990). The natural history of rhizomyid rodents. In E. Nevo & O. A. Reig (Eds.), *Evolution of Subterranean Mammals at the Organismal and Molecular Levels* (pp. 155–183). A. R. Liss, New York, NY.

Flynn, L. J., Heintz, E., Sen, S., & Brunet, M. (1983). A new Pliocene tachyoryctine (Rhizomyidae, Rodentia) from Lataband, Sarobi Basin, Afghanistan. *Proc. Kon. Ned. Akad. Wetensch*. B 86, 61–68.

Flynn, L. J., Sahni, A., Jaeger, J.J., Singh, B., & Bhatia, S.B. (1990). Additional fossil rodents from the Siwalik Beds of India. *Proc. Kon. Ned. Akad. Wetensch*., 93, 7–20.

Flynn, L. J. & Jacobs, L. L. (1999). Late Miocene small-mammal faunal dynamics: the crossroads of the Arabian Peninsula. In P. J. Whybrow & A. Hill (Eds.), *Fossil vertebrates of Arabia* (pp. 410–419). New Haven: Yale University Press, New Haven.

Flynn, L. J., Kimura, Y., & Jacobs, L. L. (2020). The murine cradle. In G. V. R. Prasad & R. Patnaik (Eds.), *Biological Consequences of Plate Tectonics: New Perspectives on Post-Gondwanaland Break-Up* (pp. 347–362). Springer.

Gogolevskaya, I. K., Veniaminova, N. A., & Kramerov, D. A. (2010). Nucleotide sequences of B1 SINE and 4.5SI RNA support a close relationship of zokors to blind mole rats (Spalacinae) and bamboo rats (Rhizomyinae). *Gene*, 460, 30–38.

Gupta, S. S., Verma, B. C., & Tewari, A. P. (1978). A new fossil rodent *Rhizomyoides saketiensis* sp. nov. from the Tatrot member (Astian) of Siwalik fossil park, Saketi, Sirmur distt, Himachal Pradesh. *J. Paleontol. Soc. India* 21/22, 112–115.

Hinton, M. A. C. (1933). Diagnoses of new genera and species of rodents from Indian Tertiary deposits. *Annals and Magazine of Natural History*, 12(72), 620–622.

Jacobs, L. L. (1978). Fossil rodents (Rhizomyidae and Muridae) from Neogene Siwalk deposits, Pakistan. *Museum of Northern Arizona*, 52, 1–103.

Jacobs, L. L, Flynn, L. J., & Downs, W. R. (1989). Neogene rodents of Southern Asia. In C. C. Black & M. R. Dawson (Eds.), *Papers on Fossil Rodents in Honour of Albert Elmer Wood* (pp. 157–177). Science Series 33, Natural History Museum of Los Angeles County.

Jacobs, L. L., Flynn, L. J., Downs, W. R., & Barry, J. C. (1990). Quo vadis, Antemus? The Siwalik muroid record. In E. H. Lindsay, V. Fahlbusch, & P. Mein (Eds.), *European Neogene Mammal Chronology* (pp. 573–586). Plenum Press, New York, NY.

Kimura, Y., Jacobs, L. L., & Flynn, L. J. (2013). Lineage-specific responses of tooth shape in murine rodents (Murinae, Rodentia) to late Miocene dietary change in the Siwaliks of Pakistan. *PlOS ONE*, 8(10), e76070.

Kimura, Y., Flynn, L. J., & Jacobs, L. L. (2017). Early Late Miocene Murine Rodents from the Upper Part of the Nagri Formation, Siwalik Group, Pakistan, with a new fossil calibration point for the Tribe Apodemurini (*Apodemus*/*Tokudaia*). *Fossil Imprint*, 73(1–2), 197–212.

Kimura, Y., Flynn, L. J., & Jacobs, L. L. (2021). Tempo and mode: evidence on a protracted split from a dense fossil record: *Frontiers in Ecology and Evolution*, v. 9, 642814. doi: 10.3389/fevo.2021.642814

Lang, J. & Lavocat, R. (1968). Première découverte d une faune de vertébrès dans le Tertiaire d'Afghanistan et datation de la série de Bamian. *C. R. Acad. Sci*., Sér. D 266, 79–82.

López Antoñanzas, R. & Wesselman, H. B. (2013). *Tachyoryctes makooka* (Tachyoryctini, Spalacidae, Rodentia) and its bearing on the phylogeny of the Tachyoryctini. *Palaeontology*, 56(1), 157–166.

López Antoñanzas, R., Flynn, L. J., & Knoll, F. (2013). A comprehensive phylogeny of extinct and extant Rhizomyinae (Rodentia): evidence for multiple intercontinental dispersals. *Cladistics*, 29, 247–273.

López Antoñanzas, R., Knoll, F., Wan, S., & Flynn, L. (2015). Causal evidence between monsoon and evolution of rhizomyine rodents. *Scientific Reports*, 5, 9008.

Lydekker, R. (1884). Rodents and new ruminants from the Siwaliks, and synopsis of Mammalia. *Palaeontol. Indica*, 10, 105–134.

Maddison, W. P. & Maddison, D. R. (2009). Mesquite: A Modular System for Evolutionary Analysis, *ver. 2.6. Mesquite Project*, Vancouver.

Patnaik, R. (2001). Late Pliocene micromammals from Tatrot Formation (Upper Siwaliks) exposed near Village Saketi, Himachal Pradesh, India. *Palaeontographica.*, 261, 55–81.

Patnaik, R. (2003). Tooth enamel microstructure in some fossil gerbillids and rhizomyids from India: functional and taxonomic significance. *Archives of Comparative Biology of Tooth Enamel*., 8, 59–66.

Patnaik, R. (2020). New Data on the Siwalik Murines, Rhizomyines and

Ctenodactylines (Rodentia) from the Indian Subcontinent In G. V. R Prasad & R. Patnaik (Eds.), *Biological consequences of plate tectonics: New perspectives on post Gondwana break-up.* Vertebrate Palaeontology and Paleoanthropology Series, Springer, New York.

Swofford, D. L. (2002). PAUP: phylogenetic analysis using parsimony, *ver, 4.0 b10.* Vancouver.

Tandon, S. K., Kumar, R., Koyama, M., & Niitsuma, N. 1984. Magnetic polarity stratigraphy of the Upper Siwalik Subgroup, east of Chandigarh, Punjab Sub-Himalaya, India. *J Geol Soc India*, 25, 45–55.

Vasishat, R. N. (1985). *Antecedents of Early Man in Northwestern India: Paleontological and Paleoecological Evidences.* Inter-India Publications, New Delhi. 230 pp.

WINDOWS INTO SAUROPSID AND SYNAPSID EVOLUTION
Essays in honor of Prof. Louis L. Jacobs, pp. 306–331, 2023

LATE MIOCENE AND EARLY PLIOCENE RODENTS FROM THE TUGEN HILLS, WESTERN KENYA

ALISA J. WINKLER*

Roy M. Huffington Department of Earth Sciences, Southern Methodist University, Dallas, Texas, 75275, U.S.A, awinkler@smu.edu;
Department of Surgery, University of Texas Southwestern Medical Center, Dallas, Texas, 75390, U.S.A.

ABSTRACT Neogene deposits in the Tugen Hills, Kenya, have yielded a minimum of four genera of rodents from the late Miocene (Kapcheberek locality, 5.9-5.7 Ma) and eight genera from the early Pliocene (Tabarin locality, 4.5-4.4 Ma). These faunas are significant in including some of the earliest fossil records of several extant African rodent genera including the sciurid *Paraxerus* (4.5-4.4 Ma), and the murines *Arvicanthis* (5.9-5.7 Ma) and either *Grammomys* or *Thallomys* (4.5-4.4 Ma). If a specimen of cf. *Heliosciurus* from Tabarin is indeed referrable to that genus, then it would be the earliest record of this exclusively sub-Saharan African squirrel. If cf. *Mus* from Tabarin is referrable to that genus, then it is one of the earlier records of *Mus* in Africa. Assignment of the Tabarin murine *Saidomys* to the same species as that from the Manonga Valley, Tanzania, further supports affinities of these two faunas. The rodent sample from the Kapcheberek locality is very small, but the affinities of modern analogues are supportive of a savanna habitat. Rodents from the Tabarin locality suggest a woodland environment.

KEYWORDS Rodentia, late Miocene, early Pliocene, Systematics, Kenya

INTRODUCTION

Fossil vertebrates were first reported from the Tugen Hills, Baringo Basin, Kenya, by Fuchs (1950). Since then, the area has yielded fossiliferous deposits dating from 15.5 Ma to <200 ka (summarized in Hill, 1999, 2002). The area has received considerable attention because it has produced abundant fossil remains from a long Neogene stratigraphic sequence that is well calibrated by radiometric and magnetostratigraphic techniques. Hominoids occur sporadically throughout the sequence, including the critical period from the middle Miocene to early Pliocene during which hominids differentiated. Although the Tugen Hills hominoids from this period are well studied (e.g., Pickford et al., 1983; Hill, 1985; Ward & Hill, 1987; Hill et al., 1991; Ward et al., 1999; Senut et al., 2001; Hill et al., 2002; Pickford et al., 2022), other taxa, such as rodents, have received much less attention. Rodents have, however, been recovered from throughout the sequence, from sites dating from 15.5 Ma to less than 1 Ma, and they are numerically abundant and taxonomically diverse (e.g., Winkler, 1990, 1992, 2002; Mein & Pickford, 2006). Through the sequence, rodent faunas show major changes in composition and relative abundance, changes likely reflecting the immigration of new taxa from Eurasia and other parts of Africa, and *in situ* evolution and extinction (Winkler, 1994, 2002). The documentation of faunal change through time in the Tugen Hills sequence, and the development of hypotheses to explain those changes, aids in an understanding of the evolution of the East African fauna, and to a synthesis of the ecological history of East Africa.

The Tugen Hills sequence includes, from oldest to youngest, six major sedimentary units that have produced fossil vertebrates (Hill, 1999, 2002): Muruyur Formation (15.5-15 Ma), Ngorora Formation (13-8.5 Ma), Mpesida Beds (7-6.2 Ma), Lukeino Formation (6.2-5.6 Ma), Chemeron Formation (5.6-1.6 Ma), and Kapthurin Formation (700-<200 ka). Sediments intercalated with volcanic units provide age control through radiometric and magnetostratigraphic methods. Stratigraphy and paleontology of the Tugen Hills section are summarized by Hill (1999, 2002). Prior to studies by Winkler (1990), rodents were reported from the sequence (e.g., Bishop and Pickford, 1975; Pickford, 1978; Jaeger et al., 1985, Flynn et al, 1983, 1985; Hill et al., 1986; McBrearty, 1999, Denys, 1999), but not formally and/or fully studied. Winkler (1992)

*Corresponding author

published on rodents from the Muruyur Formation and named a new rodent from the Chemeron Formation (*Tectonomys africanus*; Winkler, 1997). Mein & Pickford (2006) described an extensive collection of micromammals from several localities (Aragai, Kapsomin, Kapcheberek) sampling the Lukeino Formation that yielded (among other taxonomic groups) 16 species of rodents.

The present paper describes the rodent fauna collected by Winkler (1990) and colleagues (in particular, Louis Jacobs) from the Lukeino (Kapcheberek locality) and Chemeron (Tabarin locality) Formations, primarily in 1987. This paper follows Deino et al. (2002) in considering Tabarin locality BPRP#77 to sample the Chemeron Formation as opposed to the Mabaget Formation. Table 1 presents the composite rodent faunal list from these collections. Figure 1 shows the location of Kapcheberek and Tabarin in the context of some other Baringo localities (e.g., Kipsaramon, Muruyur Beds; Kabarsero, Ngorora Formation). The focus of this paper is on systematics; paleobiogeographic and paleoenvironmental interpretations based on these fossils have been discussed elsewhere (Winkler 1994, 2002). Rodents from the Ngorora Formation will be described in a subsequent paper. The Mpesida Beds have not yet yielded rodents, and those from the Kapthurin Formation have not been formally described (Denys, 1999; McBrearty, 1999).

Table 1. Composite rodent fauna for the Kapcheberek (Lukeino Formation) and Tabarin localities (Chemeron Formation), Tugen Hills, Kenya, based primarily on collections described in this paper

Taxon	Locality	
	Kapcheberek (BPRP#76c)	Tabarin (BPRP#77a except as noted)
Family Sciruidae		
Cf. *Heliosciurus* sp.		X
Paraxerus meini		X
Family Nesomyidae		
Subfamily Dendromurinae		
Dendromus sp.	X	
Steatomys minus sp.	X	
Family Muridae		
Subfamily Deomyinae		
Tectonomys africanus		X
Subfamily Murinae		
Saidomys alisae	X	
Saidomys parvus		X
Arvicanthis sp.	X	
Cf. *Mus* sp.		X
Grammomys or *Thallomys* sp.		X
Family Thryonomyidae		
Thryonomys sp.		X
Family Hystricidae		
Hystrix[a] sp.		X

[a]Specimen from Tabarin sub-locality BPRP#77c

MATERIALS AND METHODS

Rodent remains of the Lukeino Formation were recovered from about 130 kilograms of matrix from the Kapcheberek locality, BPRP#76c (equivalent to Pickford's locality 2/226, in his member B, Pickford, 1975). Matrix was also collected from higher in the Lukeino section (BPRP#76d; likely near Pickford [1975] locality 2/227): that matrix yielded only fragmentary rodent teeth but looked promising. Kapcheberek locality BPRP#76c is dated between 5.9-5.7 Ma (Deino et al., 2002).

Rodents were collected near the top of BPRP#76c in a massive light tan to gray-green fossiliferous muddy fine to very fine-grained sand. This sandy matrix also produced fragments of larger vertebrates (e.g., hippopotamus), gastropods and ostracods. Ostracods were identified by Andrew Cohen and Koen Martens (pers. comm. from A. Cohen, 1988, 1989) as belonging to the genus *Sclerocypris*. This taxon suggests presence of a quiet water, moderate alkalinity lake, in addition to the fluvial input suggested by the sedimentology (see also Pickford, 1975). Pickford (1975) suggested Kapcheberek sampled a lakeshore environment.

Rodents from the Tabarin locality (BPRP#77; near the base of the Chemeron Formation) were recovered from fluvial sediments that have also yielded abundant vertebrate remains. The Tabarin locality can be divided into two main sub-localities, a and b (Mark Monaghan, pers. comm., 1987). Rodents described in this study are from sublocality BPRP#77a. Hystricids have been recovered from outside the main Tabarin area in BPRP#77c (Sagatia locality, 1.5 km south of Tabarin, in the same fossiliferous horizon; Ward & Hill, 1987), and from an undetermined Chemeron locality: those specimens are not described in this paper. Rodents from BPRP#77a were recovered from approximately 48 kilograms

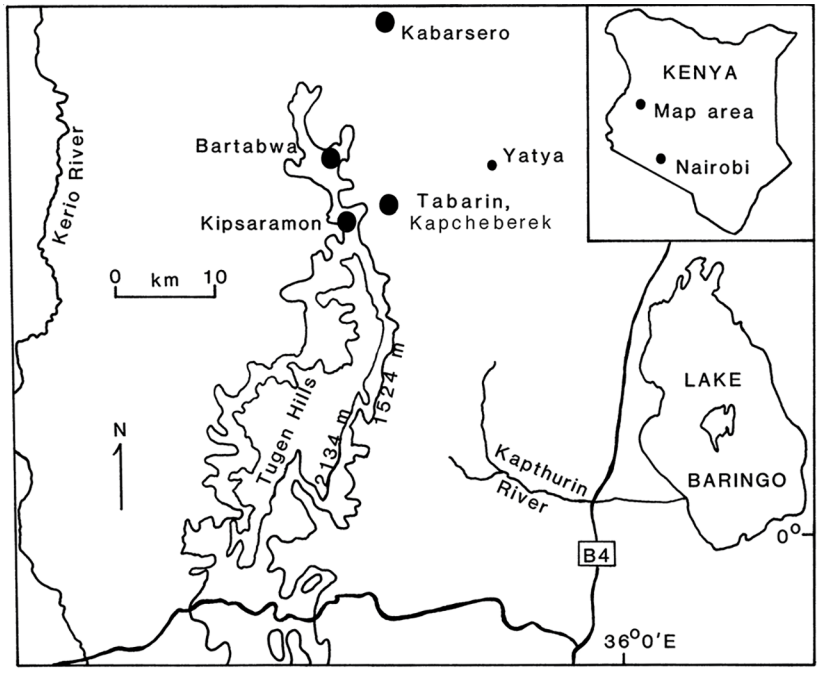

Figure 1. Location map of the Tabarin and Kapcheberek localities in the Tugen Hills, Baringo County, Kenya (after Hill, 1985).

of tan to brown fossiliferous muddy clayball and lithic gravel to very coarse-grained sand. These fluvially derived gravels extend about 181 m along strike. Below them are silts and sands, which overlie a thick tuff. Above the gravels is a brownish orange, organic-rich paleosol. The Tabarin rodents are considered 4.5-4.4 Ma based on dates for a Tabarin hominid (KNM-TH 13150), which was recovered about 10 m below the rodent level (Hill, 1999; Deino et al., 2002).

The fossiliferous matrix was processed by washing through tandem screen boxes. Most of the fine concentrate was further processed using heavy liquids (sodium polytungstate).

Most recovered specimens are isolated teeth; jaws, maxillary fragments, and post-crania are rare. Fossil teeth were measured using a microscope fitted with a reticule. Accuracy of measurement averages +/− 0.04 mm. Measurements record maximum occlusal length and width unless otherwise specified.

Fossils from the Tugen Hills were cataloged into collections at the Nairobi National Museum, Nairobi, Kenya. Casts are deposited at the Nairobi National Museum and at the Shuler Museum of Paleontology, Roy M. Huffington Department of Earth Sciences, Southern Methodist University, Dallas, Texas.

Institutional Abbreviations — **BPRP**, Baringo Paleontological Research Project; **KNM-**Nairobi National Museum collections, Nairobi, Kenya; **KNM-BC**, Baringo Basin, Chemeron Formation localities; **KNM-LT**, Lothagam localities, Kenya; **KNM-LU**, Baringo Basin, Lukeino Formation localities; **KNM-TH**, Baringo Basin, Tugen Hills localities; **LAET**, Laetoli, Tanzania, specimens formerly deposited at the Nairobi National Museum, Nairobi, Kenya, but later moved to the National Museum of Tanzania (specimens were studied while housed in Kenya).

Anatomical Abbreviations — **M**, upper molar; **m**, lower molar; **P**, upper premolar; **p**, lower premolar.

SYSTEMATIC PALEONTOLOGY

Lukeino Formation rodents.

The relatively small sample from the Kapcheberek locality yielded a minimum of four taxa of rodents. Two of these are nesomyines, *Dendromus* and *Steatomys*, and two are murines, *Saidomys* and *Arvicanthis*.

Family NESOMYIDAE Forsyth Major, 1897
Subfamily DENDROMURINAE Allen, 1939
Genus *DENDROMUS* A. Smith, 1829
DENDROMUS sp.
(Fig. 3A)

Referred material — Left M1, KNM-TH 19464, from the Kapcheberek locality, BPRP#76c, Lukeino Formation.

Description — Measurements are given in Table 2. Tooth terminology used here refers to two different systems: see Fig. 2 and Denys & Winkler (2015). This tiny tooth is longer than wide and heavily worn. There is a distinct low median anterior cusp nestled between the labial and lingual anterocones. The latter two cusps are roughly similar in size with the labial anterocone slightly larger and extending slightly further posteriorly than the lingual lobe. The protocone (t5) is the largest cusp; wear has caused it to contact both the lingual anterocone and the enterostyle (t4). The paracone (t6) is displaced posteriorly relative to the protocone. There is a large labiolingually compressed enterostyle (t4) posterolingual to the protocone. There is a short crest connecting the paracone and metacone (t9) and a shorter indistinct crest connecting the protocone and hypocone. A protoloph joins the protocone and paracone, and a metaloph joins the metacone and hypocone. A well-developed posterior cingulum is present, connecting the two posterior-most cusps. The tooth has three large roots: anterior, lingual, and posterior. Presence or absence of a labial rootlet is indeterminate.

Discussion — KNM-TH 19464 was mentioned by Mein and Pickford (2006) in association with two other specimens of *Dendromus* (an M1 and m1) recovered from their Kapsomin locality, Lukeino Formation. It is difficult to make detailed comparisons of the Kapsomin and Kapcheberek teeth based on the published image in Mein & Pickford (2006: Plate 1, 20), but the hypocone (t8) of the Kapsomin tooth appears proportionally larger relative to the metacone (t9), compared to their relationship on the Kapcheberek tooth. The Kapsomin tooth is slightly larger (1.54×0.91 mm) than that from Kapcheberek (1.46×0.81 mm). With such a small sample, the significance, if any, of those differences is unknown (for example, see the variability noted by Denys [1994] in size and morphology of fossil and extant *Dendromus*).

Dendromus is currently a widely distributed taxon in sub-Saharan Africa (e.g., Musser & Carleton, 2005; Voelker et al,

Table 2. Occlusal measurements (in mm) of Dendromurinae from the Kapcheberek and Kapsomin localities, Lukeino Formation, Kenya, and comparative fossil and extant taxa.

Taxon	Locality	Tooth position	N	Length	Width	M1 L/W
Dendromus sp.	Kapcheberek	LM1	1	1.46	0.81	1.80
Dendromus[a] sp. nov.	Kapsomin	LM1	1	1.54	0.91	
Dendromus sp.	Laetoli	LM1	1	1.92	1.13	1.70
D. mesomelas	Kenya	M1	5	1.81-2.35	1.01-1.19	1.74-2.01
D. mystacalis	Kenya	M1	2	1.93-2.00	0.96-1.04	1.92-2.01
D. melanotis	southern Africa	M1	11	1.61-1.82	0.92-1.05	1.60-1.90 X=1.75
S. minus	Kapcheberek	Lm1	1	1.71	1.08	-
S. minus[a]	Kapsomin?	m1	9 length 8 width	1.62-1.82 X=1.69	1.00-1.17 X=1.17	-
"K. minus"[b]	Ch'orora	m1	22	1.59-1.89 X=1.68	1.04-1.22 X=1.10	-
S. cf. *intermedius*[a]	Kapsomin?	m1	2	1.89-1.97	1.34-1.36	-
S. sp. indet.	Laetoli	Rm1	1	1.54	1.00	
S. minus	Kapcheberek	Rm2	1	1.22	1.12	-
S. minus[a]	Kapsomin?	m2	4	1.27-1.31 X=1.29	1.07-1.18 X=1.12	-
"K. minus"[b]	Ch'orora	m2	11	1.22-1.34 X=1.28	1.10-1.22 X=1.14	-
S. cf. *intermedius*[a]	Kapsomin?	Rm2	1	1.33	1.24	-

[a]Measurements from Mein & Pickford (2006)
[b]Measurements from Geraads (2001)

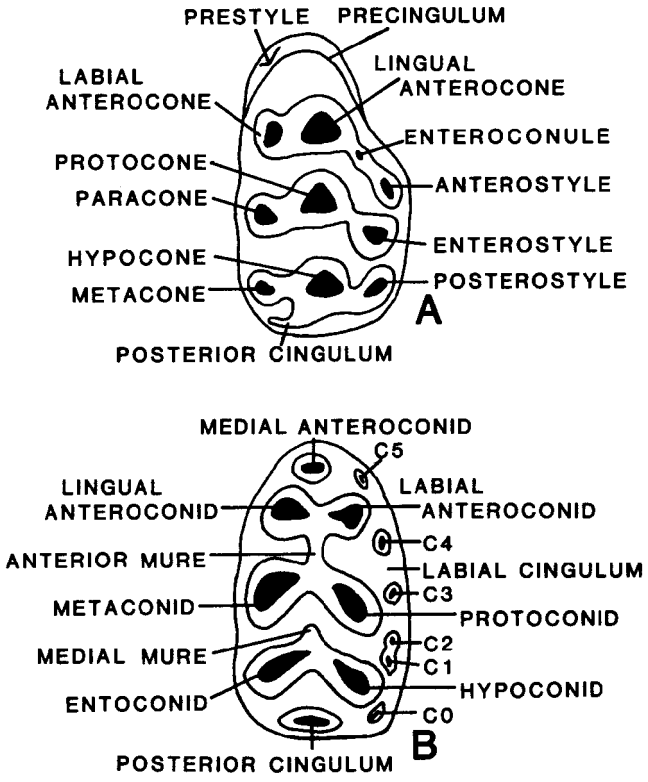

Figure 2. Murid rodent tooth terminology (from Jacobs, 1978) for A) upper right and B) lower right molars.

2021). KNM-TH 19464 was compared with five (*D. lovati*, *D. nyikae*, *D. melanotis*, *D. mesomelas*, and *D. mystacalis*) of the many extant species: it is distinct from these species primarily because the labial cusps are not strongly compressed labial-lingually as are those of the extant taxa. Among those taxa, the fossil *Dendromus* is most similar to *D. melanotis* based on its small size and relatively low length:width ratio (Table 2).

Denys (1987) partially summarizes the fossil record of *Dendromus* in eastern (Laetoli, and Olduvai, Tanzania) and southern Africa (Sterkfontein, Makapansgat, and Langebaanweg, South Africa; Langebaanweg ca. 5.2-5.0 Ma [Denys, 1994], Sterkfontein and Makapansgat date to later in the Pliocene), as well as a late Miocene record from Salobrena, Spain. Other southern African records include Gcwihaba C Hill, Botswana (similar age as Makapansgat based on faunal correlation; Pickford and Mein, 1988), Kromdraai (Pocock, 1987), Taung (Broom, 1948), and Cooper's Cave (1.4 Ma; Linchamps et al., 2023), South Africa. An isolated M2 of a large *Dendromus* is mentioned, but not described (Jaeger & Wesselman, 1976), from the Shungura Formation, lower Omo valley, Ethiopia. However, no dendromurines are reported in Wesselman's (1984) comprehensive study of the Omo micromammals. Mein et al. (2004) further summarized the fossil record of the genus, including reports from Namibia, Abu Dhabi, and Bolt's Farm, South Africa. Geraads (2001) considers two teeth from Ch'orora (8-10 Ma) to be aff. *Dendromus* sp. *Dendromus* is also reported (but not described) from Aramis, Ethiopia (4.4 Ma; Louchart et al., 2009).

Mein & Pickford (2006) briefly made comparisons of the Lukeino material to that of *D. denysae* from the late Miocene of Harasib, Namibia (Mein et al., 2004). A comparison is also made here of KNM-TH 19464 to the description and illustration of a less worn M1 (ARI 129) from Harasib. The teeth are similar overall with the following differences: the Harasib tooth 1) is larger in size (1.78×0.95 mm); 2) has a more distinct crest between t5 (protocone) and t8 (hypocone); 3) has a proportionally larger t8 (hypocone) versus the size of t9 (metacone); and 4) has a posterior cingulum that opens labially (although connection of that crest to t9 in KNM-TH 19464 may be a function of occlusal wear). The measurements in Mein et al. (2004: Table 4) for all remains of *D. denysae* are accidentally a duplication of those for another taxon. Mein & Pickford (2010) report *D.* cf. *denysae* from the late Miocene of Sheikh Abdallah, Egypt. The M1 from that site (n = 3; mean L = 1.75; mean W = 0.97) are also larger than those from Laetoli and they are described as having poorly developed crests between t5 (protocone) and t8 (hypocone) and between t6 (paracone) and t9 (metacone).

Compared to a cast of the M1 of the genus from Laetoli (Denys, 1987) and to observed individuals of some extant species, the Lukeino specimens (and *D. denysae*) lack strongly compressed labial cusps. This character may be primitive for the genus. Denys (1987) lists several characters of the Laetoli M1 to differentiate it from extant *Dendromus* and suggests the Laetoli species may also have characters primitive for the genus. These characters (orientation of the longitudinal groove, compression of the metacone and its connection to the paracone, presence of a crest between the protocone and hypocone, and a small, low, isolated enterostyle) are, however, within the range of variation observed in extant specimens. Measurements of the Laetoli tooth (Denys, 1987:127) are also within the range of variation seen in extant forms (Table 2). Thus, while the less compressed labial cusps of the Lukeino M1s appear primitive for the genus, the Laetoli *Dendromus* appears of more similar

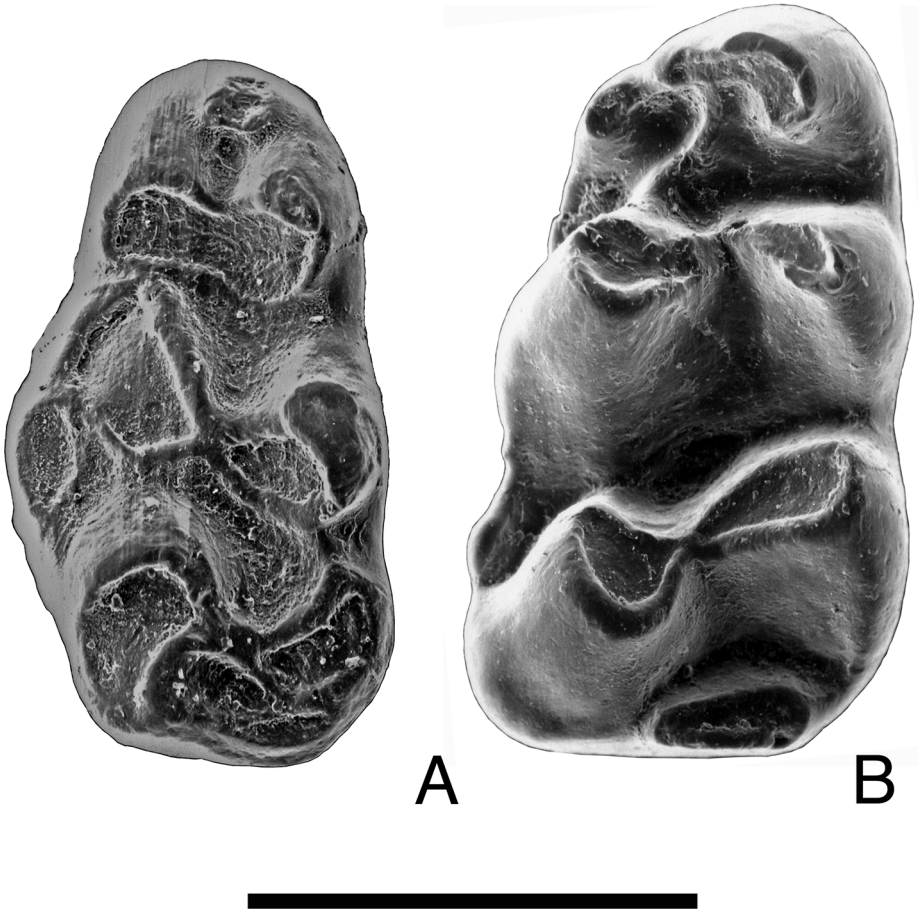

Figure 3. Dendromurine rodents from the Kapcheberek locality, Lukeino Formation, Kenya. A) *Dendromus* sp., left M1, KNM-TH 19464. B) *Steatomys minus*, left m1, KNM-TH 19467. Bar scale is 1 mm.

evolutionary grade as modern *Dendromus* compared to the Lukeino tooth.

Voelker et al. (2021) noted that the extant genus is widely distributed in sub-Saharan African and found in a variety of habitats 'ranging from tall grassland and savannah, to dense scrub, grassy wetlands and subalpine or alpine vegetation" and even Afrotropical lowland forests. *Dendromus melanotis* is found in habitats ranging from dry-grass savannas to montane forests but is most commonly present in fairly open dry savannas (Kingdon, 1974).

Genus *STEATOMYS* Peters, 1846
STEATOMYS MINUS Geraads, 2001
(Fig. 3B)

Referred material — Left m1, KNM-TH 19467; right incomplete m1 (anteroconid through the first row of major cusps), KNM-TH 19461; right incomplete m1 (missing the anteroconid), KNM-TH 19463; right m2, KNM-TH 19441; all from Kapcheberek, BPRP#76c, Lukeino Formation.

Description — Measurements of the complete Lukeino specimen (and the m2, TH-19441) are in Table 2. The m1 has a large medial anteroconid that extends labially as an anterior cingulum that contacts the protoconid. The valley between this cingulum and protoconid is deep. On KNM-TH 19467 (very lightly worn) the anteroconid is weakly bilobed with a larger lingual lobe and a much smaller labial lobe. There is another cuspid lateral to the labial lobe that continues as a cingulum to contact the protoconid. With occlusal wear, these multiple components of the anterior end of the tooth would likely fuse into a single structure. An anterior longitudinal crest (mure) runs obliquely posterolabially to join the labial lobe of the anteroconid with the protoconid. KNM-TH 19461 (more heavily worn) has a single anteroconid

with a long labial cingulum that almost contacts the protoconid. On this specimen a wide median anterior longitudinal crest connects the anteroconid to the first row of major cusps. On both specimens, the first row of major cusps is only slightly oblique: the protoconid is slightly larger in size than the metaconid. The hypoconid and entoconid are large, with the hypoconid conical and the entoconid more transversely elongate. These latter two cusps are aligned obliquely, with the hypoconid posterior. There is a moderately developed ectostylid between the protoconid and hypoconid: this cuspid is indistinct on the more heavily worn KNM-TH 19463. A short indistinct posterior longitudinal crest connects the protoconid and hypoconid on KNM-TH 19467. The posterior cingulum is a well-developed flattened oval located toward the lingual side of the tooth. KNM-TH 19467 has a low weak posterolabial shelf on the hypoconid. This tooth has large anterior and posterior roots.

A slightly worn M2, KNM-TH 19441, is almost square in outline. The protoconid is slightly larger and more rounded than the transversely elongate metaconid. The elongate entoconid and larger and more rounded hypoconid are oriented obliquely, with the entoconid approaching the metaconid. The hypoconid is separated from the protoconid by a deep valley. There is a well-developed anterolabial cingulum; the cingulum originates from the metaconid and extends across the anterior two-thirds of the tooth. A prominent posterior cingulum is located posterolingually. There are large anterior and posterior roots.

Discussion — The Lukeino specimens were compared briefly with dentitions of extant *Steatomys*, including the species *S. pratensis*, *bocagei*, *caurinus*, and *parvus*. Taxonomy of modern *Steatomys* is complex and in need of revision (Coetzee, 1977; Musser & Carleton, 2005). Examination of extant specimens was informative regarding the extent of individual variation, which is important when considering the significance of character differences in small samples of fossil taxa. Characters such as the extent of bilobing of the anteroconid and development of the anterior cingulum of m1 are variable. All extant specimens examined had an ectostylid, and in most it was similar in size to that of KNM-TH 19467. All extant specimens also had a well-developed posterior cingulum on m1. Presence or absence of an anterior longitudinal crest on Recent material was generally indeterminate because *Steatomys* teeth wear quickly; of 17 extant individuals, one had a short anterior longitudinal crest, four probably lacked this crest, and 12 were indeterminate. An anterior longitudinal crest did not contact the protoconid on the extant specimens examined by Denys (1987). Presence of anterior (and posterior) longitudinal crests on KNM-TH 19467 is considered a primitive trait.

Mein & Pickford (2006) considered their sample of *Steatomys* from other localities in the Lukeino Formation to be most comparable to "*Dendromus*" [Gen. nov. "*K*." Winkler] *minus* n. sp. and "*Dendromus*" [Gen. nov. "*K*." Winkler] *intermedias* n. sp. from Ch'orora, Ethiopia (8-10 Ma; Geraads, 2001): they considered these Ch'orora species best referred to *Steatomys*. The Kapcheberek specimens are comparable in size to *S. minus* as recorded by Mein & Pickford (2006) and Geraads (2001) but are smaller than *Steatomys* cf. *intermedius* (Table 2). General morphology also seems comparable to *S. minus*, although the disposition of anterior and posterior longitudinal crests on m1 was unclear from the descriptions and photographs from the larger Lukeino sample examined by Mein & Pickford (2006). All three m1s illustrated by Geraads (2001: Plate 3, figs 14-16) have an anterior longitudinal crest, and one of the three also has a short posterior crest.

Other extinct species of *Steatomys* (*S. harasibensis*, *S. jaegeri*) were described by Mein et al. (2004) from Harasib, Namibia (ca. 10.5-9.5 Ma). Mein & Pickford (2010) also named *S. bartheli*, from Sheikh Abdallah, Egypt (ca. 11 Ma). These authors briefly compared those species to *S. minus*.

The Kapcheberek m1s were compared also with *Steatomys* sp. indet (including a cast of #79/A641.2; Denys, 1987) from Locality 6, Laetolil Beds, Laetoli, Tanzania (and see a measurement in Table 2). The Laetoli m1 is similar in overall morphology although slightly smaller in size than the Kapcheberek m1. Samples from both sites have distinct anterior longitudinal crests ("small distal crest" of Denys, 1987). The Laetoli specimen lacks an ectostylid and a posterior longitudinal crest). Development of the anterior cingulum of the Laetoli specimen is similar to that of KNM-TH 19461. Sample sizes from Kapcheberek and Laetoli are small, and the differences between the two samples may reflect individual or geographic variation and may not be of taxonomic significance.

There is a very small sample of *Steatomys* reported from Kanapoi, but these specimens have not yet been described (4.19 Ma; Manthi & Winkler, 2020). *Steatomys* has been reported from several Plio-Pleistocene sites in South Africa.

Steatomys cf. *S. pratensis* is known from Rodent Cave, Makapansgat Limeworks, and Cave of Hearths (de Graaff, 1960; Pocock, 1987). Pocock (1987) reported *Steatomys* sp. from Kromdraai A and B and from Sterkfontein. Linchamps et al. (2023) recorded *Steatomys* in their sample from Cooper's Cave, South Africa. *Steatomys* sp. or *Malacothrix* sp. is also known from Langebaanweg (ca. 6 Ma; Hendey, 1981), South Africa. Pickford and Mein (1988) reported *Steatomys* cf. *S. opimus* from Gcwihaba C Hill, Botswana.

Steatomys is currently widely distributed in sub-Saharan Africa. It is known from habitats ranging from subdesert to degraded forest or forest edge, but it is most commonly found in savannas (Swanepoel and Schlitter, 1978).

Family MURIDAE Illiger, 1815
Subfamily MURINAE Illiger, 1815
Genus *SAIDOMYS* James and Slaughter, 1974
SAIDOMYS ALISAE Mein & Pickford, 2006
(Fig. 4A)

Referred material — Incomplete right mandible with m1-m3 and the posterior aspect of the incisor, missing the anterior end of the jaw, ascending ramus and coronoid process, KNM-TH 18476; left m1, KNM-TH 19465; both from Kapcheberek, BPRP#76c, Lukeino Formation.

Description — Measurements of the Kapcheberek and Tabarin *Saidomys*, as well as comparative material, are given in Table 3.

The first lower molars have distinct cusps in three separate transverse chevrons separated by wide valleys. The lingual cusps are slightly larger than, and located slightly anterior to, the labial cusps. There is a weakly developed (i.e., in comparison to *Saidomys* from Tabarin) medial anteroconid connected to the lingual anteroconid. A distinct labial cingulum extends from the labial anteroconid to the prominent C1 adjacent to the hypoconid. The cingulum includes C4 attached to the labial anteroconid and a tiny C2 anterior to C1. The posterior cingulum is a distinct midline low flatted oval. KNM-TH 18476 has large anterior and posterior roots: presence or absence of other roots is indeterminate. KNM-TH 19465 has large anterior and posterior roots and a smaller lingual root: presence or absence of a labial root is indeterminate.

The second lower molar is almost square in outline and has two well-separated transverse chevrons. The labial cusps are slightly larger and displaced slightly posterior to the lingual cusps. There is a prominent conical labial anteroconid that has a narrow valley between it and the protoconid. A strong labial cingulum extends from the labial anteroconid to the hypoconid. This cingulum includes small accessory cusps: tiny C4, C2, and C1, and slightly larger C3. C1 is about half the size that it is on the m1s. The elongate posterior cingulum is about 30% wider than it is on the m1 of KNM-TH 18476. There are large anterior and posterior roots.

The third lower molar is triangular in outline with a labial anteroconid that is adjacent to the protoconid and about half the size of the labial anteroconid of m2. An anterior loph is slightly crescentic in orientation: it is formed by fusion of the metaconid and a slightly larger protoconid. There is a large elongate hypoconid that is connected to the metaconid by a very short crest. A very narrow low posterior cingulum is present on the posterolabial aspect of the tooth. There is a large posterior root and likely two large anterior roots.

Discussion — Morphology of the very limited remains of *Saidomys* from Kapcheberek fits well within the diagnosis and description of *S. alisae* from the Kapsomin locality, collected and described by Mein & Pickford (2006; KNM-TH 18476 was included in their "Other material"). The Kapcheberek specimens can be assigned to *S. alisae* based on the following similarities: 1) similar size (see Table 3); 2) m1 with a weak medial anteroconid (=anterior median tubercle) that is connected to the lingual anteroconid, labial cingulum extending from the labial anteroconid to C1 (=posterior accessory cusplet), presence of a distinct posterior cingulum (=posteroconid) developed as a flattened oval (2006: Plate 2, fig. 26); 2) m2 with distinct labial anteroconid, labial cingulum extending from the labial anteroconid to C1, and posterior cingulum larger than on m1; and 3) m3 with a distinct labial anteroconid. The m3 of KNM-TH 18476 lacks a posterior cingulum but does have a weak low stylar shelf on the posterolabial side of the tooth. On the m3 figured by Mein & Pickford (2006: Plate 2, fig. 28), there is a low median shelf on the posterior end of the tooth. Root development cannot be accurately compared for the two samples since the teeth on KNM-TH 18476 are embedded in the bone and TH 19465 lacks roots.

The five generally accepted species of *Saidomys* include: *S. natrunensis* from Wadi el Natrun, Egypt (James & Slaughter, 1974; Slaughter & James, 1979), *S. afarensis* from two localities in the Sidi Hakoma Member, Hadar Formation,

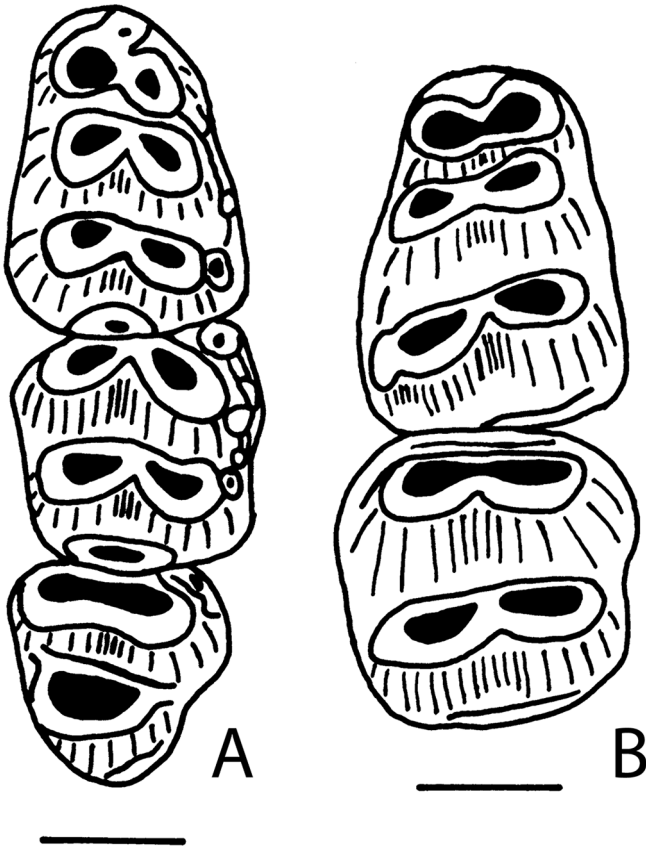

Figure 4. Murine rodents from the Kapcheberek locality, Lukeino Formation, Kenya. A) *Saidomys alisae*, right lower tooth row with m1-m3, KNM-TH 18476. B) *Arvicanthis* sp., left lower tooth row with m1-m2, KNM-TH 19462. Bar scale is 1 mm.

Ethiopia (Sabatier 1982), *S. afghanensis* (Sen 1983), from Pul-e Charkhi and Dawrankhel 14 and 15, Afghanistan, and *S. parvus* from Tanzania (Winkler, 1997). The chronologic range of the genus is from circa 6.5-2 Ma. Mein & Pickford (2006) made comparisons of *S. alisae* with these other species. Winkler (1997) discussed relationships among different species of *Saidomys* with respect to *S. parvus*. Small samples of *Saidomys* have also been reported from Lemudong'o (ca. 6 Ma; Manthi, 2007) and Kanapoi (4.19 Ma; Manthi, 2006; Manthi & Winkler, 2020), Kenya, as well as Aramis, Ethiopia (4.4 Ma; Louchart et al., 2009), but this material has not yet been described.

Genus *ARVICANTHIS* Lesson, 1842

ARVICANTHIS sp.

(Fig. 4B)

Referred material — Left incomplete mandible with m1, m2, the anterior end of the alveolus for m3, and the proximal portion of the coronoid process; KNM-TH 19462, BPRP #76c.

Description — Measurements of the Lukeino *Arvicanthis* and comparative material are given in Table 4. The specimen has wide molars with cusps elongated transversely. Labial and lingual cusps join to form transverse lophs.

The first lower molar has three separate transverse rows of cusps and lacks a medial anteroconid. C1 is present, moderate in size, and fused with the hypoconid. There are indistinct posterolabial spurs off the labial anteroconid and protoconid. A narrow posterior cingulum forms a shelf along the posterior end of the tooth. There is a large anterior root, one or two large posterior roots, and a smaller lingual root under the metaconid. Bulging of the base of the crown under the protoconid suggests a small labial root, but its presence is obscured by bone.

The second lower molar has two transverse chevrons formed by elongate cusps. There is a narrow anterior cingulum and a small labial anteroconid. C1 may be represented by a slight inflection of the enamel on the labial side of the hypoconid. A narrow posterior cingulum extends as a shelf along the posterior border of the tooth. The tooth has two anterior and two posterior roots. Presence of a labial root is obscured by bone.

Discussion — KNM-TH 19462 is assigned to *Arvicanthis* based primarily on the transverse orientation of the major rows of cusps on both m1 and m2, as well as the lack of a medial anteroconid on m1, reduced posterior cingula and poorly developed labial cingula on both teeth, and a reduced labial anteroconid on m2 (Misonne, 1969). Measurements of KNM-TH 19462 are within the size range seen in a small sample of extant *Arvicanthis* (Table 4).

Arvicanthis is presently a widespread and abundant taxon in savanna habitats. It ranges from south of the Sahara (although found along the Nile River) to the southern border of Zambia (Kingdon, 1974; Nowak, 1999; Monadjem et al., 2015). The sample from Lukeino is too small to assign to an extant species but the specimen appears distinct from several extinct taxa.

In East Africa *Arvicanthis primaevus* is known from Olduvai Bed I, Tanzania (Jaeger, 1976). *Arvicanthis primaevus* is diagnosed as smaller in size and having a simpler root

Table 3. Occlusal measurements (in mm) of *Saidomys alisae* from the Kapcheberek and Kapsomin localities, Kenya, and *Saidomys parvus* from the Tabarin locality, Kenya, and the Inolelo 1 locality, Tanzania.

	Length			Width		
Tooth & taxon	N	Mean	Observed range	N	Mean	Observed range
M1						
S. alisae[a]	-	-	-	-	-	-
S. alisae[b]	34	2.62	2.39-3.00	38	1.90	1.76-2.06
S. parvus[c]	4	2.58	2.50-2.65	3	2.04	2.00-2.12
S. parvus[d]	2	-	2.42-2.50	2	-	1.83-1.92
M2						
S. alisae[a]	-	-	-	-	-	-
S. alisae[b]	32	1.83	1.62-2.03	33	1.95	1.84-2.16
S. parvus[c]	2	-	2.06-2.12	2	-	1.88-2.00
S. parvus[d]	5	1.94	1.72-2.16	5	1.97	1.80-2.20
M3						
S. alisae[a]	-	-	-	-	-	-
S. alisae[b]	16	1.64	1.41-1.80	18	1.53	1.38-1.70
S. parvus[c]	1	-	1.88	2	-	1.62-1.65
S. parvus[d]	1	-	2.08	1	-	1.88
m1						
S. alisae[a]	2	-	2.36-2.41	2	-	1.59-1.71
S. alisae[b]	30	2.46	2.30-2.63	31	1.61	1.51-1.73
S. parvus[c]	1	-	2.67	1	-	1.83
S. parvus[d]	3	2.52	2.33-2.67	3	1.73	1.67-1.79
m2						
S. alisae[a]	1	-	1.82	1	-	1.76
S. alisae[b]	38	1.87	1.72-2.15	38	1.81	1.62-1.92
S. parvus[c]	2	-	1.92-2.04	2	-	1.88-2.04
S. parvus[d]	-	-	-	-	-	-
m3						
S. alisae[a]	1	-	1.65	1	-	1.59
S. alisae[b]	24	1.66	1.60-1.81	25	1.58	1.46-1.71
S. parvus[c]	3	-	1.71-1.82	3	-	1.59-1.71
S. parvus[d]	-	-	-	-	-	-

[a]*Saidomys alisae* from the Kapcheberek locality, Kenya
[b]*Saidomys alisae* from the Kapsomin locality, Kenya (Mein & Pickford, 2006)
[c]*Saidomys parvus* from the Tabarin locality, Kenya
[d]*Saidomys parvus* from the Inolelo 1 locality, Tanzania (Winkler, 1997)

pattern than extant *Arvicanthis*. Jaeger considered those characters primitive for the genus. Six specimens assigned to *Arvicanthis* sp. by Black and Krishtalka (1986) from Pleistocene deposits in the Koobi Fora Formation, east Lake Turkana, Kenya, are generally similar to *A. primaevus* in size and overall morphology of the lower teeth.

The Lukeino *Arvicanthis* is distinct from *A. primaevus* because the latter is smaller in size (Table 4), has posterior

cingula as distinct cusps, has less transverse cusps, has a better developed C1 on m2, and eight of the nine m1s have a feeble anterior crest (mure) between the lingual anteroconid and metaconid. Presence of cuspate posterior cingula, an anterior crest on m1, and less transverse cusps, are plesiomorphic characters of *A. primaevus* relative to both the Lukeino specimen and extant *Arvicanthis.*

Arvicanthis sp. indet. is known from two upper molars from the Shungura Formation, Omo River valley, Ethiopia (3.03- >1.87 Ma; Wesselman, 1984). Wesselman (ibid) lists other Plio-Pleistocene reports of *Arvicanthis* from eastern, north, and southern Africa. Specimens from Olduvai Beds II and IV and Peninj (Denys, 1987), Tanzania, and from Garba IV, Ethiopia, are referred to extant taxa.

Jaeger (1975) described a new species, *A. arambourgi*, from Ternifine (middle Pleistocene), Algeria. Although comparable in size to the Lukeino jaw (Table 4), *A. arambourgi* has less transverse cusps, presence of an anterior crest (mure) on 42% (N = 36) of the m1s, and has a small cuspate posterior cingulum on at least one m2 (disposition of the posterior cingula on m1 and other m2s is uncertain).

Jaeger (1975) also named a new extinct subspecies of the extant, *A. niloticus*, from Irhoud Derbala Virage, Morocco, and Aïn Mefta, Algeria (one M1). *Arvicanthis niloticus irhoudae* was diagnosed as being 20% larger than *A. n. testicularis* (an extant subspecies) and having a simpler root pattern on M2 (Jaeger, 1975). He speculated that *A. n. irhoudae* may be ancestral to *A. arambourgi* because the former has a simpler root pattern on M2 and more isolated cusps. The validity of this subspecies needs to be reexamined. *Arvicanthis n. irhoudae* and the Lukeino teeth are overall quite similar. The single specimen (cast) of *A. n. irhoudae* examined differs in having a small medial anteroconid and larger lingual anteroconid on m1, and a better developed labial anteroconid and C1 on m2. An illustration of another m2 (Jaeger, 1975) shows a posterior cingulum developed as a moderate-sized cusp. These differences are likely within the range of individual variation seen in extant *Arvicanthis*. Individual variation in *A. n. irhoudae* is undescribed.

Tchernov (1968) mentioned (but did not describe or illustrate) *Arvicanthis ectos*, an extinct species from the Pleistocene of Israel. Jaeger (1976) stated that the upper toothrow of this species is referable to *Rattus*, but the lower toothrow corresponds to *Arvicanthis*. Size of the lower toothrow is not indicated. The specimen resembles *Arvicanthis* of modern grade based on transverse rows of cusps, lack of a medial anteroconid on m1, reduced labial cingula (only a small C1 on m1, a smaller C1 or just a cingulum on m2), and reduced posterior cingula on both m1 and m2. From occlusal morphology alone, the Israeli and Lukeino dentaries are of similar evolutionary grade, but detailed comparisons await a revision of the Israeli material.

Lavocat (1957, 1967) reported *Arvicanthis* (?) from Sterkfontein, South Africa. If substantiated, this is an important record, as the genus is not currently found in southern Africa (Kingdon, 1974; Nowak, 1999). However, there are no descriptions or illustrations of the specimen(s), and the genus is not included in faunal lists from Sterkfontein in de Graaff (1960) or Pocock (1987).

A partial maxilla, left and right mandibles and fragmentary postcrania of a single individual of an extinct species, *A. musisii,* were reported by Mein (1994) from the lower Pliocene of Uganda. *Arvicanthis musisii* is diagnosed by large size, and (in terms of m1 and m2) having: 1) an m1 with a connection between the lingual anteroconid and the metaconid (lacking in KNM-TH 19462) and a weak posterior cingulum (present as a cusp on *A. musisii* but as a low ridge on KNM-TH 19462); and 2) an m2 lacking a posterior cingular tubercle (an elongate low ridge is present along the posterior margin of the tooth on the drawing of m2 (Mein, 1994: Planche I.B). The m2 of KNM-TH 19462 also has a low posterior cingular ridge, but it is located posterolabially. Other differences (from comparison with the illustrated specimen in Mein [Mein, 1994: Planche I.B] include: on the Ugandan teeth: 1) on m1 anteroconids unequal in size (lingual is larger), while they are comparable in size on KNM-TH 19462; 2) the Ugandan specimen has a weaker C1 on m1; and 3) the m2 of the Ugandan specimen has an anterolabial cusp (only a weak crest on KNM-TH 19462) and a small C1 (absent on KNM-TH 19462). The m1 of *Arvicanthis musisii* is longer than that of KNM-TH 19462, but otherwise the size is comparable.

Manthi (2007) reported 10 dental elements (including upper and lower dentition) from Lemudong'o, Kenya (6 Ma), attributable to *Arvicanthis* sp., plus two assignable to cf. *Arvicanthis*. The remains are not illustrated, described or compared in detail. Manthi does note, however, that the material is comparable in size and morphology to that of extant *A. niloticus* and/or *A. abyssinicus*. Tooth morphology of an illustrated specimen from Lemudong'o, KNM-NK

Table 4. Measurements (in mm) of *Arvicanthis* sp. from the Kapcheberek locality, BPRP#76, Lukeino formation, Kenya, and comparative fossil and extant specimens.

Taxon	Locality	Length m1	Width m1	Length m2	Width m2
Arvicanthis sp.	BPRP#76	2.59	1.94	2.06	2.18
A. *musisii*[a]	Kazinga Channel, Uganda	2.92-2.96 N=2	1.98-2.03 N=2	1.99-2.01 N=2	2.18-2.19 N=2
A. primaevus[b]	Olduvai, Tanzania	2.15-2.33 N=8	1.47-1.65 N=8	1.56-1.63 N=4	1.56-1.65 N=4
A. sp.[c]	Lake Turkana, Kenya	2.21-2.25 N=2	1.47-1.55 N=2	1.47-1.81 N=3	1.50-1.70 N=3
A. arambourgi[d]	Ternifine, Algeria	2.56-2.95 X=2.76 N=36	1.69-2.01 X=1.89 N=36	1.85-2.07 X=1.98 N=31	1.91-2.16 X=2.03 N=31
A niloticus[e]	East & west Africa	2.46-3.00 N=4	1.77-2.25 N=4	1.77-2.00 N=4	1.92-2.58 N=4

[a]Measurements from Mein (1994)
[b]Measurements from Jaeger (1976)
[c]Measurements from Black & Krishtalka (1986)
[d]Measurements from Jaeger (1975)
[e]Extant specimens; specimen labels list them as subspecies *mordax*, *testicularis*, and *abyssinicus*

41089 (m1-m2; Manthi, 2007: fig. 4) is comparable to that of teeth of KNM-TH 19462. However, there are some differences in development of the labial cuspids on the Lukeino m2 (e.g., stronger C1 on KNM-NK 41089 than on that from Lukeino), although that may be attributable to individual variation. Measurements of the Lemudong'o teeth (Manthi, 2007: Table 1) are confusing as they are considerably lower than that for the extant and fossil *Arvicanthis* reported here (Table 4; e.g., m1 of the Lemudong'o averaging 1.7×1.1 mm). *Arvicanthis* is also reported (but not described) from Aramis, Ethiopia (4.4 Ma; Louchart et al., 2009).

In summary, the Lukeino *Arvicanthis* is one of the earlier records of the genus. For its geologic age, it, surprisingly, already possesses many derived characters of the genus such as large size, transverse cusp rows, lack of a medial anteroconid and connections between the anterior two toothrows on m1, posterior cingula developed only on m1 and m2, and reduction of other accessory cuspids. Although the sample size is very small, the Lukeino specimen appears more similar to extant *Arvicanthis* than it does to any adequately described extinct taxon. The possibility that this specimen was contamination from more recent sediments was considered, but its preservation matches that of other rodents from the Kapcheberek locality.

Chemeron Formation rodents.

Matrix from the Tabarin locality yielded a minimum of eight taxa of rodents. These include the sciurids *Heliosciurus* and *Paraxerus*, the deomyine *Tectonomys*, the murines cf. *Mus*, *Grammomys* or *Thallomys* sp., *Saidomys parvus*, and the thryonomyid, *Thryonomys*.

Family SCIURIDAE Hemprich, 1820
Subfamily XERINAE Osborn, 1910
Genus *HELIOSCIURUS* Trouessart, 1880
Cf. *HELIOSCIURUS* sp.
(Fig. 5A)

Referred material — Left p4, KNM-TH 19484, from Tabarin, BPRP#77a, Chemeron Formation.

Description — Occlusal measurements of the Tabarin sciurids are given in Table 5. The tooth is lightly worn and roughly ellipsoidal in outline. A protoconid and hypoconid are well-developed and about equal in height. The metaconid is the tallest cusp on the tooth. There is a distinct anteroconid separated by a sulcus from the protoconid and connected lingually to the metaconid. The protoconid and metaconid are connected by a short metalophid. An indistinct mesoconid is present on the ectolophid between the protoconid and

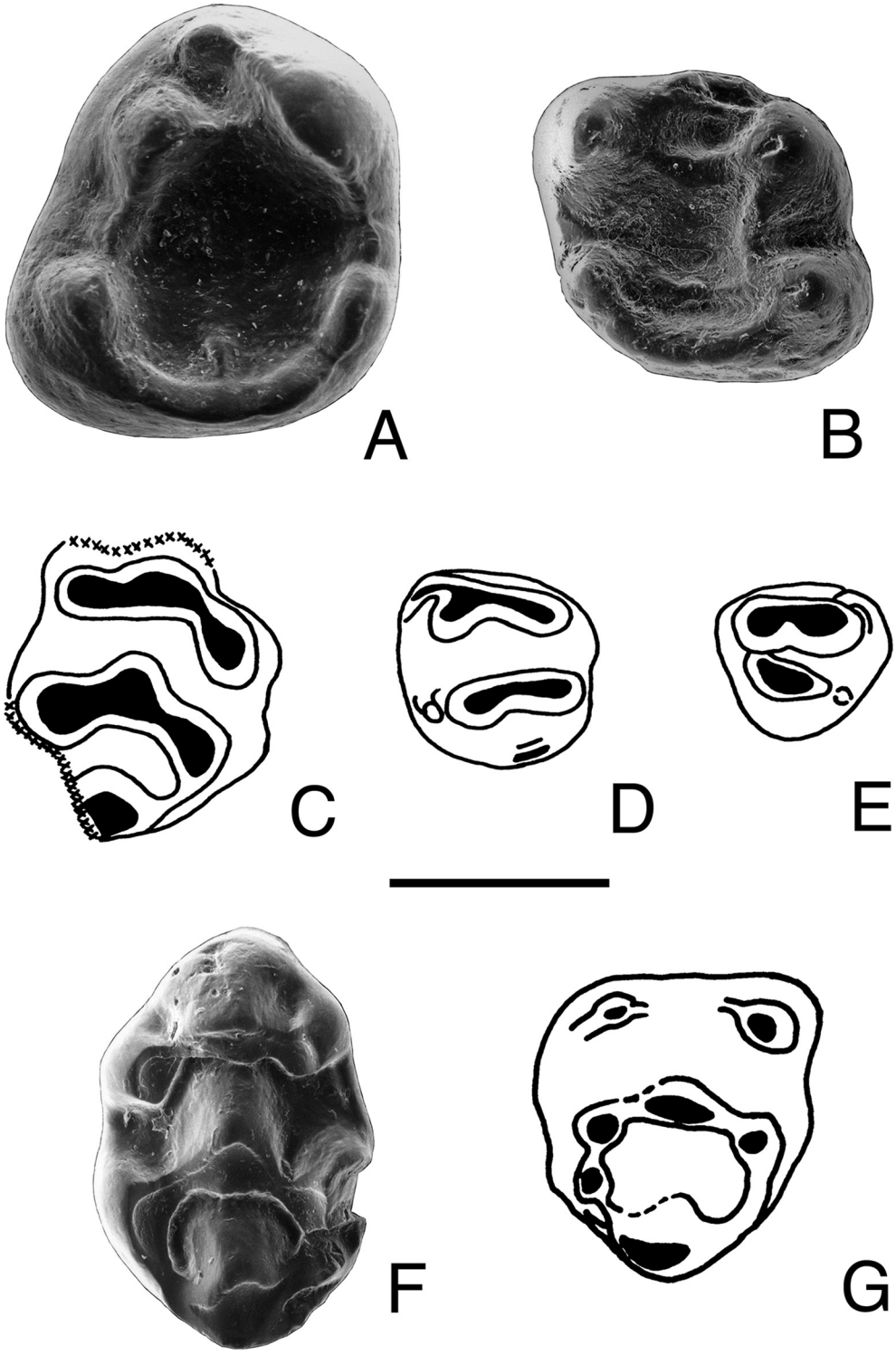

Figure 5. Sciurids (cf. *Heliosciurus*, *Paraxerus meini*), and murines (cf. *Mus*, *Grammomys* or *Thallomys*) from the Tabarin locality, Chemeron Formation, Kenya. A) cf. *Heliosciurus* sp., left p4, KNM-TH 19484. B) *Paraxerus meini*, right m1 or m2, KNM-TH 19473. C-E, cf. *Mus*, C), right M1, KNM-TH 19468, D) left m2, KNM-TH 19475, E) right m3, KNM-TH 19476. *Grammomys* or *Thallomys* sp. F) left M1, KNM-TH 22308, G) right M2, KNM-TH 19478. Bar scale is 1 mm.

Table 5. Occlusal measurements (in mm) of fossil sciurids from the Tabarin locality, Kenya, and comparative fossil and extant taxa.

Taxon	Specimen number	Locality	Tooth position	Length	Width
Cf. *Heliosciurus*	KNM-TH 19484	Tabarin, Kenya	Lp4	2.31	1.85
H. ruwenzorii	-	Extant, Congo	p4	2.00-2.08 N=3 X=2.03	1.71-2.00 N=3 X=1.69
H. gambianus	-	Extant, Congo	p4	1.77	1.69
H. rufobrachium	-	Extant, Ivory Coast	p4	2.15-2.31 N=5 X=2.21	2.15-2.46 N=5 X=2.26
Kubwaxerus pattersoni	KNM-LT 23087	Lothagam, Kenya	Rp4	2.44	2.06
Paraxerus meini	KNM-TH 19473	Tabarin, Kenya	Rm1 or m2	1.64	1.60
P. meini[a]	various	Laetoli, Tanzania	m1	1.67=1.90 N=6 X=1.77	1.57-1.76 N=6 X=1.68
			m2	1.71-1.82 N=5 X=1.75	1.71-1.90 N=5 X=1.80
P. ochraceus[b]	various	Omo, Ethiopia	m1 or m2	1.61-1.86 N=6 X=1.77	1.70-1.97 N=7 X=1.80

[a]Measurements from Denys (2011)
[b]Measurements from Wesselman (1984)

hypoconid. An entoconid is moderately developed and connected to the hypoconid by a posterolophid. A small mesostylid lies between the entoconid and metaconid. There is a weak hypoconulid just labial to the entoconid. The talonid basin is wide and relatively shallow. Short spurs extend toward its center from the metalophid and posterolophid. Root development is indeterminate.

Discussion — Among extant taxa, the Tabarin tooth is most similar to the exclusively African genus *Heliosciurus* (Sun Squirrels). The fossil tooth was compared with three of the six extant forms listed by Thorington & Hoffmann (2005), *Heliosciurus ruwenzorii vulcanius*, *H. gambianus rhodesiae*, and *H. rufobrachium rubricatus*, *coenosus* and *aubryi*. Amtmann (1975) lists 52 subspecies for these and notes that "too many subspecies are certainly recognized" for *H. gambianus* and *H. rufobrachium*. Taxonomy of the genus is extremely complicated, primarily because of the great variability in pelage color reflecting local conditions of temperature and moisture (Rosevear, 1969).

Major differences between the fossil and the extant taxa include: in the extant specimens (1) the distance between the protoconid and hypoconid is greater; (2) the labial side of the tooth between the protoconid and hypoconid slopes labially less steeply, and the ectolophid often has a lingually projecting spur; and (3) in many individuals of *H. gambianus* and some of *H. rufobrachium*, the hypoconid is proportionally larger and extends more labially. The major difference between the fossil and the extant taxa is in the development of the entoconid. The entoconid of the fossil is relatively small, distinct, and anteriorly placed. In the extant specimens of *Heliosciurus* examined, the entoconid is usually larger, less distinct, and extends farther posteriorly. A large and posteriorly placed entoconid, especially associated with a large hypoconid, gives a more triangular outline to many modern specimens. Differences in size between the Tabarin tooth and comparative material are generally one of proportion; the fossil is narrow for its length because of the relatively small hypoconid and entoconid. Root development is indeterminate.

The Tabarin cf. *Heliosciurus* tooth also shows similarities with an extinct giant squirrel, *Kubwaxerus pattersoni*, known

only from the late Miocene (7.44-6.54 Ma), upper member of the Nawata Formation, at Lothagam, Kenya (Cifelli et al., 1986; Winkler, 2003). The Tabarin specimen was compared with casts of two specimens mentioned by Winkler (2003), but not yet described. The two taxa differ in: 1) in KNM-TH 19484 the anteroconid does not contact the protoconid while in *Kubwaxerus pattersoni* the anteroconid is present as an anterior cingulum that contacts the protoconid; 2) the entoconid of KNM-TH 19484 is located relatively more anteriorly; 3) the talonid basin of KNM-TH 19484 is relatively wider; and 4) *Kubwaxerus pattersoni* is larger, with the smaller of two specimens (KNM-LT 23087) 5-10% larger than the Tabarin tooth.

Sun squirrels are exclusively African and are found from the west to east coasts from about 17° N to 20° S Latitude (Rosevear, 1969). Rosevear describes them (in West Africa) as typically inhabiting dense woodland, "fringing forest and remnant patches, as well as of secondary farm regrowth within the high forest zone itself." Amtmann (1975) notes that *H. ruwenzorii* occurs in forests between 1600 to 2400 m, *H. gambianus* in savanna woodland and secondary forest ("more of an open woodland animal," Rosevear, 1969; has a "general but not exclusive preference for drier habitats," Kingdon, 1974), and *H. rufobrachium* in rain forests ("more of a closed forest animal," Rosevear, 1969; it may occupy relatively dry habitats in East Africa according to Kingdon, 1974). The presence of *Heliosciurus* in the Tugen Hills fossil record is consistent with a savanna woodland, woodland, or dense forest habitat.

Genus *PARAXERUS* Forsyth Major, 1893

PARAXERUS MEINI Denys, 2011

(Fig. 5B)

Referred material — Right m1 or m2, KNM-TH 19473, from Tabarin, BPRP#77a, Chemeron Formation.

Description — Based on size comparison with the material from Laetoli, Tanzania (Table 5), KNM-TH 19473 is likely an m2. The Tabarin tooth is essentially square in occlusal outline with transverse crests and bunodont cusps. A ridge with multiple very small supplementary cuspids connects the metaconid to the anteroconid. There is a distinct metalophid, which is slightly concave posteriorly. The ectolophid is also distinct and slightly curved: a mesoconid may be present but is very indistinct. A low transverse entolophid connects the entoconid to the anterior part of the hypoconid. There are a few indistinct supplementary cuspids on the entolophid. There is also a long, posteriorly concave, posterolophid: this lophid lacks any supplementary cusps. Root development is indeterminate.

Discussion — The Tabarin *Paraxerus* is assigned to *P. meini*, described from the Upper Laetolil (3.8-ca.3.4 Ma) and Upper Ndolanya Beds (2.7-2.6 Ma), Laetoli, Tanzania (Denys, 1987 as *Paraxerus* sp. indet.; Denys, 2011). Comparisons of the Tabarin specimen with the Laetoli material were based on two casts (LAET-76, 4170 and 4178) as well as published illustrations and descriptions in Denys (2011). Assignment of the Tabarin tooth to *P. meini* is based on the tooth being of small size with bunodont cusps, presence of supplementary cuspids, a distinct ectolophid and a transverse entolophid directly connected to the anterior part of the hypoconid. In contrast to the Laetoli specimens, TH 19473 lacks supplementary cusps on the posterolophid. The ectolophid of the Laetoli material is described as longitudinal, but it is curved on at least one specimen (LAET 76-4178), comparable to the curvature seen on the Tabarin tooth. Denys noted the presence of a mesoconid on the ectolophid: on the two casts, the cusp appears to be lacking on the m1s, but is present on an m2. Wesselman (1984) described multiple isolated teeth of *P. ochraceus* (an extant species) from the Shungura Formation, Omo River Valley (Members B, C; 3.03-2.08 Ma) of Ethiopia. He noted the specimens from Omo were generally similar to those from Laetoli, except for some differences in tooth size. Denys (2011) also noted that the Omo material was quite similar in morphology to *P. meini* from Laetoli.

Early records of *Paraxerus* are from Lemudong'o, Kenya (Manthi, 2007; ca. 6 Ma) and Kanapoi, Kenya (Manthi, 2006; Manthi & Winkler, 2020; 4.19 Ma). The Lemudong'o record is a single isolated Lp4 (KNM-NK 44920). Based on the published image (Manthi, 2007: Fig. 10), and as noted by Denys (2011), the tooth lacks an ectolophid, a characteristic feature of the genus. The specimen also does not appear to have an entolophid. The Lemudong'o tooth does have similarities to the other sciurid from Tabarin, KNM-TH 19484: comparable small size, protoconid and metaconid close with an anteroconid between them, wide talonid basin, and relatively anterior entoconid. For now, it is recommended that the Lemudong'o tooth be re-examined before being definitively assigned to *Paraxerus*. Manthi (2006) reported a mandible (KNM-KP 46313) from Kanapoi as *Paraxerus*.

However, Manthi and Winkler (2020) consider all sciurids from Kanapoi to pertain to *Xerus*. Pending assignment of the Lemudong'o specimen, the Tabarin *Paraxerus* would be the oldest record of the genus from Africa.

Paraxerus, the African Bush Squirrel, is found exclusively in Africa. Thorington and Hoffman (2005) include 11 species in the genus. *Paraxerus ochraceus* is the only species currently found in the study area. It includes five (Kingdon, 1974) to eight (Amtmann, 1975) subspecies, which occur in a wide variety of wooded habitats. Nowak (1999: 1279) notes that the genus *Paraxerus* is currently "found in forests, plantations, and other areas where there are trees."

Family MURIDAE Illiger, 1815
Subfamily DEOMYINAE Lyddeker, 1889
Genus *TECTONOMYS* Winkler, 1997
TECTONOMYS AFRICANUS Winkler, 1997

Referred material — Right M1, KNM-TH 18477, holotype, from Tabarin, BPRP#77a, Chemeron Formation.

Description — The tooth (figured in Winkler, 1997: Fig. 4A; Winkler, 2002: Fig. 2c; Denys & Winkler, 2015: Fig. 7.3) is relatively elongate. Cusps in the longitudinal midline (lingual anterocone, protocone, and hypocone) are the largest. An anterostyle is slightly displaced posteriorly relative to the rest of the anterior chevron and is strongly compressed labio-lingually. The large lingual anterocone is situated transverse to the smaller labial anterocone. Projecting posterolabially from the labial anterocone is an elongate spur. A precingulum and stylar cusps are lacking. Cusps of the middle chevron are transverse with the paracone and enterostyle only slightly posterior to the protocone. The enterostyle is slightly oblique to the protocone and paracone. The paracone and enterostyle are rounded and similar in size. The posterior chevron includes a transversely elongate hypocone and a smaller more rounded metacone. These two cusps are at the same transverse level. The hypocone is lingual relative to the median location of the lingual anterocone and protocone. A posterostyle is lacking. The posterior cingulum is well developed, semi-lunar in shape, and posteriorly connects the hypocone to the metacone, enclosing an ellipsoidal basin. Chevrons of the tooth are separated by deep transverse valleys and the cusps of each chevron are separated by shallow wide valleys. There are three large roots: anterior, posterior, and lingual.

Discussion — *Tectonomys africanus* is based on a holotype from Tabarin and a hypodigm of two M1s and seven M2s from Inolelo 1, Ibole Member, Manonga Valley, Tanzania (Winkler, 1997). The Manonga Valley specimens date to the late Miocene or early Pliocene (ca. 6-4 Ma) based on overall faunal correlation, or to the early Pliocene using only the rodents. Teeth of *Tectonomys* are large, brachydont, and relatively elongate. The M1 is characterized by a posteriorly displaced anterostyle, cusps in the middle chevron oriented transverse to one another, an elongate lingually placed hypocone at the same transverse level as the metacone, a very strong posterior cingulum, and three roots. The phylogenetic relationships of *Tectonomys* were discussed in Winkler (1997) and Denys & Winkler (2015). *Tectonomys* was originally considered within Murinae (Winkler, 1990, 1997) but placed later within Deomyinae (Winkler, Denys & Avery, 2010; Denys & Winkler, 2015).

Subfamily MURINAE Illiger, 1815
Genus *MUS* Linneaus, 1758
cf. *MUS* sp.
(Fig. 5)

Referred material — Right incomplete M1, KNM-TH 19468 (width ~1.06 mm); left m2, KNM-TH 19475 (1.02× 1.00 mm); right m3, KNM-TH 19476 (0.94×0.72 mm). All from Tabarin, BPRP#KO77a, Chemeron Formation.

Description — These teeth are small and brachydont. The M1 (Fig. 5C) is missing the anterior end of the tooth and the posterolabial corner including the metacone and part of the hypocone. An anterior chevron consists of a smaller labial anterocone closely opposed to and transversely aligned with a larger lingual anterocone. The anterostyle is lightly compressed and is displaced posteriorly at about 70^{o} to the rest of the chevron. The middle chevron has a large protocone, and a paracone and enterostyle that are roughly similar in size and only slightly smaller than the protocone. The enterostyle is not compressed: it is displaced posteriorly relative to the rest of the chevron. The anterostyle and enterostyle are notably less compressed labiolingually compared to the condition observed in *Acomys*. There is a large inflated hypocone with the enamel on its lingual side thickened slightly. A short indistinct crest connects the hypocone to the enterostyle. A posterostyle is lacking. Presence of a posterior cingulum and the number of roots is indeterminate.

The m2 (Fig. 5D) is trapezoidal in shape and tapers posteriorly. There are two lophs formed by the protoconid and metaconid anteriorly, and the hypoconid and entoconid posteriorly. The major labial cusps are slightly larger than, and located a little posterior to, the major lingual cusps. An anterolabial cusp is elongate and connected by wear to the protoconid. This cusp is considerable smaller than that seen in *Acomys*. There is a labial cingulum between the protoconid and hypoconid which includes a small C1 adjacent to the hypoconid. The posterior cingulum is low and elongate connecting the posterior two cusps and enclosing a circular basin. There are large anterior and posterior roots.

An m3 (Fig. 5E) is triangular with the apex posterior. The larger protoconid and smaller metaconid are fused through wear to form a transverse loph. There is a low, moderately developed anterolabial cingulum. The hypoconid is large with its lingual side tilted anteriorly. A weak indentation on its anterior side demarcates an indistinct entoconid that is fused to the hypoconid. C1 is low, indistinct, and adjacent to the hypoconid. A large posterior root and one or two anterior roots are present.

Discussion — These specimens are similar to *Mus* in their small size, presence of a posteriorly displaced anterostyle and enterostyle on M1, and a strongly trapezoidal outline to m2. In extant *Mus*, however, the anterostyle tends to be more compressed labiolingually and the m3 tends to be more reduced in length relative to m2. The oldest known African records of *Mus* are from Lissasfsa, Morocco (Mio-Pliocene: Geraads, 1998), and Aramis, Ethiopia (Louchart et al., 2009). The large sample from Lissasfsa (around 150 teeth) was assigned to a new extinct species, *M. ique*. Compared to the very small sample from Tabarin, the m2 and m3 of *M. ique* (the Tabarin M1 is quite incomplete) are smaller, and from the photographs (Geraads, 1998: Fig. 12.4, 7, 8), the lophs on m2 are more oblique and there is a distinct posterior cingulum, and the m3 is proportionally longer. The Aramis material has not yet been described.

Some other African fossil records of *Mus* are from just over 3 Ma at Hadar (Sabarier, 1982) and the Omo Valley (Wesselman, 1984), Ethiopia, as well as the Plio-Pleistocene of the Maghreb, North Africa (e.g., Jaeger, 1975). Wesselman (1984) summarizes other fossil African records of *Mus*.

Presence of an anterolabial cingulum (or labial anteroconid) on the Tabarin m3 is a primitive character seen in the extinct genus *Progonomys* (a sister taxon to *Mus*) and at least some fossil *Mus* (i.e., *Mus auctor* from Pakistan [5.7 Ma, Jacobs, 1978], and some *Mus petteri* from Olduvai, Tanzania [Jaeger, 1978]). Development of this cingulum on *M. ique* is uncertain (likely very small or lacking). There are no m3s of the *Mus* from Hadar or Omo. The anterolabial cingulum is lacking in extant *Mus*. It is observed on some *Acomys* (pers. comm. C. Denys).

Genus *GRAMMOMYS* Thomas, 1915 or *THALLOMYS* Thomas, 1920

GRAMMOMYS or *THALLOMYS* sp.

(Fig. 5)

Referred material — Left M1, KNM-TH 22308 and right M2, KNM-TH 19478; both from BPRP#77a.

Description — Measurements of the Tabarin specimens and comparative material are given in Table 6. The first upper molar (Fig. 5F) is rounded in occlusal outline and has distinct cusps. The midline cusps (lingual anterocone, protocone, and hypocone) are the largest. The anterior chevron has conical cusps. The labial anterocone is relatively small and located close to the lingual anterocone. The anterostyle is slightly larger than the labial anterocone and is posterior to the rest of the chevron. A precingulum and prestyles are lacking. The middle chevron is slightly concave posteriorly. A rounded paracone (broken) is slightly posterior to the protocone. The enterostyle is similar in size to the paracone but is less rounded and located more posteriorly. The paracone and enterostyle are separated from the protocone by short crests. The posterior chevron includes a very large conical hypocone and smaller conical metacone (broken) situated anterolabially. The metacone is connected to the paracone and hypocone by short crests. The posterostyle is reduced to a long crest connecting the hypocone to the enterostyle. There is a weak posterior cingulum. There are large anterior and posterolabial roots, two closely spaced lingual roots (the most anterior is the larger), and a smaller labial root.

The second upper molar (Fig. 5G) is wide anteriorly and tapers posteriorly. There is a large conical anterostyle and a much smaller labial anterocone. The labial anterocone is joined to the protocone by a very low crest. The large protocone is connected to a smaller paracone and enterostyle by short crests. The latter two cusps are conical and located slightly posterior (especially the enterostyle) to the protocone. A

Table 6. Measurements (in mm) of *Grammomys* or *Thallomys* sp. from Tabarin, Kenya, as well as representative fossil and extant taxa.

Taxon	Locality	Length M1	Width M1	Length M2	Length M2
Grammomys or *Thallomys* sp.	Tabarin, Kenya	1.92	1.33	1.43	1.36
Grammomys dolichourus[a]	various	1.81-2.27 X=2.03 N=14	1.22-1.50 X=1.38 N=14	1.26-1.65 X=1.43 N=15	1.22-1.50 X=1.36 N=15
Grammomys cometes	Various (N=5)	1.89-2.31 X=2.13	1.36-1.52 X=1.44	1.43-1.62 X=1.50	1.39-1.50 X=1.44
Thallomys loringi	Various (N=7)	2.28-2.56 X=2.45	1.61-1.71 X=1.66	1.61-1.89 X=1.79	1.57-1.73 X=1.68
Thallomys quadrilobatus[b]	Olduvai, Tanzania	2.23-2.59 X=2.41 N=16	1.58-1.78 X=1.67 N=16	1.52-1.75 X=1.62 N=8	1.53-1.72 X=1.63 N=8
Thallomys jaegeri[c]	Omo, Ethiopia	2.06-2.08 N=2	1.35-1.38 N=2	1.46-1.54 N=4	1.34-1.40 N=4
Thallomys laetolilensis[d]	Laetoli, Tanzania	2.05-2.42 X=2.18 N=11	1.40-1.67 N=1.54 N=13	1.55-1.68 N=1.61 N=7	1.50-1.62 N=1.57 N=6

[a]Includes *G. dolichourus discolor*, *G. d. lutosus*, and *G. d. polionops*
[b]Measurements from Jaeger (1976)
[c]Measurements from Wesselman (1984)
[d]Measurements from Denys (1987)

short crest extends between the very large hypocone and smaller, conical, more anteriorly placed metacone. A short crest connects the metacone to the paracone. The posterostyle is represented by a long crest connecting the hypocone to the enterostyle. A weak posterior cingulum is present. The root pattern is indeterminate.

Discussion — One of the most distinctive characters of KNM-TH 18481 and 19478 is presence of a strong ridge connecting the hypocone to the enterostyle, which represents the posterostyle. This (along with overall morphology including stephanodonty between the middle and posterior chevrons, a weak posterior cingulum, and five roots on M1) is consistent with assignment to one of two extant genera, *Grammomys* or *Thallomys* (Davis, 1972; Misonne, 1974). The strength of the connection between the enterostyle and hypocone is more like *Grammomys*, but within the range of individual variation in *Thallomys*. The fossils are excluded from *Thamnomys* because that taxon has a distinct posterostyle and a reduced metacone (Davis, 1972; Misonne, 1974).

The Tabarin teeth were compared with two species (four subspecies) of extant *Grammomys* and with one species of *Thallomys* (sensu Misonne, 1974). From comparison of occlusal and root morphology of M1 and M2, and from published descriptions of the two genera [which state that they differ in pelage, bullae, and development of the anteroconid on m1 (Misonne, 1974)], the fossils cannot be confidently assigned to one genus or the other. The M1 and M2 of comparative specimens of *Thallomys* are longer and wider than those of *Grammomys* (and larger than the fossils; Table 6), but this difference by itself is not enough to warrant generic distinction of the fossils. Extant comparative specimens of *Thallomys* and *Grammomys* have similar length:width ratios for M1 and M2 (1.48 for M1 and 1.04-1.06 for M2). Another Tabarin M1 is proportionally wider (L/W for M1 = 1.36) compared to the extant specimens, but the significance of this is uncertain. The Tabarin teeth differ from extant taxa in that the ridge connecting the hypocone and metacone on both the fossil M1 and M2 is short. This ridge is appreciably longer on 93% (N = 20) of the M2s of extant *Grammomys*. Ridge length is similar (50%) or longer (50%) on the M1s of *Grammomys* and on M1s and M2s of *Thallomys*.

Grammomys and *Thallomys* are known from the Plio-Pleistocene of southern and eastern Africa (summarized in Denys, 1999). De Graaff (1981) reported *Grammomys* cf. *G. dolichurus* and *Thallomys* cf. *T. paedulcus* from Makapansgat (about 3.3 Ma; Denys, 1999) and Kromdraai, South Africa. Broom (1948) described an extinct species, *Thallomys debruyni*, from Taung (about 2.5 Ma; Denys, 1999), South

Africa. This taxon is based on a single specimen, the anterior two-thirds of a skull with the molars "broken off." Taxonomic assignment of this specimen needs confirmation. *Thallomys* and *Grammomys* are reported from Aigames II (1-2 Ma; *Thallomys*) and Berg Aukas I (~13 Ma; *Grammomys*), Namibia (Conroy et al., 1992). This material has not been described. Denys (1999) also noted late Pliocene-early Pleistocene records of *Thallomys* from Humpata Level 2, Leba, Angola, and *Grammomys* from Sterkfontein and Swarkkrans, South Africa. *Thallomys* has also been reported from Cooper's Cave, South Africa (1.4 Ma; Linchamps et al., 2023).

Thallomys laetolilensis was reported from the Upper Laetolil Beds, Laetoli, Tanzania (Denys, 1987, 2011). Denys also described an incomplete mandible of *Thallomys* cf. *T. laetolilensis* from the Upper Ndolanya Beds of Laetoli. Considering only the upper dentition, Denys (1984) distinguished the Laetoli material from *Grammomys* primarily on the absence of a posterostyle on *Thallomys* and on the Laetoli fossils. However, both of these taxa (personal observation) usually have the posterostyle represented by a small cusp or a ridge between the enterostyle and hypocone, although it is usually more prominent in *Grammomys*.

The specimens from Tabarin differ from *T. laetolilensis* in two derived characters. The Tabarin teeth seem to have a stronger ridge between the enterostyle and hypocone and the M1 has five roots (*T. laetolilensis* has four). The Tugen Hills M1 is close to the size range of *T. laetolilensis*, but the M2 is smaller (Table 6).

Wesselman (1984) described *Thallomys quadrilobatus* (Omo Member F, 2.08 and Member G, 1.98 Ma) and a new species of *Thallomys*, *T. jaegeri* (Member B, 3.03 and Member C, 2.48 Ma), from small samples of isolated teeth from the Omo River valley, Ethiopia. *Thallomys jaegeri* is basically similar in morphology to, but significantly smaller than, *T. quadrilobatus* (Table 6). Although similar in size (Table 6), the Tabarin specimens differ from *T. jaegeri* in having an extra root on M1. The posterior cingula on the Tabarin M1 and M2 are weak (derived condition), while those of *T. jaegeri* are described as well developed (Wesselman, 1984).

The type of the extinct species *Thallomys quadrilobatus* is from Olduvai Beds I and II, Tanzania (1.8-1.75 Ma, Jaeger, 1976). In addition to the Omo River Valley record (Wesselman, 1984), the species is also known from the Koobi Fora Formation, East Turkana, Kenya (Plio-Pleistocene, Black and Krishtalka, 1986) and the Peninj Site, West Natron, Tanzania (Denys, 1987). This species is similar in size and overall morphology (including five roots on M1) to an extant species *Thallomys paedulcus*, however, *T. quadrilobatus* differs in a number of minor characters including having an M1 with the labial anterocone closer to the lingual anterocone (Jaeger, 1976). Contra Black and Krishtalka (1986), extant *T. paedulcus* does have a posterior cingulum on M1, but it is weakly developed. Jaeger (1976) noted that extant east and South African populations of *T. paedulcus* have a number of differences, and that *T. quadrilobatus* is most similar, and probably ancestral to, the southern African populations. *Thallomys quadrilobatus* lacks a posterostyle according to Jaeger (1976), but it has distinct crests between the enterostyle and hypocone.

Grammomys or *Thallomys* from Tabarin is distinct from *T. quadrilobatus* in being noticeably smaller (Table 6). The two taxa share the synapomorphy of five roots on M1 and differ from *T. laetolilensis*, which has a primitive pattern of four roots.

Jaeger (1976) tentatively referred a small M1 and partial mandible with m1-m3 from Olduvai Middle Bed I to *Grammomys*. Contra Jaeger (1976), a cast of the M1 shows a connection between the enterostyle and hypocone. Minor differences between that material and the Tabarin teeth are probably within the range of individual variation seen in modern populations.

Denys (1987) suggested that *T. laetolilensis* is ancestral to *T. quadrilobatus* based on the former's smaller size (primitive), weaker stephanodonty (primitive), and less elongate anterior four major cusps on m1. The derived root pattern of the geologically younger *T. quadrilobatus* also suggests this relationship. Wesselman (1984) suggested that *T. jaegeri* (from Omo localities dated 3.08-2.48 Ma) may be ancestral to *T. quadrilobatus* (from Omo localities dated 2.08-1.98 Ma). Differences between these taxa from Omo localities include *T. jaegeri* having less stephanodonty (primitive), more robust posterior cingula on M1 and M2 (primitive), less developed posterior cingulum on m1, and four roots on M1 (primitive). Affinities of the Tabarin specimens are difficult to evaluate because of the small sample size and questionable generic assignment. However, the synapomorphy of five roots on M1 suggests a closer relationship with both Olduvai taxa [*T. quadrilobatus* and especially the smaller taxon, *Grammomys* sp. indet.].

Mein & Pickford (2006) established a new genus, *Lukeinomys*

(*L. cheptumoae*), from a small sample from Kapsomin, Lukeino Formation. They suggested it "could be ancestral to" (Mein & Pickford, 2006: pg 208) the *Thallomys-Grammomys* group and noted that it differed from that group by the presence of archaic characters such as the absence of stephanodonty between the paracone (t6) and metacone (t9) and a simpler root pattern. On the Tabarin teeth, the presence of stephanodonty between the paracone and metacone as well as an M1 with five roots (*L. cheptumoae* has four) precludes assignment of the Tabarin teeth to *L. cheptumoae*. Mein & Pickford (2006: p. 208) noted they have new collections of material from Tabarin (unpublished) that includes lower molars and that these specimens lack the sharp chevroning they observe in *Thallomys*, but which is lacking in *Grammomys*. Thus, they consider their Tabarin specimens to pertain to *Grammomys*. They also consider *T. laetolilensis* (Denys, 1987) to pertain to *Grammomys* for this reason. Since lower molars are unavailable in the collection described here, this character cannot be evaluated.

Thallomys is currently found in East Africa in acacia bush and woodland habitats where it lives almost exclusively in acacia trees (Kingdon, 1974). Species of *Grammomys* are found in habitats ranging from wet forests to tall grass and secondary scrub (Kingdon, 1974). Members of both genera are adept climbers.

Genus *SAIDOMYS* James and Slaughter, 1974
SAIDOMYS PARVUS Winkler, 1997
(Fig. 6)

Referred material — Left M1s, KNM-TH 18479, -18480, -19486; right M1s, KNM-TH 18478, KNM-TH 19470; left M2s, KNM-TH 18482, -19482, -19466; right M2, KNM-TH 18484 (incomplete); left M3s, KNM-TH 18483 (incomplete), 30591 (incomplete); right M3, KNM-TH 19472; left m1, KNM-TH 19465; right m1, KNM-TH 19471; left m2, KNM-TH 19488; right m2, KNM-TH 19469; left m3, KNM-TH 18487; right m3s, KNM-TH 18485, -18486; incomplete right mandible with m1-m3, KNM-TH 18476. All from Tabarin, BPRP#77a, Chemeron Formation.

Description — Measurements of the Tabarin *Saidomys parvus* as well as comparative material are given in Table 3.

First upper molar — First upper molars are broad in occlusal outline (Fig. 6A). The first two chevrons are fairly symmetrical with respect to the longitudinal axis of the tooth. The first chevron consists of a large lingual anterocone and smaller labial anterocone and anterostyle. The latter two cusps are approximately equal in size and almost transversely aligned with the lingual anterocone. There is a precingulum on three of four specimens; it extends all along the anterior side of the lingual anterocone. The precingulum may contact the labial anterocone (KNM-TH 18479) or both the labial anterocone and anterostyle (KNM-TH 18480). A small labial prestyle is present on KNM-TH 18478. The middle chevron includes a large protocone (similar in size to the lingual anterocone) and slightly smaller paracone and enterostyle. The latter two cusps are similar in size and located slightly posterior to the protocone. A large hypocone is somewhat elongate transversely and connected to a smaller anteriorly placed metacone. A short posterior cingulum is present on all five specimens. The posterostyle is lacking but may be represented by a thickening of the enamel. A short crest connects the enterostyle and hypocone on three of four specimens. Large anterolabial and posterolabial, two fused lingual, and a small labial root are present.

Second upper molars are broad anteriorly and taper posteriorly (Fig. 6B). Anteriorly, the teeth have a small conical labial anterocone and a conical anterostyle which is at least twice the size of the labial anterocone. The middle row of cusps includes a large protocone and smaller posteriorly placed paracone and enterostyle. The hypocone is the largest cusp. It is connected to a much smaller anteriorly placed metacone. A distinct posterostyle is absent, but enamel on the lingual side of the hypocone is thickened. There is a short crest connecting (or almost connecting) the enterostyle and hypocone. A posterior cingulum is vestigial on the two specimens where this area is preserved. Root pattern is indeterminate.

The third upper molars are wide anteriorly and taper posteriorly, and are noticeably longer than wide (Fig. 6C). There is a large anterostyle and a much smaller labial anterocone. The enterostyle is large (compared to the protocone and paracone) and transversely elongate. A short low lingual cingulum connects the anterostyle and enterostyle. The hypocone is large and transversely elongate; it is connected to a smaller conical metacone. A posterostyle is lacking. The posterior cingulum is also absent but, there is a low indistinct posterior stylar shelf. The root pattern is indeterminate.

Part of the lower incisor and mandible is preserved on KNM-TH 18476. The incisor is ungrooved and in cross-section is shaped like a flattened oval. The indistinct

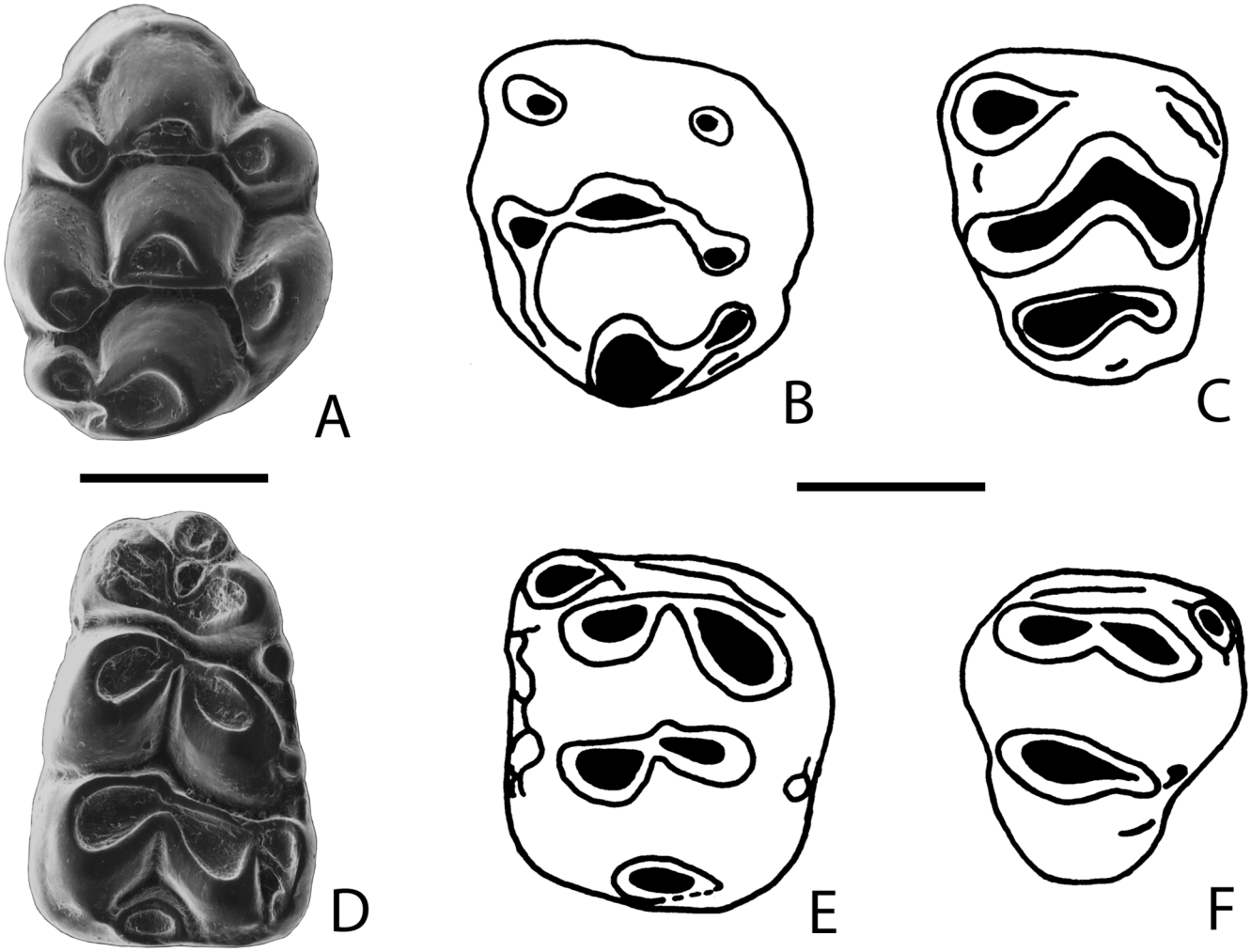

Figure 6. *Saidomys parvus* from the Tabarin locality, Chemeron Formation, Kenya. A) right M1, KNM-TH 18478, B) left M2, KNM-TH 18482, C) left M3, KNM-TH 18483, D) right m1, KNM-TH 19471, E) left m2, KNM-TH 19488, F) right m3, KNM-TH 18485. Both bar scales are 1 mm. The scale on the left is for the scanning electron photomicrographs: that on the right is for the drawings.

posterior end of the mental foramen is preserved. It is located anterior to and under M1. The masseteric crest is strong and does not reach the mental foramen.

Both lower first molars have moderate occlusal wear. Their major cusps are arranged in three transverse rows, separated by moderately deep furrows (Fig. 6D). The labial cusps are located slightly posterior to, and are a little smaller than, the lingual cusps. There is a large medial anteroconid, nestled between the lingual and labial anteroconids: on KNM-TH 19481 it is more closely associated with the lingual anteroconid. The posterior cingulum is a small, somewhat flattened oval. A labial cingulum includes a well-developed C1: on KNM-TH 19481 this cingulum also includes small C2 and C4. On KNM-TH 19481 there is only a very small C3 in addition to C1. There are large anterior and posterior roots (the posterior formed by two fused roots), as well as a small labial root and smaller lingual root.

Second lower molars are almost square to rectangular in outline and have two rows of cusps (protoconid, metaconid, and hypoconid, entoconid) separated by a furrow (Fig. 6E). The labial cusps are oriented somewhat posterior to the lingual cusps. A small labial anteroconid is present. KNM-TH 19488 has a low distinct anterior cingulum along most of the anterior side of the tooth. This cingulum is faint on KNM-TH 19469, which also has a tiny accessory conule anterolingual to the labial anteroconid. The posterior cingulum is as described for M1. There is a low cingulum between the metaconid and entoconid on KNM-TH 19488; this cingulum

is absent on KNM-TH 19469. Both specimens have a posterior spur off the labial anteroconid. On KNM-TH 19469 (which is more heavily worn) C1 is similar in size to the labial anteroconid and in contact with the hypoconid. On KNM-TH 19488 an accessory labial cuspule is about half the size of the labial anteroconid and is not in contact with the hypoconid. Root development is indeterminate.

Third lower molars are triangular in outline and are formed primarily by three cusps (protoconid, metaconid, hypoconid; Fig. 6F). Along the anterior side of the tooth is a small labial anteroconid and a long low anterior cingulum. A chevron is formed by the protoconid and metaconid, which are similar in size. These two cusps are distinct but they are almost completely fused on KNM-TH 18486. This chevron is separated by a deep furrow from the large hypoconid which forms the apex of the triangle. On KNM-TH 18485 and -18487, C1 is present and fused with the hypoconid. KNM-TH 18486 lacks C1 but has a small labial cingulum between the metaconid and hypoconid. A reduced posterior stylar shelf is present on KNM-TH 18486 and along the posteriolabial side of KNM-TH 18485 but is lacking on KNM-TH 18487. Two anterior and one posterior roots are present.

Discussion — Morphology and size of the Tabarin *Saidomys* fits well within the diagnosis and description of *S. parvus* from the Inoleleo 1 and Shoshamagai 2 (tentatively referred specimen) localities, Ibole Member, Manonga Valley, Tanzania (Winkler, 1997). The age of this material is considered as late Miocene/early Pliocene based on overall faunal correlation or early Pliocene based on faunal correlation using only the rodents.

The sample sizes are limited for the two populations: this is especially true for the Manonga sample, which does not include m2 or m3. The following differences for the other teeth between the two samples were noted: 1) M1 – the Manonga sample (n = 2) has a weaker posterior cingulum (Tabarin sample n = 5); 2) M3 – the single Manonga specimen has a small conical posterior cingulum versus an indistinct shelf seen in this area on the single Tabarin tooth. Also, on the Manonga tooth the metacone and hypocone appear more similar in size (although fused from heavy occlusal wear) compared to the smaller metacone and larger hypocone on the less worn Tabarin tooth; and 3) m1 – three of four Manonga m1s have a conical posterior cingulum compared to the flattened ovals observed on the two Tabarin teeth. However, those three Manonga m1s have light occlusal wear and the more worn specimen with heavier wear has a flattened oval more similar to the m1s from Tabarin. Both populations have strong labial cingula with a distinct c1, but there is variable development of other cingular cusps even within each population.

As noted for *S. alisae*, Winkler (1997) made comparisons of *S. parvus* with *S. natrunensis*, *S. afarensis*, and *S. afghanensis*. Mein & Pickford (2006) made comparisons of *S. alisae* with *S. parvus* from Tanzania. One of the major differences they noted (and this applies also to *S. parvus* from Tabarin) is that *S. alisae* has an m1 with a weak medial anteroconid (=anterior median tubercle) compared to a larger one (sometimes more centrally located) on *S. parvus*.

Family THRYONOMYIDAE Pocock, 1922

Genus *THRYONOMYS* Fitzinger, 1867

THRYONOMYS sp.

Referred material — Incomplete right upper M1 or M2, KNM-TH 19483, from Tabarin, BPRP#77a. Right lower incisor, KNM-TH 13628, from Tabarin c (specimen not described here). Both from the Chemeron Formation.

Description and discussion — If complete, this specimen would be roughly square in occlusal outline. It consists of the area anterolingual to a diagonal line running from the anterolabial corner to the posterolingual corner. The roots are not preserved. Minimum measurements are 3.42 mm length by 3.42 mm width. Extremely heavy wear has obscured all surface features except for a wide lingual reentrant that extends anterolabially almost half-way across the tooth.

The Tabarin tooth is assigned to *Thryonomys* based on size and morphology including the transverse orientation of the anterior end of the tooth, relatively compressed lophs, and extent of the lingual reentrant. The tooth is, however, too incomplete for specific comparisons or assignment. A small (labiolingual width 4.0 mm) left upper incisor (KNM-LT 26734) of *Thryonomys* was recovered from BPRP#75A (Sagatia locality). An autapomorphy of *Thryonomys* is the presence of three grooves on the upper incisor. On this specimen, the three grooves are distributed relatively equally (of the two extant genera, more similar to the pattern seen in *T. gregorianus*; see Kingdon, 1974: pg. 696; Denys, 2011).

Thryonomys sp. is known from the Pleistocene Kapthurin Formation, Baringo District (Denys, 1999; McBrearty, 1999).

A right upper incisor of *Thryonomys* from the Kapthurin Formation has three grooves in the pattern seen in extant *T. swinderianus* (grooves concentrated on the lingual side of the tooth making the lateral most ridge distinctly larger than the others).

Thryonomys has been reported from several sites in East Africa (see discussion in Denys, 2011). Some of the oldest records of the genus are from Lemudong'o, Kenya (6 Ma, material not yet fully described; Manthi, 2007) and the late Miocene (5.7 Ma) of the Middle Awash, Ethiopia (Wesselman et al., 2009). It should be noted that the Middle Awash material, assigned to an extinct species, *T. asakomaae*, has an upper incisor with two grooves (as observed in the extinct genera *Paraulacodus* and *Protohummus* [Wesselman et al., 2009; Kraatz et al., 2013]).

Thryonomys is currently represented in Africa by two species (Kingdon, 1974). *Thryonomys gregorianus* is found in moist savannas from northern Cameroon to the East African coast. The generally larger *T. swinderianus* is more widely distributed in sub-Saharan Africa. It is essentially semi-aquatic and is associated with reed beds and grassy areas. Both species are dependent on a permanent source of water.

CONCLUSIONS

The rodents described in this paper augment our knowledge of late Miocene/early Pliocene faunas in East Africa, and the origins of some extant African rodent genera. The sample from the Kapcheberek locality (5.9-5.7 Ma) is very small, but it complements the larger sample published by Mein & Pickford (2006), which is derived primarily from their Kapsomin locality. Three of the four taxa from the Kapcheberek collection described here were also collected by Mein & Pickford (2006): *Dendromus*, *Steatomys minus* and *Saidomys alisae*. Mein & Pickford (2006) do not report *Arvicanthis*, but multiple specimens of that genus were found (not yet formally described) from the 6 Ma Lemudong'o locality, Kenya (Manthi, 2007). The Kapcheberek and Lemudong'o reports of *Arvicanthis* are some of the earliest for this genus. The Kapcheberek rodents described in the present paper suggest the presence of a savanna habitat ca. 5.9-5.7 Ma. Based on the overall small mammal fauna from the Kapsomin locality, Mein & Pickford (2006) suggested the presence of well-wooded to forested habitats, in addition to some relatively more open habitats.

Rodents from the Tabarin locality (4.5-4.4 Ma) reported here are more abundant and diverse than those from Kapcheberek. Significantly, the fauna includes some of the earliest records of several extant African rodent genera (*Paraxerus*, and either *Grammomys* or *Thallomys*). If cf. *Heliosciurus* is referrable to *Heliosciurus*, it may be the earliest record of this genus in Africa. The rodents from the Tabarin locality are suggestive of a woodland habitat in this area in the early Pliocene.

ACKNOWLEDGMENTS

This manuscript is dedicated to my dissertation supervisor and colleague, Lou Jacobs, who has provided many years of encouragement, support, patience, and friendship. Financial support was generously provided by the Institute for the Study of Earth and Man and the Roy M. Huffington Department of Earth Sciences, Southern Methodist University, the Geological Society of America, and Sigma Xi. Collection study grants were courtesy of the Smithsonian Institution, Washington, D.C., and the American Museum of Natural History, New York. I thank the government of the Republic of Kenya for research permission and the staff of the Nairobi National Museum (in particular the late K. Cheboi), Nairobi, Kenya, for their assistance. This study benefitted from discussions with the late A. Hill. Dwight Deuring (formerly with SMU) assisted with the photomicrographs. D. Winkler generously prepared the figures for the manuscript. I thank Yuong-Nam Lee for the kind invitation to contribute to this volume, and for his suggestions to improve the manuscript. The manuscript benefited from constructive reviews by L. Flynn and C. Denys. This research was in partial fulfillment for a Doctorate in Philosophy in Geology at Southern Methodist University, Dallas, Texas, under the supervision of Louis Jacobs.

LITERATURE CITED

Amtmann, E. (1975). Family Sciuridae. In J. Meester & H. W. Setzer (Eds.), *The Mammals of Africa, an Identification Manual* (pp. 1–12). Smithsonian Institution Press.

Bishop, W. W. & Pickford, M. H. L. (1975). Geology, fauna and palaeoenvironments of the Ngorora Formation, Kenya Rift Valley. *Nature*, 254, 185–192.

Black, C. C. & Krishtalka, L. (1986). Rodents, bats, and insectivores from the Plio-Pleistocene sediments to the east of Lake Turkana,

Kenya. *Natural History Museum of Los Angeles County, Contributions in Science*, 372, 1–15.

Broom, R. (1948). Some South African Pliocene and Pleistocene mammals. *Annals of the Transvaal Museum*, 21, 1–38.

Cifelli, R. L., Ibui, A. K., Jacobs, L. L., & R. Thorington, Jr., W. (1986). A giant tree squirrel from the late Miocene of Kenya. *Journal of Mammalogy*, 67, 274–283.

Coetzee, C. G. (1977). Genus *Steatomys*. In J. Meester & H. W. Setzer (Eds.), *The Mammals of Africa, an Identification Manual* (pp. 1–4). Smithsonian Institution Press.

Conroy, G. C., Pickford, M., Senut, B., Van Couvering, J., & Mein, P. (1992). *Otavipithecus namibiensis*, first Miocene hominoid from southern Africa, Nature, 356, 144–148.

de Graaff, G. (1960). A preliminary investigation of the mammalian microfauna in Pleistocene deposits of caves in the Transvaal system. *Palaeontologia Africana*, 7, 59–118.

de Graaff, G. (1981). *The Rodents of Southern Africa*. Butterworths and Company.

Deino, A., Tauxe, L. L., Hill, A., & Monaghan, M. (2002). $^{40}Ar/^{39}Ar$ geochronology and paleomagnetic stratigraphy of the Lukeino and lower Chemeron succession at Tabarin and Kapcheberek, Tugen Hills, Kenya. *Journal of Human Evolution*, 42 (1–2), 117–140.

Denys, C. (1987). Fossil rodents (other than Pedetidae) from Laetoli. In M. D. Leakey & J. M. Harris (Eds.), *Laetoli: a Pliocene site in northern Tanzania* (pp. 118–170). Oxford University Press.

Denys, C. (1987). Micromammals from the West-Natron Pleistocene deposits (Tanzania). Biostratigraphy and Paleoecology. *Sciences Géologiques, Bulletin*, 40(1–2), 185–201.

Denys, C. (1994). Nouvelles espèces de *Dendromus* (Rongeurs, Muroidea) à Langebaanweg (Pliocene, Afrique du Sud): consèquences stratigraphiques et paléoécologiques. *Palaeovertebrata*, 23(1–4), 153–176.

Denys, C. (1999). Of mice and men: evolution in east and South Africa during Plio-Pleistocene times. In T. G. Bromage & F. Schrenk (Eds.), *African Biogeography, Climate Change and Human Evolution* (pp. 226–252). Oxford University Press.

Denys, C. (2011). Chapter 2. Rodents. In T. Harrison (Ed.). Paleontology and Geology of Laetoli: Human Evolution in Context. Volume 2: Fossil Hominins and the Associated Fauna. *Vertebrate Paleobiology and Paleoanthropology Series* (pp. 15–53). Springer Dordrecht.

Denys, C. & Winkler, A. (2015). Advances in integrative taxonomy and evolution of African murid rodents: how morphological trees hide the molecular forest. In P. G. Cox & L. Hautier (Eds.), *Evolution of the Rodents, Advances in Phylogeny, Functional Morphology and Development* (pp. 186–220). Cambridge University Press.

Flynn, L. J., Jacobs, L. L., & Sen, S. (1983). La diversité de *Paraulacodus* (Thryonomyidae, Rodentia) et des groupes apparentés pendant le Miocène. *Annales de Paléontologie*, 69, 355–366.

Flynn, L. J., Jacobs, L. L., & Lindsay, E. H. (1985). Problems in muroid phylogeny: relationship to other rodents and origin of major groups. In W. P. Luckett & J. -L. Hartenberger (Eds.), *Evolutionary relationships among rodents, a multidisciplinary analysis* (pp. 589–616). NATO ASI Series A, Life Sciences Vol. 92.

Geraads, D. (1998). Rongeurs du Mio-Pliocène de Lissasfa (Casablanca, Maroc). *Geobios*, 31, 229–245.

Geraads, D. (2001). Rongeurs du Miocène superiéur de Ch'orora, Ethiopie: Murinae, Dendromurinae et conclusions. *Palaeovertebrata*, 30, 89–109.

Hendey, Q. B. (1981). Palaeoecology of the late Tertiary fossil occurrences in E Quarry, Langebaanweg, South Africa, and a reinterpretation of their geological context. *Annals of the South African Museum*, 84, 1–104.

Hill, A. (1985). Early hominid from Baringo, Kenya. *Nature*, 315, 222–224.

Hill, A. (1999). The Baringo Basin, Kenya: from Bill Bishop to BPRP. In P. Andrews & P. Banham (Eds.), *Late Cenozoic Environments and Hominid Evolution: a Tribute to Bill Bishop* (pp. 85–97). Geological Society.

Hill, A. (2002). Introduction. Paleoanthropological research in the Tugen Hills, Kenya. *Journal of Human Evolution*, 42, 1–10.

Hill, A., Curtis, G., & Drake, R. (1986). Sedimentary stratigraphy of the Tugen Hills, Baringo, Kenya. In L. E. Frostick, R. W. Renaut, I. Reid, & J. J. Tiercelin (Eds.), *Sedimentation in the African Rifts* (pp. 285–295). Geological Society of London, Special Publication No. 25.

Hill, A., Behrensmeyer, K., Brown, B., Deino, A., Rose, M., Saunders, J., Ward, S., & Winkler, A. (1991). Kipsaramon: a lower Miocene hominoid site in the Tugen Hills, Baringo District, Kenya. *Journal of Human Evolution*, 20, 67–75.

Jacobs, L. L. (1978). Fossil rodents (Rhizomyidae & Muridae) from Neogene Siwalik deposits, Pakistan. *Museum of Northern Arizona Press, Bulletin Series*, 52, 1–103.

Jaeger, J. -J. (1975). *Les Muridae (Mammalia, Rodentia) du Pliocène et du Pléistocène du Maghreb: Origine, évolution, données biogéographiques et paléoclimatiques* [Unpublished doctoral dissertation]. Université des Sciences et Techniques du Languedoc.

Jaeger, J. -J. (1976). Les rongeurs (Mammalia, Rodentia) du Pléistocène Inférieur d'Olduvai Bed I, Ière Partie: les muridés. In R. J. G. Savage & S. C. Coryndon (Eds.), *Fossil Vertebrates of Africa, Volume 4* (pp. 57–120). Academic Press.

Jaeger, J. -J., & Wesselman, H. B. (1976). Fossil remains of micromammals from the Omo Group deposits. In Y. Coppens, F. C. Howell, G. L. Isaac, & R. E. F. Leakey (Eds.), *Earliest man and environments in the Lake Rudolf Basin* (pp. 351–360). University of Chicago Press.

Jaeger, J. -J., Tong, H., Buffetaut, E., & Ingavat, R. (1985). The first fossil rodents from the Miocene of northern Thailand and their bearing on the problem of the origin of the Muridae. *Revue de Paléobiologie*, 4, 1–7.

James, G. T. & Slaughter, B. H. (1974). A primitive new middle Pliocene murid from Wadi el Natrun, Egypt. *Annals of the Geological Survey of Egypt*, 4, 333–362.

Kingdon, J. (1974). *East African Mammals: an Atlas of Evolution in Africa. Volume IIB (Hares and Rodents).* University of Chicago Press.

Kraatz, B. P., Bibi, F., Hill, A., & Beech, M. (2013). A new fossil thryonomyid from the Late Miocene of the United Arab Emirates and the origin of African cane rats. *Naturwissenschaften*, 100, 437–449. DOI 10.1007/s00114-013-1043-4

Lavocat, R. (1957). Sur l'âge des faunes de rongeurs des grottes à Australopithèques. In J. D. Clark (Ed.), *Proceedings 3rd Pan-African Congress on Prehistory* (pp. 133–134). Chatto and Windus.

Lavocat, R. (1967). Les microfaunes du quaternaire ancient d'Afrique orientale et austral. In W. W. Bishop & D. D. Clark (Eds.), *Background to Evolution in Africa* (pp. 67–72). University of Chicago Press.

Linchamps, P., Stoetzel, E., Cornette, R., Denys, C., Hanon, R., Maringa, N., Matthews, T., & Steininger, C. (2023). Fossil micromammals

and the palaeoenvironments of the *Paranthropus robustus* site of Cooper's Cave. *Historical Biology*. DOI:10.1080/08912963.2023.2196677

Louchart, A., Wesselman, H., Blumenschine, R. J., Hlusko, L. J., Njau, J. K., Black, M. T., Asnake, M., & White, T. D. (2009). Taphonomic, avian, and small-vertebrate indicators of *Ardipithecus ramidus* habitat. *Science*, 326, 66e1–66e4. DOI: 10.1126/science. 1175823

Manthi, F. Y. (2006). *The Pliocene micromammalian fauna from Kanapoi, northwestern Kenya, and its contribution to understanding the environment of Australopithecus anamensis* [Unpublished doctoral dissertation]. University of Cape Town.

Manthi, F. K. (2007). A preliminary review of the rodent fauna from Lemudong'o, southwestern Kenya, and its implication to the late Miocene paleoenvironments. *Kirklandia*, 56, 92–105.

Manthi, F. K. & Winkler, A. J. (2020) Rodents and other terrestrial small mammals from Kanapoi, north-western Kenya. *Journal of Human Evolution*, 140. DOI: 10.1016/j.jhevol.2019.102694.

McBrearty, S. (1999). The archaeology of the Kapthurin Formation. In P. Andrews & P. Banham (Eds.), *Late Cenozoic Environments and Hominid Evolution: a Tribute to Bill Bishop* (pp. 143–156). Geological Society.

Mein, P. (1994). Micromammifères du Miocène superiéur et du Pliocène du Rift Occidental, Ouganda. In B. Senut & M. Pickford (Eds.), *Geology and Palaeobiology of the Albertine Rift Valley, Uganda-Zaire* (pp. 187–193). Vol. II: Palaeobiology. Orléans, CIFEG Occasional Publication 1994/29.

Mein, P. & Pickford, M. (2006). Late Miocene micromammals from the Lukeino Formation (6.1 to 5.8 Ma), Kenya. *Bulletin Mensuel Société Linnéenne de Lyon*, 75(4), 183–223.

Mein, P. & Pickford, M. (2004). Vallesian rodents from Sheikh Abdallah, Western Desert, Egypt. *Historical Biology*, 22, 224–259.

Mein, P., Pickford, M., & Senut, B. (2004). Late Miocene micromammals from the Harasib karst deposits, Namibia. Part 2b - Cricetomyidae, Dendromuridae and Muridae, with an addendum on the Myocricetodontinae. *Communs geol. Surv. Namibia*, 13, 43–61.

Misonne, X. (1969). African and Indo-Australian Muridae, evolutionary trends. *Musee Royal de l'Afrique Centrale Annales, Serie 8, Sciences Zoologiques*, 172:1–219.

Misonne, X. (1974). Part. 6. Order Rodentia In J. Meester & H. W. Setzer (Eds.), *The Mammals of Africa, an Identification Manual* (pp. 1–39). Smithsonian Institution Press.

Monadjem, A., Taylor, P. J., Denys, C., & Cotterill, F. P. D. (2015). *Rodents of Sub-Saharan Africa, a Biogeographic and Taxonomic Syntheses*. De Gruyter.

Musser, G. G. & M. D. Carleton. (2005). Superfamily Muroidea. In D. E. Wilson & A. M. Reeder (Eds.), *Mammal Species of the World, A Taxonomic and Geographic Reference*, 3rd Edition, Vol. 2 (pp. 894–1531). John Hopkins University Press.

Nowak, R. M. (1999). *Walker's Mammals of the World. 6th Edition*. The Johns Hopkins University Press.

Pickford, M. H. L. 1975. *Stratigraphy and palaeoecology of five late Cainozoic formations in the Kenya Rift Valley* [Unpublished doctoral dissertation]. University of London.

Pickford, M. (1978). Stratigraphy and mammalian palaeontology of the late-Miocene Lukeino Formation, Kenya. In W. W. Bishop (Ed.), *Geological Background to Fossil Man* (pp. 263–278). Scottish Academic Press.

Pickford, M. & Mein, P. (1988). The discovery of fossiliferous Plio-Pleistocene cave fillings in Ngamiland, Botswana. *Comptes rendus des séances de l'Académie des Sciences* 307, Série 2, 1681–1686.

Pickford, M. H. L., Johanson, D. C., Lovejoy, C. O., White, T. D., & Aronson, J. L. (1983). A hominoid humeral fragment from the Pliocene of Kenya. *American Journal of Physical Anthropology*, 60, 337-346.

Pickford, M., Senut, B., Gommery, D., & Kipkech, J. (2022). New Pliocene hominid fossils from Baringo County, Kenya. *Fossil Imprint*, 78(2), 451–488.

Pocock, T. N. (1987). Plio-Pleistocene fossil mammalian microfauna of southern Africa - a preliminary report including description of two new fossil muroid genera (Mammalia: Rodentia). *Palaeontologia Africana*, 26, 69–91.

Robinson, P. & Black, C. C. (1973). A small Miocene faunule from near Testour, Beja gouvernorat, Tunisia. *Annales des Mines et de la Géologie, Tunis*, 26, 445–449.

Rosevear, D. R. (1969). *The Rodents of West Africa*. British Museum (Natural History).

Sabatier, M. (1982). Les rongeurs du site Pliocène a hominidés de Hadar (Ethiopie). *Palaeovertebrata*, 12, 1–56.

Sen, S. (1983). Rongeurs et lagomorphes du gisement pliocène de Pul-e Charkhi, bassin de Kabul, Afghanistan. *Bulletin du Museum National d'Histoire Naturelle, série 5, section C*, 1, 33–74.

Senut, B., Pickford, M., Mein, P., Conroy, G., & Couvering, J. V. (1992). Discovery of 12 new Late Cainozoic fossiliferous sites in palaeokarsts of the Otavi Mountains, Namibia. *Comptes rendus des séances de l'Académie des Sciences* 314, Série 2, 727–733.

Senut, B., Pickford, M., Gommery, D., Mein, P., Cheboi, K., & Coppens, Y. (2001). First hominid from the Miocene (Lukeino formation, Kenya). *Comptes rendus des séances de l'Académie des Sciences* 332, Série 2, 137–144.

Slaughter, B. H. & James, G. T. (1979). *Saidomys natrunensis*, an arvicanthine rodent from the Pliocene of Egypt. *Journal of Mammalogy*, 60, 421–425.

Swanepoel, P. & D. A. Schlitter. (1978). Taxonomic review of the fat mice (Genus *Steatomys*) of West Africa (Mammalia: Rodentia). *Bulletin of Carnegie Museum of Natural History*, 6, 53–76.

Tchernov, E. (1968). *Succession of rodent faunas during the upper Pleistocene of Israel*. Verlag Paul Parey.

Thorington, R. W. & Hoffmann, R. S. (2005). Family Sciuridae. In D. E. Wilson & A. M. Reeder (Eds.), *Mammal Species of the World, A Taxonomic and Geographic Reference*, 3rd Edition, Vol. 2 (pp. 754–818). John Hopkins University Press.

Voelker, G., Huntley, J. W., Bryia, J., Denys, C., Sumbera, R., Demos, T. C., Lavrenchenko, L., Nicolas, V., Gnoske, T. P., & Kerbis Peterhans, J. C. (2021). Molecular systematics and biogeographic history of the African climbing-mouse complex (*Dendromus*). *Molecular Phylogenetics and Evolution*, 161. doi.org/10.1016/j.ympev.2021.107166

Ward, S. & Hill, A. (1987). Pliocene hominid partial mandible from Tabarin, Baringo, Kenya. *American Journal of Physical Anthropology*, 72, 21–37.

Ward, S., Brown, B., Hill, A., Kelley, J., & Downs, W. (1999). *Equatorius*: a new hominoid genus from the Middle Miocene of Kenya. *Science* 285, 1382–1386.

Wesselman, H. B. (1984). The Omo micromammals, systematics and paleoecology of early man sites from Ethiopia. *Contributions to Vertebrate Evolution*, 7, 1–219.

Wesselman, H. B., Black, M. T., & Asnake, M. (2009). Chapter 5. Small mammals. In Y. Haile-Selassie & G. WoldeGabriel (Volume Eds.),

T. D. White (Series Ed.), *Ardipithecus kadabba in Africa: Miocene Evidence from the Middle Awash, Ethiopia* (pp. 105–134). University of California Press.

Winkler, A. J. (1990). *Systematics and biogeography of Neogene rodents from the Baringo District, Kenya* [Unpublished doctor dissertation]. Southern Methodist University.

Winkler, A. J. (1992). Systematics and biogeography of middle Miocene rodents from the Muruyur Beds, Baringo District, Kenya. *Journal of Vertebrate Paleontology*, 12, 236–249.

Winkler, A. J. (1994). The middle/upper Miocene dispersal of major rodent groups between southern Asia and Africa. In Y. Tomida, C. Li, & T. Setoguchi (Eds.), *Rodent and Lagomorph Families of Asian Origins and Diversification. National Science Museum Monographs No. 8* (pp. 173–184). National Science Museum, Tokyo.

Winkler, A. J. (1997). Systematics, paleobiogeography, and paleoenvironmental significance of rodents from the Ibole Member, Manonga Valley, Tanzania. In T. Harrison (Ed.), *Neogene Paleontology of the Manonga Valley, Tanzania: A Window into East African Evolution* (pp. 311–332). Plenum Press.

Winkler, A. J. (2002). Neogene paleobiogeography and East African paleoenvironments: contributions from the Tugen Hills rodents and lagomorphs. *Journal of Human Evolution*, 42(1–2), 237–256. DOI: 10.1006/jhev.2001.0501

Winkler, A. J. (2003). Rodents and lagomorphs from the Miocene and Pliocene of Lothagam, Northern Kenya. In M. G. Leakey & J. Harris (Eds.), *Lothagam: The Dawn of Humanity in Eastern Africa* (pp. 169–198). Columbia University Press.

Winkler, A. J., Denys, C., & Avery, D. M. (2010). Chapter 17. Rodentia. In L. Werdelin & W. J. Sanders (Eds.), *Cenozoic Mammals of Africa* (pp. 262–304). University of California Press.

WINDOWS INTO SAUROPSID AND SYNAPSID EVOLUTION
Essays in honor of Prof. Louis L. Jacobs, pp. 332–340, 2023

A NEW SPECIES OF *PLIOPENTALAGUS* (LAGOMORPHA, MAMMALIA) FROM THE PLIOCENE KOBIWAKO GROUP, CENTRAL JAPAN

YUKIMITSU TOMIDA[1,*] and KEIICHI TAKAHASHI[2]

[1]Curator Emeritus, National Museum of Nature and Science, Tsukuba, Ibaraki 169-0073, Japan, aztlanolagus@yahoo.co.jp
[2]Director, Lake Biwa Museum, Kusatsu, Shiga 525-0001, Japan, takahashi-keiichi@biwahaku.jp

ABSTRACT Reported here is the discovery of a new species of leporid mammal from the Pliocene Kobiwako Group in central Japan. *Pliopentalagus okuyamai*, sp. nov., is described based on a partial skull and upper dentition alone. In case of extinct Leporidae, no taxon has been described without the lower dentition, especially the lower third premolar. However, *Pliopentalagus okuyamai* can be distinguished from all known extant and extinct genera (except for *Pliopentalagus*) by characteristics of the palatal bridge and upper dentition alone. Among the genera of the Leporidae, *Pentalagus furnessi* is most closely related to *Pliopentalagus*. However, the extremely deep secondary enamel folds of the internal reentrant and the more squared outline of upper molariform teeth in *Pentalagus furnessi* can be easily distinguished from *Pliopentalagus*. Although the genus *Aztlanolagus* may be congeneric with *Pliopentalagus*, *A. agilis* can be distinguished by the much shallower depth of the secondary enamel folds of upper molariform teeth and much smaller size than *Pl. okuyamai*. Among the known species of *Pliopentalagus*, *Pl. okuyamai* is distinguished by its largest size, the deepest and most densely arranged secondary folds, and the largest length/width ratio of the palatal bridge. *Pl. okuyamai* is the first and oldest record of the family Leporidae in Japan, and may be a possible ancestral form of, or most closely related to, *Pentalagus furnessi*.

KEYWORDS *Pliopentalagus,* new species, Pliocene, Japan

INTRODUCTION

An isolated upper molariform tooth of a leporid was collected, by Mr. Shigemi Okuyama, from the upper part of Ueno Formation of the Kobiwako Group, which is exposed on the river floor of Hattori River in Ohyamada Village (currently Iga City), Mie Prefecture in March 1990 (Fig. 1). In November of the same year, he collected a fragmentary skull of a leporid from the same locality, but it was broken into various parts. Based on the condition of fossil occurrence, components of the material, and relative size and morphology of the left and right teeth, it is assumed that all these fragmentary parts belong to a single skull. The isolated tooth first found is a left upper 4th premolar (P4), and the skull also includes left P4. Based on the general morphology and enamel pattern of the teeth, both the isolated P4 and the skull belong to the same species. Thus, the leporid fossils from this locality represent two individuals of a single species. These specimens were donated to the Lake Biwa Museum (LBM) by Mrs. Kimiyo Okuyama after Mr. S. Okuyama passed away in 2003. Mr. Okuyama was collecting fossils mainly in Mie Prefecture and surrounding area before his death, and his collection was officially donated to the LBM in September, 2010 (Tanimoto and Kitada, 2011). However, the majority of his collection (including those two leporid specimens mentioned above) had already been accessioned by the LBM by early in 2008.

These specimens were briefly studied by Kawamura and Okuyama in 1995 (Kawamura and Okuyama,1995), but no further study was conducted since then. The second author (KT, then Head Curator of the LBM) recommended in 2008 that YT study and describe the specimens. We nearly completed the descriptive part with photos. However, the study was delayed for various reasons in late 2008. The present paper is the completed study after 15 years of silence.

As commonly known among scholars of lagomorph fossils, lower third premolar (p3) is the most important tooth in classification of Leporidae, and p4-m2 are also important in classification of some genera including *Pentalagus* and *Pliopentalagus*. Although the specimens described below do

*Corresponding author

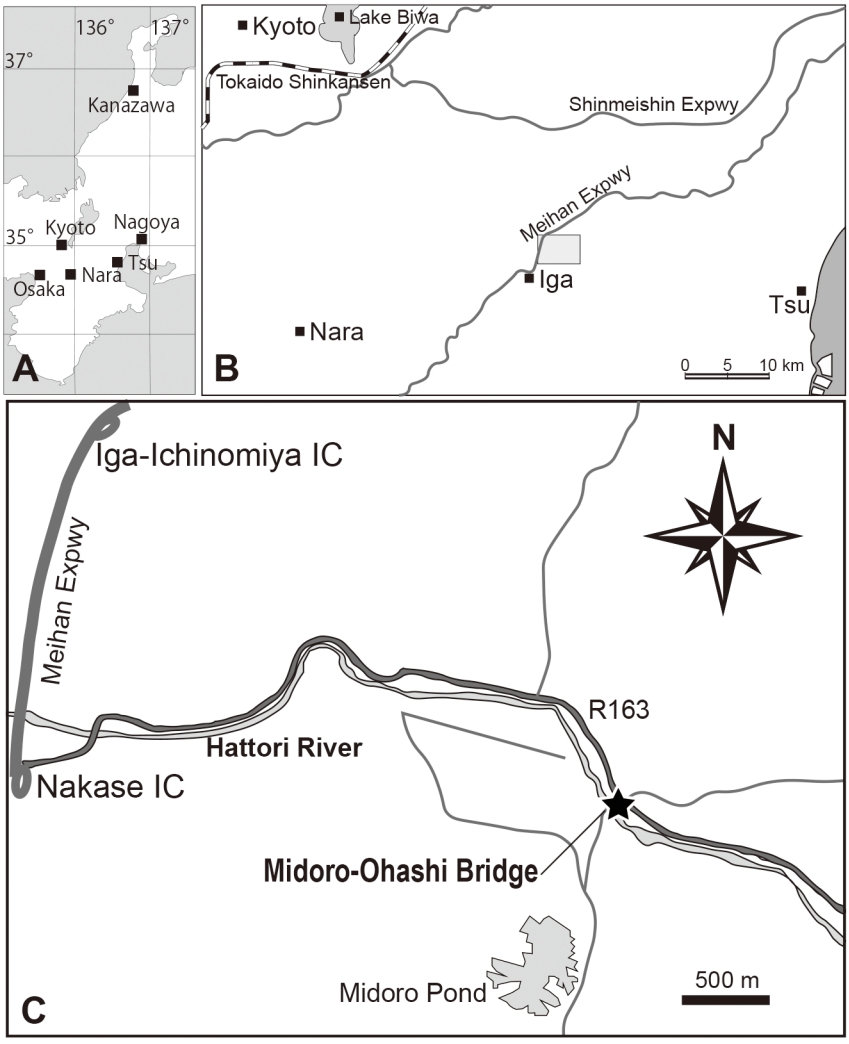

FIGURE 1. Geographic location of the type locality (solid star) of *Pliopentalagus okuyamai*. A, central part of the Honshu, Japan; B, enlargement of between Kyoto and Tsu area; C, enlargement of rectangular grey area near center of B, and the solid star indicates the type locality.

not include any lower dentition, the fragmentary skull preserves nearly complete palatal bridge and most of the upper dentition. Fortunately, both the palatal bridge and enamel pattern of upper dentition of those specimens are characteristic enough to distinguish them from other leporid taxa, and therefore they are described as a new species below.

No leporid fossil has been known from the Tertiary in Japan, and the material described below is the first and oldest record of the family Leporidae in Japan. In addition, it may be a possible ancestral form of, or rather most closely related to, *Pentalagus furnessi* (living Amami Rabbit), rather than of a Chinese species of *Pliopentalagus* described by Tomida and Jin (2009).

METHOD

Measurements of skull were made following Averianov et al. (2000), using a reticule in a Wild M5 stereomicroscope. Measurements of the teeth were also made using a reticule in the same stereomicroscope. For measurement, teeth were held with the portion of the tooth closest to the occlusal surface perpendicular to the table supporting the microscope. Illustrations of the occlusal surface of each tooth were made with the tooth in the same orientation used for measurement. Pencil drawings were made by YT using a camera lucida. Final illustrations were made by tracing these pencil drawings using Adobe Illustrator CS2.

YT examined and collected data (including measurements of teeth and skulls and pencil drawings of the teeth) from all the extant genera of the family Leporidae at The Natural History Museum in London, Museum of Comparative Zoology at Harvard University, and the National Museum of Nature and Science (Japan), and from extinct *Aztlanolagus agilis* at the University of Texas at El Paso. These data are used in comparison with the specimens described in this paper.

Institutional Abbreviations — **LBM**, Lake Biwa Museum, Kusatsu Japan; **NMNS-Z**, National Museum of Nature and Science, Department of Zoology, Tsukuba, Japan

Anatomical Abbreviations — **EAR**, external anterior reentrant; **I**, upper incisor; **IAR**, internal anterior reentrant; **IRF**, internal reentrant fold; **M**, upper molar; **m**, lower molar; **MAR**, main anterior reentrant; **P**, upper premolar; **p**, lower premolar.

SYSTEMATIC PALEONTOLOGY

Order LAGOMORPHA Brandt, 1885
Family LEPORIDAE Gray, 1821
Subfamily LEPORINAE Trouessart, 1880
Genus *PLIOPENTALAGUS* Gureev et Konkova, 1964

Type Species — *Pliopentalagus moldaviensis* Gureev et Konkova, 1964 (in Gureev, 1964), p. 129.

Comments — For detail, see Tomida and Jin (2009).

PLIOPENTALAGUS OKUYAMAI, sp. nov.

(Figs. 2 and 3; Tables 1 and 2)

Holotype — NOTE: The fragmentary skull broken into several parts is considered as a single specimen. However, the LBM catalogued and gave independent numbers to them when they were officially donated, so we give those numbers (below), but we use the term "holotype" (instead of numbers). The catalog numbers consist of ten digits (e.g. 0142001184), and the first 6 digits indicate information like geological age and locations. They are same to all parts mentioned below, but in most cases we use only last 4 digits.

The holotype is a fragmentary skull consisting of following parts: palatal portion with nearly complete palatal bridge and left P2-M1 in place and right P3-P4 (broken but nearly in place) and M1-M2 (broken and dislocated; M2 is only the occlusal tip) (LBM 0142001184), fragmentary premaxillae with left and right broken small I2s (1188), fragmentary left large I1 (1185), left M2 with maxillary fragment (1187), fragmentary right M2 without occlusal surface (part of 1184), and several unidentifiable bone fragments (1189, 1190).

Etymology — In honor of Mr. Shigemi Okuyama who found the holotype and referred specimen and donated them to LBM (through his wife after his death).

Referred specimen — An isolated left P4 with slight weathering near the occlusal surface (LBM 0142001186).

Locality and age — River floor of Hattori River near Midoro O'hashi bridge in Ohyamada Village (currently Iga City), Mie Prefecture, central Japan (Fig. 1). Dark grey mudstone between two tuff beds called Hattori River I and II, upper part of Ueno Formation, Kobiwako Group (Kawamura and Okuyama, 1995), which is correlated near the boundary between Gauss and Gilbert paleomagnetic chrons, about 3.6 Ma (Satoguchi et al., 2005; Satoguchi, 2020).

Diagnosis — Largest known species of the genus. In P3-M2, the secondary folds of IRF are deepest and most densely arranged (counts 10 to 12 on both anterior and posterior walls) among known species of the genus, and the depth of the secondary folds is nearly equal on anterior and posterior walls. The ratio of length/width of the palatal bridge is largest among the known species of the genus and is almost same as that of *Pentalagus furnessi*.

Measurements — See table 1.

Description of holotype — The holotype preserves the palatal bridge, left side of which is nearly complete, while right side is broken somewhat right of the midline; in addition, alveolus of right P3 is unclear (Fig. 2A). Thus, "width" of the palatal bridge (= distance of lingual borders of left and right P3 alveoli; C4 of Fig. 2 in Averianov et al., 2000) is estimated by [the distance between midline, from the suture line of left and right maxillae to the posterior projection of the posterior edge, of palatal bridge and left P3 alveolus] x 2, and it is 13.7 mm. Both anterior and posterior edges of the palatal bridge are preserved on the left side, and the length is measured as 13.84 mm. Thus, the ratio of length/width is estimated as 1.01, which is almost exactly same as that of *Pentalagus furnessi*. Contribution of palatine to the length of palatal bridge is considerable, and proportional contribution of maxilla and palatine to the length is about

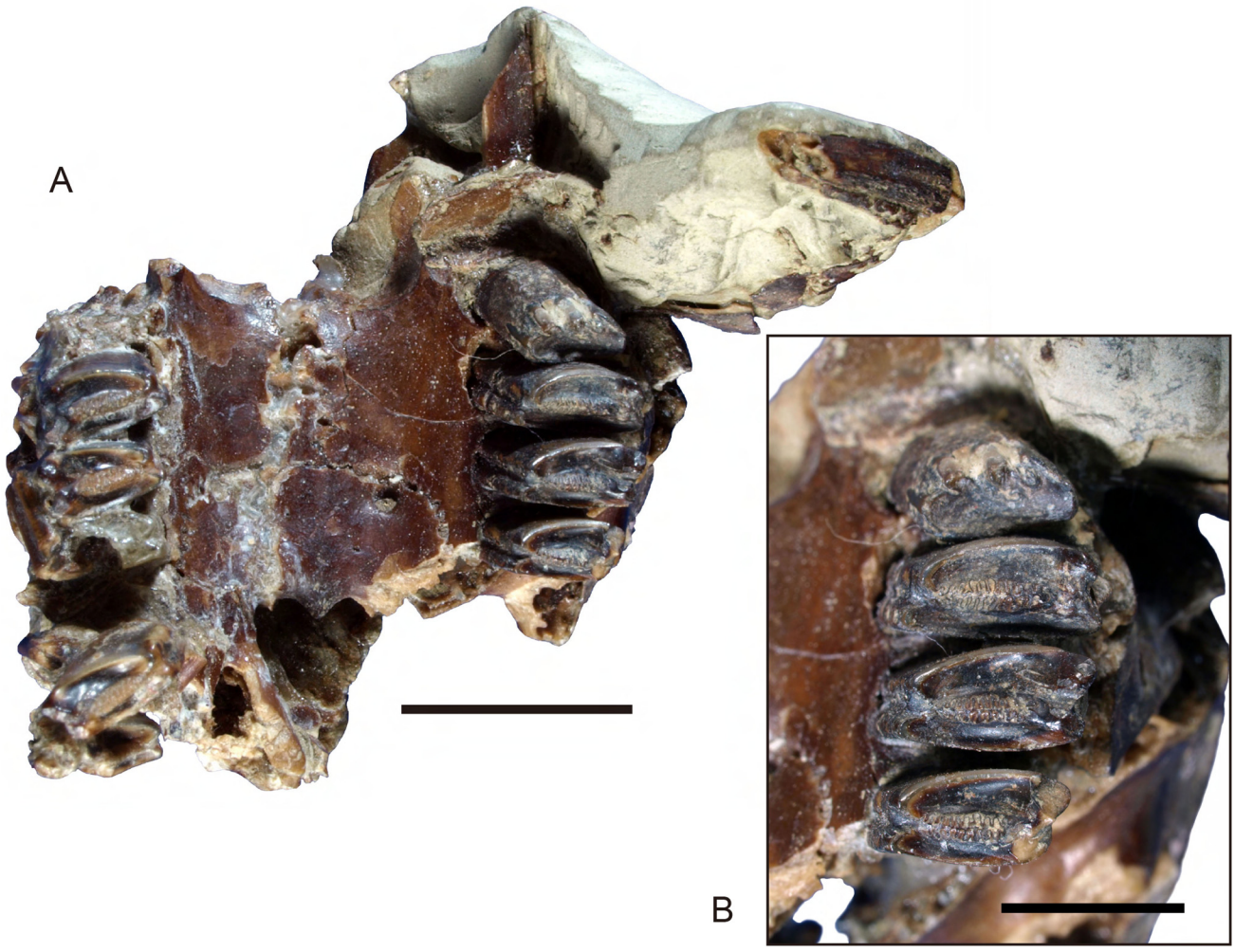

FIGURE 2. Photographs of major portion (LBM 0142001184) of the holotype. **A**, ventral view of the partial skull with palatal bridge, left P2-M1, and right P3-4, tip of M1; **B**, enlargement of occlusal surfaces of left P2-M1. Scale bars are 10 mm and 5 mm for A and B, respectively.

6:5, respectively (Fig. 2A). Posterior part of incisive foramen is observable, and the maximum width of that part is estimated as 9.7 mm, while the width of mesopterygoid fossa is estimated as 5.6-6.0 mm based on the curvature of the posterior edge of palatal bridge. Although the latter is rather inaccurate, it is obvious that the maximum width of incisive foramen is much wider than that of mesopterygoid fossa.

Left and right premaxillae are partly preserved, especially ventral side, and both left and right small second upper incisors are partly observable on the dorsal broken face. A cross section of right one is observable, and it is slightly antero-posteriorly flattened circular in outline with the middle part of the posterior face somewhat swollen. Thin enamel surrounds the tooth (Fig. 3E).

The large first upper incisor (Fig. 3D) is a rounded rectangle (wider than long and more rounded on buccal side), with ratio of about 7 : 10, in cross section, and has a groove on the anterior surface without cement filling. The groove is a wide V shape in cross section, and the apex of the groove lies somewhat medial to the midline of the tooth width (about 45% across the tooth width from the medial edge). Relatively thin enamel covers the anterior face and the anterior 1/3 and anterior half of medial and lateral sides, respectively.

Only one P2 is preserved (Figs. 2B, 3A). The tooth column curves antero-dorsally, then further curves postero-dorsally toward the base of the tooth. P2 is oval in outline in occlusal view, with the posterior face more flattened. There are three reentrant folds on the anterior face, EAR, MAR, and IAR, all of which are filled with cement, and cement further develops

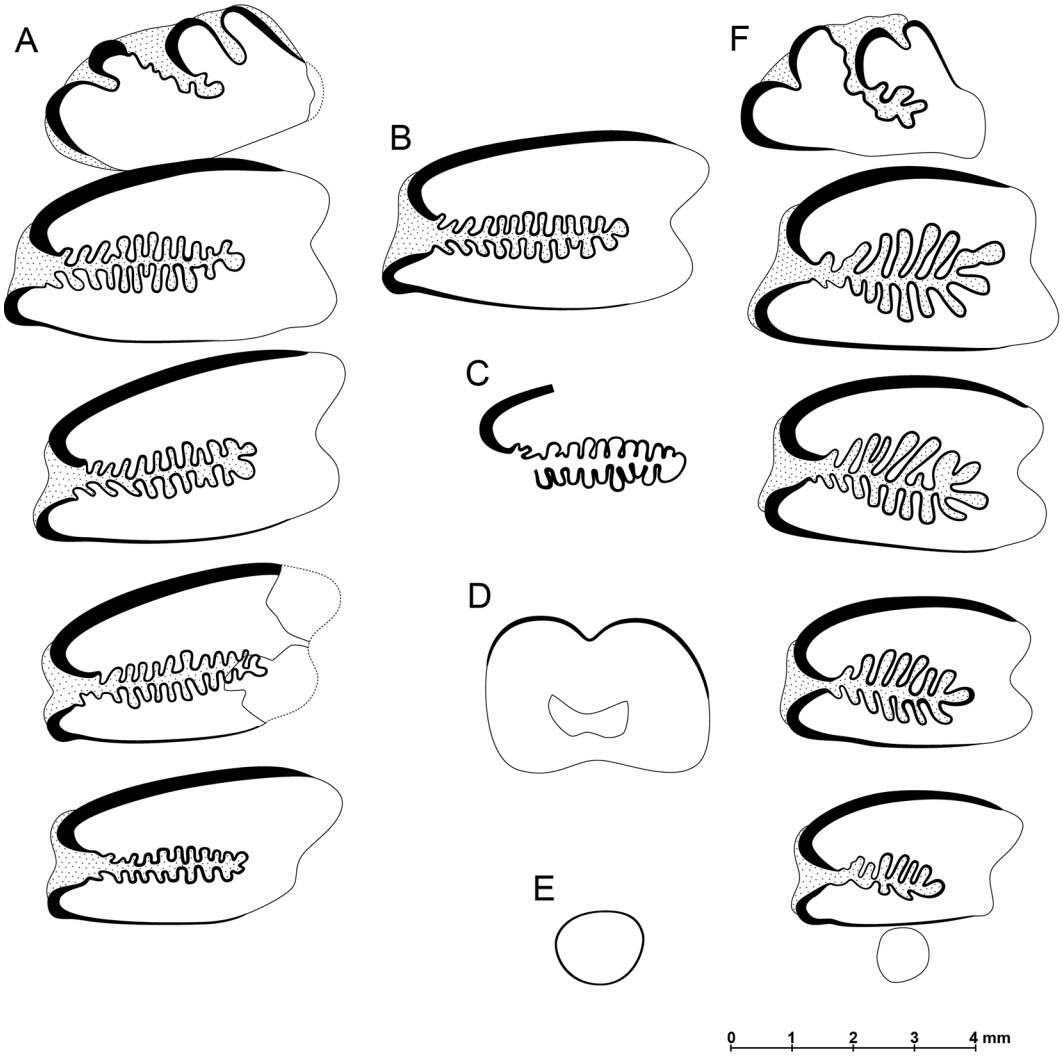

FIGURE 3. Diagrams of the upper dentition of *Pliopentalagus okuyamai* (A to E) and *Pentalagus furnessi* (F). **A**, occlusal surfaces of left P2-M2 of the holotype; **B**, occlusal surface of left P4 of LBM 0142001186; **C**, distal view of right M2 of the holotype; **D**, cross section of left first upper incisor of the holotype; **E**, cross section of left second upper incisor of the holotype; **F**, occlusal surfaces of left P2-M3 of NMNS-Z 1831.

on the anterior face, toward the base of the tooth. MAR is deepest, extends postero-buccally over 60% of the tooth length, and the enamel walls are crenulated. EAR and IAR are both shallower than MAR, extend postero-buccally about 45 and 30% of the tooth length, respectively, and the enamel walls are without crenulations. Thick enamel covers the lingual corner of the tooth and anterior ends of two dentine lobes in the middle, while moderately thick enamel covers the antero-buccal corner.

The holotype includes left and right P3s. P3 is the largest tooth in each cheek tooth row, and the general outline in occlusal view is typical for other leporines. The length/maximum width ratio is 0.55 and 0.53 in left and right P3, respectively, and it is also rather typical. Anterior loph is narrower than posterior at both lingual and buccal ends. Thick enamel covers over 80% of anterior surface of the tooth and the lingual corners of both anterior and posterior lophs. Thin enamel continues on the posterior wall of the posterior loph, reaching across about 2/3 the tooth width. Deep IRF is locating somewhat posterior to the midline of the tooth, reaching nearly 3/4 of the way across the tooth width. The secondary enamel folds are very deep (but still shallower than *Pentalagus furnessi*) on both anterior and posterior walls, and both walls are aligned very closely to

TABLE 1. Measurements of the teeth of holotype and LBM 0142001186. (*) indicates to be measured on the tooth shaft

		Length	Ant. Width	Post. Width	Max. width
Holotype					
Left	I1	2.64			3.76
	P2	2.16	4.58		
	P3	3.08	5.08	5.58	5.58
	P4	3.12	5.08	5.08	5.48
	M1	2.84	5.00	4.58	5.06
	M2	2.56	4.92	4.12	5.17
Right	I2	1.20			1.44
	P3	3.16	5.42	6.00	6.00
	P4	3.16	5.33	5.42	5.62
	M1	2.84	5.25	4.92	5.42
	M2	2.52			
LBM 0142001186					
Left	P4*	3.04	5.25	5.17	5.72

TABLE 2. Comarisons of the palatal bridges among *Pliopentalagus*, *Pentalagus*, and *Aztlanolagus*. (*) indicates estimated value

Taxa	Numbe of specimens	Length of palatal brige (C4) in range	Distance of P3s alveoli (C5) in range	Ratio C4/C5 in average
Pliopentalagus huainanensis	1	8.21	9.67*	0.85
Pliopentalagus dajushanensis	9	7.48-8.96	9.89-11.29	0.74
Pliopentalagus anhuiensis	2	5.69-6.01	8.99-9.71	0.63
Pliopentalagus okuyamai	1	13.84	13.7*	1.01
Pentalagus furnessi	7	10.60-12.90	10.93-12.54	1.02
Aztlanolagus agilis	1	6.68	7.47	0.89

each other. Ratio between maximum total length of both anterior and posterior folds and the tooth length is ca. 33% in left P3. In addition, the secondary enamel folds are densely arranged; they count 11 on the anterior wall and 11 (there is a twelfth small one) on the posterior wall in left P3 (Fig. 3A); 12 and 11 in right P3. The depth of the secondary folds is about the same on the anterior and posterior walls.

Morphology of P4 through M2 is quite similar to that of P3 in general, and the following description includes mainly differences between each tooth and P3. The holotype also includes left and right P4s. P4 is the second largest tooth in each cheek tooth row, and the length/maximum width ratio is 0.57 and 0.56 in left and right P4, respectively. Anterior loph is narrower than posterior loph lingually, while the former is slightly wider than the latter buccally. Thick enamel covers nearly 90% of anterior surface of the tooth, while thin enamel continues on the posterior wall of the posterior loph, reaching over 80% of the tooth width. Secondary enamel folds are slightly shallower than P3, and the ratio between maximum total length of both anterior and posterior folds and the tooth length is ca. 30% in left P4. Enamel folds count 11 on the anterior wall and 10 on the posterior in left P4; 10 and 11 in right P4. The depth of the secondary folds is about the same on the anterior and posterior walls, as in P3.

In M1, the length/maximum width ratio is 0.56 and 0.52, left and right, respectively. Anterior loph is only slightly narrower than posterior loph lingually, while the former is obviously wider than the latter buccally, thus the anterior loph is clearly wider than the posterior. Thin enamel covering posterior wall of the posterior loph reaches nearly 80% of the width of posterior loph (or ca. 73% of the maximum tooth

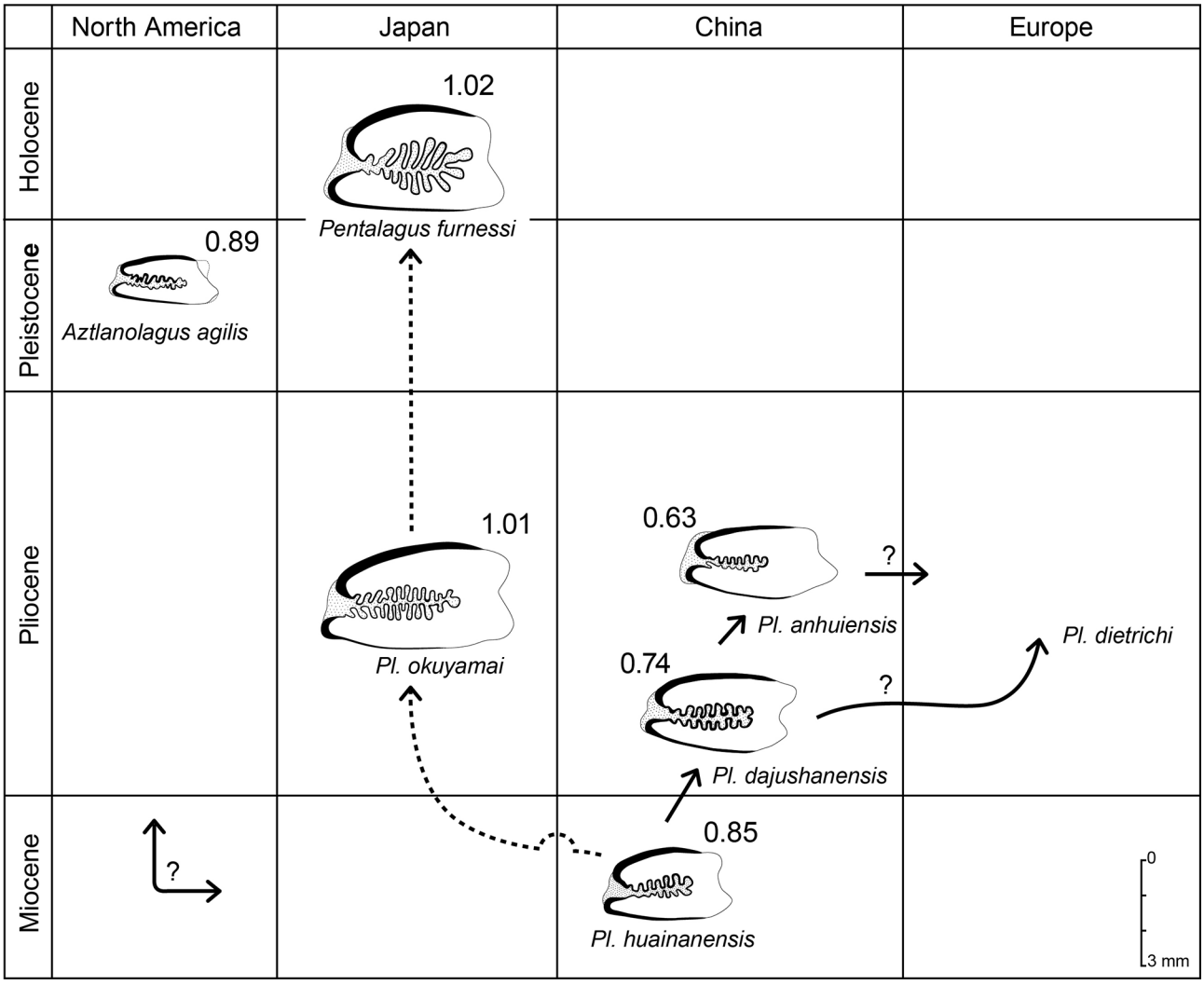

FIGURE 4. Proposed phylogeny of *Aztlanolagus agilis*, *Pliopentalagus* spp, and *Pentalagus furnessi*. Time and place of the *Aztlanolagus*/*Pliopentalagus* transition are unkown so far. Number above each tooth illustration indicates average of width/length ratio of the palatal bridge for each.

width). Secondary enamel folds are slightly shallower than P4, but tooth length is also somewhat shorter, so the ratio between maximum total length of both anterior and posterior folds and the tooth length in left M1 (ca. 29%) is almost same as in left P4. Secondary enamel folds are still densely arranged and count 11 on the anterior wall and 12 on the posterior wall in left M1; 10 and 10 in right M1.

In left M2, the length/maximum width ratio is 0.50, while it is not available in right M2 because of breakage. Anterior loph is slightly narrower than posterior loph at lingual end, while the former is much wider than the latter at buccal end, thus the anterior loph is definitely wider than posterior. Thick enamel covers over 90% of anterior surface of the tooth width, while thin enamel covers nearly 80% of the posterior wall. Secondary enamel folds are somewhat shallower than in M1, and the ratio between maximum total length of both anterior and posterior folds and the tooth length in left M2 is ca. 26%, somewhat less than in left M1; but they are still densely arranged and count 11 on the anterior wall and 10 on the posterior wall in left M2. Right M2 is broken into two parts, and the enamel pattern of distal end is visible on the isolated part (Fig. 3C). The secondary enamel crenulations are already being formed but enamel deposition is not yet complete at this stage and cement is not yet deposited.

Description of Referred Specimen — This tooth fragment is somewhat weathered, with some thick enamel and dentine

around the tooth missing on and near the occlusal surface. However, the tooth is otherwise normal and the illustration (Fig. 3B) is made with the enamel estimated based on the normal part of the tooth, which is visible through a stereo-microscope.

General outline of occlusal surface including the fact that anterior loph is narrower than posterior loph at lingual end while the former is slightly wider than the latter at buccal end, indicates that LBM 0142001186 is a left P4 of a leporine. Compared to P4 of the holotype, LBM 0142001186 is similar in size, but relative width is slightly greater (the length/maximum width ratio is 0.53). Thick enamel covers about 90% of anterior surface of the tooth and the lingual corners of both anterior and posterior lophs. Thin enamel continues posterior wall of the posterior loph, reaching about 80% of the width of the loph. Deep internal reentrant fold is somewhat posterior to the midline of the tooth, reaching about 3/4 way across the tooth width. Secondary enamel folds are as deep as in the holotype, and the ratio between maximum total length of both anterior and posterior folds and the tooth length is ca. 29%. Enamel folds count 12 (13 counting the first tiny one) on the anterior wall and 11 on the posterior. The depth of the secondary folds is about the same on the anterior and posterior walls. The above detailed description strongly suggests that LBM 0142001186 and the holotype represent the same species.

DISCUSSION

As commonly recognized among scholars of lagomorph fossils, lower third premolar (p3) is the most important tooth in classification of the Leporidae, and p4-m2 are also important in classification of some genera. Probably, as far as we know, no taxon of the family has been described based on the upper dentition alone. However, combinations of the following characters among the upper dentition of the Leporidae can identify the specimens described above as the genus *Pliopentalagus*: (1) presence/absence of cement in the groove on I1, (2) number of anterior reentrants on P2, (3) presence/absence of crenulation and the depth of MAR on P2, (4) depth of IRF in P3-M1, (5) condition of enamel walls of IRF in P3-M1, and (6) number of secondary enamel folds (both anterior and posterior) of the IRF on P3-M1.

Among the extant and extinct genera of the Leporidae, *Pentalagus furnessi* is morphologically the most closely related taxon to the genus *Pliopentalagus*. However, the depth of the secondary folds of IRF of P3-M1 is much deeper in *Pentalagus* than *Pliopentalagus* in general, and number of secondary folds in P3-M1 is obviously fewer in *Pentalagus furnessi* than *Pl. okuyamai*, at least (Fig. 3A, F). Also, general outline of P3-M1 is more squared (antero-posteriorly long) in *Pentalagus* while that of *Pliopentlagus* is more rectangular (antero-posteriorly short) (Fig. 3). Thus, we conclude that *Pl. okuyamai* is a species of the genus *Pliopentalatus*, not the genus *Pentalagus*.

The genus *Aztlanolagus* known from North America may be con-generic with *Pliopentalagus* (Tomida and Jin, 2004, 2008). Discussion of these two genera and *Pentlagus*, including phylogenetic and paleogeographic relationships, is currently being prepared as a separate paper by YT. Therefore, we note morphological differences between *Pl. okuyamai* and *A. agilis* alone in this paper. The secondary folds of IRF of P3-M1 in *A. agilis* are obviously shallower than in *Pl. okuyamai*, especially the posterior secondary folds which are even shallower than the anterior. In addition, the size of the teeth is much smaller than *Pl. okuyamai*.

Four other species are recognized in the genus *Pliopentalagus*: *Pl. dietrichi*, *Pl. anhuiensis*, *Pl. dajushanensis*, and *Pl. huainanensis*. (Daxner and Fejfar, 1967; Tomida and Jin, 2009). In terms of the size of upper P3-M1, these four species are all obviously smaller than *Pl. okuyamai*. Also, the depth and number of the secondary enamel folds of IRF are shallower and fewer, respectively, than *Pl. okuyamai* (Fig. 4).

Other than the largest tooth size and very deep and densely arranged secondary enamel folds of P3-M1 in *Pl. okuyamai* among the species of the genus, another characteristic feature of the species is the extremely long palatal bridge. As described above, the length (C4) and width (C5) of the palatal bridge are 13.84 and 13.7 mm, respectively, and the ratio of C4/C5 is 1.01, which is almost exactly same ratio as in *Pentalagus furnessi* (Table 2). On the other hand, the ratio in other species (as far as known) of the genus is less than 0.85, and that of *Aztlanolagus agilis* is 0.89 (Table 2). In addition, the ratio becomes smaller from the older species to younger species in Chinese lineage, while it is large in *Pl. okuyamai* (Fig. 4).

As described above, it is obvious that the maximum width of incisive foramen is much wider than that of mesopterygoid fossa in *Pl. okuyamai*, while the former is narrower than the latter in *Pentalagus furnessi*, thus the relationships of the two

widths are opposite in these two taxa. Parenthetically speaking, the maximum width of incisive foramen is also wider than that of mesopterygoid fossa in *Pl. dajushanensis*, but the difference is smaller. In addition, the proportional contributions of the maxilla and palatine to the palatal bridge length is about 6:5, respectively, in *Pl. okuyamai*, while it is about 8:2 in *Pentalagus furnessi*. Thus, these taxa are dissimilar in the two characteristics mentioned above.

Combining all the characteristics mentioned above, we propose phylogenetic relationships among these taxa (Fig. 4). We do not know where and when *Aztlanolagus*/*Pliopentalagus* originated, but *Pl. huainanensis* is the oldest and most primitive species within the Asian lineages, and *Pl. dajushanensis* and *Pl. anhuiensis* gradually evolved within China (Tomida and Jin, 2009). Sometime before 3.6 Ma, *Pl. huainanensis* or similar species migrated to Japan and evolved into *Pl. okuyamai* by 3.6 Ma with the characteristics of larger size, deeper and densely arranged secondary folds of IRF of P3-M1, and the length/width ratio of palatal bridge toward 1. If the secondary folds of IRF of P3-M1 deepen, and general outline of P3-M1 becomes squared (antero-posteriorly longer), the new species becomes more similar to *Pentalagus furnessi*. But, how or why the relationships in widths of incisive foramen and mesopterygoid fossa have changed is unclear so far. At any rate, we conclude that *Pl. okuyamai* may be a possible ancestral form of, and at least most closely related to *Pentalagus furnessi*.

ACKNOWLEDGMENTS

We thank Y. N. Lee for inviting us to contribute the Dr. Jacobs' festschrift volume and for providing an opportunity to complete this study. We are also grateful to reviewers L. J. Flynn and M. Erbajeva who made constructive suggestions for improvement of the manuscript. YT thanks P. Jenkins, D. Hills, and L. Tomsett of the Department of Mammalogy at The Natural History Museum in London, L. J. Flynn of Harvard University, S. Kawada of the National Museum of Nature and Science Japan, and A. H. Harris of the University of Texas at El Paso, for his examinations of the specimens under their care. Figures 1 to 4 were prepared by M. Oshima, and line drawings of teeth using Adobe Illustrator CS2 were made by S. Yamamoto. We thank them for their help.

AUTHOR CONTIBUTIONS

YT described the original specimens, made comparisons with other taxa, and drafted the manuscript. KT arranged this project and took photos. Both authors edited the manuscript.

LITERATURE CITED

Averianov, A., Abramov, A. V., & Tikhonov, A. N. (2000). A new species of *Nesolagus* (Lagomorpha, Leporidae) from Vietnam with osteological description. *Contributions from the Zoological Institute, St. Petersburg*, 3, 1–22.

Daxner, G. & Fejfar, O. (1967). Über die Gattungen *Alilepus* Dice, 1931 und *Pliopentalagus* Gureev, 1964 (Lagomorpha, Mammalia). *Annals Naturhistorishes Museum Wien*, 71, 37–55.

Kawamura, Y. & Okuyama, S. (1995). Pliocene leporid remains (Lagomorpha, Mammalia) from the Ueno Formation of the Kobiwako Group, at Oyamada, Mie Prefecture, central Japan: the oldest rabbit remains in Japan. *Abstracts of the 1995 Annual Meeting of the Palaeontological Society of Japan (Nagoya)*, 90. (In Japanese)

Satoguchi, Y. (2020). Geological history of paleo- and present Lake Biwa. In H. Kawanabe, M. Nishino, & M. Maehata (Eds.), *Lake Biwa: Interactions between Nature and People (Second Ed.)* (pp. 17–24). Springer.

Satoguchi, Y., Higuchi, Y., & Kurokawa, K. (2005). Correlation of the Ohta Tephra Bed in the Tokai Group with a tephra bed in the Miura Group, central Japan. *Journal of the Geological Society of Japan,* 111(2), 74–86. [in Japanese with English abstract].

Tanimoto, M. & Kitada, M. (2011). The record of "Dinosaur and Fossils of Iga 2010" held at Ueno History and Folklore Museum. -The commemorative exhibition of the donation of Okuyama Fossil Collection to the Lake Biwa Museum-. *Iga Basin Fossil Club Bulletin*, 6, 2–13. [in Japanese].

Tomida, Y. & Jin, C. Z. (2004). *Aztlanolagus* (Lagomorpha, Mammalia) revisited: origin, migration, evolution, and taxonomy. *Journal of Vertebrate Paleontology,* 24(3) supplement, 121A.

Tomida, Y. & Jin, C. Z. (2008). Can morphological differences among extinct species be explained by means of genetics? An example from fossil rabbits. *Journal of Vertebrate Paleontology*, 28(3) supplement, 152A.

Tomida, Y. & Jin, C. Z. (2009). Two new species of *Pliopentalagus* (Leporidae, Lagomorpha) from the Pliocene of Anhui Province, China, with a revision of *P. huainanensis*. *Vertebrata PalAsiatica*, 47(1), 53–71.

WINDOWS INTO SAUROPSID AND SYNAPSID EVOLUTION
Essays in honor of Prof. Louis L. Jacobs, pp. 341–365, 2023

PROCYONIDAE (MAMMALIA, CARNIVORA) AND THE GREAT AMERICAN BIOTIC INTERCHANGE

JON BASKIN[1,*] and ALBERTO VALENCIANO[2,3]

[1]Department of Biological and Health Sciences, Texas A&M University-Kingsville, Kingsville, Texas 78363, U.S.A., Jon.Baskin@retiree.tamuk.edu;
[2]Departamento de Estratigrafía, Geodinámica y Paleontología, Facultad de Ciencias Geológicas, Universidad Complutense de Madrid, C/José Antonio Novais 12, 28040, Madrid, Spain, albvalen@ucm.es
[3]Research and Exhibitions, Iziko Museums of South Africa, P.O. Box 61, Cape Town, 8001, South Africa

ABSTRACT Members of the family Procyonidae were the first placental carnivorans to migrate from North America to South America, during the first part of the Great American Biotic Interchange (ProtoGABI). The *Cyonasua* group is an endemic South American radiation of procyonids, known from the Late Miocene to Middle Pleistocene. It includes *Cyonasua argentina*, perhaps four species of *Amphinasua*, one of *Brachynasua*, and two species of the remarkable, bear-like *Chapalmalania*. Some of the characters used to distinguish these taxa are likely caused by individual variation and sexual dimorphism. Early records of the *Cyonasua* group include fossils collected in 1926-27 by an expedition from the Field Museum of Natural History to Catamarca Province, Argentina. We illustrate and discuss the most important of these specimens. The *Cyonasua* group is the sister taxon of the North American Middle and Late Miocene *Arctonasua*. The extant genera *Nasua* and *Procyon* have a Pliocene record in North America and first occur in South America in the Early-Middle Pleistocene. The fossil record indicates that, for the most part, the genera of procyonids evolved in North America before migrating to South America. Divergence dates determined from the fossil record are younger than those of the molecular clock.

KEYWORDS Miocene, Pliocene, GABI, Carnivora, *Cyonasua*

INTRODUCTION

In the Late Miocene, land mammals from North and South America began crossing the narrowing gap between Central and South America, first by island hopping and later along the dry land corridor of the Isthmus of Panama (Simpson, 1950, 1952, 1980). This exchange and interaction of northern and southern taxa greatly altered the Neotropical and Nearctic faunas and floras. The "heralds" of the Great American Biotic Interchange (GABI) included ground sloths migrating northward from South America and procyonids migrating southward from North America (Webb, 1985). Woodburne et al. (2010) placed the heralds in the pre-GABI followed by GABI 1 to 4. We follow Cione et al. (2015) in dividing the Interchange into the Late Miocene to Early Pliocene ProtoGABI and the Late Pliocene to Early Holocene GABI 1 to 4 (Fig. 1).

The extant Procyonidae include 14 species and 6 genera of small to medium size, mainly Neotropical carnivorans (e.g., Koepfli et al., 2017). Procyonids are adapted to terrestrial and arboreal habitats, and their dietary ecology ranges from frugivory (*Potos*, *Bassaricyon*), to omnivory (*Nasua*, *Nasuella*, *Procyon*), and to omnivory, but with a significant proportion of insects and small vertebrates (*Bassariscus*) (e.g., Kays, 2009; Koepfli et al., 2017; Kitchener et al., 2017). Beginning in the Late Miocene (ca. 7 Ma) to middle Pleistocene (ca. 1 Ma), the extinct procyonids of the *Cyonasua* group diversified in South America (e.g., Patterson & Pascual, 1968; Simpson, 1980; Webb, 1985; L. Soibelzon & Prevosti, 2007; Forasiepi et al., 2014; Cione et al., 2015). During GABI 1-4, extant procyonids migrated south and diversified in South America (e.g., Simpson, 1980; Woodburne, 2010; Forasiepi et al 2014). The aim of our present research is to summarize the diversity of fossil procyonids in the Americas, update the taxonomic attributions, and summarize the evolutionary history of the procyonids, placing special emphasis on the *Cyonasua* group.

*Corresponding author

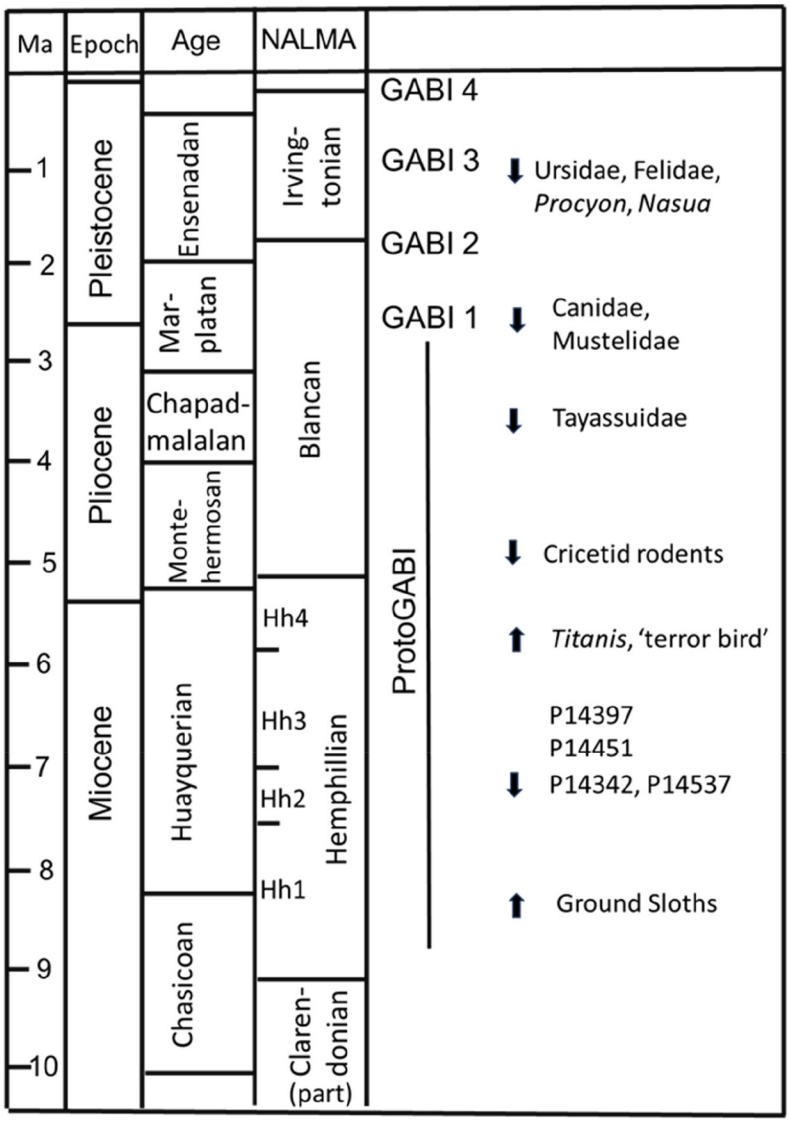

FIGURE 1. Biostratigraphic and chronostratigraphic chart of migration events to South America (↓) and to North America (↑) during the GABI and stratigraphic occurrence of FMNH P specimens.

Abbreviations — AMNH F:AM, Frick Collection, Division of Vertebrate Paleontology, American Museum of Natural History, New York City, USA; FMNH, Field Museum of Natural History, Chicago, USA; MACN, Museo Argentino de Ciencias Naturales 'Bernardino Rivadavia,' Buenos Aires, Argentina; MLP, Museo de La Plata, La Plata, Argentina; MMP, Museo Municipal de Ciencias Naturales "Lorenzo Scaglia", Mar del Plata, Argentina; NRM, Naturhistoriska Riksmuseet, Stockholm, Sweden; UCMP. University of California Museum of Paleontology, Berkeley, USA; UF, Vertebrate Paleontology Collection of the Florida Museum of Natural History (FLMNH), University of Florida, Gainesville, USA; GABI, Great American Biotic Interchange; NALMA, North American Land Mammal Age.

SYSTEMATIC PALEONTOLOGY

Family PROCYONIDAE (Gray, 1825)

Included Taxa — *Broiliana* Dehm 1950, Procyoninae Gill, 1872, and Potosinae, Trouessart 1904.

Distribution — Early Miocene (MN3, Orleanian and Agenian) of Europe; Early Miocene-Recent (Hemingfordian-Recent) of North America; Late Miocene-Recent (Huayquerian-Recent)

of South America.

Diagnosis — In the Procyonidae and Ailuridae, the dental formula is I3/i3, C1/c1, P4/p4, M2/m2. The procyonid and ailurid dentition is distinguished from that of primitive mustelids in having the second molars enlarged. The m2 has a short trigonid and an elongated talonid. The m1 primitively has a relatively prominent metaconid and a basined talonid. P4 has a lingualinternal cingulum and a small parastyle. M1 retains a postprotocrista and metaconule, the primitive arctoid state. Procyonids are derived relative to ailurids in having a Type B auditory bulla (Hunt, 1974) with an inflated entotympanic, greater separation of the posterior lacerate and posterior carotid foramina, a deep suprameatal fossa, and loss of the alisphenoid canal. Relative to *Broiliana*, the New World Procyonidae (Potosinae + Procyoninae) are further derived in having P4 with a better developed parastyle, and m2 hypoconulid postero-lingual and anterior cingulum reduced.

Discussion — In his classification of mammals, Gray (1825) listed, without comments, the Tribe Procyonina for *Procyon*, *Nasua*, and ?*Potos*. The Tribes Procyonina, Ursina (bears), and the Gulonina, Myadina, and Taxina (various mustelids) were placed in the Family Ursidae. Turner (1848) discussed the cranial and dental characters uniting *Procyon*, *Bassaris* (=*Bassariscus*), *Nasua*, and *Cercoleptes* (=*Potos*) in the ursid subfamily Procyonina. Bonaparte (1850) established the Family Procyonidae for the Procyonina (*Potos* was placed in its own family Cercoleptidae), Melina (certain mustelids) and Ailurina (red panda). Flower (1869) restricted Procyonidae to *Procyon*, *Bassaris* (=*Bassariscus*), *Nasua*, and *Cercoleptes* (=*Potos*) and discussed characters that united this family. Pocock (1921) added *Bassaricyon* and further discussed the 18th and 19th century history of the recognition and diagnosis of members of this family. Koepfli et al. (2017) elaborated further on this and added developments in the 20th century.

Subfamily PROCYONINAE Gill, 1872

Distribution — Early Miocene-Recent (Hemingfordian-Recent) of North America; Late Miocene-Recent (Huayquerian-Recent) of South America.

Diagnosis — Primitive Procyoninae are distinguished from primitive Potosinae in having M1 with a more posteriorly situated hypocone, M1 with a better developed metaconule, and bulla with a more inflated entotympanic. The extinct South American procyonines of the *Cyonasua* group share with the extant *Nasua*, *Nasuella*, and *Procyon* the following characters: m1 with an entoconulid and a low trigonid with paraconid and metaconid close together; m2 with entoconid, a postero-lingual hypoconulid forming a heel, and a reduced anterior shelf; P4 with enlarged protocone and parastyle and with shortened metaconid blade; and M2 with broadened protocone.

Comment — Gill (1872) established this subfamily solely for *Procyon*, with *Nasua* placed in its own procyonid subfamily, and *Potos* and *Bassariscus* in own families. The Procyoninae was later expanded to include many more genera (e.g., Simpson, 1945).

CYONASUA GROUP Patterson & Pascual, 1968

Diagnosis — Medium to very large-sized procyonids with a shortened rostrum (relative to *Procyon*) and deep mandible, I3 enlarged, P4 triangular with hypocone absent and with reduced to absent parastyle and reduced metacone (=metastyle), M1 and M2 with greatly reduced to absent hypocone, and m1 with a complex paraconid except in the most primitive species.

Comments — Patterson & Pascual (1968) coined the term *Cyonasua* group for the endemic South American Late Miocene to Middle Pleistocene (Huayquarian to Ensenadan Ages) procyonids. From the late 19th into the 21st century the systematics of this group has been contentious. The two most important 20th century works describing and illustrating the members of the *Cyonasua* group are Kraglievich & Reig (1954) and Kraglievich & Olazábal (1959). Berta & Marshall (1978) provided a useful summary of the synonymies and references concerning South American fossil procyonids up to that time. In the 21st century, Argentinian paleontologists have greatly increased our knowledge of this group. Prevosti & Forasiepi (2018) includes the most comprehensive review of South American fossil procyonids to date and should be consulted for further information. *Cyonasua argentina* was the first member of this group to be described (F. Ameghino, 1885). F. Ameghino noted the similarity of *Cyonasua* to *Nasua*, the coatimundi. F. Ameghino (1891) synonymized *Amphinasua brevirostris* (Moreno & Mercerat, 1891) with *C. argentina*, but later (1906) considered *Cyonasua*, *Amphinasua*, and *Pachynasua* (F. Ameghino, 1904) distinct genera from different time periods forming a lineage to *Ailurus*, the red panda. C. Ameghino & Kraglievich (1925) placed their new genus *Brachynasua* in the Potosinae. *Cyonasua* was recognized as the senior synonym of *Amphinasua* and *Pachynasua* (Riggs &

Patterson, 1939; Kraglievich & Reig, 1954; Kraglievich & Olazábal, 1959). Kraglievich & Olazábal (1959) determined that the bear-sized *Chapalmalania* (F. Ameghino, 1908a) was a procyonid (rather than an ursid) that was very closely related to *Cyonasua*. Berman (1994) added *Brachynasua* to the junior synonyms of *Cyonasua*. Baskin (2003, 2004) retained four genera in this group, with *Cyonasua* the primitive sister taxon of *Amphinasua, Brachynasua* and *Chapalmalania*. Others (e.g., Berman, 1994; L. Soibelzon & Prevosti, 2007; J. Tarquini et al., 2018) recognized only two valid genera: *Cyonasua* with at least eight valid species (*C. argentina, C. brevirostris, C. longirostris, C. clausa, C. pascuali, C. groeberi C. lutaria*, and *C. meranii*) and *Chapalmalania*, with two, *Ch. ortognatha* and *Ch. altaefrontis*. Prevosti & Forasiepi (2018) included seven species in *Cyonasua*, with *C. longirostris* a junior synonym of *C. brevirostris*. L. Soibelzon, (2011, fig. 1) displayed the temporal distribution of these taxa. We recognize those species assigned to *Cyonasua* as belonging to *Cyonasua, Amphinasua,* and *Brachynasua*.

CYONASUA F. Ameghino, 1885

Type species — *Cyonasua argentina* F. Ameghino, 1885, p. 17

Holotype — MLP 10-171, left mandible with a broken canine and p2-p3; MLP 69-XII-14-1, anterior mandible with p4 (L. Soibelzon, & Bond, 2013, figs. 2.1, 2.2).

Type locality — Lower Member of the Ituzaingó Formation (Late Miocene; traditionally known as "Mesopotamiense" or "Conglomerado osífero"; Brunetto et al. 2013), Barrancas del río Paraná, Department of Paraná, Entre Ríos Province (Cione et al., 2000; L. Soibelzon, & Bond, 2013). The fossil mammals of the Conglomerado osífero are the basis for the Piso Mesopotamiense (Ameghino, 1883). Cione et al. (2000) assigned the "Mesopotamiense" to the Huayquerian Age. Schmidt et al. (2020) further discussed the different interpretations of the age of the "Mesopotamiense." Sr-isotope dates of 11.9 to 6.00 Ma for the underlying Paraná Formation set a maximum age for the Ituzaingó Formation (del Río et al., 2018; Schmidt et al., 2020).

Diagnosis — The most primitive genus of the *Cyonasua* group. Medium-sized procyonid with paraconid of m1 simple, conical; p1 present; p2-p4 with poorly-developed posterior accessory cusps.

Distribution — *Cyonasua* (*sensu* Kraglievich & Reig, 1954) is well represented in the Late Miocene to Pliocene of Argentina (e. g., Berta & Marshall, 1978; Berman, 1994; J. Tarquini et al. 2016). Elsewhere it is known from the Late Pliocene of Venezuela (Forasiepi et al., 2014), Late Miocene of Uruguay (L. Soibelzon, et al., 2019), Late Miocene of Bolivia (L. Soibelzon, et al., 2020), and Late Miocene of Peru (J. Tarquini et al., 2020). Huayquerian, Montehermosan, and Chapadmalan Ages.

Comments — F. Ameghino (1885) distinguished *Cyonasua* from *Nasua* and provided measurements of the type material. While this material was sufficient to diagnose the genus, it is insufficient to determine if any of the other nominate species of *Cyonasua* are junior synonyms of the genotype. However, *C. argentina* has only been recorded with certainty in the "Mesopotamiense" (L. Soibelzon, & Bond, 2013). MACN-A-53-6 is a mandible fragment with m1, m2 of *Cyonasua* from Paraná. The m1 has "V"-shaped trigonid, the paraconid is a simple cuspid, and the entoconid prominent (Kraglievich & Reig, 1954, fig. 4). This can be used to diagnose the species. Although the illustration makes the m1 appear smaller than the other specimens, the m1 lengths are similar (Kraglievich & Reig, 1954, unnumbered table). Other specimens of *C. argentina* from Catamarca Province (Kraglievich & Reig, 1954; Kraglievich & Olazabel, 1959) are discussed below.

AMPHINASUA Moreno & Mercerat, 1891

Type species — *Amphinasua brevirostris* Moreno & Mercerat, 1891:235.

Included species — *Amphinasua brevirostris*, *A. clausa*, *A. lutaria*, *A. groeberi*, *A. pascuali*.

Diagnosis — Medium- to large-sized procyonids with paraconid of m1 complex as result of the development of at least a lingual crest of the paraconid; paracone of m1 situated anterolingually. Characters of the skull and upper dentition are discussed with *Amphinasua brevirostris*. An m1 with a complex paraconid also characterizes *Chapalmalania* (Kraglievich & Reig, 1954; Kraglievich & Olazabel, 1959).

Amphinasua brevirostris Moreno & Mercerat, 1891

Holotype — MLP 10-52.

Type locality—"bajo de Andalhualá" near Valle Santa María, Catamarca Province.

Additional material — MACN 8209, holotype of *Amphinasua*

longirostris Rovereto, 1914, p. 81; MACN 8210, holotype of *Pachynasua*? *robusta* Rovereto, 1914, p. 82.

Diagnosis — Medium-sized procyonid with m1 paraconid situated antero-lingually close to the metaconid and with a low crest extending postero-lingually; I3 much larger than I1 or I2; P1/p1 reduced to absent; P4 with a low protocone directly opposite the subcentral paracone, which is flanked by a very small parastyle and metacone; M1 with hypocone very reduced to absent; M2 relatively small; cranium with expanded frontal sinuses.

Distribution — Andalhuala and Chiquimil Formations, Catamarca Province, Huayquerian Age.

Descriptions — The holotype of *Amphinasua brevirostris* is a skull with a damaged rostral region (Moreno & Mercerat, 1891, Lamina IX; Reguero & Candela 2011, fig. 4). The P1 is small; P2 and P3 are simplified, lacking accessory cusps; P4 is triangular, with the paracone situated subcentrally on the buccal margin opposite a low protocone, a very small metacone, that is shorter than the parastyle, and no hypocone; M1 with buccal cingulum absent and a narrow posterolingual hypoconal shelf; M2 triangular, with a relatively prominent posterolingual hypoconal shelf.

The holotype of *Amphinasua longirostris* is a skull with two hemimandibles (Rovereto, 1914, plate VII, figs. 5, 5a, 5b). It has P1 small, P2/p2 and P3/p3 without accessory cusps, and m1 paraconid antero-medial, with a low postero-lingual extension (see Foresiepi et al., 2014, fig. 2D). Baskin (2004) interpreted this as a paraconid with a lingual extension from an illustration of the m1 (Kraglievich & Reig, 1954, fig. 4 A) and from a poor-quality plaster cast (UCMP 38435). The holotype of *Pachynasua*? *robusta* is an anterior mandible with c1, p3, p4 (Rovereto, 1914, plate VII, figs. 6a). The mandible is deep, the canine is broken, p1 is absent, and the worn p3 and p4 do not have accessory cusps.

Comments — The holotypes of *Amphinasua brevirostris, A. longirostris*, and *Pachynasua*? *robusta* are from unknown levels of the Andalhuala Formation, Valle de Santa María, Catamarca Province. Although there are morphological differences between the first two (Forasiepi et al., 2014) and the third consists of a worn, anterior dentition "without any systematic value" (Soibelozon et al. (2019, p. 368), we follow Kraglievich & Reig (1954) in synonymizing the three.

Moreno & Mercerat (1891) compared *Amphinasua brevirostris* favorably to *Cyonasua* and *Nasua*. F. Ameghino (1891, p. 204-207) synonymized *A. brevirostris* with *C. argentina*. He illustrated the skull of *A. brevirostris* with a hemimandible attributed to *C. argentina* from Paraná (F. Ameghino, 1891, fig. 76). To the best of our knowledge, the provenance of that jaw has not been published. Ameghino emphasized that *Cyonasua* had the four premolars and two molars of procyonids rather than three premolars and three molars used in the descriptions of *A. brevirostris*. Mercerat (1895) defended the distinctness of the two genera, having previously noted *Amphinasua* was most similar to *Nasua* and that an antiquated tooth numbering system was used for the cheek teeth.

Forasiepi et al (2014) constructed a data matrix with 78 characters based on Ahrens (2012) with the addition of members of the *Cyonasua* group. *Cyonasua brevirostris* and *C. longiramus* (represented by the type specimens) have a deep zygomaticus muscle fossa in orbital wall (derived) relative to its absence in *Chapalmalania altaefrontis*. The P4 hypocone is present (scored as derived) in *A. longirostris* and absent (scored as primitive) in *A. brevirostris*, the only difference of these sister taxa. The m1 paraconid of *A. longirostris* is scored as not divided.

Amphinasua clausa (F. Ameghino, 1904 p. 268)

Holotype — MACN 7955. Mandible with left i1, i3 c1, p2-m2; right i2, i3, p3-m2 described as *Pachynasua clausa*, new genus and species (F. Ameghino, 1904). Figure in Rovereto (1914, fig. 67). Measurements in Sobelzon et al. (2020, table 1).

Type locality — "Farola Monte Hermoso", Buenos Aires Province, Argentina, the type locality of the Monte Hermoso Formation. L. Soibelzon, (2011) described eight deciduous teeth of *Cyonasua* sp. collected by Sergio Bogan from the 'Miembro de las Limolitas claras' of the Monte Hermoso Formation, close to the site where MACN 7955 was found. The Miembro de las Limolitas claras had been assigned to the Chapadmalalan Age (Cione & Tonni, 1996). Tomassini et al. (2013) assigned *Amphinasua clausa* to the *Eumysops laeviplicatus* Zone, the only biozone of the Montehermosan Age. The Montehermosan is Early Pliocene, 4.7-3.7 Ma (Prevosti et al., 2021).

Description — MACN 7955 is from an old individual with a very worn dentition, such that the cusp patterns are not visible (Rovereto, 1914, fig. 67). The p1 alveolus is very small. The p2 and p3 are crowded and set at an angle. *Amphinasua clausa* is similar in size to *A. groeberi* and *A.*

brevirostris. The offset and overlapping p2 and p3 are similar to those of *A. lutaria* (Cabrera, 1936) which is smaller and lacks p1.

Comment — Because the dentition is so worn, *Cyonasua clausa* has been considered *Cyonasua incertae sedis* (Kraglievich & Reig, 1954) and "without any systematic value" (Soibelozon et al., 2019, p. 368). However, the holotype of *Amphinasua clausa* is at least as informative as the holotype of *Cyonasua argentina*.

Amphinasua lutaria (Cabrera, 1936, p. 304)

Holotype — MLP 34-VI-20-6, left premaxilla and maxilla with i3-m2; left and right mandible with i1-m2; right tibia and fibula (Tarquini, 2018). It was described as a new species of *Pachynasua* and later transferred to *Cyonasua* (Kraglievich & Reig, 1954).

Type locality — Atlantic coast of Miramar, *Paraglyptodon chapadmalensis* biozone of the Chapadmalal "formation", Buenos Aires Province (Cione & Tonni, 1995; Cenizo et al., 2016).

Description — P1/p1 absent; P4 with small parastyle and larger metacone flanking the prominent paracone, small twinned cuspules posterolingually placed to the protocone; M1 with a reduced lingual cingulum and a small parastyle; lower premolars with prominent posterior accessory cuspids; p2 and p3 crowded and offset in the mandible, and m1 with a complex paraconid (Prevosti & Reguero, 2000, fig. b, c; Forasiepi et al., 2014, fig. 4a, c; Engelman & Croft, 2019, figs. 3A, 4A).

Amphinasua groeberi (Kraglievich & Reig, 1954, p. 217)

Holotype — MMP S-645, left mandible with p2-m2 and anterior right mandible c1, p2, and partial p3. Described as *Cyonasua groeberi* (Kraglievich & Reig, 1954).

Type locality — Tuclame Quarry, La Playa Formation of Córdoba Province, Huayquerian–Montehermosian in age (Bondesio & Pascual, 1981) or younger (Deschamps et al., 2013).

Description — The p1 alveolus is for a small, single-rooted tooth. The premolars are wider posteriorly. The p3 and p4 possess well-developed anterior and posterior accessory cuspids. The m1 has a complex paraconid. (Kraglievich & Reig, 1954, figs. 1-3, 4D).

Amphinasua pascuali (Linares, 1982, p. 118)
Figure 2

Holotype — AMNH F:AM 45985, right mandible with p2-m2. Described as *Cyonasua pascuali* (Linares, 1982, figs. 3, 4c; L. Soibelzon, 2020, fig. 4) from the Huayquerías Formation, Mendoza Province is Huayquerian in age, greater than 5.8 Ma (Marshall, 1985). *Amphinasua* cf. *pascuali* has been reported from the Huauquerian Tariquía Formation of Bolivia (L. Soibelzon, et al., 2020).

Referred specimens — AMNH F:AM 45984, left mandible with p2 and broken dentition, possibly from the same individual as AMNH F:AM 45985; AMNH F:AM 45986, right mandible with broken p3, and complete p4-m2.

Type locality — San Carlos, Mendoza, Huayquerías Formation.

Description and Comparison — AMNH F:AM 45985 is significantly smaller than the holotypes of other species of *Cyonasua*. There is no alveolus for a p1. The posterior accessory cusp is absent on p2, weakly developed on p3, and better developed on p4. The p4 has a very small anterior accessory cusp. The premolars are not expanded postero-lingually. The m1 has a small antero-lingually situated paraconid with a prominent lingual extension. In the m1 talonid, the hypoconid is the most prominent cusp, followed by the entoconid (identified by Linares, 1982, as the entoconulid), and a smaller hypoconulid. The m2 metaconid is situated distinctly posterior to the protoconid and the protoconid is separated from the hypoconid by a V-shaped notch, and the hypoconulid is situated postero-centrally.

AMNH F:AM 45986 is larger than AMNH F:AM 45985, with a p2-m1 length similar to *Cyonasua lutaria* but with a longer m1 and a longer m2 (Table 1). The p4 length and width are similar to the holotype of *Cyonasua argentina*. The p4 lacks an anterior accessory cusp. The m1 has a better developed antero-internal cingulum of the paraconid than AMNH F:AM 45985; the hypoconid is the largest cusp of the talonid; and the entoconid is connected anteriorly to a small entoconulid and posteriorly to a small hypoconulid. The m2 metaconid is situated almost opposite the protoconid; the protoconid and hypoconid are connected by a narrow ridge; and the hypoconulid is situated postero-lingually.

Causes of Variation

Rodriguez et al. (2016) have pointed out that for *Cyonasua*

FIGURE 2. *Amphinasua pascuali* from San Carlos, Mendoza, Argentina, Huayquerias Formation. A-C. AMNH F:AM 45985, right hemimandible in buccal (A), lingual (B), and occlusal (C) views; D. AMNH F:AM 45984, left hemimandible with p2 and broken dentition in buccal (D), lingual I, and occlusal (F) views; G-I. AMNH F:AM 45986, right hemimandible from Mendoza in buccal (G), lingual (H), and occlusal (I) views.

(*sensu lato*) a "large number of taxa have been described for a relatively short time span, collected from a restricted geographical area, and based on badly preserved specimens raises reasonable doubt about the validity of these taxa." They proposed that sexual dimorphism was a factor for some of these differences. Males of *Nasua* are consistently larger than females (Decker, 1991). Adult males of *Bassariscus astutus* were significantly larger than females for 12 of 17 cranial and dental measurements

TABLE 1. Measurements (mm) of AMNH 45986; the holotypes of *Cyonasua pascuali* (AMNH F:AM 45985), *C. argentina* (MLP 69-XII-14-1), *C. longirostris* (MACN 8209), *C. lutaria* (MLP 34-VI-20-6), *C. clausa* (MACN 7955), and *C. groeberi* (MMMP S-645), data from Soibelzon et al., (2020); *A. brevirostris* (FMNH P14342 and P14397); and *C. argentina* (MACN 6689, 13284), and *C.* cf. *argentina* (MACN 6692) from the "Araucanense" of Catamarca Province as identified in Kraglievich and Reig (1954)

	p4L	p4W	p4W/p4L	m1L	m1W	m2L	m2W	p2m2	p4L/m1L	m2L/m1L
AMNH F:AM 45986	9.6	6.2	0.64	12.1	7.3	9.6	5.9	43.0	0.79	0.79
C. pascuali	7.1	4.0	0.56	8.9	4.8	7.0	3.9	34.0	0.80	0.79
C. argentina	9.5	6.0	0.63							
C. longirostris				12.5	7.1	9.8	5.6	47.8		0,78
C. lutaria	9.5	5.4	0.57	10.8	6.0	8.4	5.4	43.0	0.88	0.78
C. clausa	9.8	6.9	0.70	12.5	7.2	8.6		49.0	0.77	0.69
C. groeberi	10.8	7.6	0.70	12.2	7.7	8.7	6.0	48.5	0.89	0.71
FMNH P14342	9.2	6.4	0.70	11.3	6.6	9.9	4.9	48.0	0.81	0.88
FMNH P14397	11.0	6.0	0.55	12.2	7.0	9.6	5.3	48.2	0.90	0.79
MACN 6689	9.1			10.7		8.8		45.0	0.85	0.82
MACN 13284	9.2	5.8	0.63					42.0		
MACN 6692	9.3	6.1	0.66	11.6	6.5	9.5	5.0	44.5	0.80	0.83

(Stangl et al., 2014). The 52% body size difference in two specimens of the ailurid *Pristinailurus bristoli* from the Hemphillian Gray Fossil Site in Tennessee is most plausibly explained by sexual dimorphism (Fulwood & Wallace, 2015). The borophagine canid *Epicyon saevus* from the late Clarendonian of Florida varies in the development of accessory cusps and size of the lower premolars (Baskin, 1998a). The following are examples where further research is needed to determine whether size (Table1) and/or morphological differences may represent different, possibly new, species or are evidence of individual variation or sexual dimorphism.

Linares (1982) did not include AMNH F:AM 45986 in the hypodigm of *Cyonasua pascuali* or discuss it in his paper. The catalogue label from AMNH states it came from the locality of San Carlos (Mendoza). Although AMNH F:AM 45986 has a 34% greater m1 length and a 26% greater p2-m2 length than AMNH F:AM 45985, the width to length proportions for the p4, for the m1, and for the m2, respectively, are similar.

Two species of *Cyonasua* were presumed present in the "Araucanense" of Catamarca Province (Kraglievich & Reig, 1954; Kraglievich & Olazabel, 1959). *Cyonasua argentina*, the smaller of the two (Table 1), has a lower horizontal ramus, more complicated premolars, m1 with a simple conical paraconid and talonid without well-defined cuspids on the margins, and m2 proportionally well-developed. MACN 6692, illustrated by F. Ameghino (1906, fig. 259) as *Amphinasua brevirostris*, was reidentified as *Cyonasua* cf. *argentina* by Kraglievich & Reig (1954). *Cyonasua brevirostris* (represented by the holotype of *Amphinasua longirostris*) is larger with simpler premolars; m1 with paraconid formed by two to three cusps, metaconid more reduced, the talonid postero-lingual border with an entoconid and hypoconulid; and m2 tending to be proportionately reduced in size (Kraglievich & Reig, 1954, p. 224, fig. 4A). These differences may be of taxonomic significance or may represent individual variation or sexual dimorphism within *Amphinasua brevirostris*.

Both *Amphinasua clausa* (F. Ameghino, 1904) and *A. lutaria* (Cabrera, 1936) were first assigned to *Pachynasua.* Both have premolars that are offset. *Amphinasua clausa* is 14% larger than *A. lutaria*. *Amphinasua lutaria* lacks p1 and there are no gaps between the premolars. The stratigraphic ranges of *Amphinasua clausa* and *A. lutaria* may have overlapped (L. Soibelzon, 2011, fig. 1b).

Problematic Taxon Names

Parahyaenodon argentinus (F. Ameghino, 1904, p. 266) and *Tetraprothomo argentinus* (F. Ameghino, 1908b) are from unknown levels of the Monte Hermoso Formation (Tomassini et al., 2013). *Parahyaenodon argentinus* is a procyonid allied to *Cyonasua*, not a metatherian borhyaenid carnivore

(Forasiepi et al., 2007). The holotype of *Tetraprothomo* is a procyonid femur (Bordas, 1942; Forasiepi et al., 2007). Examples of *Cyonasua* recorded as *Cyonasua* sp., with little or no further information, make it difficult to determine anything further.

The holotype and only specimen of *Oligobunis argentinus* is an anterior mandible fragment with i3, c1, p2-p3 (Burmeister, 1891, p. 378, plate VII, fig. 2; L. Soibelzon, & Bond 2013, fig. 2.3). It is from Ituzaingó Formation at Barrancas del río Paraná, Entre Ríos Province (L. Soibelzon, & Bond, 2013), the same general locality as the holotype of *Cyonasua argentina*. Burmeister (1891) named his species *Oligobunis argentina* but labeled the figure caption (Burmeister, 1891, p. 400) *Oligodens argentinus*. He compared his specimen favorably to the North American *Oligobunis crassivultus* (Cope, 1881). Cope considered his species a canid and had initially assigned it to *Icticyon*. *Icticyon* is a junior synonym of *Speothos*, the hypercarnivorous Latin American bush dog. However, *Oligobunis crassivultus* is an oligobunine mustelid (Valenciano et al., 2016). Ameghino (1891) recognized Burmeister's species as a junior synonym of his *Cyonasua argentina*. Later work which distinguished the two referred to it as *C. argentinus*. Its provenance suggests it is *C.* cf. *argentina*.

MACN-PV 6229 is an incomplete skull, mandible with canine and molars, and astragalus (Kraglievich & Olazábal 1959; J. Tarquini et al., 2018) from the Huayquerian, Epecuén Formation, La Pampa province, Argentina (Tonni et al., 1992). One of us (JB) made brief observations of it and other specimens at the MACN. It has the m1 (Kraglievich & Reig, 1954, fig. 4E) paraconid smaller and lower than the metaconid. The paraconid and metaconid are close together almost closing off the trigonid. The paraconid has a slightly more lingual, very small accessory cuspid. And very close to the slightly smaller and lower metaconid. In a footnote, Kraglievich & Olazábal (1959, p. 39) suggested it might be a new species. Zetti (1972) proposed a name in his dissertation, but never published it (J. Tarquini et al., 2020). Because m1 lacks a prominent cingulid extending from the paraconid, it is tentatively referred to *C.* cf. *argentina*.

BRACHYNASUA C. Ameghino & Kraglievich, 1925

Type and only species — *Brachynasua meranii* C. Ameghino & Kraglievich, 1925.

Diagnosis — A procyonid of the size of *A. pascuali*; very short rostrum, P1/p1 absent; no postcanine diastema; P2/p2 anterior root offset; P4 with virtually no parastyle anterior to the paracone, the metacone is a small, very low cusp, the protocone is low, and the tooth is relatively wide posterobucally; and the M1 has no paraconule or metaconule, the paracone is larger than the metacone, both lingual and buccal cingula are present, and the lingualcingulum is slightly expanded posterolingually; M2 very small to absent (Zetti, 1966).

Distribution — "las toscas del Rio de La Plata" (E. Soibelzon et al. 2008), Buenos Aires Province. Ensenadan Age (middle Pleistocene).

Comment — The illustrated holotype lacks the M1 (C. Ameghino & Kraglievich, 1925, p. 185). However, an M1, probably collected at a later date, is present in the specimen (Kraglievich & Olazábal, 1959). *Brachynasua* has many features that are convergent with *Potos* which led C. Ameghino & Kraglievich assigning it to the Potosinae. Kraglievich & Olazábal (1959) stated that *Brachynasua* was likely more closely related to *Procyon* than to *Potos*. The fossil record shows that these features developed independently and much earlier in the North American lineage that gave rise to *Potos* and possibly *Bassaricyon* (Baskin, 2003).

CHAPALMALANIA F. Ameghino, 1908a

Type species — *Chapalmalania ortognatha* F. Ameghino, 1908a, p. 424.

Included species — *Chapalmalania ortognatha* F. Ameghino, 1908a; *Ch. altaefrontis* Kraglievich & Olazábal, 1959.

Distribution — Buenos Aires Province, Mendoza Province, and Catamarca Province, Argentina; Ware Formation, Colombia; and San Gregorio Formation, Venezuela. Late Pliocene (Chapadmalalan to Marplatan Ages).

Diagnosis — A bear-sized procyonid, with a short, broad rostrum and a high skull; P1/p1 present; P1-P3 offset, expanded transversely; P4 with a well-developed buccal cingulum and with very low parastyle and metacone. M1 without a hypocone, but with well-developed lingual and buccal cingula and the paracone and metacone are close together. The M2 is a relatively small, transversely elongated tooth. The p1 alveolus is small. The m1 with bifid paraconid and reduced metaconid.

Comment — F. Ameghino (1908a) created the Piso Chapalmalense for the fauna collected from the coastal cliffs between Mar del Plata and Miramar in Buenos Aires Province.

Kraglievich (1952) named this unit the Chapadmalal Formation. The fauna of this unit, including *Chapalmalania ortognatha*, defined the Chapadmalalense (Chapadmalalan in English) Age (Cione & Tonni, 1996; Tonni, 2009). Since the mid 1990's some references to *Chapalmalania* have spelled it *Chapadmalania.* According to the rules of the International Commission on Zoological Nomenclature (ICZN, 1999), "The original spelling of a name is the "correct original spelling", unless it is demonstrably incorrect" (Article 32.2), such as "an inadvertent error, such as a lapsus calami or a copyist's or printer's error" (Article 32.5).

Discussion — *Chapalmalania* is known exclusively from cranial and dental remains, the postcranial skeleton is unknown (J. Tarquini et al., 2018). The type specimen of *Chapalmalania ortognatha* is an anterior rostrum with incisors and a canine (F. Ameghino, 1908a; Kraglievich & Olazábal, 1959, fig. 3a; Agnolín, 2022, fig. 1A) that Ameghino thought was from a giant short-faced bear. The type specimen is from the Chapadmalal Formation, Buenos Aires Province, Argentina, and is 'probably no older than 2.8 Ma' (Marshall et al., 1986, p. 456). A P4 of *Chapalmalania* cf. *ortognatha* (Kraglievich & Olazábal, 1959, fig. 4) is from the Chapadmalal Formation or from the Uquian (=Marplatan) Age Barranca de los Lobos Formation (Marshall et al., 1986). There is an undescribed, but illustrated, skull of *Ch. ortognatha* from the Chapadmalal Formation (Berman, 1994; Prevosti et al., 2013, fig. 4j). Berman (1993) noted a mandible of *Ch. ortognatha* from the Vorohué Formation (Marplatan Age) in the Miramar region, that he discussed in detail in his dissertation (Berman, 1994).

The larger *Ch. altaefrontis* is based on a partial skull from the Tunuyán Formation, Mendoza Province (Kraglievich & Olazábal, 1959). It was initially considered Montehermosan in age (Kraglievich & Olazábal, 1959). Marshall (1985; *et al*., 1986) interpreted this specimen came from between two tuffs, dated at 2.4 and 2.6 Ma. Yrigoyen (1994) regarded that this specimen came from approximately 180 m below the lower tuff, and to be probably older than 3.8 Ma, but Chapadmalalan in age. North of Argentina, *Chapalmalania* sp. occurs in the Late Pliocene San Gregorio Formation, Venezuela (Carrillo-Briceño et al., 2021) and Late Pliocene Ware Formation, Colombia (Forasiepi et al. 2014).

Berman (1994) suggested that *Chapalmalania* could be seen as a scavenger. De los Reyes et al. (2013) described a skull of a glyptodont from sediments in Buenos Aires Province that are Chapadmalalan or younger in age that had bite marks that correspond to the dentition of *Chapalmalania* sp. They inferred that *Chapalmalania* was an omnivore with hyena-like scavenger habits.

Procyonids with a North and South American Fossil Record

PROCYON Storr, 1780

Fossil Distribution — late Hemphillian to Rancholabrean of United States of America; Rancholabrean of Canada; Irvingtonian and Rancholabrean of Mexico; Lujanian of Argentina (L. Soibelzon et al., 2010); Pleistocene of Brazil (Rodriguez et al., 2013); and Marplatan? of Venezuela (Ruiz-Ramoni et al., 2018). See Prevosti & Forasiepi (2018) for complete information.

Diagnosis — Rostrum of skull not greatly elongate; P2-3/p2-3 tall, anterioposteriorly compressed; P4 subquadrate, with prominent hypocone and parastyle; M1 with prominent metaconule posterior to protocone; m1 with closed trigonid; angular process of dentary above level of tooth row.

NASUA Storr, 1780

Fossil Distribution — late Hemphillian (Latest Miocene) to Rancholabrean of United States of America; Marplatan? of Venezuela (Ruiz-Ramoni et al., 2018); Late Pleistocene (Lujanian?), Brazil (Rodrigues et al., 2014); Middle Pleistocene, (?Ensenadan), Bolivia (Berta & Marshall, 1978). Prevosti & Forasiepi (2018) conclude that earliest South American record of *Nasua* is Late Pleistocene.

Diagnosis — Cranium with elongate and laterally compressed rostrum; Canines compressed, upper canines buccally laterally flared; P1 two-rooted; P4 subquadrate, with prominent hypocone and parastyle; M1 with prominent metaconule posterior to protocone; m1 with closed trigonid; angular process of dentary above level of tooth row.

PROCYONIDAE AND THE GREAT AMERICAN BIOTIC INTERCHANGE

First Appearances of members of the *Cyonasua* group

Procyonids, the first placental carnivorans in South America, dispersed across a narrowed seaway between Panama and Colombia as heralds of the GABI (Patterson & Pascual, 1968; Simpson, 1980; Webb, 1985; Woodburne et al., 2006; Cione et

al., 2015). Their oldest records are from the Huayquarian Age in Argentina (Prevosti et al., 2021). In 1926, Elmer Riggs led a paleontological expedition for the Field Museum of Chicago to Catamarca Province, Argentina (Riggs & Patterson, 1939; Butler et al, 1984). There they made extensive collections of fossils from the "Araucanense", including, most famously, the saber-toothed marsupial *Thylacosmilus atrox* (Riggs, 1934) and a nearly complete skeleton of the "terror-bird" *Andalgalornis ferox* (Patterson & Kraglievich, 1960; Marshall, 1978). The procyonids they collected were only briefly mentioned (Riggs & Patterson, 1939) and it wasn't until radiometric and paleomagnetic dating assigned absolute ages to them that their significance was recognized (Marshall et al., 1979).

FMNH P14342 and P14537 were collected from units XVIIIa and XIX, respectively, of the Chiquimil Formation near Chiquimil (Entre Ríos), in the Valle de Santa María, (Marshall et al., 1979). Reguero & Candela (2011) reported FMNH P14342 and P14537 (nec P14357) were from a few meters above the base of the Andalhuala Formation at Chiquimil. They are instead from the El Jarillal Member, the uppermost member of the Chiquimil Formation (Esteban et al, 2014; Prevosti et al., 2021). They were initially assigned an average age date of 6.02 Ma (Marshall et al., 1979; Butler et al., 1984). The radiometric dates have been revised to 7.31-7.14 Ma, making them the oldest securely dated procyonids in South America (Esteban et al, 2014; Prevosti et al., 2021). These two are "morphologically similar and resemble *C. brevirostris*" (Tedford in Marshall et al., 1979, p. 275). In FMNH P14342 (Figure 3A-H), the dentition is moderately worn. The p2 and p3 do not have anterior and posterior accessory cuspids. The p4 has a lingually situated posterior accessory cuspid and a well-developed heel. The postero-lingual extension of the paraconid of the left m1 is expanded terminally into a smaller cusp. The trigonid of the right m1 is damaged. The talonid has an entoconid and entoconulid. The m2 is large, but not as large as m1. The forelimb was described by J. Tarquini et al. (2019).

In FMNH P14537 (Fig. 3 I-J; Hough, 1948, figs. 7, 8; Prevosti et al., 2013, fig. 4f-h), the teeth are heavily worn. P1/p1 are apparently absent, perhaps as a result of age. The worn and damaged P4 appears to be triangular in shape and lacking a hypocone. The premolars are separated by diastemata. Because of wear, it is not possible to determine the presence of accessory cusps.

FMNH P14451 and FMNH P14397 were collected at Puerta de Corral Quemado from two levels of the "Araucanense" Formation (Butler et al., 1984), now the Andalhuala Formation (Reguero & Candela, 2011). Marshall et al. (1979) had wrongly assigned them to the younger Corral Quemado Formation (Butler et al., 1984). FMNH P14451, a lower jaw with deciduous dentition (Fig. 4), is from just above unit 14 of the Andalhuala Formation (Reguero & Candela, 2011) and has been age dated at 7.0 to 7.5 Ma (Butler et al., 1984), making it one of the oldest well-dated members of the *Cyonasua* group. This deciduous dentition is not further identifiable beyond *Cyonasua* sp. (Marshall et al., 1979). FMNH P14397 (Fig. 5) is from unit 16 or 17 of the Andalhuala Formation, age dated at 6.4 to 6.9 Ma (Marshall et al., 1979; Butler et al., 1984). The p1 alveolus is very small. The p2 has a weakly developed posterior accessory cuspid. The p4 anterior accessory cuspid is small; the prominent posterior accessory cuspid is situated postero-labial to the protoconid; and the talonid has two small cuspids on its posterior margin. The m1 protoconid is the most prominent cusp; the metaconid is lower than the protoconid; the hypoconid is the most prominent cusp of the talonid, entoconid and smaller entoconulid are distinct cuspids.

FMNH P14397 was described as having "a simple connate m1 paraconid rather than the more complex divided cuspid present in the type of *C. lutaria*" or the bifid m1 paraconid of *Amphinasua groeberi*; and in having "longer and more complex lower premolars bearing stronger anterior and posterior cuspids and having a shorter m2 than m1" (Marshall et al., 1979, p. 276). We interpret that the m1 paraconid is complex: the paraconid is a small cusp situated on the antero-medial flank of the protoconid at the front of the tooth. A low ridge extending posteriorly from it terminates in a lower cusp on the lingual margin; this extension of the paraconid is separated from the metaconid by a narrow gap. Although the anterior and posterior accessory cusps of p4 are prominent as in *Amphinasua groeberi*, the dimensions of the m1 and m2 are more similar to those of the type *Amphinasua longirostris* (Table 1). The complex m1 paraconid suggests assignment to *Amphinasua brevirostris*.

Other early examples of the *Cyonasua* group include *Amphinasua pascuali* (Linares, 1982), from the Huayquerias Formation, Mendoza Province, which is 5.8 Ma or older (Marshall et al., 1986). *Cyonasua* has been recorded from three localities of the Cerro Azul Formation, Salinas Grandes de Hidalgo, La Pampa Province (Goin et al., 2000; Romano et al., 2023). Salinas Grandes de Hidalgo has a median inferred age of 6.83 Ma (range 7.31-6.47 Ma); Quehué, 6.61 Ma (range

FIGURE 3. *Amphinasua brevirostris* from Valle de Santa María and Río Corral Quemado, Catamarca Province, Argentina. A-H. FMNH P14342. Fragmented skull, mandibles and postcranial skeleton. Skull in occlusal view (A), detail of the dentition in occlusal view (B), left humerus in cranial view (C), and right femur in cranial view (D); Right hemimandible with p2-m2 in buccal (E), lingual (F) and occlusal (G) views. Left hemimandibles with p4-m2 in occlusal view (H); I-J. FMNH P14537. Skull and mandible in lateral view (I), detail of the maxilla, note upper canines are reconstructed (J). Bar scales shared in (B, E-H, J), and (C, D, I).

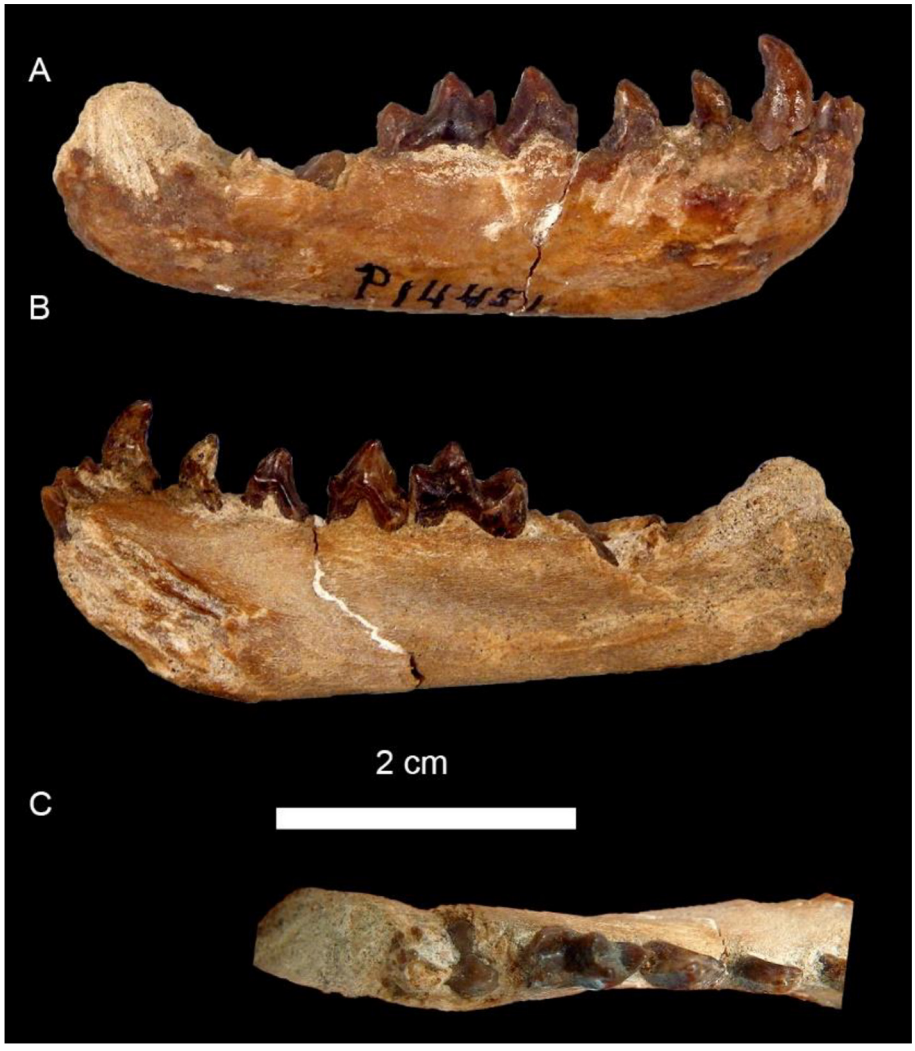

FIGURE 4. FMNH P14451, right hemimandible with deciduous dentition comprising dc, dp1-dp4 of *Cyonasua* sp. in buccal (A), lingual (B) and occlusal views (C).

7.05-6.32 Ma); and Telén, ca. 7.09 Ma (range 7.21-6.95 Ma) (Prevosti et al., 2021; Romano et al., 2023). Berman (1989) noted *Cyonasua* n. sp. from the Maimará Formation, Jujuy province. Although the specimen is currently lost, its estimated age is between c. 6.6 and c. 6.4 Ma (Candela et al., 2023). In Peru, postcranial elements of *Cyonasua* sp. from two levels in the Pisco Formation have been age dated at 6 to 7 Ma (J. Tarquini et al. (2020). L. Soibelzon, et al. (2019) accepted that 11-9 Ma was the best estimate available at the time for the Late Miocene Camacho Formation of Uruguay which has produced an m2 of *Cyonasua* sp. del Río et al. (2018) and del Río & Martínez (2021) assigned age dates of 7.20 Ma-6.92 Ma for the San Pedro Member of the Camacho Formation. This widespread distribution around 7 Ma suggests they may have entered South America earlier in the Huayquerian. Those evidences clearly demonstrate that the *Cyonasua* group of procyonids preceded the entrance of other members of the Carnivora from North America to South America by approximately five million years (Fig. 1), as has been noted by many others beginning with Patterson & Pascual (1968).

FMNH P14401, a left mandible (Fig. 6) of *Chapalmalania* cf. *altaefrontis* (Kraglievich & Olazábal, 1959, fig. 11b; Prevosti et al., 2013, fig.4i), may represent the first occurrence of *Chapalmalania*. It was collected from the Corral Quemado Formation at Puerta de Corral Quemado Catamarca Province by the Riggs expedition (Riggs & Patterson, 1939; Marshall et al. 1979). It is presumably from level 21, which has been dated at 5.4-5.8 Ma (Butler et al., 1984), but according to Marshall

FIGURE 5. FMNH P14397, *Amphinasua brevirostris* from unit 16 or 17 of the Andalhuala Formation, in buccal (A), lingual (B) and occlusal views (C).

& Patterson (1981), could be as old as unit 15 (6.5 Ma) or as young as unit 32 (younger than 3.5 Ma). Reguero & Candela (2011) included *Chapalmalania* in the Andalhuala Formation Fauna of the Montehermosan to Chapadmalalan Ages. Accurately determined occurrences of *Chapalmalania* are limited to the Chapadmalalan with a possible younger occurrence in the Marplatan Age (L. Soibelzon, 2011, fig. 1; L. Soibelzon & Prevosti, 2012; Forasiepi et al., 2014).

Origin of the *Cyonasua* group

The *Cyonasua* group is not directly related to the extant procyonids. Baskin (1982, 2004) proposed a sister-group relationship for it and the North American Barstovian to Hemphillian Miocene *Arctonasua*. Forasiepi et al. (2014) strongly supported the monophyly of the *Cyonasua* group but rejected a sister-group relationship of it with *Arctonasua*. The *Cyonasua* group and *Arctonasua* share nine possible synapomorphies (Baskin, 1982, 1989, 2004). *Arctonasua* differs from *Cyonasua* in having an elongate rostrum, P4 with a more anteriorly placed and larger protocone, upper molars with a better developed hypocone, m2 with the protoconid smaller than the metaconid, and a simple paraconid on m1, all primitive characters. *Cyonasua* may be derived from a taxon similar to the early Barstovian (ca. 16 Ma) *Arctonasua minima* (Baskin, 1982; Fig. 7). The P4 of *A. minima* has a greatly reduced hypocone, approaching the state of the *Cyonasua* group. However, in this species the P4 metacone is absent, an even more derived condition than in primitive *Amphinasua*. The m1 of *Arctonasua minima* is similar in size and morphology to that of FMNH P14397 from Catamarca (Fig.

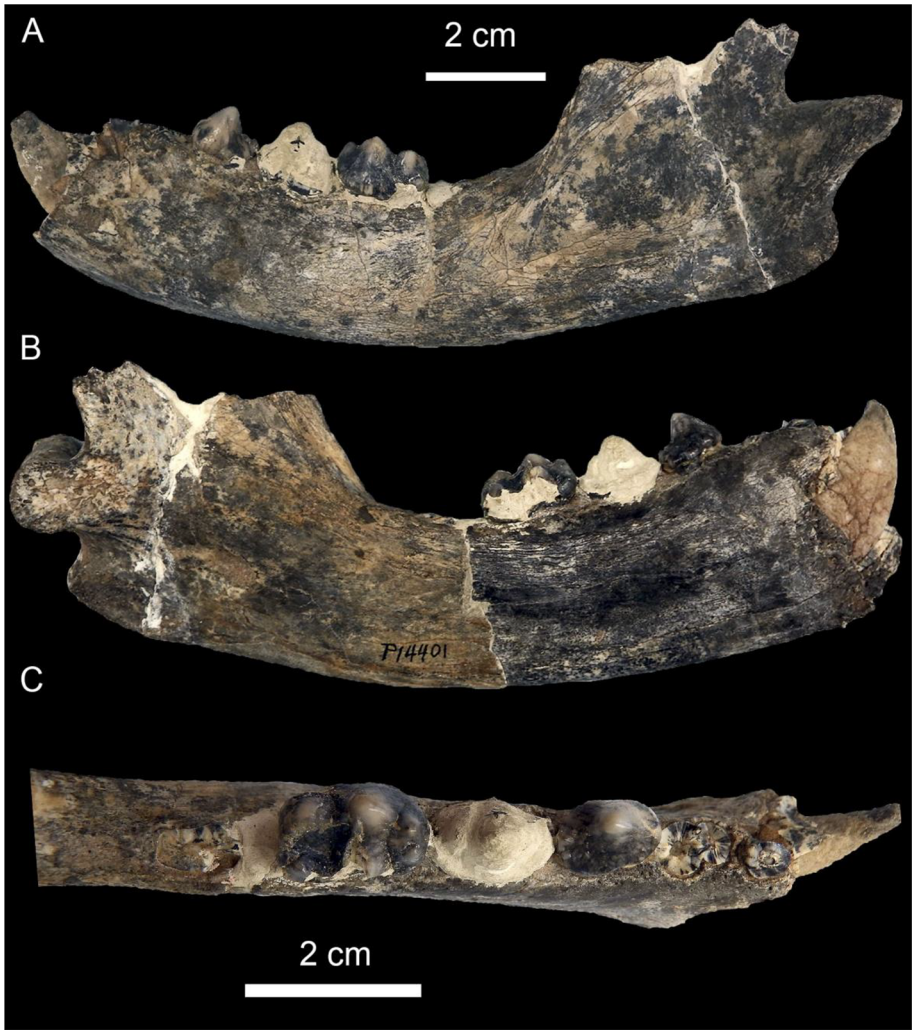

FIGURE 6. *Chapalmalania* cf. *altaefrontis* FMNH P14401; from Corral Quemado, level 2, Catamarca (Argentina), left mandible with fragmented c, complete p3, p4 (reconstructed) and fragmented m1, in buccal (A), lingual (B) and occlusal views (C) Scale bar is the same in A and B.

5). In FMNH P14397, the paraconid is somewhat more separated from the metaconid (but is situated mostly at the same level labial to the metaconid) and the entoconid and entoconulid are less bulbous than in *A. minima*. The mandible is much more massive.

Chapalmalania and *Amphinasua* share the unique morphology of the m1 paraconid (which is unknown in *Brachynasua*). C. Ameghino & Kraglievich (1925) suggested that *Brachynasua* was related to *Potos*. Kraglievich & Olazábal (1959, p. 45) concluded *Brachynasua* was more closely related to *Procyon*. Baskin (1990) suggested it was more closely related to *Cyonasua*. *Brachynasua* is interpreted to be the sister taxon of advanced *Amphinasua* such as *A. lutaria*, because of loss of P1/p1 and similar P4 and M1 morphology. *Chapalmalania* is also similar to *Brachynasua* in having P4 with parastyle greatly reduced to absent. However, in *A. lutaria*, the parastyle is reduced, approaching the condition of *Brachynasua*. Linares (1982) stated that the Clarendonian (Late Miocene) *Protoprocyon* was ancestral *Cyonasua* group and to *Nasua*, *Procyon*, and *Bassaricyon*. However, in our opinion *Protoprocyon* is most closely related to *Paranasua*, *Nasua*, and *Procyon* (Figure 8) on the basis of the shared derived m2 morphology.

Morphological vs. molecular phylogenies of the Procyonidae

Decker & Wozencraft (1991) used 37 cranial characters, 14 dental characters, seven postcranial characters, and six soft tissue characters of extant procyonids to generate the following

FIGURE 7. *Arctonasua minima* from Observation Quarry, Dawes County, Nebraska, Olcott Formation equivalent, early Barstovian. A-C. AMNH F:AM 49116, left hemimandible with p2 and m1 in buccal (A), lingual (B), and occlusal (C) views; D. AMNH F:AM 25378, left m1 in occlusal view; E-F. AMNH F:AM 105249, left P4 in occlusal (E) and anterior (F) views; G. AMNH F:AM 61006a, left M1 in occlusal view.

tree: (*Potos*-*Bassaricyon*)-(*Bassariscus*-(*Procyon*-(*Nasua*-*Nasuella*))). Ahrens (2012) used 78 cranial and dental characters to develop similar trees supporting the homology of the morphological characters. In addition to dental characteristics (which may be the result of convergence for a frugivorous diet). Decker & Wozencraft (1991) used nine cranial synapomorphies to unite *Potos* and *Bassaricyon* in the Potosinae. Ahrens (2012) recognized eight unambiguous synapomorphies, including cranial characters, uniting *Potos* and *Bassaricyon* in the Potosinae. *Potos* is in many ways the most specialized of the procyonids, having New World primate post-cranial characters such as a prehensile tail (Ford & Hoffmann, 1988).

Baskin (1982) developed a phylogenetic tree based on dental characters of living and fossil procyonids: (*Potos*)-(*Bassariscus*-((*Cyonasua*-*Arctonasua*)-(*Bassaricyon*-(*Procyon*-(*Nasua*-*Nasuella*))). His 1989 and 1998b phylogenies omitted *Potos* and *Bassaricyon*, but were otherwise similar. Baskin (2004) added *Parapotos* (Baskin, 2003), *Bassaricyonoides* (Baskin, 2003), and *Bassaricyon* to the Potosinae and expanded the discussion of the sister-group relationship of *Arctonasua* and *Cyonasua* to include the other three genera of the Cy*onasua* group.

DNA phylogenies of extant procyonids produce different results from morphological ones. In them *Bassariscus* is the sister taxon of *Procyon*; *Bassaricyon* is the sister taxon of

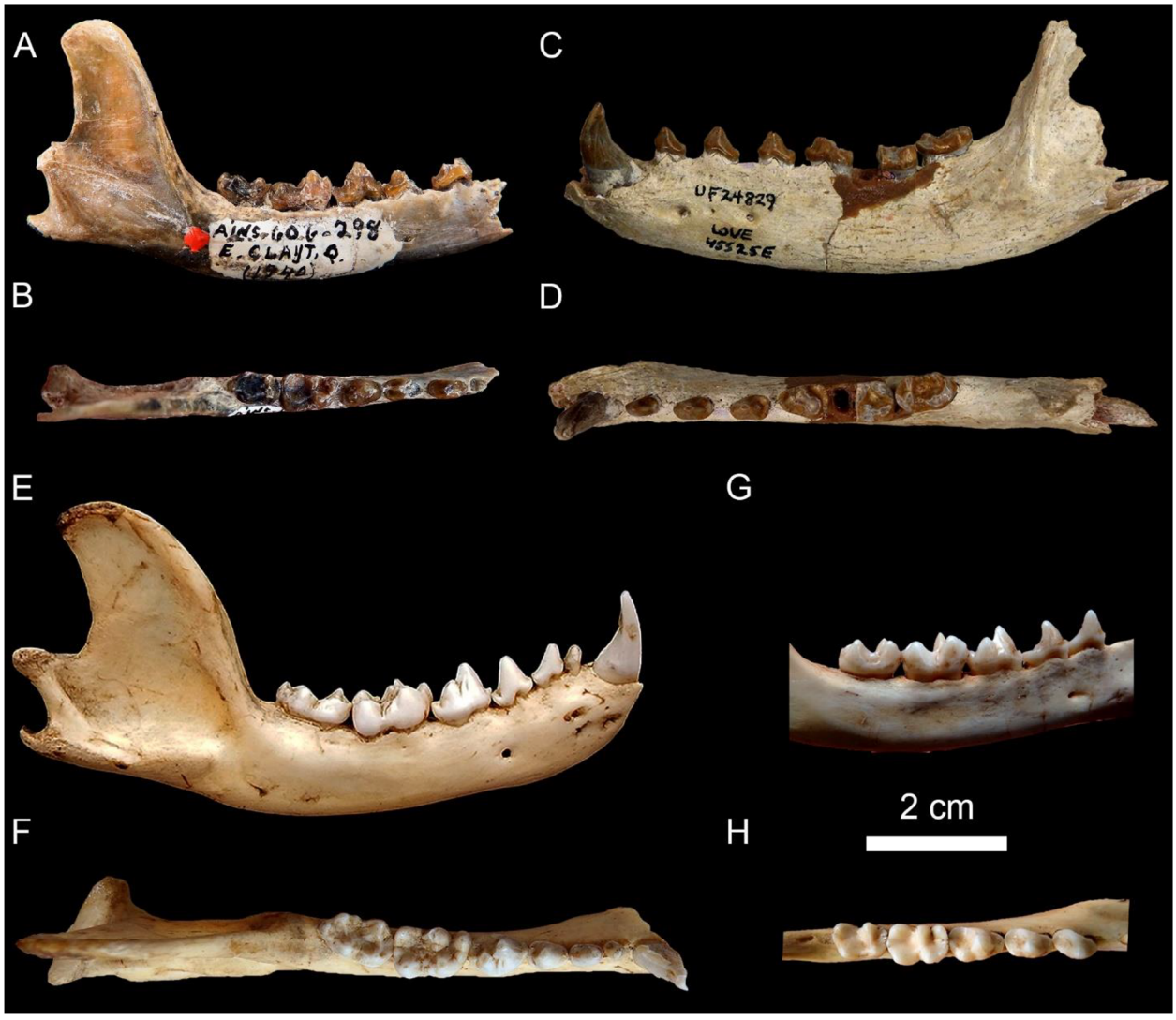

FIGURE 8. Mandibles of extinct and extant procyonids. A-B. *Protoprocyon savagei* AMNH F:AM 25210 (Holotype) from E. Clayton Quarry (Brown County, Nebraska, Early Clarendonian) in buccal (A), and occlusal (B) views; C-D. *Paranasua biradica* UF 24829 (Holotype) from Love Bone Bed (Alachua County, Florida, latest Clarendonian) in buccal (C), and occlusal (D) views; E-F. Extant *Procyon lotor* (raccoon) NRM-MA582011 in buccal, (E) and occlusal (F) views; G-H. Extant Nasua nasua (coati) NRM-MA585504, in buccal (G), and occlusal (H) views.

Nasua. These four genera are the sister-group of *Potos* (Fulton and Strobeck, 2007; Koepfli et al. 2007, 2017; Eizirik et al., 2010). According to Koepfli et al. (2017), similarities of dental characters, such as those uniting *Procyon* and *Nasua*, are not shared derived characters, but are caused by developmental genetic correlation. This caused the morphology-based phylogenies to differ from the molecular phylogeny. We cannot offer further evidence on which phylogenies may be more accurate and we agree "that a substantial portion of the procyonid fossil record may yet be uncovered" (Koepfli et al., 2017, p. 89). The molecular clock divergence between the *Nasua* and the *Bassaricyon* lineages and the molecular clock divergence between the *Procyon* and the *Bassariscus* lineages averages 11-12 Ma; that between the (*Nasua-Bassaricyon*) and the (*Procyon-Bassariscus*) lineages averages 18-20 Ma; and that between *Potos* and the other procyonids is in the Early Miocene or perhaps the Oligocene, ca. 21-25 Ma (Koepfli et al., 2007). The fossil record places the divergence of *Procyon* and *Nasua* at 10-12 Ma (i.e., at least 6 Ma younger than the molecular date); that of (*Procyon-Nasua*) and *Bassariscus* at 12-14 Ma (i.e., similar to the *Procyon* and *Bassariscus* molecular divergence date); and that of the Potosinae and Procyoninae at

18-20 Ma (Baskin,2003, 2004).

Origin of the present-day genera and species of Procyonidae found in South America

Procyon (raccoons) is widely distributed throughout the Americas, from Canada to northern Argentina. *Nasua* (coatis) ranges from the southwestern United States to Uruguay and northern Argentina. *Nasuella* is endemic to South América, in the Andes of Colombia, Ecuador and Venezuela (Helgen et al. 2009). It has recently been considered a junior synonym of *Nasua* (Ruiz-García et al., 2022a, 2022b). *Bassaricyon* and *Potos* are restricted to Central and South America. Koepfli et al. (2017:90) noted that molecular data leave unanswered whether "the lineages representing the extant procyonid genera evolved and diversified first in North America, South America, or some combination of the two." *Nasua narica* is known from southern Arizona, New Mexico, and Texas to far northwestern Colombia. It is widespread in Mexico and Central America. Nigenda-Morales et al. (2019) used molecular evidence to demonstrate that *Nasua narica* is more closely related to the South American endemic *Nasuella* than it is to the South American endemic *Nasua nasua*, both of which are allopatric to *N. narica*. The mitochondrial DNA also indicated the following (Nigenda-Morales et al., 2019): (1) the most recent common ancestor of the coatis most likely occurred in South or Central America around 6 Ma; (2) the diversification of other extant procyonid lineages may have occurred in South America; (3) the dispersal of *N. narica* was south-to-north beginning in the Pliocene of South America; and (4) the diversification of extant procyonid lineages may have occurred in South America. Ruiz-García et al. (2022a, b) concluded that the mitochondrial DNA diversification of the coatis began around 13 Ma in the Northern Andes where *N. narica* originated and then later migrated to Central America.

The fossil record demonstrates that most of, if not all of, the direct ancestors of the extant genera of procyonids evolved in North America or Central America during the Miocene. During the Late Pliocene and Pleistocene, they crossed the Panamanian land bridge and further diversified in South America. Some species may have migrated back into Central and perhaps North America. *Bassariscus* has an extensive fossil record in North America, from the Barstovian (middle Miocene, 16 Ma) to Recent of North America and the Recent of Central America (Baskin, 2004), but is only known from a few Late Pleistocene localities in Mexico, and none from Central or South America. It is morphologically the most primitive of the living procyonids (Decker and Wozencraft, 1991; Baskin, 2004; Ahrens, 2012). The late Clarendonian (Late Miocene, 9 Ma) genus *Paranasua* is the sister taxon to *Procyon* and *Nasua* (Baskin, 1982). The oldest records of *Procyon* are from the Late to Latest Miocene (ca. 5 Ma) of North America: ?*Procyon* sp. from the late Hemphillian Mt. Eden Local Fauna in southern California (Baskin, 1982); *Procyon* sp. from the late Hemphillian Modesto Local Fauna, Mehrten Formation of California (Wagner, 1976, 1981); and *Procyon* sp. from the latest Hemphillian of Florida (Baskin, 1982; Webb et al. 2008). *Procyon rexroadensis* (Hibbard, 1941), from the early Blancan (Early Pliocene, 3-5 Ma) Rexroad Formation of Kansas, was synonymized with the extant *P. lotor* because of its lack of distinguishing characteristics (Emmert & Short, 2018). *Procyon gipsoni* and *P. megalokolos* are from the late Blancan (late Pliocene, 2-3 Ma) of Florida (Emmert & Short, 2018). *Procyon* sp. has been reported from numerous other Blancan and Irvingtonian localities in the United States. *Procyon lotor* is widespread in the Pleistocene of North America (Kurtén & Anderson, 1980).

Nasua sp. is present in the latest Hemphillian of Florida (Baskin, 1982; Webb et al. 2008). *Nasua pronarica*, described from a p4, is from the early Blancan Beck Ranch Local Fauna of Texas (Dalquest, 1978); *Nasua mastodonta* is from the late Blancan (Late Pliocene) of Florida (Emmert & Short, 2018). *Nasua narica* and *P. lotor* are known from the Late Pleistocene of Mexico (Ferrusquía-Villafranca et al., 2010). *Procyon* and *Nasua* have been reported from several Pleistocene localities in South America (see references in Ruiz-Ramoni et al., 2018). Their possible earliest occurrences in South America are from the Late Pliocene-Early Pleistocene (Marplatan) of El Breal De Orocual of Venezuela (Ruiz-Ramoni et al., 2018). The Marplatan Age is dated at ca. 3.2-2.0 Ma (Cione & Tonni, 2005) and correlates with the late Blancan NALMA (Woodburne et al., 2006). However, the tar deposits at Orocual range in age from Late Pliocene to Late Pleistocene (Solórzano et al., 2015). The earliest well-dated (and not contentious) for records for *Procyon* are from the Late Pleistocene of Argentina and Brazil (L. Soibelzon, et al. 2010; Rodriguez et al. 2013; Prevosti & Forasiepi, 2018).

Emmert & Short (2018) noted that because there are similar and older records in North America, a North American origin more likely, supporting an entry into South America after the completion of the land bridge during GABI I (Woodburne,

2010; Cione et al., 2015). *Potos* and *Bassaricyon* are not represented in the fossil record. As discussed above, molecular evidence indicates *Bassaricyon* is a procyonin, the sister taxon of *Nasua*; morphological evidence, a potosin, the sister taxon of *Potos*. Both are arboreal frugivores and we would not be surprised if their dental and skeletal similarities are the result of ecological convergence. *Bassaricyonoides* (Hemingfordian, Early Miocene of Panama, Nevada, and Florida) and *Parapotos* (Barstovian, middle Miocene) of Texas are the only known fossil Potosinae (Baskin, 2003). Besides several derived dental characteristics, *Parapotos* and *Potos* have a mandible that is massive, deeper anteriorly and with a large symphysial region, unlike the unspecialized mandible of *Bassaricyon*. Although the fossil record is limited, this does support a North American origin.

CONCLUSION

During the Late Oligocene, primitive musteloids (such as *Amphictis ambigua*, *Pseudobassaris riggsi*, and *Stromeriella franconica*) with affinities to the Procyonidae and Ailuridae appear in Europe (e.g., Cirot & de Bonis, 1993; Wolsan & Lange-Badré, 1996; Wang et al., 2023). *Broiliana nobilis* from the Early Miocene (MN3) of Germany (Dehm, 1950) is the sister taxon of the New World Procyonidae (Baskin, 1982, 1989). *Bassaricyonoides* from the Hemingfordian (Early Miocene, ca, 17-19 Ma) of Nevada, Florida, and Panama is the earliest record of the Potosinae. A second potosine, *Parapotos tedfordi*, is present in the middle Miocene (Barstovian) of Texas (Baskin, 2003). The presence of a New World monkey in the Early Miocene (late Arikareean) Las Cascadas Formation of Panama (Bloch et al., 2016) and *Bassaricyonoides* in the overlying Hemingfordian Centenario Fauna (MacFadden et al., 2014) raises the possibility that potosin procyonids entered South America before ProtoGABI.

The Hemingfordian *Edaphocyon lautus* from the Running-water Formation of Nebraska (Baskin, 1982), *Bassariscus antiquus* from the Mascall Formation of Oregon (Barrett et al., 2020), and cf. *Probassariscus* from the Thomas Farm Local Fauna of Florida (Holte, 2008) are the earliest Procyoninae. The Barstovian is the Last Appearance Datum for *Edaphocyon* and *Probassariscus* and First Appearance Datum for *Arctonasua* (Baskin 1982, 1998b, 2004). *Protoprocyon* (Linares, 1982; Baskin, 1989) is restricted to the Clarendonian; *Paranasua*, to the Clarendonian and Hemphillian (Baskin 1982). The late Hemphillian is the Last Appearance Datum for *Arctonasua* (Baskin 1982). The latest Hemphillian (Hh4, Early Pliocene) is the first definite record of the extant *Procyon* and *Nasua*. Thus, the fossil record reveals that the ancestors of the extant genera of procyonines evolved in North America or Central America during the Miocene, crossed the Panamanian land bridge in the Pleistocene, and underwent further diversification in South America.

The *Cyonasua* group, composed of *Cyonasua argentina*, *Amphinasua* spp., *Brachynasua meranii*, and *Chapalmalania* spp., is an endemic South American radiation of Late Miocene to Middle Pleistocene (Huayquarian-Ensenadan) procyonids. *Amphinasua brevirostris* from the Chiquimil Formation, Cartamarca Province, Argentina (FMNH P14342 and P14537, 7.31-7.14 Ma), is the oldest record of a procyonid (and the Carnivora as well) in South America (Marshall et al., 1979; Reguero & Candela, 2011; Prevosti et al., 2021). The arrival of procyonids in South America coincided with the decline of the Sparassodonta, a group of borhaenid marsupials (Soibelizon, 2011, fig. 1). Although the Huayquerian members of the *Cyonasua* group were more carnivorous than extant procyonids other than *Bassariscus*, they were more omnivorous than the larger, hypercarnivorous sparassodonts (Forasiepi et al., 2007; Prevosti et al. 2013). Engelman and Croft (2019) posit that ecological dissimilarity enabled the *Cyonasua* group to successfully invade and diversify in South America without competition from the sparassodonts. Competitive replacement was also probably not a factor in the extinction of the *Cyonasua* group. The last appearance of *Amphinasua* in the Chapadmalalan preceded the first appearance in the Marplatan of the Canidae, Mustelidae, *Nasua*, and *Procyon* (Fig. 1). The extinction of *Chapalmalania* in the Pliocene preceded the appearance of Ursidae in South America. The presumably frugivorous *Brachynasua meranii* is known from a single Ensenadan record. Because the frugivorous *Potos* and *Bassaricyon* lack a fossil record in South America, it cannot be shown if there was competition with *Brachynasua*. Climate change was an important factor in the extinction of the hathliacynid sparassodonts (Zimicz, 2014). S. Tarquini et al. (2022) attributed the extinction of the sparassodonts to multiple factors, including uplift of the Andes, not to competition. Pino et al. (2022) concluded that regional climatic change caused by the uplift of the Andes led to the extinction of the sparassodonts. The last members of the *Cyonasua* group, other than *Brachynasua*, occurred at the same time as the last

sparassodonts (Cione et al., 2015), perhaps going extinct for the same reasons.

ACKNOWLEDGMENTS

The late Drs. Rosendo Pascual of the Museo de La Plata, Jose Bonaparte of the Museo Argentino de Ciencias Naturales, and Richard Tedford of the American Museum of Natural History kindly allowed the first author (J.B.) to study specimens in their institutions. I am privileged to have known them, George Simpson, Bryan Patterson and David Webb and to have benefited from their knowledge of the GABI. We also thank the following curators and collection managers for access to the material under their care: D. Kalthoff (NRM, Stockholm, Sweden), W. Simpson, and K. Angielczyk (FMNH), Hulbert Jr (FLMNH), as well as J. Flynn, J. Meng and R. O´leary (AMNH). This research received support to AV from SYNTHESYS + Project http://www.synthesys.info/ which is financed by European Community Research Infrastructure Action under the H2020 Integrating Activities Programme, Project number 823827. AV is also grateful for support from FLMNH by an International Travel Grant Vertebrate Paleontology Program (2015), FMNH Visiting Scholarship (2016), AMNH through Theodore Roosevelt Memorial Scholarship 2022 and Collection Study Scholarship Program 2022, the project PID2020-116220GB-I00 funded by MCIN/AEI/10.13039/501100011033 (Ministerio de Investigación e Innovación), as well as the Research Group UCM 910607. Francisco Prevosti and Juliana Tarquini reviewed the manuscript and improved it with constructive comments despite our taxonomic differences in interpretation.

Dedication to LLJ by JB. I met Louis Jacobs in 1972 when he was a second year and I was a new Master's student in the Department of Geosciences at the University of Arizona. Our theses, supervised by Everett Lindsay (the "Dock") were both on small mammals, mostly rodents, from the Hemphillian of Arizona. I learned a lot from Louis and both of us a lot from the Dock, whose dissertation was on small mammals, especially rodents, from the Barstow Formation. Dock and his students formed the "Red Fireballs", a group whose mission was to socialize together and help each other with our research. In furthering these two aims we met on Friday afternoons at the home of George Simpson, who had retired to Tucson and was on our thesis committees. One of the topics Dr. Simpson discussed with us was the history of the mammalian fauna of South America. Louis and I became more interested in what Simpson (1950, 1953) termed the third major stratum of mammalian immigrants to South America, consisting of "late island-hoppers" and "late immigrants", what is now called the Great American Biotic Interchange. Louis has a continuing interest in faunal interchange between zoogeographic realms, including the role of sigmodontine rodents in the GABI (Jacobs & Lindsay, 1981, 1984; Jacobs & Flynn, 2005; Lindsay et al., 2006). Whatever group of fossils Louis has studied, be it North American cricetid rodents, South Asian murid rodents, dinosaurs from Texas and Malawi, mosasaurs from Texas, Angola and the Netherlands, a snake with limbs, etc., etc., etc., he has tackled with great enthusiasm which he brings to all of us who have heard him talk about his research.

AUTHOR CONTRIBUTIONS

JB developed the initial concept for the research and wrote the first draft of the manuscript. JB and AV performed the data collection, the analysis and wrote the final draft.

LITERATURE CITED

Ahrens, H. E. (2012). Craniodental characters and the relationships of Procyonidae (Mammalia: Carnivora). *Zoological Journal of the Linnean Society*, 164(3), 669–713.

Ameghino, C. & Kraglievich, L. (1925). Un nuevo prociónido cercoleptoide en el Pampeano inferior de la Argentina, *Brachynasua meranii*, n. gen., n. sp. *Comunicaciones Museo Nacional de Historia Natural*, "*Bernadino Rivadavia*", *Buenos Aires*, 2(18), 181–191

Ameghino, F. (1883). Sobre una colección de mamíferos fósiles del Piso Mesopotámico de la Formación Patagónica recogidos en las barrancas del Paraná por el Profesor Pedro Scalabrini. *Boletín de la Academia Nacional de Ciencias en Córdoba*, 5, 1-226

Ameghino, F. (1885). Nuevos restos de mamíferos fósiles Oligocenos, recogidos por el profesor Pedro Scalabrini y pertenecientes al Museo Provincial de la Ciudad de Paraná. *Boletín de la Academia Nacional de Ciencias en Córdoba*, 8, 3–207.

Ameghino, F. (1891). [Revista crítica y bibliográfica] Exploración arqueológica de la provincia de Catamarca. Primeros datos sobre su importancia y resultados, por F. P. Moreno. *Revista Argentina de historia natural*, 1, 199–206

Ameghino, F. (1904). Nuevas especies de mamíferos cretáceos y terciarios de la República Argentina (conclusión). *Anales de la Sociedad Cientifica Argentina*, 58, 241–291.

Ameghino, F. (1906). Les formations sédimentaires du Crétacé supérieur et du Tertiare de Patagonie. *Anales del Museo Nacional de Buenos Aires*, 3(8), 1–568.

Ameghino, F. (1908a). Las formaciones sedimentarias de la región litoral

de Mar del Plata y Chapalmalán. *Anales del Museo Nacional de Buenos Aires*, 3(10), 334–428.

Ameghino, F. (1908b). Notas preliminaries sobre el *Tetraprothomo argentinus* un precursor del hombre del Mioceno Superior de Monte Hermoso. *Anales del Museo Nacional de Buenos Aires*, 9, 1–82.

Agnolín, F. L. (2022). Chapadmalal: una pieza más en los esquemas biogeográficos y evolutivos de Ameghino. In F. Agnolín, D. Bohy & C. Quintana (Eds.), *Trabajos de 1as Primeras Jornadas, Paleontológicas Chapadmalenses* "*Chapadmalal en la visión de Florentino Ameghino*" (pp. 13–22).

Barrett, P. Z., Finkelman, L., Perdue, G., Mclaughlin, W. N. F., Reuter, D. M. & Hopkins, S. S. B. (2020). Small carnivoran fauna of the Mascall Formation, Crooked River Basin, central Oregon. *Journal of Vertebrate Paleontology*, DOI: 10.1080/02724634.2020.1717506.

Baskin, J. A. (1982). Tertiary Procyoninae (Mammalia: Carnivora) of North America. *Journal of Vertebrate Paleontology*, 2, 71–93.

Baskin, J. A. (1989). Comments on New World Tertiary Procyonidae (Mammalia, Carnivora). *Journal of Vertebrate Paleontology*, 9, 110–17.

Baskin, J. A. (1990). Procyonidae and Mustelidae and the Great American Interchange. *Abstracts of the Joint Meeting of the Sociedad Argentina para el Estudio de los Mamíferos and the American Society of Mammalogists, Buenos Aires*, p. 42.

Baskin, J. A. (1998a). Evolutionary trends in the late Miocene hyena-like dog *Epicyon* (Carnivora, Canidae). In Y. Tomida, L. J. Flynn, & L. L Jacobs (Eds.), *Advances in vertebrate paleontology and geochronology* (pp. 189–211). National Science Museum, Tokyo, Monographs, 14.

Baskin, J. A. (1998b). Procyonidae. In C. M. Janis, K. M. Scott, & L.L. Jacobs (Eds.), *Evolution of Tertiary Mammals of North America, Volume 1: Terrestrial Carnivores, Ungulates, and Ungulatelike Mammals* (pp. 144–151). Cambridge University Press.

Baskin, J. A. (2003). New procyonines from the Hemingfordian and Barstovian of the Gulf Coast and Nevada, including the first fossil record of the Potosini. *Bulletin of the American Museum of Natural History*, 279, 125–146.

Baskin, J. A. (2004). *Bassariscus* and *Probassariscus* (Mammalia, Carnivora, Procyonidae) from the early Barstovian (middle Miocene). *Journal of Vertebrate Paleontology*, 24(3), 709–720.

Berman, W. D. (1989). Notas sobre la sistemática y paleobiografia del grupo *Cyonasua* (Carnivora, Procyonidae) de la Argentina. *Actas*, *VI Jornadas Argentinas de Paleontologia de Vertebrados*, 6, 17–18.

Berman, W. D. (1993). Diversidad de carnívoros placentarios en paleocomunidades del Plio-Pleistoceno en la provincia de Buenos Aires, Argentina. *X Jornadas Argentinas de Paleontologia de Vertebrados*, *Ameghiniana*, 30, 324.

Berman, W. D. (1994). Los carnívoros continentales (Mammalia, Carnivora) del Cenozoico en la provincia de Buenos Aires. *Tesis Doctoral, Facultad de Ciencias Naturales y Museo, Universidad Nacional de La Plata (Inédito)*.

Berta, A. & Marshall, L. G. (1978). South American Carnivora. *Fossilium Catalogus I*, *Animalia*, Part 125: 1–48. Dr. W. Junk.

Bloch, J. I., Woodruff, E. D., Wood, A. R., Rincon, A. F., Harrington, A. R., Morgan, G. S., Foster, D. A., Montes, C., Jaramillo, C. A., Jud, N. A. & Jones, D. S. (2016). First North American fossil monkey and early Miocene tropical biotic interchange. *Nature*, 533(7602), 243–246.

Bonaparte, C. L. (1850). Conspectus systematis Mastozoologie. *Nuovi Annali delle Scienze Naturali*, 3, 472–479.

Bondesio, P. & Pascual, R. (1981). Un Cardiatheriinae (Mammalia, Rodentia, Hydrochoeridae) de los alcáreos travertínicos de Las Playas (Córdoba). Edad y correlaciones. *Ameghiniana*, 18, 169–175.

Bordas, A. F. (1942). La posición sistemática del fémur del *Tetraprothomo argentinus*. *Relaciones de la Sociedad Argentina de Antropología*, 3, 53–58.

Brunetto, E., Noriega, J. I., & Brandoni, D. (2013). Sedimentología, estratigrafía y edad de la Formación Ituzaingó en la Provincia de Entre Ríos, Argentina. In D. Brandoni & J. I. Noriega (Eds.), *El Neógeno de la Mesopotamia Argentina* (pp. 13–27). Asociación Paleontológica Argentina, Publicación Especial, 14.

Burmeister, G. (1891). Adiciones al examen crítico de los mamíferos fósiles tratados en el artículo IV anterior "Examen crítico de los mamíferos y reptiles fósiles denominados por Don Augusto Bravard". *Anales Museo Nacional de Buenos Aires*, 3, 375–400. [https://www.biodiversitylibrary.org/page/45614751#page/414/mode/1up]

Butler, R. F., Marshall, L. G., Drake, R. E., & Curtis, G. H. (1984). Magnetic polarity stratigraphy and ^{40}K-^{40}Ar dating of late Miocene and early Pliocene continental deposits, Catamarca Province, NW Argentina. *Journal of Geology*, 92, 623–636.

Cabrera, A. (1936). Un nuevo carnívoro del Chapadmalense de Miramar. Instituto del Museo de la Universidad Nacional de La Plata; *Notas del Museo de La Plata*, 1, 303–308.

Candela, A. M., Abello M. A., Reguero, M. A., García Esponda, C. M., Pardiñas, U. F. J., Zurita, A. A., Pujos, F., Miño-Boilini, A., Quiñones, S., Galli, C. I., Luna, C., Voglino, D., De Los Reyes, M. & Cuaranta, P. (2023). The Late Miocene mammals from the Humahuaca Basin (northwestern Argentina) provide new evidence on the initial stages of the Great American Biotic Interchange. *Papers in Palaeontology*, 9(4), DOI: 10.1002/spp2.1527

Carrillo-Briceño, J. D., Sánchez, R., Scheyer, T. M., Carrillo, J. D., Delfino, M., Georgalis, G. L., Kerber, L., Ruiz-Ramoni, D., Birindelli, J. L., Cadena, E. A., Rincón, A. F., Chavez-Hoffmeister, M., Carlini, A. A., Carvalho, M. R., Trejos-Tamayo, R., Vallejo, F., Jaramillo, C., Jones, D. S., & Sánchez-Villagra, M. R. (2021). A Pliocene-Pleistocene continental biota from Venezuela. *Swiss Journal of Palaeontology*, 140(1), 1–76.

Cenizo, M., Soibelzon, E., & Magnussen Saffer, M. (2016). Mammalian predator-prey relationships and reoccupation of burrows in the Pliocene of the Pampean Region (Argentina): new ichnological and taphonomic evidence. *Historical Biology*, 28(8), 1026–1040.

Cione, A. L. & Tonni, E. P. (1995). Chronostratigraphy and "land mammal ages" in the Cenozoic of southern South America: Principles, practices, and the "Uquian" problem. *Journal of Paleontology*, 69, 135–159.

Cione, A. L. & Tonni, E. P. (1996). Reassessment of the Pliocene-Pleistocene continental time scale of Southern South America. Correlation of the type Chapadmalalan with Bolivian sections. *Journal of South American Earth Sciences*, 9(3–4), 221–236.

Cione, A. L. & Tonni, E. P. (2005). Bioestratigrafía basada en mamíferos del Cenozoico superior de la provincia de Buenos Aires, Argentina. *Geología y recursos minerales de la provincia de Buenos Aires*, 11, 183–200.

Cione, A. L., Gasparini, G. M., Soibelzon, E., Soibelzon, L. H., & Tonni, E. P. (2015). *The Great American Biotic Interchange. A South American Perspective.* Springer Briefs in Earth System Sciences; South America and the Southern Hemisphere. Springer.

Cione, A .L., Azpelicueta, M. D. L. M., Bond, M., Carlini, A. A., Casciotta, J .R., Cozzuol, M. A., de la Fuente, M., Gasparini, Z., Goin, F.

J., Noriega, J., Scillato-Yané, G. J., Soibelzon, L., Tonni, E. P., Verzi, D., & Vucetich, G. (2000). Miocene vertebrates from Entre Ríos province, eastern Argentina. *El Neógeno de Argentina. Serie Correlación Geológica*, 14, 191–237.

Cirot, E. & de Bonis, L. (1993). Le crâne d'*Amphictis ambiguus* (Carnivora, Mammalia): son importance pour la compréhension de la phylogénie des mustéloïdes. *Comptes rendus de l'Académie des Sciences de Paris* Série II 316, 1327–1333.

Cope, E. D. (1881). Miocene dogs. *American Naturalist*, 15, 497.

Dalquest, W. W. (1978). Early Blancan mammals of the Beck Ranch Local Fauna of Texas. *Journal of Mammalogy*, 59, 269–298.

Decker, D. M. (1991). Systematics of the coatis, genus Nasua (Mammalia: Procyonidae). *Proceedings of the Biological Society of Washington*, 104(2), 370–386.

Decker, D. M. & Wozencraft, W. C. (1991). Phylogenetic analysis of Recent procyonid genera. *Journal of Mammalogy*, *72*, 42–55.

Dehm, R. (1950). Die Raubtiere aus dem Mittel-Miocän (Burdigalium) von Wintershof-West bei Eichstät in Bayern. *Abhandlungen der Bayerischen Akademie der Wissenschaften*, 58, 1–141.

De los Reyes, M., Poiré, D., Soibelzon, L. H., Zurita, A. E., & Arrouy, M. J. (2013). First evidence of scavenging of a glyptodont (Mammalia, Glyptodontidae) from the Pliocene of the Pampean region (Argentina): taphonomic and paleoecological remarks. *Palaeontología Electrónica, 16.2.15.A*., doi.org/10.26879/331

del Río, C. J. & Martínez, S. (2021). Diversity and biostratigraphy of the late Oligocene-late Miocene sand dollars (Echinoidea: Scutelliformes) of Argentina and Uruguay. *Revista de Biología Tropical*, 69(S1), 35–50. DOI 10.15517/rbt.v69iSuppl.1.46324

del Río, C. J., Martínez, S. A., McArthur, J. M., Thirwall, M. F., & Pérez, L. (2018). Dating late Miocene marine incursions across Argentina and Uruguay with Sr-isotope stratigraphy. *Journal of South American Earth Sciences*, 85, 312–324.

Deschamps, C. M., Vucetich, M. G., Montalvo, C. I., & Zárate, M. A. (2013). Capybaras (Rodentia, Hydrochoeridae, Hydrochoerinae) and their bearing in the calibration of the late Miocene–Pliocene sequences of South America. *Journal of South American Earth Sciences*, 48, 145–158.

Eizirik, E., Murphy, W. J., Koepfli, K.-P., Johnson, W. E., Dragoo, J. W., Wayne, R. K., & O'Brien, S. J. (2010). Pattern and timing of diversification of the mammalian order Carnivora inferred from multiple nuclear gene sequences. *Molecular Phylogenetics and Evolution*, 56(1), 49–63.

Emmert, L. G. & Short, R.A. (2018). Three new procyonids (Mammalia, Carnivora) from the Blancan of Florida. *Bulletin of the Florida Museum of Natural History*, 55(8), 157–173.

Engelman, R. K. & Croft, D. A. (2019). Strangers in a strange land: Ecological dissimilarity to metatherian carnivores may partly explain early colonization of South America by *Cyonasua*-group procyonids. *Paleobiology*, 45(4), 598–611.

Esteban, G. I., Nasif, N., & Georgieff, S. M. (2014). Cronobioestratigrafía del Mioceno tardío-Plioceno temprano, Puerta de Corral Quemado y Villavil, provincia de Catamarca, Argentina. *Acta geológica lilloana*, 26(2), 165–192.

Ferrusquía-Villafranca, I., Arroyo-Cabrales, J., Martínez-Hernández, E., Gama-Castro, J., Ruiz-Gonzalez, J., Polaco, O. J., & Johnson, E. (2010). Pleistocene mammals of Mexico: A critical review of regional chronofaunas, climate change response and biogeographic provinciality. *Quaternary International*, 217(1–2), 53–104.

Flower, W. H. (1869). On the value of the characters of the base of the cranium in the classification of the order Carnivora, and on the systematic position of *Bassaris* and other disputed forms. *Proceedings of the Zoological Society of London*, 1869, 4–37.

Forasiepi, A. M., Martinelli, A. G., & Goin, F. J. (2007). Revisión taxonómica de *Parahyaenodon argentinus* Ameghino y sus implicancias en el conocimiento de los grandes mamíferos carnívoros del Mio-Plioceno de América de Sur. *Ameghiniana*, 44, 143–159.

Forasiepi, A. M., Soibelzon, L. H., Gomez, C. S., Sánchez, R., Quiroz, L. I., Jaramillo, C., & Sánchez-Villagra, M. R. (2014). Carnivorans at the Great American Biotic Interchange: new discoveries from the northern Neotropics. *Naturwissenschaften*, 101(11), 965–974.

Ford, L. S. & Hoffmann, R. S. (1988). *Potos flavus*. *Mammalian species,* 321, 1-9.

Fulton, T. L. & Strobeck, C. (2007). Novel phylogeny of the raccoon family (Procyonidae: Carnivora) based on nuclear and mitochondrial DNA evidence. *Molecular Phylogenetics and Evolution*, 43, 1171–1177.

Fulwood, E. L. & Wallace, S. C. (2015). Evidence for unusual size dimorphism in a fossil ailurid. *Palaeontologia Electronica* 18.3.45A: 1-6. doi.org/10.26879/526

Gill, T. (1872). Arrangements of the families of mammals with analytical tables. *Smithsonian Miscellaneous Collections*, 11(1), vi + 1–998.

Goin, F. J., Montalvo, C. I., & Visconti, G. (2000). Los marsupiales (Mammalia) del Mioceno Superior de la Formación Cerro Azul (Provincia de La Pampa, Argentina). *Estudios geológicos*, 56(1-2), 101–126.

Gray, J. E. (1825). An outline of an attempt at the disposition of the Mammalia into tribes and families, with a list of the genera apparently pertaining to each. *Annals of Philosophy*, (*new series*), 10, 337–344.

Helgen, K. M., Kays, R. W., Helgen, L. E., Tsuchiya-Jerep, M. T., Pinto, C. M., Koepfli, K. P., Eizirik, E., & Maldonado, J. E. (2009). Taxonomic boundaries and geographic distributions revealed by an integrative systematic overview of the mountain coatis, *Nasuella* (Carnivora: Procyonidae). *Small Carnivore Conservation*, 41, 41–64.

Hibbard, C. W. (1941). New mammals from the Rexroad fauna, Upper Pliocene of Kansas. *American Midland Naturalist*, 26, 337–368.

Hollister, N. (1915). The genera and subgenera of raccoons and their allies. *Proceedings of the United States National Museum*, 49, 143–150.

Holte, S. E. (2018). *Understanding Carnivoran Ecomorphology through Deep Time, with a Case Study during the Cat-Gap of Florida*, Doctoral dissertation, University of Florida, 275 pp.

Hough, J. R. (1948). R., 1948. The auditory region in some members of the Procyonidae, Canidae and Ursidae: its significance in the phylogeny of the Carnivora. *Bulletin of the American Museum of Natural History*, 92(2), 67 –118.

Hunt, R. (1974). The auditory bulla in Carnivora: an anatomical basis for reappraisal of carnivore evolution. *Journal of Morphology*, 143, 21–76.

ICZN. (1999). International Code of Zoological Nomenclature. 4th ed. [available online at iczn.org/iczn/index.jsp]

Jacobs, L. L. & Flynn, L. J. (2005). Of mice… again: the Siwalik rodent record, murine distribution, and molecular clocks. In D. E. Leiberman, R. J. Smith & J. Kelley (Eds.), *Interpreting the past: essays on human, primate, and mammal evolution in honor of David*

Pilbeam (pp. 63–80). Brill Academic Publishers Inc.

Jacobs, L. L. & Lindsay, E. H. (1981). *Prosigmodon oroscoi*, a new sigmodont rodent from the late Tertiary of Mexico. *Journal of Paleontology*, 1, 425–430.

Jacobs, L. L. & Lindsay, E. H. (1984). Holarctic radiation of Neogene muroid rodents and the origin of South American cricetids. *Journal of Vertebrate Paleontology*, 4(2), 265–272.

Kays, R. (2009). Family Procyonidae (raccoons). In D. E. Wilson, & R. A. Mittermeier (Eds.), *Handbook of Mammals of the World. 1. Carnivores* (pp. 504–530). Lynx Editions.

Kitchener, A. C., Meloro, C., & Williams, T. M. (2017). Chapter 3. Form and function of the musteloids. In D. W. Macdonald, C. Newman, & L.A. Harrington (Eds.), *Biology and Conservation of Musteloids* (pp. 92–128). Oxford University Press.

Koepfli, K.-P., Dragoo, J. W., & Wang, X. (2017). Chapter 2. The evolutionary history and molecular systematics of the Musteloidea. In D. W. Macdonald, C. Newman, & L. A. Harrington (Eds.), *Biology and Conservation of Musteloids* (pp. 75–91). Oxford University Press.

Koepfli, K.-P., Gomper, M. E., Eizirik, E., Ho, C.-C., Linden, L., Maldonado, J. E., & Wayne, R. K. (2007). Phylogeny of the Procyonidae (Mammalia: Carnivora): Molecules, morphology and the Great American Interchange. *Molecular Phylogenetics and Evolution* 43(3), 1076–1095.

Kraglievich, J. L. (1952). El perfil geológico de Chapadmalal y Miramar, provincia de Buenos Aires. *Revista Museo Municipal Ciencias Naturales y Tradicional Mar del Plata*, 1(1), 8–37.

Kraglievich, J. L. & Olazábal, A. G. de. (1959). Los prociónidos extinguidos del género *Chapalmalania* Amegh. *Revista del Museo Argentina de Ciencias Naturales,* "*Bernadino Rivadavia*", (*Ciencias Zoológicos*), 6(1), 1–59.

Kraglievich, J. L. & Reig, O. A. (1954). Un nuevo prociónido del Plioceno de las Playas Provincia de Córdoba). *Revista del Asociación Geológica Argentina*, 9(4), 210–231.

Kurtén B. & Anderson E. (1980). *Pleistocene Mammals of North America*. Columbia University Press.

Linares, O. J. (1982) Tres nuevos carnívoros prociónidos fósiles del Mioceno de Norte y Sudamérica. *Ameghiniana*, 18, 113–121.

Lindsay, E. H., Jacobs, L. L., & Tessman, N. D. (2006). Vertebrate fossils from Yepómera, Chihuahua, Mexico. In O. Carranza-Castañeda & E. H. Lindsay (Eds.), *Advances in Late Tertiary Vertebrate Paleontology in Mexico and the Great American Biotic Interchange* (pp. 19–32). Publicación Especial 4. Universidad Nacional Autónoma de México, Instituto de Geología and Centro de Geociencias.

MacFadden, B. J., Bloch, J. I., Evans, H., Foster, D. A., Morgan, G. S., Rincon, A., & Wood, A. R. (2014). Temporal calibration and biochronology of the Centenario Fauna, early Miocene of Panama. *The Journal of Geology*, 122(2), 113–135.

Marshall, L. G. (1978). The terror bird. *Field Museum of Natural History Bulletin*, 49(9), 6-15.

Marshall, L. G. (1985). Geochronology and land-mammal biochronology of the Transamerican faunal interchange. In F. G. Stehli & S. D. Webb (Eds.), *The Great American Biotic Interchange* (pp. 49–85). Plenum Press.

Marshall, L. G., Butler, R. F., Drake, R. E., Curtis, G. H., & Tedford, R. H. (1979). Calibration of the Great American Interchange. *Science*, 204, 272–279.

Marshall, L. G., Drake, R. E., & Curtis, G. H. (1986). ^{40}K-^{40}Ar age calibration of late Miocene-Pliocene mammal-bearing Huayquerias and Tunuyan Formations, Mendoza Province, Argentina. *Journal of Paleontology*, 60, 448–457.

Marshall, L. G. & Patterson, B. (1981). Geology and geochronology of the mammal-bearing Tertiary of the Valle de Santa María and Río Corral Quemado, Catamarca Province, Argentina. *Fieldiana: Geology*, 9, 1–80.

Mercerat, A. (1895). Amphinasua Brevirostris Mor. et Merc. *Revista del Museo de La Plata*, 6, 253–264.

Moreno, F. P. & Mercerat, A. (1891). Esploración arqueológica de la Provincia de Catamarca. Paleontología. *Revista del Museo de La Plata*, 1, 222–236.

Nigenda-Morales, S. F., Gompper, M. E., Valenzuela-Galván, D., Lay, A. R., Kapheim, K. M., Hass, C., Booth-Binczik, S. D., Binczik, G. A., Hirsch, B.T., McColgin, M., & Koprowski, J. L. (2019). Phylogeographic and diversification patterns of the white-nosed coati (*Nasua narica*): Evidence for south-to-north colonization of North America. *Molecular phylogenetics and evolution*, 131, 149–163.

Patterson, B. & Kraglievich, J. L. (1960). *Sistemática y nomenclatura de las aves fororracoideas del Plioceno Argentino.* Publications del Museo municipal de ciencas naturales y tradicional de Mar del Plata 1, 1-51.

Patterson, B. & Pascual, R. (1968). The fossil mammal fauna of South America. *The Quarterly Review of Biology*, 43, 409–451.

Pino, K., Vallejos-Garrido, P., Espinoza-Aravena, N., Cooper, R. B., Silvestro, D., Hernández, C. E., & Rodríguez-Serrano, E. (2022). Regional landscape change triggered by Andean uplift: The extinction of Sparassodonta (Mammalia, Metatheria) in South America. *Global and Planetary Change*, *210*, doi.org/10.1016/j.gloplacha.2022.103758.

Pocock, R. I. (1921). The auditory bulk and other cranial characters in the Mustelidae. *Proceedings of the Zoological Society of London.* 1921, 473–486.

Prevosti, F. J. & Forasiepi, A. M. (2018). *Evolution of South American mammalian predators during the Cenozoic: paleobiogeographic and paleoenvironmental contingencies*. Springer.

Prevosti, F. J., Forasiepi, A., & Zimicz, N. (2013). The evolution of the Cenozoic terrestrial mammalian predator guild in South America: competition or replacement *Journal of Mammalian Evolution*, 20(1), 3–21.

Prevosti, F. J. & Reguero, M. A. (2000). Catálogo de tipos de vertebrados fósiles del Museo de La Plata. I. Carnivora. *Serie Técnica y Didáctica del Museo de La Plata*, 28, 1–12.

Prevosti, F. J., Romano, C. O., Forasiepi, A. M., Hemming, S., Bonini, R., Candela, A. M., Cerdeño, E., Madozzo Jaén, M., Ortiz, P. E., Pujos, F., & Rasia, L. (2021). New radiometric ^{40}Ar-^{39}Ar dates and faunistic analyses refine evolutionary dynamics of Neogene vertebrate assemblages in southern South America. *Scientific Reports*, 11(1), 1–14.

Reguero, M. A. & Candela, A. M. (2011). Late Cenozoic mammals from the northwest of Argentina. In J. A. Salfity & R. A. Marquillas (Eds.), *Cenozoic geology of the Central Andes of Argentina* (pp. 411–426) Salta: INCE, Instituto del Cenozoico.

Riggs, E. S. (1934). A new marsupial saber-tooth from the Pliocene of Argentina and its relationships to other South American predacious marsupials. *Transactions of the American Philosophical Society*, 24(1), 1–32.

Riggs, E. S. & Patterson, B. (1939). Stratigraphy of the Late-Miocene and Pliocene deposits of the province of Catamarca (Argentina), with notes on the faunae. *Physis*, 14, 143–162.

Rodrigues, S., Avilla, L. S., Soibelzon, L. H., & Bernardes, C. (2014). Late Pleistocene carnivores (Carnivora: Mammalia) from a cave sedimentary deposit in northern Brazil. *Anais da Academia Brasileira de Ciências*, 86, 1641–1655.

Rodriguez, S. G., Soibelzon, L. H., Rodrigues, S., Morgan, C. C., Bernardes, C., Avilla, L., & Lynch, E. (2013). First record of *Procyon cancrivorus* (G. Cuvier, 1798) (Carnivora, Procyonidae) in stratigraphic context in the Late Pleistocene of Brazil. *Journal of South American Earth Sciences*, 45, 1–5.

Rodriguez, S. G., Morgan, C. C., Soibelzon, L. H., & Lynch, E. (2016). Intra- and interspecific variation in tooth morphology of *Procyon cancrivorus* and *P. lotor* (Carnivora, Procyonidae), and its bearing on the taxonomy of fossil South American procyonids. *Hystrix, the Italian Journal of Mammalogy*, 27, doi:10.4404/hystrix-27.2-11647.

Romano, C. O., Bonini, R., Hemming, S., Cenizo, M., Pardiñas, U. F. J., & Prevosti, F. J. (2023). Advances in the understanding of Neogene mammalian fauna in the Pampean Region (Central Argentina) through revising "biozone" hypotheses based on new dates and biochronological analyses. *Ameghiniana*, doi: 10.5710/AMGH.07.07.2023.3551

Rovereto, C. (1914). Los estratos Araucanos y sus fósiles. *Anales del Museo Nacional de Historia Natural de Buenos Aires*, 25, 1–250.

Ruiz-García, M., Jaramillo, M. F., & Shostell, J. M. (2022a). How many taxa or groups are within *Nasua nasua* and *Nasuella olivacea* (Procyonidae, Carnivora)? The mitochondrial reconstruction of the complex evolutionary history of the coatis throughout the neotropics and some insights into the systematics of the genus *Bassarycion*. *Journal of Phylogenetics & Evolutionary Biology*, 10(3), DOI: 10.37421/2329-9002.2022.10.206.

Ruiz-García, M., Jaramillo, M. F., López, J. B., Rivillas, Y., Bello, A., Leguizamon, N., & Shostell, J. M. (2022b) Mitochondrial and karyotypic evidence reveals a lack of support for the genus *Nasuella* (Procyonidae, Carnivora). *Journal of Vertebrate Biology*, 71, 21040, 1–25. https://doi.org/10.25225/JVB.21040

Ruiz-Ramoni, D., Rincon, A., & Montellano-Ballesteros, M. (2018). Evidencias del origen de *Nasua* y *Procyon* (Procyonidae: Carnivora) en América del Sur. *Revista Brasileira de Paleontologia*, 21(1), 87–94.

Schmidt, G. I., Diederle, J. M., Góis, F., Vallone, E. R., Tarquini, J., Osuna, M. F., Gottardi, M. G., & Brandoni, D. (2020). New vertebrates from the Late Miocene of Entre Ríos Province, Argentina: diversity, age, and paleoenvironment. *Journal of South American Earth Sciences*, 101, doi.org/10.1016/j.jsames.2020.102618.

Simpson, G. G. (1945). The principles of classification and a classification of mammals. *Bulletin of the American Museum of Natural History*, 85, 1–350

Simpson, G. G. (1950). History of the fauna of Latin America. *American Scientist*, 38(3), 361–389.

Simpson, G. G. (1953). *Evolution and Geography: An Essay on Historical Biogeography with Special Reference to Mammals*. Condon Lectures. Eugene, Oregon, pp. 1–64.

Simpson, G. G. (1980). *Splendid Isolation, the Curious History of South American Mammals*. Yale University Press.

Soibelzon, E., Gasparini, G. M., Zurita, A., & Soibelzon, L. (2008). Análisis faunístico de vertebrados de las toscas del Río de La Plata (Buenos Aires, Argentina): un yacimiento paleontológico en desaparición. *Revista del Museo Argentino de Ciencias Naturales nueva serie*, 10(2), 291–308.

Soibelzon, L. H. (2011). First description of milk teeth of fossil South American procyonid from the lower Chapadmalalan (Late Miocene–Early Pliocene) of "Farola Monte Hermoso," Argentina: paleoecological considerations. *Paläontologische Zeitschrift*, 85(1), 83–89.

Soibelzon, L. H. & Bond, M. (2013). Revisión de los carnívoros (Carnivora, Mammalia) acuáticos y continentales del Mioceno de la Mesopotamia argentina. In D. Brandoni & J. I. Noriega (Eds.), *El Neógeno de la Mesopotamia argentina* (pp. 170–178). Asociación Paleontológica Argentina, Publicación Especial, 14.

Soibelzon, L. H. & Prevosti, F. J. (2007). Los carnívoros (Carnivora, Mammalia) terrestres del Cuaternario de América del Sur. In G. X. Pons, and D. Vicens (Eds.), *Geomorphologia Litoral I Quaternari. Homenatge a D. Joan Cuerda Barceló* (pp. 49–68). Monografies de la Societat d'Història Natural de les Balears, 14.

Soibelzon, L. H. & Prevosti, F. (2012). South American Fossil Land Carnivores (Carnivora, Mammalia): State of the Art. In M. Ruiz-Garcia & J. M. Shostell (Eds.), *Molecular population genetics, evolutionary biology and biological conservation of neotropical carnivores* (pp. 509–530). Nova Science Publishers

Soibelzon, L. H., Rinderknecht, A., Tarquini, J., & Ugalde, R. (2019). First record of fossil procyonid (Mammalia, Carnivora) from Uruguay. *Journal of South American Earth Sciences*, 92, 368–373.

Soibelzon, L. H., De los Reyes, M., Tarquini, J., Tineo, D. E., Poiré, D. G., González, G., & Vergani, G. D. (2020). First record of a fossil procyonid (*Cyonasua* cf. *C. pascuali*), Mammalia, Procyonidae) in Bolivia, Tariquía Fm., Late Miocene. *Journal of South American Earth Sciences*, 99, /doi.org/10.1016/j.jsames.2019.102492.

Soibelzon, L. H., Zurita, A. E., Morgan, C. C., Rodríguez, S., Gasparini, G. M., Soibelzon, E., Schubert, B. W., & Miño-Boilin, Á. R. (2010). Primer registro fósil de *Procyon cancrivorus* (G. Cuvier, 1798) (Carnivora, Procyonidae) en la Argentina. *Revista mexicana de ciencias geológicas*, 27(2), 313–319.

Solórzano, A., Rincón, A. D., & McDonald, H. G. (2015). A New Mammal Assemblage from the Late Pleistocene El Breal de Orocual, Northeast of Venezuela. *Science Series, Natural History Museum of Los Angeles County*, 42, 125–150.

Stangl, F. B., Henry-Langston, S., Lamar, N., & Kasper, S. (2014). Sexual dimorphism in the ringtail (*Bassariscus astutus*) from Texas. *Occasional Papers, Museum of Texas Tech University*, 328, 1–8.

Storr, G. C. C. (1780). *Prodromus methodi Mammalium.* Tübingen: Reissianis.

Tarquini, J. (2018). *El esqueleto poscraneano de los Procyonidae (Mammalia, Carnivora) vivientes y extintos de América del Sur: análisis morfo-funcional y ecomorfológico*. [Unpublished doctoral dissertation]. Universidad Nacional de La Plata, Facultad de Ciencias Naturales y Museo, La Plata.

Tarquini, J., Vilchez Barral, M. G., & Soibelzon, L. H. (2016). Los prociónidos fósiles de América del Sur. *Contribuciones científicas del Museo Argentino de Ciencias Naturales*, 6, 359–365.

Tarquini, J., Toledo, N., Soibelzon, L. H., & Morgan, C. C. (2018). Body mass estimation for †*Cyonasua* (Procyonidae, Carnivora) and related taxa based on postcranial skeleton. *Historical Biology*, 30(4), 496–506. dx.doi.org/10.1080/08912963.2017.1295042

Tarquini, J., Morgan, C. C., Toledo, N., & Soibelzon, L. H. (2019). Comparative osteology and functional morphology of the forelimb of *Cyonasua* (Mammalia, Procyonidae), the first South American carnivoran. *Journal of Morphology*, 280(3), 446-470.

Tarquini, J., Soibelzon, L. H., Salas-Gismondi, R., & De Muizon, C. (2020). *Cyonasua* (Carnivora, Procyonidae) from late Miocene of

Peru shed light on the early dispersal of carnivorans in South America. *Journal of Vertebrate Paleontology*, 40(5), p. e1834406.

Tarquini, S. D., Ladevèze, S., & Prevosti, F. J. (2022). The multicausal twilight of South American native mammalian predators (Metatheria, Sparassodonta). *Scientific Reports*, 12(1), 12–24.

Tomassini, R. L., Montalvo, C. I., Deschamps, C. M., & Manera, T. (2013). Biostratigraphy and biochronology of the Monte Hermoso Formation (early Pliocene) at its type locality, Buenos Aires Province, Argentina. *Journal of South American Earth Sciences*, 48, 31–42.

Tonni, E. P. (2009). Los mamíferos del Cuaternario de la región pampeana de Buenos Aires, Argentina. In M. T. Alberdi, G. Leone, & E. P. Tonni (Eds.), *Quaternario Do Rio Grande do Sul: integrando conocimientos* (pp. 193-205). Monografias da Sociedade Brasileira de Paleontologia, Porto Alegre.

Tonni, E. P., Alberdi, M. T., Prado, J. L, Bargo, M. S., & Cione, A. L. (1992). Changes of mammal assemblages in the Pampean region (Argentina) and their relation with the Plio-Pleistocene boundary. *Palaeogeography, Palaeoclimatology, Palaeoecology*, 95, 179–194.

Trouessart, E. L. (1904). *Catalogus mammalium tam viventium quam fossilum*. Quinquennale Supplementum, Fasciculus I. Primates, Prosimiae, Chiroptera, Insectivora, Carnivora, Pinnipedia. R. Friedländer und Sohn.

Turner, H. N. (1848). Observations relating to some of the foramina at the base of the skull in Mammalia, and on the classification of the order Carnivora. *Proceedings of the Zoological Society of London*, 1848, 63–88.

Valenciano, A., Baskin, J. A., Abella, J., Pérez-Ramos, A., Álvarez-Sierra, M. A., Morales, J., & Hartstone-Rose, A. (2016). *Megalictis*, the bone-crushing giant mustelid (Carnivora, Mustelidae, Oligobuninae) from the Early Miocene of North America. *PLoS ONE*, 11(4), e0152430.

Wagner, H. (1976). A new species of *Pliotaxidea* (Mustelidae: Carnivora) from California. *Journal of Paleontology*, 50, 107–127.

Wagner, H. M. (1981). *Geochronology of the Mehrten Formation in Stanislaus County, California*. Ph.D. dissertation, Department of Geology, University California, Riverside, 342 pp.

Wang, X., Emry, R. J., Boyd, C. A., Person, J. J., White, S. C., & Tedford, R. H. (2023). An exquisitely preserved skeleton of *Eoarctos vorax* (nov. gen. et sp.) from Fitterer Ranch, North Dakota (early Oligocene) and systematics and phylogeny of North American early arctoids (Carnivora, Caniformia), *Journal of Vertebrate Paleontology*, 42, sup1, 1–123, DOI: 10.1080/02724634.2022.2145900.

Webb, S. D. (1985). Late Cenozoic mammal dispersals between the Americas. In F. G. Stehli and S. D. Webb (Eds.), *The Great American Biotic Interchange* (pp. 357–386). Plenum Press, New York.

Webb, S. D., Hulbert Jr, R., Morgan, G. S., & Evans, H. F. (2008). Terrestrial mammals of the Palmetto Fauna (early Pliocene, latest Hemphillian) from the central Florida phosphate district. *Natural History Museum Los Angeles County Science Series*, 41, 293–312.

Wolsan, M. & Lange-Badré, B. (1996). An arctomorph carnivoran skull from the Phosphorites du Quercy and the origin of the procyonids. *Acta Palaeontologica Polonica*, 41, 277–298.

Woodburne, M. O. (2010). The Great American Biotic Interchange: dispersals, tectonics, climate, sea level and holding pens. *Journal of Mammalian Evolution*, 17(4), 245–264.

Woodburne, M. O., Cione, A. L., & Tonni, E. P. (2006). Central American provincialism and the Great American Biotic Interchange. In Ó Carranza-Castañeda & E. H. Lindsay (Eds.), *Advances in late Tertiary vertebrate paleontology in Mexico and the Great American Biotic Interchange* (pp. 73–101). Universidad Nacional Autónoma de México, Instituto de Geología and Centro de Geociencias, Publicación Especial, 4.

Yrigoyen, M. R. (1994). Revisión estratigráfica del Neógeno de las Huayquerías de Mendoza septentrional, Argentina. *Ameghiniana*, 31(2), 125–138.

Zetti, J. (1966). Carnivora. In R. Pascual, E. J. Ortega Hinojosa, D. Gondar, & E. Tonni (Eds.) *Vertebrata*. *in* (Borello, A. V., ed.) *Paleontografia Bonaerense*. IV (pp. 146–160). La Plata.

Zetti, J. (1972). *Los mamíferos fósiles de edad Huayqueriense (Plioceno medio) de la región pampeana*. [Unpublished doctoral dissertation]. Universidad Nacional de La Plata, Facultad de Ciencias Naturales y Museo, La Plata.

Zimicz, N. (2014). Avoiding competition: the ecological history of late Cenozoic metatherian carnivores in South America. *Journal of Mammalian Evolution*, 21, 383–393.